Serbian Association for Geometry and Graphics

The 7th International Scientific Conference on Geometry and Graphics

moNGeometrija 2020

September 18th - 21st, Belgrade, Serbia

PROCEEDINGS

Serbian Association for Geometry and Graphics

The 7th International Scientific Conference on Geometry and Graphics

moNGeomatrija2020

PROCEEDINGS

September 18th – 21st 2020, Belgrade, Serbia

ISBN 978-86-6060-046-4

SUGIG

Beograd, 2020.

The 7th International Scientific Conference on Geometry and Graphics

moNGeomatrija2020

Publishers

Serbian Society for Geometry and Graphics (SUGIG)
Faculty of Mechanical Engineering, University of Belgrade

Title of Publication
PROCEEDINGS

Editor-in-Chief
Zorana Jeli

Co-Editors
Branislav Popkonstantinović
Slobodan Mišić
Djordje Djordjević
Maja Petrović

Graphic design
Djordje Djordjević
Maja Petrović

Formatters
Djordje Djordjević
Maja Petrović
Ivana Cvetković
Nikola Popović

Print
Planeta print, Belgrade

Dean's decision number 13/20 from 20.08.2020.

Number of copies: 80

ISBN 978-86-6060-046-4

The 7th International Scientific Conference on Geometry and Graphics

moNGeomatrija2020

Conference Organizers

Serbian Society of Geometry and Graphics (SUGIG)

Faculty of Mechanical Engineering, University of Belgrade

Co-organizers

Faculty of Civil Engineering, University of Belgrade

Faculty of Architecture, University of Belgrade

Faculty of Forestry, University of Belgrade

Faculty of Applied Arts, University of Arts in Belgrade

Faculty of Transport and Traffic Engineering, University of Belgrade

Under the auspicies of

Ministry of Education, Science and Technological Development of Republic of Serbia

Scientific Committee:

Hellmuth Stachel – Austria
Emil Molnar – Hungary
Gunter Weiss – Germany
Djuro Koruga– Serbia
Naomi Ando – Japan
Radovan Štulić – Serbia
Branislav Popkonstantinović – Serbia
Ratko Obradović – Serbia
Branko Malešević – Serbia
Lidija Matija – Serbia
Grga Djurica – Serbia
Daniel Lordick – Germany
Albert Wiltsche – Austria
Milena Stavric – Austria
Ajla Aksamija– USA
Olga Timcenko – Denmark
Ema Jurkin – Croatia
Alina Duta – Romania
Dragos-Laurentiu Popa – Romania
Carmen Marza – Romania
Laszlo Voros – Hungary
Zsuzsanna Balajti – Hungary
Monika-Sroka Bizon – Poland
Tashko Rizov – Macedonia
Milan Petrović – Serbia
Maja Čavić – Serbia
Vesna Stojaković – Serbia
Aleksandar Čučaković – Serbia
Marija Obradović – Serbia
Sonja Krasić – Serbia
Milan Ristanović – Serbia
Slobodan Mišić – Serbia
GianLucca Stasi – Spain
Maja Ilić – Republic of Srpska, Bosnia and Herzegovina
Djordje Djordjević – Serbia
Mirjana Devetaković – Serbia
Marijana Paunović – Serbia
Magdalena Dragović – Serbia
Gordana Djukanović – Serbia
Maja Petrović – Serbia
Emil Veg – Serbia
Miša Stojićević – Serbia
Bojan Banjac – Serbia

Organizing Committee:

Zorana Jeli
Aleksandar Čučaković
Marija Obradović
Slobodan Mišić
Djordje Djordjević
Mirjana Devetaković
Marijana Paunović
Magdalena Dragović
Gordana Djukanović
Maja Petrović
Emil Veg
Miša Stojićević
Bojan Banjac
Ana Petrović
Boris Kosić
Ivana Vasiljević
Ivana Cvetković
Aleksandra Dragićević
Aleksandra Joksimović

Reviewers:

Prof. Hellmuth Stachel – Austria
Prof. Gunter Weiss – Germany
Prof. Naomi Ando – Japan
Prof. Radovan Štulić – Serbia
Prof. Branislav Popkonstantinović – Serbia
Prof. Ratko Obradović – Serbia
Prof. Branko Malešević – Serbia
Prof. Lidija Matija – Serbia
Associate Prof. Milena Stavrić – Austria
Associate Prof. Ajla Aksamija – USA
Associate Prof. Ema Jurkin – Croatia
Associate Prof. Alina Duta – Romania
Associate Prof. Dragos-Laurentiu Popa – Romania
Associate Prof. Carmen Marza – Romania
Associate Prof. Laszlo Voros – Hungary
Associate Prof. Zsuzsanna Balajti – Hungary
Associate Prof. Monika-Sroka Bizon – Poland
Associate Prof. Tashko Rizov – Macedonia
Associate Prof .Aleksandar Čučaković – Serbia
Associate Prof. Marija Obradović – Serbia
Associate Prof. Sonja Krasić – Serbia
Associate Prof. Slobodan Mišić – Serbia
Associate Prof. Vesna Stojaković – Serbia
Associate Prof. GianLucca Stasi – Spain
Associate Prof. Zorana Jeli – Serbia
Ass. Prof. Maja Ilić – Republic of Srpska, Bosnia and Herzegovina
Ass. Prof. Magdalena Dragović – Serbia
Ass. Prof. Emil Veg – Serbia

Ass. Prof. Miša Stojićević – Serbia
Ass. Prof. Djordje Djordjević – Serbia
Ass. Prof. Mirjana Devetaković – Serbia
Ass. Prof. Marijana Paunović – Serbia
Ass. Prof. Gordana Djukanović – Serbia
Ass. Prof. Bojan Banjac – Serbia
Ass. Prof. Maja Petrović – Serbia

PROCEEDINGS

CONTENT

TOPIC 1: THEORETICAL GEOMETRY AND GRAPHICS

CONTENT

- INVITED LECTURE -

GEOMETRIC PROPERTIES OF THE "FLOWER" CONCAVE ANTIPRISMS OF THE SECOND SORT

Marija Obradović
University of Belgrade, Faculty of Civil Engineering
PhD., Associate Professor, marijao@grf.bg.ac.rs

ABSTRACT

This study presents a continuation of the research on the concave polyhedra of the second sort, adding to this family a new group of related polyhedra. They are formed over a specific type of isotoxal concave polygons that allow geometric arrangement of a double row of equilateral triangles into formations which enclose a deltahedral lateral surface without overlaps and gaps. As in all other representatives of the concave polyhedra of the second sort, we expect to find here the "major" and "minor" type, depending on the way we fold the net. This research has identified both these polyhedra types, which have the same planar net, but are formed over different basic concave polygons. The origination, constructive methods and properties of these solids are elaborated in the paper.

Keywords: concave polyhedron; concave polygon; polygon elevation; antiprism; isotoxal; constructive geometry

INTRODUCTION

Triangulated surfaces, as one of the most common ways of visualizing complex free-form shapes, as well as parametric and implicit surfaces are among the most recognizable features of computer graphics in recent decades. Numerous software programs use algorithms that can represent any shape by a series of connected triangles, so that irregular deltahedral surfaces, made up of arbitrary (scalene) triangles, form the weft of any free-form shape. Thus, triangular nets have the ability to obediently apply our ideas via digital tools and adapt to any desired surface, discretizing it. However, if we introduce more geometric regularities into the process of forming the net itself and also increase the level of the regularities expected from the resulting shapes, the free form inevitably gives way to the geometric one.

If we introduce a requirement that each triangle should be equilateral, the surface continuous and convergent, we will pose a problem that can be solved by a different, perhaps simpler approach. Knowing the properties and relations of linear and angular measures within an equilateral triangle, we can solve the task with classical geometric methods, from trigonometry to constructive geometry. Given an additional condition: that these regular deltahedral surfaces should also encompass regular polygonal bases, we come to a few convex solutions, such as Platonic solids: tetrahedron, octahedron and icosahedron, and Johnson solids: J12 and J13 (Johnson, 1966) while convexity alone adds three Johnson solids more: J17, J51 and J84. However, if we exclude convexity as a criterion, we are left with various other possibilities. Some of them have been described in a series of papers (Obradović et al.., 2013-II; Mišić et al.., 2015, Obradović et al.., 2017) dealing with composite concave deltahedra based on the geometry of concave polyhedra of the second (or higher) sort with regular polygonal bases. The later solids, the concave polyhedra of the second sort, serve as a foundation of this research as well. They include: concave cupolae (Obradović et al.., 2008), concave pyramids (Obradović et al.., 2014; Obradović et al.., 2015) and concave antiprisms of the second sort (Obradović et al.., 2013-I). The sort is determined by the number of rows of equilateral triangles in the lateral surface, which is directly related to the number of resulting solutions (ergo, heights of those solutions). The 'sorts' are regularly of an even number (Mišić, 2013), so we have concave polyhedra of the second, fourth, sixth, etc. sorts, except for the antiprisms which are always of the second sort.

In this paper, as an addition to the above concave polyhedra formed over regular *convex* polygonal bases, we look for concave polyhedra that are formed in a similar way, but with *concave* polygon of multilateral *k*-fold symmetry as the basic one. We start from the ones that can create an infinite deltahedron (Wachman et al..,

1974). Those are (concave) antiprisms, formed over two identical polygonal bases. Given that their star-like bases are not actually stellations of convex polygons, the solutions obtained will not be polygrammatic antiprisms (Huybers, 2001), but original solids with all edges of equal length and with deltahedral lateral surfaces. This paper explores the shapes of these bases and the ways to form the solids out of the same triangular net so that we get feasible solutions without gaps or overlaps of the triangular faces.

2. RESULTS OF PREVIOUS RESEARCH

Two previous studies are crucial to understanding the method and the results of this research. The first one (Obradović et al.., 2013-I) concerns the definition of the forms and measures of the concave antiprism of the second sort, CA-II. We have shown that they are formed, similarly to the concave cupolae or concave pyramids of the second sort, by folding a net of double series of equilateral triangles, and that, depending on the way the net is folded, they may be higher (major, M) or lower (minor, m) in height. In other words, they can exist as two types of the concave antiprisms, denoted by: CA-II-nM and CA-II-nm. Fragments of these solids' surface were used to obtain concave rings-like surfaces, crucial for the next study.

The second study (Obradović et al.., 2019) considers a special way of assembling the major type of the solids mentioned above, CA-II-nM, so that their lateral surfaces form deltahedral closed rings. These rings are consequently of the second sort, thus denoted by CDR-II. They are formed by closing the full circle via 2π polar array of unit *spatial decahedral cells*, shown in Fig. 1 a) and b), formed by two partly overlapped unit hexahedral cells of two adjacent CA-II-nMs (Obradović et al.., 2019, Fig. 2). To perform a precise array, we have determined the angle $\boldsymbol{\omega}$ (or $\boldsymbol{\varphi}$) found between the symmetry planes (σ or τ) of the adjacent pair of CA-II-nMs (Fig 1 c and d). The planes, seen as the axes of symmetry in the top orthogonal view are defined by the outermost points of the unit decahedral cells. Their multiplication by an integer $\boldsymbol{K}$ gives a full circle, so that the ring is obtained.

In this paper, only the angle $\boldsymbol{\omega}$ is relevant for the calculus and the construction of the lateral surface.

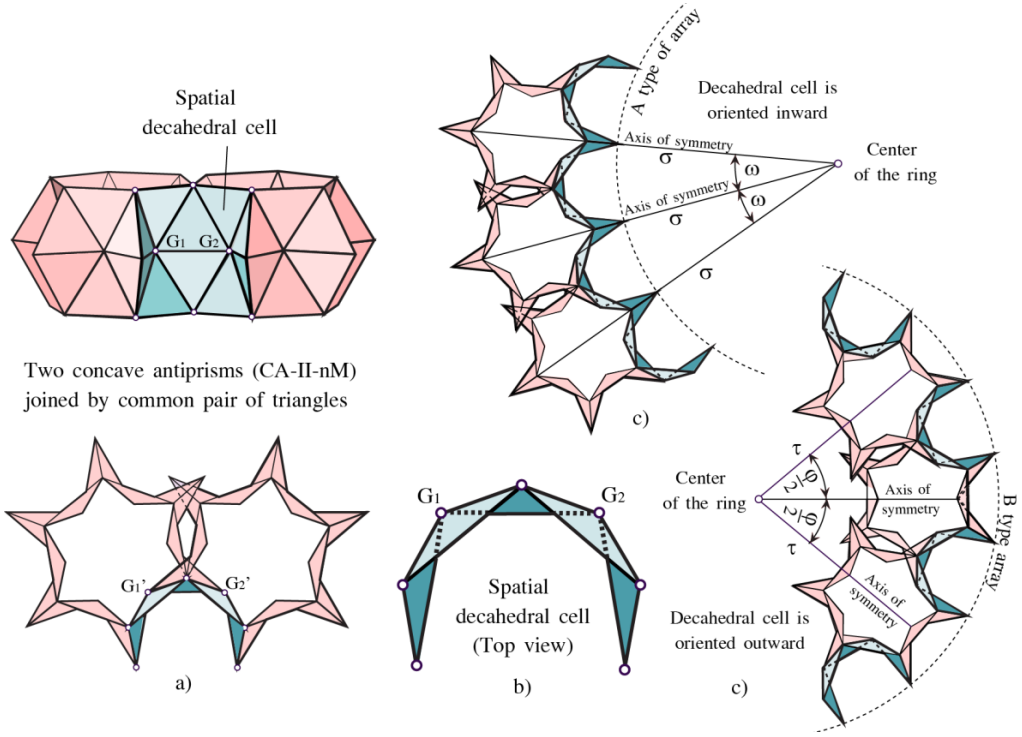

Figure 1: (a) Two paired concave antiprisms of the second sort (CA-II-nM) (b) Unit spatial decahedral cell (c) Two ways of forming concave deltahedral rings (CDR-II) using the unit decahedral cells (Source: Obradović et al. (2019); illustration is modified Fig. 2)

The obtained rings share key features of concave polyhedra of the second sort: multilateral *k*-fold symmetry, deltahedral lateral surface and the same folding methods, which produce its major and minor type. Naturally, since they are derived from CA-II-nM's fragments, they share their linear and angular dimensions.

In the top view, the shapes of CDR-II can be flower-like or star-like, with distinct shapes (A, B) or even more complex, mixed with fragments of CA-II-nMs (A_f, B_f) in between "petals" or "star-points", depending on the

number of sides (n) in the CA-II-nM's base polygon from which the rings originate. The number n conditions the number k, which represents the number of decahedral cells in the ring. If the full ring is closed with k unit cells, then $k=K$, which is the number of "petals" or "star points" in the newly obtained rings. Based on the formulae (1) and (3) in (Obradović et al.., 2019), for the angle $\boldsymbol{\omega}$, and having that: $k_{A,B} = \frac{2\pi}{\omega}$ the interdependence between n and k can be expressed as:

$$\boldsymbol{k} = \frac{3\boldsymbol{n}}{\boldsymbol{n}-5};\ \boldsymbol{n} \in \mathbb{N} \qquad \text{(Eq.1)}$$

The aforementioned study, of which this research is a continuation, considered only the forms of rings obtained by using (decahedral) fragments of CA-II-nM, without dealing with geometry of the bases thus obtained, since eight different possible ring shapes can be identified: A, A_f, A_a, B, B_f, B_{f3}, C and C_f. Thus, n had to be an integer, as the number of sides in the basic regular polygon of the CA-II-nM, while k was usually a rational number, and in only a few special cases an integer too (when the pure forms A and B of the ring are obtained). Therefore, in general case, we needed to correct k by a factor j to convert the fraction k to an integer K, which represents the number of "petals" or "star points" in the deltahedral rings.

In this study, the subject of the research are solids whose lateral surfaces are just pure forms (A and B) of concave deltahedral rings, with a number of "petals" that can be of any integer $k \in \mathbb{N}$ (CDR-II-k). Also, unlike the previous research, we do not examine only the lateral surfaces, but the whole solid, including the shapes of the base polygons. In addition, we are looking for a connection between the A and B ring shapes and the major and minor solid types.

3. INITIAL SETTINGS OF THE RESEARCH

This paper investigates an entire group of polyhedra generated with a precise polar array of k spatial decahedral cells, with no additional cells in between. Hence, we are looking for the distinct forms of "flowers" only, which are obtained by folding the net of the deltahedral lateral surface. In this case, the number n will not always be an integer as it was with CDR-II, but the number k will, as an assigned number of sides in the regular k-sided polygon which we elevate[1] (Grünbaum et al.., 1986) by triangles, i.e. "petals" of the new non-convex, $2k$-sided polygon. This $2k$-sided, star-like isotoxal[2] polygon will be the base polygon of the "flower" concave antiprism, and finding its geometrical properties is one of the foci of this paper.

We are investigating a special type of concave polygons that arise as elevated k-sided regular convex polygons, and have the property that their concave angles are conjugate to the interior angles of the n-sided convex polygon.

3.1. Minor Type of Floral antiprisms of the second sort

Although in the previous research we used CA-II-nM, i.e. the antiprisms of the **major** height for the procedure of obtaining CDR-II-K, the resulting structures came out to have all the characteristics of the lower-height solid type. Why? Because the disposition of protruding and indented vertices and edges, when viewed from the exterior, gives the result that corresponds to the way the triangular net is folded to get the minor type of concave polyhedra of the second sort. The central vertices G_1 and G_2 of the unit decahedral cell (Fig. 1a, b), originating from the central vertex G of the hexahedral cell in the CA-II-nM are protruding, which gives a lower height (Obradović et al.., 2013-I), as it is the case with all the other C-II-n representatives (Obradović et al.., 2008; Obradović et al.., 2014; Obradović et al.., 2015). Given that we are here applying the same method of folding the triangular net in two different ways, major and minor, with this we obtain the lateral surface of minor height, which will be evidenced by the elaboration of the major type, discussed later.

Let us first look at the geometric properties and the method of generating the "flower" antiprisms of the second sort with k petals, of minor type (FA-II-km). Inverting the procedure of the previous research, now the input is k - the number of "petals" we wish to obtain, so the number n - the assumed number of the sides in CA-II-nM that produces this deltahedral surface is derived from the above formula (Eq. 1):

[1] Grünbaum used the term „elevatum" for the positive height, i.e. pointing outward pyramids in augmentations (Weisstein https://mathworld.wolfram.com/Augmentation.html) .

[2] Isotoxal polygon is an equilateral, edge transitive polygon, i.e. it has only one type of edge.

$$n_m = \frac{5k}{k-3};\ k \in \mathbb{N} \qquad \text{(Eq.2)}$$

Although n will not be an integer in most cases, this will not interfere with the formation of deltahedral ring (CDR-II-k) for any $k \in \mathbb{N}$. In all cases, the interior angles of n-sided polygon define the exterior angles of the star-like $2k$-sided polygon.

In Fig. 2 we see the starting setup with the elements we use to trigonometrically determine all the necessary angular measures for defining the basis $2k$-sided polygon.

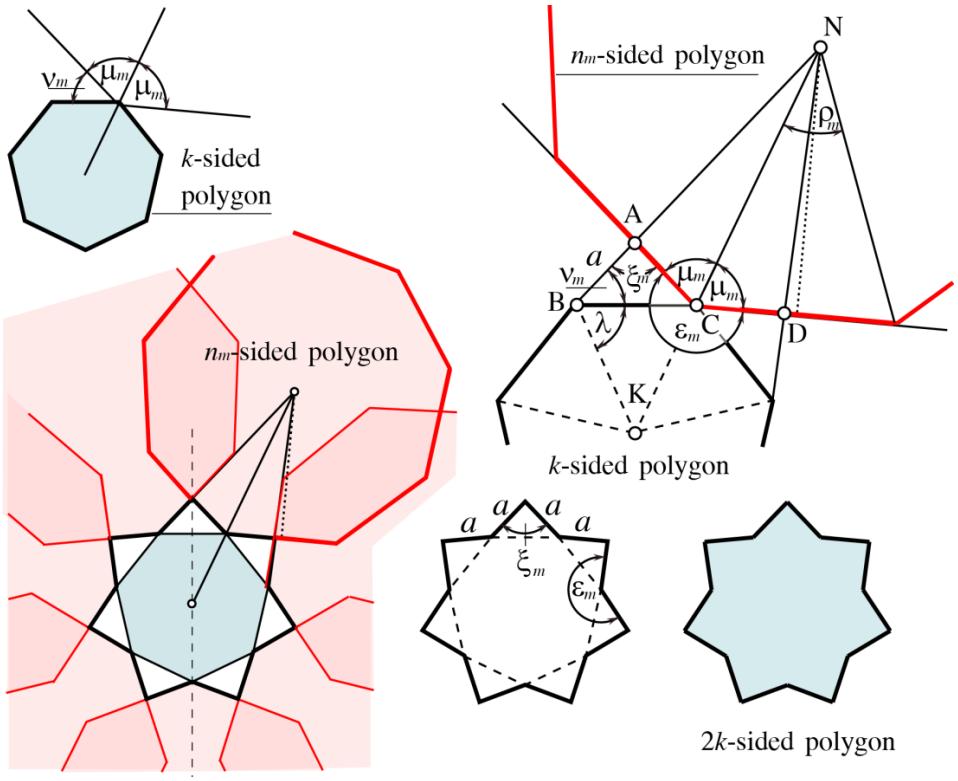

Figure 2: The way of forming the basic 2k-sided star-like polygon based on the k-sided regular convex polygon, the key angles and the final shape of the polygon (the example of heptagon)

We first need to determine the value of the angle μ_m, the interior angle of the n-sided polygon, then to define the other necessary angles depending on it, above all the angle ε_m in the "star-polygon" as its conjugate angle, and the angle υ_m as the base angle of the elevatum triangle. This way, a special type of concave, isotoxal polygon arises as an elevation of the k-sided regular convex polygon.

The calculated values of the angles: ρ_m, λ, μ_m, υ_m, ξ_m and ε_m (Fig. 2) relevant for determining the interdependence between the n-sided and $2k$-sided polygons are given by the formulas in Table 1.

Table 1: Overview of all the angles relevant for determining the 2k-sided star-like concave polygon (base "flower" polygon) for the minor type of "flower antiprism" FA-II-km

Angle	=	$f(k)$	*Equation*
ρ_m	=	$\frac{2\pi(k-3)}{5k}$	(Eq.3)
λ	=	$\frac{\pi(k-2)}{2k}$	(Eq.4)
μ_m	=	$\frac{3\pi(k+2)}{10k}$	(Eq.5)
υ_m	=	$\frac{\pi(k+2)}{5k}$	(Eq.6)
ξ_m	=	$\frac{\pi(3k-4)}{10k}$	(Eq.7)

ε_m	=	$\frac{\pi(7k-6)}{5k}$	(Eq.8)

The obtained polygon will be neither a regular star polygon[3] (Kepler, 1619/1968; Coxeter, 1969) i.e. stellation, or polygram, nor a regular compound polygon (see: Bowers, 2012), except in two special cases. It is an equilateral, isotoxal star polygon with angles such that:

$$\varepsilon_m = \frac{\pi}{2} + 3\xi_m \qquad \text{(Eq.9)}$$

Table 2 shows the interdependencies of the numbers *k* and *n*. We can see how the values of *n* in the outer polygon change as the values of *k* increase. We notice that when *k* tends to infinity, *n* tends to number 5, which can also be verified by the Eq. 1.

Table 2: Minor type of FA-II-k; Interdependence of the number of sides of two conjugated polygons: *k*-sided and *n*-sided

k	3	4	5	6	7	8	9	10	11	12	13	14	15	16	17	18	19	20	21	22
n_m	∞	20	12.5	10	8.75	8	7.5	7.14	6.875	6.66	6.5	6.36	6.25	6.15	6.07	6	5.94	5.88	5.94	5.88

We find that both *k* and *n* are integers only in 4 cases (plus 2 in which the associated number is infinite), as shown in Table 3. This, however, does not in any way interfere with the formation of the star polygon for any value of $k \in \mathbb{N}$. These 4 cases are the ones where CA-II-nM and FA-II-km can be adjoined and match face to face so that they can be arranged as modular elements.

Table 3: Minor type of FA-II-k - Cases when both k and n are integers

k	3	4	6	8	18	∞
$n_m = \frac{5k}{k-3}$	∞	20	10	8	6	5

In the case of $k = 8$, there is a unique situation when the *2k*-sided polygon is simultaneously a stellated polygon - obtuse octagram {8/2} (Grünbaum, et al.., 1986), a regular compound polygon and a flower (minor) polygon.

As stated above, the sides of this "flower" star polygon are all of equal length, *a*, which is the side of an equilateral triangle in the lateral surface. The question we have to resolve now is what the arrangement of equilateral triangles in the deltahedral surface of such an FA-II-km will look like.

3.2. Description of the Constructive Procedure

Each "petal" of the "flower" antiprism consists of ten equilateral triangles, organized as described in (Obradović et al.., 2019) and forming a unit decahedral cell (see Fig. 1). These cells are connected to the adjacent ones by the outermost edges and, thus arrayed, they close the annular lateral surface.

The decahedral unit cell has two planes of symmetry:

- the vertical one, passing through the midpoint of the edge G_1G_2 and the centroid (K) of the base polygon,
- the horizontal one, passing through the vertices G_1 and G_2, parallel to the planes of the bases.

Due to the later, in the top view, the triangles that constitute it are seen as overlapped, two by two. Thus, we will see only 5 triangles organized around each "star elevatum" ABC of the initial *k*-sided polygon, the matrix for the *2k*-sided isotoxal "flower" polygon (Fig. 3 c).

It is imperative that in the first projection (top view) all the triangles from the lateral surface should be projected into congruent triangles, since both bases of the concave antiprism are, by definition, congruent and all the

[3] According to one of Kepler's definitions, not only stelations, but isotoxal concave polygons are also named 'star polygons'.

triangles are set at the same angle with respect to them, in order to span the same height (Fig 3 b). Therefore, the base angles in these isosceles triangles are all equal and amount to the value denoted by α.

The 5 visible triangles (seen in top view) from the unit decahedral cell are arrayed in an open polygon with 7 vertices: H_1, C, G_1, A, G_2, B and H_2 (enumerated clockwise) as shown in Fig 3 a) and b). Given that 3 of these 7 vertices coincide with the vertices ABC of the base star polygon, we come to the conclusion that all the (projected) vertices of the decahedral unit cell lie on the same circle *c*, determined by the vertices A, B, and C. The vertices G_1 and G_2 are easily found in the intersection of the normals of the sides AB and BC respectively, with the circle *c* itself (Fig. 3 a), while the vertices H_1 and H_2 are found at the intersection points of the circle *c* and the symmetry axes - planes (σ) of the base polygon, set through the vertices B and C respectively.

Then, with the polar array of *k* identical decahedral cells, and with the center in the intersection point (K) of their symmetry planes (σ), we form the entire ring (Fig. 3 d).

In Fig. 3 e) we can see the first orthogonal projection of the "flower" antiprism's lateral surface thus obtained.

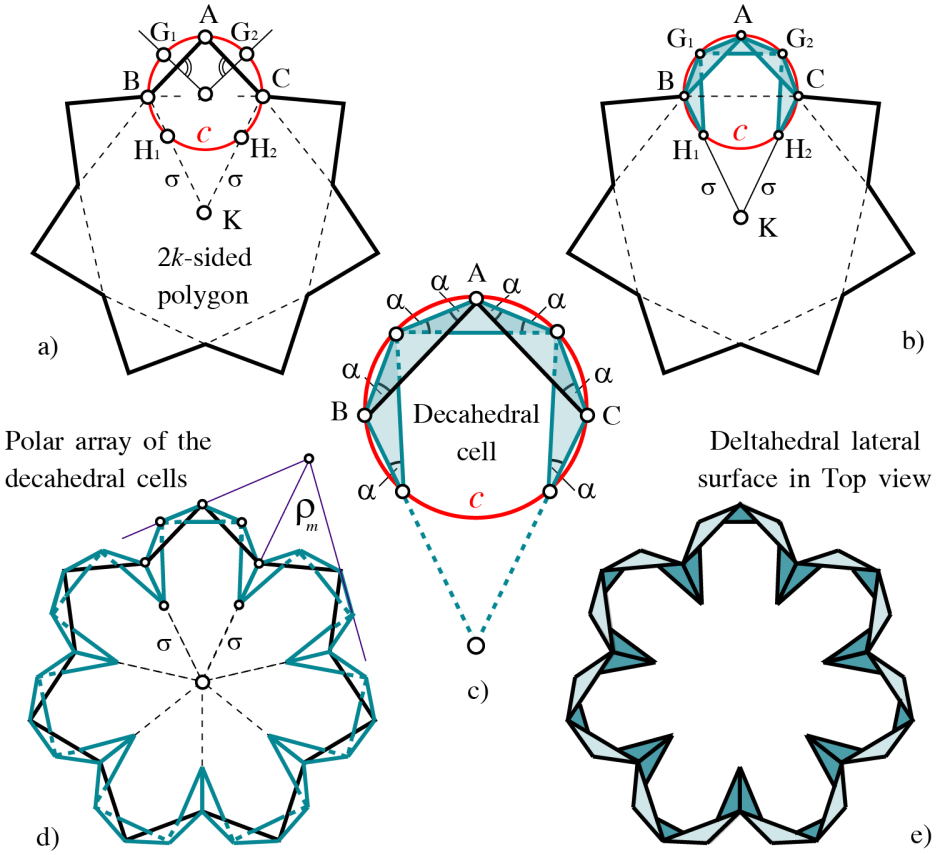

Figure 3. Construction and polar array of a single decahedral cell

3.3. Determining the height of the solid

In order to fully define the solid, we need to determine the heights of the vertices. According to formula (1) in (Obradović et al.., 2019), the angles α seen in the first projection are the base angles in the isosceles triangle, which every triangle from the deltahedral surface is projected into. We can now calculate this angle α as $f(k)$.

$$\alpha_m = \frac{\pi(k+2)}{10k} \qquad \text{(Eq.10)}$$

Based on this angle, we can calculate the height of the solid itself. On the other hand, we can easily obtain it via constructive procedures based on the 3D transformations of an equilateral triangle (Fig. 4 a).

$$h = \frac{a}{2}\sqrt{3-(tg\alpha)^2} \qquad \text{(Eq.11)}$$

The constructive - geometric procedures for obtaining the height of the "flower" antiprism (h_{FA}), i.e. the heights of the vertices A, B and C, start from the assumption that the vertices G_1, G_2, H_1 and H_2 lie in the horizontal plane at height h=0. Two of them are shown in Figure 4. We can use:

- the method of introducing a new transformation plane (2') in the orthogonal view, given in Fig. 4 a)
- the method of 3D rotation of the equilateral triangle's edge (H_1B) in a 3D environment, given in Fig. 4 b).

With the obtained heights of the vertices A, B and C we easily form lateral triangles (Fig. 4 b), and then the whole lateral surface, considering that the entire structure should be repeated, i.e. "mirrored", with respect to the horizontal plane of symmetry (Fig. 4 c).

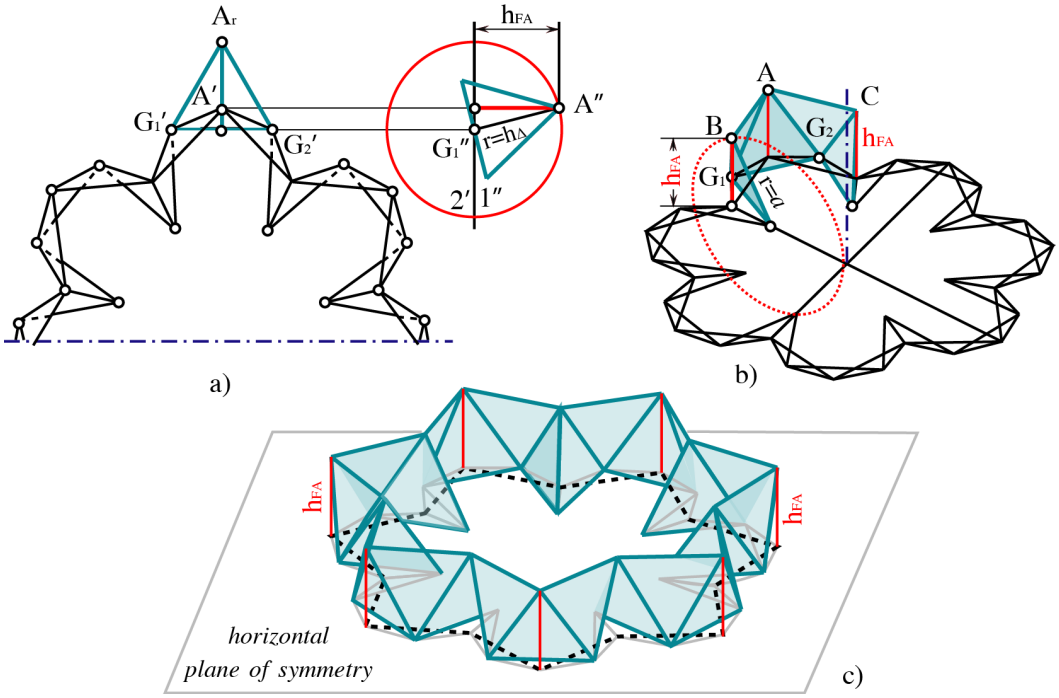

Figure 4: Construction of the vertex heights: (a) transformation plane method, (b) 3D rotation method (c) half of the lateral surface

With this constructive procedure we can create a "flower" antiprism for any k. Examples of several "flower" antiprisms of minor type (FA-II-km), for initial $k \in \{3, 4, 5, 6, 7, 8\}$ are shown in Fig. 5. We can observe the outlines of the $2k$-sided "flower" polygons in top view, as well as the models of k-merous "flower" antiprisms themselves in axonometric view.

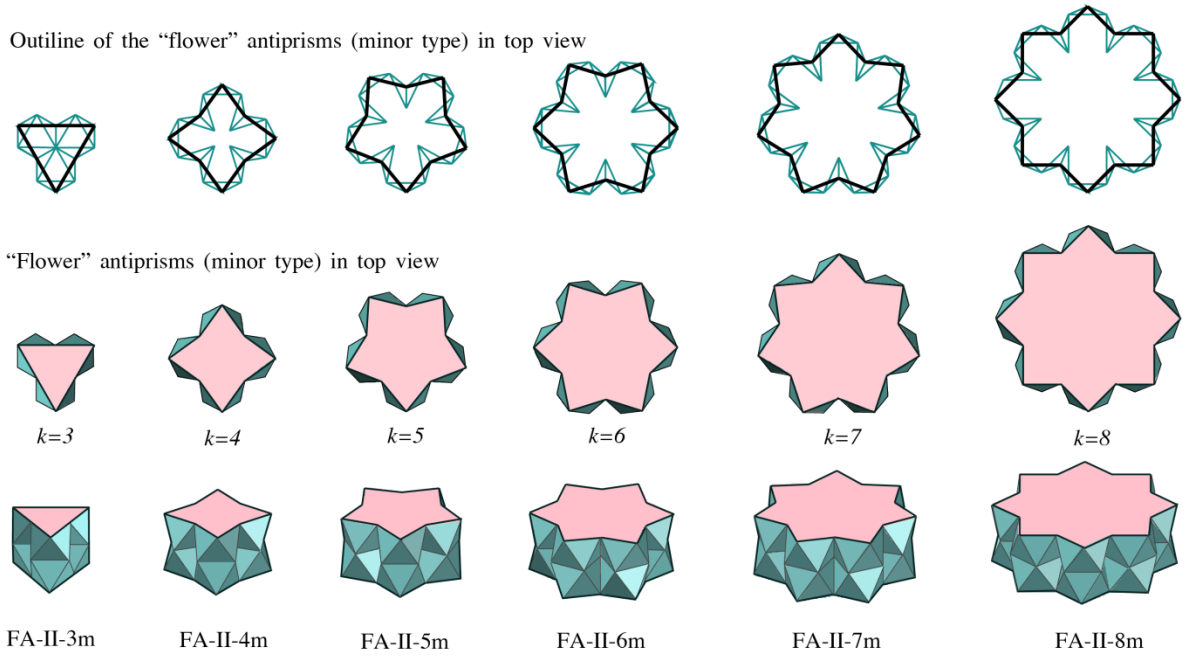

Figure 5: Some representatives of "flower" antiprisms, with $k \in \{3, 4, 5, 6, 7, 8\}$

All the solids shown are verified through 3D models performed in AutoCAD application. In Fig. 6 a) we see FA-II-7m as a rendered image of a 3D model, while in Fig. 6 b) we see a photograph of a physical model of the same solid.

In this way, we prove the accuracy and feasibility of these forms.

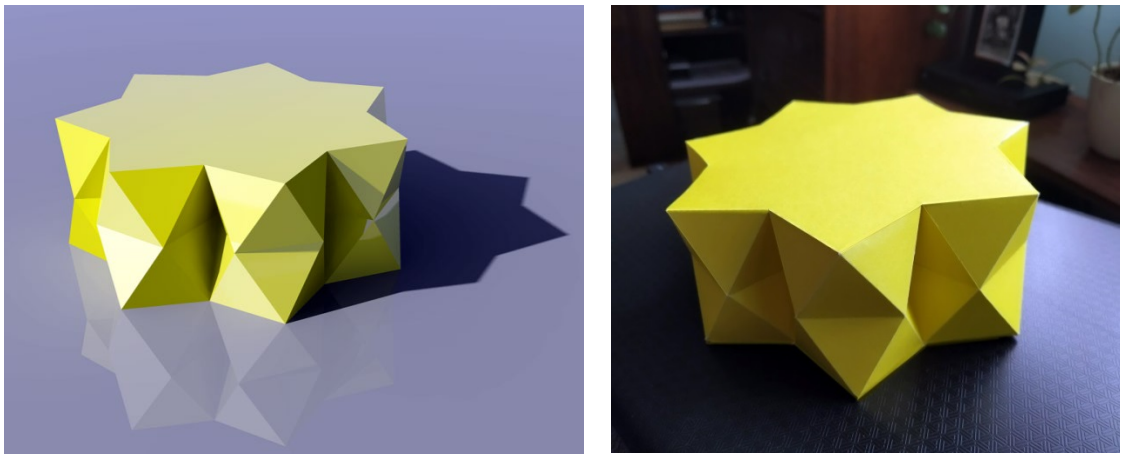

(a) (b)

Figure 6. An example of FA-II-7m: (a) Rendered image of a 3D model, (b) Photograph of a physical model

4. MAJOR TYPE

As stated above, and according to all the previous research on concave polyhedra of the second sort (Obradović et al.., 2008; Obradović et al.., 2013-I; Obradović et al.., 2014; Obradović et al.., 2015), two types of lateral surface, major and minor, can be formed from a single net of double-rowed equilateral triangles, depending on the folding mode. The situation here will be similar to that described above. From a triangular grid, we separate a segment corresponding to k connected decahedral cells and thus again obtain $10 \cdot k$ equilateral triangles organized in two rows. The net of the 7-merous "flower" antiprism is given in Fig.7. By folding it in the manner that the vertices G_1 and G_2 of the unit decahedral cell are protruding into exterior, we get a minor type of "flower" antiprism, described in the previous.

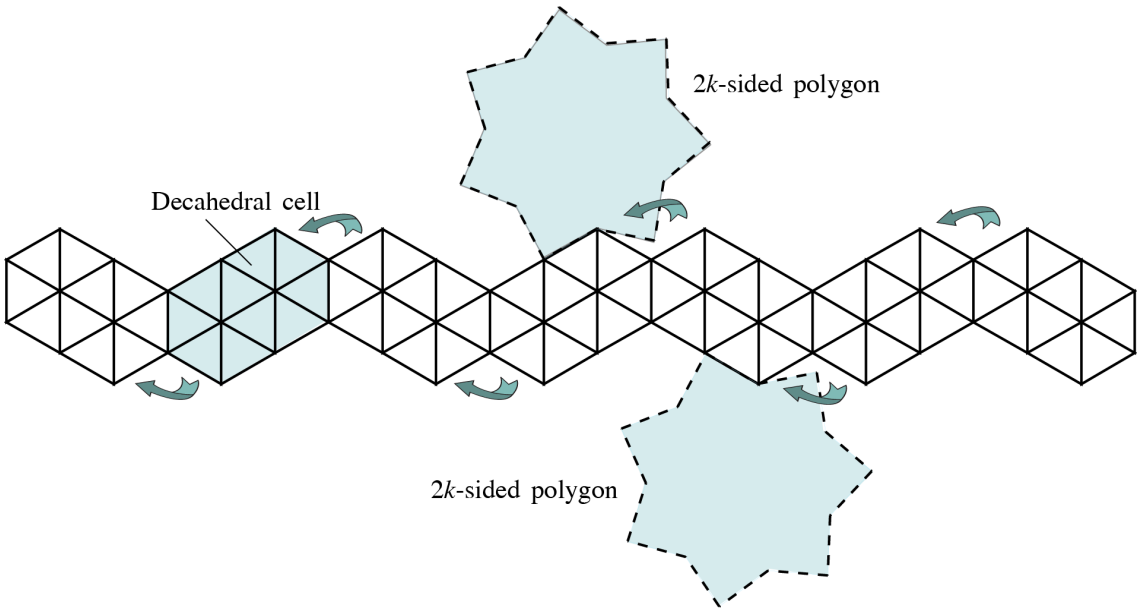

Fig. 7: Net of the "flower" antiprism

Now, to get the major type, we fold the net in the alternative way so that the vertices G_1 and G_2 become indented, as viewed from the outside.

However, if we keep the same base polygon, we will find that it is not possible to obtain the equilateral deltahedral surface, due to constructive and trigonometric paradoxes. Let us look further into this.

From Fig. 8 we can see that angle χ, viewed as angle NH_1A in the quadrilateral (deltoid) NH_1AG_1, is:

$$\chi_1 = \frac{2\pi-\rho}{4} = \frac{\pi(4k+3)}{10k} \qquad \text{(Eq.12)}$$

At the same time, this angle must satisfy the condition from the quadrilateral NH_1QC, that as the angle NH_1Q it is:

$$\chi_2 = 2\pi - \frac{3\rho_m}{2} - \upsilon_m - \mu_m - \frac{\pi}{2} = \frac{2\pi(k+2)}{5k} \qquad \text{(Eq.13)}$$

These two values, χ_1 and χ_2 of the angle χ, cannot be equal for any value of k, (Fig. 8 a) if the values of ρ_m, μ_m and υ_m are expressed as functions of n_m, because its relation to k is defined by Eq. 2, for the minor type. The given relation does not simultaneously satisfy the setting for the major type. Therefore we must look for other value, n_M, and consequently all the related angles, to satisfy the above condition.

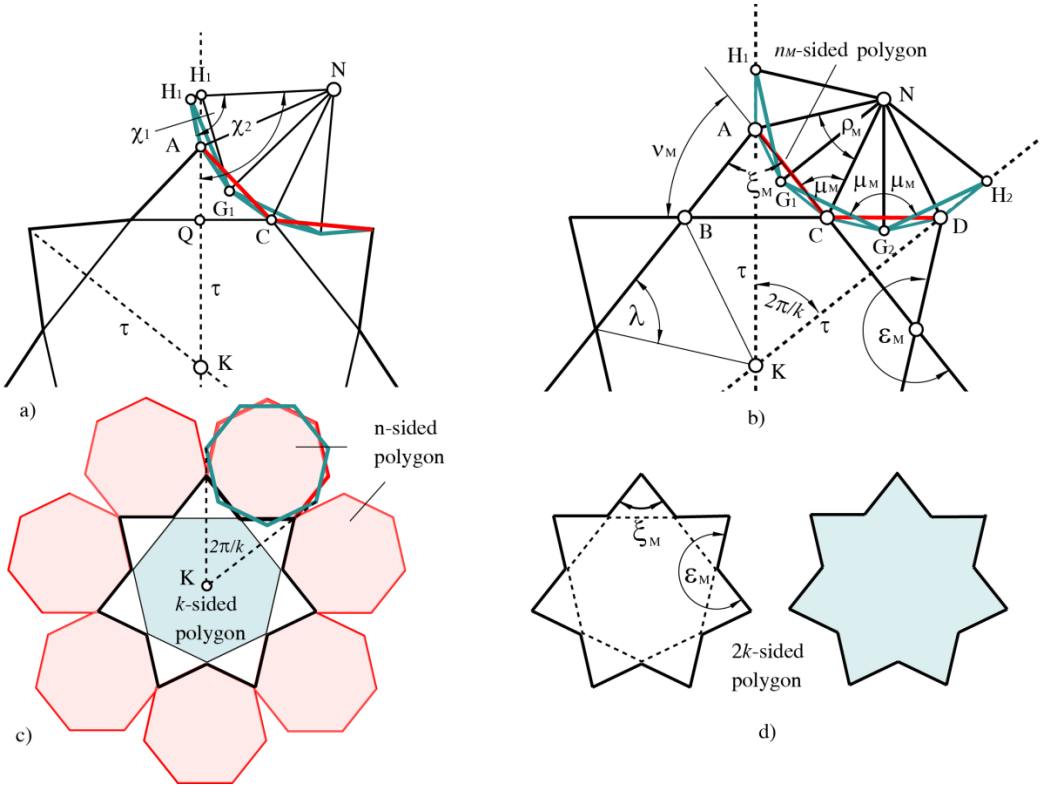

Figure 8. Starting elements for determination of FA-II-kM

Although it will not be feasible to use the same "minor" polygonal basis, we can still assemble a major type of lateral surface out of the same net, with the same number of "petals", and with the central vertices G_1 and G_2 being indented. Accordingly, the basic star polygon will be slightly different.

The outmost edges (AH_1 and DH_2) of the decahedral cells must lie on the planes of symmetry (τ) of the basic star polygon, and at the same time, the vertices of the lateral triangles (H_1, A, G_1, C, G_2, D and H_2), projected into vertices of the isosceles triangles, must form a *2n*-sided polygon, whose 6 consecutive sides form the contour of the major "flower" antiprism (Fig. 8 b). This means that the n_M-sided polygon is determined by the angle between the planes τ, which is $2\pi/k$.

The value of n_M is given by Eq. 14, and the value of the base angle α of the projected isosceles triangle in Eq. 15.

$$n_M = \frac{5k}{k-2};\ k \in \mathbb{N} \qquad \text{(Eq.14)}$$

$$\alpha_m = \frac{\pi(k-3)}{10k} \qquad \text{(Eq.15)}$$

If we apply rotational symmetry on the n_M-sided polygon by the angle $2\pi/k$ and with the center of the rotation in the centroid K of the *k*-sided base polygon, the new arrangement of n_M-sided polygons accurately plot the sides, "petals" of the basic *2k*-sided polygon (Fig. 8 c).

The major-type of the *2k*-sided polygon, now with a different n_M-sided conjugate polygon, obtains its final appearance, given in Fig. 8 d.

The calculated values of the angles: ρ_M, λ, μ_M, υ_M, ξ_M and ε_M (Fig. 8 b) relevant for determining the n_M-sided and *2k*-sided polygons are given by the formulas in Table 4.

Table 4: Overview of all the angles relevant for determining the *2k*-sided star-like polygon (base "flower" polygon) for the major type of "flower antiprism" FA-II-kM

Angle	=	$f(k)$	*Equation*
ρ_M	=	$\frac{2\pi(k-2)}{5k}$	(Eq.16)
λ	=	$\frac{\pi(k-2)}{2k}$	(Eq.17)
μ_M	=	$\frac{\pi(2k+1)}{5k}$	(Eq.18)
υ_M	=	$\frac{\pi(k+3)}{5k}$	(Eq.19)
ξ_M	=	$\frac{3\pi(k-2)}{5k}$	(Eq.20)
ε_M	=	$\frac{\pi(7k-4)}{5k}$	(Eq.21)

Table 5 shows the relationship between numbers of sides in *k*-sided and n_M-sided polygons, if we assign *k* to be an integer.

Table 5: Major type of FA-II-k; Interdependence of the number of sides between two conjugated polygons: *k*-sided and *n*-sided

k	3	4	5	6	7	8	9	10	11	12	13	14	15	16	17	18	19	20	21	22
n_M	**15**	10	8.33	7.5	7	6.67	6.43	6.25	6.11	6	5.91	5.83	5.77	5.71	5.67	5.62	5.59	5.55	5.59	5.55

Only in four cases are both *k* and n_M integers, as it is shown in Table 6. There we see that if *k* tends to infinity, n_M tends to number 5, as for the minor type of "flower" antiprism, but now there are no cases when n_M is infinite, since the condition for that is *k*=2, which is not possible for a polygon.

Table 6: Major type of FA-II-k – Cases when both k and n are integers

k	2(-)	3	4	7	12	∞
$n_M = \frac{5k}{k-2}$	∞	15	10	7	6	5

Once again, just like for the minor type, in the first projection (top view) all the triangles from the lateral surface are projected into congruent triangles (Fig 9 c). In this case also 3 out of 7 visible vertices of the unit cell coincide with the vertices A, C and D of the "flower" polygon, i.e. belong to both *k*-sided and n_M-sided polygons (Fig 8 b and Fig 9 a). The vertices G_1 and G_2 can also be found in the intersection of the normals of the sides AC and CD respectively with the circle *c* itself, while the vertices H_1 and H_2 are found at the intersection points of the circle $\boldsymbol{c}$ and the symmetry plane (τ) of the base polygon, set through the vertices A and D respectively (Fig 9 a). The remaining 4 vertices belong to an identical but gyrated polygon to the n_M-sided one, so one more time all the 7 vertices of the unit cell, seen in the top view, will lie on the same circle *c*, determined by the vertices A, C, and D (Fig. 9 b).

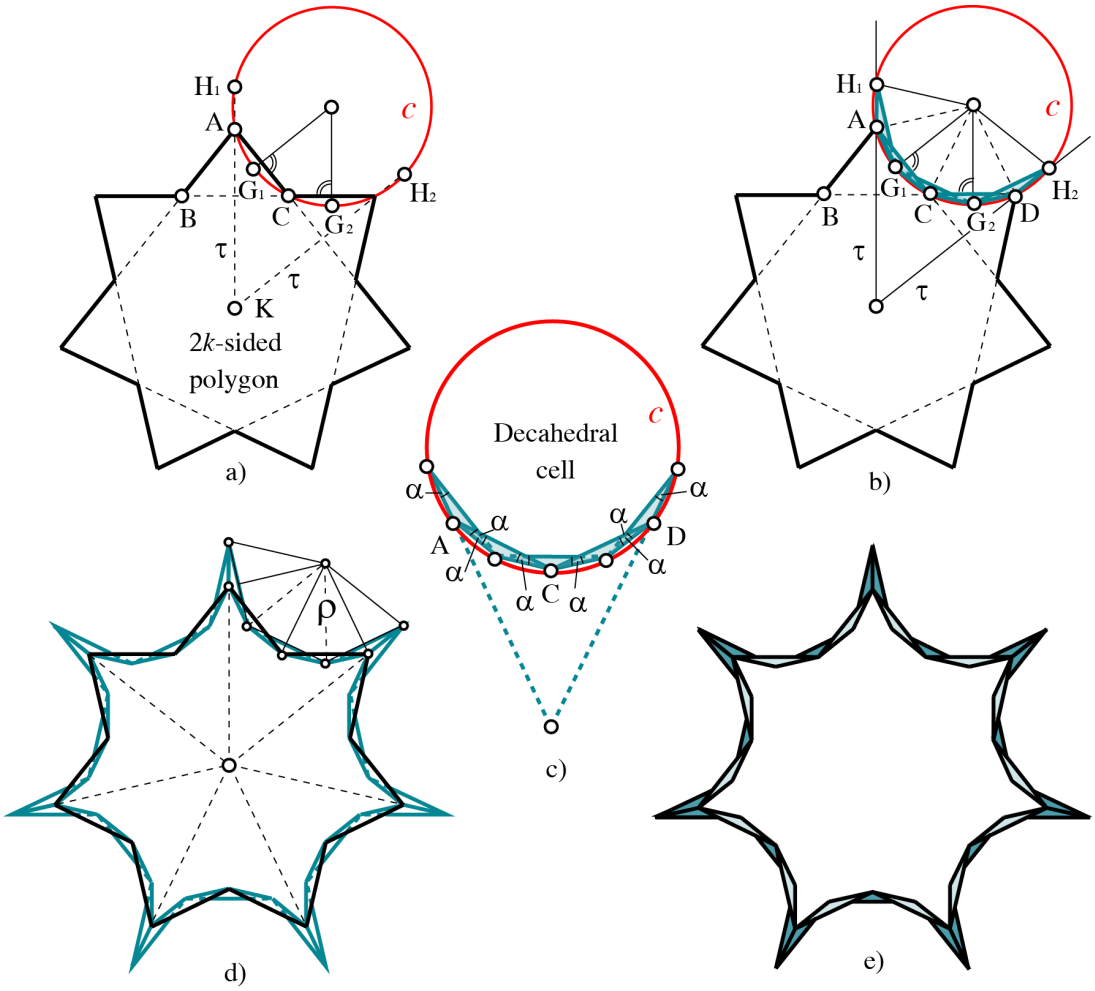

Fig 9: The construction and origination of "flower" antiprism of the major type

Accordingly, another way to create the contour of a "flower" antiprism's unit cell of the major type is to have the polygon n_M girated. Then, with its polar array, we form the entire ring, observed in top view (Fig 9 d). In Fig. 9 e) we can see in the final contour outlook of the lateral surface with the obtained k (7) "petals" of the "flower" antiprism, also in the top orthogonal view.

Next we proceed to determination of vertices' heights in order to obtain all the necessary elements for construction of the solid. We apply the same methods as for finding the height of the minor type, described in the section 3.3.

It is interesting to note that the minor and major types differ not only in height and in the way the net is folded and assembled, but also in two additional interesting details:

- the area of the major polygon is larger than that of the minor polygon,
- surfaces whose fragments form the lateral surface of the major type of the "flower" antiprism, with the equivalent role that CA-II-nms had in the formation of the minor type of the "flower" antiprism, are nothing else than double convex antiprisms. In this way, the connection between convex and concave antiprisms is confirmed again, as shown by Obradović et al (2019), but in the inverse procedure, where double convex antiprisms occurred as a consequence of the polar arrangement of CA-II-nm fragments.

Also, we will notice another link between the present and the previous studies: the case B of the CDR-II (illustrated only by the example with fragments of CA-II-4ms) described in Obradović et al (2019) is nothing but the lateral surface of the major type of "flower" antiprism, and the case A of those CDR-II-Ks is in fact the lateral surface of the minor type.

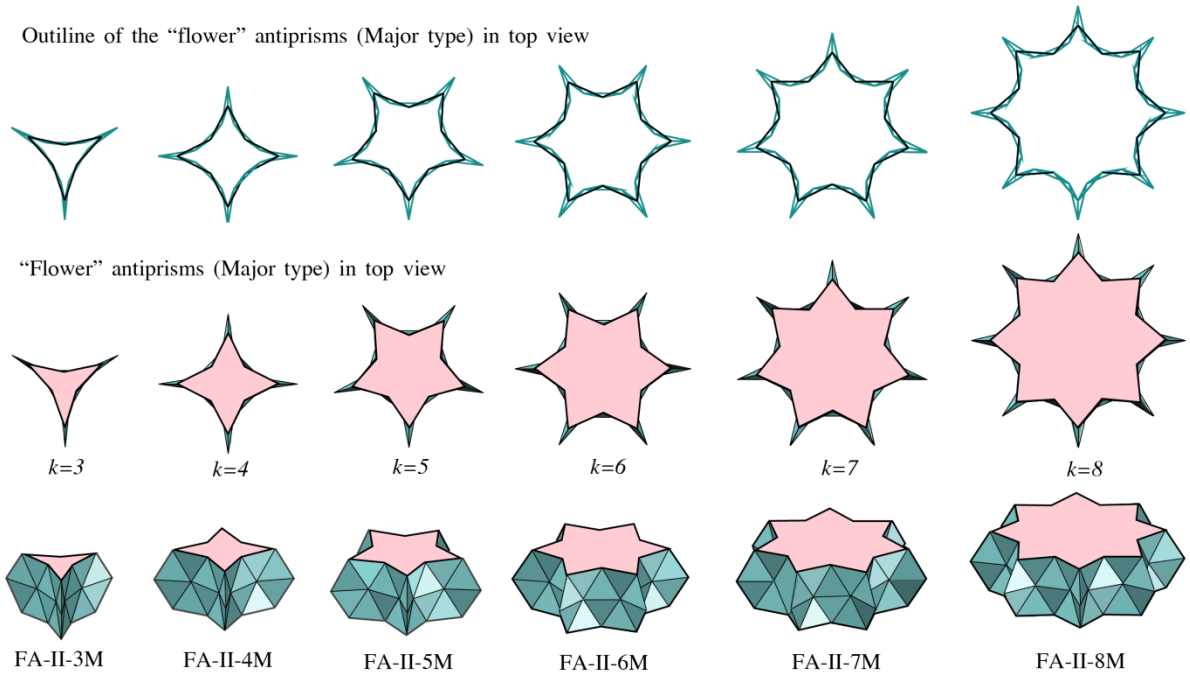

Figure 10. Some representatives of "flower" antiprisms, major type, with k=3 to k=8

Examples of several "flower" antiprisms of major type (FA-II-kM), for initial $k \in \{3, 4, 5, 6, 7, 8\}$ are shown in Fig. 10. We can observe the outlines of the $2k$-sided "flower" polygons in top view, as well as the k-merous "flower" antiprisms themselves in top and axonometric views.

In Fig. 11 a) we see a rendered image of a 3D model of the FA-II-7M performed using AutoCAD application, while in Fig. 11b) a photograph of the same solid's physical model is presented.

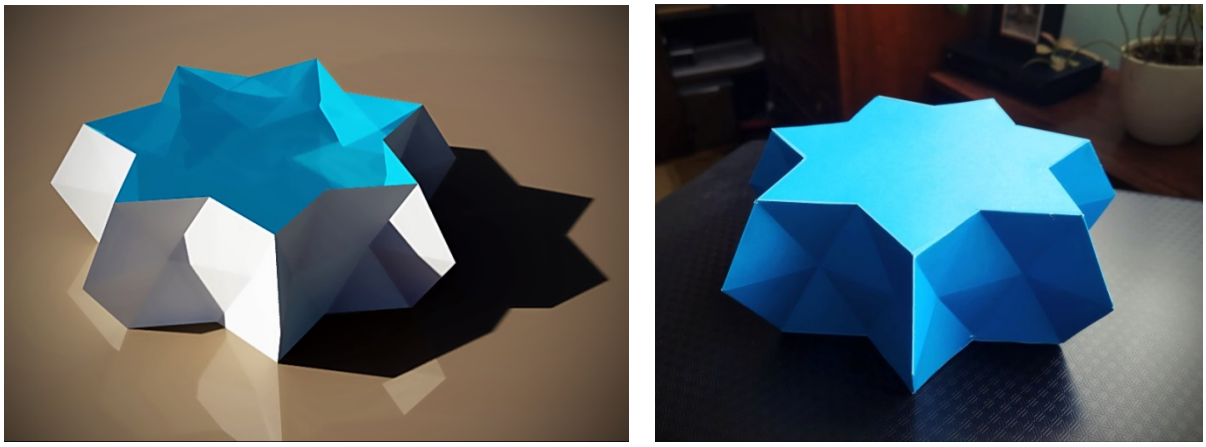

a) b)

Fig. 11: a) Rendered the 3D model of the FA-II-7M; b) photograph of the physical model of the FA-II-7M

Finally, comparing the basic "flower" polygons of the FA-II-km and FA-II-kM representatives, with the same initial k-sided polygon (Fig. 12), we can observe that although they are not congruent, the divergence between major and minor polygons decreases with increasing the number k. The minor type of the polygon is given in red, and the major is given in black. The polygons equalize when $n=5$, while k is tending to infinity.

Note: If we compared these polygons for the same triangle edge a, the differences would be even less noticeable. Also, we will find that stellar polygons (polygrams) appear in two special cases only: for $k=8$ in the minor case, where obtuse octagram {8/2} (Grünbaum, et al.., 1986) appears, and for $k=7$ in the major case, where obtuse heptagram {7/2} is obtained.

In this way, the properties and measures of "flower" antiprisms of the second sort are completely defined.

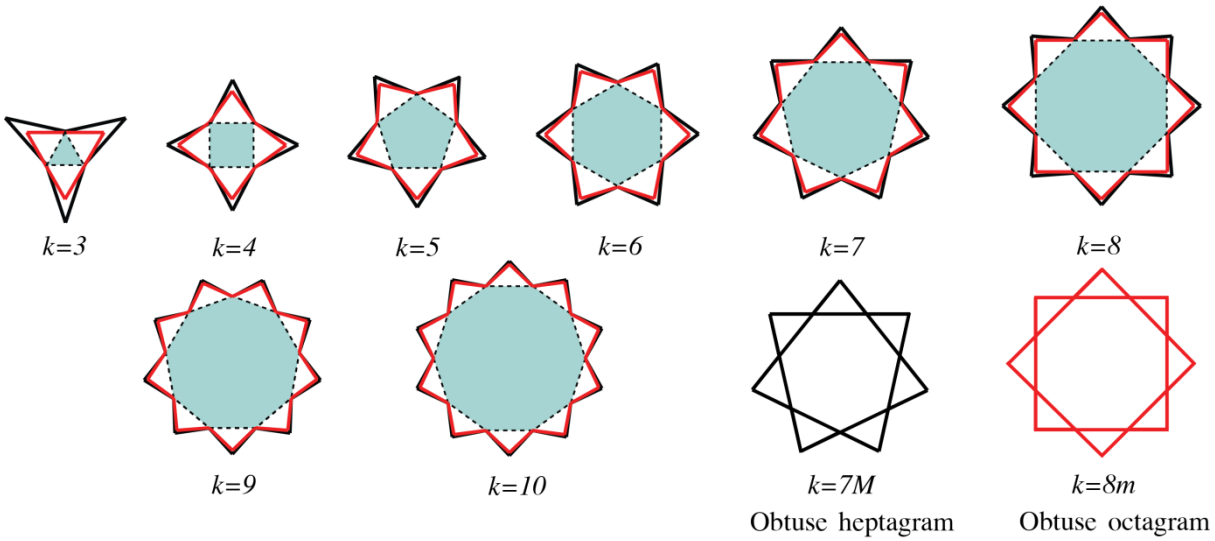

Fig. 12: Comparison of Major and minor representatives of FA-II-k with two special cases (k=7 for M, and k=8 for m) - polygrams

We can use these polyhedral surfaces to form infinite polyhedra, more precisely: infinite deltahedra, but only of the same type FA-II-k, without combining the major and minor types, as it was possible with CA-II-ns.

CONCLUSIONS

Based on all the above presented in the paper, the following conclusions are drawn:

- By using unit decahedral cells made of equilateral triangles, analogously to those formed by the use of CA-II-nM's lateral surface fragments, we can take any integer k of them to form a closed deltahedral surface with multilateral k-fold symmetry.
- We can form a solid, a "flower" concave antiprism, enclosing these annular lateral surfaces by bases which are isotoxal concave $2k$-sided star polygons.
- These star polygons are not stellations (except in two special cases), but elevations of regular k-sided convex polygons. This special type of isotoxal star polygon has concave angles that are conjugate to the interior angles of an n-sided polygon, where $n=f(k)$, and n does not have to be an integer. The number k indicates the number of "petals" in the "flower" antiprism itself.
- By an alternative way of folding the net of the lateral surface, we can get another type of "flower" antiprism. If we fold the net so that its central vertices (G_1 and G_2) of the decahedral unit cells are protruding into exterior, we get a lower height of the solid, i.e. the minor type, and if these vertices are indented, we get a greater height of the solid, i.e. the major type. This corresponds to the way all other concave polyhedra of the second sort are formed.
- The bases of the major and minor types will not be congruent in this case, and the aberrations occur in the angles of these polygons, so that the differences will disappear only when $k = \infty$ and $n=5$.
- For the minor type of "flower" antiprisms, conjugate solids are concave antiprisms of the second sort (CA-II-nM), and for the major type, the conjugate solids are double convex antiprisms. For both the major and minor types, there are only 4 cases where both k and n are of an integer value, whereupon the conjugate solids can modularly fit.

With this research, it is shown that the world of concave polyhedra of the second sort is not depleted with the ones having convex polygons as bases, and that there is a clear relationship between concave antiprisms of the second sort (CA-II-nM), concave "flower" antiprisms (FA-II-k) and convex antiprisms.

For the further research, one might focus on: what happens if we apply the procedure analogous to the one described in this paper to the minor type of the concave antiprisms of the second sort, CA-II-nm, using their fragments for obtaining deltahedral rings? What kind of rings, and "flower" antiprisms would be produced by such an array of their fragments? In this case, even more curiosities occur. Such "flower" antiprisms might even include regular convex polygons as their bases, which is to be explored.

Acknowledgements

The research is financially supported by Ministry of Education, Science and Technological Development of the Republic of Serbia.

REFERENCES

1. Bowers J. (2012). Regular Polygons and Other Two Dimensional Shapes, Page created by, 2012. Polytope.net http://www.polytope.net/hedrondude/polygons.htm
2. Coxeter, Harold Scott Macdonald. (1969) Introduction to geometry, Second edition, 2.8 *Star polygons* p.36-38.
3. Grünbaum, B., & Shephard, G. C. (1986). *Tilings and patterns.* WH Freeman & Co.
4. Grünbaum, Branko, Geoffrey C. Shephard. (1977). Tilings by regular polygons, Mathematics Magazine Vol. 50. No5: 227-247.
5. Huybers, P. (2001) Prism based structural forms. Engineering structures, 23(1), 12-21.
6. Johnson, N. W. (1966). Convex polyhedra with regular faces. Canadian Journal of Mathematics, 18(1), 169-200.
7. Kepler, Johannes. 1619/ 1968. Harmonices mundi. Libri V. Culture et Civilisation.
8. Mišić S. 2013. Constructive – geometric generating of cupolae with concave polyhedral surfaces, Doctoral Dissertation, University of Belgrade - Faculty of Architecture, 2013.
9. Mišić S., Obradović M., Đukanović G., 2015. Composite Concave Cupolae as Geometric and Architectural Forms, Journal for Geometry and Graphics, Vol.19. No 1. pp 79-91. Heldermann Verlag 2015.
10. Obradović M., Mišić S. (2008). Concave Regular Faced Cupolae of Second Sort, In: Proceedings of 13th ICGG (ICGG 2008, Dresden, August 2008), ed. Gunter Weiss, Dresden: ISGG/ Technische Universität Dresden El. Book: 1-10.
11. Obradović M. 2012. A Group Of Polyhedra Arised As Variations Of Concave Bicupolae Of Second Sort, In: Proceedings of the 3rd International Scientific Conference MoNGeometrija 2012, ed. Ratko Obradović, FTN Novi Sad, June 21-24. 2012. pp. 95-132.
12. Obradović M., Mišić S., (2019). Concave deltahedral rings based on the geometry of the concave antiprisms of the second sort, GEOMETRIAS'19: Polyhedra and beyond, Porto, 05 - 07 September 2019. Book of abstracts, Aproged, pp. 85-89 .
13. Obradović M., Mišić S., Popkonstantinović B. (2014). Concave Pyramids of Second Sort - The Occurrence, Types, Variations, In: Proceedings of the 4th International Scientific Conference on Geometry and Graphics, 2. MoNGeometrija 2014, June 20-22.Vlasina, Serbia, ed. Sonja Krasić, Faculty of Civil Engineering and Architecture in Niš and Serbian Society for geometry and graphics (SUGIG), 157-168.
14. Obradović M., Mišić S., Popkonstantinović B. (2015). Variations of Concave Pyramids of Second Sort with an Even Number of Base Sides, Journal of Industrial Design and Engineering Graphics (JIDEG) – The SORGING Journal, Volume 10, Special Issue, 1, 45-50.
15. Obradović M., Popkonstantinović B., Mišić S. (2013-I). On the Properties of the Concave Antiprisms of Second Sort, FME Transactions, 41(3), 256-263.
16. Obradović M., Mišić S., Popkonstantinovič B., Petrović M., Malešević B., Obradović R., (2013- II). Investigation of Concave Cupolae Based Polyhedral Structures and Their Potential Application in Architecture, *Technics Technologies Education Management*, Vol. 8. No.3. 8/9 2013. pp. 1198-1214.
17. Obradović M., Stavrić M., Wiltsche A., 2017. Polyhedral Forms Obtained by Combining Lateral Sheet of CP II-10 and Truncated Dodecahedron, *FME Transactions* Vol. 45, No 2, pp. 256-261.
18. Wachman A., Burt M. and Kleinmann M., *Infinite Polyhedra*, Technion, Haifa, 1974.
19. Weisstein, Eric W. "Augmentation." From *MathWorld*--A Wolfram Web Resource. http://mathworld.wolfram.com/Augmentation.html [Accessed 1st April 2020].

SETS OF PLANAR AND SPATIAL TESSELLATIONS BASED ON COMPOUND 3D MODELS OF THE 8D AND 9D CUBES AND ON RE-STRUCTURED CONVEX UNIFORM HONEYCOMBS

László Vörös
Department of Visual Studies, University of Pécs, Hungary
DLA, Associate Professor, vorosl@mik.pte.hu

ABSTRACT

A set of the convex uniform honeycombs consists of combinations of some Platonic and Archimedean solids as well as regular octagon based prisms. The edges of these solids are parallel to these ones of the Archimedean truncated cuboctahedron. It is the hull of a 3D model of the 9D cube. Special, symmetric 3D models of the 8D and 9D cubes and those of its lower-dimensional parts provide other sets of stones for further periodical space-filling mosaics. Subsets of these stones are building boxes of compound models of the elements applied in the tessellations of the above initial solids or models. The rebuilt tessellations can have fractal like structures as well.

Keywords: constructive geometry; hypercube modelling; convex uniform honeycomb; tessellation; fractal

INTRODUCTION

The 3-dimensional framework (3-model) of any k-dimensional cube (k-cube) can be produced based on starting k edges arranged even by rotational symmetry, whose Minkowski sum can be called zonotope [1], [3], [4]. Combining $2<j<k$ edges, 3-models of j-cubes can be built, as parts of a k-cube. The suitable combinations of these zonotope models can result in 3-dimensional space-filling mosaics. The investigated periodical tessellations always hold the 3-model of the k-cube and necessary j-cubes derived from it [8]. The tessellations may be mentioned further as mosaics and the cells as stones.

The mosaics can have fractal or fractal like structure as well, since the stones can be replaced with restructured ones. The hulls of 3-models of k- and $3<j$-cubes can be filled with different sets of 3-models of $2<j<(k\text{-}1)$ or $2<i<(j\text{-}1)$ -cubes touching each other at congruent faces [6]. Another possibility is if the 3-models of the given k- and of the derived j-cubes are arranged along the outer edges of the restructured models and the faces are replaced with central symmetrically arranged sets of the above elements. The inner spaces of the new compound models are filled also with the initial models. The elements can have different colours and different tones of these according to their shape and role like edge, face and inner elements [11].

If also the inner edges are followed by 3-models of the k- and j-cubes [10], the construction can require unmanageable quantity of the elements, from practical points of view, but the restructured mosaics can have a more consequent fractal like structure. The intersections of the mosaics with planes allow unlimited possibilities to produce periodical symmetric plane-tiling. Moving intersection planes result in series of tessellations or grid-patterns transforming into each other. These can be shown in varied animations [8], [9]. This contribution deals partly with these possibilities based on compound 3D models of the 8D and 9D cubes.

A set of the convex uniform honeycombs consists of combinations of some Platonic and Archimedean solids as well as regular octagon based prisms [2]. The edges of these solids are parallel to these ones of the Archimedean truncated cuboctahedron (4;6;8). It is the hull of a 3D model of the 9D cube [6]. The affine pairs of the above solids can have compound models if the edges are replaced with sequences of the rotational symmetric 3D model of the 8D cube and its derived parts. The inner spaces of the models are filled with the same stones that are applied in the former compound rotational symmetric model of the 8D and the 9D cube [12]. The new space-filling mosaics have only two different unit parts if the stones are coloured only according to their different shapes.

2. OPERATIONS BASED ON 3D MODELS OF THE 8D AND 9D CUBES

2.1. Centrally and Rotation Symmetric Models

The initial edges of the 3-model of the 8-cube are arranged rotation symmetrically around an axis. The directions of parallel shifts of model elements are defined by these edges. So the model will be rotation and centrally symmetric (Figure 1(a)). It has inner coinciding vertices and edges intersecting each other between their endpoints (Figure 1(b)). The faces have four different rhombic shapes. The models of lower-dimensional parts of the cubes can be constructed by combinations of the initial edges. All models can touch each other at congruent faces. A 3-model of the 9-cube can be derived from the above one if the ninth initial edge is a segment of the rotation axis (red line in Figure 3(a)).

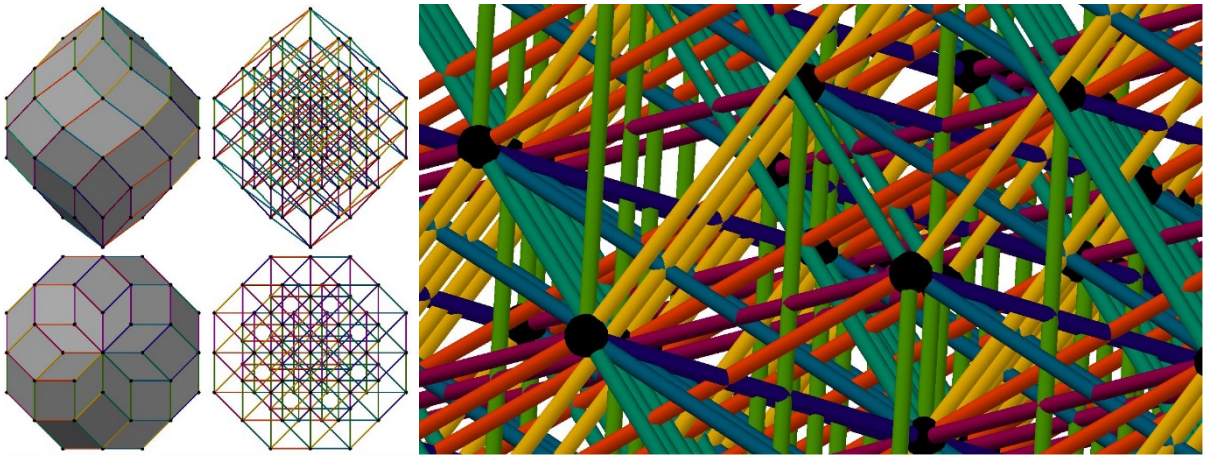

(a) (b)

Figure 1: (a) The central and rotation symmetric 3D model of the 8D cube in front and top views (b) Intersections of the inner edges

2.2. Compound Models

A sequence of the above models of the 8-cube and 3-models of its lower dimensional parts can substitute for all edges of the whole compound model. According to the introduced example, the endpoints and the intersection points of the edges have to be centre points of 8-cube models that ensure the junctions in all possible directions. There are placed 3-models of 4-cubes among these elements as well as an 8-cube model at the midpoints of the segments among the intersection points (Figure 2). A sequence consists of 31 elements. All outer and inner edges of the whole model need almost 30 thousand elements. Together with the compound faces and inner spaces, filled with 3-models of the 8-cube and of the needed *j*-cubes, the model requires an unmanageable amount of the elements, from practical points of view.

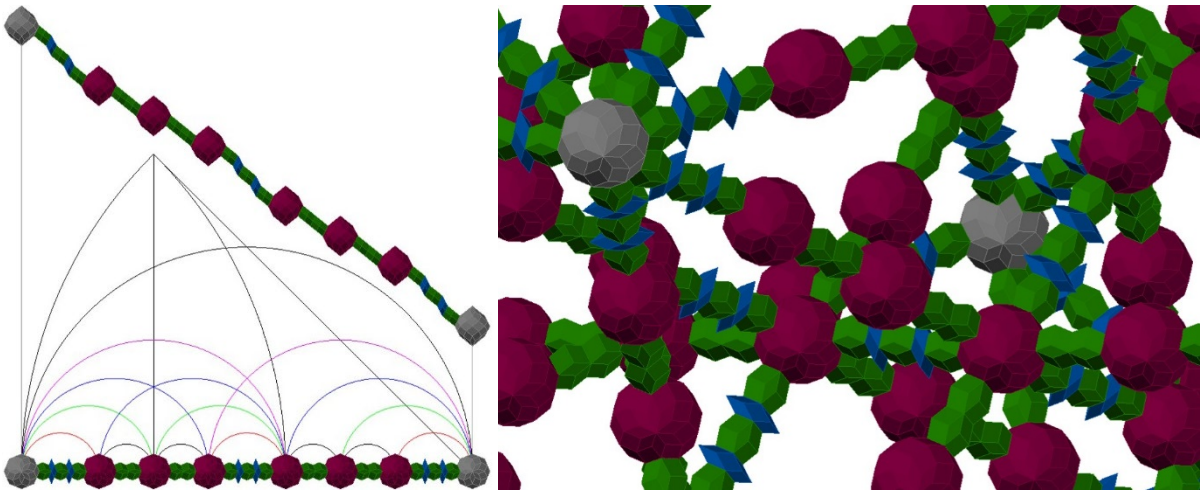

(a) (b)

Figure 2: (a) The construction of the model sequence along the edges of the compound 3D model of the 8D cube (b) Some intersecting inner edges of this compound model

A limited solution can be if only the outer edges and faces have compound models and the inner space is filled with 3-models of the 8-cube and of needed *j*-cubes. These models are called further compound models. The layout of the compound edge is defined by the next rules. The sequence of edge elements has to be centrally symmetric to the midpoint of the edge and must have a symmetry plane consisting of the initial edge (Figure 3(a)). The four differently shaped rhombic faces of the compound 8-cube model have to be reconstructed with central symmetrically arranged sets of stones around the centre points of the faces (Fig. 3 (b)). The layout of the edges and of the differently shaped faces, joining the hulls of 3D models of the 8D and 9D cubes, can be seen in Figure 4. The net of the compound outer edges consists of 788 elements between the pairs of 54 vertex solids. The whole filled model is built up with 36-37 thousand elements (Fig. 5(a)). The compound model of the 9-cube requires an additional vertical edge with a sequence of initial 3-models of 8-cubes (Fig. 3(a)). This way it needs the same set of stones like the above model of the 8-cube. These compound models consist of the initial 3-model of the 8-cube and of 9 derived *j*-cubes as building stones (Fig. 5(b)). There is the same angle between the 8 neighbour initial strait line edges. The notation of the *j*-cubes shows the multiplication of this angle between the initial edges needed for the construction of these stones (Fig. 5(c)) that can have different colours and different tones of these according to their shape and role like edge, face and inner elements (Fig. 5(c)).

The 3-model of the 8-cube and of each *j*-cube can be rebuilt with the above compound edges and faces and with the filling stones shown in Figure 5(b). However some stones of faces of thin initial *j*-cube models can require modifications. The 3-models of *k*- and *j*-cubes can be replaced also with sets of *j*- and <*j*-cubes [5]. This operation can be solved here with the stones of the compound model and the stones of penetrated parts are omitted. The initial 3-models of the 8-cube and its *j*-cubes as well as the mosaics built with these can be rebuilt with the compound models and the stones of these can be rebuilt again and again. This way the new constructions will have fractal like structure. It will be more consistent if the initial set of stones is equal to this one used for the compound models. More about it can be read in section 4.

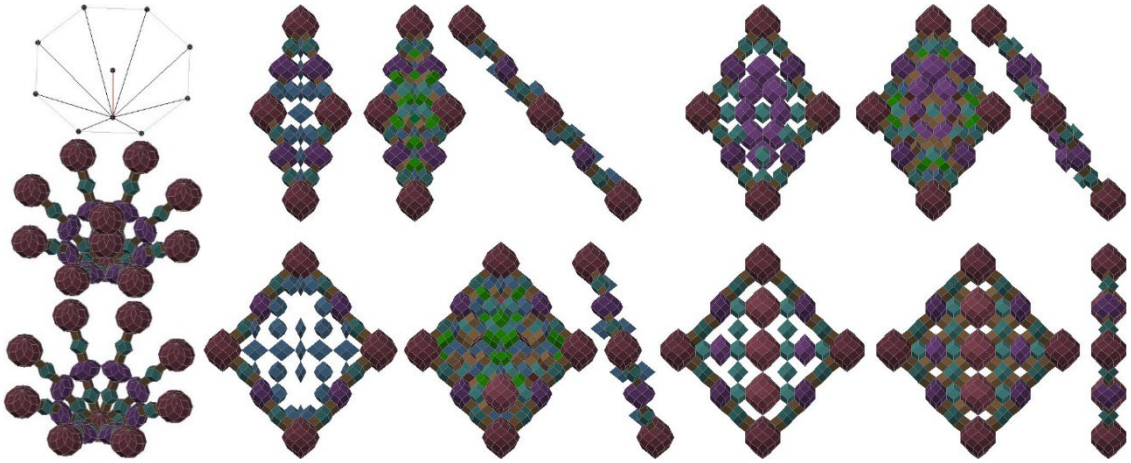

(a) (b)

Figure 3: (a) Sequences of the initial models along the edges of the limited compound 3D model of the 8D and 9D cubes (b) The structure of the compound, centrally symmetric faces of the limited compound 3D model of the 8D cube in front and side views

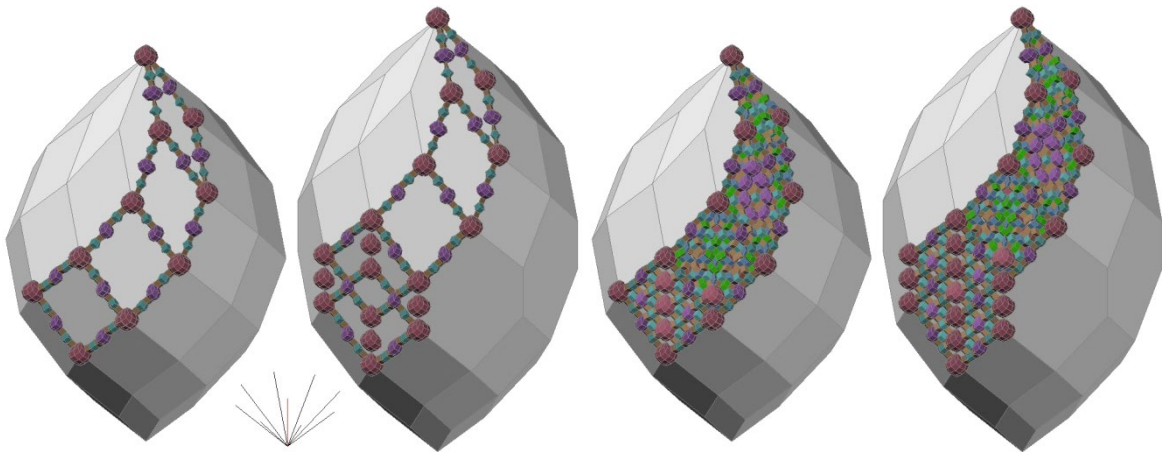

Figure 4: Centrally symmetric compound models of the edges and of the differently shaped faces joining the hulls of 3D models of the 8D and 9D cubes

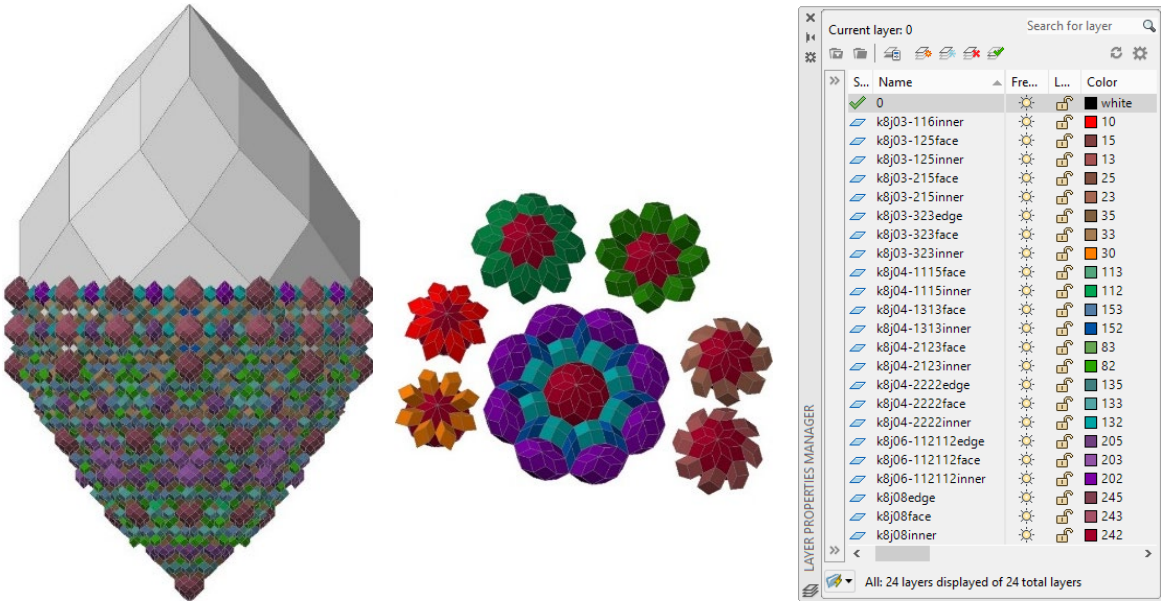

(a) (b) (c)

Figure 5: (a) The half part of the symmetric whole compound model and the hull of the initial model of the 8D cube (b) The differently shaped elements needed for the filled models of the 8D and 9D cubes (c) The elements can be coloured according to their roles as well.

All fourth layers of all compound models have a horizontal symmetry plane and use the same set of stones having a horizontal and more vertical symmetry planes. Figures 6(a) and 6(b) show all these layers of the half part of the compound model of the 8-cube. The first one is on the middle level, the other ones are mirrored to this one inside of the whole model. This layer has congruent pairs placed on higher and lower neighbour levels inside of the compound 3-model of the 9-cube. The central parts of all these layers are mirrored into the higher one. The border parts are then completed according to the surrounding faces. Unit, prism shaped parts can be found between two accidently chosen layers (Figures 6(b), 7 and 8). These can create larger compound unit parts as well (Figures 9 and 10).

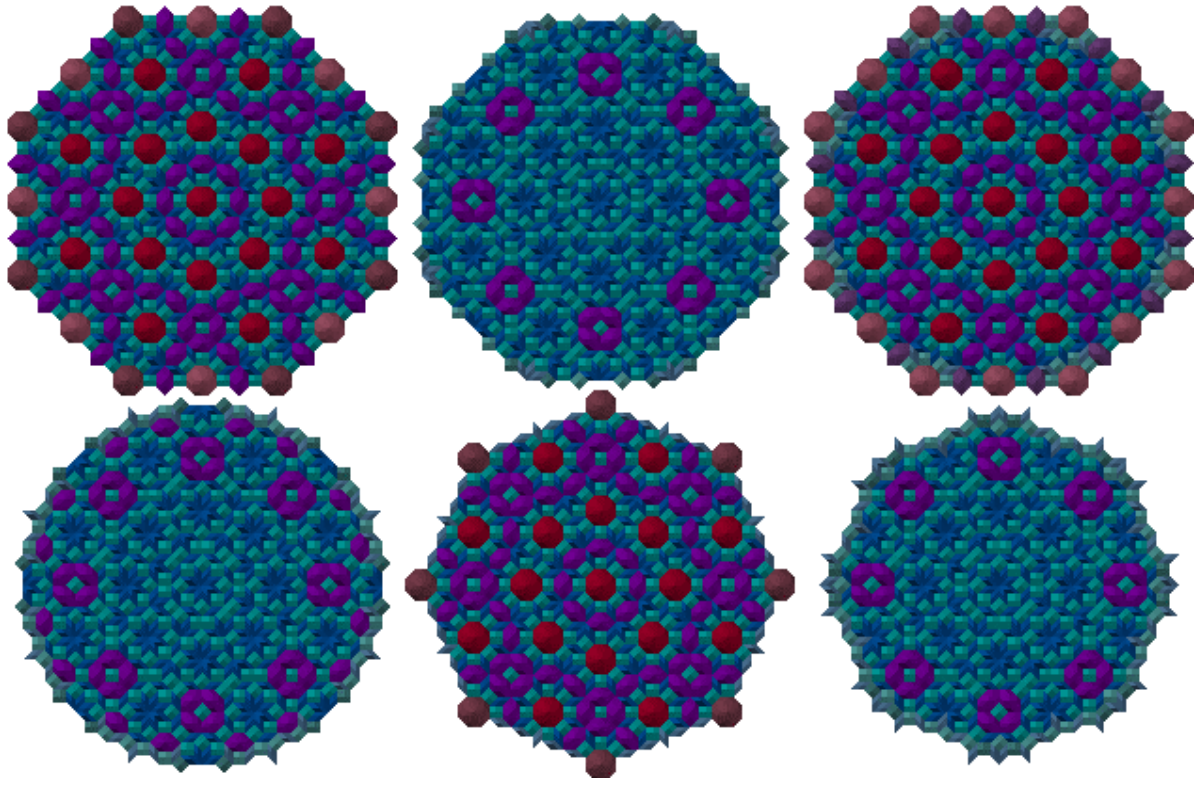

Figure 6(a): Layers of stones having a horizontal symmetry plane inside of the half part of the compound 3-model of the 8D and 9D cube. These are mirrored to the level plane of the first, i.e. middle level layer inside of the whole models.

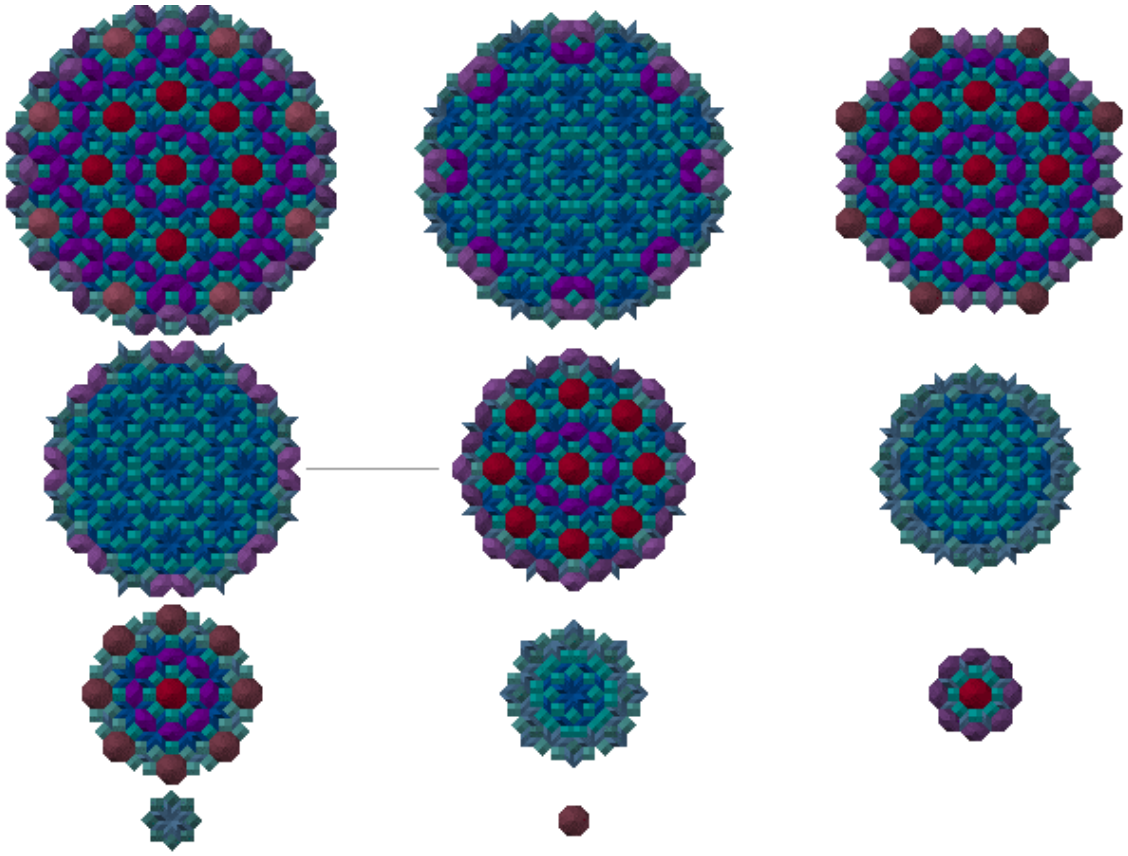

Figure 6(b): Layers of stones having a horizontal symmetry plane inside of the half part of the compound 3-model of the 8D and 9D cube.

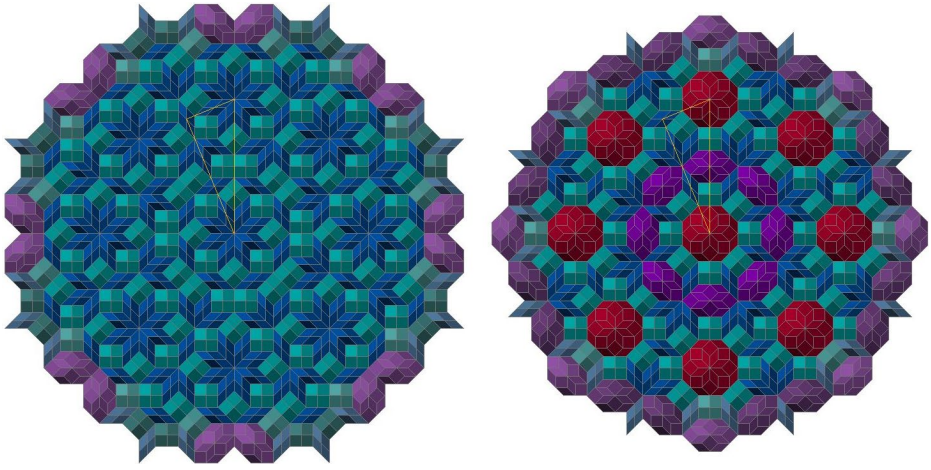

Figure 7: An accidently chosen pair of plane symmetric layers of stones and the common border of repeatable parts.

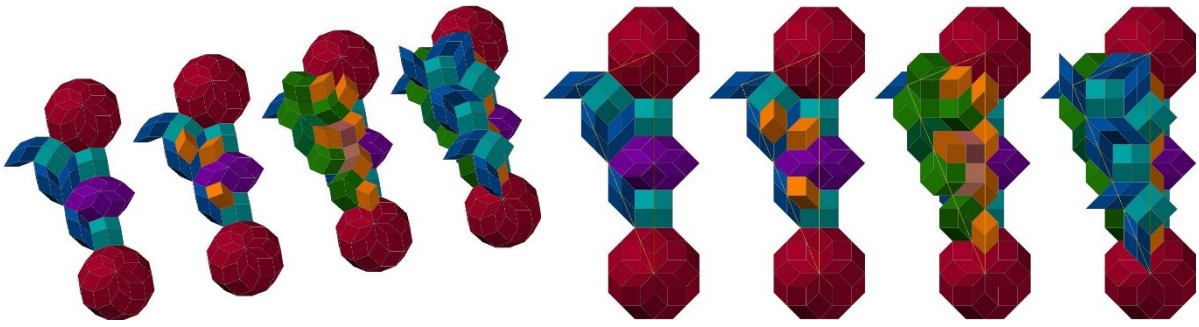

Figure 8: Construction of the honeycomb based on the above layers of stones (axonometric projection and top view)

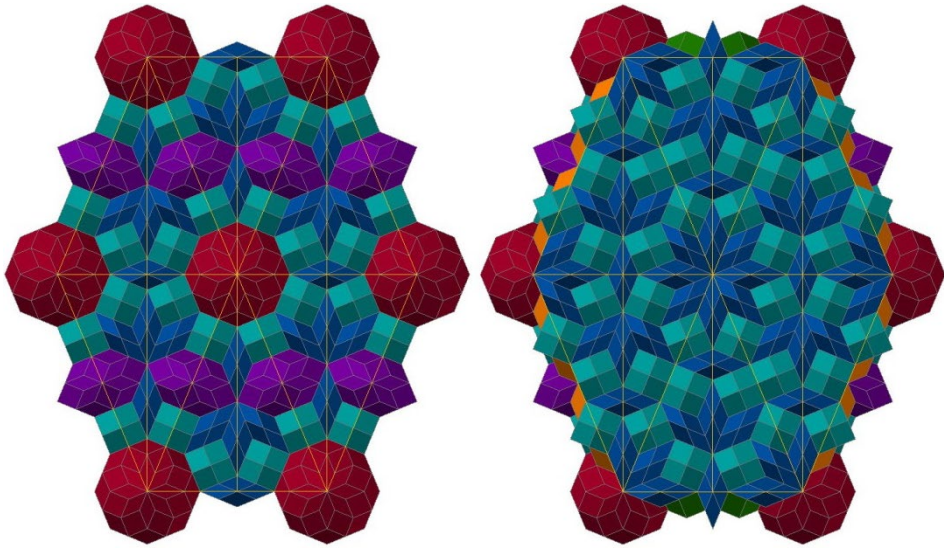

Figure 9: Construction of a compound unit part of the new spatial mosaic built up with the above honeycomb

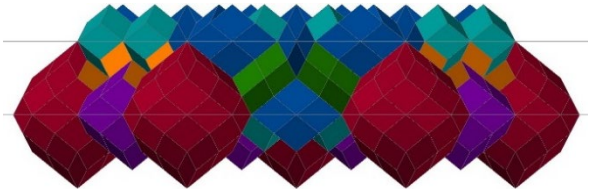

Figure 10: The front view of the above compound unit part

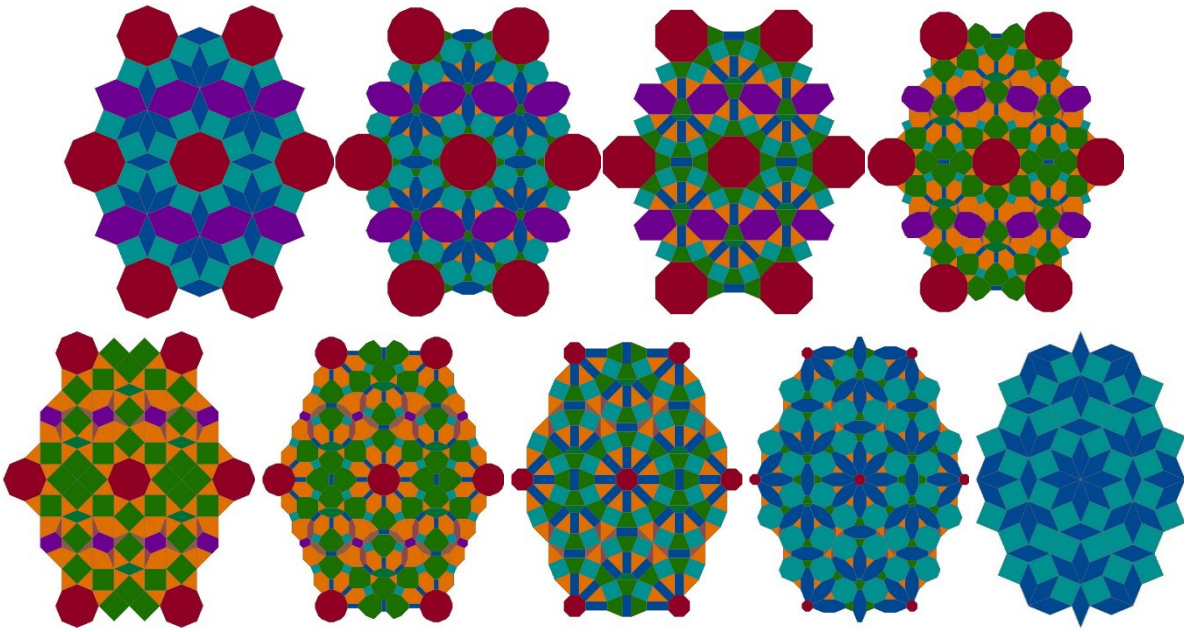

Figure 11: Nine tessellations gained as equidistant horizontal sections of the above compound unit part of a periodical space-filling mosaic

The intersections of the mosaics with planes allow unlimited possibilities to produce periodical symmetric plane-tiling. Moved intersection planes result in series of tessellations or grid-patterns transforming into each other (Figure 11). These can be shown in varied animations [9].

The unit mosaics and the compound ones can be mirrored to horizontal and vertical planes bearing the border stones. New space-filling periodical mosaics can be constructed this way. The above method is applicable also for all former mentioned tessellations derived from the introduced initial and compound 3-models of the 8D and 9D cubes. In section 4 are described other possibilities to create further tessellations based on these models.

3. OPERATIONS BASED ON A 3D MODEL OF THE 8D CUBE AND ON A SET OF CONVEX UNIFORM HONEYCOMBS

The 3-model of the 8-cube and of its *j*-cubes are the same like this ones applied as stones of the compound models described in the former section 2. The uniform convex honeycombs of Platonic and Archimedean solids consist of the cube, i.e. Platonic hexahedron, and the solids shown in Figure 12. Their edges are parallel to the 9 differently oriented edges of the solid (4;6;8). It is true also to the right prisms having regular octagon base face oriented horizontally or vertically.

3.1. Compound Models of the Elements of the Considered Honeycombs

The compound models of the affine pairs of these considered solids can be constructed based on the compound edge models (Figure 13(a)). Two examples of the compound solid models are showed in Figure 14. All compound models consist of the 3-models of the 8-cube and of 7 derived *j*-cubes (Figure 13(b)). The stones have different colours and different tones of these depending on shape and role, given in Figure 5(c).

The edges of the 3-cube have 3 different orientations. Our first set [group 3] has only 1 element but, because of the above modifications, the bearing solid of the compound model of the cube has 2 different shapes. Thus the modified set is called [group 3]' and has 2 elements. In Figure 15, are given their compound models and deviations of edge lengths in % and of angles in degrees, related to the regular cube. These can illustrate the deviations regarding the considered Platonic and Archimedean solids and their affine pairs as well that give the base of the compound models. The edges of members of the next set of Platonic and Archimedean solids have 6 different spatial orientations: (3;3;3), (3;3;3;3), (3;4;3;4), (3;6;6), (4;6;6). This set is called here as [group 6] and the set of the modified solids as [group 6]'. It has 5 elements, like [group 6] (Figure 12(a)). The edges of the next polyhedrons have 9 different orientations, 3+6 of the above edges: (3;4;4;4), (3;8;8), (4;6;8). This set is called [group 9] shown in Figure 12(b) and has 3 elements like [group 9]' as well.

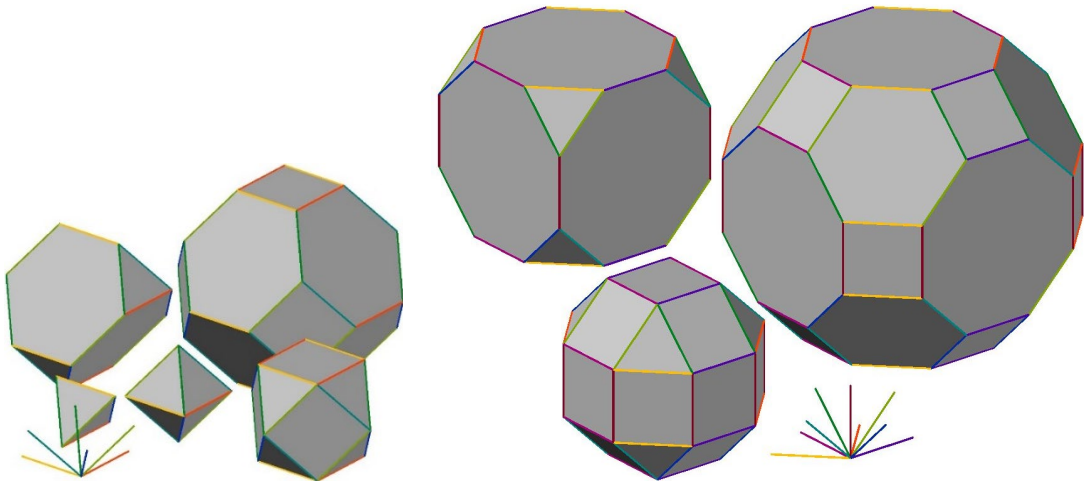

(a) (b)

Figure 12: Platonic and Archimedean solids, elements of the considered convex uniform honeycombs (a) [group 6] (b) [group 9]

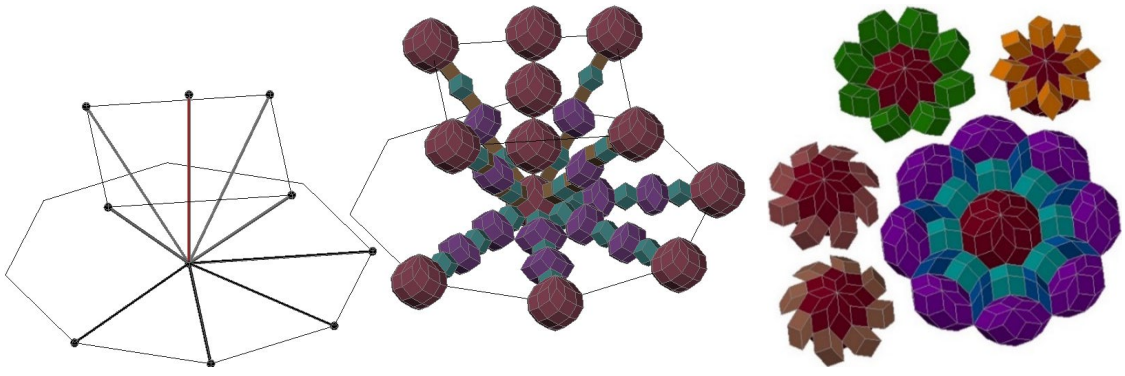

(a) (b)

Figure 13: (a) The construction of the 9 compound edges (b) All compound models consist of this set of the initial models.

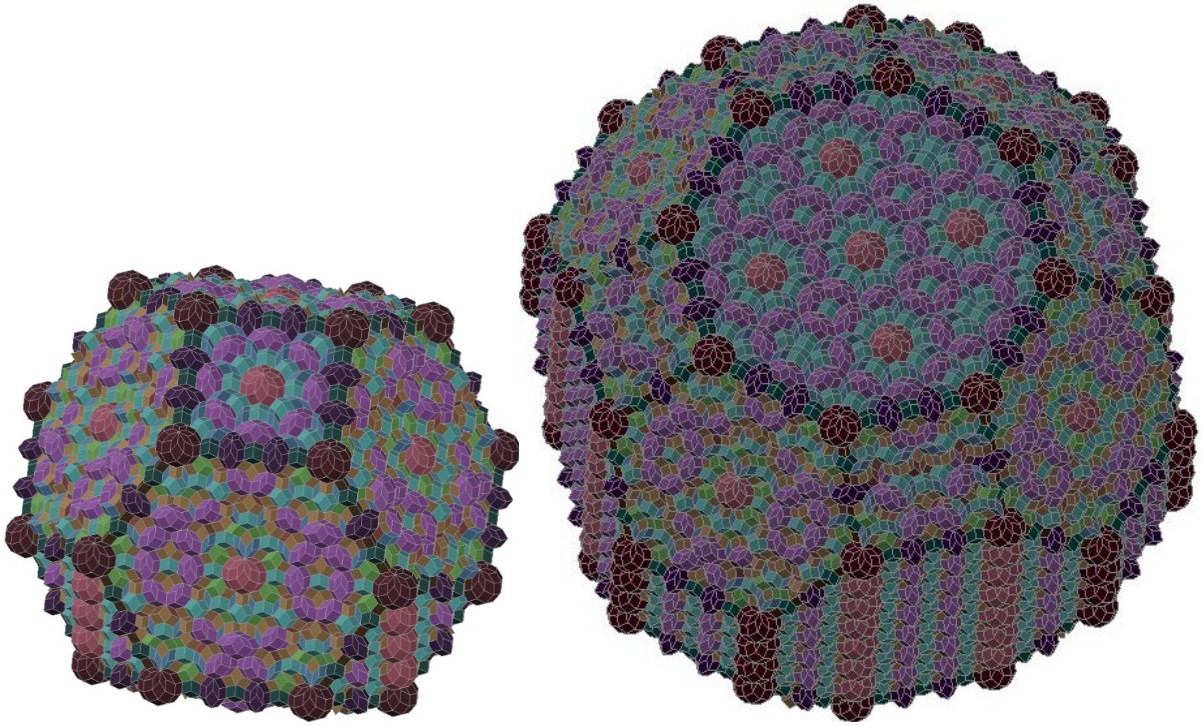

Figure 14: The filled compound 3-models of the Archimedean solids: truncated octahedron (4;6;6), 16117 stones and truncated cuboctahedron (4;6;8), 29826 stones

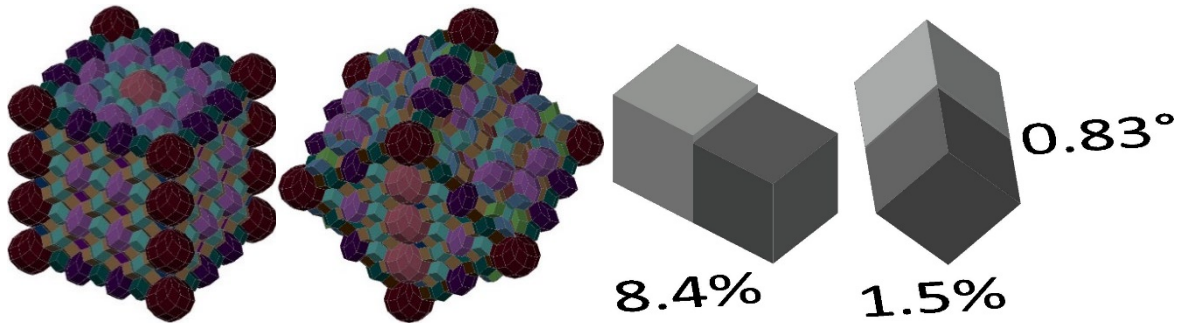

(a) (b)

Figure 15: (a) The compound models of the affine pairs of the cube oriented in two different ways. (b) Their bearing solids can illustrate the deviations regarding the considered Platonic and Archimedean solids (dark grey) and their affine pairs (light grey).

The inner spaces of all compound models are filled with layers of stones chosen from the used set of elements. Figure 16 shows the construction steps from the first horizontally symmetric layer up to the second one in the compound model of the Archimedean solid (4;6;8). The structure of the layers in all models is equal to this one of the above compound models introduced in section 2. So the method of construction of new tessellations, described there and illustrated in Figure 6 up to Figure 11, is applicable based on these models as well.

It is possible to construct periodical space-filling mosaics based on the convex uniform honeycombs. Its rectangular unit parts can be replaced with their affine pairs cut out from the appropriate combinations of solids, bearing the compound models of the considered initial solids. These are the repeated parts of the new tessellations using the stones derived from the 3-model of the 8-cube introduced in Figure 1. The key of the notation in Figure 17: P=Platonic, A=Archimedean, h=regular octagon based right prism, the digits denote the set of regular polygon faces joining the vertices of the given solid.

Figure 18 shows the structure of a mosaic, chosen as an example, and the compound models of the applied Platonic solids, (3;3;3) and (3;3;3;3). The compound model of the rectangular unit part of the initial mosaic can be seen in Figure 19 in axonometric projection and in front view with horizontal symmetry planes. Figure 20 shows plane-tiling patterns cut out from the above unit mosaic, here by five equidistant planes. The first and the fifth ones are adjacent symmetry planes. These patterns, further called paired patterns, define exactly the spatial structure of this part of the tessellation, knowing the above introduced construction steps and the common properties of the considered compound mosaics if the stones are coloured only according to their shape.

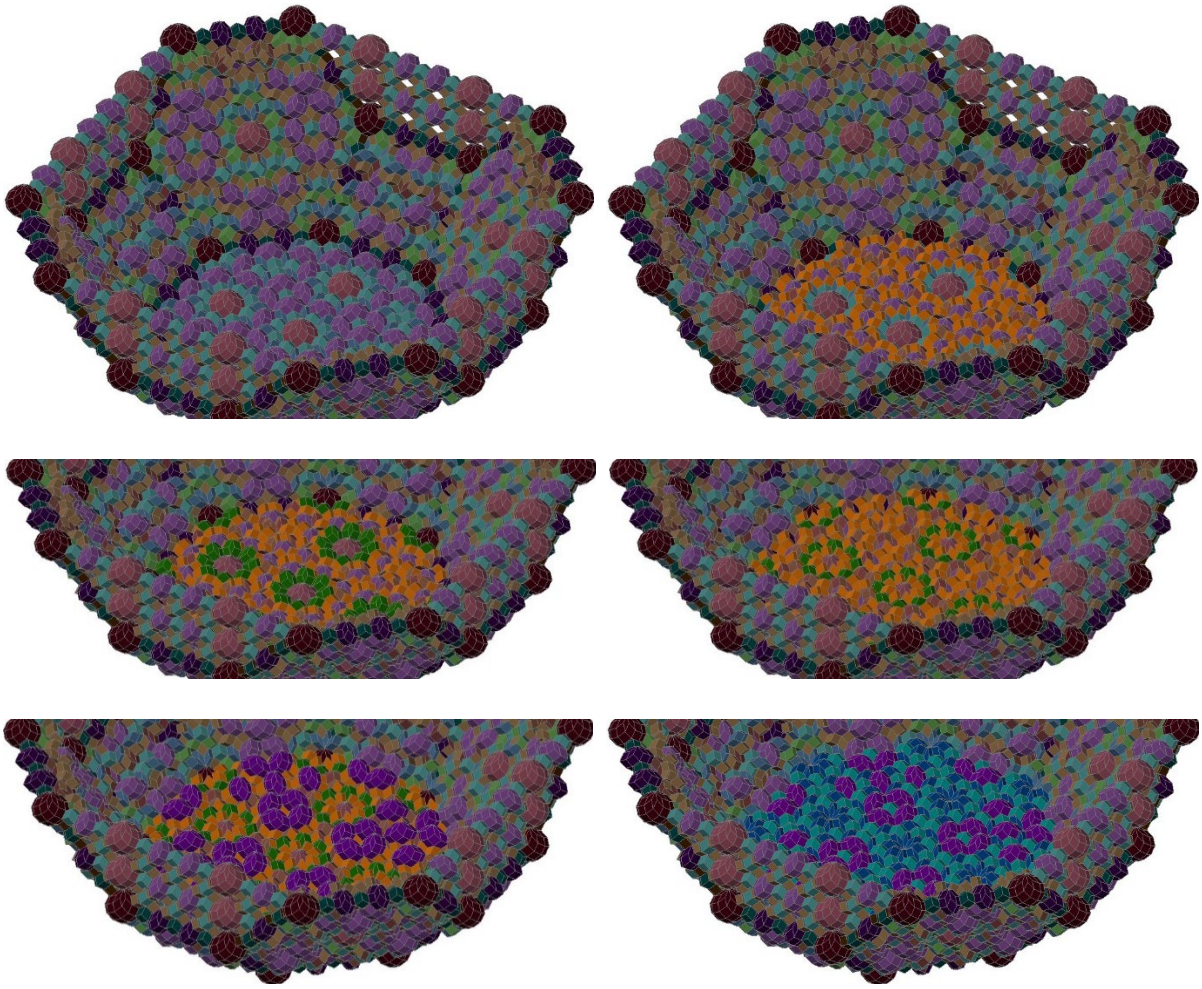

Figure 16: The inner spaces of all compound models are filled with layers of stones chosen from the used set of elements.

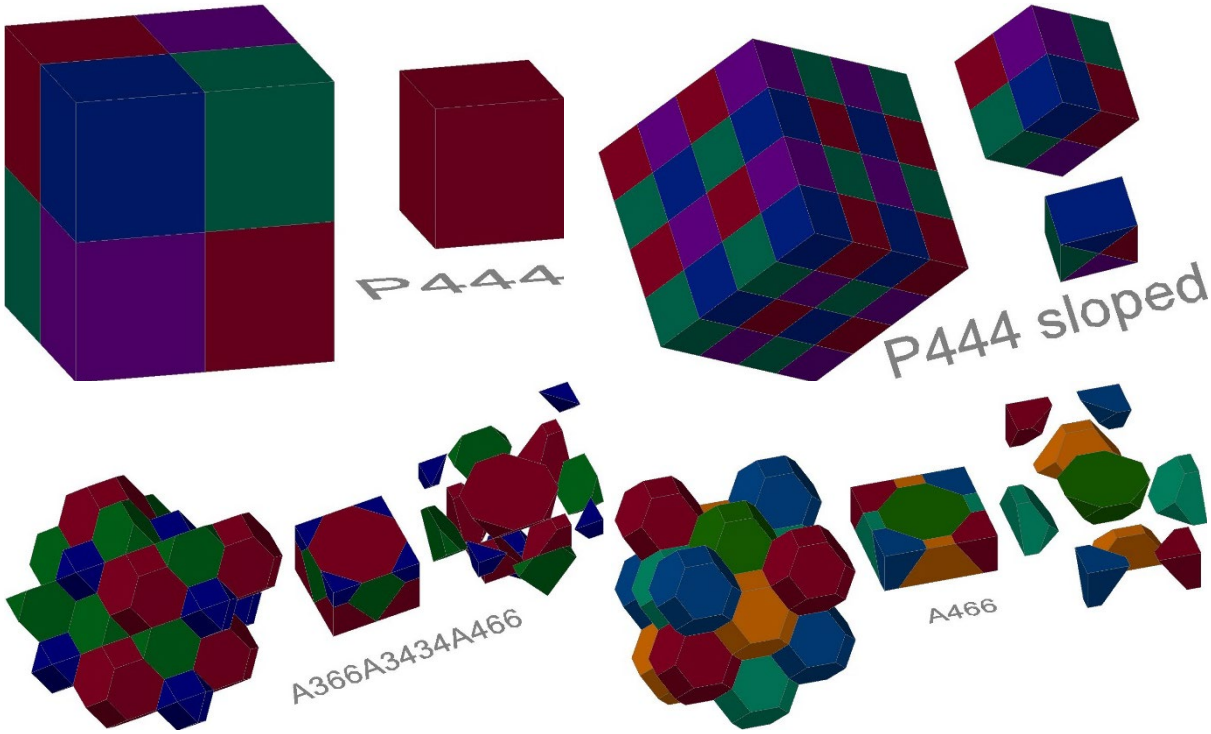

Figure 17(a): The structure of the space-filling mosaics of the considered convex uniform honeycombs and their rectangular unit parts

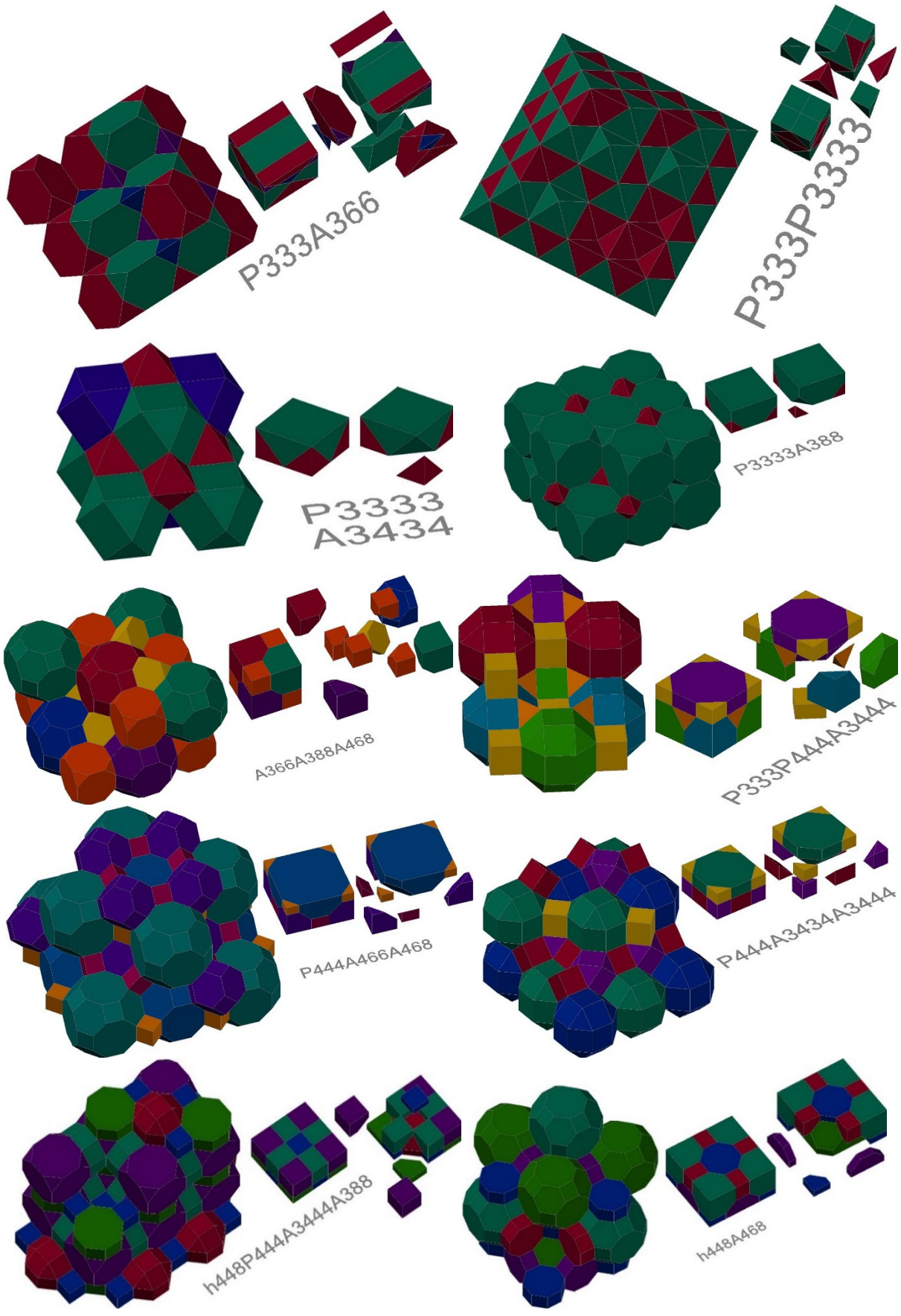

Figure 17(b): The structure of the space-filling mosaics of the considered convex uniform honeycombs and their rectangular unit parts

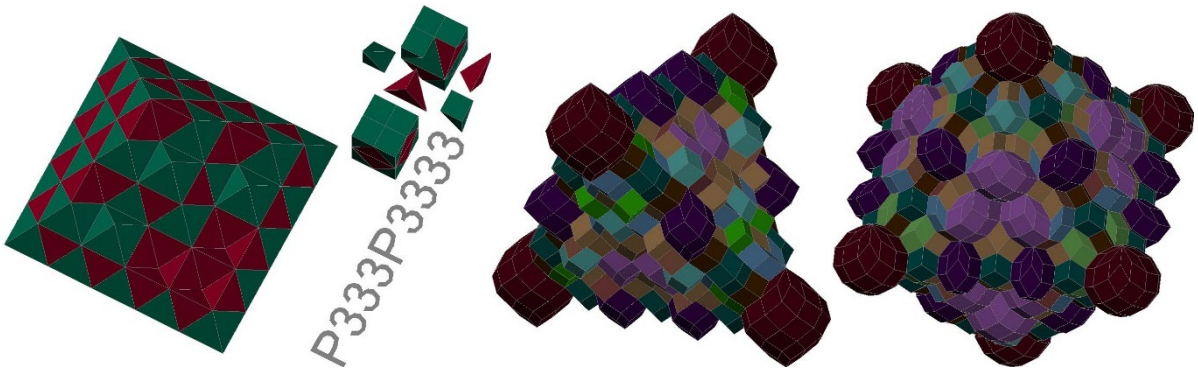

Figure 18: The structure of a mosaic, chosen as an example, and the compound models of the applied Platonic solids

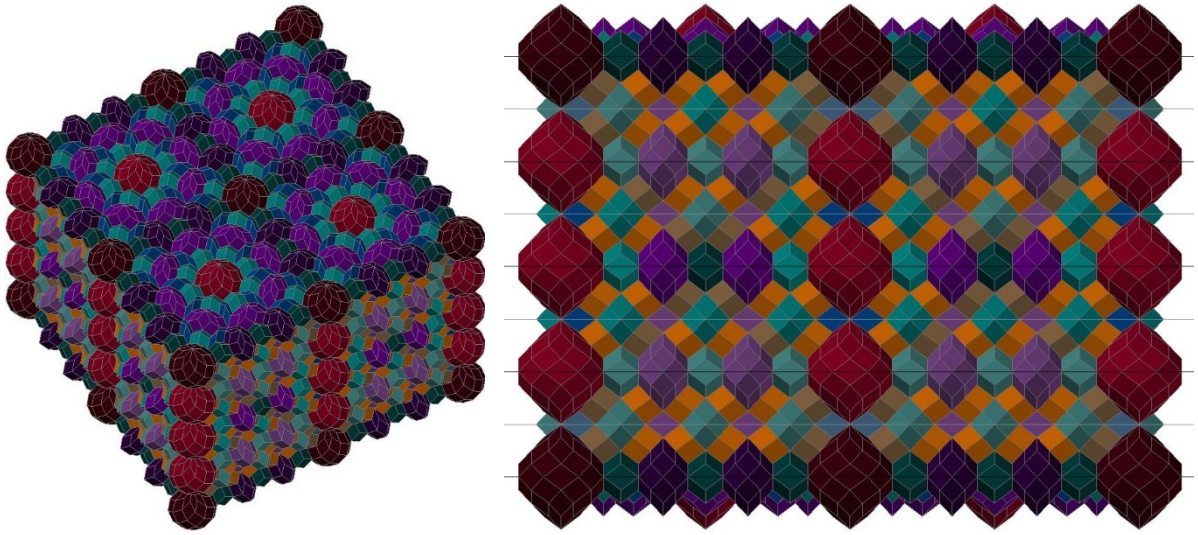

(a) (b)

Figure 19: (a) The compound model of the rectangular unit part of the above mosaic.
(b) The model in front view with horizontal symmetry planes.

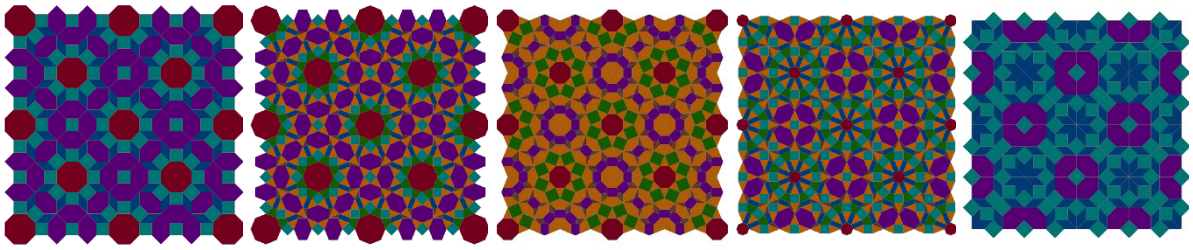

Figure 20: Plane-tiling patterns cut out from the above unit mosaic in five steps between two adjacent symmetry planes

In section 4 are described other possibilities to create further tessellations based on the initial 3-model of the 8-cube and on these compound 3-models of the considered solids.

3.2. The Base Structure of the Obtained Tessellations

The tessellations of the above defined paired patterns of the compound models of all rectangular unit mosaics, depicted in Figure 17, can be divided into congruent triangular and rectangular parts. These are arranged again in different patterns according to the used sets of the bearing solids of compound models that build up a given mosaic (Figure 21). These solids are the affine pairs of Platonic and Archimedean solids as well as of a regular octagon based right prism as it is described above. The key of the notation for Figure 21: the first digit gives the highest number of differently oriented solid edges, P=Platonic, A=Archimedean initial solid, h= prism with horizontal base face, v= prism with vertical base face, s= cube with sloped faces, the groups of digits denote the set of regular polygon faces joining the vertices of the given solid.

The compound mosaics based on the elements of [group 3]' define the congruent triangular T and rectangular R parts of the paired patterns. These parts are bordered by yellow lines in Figure 21. The same combination of T is repeated inside of the paired patterns of the spatial mosaic based on P444 and in tessellations of patterns based on the spatial mosaics consisting of the elements of [group 6]' only. Seven combinations of T and R give the tessellations of paired patterns of compound mosaics based on sets of bearing solids consisting of one of the elements of [group 9]' at least. In Figures 21 (c) up to (h), the grey lines show the borders of the repeated patterns and these tessellations are divided into the above determined triangle and rectangle shaped unit patterns by the yellow lines. Their combinations consist of some common larger parts as well. The net of bordering lines of T and R parts can be drawn in all plane-tiling patterns cut out from the given compound mosaic by other horizontal planes as well. The following spatial analysis lead to the definition of the two smallest unit parts needed to build up the tessellations of the compound models of the considered solids.

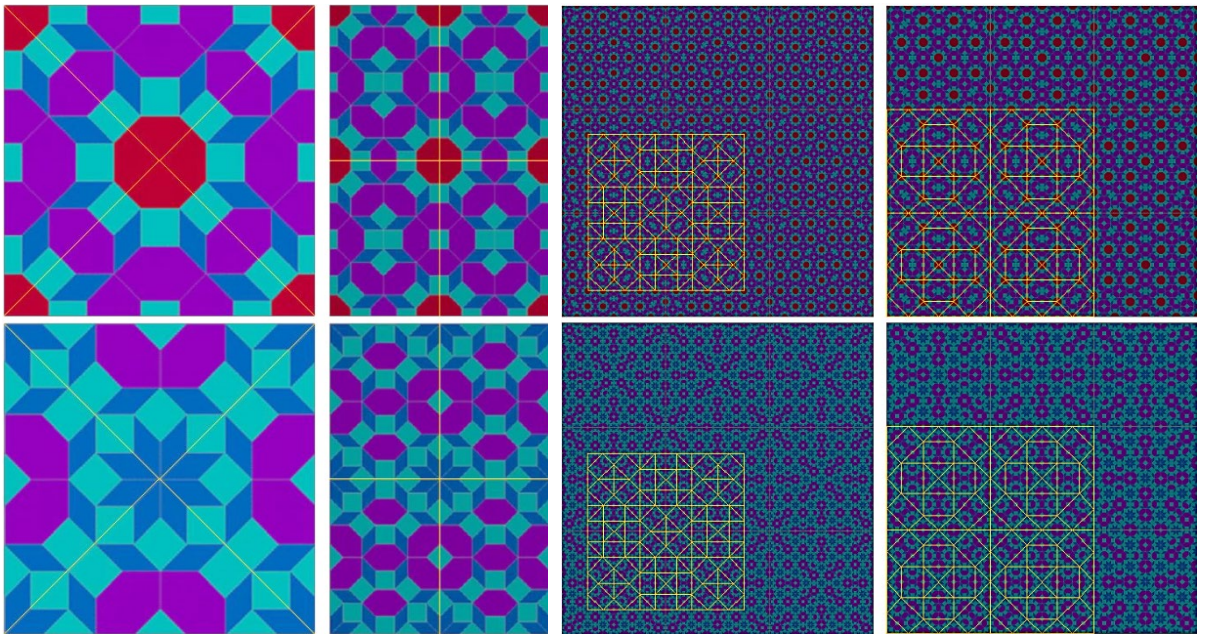

(a) (b) (c) (d)

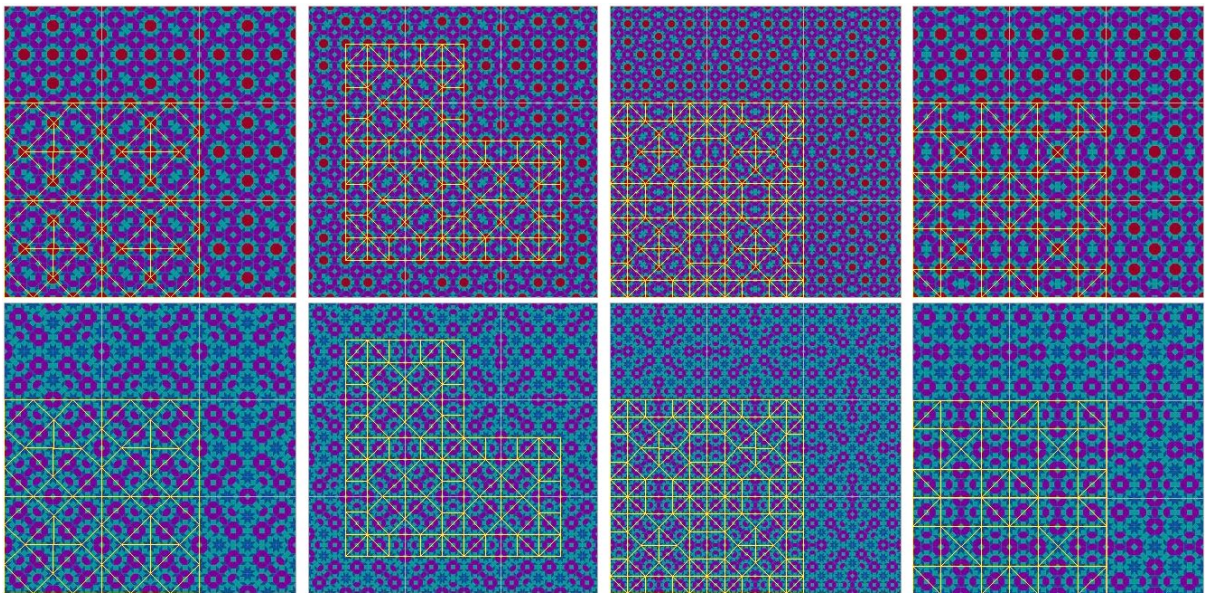

(e) (f) (g) (h)

Figure 21: The patterns defining the compound models of the above rectangular unit mosaics can be divided into congruent triangular and rectangular parts. These are arranged again in different patterns according to the used sets of the bearing solids in a compound mosaic.
(a) 3P444 (b) 3P444s (c) 9h448v448A468 (d) 9h448v448P444A3444A388
(e) 9P333P444A3444 & 9P3333A388 (f) 9A366A388A468 (g) 9P444P444sA466A468 (h) 9P444P444sA3434A3444
The pattern (a) is repeated in tessellations of patterns based on the elements of [group 6]'.

The investigation of the above described structures, helped by the paired patterns as well, show that only two different unit mosaics or their plane or centrally symmetric pairs are needed to build two compound prisms (Figure 22) that give periodical space-filling mosaics in different arrangements, not only those that are described in this section. The used stones are derived from the special 3D model of the 8D cube described in the introduction and in section 2. The above unit mosaics can be cut with border and symmetry planes of the bearing solids of the compound prisms (Figure 23). These can be divided into further triangle as well as rectangle based unit parts. The cutting vertical planes are marked with axis lines in top view in Figure 23. The finally defined unit parts are the smallest ones that build up all compound mosaics introduced in this section. These parts and their symmetric pairs are depicted in ordered front, left side and top views as well as in axonometric projection in Figures 24 and 25.

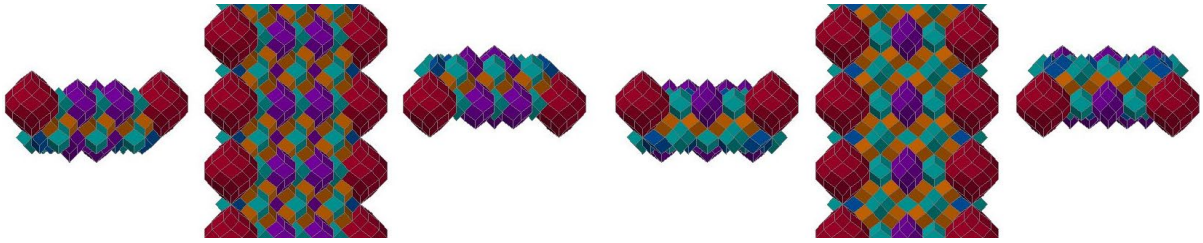

Figure 22: The above mosaics can be built up with two different compound prisms (front view).
Only two different unit mosaics or their plane or centrally symmetric pairs are repeated along the axes of these prisms.

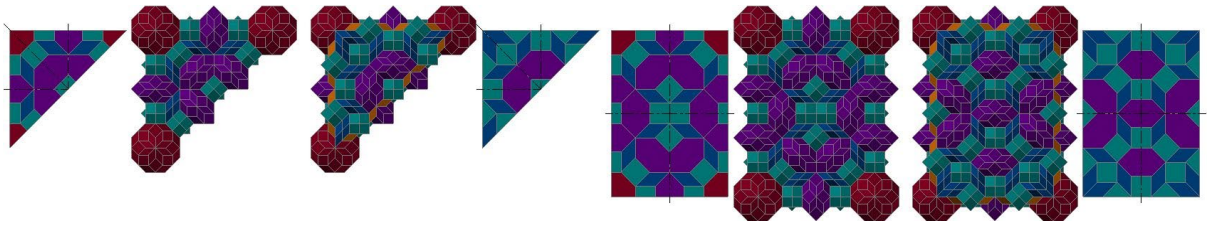

Figure 23: The above unit mosaics cut with border and symmetry planes of the bearing solids of the compound prisms (top view).
These can be divided into the smallest, triangle as well as rectangle based unit parts of all compound mosaics described in this section.

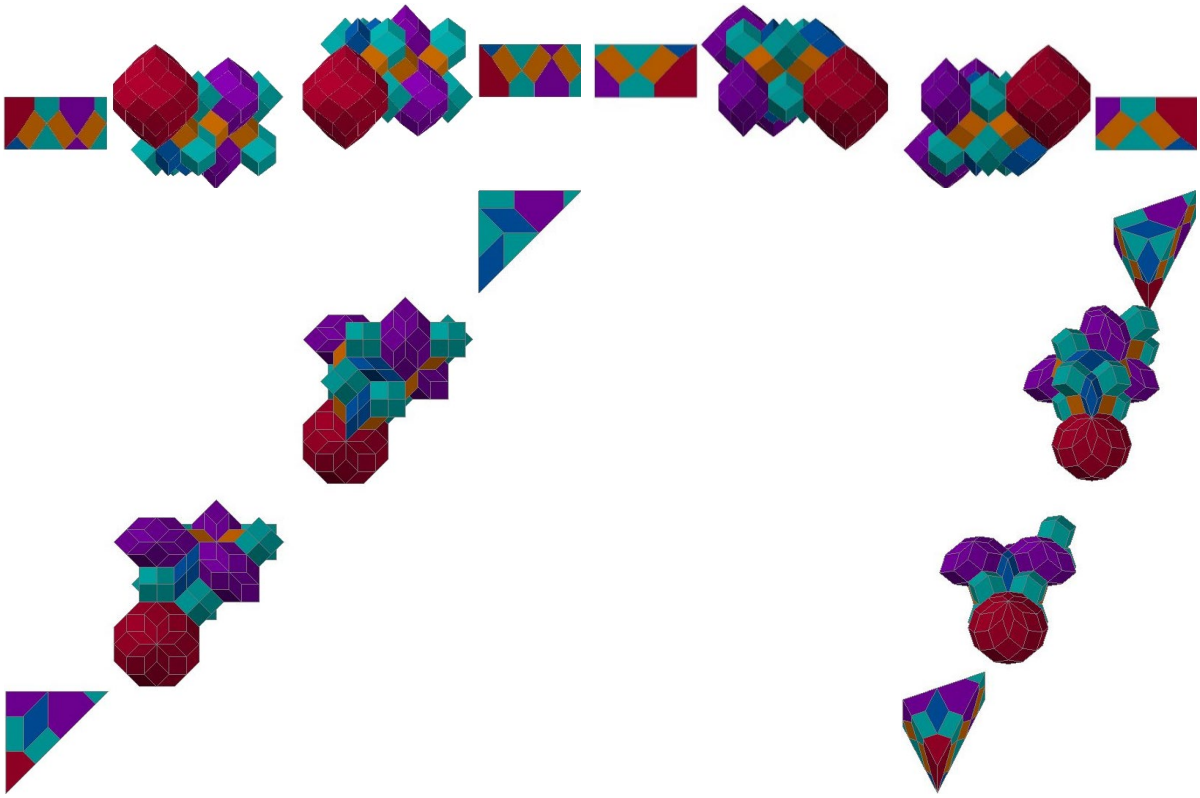

Figure 24: The smallest, triangle based unit part and its symmetric pair in front, left side and top views as well as in axonometric projection.

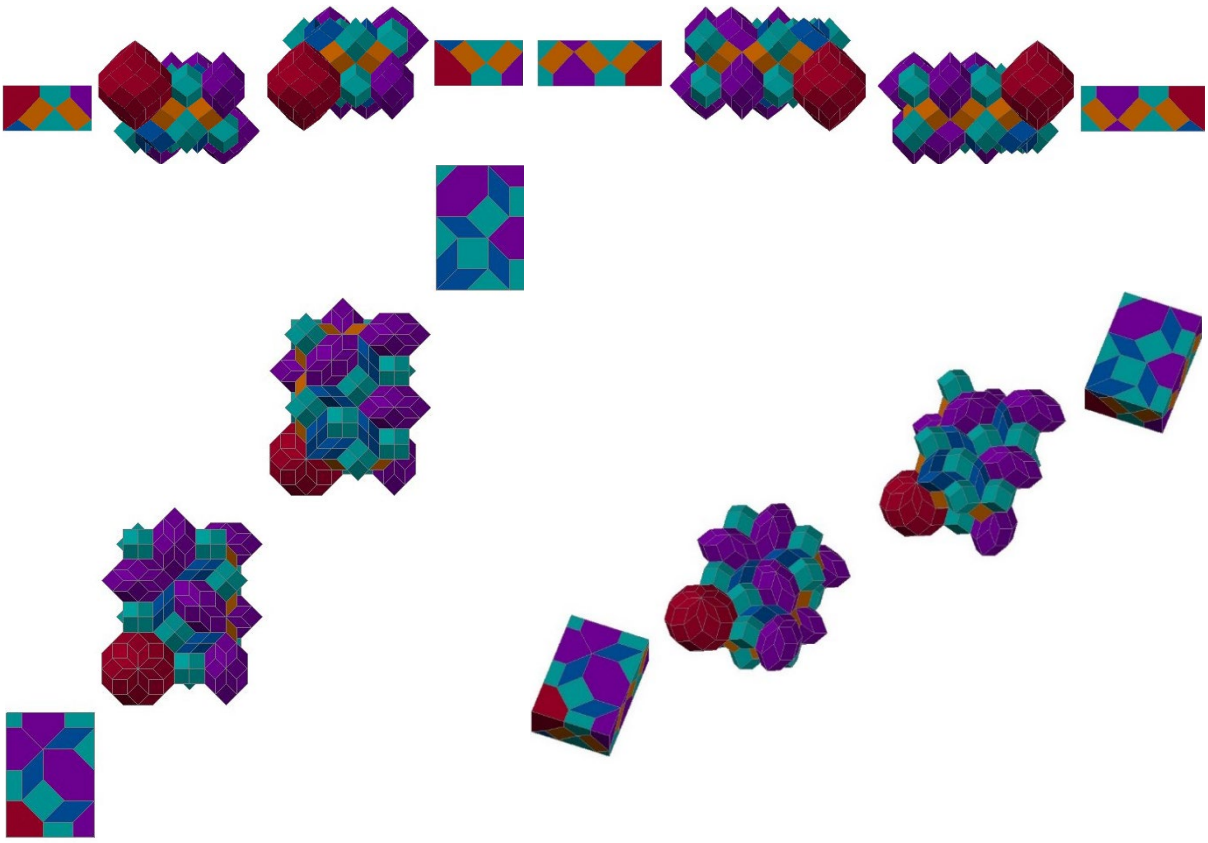

Fig. 25: The smallest, rectangle based unit part and its symmetric pair in front, left side and top views as well as in axonometric projection.

4. ON THE SPATIAL TESSELLATIONS AND FRACTAL LIKE STRUCTURES

This section summarises the process of the already introduced tessellations and describes further possibilities to create more complex ones having fractal like structures as well.

Let's call the set of initial 3-models of the 8-cube and of its *j*-cubes, described in section 2, **iM8**. Its subset is used to construct compound 3-models of the elements of **iM8**. It can be called **siM8** (Figure 5(b)). The set of the compound models will be called **cM8**. In case of the 9-cube, the notation can be **iM9** and **cM9**. (The set **iM9** consists of **iM8**. Its further elements are derived from the elements of **iM8**, using one additional initial edge (Figure 3(a)) in order to the modelling.) The construction of the elements of **cM9** needs also **siM8**. The bearing solids of **cM8** and **cM9** are affine pairs of the elements of **iM8** and **iM9**, these can be called **aM8** and **aM9**. So the cells of all possible tessellations of **iM8** or **iM9** elements can be changed to **aM8** or **aM9** elements. The application of **cM8** as well as **cM9** elements instead of **aM8** or **aM9** elements results in a mosaic **cM8** as well as **cM9** stones. This process can be repeated. A fractal like structure can be obtained by colouring of the stones according to their shapes and roles. It will be more consequent if the stones used in the first step are **siM8** elements. The modifications because of penetrations, mentioned in section 2, are avoidable if the notations of the initial 3-models dose not consist of a digit 1 (Figure 5(c), because in that case the compound model of the acute angled rhombic face needs the *j*-cube k8j04-1115 (Figure 3(b)). The initial construction steps of a very simple example for a more consequent fractal like tessellation, using the *j*-cube k8j04-2222 only, can be seen in Figure 26. The structure of the introduced unit part of the tessellation and the layout of its **iM8** elements are depicted in Figures 27, 28 and 29 coloured according to the shapes of the stones.

The set of the solids, applied in the considered convex uniform honeycombs, is called **iC9** following the above way of notation. The construction of the compound models, elements of **cC9**, needs a subset of **siM8**. It is called **ciM8** (Figure 13(b)). The name of the set of the bearing solids of **cC9** elements is **aC9**. The set **aC9** can substitute for **iC9** because the faces of their elements are affine pairs of each other. Using **cC9** elements instead of **aC9** ones, are created the compound pairs of tessellations of **iC9** elements and the unit parts introduced in section 3. The applied **ciM8** elements can be changed to **cM8** models and this step can be repeated as it is described above. This process needs already the local modifications because of penetrations. The new, more compound unit parts can be varied in order to get more complex periodical space-filling mosaics. The different structures inside of these tessellations can be shown again by colouring of the elements.

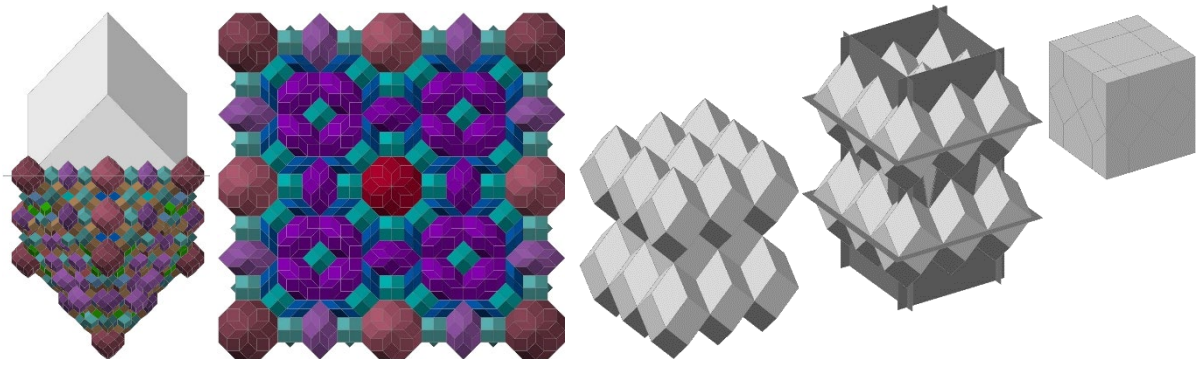

(a) (b)

Figure 26: (a) The compound model of the *j*-cube k8j04-2222 in front and top views (b) The construction of a unit part of the **aM8** models

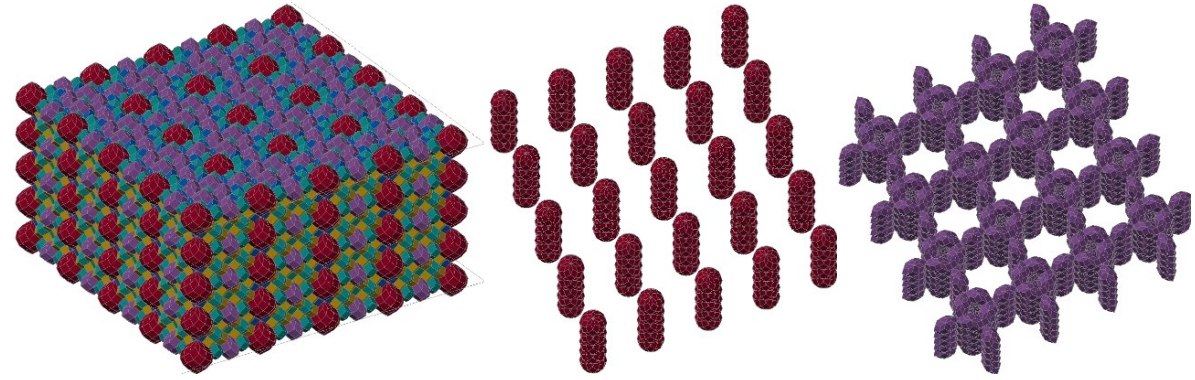

(a) (b)

Figure 27: (a) The compound model of the above rectangular unit part of the periodical space-filling mosaic.
(b) The layout of the **iM8** models k8j08 and k8j06-112112 inside of the compound unit mosaic in axonometric projection.

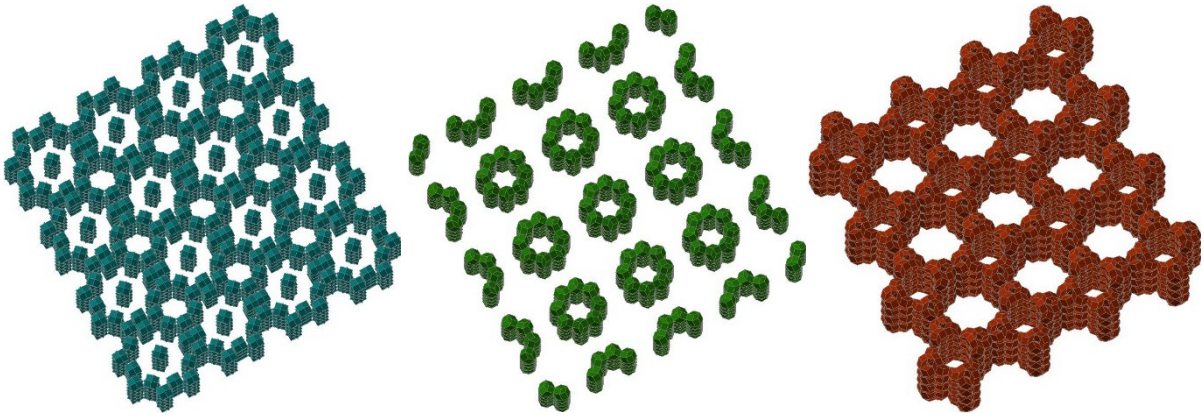

Fig. 28: The layout of the **iM8** models k8j04-2222 and k8j04-2222 as well as k8j03-125 and k8j03-215 together, in axonometric projection.

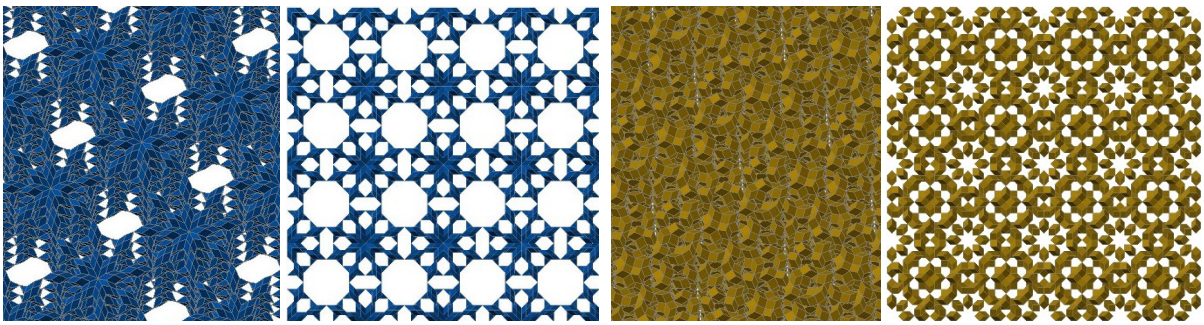

Figure 29: The layout of the **iM8** models k8j04-1313 and k8j03-223 inside of the unit part
of the periodical space-filling mosaic, in axonometric projections and in top views.

5. CONCLUDING REMARKS

The investigation of the base structure of the above introduced more complex tessellations requires the application of further possible features of the used computer and CAD program. Similar but not so detailed description regarding the 5D and 6D cubes is given already by the author in [7]. It deals especially with the helical structure of the considered tessellations that can be discovered also in the here studied constructions. All of these investigations could be extended to other hypercube models as well.

The creation of the constructions and figures required for this topic was aided by the AutoCAD program as well as by AutoLisp routines developed by the author.

REFERENCES

1. Coxeter, H. S. M., 1963. Regular Polytopes. Second edition. The MacMillan Company, New York
2. Grünbaum, B., 1994. Uniform tilings of 3-space. *Geombinatorics*, 4. pp 49–56.
3. Towle, R., Zonotopes, symmetrical structures. 2008. http://zonotopia.blogspot.com [Accessed: 20th March 2020]
4. Vörös, L., 2005. Reguläre Körper und mehrdimensionale Würfel. *KoG* 9. pp 21–27. http://master.grad.hr/hdgg/kog_stranica/kog9.pdf [Accessed: 20th March 2020]
5. Vörös, L., 2006. Two- and Three-dimensional Tilings Based on a Model of the Six-dimensional Cube. *KoG* 10. pp 19–25. http://master.grad.hr/hdgg/kog_stranica/kog10.pdf [Accessed: 20th March 2020]
6. Vörös, L., 2011. Structures in the Space of Platonic and Archimedean Solids. *Serbian Architectural Journal*, issue: 2011/2 Vol. 3 pp 140–151 https://www.researchgate.net/publication/326782715_Structures_in_the_Space_of_Platonic_and_Archimedean_Solids [Accessed: 20th March 2020]
7. Vörös, L., 2014. Helical structure of space-filling mosaics based on 3D models of the 5D and 6D cubes. Proceedings of the 9th International Conference on Applied Informatics Eger, Hungary. Vol. 1. pp 141–149, http://icai.ektf.hu/?p=papers [Accessed: 20th March 2020]
8. Vörös, L., 2018. New Space-filling Mosaics Based on 3D Models of Higher-Dimensional Cubes. Proceedings, 6th International Conference on Geometry and Graphics, Mongeometrija 2018, Novi Sad, Serbia. pp 465–477, ISBN 978-86-6022-055-6
9. Vörös, L., 2018. Inventory of Mosaics and Stones. http://geometria.mik.pte.hu/videok.html [Accessed: 20th March 2020]
10. Vörös, L., 2018. Geometrical Structures of Planar and Spatial Tessellations Based on 3D Models of Higher Dimensional Cubes. ICGG 2018 - Proceedings of the 18th International Conference on Geometry and Graphics, Milan, Italy. pp 458–470, Springer, Heidelberg, , ISSN 2194-5357 ISSN 2194-5365 (electronic) Advances in Intelligent Systems and Computing ISBN 978-3-319-95587-2 ISBN 978-3-319-95588-9 (eBook) https://doi.org/10.1007/978-3-319-95588-9 Library of Congress Control Number: 2018948129 [Accessed: 20th March 2020]
11. Vörös, L., 2018. A Set of Planar and Spatial Tessellations Based on a Compound 3D Model of the 8D Cube. Abstracts − 4th Croatian Conference on Geometry and Graphics, Vodnjan (Peroj), Croatia. p 48, http://www.hdgg.hr/vodnjan/abstracts2.pdf [Accessed: 20th March 2020]
12. Vörös, L., 2019. A Set of Planar and Spatial Tessellations Based on Compound 3D Models of the 8D and 9D Cubes. Abstracts − 21st Scientific-Professional Colloquium on Geometry and Graphics, Sisak, Croatia. p 32, http://www.hdgg.hr/sisak/abstracts.pdf [Accessed: 20th March 2020]

OBTAINING PENCILS OF CURVES OF HIGHER ORDER BY APPLYING A SUPERSYMMETRY TO PENCILS OF CONICS

Gordana Djukanović
Faculty of Forestry, University of Belgrade, Serbia
PhD, Assistant Professor, gordana.djukanovic@sfb.bg.ac.rs

Djordje Djordjević
Faculty of Architecture, University of Belgrade, Serbia
PhD, Assistant Professor, djordje@arh.bg.ac.rs

Mirjana Devetaković
Faculty of Architecture, University of Belgrade, Serbia
PhD, Assistant Professor, mirjana.devetakovic@gmail.com

ABSTRACT

In this work, pencils of conics are mapped into pencils of curves of the higher orders, using supersymmetry. A Model of basic transformation for mapping of dots (inversion) is shown graphically and using equation as well. The conics were mapped using a chain of inversions where the order of obtained curves was being doubled. The inversion was interpreted in two ways: as quadratic transformation in the classical projective geometry and as pure symmetry in the relativistic geometry. The recognition of the equivalence between inversion and harmonic symmetry has created numerous possibilities for mapping curves and obtaining new forms. Two types of pencils of conics which have not been mapped before are mapped in this work. Research studies in the field of enlarged symmetries offer inexhaustible space for further discoveries about plain and spatial forms. Obtained results will be of use in the theory of geometry and in the practice of architecture.

The mapping model was used to create the Lisp routine, which was then used in the AutoCAD software, for the purposes of computer drawing of pencils of conics and equivalent pencils of curves of the higher order. The order and the shape of the obtained curves depend on where the center of inversion has been constructed related to the base points of the pencil of conics. It is shown that the obtained pencils of curves intersect at the same number of base points as the original pencils of conics.

Keywords: inversion; supersymmetry; pencils of conics, pencils of curves of the higher orders

INTRODUCTION

In relativistic geometry, the basic terms “straight line” and “plane” are replaced with the terms “circle” and “sphere” where the size of the sphere does not affect the generality of conclusions. It also introduces a new term “observer” (hence the term “relativistic geometry”). Perception and interpretation of geometric elements are based solely on the observer’s position. Through the observer’s standing point on the “plane”, a pencil of his “straight” geodesics cuts through. Every single one of these biggest circles on the sphere defines a pencil of “straight lines” that are parallel to them but are not geodesics. By moving away from the geodesics on both sides, the diameter of the circles decreases. For each direction in the antipode, there is one infinitesimal circle. Thus, we come to an unusual conclusion: Unlike the projective plane which has only one infinitely distant straight line for all observers, the relativistic “plane” has infinitely many infinitesimal antipodal “straight lines” for each (of ∞^2) observer

individually. However strange it may be, this fact paves the way for creating a simple mechanism for the construction and deconstruction of singular points of curves.

In relativistic geometry, curves are classified into harmonic groups. All curves belonging to the same group are symmetrical to each other and the initial curve, but they can be of a different order. Symmetry in the "plane" can also be performed spatially. As all characteristics of one curve isomorphically transfer to another curve, it becomes certain that the classification of curves into harmonic groups is the way to achieve their comprehensive classification. While the curves in the most classical group of conic sections (ellipse, parabola, and hyperbola) belong to the same order but differ in many other aspects, the curves of the same relativistic group of mutually harmonically-symmetric curves differ only in shape, while they have everything else in common. The classification of curves into harmonic groups is of great value. If we determine that a curve belongs to a certain group, we can, according to the law of symmetry, apply to that curve everything that we already know about the most typical member of that group.

In relativistic geometry, the "straight line" and circle are second-order curves because a "straight line" is a circle passing through the observer's antipodal point. If a classical second-order curve has two asymptotes, it passes through the antipode twice and has a double point in it, which makes it a fourth-order curve in relativistic geometry. The curves of the third order pass through the antipode once and consequently, one order is added to them, while the curves of the classical fourth-order (one-part and two-part curves) remain the same order. The curves to which the rule doesn't apply are Newton's diverging cubic parabola (it is of the classical third order, but has one isolated double point and passes through the antipodal point once, therefore in relativistic geometry the order increases by three) and Menger's folium (Karl Menger, 1902-1985), an oval of the classical fourth order that inverted becomes a sixth-order curve). Thus, when mapped, they turn into sixth-order curves. It is important to emphasize that after the regrouping, they are all curves of the even order. (Dovniković L., 2010).

The explanation begins with mapping a straight line as a curve of $n=1$ order. A straight line can be mapped into itself if the center of harmonic symmetry is on the straight line itself because in that case, the straight line is the mapping ray. If the center of harmonic symmetry is outside the straight line, it is mapped into a curve of $2n$ order, i.e., a circle. By further harmonic symmetry of the circle, i.e., the curve of $2n$ order, where the center of mapping is on the circle, we obtain a straight line, i.e., a curve of $2n/2$ order. If the center of harmonic symmetry is outside the circle, i.e., outside the curve of $2n$ order, the curve is mapped into a curve of the same order, i.e., a circle. This means that the order of the mapped curve can be maximally doubled by harmonic symmetry.

Quadratic transformations map a rational plane curve of n order from one field of points into a rational plane curve of $2n$ order. The relativistic geometry of harmonic equivalents replaces the basic elements of projective space with the concepts of a circle and sphere, introducing the concept of relativity when considering shapes. The analysis and understanding of the spatial essence of the perspective quadratic transformation indicate the transition of this transformation into a central inversion on the sphere as a harmonic symmetry. This bijective transformation is performed by polarity which pairs points involuntarily and harmonically (hence the name harmonic symmetry) relative to the absolute while maintaining the invariance of the mapped angles. Namely, a plane curve of n order, depending on the position of the center of harmonic symmetry (the center can be on the curve or beyond it), can be mapped into a curve of n, $2n-1$, or $2n$ order in the second field.

Conics are circular curves because they can be obtained as intersections of pairs of circles. The points of an ellipse are determined as the intersection of a pair of associated circles with centers in the foci of the ellipse and the sum of the radii equal to the major axis of the ellipse. In a hyperbola, the centers of circles are also in its foci, but now the difference in radii equals the real axis of the hyperbola. In relativistic geometry, a conic is a fourth-order curve because it is "added" a double point that is in the antipode since the ellipse is obtained as an intersection of a sphere and the elliptical cylinder that touches the sphere in the antipode. Thus, the spatial curve of the fourth order is "disintegrated" into a spatial curve and an isolated double point at which the intersecting quadrics touch. Only if the isolated double point is in the antipode, will the observer see this curve as a conic. If the observer moves to another point on the sphere, he will see the intersection curve as a fourth-order curve with an isolated double point. A circle is obtained as an intersection of a sphere and a horizontal "plane", which is also a sphere in relativistic geometry. Thus we can conclude that a circle also has a double point, but it is a circular point where two spheres touch (these are the same points in the "plane" and on the sphere).

Professor Lazar Dovniković has made a great contribution to the study of curves.

Figure 1 shows mappings of the points M and N by perspective collineation, inversion and axial symmetry for the center S and the circular axis s (by supersymmetry).

In Figure 1, we can see the way singular points are created by perspective collineation, by mapping the plane (1) into the plane (2). If the circle we map touches the vanishing line $u_1 = v_2$, it maps into a parabola. If it intersects

the vanishing line, it maps into a hyperbola, and if it touches it, it maps into a parabola. Homology is centrally symmetric. The vanishing lines $u_1 = v_2$ overlap exactly at the midpoint of the vertical distance between S and the planes 1 and 2. This is shown in the frontal view as a semicircle. The point M_1 is mapped into the point M_2 by perspective collineation, which can be seen in the same view. Looking at the base of Figure 2, we can further see that point M_2' maps into point M_2 by inversion (S, s_s), and point M_1' into M_1 by the same inversion. Figure 2 shows that the same points M_1 and M_2 can be obtained by supersymmetry with the same center S and the circular axis s that is twice smaller than the axis ss. In order to map the point M_1 to M_2 by supersymmetry, M_1 is connected to the center S whereby we obtain the center of the circle that is marked red "c" in the drawing. By mapping the point M_1 by the red semicircle, we obtain the point M_2 by supersymmetry. This figure is, in fact, proof that inversion (S, s_s) can be replaced by supersymmetry relative to the center S and the circular axis s. This fact greatly simplifies the mapping of curves because simple symmetrical transferring of points relative to the circular axis "s" enables us to obtain the point M_2 from the point M_1. The figure also shows the mapping of another point N_1 to the point N_2.

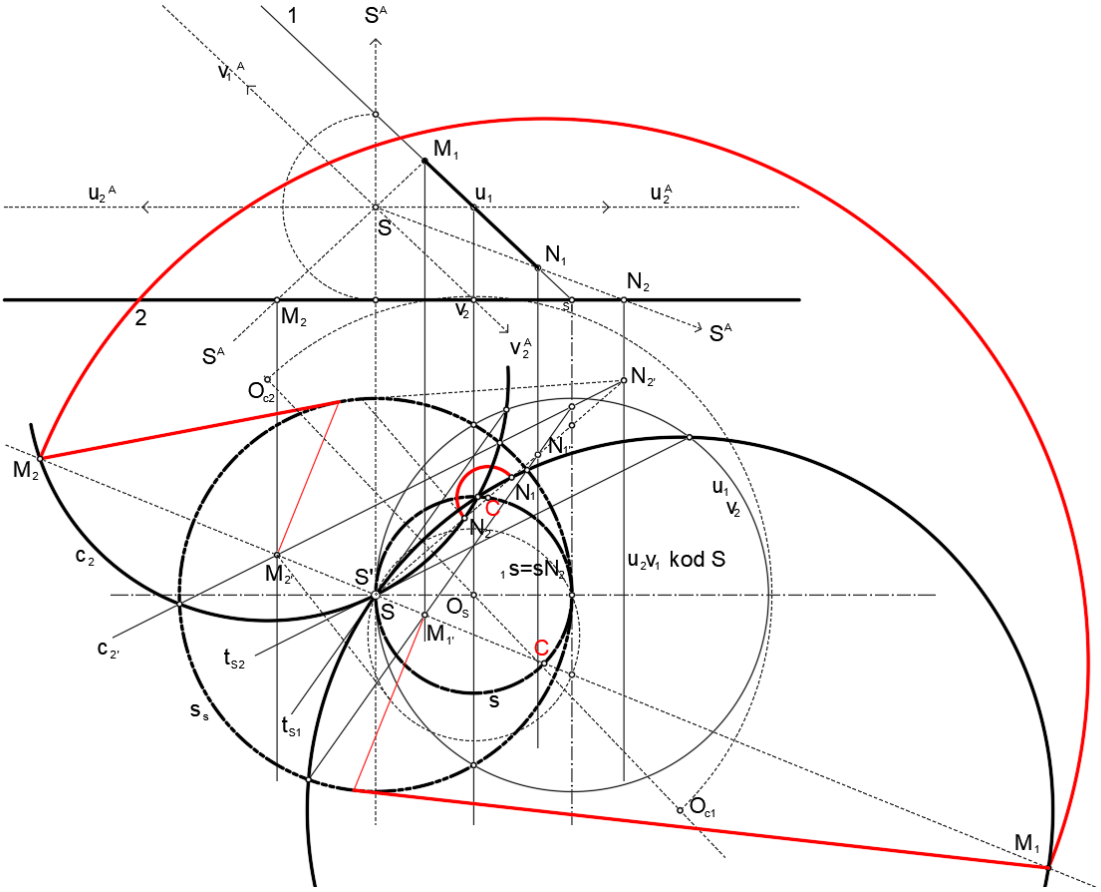

Figure. 1: Mapping of points by perspective collineation, inversion (S,s_s) and supersymmetry (S,s)

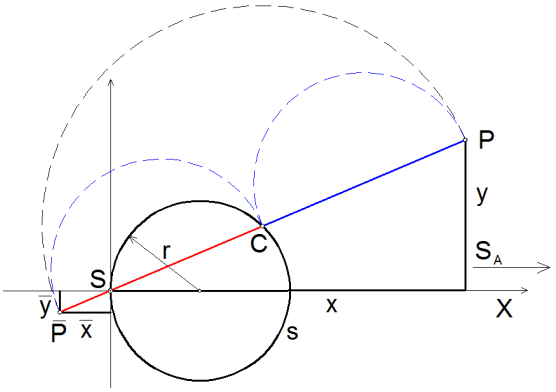

Figure. 2: Mapping of points by supersymmetry relative to the center C and the circular axis s

These are the equations for the coordinates of the mapped point $\overline{P}(\overline{x}, \overline{y})$, if the point to be mapped is P (x, y):

$$\overline{x} = \frac{4rx^2}{x^2 + y^2} - x \qquad (Eq.1)$$

$$\overline{y} = \frac{4rxy}{x^2 + y^2} - y \qquad (Eq.2)$$

A graphical model for mapping points by supersymmetry relative to the center S and the circular axis s is given in Fig. 2.

2. MAPPING OF PENCILS OF CONICS BY SUPERSYMMETRY

There are Lisp programs for drawing conics from pencils. The final result is a polyline (hyperbola, parabola, and ellipse). A step of 0.5mm is set so that the conics have the required smoothness. In this paper, elliptic-elliptic (EE) and parabolic-elliptic (PE) pencils of conics are mapped by supersymmetry. In Figure 4, an EE pencil of conics is mapped by symmetry for the center S and the circular axis s_{12}. In the EE pencil, the conics intersect at two pairs of conjugate imaginary points. The pencil of conics is drawn in blue and the marked curves are: hyperbola - h_1, parabola - p_2, and ellipse - e_3. The center of supersymmetry is placed at the vertex point of the hyperbola so that the hyperbola is mapped into a curve of the eighth order (h_1s).

The pencil of the mapped curves has the same number and type of intersecting points as the initial EE pencil of conics, two pairs of conjugated imaginary points. In relativistic geometry, a hyperbola is a fourth-order curve. The classical order of a hyperbola (2) is increased by the number of passes through the antipode, which is 2^A for the hyperbola (the order is $2 + 2^A$). The mapping of a hyperbola (h) from a pencil by symmetry for the center S and the circular axis s_{12} into a curve of the eighth order (hs) is shown in Figure 5. The double point in the antipodal center of symmetry is common to both curves and, therefore, their corresponding asymptotes are parallel.

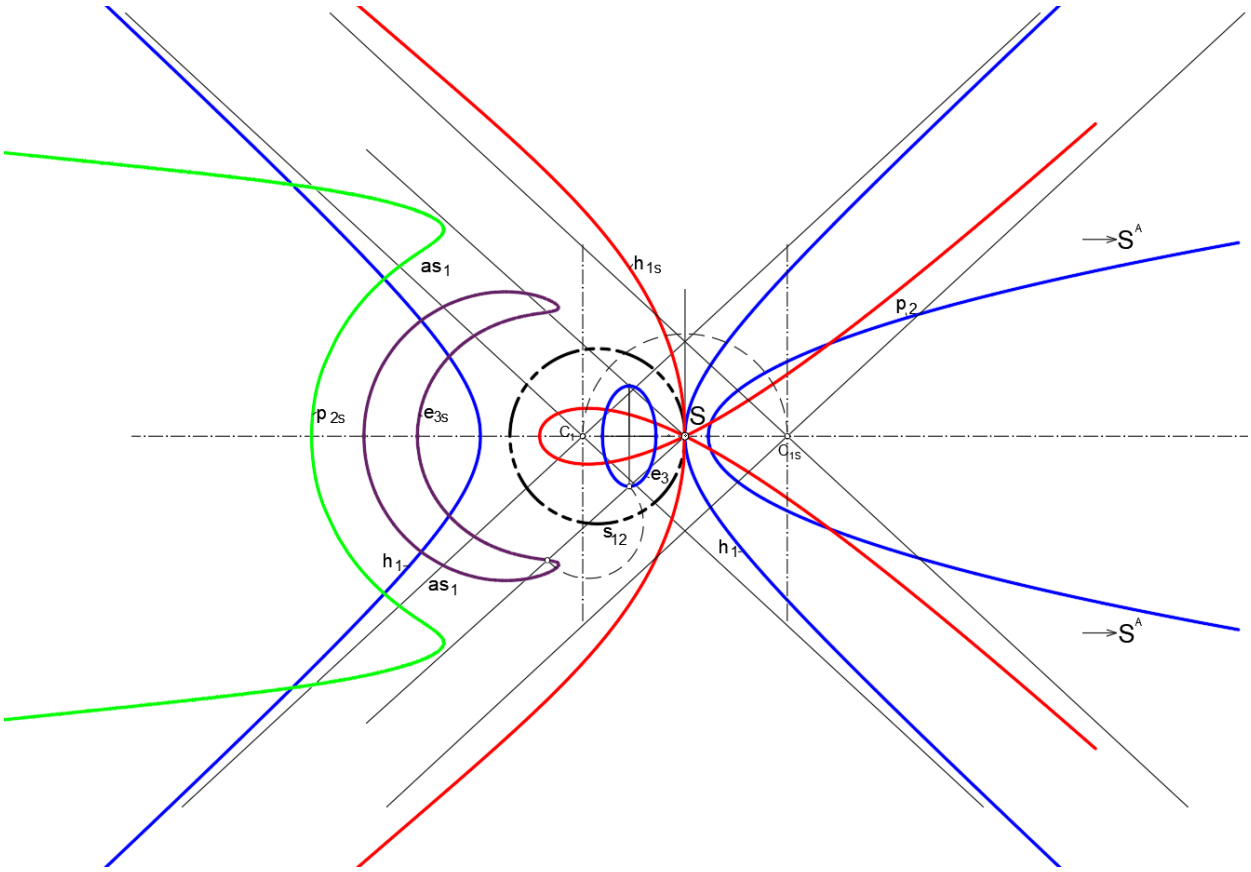

Figure. 3: An EE pencil of conics mapped by symmetry with the center S and the circular axis s

Since v_1 cuts and touches the hyperbola, a fourfold point is composed of an H-point (node) and a P-point (cusp). The total orders of the two curves are related in the following way: $n_2 = n_1 - m_{1S} + m_{2S}$, which means that the order of the starting curve decreases by the n-foldness of its (eventual) point in S (which is untied or if it is a single point, it is just displaced from *S*) and increases by the n-foldness of the new point generated in *S*. Since the "straight line" and circle are equivalent curves of the second order, they intersect the conic and its equivalent curves of the fourth order at the same number of points, i.e., four, which means that the n-foldness of the newly-created point always equals the order of the initial curve decreased by the number of its passes through *S* (because these points do not create the new singular point). The curve of the eight order (marked in black $6+2^A$) is mapped by inversion (Si, s) into the curve of the twelfth order (marked in red) with a 6-fold point in the point S. The fourfold point in the node S, together with the points 5_1 and 6_1, constricts the vanishing circle v_1 into a 6-fold point at Si. The double point at S^A of the curve hs is decomposed into ordinary points of the curve h_{inv}.

The curve of the twelfth order (the red curve marked with number 1) is mapped into a curve of the sixteenth order by supersymmetry for the center S and the circular axis s_{12} (Figure 5). The blue curve marked with number 2 has an eightfold point in S. An eightfold point in S has two cusps, two nodes, and one isolated double point (of a pair of conjugate imaginary points). The beauty and abundance of the shape of the mapped curves can be seen in the three examples with variable radius and position of the circle s_{12}.

The pencil of curves of the eighth order created by mapping the PE pencil of conics is given in Figure 6. The resulting pencil of curves of the eighth order intersects in the same number of base points as the starting pencil of conics, i.e., two real overlapping and two conjugate imaginary points.

The curves in the pencil are marked in blue. The hyperbola (h) is mapped into the curve h_s with a fourfold point in S (the curve is coloured red). The parabola (p) is mapped into the curve that is colored green and marked with p_s. The ellipse (e) is mapped by supersymmetry in the cyclamen coloured curve marked with e_s.

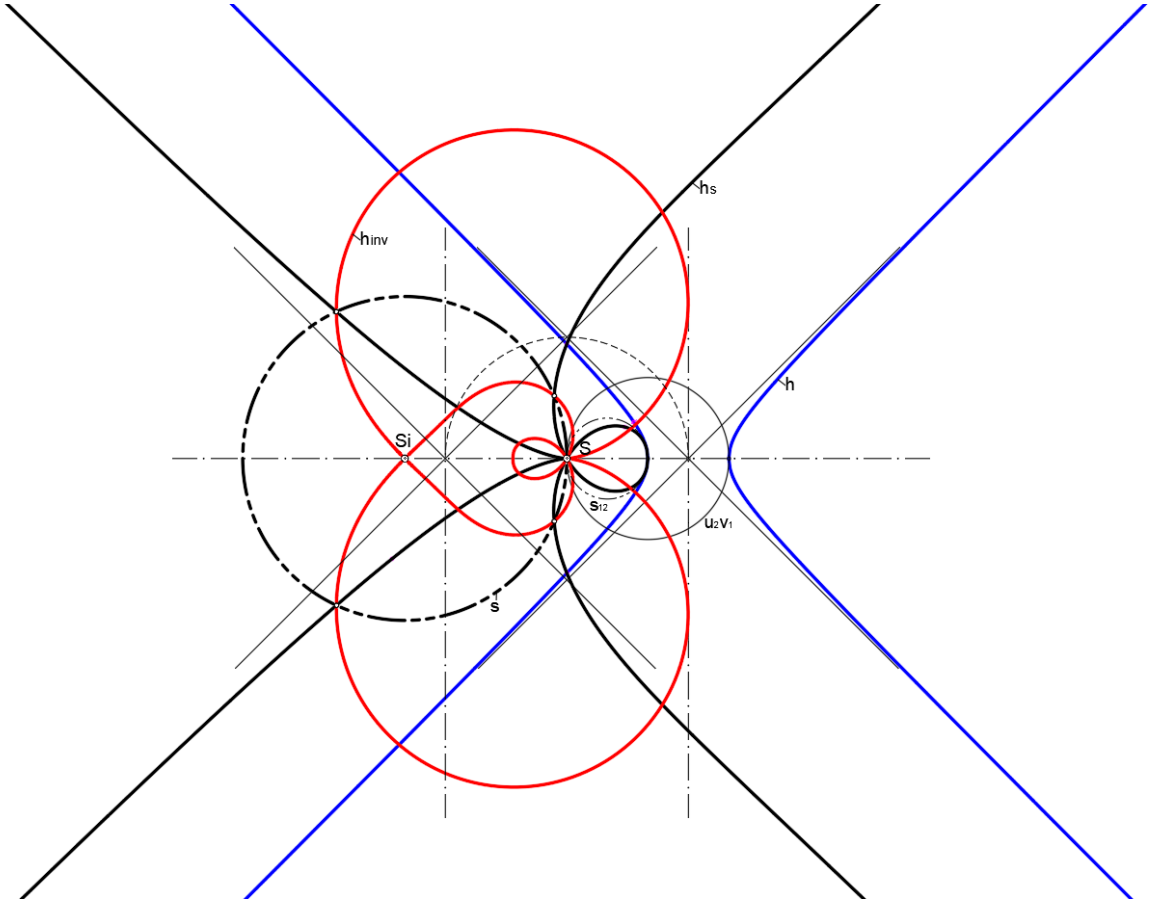

Figure. 4**:** Symmetry mapping of a hyperbola for the center S and the circular axis s_{12} into a curve of the eight order and its inversion into a curve of the twelfth order (Si, s)

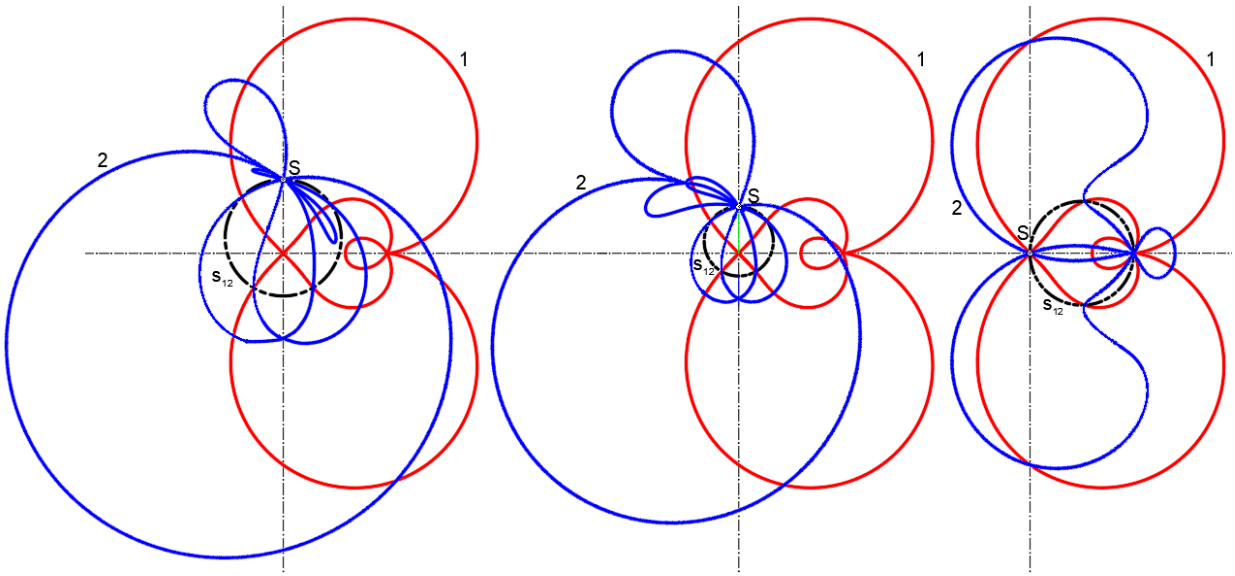

Figure. 5: Three examples of mapping a twelfth-order curve into a sixteen-order curve using symmetry for the center S and the circular axis s_{12}

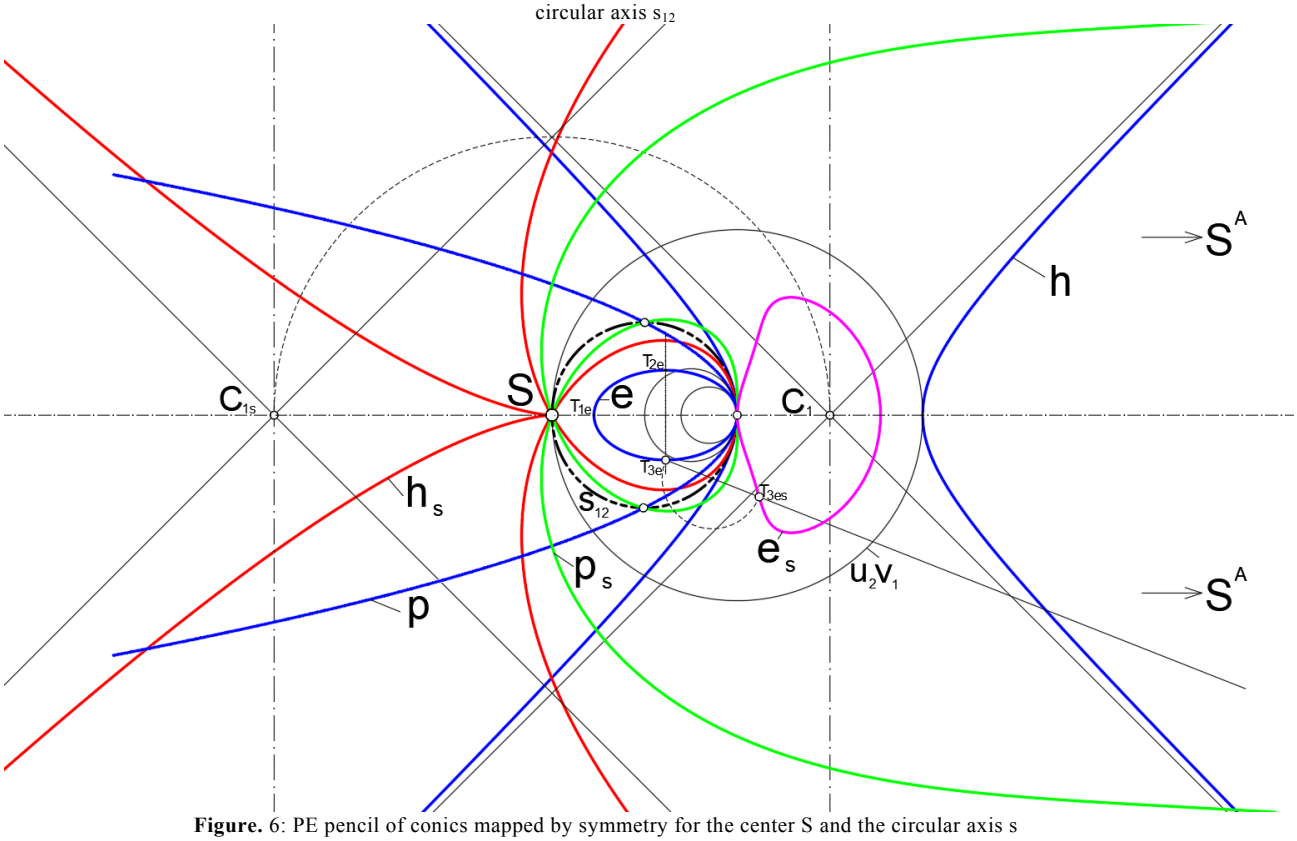

Figure. 6: PE pencil of conics mapped by symmetry for the center S and the circular axis s

2.1. CONCLUSION

This article proves that different classical constructions of "different" curves can be replaced by one conformal symmetry (inversion), by which a whole set of its conformally equivalent forms can be produced from one conic. Different types of symmetry of pencils of conics, both conformal (axial and central) and nonconformal (central-axial, i.e., polarity), as well as their transformations into corresponding harmonic symmetries for equivalent higher-order curves were also analyzed. It is shown how a specific construction of a curve is transferred to its equivalents by symmetry.

While classical inversion as a quadratic transformation is neither completely bijective (three lines are mapped into three points, and vice versa) nor completely conformal because it connects or disconnects singular points, relativistic inversion is, as pure symmetry, completely bijective and conformal. Thus it provides not only an incomparably simpler mapping but also a completely consistent and graphically precise transformation. Consequently, there is no doubt that a comparison between classical and relativistic geometry will always give the preference to the latter.

AutoCAD was used to draw pencils of conics, as well as their harmonic equivalents. Visual LISP was used to write a program for drawing conics and mapping second-order curves into higher-order curves.

2.2. ACKNOWLEDGMENT

This research has been completed within the following three research projects – COST Action 16235 Performance and Reliability of Photovoltaic Systems: Evaluations of Large-Scale Monitoring Data, funded by EU, III 47014 and TR37002, funded by the Ministry of Education and Science of the Republic of Serbia.

REFERENCES

Referencing to articles that have appeared in periodicals:

1. Dovniković, L, 2004. Relativistic Homology as a Way of Tying or Untying Singular Points, Journal for Geometry and Graphics, Vienna, Volume 8, No.2, 2004, pp 151-162
2. Đukanović G. et al, 2012. The Pencil of the 4th and 3rd Order Suraces Obtained as a Harmonic Equivalent of the Pencil of Quadrics throught a 4th Order Space curve of the 1st Category, Facta Universitatis, Series: Architecture and Civil Engineering, VOL.10 N^0 2.2012, pp. 193-207.

Referencing to books:

3. Dovniković L., 1999. The Harmony of the Spheres, The Relativistic Geometry of Harmonic Equivalents, Matica srpska, Novi Sad.
4. Dovniković L. 1977. Descriptive Geometrical Treatment And Classification Of Plane Curves Of The Third Order – Doctoral disertation, Matica Srpska, Novi Sad.
5. Đukanović G., 2012. The Pencils of Curves of the Third and Fourth Order obtained by Mapping the Pencils of Conics, Doctoral dissertation, Faculty of Architecture , Belgrade.
6. Nicholas M. P. et al, 2009. Shape Interrogation for Computer Aided Design and Manufacturing, Springer Science & Business Media

Referencing to Papers that have appeared in a long-running series of various Archives, even if they appeared on CD-ROM firstly or as to a loose Papers at the Workshops, Symposiums or Congresses

7. Benton B., 2011. Advanced Auto-CAD 2011 Training DVD-Tutorial, Infinite Skills.

Referencing to edited Conference Proceedings:

8. Dovniković L., 2010. Quantum-Relativistic Geometry as a new Scientific Paradigm, Proceedings of 2nd international Scientific Conference moNGeometrija 2010, Beograd

9. Đukanović G. et al, 2014, Mapping of the Pencils of Conics Using Supersymmetry – Inversion of Harmonic Homology, 4th International Scientific Conference on Geometry and Graphics moNGeometrija 2014, proceedings volume 2. str.180-193, June 20th - 22nd, Vlasina, Serbia

10. Đukanović G. et al, 2012. Graphic transformation of `asymmetrical` pencils of conics into pencils of curves of the 4th and 3rd order, Proceedings of 3rd International Scientific Conference moNGeometrija 2012., Novi Sad, pp 353-360

Referencing to Web-sites:

11. A Gallery of Cubic Plane Curves, http://www.milefoot.com/math/planecurves/cubics.htm [Accessed: 1st December 2019].

moNGeometrija 2020

PLÜCKER'S CONOID, HYPERBOLOIDS OF REVOLUTION, AND ORTHOGONAL HYPERBOLIC PARABOLOIDS

Hellmuth Stachel
Institute of Discrete Mathematics and Geometry, Vienna University of Technology
Professor emeritus, stachel@dmg.tuwien.ac.at

ABSTRACT

Plücker's conoid $\mathcal{C}$, also known under the name cylindroid, is a ruled surface of degree three with a finite double line and a director line at infinity. The following two properties of $\mathcal{C}$ play a major role in the geometric literature:

The bisector of two skew lines ℓ_1, ℓ_2 in the Euclidean 3-space, i.e., the locus of points at equal distance to ℓ_1 and ℓ_2, is an orthogonal hyperbolic paraboloid $\mathcal{P}$. All generators of $\mathcal{P}$ are axes of one-sheeted hyperboloids of revolution $\mathcal{H}$ which pass through ℓ_1 and ℓ_2. Conversely, the locus of pairs of skew lines ℓ_1, ℓ_2 for which a given orthogonal hyperbolic paraboloid $\mathcal{P}$ is the bisector, is a Plücker conoid $\mathcal{C}$.

In spatial kinematics, Plücker's conoid $\mathcal{C}$ is well-known as the locus of axes ℓ_{12} of the relative screw motion for two wheels which rotate about fixed skew axes ℓ_1 and ℓ_2 with constant velocities. The axodes of the relative screw motion are one-sheeted hyperboloids of revolution $\mathcal{H}_1$, $\mathcal{H}_2$ with mutual contact along ℓ_{12}. The common surface normals along ℓ_{12} form an orthogonal hyperboloid paraboloid $\mathcal{P}$ passing through the axes ℓ_1 and ℓ_2.

The underlying paper aims to discuss these two main properties. It seems that there is no close relation between them though both deal with Plücker's conoid, orthogonal hyperbolic paraboloids, and hyperboloids of revolution – however in different ways.

Keywords: Plücker's conoid; cylindroids; bisector; one-sheeted hyperboloid of revolution; orthogonal hyperbolic paraboloid

1. PLÜCKER'S CONOID

Plücker's conoid $\mathcal{C}$, also known under the name *cylindroid*, is a ruled surface of degree three with a finite double line and a director line at infinity. Using cylinder coordinates (r, φ, z), the conoid can be given by

$$z = c \sin 2\varphi \tag{1}$$

with a constant $c \in \mathbf{R}_{>0}$. All generators of $\mathcal{C}$ are parallel to the $[x,y]$-plane. The z-axis is the double line of $\mathcal{C}$ and an axis of symmetry. The conoid passes through the x- and y-axis. These two lines can be called *central generators* of $\mathcal{C}$ since both are axes of symmetry of $\mathcal{C}$, too. The Plücker conoid $\mathcal{C}$ is the trajectory of the x-axis under a motion composed from a rotation about the z-axis and a harmonic oscillation with double frequency along the z-axis (Wunderlich, 1967, p. 37).

The substitution $x = r \cos \varphi$ and $y = r \sin \varphi$ in (1) yields the Cartesian equation

$$(x^2 + y^2)\, z - 2cxy = 0, \tag{2}$$

which reveals that reflections in the planes $x \pm y = 0$ map $\mathcal{C}$ onto itself. The origin O is called the *center* of $\mathcal{C}$.

The right cylinder $x^2 + y^2 = R^2$ intersects the Plücker conoid $\mathcal{C}$ along a curve c_{cyl} of degree 4[1] (see Fig. 1, left), which in the cylinder's development (in the [ξ,η]-plane with $\xi = R\varphi$ and $\eta = z$) appears as the Sine-curve

$$\eta = c \sin\frac{2\xi}{R}, \quad 0 \le \xi \le 2R\pi$$

with amplitude c and wavelength $R\pi$. The generators of $\mathcal{C}$ connect points c_{cyl} which are symmetric with respect to (henceforth abbreviated as w.r.t.) the z-axis. The conoid is bounded by the planes $z = \pm c$, which contact $\mathcal{C}$ along the torsal generators t_1 and t_2 in the planes $x \pm y = 0$. We call $2c$ the *width* of the conoid.

The tangent plane $\tau_{X|\mathcal{C}}$ at any point $X \in \mathcal{C}$, $X \notin t_1, t_2$, with position vector

$$\mathbf{x}(r,\varphi) = (r\cos\varphi, r\sin\varphi, c\sin 2\varphi), \text{ where } r > 0, \tag{3}$$

is orthogonal to the vector product $\mathbf{x}_r \times \mathbf{x}_\varphi$ of the partial derivates

$$\mathbf{x}_r = \frac{\mathrm{d}\mathbf{x}}{\mathrm{d}r} = \begin{pmatrix} \cos\varphi \\ \sin\varphi \\ 0 \end{pmatrix} \quad \text{and} \quad \mathbf{x}_\varphi = \frac{\mathrm{d}\mathbf{x}}{\mathrm{d}\varphi} = \begin{pmatrix} -r\sin\varphi \\ r\cos\varphi \\ 2c\cos 2\varphi \end{pmatrix}.$$

This yields the equation

$$\tau_{X|\mathcal{C}}: \quad 2c\cos 2\varphi\,(x\sin\varphi - y\cos\varphi) + rz = rc\sin 2\varphi. \tag{4}$$

The tangent plane $\tau_{X|\mathcal{C}}$ has a 45°-inclination against the $[x,y]$-plane if r or $-r$ equals the distribution parameter

$$\delta := \frac{\mathrm{d}z}{\mathrm{d}\varphi} = 2c\cos 2\varphi$$

of the generator through X.

For points $X \in \mathcal{C}$ outside the torsal generators, the intersection $\tau_{X|\mathcal{C}} \cap \mathcal{C}$ splits into the generator g_X through X and an ellipse e_X with principal vertices on the torsal generators and the minor axis in the $[x,y]$-plane (Fig. 1, left). After orthogonal projection into the $[x,y]$-plane, the ellipse appears as the circle e_X' (see Fig. 1, right) satisfying

$$\cos 2\varphi\,(x^2 + y^2) + r\,(y\sin\varphi - x\cos\varphi) = 0,$$

hence

$$\left(x - \frac{r\cos\varphi}{2\cos 2\varphi}\right)^2 + \left(y + \frac{r\sin\varphi}{2\cos 2\varphi}\right)^2 = \frac{r^2}{2\cos^2 2\varphi} \quad \text{if} \quad \cos 2\varphi \neq 0.$$

All ellipses $e_X \subset \mathcal{C}$ have the same excentricity c, since it equals the difference of the z-coordinates of the respective principal and secondary vertices on the vertical cylinder (Müller and Krames, 1931, p. 208).

For all points P in space with a top view $P' \in e_X'$ opposite to the top view of the double line (see Fig. 1, right), the *pedal curve* on $\mathcal{C}$, i.e., the locus of pedal points of P on the generators of $\mathcal{C}$, coincides with e_X. This holds since right angles enclosed with generators of $\mathcal{C}$ appear in the top view again as right angles, provided that the

[1] The remaining part of the curve of intersection consists of two complex conjugate lines at infinity in the plane $x \pm iy = 0$.

spanned plane is not parallel to the z-axis. Thus, all pedal curves of a Plücker conoid are planar. Furthermore, all surface normals of $\mathcal{C}$ at points of e_X meet the vertical line through P'.

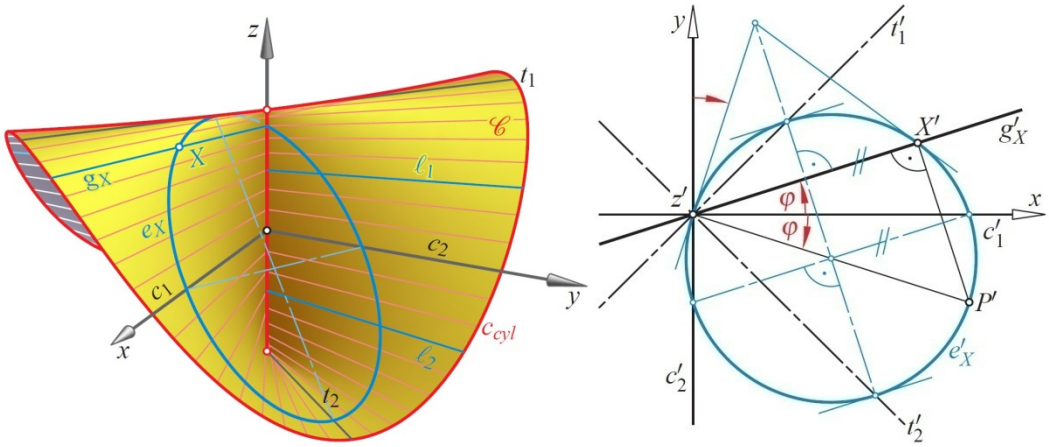

Figure 1. Plücker's conoid $\mathcal{C}$ (left: axonometric view, right: top view) with central generators c_1 and c_2, torsal generators t_1 and t_2, the generator g_X through X, and the ellipse $e_X \subset \mathcal{C} \cap \tau_{X|\mathcal{C}}$.

Remark 1: Another remarkable property of the cylindroid is reported in Stachel (1995): Let four generators g_1, ..., $g_4 \subset \mathcal{C}$ be called *cyclic* if their points of intersection with any fixed tangent plane $\tau_{X|\mathcal{C}}$ are concyclic, i.e., located on a circle (and on the ellipse e_X). Then, in each tangent plane their points of intersection are located on a circle. Moreover, there is an infinite set of spheres which contact these four lines, and, apart from four generators of a one-sheeted hyperboloid of revolution, this is the only choice of four lines in space with this property.

2. BISECTOR OF TWO SKEW LINES

For two given point sets S_1, S_2 in the Euclidean plane $\mathbb{E}^2$ or three-space $\mathbb{E}^3$, the set of points X being equidistant to S_1 and S_2 is called the *bisector* of S_1 and S_2.

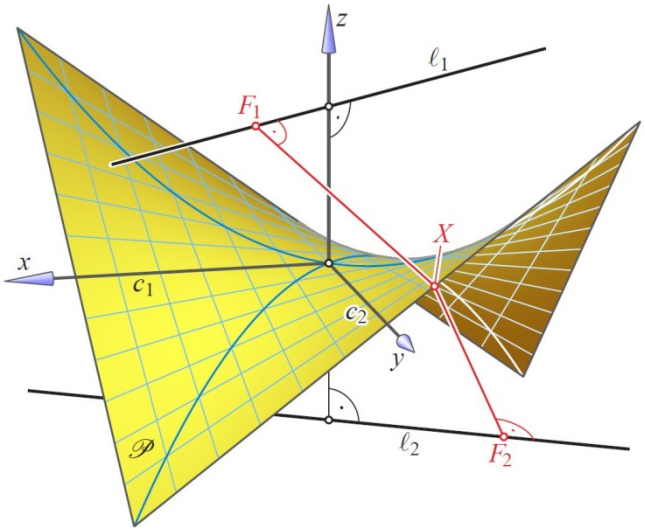

Figure 2. Points X of the bisector $\mathcal{P}$ of the two lines ℓ_1 and ℓ_2 satisfy $\overline{X\ell_1} = \overline{XF_1} = \overline{XF_2} = \overline{X\ell_2}$.

In the case of two given points $P,Q \in \mathbb{E}^3$, the bisector is the orthogonal bisector plane σ_{PQ} of P and Q. The standard definition of a parabola in $\mathbb{E}^2$ as the bisector of its focal point and directrix reveals that each paraboloid of revolution in $\mathbb{E}^3$ is the bisector of a point F and a plane not passing through F. However, also the equilateral hyperbolic paraboloid is a bisector, as reported, e.g., in Salmon and Fiedler, 1863, p. 154, and stated in the theorem below.

Theorem 1: *Let ℓ_1 and ℓ_2 be two skew lines in $\mathbb{E}^3$ with $2\varphi := \measuredangle \ell_1\ell_2$ and shortest distance $2d := \overline{\ell_1\ell_2}$.*

1. *The bisector of ℓ_1 and ℓ_2 is an orthogonal hyperbolic paraboloid $\mathscr{P}$ (Fig. 2). If ℓ_1 and ℓ_2 are given by $z = \pm d$ and $x \sin\varphi = \pm y \cos\varphi$, then*

$$\mathscr{P}: \quad z + \frac{\sin 2\varphi}{2d} xy = 0. \tag{5}$$

2. *The axes of symmetry c_1 and c_2 of the two skew lines ℓ_1, ℓ_2, which coincide with the x- and y-axis of our coordinate frame, are the vertex generators of $\mathscr{P}$; the common perpendicular of ℓ_1 and ℓ_2 is the paraboloid's axis. The lines ℓ_1 and ℓ_2 are polar w.r.t. $\mathscr{P}$, i.e., each point $X_1 \in \ell_1$ is conjugate w.r.t. $\mathscr{P}$ to all points $X_2 \in \ell_2$, and vice versa.*

3. *At any point $X \in \mathscr{P}$, the tangent plane $\tau_{X|\mathscr{P}}$ to $\mathscr{P}$ is the orthogonal bisector plane $\sigma_{F_1F_2}$ of the pedal points F_1, F_2 of X on the lines ℓ_1 and ℓ_2, respectively. Hence, $\mathscr{P}$ is the envelope of the bisecting planes $\sigma_{F_1F_2}$ for all points $F_1 \in \ell_1$ and $F_2 \in \ell_2$.*

4. *The generators of $\mathscr{P}$ are the axes of rotations in $\mathbb{E}^3$ which send the line ℓ_1 to the line ℓ_2. Therefore, the generators of $\mathscr{P}$ are axes of one-sheeted hyperboloids of revolution passing through the given pair of skew lines (ℓ_1, ℓ_2). These hyperboloids are centered on the vertex generators c_1, c_2 of $\mathscr{P}$ and share the secondary semiaxis $b = d \cot\varphi$ (Fig. 4 and 5).*

Proof: 1. Let any line ℓ be given in vector form as $\mathbf{p} + \mathbb{R}\mathbf{v}$ with $\|\mathbf{v}\| = 1$. Then, its distance to any point X with position vector $\mathbf{x}$ satisfies

$$\overline{X\ell}^2 = \|\mathbf{x}-\mathbf{p}\|^2 - \langle \mathbf{x}-\mathbf{p}, \mathbf{v}\rangle^2, \tag{6}$$

where $\langle\,,\rangle$ denotes the standard dot product. If ℓ is replaced with one of the given lines ℓ_1, ℓ_2 with

$$\mathbf{p} = (0, 0, \pm d) \text{ and } \mathbf{v} = (\cos\varphi, \pm\sin\varphi, 0) \text{ for } 0 < \varphi < \pi/2 \text{ and } d > 0,$$

then $\overline{X\ell_1} = \overline{X\ell_2}$ is equivalent to

$$x^2 + y^2 + (z-d)^2 - (x\cos\varphi + y\sin\varphi)^2 = x^2 + y^2 + (z+d)^2 - (x\cos\varphi - y\sin\varphi)^2,$$

and consecutively, to

$$\mathscr{P}: \; 2dz + xy\sin 2\varphi = 0. \tag{7}$$

This is the equation of an orthogonal hyperbolic paraboloid (Fig. 2). The rotation $(x, y, z) \mapsto (x', y', z')$ about the z-axis through $\pi/4$ with

$$x = \frac{1}{\sqrt{2}}(x' - y'), \qquad y = \frac{1}{\sqrt{2}}(x' + y'), \qquad z = z',$$

yields the standard equation

$$2z' + \frac{\sin 2\varphi}{2d}\,(x'^2 - y'^2) = 0.$$

2. Two points $X_1 = (x_1, y_1, z_1)$ and $X_2 = (x_2, y_2, z_2)$ are conjugate w.r.t. the paraboloid $\mathcal{P}$ (7) if and only if

$$\frac{\sin 2\varphi}{2d}(x_1 y_2 + x_2 y_1) + (z_1 + z_2) = 0.$$

This is satisfied by each $X_1 \in \ell_1$ and $X_2 \in \ell_2$ since

$$X_1 = (r_1 \cos\varphi, r_1 \sin\varphi, d) \text{ and } X_2 = (r_2 \cos\varphi, -r_2 \sin\varphi, -d).$$

The origin is the vertex of the paraboloid $\mathcal{P}$; the x- and y-axis are the two vertex generators c_1 and c_2.

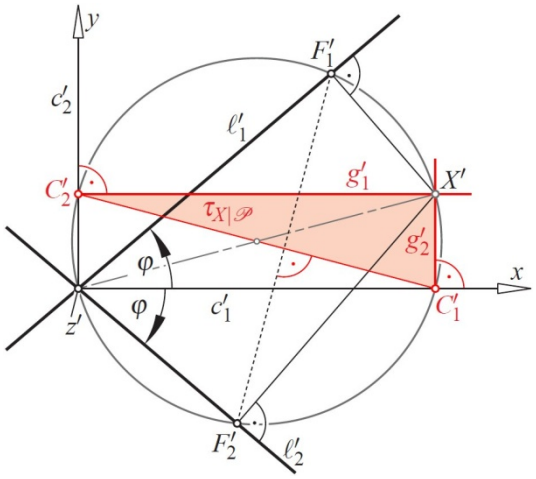

Figure 3. The tangent plane $\tau_{X|\mathcal{P}}$ at X to the bisecting paraboloid $\mathcal{P}$ is the orthogonal bisector plane $\sigma_{F_1F_2}$ of the respective pedal points F_1 and F_2 of X on the lines ℓ_1 and ℓ_2.

3. Let F_1 and F_2 be the pedal points of $X \in \mathcal{P}$ on the lines ℓ_1 and ℓ_2, respectively. Then, X is uniquely defined as the point of intersection between the orthogonal bisector plane $\sigma_{F_1F_2}$ of F_1 and F_2 and the planes orthogonal to ℓ_1 and ℓ_2 through the respective points F_1 and F_2. The generators g_1, g_2 of $\mathcal{P}$ through X pass through the pedal points C_1, C_2 of X on the vertex generators c_1 and c_2 of $\mathcal{P}$. The tangent plane $\tau_{X|\mathcal{P}}$ to $\mathcal{P}$ at X is spanned by g_1 and g_2.

Now, we project the scene orthogonally into the $[x,y]$-plane (Fig. 3): The top view of the z-axis is the common point of ℓ_1' and ℓ_2'. Since F_1 and F_2 are at equal distance to the $[x,y]$-plane, but on different sides, the bisecting plane $\sigma_{F_1F_2}$ intersects the $[x,y]$-plane along the orthogonal bisector line of the top views F_1' and F_2'. The Thales circle with diameter $X'z'$ passes through F_1' and F_2', and also through the pedal points C_i' of X' on c_i' for $i = 1, 2$. Since the arcs from C_1' to F_1' and to F_2' are of equal lengths, point C_1 lies on the trace of $\sigma_{F_1F_2}$, which must be a diameter of the Thales circle. Hence, this diameter coincides with the trace $[C_1,C_2]$ of $\tau_{X|\mathcal{P}}$, which proves the coincidence of $\tau_{X|\mathcal{P}}$ and $\sigma_{F_1F_2}$.

4. If g is the axis of a rotation which sends ℓ_1 to ℓ_2, then each point $X \in g$ has equal distances to ℓ_1 and ℓ_2, which implies $g \subset \mathcal{P}$.

Conversely, let g be the generator of $\mathcal{P}$, which intersects c_1 orthogonally at any point M. The reflection in c_1 exchanges ℓ_1 and ℓ_2 while g is mapped onto itself. Consequently, there are equal distances $\overline{g\ell_1} = \overline{g\ell_2}$ and congruent angles $\measuredangle\, g\ell_1 = \measuredangle\, g\ell_2$. The reflection in c_1 exchanges also the pedal points N_1, N_2 of M on ℓ_1 and ℓ_2; the midpoint of N_1N_2 lies on c_1 (Fig. 4).

The generator g is orthogonal to c_1 and also to N_1N_2, since $g \subset \tau_{M|\mathcal{P}}$ lies in the orthogonal bisector plane $\sigma_{N_1N_2}$. Therefore, g is orthogonal to the plane connecting M, N_1, and N_2. Furthermore, the lines $[M,N_1]$ and $[M,N_2]$ are the common perpendiculars of g with ℓ_1 and ℓ_2, respectively.

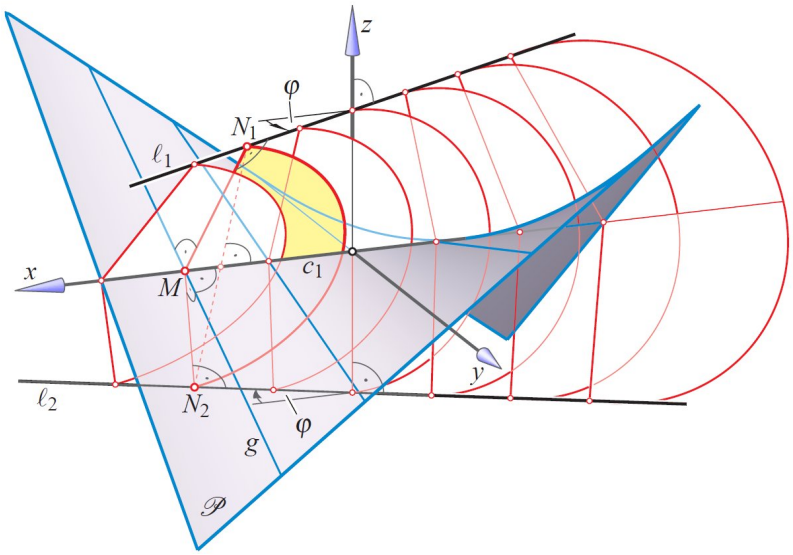

Figure 4. Gorge circles of hyperboloids of revolution through ℓ_1 and ℓ_2. The axes of the hyperboloids form a regulus of the bisecting orthogonal hyperbolic paraboloid $\mathcal{P}$ (Theorem 1,4. or Krames, 1983).

There is a rotation about g which sends N_1 to N_2. This rotation takes ℓ_1 into a line $\tilde{\ell}$ through N_2, which is orthogonal to MN_2 and includes with g an angle congruent to $\measuredangle\, g\ell_2$. We obtain $\tilde{\ell} = \ell_2$, since otherwise $\tilde{\ell}$ would be symmetric to ℓ_2 w.r.t. the meridian plane gN_2 and therefore, as a member of the complementary regulus, intersect ℓ_1.

Under a continuous rotation about g, the line ℓ_1 forms one regulus of a one-sheeted hyperboloid of revolution $\mathcal{H}$ (see Fig. 5). It is centered at M and its gorge circle passes through the pedal points N_1 and N_2 of M on the given lines ℓ_1, ℓ_2.

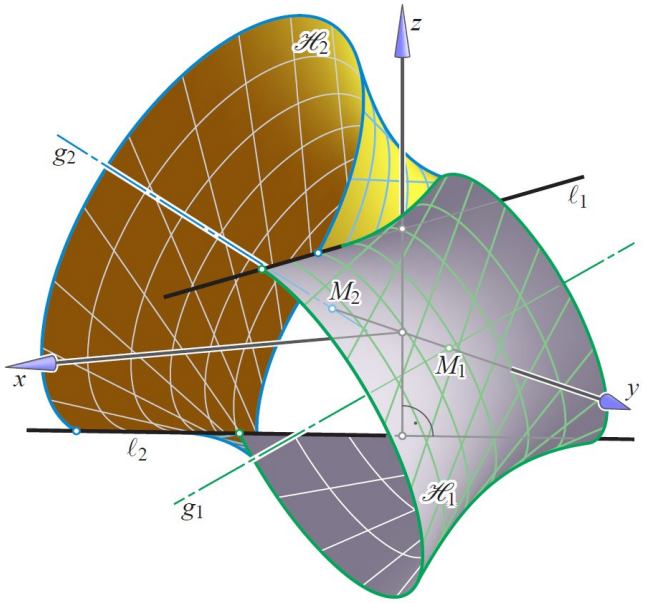

Figure 5. Two hyperboloids of revolution $\mathcal{H}_1$, $\mathcal{H}_2$ through two skew lines ℓ_1 and ℓ_2. The hyperboloids share the secondary semiaxis b and the distribution parameters $\pm b$ of their generators.

When M varies on c_1, we obtain a one-parameter family of one-sheeted hyperboloids of revolution through the skew generators ℓ_1 and ℓ_2 (Fig. 5). Due to a result of Wunderlich (1982) and Krames (1983), these two skew generators ℓ_1, ℓ_2 define already the secondary semiaxis b of these hyperboloids, namely $b = d \cot \varphi$, where $2d =$

$\overline{\ell_1\ell_2}$ and $2\varphi = \measuredangle\, \ell_1\ell_2$ (see also Odehnal et al, 2020, p. 37). Of course, the same holds for points $M \in c_2$. By the same token, $+b$ or $-b$ equals the distribution parameter of all generators of the hyperboloids. □

Remark 2: The complete intersection of any two hyperboloids of revolution $\mathcal{H}_1$, $\mathcal{H}_2$ through the two skew lines ℓ_1 and ℓ_2 (according to Theorem 1, 4., see Fig. 5) consists of two more lines which need not be real. They can be found as common transversals of ℓ_1, ℓ_2, and two other generators of the hyperboloids, one of each, and both skew to ℓ_1 and ℓ_2.

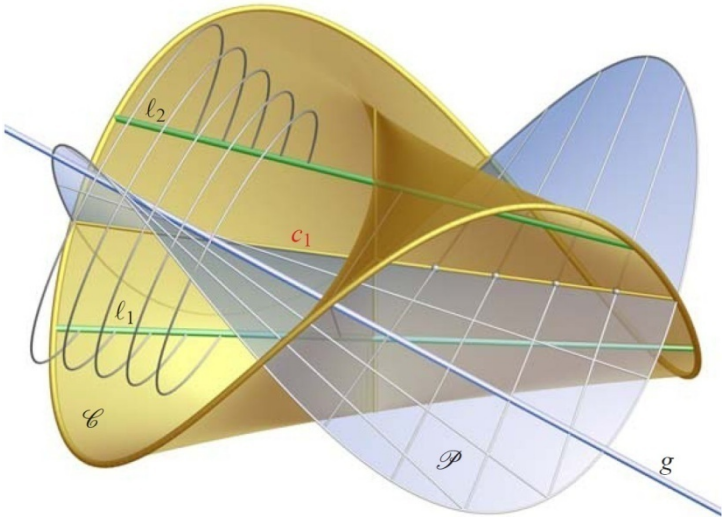

Figure 6. All pairs of skew lines (ℓ_1, ℓ_2) which share the bisecting orthogonal hyperbolic paraboloid $\mathcal{P}$ are located on a Plücker conoid $\mathcal{C}$. Generators g of $\mathcal{P}$ are axes of rotations with $\ell_1 \mapsto \ell_2$ (courtesy: G. Glaeser).

Let us focus on the paraboloid $\mathcal{P}$ with the equation (5) and ask the following: Where are all pairs (ℓ_1, ℓ_2) of lines for which $\mathcal{P}$ is the bisector? The answer, as given in the theorem below, was disclosed in Husty and Sachs (1994), but already reported at the turn to the 20th century in Schilling (1911), p. 54.

Theorem 2: *All pairs of skew lines (ℓ_1, ℓ_2) which share the bisecting orthogonal hyperbolic paraboloid $\mathcal{P}$ are located on a Plücker conoid (cylindroid) $\mathcal{C}$ in symmetric position w.r.t. the vertex generators c_1 and c_2 of $\mathcal{P}$.*

Proof. Let the lines ℓ_1 and ℓ_2 be given in the same way as in Theorem 1. Then, the bisector $\mathcal{P}$ remains the same if the quotient $(\sin 2\varphi)/d$ does not change. Obviously, all points of ℓ_1 and ℓ_2 satisfy

$$\mathcal{C}: \quad (x^2 + y^2)\, z - 2c\, xy = 0 \quad \text{where} \quad c := \frac{d}{\sin 2\varphi}. \tag{8}$$

This equation defines a Plücker conoid $\mathcal{C}$, as introduced in (2) (see Fig. 6). The surface $\mathcal{C}$ has the x- and y-axis as central generators c_1 and c_2 and the z-axis as double line. All pairs (ℓ_1, ℓ_2) are symmetric w.r.t. c_1 and c_2 and polar w.r.t. $\mathcal{P}$. □

Schilling's famous collection of mathematical models contains as model XXIII, no. 10, the pair of surfaces $\mathcal{C}$ and $\mathcal{P}$, each represented by strings with endpoints on a closed boundary curve of degree four (see Fig. 7[2] and compare with Fig. 8). The two boundary curves are even congruent, as we confirm below in Theorem 3.

[2]The displayed model belongs to the collection of the Institute of Discrete Mathematics and Geometry, Vienna University of Technology, \url{https://www.geometrie.tuwien.ac.at/modelle/models_show.php?mode=2&n=100&id=0}, retrieved March 2020.

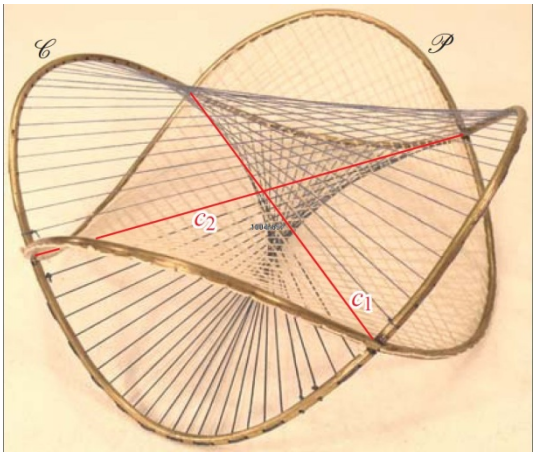

Figure 7. String model of a Plücker conoid $\mathcal{C}$ together with the surface formed by its normals along the central generators c_1 and c_2, an orthogonal hyperbolic paraboloid $\mathcal{P}$. This is model XXIII, no. 10, out of Schilling's famous collection of mathematical models. In addition, the lines c_1 and c_2, which are also vertex generators of $\mathcal{P}$, are marked in red color.

By the same token, all generators of the orthogonal hyperbolic paraboloid $\mathcal{P}$ are surface normals of the Plücker conoid along any central generator. This follows from (4): For $\varphi = 0$, the surface normal at the point $(r, 0, 0)$, $r \in \mathbb{R}$, has the direction of $(0, -2c, r)$. For $\varphi = \pi/2$, the normal at $(0, r, 0)$ has the direction of $(-2c, 0, r)$. Now we can confirm that the points $(r, -2ct, rt)$ and $(-2ct, r, rt)$ for all $(r,t) \in \mathbb{R}^2$ satisfy the paraboloid's equation

$$\mathcal{P}: \quad xy + 2cz = 0 \tag{9}$$

according to (5) in the case

$$c = \frac{d}{\sin 2\varphi} \, . \tag{10}$$

The same follows from Theorem 1,4. as the limit $\ell_1 \to \ell_2$, i.e., $d \to 0$: All generators of $\mathcal{P}$ are axes of one-sheeted hyperboloids of revolution which contact the conoid $\mathcal{C}$ along one of the central generators.

We summarize some properties of the pair of surfaces $\mathcal{C}$ and $\mathcal{P}$ (see Figs. 7 and 8), which share the distribution parameter $\delta = 2c$ at c_1 and c_2:

Theorem 3. *Let $\mathcal{P}$ be the orthogonal hyperbolic paraboloid* (9) *and $\mathcal{C}$ be the Plücker conoid satisfying* (8).

1. *The generators of $\mathcal{P}$ are the surface normals of $\mathcal{C}$ along its central generators c_1 and c_2.*
2. *Each generator g of $\mathcal{P}$ is the axis of concentric one-sheeted hyperboloids of revolution which intersect $\mathcal{C}$ along two skew generators ℓ_1, ℓ_2 being symmetric w.r.t. c_1 and c_2. The gorge circles lie in the tangent plane to $\mathcal{C}$ at the point M where $g \subset \mathcal{P}$ intersects the vertex generator of the complementary regulus.*
3. *The right cylinder $x^2 + y^2 = 4c^2$ with radius $2c$ equal to the width of $\mathcal{C}$ intersects $\mathcal{P}$ and $\mathcal{C}$ along two quartics which are symmetric w.r.t. the $[x,y]$-plane (Fig. 7).*
4. *The polarity in the paraboloid $\mathcal{P}$ maps the Plücker conoid $\mathcal{C}$ onto itself. Outside the torsal generators, there is a symmetric one-to-one correspondence between points Q_1, Q_2 on $\mathcal{C}$ such that Q_2 is the pole w.r.t. $\mathcal{P}$ of the tangent plane to $\mathcal{C}$ at Q_1, and vice versa.*

Proof. 2. We vary d and φ such that $c = d / \sin 2\varphi$ remains constant. The hyperboloids with the same axis g through $M \in c_1$ share the plane $[M, N_1, N_2]$ of the gorge circle, where the points N_1, N_2 are the pedal points of M on the corresponding pair of lines ℓ_1, ℓ_2. This plane orthogonal to g is tangent to $\mathcal{C}$ at M. The pedal points N_1 and N_2 belong to the pedal curve of M on $\mathcal{C}$, which is an ellipse with the minor axis OM along c_1 (note Fig. 1, right).

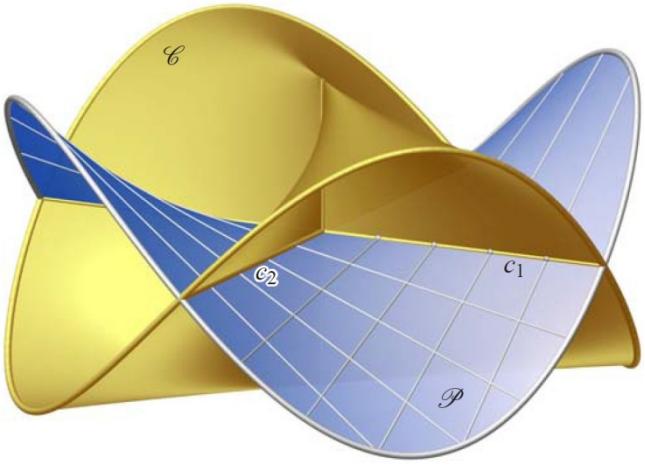

Figure 8. The surface normals of the Plücker conoid $\mathscr{C}$ along the two central generators c_1 and c_2 form the two reguli of an orthogonal hyperbolic paraboloid $\mathscr{P}$ (courtesy: G. Glaeser).

3. We plug $x = R \cos \varphi$ and $y = R \sin \varphi$ into the equation (9) of $\mathscr{C}$ and obtain $R^2 z - 2cR^2 \sin \varphi \cos \varphi = 0$. The same substitution in the equation (9) of $\mathscr{P}$ results in $R^2 \sin \varphi \cos \varphi + 2cz = 0$. The choice $R = 2c$ gives rise to two symmetric curves $z = \pm c \sin 2\varphi$ (Figs. 7 and 8).

4. We use the parametrization $\mathbf{x}(r, \varphi)$ from (3) and set $Q_i = (r_i, \varphi_i)$ for $i = 1,2$. Then, the tangent plane at Q_1 to $\mathscr{C}$ satisfies (4),

$$\tau_{Q_1|\mathscr{C}}: \; 2c \cos 2\varphi_1 \, (x \sin \varphi_1 - y \cos \varphi_1) + r_1 z = r_1 c \sin 2\varphi_1.$$

The polar plane of Q_2 w.r.t. $\mathscr{P}$ in (9) is given by

$$r_2 \, (x \sin \varphi_2 + y \cos \varphi_2) + 2cz = -2c \sin 2\varphi_2.$$

We obtain an identity of the two planes when we set

$$\varphi_2 = -\varphi_1 \;\text{ and }\; r_1 r_2 = -4c^2 \cos 2\varphi. \qquad \square \qquad (11)$$

The correspondence of item 4 reveals: If points Q_1 is at the distance $r_1 = 2c$ to the double line, i.e., on the quartic c_{cyl} as mentioned in item 3, then the corresponding point Q_2 has a tangent plane which is inclined under 45°, since $r_2 = \delta = 2c \cos 2\varphi_2$. The polarity in $\mathscr{P}$ maps the ellipse $e_{Q_1} \subset (\mathscr{C} \cap \tau_{Q_1|\mathscr{C}})$ onto the quadratic tangent cone of $\mathscr{C}$ with the apex Q_2. The tangent planes of this cone, i.e., the planes spanned by Q_2 and any generator of $\mathscr{C}$, intersect $\mathscr{C}$ in ellipses passing through Q_2. All points of the ellipse e_{Q_1} are conjugate w.r.t. $\mathscr{P}$ to the point Q_2.

Remark: If $g_1, \ldots, g_4$ are concyclic generators of $\mathscr{C}$ (cf. Remark 1), then the bisecting paraboloids for any two of these four belong to a pencil of quadrics. Their common curve is a quartic with a double point at the ideal point of the z-axis. The infinitely many spheres which contact $g_1, \ldots, g_4$ are centered on this quartic. The top view of this spine curve is an equilateral hyperbola. For proofs and further details see Stachel (1995).

3. PLÜCKER'S CONOID AS LOCUS OF INSTANT SCREW AXES FOR SKEW GEARS

In spatial kinematics, the Plücker conoid $\mathscr{C}$ is well-known as the locus of instant axes ℓ_{12} of the relative screw motion for two wheels which rotate with constant velocities ω_1 and ω_2 about fixed skew axes ℓ_1 and ℓ_2, respectively. The axes of symmetry of the two axes of rotation ℓ_1 and ℓ_2 coincide with the central generators c_1,

c_2 of $\mathcal{C}$. The axodes of the relative screw motion are hyperboloids of revolution $\mathcal{H}_1$, $\mathcal{H}_2$ with mutual contact along ℓ_{12} (Fig. 9).[3] They are solutions of the purely geometric problem: For given skew axes ℓ_1, ℓ_2, find pairs of hyperboloids of revolution which contact each other along a line.

A standard proof of this result uses dual vectors for the representation of oriented lines and screws (see, e.g., Figliolini et al, 2007). Here we present another proof:

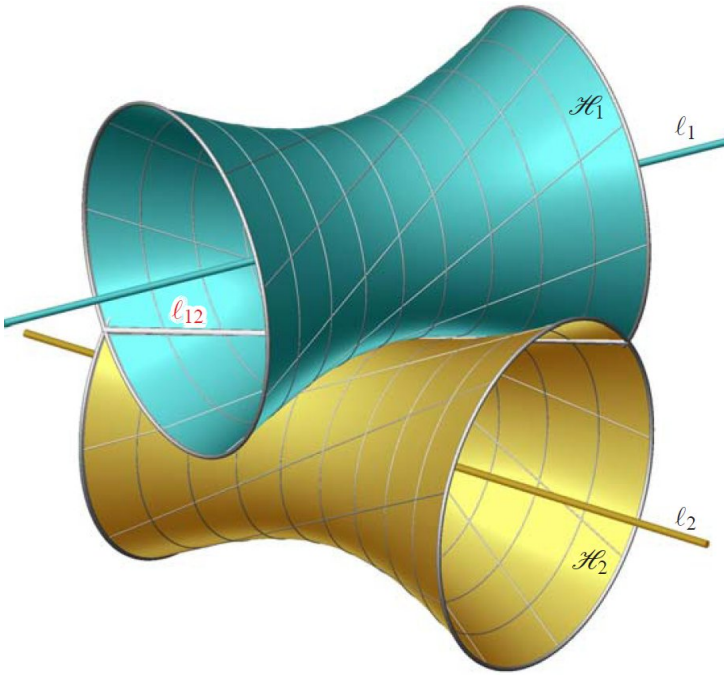

Figure 9. Two hyperboloids of revolution in contact along the line ℓ_{12} (courtesy: G. Glaeser).

The common surface normals of the two hyperboloids $\mathcal{H}_1$ and $\mathcal{H}_2$ along the line of contact ℓ_{12} form one regulus of an orthogonal hyperbolic paraboloid $\mathcal{P}$ which passes through the axes ℓ_1 and ℓ_2. The line ℓ_{12} is the vertex generator of the complementary regulus on $\mathcal{P}$. The other vertex generator of $\mathcal{P}$ intersects all three lines ℓ_{12}, ℓ_1, and ℓ_2 orthogonally. Therefore, it is the common perpendicular of ℓ_1 and ℓ_2. These conditions will prove to be sufficient for identifying the locus of the lines ℓ_{12} as a Plücker conoid.

We use the coordinate frame of Section 2 and define ℓ_1 and ℓ_2 by $z = \pm d$ and $x \sin\varphi = \pm y \cos\varphi$. Then the z-axis is the common perpendicular, and we can assume that ℓ_{12} is given by

$$z = a \quad \text{and} \quad x \sin\alpha = y \cos\alpha$$

(see Fig. 10). Now we intersect the orthogonal plane to ℓ_{12} through any point $X = (r \cos\alpha, r \sin\alpha, a) \in \ell_{12}$ with ℓ_1 and ℓ_2, and we obtain

[3] The various relations between the two fixed axes of rotations ℓ_1, ℓ_2, the relative axis ℓ_{12}, the angular velocities ω_1, ω_2, and the pitch of the relative screw motion can be visualized in the so-called *Ball-Disteli diagram*, which arises from $\mathcal{C}$ by a particular projection (see Figliolini et al., 2007, Fig. 7). It is noteworthy that we still obtain a Plücker conoid as the locus of relative screw axes when the two wheels perform helical motions with fixed pitches about fixed axes (Figliolini et al., 2007, Fig. 10). This is also a consequence of the following classical result Plücker's in connection with linear line complexes: The axes of all linear line complexes which are contained in a pencil belong to a Plücker conoid (Müller and Krames, 1931, p. 214).

$$X_1 = \left(\frac{r\cos\varphi}{\cos(\alpha-\varphi)},\ \frac{r\sin\varphi}{\cos(\alpha-\varphi)},\ d \right) \in \ell_1 \quad \text{and} \quad X_2 = \left(\frac{r\cos\varphi}{\cos(\alpha+\varphi)},\ \frac{-r\sin\varphi}{\cos(\alpha+\varphi)},\ -d \right) \in \ell_2 .$$

In the top view, the three points X, X_1, and X_2 appear already aligned. Therefore, they are collinear in space if and only if the segments X_1X and XX_2 have the same slope. This means,

$$\frac{a-d}{\tan(\alpha-\varphi)} = \frac{a+d}{\tan(\alpha+\varphi)},$$

hence

$$a\,\frac{\sin 2\varphi}{\cos(\alpha-\varphi)\cos(\alpha+\varphi)} = d\,\frac{\sin 2\alpha}{\cos(\alpha-\varphi)\cos(\alpha+\varphi)} .$$

After exclusion of the cases where $\cos(\alpha-\varphi)\cos(\alpha+\varphi) = 0$, i.e., $\alpha = \varphi \pm \pi/2$, we conclude

$$a = \frac{d}{\sin 2\varphi}\sin 2\alpha$$

as the relation between the altitude a and the polar angle α of the wanted line ℓ_{12} of contact. This is the equation (1) of a Plücker conoid in cylinder coordinates. In the excluded cases, the line ℓ_{12} intersects one of the given axes and is orthogonal to the other. Then, one hyperboloid degenerates into a cone and the other into a plane.

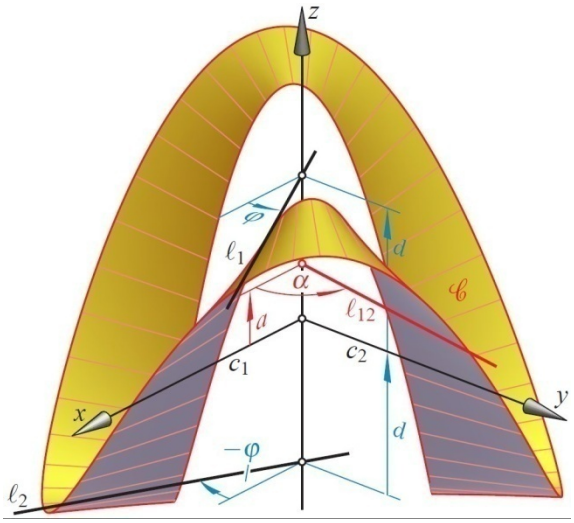

Figure 10. The axes ℓ_1, ℓ_2, the line of contact ℓ_{12}, and a portion of the Plücker conoid $\mathcal{C}$.

Theorem 4. *If the given skew lines ℓ_1 and ℓ_2 are axes of hyperboloids of revolution which contact each other along any line ℓ_{12}, then the lines ℓ_{12} are located on a Plücker cononoid $\mathcal{C}$ with the axes of symmetry of ℓ_1 and ℓ_2 as central generators. Conversely, on $\mathcal{C}$ each generator which is skew to ℓ_1 and ℓ_2 serves as a line of contact between such hyperboloids.*

Corollary 5. *Let g be any generator of the Plücker conoid $\mathcal{C}$ and n be an orthogonal transversal of g. If all points of intersection between n and $\mathcal{C}$ are real, then n meets two generators ℓ_1, ℓ_2 of $\mathcal{C}$ which are symmetric w.r.t. the central generators. In particular, at each point X of any central generator $c \subset \mathcal{C}$ the orthogonal transversals to other generators g of $\mathcal{C}$ are tangents of $\mathcal{C}$.*

Proof. According to the proof of Theorem 4, we can state: If an orthogonal transversal n of g meets any generator $\ell_1 \subset \mathcal{C}$, then it meets also the symmetric line ℓ_2.

However, we can also use the top view in Fig. 1, right, and argue as follows: The lines g and n span the tangent plane at any point $X \in g$. Each line $n \perp g$ sufficiently close to the double line intersects e_X at two points

symmetric w.r.t. the minor axis of e_X. This shows that Theorem 4 can be concluded directly from the planar pedal curves e_X on the Plücker conoid. □

Remark. The complete intersection of the two contacting hyperboloids $\mathcal{H}_1$ and $\mathcal{H}_2$ in Fig. 9 consists of the line of contact ℓ_{12} with multiplicity two and two complex conjugate generators of the complementary regulus (cf. Phillips, 2003, pp. 119–122, and compare with Remark 2).

4. CONCLUSIONS

As explained above, there are various relations between Plücker conoids $\mathcal{C}$, one-sheeted hyperboloids of revolution $\mathcal{H}$, and orthogonal hyperbolic paraboloids $\mathcal{P}$. However, they show up in different, almost contrary ways:

In Section 2, the axes of the involved hyperboloids of revolution $\mathcal{H}$ are generators of $\mathcal{P}$, and the hyperboloids pass through pairs of lines (ℓ_1, ℓ_2) on $\mathcal{C}$ symmetrically placed w.r.t. the central generators c_1, c_2 (note Figs. 4 and 5). The orthogonal hyperbolic paraboloid $\mathcal{P}$ is orthogonal to $\mathcal{C}$ along the central generators (Fig. 8).

In Section 3, the axes ℓ_1, ℓ_2 of the hyperboloids $\mathcal{H}_1$ and $\mathcal{H}_2$ are two symmetrically placed generators of $\mathcal{C}$, and the hyperboloids contact each other along another generator ℓ_{12} of $\mathcal{C}$ (Fig. 9).

REFERENCES

1. Figliolini, G., Stachel, H. and Angeles, J., 2007. A new look at the Ball-Disteli diagram and its relevance to spatial gearing. Mech. Mach. Theory, 42(10), pp. 1362–1375.
2. Husty, M. and Sachs, H., 1994. Abstandsprobleme zu windschiefen Geraden I. Sitzungsber., Abt. II, österr. Akad. Wiss., Math.-Naturw. Kl., 203, pp 31–55.
3. Krames, J., 1983. Über die in einem Strahlnetz enthaltenen Drehhyperboloide. Rad, Jugosl. Akad. Znan. Umjet., Mat. Znan., 2, pp. 1–7.
4. Müller, E. and Krames, J.L., 1931. Vorlesungen über Darstellende Geometrie. Band III: Konstruktive Behandlung der Regelflächen. B.G. Teubner, Leipzig, Wien.
5. Odehnal, B., Stachel, H. and Glaeser, G., 2020. The Universe of Quadrics. Springer Verlag, Berlin, Heidelberg.
6. Phillips, J., 2003. General Spatial Involute Gearing. Springer, Berlin, Heidelberg.
7. Salmon, G. and Fiedler, W., 1863. Die Elemente der analytischen Geometrie des Raumes. B.G. Teubner, Leipzig,
8. Schilling, M., 1911. Catalog mathematischer Modelle. 7. Auflage, Martin Schilling, Leipzig.
9. Stachel, H., 1995. Unendlich viele Kugeln durch vier Tangenten. Math. Pannonica 6, pp. 55–66.
10. Wunderlich, W., 1967. Darstellende Geometrie II. BI Mannheim.
11. Wunderlich, W., 1982. Die Netzflächen konstanten Dralls. Sitzungsber., Abt. II, österr. Akad. Wiss., Math.-Naturw. Kl., 191, 59–84.

THE BIJECTIVE PART OF THE MONGE CUBOID FOR THE MAPPING OF THE HELIX AND THE SPATIAL CURVE ARC

Zsuzsa Balajti
Department of Descriptive Geometry, Institute of Mathematics, University of Miskolc, Egyetemváros, Hungary
PhD, Associate Professor, balajtizs@uni-miskolc.hu

József Ábel
Department of Descriptive Geometry, Institute of Mathematics, University of Miskolc, Egyetemváros, Hungary
PhD student, abel.jozsef16@gmail.com

ABSTRACT

The paper deals with the examination of Monge's theory for ensuring the reconstruction of curves. There are many ways to add an image plane system to a given curve. The aim is to provide a mathematically correct condition for these image plane systems added to a given curve for ensuring the reconstruction of the representation of the curve. In engineering practice, images of a given object have the same properties in terms of reconstructability in image plane systems that can be moved into each other by parallel displacement. Therefore, from our point of view, related to the examinations, the image plane systems that can be moved into each other with parallel shifting are classified into one class during development. A class of image plane systems is defined by a pair of projection lines, perpendicular to the corresponding image planes, fitting to the starting point O of a fixed Cartesian coordinate system. This pair of projection lines is determined by three free angle parameters. These angle parameters create a Monge cuboid. Image plane systems are determined for a given helix, in which any piece of the described helix can be reconstructed from only two images. The Monge cuboid points of these image plane systems are visualised. Mathematical determination of the positions of two CCD cameras is also presented in this paper to ensure the reconstruction of the cutting edge curve from its two images.

Keywords: Monge mapping; Monge cuboid; reconstruction; helix; Hermite arc; cutting edge

1. INTRODUCTION

The representation of a point in Monge mapping is unambiguous, provided the well-known conventions are fulfilled. Due to the practice of descriptive geometry, anomalies occur during the representation of lines, of which we are aware. For example, the representation of a circle of a general position and a profile line is not bijective. For such and similar cases, descriptive geometry provides special solutions to ensure bijectivity. In our approach, it can be argued that all image planes and their projection lines, which can be movable to each other with parallel displacement, are members of one class of Monge mappings. We have named this class a Monge projection. At present, the need for the examination of bijectivity has been brought about by the demand for reconstruction based on digitised Monge-projections. As long as we consider Monge-projections as identical, i.e. as those which can be translated into each other, the number of Monge-projections for a given curve can be described using three free real parameters. Each Monge-projection corresponds to a point of a rectangular prism. Such a rectangular prism is called a Monge-cuboid. Each point of a Monge-cuboid defines a triplet of real numbers, which is in fact a triplet of angles providing a Monge-projection with respect to a given curve. The points of a Monge-cuboid can be divided into two subsets. One subset corresponds to Monge-mappings of the curve and the other corresponds to the non-bijective mappings.

Many tasks are allocated to the production of worm gear drives in our Worm Scientific School in DifiCAD Engineering Office, which has a cooperation agreement with the University of Miskolc. One of our aims is the

supervision of wear on the edge of the hob. The correct positions of CCD cameras have been determined to ensure the reconstruction of the curve of hob cutting edge, and test the wear.

2. PROBLEM

The point representation in the Monge mapping is unambiguous, provided that the well-known conventions are fulfilled [5]. The representation has been made in two image planes $\underline{K}_1$ and $\underline{K}_2$ perpendicular to each other, with the projection directions v_1 and v_2 perpendicular to them. Then, the two image planes are rotated into each other. The names of the two images of the point are the same as the name of the point, of which the first image point is marked by the sign ′ and the second image point by the sign ″.

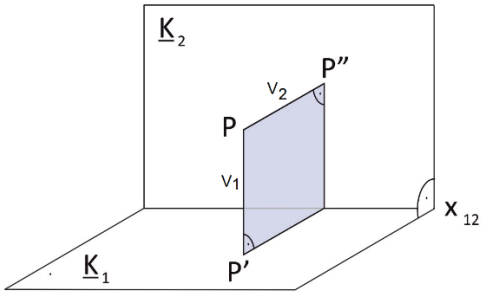

Figure. 1: The mapping of the point P on image plane system $\{\underline{K}_1, \underline{K}_2\}$

The image points are located on a straight line perpendicular to the x_{12} axis. Thus, a point P has only one ordered pair of points (P′, P″), and an ordered pair of points (P′, P″) has a single point P. Numerous theories for the modelling of the spatial figures have been given off, which we hold in great esteem [6]. The Monge projection itself is more general in mathematical terms than described above [2], but the case outlined above is generally used in technical practice. In the practice of descriptive geometry, anomalies occur during the representation of lines and circles, of which we have to be aware. Thus, the representation of a circle of a general position and a profile line is not bijective. For such and similar cases descriptive geometry has found special solutions to ensure bijectivity. In other words, mutual clarity must be ensured. There are infinite ways to add an image plane system to a given curve [4]. The aim is to provide certain conditions referring to these image plane systems with respect to bijectivity of the curve representation.

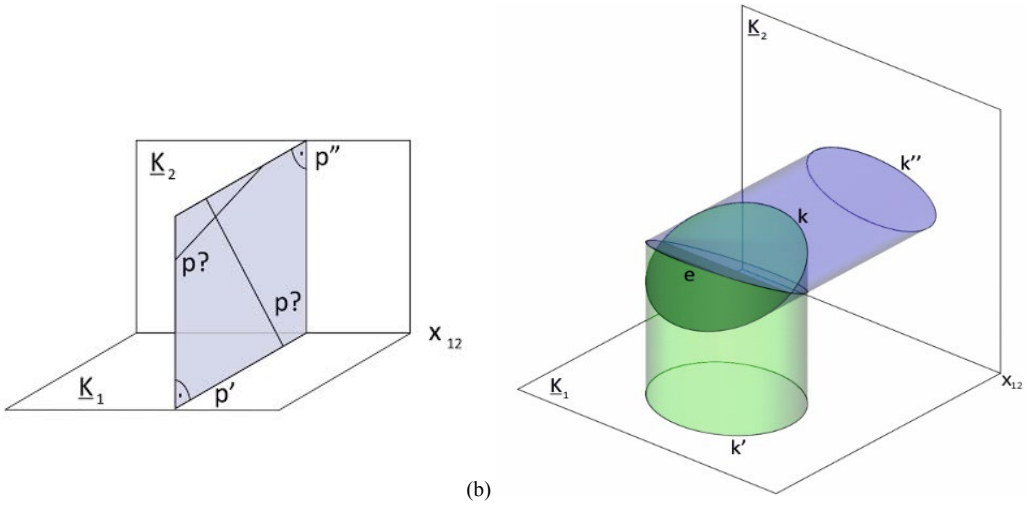

Figure. 2: The reconstruction anomalies of: (a) the line in profile position, (b) the circle in general position

3. SOLUTION

Monge's representation of an object, i.e. the *Monge projection* is determined by image planes $\underline{K}_1$ and $\underline{K}_2$ with the projection lines v_1 and v_2 perpendicular to image planes. Hence, for the curve *g*, not only the image plane system but also the *Monge projection* can be added in infinitely many ways. These may include *Monge*

projections, in which the representation of any part of the curve is bijective, or those in which there is a piece of the curve whose representation is not bijective. Our goal is to provide certain conditions about these Monge projections regarding the bijectivity of the curve representation.

Theorem: If a Monge projection is bijective or non-bijective for a given curve, this particularity does not change if the image planes of the Monge projection are shifted parallel to themselves.

Proof: The parallel offset is a congruence transformation, so the offset does not change the image curves.

Therefore, in the following analysis, we consider two Monge projections to be identical if their image plane systems $\{\underline{K}_1,\underline{K}_2\}$ can be dislocated to each other in parallel.

Based on the above, to facilitate further examination, an point O in space has been fixed and the image planes and projection lines of the Monge projections must be required to fit into it. While the x_{12} axis, the intersection of two image planes, can be characterized by two free parameters such as the coordinates of two spheres, the image planes can be described by one free parameter in the possibilities of rotation about the x_{12} axis. Consequently, the Monge projections can be described by three free parameters, in addition to previous constraints.

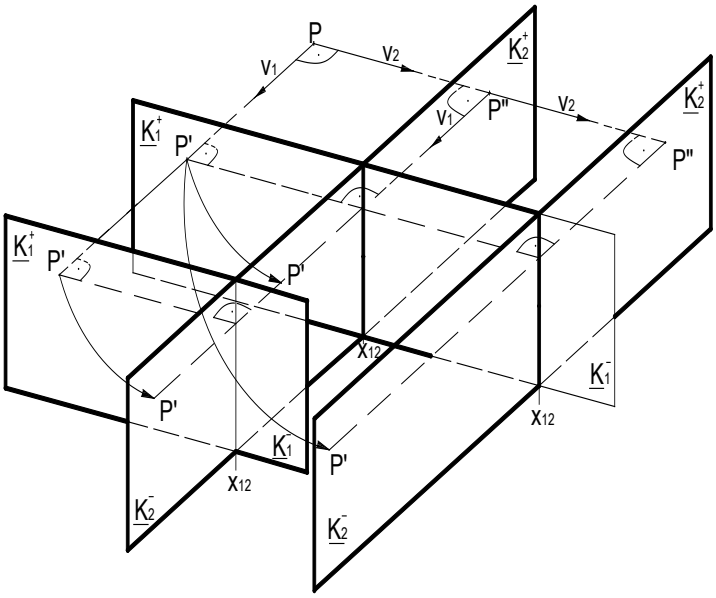

Figure. 3: The Monge projections that can be moved into each other with a parallel shift

Therefore, a triplet of numbers can be ordered to each Monge projection, *the geometric meaning of its members being an angle*. For all this, the *direction angles* of the line must be determined.

Definition 1: The first direction angle of the line e fitting the origin point O is the angle α ($0\leq\alpha\leq\pi$), by which the axis x^+ can be turned into the first projection e′ of the line e on the plane [xy] towards the direction y^+. Let $\alpha=0$ if the line e is identical to the axis z. The first direction angle of a line missing point O is identical with the first direction angle of its parallel line fitting point O.

Definition 2: The second direction angle of the line e fitting the origin point O is the angle β ($0\leq\beta\leq\pi$), by which the axis y^+ can be turned into the second projection e″ of the line e on the plane [yz] towards the direction z^+. Let $\beta=0$ if the line e is identical to the axis x. The second direction angle of a line missing point O is identical with the second direction angle of its parallel line fitting point O.

Definition 3: The third direction angle of the line e fitting the origin point O is the angle γ ($0\leq\gamma\leq\pi$) , by which the axis z^+ can be turned into the third projection e‴ of the line e on the plane [zx] towards the direction x^+. Let $\gamma=0$ if the line e is identical to the axis y. The third direction angle of a line missing point O is identical with the third direction angle of its parallel line fitting point O.

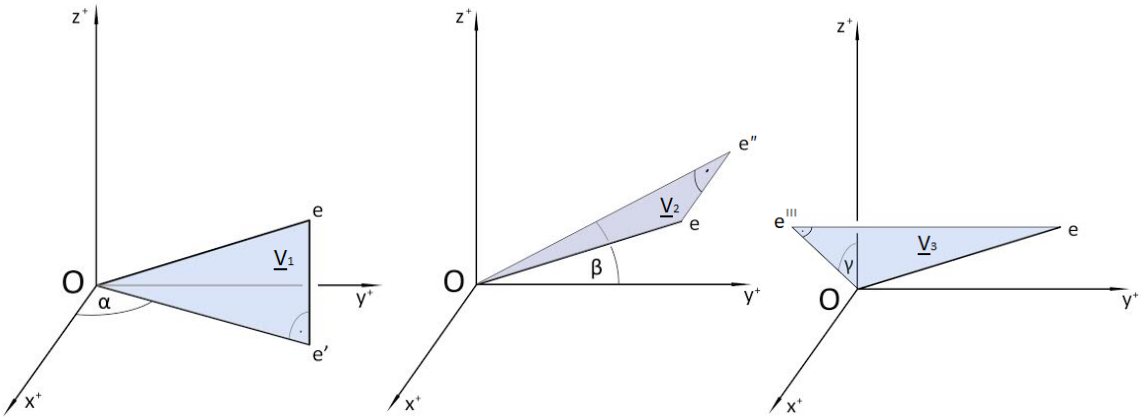

(a) (b) (c)

Figure. 4: The first direction angle α in (a), the second direction angle β in (b) and the third direction angle γ in (c) of the line e

A class of the Monge projection is defined by its image plane system $\{\underline{K}_1, \underline{K}_2\}$, or its projection lines v_1, v_2 fitting to the origin point O of the fixed coordinate system. In the remainder of the paper, the Monge projection has been determined by its projection lines v_1, v_2 fitting to the origin point O in Figure 5.

In this approach, a Monge projection can be described by using three free real parameters defined during the research. These triplets of real numbers create the Monge mapping in the following way:

α is the first direction angle and β is the second direction angle of the first projection line v_1, while angle γ is the third direction angle of the second projection line v_2 of the Monge projection.

The projection lines of the Monge mapping and the Monge projection itself have been determined by the triplet of angles (α,β,γ) defined as shown in Figure 5. The projection line v_1 is determined by the intersection of the first projection plane $\underline{V}_1$ fitting on the v_1' and the second projection plane $\underline{V}_2$ fitting on the v_1'', as can be seen in Figure 5. The projection line v_2 is determined by the intersection of the normal plane $\underline{N}$ of the first projection line v_1 at O, and the third projection plane $\underline{V}_3$ fitting on the v_2''', as can be seen in Figure 5.

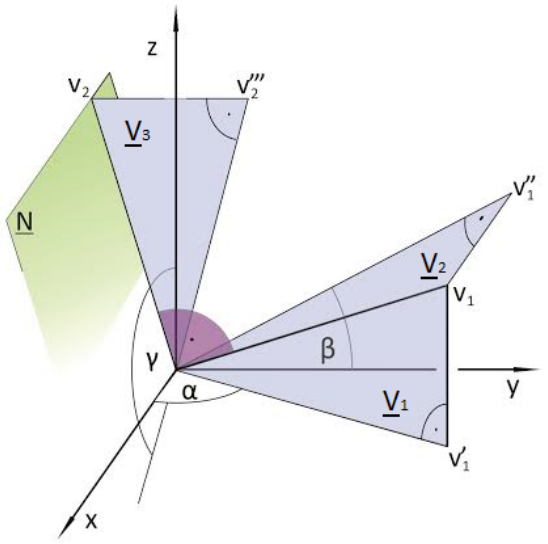

Figure. 5: The relation between the triplet of angles (α, β, γ) and the projection lines v_1, v_2 of the Monge projections in the fixed Descartes coordinate system

Definition 4: The subsets of values α, β and γ in the interval [0, π], which can clearly be linked to a Monge projection, are described in another Descartes coordinate system O[α, β, γ], which we have named *the Monge cuboid*.

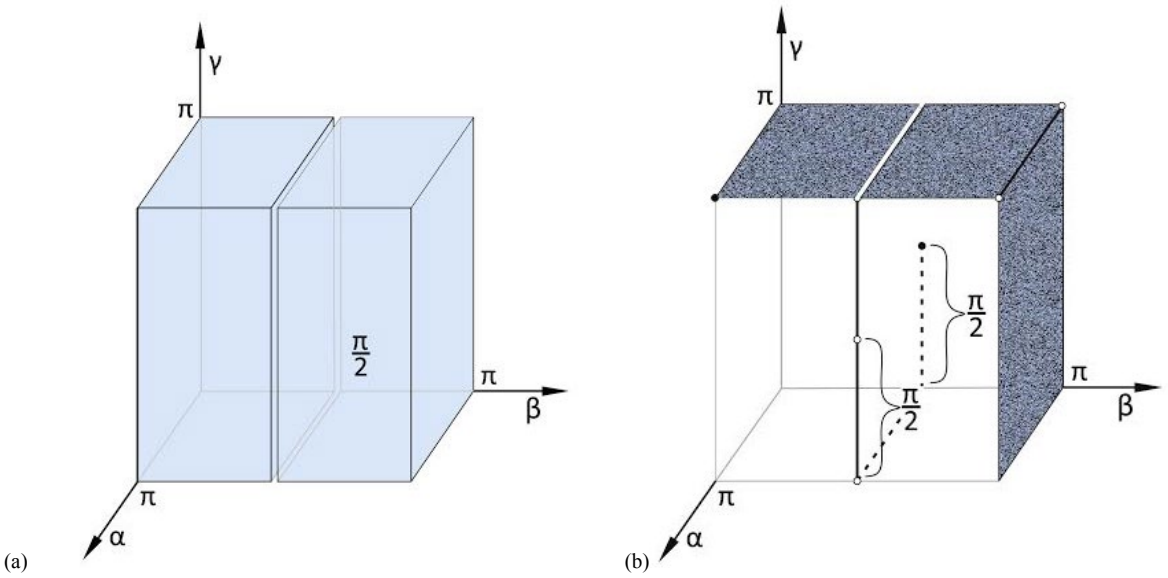

Figure. 6: The inner points (a) and border points (b) of the Monge cuboid

The inner points of the Monge cuboid satisfy the condition

$$0 < \alpha < \pi, \quad 0 < \beta < \pi/2 \quad or \quad \pi/2 < \beta < \pi, \quad 0 < \gamma < \pi \qquad \text{(Eq.1)}$$

The border points of the Monge cuboid satisfy the following conditions

$$\left.\begin{array}{l} -\ 0 < \alpha < \pi, \quad \beta = \pi, \quad 0 < \gamma < \pi, \\ -\ 0 < \alpha < \pi, \quad 0 < \beta < \pi/2, \quad \pi/2 < \beta < \pi, \quad \gamma = \pi, \\ -\ \alpha = \pi, \quad \beta = \pi/2, \quad 0 < \gamma < \pi/2, \quad \pi/2 < \gamma < \pi, \\ -\ \alpha = 0, \quad \beta = \pi/2, \quad \gamma = \pi/2, \\ -\ \alpha = \pi, \quad \beta = 0, \quad \gamma = \pi. \end{array}\right\} \qquad \text{(Eq.2)}$$

One Monge projection corresponds to a point of the Monge cuboid in a defined way. In the opposite direction, any point of the Monge cuboid defines a triplet of real numbers which is in fact a triplet of angles providing a Monge projection. The connection between the Monge projections and the points of the Monge cuboid is a mathematical mapping.

Theorem: If, for a given curve *g*, a given Monge projection is bijective or non-bijective, then the Monge projection obtained by exchanging the image planes $\underline{K}_1$ and $\underline{K}_2$ and the projection lines v_1 and v_2 is also bijective and non-bijective for the given curve *g*.

Proof: By interchanging the image planes $\underline{K}_1$ and $\underline{K}_2$ and the projection lines v_1 and v_2, the image curves *g*′ and *g*″ of the curve *g* do not change, only their notations are reversed, i.e. g′ becomes g″ and g″ becomes g′.

All Monge projections are discussed during the procedure, except those whose projection lines satisfy the conditions $v_1 \perp$ [z, x] and $v_2 \perp$ [z, x] at the same time. This method does not discuss all Monge projections, but covers all two perpendicular projections that are relevant in engineering work. This proves to be enough for our

examination, because the examination of bijectivity with respect to the given curve gives us the same result if the first and the second image are exchanged [1].

3. 1. The method of examination of curves

Simple curves will be examined through the following steps:

- positioning the curve in the fixed coordinate system O(xyz),
- creating the direction cone by moving its tangents parallel to the origin point O,
- examining the bijective and non-bijective regions of the Monge cuboid for a given curve by the relative position of the direction cone and the profile planes in the fixed coordinate system.

3.1.1. The examination of the bijectivity of the helix

Due to the cyclicity of the helix, it is sufficient to examine one thread. The axis of the helix must fit on the axis z of the Cartesian coordinate system, starting on the axis x.

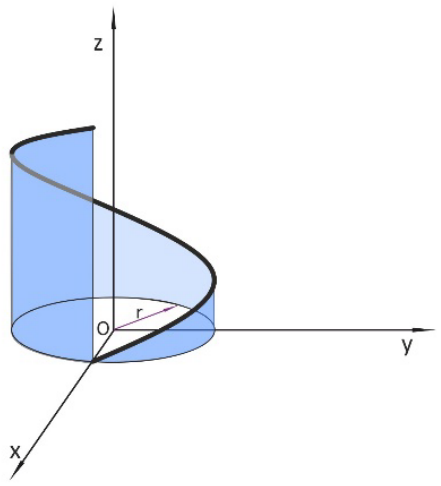

Figure. 7: The border points of the Monge cuboid

The parametric equation for a thread of a helical line with the parameter *p* on a z-axis cylinder of radius *r*

$$\left.\begin{aligned} x &= r\cdot\cos\varphi \\ y &= r\cdot\sin\varphi \\ z &= p\cdot\varphi \end{aligned}\right\} \qquad \text{(Eq.3)}$$

where $p \in \mathbb{R}\setminus\{0\}$, $r \in \mathbb{R}^{+}$, $0 \le \varphi < 2\pi$.

The coordinates of the tangent vectors r_e of the helix are obtained by the derivation

$$\left.\begin{aligned} x_e &= r\cdot\sin\varphi \\ y_e &= -r\cdot\cos\varphi \\ z_e &= p \end{aligned}\right\} \qquad \text{(Eq.4)}$$

These tangent vectors, passing through the origin point O, create the direction cone of the curve, as can be seen in Figure 8. The constant angles enclosed by the tangent vectors and the axis z are called ω.

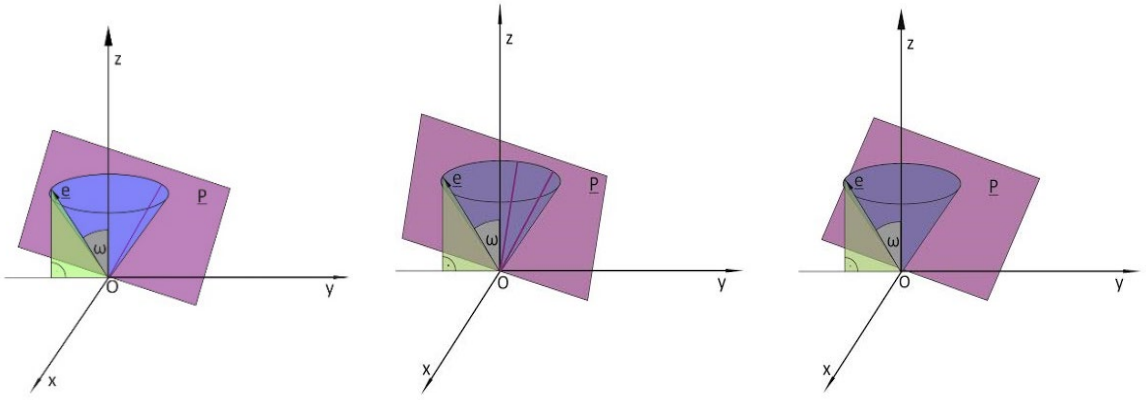

(a) (b) (c)

Figure. 8: The direction cone and the profile plane P of the Monge projection at the origin point O with two common cone-creators in (a), with one common cone-creator in (b) and no common cone-creator in (c)

In any Monge projection, the profile plane P contains one or two straight lines of cone-creators andthere is a tangent in the profile direction to the curve. All this implies that it may be a piece of the curve whose description is not necessarily bijective in this Monge projection. If the profile plane P of a Monge projection does not contain any tangents to the helix (Figure 8(c)), then the images of the helix are elongated cycloid, or affine plane-curves, and contain inflection points. In this case, any piece of the helix can be clearly reconstructed from its two images.

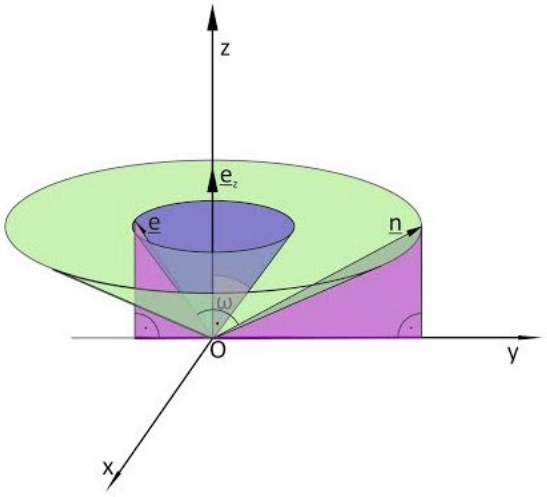

Figure. 9: The direction cone and its normal cone

The normal cone of the direction cone has been created by the normal vectors $\mathbf{n}(n_x, n_y, n_z)$ of the tangent planes of the direction cone in the point O, as can be seen in Figure 9. The cone creators of the normal cone of the helix are the normals of the profile planes, touching the direction cone of the helix.

Let $\mathbf{n}(n_x, n_y, n_z)$ be a unit vector, so that length is $|\mathbf{n}| = 1$, and $\mathbf{z}(0, 0, 1)$is the unit vector in the direction of the axis z.

Internal product of the two vectors

$$\mathbf{n} \cdot \mathbf{z} = \sin \omega \qquad \text{(Eq.5)}$$

and

$$\mathbf{n} \cdot \mathbf{z} = n_x \cdot 0 + n_y \cdot 0 + n_z \cdot 1 \qquad \text{(Eq.6)}$$

so

$$n_z = \sin\omega \qquad \text{(Eq.7)}$$

Using the condition $|\mathbf{n}| = 1$

$$n_x^2 + n_y^2 + \sin^2\omega = 1 \qquad \text{(Eq.8)}$$

transforming this

$$n_x^2 + n_y^2 = \cos^2\omega \qquad \text{(Eq.9)}$$

The (Eq. 9) is an equation of a circle with the value $\cos\omega$ of the radius.

It can be determined that the direction cone of the helix and the profile plane of a Monge projection in case

$$n_x^2 + n_y^2 > \cos^2\omega \qquad \text{(Eq.10)}$$

have two common cone creators,

$$n_x^2 + n_y^2 = \cos^2\omega \qquad \text{(Eq.11)}$$

have one common cone creator, while

$$n_x^2 + n_y^2 < \cos^2\omega \qquad \text{(Eq.12)}$$

have no common cone creators.

The aim is to determine the Monge projections for profile planes with the n normal vector which satisfy the (Eq.11) and (Eq.12) and determine the conditions for the coordinates (α,β,γ) of the Monge cuboid, since in these Monge projections ordered to these points the representation of the helix is bijective.

Since the direction vectors $\mathbf{v}_1$ and $\mathbf{v}_2$ of projection lines are perpendicular to each other, the following equation is satisfied

$$\mathbf{v}_1 \cdot \mathbf{v}_2 = 0 \qquad \text{(Eq.13)}$$

which can be written in the following form, if $\mathbf{v}_1(v_{1x}, v_{1y}, v_{1z})$ and $\mathbf{v}_2(v_{2x}, v_{2y}, v_{2z})$

$$v_{1x} \cdot v_{2x} + v_{1y} \cdot v_{2y} + v_{1z} \cdot v_{2z} = 0 \qquad \text{(Eq.14)}$$

Also, according to Figure 5, the following simple relationships can be read in the case $\alpha, \beta, \gamma \neq 0, \pi$

$$\left.\begin{aligned} &tg\alpha = v_{1y}/v_{1x} \\ &tg\beta = v_{1z}/v_{1y} \\ &tg\gamma = v_{2x}/v_{2z} \end{aligned}\right\} \qquad \text{(Eq.15)}$$

and in the case $\alpha, \beta, \gamma \neq \pi/2$

$$\left.\begin{aligned} &ctg\alpha = v_{1x}/v_{1y} \\ &ctg\beta = v_{1y}/v_{1z} \\ &ctg\gamma = v_{2z}/v_{2y} \end{aligned}\right\} \qquad \text{(Eq.16)}$$

Derived from all this, the conditions determining the bijective part can be stated, taking into account the appropriate limitations.

If the axis of a helix and its tangents create the angle ω, then the bijective part of the Monge cuboid with respect to the helix is formed by number triplets (α, β, γ) satisfying the following conditions

– in case $\alpha, \beta, \gamma \neq 0, \pi/2, \pi$:
$$((\mathrm{tg}\alpha \cdot \mathrm{ctg}\,\gamma + \mathrm{tg}\,\beta + \mathrm{tg}\,\alpha \cdot \mathrm{tg}^2\,\beta \cdot \mathrm{ctg}\gamma)/(-\mathrm{ctg}\alpha - \mathrm{tg}\beta \cdot \mathrm{ctg}\gamma - \mathrm{tg}\alpha))^2 +$$
$$+ ((\mathrm{tg}\alpha \cdot \mathrm{tg}\beta - \mathrm{ctg}\gamma)/(-\mathrm{ctg}\alpha - \mathrm{tg}\,\beta \cdot \mathrm{ctg}\,\gamma - \mathrm{tg}\alpha))^2 \leq \mathrm{ctg}^2\,\omega$$

– $0 < \alpha < \pi; \beta = \pi; \gamma = /2$

– in case $0 < \alpha < \pi; \beta = \pi; 0 < \gamma < \pi/2, \pi/2 < \gamma < \pi$:
$$\sin^4\alpha \cdot \mathrm{tg}^2\,\gamma + \cos^2\alpha \cdot \sin^2\alpha \cdot \mathrm{tg}^2\,\gamma \leq \mathrm{ctg}^2\,\omega$$

– in case $0 < \alpha < \pi/2, \pi/2 < \alpha < \pi; 0 < \beta < \pi/2, \pi/2 < \beta < \pi; \gamma = \pi$:
$$(-\mathrm{tg}\beta - \mathrm{ctg}\beta)^2/\mathrm{ctg}^2\alpha + \mathrm{ctg}^2\beta \leq \mathrm{ctg}^2\,\omega$$

– in case $\alpha = \pi/2; 0 < \beta < \pi/2, \pi/2 < \beta < \pi; \gamma = \pi/2$:
$$\mathrm{tg}^2\beta \leq \mathrm{ctg}^2\,\omega$$

– in case $\alpha = \pi/2; 0 < \beta < \pi/2, \pi/2 < \beta < \pi; 0 < \gamma < \pi/2, \pi/2 < \gamma < \pi$:
$$\left((\mathrm{ctg}\beta + \mathrm{tg}\beta) + \mathrm{tg}^2\gamma\right)^2/\mathrm{ctg}^2\beta \cdot \mathrm{tg}^2\gamma \leq \mathrm{ctg}^2\,\omega$$

– in case $0 < \alpha < \pi/2, \pi/2 < \alpha < \pi, 0 < \beta < \pi/2, \pi/2 < \beta < \pi, \gamma = \pi/2$:
$$\mathrm{tg}^2\beta \cdot (1 + \mathrm{tg}^2\alpha)/(-\mathrm{tg}\beta - \mathrm{tg}\alpha) \leq \mathrm{ctg}^2\,\omega$$

(Eq.17)

The bijective part of the Monge cuboid with respect to the helix in case ω=π/4 is visualized by green inner points, the blue border and bisecting plane points, as shown in Figure 10.

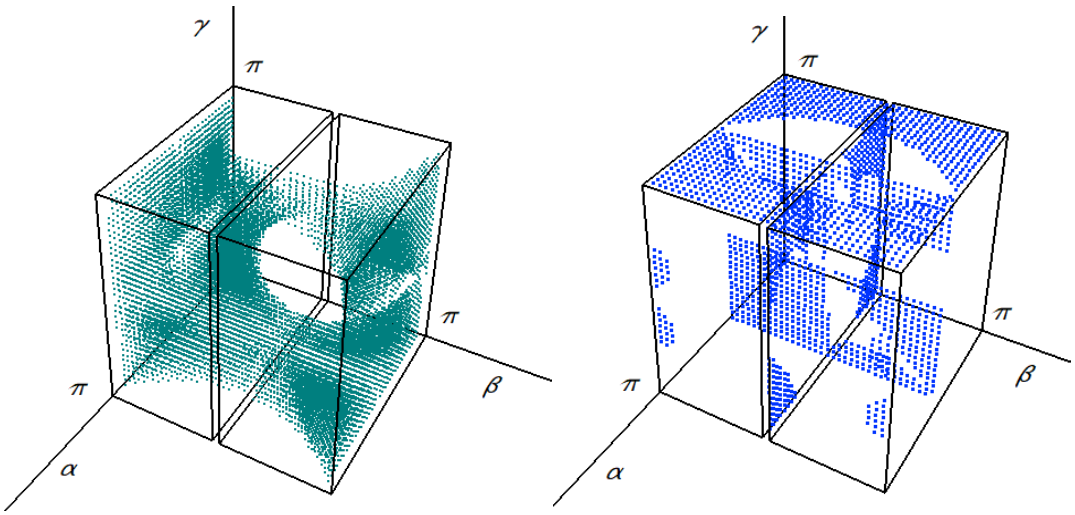

Figure. 10: The bijective part of the Monge cuboid

The triplet *α=π/4, β=π/4, γ=π/4* satisfies the conditions, so that in the Monge projection belonging to it, any piece of the helix can be clearly reconstructed from only two pictures, as shown in Figure 11(a). The triplet *α=π/3, β=π/3, γ=π/2 does not* satisfy the conditions, so that in the Monge projection belonging to this triplet, the helix has a piece which cannot be reconstructed unambiguously from only two pictures, as shown in Figure 11(b).

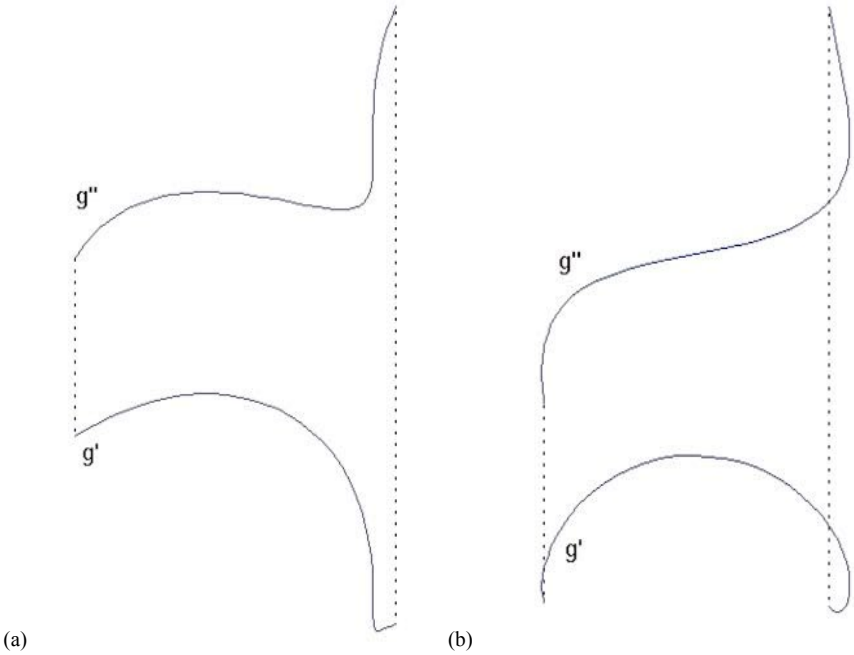

Figure. 11: In case ω=π/4, the bijective (a) and non-bijective (b) mapping of the helix

3.1.2. The condition of the reconstruction for a spatial curve

The analysis of a spatial curve has been carried out using the Hermite arc, which has been formed by points $\mathbf{p}_0$, $\mathbf{p}_3$ and their tangents $\mathbf{t}_0$, $\mathbf{t}_3$.The Hermite arc can be formulated in the form of a third-order polynomial as follows

$$\mathbf{r}(u) = \mathbf{a}_3 \cdot u^3 + \mathbf{a}_2 \cdot u^2 + \mathbf{a}_1 \cdot u + \mathbf{a}_0 \qquad \text{(Eq.18)}$$

where $u \in [0,1]$. Completing the appropriate substitutions and rearrangements, we obtain the equations

$$\left.\begin{aligned} \mathbf{a}_0 &= \mathbf{p}_0 \\ \mathbf{a}_1 &= \mathbf{p}_3 \\ \mathbf{a}_2 &= -3\cdot\mathbf{p}_0 + 3\cdot\mathbf{p}_3 - 2\cdot\mathbf{t}_0 - \mathbf{t}_3 \\ \mathbf{a}_3 &= 2\cdot\mathbf{p}_0 - 2\cdot\mathbf{p}_3 + \mathbf{t}_0 + \mathbf{t}_3 \end{aligned}\right\} \qquad \text{(Eq.19)}$$

The tangent vectors can be described in the following form

$$\mathbf{r}_e(u) = \mathbf{e}_1 \cdot u^2 + \mathbf{e}_2 \cdot u + \mathbf{e}_3 \qquad \text{(Eq.20)}$$

where

$$\left.\begin{aligned} \mathbf{e}_1 &= 6\cdot\mathbf{p}_0 - 6\cdot\mathbf{p}_3 + 3\cdot\mathbf{t}_0 + 3\mathbf{t}_3 \\ \mathbf{e}_2 &= -6\cdot\mathbf{p}_0 + 6\cdot\mathbf{p}_3 - 4\cdot\mathbf{t}_0 - 2\cdot\mathbf{t}_3 \\ \mathbf{e}_3 &= \mathbf{t}_0 \end{aligned}\right\} \qquad \text{(Eq.21)}$$

The vectors $\mathbf{n}$ are normal to the planes fitting the tangent vectors $\mathbf{r}_e$, thus satisfying the equation

$$\mathbf{n}\cdot\mathbf{r}_e(u) = 0 \qquad \text{(Eq.22)}$$

If $\mathbf{n}(n_x, n_y, n_z)$, $\mathbf{e}_1(e_{1x}, e_{1y}, e_{1z})$, $\mathbf{e}_2(e_{2x}, e_{2y}, e_{2z})$, $\mathbf{e}_3(e_{3x}, e_{3y}, e_{3z})$, the equation (Eq. 22) can be written in the next form

$$\left(n_x\cdot e_{1x} + n_y\cdot e_{1y} + n_z\cdot e_{1z}\right)\cdot u^2 + \left(n_x\cdot e_{2x} + n_y\cdot e_{2y} + n_z\cdot e_{2z}\right)\cdot u + \left(n_x\cdot e_{3x} + n_y\cdot e_{3y} + n_z\cdot e_{3z}\right) = 0 \qquad \text{(Eq.23)}$$

The vectors $n(n_x, n_y, n_z)$ are searched for the given e_{ij} values, to which the second-degree equation considering the parameter u in (Eq.23) does not have a solution. This is only fulfilled if the discriminant of the second-degree equation considering u is a negative number, hence

$$\left(n_x\cdot e_{2x} + n_y\cdot e_{2y} + n_z\cdot e_{2z}\right)^2 - 4\cdot\left(n_x\cdot e_{1x} + n_y\cdot e_{1y} + n_z\cdot e_{1z}\right)\left(n_x\cdot e_{3x} + n_y\cdot e_{3y} + n_z\cdot e_{3z}\right) < 0 \qquad \text{(Eq.24)}$$

In addition, the normal vector n of the profile plane P of the Monge-projection is perpendicular to the direction vectors of the projection lines, hence

$$\mathbf{n} = \mathbf{v}_1 \times \mathbf{v}_2 \qquad \text{(Eq.25)}$$

The final result has been obtained with suitable replacements and trigonometric identities. Based on this, the directions of the projection lines, and, thus, the positions of the CCD cameras, are determined to ensure the reconstruction of the cutting edge of the hob using the interpolated Bezier curve.

The connection between the Bezier curve and the Hermite arc is shown by the following equations

$$\left.\begin{aligned} \mathbf{p}_0 &= \mathbf{b}_0 \\ \mathbf{p}_3 &= \mathbf{b}_3 \\ \mathbf{t}_0 &= 3\cdot\mathbf{b}_1 - 3\cdot\mathbf{b}_0 \\ \mathbf{t}_3 &= 3\cdot\mathbf{b}_3 - 3\cdot\mathbf{b}_2 \end{aligned}\right\} \qquad \text{(Eq.26)}$$

Points $\mathbf{p}_3$ and $\mathbf{p}_0$ of the cutting edge of the tool have been selected on the addendum and root cylinder and between them the points $\mathbf{p}_2$ and $\mathbf{p}_1$ have been appointed proportionally.

The Bezier curve has to be interpolated to four selected points $\mathbf{p}_0$, $\mathbf{p}_1$, $\mathbf{p}_2$, $\mathbf{p}_3$ on the cutting edge of the hob, where the parameters u_0, u_1, u_2, u_3, and $u_i \neq u_j$ if i ≠ j, as well as $u_0 = 0$ and $u_3 = 1$.

Finding the control points $\mathbf{b}_0$, $\mathbf{b}_1$, $\mathbf{b}_2$, $\mathbf{b}_3$ is necessary to determine the interpolation Bezier curve fitting to the selected points $\mathbf{p}_0$, $\mathbf{p}_1$, $\mathbf{p}_2$, $\mathbf{p}_3$, thus the following equation is satisfied

$$\mathbf{b}(u_i) = \mathbf{p}_i \qquad (i = 0,\ldots,3) \qquad \text{(Eq.27)}$$

The equation of the Bezier curve can be given using the well-known Bernstein polynomials

$$\mathbf{b}(u) = \sum_{j=0}^{n} B_j^n(u)\mathbf{b}_j \qquad B_j^n(u) = \binom{n}{j} u^j (1-u)^{n-j} \quad (i = 0,\ldots,3) \qquad \text{(Eq.28)}$$

from which the following linear inhomogeneous equation system can be obtained

$$\begin{bmatrix} \mathbf{p}_0 \\ \mathbf{p}_1 \\ \mathbf{p}_2 \\ \mathbf{p}_3 \end{bmatrix} = \begin{bmatrix} B_0^3(u_0) & B_1^3(u_0) & B_2^3(u_0) & B_3^3(u_0) \\ B_0^3(u_1) & B_1^3(u_1) & B_2^3(u_1) & B_3^3(u_1) \\ B_0^3(u_2) & B_1^3(u_2) & B_2^3(u_2) & B_3^3(u_2) \\ B_0^3(u_3) & B_1^3(u_3) & B_2^3(u_3) & B_3^3(u_3) \end{bmatrix} \cdot \begin{bmatrix} \mathbf{b}_0 \\ \mathbf{b}_1 \\ \mathbf{b}_2 \\ \mathbf{b}_3 \end{bmatrix} \qquad \text{(Eq.29)}$$

The $u_i \neq u_j$ condition provides us with a clear result [8] to all $\mathbf{b}_i$ (i,j=0,…,3). The resulting Bezier curve written with control points $\mathbf{b}_0$, $\mathbf{b}_1$, $\mathbf{b}_2$, $\mathbf{b}_3$ passes through the points $\mathbf{p}_0$, $\mathbf{p}_1$, $\mathbf{p}_2$, $\mathbf{p}_3$.

The examination of the cutting edge curve can only be performed with two CCD cameras if any piece of the curve can be unambiguously reconstructed from its two pictures [3].

The spatial positions of the points P_n, …, P_0 of the cutting edge are determined from its images that can be considered as perpendicular projections [7].

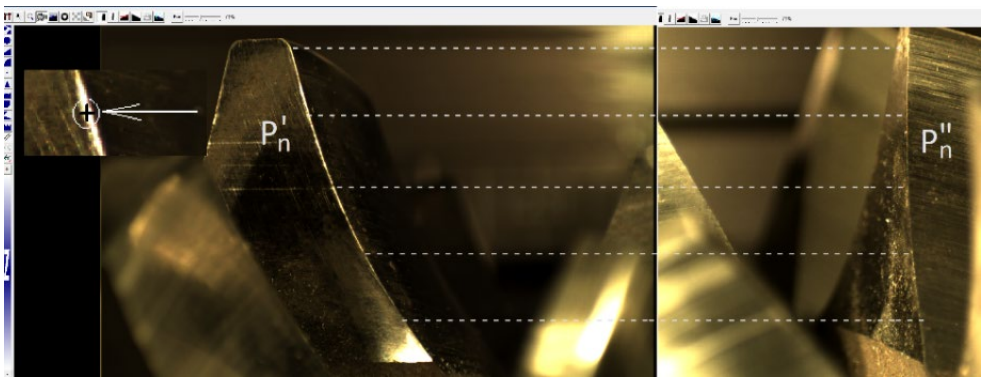

Figure. 12: Photos taken by CCD cameras in an ordered position

4. CONCLUSION

The paper gives a special solution to the anomalies' concept of the reconstruction problem from two photos and two perpendicular projections. The Monge projections, which can be translated into each other, have been considered identical. The Monge projections can be described by three free real parameters. The three real parameters have been defined by the direction angles of the projection lines of the Monge projections in a fixed coordinate system. One triplet of free real parameters corresponds to one Monge projection, and it is completed in the opposite direction. The applied triplets of free parameters create the Monge cuboid. All perpendicular images have been discussed by this method. The Monge cuboid has two subsets which give us the bijective and non-bijective Monge projections. This method determines the correct positions of CCD cameras to reconstruct the curve of the cutting edge of the tool. This method is a necessary condition for the possibility of feedback during machining, as well as a continuous comparison with the mathematical form of the tool edge.

5. REFERENCES

1. Balajti, Z., Dudás, I. 2017. The Monge Theorem and Its Application in Engineering Practice. *International Journal of Advanced Manufacturing Technology*, 91. pp 739–749. DOI: 10.1007/s00170-016-9763-1
2. Cvetković, I. D., Stojićević, M. D., Stachel, H., Milićević R. G., Popkonstantinović B. D.: *The Man who Invented Descriptive Geometry*, FME Transactions (2019) VOL. 47, No 2, 331-336. 2019., DOI:10.5937/fmet1902331C
3. Hungarian Scientific Research Fund No. T026566. Development of CCD cameras systems to the area of machine industry. Miskolc, 2002. (Lead investigator: Prof. Dr. Dr. h. c. Dudás I. DSc.)
4. Jeli, Z., Komatin, M., Popkonstantinovic, B., Regodic, M. 2012. Usage of modern graphical presentations in development of technical systems. 3th International Conference moNGeometrija, Novi Sad, Serbia. ISBN 978-86-7892-405-7 pp. 553-564.
5. Monge, G. 1799. Géometrie descriptive. Lecon données aux Ecoles normales. l'an 3 de la République, Paris, Baudouin, an VII. ISBN ; 978-2-87647-065-1, p. 142.
6. Popkonstantinovic, B., Stojicevic, M., Jeli, Z., 2019. Obradovic, M., Dragos-Laurentiu P.: Simulation and Motion Study of Mechanical Integrator 3D Model, *FME Transactions*, 47, No 2, pp. 299-303. doi:10.5937/fmet1902299P
7. Stachel, H., 2006. Descriptive Geometry Meets Computer Vision – The Geometry of Two Images. Journal for Geometry and Graphics. 10(2). pp 137–153.
8. Vadászné Bognár, G., 2003. Mathematic for IT specialists and Engineerings 2., Miskolc, Hungary. University Presss of Miskolc, ISBN: 9636615764. p. 347.

CONCAVE PYRAMIDS OF FOURTH SORT

Slobodan Mišić
Faculty of Applied Arts, University of Arts in Belgrade, Serbia
PhD., Associate Professor, slobodan.misic@fpu.bg.ac.rs

Marija Backović
Military Technical Institute, Electronic Systems Sector, Belgrade, Serbia
MSc., Researcher, mbbackovic@gmail.com

ABSTRACT

The paper discusses the generation of a specific group of polyhedra, Concave Pyramids of Fourth Sort (CP IV). Correspondingly to the method of generating the Concave Cupolae of Fourth Sort (CC IV), the Concave Pyramids of fourth sort have the similar logic of origination, and their counterpart in regular faced convex pyramids. The concave polyhedral surface consists of a series of equilateral triangles, grouped into spatial pentagons and hexagons. Positioned polarly around the central axis of the regular polygon in the polyhedron's basis and linked by connected triangles, the spatial pentagons and hexagons form the deltahedron's surface area. The criterion of face regularity is respected, as well as the criterion of multiple axial symmetry. Distribution of the triangles is based on strictly determined and mathematically defined parameters, which allows the creation of such structures in a way that qualifies them as an autonomous group of polyhedra – concave pyramids. The sort of the Concave Pyramids is determined by the number of equilateral triangle rows in thus obtained polyhedron's net. The parameters of the solids were determined constructively by geometric methods.

Keywords: concave pyramids; polyhedral; equilateral triangle; regular polygon.

INTRODUCTION

Concave pyramids belong to the family of previously studied polyhedral structures comprising Concave cupolae of the second sort (Obradović, 2019; Obradović et al., 2008, 2019), Concave cupolae of the fourth (and higher) sorts (Mišić, 2013; Mišić et al., 2010, 2013, 2014), Concave antiprisms of the second sort (Obradović et al., 2013) and composite polyhedra obtained by means of their mutual combination (Mišić et al., 2015). The results of the exploration of the application of these polyhedral structures in architecture and engineering were presented in (Obradović et al., 2011, 2013). The common characteristics of the polyhedra above are as follows:

- The polyhedral net is a developmental deltahedral surface
- Deltahedral net of the polyhedron is formed above the regular polygonal base
- The polyhedron has an axis that is orthogonal to the polygonal base plane and crosses the center of the incircle of the polygonal base
- The deltahedral net is obtained by means of polar distribution of the unit cell(s) around the axis of the polyhedron
- The unit cell consists of equilateral triangles grouped around a common vertex
- Two faces of the surface net meet on each edge of the polyhedron
- The faces of the polyhedron may not protrude each other or intersect, except on the edges
- The edges do not intersect, except in vertices
- The planes to which the sides belong may pass the inner space of the polyhedron – the surface area is a concave polyhedral area
- Each face is visible from outside – there are no inner sides

- There are no two neighboring coplanar faces
- The type of the polyhedron is determined by the number of rows of equilateral triangles in the planar net of deltahedral surface.

The previous studies have examined the Concave pyramids of the second sort (Obradović et al., 2014, 2015, 2017). The unit cell consists of five equilateral triangles grouped around the common vertex. All the unit cells in thus formed deltahedral net of concave pyramids of the second sort have a common vertex located on the rotation axis, orthogonal to the plane of the polygon's base. Due to the manner in which the vertex is formed and the surface area which is a developmental concave deltahedral surface, these polyhedra are termed Concave pyramids.

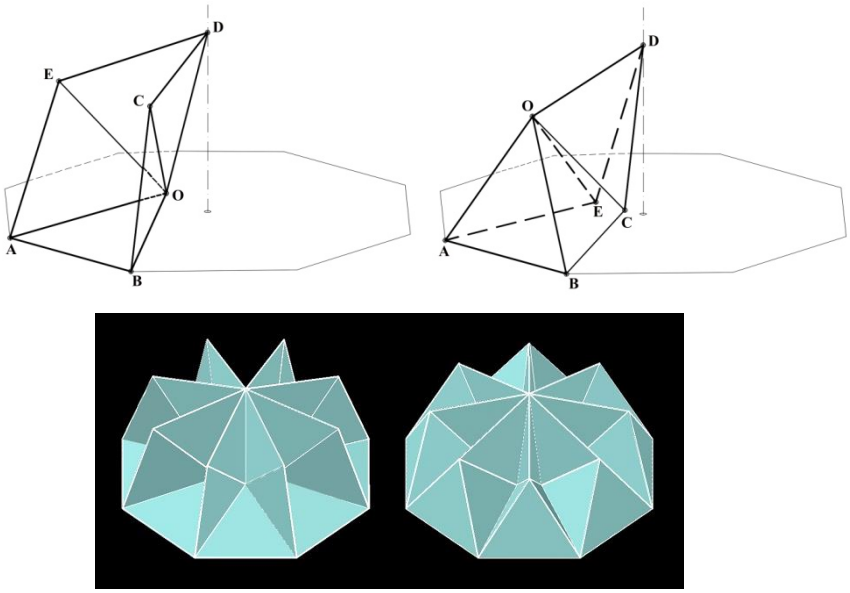

Figure 1: Method of generating the Concave pyramids of second sort by folding and creasing the plane net, obtaining two different types: CP-8M, and CP-8m

Geometrical generation of concave pyramids of the second sort is based on finding the precise position of the spatial pentagon's vertex which meets the condition that the vertices A and B are located on the sides, while the vertex D lies on the axis of polygonal base (Fig. 1). Previous research has shown that there are two types of concave pyramids of the second sort above the same polygonal base. If the common vertex O is indented, the concave pyramid of greater height is obtained (CP-II-nM). Conversely, if the common vertex O protrudes, the distribution of the other vertices in the spatial pentagon is such that it generates a concave pyramid of a smaller height (CP-II-nm).

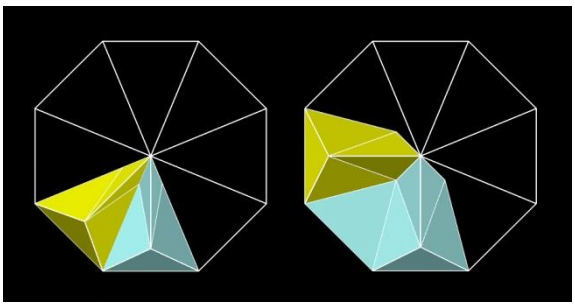

Figure 2: Method of generating the Concave pyramids of second sort, tip A and tip B

Apart from this classification of the concave pyramids of the second sort into those with smaller and larger height, resulting in differently shaped polyhedron, there also two ways in which concave pyramids can be generated. In the first manner, termed "type A" the number of unit cells in the net is equal to the number of sides (n) of the polygonal base (Fig. 2) - the unit cell is developed above every side of the polygonal base. In the

second manner, or "type B", the unit cell is developed above every other side, and they are mutually connected by means of equilateral triangles. The second manner of generation can only be applied to concave pyramids of the second sort which are formed above the polygonal base with even number of sides.

Table 1: All possible shapes of concave pyramids of the second sort

CP II	*n*=6	*n*=7	*n*=8	*n*=9
CP II-mA	•	•	•	
CP II-MA	•	•	•	•
CP II-B	•		•	

Table 1 shows all possible shapes of concave pyramids of the second sort. As can be seen, they can be developed above polygonal base $6 \leq n \leq 9$. The net CP II-10B and CP II-9mA protrudes the plane of the polygon's base so that the polyhedron itself cannot be formed, but it is possible to generate the net, which has been used (Mišić et al., 2015) to form composite polyhedral structures (Emmerich, 1986).

2. CONCAVE PYRAMIDS OF THE FOURTH SORT

This paper presents the results of the study of 'type B' concave pyramids of the fourth sort. The generation of the concave pyramids of the fourth sort is based on predefined conditions described in the introduction, which classify those polyhedrons into a unique family of concave polyhedral structures. The unit cell consists of the spatial hexagon ABCDEF (six equilateral triangles grouped around the common vertex O_1 and the spatial pentagon EDGHJ (five equilateral triangles grouped around the common vertex O_2), with the common edge ED (Fig. 3). Thus formed unit cell in turn forms the surface of the concave pyramid by planar distribution around the axis orthogonal to the base plane. In the deltahedral surface area CP-IV two neighboring unit cells are joined by means of an equilateral triangle (with which they share the common edge BC, or AF) and the spatial tetrahedron (four equilateral triangles grouped around a common vertex Q) with which they share the common sides CD, DG, or FE, EJ. The common vertex of all unit cells (marked as vertex H in Fig. 3) lies on the polyhedron's axis.

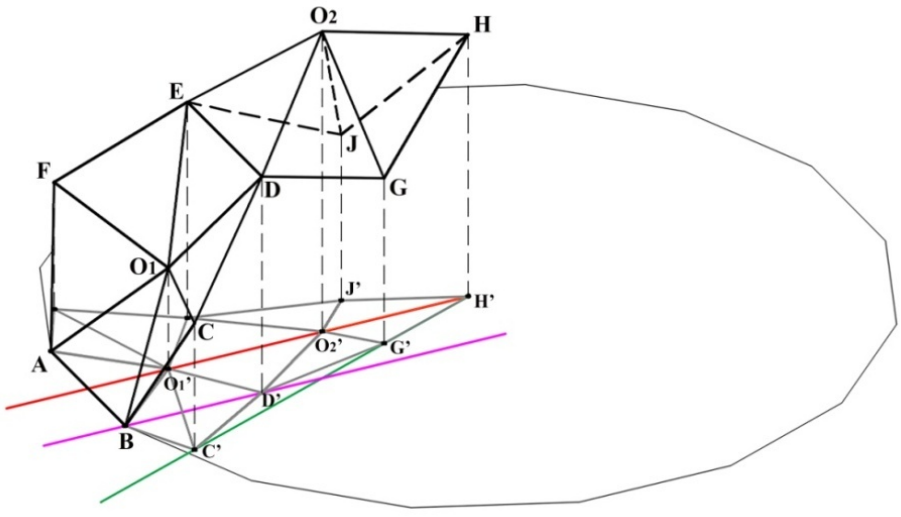

Figure 3: The unit cell of the concave pyramid of the fourth sort and orthogonal projection onto the base plane

The geometry of the unit cell defines the possible size of the polygonal base. The condition that the radius of polygon's base incircle must be:

$$r < \frac{3a\sqrt{3}}{2} + a \qquad \text{(Eq. 1)}$$

leads us to the conclusion that concave pyramids of the fourth sort can be formed above the polygonal base whose number of sides is $10 \leq n \leq 22$.

Geometrical generation is based on finding the unit cell vertex position which meets the following conditions:

- The vertices A and B are located on the sides, while the vertex H is on the axis of the polygonal base,
- The vertices O_1, O_2 and H lie on the common plane α,
- The vertices B and D lie on the common plane β,
- The vertices C, Q, G and H are on the common plane γ,
- The planes α, β and γ are orthogonal to the plane of the polygonal base of the concave pyramid.

The construction itself relies on the constructive procedure for generating Concave cupolae of the fourth sort (Mišić, 2013). In other words, it relies on the fact that the distance between the neighbouring vertices of the unit cell is always the same and equal to the side of the unit equilateral triangles. To illustrate, let us look at the construction of the position and height of the vertex D. The auxiliary spheres whose centers are located in the neigh boring vertices of the spatial hexahedron (vertices $O_1$and C) are cut by the plane β containing vertices B and D. Mutual intersection of thus obtained intersecting circles ($k_1$and k_2) determines the position of vertex D, following the condition that vertex B must be located on the polygonal plane. By repeating the constructive procedure above and by determining the position for every unit cell for multiple initial positions of vertex O_1, we generate the trajectory of vertex H. When thus produced vertex H trajectory is intersected by the plane containing the polyhedron's axis, we obtain the sought position of vertex H, and the final position of all the other vertices of the unit cell.

The constructive procedure to generate the vertex H trajectory allows us to choose the position of vertices C, Q and O_2 with a larger or a smaller height, which results in 8 possible variations of the constructive procedure for CP IV. The same holds for the construction of Concave cupolae of the fourth sort, for which reason the same manner of denotation of the variants of the constructive procedure has been adopted:

1. **CP IV-B (CQO_2)** smaller height for **C**, **Q** and **O_2**
2. **CP IV-B ($CQ^*O_2^*$)** smaller height for **C**, larger height for **Q** and **O_2**
3. **CP IV-B (CQ^*O_2)** smaller height **C** and **O_2**, larger height for **Q**
4. **CP IV-B (CQO_2^*)** smaller height for **C** and **Q**, larger height for vertex **O_2**
5. **CP IV-B (C^*QO_2)** larger height for **C**, smaller height for **Q** and **O_2**
6. **CP IV-B ($C^*Q^*O_2$)** larger height for **C** and **Q**, smaller height for **O_2**
7. **CP IV-B ($C^*QO_2^*$)** larger height for **C** and **O_2**, smaller height for **Q**
8. **CP IV-B ($C^*Q^*O_2^*$)** larger height for **C**, **Q** and **O_2**.

The change of the shape of the concave pyramids of the fourth sort depending on the choice of the constructive procedure is in this study illustrated by the case of the concave pyramid above the dodecagonal base. The planar net CPIV-12B is shown in Fig. 4.

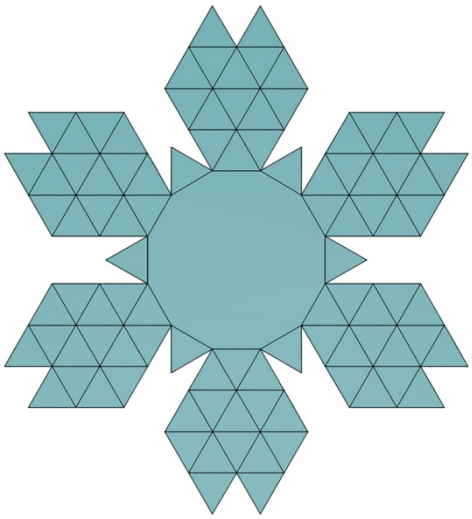

Figure 4: The planar net CP IV-12B

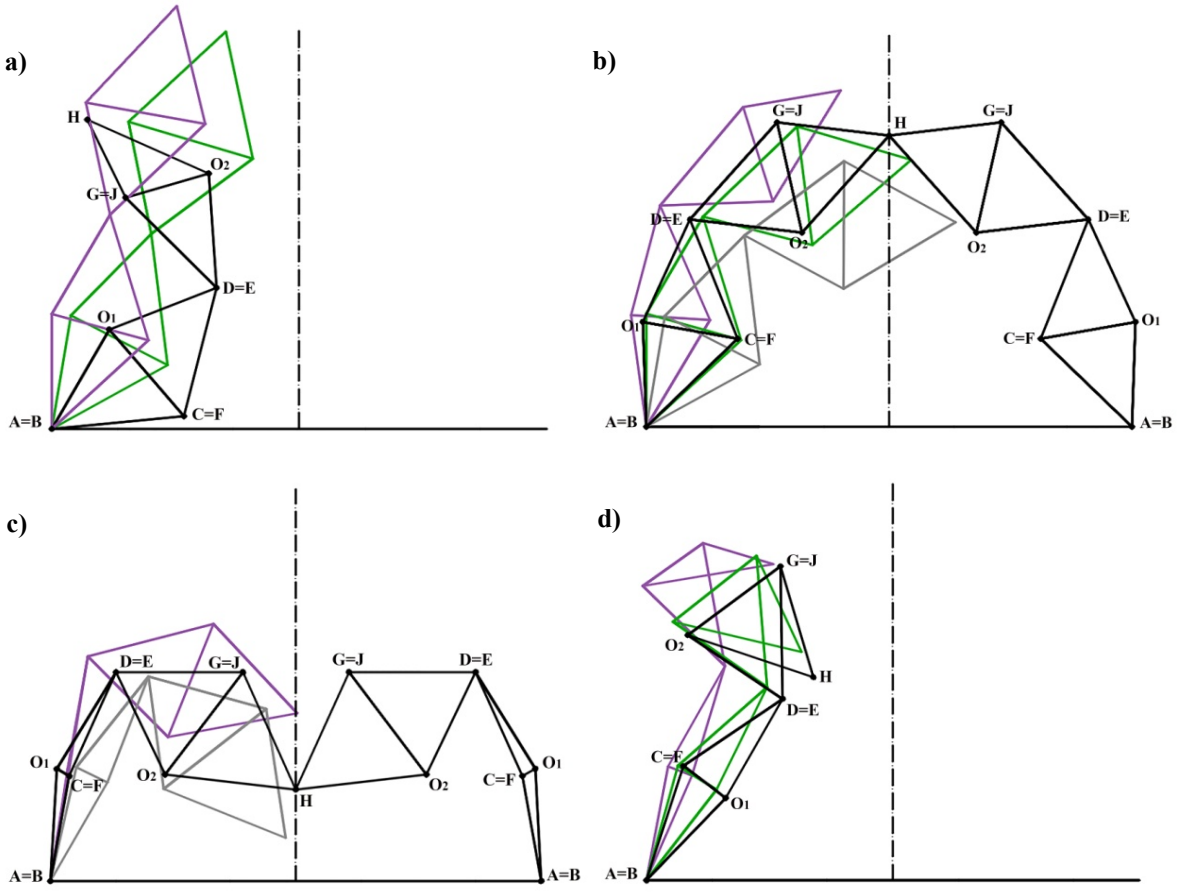

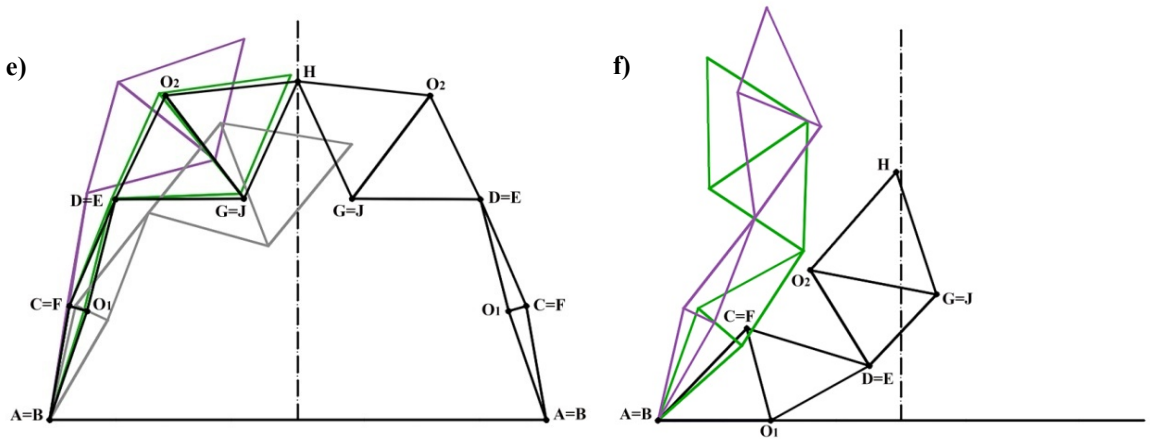

Figure 5: The change of the shape of CC IV-12B depending on the choice of the constructive procedure (vertical section of three positions of a unit cell) **a)** CP IV-12B ($CQ^*O_2^*$), **b)** CP IV-12B (CQ^*O_2), **c)** CP IV-12B (C^*QO_2), **d)** CP IV-12B ($C^*Q^*O_2$), **e)** CP IV-12B($C^*QO_2^*$), **f)** CP IV-12B ($C^*Q^*O_2^*$)

Concave pyramids of the fourth sort above the dodecagonal polygonal base can be formed by using the following variations of the constructive procedure: CP IV-B (CQ^*O_2), CP IV-B (C^*QO_2) and CP IV-B ($C^*QO_2^*$) (Fig. 5-8). In other cases the vertex H trajectory does not intersect the plane to which the polyhedron's axis belongs or the faces of the polyhedron protrude each other or intersect - constructive procedure variations CP IV-B (CQO_2) and CP IV-B (CQO_2^*), so that it is not possible to generate a concave pyramid which meets the predefined starting conditions. The trajectory passes by the plane - constructive procedure variations CP IV-12B (C^*Q^*O2) and CP IV-12B ($C^*Q^*O2^*$), or distances itself from the plane of the polyhedron's central axis when the position of vertex O_1 is altered (constructive procedure variations: CP IV-12B ($CQ^*O_2^*$) (Fig. 5).

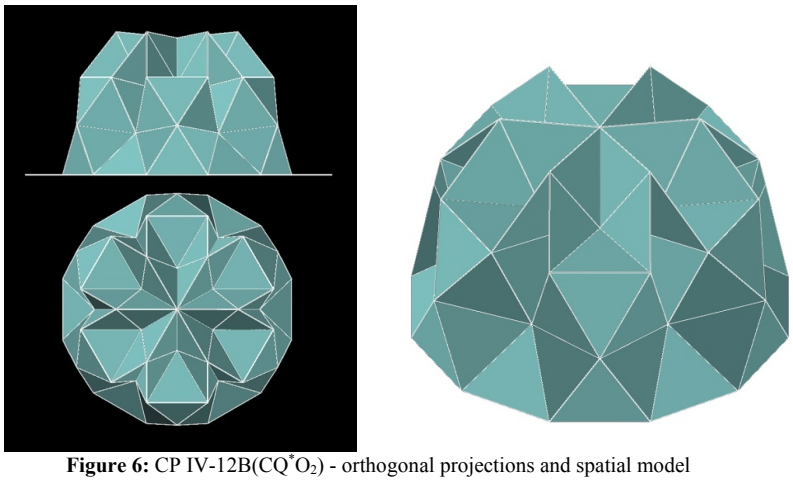

Figure 6: CP IV-12B(CQ^*O_2) - orthogonal projections and spatial model

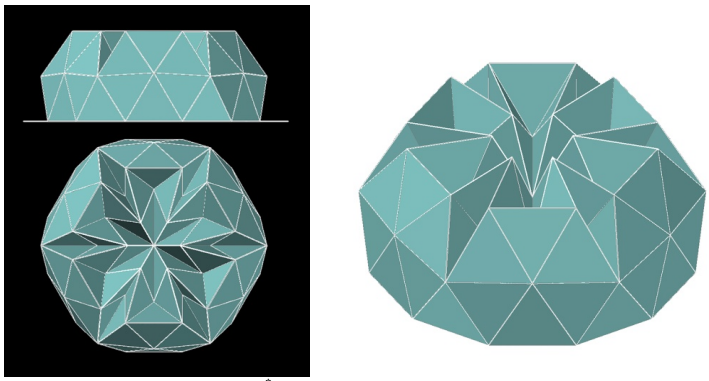

Figure 7: CP IV-12B(C^*QO_2) - orthogonal projections and spatial model

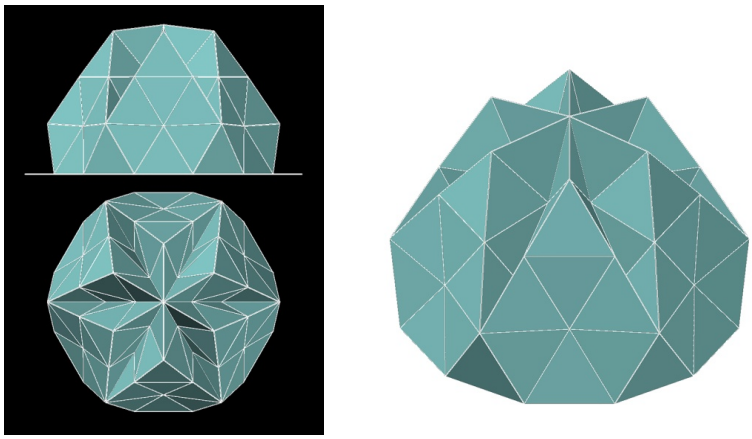

Figure 8: CP IV-12B($C^*QO_2^*$) - orthogonal projections and spatial model

The study has shown that above every polygonal base $10 \leq n \leq 22$ it is possible to generate CP-IV by applying different variations of the constructive procedure. However, this research has not uncovered the rule which defines the possibilities for forming CP IV for the given polygonal base and the given variation of the construction procedure. For that reason, we examined all the possible cases, and the results are shown in Tab. 2.

Table 2:. Concave pyramids of the fourth sort – the possibilities of their generation above different polygonal base by applying different construction procedure

CP IV-B	*n*=10	*n*=12	*n*=14	*n*=16	*n*=18	*n*=20	*n*=22
CP IV-B (CQO_2)				•			
CP IV-B ($CQ^*O_2^*$)							
CP IV-B (CQ^*O_2)	•	•	•				
CP IV-B (CQO_2^*)						•	
CP IV-B (C^*QO_2)		•					
CP IV-B ($C^*Q^*O_2$)						•	
CP IV-B ($C^*QO_2^*$)	•	•	•	•	•		
CP IV-B ($C^*Q^*O_2^*$)							

Bearing in mind that the above described generation procedure for concave pyramids of the second and fourth sort, we maintain that for any concave pyramid above an n-sided polygonal base the following applies:

- The number of vertices is calculated by means of the formula:

$$v = \frac{9n}{2} + 1 \qquad \text{(Eq. 2)}$$

- The number of edges is calculated by means of the formula:

$$e = \frac{25n}{2} \qquad \text{(Eq. 3)}$$

- The number of faces is calculated by means of the formula:

$$f = 8n + 1 \qquad \text{(Eq. 4)}$$

CONCLUSION

By observing predefined conditions for generating the family of concave polyhedral structures which include the previously studied concave cupolae of the second and higher sort, concave antiprisms of the second sort and concave pyramids of the second sort it is possible to constructively generate type B concave pyramids of the fourth sort. There are 12 polyhedrons of this type whose generation relies on the constructive procedure for forming the concave cupolae of the fourth sort. It has been proven that for the same polygonal base it is possible to generate more than one CPIV-nB. The presentation of thus formed new polyhedrons and the

confirmation of accuracy of the selected constructions was performed by means of the software package AutoCAD 3D models. Future research may focus on the confirmation of the results presented in this paper, as well as on analytical methods, application of appropriate iterative numerical procedures and the exploration of the applicative potential of these polyhedrons in architectural geometry.

REFERENCES

1. Emmerich D.G., 1986. Cimposite polyhedral. *Topologie Strucutrale*, 13. pp. 5-32.
2. Mišić, S., Obradović, M., Đukanović, G., 2015. Composite Concave Cupolae as Geometric and Architectural Forms. *Journal for Geometry and Graphics*, 19 (1). pp. 79-91.
3. Mišić, S., Obradović, M., 2010. Forming the Cupolae With Concave Polyhedral Surfaces by Corrugating a Fourfold Strip of Equilateral Triangles. Proceedings of International Conference for Geometry and Graphics moNGeometrija 2010, Belgrade, Serbia. pp. 363-374.
4. Mišić, S., 2013. Konstruktivno-geometrijsko generisanje kupola sa konkavnim poliedarskim površima. (Generation of the cupolae with concave polyhedral surfaces), PhD thesis. University of Belgrade, Faculty of Architecture, Belgrade, Serbia.
5. Mišić, S., Obradović, M., Lazović, G., Popkonstantinović B., 2013. Generating a Type of Concave Cupolae of Fourth Sort. Proceedings of International Conference on Engineering Graphics and Design - ICEGD 2013., Timişoara, Romania. pp. 79-82.
6. Mišić, S., Obradović, M., Popkonstantinović, B., 2014. The Structural Transformation of Concave Cupolae of Fourth Sort Using Different Variants of Constructive Procedure. Proceedings of the 4th International Scientific Conference moNGemetrija 2014, Vlasina, Serbia. pp. 147-156.
7. Obradović, M., Mišić, S., 2008. Concave Regular Faced Cupolae of Second Sort, Proceedings of 13th ICGG, Dresden, Germany, El Book, pp. 1-10.
8. Obradović, M., Mišić, S., Popkonstantinović, B., Petrović, M., 2011. Possibilities of Deltahedral Concave Cupola Form Application in Architecture. Proceedings of ICEGD Conference, Iasi, Romania. pp. 123-140.
9. Obradović, M., Mišić, S., Popkonstantinović, B., Petrović, M., Malešević B., Obradović, R., 2013. Investigation of Concave Cupolae Based Polyhedral Structures and Their Potential Application in Architecture, *Technics Technologies Education Management* 8 (3). pp. 1198–1214.
10. Obradović, M., Popkonstantinović B., Mišić S., 2013. On the Properties of the Concave Antiprisms of Second Sort, *FME Transactions*, 41(3). pp 256-263.
11. Obradović, M., Mišić, S., Popkonstantinović, B., 2014. Concave Pyramids of Second Sort - the Occurrence, Types, Variations. Proceedings of the 4th International Scientific Conference moNGemetrija 2014, Vlasina, Serbia. pp. 157-168.
12. Obradović, M., Mišić S., Popkonstantinović B., 2015. Variations of Concave Pyramids of Second Sort With an Even Number of Base Sides. *Journal of Industrial Design and Engineering Graphics* (JIDEG), 10 (1) Special Issue. pp 45-51.
13. Obradović, M., Stavrić, M., Wiltsche, A., 2017. Polyhedral forms obtained by combinig lateral sheet of CP II-10 and truncated dodecahedron. *FME Transactions*, 45(2). pp. 256-261.
14. Obradović, M., 2019. Tiling the Lateral Surface of the Concave Cupolae of the Second Sort. *Nexus Network Journal*, 21. pp. 59-77.
15. Obradović, M., 2019. Geometric Redesign of the Subdivided Surface of CC II: Application In Architecture. *Journal of Industrial Design and Engineering Graphics* (JIDEG), 14 (1). pp. 79-84.

SPATIAL INTERPRETATION OF ERDÖS-MORDELL INEQUALITY FOR POLYGONS OVER WEBERIAN FOCAL-DIRECTORIAL SURFACES

Maja Petrović
University of Belgrade – The Faculty of Transport and Traffic Engineering, Belgrade, Serbia
PhD, Assistant Professor, majapet@sf.bg.ac.rs

Branko Malešević
University of Belgrade – School of Electrical Engineering, Belgrade, Serbia
PhD, Full Professor, malesevic@etf.bg.ac.rs

Radovan Štulić
University of Novi Sad – Faculty of Technical Sciences, Novi Sad, Serbia
PhD, Full Professor, stulic@uns.ac.rs

Ema Jurkin
University of Zagreb – Faculty of Mining, Geology and Petroleum Engineering, Zagreb, Croatia
PhD, Associate Professor, ema.jurkin@rgn.hr

Radomir Mijailović
University of Belgrade – The Faculty of Transport and Traffic Engineering, Belgrade, Serbia
PhD, Full Professor, radomirm@sf.bg.ac.rs

ABSTRACT

In the paper we deal with a geometrical problem which originates from the Erdös-Mordell inequality (EMI) for regular polygons generalizing it by defining Weberian focal-directorial surfaces (WFDS). Furthermore, we derive such surfaces in a way suitable for their visualization and present possibilities of the application of Weber's surfaces generated by eight foci and eight directrix lines at most.

Keywords: algebraic equation; Erdös-Mordell inequality; Erdös-Mordell curve and surfaces; Weberian focal-directorial curves and surfaces

INTRODUCTION

The research of trifocal and tridirectorial curves paired with the research of geometrical Erdös-Mordell type inequalities for triangles, published in the paper of Malešević et al. (2014), has brought about the unification of these two areas into a general Weber-type location problem. In the papers (Petrović 2016, 2019) defines Weberian focal-directorial curves (WFDC) as locus of points in a plane with a constant sum of distances to m foci and n directrices. Obtained in such a way, the locus of points in a plane, of the combined multifocal and multi-directorial curves, are tied to location problems and are otherwise called isocost curves. In this paper, through setting foci/directrices in such a way that they coincide with vertices/sides of regular polygons and through the analysis of positive and negative scaling coefficients, i.e. Weber weight factors corresponding to their respective distances, a new visual interpretation of the Erdös-Mordell inequality for regular polygons is shown.

The proofs of Erdös-Mordell inequality are often based on the proofs of various other inequalities, as given in the papers (Liu, 2020, 2019, 2018a, 2018b; Minculete, 2012; Obradović et al., 2012; Gueron and Shafrir, 2005; Pech, 1994). In the paper of Banjac et al. (2014), authors described one approach for the visualization of Weber's curve and surface. In the paper (Banjac et al. 2013), authors verified one conjecture that relates to the Erdös-

Mordell curve. The paper (Petrović et al., 2018) deals with the simplest representatives of Weberian focal-directorial generated two-dimensional entities – conic sections.

2. THE RESEARCH

2.1. Analytical representation

The Erdös-Mordell inequality for a triangle $R_1 + R_2 + R_3 \geq 2(r_1 + r_2 + r_3)$ when interpreted as the Fermat-Torricelli-Weber problem has the following formulation: the trifocal distances' sum of a triangle is larger than or equal to the double value of the tri-directorial distances' sum of the triangle (foci are the vertices, and directrices are the sides of the triangle). The above expression for the case of equality can be formulated as the following:

$$a_1R_1 + a_2R_2 + a_3R_3 + b_1r_1 + b_2r_2 + b_3r_3 = S, \tag{1}$$

where R_1, R_2, R_3 are the Euclidean distances to the foci (polygon vertices) and r_1, r_2, r_3 are the Euclidean distances to the directrices (polygon sides). The Weber weight coefficients corresponding to the distances from the foci are equal to unit coefficients $a_1 = a_2 = a_3 = 1$, while the Weber weight coefficients corresponding to the distances from the directrices are also equal, albeit with negative weight values $b_1 = b_2 = b_3 = -2$ and the parameter S equals zero.

We generate a Weberian focal-directorial 3D element in such a way that, for every point on the surface $T(x, y, z)$, it holds that its first projection coincide with the respective point $M(x, y)$ of the triangle plane $(T'(x, y) \equiv M(x, y))$, while its z-coordinate is represented with the difference between the focal distances' sum and the double value of the directorial distances' sum:

$$z = R_1 + R_2 + R_3 - 2(r_1 + r_2 + r_3). \tag{2}$$

Furthermore, we generalize this problem by defining Weberian focal-directorial surfaces (WFDS) which originates from the Erdös-Mordell inequality (EMI) for regular polygons:

$$z = R_1 + \cdots + R_k - w(r_1 + \cdots + r_k), \tag{3}$$

where k is the number of sides of a regular polygon and $w = 1/\cos(\pi/k)$ is the Weber weight coefficient.

Let R_i be the Euclidean distances to the foci $F_i(x_i, y_i)$ i.e. polygon vertices

$$R_i = \sqrt{(x - x_i)^2 + (y - y_i)^2}, \tag{4}$$

and let r_i be the Euclidean distances to the directrices $d_i\big(F_i(x_i, y_i),\ F_{i+1}(x_{i+1}, y_{i+1})\big)$ i.e. polygon sides

$$r_i = \frac{|y(x_{i+1} - x_i) + x(y_i - y_{i+1}) + x_i y_{i+1} - x_{i+1} y_i|}{\sqrt{(x_{i+1} - x_i)^2 + (y_{i+1} - y_i)^2}}, \tag{5}$$

where $i = 1, \cdots, k$. The coordinates of regular polygon vertices are $x_i = \cos(2\pi i/k)$ and $y_i = \sin(2\pi i/k)$, if the polygon inscribed into unit circle and $F_1 \equiv F_{k+1}$ is satisfied.

2.2. Graphical representation

In this section of our paper we present the graphical representation of WFDS which are defined by the equation *(3)* for $k = 3\ldots6$. Each surface is represented in three orthogonal projections and an axonometry (Fig. 1 – Fig. 4).

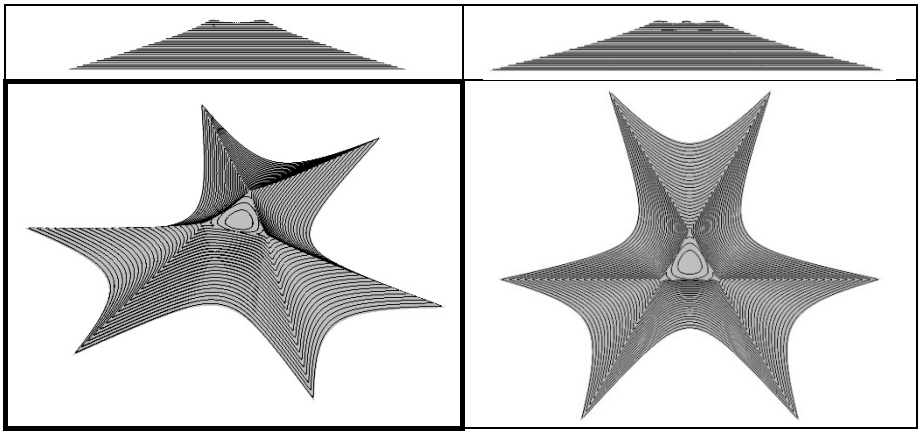

Figure 1. WFDS: $k = 3$;

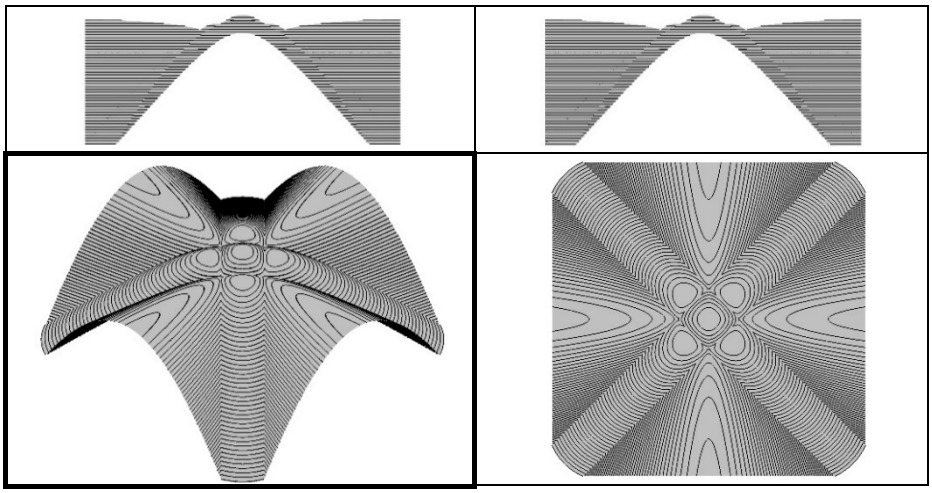

Figure 2. WFDS: k = 4;

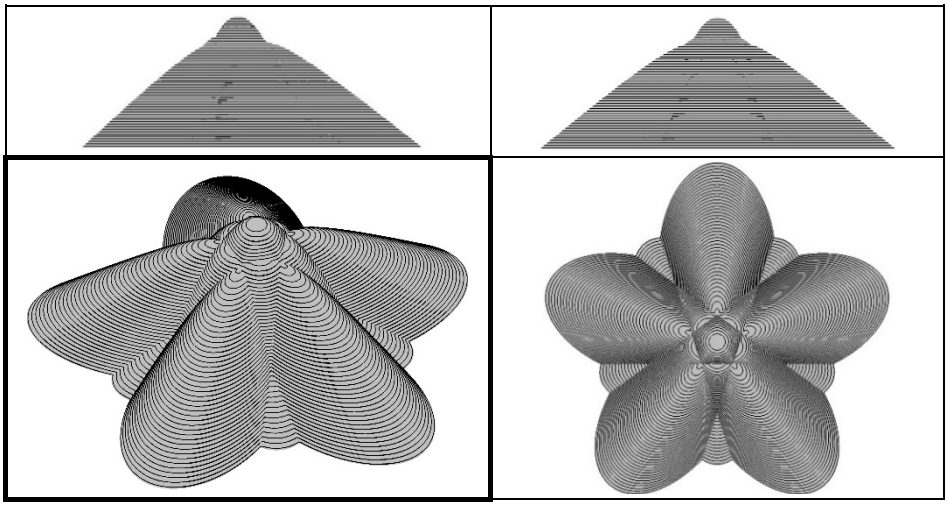

Figure 3. WFDS: $k = 5$;

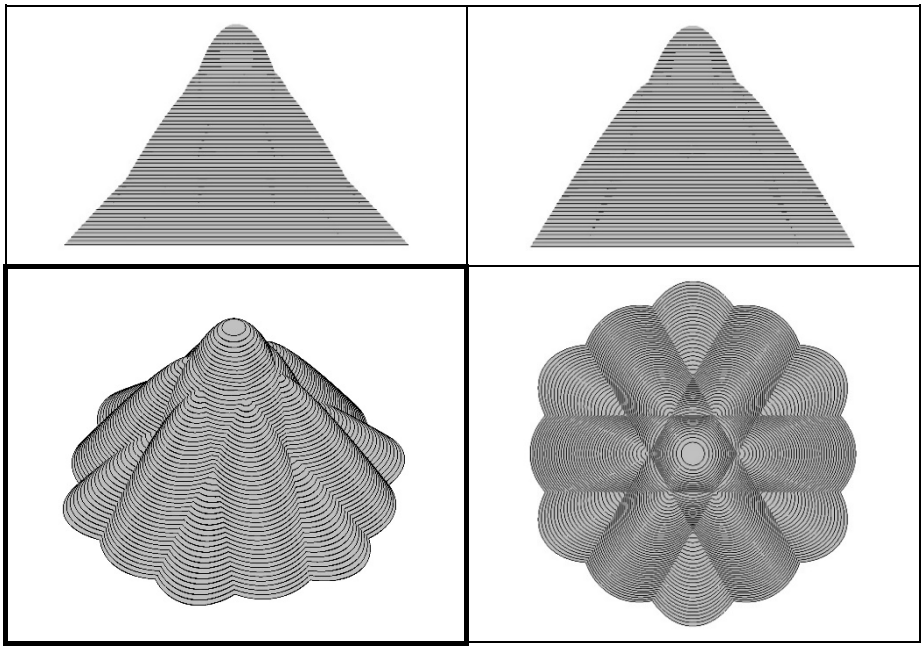

Figure 4. WFDS: $k = 6$.

Geometrical forms which are obtained from the equation (3) and given in Figures 1 – 4 are generated by the free mathematics visualization tool VisuMath 3.0 (2015).

2.3. Possibility of application in architecture

Fig. 5 (a and b) shows parts of surfaces which belong to the group of surfaces (WFDS) generated as a visual interpretation of the Erdös-Mordell inequality for a square (Fig. 2). The modelled part of the surface is reminiscent of a bird with its wings spread out (Fig. 5a). The use of the skeletal system in the structural formation of a building can be found in the works of the Spanish architect Santiago Calatrava.

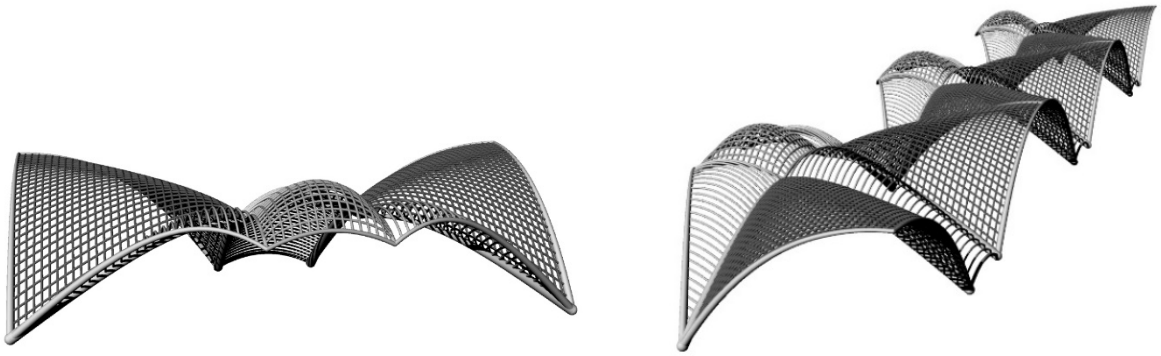

Figure 5. WFDS: a) $k = 4$; part of surface (Fig. 2) b) $k = 4$; multiplication of surface (a)

WFDS generated in this way, for values of $k > 4$, can have a geometrically bionic form (Fig. 3 and Fig 4) and as such may have uses in architectural design (Fig. 7).

The regular octagon as the base for obtaining WFDS enables us to create various bionic forms which in its totality incorporates multitude close/open spatial curved polygons. In the Fig. 6 it can be noticed, apart from the base regular octagon, spatial curved triangles and quadrilaterals, either open or close, appear.

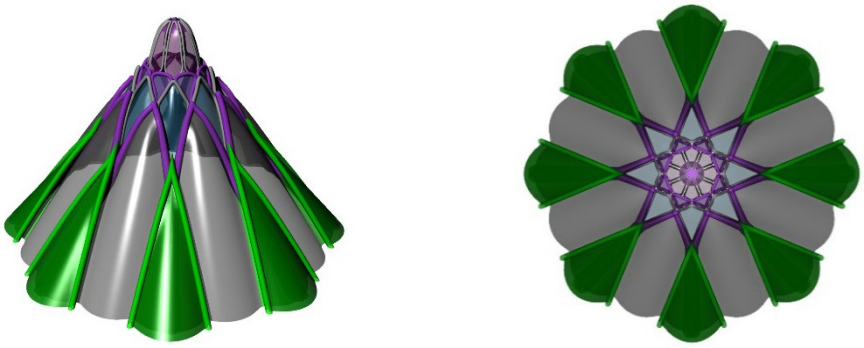

Figure 6. WFDS: a) $k = 8$; b) $k=8$; top view

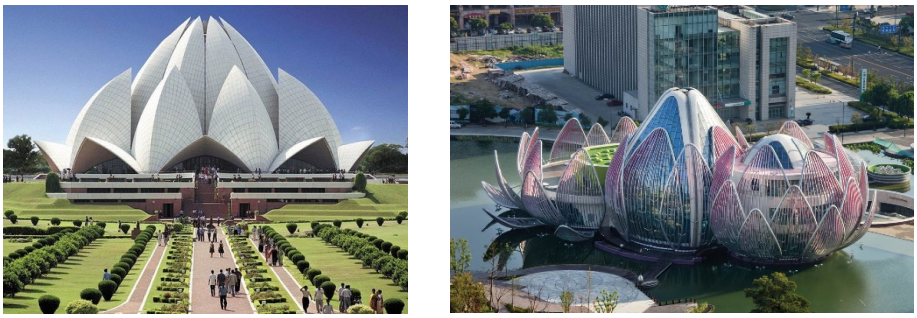

Figure 7. Bionic architecture (left: the Lotus Temple in New Delhi, India, by Fairiborz Sahba (1986), Source: https://www.archdaily.com/158522/ad-classics-lotus-temple-fariborz-sahba/; right: the Lotus Building in Wujin, China, by Studio 505 (2013) , Source: https://www.db-a.co/work/the-lotus-building/)

3. CONCLUSIONS

In this paper focal-directorial generated 3D elements as spatial interpretation of certain geometric inequalities for regular polygons have been presented. Due to their geometrically deterministic forms, flexibility of shapes and compatibility with feasible structure featuring in recent trends in design, focal-directorial 3D generated elements may be characterized as a designing pattern of an architectural-urban space.

Acknowledgements. This research was supported by the Ministry of Education, Science and Technological Development of the Republic of Serbia.

REFERENCES

1. Banjac, B., Malešević, B., Petrović, M. and Obradović, M., 2013. A Computer Verification of a Conjecture About the Erdös-Mordell Curve. In Proceedings of 21st Telecommunications Forum TELFOR 2013, Belgrade, Serbia, pp. 1031–1034.
2. Banjac, B., Petrović, M. and Malešević, B., 2014. Visualization of Weber's curves and surfaces with applications in some optimization problems. In Proceedings of 22nd Telecommunications Forum TELFOR 2014, Belgrade, Serbia, pp. 1003–1006.
3. Gueron, S. and Shafrir, I., 2005. A weighted Erdős–Mordell inequality for polygons. Am. Math. Monthly 112(3), pp. 257–263.
4. Liu, J., 2020. An improved result of a weighted trigonometric inequality in acute triangles with applications. Journal of Mathematical Inequalities, 14(1), 147–160.
5. Liu, J., 2019. New Refinements of the Erdös–Mordell Inequality and Barrow's Inequality. Mathematics 2019, 7(8), 726, pp. 1–12.

6. Liu, J., 2018a. New Refinements of the Erdös–Mordell Inequality. Journal of Mathematical Inequalities, 12(1), 63–75.
7. Liu, J., 2018b. Two New Weighted Erdős–Mordell Type Inequalities. Discrete & Computational Geometry 59(3), pp. 707–724.
8. Malešević, B., Petrović, M., Obradović, M. and Popkonstantinović B., 2014. On the Extension of the Erdös-Mordell Type Inequalities. Mathematical Inequalities and Applications 17 (1), pp. 269–281.
9. Minculete, N. (2012). Several geometric inequalities of Erdös-Mordell type in the convex polygon, In International Journal of Geometry 1(1), pp. 20–26.
10. Obradović, M., Malešević, B., Petrović, M. and Popkonstantinović, B., 2012. One application of the cone surfaces on the Erdös-Mordell inequality. In Proceedings of 3rd International Scientific Conference moNGeometrija 2012, Novi Sad, Serbia, pp. 335–351.
11. Pech, P., 1994. Erdös–Mordell inequality for space n-gons. Math. Pannon. 5(1), pp. 3–6.
12. Petrović, M., 2019. Geometric Genesis and Form Variation of Focal-Directorial Curves and Surface - Plenary lecture. In: Book of Abstracts of the 21st Scientific-Professional Colloquium on Geometry and Graphics, Sisak, Croatia, pp. 5–7.
13. Petrović M., 2016. Generating the focal-directorial geometric forms as a designing pattern of the architectural-urban space (in Serbian: Generisanje fokalno-direktrisnih geometrijskih formi kao obrasca za oblikovanje arhitektonsko-urbanističkog prostora), Doctoral dissertation, University of Belgrade, Faculty of Architecture, 2016, available at: http://nardus.mpn.gov.rs/handle/123456789/8043
14. Petrović, M., Malešević, B., Štulić, R., Vučić, M. and Mijailović, R., 2018. Spatial Interpretation of Fermat-Weber's Set of Points over Conic Sections. In Proceedings of 6th International Scientific Conference MoNGeometrija 2018, Novi Sad, Serbia, pp. 440–445.
15. VisuMath 3.0 by Ignace Van de Woestyne (Downloads a free mathematics visualization tool designed for research and educational purposes), 2015. http://www.visumath.be/ [Accessed: 30th May 2015].

VISUALIZATION OF SINGULAR QUADRIC SECTIONS OF FOUR-DIMENSIONAL CONES

Michal Zamboj
Department of Mathematics and Mathematics Education, Charles University, Prague, Czech Republic
Ph.D., Assistant Professor, michal.zamboj@pedf.cuni.cz

ABSTRACT

Recently, we have studied four-dimensional synthetic constructions of real regular quadric sections of four-dimensional cones with an ellipsoidal (for unruled quadrics) and a one-sheet hyperboloidal (for ruled quadrics) directrix in the affine classification. The four-dimensional space is visualized in the double orthogonal projection onto two mutually perpendicular 3-spaces, in which a four-dimensional object is represented by its two conjugated three-dimensional images in one modeling 3-space. This way, tools of the classical descriptive geometry are generalized and conveniently used with interactive computer graphics for synthetic constructions in the four-dimensional space. In this contribution, synthetic constructions of all the real singular quadrics in the double orthogonal projection are carried out. Each singular three-dimensional quadric is ruled, and hence for finding the most of real cases, we choose hypercones containing a one-sheet hyperboloid. Spatial sections of a one-sheet hyperboloidal hypercone through its singular point (vertex) are three dimensional real cones or two real planes intersecting in a line. Considering a hypercone with an improper singular point (i.e. four-dimensional hypercylinder) with a one-sheet hyperboloidal directrix, the following spatial sections: an elliptic, parabolic, and hyperbolic cylinder, or two parallel planes; can be derived. Furthermore, to obtain a double plane, or a proper and improper planes, as spatial sections, we choose a singular four-dimensional quadric with at least a singular line. We visualize hyperquadrics with their spatial sections in the double orthogonal projection and support the constructions with their analytic derivations in the projective extension of the real space. All visualizations are supplemented with interactive 3D models with step-by-step constructions. The purpose of the presented work is to show how a generalization of descriptive geometry methods of Monge's projection is applied for a deeper understanding and investigation of the properties of four-dimensional hyperquadrics.

Keywords: four-dimensional visualization; double orthogonal projection; descriptive geometry; quadrics; computer graphics

INTRODUCTION

Conics are often defined as planar sections of quadratic conical and cylindrical surfaces. Constructions of their images in various projections are fundamental parts of descriptive geometry or methods of visualization. The study of these images is important for a deeper understanding of synthetic properties of conics. We use a similar method to construct images of quadrics as spatial sections of quadratic conical or cylindrical hypersurfaces in the four-dimensional space. For a comprehensive study of synthetic and analytic properties of conics and quadrics with the emphasis on the visual aspect see (Glaeser et. al. 2016; Odehnal et al. 2020). For a detailed synthetic view on the projective geometry of quadrics see (Baker; 1923). For the analytic geometry of quadrics in the projective extension of the real space see (Semple et al; 1952, Part II, Chapter IX) or (Cassas-Alvero, 2014, Chapters 6–7).

To visualize images of objects in the four-dimensional space, we use the method of the double orthogonal projection of the 4-space onto two mutually perpendicular 3-spaces. The method is an analogy to Monge's orthogonal projection of 3-dimensional objects onto two mutually perpendicular planes. Constructions of three-dimensional images of elementary four-dimensional objects are described in (Zamboj; 2018a), constructions of spatial sections of polytopes in (Zamboj; 2018b).

As same as regular conics are collinear images of the directing circle of a circular cone, regular quadrics are collinear images of the directing quadric of the given hypercone. Furthermore, collineation preserves collinearity, and hence we need different directing quadrics to derive ruled and unruled quadrics. Particularly, unruled regular quadrics: an ellipsoid, two-sheet hyperboloid, and paraboloid are spatial sections of a conical hypersurface with a spherical directrix, i.e. a surface generated by joining points of a sphere with noncospatial vertex. Ruled regular quadrics: a one-sheet hyperboloid and hyperbolic paraboloid, are spatial sections of a conical hypersurface with a one-sheet hyperboloidal directrix. The affine classification and constructions of regular quadric sections of conical hypersurfaces are described in (Zamboj; 2019). Parallel sections of hypercones and multidimensional analogies are discussed in (Zamboj; 2020). In this contribution, the classification and constructions of real singular cases of quadric sections are finalized.

2. PRELIMINARIES

2.1. The double orthogonal projection of the 4-space onto two mutually perpendicular 3-spaces

Some necessary preliminary constructions in the double orthogonal projection are summarized from the references above in the following lines. In Monge's projection, a point $P(x_P, y_P, z_P)$ is orthogonally projected into the horizontal plane $\pi(x, y)$ and vertical plane $\nu(x, z)$. The plane ν is chosen to be the *drawing* (*picture*) *plane*, and the plane π is rotated about the x-axis to the drawing plane such that the axes z and y have opposite directions. After the rotation, both orthogonal images – the top view $P_1(x_P, y_P)$ in π and the front view $P_2(x_P, z_P)$ in ν, lie on the *ordinal line* (or *line of recall*) perpendicular to the x-axis in the drawing plane. The principle of Monge's projection of a circular cone of revolution with its base in π is visualized in Figure 1a.

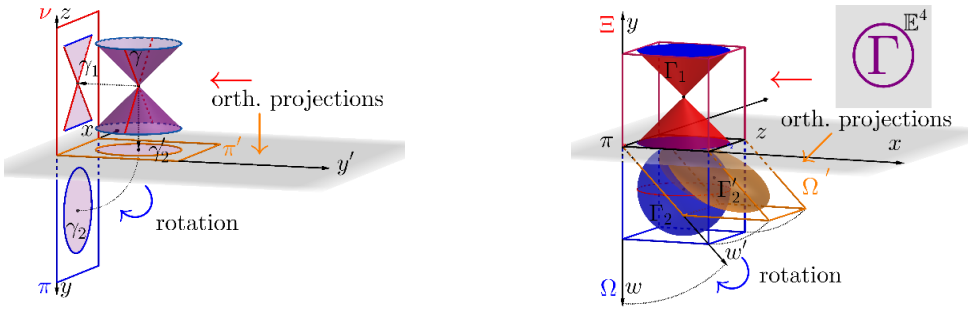

(a) **(b)**

Figure. 1: (a) Principle of Monge's projection – visualization of a circular cone, and (b) principle of the double orthogonal projection – visualization of a spherical hypercone.

In the four-dimensional case with the coordinate axes x, y, z, w, a point $P(x_P, y_P, z_P, w_P)$ is orthogonally projected into mutually perpendicular 3-spaces $\Xi(x, y, z)$ and $\Omega(x, y, w)$. Let Ω be a modeling 3-space and Ξ is rotated about the plane $\pi(x, y)$ into this *modeling 3-space*. After the rotation, the images $P_3(x_P, y_P, z_P)$ (Ξ-image) and $P_4(x_P, y_P, w_P)$ (Ω-image) lie in the modeling 3-space on a perpendicular to $\pi(x, y)$ – *ordinal line*. The principle of the double orthogonal projection of spherical hypercone with its spherical base in the 3-space Ξ is visualized in Figure 1b.

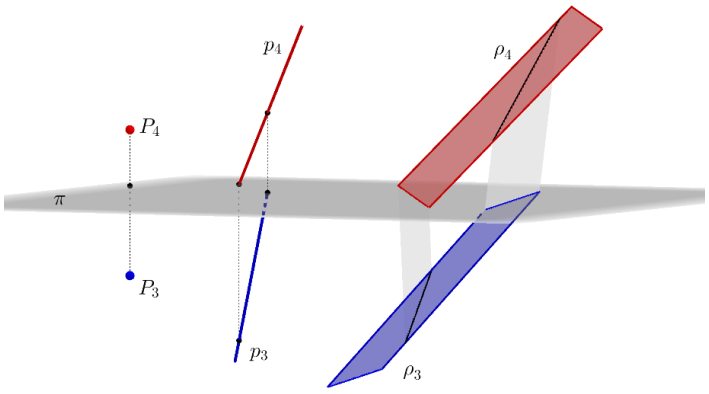

Figure. 2: Conjugated images of a point, line, and plane. Intersections with reference 3-spaces are highlighted
Interactive model: https://www.geogebra.org/m/zhztkfnp

The modeling 3-space, in which we perform our constructions is a virtual three-dimensional space. The observer can move in this 3-space to any point. For this reason, we supplement our (two-dimensional) figures with 3D interactive models in the GeoGebra Book (Zamboj, 2020b).[1]

Similarly to Monge's projection, points, lines, and planes in general positions (with respect to the reference system) in the 4-space have two conjugated images (Figure 2).

A 3-space is represented by its intersections with the 3-spaces Ξ and Ω, called *traces* (Figure 3).

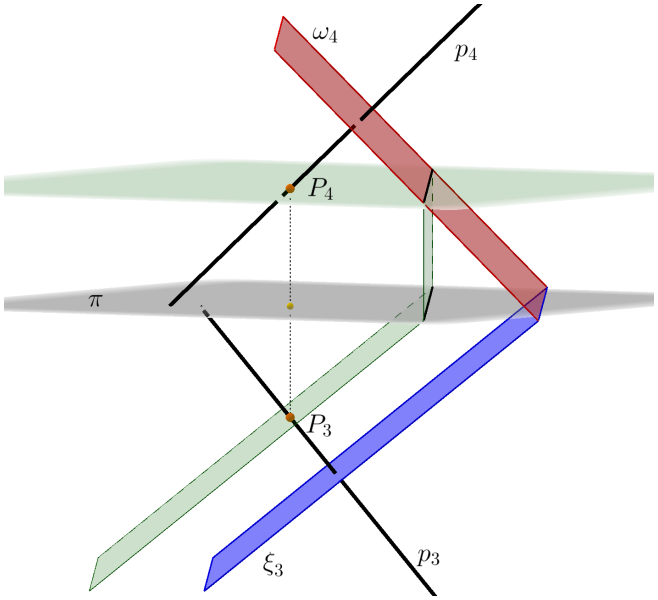

Figure. 3: A visualization of a 3-space **Σ** given by its traces **ω** and **ξ**. A point ***P*** lies in **Σ** and is located in a plane parallel to **ξ**. Images of a perpendicular ***p*** to **Σ** through ***P*** are perpendiculars to images of the traces
Interactive model: https://www.geogebra.org/m/yduyywqe

Constructions of true shapes, measuring lengths and angles in the double orthogonal projection are straightforward generalizations of constructions in the Monge's projection.

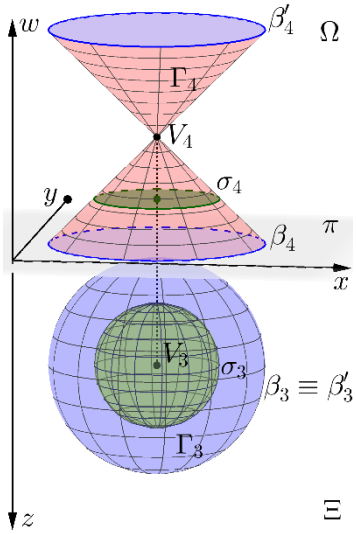

Figure. 4: Conjugated images of a spherical hypercone **Γ** with a base sphere ***β*** and a spherical section ***σ*** of **Γ** and a 3-space parallel to the reference 3-space $\Xi(x, y, z)$
Interactive model: https://www.geogebra.org/m/unmtdar5

To understand further constructions of images of various hypercones and hypercylinders, we demonstrate the visualization on a spherical hypercone described above. Let Γ be a right spherical hypercone with a directing

[1] Since the figures are only projections of three-dimensional models, we highly recommend the reader to follow the interactive visualizations.

sphere β in the 3-space Ξ and a vertex V on the axis perpendicular to Ξ, through the center of β (Figure 4). We restrict the hypercone between the 3-spaces Ξ and a parallel 3-space Ξ' such that V has the same distance from either of them. Consecutive parallel sections of Γ from Ξ to Ξ' are spheres shrinking to a point V and extending back to the same size in Ξ'. Their Ξ-images fill a ball with the apparent contour being the bounding sphere β. Their Ω-images are discs filling the double cone with the vertex V.

2.2. Analytic representation of singular quadric hypersurfaces

It is suitable to support synthetic constructions in the next section with their analytic derivations. In the projective extension of the real four-dimensional space $\mathbb{RP}^4$ with homogenous coordinates x_1, x_2, x_3, x_4, and x_0, the 3-space $\Xi(x, y, z)$ is extended to $\Xi(x_1, x_2, x_3, x_0)$ and the 3-space $\Omega(x, y, w)$ to $\Omega(x_1, x_2, x_4, x_0)$. For the affine classification, we assume that improper (infinite) points have the last coordinate $x_0 = 0$. Four-dimensional quadratic conical and cylindrical hypersurfaces are hyperquadrics with a unique proper or improper singular point, respectively. For example, the conical hypersurface with a spherical (or affinely ellipsoidal) directrix used in the previous section has the canonical equation for the vertex translated into the origin:

$\Gamma: x_1^2 + x_2^2 + x_3^2 - x_4^2 = 0$ (Eq. 1)

For a derivation of singular quadric sections: a quadratic cone and intersecting planes, we use the conical hypersurface with a one-sheet hyperboloidal directrix with the following canonical equation:

$\Gamma: x_1^2 + x_2^2 - x_3^2 - x_4^2 = 0$ (Eq. 2)

For a derivation of singular quadric sections: an elliptic, parabolic, and hyperbolic cylinder, and parallel planes, we use the cylindrical hypersurface with a one-sheet hyperboloidal directrix and an improper vertex with the following equation:

$\Gamma: x_1^2 + x_2^2 - x_4^2 - x_0^2 = 0$ (Eq. 3)

For a derivation of a double proper plane, double improper plane, or intersecting proper and improper planes, we use the following quadric hypersurface with an improper singular line and the equation:

$\Gamma: x_1^2 - x_4^2 + x_0^2 = 0$ (Eq. 4)

Quadric hypersurfaces Γ given by Equations 2 – 4 will be consecutively cut with 3-spaces Σ in different positions. We intentionally skip the hypersurface Γ given by Equation 1, since its real intersections with a 3-space are derived from the other cases. Imaginary singular quadric sections are not visualized and also omitted in the analytic derivation. They could be derived in the similar fashion: an imaginary quadratic conical surface (with a real vertex) and imaginary intersecting planes as sections of Γ given by Equation 1; imaginary parallel planes as a section of Γ given by Equation 4; and for an imaginary quadratic cylindrical surface we could use an equation of another hypersurface, e.g. the following cylindrical hypersurface with a two-sheet hyperboloidal directrix and an improper singular point:

$\Gamma: x_1^2 + x_2^2 - x_4^2 + x_0^2 = 0$ (Eq. 5)

3 SINGULAR QUADRIC SECTIONS

Analytic derivations and synthetic constructions of images of quadric hypersurfaces and their sections are discussed in the following section. For the sake of simplicity, analytic equations are given in their canonical forms. On the other hand, for the sake of visualization in the constructions of images in the double orthogonal projection, the reference system is translated such that Ξ and Ω-images do not overlap.

3.1. Singular quadric sections of a one-sheet hyperboloidal conical hypersurface with a 3-space

Analytic derivation

Let us have a one-sheet hyperboloidal conical hypersurface Γ defined by Equation 2 and a 3-space Σ, perpendicular to Ω through the vertex V, given by the equation:

$\Sigma: x_4 = \alpha x_1, \alpha \in \mathbb{R}$ (Eq. 6)

By substituting Equation 5 into Equation 2, we obtain sections of Γ with Σ, dependant on the parameter α:

$\kappa: x_1^2(1 - \alpha^2) + x_2^2 - x_3^2 = 0$ (Eq. 7)

In the 3-space $\Xi(x_1, x_2, x_3, x_0)$, Equation 7 is the equation of a singular quadric κ. For $\alpha \neq \pm 1$, the equation represents a quadratic conical surface, and in the case of $\alpha = \pm 1$, two proper intersecting planes.

In our visualizations, each conical hypersurface is represented by a spatially restricted hypercone (Figure 5). Images of the hypercone are defined by their apparent contours, which are projections of contour generators into the 3-spaces of projection (Ξ and Ω) in orthogonal directions of w and z axes, respectively. Let $\boldsymbol{A}$ be the matrix of the conical hypersurface Γ defined by Equation 2. The polar 3-space of the point Z_∞ with respect to Γ has coordinates:

$$Z_\infty^T \boldsymbol{A} = (0,0,1,0,0) \begin{pmatrix} 1 & 0 & 0 & 0 & 0 \\ 0 & 1 & 0 & 0 & 0 \\ 0 & 0 & -1 & 0 & 0 \\ 0 & 0 & 0 & -1 & 0 \\ 0 & 0 & 0 & 0 & 0 \end{pmatrix} = (0,0,-1,0,0)^T,$$

and hence the contour generator in the z-direction is the intersection of the polar 3-space $x_3 = 0$ and Γ, with the equation:

$$x_1^2 + x_2^2 - x_4^2 = 0 \qquad \text{(Eq. 8)}$$

The apparent contour Γ_4 – orthogonal projection of the contour generator in the direction of the z-axis into the 3-space Ω is the asymptotic elliptical quadratic cone with the same equation. By restriction of Γ with the 3-spaces $x_3 = \pm x_0$, parallel to Ξ, we obtain overlapping bounding one-sheet hyperboloids in Ω carrying the same equation as their orthogonal projection into Ω:

$$x_1^2 + x_2^2 - x_4^2 - x_0^2 = 0 \qquad \text{(Eq. 9)}$$

With respect to the symmetry of the coordinates x_3 and x_4 in the equation of Γ, the apparent contour Γ_3 is also the asymptotic elliptical cone in Ξ with the equation:

$$x_1^2 + x_2^2 - x_3^2 = 0 \qquad \text{(Eq. 10)}$$

Similarly, boundaries of Γ after the restriction with the 3-spaces $x_4 = \pm x_0$, parallel to Ω are overlapping one-sheet hyperboloids in Ξ with the equation:

$$x_1^2 + x_2^2 - x_3^2 - x_0^2 = 0 \qquad \text{(Eq. 11)}$$

Synthetic construction (Figure 5)

Let us have a one-sheet hyperboloidal hypercone Γ given by a directing one-sheet hyperboloid of revolution in the 3-space Ξ with the axis of revolution perpendicular to π, and a noncospatial vertex V on a line in the w-direction through the center of the hyperboloid. From the analytic derivation, the conjugated images Γ_3 and Γ_4 are bounded by one-sheet hyperboloids of revolution (cf. Equation 9, 11) and their asymptotic cones (cf. Equation 8, 10). In the given position, the angle ψ of a generatrix z of the asymptotic cone with the reference plane π appears in its true size in the Ω-image.

The 3-space Σ, perpendicular to Ω through V (cf. Equation 6), is given by its traces ω_4^Σ and ξ_3^Σ, and the angle φ between Σ and Ξ is the same as the angle between ω_4^Σ and π. In this position, Ω-images of all points in Σ are in ω_4^Σ. The resulting quadric section depends on the relation between φ and ψ (cf. Equation 7 with the parameter α).

(a) For $\varphi \neq \psi$, the resulting section κ is a right elliptical quadratic cone. For $\varphi < \psi$ (Figure 5a), the image κ_4 is the intersection of Γ_4 with ω_4^Σ, which is an ellipse with vertices A_4, B_4, C_4, and D_4,with its inner points, given as the intersection of the plane ω_4^Σ and the bounding one-sheet hyperboloid of Γ_4. The Ξ-image κ_3 is a right elliptical cone with the axis through V_3 perpendicular to π, and vertex V_3. The Ξ-images A_3, B_3, C_3, and D_3 of vertices of the bounding ellipse of κ_4 lie in π. They are vertices of the directing ellipse of the cone κ_3. For $\varphi > \psi$ the intersection κ_4 of Γ_4 with ω_4^Σ is a hyperbola, and the corresponding right elliptical quadratic cone κ_3 has its axis parallel to the x-axis.

(b) For $\varphi = \psi$ (Figure 5b), the intersection κ_4 of Γ_4 with ω_4^Σ consists of two intersecting planes (restricted to rectangles). In the Ω-image, the trace ω_4^Σ is tangent to a generatrix of the asymptotic cone of Γ_4 and intersects its bounding one-sheet hyperboloid in a rectangle κ_4, or explicitly $A_4B_4C_4D_4$ with sides A_4B_4 and C_4D_4 on parallel generatrices. Since the bounding hyperboloid is the Ω-image of the intersection of restricting 3-spaces with the conical hypersurface, the rectangle $A_4B_4C_4D_4$ overlaps with $A'_4B'_4C'_4D'_4$. The Ξ-images $A_3B_3C_3D_3$ and $A'_3B'_3C'_3D'_3$ are rectangles

symmetrical with respect to the plane parallel to π through V_3. The sides A_3D_3 and B_3C_3 lie on the generatrices of the bounding one-sheet hyperboloid of Γ_3.

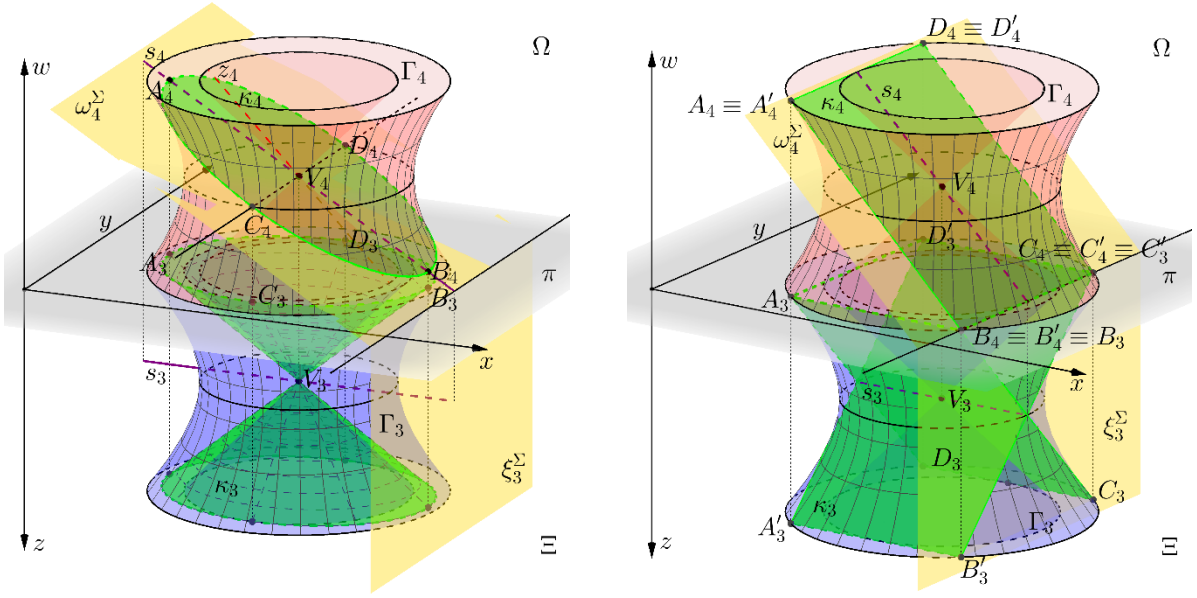

(a) **(b)**

Figure. 5: Singular quadric sections **κ**: (a) an elliptical cone, (b) intersecting rectangles; of a one-sheet hyperboloidal hypercone **Γ** with a 3-space **Σ**
Step-by-step constructions: (a) https://www.geogebra.org/m/jkya2t5k (b) https://www.geogebra.org/m/rrf9kz8b

3.2. Singular quadric sections of a one-sheet hyperboloidal cylindrical hypersurface with a 3-space

Analytic derivation

For the second case, let us have a one-sheet hyperboloidal conical hypersurface Γ defined by Equation 3, and, again, a 3-space Σ, perpendicular to Ω, given by Equation 5. The quadric κ of intersection of Γ and Σ has the following form:

$$\kappa: x_1^2(1-\alpha^2) + x_2^2 - x_0^2 = 0 \qquad \text{(Eq. 12)}$$

In case of $\alpha \in (-1,1)$, κ is an elliptic cylindrical surface, in case of $\alpha \in (-\infty,-1) \cup (1,\infty)$, κ is a hyperbolic cylindrical surface, and if $\alpha = \pm 1$, κ consists of two parallel planes.

To obtain a parabolic cylindrical surface, we choose the cutting 3-space Σ in the following form:

$$\Sigma: x_4 = x_1 - x_0 \qquad \text{(Eq. 13)}$$

After the substitution into Equation 3 of Γ, the quadric section κ is a parabolic cylinder with the equation:

$$\kappa: x_2^2 + 2x_1x_0 - 2x_0^2 = 0 \qquad \text{(Eq. 14)}$$

The directrix of the one-sheet hyperboloidal cylindrical hypersurface Γ is the one-sheet hyperboloidal surface given by Equation 3 in the 3-space Ω. Therefore the Ω-image is the given one-sheet hyperboloidal surface itself.

The Ξ-image Γ_3 is given by the apparent contour – elliptic cylindrical surface:

$$x_1^2 + x_2^2 - x_0^2 = 0 \qquad \text{(Eq. 15)}$$

and restricted between the parallel 3-spaces $x_4 = \pm x_0$ by another overlapping elliptic cylindrical surface:

$$x_1^2 + x_2^2 - 2x_0^2 = 0 \qquad \text{(Eq. 16)}$$

Synthetic construction

Let us have a one-sheet hyperboloid in the 3-space Ω, and let the one-sheet hyperboloidal cylinder Γ be generated by this one-sheet hyperboloid and the direction of the z-axis (improper singular point). Moreover, Γ is restricted between the 3-space Ξ and a 3-space parallel to Ξ, and Ω and parallel to Ω. The Ω-image Γ_4 is given by the set of points between the asymptotic cone (cf. Equation 15) and restricting one-sheet hyperboloid (cf. Equation 16), analogically to the case of the one-sheet hyperboloidal hypercone in Section 3.1. The angle ψ between a generatrix z of the asymptotic cone and π is in its true size in the Ω-image. The Ξ-image Γ_3 is the cylindrical shell between coaxial boundary circular right cylinders. The radius of the circular base of the inner cylinder is the same as the radius of the neck circle of the base hyperboloid that is in the true shape in the Ω-image. The radius of the circular base of the outer cylinder is given by the restricting 3-spaces.

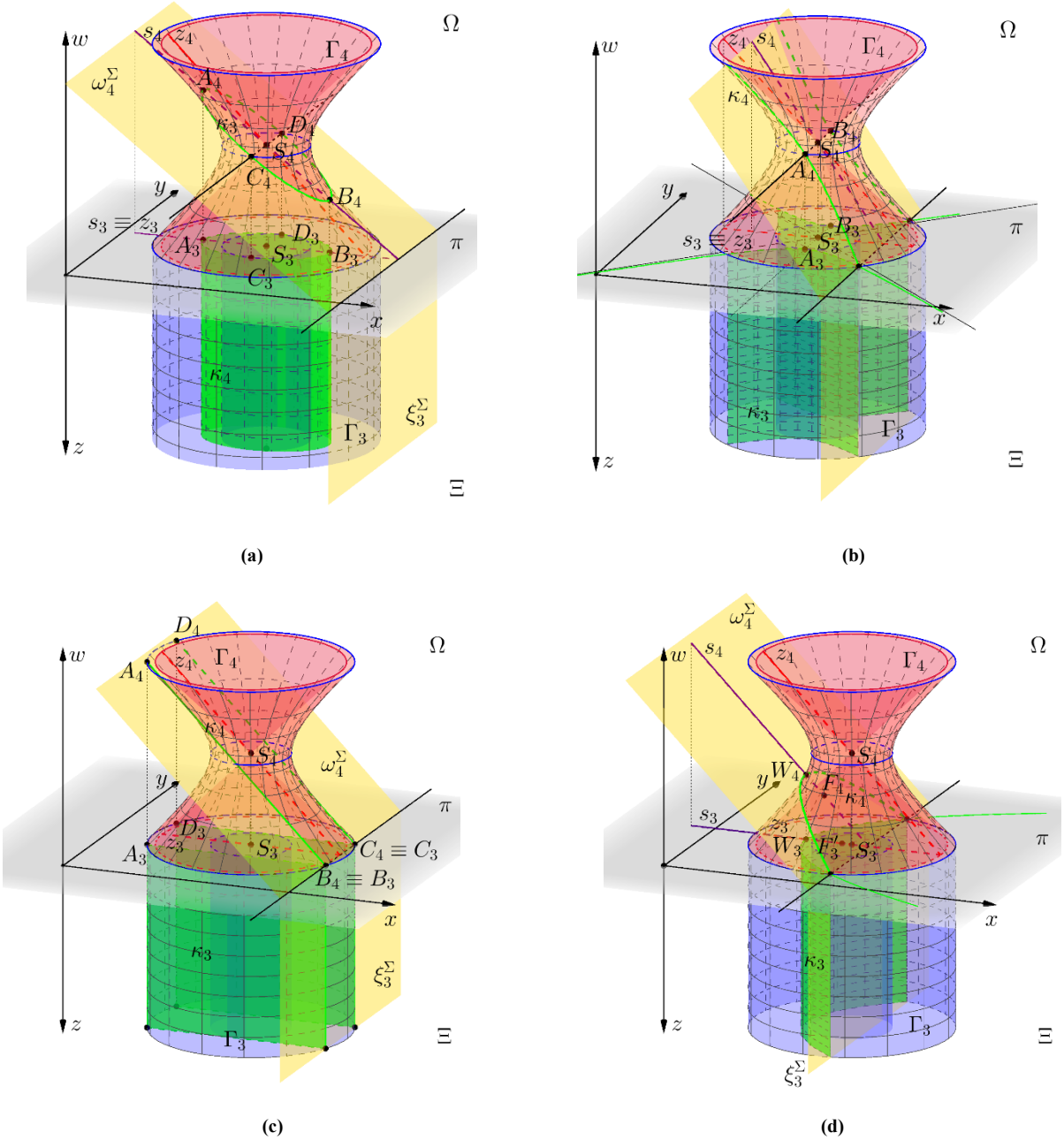

Figure. 6: Singular quadric sections **κ**: (a) an elliptic cylinder, (b) a hyperbolic cylinder, (c) parallel rectangles, (d) a parabolic cylinder; of a one-sheet hyperboloidal hypercylinder **Γ** with a 3-space **Σ**
Step-by-step constructions: (a) https://www.geogebra.org/m/xqgs4dfq (b) https://www.geogebra.org/m/kvxzecka
(c) https://www.geogebra.org/m/g6zynzqc (d) https://www.geogebra.org/m/ap6uxt7f

The cutting 3-space Σ is perpendicular to Ω, and so the angle φ between Σ and Ξ is preserved in the Ω-image. Different kinds of singular quadric sections are obtained by the following choices of Σ:

Let the center S of the hyperboloidal base lie in Σ (cf. Equation 12).

(a) In the case of $\varphi < \psi$, the section κ is an elliptic cylinder (Figure 6a). The difference between the angles φ and ψ is constructed with the use of the slope line s of Σ (i.e. a line of the 3-space perpendicular to its trace) through S and the generatrix z of the asymptotic cone in the ordinal plane of s. The Ω-image κ_4 is the intersecting ellipse of the one-sheet hyperboloid Γ_4 and the plane ω_4^Σ with vertices A_4, B_4, C_4, and D_4. The vertices of the directing ellipse of the elliptic cylinder κ_3 in the Ξ-image are the Ξ-images A_3, B_3, C_3, and D_3.

(b) If $\varphi > \psi$, the quadric section κ is a hyperbolic cylinder (Figure 6b). Again, the relation between φ and ψ can be derived from the Ω-images of the generatrix z of the asymptotic cone and the slope line s of Σ through S. The section of the one-sheet hyperboloid Γ_4 and the trace ω_4^Σ is a hyperbola κ_4. For the construction of the Ξ-image κ_3, we construct the image of the directing hyperbola of the cylinder. The vertices A_3 and B_3 of the directing hyperbola are Ξ-images of the vertices of κ_4, to construct the hyperbola, we can conveniently use its asymptotes, which are images of the asymptotes of κ_4.

(c) In the case of $\varphi = \psi$, the resulting section κ consists of two parallel planes (restricted to rectangles) (Figure 6c). The trace ω_4^Σ is tangent to the asymptotic cone. Therefore, κ_4 is the intersection of ω_4^Σ with the one-sheet hyperboloid Γ_4 composed of two parallel segments A_4B_4 and C_4D_4. In the Ξ-image, the segments A_3B_3 and C_3D_3 generate two rectangles parallel with the z-direction.

For the last case, the center S is not incident with Σ (cf. Equations 13,14).

(d) To obtain a parabolic cylinder κ, let again $\varphi = \psi$ (Figure 6d). The slope line s_4 of Σ is parallel to the generatrix z_4 of the asymptotic cone of Γ_4. The section κ_4 of Γ_4 with ω_4^Σ is a parabola, with the vertex W_4 on s_4. The Ξ-image W_3 is the vertex of the directing parabola of the parabolic cylinder. To construct the directing parabola and its fundamental elements, we can use the tangent and normal of the parabola at the point of intersection with the directing circle of the restricting cylinder.

3.3. Singular quadric sections of a cylindrical hypersurface with a directing hyperbolic cylinder with a 3-space

Analytic derivation

Let a hypersurface Γ be defined by Equation 4. To obtain the proposed singular quadrics composed by planes, we choose special positions of the cutting 3-space Σ. Let the 3-space Σ be in the form of Equation 13:

$\Sigma: x_4 = x_1 - x_0$

In this special position, the quadric κ of intersection of Γ and Σ is formed by a proper and improper plane reduced to the form:

$\kappa: 2x_1x_0 = 0$ (Eq. 17)

Next, if Σ is given by the equation:

$\Sigma: x_4 = x_0$ (Eq. 18)

the quadric section κ is a double plane with the equation:

$\kappa: x_1^2 = 0$ (Eq. 19)

The last case is given by the following choice of the equation of the cutting 3-space Σ:

$\Sigma: x_4 = x_1$ (Eq. 20)

The corresponding intersection of Σ and Γ is the quadric κ formed by the double improper plane:

$\kappa: x_0^2 = 0.$ (Eq. 21)

The directrix of the hypersurface Γ is a hyperbolic cylindrical surface defined by Equation 4 in the 3-space Ω. Therefore, it is also the Ω-image Γ_4. The Ξ-image would fill the whole 3-space Ξ, and so we restrict it to a prism.

Synthetic construction

Let a right hyperbolic cylinder in the 3-space Ω with the axis of the cylinder parallel to the y-axis be the directrix of a hypercylinder Γ generated in the direction of the z-axis. The Ω-image Γ_4 is the directing hyperbolic cylinder and the Ξ-image is restricted to a rectangular cuboid. The angle ψ between an asymptotic plane ζ of the hyperbolic cylinder and the 3-space Ξ appears in its true size between ζ_4 and π in the Ω-image.

Let the 3-space Σ be perpendicular to Ω, and hence the size of the angle φ between Σ and Ξ is the same as between the trace ω_4^Σ and π. To finish the affine classification, we only need to visualize sections given by the following positions of the 3-space Σ:

(a) In the case of $\varphi = \psi$ and the axis of the hyperbolic cylinder Γ_4 does not lie in ω_4^Σ (cf. Equations 13 and 17), the quadric section κ is a proper plane and improper plane (Figure 7a). The intersection of Γ_4 and ω_4^Σ is a segment κ_4. The Ξ-image κ_3 of the section is a rectangle generated by the Ξ-image of the segment and the direction of the z-axis inside the area of the rectangular cuboid Γ_3.

(b) If the trace ω_4^Σ is a tangent plane to the hyperbolic cylinder Γ_4 (cf. Equations 18 and 19), the resulting quadric section κ consist of a double plane (Figure 7b). The construction of the Ξ and Ω-images is identical to the previous case.

(c) At last, if the trace ω_4^Σ is one of the asymptotic planes of the hyperbolic cylinder Γ_4 (cf. Equations 20 and 21), the intersection of Γ and Σ lie in the infinity on the double improper plane.

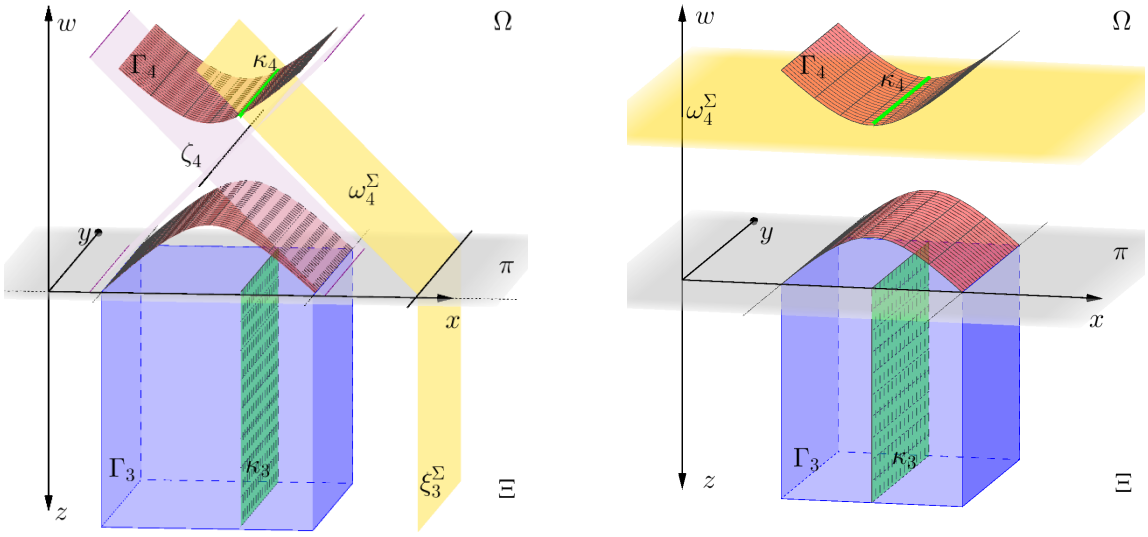

(a) **(b)**

Figure. 7: Singular quadric sections **κ**: (a) a rectangle and (b) a double rectangle; of a hypercylinder **Γ** with a hyperbolic cylindrical directrix with a 3-space **Σ**
Step-by-step constructions: (a) https://www.geogebra.org/m/p5dunny7 (b) https://www.geogebra.org/m/frq9mrcz

4 CONCLUSION

Throughout the paper, we have shown a synthetic method to visualize all the real singular quadrics with proper points as sections of singular quadratic hypersurfaces in the four-dimensional space. The provided graphical constructions were created in the double orthogonal projection of the 4-space onto two perpendicular 3-spaces. We tried to introduce the method of projection as a reliable way to study complicated four-dimensional objects synthetically, with the current possibilities of interactive 3D modeling software. In four-dimensional constructions, it is often easy to slip into faulty intuitive conclusions, and therefore our visualizations are always supported with analytic verifications. The affine classification of quadrics is usually treated analytically, and our

aim was not to discuss the classification itself but to perform their precise constructions as sections of hypersurfaces, and, also, to show the power of classical methods of descriptive geometry in a novel way.

ACKNOWLEDGMENT

The work was supported by the grant No. CZ.02.3.68/0.0/0.0/16_038/0006965, Faculty of Education, Charles University.

REFERENCES

Baker, H. F., 1923. Principles of geometry, vol. III. Cambridge University Press.

Cassas-Alvero, E., 2014. Analytic projective geometry. European Mathematical Society Publishing House, Zürich.

Glaeser, G., Stachel, H., and Odehnal, B., 2016. The Universe of Conics. Springer-Verlag Berlin Heidelberg.

Odehnal, B., Stachel, H., and Glaeser, G., 2020. The Universe of Quadrics. Springer-Verlag Berlin Heidelberg.

Semple, J. G. and Kneebone, G. T., 1952. Algebraic Projective Geometry. Oxford University Press, New York, USA.

Zamboj, M., 2018a. Double Orthogonal Projection of Four-Dimensional Objects onto Two Perpendicular Three-Dimensional Spaces. *Nexus Network Journal*, 20. pp. 267–281.

Zamboj, M., 2018b. Sections and Shadows of Four-Dimensional Objects. *Nexus Network Journal*, 21. pp. 475–487.

Zamboj, M., 2019. Quadric Sections of Four-Dimensional Cones. Proceedings of the 18th International Conference on Geometry and Graphics. ICGG 2018. Advances in Intelligent Systems and Computing, vol 809. Springer, Cham. pp. 500–513.

Zamboj, M., 2020a. Visualizing Objects of Four-Dimensional Space: From Flatland to the Hopf Fibration. Proceedings of the 19th Conference on Applied Mathematics Aplimat 2020. Slovak University of Technology, Bratislava, Slovakia. pp. 1140–1164.

Zamboj, M., 2020b. https://www.geogebra.org/m/vxzkjspw [Accessed: 22nd March 2020].

TOPIC 2: APPLIED GEOMETRY AND GRAPHICS

CONTENT

ABOUT THE GEOMETRY OF SOME FITTINGS USED IN FLAT-OVAL DUCTS

Carmen Mârza
Department of Building Services Engineering, Technical University of Cluj Napoca, Cluj Napoca, Romania
PhD., Associate Professor, Carmen.Marza@insta.utcluj.ro

Georgiana Corsiuc
Department of Building Services Engineering, Technical University of Cluj Napoca, Cluj Napoca, Romania
PhD., Lecturer, Georgiana@mail.utcluj.ro

Ana Maria Graur
Faculty of Architecture and Urban Planning, Technical University of Cluj-Napoca, Romania
PhD., Assistant, arh.anamariarusu@gmail.com

ABSTRACT

The classic solutions for the ventilation or air conditioning installations, which transport fresh, treated or polluted air, are realized by means of circular or rectangular ducts. A current solution is represented by the use of flat-oval channels, which combines the advantages of the previous types, among which, one can mention: the reduced height of the section for the same area compared to the circular sections, respectively, low pressure losses and reduced risk of depositing impurities compared to the rectangular sections. Despite these advantages, their use has not become widespread on the market in our country due to the reluctance of designers and manufacturers. The subject about the flat-oval sections was approached by the authors in a previous paper. In this paper, the attention is focused on the geometrical solving of some pieces used for changing the flow direction such as elbows, branches or bifurcations. By default, these parts introduce local load losses, which means increased energy costs. The pressure losses in fittings are described using the K-factor and the equivalent length concept. By selecting suitable geometric solutions the pressure losses can be reduced. Solving these pieces requires knowledge of descriptive geometry regarding cylindrical surfaces, namely, plane sections, developments and intersections between cylinders. Based on the graphical and/or analytical solutions of fittings developments, calculation programs are made to be implemented on numerical control machines, increasing in this way the production efficiency and also the execution precision.

Keywords: descriptive geometry; applied geometry; cylindrical surfaces; flat-oval ducts; elbows; branches.

GENERAL INFORMATION

The pipes used in the field of building services have in most cases, as it is known, circular sections. When transporting large fluid flows, which involved large sections, depending on the possibilities of installing the pipes, apparent, buried or concealed in technical spaces, there was a need to find other types of sections.

For example, in the case of wastewater ducts, the use of cross-sections as perfect oval, ovoid or other technical curves composed from circle arches was allowed. Another type of section is the flat-oval type - with various ratios between the circular area and the flat area. In fact, some cross-sections of this type have been standardized in Germany, and then in our country. They are mounted upright - Figure 1.a, so that the pressure of the earth on the walls of the pipes is favourable and the risk of depositing impurities on the bottom of the pipes is minimal, to avoid their rapid clogging.

With the development of the occupational hygiene concept at the beginning of the 20th century, the ventilation/air conditioning installations began to be used on a large scale in buildings with different destinations: industrial, administrative, commercial. Even in residential buildings, located in hot and/or humid climatic areas, this type of installations are used. Moreover, the contemporary man, sensitive to the micro-climate, demands working and living conditions that meet the imposed parameters by the thermal comfort. In many situations, the technical solutions of the specialists recommend complementary installations of heating, cooling, air conditioning, ventilation with the possibility of recovering energy from the extracted air. The ventilation/air conditioning installations use air as thermal agent and require sections of pipes with a wide range, respectively about 100… 2000 mm. Thus, the shape of the cross-section used can be circular, rectangular and flat-oval. The last one combines the advantages of the circular or rectangular types, among which, one can mention: the reduced height of the section for the same area compared to the circular sections, respectively, low pressure losses and reduced risk of depositing impurities compared to the rectangular sections. As a rule, they are mounted in the position indicated in Figure 1.b. In this regard, ASHRAE Advanced Energy Design Guides recommend the use of flat-oval pipes instead of rectangular ones, when the height is limited. Among the advantages of flat-oval sections, we mention that for the same section, thus implicitly the same air flow rate, it requires significantly reduced installing heights compared to the circular section tube, which leads to more efficient use of the space. Consequently, for the same useful section results a decrease in the height of the tubing, inclusively of the technical space, between 50 and 88 %. (Mârza et al., 2019)

The following notations were used:

r = radius of the circular portion of the flat-oval pipe

b = flat span length (b= MA-ma);

MA = length of major axis (MA = b+2r);

ma = length of minor axis (ma = 2r).

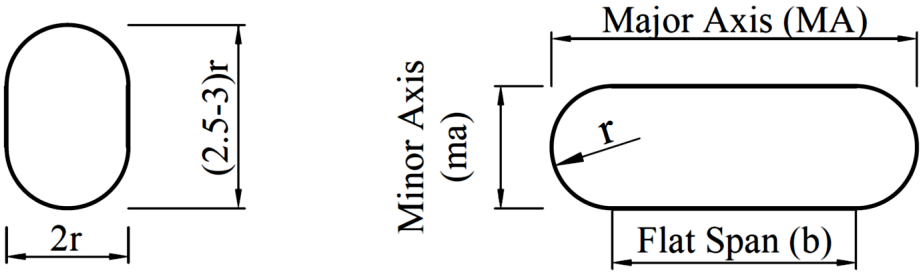

(a) (b)

Figure. 1: Mounting positions of flat-oval pipes

The flat-oval tubing can be made from galvanized sheet processed and joined longitudinally. Another method consists in processing circular spiral tubing in special machines where the pressing takes place, respectively the stretching until the desired shape of the cross-section is obtained. The execution technology is chosen according to the type of agent transported through the channels. The tubes with spiral folding and the related fittings are executed on computer numerical control (CNC) machines.

The use of rubber gaskets gives the tubes a very good sealing.

In accordance with ASHRAE recommendations, most commonly circular tubes are used, and in the areas where the installation height does not allow their use, the transition to the flat-oval section is made, returning then to the circular section (ASHRAE, 2011). Therefore, it is necessary to use some fittings, which will allow to follow the route required for the distribution of the fresh/treated air, respectively the evacuation of the polluted air. For this reason, most comparative analyzes presented by the authors will refer to the circular and flat-oval sections.

In a previous paper, the authors studied the geometry of the transition parts between circular and flat-oval, rectangular and flat-oval or between flat-oval of different sections, following in this paper to deal with the pieces that change the transport direction in flat-oval ducts.

2. PHYSICAL MEASUREMENTS REGARDING HYDRAULIC CALCULATIONS IN FLAT-OVAL DUCTS

2.1. Ducts cross-section

An important size in the various sizing calculations of ducts is represented by the cross-section area. If we make a comparative analysis between the geometry of the circular ducts and the flat-oval ones, knowing that the perimeter remains constant, according to elementary algebraic calculations result cross-section areas specified in Table 1.

Table 1: Geometric dimensions of different cross-section

Cross-section type	*Perimeter*	*Radius*	*Area*	*Percent*
	***2πR***	***R***	***π·R²***	***100%***
	***2r(π+2)***	***0.61·R***	***2.65·R²***	***84%***
	***2r(π+3)***	***0.51·R***	***2.37·R²***	***75%***

One notice that with the elongation of the circular section, the effective flow section of the fluid is reduced. However, where the mounting height does not allow the installation of the circular ducts, the flat-oval sections are used.

2.2. Equivalent diameter

Usually, for design purposes (friction loss calculations), it is necessary to "convert" rectangular or flat oval ducts to round ducts. This substitution is possible by the means of the **equivalent diameter.**

By definition, the equivalent diameter (D_{eq}) is the diameter of a circular duct that will give the same pressure drop at the same air flow as the flat oval duct (Bhatia).

Heyt and Diaz (1975), used the following equation to convert flat oval ducts to and from round cross-sections (ASHRAE, 1989):

$$D_{eq} = \frac{1.55 \cdot A^{0.625}}{P^{0.250}} \quad \text{(Eq.1)}$$

Where,
A – cross-section of the flat-oval duct,
P – perimeter of the flat-oval duct.

The cross section, respectively the perimeter are calculated using Eq.2 and Eq.3:

$$A = \pi r^2 + ma(MA - ma) \quad \text{(Eq.2)}$$

$$P = 2\pi r + 2(MA - ma) \quad \text{(Eq.3)}$$

Where MA, ma, r were previously defined.

For example, a flat oval duct having MA=320 mm and ma= 76 mm is equivalent to a Ø 160 mm round duct.

2.3. Pressure losses

The pressure losses on a path are composed of linear and local losses. In the case of fittings that change direction, are of interest the local losses that are introduced. These can be quantified in two ways:

a) By means of a local coefficient, called **K factor**, the pressure loss is calculated using the equation:

$$\Delta p = K \cdot \frac{\rho \cdot V^2}{2} \qquad \text{(Eq.4)}$$

where:
Δp- dynamic pressure losses [Pa];
K - non-dimensional coefficient for local losses;
ρ - air density [kg/m^3];
V - air velocity [m/s]

Every fitting has its own K factor, which is measured experimentally and reported by the fitting manufacturers. Design handbooks are presenting those coefficients in the form of tables or nomographs. More recently, engineers may search for K factors in a very specialized database, the ASHRAE Duct Fitting Database Program. It is a menu-driven database, including loss coefficient values for more than 200 round, rectangular and flat oval fittings. As input, fitting type, geometry and flow rate are necessary. Pictorial outlines of each fitting are included in documentation and may be displayed on screen (Duct System Design Guide, 2003). Unfortunately, it is not a free application.

b) Often for simplicity in evaluating the local pressure losses, an "**equivalent length"** method -is used (Bhatia). It is like a replacement of a local loss with a friction loss, when a fitting such as an elbow is assigned a number that represents a length of a straight duct that has an equal pressure drop. For example, a 90^o elbow might have an equivalent length of 4.5 m (TECA). This additional length is then added to the straight length of the duct to obtain the total design length (Bhatia).

3. THE GEOMETRY OF SOME FITTINGS USED TO CHANGE THE DIRECTION FOR FLAT-OVAL DUCTS

On the route of the ventilation / conditioning ducts having a flat-oval section it is necessary to provide parts for changing the direction such as elbows and different types of branches.

3.1. Elbows

Regarding elbows, these can be of two types (SPOT, 2017):

- Hard bend - if the axis of the piece is contained in a horizontal plane - Figure 2
- Easy bend - if the axis of the piece is contained in a frontal or profile plane - Figure 3

(a)

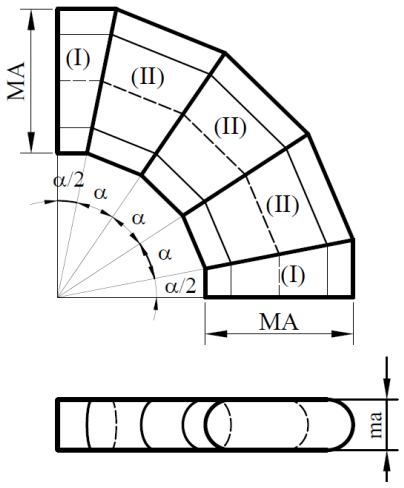

(b)

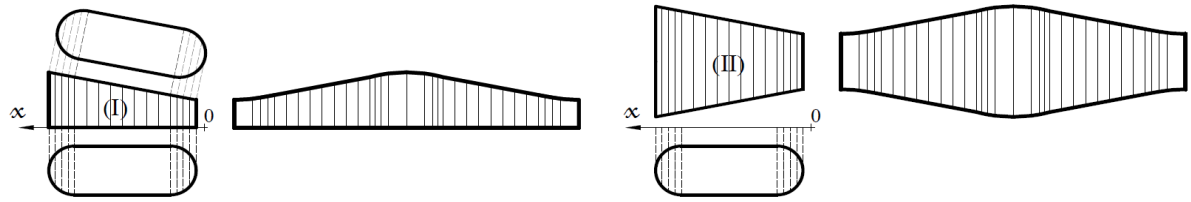

(c) (d)

Figure. 2: Hard bend elbow

In Figure 2.a a hard bend type elbow is represented in axonometry and in Figure 2.b it is represented in double projection. The given solution represents a 90º elbow consisting of five segments: two equal end segments (noted I), having the angle between the limiting vertical projecting planes of 11.25º and three identical intermediary segments (noted II), having a 22.5º angle between the limiting planes (Mârza et al., 2016).

In the Figures 2.c and d the developments of the two types of segments were represented, including the true size of the sections composed of flat areas and elliptical parts (Moncea et al., 1975). The elliptical area is similar to the circular cross-section as the angle between the vertical projecting planes is lower.

Figure 3 represents an easy bend type elbow, respectively in Figure 3.a the axonometry, in Figure 3.b the double projection and in Figures 3.c, d the developments of the two types of segments which compose the elbow. The geometric solution is similar to the previous case.

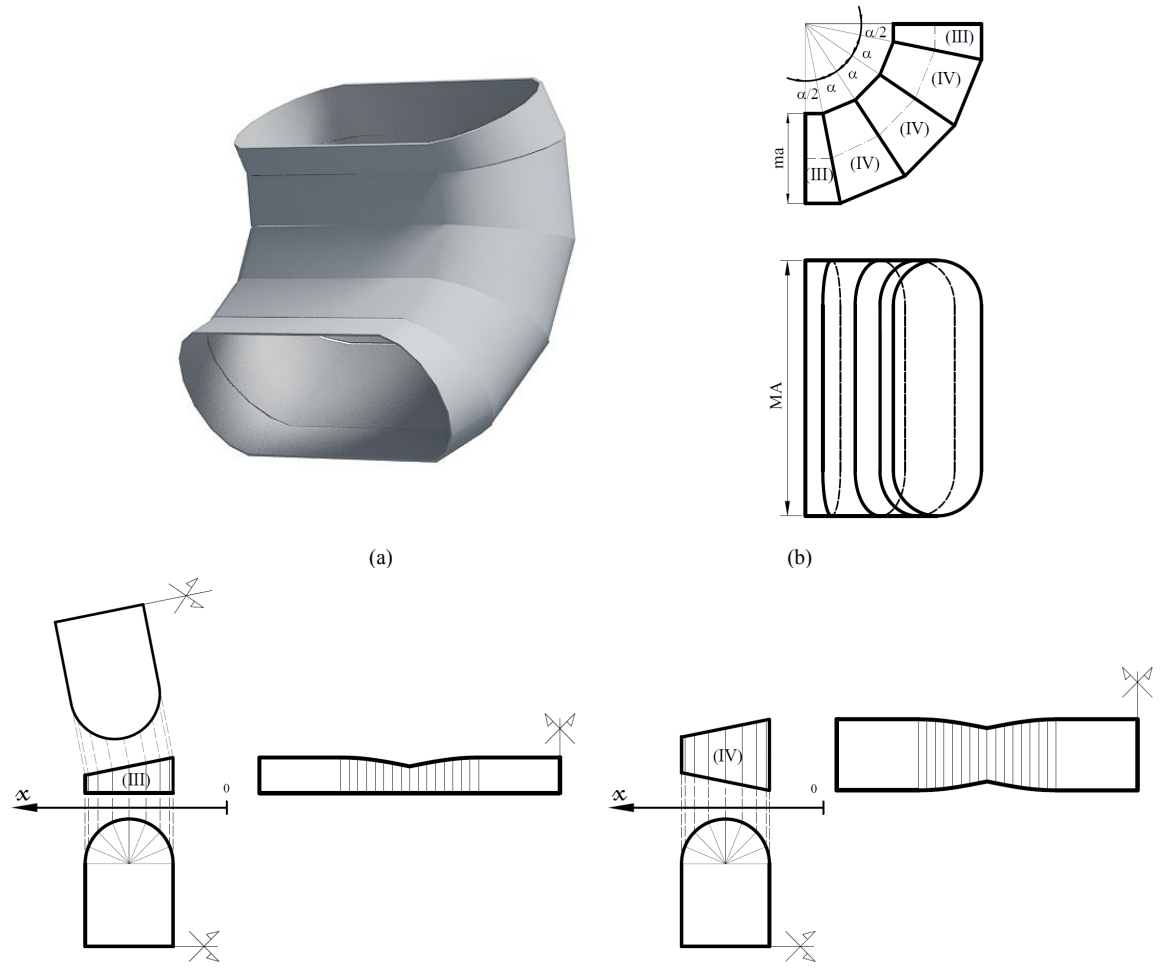

(a) (b)

(c) (d)

Figure. 3: Easy bend elbow

3.2. Tee Branches

If the design requires the existence of several sectors to ensure the inlet or outlet of the air through uniformly distributed jets in a large space, it is necessary for the tubing route to branch in several directions. Thus, the most often used branches are the tees that make 90º between the axes of the cross-sections. Depending on the pipeline route, lateral branches can be used, with the angles between the axes of the cross-sections different values, the most common being 30º, 45º or 60º.

In Figure 4.a, a tee branch, with perpendicular axes, was represented in orthogonal projection on three planes of projection. Due to the fact that, usually, the air flows carried on the secondary section are smaller, the geometric solution is selected so that the minor axis of the secondary section to be equal to that of the main section, changing as needed only the major axis. This solution is advantageous from a geometrical and technical point of view. In this way, the intersection curve between the two duct segments will be composed of flat and curve lines, with the mention that in the vertical projection the intersection curve is projected, in this case, about straight lines.

In Figures 4.b and 4.c were represented the developments of the two parts of the tee branch and in Figure 4.d the piece is represented in 3D.

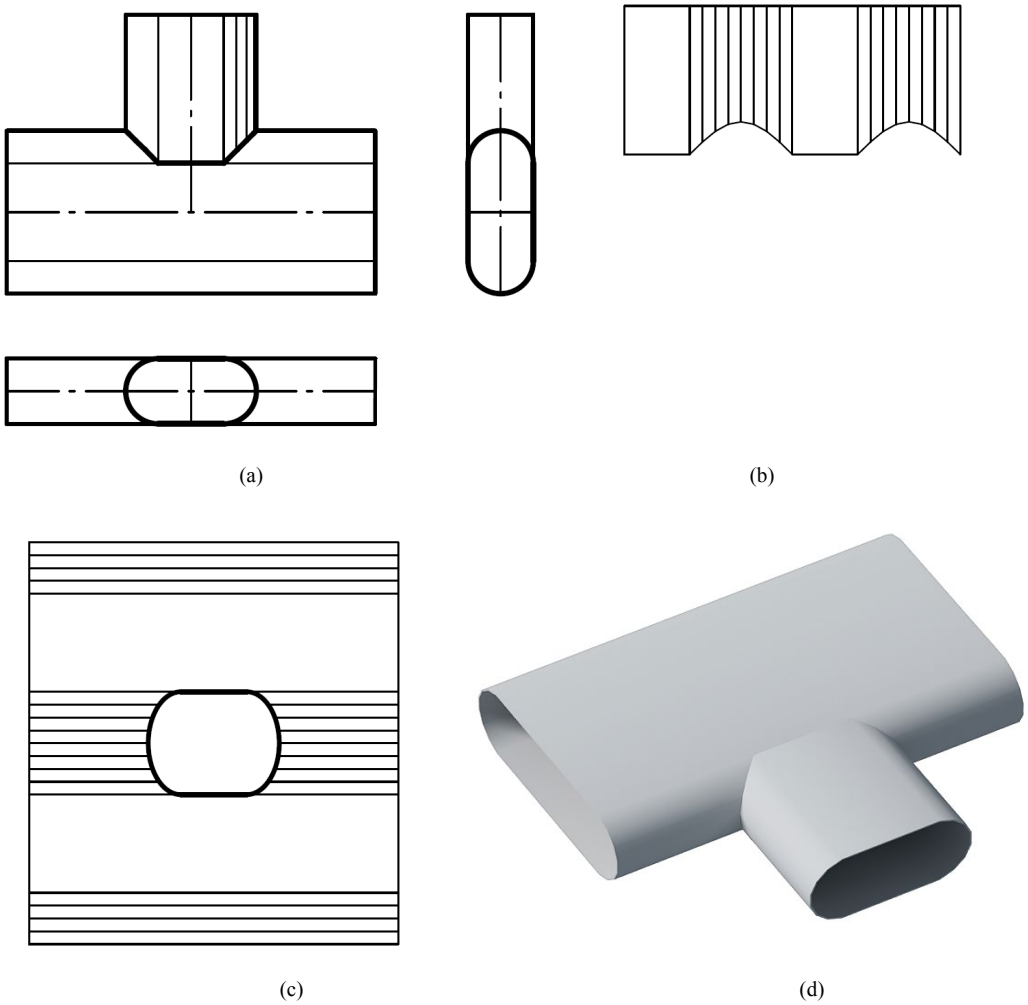

(a) (b)

(c) (d)

Figure. 4:. „T" Branch

3.3. Y Branches

In Figure 5 an Y branch is represented, used when the main pipeline route divides in two directions. Usually, the secondary sectors transport reduced air flows. The piece was represented in front view (Figure 5.a), respectively in axonometry (Figure 5.b). It was selected the solution consisting in four types of segments, respectively type I and II used at the hard bend elbow and two other types of segments noted V and VI.

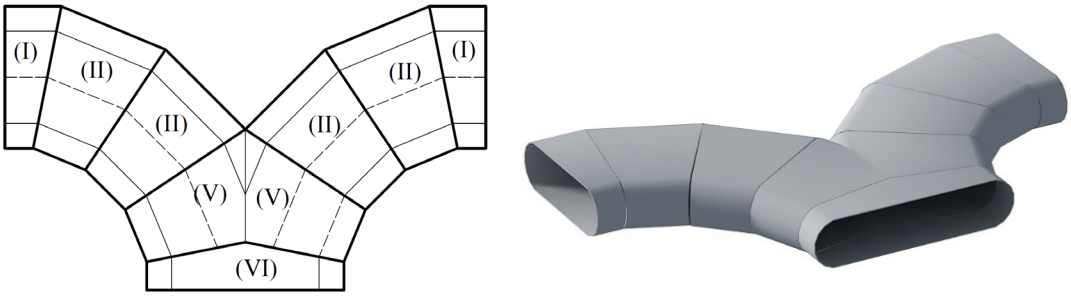

a) b)

Figure. 5: „Y" branch

4. CONCLUSIONS

The authors considered important to study the flat-oval channels and the corresponding fittings, since in Romania and even in Europe these were not widely implemented. These types of ducts were introduced in the design handbooks of the last years without carrying out a hydraulic and geometric study of them. For this reason, these have not been implemented either, as it happened in countries from America and Asia, which recommend and use them due to the advantages offered. Of course, their construction, which is carried out on computer numerical control machines, prior involve a more elaborate geometric study, which requires the application of some knowledge of descriptive and surface geometry, especially in fittings manufacturing.

The solutions presented in the paper are not unique. The fittings can be composed of more or less segments, having different angles, depending on the situation imposed by the duct's routes. When selecting the proposed solution, consideration was given to ensure an air flow with reduced turbulences. At the same time, by repeating some modules, for the same cross-section of the duct, it ensures increased efficiency and flexibility in production.

REFERENCES

1. Bhatia, A., HVAC - How to Size and Design Ducts, Course No: M06-032, Continuing Education and Development, Inc., Available online at: https://www.cedengineering.com/userfiles/How%20to%20Size%20and%20Design%20Ducts.pdf [Accessed: February 2020].
2. Heyt, J. W., Diaz, M. J., 1975. Pressure drop in flat oval spiral air duct. *ASHRAE Transactions,* pp. 221–232.
3. Mârza, C., Corsiuc, G., Graur, A. M., 2019. About the geometry of transition pieces relative to the flat-oval tubing. *FME Transactions*, 47 (2), pp: 337-342.
4. Mârza, C., Corsiuc, G., 2016. Study regarding the geometry of some connecting pieces for circular ducts. Proceedings of the 5th International Scientific Conference on Geometry and Graphics moNGeometrija 2016, Belgrade, Serbia. pp. 403-409.
5. Moncea, J., Alămoreanu, I., 1975. Desfășurarea suprafețelor (Development of surfaces), Editura Tehnică, Bucharest, Romania.
6. ASHRAE, 1989. Handbook: Fundamentals, American Society of Heating, Refrigeration and Air-conditioning Engineers.
7. ASHRAE, 2011. Advanced Energy Design Guides, available online at: http://www.arch.ttu.edu/people/faculty/hill_g/DesignStudioResources/AEDG50-SmallMedOfficeBldgs_2011.pdf [Accessed: February 2020].
8. Duct System Design Guide, 2003. First Edition, McGill AirFlow Corporation, Groveport, Ohio.
9. TECA Oval Fitting Summary, Thermal Environmental Comfort Association, Available online at: http://eccomfg.com/pdf/News/OVAL%20FITTING%20STUDY_rev3.pdf [Accessed: February 2020].
10. SPOT, 2017. Single-Wall Flat Oval Fittings, Spiral Pipe of Texas, Available online at: https://www.spotusa.com/wp-content/uploads/2017/05/Flat-Oval-Terms.pdf [Accessed: February 2020].

INTERACTIVE PRESENTATION IN ARCHITECTURE BY VIRTUAL REALITY

Miloš Obradović
Faculty of Technical Sciences, University of Novi Sad, Republic of Serbia
M.Sc., Teaching Assistant, milos_obradovic@uns.ac.rs

Jelena Kićanović
Faculty of Technical Sciences, University of Novi Sad, Republic of Serbia
M.Sc., Researcher, kicanovicj@uns.ac.rs

Vesna Stojaković
Faculty of Technical Sciences, University of Novi Sad, Republic of Serbia
PhD, Associate Professor, vesna100@uns.ac.rs

ABSTRACT

The aim of this paper is the presentation of a house using interactive virtual reality, as well as to discuss general control, movements and interaction with objects in a virtual environment. The paper presents and analyzes the workflow starting from the design of the house to the process of applying interactive virtual reality in architecture by using Unreal Engine software. It describes and explains the way of making a scene for an interactive architectural visualization, the possibilities of user interaction with virtual space, the usage of VR in architectural visualization, as well as moving (teleportation) through virtual space, interactive (moveable) assets and interactive (changeable) assets via controllers. As a result, it also explains the segments that affect the quality of experiencing a virtual space and the ways to improve the segments that produce inadequate results. It shows the advantages and disadvantages of experiencing space through virtual reality, the pros and cons of interactive architectural visualization and it makes a comparison between the VR presentation and other forms of presentation. Also, it presents the problems that originate during the creation process of an interactive virtual walk and the way of solving them. The presented method of creating an interactive scene can be useful for the architects, designers and in the real estate sales, because it can place the user in the virtual space, visualizing the design before it is built.

Keywords: Virtual Reality; Interactive Visualization; Architectural Visualization

1. INTRODUCTION

Virtual Reality (VR) is a term used to describe a computer-generated three-dimensional environment that a person can explore and interact with (Donovan A., 2019). With the development of technology, architecture has evolved. The possibilities of user interaction with the virtual scene are based on moving through space and interacting with objects by changing them, lifting or capturing them, as well as using it as a way of reviving cultural heritage (Ferdani D. et al., 2020; Gaitatzes A. et al., 2001; Whyte J. et al., 1999; Gaoliang P. et al., 2010). For many industries that rely on design, the biggest challenge is often to convince the client that the finished project will look at least the same, or even better, than the 3D presentation. Nowadays VR technology has a lot of potential for application in architecture (TMD STUDIO LTD, 2017).

In the world of architecture, visualization has always been a central part of architectural design, and any project can be presented in many ways - using orthogonal drawings, 3D rendering, photorealistic renders, animation, Augmented Reality, Virtual Reality etc. One of the ways in which visualization and the experience of space benefit in terms of quality of the experience is Virtual Reality which is increasingly present as an integral part of any architectural project. With VR, the user is transported to a different space in which he/she interacts with digital objects, using assets in his/her virtual environment. In this way, the users change the way they look at a particular event, place and space, by participating in it.

The aim of this paper is the presentation of a house using interactive virtual reality. The paper presents and analyzes the workflow starting from the design of the house to the process of applying interactive virtual reality in architecture. The way of making a scene for an interactive architectural visualization, the possibilities of user interaction with virtual space, the usage of VR in architectural visualization, as well as moving (teleportation) through virtual space, interactive (moveable) assets and interactive (changeable) assets via controllers are described and explained. The segments that affect the quality of experiencing a virtual space and the ways to improve the segments that produce inadequate results are presented. The advantages and disadvantages of experiencing space through virtual reality, the pros and cons of interactive architectural visualization and it makes a comparison between the VR presentation and other forms of presentation are shown. Also, the problems that originate during the creation process of an interactive virtual walk and the way of solving them are presented.

2. METHODS USED FOR CREATING AN INTERACTIVE SCENE

In this paper 3ds Max and Unreal Engine software are used. 3ds Max is a powerful 3D modeling and animation solution used by game developers, visual effects artists, and graphic designers to create massive worlds, stunning scenes, and engaging virtual reality (VR) experiences (3DS MAX, 2020). The Unreal Engine is a game engine developed by Epic Games, first showcased in the 1998 first-person shooter game Unreal. Although initially developed for first-person shooters, it has been successfully used in a variety of other genres, including platformers, fighting games, MMORPGs, and other RPGs. With its code written in C++, the Unreal Engine features a high degree of portability and is a tool used by many game developers today, with it being source-available. The most recent version is Unreal Engine 4, which was released in 2014 (Computer Hope, 2019).

Unreal Engine was selected as the VR environment due to the amount of available information that can be used in order to create it. Also, there are predefined templates that facilitate the process of creating a scene, such as first person controller, the ability to move through objects and lift objects. Other VR environments can be used for virtual walks, and one way of application can be to display a virtual environment for the sale of apartments under construction.

In this paper possibilites how to create an interactive architectural visualization, as well as the possibilities of user interaction with virtual space are explored. Also, it is necessary to determine the relationship between the two programs mentioned above, as well as to find a way of implementing all the assets into a virtual scene. The user experience in the virtual space is different from the experience in the real world, and it is necessary to determine how practical the use of headset is to obtain a visual effect, and to what extent the effects affect the perception of the space. The analysis can determine whether the result can be corrected, and to what extent. Also, the way of improving segments that produce substandard results needs to be explored, so that the end result is of the highest quality. The goal is to create an interactive virtual walk through the object using headset and controllers for specific interactions in the virtual space. Within the research, certain segments of interactive architectural visualization were used that can affect the quality of experiencing the space, such as the ability to move through space, lift elements, change elements, etc.

3. VR INTERACTIVE PRESENTATION IN ARCHITECTURE

The selection of the analyzed examples was made on the projects based on the use of VR, more precisely, the examples that were analyzed had the benefit of using VR as a presentation method. These are two examples of residential properties that have been implemented in VR with the help of the Unreal Engine software.

3.1. A virtual walk through a residential building

A virtual walk through a building was created in Unreal Engine, and two scenes can be viewed simultaneously throughout the video. One of them is a virtual scene, through which the user teleports within the 3D model, leaving viewers with the impression that they are actually there. The second, real scene, can be seen at the bottom right of the screen, where he can see that his virtual walk is based on standing in a place from which he moves with the controllers in the virtual scene. This kind of movement through the virtual scene is beneficial because it does not require much physical movement while carrying the equipment.

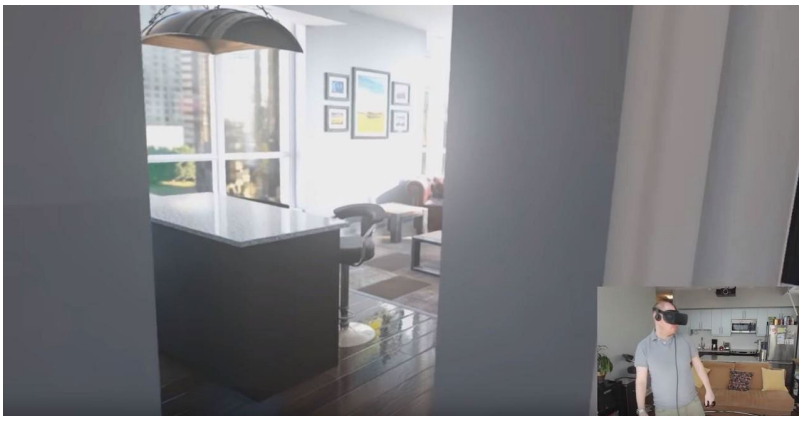

Figure 1. Virtual walk through a residential building (Screenshot)

3.2. An interactive virtual walk

Another example was created in the Unreal Engine software. As in the previous example, two scenes can be followed during the video. In the lower right corner is the user with the equipment, while the virtual scene is on the rest of the screen. Except from the teleportation, the user controls the hands that appear in the virtual scene by using the controllers. With the help of these, there is a possibility of interaction between the users and certain parts of digital objects, where the sense of being in the virtual space becomes even more important.

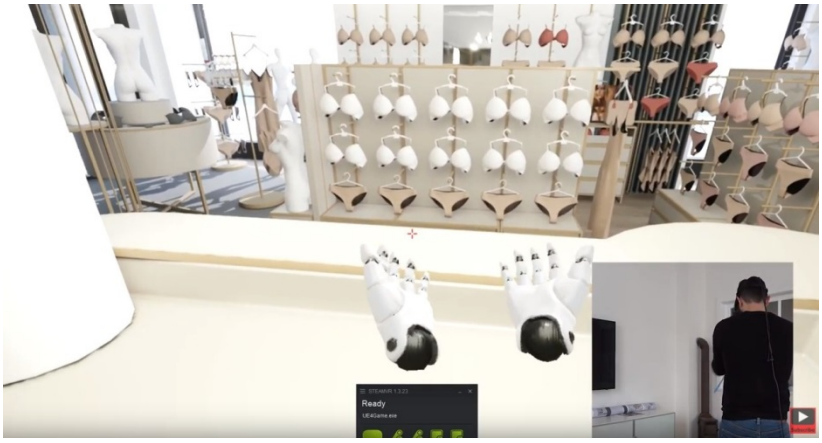

Figure 2. Interactive virtual walk (Screenshot)

4. APPLICATION OF VR TECHNOLOGY FOR ARCHITECTURAL VISUALIZATION

The combination of software and VR equipment allows the interaction of users with space. The final presentation, i.e., the experience of the space through virtual reality, will affect the end result. Traverse to Unreal Engine from 3ds Max (Whyte J. et al., 1999) is the first step toward solving the goal. For the interactive architectural scene to be created, it is necessary to determine the relation between the 3D modeling software and the Unreal Engine. The method of creating interactive architectural visualization, as well as the possibility of

user interaction with the virtual space, must be determined. In order to create the virtual scene, there must be a certain way of implementing the physical scene into a virtual scene, as well as a way of moving users through space. Emphasis should be placed on headset and controllers, how the use of equipment affects the perception of space and whether the results obtained can be corrected. The game engine Unreal Engine 4 was used to create the overall environment which is suitable for HMD (Head-Mounted Display) and motion controllers, which were tested on Oculus Rift.

4.1. The way of creating an interactive scene

In order for the scene created to be interactive, it is necessary to determine which segments of the scene should be interactive, and to what extent. The possibilities of movement through space should be limited, as well as the ability to interact with certain elements in the scene. There must be a difference between how a user can interact with a scene in a software and by using VR equipment. One way is to take part in a scene using a computer when interacting with a first-person template (Gaoliang P. et al., 2010), and another way is to interact with a VR template when the user, in addition to the computer, needs the right equipment for the interaction to be complete.

4.2. The possibilities of interaction with virtual space

Only when the model is arranged, when the materials are adequately fitted to the model and when there are appropriate lights can it be possible to switch to the application of VR in architectural visualization. When inserting models into the scene and further arranging them, it is necessary to pay attention to the segments that will be used during interactive visualization. In this paper interactivity is based on the possibility of teleporting through space, the ability to capture, pick up and throw certain elements in the scene, as well as the ability to change furniture by using a controller.

4.3. Movement through the house using controllers

In order to navigate through the scene (Obradović M., 2019), the user needs to use the controllers (Ferdani D. et al., 2020; Avşar E. Ö. et al., 2008). Within a predefined range of motion, pressing a specific controller button, the teleport to the desired location is enabled. Inability to teleport is the main problem that most often occurs in practice (Ferdani D. et al., 2020). Creating a volume of the desired dimensions, which is placed below those parts of the scene in the frame, is the way of solving the problem of not being able to move. It is a transparent, four-sided prism, that is not visible during the walk, and it allows the user to navigate seamlessly through 3D space (Fig. 4).

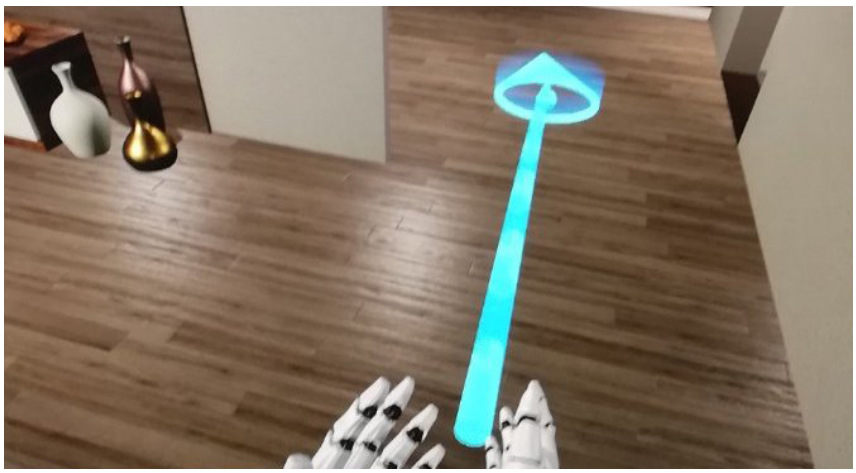

Figure 3. Teleportation through the space

By tracking the head and hand movement of the user and monitoring the controllers, it is possible to know exactly where the user is positioned and where they are looking (Ferdani D. et al., 2020; Gaitatzes A. et al., 2001). Teleportation through a scene is easy for the users because they are not required to navigate via joystick on the controllers. However, the user in real life is standing in one spot and the distance to be moved can be chosen with just one click of a button, as well as the direction they want to turn after the teleportation is done.

Collision is of great importance in this part of the project, because of which walls, ceilings, floors and objects must be covered in order to prevent teleportation through those parts of the scene. Sensors do not always detect controllers and it takes some time for the detection to run smoothly.

4.4. Interactive objects

The Motion Controller Template contains a box that can be used interactively. It is an asset that is programmed so that with the help of virtual hands it can be moved (Obradović M., 2019), lifted and thrown, all during a virtual walk through the scene. These capabilities are provided by Blueprint, which can be applied to assets as desired. What is important is that the collision for the given objects is applied in as much detail as possible. For example, a complex collision has to be used on a particular high-poly model, since it is possible that placing a normal collision on a more complex asset will not have the same effect as when a complex collision is placed on a more complex object.

The advantage of being able to pick up individual elements is that they can be moved to another part of the scene, and the user can, at their request, change the positions of the elements within the scene - move, add, or move some of them (Fig. 5). The disadvantage is that the pickup option must be adjusted for each individual element, and if the user wanted the whole scene to be interactive, it would take a long time for such a process. A collision must exist in every segment that the user wants to raise and for each individual element it must be applied separately. Although the effect of raising and dropping individual models seems interesting, the very process of creating an interactive model takes a long time. To get a great effect, it is necessary to repeat the same process countless times, because Blueprint cannot be added to multiple models at once.

Figure 4. Picking up the chair by using the controllers

4.5. Changing elements and colors

In order to change the model (Zhang Y. et al., 2019; Obradović M., 2019) completely, the user would have to get close to it (predetermined) so that the model could react to the controllers, and, by pressing a specific button, it would be replaced. This way of choosing between the two models may be of interest to the users. The principle is the same when it comes to lifting individual elements. The disadvantage here is that a separate Blueprint needs to be created for each individual segment which has to be replaced. For this reason, in this paper, it is possible to replace the sofa in the living room by clicking on a specific controller button.

The Blueprints Visual Scripting system in Unreal Engine is a complete gameplay scripting system based on the concept of using a node-based interface to create gameplay elements from within Unreal Editor. As with many common scripting languages, it is used to define object-oriented (OO) classes or objects in the engine. Objects defined using Blueprint are colloquially referred to as just Blueprints (Introduction to Blueprints, 2019).

Figure 5. Modifying the model interactively

4.6. The advantages and disadvantages of using VR in interactive visualization

It can be concluded that the created interactive architectural visualization has its advantages and disadvantages which will be presented in the text that follows.

4.6.1. The advantages

VR is a specific way of experiencing space and one of the benefits of participating in space through VR is the kind of interactivity the user has in virtual space (Qi S., 2012). It cannot be compared to other segments of virtual observing of an interior, because it gives the impression of being present in a given, virtual space. Virtual reality technology provides a real-world view of the existing world, augmenting the user's perception of computer-generated digital content. This research gives a representation of the house which uses virtual environment to generate virtual content by offering the users additional content that complements the information about the real environment. Part of the analyzed work refers to the implementation which would increase the degree of realism of three-dimensional models by using normal maps and textures with high level of details. The problem was that some of the versions of game engine do not support the specified *tiff* format which gives more complex details. Having adequate equipment, as well as the computers with good hardware performance, represents some of the advantages of VR. Regarding performances, one of the key shortcomings is the speed of data processing, which is then transmitted to the HMD.

The feeling of being present in a virtual space where the user is physically not present can be achieved through virtual reality in a very good way. The ability to interact with a scene during a virtual presence can only be achieved through virtual reality as one type of the presentation of an architectural object. The relationship between users and changing elements in space is easy to use and the space experience of a particular space is better than, for example, with a photorealistic render. Interactive architectural visualization contains some degree of photorealism. Also, the shadows resulting from moving or changing certain models are interactive.

4.6.2. The disadvantages

One of the disadvantages while working in the Unreal Engine program is that materialization has to be selected for each segment separately, and materialization for unclassified objects takes a long time. Each interactive element must have a collision and a corresponding Blueprint in order to be used in a virtual space in a certain way, and it is not possible to apply one script for several segments at a time. For each segment it is necessary to do the whole process from the beginning. Although VR is a way of presenting architectural visualization that is increasingly accessible, the users who have not encountered VR equipment may experience certain problems when using it, such as motion sickness. In addition to the possible nausea and dizziness, the preparation of a scene for an interactive virtual walk can take a long time.

4.7. Research opportunity in order to enhance interactive walk

Based on the research and use of virtual reality in the form of interactive architectural visualization, it can be concluded that there are more advantages than disadvantages of this type of presentation. Additional VR research can enhance the virtual experience. Some of the problems encountered by the user are described earlier in the text, and each has been properly addressed. By exploring Unreal Engine in order to create a virtual walk through space, the user experience in the virtual space could be enhanced.

5. CONCLUSION

Firstly, it was necessary to design a model of single-family residential building. ArchiCAD and 3ds Max software were used to prepare the model, as well as the assets downloaded from the Internet. The next step was to import the model into the Unreal Engine program, and after working in the same project, it was ready for execution in VR.

The level of detail of the final project depends on the time invested, materialization, as well as lighting. The detail of the model processing before preparing for VR is not always the same. Depending on the level of detail of the object, as well as its environment, depends on what the primary goal of virtual reality is. The surroundings of the building contain a satisfactory level of detail and in no segment leave the user in unfinished space, while the space that cannot be accessed is adequately marked. In order for a virtual walk to be created, it is necessary to go through three steps, where the first step is represented by the creation of an idea, the second by the creation of a 3D model, and the third by the implementation and connection with the virtual space. Based on VR research in architecture, one of the advantages is a sense of presence in a virtual space in which the user is not physically present, an interactive relationship between users and elements in the virtual space, the existence of a photorealism, a large number of pre-created materials, as well as interactive shadows, are some of the benefits of VR.

In order to be able to access the virtual walk, the user needs to have the appropriate equipment, while there is also the possibility of nausea while wearing the equipment. It is common for software to slow down in scenes with lots of assets, and some problems are related to an inadequate way of applying material to elements in a scene. Through a series of research on the topic of virtual reality, it is concluded that the effectiveness of VR depends on the photorealism of the project, as well as on the author's desire to focus on particular segments of the project. The conclusion of the paper is that the implementation of VR in Unreal Engine has more advantages than disadvantages, and one of the biggest disadvantages is that this topic is still under-researched and little-applied in Serbia. In addition to good visual effects, the advantages include the ability of users to communicate with virtual space, the accessibility to the program, a wide range of possibilities related to using it, as well as significantly better visual effect than Unity program, for a relatively similar time of use of the software. The result obtained differs from the usual presentation methods because the user has the ability to interact with the space. VR in architecture shows a positive effect on users, and its effectiveness will certainly affect the improvement and expansion of architectural visualization capabilities in the future.

REFERENCES

3DS MAX. https://www.autodesk.com/education/free-software/3ds-max [Accessed: 3th March 2020]

Avşar E. Ö. et al. 2008. MODELING OF THE TEMPLE OF APOLLO SMINTHEUS USING PHOTOGRAMMETRY AND VIRTUAL REALTY. *The International Archives of the Photogrammetry, Remote Sensing and Spatial Information Sciences 2008*. Vol. XXXVII, Part B5 Beijing, pp. 357-361

Computer Hope. Unreal Engine, 2019. https://www.computerhope.com/jargon/u/unreal-engine.htm [Accessed: 14th October 2019]

Donovan A. How VR Technology Is Changing the Way Architects Design Your Home, 2019. https://interestingengineering.com/how-vr-technology-is-changing-the-way-architects-design-your-home [Accessed: 5th October 2019]

Ferdani D. et al. 2020. 3D reconstruction and validation of historical background for immersive VR applications and games: The case study of the Forum of Augustus in Rome. *Journal of Cultural Heritage 2020*, In Press, Corrected Proof

Gaitatzes A. et al. 2001. Reviving the Past: Cultural Heritage Meets Virtual Reality. *Proceedings of the 2001 conference on Virtual reality, archeology, and cultural heritage 2001*, pp. 103-110

Gaoliang P. et al. 2010. A desktop virtual reality-based interactive modular fixture configuration. *Computer-Aided Design*. Vol. 42, pp. 432-444

Introduction to Blueprints. https://docs.unrealengine.com/en-US/Engine/Blueprints/GettingStarted/index.html [Accessed: 15th October 2019]

Obradović M. 2019. Interactive presentation of a house by Virtual Reality. *Proceedings of the Faculty of Technical Sciences*, In press

Qi S., 2012. Virtual Interior Design Based On VRML AND JAVA. *2012 International Conference on Medical Physics and Biomedical Engineering*. Physics Procedia 33 (2012), pp. 1614 – 1620

TMD STUDIO LTD. Virtual Reality Uses in Architecture and Design, 2017. https://medium.com/studiotmd/virtual-reality-uses-in-architecture-and-design-c5d54b7c1e89 [Accessed: 5th October 2019]

Whyte J., et al. 1999. From CAD to virtual reality: modelling approaches, data exchange and interactive 3D building design tools. *Automation in Construction*. Vol. 10, pp. 43–55

Zhang Y. et al. 2019. User-centered interior finishing material selection: An immersive virtual reality-based interactive approach. *Automation in Construction*. Vol. 106, 102884

moNGeometrija 2020

REVERSE PERSPECTIVE – DIFFERENT APPROACHES AND APPLICATIONS

Ivana Marcikić
Faculty of Applied Arts, University of Arts in Belgrade, Belgrade, Serbia
PhD., Full Professor, marcikicivana@yahoo.com

Marijana Paunović
Faculty of Applied Arts, University of Arts in Belgrade, Belgrade, Serbia
PhD., Assistant Professor, marijanavpaunovic@gmail.com

ABSTRACT

Due to the paucity of medieval sources which could provide answers to why after ancient knowledge of perspective, was applied a new method for representing space in Byzantine painting. Nowadays exist different interpretations of the reverse perspective method. Many of these interpretations date from the first half of the twentieth century. The goal is to show the application of reverse perspective in modern visual arts.

In addition to reverse perspective, elements of artistic perspective and visual effects were used in the comparative analysis of examples of Serbian medieval painting and modern visual art. Of note are the works of contemporary Spanish, British and Serbian artists such as Perez Villalta, David Hockney, Aleksandar Tomašević.

Keywords: inverse perspective; fish-bone perspective; axonometric projection; optical-physiological perspective; representation of architecture

1. INTRODUCTION

Inverse, reverse or inverted perspective are the terms which refer to the principle of representing space in Byzantine painting as well as Serbian medieval icons and frescoes. How this principle was used before Renaissance linear perspective, in relation to which it compares, the terms above are questionable.

An interesting study conducted by Clemena Antonova (Antonova, 2010) points to various theses that explain the reverse perspective. In the approach by Oskar Wulff the viewer of the icon is “inside” of the pictorial space as a result of the inversion of linear perspective. The second approach refers to the position of the figures on the fresco above the viewer’s eyes, the scenography thesis which goes back to ancient murals. Furthermore is the reverse fish-bone perspective thesis, which means connection with Pompeian perspective. All these theses are based on ideas to explain reverse perspective by a mathematically correct method – linear perspective or its combination with oblique projection. In this sense, the most extreme approach is the Russian analogy of space in the icon with a non-Euclidean geometry. The optical view thesis is based on the idea that space in the icon is solved as anamorphosis.

This brings us to the question of the aim of Byzantine as well as Serbian medieval painting, which is opposite to the decorative illusion task to deceive observers. The expansion of depicted space by increasing distance in a Byzantine painting is paradigm of Byzantine perspective. It is opposed to the rules of Renaissance perspective, but is in line with laws of nature and the dimensions in real space. On the other hand, compositions enable canonical laws to be obeyed and respect the hierarchy according to which figures are always dimension

strictly by their importance, i.e. perspective of importance. The examples of reverse perspective in Serbian medieval painting are shown in the compositions in our monasteries. That examples define visual effects of reverse perspective including: enlargement of the space in the picture when the distance is enlarged, the multiocular principle - the effect of the film image, synergy of the fresco and architectural elements and several "horizons" which divide the image vertically into several zones.This paper points to different approaches of applying the inverse perspective through Eastern and Western interpretation and the sence of space and comprehension of the world around us.

2. APPLICATION OF INVERSE PERSPECTIVE IN CONTEMPORARY SERBIAN ART

Characteristic examples of works of our modern artists were chosen, on which the method of the medieval inverse perspective is directly applied.

2.1. Inspiration in tradition

We emphasize the authors who have dedicated the period of their work to the study of our medieval cultural heritage.

2.1.1. Aleksandar Tomašević

The table's horizontal edge line (Fig.1), depicted as a vertical rectangle in the lower portion of Aleksandar Tomašević's *Black Chalice* is the golden ratio line. The decorative cloth under the chalice is a rectangle, shaped like a trapezoid in reverse perspective, while the borders follow the shorter edges of the trapezoid in an axonometric projection, retaining their parallel position. The reason behind the deviation from the reverse perspective is clear; the observer would otherwise have the impression of an irregular pattern, while in this way, the geometrics are emphasised and "preserved". The base, i.e. the chalice's handle has a frontal appearance and the highest horizontal circle is in inverse perspective as if "tilted" towards the observer. What is interesting is that it is represented only by the irregularly shaped semi-ellipse, while the front half of the circle is its diameter. This method is directly taken from Byzantine painting. The background is resolved with a surface ornament (these elements are rectangles, squares and squares rotated by 45°) which indirectly adds the effect of depth to the composition.

Figure.1. *Black Chalice*, 1963, mosaic, 62x120cm, (Vojinović at al. 1988)

In the composition *Still Life with Two Fishes*, 1961, mosaic, 55x92cm, by the same artist, the chalice is depicted in a frontal projection, and the fish-filled bowl is in a combined one (inverse perspective and frontal appearance). The construction of the highest horizontal circle is a geometrically, accurately positioned ellipse drawn inside a trapezoid as an inverse square painting.

The Russian theoretician L.F. Zhegin dedicated his most important study "The Language of a Pictorial Work (Conditionality of Ancient Art)" to analysing the Byzantine perspective in Russian iconography. His schematics with objects that stand in the center of the table and moving toward the observer and deformation of circle in a bevel position (Жегин, 1970:48,51) correspond to the projections of analysed objects in inverse perspective in painting, mosaic and graphics techniques.

2.2.2. Branislav Makeš

In the graphic *Byzantine V*, 1994, graphic, 13x10cm by the artist Branislav Makeš, the altar spread is constructed in inverse perspective. The depiction of each of the three chalices, placed on top of it, follows a combined projection – the frontal appearance for their bases and the reverse perspective for depicting their highest horizontal circles.

The depiction of the cross-shaped incense burner in Makeš's graphic (Fig.2) is the same as the stone baptistery in the fresco in Narthex of Arch. Danilo II, 1565, The Patriarchate of Peć. In both examples it was important to "tilt" the highest horizontal plane towards the observer in order for them to see what shape it is, which is enabled by the use of inverse perspective. The remaining parts are depicted with a frontal appearance, sufficient to complete the form overview.

Figure. 2. *Byzantine XII*, 1994, graphic, 13x10cm, Serbian Orthodox Church Museum, Belgrade (with geometric analyses of vanishing points) (Макилатуре, 2016)

In the graphic *Byzantine I* 2001, 21x28cm, from the "An Obol for Byzantium" cycle by Makeš, a hexagonal chalice is depicted in reverse perspective. Without inverse perspective the chalice's hexagonal shape would be unrecognisable, as its frontal projection would be turned into a polygon's diagonal line. In this composition, the base of the chalice is depicted with a frontal appearance, as with both Byzantine and our icons. The horizontal altar surface, on which the chalice stands, is depicted as being vertical. The effect of a kinetic viewpoint which follows the movement of the projection planes is created.

In the composition *Byzantine XXV* 1995, acrylic on canvas, 80x100cm, National museum, Belgrade, the painter Makeš creates depth by using several parallel rectangular shapes which provide the effect of theatre soffits. Through careful analysis and by connecting their vertices, we come up with the vanishing points of a cuboid's inverse perspective, to which they belong as frontal sides. The second inverse vanishing point is the intersection point of the rectangle's diagonals which are centrally positioned within the composition. The shading scale helps create the inverse perspective of the cuboid's two outer horizontal and outer profile sides. In the lower right hand corner of the composition part of a semicircular niche is represented in an exact constructive geometric manner, in inverse perspective.

From the "Graphic Études" collection, the graphic "Still Life with an Ewer" 1991, graphic, 31x26cm, has all the elements of a reverse fishbone perspective, as well as a Byzantine projection of the central object – the ewer. The artist even hints at the fishbone perspective through the shape of the object's shadow being cast. The plaid tablecloth, depicted in the almost vertical position of the rotated horizontal plane, also evokes this. The grooves on the furniture, on both the left and right sides, also direct one's gaze towards the fishbone perspective. The ewer's highest circle is depicted in an inverse perspective with an emphatically large ellipse axis going through the centre of the surrounding trapezoid. With this, the artist gives a geometrically accurate analysis of the inverse perspective employed in which he uses Cézanne's wedge. A base which Cézanne used to set the model object in a position which was inclined towards the viewer, in order to establish several sides, known as the Cézanne wedge. Cézanne's methods of inverse perspective are research and shown in our paper "Inverse Perspective in Cézanne's Art" (FME Transactions (2017) 45, 301-306).

2.2.3. Ljubinka Jovanović

The composition (Fig.3) by the artist Ljubinka Jovanović, is characterised by a large viewing angle, i.e. a wide-angle reverse perspective. The simultaneous overview of the left and right sides of the object are present here as a characteristic of the Byzantine perspective. The schematic *Simultaneous perception of frontal and profile layout* by theorist L.F. Zhegin (Жегин, 1970:89) confirms that rule.

Figure.3. *La fabrique*, 1983, acrylic on paper, 200x150cm (Михаиловић, 2002)

The diptych *Les docks*, 1999/2000, acrylic (195x130cm) x 2 by the same artist, has the colourings of a Byzantine painting (Byzantine blue, gold and silver) with discreet contour lines on a scale from umbra to purple. The curves of the composition's right wing are calmed by the rectangles on the left side, in which the bifora has two pronounced rectangular frames with embedded arched windows. The wing of the window on the right is open, shown in a light tone and in a Byzantine perspective. The cuboid on the diptych's left side, whose frontal

basis has the same height as the composition, is also given in inverse perspective. Two of its profile planes (the left and right triangle) are at odds with each other, as one is completely dark – black – and the other is brightly illuminated in a golden hue. The horizontal triangles of the floor and ceiling are depicted by combining the golden-silver sections. The lower horizontal bifora of the diptych's left wing is the highest tangent of the right wing's circular arch. The connection between the left and right sides of the composition is made through the joint horizontal line of the two semi-circular portals. The larger one, on the left side, is dark and thereby closer in size to the smaller one located in the right half.

The name *Kolo without Music* oil, 1952, 110 x 97cm, originally known as the *Deaf Kolo*, and the painting's place in the "Kosovo" cycle, are stressed through the use of colour. The scene is placed in the foreground, illuminated by the fire coming off a burning field; the figures have a placement similar to that of a Byzantine fresco or icon. The feet, which here resemble bird wings with their shape, or those of a black raven, are placed in the composition's lower edge, while the height of the figures equals that of the painting. We see a similar resemblance to a bird's shape when observing the hands of these feminine figures. Their faces are darkened by pain; their arms are intertwined into a garland with which they lean on each other. Parts of their shawls fall over their arms, obscuring the basis of this ornament.

In the composition *Serbian Women* oil, 1950, 130 x 100cm, also from the "Kosovo" cycle, we see the same placement of female figures, but in the dark of night, their faces are less intimidated; they are more secure and the faces are much brighter. The arms are raised high, while the colour of their garb is dark, further emphasising the night's atmosphere. The joined waistline divides the composition into a bottom square and the golden rectangle in the upper zone. The monumentality of the composition *Inner space II*, Lj. Jovanović, triptych, 1999/2000, (195x130cm) x 3, is emphasised by the dimensions of the painted architecture which traces the object's real size. The spatial elements are depicted in inverse perspective, as the wings on the sides (left and right, shown in a light silvery hue) are smaller than half of the portal – left ajar, meaning foreshortened towards the observer. On the left side, in the foreground, is a smaller arched opening that confirms the reversed perspective, while in the triptych's right corner is a symmetrical square whose diagonals, as the edges of the cuboid's four outer sides – the aforementioned square being its basis in a frontal position – lead into an inverse vanishing point.

2.2.4. Kosta Bogdanović

In the sculpture *Vizantema 18* (Fig.4), artist Kosta Bogdanović depicts architecture in an inverse relief perspective. The background is in a Byzantine-blue hue, directly associating it with Byzantium, to which both the inverse perspective and the work's title themselves, can be associated. What is interesting is the use of combined materials and colour with the added visual effects of a natural metallic sheen.

Figure.4. *Vizantema 18*, sculpture, K Bogdanović, (with geometric analyses of vanishing points) (Јовановић, 2011)

2.2. Influence of Cézanne's inverse perspective

Immediate influence of Cézanne's art we can see in the next two works. In the example of *The City's High Skyscrapers* (Fig.5, a) by artist Zoran Grebenarović, with several of Belgrade's prominent architectural landmarks, the inverse perspective has also been applied. This projection serves to help us see the highest horizontal plane of the *Beogradjanka* building from the top. Its inverse perspective was emphasised by the artist with the larger surface of the more distant zone – had he used the axonometric projection of the semi-regular polyhedron's symmetrical surface, they would have been depicted as corresponding. In the composition *Still Life with a Frying Pan* (Fig.5, b) by artist Miodrag Rogić, a table which contains several utilitarian objects of different shapes and sizes is depicted in an inverse perspective. The chosen projection system provides the opportunity to clearly define each one of them individually.

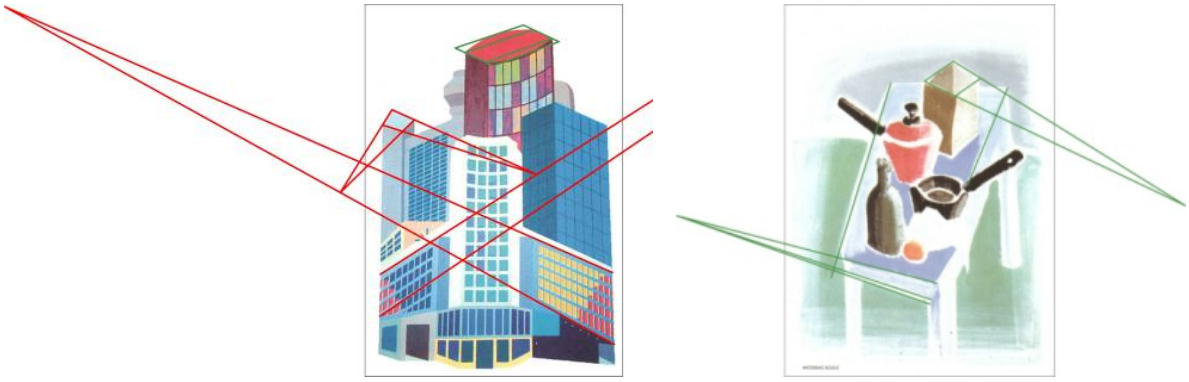

(a) (b)

Figure.5. (a) The City's High Skyscrapers, Z. Grebenarović and (b) *Still Life with a Frying Pan,* M. Rogić, 2002, acrylic on canvas, 100x73cm (with geometric analyses of vanishing points) (Јовановић, 2011)

In the indirect way, the painter Čedomir Vasić has used two types of projection: orthogonal to the horizontal plane, and the frontal oblique projection for the triumphal arch (Fig.6, a). He has achieved the visual effect of the Byzantine method of representing space with the kinetic eye, which moves from the infinitely far position of the distant point, into the vertical position of the frontal observation of the central object. With choice of the projections that have been mentioned, the painter provides data on the main building and a circular urban complex, while presenting the circle with an ellipse in order to avoid causing confusion about its real form.

Cubist intention to observe the object from several view-points is applied in the painting (Fig.6, b). Two sailboats, represented in inverse perspective, look like as a central symmetrical figure.

(a) (b)

Figure. 6. (a) *Place de L'Etoile*, Č. Vasić, 1985, acrylic on canvas, 61x73cm and (b) *The Hand Cuts- the Angel of History I,* M. Prodanović,1997, acrylic on canvas, 218 x 298cm (Јовановић, 2011)

3. APPLICATION OF INVERSE PERSPECTIVE IN WESTERN ART

Giotto's fresco painting contained a Byzantine perspective, hinting at a Renaissance perspective method with a specific depiction of space and the arrangement of objects and figures in it. Giotto achieved the rhythm in his compositions by the axial symmetry of parts of architectural objects according to the vertical. In the Scrovegni Chapel he achieved a symbiosis of the real interior with the space shown in it, a one century before the foundation of the mathematical theory of constructive perspective.

3.1. Early Examples

The pool edges in the painting (Fig.7, a) by Matteo Giovannetti (1300 - 1368) are depicted in the inverse perspective. The pool seems to have been rotated into an oblique position towards the observer in order for it to be more visible. The vertical line of the trees in the foreground divides the composition along the golden ratio. Obeying the rules of reverse perspective, this tree is depicted as being thinner than the remaining, more distant ones, thereby enhancing the visual effect of inverted space in the fresco.

(a) (b)

Figure.7. (a) *Four People Around Pond Catching Fish*, detail from frescoe, M. Giovannetto, XIVc, Popes' Palace in Avignon, France and (b) *December,* Limbourg Brothers' Calendar, 1412-1416, (https://commons.wikimedia.org)

In the *December* painting of the Limbourg Brothers' Calendar (Fig.7, b), the tree crowns are magnified the further away they are from the observer, and the terrain with the main hunting scene, depicting it as though it has just finished, is "elevated" to allow the observer a better view of what is being portrayed.

3.2. Contemporary Examples

3.2.1. David Hockney

The inverse perspective of the chair (Fig.8) and armchair depicted by the artist David Hockney *The Chair,* 1985, oil on canvas, 122x91cm, have "changed" the geometry of their cube, turning the shown forms into something particularly interesting.

Figure.8. *Chair, Jardin de Luxembourg, Paris 10th August 1985*, photo collage, 1985 (Hockney, 1977)

In his composition *Large Interior,* Los Angeles, 1988, oil, paper and ink on canvas, 183x305cm, a visual effect is created by also combining different projection systems. The elements of the interior (walls, floor, ceiling) and the objects themselves are depicted in several different projection types such as inverse perspective, the Renaissance perspective, the axonometric projection, etc. In the photo-collage *The Desk,* 1984, where a stylish commode is shown, the visual effect of ambiguity, the concave- convex, is created through the use of inverse perspective.The central object of the composition *A Visit with Christopher and Don, Santa Monica Conyon 1984*, 1984 also by Hockney, is a round stylised table whose base appears as three paws of a sluggish, moving animal. The tabletop is depicted in a constructed inverse perspective. The inverted relief comes to the fore in the examples of the armchairs, while the spatial "disorder" enhances the impression that this is about a psycho-drama's scenography, where each prop has its own inversely projected vanishing point. The panoramic inverse perspective with a 360° viewing angle isn't an often used projection system, but in the example by the same artist *A Walk Around the Hotel Courtyard*, Acatlan 1985 oil on 2 canvases, 183x610cm, who points to the extraordinary visual effects created by using an agitated space. As if there are no obscured zones, we can peer into each part of the depicted interior or exterior.

3.2.2. David Belmonte

In the drawing by the artist David Belmonte *Inverse Perspective*, ~2010, Sevilla, a schematic depiction of a forest is given by using the tree crowns depicted in a constructive inverse perspective, which means that the tree crowns become magnified with distance from the observer.

Figure. 9. *Bodegón perspectiva inversa* 1, painting, ~2010, Sevilla**,** (http://davidrbelmonte.blogspot.com/2010/03/perspectiva-inversa.html)

The constructive drawing *Perspectiva inversa*, ~2010, Sevilla by the same artist, shows an object and figures in an inverse perspective, with a prominent vanishing point in the viewpoint. In a correct spatial grid, where all the silhouettes of human figures and birds in flight are placed, those depicted as belonging to planes perpendicular to the painting plane are of particularly interesting. As opposed to the rules of the Renaissance perspective, the dimensions grow larger with distance moving further away from the observer. A composition, by the same artist, of a filter coffee maker (Fig.9) whose lid has an octagonal shape, and which is depicted in inverse perspective, proves the advantages of this system. This artist, while dealing with inverse perspective, has resolved space through different media. His computer graphics *Peras*, computer graphic, ~2010, Sevilla indicate a significant predisposition to using inverse perspective.

3.2.3. Guillermo Pérez Villata

The little table with a lamp, a chandelier and a chair (Fig.10), by artist Guillermo Pérez Villata, are also depicted in inverse perspective with a prominent change in their dimensions (elongation) in order to create the visual effect of impossible objects. The Corrida *Año 2000 Cartel Taurino*, 1999 by the same artist is depicted in inverse perspective with a joint contact point of horizontal intersecting curves, obscured in the composition by the entry objects. The inverse projection enables an emphasised "top-down" view, while simultaneously making the object's appearance seem more interesting than it would be with an axonometric projection, where all the intersecting curves would be congruent, and only move in a translatory way.

Figure.10. *S/T,* 1989, serigraphy, 103x74cm, Valencia, (http://www.twoartgallery.com/obras/guillermo-perez-villalta-st-serigrafia-103-x-74-cm-1989/)

4. COMPARATIVE ANALYSES

These four examples show galleons, two in a Renaissance perspective (Fig. 11. a and b) and two in inverse perspective (Fig. 11. c and d). Side-by-side analysis points to the inverse perspective enabling the "deck" to be depicted, as well as the ship's "interior" with more precision, thereby creating an additional "narrative" perspective.

(a) (b) (c) (d)

Figure.11. (a) *Fall of Icarus*, detail, P. Bruegel, ~ 1565, Musées Royaux, des Beaux Arts de Belguque, Brussels (Vöhringer,1999); (b) *Ulysses Deriding Polyphemus*, detail, J. Turner, 1829, National Gallery, London (Vöhringer,1999); (c) *Belles Heures,* Limburg Brothers, c. 1405–1409, Metropolitan Museum of Art at the Cloisters and (d) *Battle Ship*, David Belmonte, ~2010, Sevilla

(a) (b)

Figure.12. (a) *Life and Miracles of St. Nicholas (detail)*, frescoe in St. Nicholas capel, 1639, Morača and (b) *Temptation of Christ,* Limbourg Brothers, XVc (http://www.wikigallery.org/)

On the frescoe from Monastery Morača (Fig.12, a) horizontal plane of the water is shown as oblique plane. The relief of the coast is in the byzantine inverse perspective. On the similar way the water plane is painted in the example (Fig. 12, b).

The same spatial position of painted chess boards, one (Fig.13, a) made in the 14th century, and the other (Fig.13, b) six centuries later, represents the same intent of the painter to make all the fields of the chess boards visible to us. That is why they are flipped from a horizontal position to a vertical plane in both examples, while the sitting figures of the chess players retain their original position.

(a) (b)

Figure. 13. (a) *Manesse codex*, XIV c, Heidelberg University Library © Universitätsbibliothek Heidelberg, (https://digi.ub.uni-heidelberg.de/diglit/cpg848/0021) and (b) *Fišer- Spaski,* M. Srbinović, 1972, triptych, oil on canvas, 208x370cm

The artist Mladen Srbinović, in his tapestry *Nymph* 1976, tapestry, 207x198cm, creates the effect of inverse perspective in an indirect manner, i.e. by enlarging the vertical surfaces, proportional to their distance from the observer. This method of depiction allows us to view the ornaments in all of their details in the aforementioned surfaces.

5. CONCLUSION

At the recent "2016" international symposium in Belgrade, discussion on the topic of Byzantine perspective in a pair of Monge's projections (Huylebrouck, 2016) prompted the question of, what the purpose is of interpreting the projection used in medieval painting with geometric methods discovered several centuries later, more precisely in the 18th century. Our response would be that the importance and influence of Byzantine perspective today, as well as its immediate application in the fine arts of the 20th and 21st centuries, doesn't only justify the present interest that geometricians have in this method of depicting the third dimension, but also encourages more complex studies. What we are searching for, is one precise interpretation of inverse perspective depiction, which would provide, on a scientific basis, all the elements, as necessary and sufficient conditions, for establishing inverse perspective as a constructive – geometrical projection method.

REFERENCES

Antonova, C., 2010. On the Problem of "Reverse Perspective": Definitions East and West, Leonardo 43/5, pp. 464-469.

Макеш, Б., 2016. Макилатуре. Галерија Графички колектив, Београд.

Huylebrouck, D., 2016. Reverse Fishbone Perspective, Proceedings of The 5th ICGG Conference Mongeometrija 2016, Proceedings, Belgrade, Serbia, pp. 380-386.

Marcikić, I. J. and Paunović M., 2017. Inverse Perspective in Cézanne's Art, FME Transactions 45, pp. 301-306

Војиновић. В. 1988. Александар Томашевић, УЛУС, Београд.

Марцикић, И. 2002. Ефекти конструкције простора у визуелним уметностима, Doctoral dissertation, Универзитет уметности у Београду, Београд.

Јовановић, З. М., 2011. Византина у савременој српској уметности. Службени гласник, Београд.

Kusovac, N. at all. 2000. Izazov tradicije. Radionica duše, Beograd.

Hockney, D. 1977. David Hockney by David Hockney. Thames and Hudson, London.

Жегин., Л. Ф., 1970. Язык живописного произведения. (Условность древнего искусства). Искусство, Москва.

Михаиловић, М. 2002. Љубинка. УЛУС – Карић фондација, Београд.

Villata http://www.twoartgallery.com/obras/guillermo-perez-villalta-st-serigrafia-103-x-74-cm-1989/ [Accessed: 10th December 2019].

Belmonte, D. 2010. http://davidrbelmonte.blogspot.com/2010/03/perspectiva-inversa.html [Accessed: 5th April 2015].

Universitätsbibliothek Heidelberg, https://digi.ub.uni-heidelberg.de/diglit/cpg848/0021 [Accessed: 10th April 2015]

Limbourg. http://www.wikigallery.org/ [Accessed: 1st May 2020]

POLYHEDRA IN ARCHITECTURAL DESIGN

Ana-Maria Graur
Faculty of Architecture and Urban Planning, Technical University of Cluj-Napoca, Romania
PhD., Assistant, Anamaria.RUSU@arch.utcluj.ro

Carmen Mârza
Department of Building Services Engineering, Technical University of Cluj Napoca, Cluj Napoca, Romania
PhD., Associate Professor, Carmen.Marza@insta.utcluj.ro

Georgiana Corsiuc
Department of Building Services Engineering, Technical University of Cluj Napoca, Cluj Napoca, Romania
PhD., Lecturer, Georgiana.Iacob@insta.utcluj.ro

ABSTRACT

With the advent of the computer are dramatically influenced, both the shape and materialization of architecture, and of course the representation in architectural design. New trends, theories and styles appear in the architecture produced by digital. A new language of architectural forms, the so-called free forms, makes its presence felt in the built environment. The relationship between the shape of these free volumes and simple geometric volumes represents an evolution whose result is the change of the architectural paradigm towards a digital architecture. At the base of this new architecture is geometry, with its primary volumes. In this paper we want an inventory of buildings that use irregular and regular polyhedra as geometry. These polyhedral volumes allow modularity and repetitiveness, and this process can be extended to give rise to more complex forms such as free forms. Descriptive geometry must provide basic knowledge about the creation of space, shapes and methods by which they can be represented.

Keywords: irregular polyhedrons; regular polyhedrons; architectural design; descriptive geometry; applied geometry

INTRODUCTION

Over the course of time, from antiquity to the present, the relationship between geometry and architecture has been intensively studied and theorized, but only since the 16th century, starting with architect Andrea Palladio[1] (1508-1580), geometry becomes the basis of all architectural rules and typologies. As well noted by Galileo Galilei (1564-1642), also during that period: [The universe] cannot be read until we have learnt the language and become familiar with the characters in which it is written. It is written in mathematical language, and the letters are triangles, circles and other geometrical figures, without which means it is humanly impossible to comprehend a single word.

Later, in 1784, Étienne-Louis Boulléems (1728-1799), the visionary french neoclassical architect, has developed a distinctive architecture based on pure geometrical forms, characteruzed by the removal of all unnecessary ornamentation and inflating geometric shapes to a huge scale. At the beginning of the 20th century, the Formalism, as its name suggests, emphasizes the form, and the architect becomes interested in the visual relationship between the parts of the architectural object and the object as a whole. The shape, often on a monumental scale, is the center of attention, which is dominated by rigid geometric lines and shapes. In the same direction, the Bauhaus style and modernism are oriented, which through the visual vocabulary of straight,

[1] Appeared in 1570 in Venice, the treatise I quattro libri dell'architettura, in chapters XXI-XXIX deals with elements of morphology of the construction and the way of decorating them, noting compositional concepts such as hierarchy, symmetry, functional zoning, vertical structuring.

curved and diagonal lines of Friedrich Wilhelm August Fröbel (1782-1852), were oriented towards a purist image of geometry. A number of common features can be identified from the analysis of these examples: the use of simple and primary geometries, capable of symbolizing by themselves monumentality. At the end of the twentieth century, the computer appeared, and architecture began to operate with increasingly complex geometries, abandoning traditional Platonic forms in favor of formal complexity. In this paper we want to show that complex shapes can be obtained precisely by using simple geometric volumes. For a start, we will present some examples of buildings that use as architectural language irregular and regular volumes of polyhedra, being able to indicate new directions for the development of these geometric shapes.

2. IRREGULAR POLYHEDRONS

Throughout history, architects and builders have sought to perfect the shapes of buildings, but the built environment is mainly composed of primary volumes, polyhedra. A polyhedron is the natural generalization of the polygon from two-dimensional space to three-dimensional space: it is a region of space whose boundary is composed of a finite number of polygonal surfaces, any two polygonal surfaces are disjoint or have common edges and vertices. The polyhedra can be convex or concave, Figure. 1. Convex polyhedra are those polyhedra that cannot be sectioned by the planes of their faces.

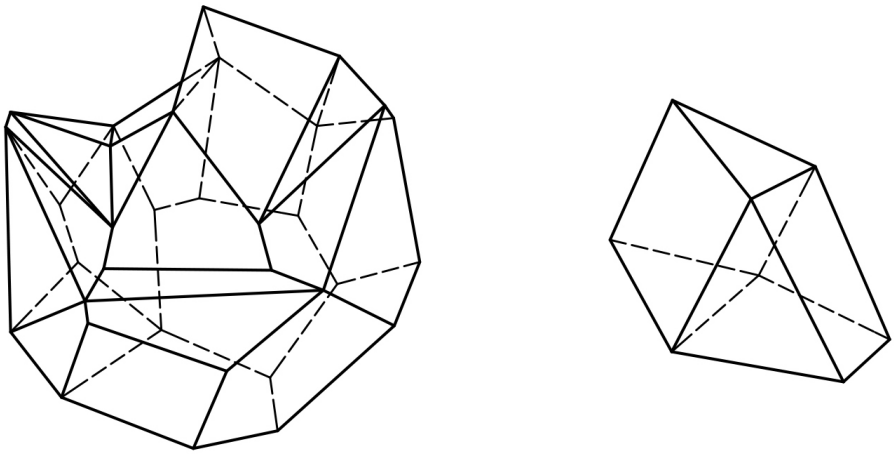

(a) (b)

Figure. 1: (a) concave polyhedra, and (b) convex polyhedra

2.1. The graphical/descriptive representation of the irregular polyhedrons

An irregular polyhedron is that polyhedron that does not meet the conditions of the regular one. It is a geometric volume bordered by flat faces, various polygons. His faces can be polygons with a certain number of sides. The sides of these polygons determine the edges of the polyhedron and result from the intersection of two adjacent faces of the polyhedron. Several edges of a polyhedron are competing in a polyhedron vertex, which is also common for at least three faces of the polyhedron Figure. 2a.

2.2. Achievements in the field of architecture

In nature we can rarely see order and symmetry, the elements of nature are in a relationship of asymmetry, implicitly, dynamism. Extrapolating we can say that the built environment adapted to nature will approach a complex, asymmetrical volume. It will allow the planimetry a greater freedom, than in the case of using the symmetry. Each architectural volume will be able to develop freely, presenting different images depending on the facade we are looking at. The building is much better adapted to the site where it is located and will be able to respect the requirement of the architectural theme. This image is also presented by Futuroscope, theme park in Poitiers, Poitou-Charentes Region, France, opened on May 31, 1987, which uses as a formal design, the prism Figure. 2b. Architect Denis Laming led the design of the pavilions, which include buildings shaped like spaceships, crystals formations emerging from the ground, and triangular wedges. What we study are the crystals formations that seem to come out of the site, giving the feeling of a continuous dynamic. Irregular polyhedral surfaces are most often found in the materialization of complex architectural forms due to flat faces Figure. 2c. One such case is the folded facade that can generate free forms. It has the advantage of generating more visual directions by the different inclination of the various planes, it can be molded on an already existing structure or it can take over the load-bearing structure by its own shape. Folded plate geometries cand take a

varieety of patterns, such as saw-tooth or polyhedral facets. [1] As we see multiplication of irregular prismatic volumes can generate a complex architecture.

(a) (b) (c)

Figure. 2: (a)irregular polyhedron (b) Futuroscope Theme Park, Poitiers, France (c) Basque Health Department Headquarters, Bilbao, Spain (b) https://jfalison.wordpress.com/2011/08/26/maddie-post-futuroscope-2/2011 (c) https://www.archdaily.com/7093/basque-health-department-headquarters-in-bilbao-coll-barreu-arquitectos?ad_medium=gallery

3. REGULAR POLYHEDRONS

These polyhedra have been studied for hundreds of years. The regular polyhedrons (platonic) have the faces formed by regular polygons with the same number of sides, and all dihedral and polyhedral angles are equal. We can say that this concept of regularity is related to the repetition of the chosen geometric elements (equilateral triangle, square, pentagon) that generates a symmetry, both in the geometric figure and in the regular volume. The regular polyhedra are inscribed to a sphere and are circumscribed to a sphere of the same center. In three-dimensional space there are five regular polyhedra, Figure. 3 namely: regular tetrahedron (4 equilateral triangle faces), octahedron (8 faces are equal equilateral triangles), cube or hexahedron (6 equal square faces), icosahedron (20 faces equal equilateral triangles), dodecahedron (12 faces equal pentagons).

This fact is a result of Euler's theorems as follows: if a convex polygon is divided into a certain number of polygons, then the sum between the faces of the polygons and the number of the vertices exceeds by one unit the number of the sides; in any convex polyhedron the sum between the number of faces and that of the vertices is equal to the number of edges increased by 2; there can be no more than five covex polyhedra having all faces having the same number of sides and all angles polyhedrons having the same number of edges [2]. Regular polyhedra are polyhedra that enjoy the following properties: all faces are equal regular polygons; the vertices are equal solid regular angles; they can be inscribed or circumscribed to spheres with the same center.

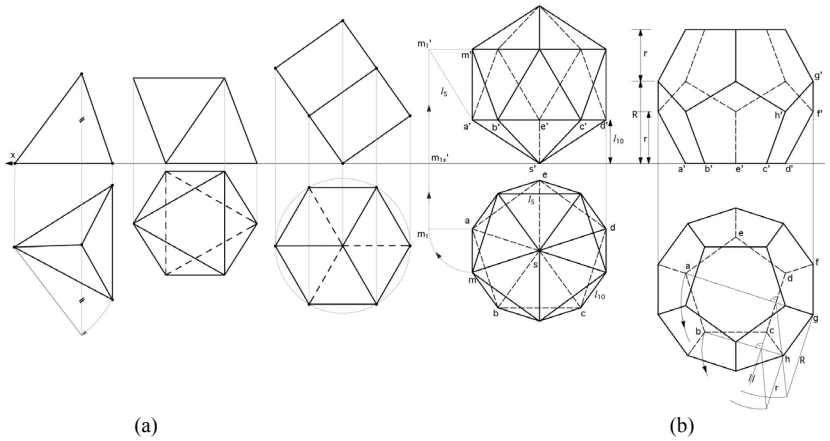

(a) (b)

Figure. 3: Platon’s polyhedra - tetrahedron, octahedron, hexahedron, icosahedron and dodecahedron

3.1. Achievements in the field of architecture

The architectural object is unique in relation to nature, more precisely to the site, and in relation to the city, socio-cultural, historical context. In this sense, the architecture uses the same interface language that also describes the physical reality, which it simulates and even more competes with through the organic architecture. But beyond the copying of nature, architecture aims, the other operating language of reality, geometry. When the geometry of regular polyhedra is used, harmony appears in the architecture, symmetry and regularity appear.

3.2.1. The Tetrahedron

Looking at The Great Pyramid of Giza we see a wonder of the ancient world that today still attracts people from all over the world. The pyramid managed to survive the present, defining our attractiveness to this simple and powerful form. Architects continue to design pyramids, in other forms, for example an identical repetitive linear sequence of a tetrahedron structure to generate a bridge. It is the case The Tetrahedron project by Christopher Charles Benninger Architects in 2011, Kolkata, West Bengal, India, Figure. 4b.

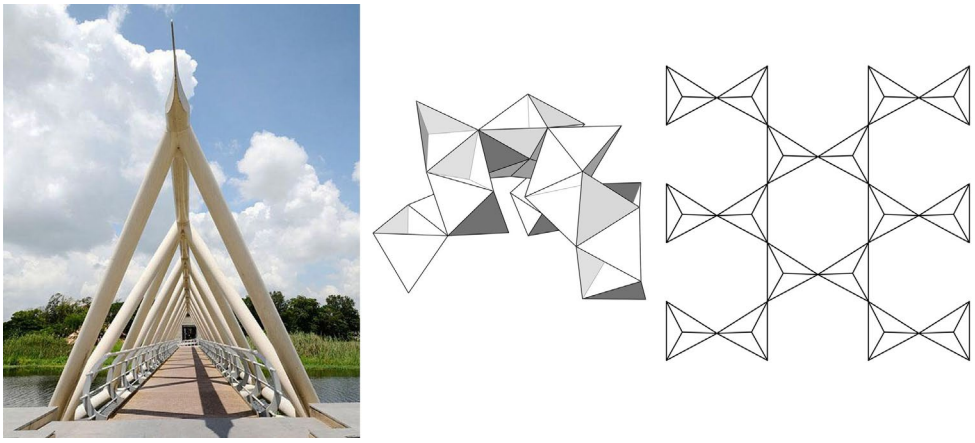

(a) (b)

Figure. 5: (a) The Tetrahedron, West Bengal, India (b) Multiplication of the Tetrahedron
(a) https://ebuild.in/the-tetrahedron-new-steel-bridge-kolkota 2018

The architect invented a system of interconnected tetrahedrons along a line. He eventually called this unique structure The Tetrahedron. The result is a number of geometries within one another, at one level being composed of three parallel and horizontal pipes, forming in section a triangle, with two pipes below a carriageway hung between them for pedestrian movement. The users walk under the third pipe above their heads, and amongst the diagonal pipes forming the tetrahedrons [3].

Finally we see that the triangular polyhedrons are not deformable, and among them the tetrahedron is the only one which can constitute on it own a covering surface [4]. To generate a complex architecture we will use the tetrahedron in a chaotic assembly. In this way we can obtain spaces both inside the tetrahedra and outside them, by joining several tetrahedra Figure. 4b. We can use this design on office or apartment buildings, which can be developed both horizontally and vertically, multi-storey buildings. Tetrahedron can be used to create a complex spatial surface or envelope resulting from joining according to the Figure 4b.

3.2.2. The Cube

The cube represents an important form in architecture because it is the basis of the geometric principle of forces in a building of most frame type structures. But we want to present a less obvious example of the use of the cube as a form of inspiration in architecture, the Kubuswoningen is located in the Oude Haven, the most historic section of Rotterdam's port, Netherland, architect Piet Blom, completed in 1984, Figure. 5a.

(a) (b)

Figure. 5: (a) The Kubuswoningen, Rotterdam, Netherland, and (b) Serpentine Pavilion and Summer Houses 2016
(a)https://www.reddit.com/cubic_houses_rotterdam_netherlands/2019 (b) https://archello.com/project/serpentine-pavilion-2016

Inside, the houses are divided into three levels accessed via a narrow staircase.The lower level is a triangular area used as the living room. The middle level houses the sleeping and bathing area, and the highest level is a spare area used either as a second bedroom or another living area [5]. Such an agglomeration of cubic spaces uses proximity to relate the spaces to each other. There are cellular spaces, repetitive with the same use. Using the cube as a closing surface, by a slight sliding or translating, you obtain tubes that vary in size, and the generated surface constantly surprises. This is also the case of the Serpentine Pavilion 2016 project, Figure. 5b. Bjarke Ingels declares: "we have attempted to design a structure that embodies multiple aspects that are often perceived as opposites: a structure that is free-form yet rigorous, modular yet sculptural, both transparent and opaque, both box and blob". [6] In this example we are dealing with the principle of reverberation, like an increasing repetition, which has to do with elements similar in shape but different in size, hierarchically graded.

3.2.3. The Octahedron

The architect Christian Norberg-Schulz (1926-2000) said that the purpose of the architecture is to give meaning to a solid and implicit matter, obtaining an identity resulting by uniqueness and identification. One of the projects we will present is an interactive and experimental pavilion made in United States, in 2013 by LMNTechStudio, Figure. 6a. This architectural object attracts the passer-by and invites the Seattle community to interact. The pavilion is clad with over 400 triangular panels. The inner face was the canvas for 54 sets of CNC cut patterns generated as part of a technology training exercise. The outer face was a canvas that addressed the community, with the help of chalk, the passer-by completely transformed the outer surface of the Octahedron [7]. With the multiplication of the octahedron we can obtain a complex shape that incorporates in each octahedron an architectural space. Joining the volumes is done either on one side or on one side of the octahedron. Another approach is to join in a flat spatial network, full or aerated by octahedra, Figure. 6b. The design of roofs or facades is varied, and different sizes of geometric bodies can be combined.

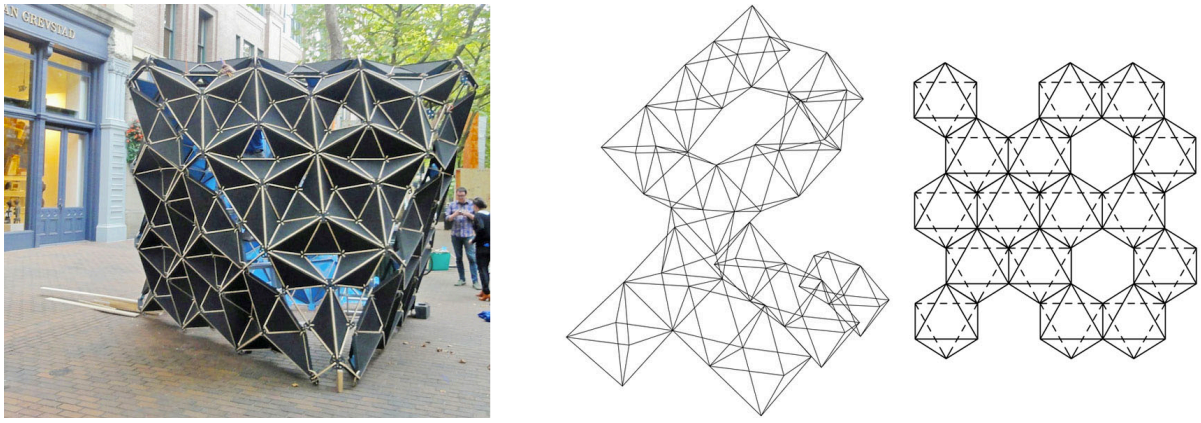

(a) (b)

Figure. 6: (a) The Octahedron, Seattle, United States, and (b) Multiplication of the Octahedron
(a) https://www.arch2o.com/the-octahedron-lmntechstudio/2013

3.2.4. The Dodecahedron

Within this section, the dodecahedron, we will present a residential project presented at a competition by the Tammo Prinz architecture office in 2014, Platonian Tower in Lima, Peru. The concept was the introduction of a cube in a dodecahedron to create a unique living space, with the possibility of extension.Obtaining such a module attempts to join them, resulting in a modular tower. The matching flat surfaces fit together perfectly for stacking. The internal cube hosts the interior spaces, while the extruded spaces can be used as additions, exterior living or just open outdoor air. Flexibility in these external sections allows for residents to change or adapt spaces as needed [7]. This repeated and combined module in terms of architectural composition generates harmony, Figure. 7a. This example deals with the singular geometric volume, but through a repetitiveness of the octahedron we can obtain an image of a complex architecture developed according to the architectural theme. A much more complex configuration can be obtained through a surface defined by the dodecahedron Figure. 7b.

(a) (b)

Figure. 7: (a) The Platonian Tower in Lima, Peru, and (b) Multiplication of The Dodecahedron
(a) https://www.archdaily.com/500635/tammo-prinz-architects-propose-platonian-tower-in-lima 2014

3.2.5. The Icosahedron

Joseph Mikrut, a graphic designer, lives in Costa Rica and initially thought of building this icosahedron structure on the ground, Figure. 8a, but he noticed the trees that attracted his attention through the branches of the branches that could sustain through the five branches the vertices of the bottom pentagon, a perfect support point. Another icosahedron structure is suspended by cables between five Melina trees [8]. These structures are grouped by proximity and have the common feature of the architectural form, the icosahedron. Here monumentality was obtained by capitalizing on only one geometric body, the icosaerd. The way to get an architecture with free forms is, as we noticed before, the repetitiveness. The geometric body has a modularity that allows the association of other icosahedrons and, thus, we extend the building in any direction we want. A surface that can become a facade can be obtained by joining icosahedrons placed on a face, Figure. 8b. Having no rigid plan, a crowded organization allows flexibility, accepting growth and change without changing its character.

(a) (b)

Figure. 8: (a) The Icosahedron Structure, Costa Rica, and (b) Multiplication of the Icosahedron
(a) http://www.hometreehome.it/icosahedron-treehouse/ 2015

5. RESEARCH DIRECTIONS

Today, the great test of architecture is the implementation of non-standard, non-Euclidean geometries, and especially those of complex sciences (fractals, strange attractors, dissipative systems). The structural efficiency and the expression or form of the building become paramount criteria in the materialization of the architecture. These complex shapes can be materialized from a geometry based on that of polyhedra, in some situations the architecture can be designed in the form of geodesic domes or parts of them, combined with other portions of free surfaces. An important feature of free-form architecture is that it structures a type of fluid space, which simultaneously forms the form, structure and facade.

The approximation of a surface with a polyhedron is more accurate as the polyhedron has smaller edges. Otherwise the two-dimensional equipartition in space lead, as particular cases, to the five regular or Platon's polyhedra.

To achieve large opening reticular domes, it is necessary to multiply the faces and vertices of these polyhedra, such as to result as many equal edges (struts) and identical solid angles (knodes). This multiplication, which is performed according to certain laws, involve that the polyhedron to follow a sphere through a series of quasi-regular polyhedra having increasingly smaller edges and faces, closer in size to the surface of the sphere or, in generally to the curved surface which supports. The reticular surfaces can be treated as a succession of joined polygons, lying on a surface [10]. We can make an infinite number of polygons that are regular, so that their peaks are located on the circumscribed circle and all their faces reach the inscribed circle.

6. CONCLUSIONS

People have always studied nature and found inspiration in everything around them. This imitation finds its answer in the geometry of the construction and in the optimization of the design solution in terms of structural and functional efficiency. Fernand Léger (1881-1955) said "Architecture is not an art, but an organic function. It grows on the ground like animals and plants, it is a function of social order. " This organic function denotes an increase and development of the architectural form, from simple to complex derived from simple geometric solids, polyhedra. Thus, we can extract some features from this analysis: first of all the call in architecture to simple, primary geometries, polyhedra of all types, capable of symbolizing by themselves the monumentality and symmetry in architecture. But in the complex architectural programs that lead to compositions with large proportions, to follow the geometric symmetry becomes a nonsense, due to the proportions it would be difficult to observe the symmetry visually. Thus, in the second variant one resorted to complex geometries using the multiplication of the same geometric volume or combined with other geometric volumes resulting in complexity, dynamism, growth, asymmetry. The possibility to multiply polyhedra in order to obtain free forms in architecture offers flexibility and can directly meet the requirements of the place, the site, becomes a spontaneous, more interesting, more natural architecture and allows in the future a possible expansion / extension of space, but without changing the original character of the architecture.

REFERENCES

Hachem-Vermette, C., 2020. Solar Buildings and Neighborhoods: Design Considerations for High Energy Performance, Springer, Calgary, Canada, pp. 149.

Tănăsescu, A., 1975. Descriptive geometry. Perspective. Axonometry, Didactic and Pedagogical Publishing House, Bucharest, Romania, pp.119-124.

Dumitrescu C., 1995. Descriptive geometry. Politehnica University of Timisoara, Romania, pp.87-90.

TETRAHEDRON, 2014 https://worldarchitecture.org/architecture-projects/hzhfn/the_tetrahedron_new_steel_bridge_at_the_indian_institute_of_management_calcutta-project-pages.html [Accessed: 3 March 2020].

Ankel, G., 1981. Experimental Sociology of Architecture: A Guide to Theory, Research and Literature. Walter de Gruyter GmbH & Company KG, Germany, pp 195.

CUBIC, 2011 https://allthatsinteresting.com/cubic-houses-rotterdam [Accessed: 3 March 2020].

CUBIC, 2016 https://archello.com/project/serpentine-pavilion-2016 [Accessed: 3 March 2020].

OCTAHEDRON, 2013 https://architizer.com/projects/the-octahedron-1/ [Accessed: 3 March 2020].

DODECAHEDRON, 2014 https://www.archdaily.com/500635/tammo-prinz-architects-propose-platonian-tower-in-lima [Accessed: 6 March 2020].

ICOSAHEDRON, 2015 http://www.hometreehome.it/icosahedron-treehouse/[Accessed: 3 March 2020].

Marza, C., Corsiuc, G. and Graur A.M., 2017. Applying the theory of the plane in the civil engineering field. JIDEG, VOLUME 12 ISSUE 1, pp 59-64.

moNGeometrija 2020

SOLVING THE 3D BIN PACKING PROBLEM TO IMPROVE TRANSPORT EFFICIENCY

Dragan Lazarević
University of Belgrade – The Faculty of Transport and Traffic Engineering, Belgrade, Serbia
PhD., Assistant, d.lazarevic@sf.bg.ac.rs

Maja Petrović
University of Belgrade – The Faculty of Transport and Traffic Engineering, Belgrade, Serbia
PhD., Assistant Professor, majapet@sf.bg.ac.rs

Aleksandar Trifunović
University of Belgrade – The Faculty of Transport and Traffic Engineering, Belgrade, Serbia
M.Sc., Assistant, a.trifunovic@sf.bg.ac.rs

Momčilo Dobrodolac
University of Belgrade – The Faculty of Transport and Traffic Engineering, Belgrade, Serbia
PhD., Associate Professor, m.dobrodolac@sf.bg.ac.rs

ABSTRACT

The application of geometric modelling in order to improve the efficiency of utilization of cargo space of vehicles is one of the steps forward in the practical application of the synthesis of basic geometric principles and computer programming. The paper presents the concept of solving a three-dimensional packing problem – the 3D Bin Packing Problem. The final result of the implementation of the aforementioned concept is the formation of a three-dimensional model of the packing plan, on the basis of which the compactness of cargo and the maximum utilization of cargo space is achieved. The applicability is shown in the example of packing packages within a company that deals with the transfer of postal express items. In such systems, solving the 3D Bin Packing Problem produces significant results. The reason for this is the stochastic nature of the transport requirements, which is primarily reflected in the different physical characteristics of the packages being transported. The efficient utilization of cargo space within transport systems contributes to the improvement of the realization of business activities and the reduction of costs.

Keywords: packing problems; 3D CAD model; cargo space engineering; transportation; postal items

INTRODUCTION

Modern transportation systems represent a significant link in the goods distribution chain. They are faced with numerous challenges which often deviate from certain standardization criteria. This primarily refers to deadlines and the structure of the transported goods. Depending on their size and business policy, companies can use their own distribution systems or the systems hired from a third party. As a consequence, distribution chains and transportation networks of different complexity are created.

The postal network is one of the most developed logistics networks which daily transports a large number of consignments from one location to another. The realization of this process requires expenses in terms of money, energy, time, as well as other necessary resources. On the other hand, all companies believe that the successful business operation is reflected in the realized profit. It can be thus concluded that the efficient performance of activities and the responsible and justified use of resources are the pre-conditions for the successful operation of every company. Since transportation activities represent the most challenging segment of consignment shipment,

their optimization is a significant factor of success. Dispatching and packing of consignments represent the reloading activities which significantly affect the efficiency of the transportation process. The manner of packing primarily affects the consignment safety and the cargo space usage, and consequently the efficiency of the total fleet. The significance of this problem is seen in the fact that in the future the postal system will witness an increasing number of consignments of non-standardized characteristics (Lazarević et al., 2019). This paper analyzed the technological process of shipping express consignments in the postal company. This company represents one of the largest logistics and distribution systems in Serbia and the region. Specific problems and challenges were identified in the process. They occur mostly due to the increasing number of non-standardized consignments in the system. One of the main causes of this tendency is the expansion of e-commerce chains and the share of postal companies in these systems, primarily in the segment of delivering the purchased goods. One of the selected problems is related to the inefficient usage of the cargo space of transportation vehicles due to the impossibility of compact packing of non-standardized consignments. This problem leads to the situation in which all consignments that are supposed to be transported to a delivery unit of the postal network cannot be packed in the envisaged cargo space of the delivery vehicle. This can result in delayed deliveries (waiting for a vehicle to return from the fieldwork or waiting for the next transportation line) or the necessity of hiring additional resources (means of transportation and couriers), which increases the expenses. This negatively impacts the sustainable development of postal services.

In the literature, this problem is named the *3D Bin Packing Problem*, or the three-dimensional packing problem. It can also have other labels containing the following keywords - *Container Loading Problems – CLP* (Mladenović et al., 2019). This problem can be solved by means of various suitable algorithms and realization software (Lazarević et al., 2019). In order to optimize the use of the cargo space when transporting consignments, this paper proposed the introduction and application of a solving concept for the *3D Bin Packing Problem*. On the basis of this concept, a geometric model of the packing plan was created in accordance with appropriate constraints. The results of the concept application were presented using an example from a real system, and the specialized software *EasyCargo* was used for solving the task of three-dimensional packing.

2. THE CONCEPT OF THE PROBLEM OF PACKING BINS INTO THE CARGO SPACE

In the literature, the packing problem is most often called the *3D Bin Packing Problem*, i.e. the three-dimensional packing problem. However, this concept was preceded by the approaches for solving one-dimensional or two-dimensional problems. One-dimensional packing is the task of placing specific goods, objects or parcels into the corresponding cargo spaces by maintaining a high level of the cargo space usage and taking care of only one constraint – dimension (for example, the transportation vehicle capacity) (Johnson et al., 1974). The two-dimensional packing problem (2D Bin Packing Problem) is the improvement of the one-dimensional problem in terms of constraints which are considered while packing. Namely, this task considers two constraints – dimensions (for example, the parcel's length and width). One of the first tasks from this field found in the literature is packing (placing) the highest possible number of small rectangles of certain dimensions (without overlapping) on the surface of a larger rectangle (Erdös&Graham, 1975). The three-dimensional packing is a special case or a synthesis of the previously defined problems which takes into consideration the minimum of three constraints – dimensions (Martello et al., 2000). The solution to this problem is creating a geometric model of the packing plan in the defined cargo space, container, on a pallet, etc. (Lazarević et al., 2019).

The *3D Bin Packing Problem* is frequently associated with loading goods and pallets into the cargo space of a delivery vehicle or into a container, but it is also related to numerous other modifications, such as pallet packing. One of the first papers on this subject was written by Wright (1974). It offered a solution related to the most suitable configuration for loading pallets into the cargo space (Wright, 1974). The 3D packing task can have different constraints and specific characteristics, such as rotating the parcels (yes/no), defining their priority when packing, stability analyses, etc. (Dube et al., 2006; Miyazawa& Wakabayashi, 2009; Junqueira et al., 2012; Lim et al., 2012). Lin et al. (2016) partially analyzed the concept of the *3D Bin Packing Problem* in the field of parcel consignment delivery. In this study, the aim was to apply the 3D packing concept while eliminating reloading of parcels after each completed delivery (Lin et al., 2016). When it comes to the consignment delivery and postal traffic, the problem was solved using the real system of the postal company in Serbia (Lazarević et al., 2019).

A significant number of algorithms for solving the tasks of 2D and 3D packing have been developed so far (Pisinger, 2002; Egeblad&Pisinger, 2009; Joung and Do Noh, 2014; Feng et al., 2015; Junqueira&Morabito, 2015; Paquay, 2016). Some of them have been applied in the corresponding specialized software.

The general mathematical problem includes the task of packing parcels of specific dimensions into a cargo space of the pre-defined structure and capacity with the aim of its maximum exploitation, i.e. compact packing and reduction of space between the parcels (Chen et al., 1995). In order to realize the mathematical model, one should know the dimensions of the available cargo spaces, as well as the dimensions of each bin which is to be loaded. One of the important suggestions is to pack the bins in so that their edges are parallel and perpendicular to the edges of the cargo space. A general model (Chen et al., 1995) is presented in the following text. The following variables and parameters were used:

- N – the total number of bins which should be packed;
- t – the total number of available cargo spaces;
- B – an arbitrarily large number;
- u_{ij} – a binary variable defining whether the bin i is placed into the cargo space j (u_{ij} = 1, when the bin i is placed into the cargo space j; u_{ij} = 0, in other cases);
- o_j – a binary variable showing whether the cargo space j is occupied (o_j = 1, when the cargo space j is occupied; o_j = 0, in other cases);
- D_j, S_j, V_j – parameters related to the length, width and height of the cargo space j;
- p_i, q_i, r_i – parameters related to the length, width and height of the bin i;
- x_i, y_i, z_i – shows the location, or the coordinates of the front bottom left corner of the bin i in the cargo space;
- d_{xi}, d_{yi}, d_{zi} – binary variables indicating whether the length of the bin i is parallel to the axes X, Y and Z. If, for example d_{yi}= 1, it means that the length p is parallel to the axis Y, while d_{yi}= 0 is the opposite;
- s_{xi}, s_{yi}, s_{zi} – binary variables indicating whether the width of the bin i is parallel to the axes X, Y and Z. If, for example s_{yi}= 1, it means that the width q is parallel to the axis Y, while s_{yi}= 0 is the opposite;
- v_{xi}, v_{yi}, v_{zi} – binary variables indicating whether the height of the bin i is parallel to the axes X, Y and Z. If, for example v_{yi}= 1, it means that the height r is parallel to the axis Y, while v_{yi}= 0 is the opposite;

The following binary variables indicate the relative position between the bins:

- a_{ik} – has the value 1 if the bin i is to the left of the bin k;
- b_{ik} – has the value 1 if the bin i is to the right of the bin k;
- c_{ik} – has the value 1 if the bin i is behind the bin k;
- g_{ik} – has the value 1 if the bin i is in front of the bin k;
- e_{ik} – has the value 1 if the bin i is under the bin k;
- f_{ik} – has the value 1 if the bin i is above the bin k.

When it comes to the observed dimensions, length always refers to the longest dimension, height to the shortest, while width refers to the medium dimension. Figure 1 represents an arbitrary cargo space j with two bins i and k. The fact that the bins i and k are in the cargo space j makes the binary variables u_{ij} and u_{kj} have the value 1. The analysis of the relative position of the bins shows that the bin i is to the right of and behind the bin k, so the variables b_{ik} and c_{ik} have the value 1. The values of the variables a_{ik}, g_{ik}, e_{ik} and f_{ik} amount to 0 in this case.

The analysis of the location of the bin i in relation to the cargo space j shows that the length of the bin p_i is parallel to the axis X (d_{xi}=1; d_{yi}, d_{zi}=0), the width of the bin q_i is parallel to the axis Z (s_{zi}=1; s_{xi}, s_{yi}=0), while the height of the bin r_i is parallel to the axis Y (v_{yi}=1; v_{xi}, v_{zi}=0). The orientation of the bin k in relation to the cargo space j is the same as in the case of the bin i, so the variables have the following values:

$$d_{xk}=1;\ d_{yk},\ d_{zk}=0;$$

$$s_{zk}=1;\ s_{xk},\ s_{yk}=0;$$

$$v_{yk}=1;\ v_{xk},\ v_{zk}=0.$$

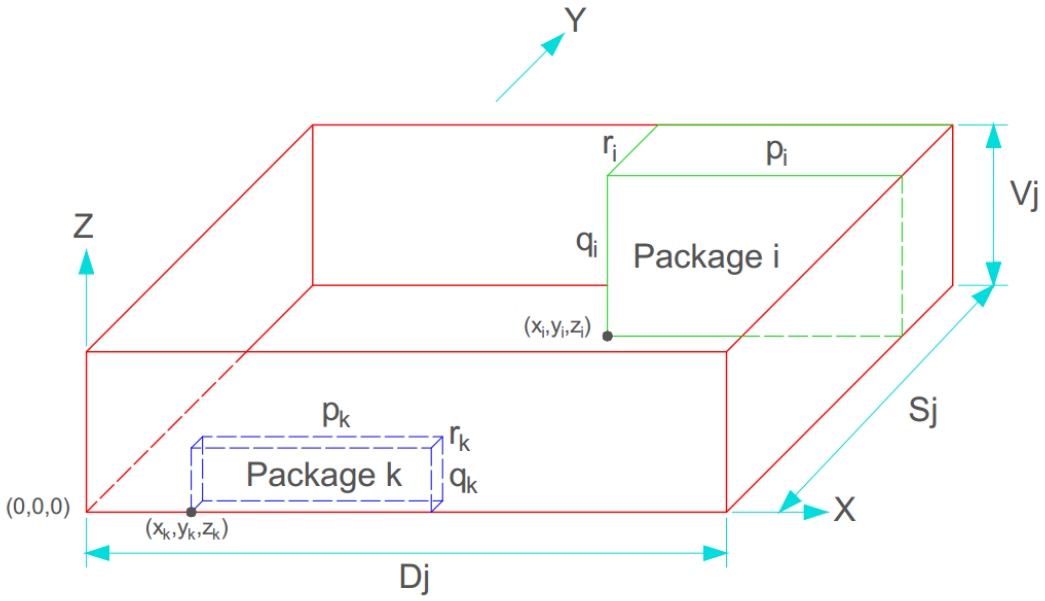

Figure. 1: The cargo space *j* with the two packed bins (package) *i* and *k*

The problem of packing bins into the cargo space is presented by means of the model of mixed integer linear programming (Chen et al., 1995):

$$\min \sum_{j=1}^{t} D_j * S_j * V_j * o_j - \sum_{i=1}^{N} p_i * q_i * r_i \qquad (1)$$

s.t.

$x_i + p_i * d_{xi} + q_i * s_{xi} + r_i * v_{xi} \leq x_k + (1- a_{ik}) * B$, for all $i, k, i < k$ (1)

$x_\kappa + p_\kappa * d_{x\kappa} + q_\kappa * s_{x\kappa} + r_\kappa * v_{x\kappa} \leq x_i + (1- b_{ik}) * B$, for all $i, k, i < k$ (2)

$y_i + q_i * s_{yi} + p_i * d_{yi} + r_i * v_{yi} \leq y_k + (1- c_{ik}) * B$, for all $i, k, i < k$ (3)

$y_k + q_k * s_{yk} + p_k * d_{yk} + r_k * v_{yk} \leq y_i + (1- g_{ik}) * B$, for all $i, k, i < k$ (4)

$z_i + r_i * v_{zi} + q_i * s_{zi} + p_i * d_{zi} \leq z_k + (1- e_{ik}) * B$, for all $i, k, i < k$ (5)

$z_k + r_k * v_{zk} + q_k * s_{zk} + p_k * d_{zk} \leq z_i + (1- f_{ik}) * B$, for all $i, k, i < k$ (6)

$a_{ik} + b_{ik} + c_{ik} + g_{ik} + e_{ik} + f_{ik} \geq u_{ij} + u_{kj} - 1$, for all $i, k, j, i < k$ (7)

$\sum_{j=1}^{t} u_{ij} = 1$, for all i (8)

$\sum_{i=1}^{N} u_{ij} \leq B * o_j$, for all j (9)

$x_i + p_i * d_{xi} + q_i * s_{xi} + r_i * v_{xi} \leq D_j + (1- u_{ij}) * B$, for all i, j (10)

$y_i + q_i * s_{yi} + p_i * d_{yi} + r_i * v_{yi} \leq S_j + (1- u_{ij}) * B$, for all i, j (11)

$z_i + r_i * v_{zi} + q_i * s_{zi} + p_i * d_{zi} \leq V_j + (1- u_{ij}) * B$, for all i, j (12)

$d_{xi}, d_{yi}, d_{zi}, s_{xi}, s_{yi}, s_{zi}, v_{xi}, v_{yi}, v_{zi}, a_{ik}, b_{ik}, c_{ik}, g_{ik}, e_{ik}, f_{ik}, u_{ij}, n_j = 0$ or 1,

$x_i, y_i, z_i \geq 0$

The objective function is used with the aim is to minimize the unused cargo space while packing. The constraints 1-6 ensure that there are no overlaps of the bin locations in the cargo space. Naturally, this constraint is valid only for the bins which are in the same cargo space, which is checked within the constraint 7. The constraint 8 guarantees that each bin can be only in one cargo space. If a bin is loaded into the cargo space, the

cargo space is considered to be used (constraint 9). The constraints 10 – 12 ensure that all the packed bins are within the physical dimensions of the cargo space.

Therefore, it can be concluded that the following applies for the variables d_{xi}, d_{yi}, d_{zi}, s_{xi}, s_{yi}, s_{zi}, v_{xi}, v_{yi}, v_{zi}:

$$d_{xi} + d_{yi} + d_{zi} = 1;$$

$$s_{xi} + s_{yi} + s_{zi} = 1;$$

$$v_{xi} + v_{yi} + v_{zi} = 1;$$

$$d_{xi} + s_{xi} + v_{xi} = 1;$$

$$d_{yi} + s_{yi} + v_{yi} = 1;$$

$$d_{zi} + s_{zi} + v_{zi} = 1.$$

Having in mind the mentioned dependencies, the variables s_{xi}, s_{zi}, v_{xi} and v_{yi} can be removed from the model, i.e. they can be expressed using other variables. Following these alterations, the model will be as follows:

$$x_i + p_i * d_{xi} + q_i * (d_{zi} - s_{yi} + v_{zi}) + r_i * (1 - d_{xi} - d_{zi} + s_{yi} - v_{zi}) \leq x_k + (1 - a_{ik}) * B \quad (1a)$$

$$x_\kappa + p_\kappa * d_{x\kappa} + q_\kappa * (d_{zk} - s_{yk} + v_{zk}) + r_\kappa * (1 - d_{xk} - d_{zk} + s_{yk} - v_{zk}) \leq x_i + (1 - b_{ik}) * B \quad (2a)$$

$$y_i + q_i * s_{yi} + p_i * (1 - d_{xi} - d_{zi}) + r_i * (d_{xi} + d_{zi} - s_{yi}) \leq y_k + (1 - c_{ik}) * B \quad (3a)$$

$$y_k + q_k * s_{yk} + p_k * (1 - d_{xk} - d_{zk}) + r_k * (d_{xk} + d_{zk} - s_{yk}) \leq y_i + (1 - g_{ik}) * B \quad (4a)$$

$$z_i + r_i * v_{zi} + q_i * (1 - d_{zi} - v_{zi}) + p_i * d_{zi} \leq z_k + (1 - e_{ik}) * B, \quad \text{za sve } i, k, i < k \quad (5a)$$

$$z_k + r_k * v_{zk} + q_k * (1 - d_{zk} - v_{zk}) + p_k * d_{zk} \leq z_i + (1 - f_{ik}) * B, \quad \text{za sve } i, k, i < k \quad (6a)$$

$$x_i + p_i * d_{xi} + q_i * (d_{zi} - s_{yi} + v_{zi}) + r_i * (1 - d_{xi} - d_{zi} + s_{yi} - v_{zi}) \leq D_j + (1 - u_{ij}) * B \quad (10a)$$

$$y_i + q_i * s_{yi} + p_i * (1 - d_{xi} - d_{zi}) + r_i * (d_{xi} + d_{zi} - s_{yi}) \leq S_j + (1 - u_{ij}) * B \quad (11a)$$

$$z_i + r_i * v_{zi} + q_i * (1 - d_{zi} - v_{zi}) + p_i * d_{zi} \leq V_j + (1 - u_{ij}) * B \quad (12a)$$

One of the additional constraints which can be included in the model, and which is particularly important for transport, is the allowed total weight of the bins, i.e. the cargo space capacity:

$$\sum_{j=1}^{t} \sum_{i=1}^{N} u_{ij} * m_i \leq M_j \quad (13)$$

where m_i is the weight of the consignment i, while M is the capacity of the observed cargo space.

The presented model is one of the general models dealing with the observed problem. These models have been developed over time. Depending on the requirements, various functionalities and constraints can be included, as in the example of defining the capacity constraint. The development of mathematical models and algorithms has considerably contributed to the development of software for solving the task of dimensional packing.

3. THE PROPOSED CONCEPT FOR SOLVING THE 3D *BIN PACKING PROBLEM* WHILE TRANSPORTING EXPRESS CONSIGNMENTS

The significance of solving the problem of three-dimensional packing while transporting express consignments relies on the fact that the transportation systems are faced with an increasing number of consignments with non-standardized dimensions. The sources of these consignments are mainly e-commerce chains. Namely, in order to improve their position in the market, attract a larger number of users and increase the profit, postal companies have to take part in the e-commerce chains. Consequently, they accept the transportation of an increasing number of non-standardized consignments. Non-standardized consignments are all the consignments whose dimensions and other features do not correspond to the regulated standards. Automated postage systems are adjusted to operate with standardized consignments so it is impossible to process non-

standardized consignments in an automated manner. Therefore, these consignments are mostly processed manually.

Significant problems arise when packing non-standardized consignments into the cargo space of a transportation vehicle. These consignments cannot be packed into the standard packaging for transporting express consignments, so they are loaded into the transportation vehicle in their own packaging (if they have one). This makes completely compact packing and minimizing the cargo space usage impossible, which can indirectly cause numerous problems. Due to the lack of space in the cargo space, it is sometimes impossible to pack all the consignments scheduled by the defined transportation timetable in accordance with the delivery deadlines. Two scenarios are possible in the mentioned situation: transportation of consignments by later departures (it can result in the delayed delivery of consignments); or engaging additional resources (transportation vehicles and couriers) in order to realize the transportation of the remaining consignments according to the pre-defined schedule. In the latter scenario, there are additional expenses which cannot be compensated through the service cost. When hiring an additional transportation vehicle, the negative impact on the environment is evident. Non-standardized consignments are subject to damages during the reloading and transportation processes. Namely, the impossibility of compact packing leaves a larger space between the consignments, which increases the possibility that the consignments will move, slide and squeeze during transportation. As mentioned above, the systems of the postal companies are faced with an increasing number of different consignments, i.e. goods of various features, sensitivity and value, which additionally aggravates the stated problem.

A concept of solving the *3D bin packing problem* has been proposed. This concept implies creating a geometric model, i.e. a plan which should be the basis for conducting packing, depending on the defined characteristics of the cargo space and consignments. The benefits of the application of this approach lie in better exploitation of the cargo space, and are primarily perceived in eliminating delays, improving consignment safety and decreasing the number of required transportation resources (reducing the costs and negative impact on the environment).

The realization of the concept for solving the 3D bin packing problem within the system of transporting express consignments can be presented in the following steps (Lazarević et al., 2019):

- Step 1: collecting information about the physical characteristics of consignments (length, width, height and weight);
- Step 2: defining the cargo space, i.e. the transportation vehicle;
- Step 3: the application of the software for solving the 3D bin packing problem;
- Step 4: the analysis of the obtained solution;
- Step 5: packing of the consignments according to the defined geometric model of the packing plan.

4. SOLVING THE 3D BIN PACKING PROBLEM USING AN EXAMPLE FROM THE REAL SYSTEM FOR TRANSPORTING EXPRESS CONSIGNMENTS

The analyzed packing task refers to an example from a real system of the postal company. The consignments were supposed to be transported from the processing centre to the corresponding unit of the postal network. The vehicle *Peugeot Partner* was available. When loading the consignments into the transportation vehicle, certain number of them (approximately 10%-15% of the total quantity) could not fit into the envisaged cargo space. The application of the proposed concept enables creating the geometric model of the packing plan, which will help all consignments to be packed, and indicating the impossibility of loading all the consignments in the envisaged cargo space. The results related to the latter situation can initiate changes in transport organization (hiring a transportation vehicle with a larger cargo space capacity, distributing the consignments to two or more transportation vehicles).

The first step involves collecting the information about the physical characteristics of consignments. This concept is not implemented in the observed company (there is no system for collecting all necessary information). Thus, in the studied case it was not possible to precisely define the required characteristics because the standard business process does not include such records. Table 1 shows the requirements, i.e. the number and characteristics of the consignments which should be packed into the cargo space of a specific transportation vehicle. Precise data about the characteristics were considered for standard consignments (packaging dimensions), while the characteristics of the remaining non-standardized consignments were defined in cooperation with the company

employees who worked on the jobs of consignment reloading and directing. Modern systems based on 3D scanners can collect precise information about the physical characteristics of consignments. Accurate data on the consignments' weights were not available, but the total weight was within the limits of the cargo load capacity of the envisaged transportation vehicle, according to the employees' estimation. This is the reason why the consignments were assigned arbitrary weight values.

Table 1: Characteristics of the requirements

Packaging type	*Dimensions (length x width x height) [mm]*	*Quantity*
Cardboard bins T1	*(250x175x100)*	*53*
Cardboard bins T2	*(350x250x120)*	*33*
Bulk bins	*(550x500x400)*	*9*
Sacks	*(1000x350x350)*	*2*
Consignments of non-standardized packaging		*47*

Step 2 defines the cargo space where the consignments are supposed to be packed. In the analyzed case, the used vehicle was *Peugeot Partner,* with the capacity of approximately 650kg, and the following dimensions of the cargo space: length - 1800mm; width - 1620mm; height - 1250mm.

In step 3, the software is applied to solve the *3D Bin Packing Problem*, i.e. the geometric model of the packing plan is created. In this specific case, the obtained solution stated that all the stored consignments could be packed in the defined cargo space. However, in the reality 10% - 15% of the total quantity of the consignments remained out of the cargo space. In the solution, the cargo space usage, presented by the occupancy rate, amounted to around 80%. The consignments requiring special handling, particularly the fragile ones, which were outside of the bulk bins, were included in the packing plan by the software users in order to increase their safety level (Lazarević et al. 2019). Figures (Fig. 2 – 4) offer the geometric presentation of the packing plan models using different views, which was obtained as the graphic output of the software.

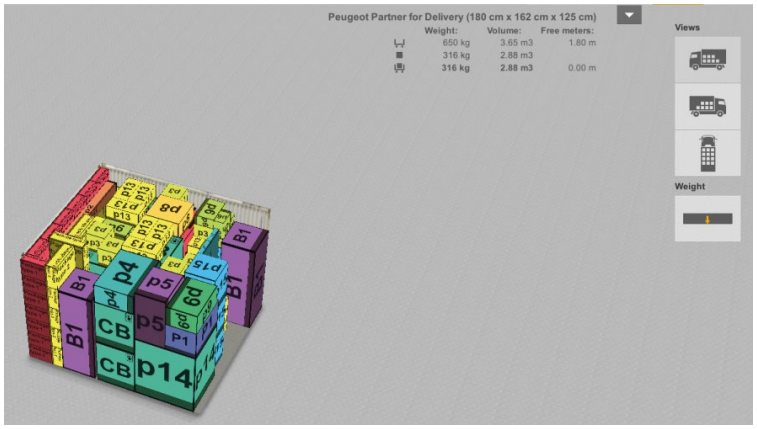

Figure. 2: The geometric model of the packing plan (perspective view 1)

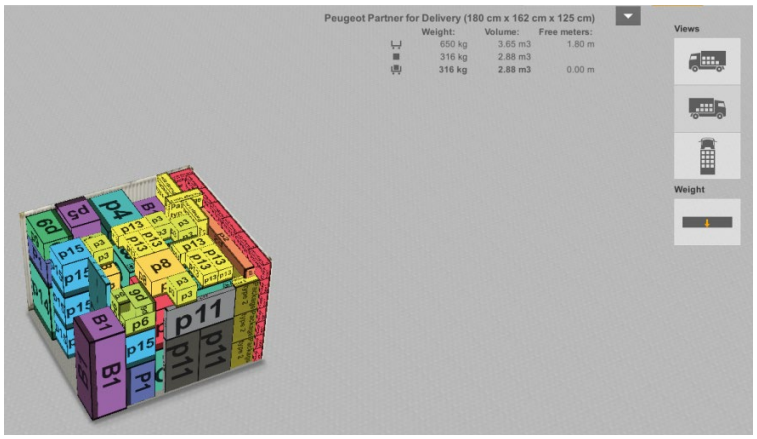

Figure. 3: The geometric model of the packing plan (perspective view 2)

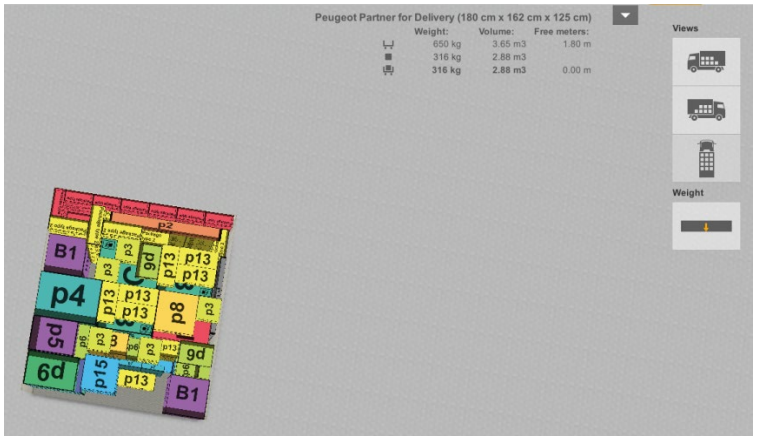

Figure. 4: The geometric model of the packing plan (perspective view 3)

Thus obtained solution can be decomposed in order to obtain a more detailed visual plan. The decomposition level depends on the consignment structure, i.e. the level of visibility of the consignments' position in the cargo space (Lazarević et al. 2019). The following figures (Fig.5 – Fig.7) show the packing plan with an arbitrary decomposition level.

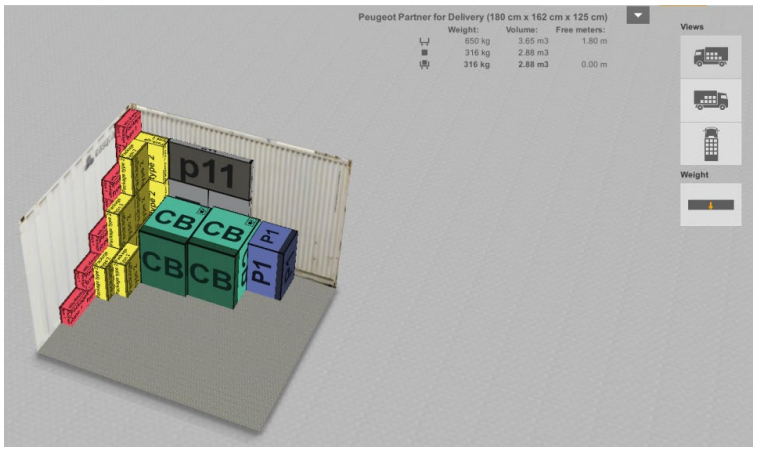

Figure. 5: The decomposed geometric model of the packing plan – level 1

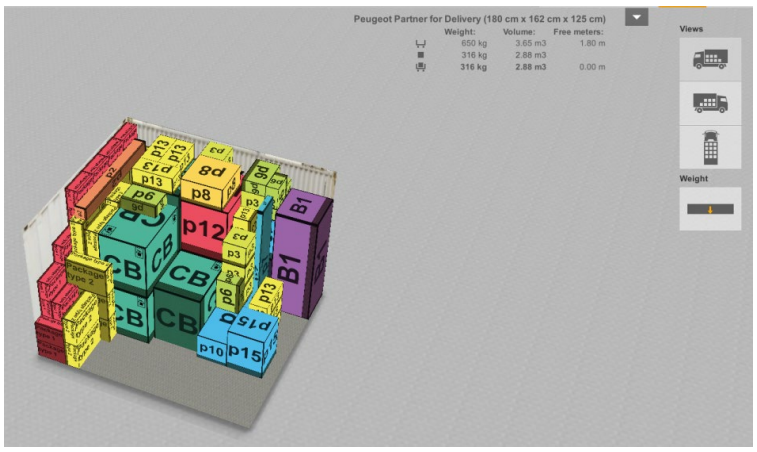

Figure. 6: The decomposed geometric model of the packing plan – level 2

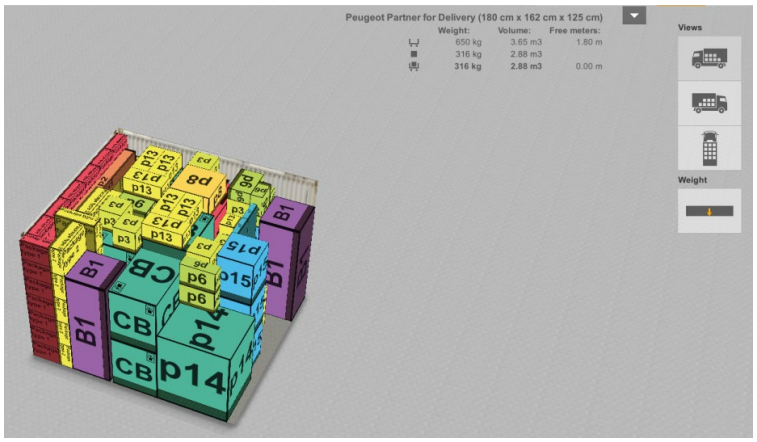

Figure. 7: The decomposed geometric model of the packing plan – level 3

The number of decomposition levels depends on the structure of the geometric model of the packing plan. In theory, the number of decomposition levels can be equal to the number of consignments which are to be packed. The last level represents the complete packing plan which is presented in this paper by means of various perspective views, as the obtained final solution.

The analysis of the solution involves checking whether all the consignments are in the packing plan, as well as checking the position of the consignments requiring special handling and including sensitive content. The software enables manual correction of the consignment position if required, as well as the generation of the records regarding their status. On the basis of the solution and created geometric model of the packing plan, transportation vehicles are analyzed in order to find out the most suitable one for transportation. In the case of the low level of the cargo space usage, a transportation vehicle of lower capacity should be considered. On the other hand, when the cargo space capacity of the transportation vehicle is insufficient for all consignments, the task to be solved is the selection of the transportation concept – a larger transportation vehicle or 2 or more small vehicles (Lazarević et al. 2019). In the studied situation, there were no significant corrections, and the ones which were conducted are part of the presented final solution of the geometric model of the packing plan.

5. CONCLUSION

Improving the sustainability of transportation systems represents a significant initiative for transportation companies and for the companies whose operation is based on transportation activities, and for society as a whole. Distribution systems ensure the transportation of various goods to specific locations, while forming a complex logistics chain based on the developed and strong infrastructure. Depending on the nature of the distributed goods, the technological process of transportation has specific characteristics. One of the common tasks is the efficient usage of the available transportation resources. This study analyzed the problem of the efficient usage of the cargo space of transportation vehicles.

The paper observed the technological process of transporting express consignments in the postal company which represents one of the largest logistics and distribution centres in Serbia and the region. The observed problem was related to packing postal consignments into the cargo space of transportation vehicles while transporting the consignments between postal centres and delivery units of the postal network. In the future, the expansion of e-commerce will result in a larger number of non-standardized consignments, which will make the packing problem even more complex. In order to solve the mentioned problem, i.e. to optimize the cargo space usage when transporting consignments, the application of a concept for solving the packing problem (*3D Bin Packing Problem),* was proposed in the paper. On the basis of this concept, a geometric model of the packing plan was created according to corresponding constraints. The application of the concept can generate a solution for compact consignment packing with a high level of the cargo space usage or indicate the insufficient cargo space capacity of the analyzed transportation vehicle. In the literature and in practice, there have been a large number of algorithms and examples of software for solving the *3D Bin Packing Problem.*

Using an example from a real system, the paper proved the applicability of the proposed concept. The results of the application of the *EasyCargo* software were presented in the form of geometric models of the packing plan.

REFERENCES

1. Chen, C. S., Lee, S. M. and Shen, Q. S., 1995. An analytical model for the container loading problem. *European Journal of Operational Research*, 80(1). pp 68-76.
2. Dube, E., Kanavathy, L. R., and Woodview, P., 2006. Optimizing Three-Dimensional Bin Packing Through Simulation. In Sixth IASTED International Conference Modelling, Simulation, and Optimization, Gaborene, Botswana.
3. Egeblad, J. and Pisinger, D., 2009. Heuristic approaches for the two-and three-dimensional knapsack packing problem. *Computers & Operations Research*, 36(4). pp 1026-1049.
4. Erdös, P. and Graham, R. L., 1975. On packing squares with equal squares. *Journal of Combinatorial Theory*, 19(1). pp 119-123.
5. Feng, X., Moon, I. and Shin, J., 2015. Hybrid genetic algorithms for the three-dimensional multiple container packing problem. *Flexible Services and Manufacturing Journal*, 27(2-3). pp 451-477.
6. Johnson, D. S., Demers, A., Ullman, J. D., Garey, M. R. and Graham, R. L., 1974. Worst-case performance bounds for simple one-dimensional packing algorithms. *SIAM Journal on computing*, 3(4). pp 299-325.
7. Joung, Y. K., and Do Noh, S., 2014. Intelligent 3D packing using a grouping algorithm for automotive container engineering. *Journal of Computational Design and Engineering*, *1*(2). pp 140-151.
8. Junqueira, L. and Morabito, R., 2015. Heuristic algorithms for a three-dimensional loading capacitated vehicle routing problem in a carrier. *Computers & Industrial Engineering*, 88. pp 110-130.
9. Junqueira, L., Morabito, R. and Yamashita, D.S., 2012. Three-dimensional container loading models with cargo stability and load bearing constraints. *Computers & Operations Research*, 39(1). pp 74-85.
10. Lazarević, D., Dobrodolac, M. and Petrović, M., 2019. Optimizacija iskorišćenja tovarnog prostora formiranjem geometrijskog modela plana pakovanja pošiljaka. Proceedings of The International Scientific Conference on Information Technology and Data Related Research Sinteza 2019, Novi Sad, Serbia. pp 45-51.
11. Lim, A., Ma, H., Xu, J. and Zhang, X., 2012. An iterated construction approach with dynamic prioritization for solving the container loading problems. *Expert Systems with Applications*, 39(4). pp 4292-4305.
12. Lin, C. C., Kang, J. R., Liu, W. Y and Li, C. C., 2016. On two-door three-dimensional container packing problem under home delivery service. *Journal of Industrial and Production Engineering*, 33(3). pp 205-214.
13. Martello, S., Pisinger, D. and Vigo, D., 2000. The three-dimensional bin packing problem. *Operations research*, 48(2). pp 256-267.
14. Miyazawa, F. K. and Wakabayashi Y., 2009. Three-dimensional packings with rotations. *Computers & Operations Research*, 36(10). pp 2801-2815.
15. Mladenović, S., Zdravković, S., Vesković, S., Janković, S., Đorđević, Ž., and Đalić, N., 2019. Development of a Novel Freight Railcar Load Planning and Monitoring System. *Symmetry*, *11*(6). pp 756.
16. Paquay, C., Schyns, M. and Limbourg, S., 2016. A mixed integer programming formulation for the three-dimensional bin packing problem deriving from an air cargo application. *International Transactions in Operational Research*, 23(1-2). pp 187-213.
17. Pisinger, D., 2002. Heuristics for the container loading problem. *European journal of operational research*, 141(2). pp 382-392.
18. Wright, P., 1974. Pallet loading configurations for optimal storage and shipping. *Paperboard and Packing*, pp 46-49.

SIMULATION ANALYSIS OF THE SPATIAL DISTRIBUTION OF MARKET STALLS IN THE PUBLIC OPEN SPACE

Tanja Mitrović
Department of Architecture and Urban Planning, University of Novi Sad, Republic of Serbia
Research Assistant, mitrovict@uns.ac.rs

Vesna Stojaković
Department of Architecture and Urban Planning, University of Novi Sad, Republic of Serbia
PhD, Associate professor, vesna100@uns.ac.rs

ABSTRACT

The design of public open spaces affects the movement of people, their behaviour and interaction. For temporary settings in public spaces, there are generally no defined rules that dictate their spatial distribution. In this study we intend to improve functionality of public open space during the events by proposing a multi-agent simulation-based model as a decision-making support tool.

Simulation analysis is based on a model in which agents in the pedestrian flow represent visitors of the event and passers-by. The results presented in this paper show that the distribution of market stalls affects the retention time of both groups of agents in the analysed public open space. The case study was conducted for a real space, the main square in Novi Sad, where we compared different spatial distributions of the same number of market stalls based on agents' spent time. The aim of the research is to contribute to better decision making and to point out the impact of things that are often overlooked in the design process.

Keywords: agent-based modelling; spatial simulation; urbanism; decision-making support

1. INTRODUCTION

The inter-relationship between the built environment and human spatial behaviour is one of the focal point of architectural and urban design (Haklay et al., 2001; Loscos, et al., 2003; Turner et al., 2002). Urban and architectural design practitioners design the physical environment in a way that is best adapted to human spatial behaviour as much as possible considering the planned use of space. This process often relies on existing knowledge of how people have used space in similar situations, anticipating users' activity in advance. When it comes to temporary settings, such as market stalls during events in public space, they are often overlooked in the planning process.

The approach that proves to be promising in overcoming these problems is computational simulations, allowing us to test hypotheses and phenomena that have proven complex in the real world (Gilbert, 2008). A specific tool in computational simulations which is extremely relevant to this field is agent-based modelling (ABM) (Karbovskii et al., 2018; Ligtenberg et al., 2001). Agent-based modelling by capturing the use of public space can help provide a controlled environment for a better understanding of human spatial activities as they manifest in the real world. ABM allows us to explore the dynamics and processes that take place in interactions between individuals, as well as interactions between individuals and the environment (Benenson, 1998; Trakulpipat et al., 2008; Zhu et al., 2008). For this reason, the ABM approach was used for the purposes of this research.

The purpose of such simulations is to enable the evaluation of multiple design iterations and optimize performance criteria, such as urban space functionality and quality, as well comfort of its users (Ewing et al., 2009). The simulated pedestrian's activities in the survey area can provide adequate feedback for urban planners, predicting pedestrian flow and examining potential scenarios. This can contribute to better decision-making during the planning process and therefore to the sustainability of the urban environment. It is reflected in the optimization of the urban planning process and the adoption of responsive design solutions.

The aim of the paper is to examine the impact of the spatial distribution of market stalls on the retention time of urban space users in order to select the layout that is most favourable to minimize the walking duration of people who pass through this area daily. To this end, the model is created with two groups of agents, visitors and passers-by, with assigned behaviour patterns. The possible layouts for a spatial distribution of market stalls for a specific real space - the main square in the Novi Sad, were selected. Simulations were performed for all spatial layouts and time analysis was carried out. The model proposed in this paper is generated in Grasshopper, linking the personal templates of PedSim, an agent-based simulator, to the geometry from Rhinoceros.

2. METHODOLOGY

For the purpose of this research, PedSim was employed since it is an agent-based simplified pedestrian simulator adapted for use by urban planners (PedSim, 2019). It is a Grasshopper add-on which working principle is based on a multiple force model. In other words, for agent's movement are used: target force, person repulsion, obstacle repulsion and anticipatory collision avoidance force. The direction of agent's movement in PedSim is defined by the starting point and the end point. Agents follow the best route that will led them to the end point. It also includes rerouting to avoid obstacles and collisions. PedSim also provides an introduction of targets that are of interest to the agents, and which they will visit if they see them on their way from the starting point to the end point. In order to perform the simulation with this tool it is necessary to enter the required input data. Person templates, targets and obstacles are the main input data and they are defined below in accordance with the needs of this research.

Since the Square is located at the meeting of six pedestrian streams (Kralja Aleksandra Street, Modene Street, Zmaj Jovina Street, Katolička porta, Njegoševa Street and Pozorišni trg), we introduced six points which represent starting and end gates for agents. One point is set up in each street. The relationship of points is defined so that each of them represents the starting gate for agents in corresponding street, but also the end gate for agents who start moving from other points. In this way, 15 intermediate routes were established. However, it was also necessary to define their movement directions and person templates so that further analyses can be made. The movement in both directions was introduced, so 30 directions of motion were obtained. The first 15 directions are determined by connecting all points to each other and for these directions are assigned person templates with identifications (ID) 1 and 3. An ID 1 represents passers-by, that is, agents moving from one point to another without delay and an ID 3 is a tag of visitors, that is, agents who will turn to one of the stalls and linger for a while and then continue to move to the end point. The other 15 directions represent opposite directions to the first ones, with agents labelled as ID 2 and ID 4. These marks represent passers-by and visitors, respectively. The pattern of their movement is the same as in the first case. In other words, we have two types of agents in the model: passers-by that include agents labelled with ID 1 and ID 3 and visitors, that is, agents labelled with ID 2 and ID 4. ID tags are necessary for further analysis of time spent. Figure 1 shows the directions of movement with corresponding person templates.

For simulation purposes four layouts of spatial distribution of market stalls are proposed. They were selected based on the closest resemblance to the most commonly used arrangement of market stalls during events in the Square. The module with a rectangular 3x4 m base was used to represent each market stall individually. All four layouts have 20 pieces of these identical modules that are arranged in different ways. They are recognized in PedSim as targets for visitors. Layouts are shown in Figure 2.

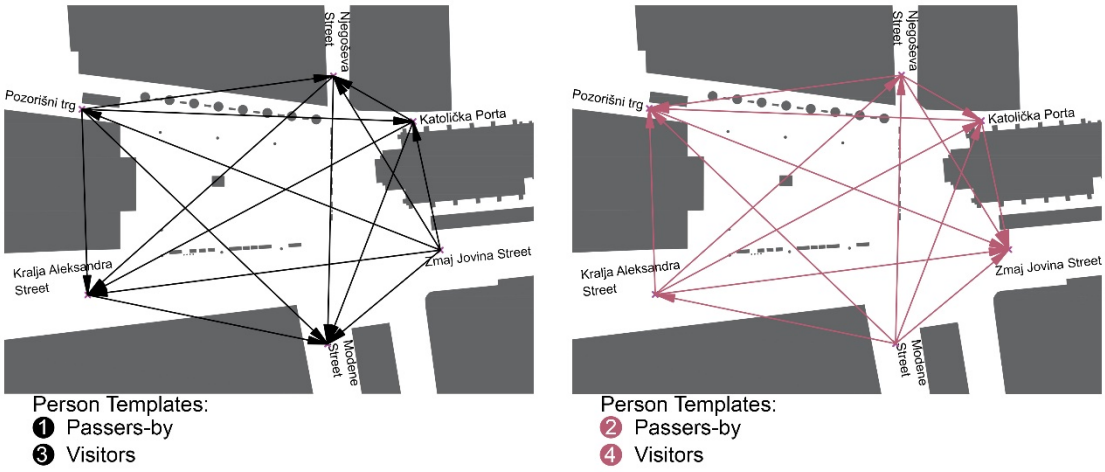

(a) (b)

Figure. 1: Directions of movements with corresponding person templates: (a) Initially established directions of movements, and (b) Opposite directions of movement (Source: Authors)

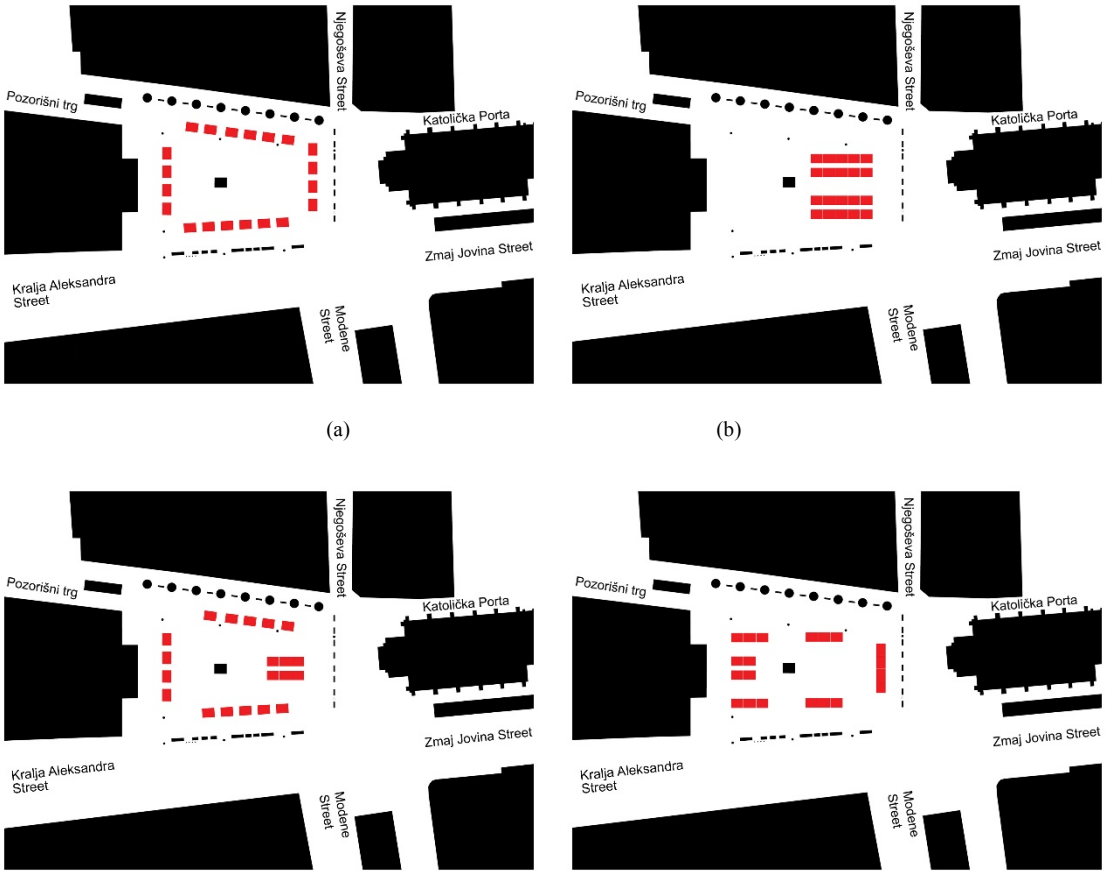

(a) (b)

(c) (d)

Figure. 2: Selected layouts of spatial disposition of market stalls to be analysed: (a) Layout 1: Stalls are placed along the rim of the Square, (b) Layout 2: Stalls are grouped into two equal clusters on the northeast side of the Square (c) Layout 3: Stalls are placed in a way which represents one of the possible combinations of the first two layouts, and (d) Layout 4: Stalls are organized into smaller groups with denser positioning on the southwest side of the Square (Source: Authors)

Stalls, along with surrounding buildings and existing fixed urban furniture, are obstacles to the movement of pedestrians. As such, they affect the movement patterns of agents and the duration of movement. All these

elements of the built environment are defined in Rhinoceros by polylines, in order to be recognized in PedSim as obstacles. One of PedSim's outputs is a record of the start time and end time of agent's movement. Not all agents are generated from the starting point at the same time, but go one after another, and therefore there are differences between start times and end times. They follow different routes, which also affects the diversity of end times. Because of that it was necessary to sort agents by using IDs in defining person templates, as shown earlier. This time records were used to calculate the duration of movement of each agent and further to calculate the total movement time of both groups of agents.

3. INPUTS

In order to run the simulation, the additional setup of following parameters was implemented: target force, body radius, population, generation time, visiting time and probability. Target force is a component that affects the speed of movement of agents and it is set for all agents to the same value. An equal body radius of 0.35 m was used for all agents. Each simulation was performed with a total of 300 agents with the same time of their generating. Visiting time for all stalls is also same. In determining the visitors' interest targets, it was also necessary to specify the exposed sides of the stalls so that each stall is assigned a point on the side from which visitors can access. Probability is defined as the proportion of people and a 60/40 ratio for the benefit of passers-by is adopted. Simulations were stopped when the total number of agents arriving at the end points was 300, where the ratio of passers-by and visitors who reached their destination may be different from 60/40 at that moment.

4. RESULTS AND DISCUSSION

Four simulations were performed for selected and already presented spatial distributions of market stalls in the main square in Novi Sad. Figure 3 shows traces of simulated movements of all agents. It is noticeable that collective movement patterns change depending on the stall layout applied.

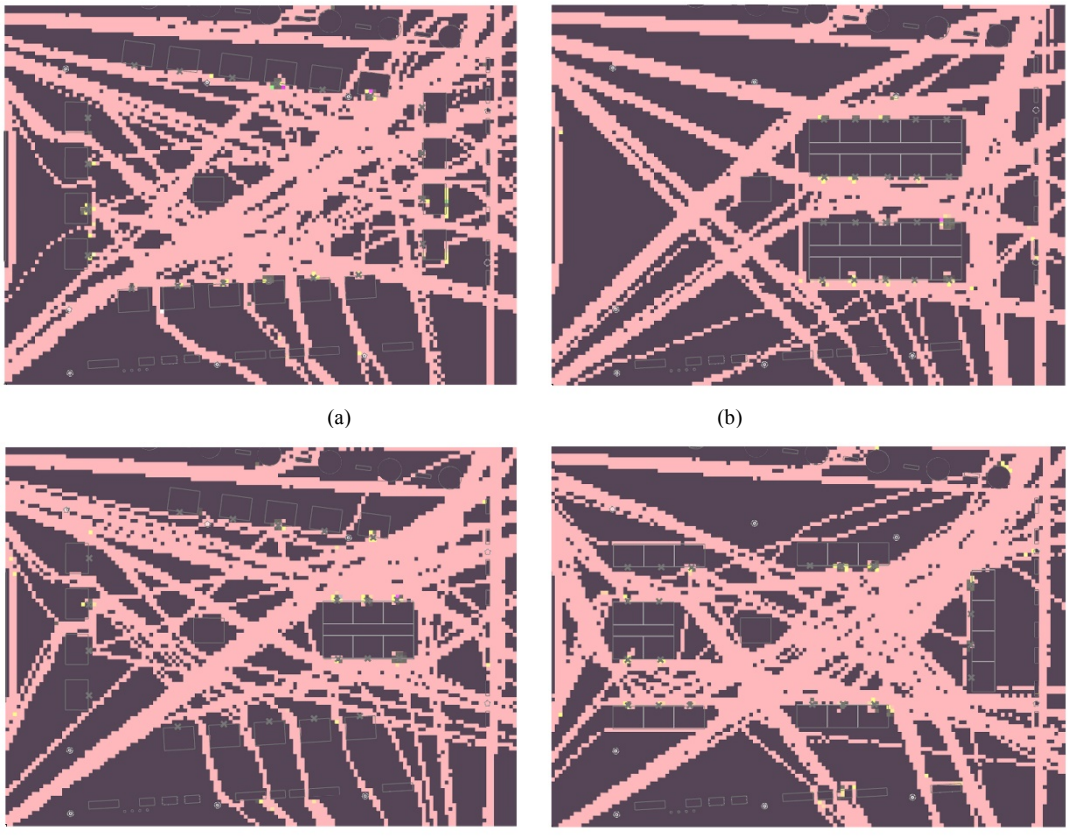

(a) (b)

(c) (d)

Figure. 3: Traces of the movement of agents in the Square shown by a heat map for the following spatial distributions of market stalls: (a) Layout 1, (b) Layout 2, (c) Layout 3, and (d) Layout 4 (Source: Authors)

Results given in Figure 4 show that the spatial distribution of the market stalls has a significant impact on the duration of movement for both group of agents. The graph shows the total score for all four person templates, with the results of the agents labelled with ID 1 and ID 2 having been summed up and displayed under the name of passers-by. Likewise, the results of the time duration for agents labelled with ID 2 and ID 3 are shown under the name visitors. The obtained results point out that the distribution of stalls with Layout 2 is convenient to saving visitors time. On the other hand, stalls arranged according to Layout 4 are well-favourable to save time for passers-by who are the focus of this paper.

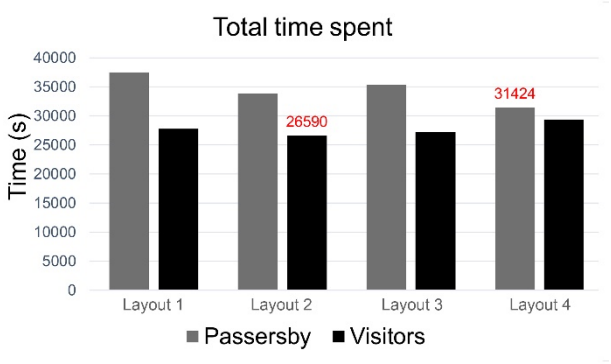

Figure. 4: The total time that all agents together spent in all four simulations.
The minimum values of time spent for both visitors and passers-by are marked. (Source: Authors)

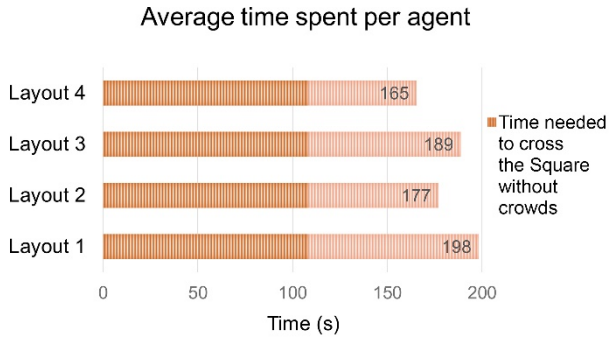

Figure. 5: Comparative representation of the average times that one agent spend crossing the Square without crowds and one passer-by spend within all four layouts (Source: Authors)

For the sake of comparison, as shown in Figure 5, a simulation of the same number of agents without market stalls was also performed and it was found that it took an average of 108 seconds for one agent to cross the Square without the crowds. The average time that one passer-by spent in the simulation of the Layout 4 (with a total of 190 passers-by) is 165 seconds, which is 12 seconds less than Layout 2 (with a total of 192 passers-by). This difference is not large, but it represents 11% of the time that one passer-by spends on average when crossing the Square without the crowds. Since this paper is tasked with finding a spatial distribution of mark stalls that reduces the duration of movement of passers-by, Layout 4 is chosen as the most appropriate solution.

5. ASSUMPTIONS AND CONSTRAINTS

The method described in this paper cannot be applied to urban areas with dynamic terrain configuration since PedSim only handles 2D scenarios. It also does not take into account the spontaneous stopping of the movement of people in the Square when meeting or taking pictures, forming smaller or larger groups. The number of agents emerging from the starting point cannot be randomly generated, but can only be set as one at a time, or two at a time, and so on. In these aspects, the limitations of PedSim can affect the accuracy of the final conclusion.

A subsequent study could be concerned with manipulating parameter values and features such as visiting time and target of interest, which would make it possible to prioritize the attractiveness of the market stalls.

Another possible direction for future developments is a more complete and sophisticated approach to social variables. This aspect is of special importance considering the use of pedestrian models in event planning. It is clear that future work will move on multiple fronts, which is made possible by the flexibility of the ABM paradigm.

6. CONCLUSION

Results obtained in this research proved that the significance of the spatial distribution of the market stalls in urban space is greater than it is believed since it is generally neglected in the design process. It is shown that the agent-based modelling approach is highly applicable to this field and the ability of the multi-agent based tool to examine urban form and to assist in decision-making is justified. The presented method supports the use of simulation based models for estimating walkability parameters, specifically duration of movement, which is an important component of urban quality. By defining person templates, this work presents a generalized model of collective human spatial behaviour, designed so that it may be more easily incorporated to specific layouts of spatial distribution of market stalls. The model was designed and implemented in two-dimensional space using simplified geometry. Future studies are encouraged to examine the use of an agent-based model as a tool to contribute to the creation of sustainable urban environment.

ACKNOWLEDGMENT

This research (paper) has been supported by the Ministry of Education, Science and Technological Development through the project no. 451-03-68/2020-14/200156: “Innovative scientific and artistic research from the FTS (activity) domain”.

REFERENCES

1. Benenson, I., 1998. Multi-agent simulations of residential dynamics in the city. *Computers, Environment and Urban Systems*, 22(1). pp 25-42.
2. Ewing, R. and Handy, S., 2009. Measuring the Unmeasurable: Urban Design Qualities Related to Walkability. *Journal of Urban Design*, 14(1). pp 65-84.
3. Gilbert, N., 2008. Agent-Based Models. Series: Quantitative applications in the social science. Los Angeles, SAGE Publications, Inc.
4. Haklay, M., O'Sullivan, D., Thurstain-Goodwin, M. and Schelhorn, T., 2001. "So go downtown": simulating pedestrian movement in town centres. *Environment and Planning B: Planning and Design*, 28(3), pp 343-359.
5. Karbovskii, V., Voloshin, D., Karsakov, A., Bezgodov, A. and Gershenson, C., 2018. Multimodel agent-based simulation environment for mass-gatherings and pedestrian dynamics. *Future Generation Computer Systems*, 79(1). pp 155-165.
6. Ligtenberg, A., Bregt, A.K. and van Lammeren, R. 2001. Multi-actor-based land use modelling: Spatial planning using agents. *Landscape and Urban Planning*, 56(1-2). pp 21-33.
7. Loscos, C., Marchal, D. and Meyer, A., 2003. Intuitive Crowd Behaviour in Dense Urban Environments using Local Laws. Proceedings of the Conference: Theory and Practice of Computer Graphics, NW Washington, DC, United States. pp 122.
8. PedSim, 2019. https://www.food4rhino.com/app/pedsim [Accessed: 25th February 2020].
9. Trakulpipat, C. and Sinthupinyo, S., 2008. Designing Market Stall Layout by Agent-Based Simulation. Proceedings of the IMECS International MultiConference of Engineers and Computer Scientists, Hong Kong, China.
10. Turner, A. and Penn, A., 2002. Encoding natural movement as an agent-based system: an investigation into human pedestrian behaviour in the built environment*, Environment and Planning B: Planning and Design*, 29(4). pp 473-490.
11. Zhu, W. and Timmermans, H., 2008. Cut-off models for the 'go-home' decision of pedestrians in shopping streets, *Environment and Planning B: Planning and Design*, 35(2). pp 248-260.

GEOMETRY OF SOLAR TOWER WITH ELLIPTICAL TORUS MIRROR

Miša Stojićević
Faculty of Mechanical Engineering, University of Belgrade, Republic of Serbia
PhD., Assistant Professor, mstojicevic@mas.bg.ac.rs

Branislav Popkonstantinović
Faculty of Mechanical Engineering, University of Belgrade, Republic of Serbia
PhD., Full - Time Professor, dr.branislav.pop@gmail.com

Zorana Jeli
Faculty of Mechanical Engineering, University of Belgrade, Republic of Serbia
PhD., Associate Professor, zjeli@mas.bg.ac.rs

Ivana Cvetković
Faculty of Mechanical Engineering, University of Belgrade, Republic of Serbia
M.Sc., Teaching Assistant, ivanacvetkovic1992@gmail.com

Boris Kosić
Faculty of Mechanical Engineering, University of Belgrade, Republic of Serbia
M.Sc., Teaching Assistant, bkosic@mas.bg.ac.rs

ABSTRACT

An intense increase of research in "green" technologies brings a variety of science fields in common goal to contribute sustainable development. Such an example is concentrated solar power (CSP) which combines knowledge of astronomy, thermodynamics, mechatronics and geometry in one final product. The solar power tower is a system that uses an array of flat, movable mirrors called heliostats to focus Sun's rays into one focal point which is usually a boiler located on top of central collector tower. This paper will present one possible design of solar power tower by using geometry to relocate its focal point. Most common solutions for solar power tower are shown and they are based on concept where boiler is in plain sight. Idea behind this relocation of focal point in novel construction is that boiler will be isolated from environment conditions and by doing so it can preserve more thermal energy during night. This can be achieved by installing additional mirror on solar power tower which has a shape as revolved partial ellipse. Here will be explained how this additional mirror can be used as economiser for fluid that is being heated in solar power. Paper also explains use of "fat point" at focal point and thus compensate errors that can occur if rays from heliostat are inaccurate.

Keywords: solar power tower; ellipse; concentrated solar power; focal point; fat point, accuracy; applied geometry

INTRODUCTION

Many papers and reviews present the latest developments in two main branches of renewable, solar energy technologies: Photovoltaic (PV) and Concentrated Solar Power (CSP). Photovoltaic system is based on using solar panels to convert sunlight into electricity via process called photovoltaic effect. Concentrate solar power system has several designs such as solar power tower, parabolic troughs, dishes and Linear Fresnel Reflectors (Stojicevic, 2019). They all have the same principle of work: to gather as much of solar energy as they can and to concentrate it in a smaller area as it is possible. This concentrated solar radiation then will be used to produce steam which will be later used for electricity generation by using steam turbines. Both of the systems have their advantages and disadvantages. For instance, PV is less complicated for montages (can be applied anywhere) but also costs more than CSP. CSP has initially lower cost of installation and has one more capability which provides cutting edge in comparison to PV: thermal storage capacity. Sun's radiation is heating thermal storage that is usually filled with molten salt. Once heated, it will take time to cool it and thus provides heat needed in the system. When Sun sets over a horizon, a PV system is not producing any more energy while CSP has a thermal energy for a few hours more.

One of CSP system that has the biggest capacity in large scale of electricity production is Solar power tower (Fig. 1). Solar power tower, sometimes referenced as Central receiver system, is system of CSP that uses a field of mirrors that reflects Sun's rays into one central receiver placed on the top of a tower. Those mirrors, that are motorized so they can track the Sun's path during the day, are called heliostats. By focusing Sun's rays into one point they can achieve temperature 1000 °C and more on a receiver. Receiver, or boiler, is a place where concentrated heat is transferred to the water, thus turning it into steam which is than transformed into mechanical energy. In last few decades solar tower power system has been subject of many researches and has been proven to be quite effective. Now, research in this area is moving towards finding better material and improving effectiveness of system (Mao, 2016; Cavallaro, 2010; Lovegrove, 2012; Fernández-García, 2014).

One interesting point of view is given by Prasad (2017) in his research regarding Linear Fresnel Reflectors. In their research, authors propose that Linear Fresnel Reflectors have additional mirror that will refocus Sun's rays into absorbing tube. Any Sun's ray that does not hit an absorbing tube will be redirected from secondary mirror again to the absorbing tube. This takes us to the interesting question: is implementation of secondary mirror possible in larger system, such as solar power tower and if so, can it be used to improve effectiveness of solar power tower systems? Recent researches are working due to the concept called Beam-Down Solar Thermal Concentrator. Such a concentrator will be presented in this paper which can, by using secondary mirror shaped like elliptical torus, to refocus Sun's ray from one point to another.

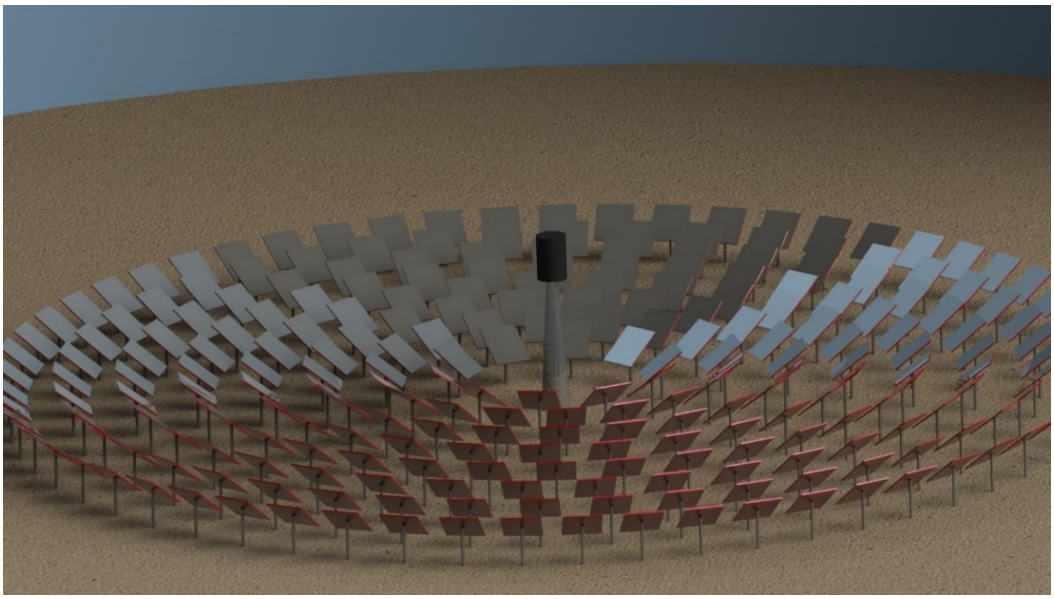

Figure. 1: Solar power tower and heliostat field

1. REFLECTING PROPERTIES OF ELLIPSE

The name, ἔλλειψις (élleipsis, "omission"), was given by Apollonius of Perga in his Treatise on Conic Sections (Stavek, 2018). There are several definition of ellipses and one of them is that ellipse is a curved line forming a closed loop, where the sum of the distances from two points (foci) to every point on the line is constant. In Figure 2, these two points (foci) are marked as F_1 and F_2. Point "*V*" represents a point on ellipse and labels "*a*" and "*b*" distances between focal points and point given "*V*". Point "*C*" marks a center of an ellipse and from this point two axis are taken into consideration: semi-minor axis and semi-major axis. One of the properties of ellipse is semi major axis length $a + b = 2$. This formula is important regarding the size of the ellipse that will be used in design of solar power tower.

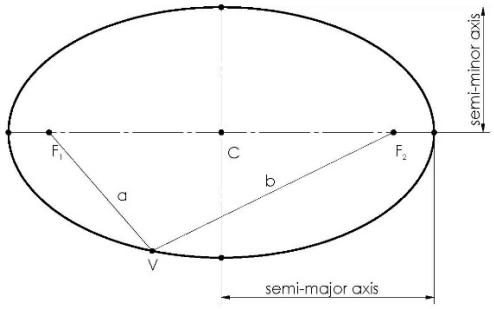

Figure. 2: Ellipse with its important points

By taking one half of the ellipse, as displayed in Figure 3, it shows a reflective property of ellipse (Berendonk 2014). When ray *a* enters ellipse through focal point F_1 it reflects in point *V* and passes through second focal point F_2 as ray *b*. This is applicable to any ray passing through one focal point that will leave through the second one, regardless of the angle at which it enters. This property is similar to reflective property of parabola.

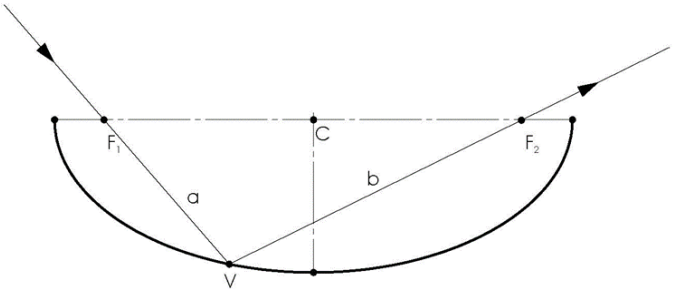

Figure. 3: Reflection property of ellipse mirror

This reflection property of ellipse is used by architects when designing halls so that quiet sounds (whispers) emitted from one particular place in the room can be clearly heard at another (remote) place. This is known as a whispering gallery or whispering room. In the Greek legend of Dionysius' ear, Dionysius made a cave shaped like an ellipse in order to hear the words whispered by a prisoner in one of the foci of the cave. Same reflective properties can be applied to the light as to the sound. Most notable application of ellipse shaped mirrors is in microscopes where entering rays represent a picture which is magnified after passing through the mirror.

2. TOWER DESIGN

Reflective properties of an ellipse can be used in reflection of Sun's rays in CSP systems especially in solar tower system towers. In Fig. 4 Sun's rays are being reflected from the surface of the heliostat, which is first reflection mirror, and pointed to elliptic mirror which can be called second reflection mirror. Ray, marked on Fig. 4 as *a*, then passes through focal point F_1 and reaches mirror at point *V*. Since second reflection mirror is shaped as ellipse ray reflect to second focal point F_2 and this ray is marked as *b*. Focal point F_2 represents a boiler, heater with molten salt that gives necessary temperature for turning water into useful steam for steam turbines.

Angle in which ray *a* hits a second reflection mirror varies from position of heliostat. If heliostat is near to solar tower, angle between ray *a* and horizontal, marked with α in Fig. 4, is closer to 90 degrees. The more heliostat is

distant from the solar tower, the angle is getting more acute. Thus, depending on distance of heliostat from solar tower position of point *V* varies on ellipse shaped mirror. In Fig. 5a an area is marked with red giving a view which area on ellipse mirror is used for refocusing Sun's rays. Concentration of Sun's rays falling into second reflecting mirror can preheat mirror if this area is too small. In order to dilute those rays from overheating mirror, partial elliptic mirror will be placed under certain angle. Partial ellipse shown in Fig. 4 is placed under an angle marked with β and size of this angle is determined by how many heliostats are pointing into focal point F_1. With the rise od number of heliostats, the angle β is going to reduce, but nevertheless it will require additional cooling.

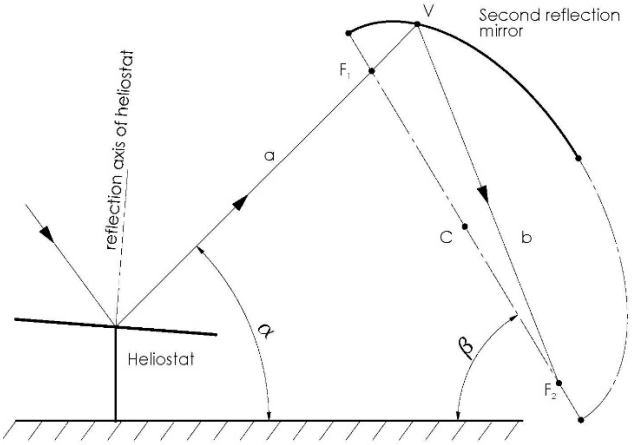

Figure. 4: Ellipse shaped mirror

As it can be seen in Fig. 1, field of heliostat is spread around solar power tower in all directions, so in order to create design of ellipse shaped mirror as second reflecting mirror there are several conditions that must be considered. Ellipse that has been shown in Fig. 4 must be oriented to this heliostat in order to refocus Sun's ray to one point. In order to accomplish this, an elliptical torus will be constructed. An elliptical torus can be generated by sweeping an ellipse about a given axis in this particular case, and that vertical axis passes though focal point F_2. Parts of ellipse that are used to refocus Sun's ray (usually of point V_{min} to point V_{max} shown on fig. 5a) revolve around this vertical axis (Fig. 5b). Revaluated partial ellipse becomes part of elliptical torus, and it will be oriented toward entire field of heliostats as it is shown in Fig. 6.

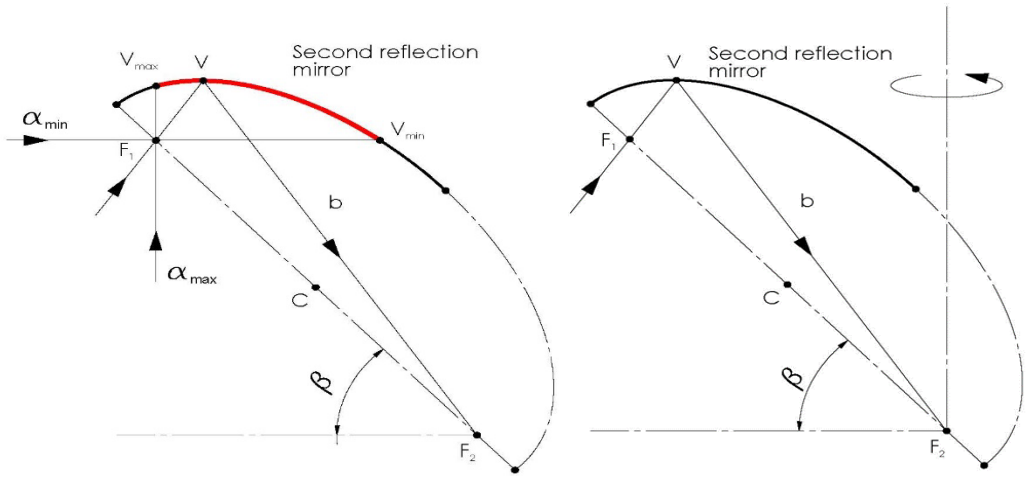

(a) (b)

Figure. 5: (a) Area on secondary mirror that is inflated by sun's rays, and (b) profile of mirror revolved around axis

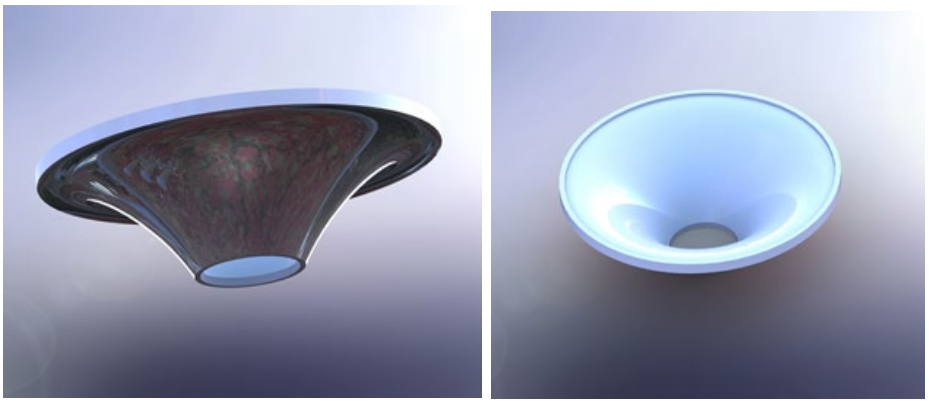

Figure. 6: Shape of partial elliptic torus created in software package Solidworks

Shaped like this, second reflecting mirror now can receive Sun's rays from all round solar power tower and focus them in one single point thus gaining one more interesting factor in optimization of CSP systems - heat energy preservation. This can be achieved in two ways: by water preheating before transferring to boiler and by isolating boiler during the night.

In Figure 7a, point *V* is placed on mirror surface and in that point Sun ray, passing focal point F_1, is redirected to focal point F_2 which is now a boiler. When field is large there may be a problem with cooling this surface (Fig. 5a). To cool down the mirror volume, this elliptical mirror is filled with water. This water is later used in steam turbines and elliptical mirror becomes kind of economiser which produces preheated water to system.

Although there are many advances in a field of material used for heat accumulation (Fernandez, 2014) the problem of cooling during the night is a big issue. During the day, elliptical mirror is in a position shown in the left figure, but when night comes there is no more heating of boiler because there are no reflected Sun heat. Boiler is then cooling down since the temperature during the night is lower than the one during the day (in deserts going even below zero). In order to preserve heat in boiler as much as it can, a special insulation cap is placed on the boiler. This cap (Fig. 7b) shows the way how to isolate boiler from environment heat and how to provide needed heat for a longer period of time in comparison to open field systems.

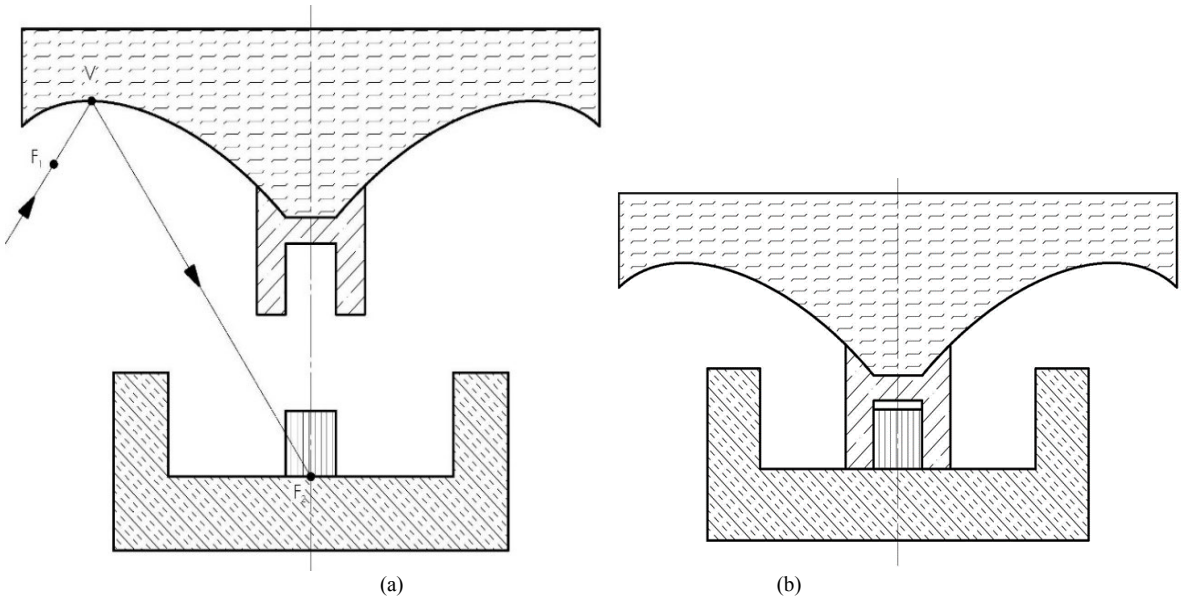

(a) (b)

Figure. 7: (a) Basic sketches for design of solar power tower during a day, and (b) during a night

To determine the shape and size of the isolation cap for boiler, there will be discussion about concept called "fat point". Accuracy of heliostat is not precise as it should be and including deviations in design process is a part creating blueprints for solar power tower. In Fig. 8 are shown 3 rays, two of them (green and blue) do not pass through focal point F_1. Ray, coloured in red, passes straight to F_1, reflects from elliptical mirror and lands in F_2. Blue and green ray, do not pass through F_1 but hit *V* point. As it can be seen, blue ray end up below F_2 and green one also misses focal point. There are many reasons why heliostat can reach required precision and that will have

impact on determining size of fat point and on shape of a boiler. By taking this into the consideration, designer can proceed to construct solar power tower with elliptical torus mirror.

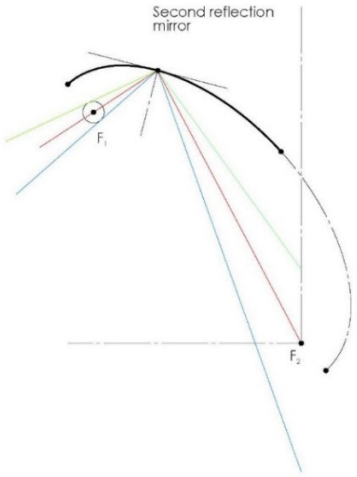

Figure. 8: Geometric representation of phenomena called "fat point" in ellipse

3. 3D MODEL OF SOLAR POWER TOWER

This particular construction will not address all of construction features such as mechanism for moving economiser up and down or type of pumps that are needed to fill economiser. Idea is to describe an application of elliptical torus mirror in design of solar power towers that can be used for smaller CSP plants. Concept presented in this paper is known as Beam down tower and it can be seen in usage in UAE concentrating solar energy to 1,100 degrees and currently producing only 100 kW (Grang, 2015). However, there are problems with this concept as well (Vant-Hull, 2014). Such a problem is overheating of secondary mirrors and this concept with elliptic torus mirror system will try to address this problem.

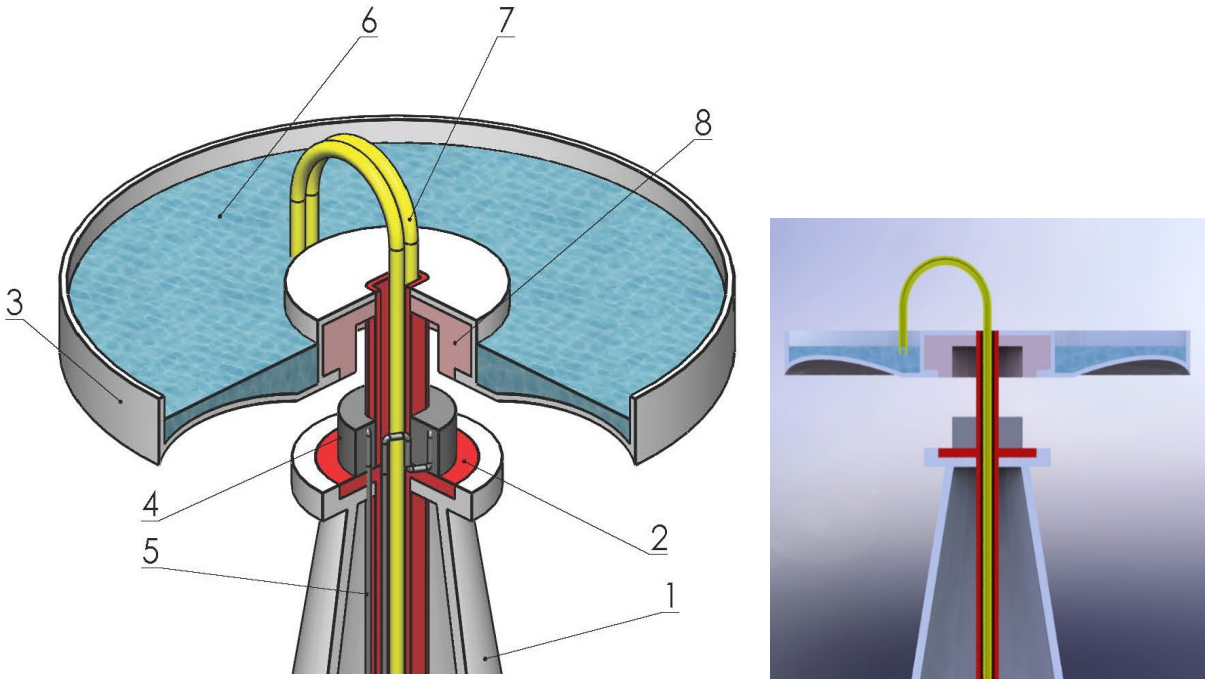

(a) (b)

Figure. 9: (a) Assembly of solar power tower with main parts, and (b) cross section of solar power tower

By applying all parameters described in previous chapters, the concept design of this solar power tower begins to emerge. In Figure 9 is shown a 3D model that is designed by using software package SolidWorks 2016. On the top of the tower (1), a carrier (2) of secondary mirror is placed. This mirror is also an economiser (3) which have

several functions. Main one is to carry elliptical torus mirror and second one is to provide cooling of that mirror. This cooling is possible through transfer of heat to water, which will be later used in boiler. Boiler (4) is basically a container of heat transfer medium that is used for most modern type solar power towers such as water/steam, molten salts, liquid sodium, oil and even air. Through this material, a pipeline (5) is taking away heat to heat exchanger in which water is heated and turned to steam. Before this process, water (6) is previously preheated in economiser (3). In order to transport this water in and out of economiser, two pipes (7) are implemented. When Sun sets down entire economiser is going down and isolation cap (8) is placed around boiler (4) thus providing necessary isolation from environmental conditions.

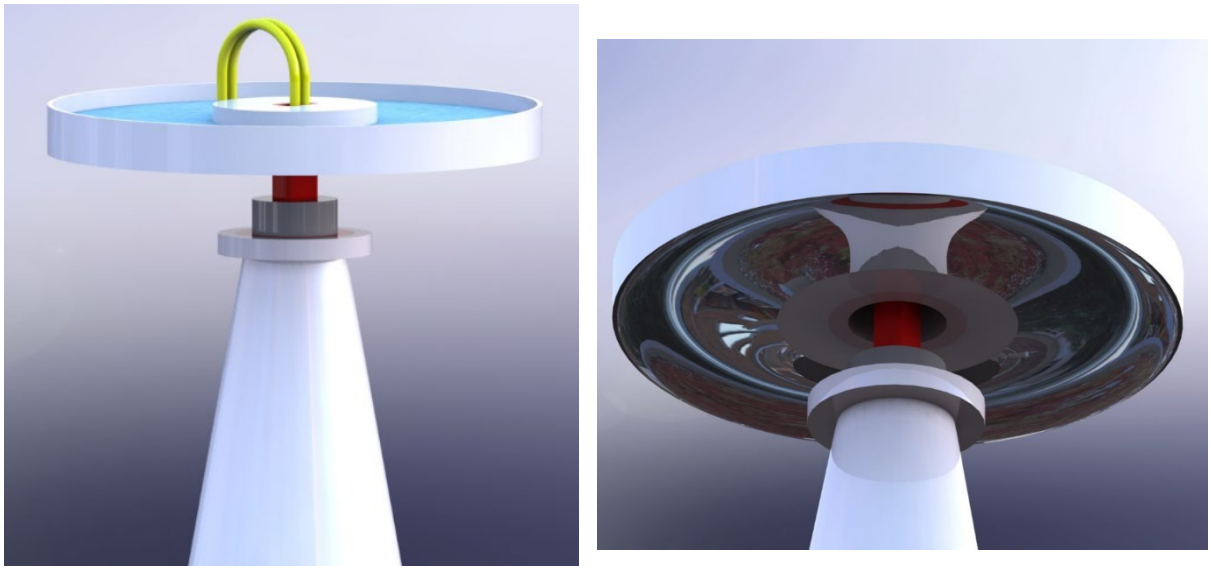

(a) (b)

Figure. 10: (a) Solar power tower with elliptical torus mirror, and (b) mirror of solar power tower

Figure 9b shows a cross section of solar power tower with elliptical torus mirror and here it can be seen how is water transported to economiser. One pipe is used to bring cold water in and other to suck it out of economiser. This flow will provide needed circulation and thus keep mirrors from overheating. Figure 10 shows a tower construction from significant angles and Figure 11 shows two position of operations of solar tower: a) during the daylight and b) during the night.

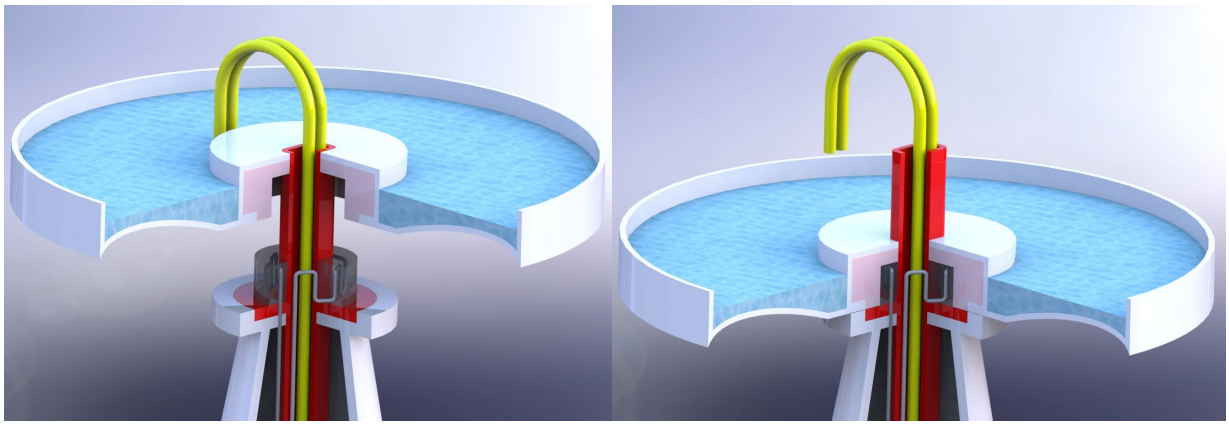

(a) (b)

Figure. 11: (a) Working positions of Solar power tower during a day, and (b) during a night

CONCLUSION AND FURTHER RESEARCH

Researchers and scientists will continue to look for methods to convert the endless energy potential of the Sun in order to create usable electricity to power the world. One of those methods of improving solar power systems, especially concentrated solar power systems, is a novel design in existing ones in order to improve them.

One advantage of CSP over PV and many other renewable energy technologies is its ability to store the Sun's energy. Molten salt, for example, can be stored and kept hot for many hours so that when electricity is needed, the heat can be used to make steam to drive a generator.

Aim of this paper is to provide few interesting approaches to modern problems about designs of solar power towers in CSP systems. As said, beam-down technology is not new but it is the latest in the design of CSP systems, but it needs to be constantly improved. PV and CSP have their advantages and disadvantages but both are needed for deferent places on Earth depending on latitude on Earth (Hernández-Moro, 2013). Future scope of research will be done in several areas. First, detailed calculation regarding thermal capacity must be done in order to determine the size of a boiler. By doing this, designers and engineers can calculate dimensions of partial ellipse needed to design an elliptical torus. Next step is to convert ellipse to series of straight line segments so that the reflection property and shape are most preserved compared to the ellipse. Second path of research will lead to finding appropriate materials which can withstand extreme temperatures.

Acknowledgement: This research is supported by the Ministry of Science and Education of the Republic of Serbia, Grant No. III 44006.

REFERENCES

1. Berendonk, S., 2014. Proving the reflective property of an ellipse. *Mathematics Magazine*, 87(4), pp.276-279.
2. Cavallaro, F., 2010. Fuzzy TOPSIS approach for assessing thermal-energy storage in concentrated solar power (CSP) systems. *Applied Energy*, 87(2), pp.496-503.
3. Fernández-García, A., Cantos-Soto, M.E., Röger, M., Wieckert, C., Hutter, C. and Martinez-Arcos, L., 2014. Durability of solar reflector materials for secondary concentrators used in CSP systems. *Solar energy materials and solar cells*, 130, pp.51-63.
4. Fernández, A.G., Ushak, S., Galleguillos, H. and Pérez, F.J., 2014. Development of new molten salts with LiNO3 and Ca (NO3) 2 for energy storage in CSP plants. *Applied Energy*, 119, pp.131-140.
5. Grange, B., Kumar, V., Gil, A., Armstrong, P.R., Codd, D.S., Slocum, A. and Calvet, N., 2015. Preliminary optical, thermal and structural design of a 100 kWth CSPonD beam-down on-sun demonstration plant. *Energy Procedia*, 75, pp.2163-2168.
6. Hernández-Moro, J. and Martinez-Duart, J.M., 2013. Analytical model for solar PV and CSP electricity costs: Present LCOE values and their future evolution. *Renewable and Sustainable Energy Reviews*, 20, pp.119-132.
7. Lovegrove, K. and Pye, J., 2012. Fundamental principles of concentrating solar power (CSP) systems. *Concentrating solar power technology* (pp. 16-67). Woodhead Publishing.
8. Mao, Q., 2016. Recent developments in geometrical configurations of thermal energy storage for concentrating solar power plant. *Renewable and Sustainable Energy Reviews*, 59, pp.320-327.
9. Prasad, G.C., Reddy, K.S. and Sundararajan, T., 2017. Optimization of solar linear Fresnel reflector system with secondary concentrator for uniform flux distribution over absorber tube. *Solar Energy,* 150, pp.1-12.
10. Stavek, J., 2018. Kepler's Ellipse Generated by the Trigonometrically Organized Gravitons. *Appl. Phys. Res*., 10, p.p26.
11. Stojicevic, M., Jeli, Z., Obradovic, M., Obradovic, R. and Marinescu, G.C., 2019. Designs of solar concentrators. *FME Transactions*, 47(2), pp.273-278..
12. Vant-Hull, L., 2014. Issues with beam-down concepts. *Energy Procedia*, 49, pp.257-264.

IS THE EARTH ROUND?

Iva Kodrnja
Institute of Geomatics at Faculty of Geodesy, University of Zagreb, Croatia
PhD., Assistant Professor, iva.kodrnja@gmail.com

ABSTRACT

In this two part exposition on the importance of philosophy in science and thought in general, we will explore the mathematics of the recent philosophical issue of the Earth being round or flat, the problem answered millennia ago, but that has recently re-emerged as a question in our society.

The first part is the discussion on philosophy and affiliation towards knowledge in general. The historic solution of the problem, known in ancient Greece and probably to other much older civilizations, is founded in astronomy and is the undoubtable principle that we are living in Space, and that the Earth, as well as other visible celestial bodies, must be of round shape, rotating and revolving. This shape is the only shape suitable to the revolving motion.

In the second part we present the mathematics of the problem; sphere as a three-dimensional object and its planar projection - stereographic projection; spherical geometry; sphere as a Riemann surface, Gaussian map, cartography and its general link to geodesy.

We will reveal the true cause of this misapprehension of reality through our mathematical reasoning in the conclusion of the paper.

Keywords: philosophy; spherical geometry; Riemann surface; stereographic projection; geodesy

1. INTRODUCTION

We will not dwell on whether the Earth is round. That is not the issue. Why not, you may ask? Because of thousands of years of history, starting from the ancient Greeks who are considered to be the cradle of today's civilization in a scientific sense or maybe even further in the past, with Egyptian walls to indicate that maybe they knew more about Space than we do. The Greeks even measured the diameter of Earth, in Egypt though, by first knowing the relation between Earth and Sun, the rotation, and two sticks placed some 800 km apart by measuring the lengths of their shadows.

But the issue is how can it happen that today, in this modern times, when informations are available around any corner, with internet news, compulsory schooling, millions of books and libraries, in the times when space travel is becoming a (very expensive) touristic adventure, we still have a considerable amount of people who do not believe the Earth is round. How is it possible that such informations, various false theories, can exist and be credible to some? Doesn't that say something about the quality of the information level of our civilization? Of the level of our knowledge in general?

On the other hand, we will try to penetrate into this matter from the philosophical side, to consider mathematically why this kind of misinformation appears, and even the quality of the information. The mathematical side of the issue is that the sphere is not flat and the question of flattening the sphere. Why is that important? Because the Earth is round and from time immemorial humans were travelling the Earth. To do so, if we want to go from point A to point B, unless we are wandering about, we desire to know the route. Mathematically, we are speaking of curves on a sphere. And to pass the information, we use carts, maps. And here lies the essence of the problem. We will deal with this in Section 3 by seeing the metaphysical level of the mathematics of spheres and their planar projections to find the conception of the false ideas on the nature of Earth. We will consider the geometry of

spheres, notion of curvature, 19th century geometrical revolution (Gray, 2010.), Gauss and Riemann (de Saint-Gervais, 2007.), cartography and stereographic projection (Casey, 1889.).

Figure. 1: A photograph from the exhibition Imaginary 2017. in Edinburgh, stereographic projection using rays of light projecting through a model of the globe onto a large nearby wall, (IMAG, 2017.)

In a healthy, advanced civilization knowledge is fluent to and through all, there is no such misconceptions as the one we currently discuss, they are a symptom of disturbance of the flow, and this paper is to be a play of knowledge. If in a play you desire an opponent than knowledge versus deviation, but we do not wish to attack or belittle anyone individually. This is on a civilizational level, where the standards of information levels should and must be high and such deviations mustn't sustain. Our goal is advancement of standards of life, by which we mean unassailable understanding of the principles of life and living by them.

2. IMPORTANCE OF PHILOSOPHY

We start the discussion with an etymological introduction, exploring its Greek origin but we will go no further into historical or even modern definitions. We will remain in the origins of the richness of the notion of philosophy and will not succumb to anything less, refraining in this way from the modern deflating definitions.
All notions have a name. The name itself, if it is appropriate, carries the metaphysical meaning of the notion. The origin of the notion of philosophy is surely not Greek, it is an eternal metaphysical concept, but the word philosophy is.
Philosophy, φιλοσοφία consists of two words; φιλο (philo) which is love, attraction, affection and σοφία (sophia), which is wisdom, knowledge, (ETYM, 2020.,). Therefore, philosophy is the love, attraction towards knowledge. I would argue it is not a science itself but a 'metascience', a guiding feeling for anyone who desires knowledge in any discipline. It must always be present, be the starting point of all sciences. Science itself is a set of methods or means of obtaining knowledge on specific sections of life. Isn't it true that science itself is impossible without philosophy, the desire for knowledge? Philosophy is also the basis of art, which is the exposition of internal knowledge and cognition, internal beauty exposed and put into motion. The motivation then must be the love for knowledge and desire for it to be spread. Isn't it true that art itself is impossible without philosophy, the desire for knowledge?
Having a healthy basis must not be avoided in all explorations, actions and constructions. When we are motivated by a clean desire and attraction to wisdom, then our actions will be such that their consequences are wisdom. It is a natural phenomenon; a healthy apple has healthy seeds and its fruits will also be healthy since they are endowed with their ancestor's health. Philosophy is the healthy ancestor of all sciences; therefore it is not a science but a 'metascience'. It is the pleasure we feel in any true cognition which than becomes a sort of mental art piece. Philosophy contains within, as a set of its themes, all disciplines and should be the measure of all disciplines of mind and its actions, as the seed of an apple is the measure of its fruits. It is the agreement that we will be devoted exclusively to knowledge and its propagation into all areas through our actions. It should be to a scientist precisely what the Hippocrates's pledge is to a doctor. An oath that all his actions will be founded in knowledge, based,

caused and put in motion by pure knowledge. This will assure that we belong to and are the knowledge and would never go against the principles of life. This is the basis of a healthy civilization.
We return to the beginning and the Greek origin of the name, since the Greek culture was closer to the true, original state of affairs which is the metaphysical reality of life. Their names for notions, ideas, concepts were alive, as the notions themselves are. They are living within us and they can be described by none less than infinity of words for they are infinite in their nature. They never vanish, there is no absolute truth except the absolute truth of the infinite life of notions and their endless existence. All else is the play of knowledge which we must release into our world. Then, the words become vivid, knowledge is alive, present and omnipresent and it becomes our present, basis for our future. Our buildings become homes, forts, fortresses and temples of knowledge and our civilization can move forward into metaphysical revolution. For our truth is we are living on or to say through the physical revolution of our home, Earth.
On the other pole, the endless stream of knowledge is the goal of philosophy and means of destruction and deconstruction of blockages of the flow of knowledge, the metaphysical wall that allows ignorance. We are living on a sphere in Space, so we should act accordingly. We are in the Universe, that is our physical and should be our metaphysical reality.

2.1 Earth's measure or measure of Earth

Once again, we begin with etymology. Philosophy starts and ends with Phi. Phi is surely one of the most popular numbers, honoured by a name referring to the highest value – the golden number. We are more interested in its interpretation than its numerical value, and this interpretation is the fractal nature of the construction which circularly is again the definition of its value. And this is the golden section, proportion, ratio, mean, altogether referring to measure. But what is measure, metaphysically? The word measure has multiple meanings, (LEX, 2020.). First, we must note the difference between measure and measurement. Notion of measure is the quantity of quality. From this we can get all other interpretations, varying the qualities, choosing and setting the standards of quantity.
In a non-mathematical sense, measure can be described as the assessment of importance, effect of value and measurement as a plan or course of actions taken to achieve a particular purpose based on the measure. Further, a measure is also judging by comparison and reaching the required standard, and in more negative tone, measure is scrutinizing someone in order to form an assessment of them. As we can see, this notion is deeply intertwined into our lives on many levels.
Returning to mathematics, geometry is, etymologically, Earth's measure, but our usual usage is in expressions of size, amounts or degrees of something. The other discipline, the one dealing with actual measuring of Earth is geodesy. Here we also have a linguistic connection, since the archaic meaning of measure is to travel over a certain distance.
The question now becomes what is our measure of Earth, what is our assessment of Earth? What is our geometry, where is our knowledge of geometry on a civilizational level, if we have doubts on the shape and position of our home, of Earth? This also reflects and propagates to all our scientific disciplines and eventually enters our lives on a daily basis, when we read articles in newspapers or on the Internet about the Earth being flat. To our scientists this is a deprecated topic, they do not deal with this. And funny as it is, most proofs of the thesis as well as refutes are based on measurement, rarely do we see measure being a part of the argument. Here we see a breach of reciprocity law. On one hand, the Earth's measure - perpetual rotation providing us with a home and possibility of life, and on the other hand our measurements of Earth and life which usually end with a desire to escape, probably from ourselves. We end this section with conclusion that philosophy is the golden measure of science, of life and our greatest necessity.

3. MATHEMATICS OF SPHERES

Everyone knows what a sphere is, or at least has an idea about it. On the most elementary level, we can say it's a ball. Of course, when we speak of shape of Earth as a sphere we do so in an ideal, Plato's cave sense, as most of mathematics does. The Earth is surely not a sphere!

3.1 Geometrical definition of a sphere

Saying the sphere is a ball can be visually gratifying but doesn't get us far in any scientific direction. The common definition of a sphere states: *A sphere is a locus of points such that their distance from one fixed point in space is constant, the same*. The one fixed point is called the center of the sphere, a point clearly not lying on the sphere. This definition implies we have a space in which all the points lie, and the means to measure distance of points, metrics. Then a sphere is an object naturally embedded in this space.

But if we respect the Earth's rotational motion, and introduce it into our investigation of a sphere, we come to another well-known definition of a sphere as a rotational surface. *A sphere is a surface generated by revolution of a semicircle about its diameter, which remains fixed*. This physical, mechanical definition yields a different approach to positions of points in space, a different, spherical coordinatization.
The generating semicircle of a sphere is called the prime meridian and in the plane in which the prime meridian lies, the 'upper' endpoint of the diameter is the *zenith* N, the North Pole and the midpoint of the diameter is the center of the sphere C, the origin of the coordinate system. The angle between the radius defined by N and a radius defined by any point on the semicircle is called *inclination* or the polar angle, denoted by ψ. All curves generated by revolution of the prime meridians are called meridians. The plane through the origin orthogonal to the diameter of the prime meridian is called the *fundamental plane* or plane of reference. In this plane or any plane parallel to it we can determine the angle between a meridian and the prime meridian. This angle is called *azimuth*, denoted by φ.

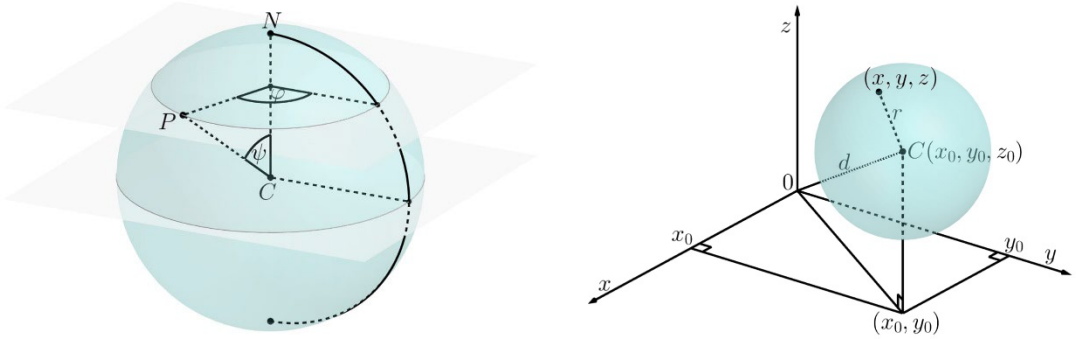

(a) (b)

Figure. 2: (a) Spherical coordinate system, (b) sphere in the Cartesian coordinate system

In the spherical coordinate system a point P is uniquely determined, Figure 2a, by three coordinates $(\boldsymbol{r}, \boldsymbol{\psi}, \boldsymbol{\varphi})$, its distance $\boldsymbol{r}$ from the origin point and the two angles, inclination $\boldsymbol{\psi} \in [\boldsymbol{0}, \boldsymbol{\pi}]$ measured in a plane determined by the three points P, N and C and the azimuth $\boldsymbol{\varphi} \in [\boldsymbol{0}, \boldsymbol{2\pi}]$ measured in the reference plane, with $\boldsymbol{\varphi} = \boldsymbol{0}$ being the equation of the prime meridian.
The equation of a sphere in the spherical system is $\boldsymbol{r} = \boldsymbol{const}$.
In the usual Euclidean space with Cartesian coordinate system with three mutually orthogonal axes x, y and z, where every point is given by three coordinates $(\boldsymbol{x}, \boldsymbol{y}, \boldsymbol{z})$ which can be interpreted as composition of two orthogonal projections of the point, first to a coordinate plane, a plane determined by two of three axes, and from there to each of the axis, Figure 2b. This provides the understanding of the usual Euclidean metric, considering the right triangles appearing while projecting orthogonally; the distance of two points $(\boldsymbol{x_0}, \boldsymbol{y_0}, \boldsymbol{z_0})$ and $(\boldsymbol{x_1}, \boldsymbol{y_1}, \boldsymbol{z_1})$ in the Euclidean plane is given by

$$\sqrt{(\boldsymbol{x_1} - \boldsymbol{x_0})^2 + (\boldsymbol{y_1} - \boldsymbol{y_0})^2 + (\boldsymbol{z_1} - \boldsymbol{z_0})^2} \qquad \text{(Eq.1)}$$

from which we easily determine the equation of the sphere with center $\boldsymbol{C} = (\boldsymbol{x_0}, \boldsymbol{y_0}, \boldsymbol{z_0})$ and radius $\boldsymbol{r}$ is

$$\sqrt{(\boldsymbol{x} - \boldsymbol{x_0})^2 + (\boldsymbol{y} - \boldsymbol{y_0})^2 + (\boldsymbol{z} - \boldsymbol{z_0})^2} = \boldsymbol{r}. \qquad \text{(Eq.2)}$$

We can conclude that in the Euclidean space, a sphere is an object defining the metrics. This is obvious to all who do planar construction with ruler and compass, the use of compass to measure and transfer lengths is a planar version of this claim.
The rectangular coordinate system makes geometry hard and complex when dealing with spheres, the sphere is clearly not an appropriate object for this system. Despite its fundamental involvement in the metric system, its equation is complicated, having both squares and roots falsely making it seem linear, but we all know that any computations regarding spheres quickly become overwhelming. Furthermore, the spherical coordinate curves are meridians, given by equation $\boldsymbol{\varphi} = \boldsymbol{const}$ and parallels given by equation $\boldsymbol{\psi} = \boldsymbol{const}$, whereas these important curves have hard to compute equations in any rectangular system, namely the equation of a parallel is similar to that of the sphere itself, just having $\boldsymbol{z} = \boldsymbol{const}$ while a meridian has to be computed as intersection curve of the sphere and a vertical plane which is defined by a linear equation in two variables $\boldsymbol{x}$ and $\boldsymbol{y}$.
All planar sections of a sphere are circles. If the plane passes through the center of the sphere, the circle's diameter is the same as the sphere's and the circle is called a *great circle*. All meridians are great circles and the one parallel

passing through the center is a great circle called *equator*. The great circles of the sphere are geodesic curves, the curves of shortest distance between two points on the sphere.

3.2 Sphere is not flat

Is it obvious that sphere is not flat, and what does this mean? First, by flat we mean planar, two-dimensional and identical in a way to the plane. As we stated in the previous subsection, a sphere is a surface, a two-dimensional subspace of a space. A plane is also a surface. But there is a difference. A sphere contains a volume of space or is a boundary to a volume of space, it is solid, three-dimensional. A plane is not. As a surface, it has infinite area, unless we observe a bounded part of a plane and then the area depends on the boundary. The sphere is bounded, the area of the sphere is $\mathbf{4\pi r^2}$. We can also measure the volume surrounded by a sphere and it is equal to $\mathbf{^4/_3\,\pi r^3}$. These measurements are done by two and three-dimensional metrics derived from the one-dimensional length metric defined by (Eq. 1).

Take for example a cylinder, regarded as a surface. It also has infinite volume and area, unless it is bounded, and then measurements depend on the boundary. But a cylinder contains lines, infinitely many lines. As a translational surface generated by a line moving along a space curve, we see there is a line contained in the surface through every point of the surface. This type of surfaces is called ruled surfaces and the lines rulings. If we cut a cylinder along one ruling, we can, without distortion of the surface, flatten the cylinder into a plane. If the curve defining the cylinder is closed, after flattening we will get a finite area. Surfaces that can be flattened are called developable surfaces, and in three-dimensional space, only ruled surfaces, generated by moving a line are developable. They are locally isometric to a plane, can be physically constructed from a piece of paper by bending so that the paper is not destroyed and the metric relations between corresponding sets of close points are the same.

The sphere doesn't contain any lines, which is obvious since it is bounded and it can't be unrolled into a plane without deformation, change of shape. If we want to be more precise, and mathematicians have always had this desire, we must introduce another notion, and this is curvature. For curves, curvature can be defined either using movement of lines, as the change of slope of tangents to a curve or in planar case by comparison to a circle, using osculating circles. Curvature measures the change of directions of a point travelling along the curve. A line has zero curvature, that why we say a straight line, while a circle's curvature is reciprocal to its radius. For surfaces, we must generalize this concept. Today we have various established ways of measuring and defining the curvature. Clearly, a plane must have zero curvature regardless of the definition of the measure and measurement of curvature and the curvature itself must indicate the difference between a plane and a generic surface. We can look at one aspect of curvature locally pointwise by the relation between the tangent plane at a regular point and the locally near part of the surface. Then we have three possibilities, three types of points, Figure 3, (Gorjanc et al., 2018.).

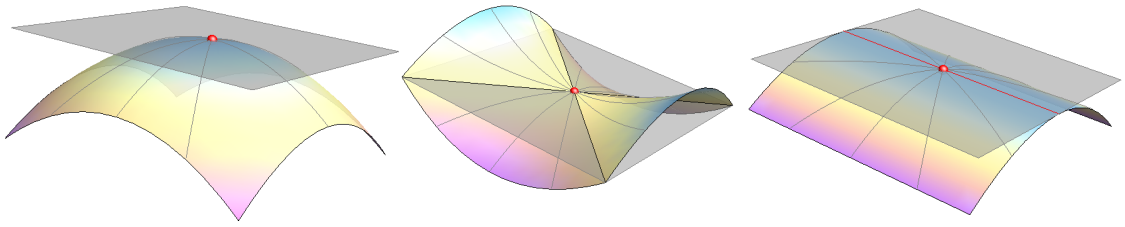

(a) (b) (c)

Figure. 3: Types of regular points (a) elliptic point, (b) hyperbolic point, (c) parabolic point
(Source: Gorjanc et al, 2018)

Elliptic points are such that all near points of the surface lie on the same side with respect to the tangent plane at the point. All points of the sphere are elliptic. *Parabolic points* are such that the tangent plane touches the surface along a curve on the surface that passes through that point and all near surface points are on the same side of the tangent plane. If all points of a surface are parabolic, then the surface is a ruled surface and it is developable. *Hyperbolic points* are such that the tangent plane intersects the surface and the points on the surface are separated by intersection curves and lie on different sides of the tangent plane. These intersection curves are called asymptotic directions. A surface with elliptic of hyperbolic points is non-developable.

If we look at curvature as a measure of change of direction when a point travels along the surfaces, it is very natural to observe curves on the surface and measure the curvature along them. There are infinitely many curves on the surface passing through a point on the surface, and the tangent plane is a plane that contains all the tangents of these curves, if the point is regular. Otherwise, the tangents don't lie in one plane but form a cone. In the case of a regular point, the tangents corresponding to two normal sections with extremal curvature are called principal directions, they are orthogonal, and the curvature of the two normal section curves, called lines of curvature, is defined by osculating circles and denoted by k_1 and k_2. The normal section curves with zero curvature are

intersections of the surface with the tangent plane and the point is either parabolic and one of the principal curvature is zero or the point is hyperbolic and the intersecting lines are the aforementioned asymptotic curves but the curvature is negative.
Every point on the sphere is regular, the normal direction is the direction of the radial line, the line from the center of the sphere and all normal sections are great circles therefore $k_1 = k_2 = 1/r$ at every point. For a plane we have $k_1 = k_2 = 0$ at every point.

3.3 How to make a sphere flat, mathematically

Trying to make a sphere flat is a problem with long history. Even the Greeks knew how to project the Earth, mostly using the stereographic projection which we will study in the next subsection. It was and still is also used to portrait the celestial sphere, the sky we see which is from our standpoint again a sphere, but we are within. With the start of colonialism, new projections appeared to be more suitable for increased naval travel. We will mention the most known, Mercator projection. Then in 19th century appeared one of the most known and celebrated mathematicians, C. F. Gauss, (Gray, 2010.). He was very much interested in astronomy and geodesy, mainly cartography. He was employed in the mapping of Hanover and since he was a brilliant mathematician, and knew the Earth was round, he made various discoveries on the issues of curvature and planar projections using the geometrical interpretation of complex points as coordinates for points in a plane, then applied it to cartography.
When making a map of say Earth, or a map from any curved surface to the plane, we must first define a set of properties we desire to preserve, which will not be distorted. The choice is usually bound by application and is always metrical – area, lengths, angles. The case of preserving angles, called conformal mapping, is the one we call similarity, meaning that form stays the same.
We will mention two of Gauss's famous theorems. The first is *Theorema Egregium*, the magnificent theorem on the intrinsic nature of what we today call Gaussian curvature. The fact that the sphere is non-developable, that the surface of a sphere cannot be represented in a plane without distortion is a direct consequence of this theorem. Before, it was assumed that curvature of the surface and the measures taken on this curved surface such as length of curves etc., are dependent and inherited from the ambient space. But Gauss showed this wasn't so.
In the modern terms of the last subsection, Gaussian curvature is the quantity $k_1 k_2$ and any two isometric surfaces must have the same Gaussian curvature. But Gauss looked at it differently. First step he took was the spherical representation of the surface, the mapping from any surface to sphere that maps the outside directed unit normals of the surface onto the unit sphere positioned at the center, as in Figure … The effect this map had locally on the area is precisely his concept of curvature, the limit of ratios of areas of smaller pieces of the starting surface and the sphere is constant along the surface.
We must mention the Gauss mapping theorem that states every (analytical) surface is locally conformally equivalent to the (Euclidean) plane, (de Saint-Gervais, 2007.). This soon led to new concepts in geometry, such as Riemann's concept of surface, with the new terminology of manifolds and is the foundation of uniformization theory. Following Gauss, Riemann had very deep philosophical thoughts on metrics and implemented many new ideas in geometry. He introduced a notion of a surface that is locally holomorphic to complex plane, namely we have homeomorphic local charts into complex plane about the neighborhood of each point that are mutually compatible, and collection of all charts is called the complex atlas, (Miranda, 1995.). All mappings on such surfaces are compositions of charts and usual mappings of the complex plane. In the terminology we see the connection with cartography.
If we extend the complex plane with one ideal point, the point in infinity, we will get a manifold, Riemann surface identical to the unit sphere embedded in real three-dimensional space, a surface called the Riemann sphere. This is also the projective complex line. The charts are stereographical projections, two of them each defined on a sphere with one point removed.
Basically, this is the reason some people believe the Earth is flat. They live locally, even if they travel far, their mindset is local and by that we mean without the concept of Space and the Solar system and the local flatness, the Gauss mapping theorem stating that locally, the Earth is flat is the strongest influence. It seems apparent to a regular person since the maps are flat and the other reason being probably the size of Earth or the ratio of a human and the planet. The planet is more than million times larger and we cannot expect to perceive the curvature from our viewpoint. The only way is to take account of the Space, as did all who were able to reach truthful conclusions on the shape of Earth.

3.4 Stereographic projection

The fact that sphere is locally isomorphic to the plane but not globally seems to be the fault or the responsibility of just one single point! This is apparent in many ways, and we have seen already that without that one point, and this could be any point on the sphere, the remaining part is isomorphic to a plane.
We choose one featured point usually called the North Pole and one plane which would be the plane of projection, positioned orthogonally to the diameter through the North Pole thus passing either through one parallel, usually the equator or through the other end or the diameter, the South Pole so that the plane is tangent at the South Pole. We project all points of the sphere except the North Pole by intersecting the line connecting a point and the North Pole with the plane of projection. This type of projection is called central projection, with the North Pole being the center of projection. It is the perspective projection and often used in fisheye lenses, Figure 4.

Figure. 4: Queens Park 360 panorama - stereographic projection, (STOLLERDOS, 2006.)

The North Pole is the vanishing point, the point which topologically brings the compactification of the plane, the adding of the ideal point or the point at infinity and the plane becomes the projective line. The meridians will map into radial lines, lines through the origin of the plane, the South Pole and the parallels map to concentric circles thus defining in the projection plane a polar coordinate system. This map is conformal but causes great distortions in relative distances in different parts of the sphere which depend on the position of the projection plane. The South Pole maps to itself, it is the fixed point, the connection point of the sphere and the plane. The North Pole cannot be mapped, it is a singularity, a point which will present the ideal point of the plane if we want to extend the map.

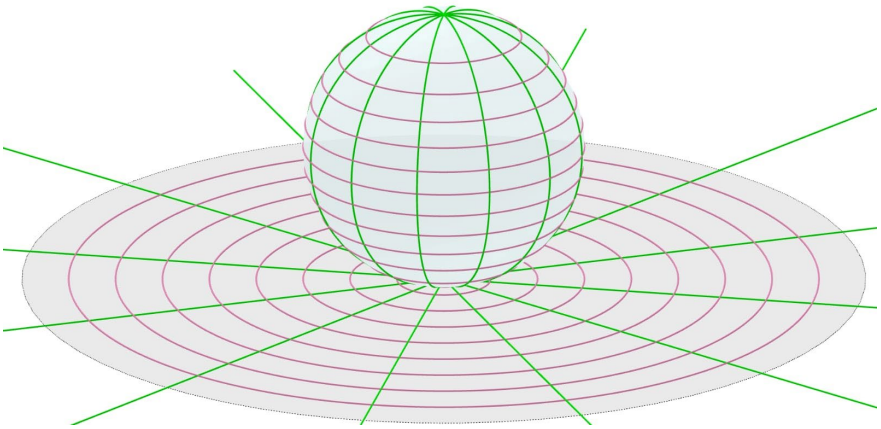

Figure. 5: Stereographic projection combines coordinate curves of the spherical system and planar polar system

We can visualize it nicely by a variant of the stereographic projection, an iterated procedure in the complex plane, (see Figure 3.1 from Mumford et al., 2015.). A logarithmic spiral cuts all the coordinate curves of the polar plane system in the same angle, it is equiangular, self-similar spiral. By lifting the spiral back to the sphere through stereographic projection, we get a loxodrome. And in this picture, we see the concept of infinity in a nicer way, Figure 5. The infinite point then becomes the 'outer border' of the plane, unreachable. The circles of the polar system with ever bigger radii will become the circles closing to the North Pole, having smaller and smaller radii. Going to infinity is closing to the singular point, the North Pole.

4. CONCLUSION

This is the metaphysical essence of the problem; the singular point representing infinity. In many flat Earth theories, this is the story; there is a border, the edge of the world, the metaphysical wall. Let us include here the mysteries of the poles, also prominent in many stories, the intrigue, the unknown, the fairytales and the various theories about the 'other side'. We have mathematically seen that the solution of the problem, of the mystery is the infinite. The infinite, the closure of the plane making it a sphere, the source of curvature is Knowledge, Knowledge is the answer. The infinite flow of Knowledge is the missing puzzle, is what is behind the singular point, is the solution, the corrective to all dilemmas. By Knowledge and through Knowledge we understand. The shape of Earth is then no longer a question. The mysteries are solved by accepting the fact we live in Space. There is the source of Philosophy, our means toward Knowledge, the desire for the truth and directions how to live it. The other side is not far away. We can then devote ourselves to the study of the true nature of our lives, life on this revolving Planet and further.

ACKNOWLEDGEMENTS

The Author would like to thank Luka Podrug for creating Figures 2 and 5.

REFERENCES

Casey, J., 1889. A Treatise on Spherical Trigonometry. Dublin University Press, Ireland.

de Saint-Gervais H. P., 2007. Uniformization of Riemann Surfaces - Revisiting a hundred-year-old theorem. EMS, Switzerland.

ETYM, 2020., https://www.etymonline.com/word/philosophy [Accessed: 21st March 2020].

Gorjanc S., Jurkin E., Kodrnja, I., Koncul, H. 2018. Descriptive Geometry - Web-textbook https://www.grad.hr/geometrija/udzbenik/

Gray J., 2010. Worlds out of Nothing - A Course in the History of Geometry in the 19th Century. Springer-Verlag London Limited, UK.

IMAG, 2017. https://imaginary.org/hands-on/stereographic-projection-globe [Accessed: 21st March 2020].

LEX, 2020. https://www.lexico.com/en/definition/measure [Accessed: 21st March 2020].

Miranda, R., 1995. Algebraic Curves and Riemann Surfaces. American Mathematical Society. USA

Mumford, D., Series, C., Wright, D., 2015. Indra's Pearls. The Vision of Felix Klein. 1st paperback edition. Cambridge University Press, UK.

STOLLERDOS, 2006., https://www.flickr.com/photos/stollerdos/304174873[Accessed: 21st March 2020].

INTRODUCING ADDITIVE MANUFACTURING AND AUGMENTED REALITY IN THE CONCEPTUAL PHASE OF THE DESIGN PROCESS

Jelena Djokikj
Faculty of Mechanical Engineering, Ss. Cyril and Methodius University in Skopje, RNM
PhD., Teaching Assistant, jelena.djokikj@mf.edu.mk

Tashko Rizov
Faculty of Mechanical Engineering, Ss. Cyril and Methodius University in Skopje, RNM
PhD., Associate Professor, tashko.rizov@mf.edu.mk

Tatjana Kandikjan
Faculty of Mechanical Engineering, Ss. Cyril and Methodius University in Skopje, RNM
PhD., Professor, tatjana.kandikjan@mf.edu.mk

Risto Tashevski
Faculty of Mechanical Engineering, Ss. Cyril and Methodius University in Skopje, RNM
PhD., Professor, risto.tashevski@mf.edu.mk

ABSTRACT

The conceptual phase is often neglected and rushed by the other departments involved in the design and production process. But the conceptual phase is of great importance for the success of the product on the market. Here, the designer incorporates all the information that he/she has about the new design, generating ideas in order for the output to be a functional and aesthetic product. It is important to make the most of it in order to assure quality result. In order to ensure short conceptual phase that will not reflect on the products' quality we propose introduction of two "new" technologies in the conceptual phase. These "new" technologies that we are proposing to be included in the conceptual phase are Additive Manufacturing (AM) and Augmented Reality (AR). AM is used for creating more realistic prototypes and proof of concepts in a short period of time. While the AR is used for more detail explanation of the products' functionality and usability.

If we apply this approach in the conceptual phase to focus groups meetings, we can be certain that the message that needs to be sent as a designer's intent is received and rightfully understood. In that manner the responses will be on the point and can be used in total, in the redesign phase or the further phases of the design process.

By incorporating new technologies in the conceptual phase, the overall time can be shortened and at the same time, the outcome can be better.

Keywords: conceptual design; additive manufacturing; augmented reality; design process

1. INTRODUCTION

In the early stages of the design process, designers use sketches to communicate their ideas. Drawings and sketches have been widely used by designers as a way to capture and develop their thoughts and ideas about a design problem (Cross, 2008). During the early stages of the design process, when the design problem is still fuzzy and abstract, designers need tools that allow them to analyse, grasp, embody and give expression to thoughts that represent partial and unfinished pieces of the object they are designing (Alcaide-Marzal et al., 2013). Sketches have traditionally been one of these tools especially during the brainstorming phase, when ideas are bursting.

In the next stages of the process the ideas can be reduced and sketches refined, leading to conceptual design and creation of a Computer-Aided Design (CAD) model. CAD software cannot compete with the freedom designers have when sketching. Nevertheless, CAD tools need to be considered in the design workflow when it comes to creativity and freshness (Robertson & Radcliffe, 2009). But sketches and drawings are not enough when an idea needs to be communicated with other sectors, or even the customer. Computer tools efficiently answer a wide range of design problems, related to embodiment desing, detail design, simulation, and manufacturing (Cross, 2008; Prats et al., 2009). The implementation of CAD simplifies things (i.e. streamlines the process), enabling designers to create 3D models and render concept ideas fast. The word “design” in CAD refers more to engineering design, which means that this kind of software is intended specifically for this type of design. That makes CAD rigid and not offering designers the freedom to create what they need.

The introduction of Computer-Aided Industrial Design (CAID) enables designers (industrial designers, in particular) to easily create any shape that they mighet have envisioned. CAID software offers a more liberated approach to design.

A prototype is an artifact that approximates a feature (or multiple features) of a product, service, or system (Otto & Wood, 2001). Several detailed taxonomies of prototypes have been proposed so far. A typical first taxonomic division is between prototypes that address form and those that address function (Otto & Wood, 2001; Pei et al., 2011). Another common distinction is the fluctuating level of fidelity of prototypes concerning the final model. A distinction is also typically drawn between virtual (simulations, visualizations, or computational approximations of behavior) and physical models. This paper shall elaborate on an expanded index and framework that provides a clearer relationship between the various distinctions (Camburn et al., 2017).

In different stages of the design and production processes, different prototypes are made to fulfill specific purposes. Camburn et al (2017) identify 10 different purposes of the prototypes: refinement, communication, exploration, active learning, timing, ideation, fixation, feedback, usability, and fidelity. Every one of these tasks is vital to the final output and the success of the product. Depending on the product, a different type of protytope is made. However, in most cases, not every one of these tasks needs to be fulfilled. But one thing has to be taken into consideration every signle time and that is timing. Both empirical and industrial studies highlight that early prototyping is critical to innovation (Jang & Schunn, 2012), specifically during the first 30% of a design project (Elsen et al., 2012), it is especially crucial to test the challenging systems (Otto & Wood, 2001). In fact, late prototyping is correlated with unsuccessful efforts (Jang & Schunn, 2012). The precise selection of when to engage prototyping should be considered strategically (Otto&Wood, 2001). This decision may depend on complexity. It is important to note that committing a larger amount of time to prototyping does not correlate to greater success (Yang 2005). Positioning efforts early on in the overall timeline is particularly critical.

As a result of the reviewed literature we are not trying to implement “new” technologies into the creative process. Our reaseach and practice locate the problem in comunication between the designers and other departments, as well as the users (customers). Research in design supports prototypes as essential to explore and enhance design usability (Barbieri et al., 2013). Prototypes enable observation of real-time interaction between users as well as between users and the design (Kurvinen, Koskinen & Battarbee 2008). Prototypes are also valuable for communicating concepts within the design team. This is why we propose the implementation of the so-called new technologies for communication purposes to better transfer information and properly gather feedback.

1.1. Additive manufacturing in conceptual design

Additive manufacturing (AM) is a group of processes used to build models by adding layers. This approach emerged in the late 1980s and early 1990s, noting constant increase in its development ever since. AM enables direct manufacturing from a design model. These technologies reduce the effort and cost to produce complex geometries. They enable mass customization and adaptive systems creation. Empirical research has

extracted several best practices from such databases for leveraging AM in prototyping, including the following heuristic guidelines: reuse features to reduce effort, employ cellular structures to increase strength and reduce mass, embed functional features in mesostructure, and employ part segmentation to increase the effective print size (Camburn et al., 2017). Figure 1 below shows an example of an appearance prototype made for a survey conducted at the Faculty of Mechanical Engineering in Skopje (Djokikj, 2020). The two models have uncanny resemblance (Figure 1-a) and the fabrication time is just two hours, no need for any tooling or any additional preparation.

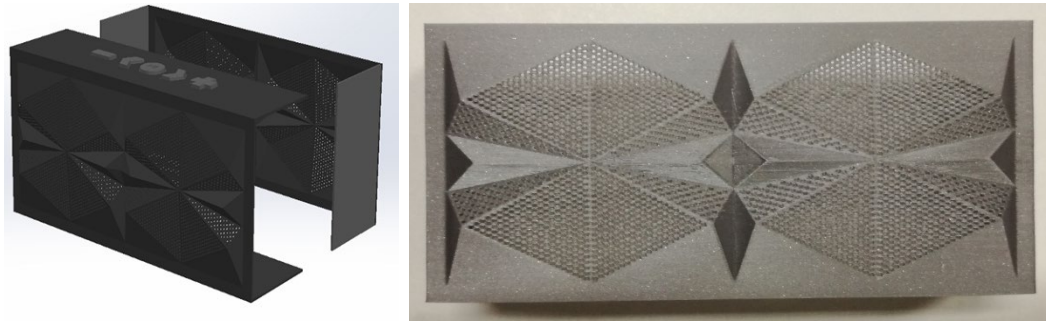

a) b)

Figure. 1: Example of use of AM in the conceptual design (Djokikj, 2020)
a) CAD model; b) Prototype fabricated with AM

The involvement of additive manufacturing in the early stages of the design process is proposed by many authors. Evans (Evans, 2002) proposes CAID/RP methodology to streamline the New Product Development (NPD) process. The use of CAID and RP in the early stages of the design process shortens the time needed to develop an idea to a finished part. When it comes to the commercial need to reduce NPD timescales and to acknowledge the extensive lead times required for the production of appearance models, potential problems need to be identified.

The use of AM in the conceptual design phase is exceptionally beneficial if these technologies are used for the manufacturing of the final part. Since the model can be designed appropriately for manufacturing at the first attempt using the design rules for AM.

Nevertheless, the use of AM in the conceptual design phase is also beneficial for the design process itself as well as the whole production process, even when the final part is being manufactured elsewhere. As stated above, the first reason for this is streamlining both the design and production processes by having functional prototypes in the early stages of the design process. The second reason is the possibility to thoroughly examine the prototype to eliminate errors in the final part. The third and maybe the most important reason for the success of the product is to communicate the idea with the customer.

1.2. Augmented reality in conceptual design

Augmented reality facilitates capturing the voice of the customer and the user experience in a uniquely quantitative fashion (Carulli et al., 2013). An augmented reality prototype might, for example, integrate eye-tracking for detailed use assessment (Bordegoni et al. 2009). It is also both cost and time effective (Ferrise et al., 2012). Augmented reality facilitates the potential to engage more senses in the user-interaction environment at an earlier stage (sight, sound, touch, and so on.) (Barbieri et al., 2013). A unique benefit is the ability to independently manipulate each sensory feedback (Ferrise et al., 2012). A controlled study found an augmented reality prototype to provide equivalent usability data from participants as a physical prototype (Bruno et al. 2010). These technologies may also enable live modification of a virtual (Ng et al., 2015) or physical model (Anderl et al., 2007).

In our previous reserch (Rizov et al., 2019) we have come across similar findings as those in the literature we reviewed. In particular, we found that implementing AR in the process engages the user, making them more involved into and interested for the product, which is a board game in this particular case. A different study demontrates (Mircheski and Rizov, 2017) the implementation of AR in a nondestructive disassembly process. The use of AR proved to be effective and easy to comperhend by users (Figure 2).

It has been noted that several authors suggest the implementation of AR in the design process. Mair et al. (2014) suggest an approach to assist the identification of suitable areas of application of AR within the product design process. This approach utilizes an established methodology for product design development that allows

each stage in the design process to be identified and considered in a logical and structured manner. These authors imply that with the proposed approach, AR is suitable for use in any stage of the design process as opposed to other well-known techniques, like drawings, basic computer-aided design, virtual reality, or rapid prototyping techniques and suchlike, to produce physical models. Ng et al. (2015) has an interesting approach for the implementation of functional 3D models into an AR environment. This approach has been developed mainly for design reasoning and evaluation, to ensure that the design is both functionally and geometrically consistent. Designers create conceptual designs by first defining how the product can be used, in the form of a Product Use Model, followed by creating basic 3D models using their bare hands in an Augmented Reality CAD Environment (ARCADE). The functional behavior of a product can be simulated as a prototype in ARCADE to demonstrate the use of the product and detect potential usability issues.

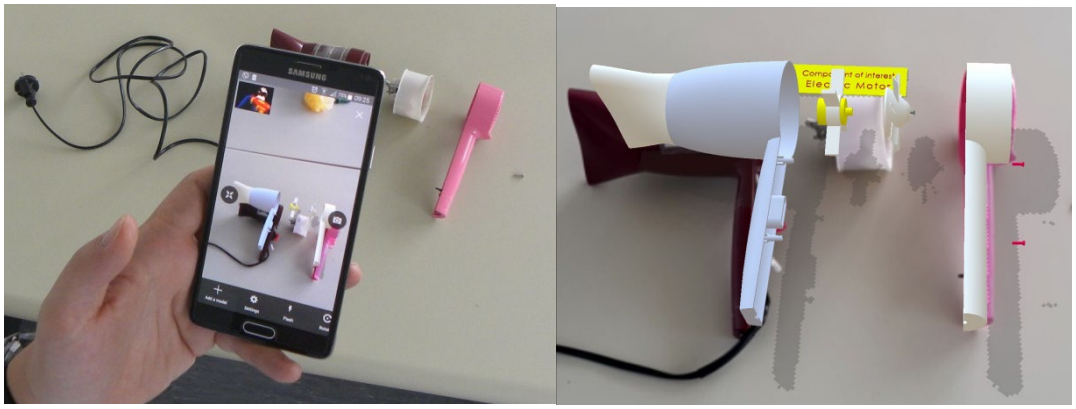

a) b)

Figure. 2: Example of use of AR for nondistructive dissasembly (Mircheski and Rizov, 2017)
a) Presentation of the process; b) AR animation showing on-screen

2. THE MODEL

The models proposed in this paper support a standard design process with added value. As it can be seen on Figure 3, the beginning is a standard design process, and the prototyping stage includes AM and AR. AM is used for both the appearance and functional prototypes. In the early stages of the design, many different models are fabricated in order to find the most appropriate one. Different models are also created for both the appearance and the functional prototypes. With the functional prototypes, specific elements of product functionality are being tested. The functional prototype does not match the look of the final product even close. This is why functional prototypes are mainly used by a closed group of professionals within the field. The appearance models are evaluated by professionals within the field or the company, but the users (customers) are also included. These models are judged based on appeal and feel (i.e. ergonomics). Everyone can have a say and the feedback goes back to the designers doing the inital sketches or the 3D models.

The implementation of AR in the conceptual design process is mainly needed for the functional prototypes, but also for the interaction models. This does not mean that AR cannot be used for the appearance prototypes. Moreover, there are cases where the use of AR in appearance prototypes is necessery. For example, if the product is equipped with new or still unknown technology, creating an AR prototype is the logical solution. If funding for the prototyping phase is limited, the use of AR is also the smart solution.

Nevertheless, AR in the conceptual phase is mainly used for interaction models. These models are essentially intended for the users, so they can exploit full functionality of the product without the part being finished. Interaction of the users with the product is of high importance, since it can give feedback to the designer about the behavioral characteristic. This kind of feedback reveals users' hidden emotions which are directly linked to the satisfactory feel of the product. Usually, this kind of experiment can be made during the last stages of the design process and prior to production. But with the implementation of AR, users can interact with the product while it is still in development.

Additionaly, AR can be implemented to demonstrate product functionality. This is again intended for the users (customers), who can have the appearance model in their hands and trigger different functionalities which can be demonstrated on-screen (mobile phone, laptop, or PC monitor).

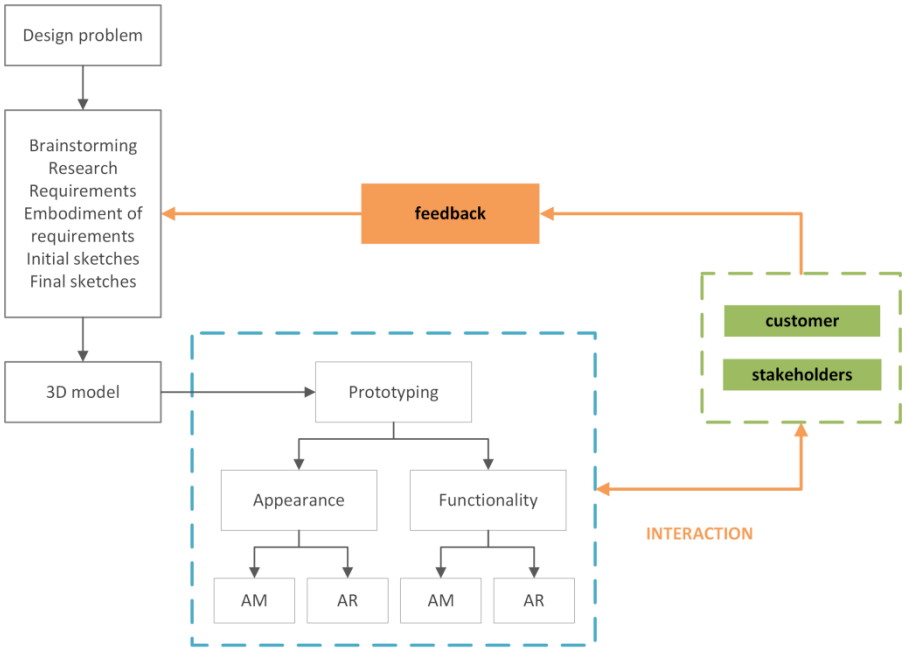

Figure. 3. The proposed model of implementation of AM and AR in the design process

4. RESULTS AND DISCUSSION

Implementation of AM and AR can speed up the design process and shorten the time to market. Having appearance and functional prototypes so early in the design process means that any design flaws can be identified and removed early in the process. Having all the potential glitches eliminated in the early stages of the process can prove to be quite effective, as any delay in the production process is equal to losing valuabale resurces such as time and money.

As explained in the last paragraph, the model that we are proposing with this paper leaves room for the design team to choose the appropriate prototype as well as the appropriate technology, depending on the product and the whole presentation plan. We are not suggesting that both technologies should be applied to any case. We simply want to demonstrate that the use of these technologies (i.e. AM and AR) is highly possible and also necessary in the conceptual phase of the design process. That is why in our flexible model, it is the design team and all the stakeholders who can decide on the appropriate strategy: what king of a prototype is needed and wether AM, AR, or both, will be used.

We believe that the use of both AM and AR is extremly beneficial because it enables communication between all those involved in the design proces: designers, customers, stakeholders, and other members in the process.

5. CONCLUSION

This paper analyses the opportunity of using two “new” technologies in the conceptual design phase. These “new” technologies to be included in the conceptual phase are Additive Manufacturing (AM) and Augmented Reality (AR). Research has shown that using AM for creating more realistic prototypes and proof of concepts also shortens the time needed to complete the process. At the same time, AR is used for a more detailed explanation of product functionality and usability. The model presented above evidently speeds up the design process, but more importantly, it provides valuble feedback to the designers from both peers and customers. Having all these tools in play in the early stages of the design process can prove to be very beneficial. It is up to the designers and the whole team to choose which one they will take into consideration.

For further research, this model has to be applied to current products, in order to evaluate the functionality of a particular design and production process of the model.

REFERENCES

1. Alcaide - Marzal J., Dieago-Mas A., Asensio-Cuesta S. and Pigueras-Fiszma B. 2013. An Exploratory study on the use of digital sculpting in the conceptual product design. *Design Studies* 34 (2). pp. 264-284. Elsevier Ltd.
2. Anderl, R., Mecke, K. & Klug, L. 2007. Advanced prototyping with parametric prototypes. In Digital Enterprise Technology, pp.503–510. Springer.
3. Barbieri, L., Angilica, A., Bruno, F. & Muzzupappa, M. 2013. Mixed prototyping with configurable physical archetype for usability evaluation of product interfaces. *Computers in Industry* 64, pp.310–323
4. Bordegoni, M., Cugini, U., Caruso, G. & Polistina, S. 2009. Mixed prototyping for product assessment: a reference framework. *International Journal on Interactive Design and Manufacturing (IJIDeM)*3,177–187.
5. Bruno, F., Cosco, F., Angilica, A .& Muzzupappa, M. 2010. Mixed prototyping for products usability evaluation. In *ASME 2010 International Design Engineering Technical Conferences and Computers and Information in Engineering Conference*, Montrel, Canada, pp.1381–1390.
6. Camburn, B., Viswanathan, V., Linsey, J., Anderson, D., Jensen, D., Crawford, R., Otto, K. and Wood, K., 2017. Design prototyping methods: state of the art in strategies, techniques, and guidelines. *Design Science*, 3.
7. Carulli, M., Bordegoni, M. & Cugini, U. 2013. An approach for capturing the voice of the customer based on virtual prototyping. *Journal of Intelligent Manufacturing* 24, pp.887–903.
8. Cross, N. 2008. Engineering design methods: Strategies for product design. Wiley.
9. Djokikj, J. 2020. Form design for Additive manufacturing. PhD Thesis. Ss. Cyril & Methodius University.
10. Elsen, C., Häggman, A., Honda, T. & Yang, M.C. 2012. Representation in early stage design: an analysis of the influence of sketching and prototyping in design projects. In *ASME 2012 International Design Engineering Technical Conferences and Computers and Information in Engineering Conference*, Chicago, IL, pp.737–747.
11. Evans, M., 2002. The integration of rapid prototyping within industrial design practice. PhD Thesis. Loughborough University.
12. Ferrise, F., Bordegoni, M. & Cugini, U. 2012. A methodology based on interactive virtual prototypes for a better design of consumer-product interaction. In ASME 2012 International Mechanical Engineering Congress and Exposition, Houston, TX, pp. 433–440.
13. Jang, J. & Schunn, C.D. 2012. Physical design tools support and hinder innovative engineering design. *Journal of Mechanical Design* 134, 041001.
14. Kurvinen, E., Koskinen, I .& Battarbee, K. 2008. Prototyping social interaction. *Design Issues* 24, pp.46–57.
15. Mair, G.M., Robinson, A. and John S. 2014. Applying Augmented Reality to the Concept Development Stage of the Total Design Methodology in R. Shumaker and S. Lackey (Eds.): VAMR 2014, Part II, LNCS 8526, pp. 414–425. © Springer International Publishing Switzerland.
16. Mircheski, I. and Rizov, T., 2017. Improved Nondestructive Disassembly Process using Augmented Reality and RFID Product/Part Tracking. *TEM Journal*.
17. Ng, L.X., Ong, S.K. & Nee, A.Y.C. 2015. Conceptual design using functional 3D models in augmented reality. *International Journal on Interactive Design and Manufacturing (IJIDeM*) 9 (2), pp.115–133.
18. Otto, K. & Wood, K. 2001. Product Design: Techniques in Reverse Engineering and New Product Design. Prentice-Hall.
19. Pei, E., Campbell, I. and Evans, M., 2011. A taxonomic classification of visual design representations used by industrial designers and engineering designers. The Design Journal, 14(1), pp.64-91.
20. Prats, M., Lim, S., Jowers, I., Garner, S.W., & Chase, S. 2009. Transforming shape in design: observations from studies of sketching. *Design Studies* 30(5), pp.503-520.
21. Rizov, T., Đokić, J. and Tasevski, M. 2019. Design of a board game with augmented reality. *FME Transactions*, 47(2), pp.253-257.
22. Robertson, B.F. & Radcliffe, D.F. 2009. Impact of CAD tools on creative problem solving in engineering design. Computer-Aided Design, 41(3), pp.136-146.
23. Stones, C. & Cassidy, T. 2007. Comparing synthesis strategies of novice graphic designers using digiteal and traditional design tools. *Design Studies*, 28(1), pp.59-72.
24. Yang, M.C. 2005.A study of prototypes, design activity, and design outcome. *Design Studies* 26, pp.649–669.

KERF BENDING: A GENEOLOGY OF CUTTING PATTERNS FOR SINGLE AND DOUBLE CURVATURE

Andriani-Melina Kalama
Department of Architecture, University of Thessaly, Volos, Greece
akalama@uth.gr

Danai Tzoni
Department of Architecture, University of Thessaly, Volos, Greece
dtzoni@uth.gr

Ioanna Symeonidou
Department of Architecture, University of Thessaly, Volos, Greece
PhD., Assistant Professor, symeonidou@uth.gr

ABSTRACT

The paper presents an ongoing research on kerf bending of sheet timber material, by removing material at strategically located areas on the surface, to weaken the material locally rendering it bendable. Through a series of experiments the aim is to understand the reciprocal relationship between the cutting pattern and characteristics such as bending curvature, material resistance under load, among others. By understanding the factors that lead to an increased degree of single or double curvature, the aim is to optimize these patterns by redesigning, combining and scaling patterns, as well as changing the direction of pattern elements. All experiments are documented, forming a genealogy of patterns that are grouped by type and geometric properties. The conclusions highlight the advantages and limitations of each cutting pattern with regards to the geometry, while they discuss the possibilities for differentiated curvature through parametrically differentiated patterns.

Keywords: kerf bending; architectural geometry; digital fabrication; curvature; cutting patterns

Introduction

Digital manufacturing technologies are evolving and becoming more accessible and widespread. New material properties and new construction techniques are steadily replacing the industrial materials and conventional construction techniques, while new designers are promoting the experimental use of new materials and the innovative use of traditional materials, such as wood.

This research explores a particular wood bending technique, which is called kerf bending or kerfing. Kerf technique refers to the removal of material at strategically located areas on a wood surface, to weaken the material locally in order to bend it. This technique is applied to produce objects of different scales and functions, from product design to small-scale architectures. (Gillkvist et al., 2016; Mitov et al., 2019)

The main goal of this research is to analyze and understand the wood curving technique, to collect pattern examples for kerf bending, to generate new patterns, to classify the patterns according to their characteristics and to discuss architectural applications of this technique. This research aims to provide recommendations and guidelines for the implementation of kerf bending and to aid in the development of digital construction prototypes and experiments for architectural applications.

Research methodology

In this research a combination of two research methods and analysis was used. The research is divided into the study of precedents study, based on findings from existing bibliography and a variety of references from experimental architecture, which aimed at investigating the curvature of wood by modifying pattern motifs. This part focuses on information about the application of the technique of kerf bending and the characteristics that govern it, the cutting machines and the clarification of the geometrical terms, such as single and double curvature, ruled and developable surfaces. The reference study is complemented by a collection of examples of application of the kerf technique in architecture and a description of the construction process, since no information on the construction process has been found for all the architectural examples, the research involved visual analysis and categorization in order to reach conclusions. Based on the knowledge gained through bibliography, the research team undertook a number of material experiments, to obtain a better insight into the process and material behaviour. The first experiments are based on existing patterns designed by Aaron Porterfield, a researcher that pioneered wood bending through kerf technique (Porterfield, 2000; Porterfield, 2005). By changing variables, such as the distances between slots, the scale of the pattern, the directions of the elements that form the pattern, and converting the linear elements into curved or dotted lines, a variety of conclusions were drawn, that were useful for further developments of the application of the technique.

Construction of curved surfaces in architecture is a time consuming and difficult process. There are many ways to construct curved surfaces, but in most cases molds are required, which results expensive for individualized production of single elements. During the last decade, a series of bending methods have been developed based on mechanical properties of the material, such as kerf bending. (Mitov et al., 2019)

Kerf bending is used in a variety of materials such as wood, plexiglass and metal. The main focus of this research is how to apply this technique to wood. Kerf bending is used in new woodworking industries and is considered a simple and fast way of bending, since it doesn't require special equipment and complex manufacturing techniques, such as thermal or chemical elaboration. The kerfs can be a part of a design or can be covered with a thin-flexible surface, such as a tap, or with a wood filler. (Güzelci etc, 2016; Moholy-Nagy, 2012)

This technique has certain advantages and disadvantages:

Advantages of kerf bending:

- Allows the generation of single and double curvature surfaces
- Provides an easy and fast way of bending, without the need for special equipment, except from cutting machines
- Suggests a manufacturing process without making an impact on the environment, as molds are not required
- It is applicable for a variety of materials such as wood, plexiglass, metal
- A wide variety of shapes may be applied for the kerfs

Disadvantages of kerf bending:

- In order to stabilize the curvature of the wood structure, fasteners like screws need to be used, as opposed to other wood bending techniques where the structure remains in curved form without further procedures
- Limitations in construction. Kerf bending is not applicable for large scale components cause to reduced strength of material
- Kerf constructions are not recommended for exterior space because of weakening of the material due to weather conditions.

Use of Kerf Bending in Architecture

Through research on examples from the literature and reference material found online, it has been observed that this technique has been used in small-scale architectural constructions, such as installations and pavilions, only during the last decade, mainly due to the reduction in timber strength and the need for high precision cutting, which is evidently improving with the development of digital manufacturing machinery. The kerf cuts are those that facilitate the bending of the material but at the same time they reduce its structural properties. As a result, in architecture it is mostly found in interiors, as well as in smaller objects such as furniture, lamps, accessories, etc.

Regarding the support of certain predetermined curvature in larger-scale constructions, there are two methodological approaches. According to the first, supporting mechanisms are being used, which are usually designed for each construction separately (e.g. The Wooden Waves, Mamu Mani, 2015), while according to the other, the construction consists of smaller repetitive elements supporting each other (e.g. Kerf Pavilion, MIT, 2012).

Regarding the texture of the curved surface, sometimes the cutting lines of kerf bending are prominent, resulting in a characteristic texture and revealing the wood bending strategy (e.g. The Wooden Waves, Mamu Mani, 2015) and sometimes the timber plates are further processed, filling the cutting gaps with special materials and paints (e.g. Mitov et al., 2019), which gives a smooth finish and hides the bending strategy on the surface.

EXPERIMENTS

The aim of the experiments is to study the characteristics of each pattern such as bending degree and strength, classify them based on the above and therefore create a database for the kerf pattens and their characteristics aiding future decisions on selecting an appropriate pattern for each construction. The first experiments were based on the kerf bending study by Aaron Porterfield (Porterfield, 2000). Each specimen is evaluated with regards to its curvature, bending strength, stretching length and twisting capacity and the required laser cutting time for its production. All specimens are 10x10cm and all their measurements are presented in tables, so that the results can be compared across patterns.

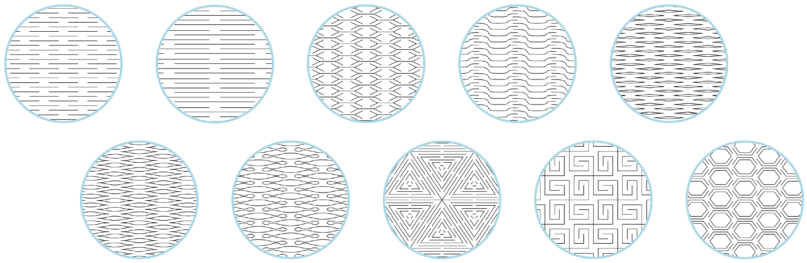

Figure. 2: Aaron Porterfield's Patterns

Calculations methodology

To measure the curvature (1/R) the specimens were photographed during maximum bending. In the photographs a curve was drawn approximating the curved shape of the specimen, and then through an algorithm the curve point with the maximum curvature was found and the curvature circle was drawn whose radius (R) was measured. Therefore, the curvature is measured based on the radius R of the circle. Double curvature specimens were measured by measuring the diagonal of the original specimen shape and the diagonal of the specimens at maximum bending.

Bending causes the specimens to deform or even break. To find the bending strength limit of the timber plates it was necessary to break them. By stabilizing the specimens and exerting a superficial force with weights to the limit of their fracture, a comparison was made between them, with weights ranging from 0,20 kg to 26,56 kg.

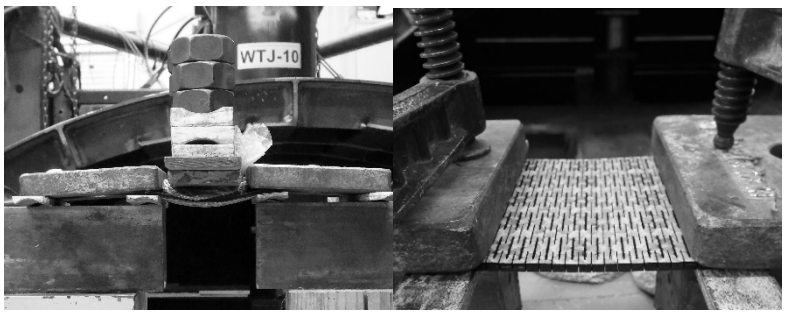

Figure. 3: Bending Strength Experiments

Some specimens during this process are elongated. This property is listed in the table as stretching length and was calculated by subtracting the original length of the specimens from the final length when stretched.

Some specimens had the ability to twist and create a ruled double curved surface. Patterns with this attribute are highlighted in the table.

To calculate the laser cutting time, a python script was used with the speed settings set to 25%. The laser cutting time was calculated algorithmically, because the timber plates were cut on three different laser cutters and if the actual time was measured the results would have not been comparable.

Experiments in different wood types

The type of wood is a very important factor in wood bending through kerfing technique. The first experiment involved cutting patterns on natural wood such as balsa and artificial wood such as plywood and MDF (Medium Density Fiberboard) to observe the differences in the characteristics of each wood. Regarding balsa wood, the specimens could not be evaluated properly, because balsa is a fragile material and the specimens were easily broken during bending. The plywood and MDF specimens were heavily curved. However, since MDF wood has been largely processed and is not governed by the characteristics of timber, the material selected for the subsequent study experiments is plywood.

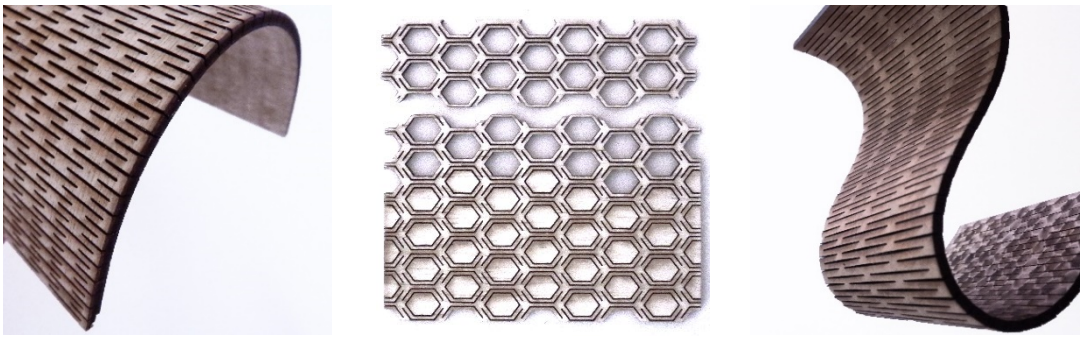

(a) (b) (c)

Figure. 4: (a) Plywood, (b) Balsa Wood and (c) MDF

Pattern experiments

Linear patterns of parallel lines

Table 1: Properties and measurements of linear pattern kerf specimens

#	Pattern	Curvature (1/R)	Double Curvature (cm)	Bending Strength (kg)	Stretching length (cm)	Twisting capacity	Laser Cutting Time
1	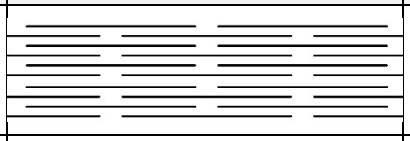	0,92	x	9,555	0,5	x	03:14
2	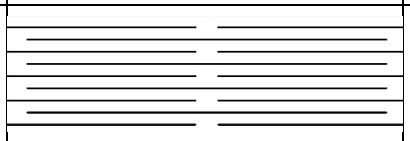	1,23	x	4,410	1,8	✓	02:32
3	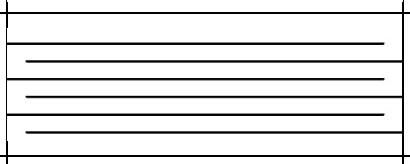	2,27	x	1,940	4,5	✓	02:09
4	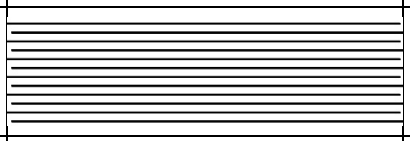	3,33	x	0,200	29	✓	04:11
5		1,42	x	1,940	3	x	04:40
6		0,59	x	1,830	1,6	x	04:40
7	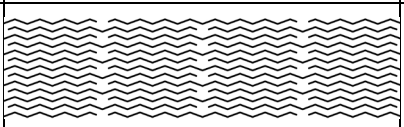	1,03	x	2,080	2,2	x	04:46
8	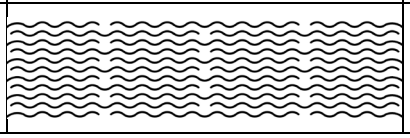	1,03	x	3,700	2	x	04:08

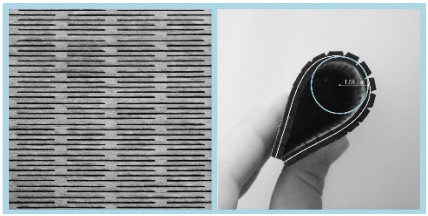

1. This pattern is designed by Aaron Porterfield and consists of horizontal parallel lines, which present discontinuity at two or three points. This is the most common pattern that has been applied to structures which use this bending method. It is observed that the specimen reaches a high degree of curvature and strength.

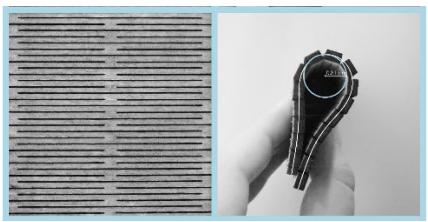

2. An inquiry that emerges from the above experiment is whether the discontinuity of the lines affects the curvature of the surface. So, a similar pattern was designed, with discontinuity at one or two points, instead of the two or three points of the original. The new pattern bends more, but its durability is affected because more material than the original is removed. The new pattern has more stretching capability.

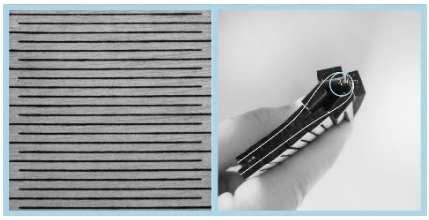

3. Subsequently, a pattern was designed consisting of parallel lines which present discontinuity at one point only, towards the boarders of the specimen right or left alternatively. The specimen reaches high bending degree and is distinguished by pliancy. In particular, when the pattern applied to 20x10cm timber plate, it can be twisted by 180^{o}.

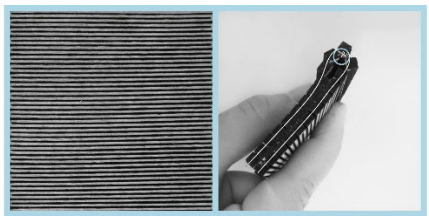

4. The same pattern, with a higher density of parallel lines, was designed. The distance between the lines was reduced from 4,4 mm to 2,2 mm. The bending degree, the pliancy and the twisting capacity are increased, compared to the previous specimen. However, this specimen appears to be brittle and faceted as the ratio between kerf lines and timber thickness is affected dramatically.

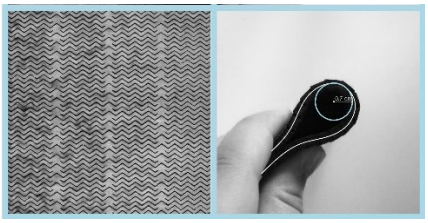

5. Based on the first linear pattern, a new pattern was designed where the straight lines were replaced by polygonal chains, with a spacing of 1,85 mm. The basic idea of the experiment was to create a single line, which would change direction and interrupt the continuity of the timber fibers in more places causing more curvature. The specimen is distinguished by pliancy. In addition, it is observed that exerting force at antisymmetric points results in twisting of the surface, creating a ruled double curved surface.

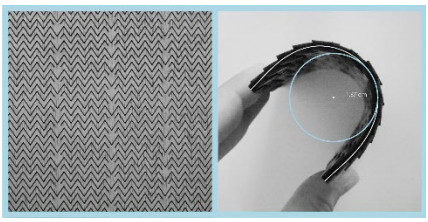

6. Subsequently, a question that arises from the above experiment is whether the angle of the polygonal chain elements affects the curvature of the surface. Therefore, a new pattern with acute angle elements is designed. The specimen is distinguished by flexibility and twisting capacity.

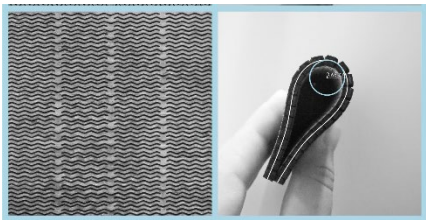

7. Meanwhile, a pattern with obtuse angle elements was designed. This specimen bends more than any of the above polygonal chain specimens, it exhibits greater strength and pliancy, but it is not capable of double curvature.

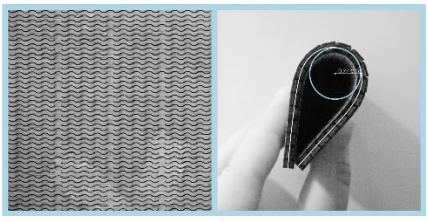

8. This pattern emerged from the original polygonal chain pattern by changing the curvature degree of the polyline. The specimen attains a lower degree of curvature than the original, but it is distinguished by more durability and flexibility.

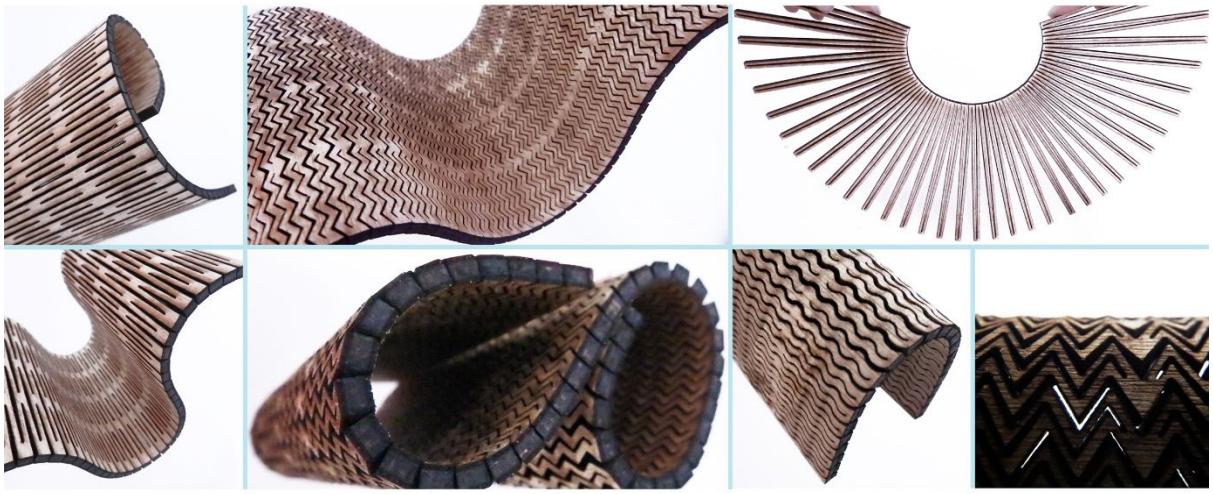

Figure. 5: Specimens of Linear Patterns

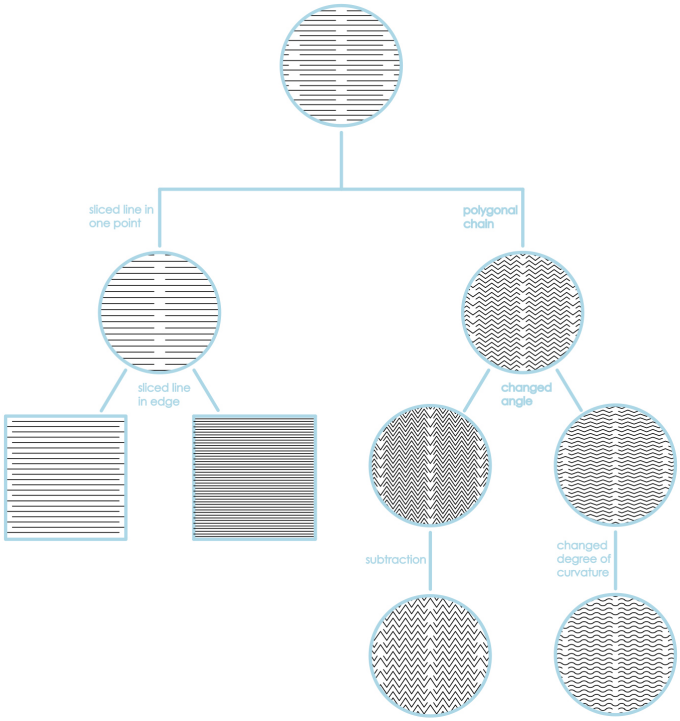

Figure. 6: Genealogy of Linear Patterns

Offset patterns

Table 2: Properties and measurements of offset pattern kerf specimens

#	Pattern	Curvature (1/R)	Double Curvature (cm)	Bending Strength (kg)	Stretching length (cm)	Twisting capacity	Laser Cutting Time
9		-	3,5	5,125	x	✓	05:13
10	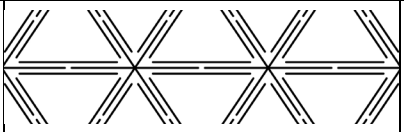	-	3,5	19,055	x	✓	02:37
11	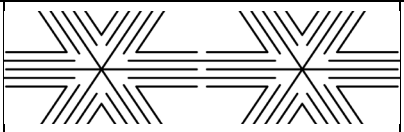	-	3,8	12,110	x	✓	02:55
12	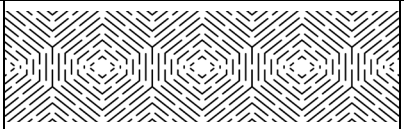	-	0,7	9,245	x	✓	04:42
13	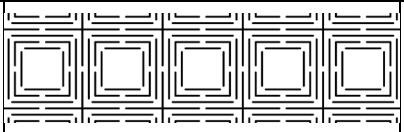	5,29	✓	18,515	x	x	04:33
14	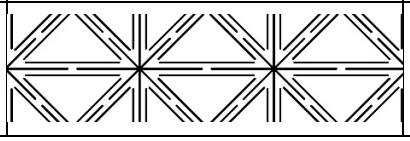	-	2,9	14,105	x	✓	03:43

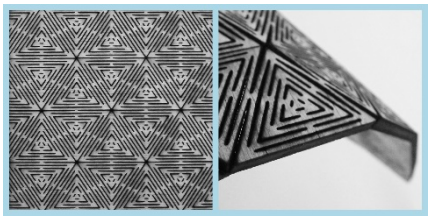

9. This pattern was designed by Aaron Porterfield and comprises of equilateral triangles with offsets of equal spacing. The pattern is distinguished by high durability and double curvature capability. The points where the lines present discontinuity are more strained during bending of the specimen and are considered as fracture points. The points that the triangles intersect, are the points of maximum curvature of the specimen, they are points of intersection of six lines and they act as a hinge connecting six flat triangles.

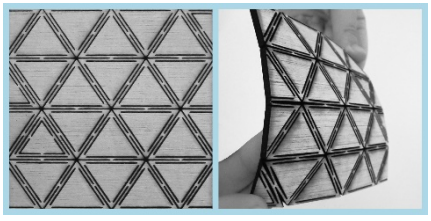

10. During the bending process of the previous specimen, it was observed that the pattern was affected only by the first and second series of the triangle offsets, and not by the following ones. Therefore, a new pattern emerged, which consists of the first two rows of the triangle offsets. Eventually, the experiment proved that the specimens reach the same degree of curvature, but the new pattern greatly increases its durability.

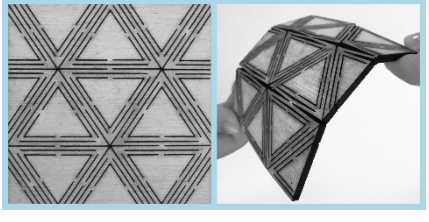

11. Subsequently, the pattern was designed on a larger scale. The basic idea of this experiment was that by increasing the length of the lines towards the points of maximum curvature, the surface would achieve a bigger curvature. The experiment shows that the specimen reaches a higher curvature degree than the original.

This double curvature pattern reaches a high curvature degree, independently of factors such as plasticity and durability. For this reason, patterns based on the same design principles but with other shapes were designed. The first shape chosen for study was the hexagon.

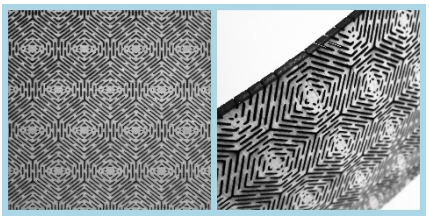

12. This pattern consists of hexagons which contain five offsets of them with equal spacing. Since this was the first attempt of redesigning the pattern shape, it was chosen to add all the hexagon offsets, to observe the reaction of the pattern. The experiment did not have the expected results. The pattern lines in different directions create double curvature, but the pattern bends only slightly. The curvature is affected, as in the previous experiment, by the first and second offset rows, so the rest can easily omitted.

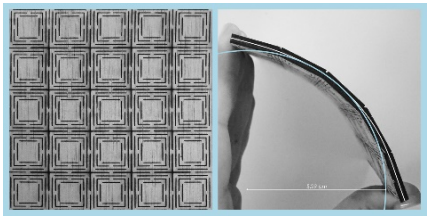

13. The design of a new pattern with squares, based on previous experiments displays a different behaviour, it is observed that this timber plate bends in two axes (x and y), due to the symmetry of the pattern. Moreover, there is only very limited double curvature.

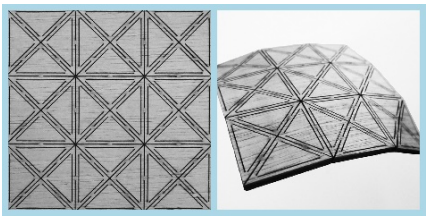

14. From the previous experiments it is deduced that the surface reaches its maximum curvature in the area where most intersecting lines are found. For this reason, a pattern with eight interesecting lines was designed, as opposed to the first pattern with six intersecting lines. The bigger the amount of intersecting lines, the bigger curvature degree will be achieved. The number of interesecting lines impact the number and the dimensions of the triangles. As a result, this specimen is bending less than the first, because of the smaller length of the lines.

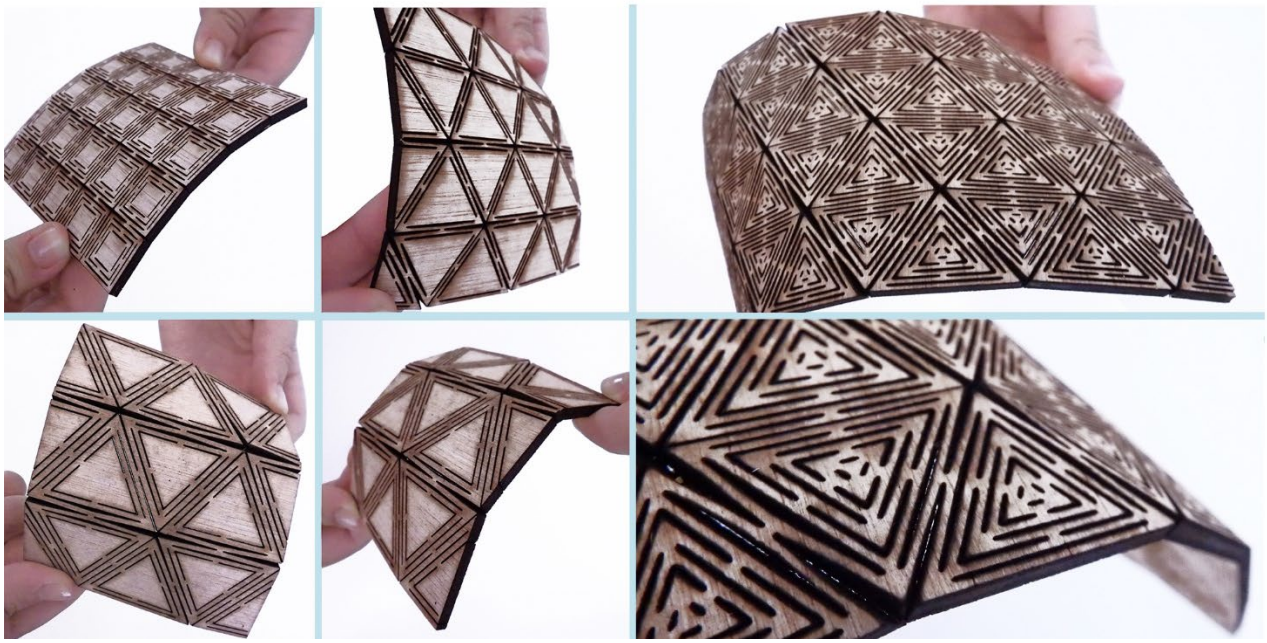

Figure. 7: Specimens of Offset Patterns

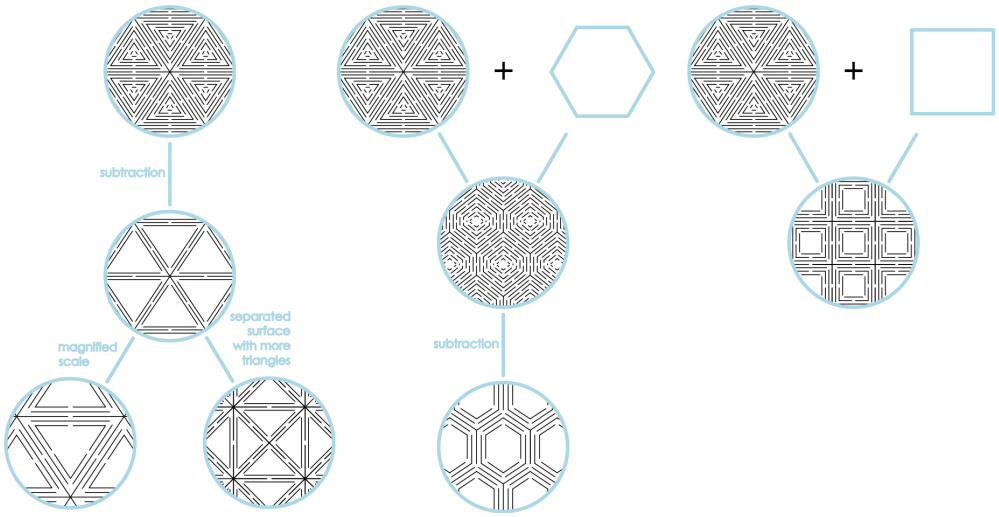

Figure. 8: Genealogy of Offset Patterns

Meander patterns

Table 3: Properties and measurements of meander pattern kerf specimens

#	*Pattern*	*Curvature (1/R)*	*Double Curvature (cm)*	*Bending Strength (kg)*	*Stretching length (cm)*	*Twisting capacity*	*Laser Cutting Time*
15	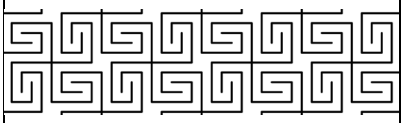	-	*3,9*	*12,155*	*x*	✓	*03:32*
16	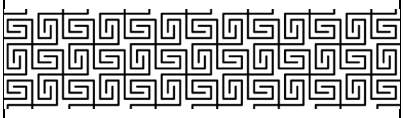	-	*8,2*	*9,755*	*x*	✓	*05:37*
17	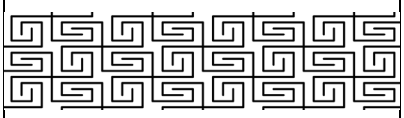	*0,48*	*x*	*9,230*	*x*	✓	*04:35*
18	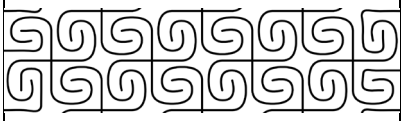	-	*2,4*	*11,210*	*x*	✓	*03:20*
19	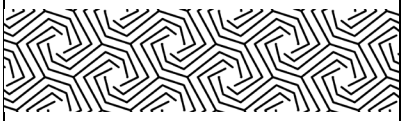	-	*4,4*	*9,560*	*x*	✓	*04:35*
20		-	*1,3*	*21,330*	*x*	✓	*03:46*
21	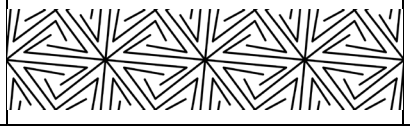	-	*3,2*	*7,220*	*x*	✓	*04:23*

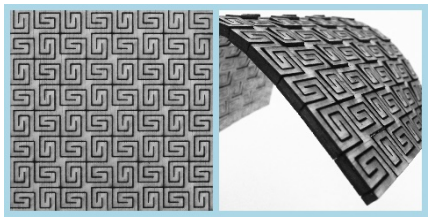

15. This first meander specimen is flexible and durable. The double curvature of this pattern is based on the long length of lines and the change of their orientation.

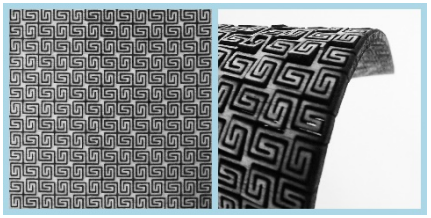

16. After conducting an experiment at a smaller scale, it emerges that as the scale of the pattern is reduced, the specimen becomes more bendable and less durable.

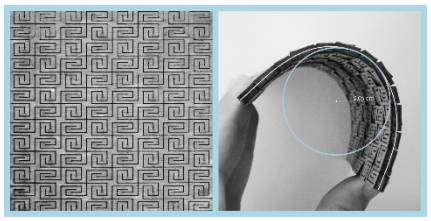

17. After scaling the original pattern in one direction, a different pattern emerged which does not display double curvature resulting in a single curvature pattern that is bendable and very durable. Consequently, the proposed fabrication strategy for double curved panels is conditioned by the dimensions of the pattern's lines and their symmetry on x and y axes.

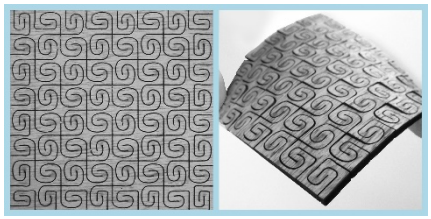

18. Drawing a meander that consists of curved segments, we observe that this pattern bends less than the original meander pattern, but it is more durable.

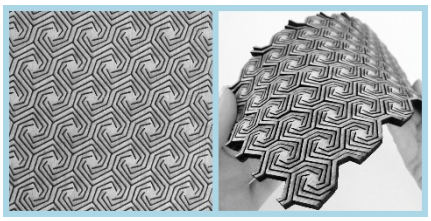

19. The shape of the original meander pattern is based on square shapes. To experiment with variations, a new meander pattern is designed based on hexagonal shapes. This is a double curvature pattern, which is bendable, but less durable than the original meander pattern. During the bending strength experiments, this timber plate broke to many pieces, as the stresses are distributed all over the surface due to the complexity of the pattern.

20. By converting the straight lines into curves, it emerges that the specimen is less bendable, but the durability is greatly increased.

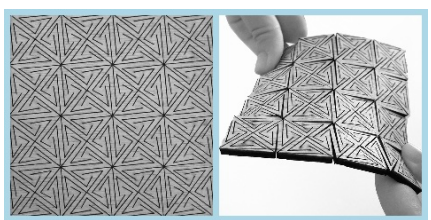

21. This pattern is a variant of the meander pattern with triangular shapes. The maximum curvature of the timber plate is at the intersection points of the eight triangles. These points operate as hinges. The specimen can be heavily curved, but easily broken due to the many lines that meet at the intersection points.

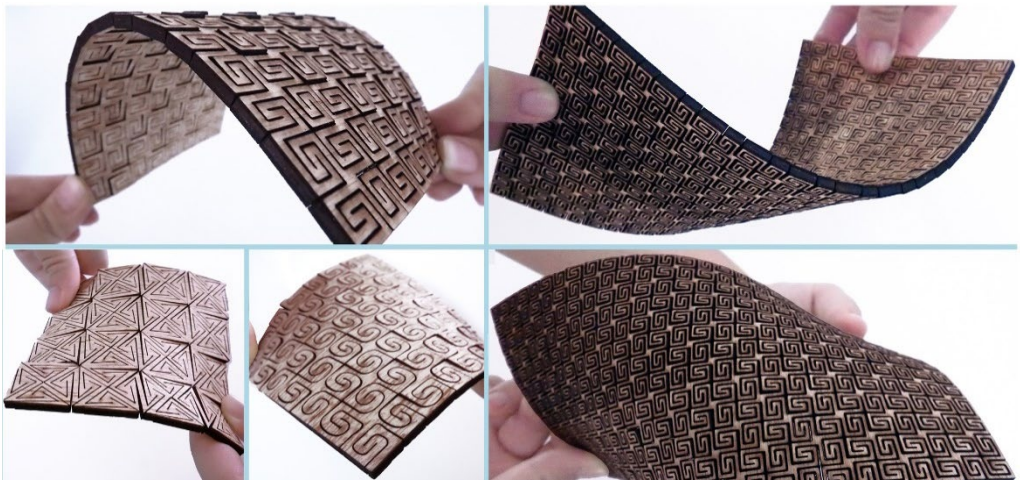

Figure. 9: Specimens of Meander Patterns

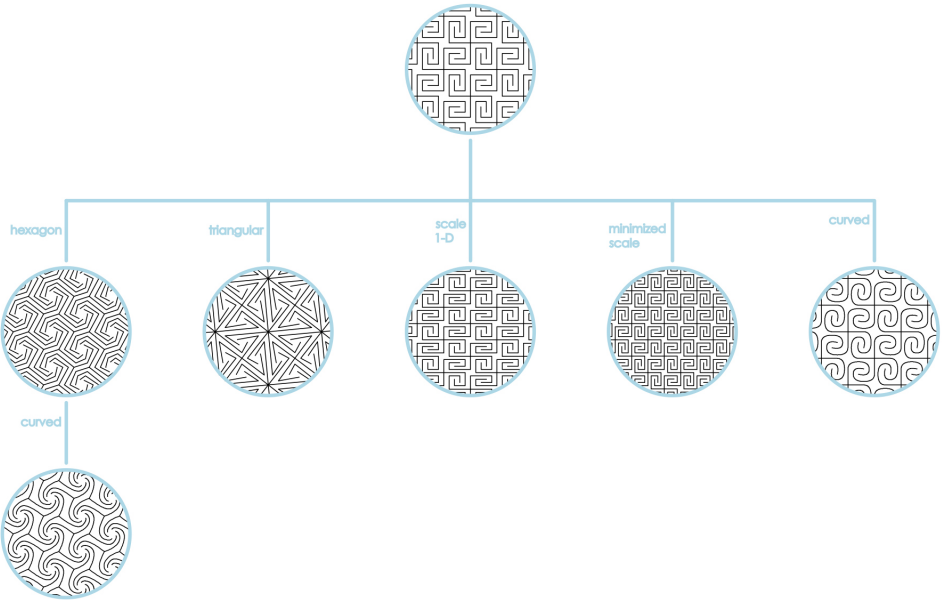

Figure. 10: Genealogy of Meander Patterns

Parametric patterns

The following experiment includes the changing of the surfaces' curvature, through variable spacing of the pattern elements. It is observed that the specimens are more flexible, as the lines of the patterns become denser, but when the distance between the patterns come close or smaller than 1mm, fracture of the specimen is possible. The specimen does not bend, when the distance between the pattern lines is high. In this experiment, the patterns are applied to a 20 x 10 cm wood surface in order to allow more space for the parametric variation of the spacing of lines. In the following diagrams, blue color gradient denotes the area of maximum curvature and in white the area of stiffness.

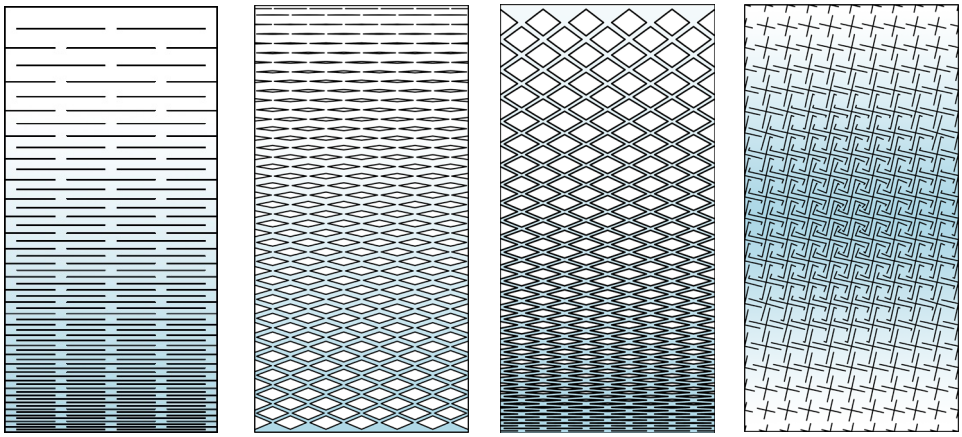

(a) (b) (c) (d)

a) This pattern is an evolution of Aaron Porterfield's linear pattern. The maximum spacing between lines is 1 cm and minimum is 0,11 cm. As the lines of the pattern become denser, the surface becomes more flexible and durable.

b) This pattern is combination of two patterns, the lines are transformed into diamonds. The first step was to set the number of the rows and the distance between them (2,9 mm), depending on the size of the larger diamond. As the shape of the diamonds grows, the lines of pattern get closer. Therefore, the specimen bends more at the point where the diamonds are larger.

c) This pattern is an evolution of the previous one, there is also a parametric transformation from lines to diamonds, but this specimen is denser. It was observed that this pattern is more bendable than the previous one, because the thickening of the lines is more noticeable.

d) Another parametric pattern was designed, based on the meander shape, by parametrically reducing the length of the pattern's lines, the meanders are transforming into crosses. This gives a rise to a pattern of double curvature, which is denser in the center of the specimen, for this reason the point of maximum curvature is located at the center of the surface. This pattern is slightly bendable, due to the short length and the lack of alignment of the lines.

As the lines of a pattern become denser, the degree of the curvature increases. The importance of the alignment of lines or shapes, their length and the distance between them must be taken into consideration while designing a pattern.

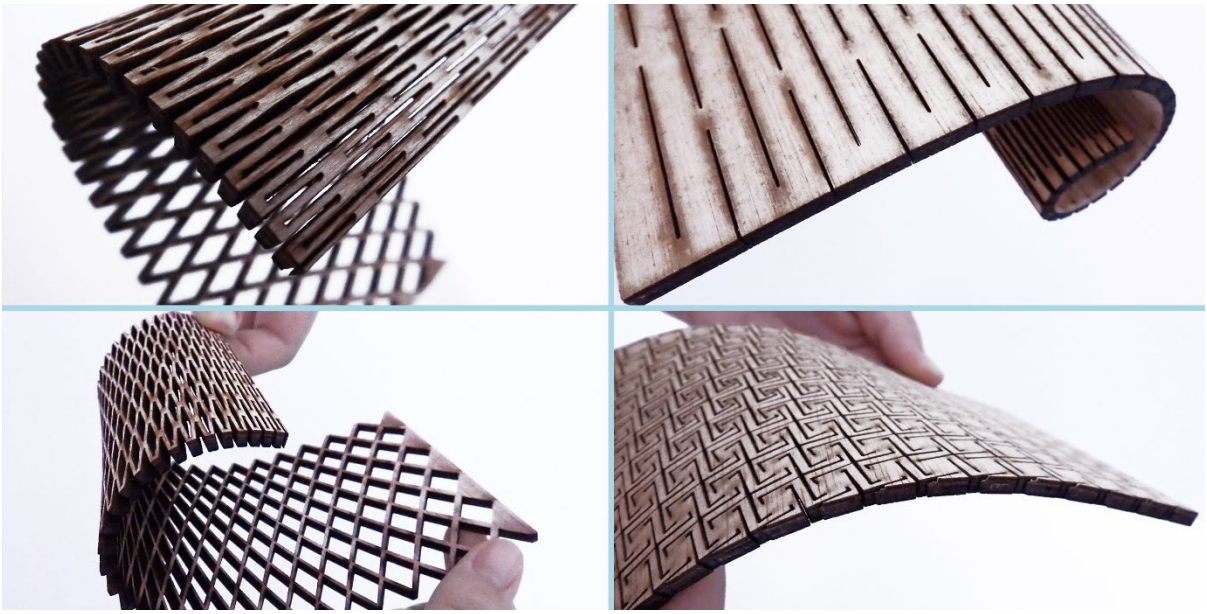

Figure. 11: Specimens of Parametric Patterns

CONCLUSIONS

Curvature

From this research it emerges that the kerf bending technique is highly dependent on the wood type. It is seen that when the kerfing is applied in natural wood, the bending is influenced by the orientation of the wood fibers. For this reason, for the single curvature patterns on natural wood, it is recommended that the pattern is applied parallel to the direction of the fibers. In case of application of the pattern perpendicular to the fibers, the fibers are seen to obstruct the bending of the timber plate. The curvature of a surface is also dependent on the thickness of the wood that is being used. The thicker the material, the sparser the applied pattern should be, in order to maintain the durability of the material.

Single curvature

Regarding the influence of a pattern on the surface curvature, it appeared that the patterns bend more when their lines are elongated and by increasing the density of the patterns. The lines of a pattern present discontinuity in order to keep the surface consistent. As the distance between the gaps of the lines is increasing, the curvature of the surface is reducing. It is necessary that some of the pattern elements are consistent until the boundaries of the surface. The more complex a pattern is, the less the surface bends.

Double curvature

It is essential that double curvature patterns are symmetrical in x and y axes, otherwise one of the two directions becomes dominant, and the pattern becomes a single curvature pattern. The double curvature patterns with offset shapes, present a high degree of bending, as the distance between the lines increases. On the other hand, the double curvature geometry motifs, such as meander, present high degree of curvature, as the distance between the lines reduces. As already mentioned previously, the durability of a surface is reduced when the curvature increases. However, this is not the case for the patterns with offset shapes, considering that their curvature increases by elongation of the length of their lines. It is possible to make a ruled surface by changing the orientation of linear patterns. Moreover, the curvature of the surface always follows the orientation of the lines of the patterns. The parametric patterns are applied to surfaces with variable curvature, their pattern dilutes where a low curvature degree is required, and where a higher degree of curvature is required the pattern becomes denser or the length of the lines extends.

Bending strength

As the curvature increases, the strength and the deformation ability of the specimens decrease. In effect, the strength of the specimen decreases by the subtraction of material. During the tests for evaluating the bending strength limit of the specimens, the creation of a cracking route which followed the lines of the pattern was observed. The specimens broke suddenly in many pieces, after bending stress. While finding the bending strength limit of double curvature patterns, we observed the fragmentation of the pattern, due to its complexity, which is distributing the tension all over the surface.

Breakpoints

According to Aaron Porterfield, the angles of the linear patterns are points of fracture. For this reason, he designed a similar pattern by replacing the angles with curves, as shown in the first row of the table (Porterfield, 2005). Therefore, the question that emerges is whether the curvature of a specimen is affected by the convexity of the pattern's shapes. The first step in this process was to choose three patterns and to redesign them with curved segments, inspired by Aaron Porterfield's experiment. Comparing the curved patterns to the linear ones, certain differences between them were observed; the linear patterns are more bendable, but the curved patterns are more durable, because of the elimination of potential break points at the angles.

Table 4: Comparison of linear and curved patterns

Linear Patterns	*Curved Patterns*
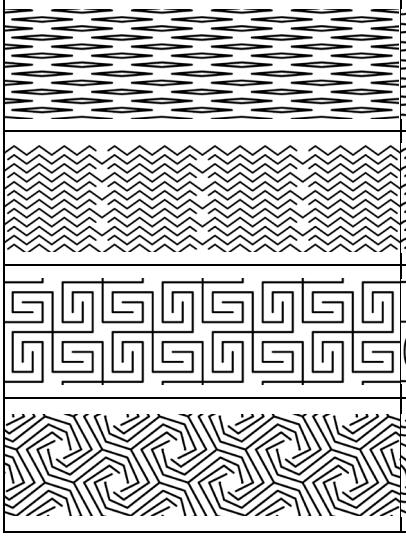	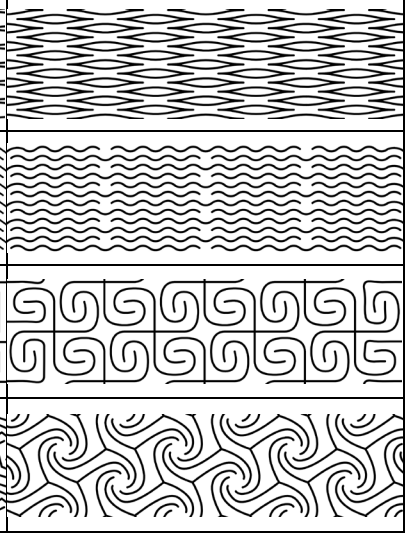

The widespread use of parametric design tools and CNC machines make the manufacturing of bended surfaces with Kerf Bending method much easier than before. As a result, new techniques for wood bending, through the removal of material, are being developed and are constantly evolving. Both the development of new patterns and the knowledge of their advantages and limitations, as well as useful remarks on their curvature, durability and other characteristics will likely lead to new architecture examples using kerf bending as a method for timber constructions of complex geometries.

ACKNOWLEDGEMENTS

This research was supported by the Department of Architecture of the University of Thessaly. It was conducted by Andriani-Melina Kalama and Danai Tzoni, under the supervision of Professor Ioanna Symeonidou. The authors would like to thank professor Dimitrios Psychogios for his valuable advice and suggestions, Professor Christos Papakonstantinou and PhD candidate Theoharis Papatheoharis of the Department of Civil Engineering of the University of Thessaly for their help and support with the experiments of bending strength in the "Laboratory of Concrete Technology" as well as the operators of the Laser Cutting Laboratory of the Department of Architecture for their feedback and advices regarding laser cutting and materials.

REFERENCES

Books

Moholy-Nagy, L., 2012. The New Vision: Fundamentals of Bauhaus Design, Painting, Sculpture, and Architecture. Courier Corporation.

Papers

Capone, M., Lanzara, E., 2018. Kerf bending ruled double curved surfaces manufacturing, in: Blucher Design Proceedings. Presented at the XXII CONGRESSO INTERNACIONAL DA SOCIEDADEIBERO AMERICANA DE GRÁFICA DIGITAL, Editora Blucher, São Carlos, BR, pp. 653–660. https://doi.org/10.5151/sigradi2018-1389 (accessed 4.7.19).

Güzelci, O., Alaçam, S., Bacınoğlu, Z., 2016. Enhancing Flexibility of 2D Planar Materials By Applying Cut Pat terns For Hands On Study Models.

Mitov, D., Tepavčević, B., Stojaković, V., Bajšanski, I., 2019. Kerf Bending Strategy for Thick Planar Sheet Materials. Nexus Netw J 21, 149–160.

Web-pages:

Furuto, A., 2012. Pavilion / EmTech (AA) + ETH [WWW Document]. ArchDaily. URL http://www.archdaily.com/221650/pavilion-emtech-aa-eth/ (accessed 12.6.19).

Gillkvist, O., Henriksson, V., Poulsen, E., 2016. Digital Wood - Design & fabrication of a full-scale exhibition structure in plywood [WWW Document]. Issuu. URL https://issuu.com/v.henriksson/docs/digitalwood (accessed 10.20.19).

Hoffer, B., Kahan, G., Crain, T., Miranowski, D., 2012. Kerf Pavilion | MIT Architecture [WWW Document]. MIT Archit. URL https://architecture.mit.edu/architectureandurbanism/project/kerf-pavilion (accessed 11.27.19).

Juc, C., 2016. The Wooden Waves | Mamou Mani Architects + Buro Happold. Arch2O.com. URL https://www.arch2o.com/wooden-waves-mamou-mani-architects-buro-happold/ (accessed 12.10.19).

Mamou-Mani, A., 2019. The Wooden Waves at BuroHappold Engineering. Mamou-Mani. URL https://mamou-mani.com/project/wooden-waves/ (accessed 12.10.19).

Menges, A., 2010. Kerf-Based Complex Wood Systems [WWW Document]. URL http://www.achimmenges.net/?p=5006 (accessed 12.6.19).

Porterfield, A., 2005. Curved Laser Bent Wood [WWW Document]. Instructables. URL https://www.instructables.com/id/Curved-laser-bent-wood/ (accessed 5.25.19).

Porterfield, A., 2000. f=f. URL https://fequalsf.blogspot.com/p/about.html (accessed 5.25.19).

BRUNO TAUT´S GLASHAUS – A MODEL FOR CONSTRUCTION TECHNIQUES OF TODAY

Martin Friedrich Eichenauer
Geometric Modeling and Visualization (GMV), Institute of Geometry, TU Dresden, Germany
research associate, Martin_Friedrich.Eichenauer@tu-dresden.de

Daniel Lordick
Geometric Modeling and Visualization (GMV), Institute of Geometry, TU Dresden, Germany
Professor, Daniel.Lordick@tu-dresden.de

ABSTRACT

The Glashaus, which Bruno Taut designed for the Werkbund exhibition in Cologne in 1914, is considered to be one of the key buildings of the 20th century. The philosophical approach, conception, and impact of the building have already been discussed in detail from an architectural point of view. No matter whether the Glashaus was inspired by nature or Gothic, the construction of the dome follows strict geometric principles and the design is strongly driven by practical building matters. The reticulated structure has only planar faces to ensure complete glazing. As such, it is a very early precursor of a non-trivial planar quad (PQ) mesh for a roof structure. We will use the Glashaus as inspiration and motive for a geometrical and structural analysis of such diagrid structures and apply the principles to modern building construction methods such as concrete printing.

At first, we propose a geometrical algorithm, which has probably been used to generate the dome. We then compare the result with an in-depth reconstruction from the plans handed down from the Historical Archive of the City of Cologne. Next, we explore the design space of the algorithm and adapt it to other surface classes like further surfaces of revolution, translational surfaces and generalized helicoids. The main focus is on the determination of the geometrical constraints, which may limit changes of the generatrix and depend on the generation method. Finally, the advantages of the proposed planar quad mesh family for large scale additive manufacturing processes will be reflected. Additional algorithms will be developed to meet the constraints of the construction process and may on the other hand push the conception for 3D-printing tools. On photographs of the erected Glashaus, unintended deformations of the dome can be detected visually. The aim of this research is, to surpass the limited accuracy of the early 20th century with contemporary manufacturing methods and trigger innovations for today's construction industry.

Keywords: dome, diagrid structure, planar quadrilateral (PQ) mesh, 3D concrete printing, Large Scale Additive Manufacturing (LSAM), parametric design

1. INTRODUCTION

The aim of this research project is to develop modules that are industrially prefabricated and assembled on site to form a shell-like construction in a simple, cost- and labour-saving manner. In order to integrate the process into a flow production, the modules get manufactured without the need for formwork. The materials used are suitable high-performance fiber composite materials based on cement that can be used in 3D printing. A good model for this are grid shells, in which predominantly planar faces are used. Due to the lack of digital construction methods the possibilities in the past were limited. In early construction examples of planar quadrilateral surfaces (PQ mesh) only surfaces were used, whose faceting is already given by the methods of construction. The term pre-rationalized has become established as a term for such a discretization, which is constructively meaningful and at the same time generally follows the surface generation. Post-rationalized, on the other hand, is a discretization that is carried out subsequently, independently of the surface generation. (Schiftner et. al., 2014) Bruno Taut's Glashaus, shown at the Werkbund exhibition in Cologne in 1914, is an early example that follows

this approach. Since concrete was also chosen as a constructive building material, Taut's glass house is an excellent model for our research project. The concrete ribbed vaults realized up to that time made use of the geometric property of rotational bodies, that their division into meridians and width lines or contour lines leads to plane facets. Even the Pantheon in Rome has a dome made of Roman concrete where the inside has a cassette structure. (Heinle et al., 1996) In many of these structures, however, the flat formation of the segments is not a guiding principle for the construction method. Only through the use of glass and the approach of having segments prefabricated did the division of surfaces into flat segments, now known as post-rationalized, come to the fore. How progressive the design of Taut's dome was can be quickly seen when comparing it with other reinforced concrete buildings of the time. An example of this is the ribbed dome of the Jahrhunderthalle in Breslau. (Vischer et al., 1928)

2. RECONSTRUCTION OF THE GLASHAUS FROM BRUNO TAUT`S – FLOOR PLANS

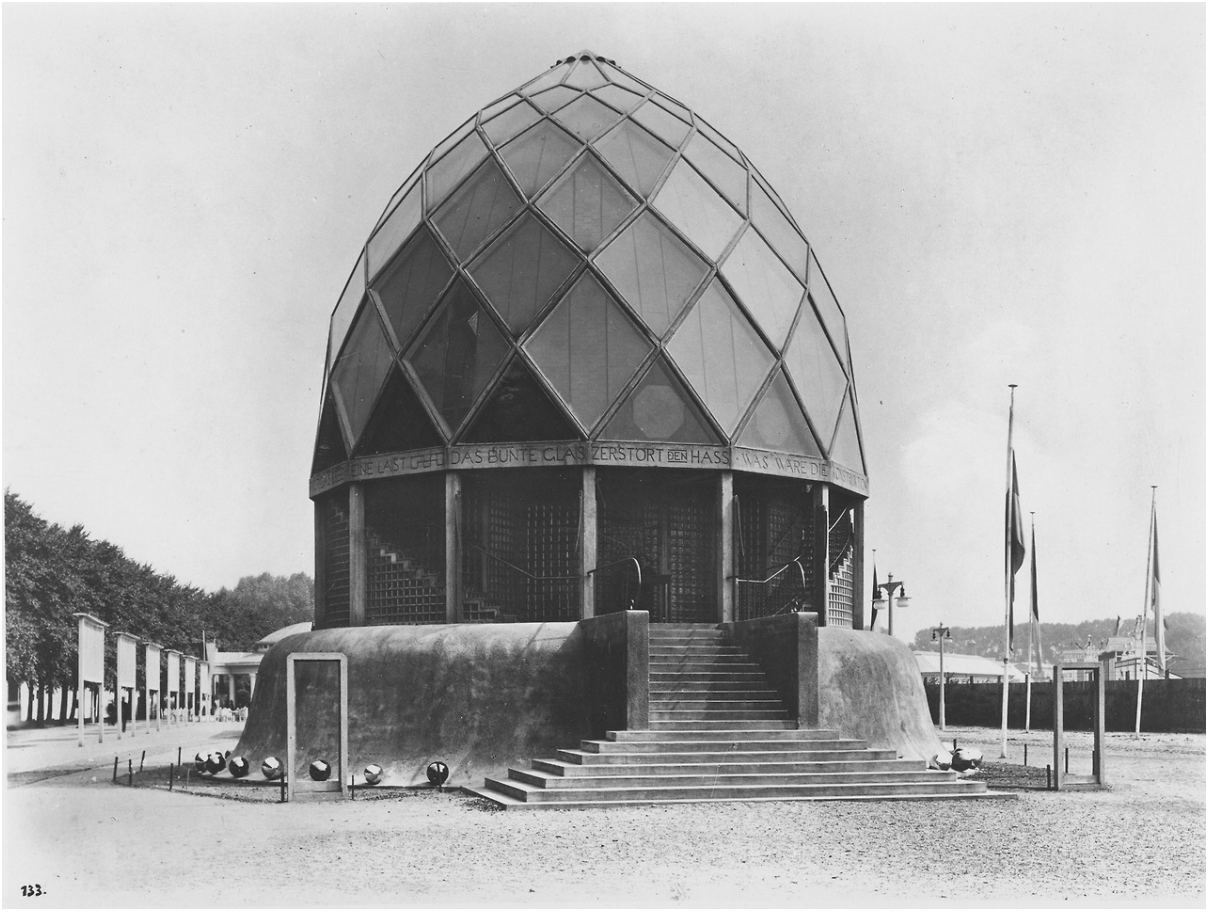

Figure. 1: A picture from 1914 of Bruno Taut`s Glass Pavilion at the Cologne Deutscher Werkbund Exhibition (Akademie der Künste)

The literature about the Glashaus documents a comprehensive study of its architectural impact. Although the construction was extremely advanced for the time, the steps of execution of the concrete work are hardly comprehensible. For an exhibition in the Martin-Gropius Bau in Berlin in 1993, a reconstruction of the glass house was carried out, which resulted in a scale model. The trigger at the time was the discovery of the building files in the Cologne City Archive. Since its holdings were largely destroyed or severely damaged in an accident, we can only rely on copies of the construction drawings. The copies with the best resolution could be taken from the CD-ROM, which was also produced for the above-mentioned exhibition, and serve as the basis for this reconstruction (Engelbert et al., 1984). It was already established at that time that there are discrepancies between Taut's constructional design and the construction drawings submitted. This is most noticeable in the staircase, which in the drawings penetrates the concrete base and, when executed, falls in all directions. The extension in the back was completely redesigned (Thiekötter et al., 1993). For our reconstruction, we follow the available plans as far as possible and use photographs of the executed building as a supplementary source of information where

necessary. The aim is to correct the construction drawings so that they are coherent. In the process, the Glashaus is reconstructed from bottom to top, i.e. from the foundation to the dome. Only the construction elements made of concrete are analysed. If reconstructed dimensions differ from the original, both values are given and the original value is marked with an asterisk. Measurements, which are not given in the original but have been measured from the plans, are also marked with an asterisk. The dimensions were taken from the original with respect to the scale of the plan. For example, the ground and basement floor plans have been scaled such that the outer ring lies on a circle with a diameter of 15.50m.

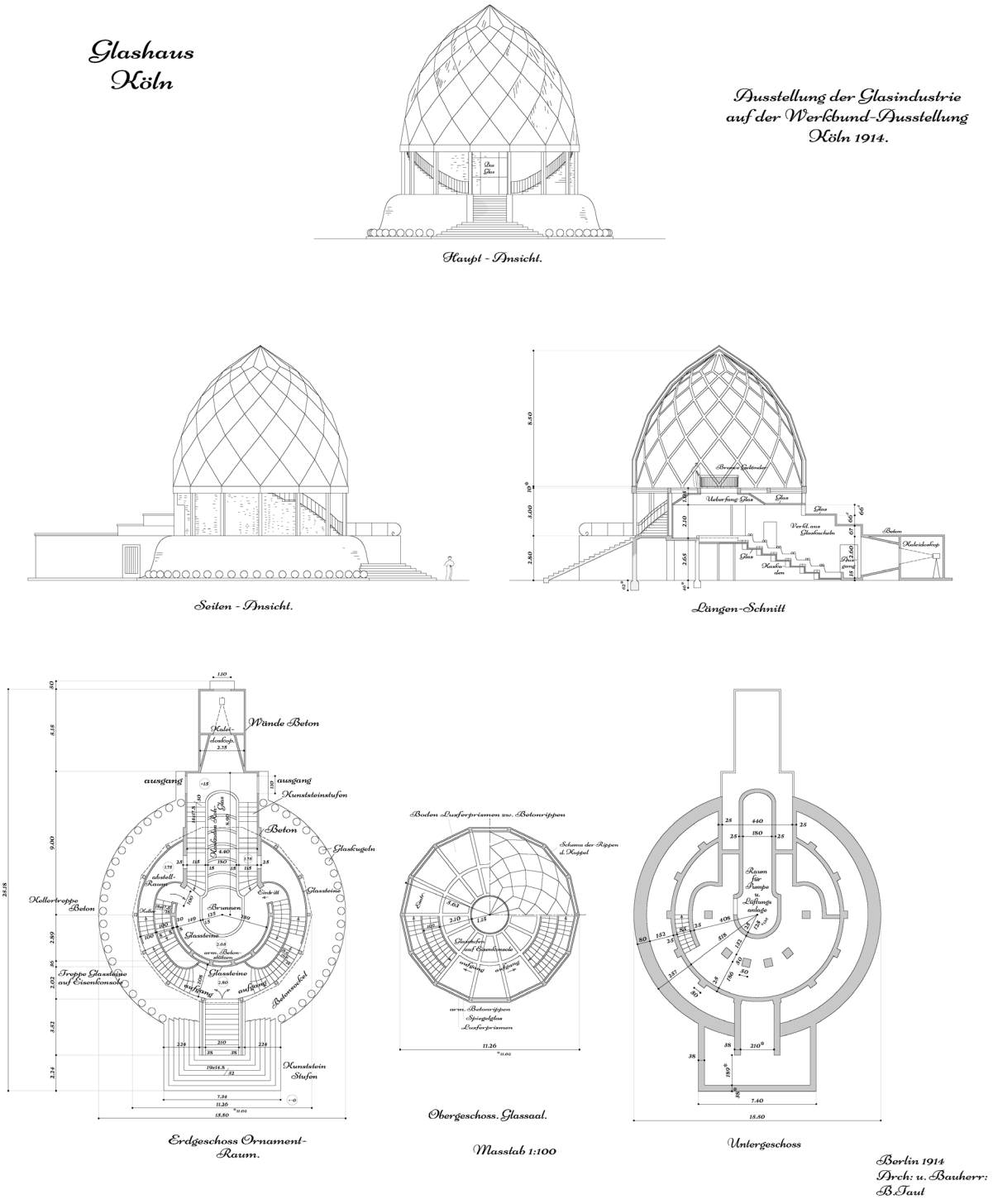

Figure. 2:Reconstruction of the building plans of Bruno Taut`s Glashaus based on Engelbert et al. (1996)

Since many lines have already faded and are rather inaccurate, the symmetry properties of the construction were used to take measurements in a particularly large number of places to obtain a consolidated average. In the basement only the space for the pump had to be reduced a bit. The correction results on the one hand from the floor above and additionally from the comparison of the dimensional chains, whose addition would otherwise not work. In the following floors there is a significant dimension that is not clear. It is the span of the dome and, consequently, the outer dimension of the floors below. It is no longer possible to clearly determine the dimensions of the Glashaus in this area. The existing plans (reinforcement plan and main plan) cannot be assigned exactly to a date. It can be assumed that the different plans are different design variants. Even on the main plans, there is a lack of clarity in the dimensioning. If one sums up the values of the dimensional chain on the ground floor to determine the cross-section of the columns, these should have a maximum of 20cm in diameter, without considering the offset to the outer edge of the tension ring. The value seems realistic, but in the photographs a clear offset to the inside can be seen. So, there would be about 20cm of installation space missing. For this reason, the span or ceiling dimension is corrected from 11.06 to 11.26m. The dimensions of the outer ring are shown in the reinforcement plan as 42cm high and 22cm deep in the top view, while in the bottom view it is about 30cm. A photogrammetric analysis of Figure 1 has shown that the column must be about 20cm wide. The height of the tension ring is about 42cm. If you look at the basement and the ground floor, you can see that the inner support ring is centred on the foundations. If one now assumes that this is also the case for the outer ring, the span of the dome would even have to be increased. This increased height can be seen in the longitudinal section by an offset of 10cm that was inserted.

3. GEOMETRIC PRINCIPAL

For the reconstruction of 1993 the determination of the dome geometry was passed on to a surveying office. Unfortunately, neither plans nor the exact methodical procedure for the analysis were published. In an explanatory report Taut himself describes the Glashaus as a rhombohedron, which strictly is not true (Herzogenrath et al., 1981). The dome nevertheless reminds one of the shapes of a crystal or a cut diamond. Even if the strict division into meridians and latitudinal rings seems to be broken up, this familiar division is nevertheless used as a guideline. In an early construction drawing this division is also hinted at (Anonymous, 1914) (See also figure 3(a)). The construction principle is now quite simple to describe: The vertices of the dome lie in a common surface which is also a surface of revolution. All vertices lie on 28 meridians. The construction drawings and pictures show that the first ring of faces is vertically oriented. This results with the condition of planar faces to a uniquely shape of the dome. In this case 28 guide curves are needed, because the base corresponds to a 14-sided polygon. If you now generate a vertically oriented plane through the end points of the successive odd counted curves, the intersection with the intermediate guide curve which counts even is clear. By two successive faces the orientation of the next section plane is now clearly defined, since three points are already known. The intersection point with the enclosed guide curve is formed again and the first square face is obtained. The principle is then repeated until the surface is closed. In the following we will investigate which surfaces can be constructed by this method.

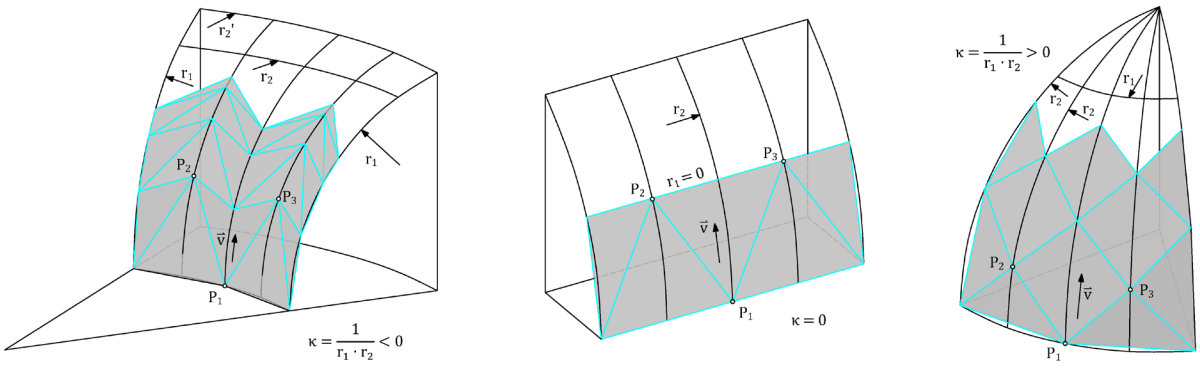

(a) (b) (c)

Figure. 3: (a) anticlastic surface, (b) cylindrical surface, (c) synclastic surface

In principle, the guide curves on which the PQ mesh is generated can be selected freely. We now want to investigate the application of the algorithm to surfaces dependent on their Gaussian curvature. The first category be negative Gaussian curvature, which includes saddle surfaces like the hyperboloid of one sheet and the hyperbolic paraboloid, the second category be Gaussian curvature zero, such as cones, and the third with positive Gaussian curvature includes classical domes or hanging shells or even a hyperboloid of two sheets. Unfortunately, one quickly realizes that only the third category, which are synclastic shapes, can be brought to a satisfying result with this method. In figure 3 the different categories are compared exemplarily. All surfaces where the curvature in one direction is zero, i.e. all cylindrical or ruled surfaces cannot be faceted.

It has to be noted that the method essentially depends on how the discrete set of directrices to generate the grid is selected. In the method described, the facets are developed in the direction of the directrices. This leads to the fact that in the case of the generators of a ruled surface, the central of the three lines defining the section plane can have either only one, or an infinite number of intersections with the plane. At this point, the algorithm stops because there is no meaningful result. However, Lordick (2009) describes a similar method that is applicable to ruled surfaces. Here the facets are developed across a set of discrete rulings. A planar quadrilateral is defined by a starting point on the first ruling and two arbitrary points on the second ruling. If the surface is skew, the three points define a plane, which intersects the third ruling in the fourth point of the quadrilateral. This algorithm can easily be distributed across any skew ruled surface and has at least two degrees of freedom in designing the grid.

If the Glashaus-principle of discretization is applied to anticlastic surfaces, the following happens. After defining the first row of panels, the next row will necessarily be shorter. If the method is continued, the quadrilaterals, which are not even convex, will become smaller and smaller until no more intersections can be found. In Figure 3(c) the principle is shown on a dome. It can be observed that a plane created adjacent to two facets is always more tilted than in the row before. From this it can be derived that the generating meridians must tilt in the same direction to achieve an attractive result. In Figure 4, the limits of the method are illustrated again on a surface. The generating parabolic arc is constant, so the shape of the rhombuses depends only on the second set of curves, which contains congruent sine curves. Those are the directrices for the algorithm. In the upper area it can be seen that the formation of the rhombuses depends on the ratio of the two main curvatures. If the two curvatures have a similar value, the facets are almost square. If one main curvature, in this case r_2, becomes smaller, the rhombuses become longer and longer until no more intersections can be found at $r_2 = 0$.

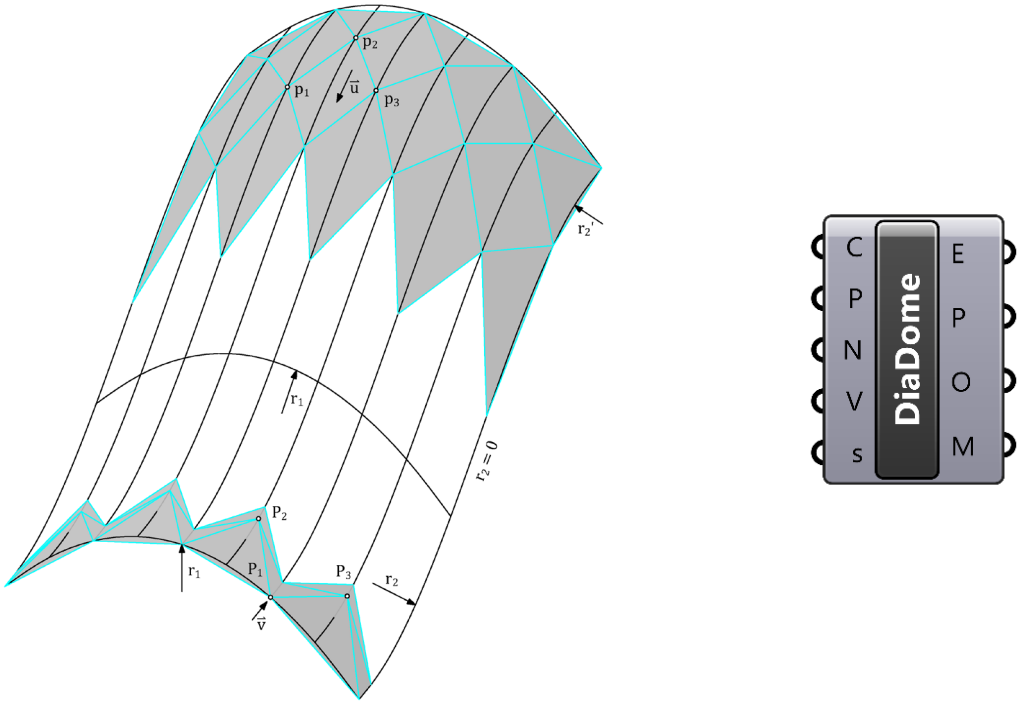

(a) (b)

Figure. 4: (a) translation surface with a sine arc and a parabola as generating, (b) Grasshopper Plug-In *DiaDome* for Rhino3D

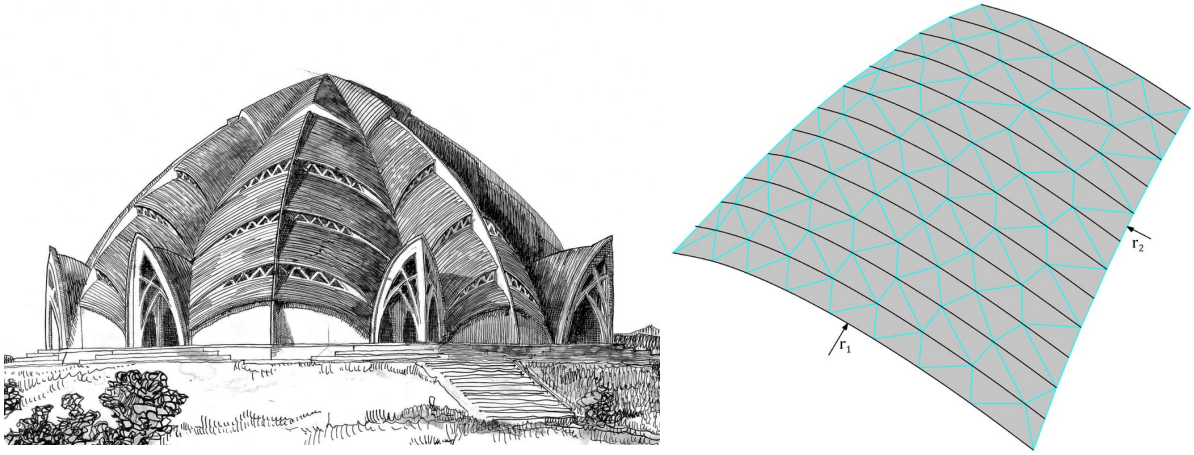

(a) (b)

Figure. 5: (a) View of the Sternkirche, a draft (cutout) by Otto Bartning from 1922 (TU Darmstadt) (b) Faceting of one roof element with the Plug-Ing DiaDome

To access the method faster, an add-on for Grasshopper3D was programmed. In Input C any curves can be fed in, at which the PQ mesh is developed. In P it is specified whether it is a closed surface (true) or an open surface (false). A closed surface is a surface that forms a "band", like most surfaces of revolution. In the input N the number of rows to be generated is specified. V is fed with vectors, which define the orientation of the first planes. For V every vector can be selected, which lies in the corresponding plane. In s the index of the first curve is given. In Output E (Error) error messages are given if the inputs are connected incorrectly. In P the outlines of the rhombuses are output as polylines and in O the outline curves of the generated PQ mesh. In M the corresponding mesh is output. The complete surface depends only on the selection of the generating curves and the initial vectors. The method and thus also the plug-in can only be applied to a small number of surface classes. Nevertheless, interesting results can be achieved. Even with synclastic surfaces, you should still avoid those where one principal curvature is too close to zero.

We want to illustrate the possibilities offered by the add-on by means of a design by Otto Bartning (see Figure. 5 (a)). For this purpose, a single roof segment was extracted and a set of discrete guide curves was distributed evenly on the surface (see Figure 5. (b)). It should be noted that the radius of curvature r_2 is much smaller than the radius r_1 and the second principal curvature is close to zero. The start vectors were chosen such that the facets end as evenly as possible at the end of the surface. Two things can be observed. When a curvature is close to zero, the individual facets tend to be very long. Next, it can be observed that one side of the quadrilaterals has a very acute angle and the other has a rather obtuse angle. The more the curvatures differ, the more the angles are different. Similar principal curvatures also lead to a more even formation of the diamond grid.

Generally, exactly four edges come together at a node. But if you analyse the discretization carefully, you can see one node with six edges. This special case occurs when a cutting plane does not create a new intersection. Figure 6 illustrates this case in more detail. The case is similar to the anticlastic surfaces, except that it is only in a single area. The points p_1, p_2, p_3 span a plane which leads to the intersection S behind the actual direction of development (here direction $\vec{d}$). If the loop is continued, the planes $\vec{u}_1\vec{v}_1$ and $\vec{u}_2\vec{v}_2$ are resulting. However, these planes are now so strongly rotated that they do not create a new intersection point. The loop would break off here. If you leave out the facet in question, you can continue the process as usual, which results in the node with six edges. This phenomenon only occurs when one of the main curvatures tends towards zero.

If you look at the faceting in Figure 5(b), you will see that the individual modules are different in shape and size, which gives the surface a very uneven character. In the case of free-form surfaces that do not have symmetry properties, an irregular formation of the diamonds can hardly be prevented. Surfaces with strong symmetry properties are particularly suitable for an even formation of the diamonds. As in the example of the Glashaus, such surfaces include surfaces of revolution, but also translation surfaces. The generating curves must also be selected so that they are symmetrical to each other. The geometric principle worked out here has many limitations. The design of the Sternkirche will demonstrate that useful results can nevertheless be achieved. In a first step, the free-form surfaces are approximated by surfaces of revolution. In the case of the Sternkirche the surfaces are best approximated when the axis of rotation is oriented parallel to the axis of rotation of the circle of curvature r_1.

The generating curves are oriented in the same direction and have to be rotationally symmetrical. Since the curvature of the generating curves is very small, it is to be expected that the diamonds get very long. With the help of the add-on, an optimization algorithm has now been applied with the aim of ensuring that one diamond vertex ends exactly at the end of the surfaces. Parameters are the orientations of the start vectors and the number of generators. The result is shown in Figure 11.

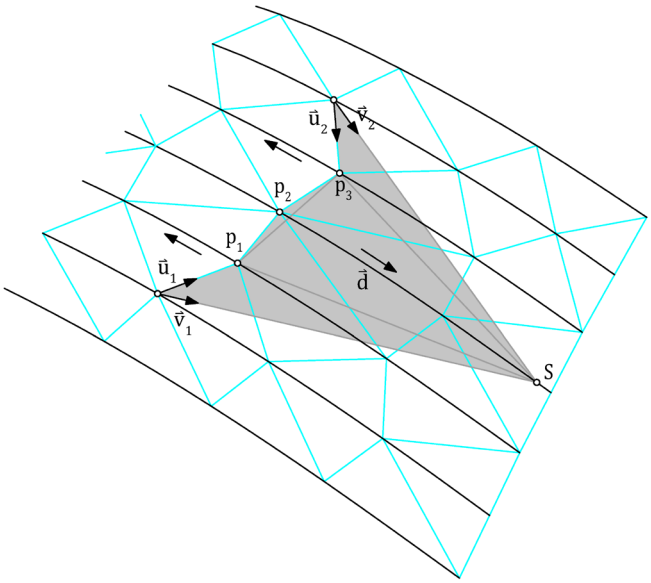

Figure. 6: Special Case – Knot with six edges

4. RECONSTRUCTION OF THE GLASHAUS FROM BRUNO TAUT - DOME

In the oldest known design for the Glashaus by Bruno Taut, the dome was still intended as a construction of iron ribs. The span of the dome was planned to be 10.5m and the height 7.5m. (Figure 3 (a)) (Anonymous, 1914). The dome is said to have actually been built of reinforced concrete ribs with a span of 8.70m and a height of 7.65m. (Thiekötter et al., 1993). In the reinforcement plan, the inner span is given as two times 4.23m (see Figure 8), but this is very different from the other scaling of the plan. The 8.70m also appears unrealistic, as the external dimensions according to the photographic sources correspond approximately to the floor plan of the storeys, which would have had to be compressed by 2m. On the basis of the proportions taken from photographs of the glass house (Figure 1), this thesis cannot be maintained. The fact that the dimensions of the reinforcement plan and the construction plans are identical is a strong indication that this scale is considered sufficiently reliable and is therefore used for further reconstruction. Its application results in a height of 8.50m inside the dome (8.83m outside). The span of 11.06m is also similar in the reinforcement plan (measured inside the tension ring). This is corrected to 11.26m as described in the second chapter.

In the previous chapter the construction method of the dome was already described. The first row of elements is vertical on the tension ring. The shape of the dome therefore depends only on the generating meridians. Mostly the shape was defined as a surface of revolution with a circle as the generating meridian, which makes the shape part of a self-intersecting spindle torus. A geometrical analysis of the front view shows that all vertices touching the surface in the contour are nested to an arc. Only the last row of facets is prolonged to the axis, such exceeds the meridian and finally gives the shape a less dull, more skyward appearance. In the first design (Figure 7 (a)) the top was not yet adjusted. In order to verify this assumption, an outline of the structure was generated based on the reinforcement drawings (Figure 3(b)). When looking at the reinforcement plan, it can be seen that it is clearly scaled. However, if you analyze the symmetry in the top view (Figure 8. below), you can see that the drawing as shown is slightly compressed in one axis. The plan was therefore straightened for the analysis. Based on this, an optimization algorithm was applied, which searches for the arc with the smallest distance to the sum of the nodes. Parameters were the radius of the arc and the distance of the center to the coordinate origin (see Figure 3 (a)). The analysis shows that the first six rows of vertices are on an arc with a radius of 912cm, an opening angle of 65° and a distance to the coordinate origin of 384cm. The average deviation from the historical plans is only about 1cm. If you continue to apply the geometric principle described in chapter 3, you will get an almost congruent result to the elevation in Figure 3(b). The construction principle is thus clearly proven. In the last row before the tip there is a clear deviation from the arc applied (a compression of the second-last row of facets), just to achieve

the slightly prominent top with the final height of the vault of 8.50m. The reinforcement plan shows the internal dimensions of the dome. As already mentioned, in order to coordinate the plans with each other, the dome is stretched slightly, which results in a radius of the arc of 925cm.

In the construction brochure for the project, Taut writes that only one company, *Beton & Eisen Gesellschaft mbH zu Berlin*, was able to carry out the calculations and to manufacture the dome. The aim was to give the structure the lightness that could be created by constructing it as a "Flechtwerk" (woven vault). The term "Flechtwerk" is no longer commonly used today. It is a framework construction in which all nodes lie on a continuously double-curved surface. A cross-section of the ribs of the vaulting of only 12 by 20 cm was praised as a special achievement (Herzogenrath et al., 1981). A closer look at the well-known photographs, however, quickly makes one doubt this. This assumption is supported by the fact that a cross-section of 15 by 22 cm can be measured relatively clearly in the reinforcement plan, which was still very ambitious in the context of the time. In the reinforcement plan, eight sections through the ribs were shown, which are almost identical in their execution. Ten bars of reinforcing steel with a diameter of 10mm were passed parallel through the ribs, which are held together every 35cm by stirrups.

If one trusts in the scale of the reinforcement plan, the distance between the reinforcement and the edge is 14mm. With a bar diameter of 10mm this would result in a concrete cover of 9mm. Today this would be almost unimaginable. Indoors, the absolute minimum for the concrete cover is 10mm and outdoors in a sprinkled area 20mm (DIN EN 1992-1-1). If one considers the construction in the context of time and with regard to its temporary character, it may well have been executed in this way. The ribs were made rectangular, whereby they also taper downwards. On the upper side of the rib is an attachment which optically serves as a closure between the glasses. It also defines the lips on which the upper glass layer rests. Two layers of glazing are very clearly visible. The first layer of clear glass rests on the ribs. The inner layer of stained glass cannot be precisely positioned. In the reinforcement plan, an unspecific line is drawn in the sections of the ribs, which could show the position of the inner glazing. How the panels are structurally connected to the ribs cannot be clarified precisely. In the front view (Figure. 8 top), wooden dowels are drawn in at regular intervals, which were probably used to fix the stained-glass windows. It can be assumed that the wooden dowels were cast into the concrete and used as a base for screwing in fastening elements. In accordance with the time, the windows were probably sealed with a putty made of mud chalk and linseed oil. In the section a-b we can see that there is also an opening for ventilation to counteract the formation of condensation.

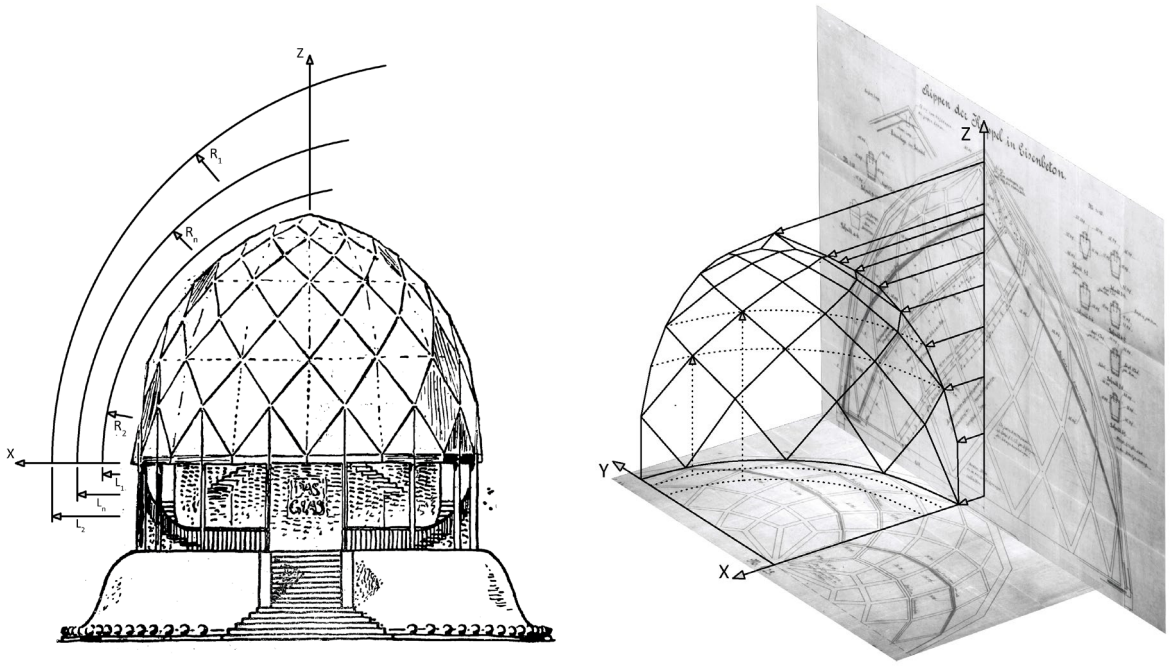

(a) (b)

Figure. 7: (a) First design of the dome (Anonymous, 1914); illustration modified, (b) Outline based on reinforcement plans from Engelbert et al. (1996)

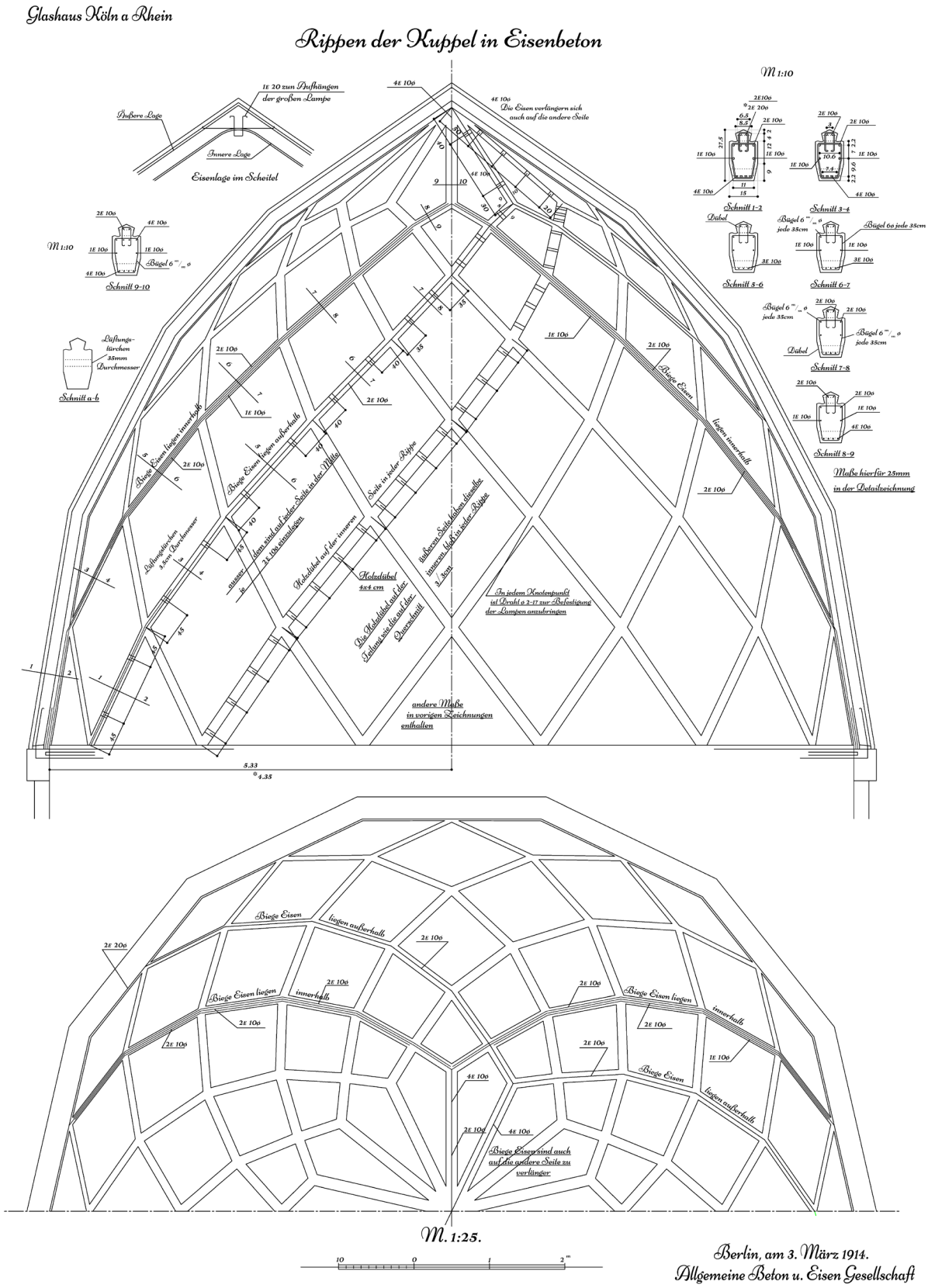

Figure. 8: Reconstruction of the reinforcement plan based on Engelbert et al. (1996)

If you now try to form the cross-sections along the geometric shape, you will quickly detect that not all edges intersect at the nodes. This is a well-known problem when offsetting PQ meshes (Pottmann et al., 2007). If you place the top edge of the ribs on the PQ mesh, the maximum deviation is 2mm. It can be assumed that this deviation of the construction of the dome was ignored or not recognized at all, because the drawings of that time did not allow such an exact representation. During the execution, skilled craftsmen were able to compensate for the minimal differences by hand. A general method to solve this problem of misalignment is not known. But it can be minimized with a variation of the guiding curves of the mesh. As an example, conical meshes have to be mentioned here, which retain their uniform edges in the event of an offset (Pottmann et al., 2008).

With regard to the mechanics of the dome, there are further interesting issues to mention: despite the filigree appearance, the weight of the dome is considerable. The concrete ribs without the support ring have a volume of about 10.5m³ which, at an average concrete density of about 2,400 kg/m³, results in a total mass of about 25 tons. This does not yet take into account the amount of reinforcing steel and the full-surface glazing. The total length of all ribs sums up to about 360 metres, whereby an average of ten reinforcing steel bars of 1 cm diameter each were laid. This is about 7.85cm² steel cross section in each rib, which adds up to a total volume of 0.28m³ steel, i.e. about 2.22t additional weight. The double glazing also plays a significant role. The installed panels are a special glass which diffuses light particularly well. However, this also gives the panes a thickness of up to 1.5cm. With a density of approx. 2,500 kg/m³ and a weight of over 12 tons, the glass accounts for a large share of the total weight of the dome of approx. 40 tons in total.

For the subsequent static calculation of the dome, the dead weight of the supporting structure, the weight of the glazing and a wind load of 0.5kN/m² were used as load cases. All nodes are rigidly connected and the dome rests without limitation in the movement on the supports. Under these conditions, the maximum load on the supporting structure is approximately 52%. This occurs - as expected - in the elements in the lower part of the dome. Except in the tension ring, only compressive forces occur as relevant loads. The maximum design moment is about 3.5kNm. Common formulas for estimating the amount of reinforcement show that the structure could even have been designed without reinforcement. However, additional forces due to imperfections are to be expected, which were not taken into account here. An interesting observation should be noted: The critical load is the dead weight of the supporting structure. A quick investigation using an algorithm for optimizing the ribs' cross-sections has revealed that the first row of ribs could be reduced to a cross-section of 16*9cm. The formation of the ribs at the tip could even be reduced to a cross-section of 9*4cm. This would reduce the total weight of the dome to 20 tons.

5. INTRODUCING THE PLANNED RESEARCH

The basic working objective of the project is the implementation of a closed flow production process into the arsenal of methods for building construction. The state of the art in the relevant flow production is characterized by a high degree of automation combined with the technically complex production apparatus. Large series of similar components are often produced for the prefabricated construction of walls and ceilings, which decisively limits the possibilities of individual adaptation of prefabricated parts with the aim of a distinctive design variety. In order to extend the design variety desired by users, the principle of "mass customization" was developed, whereby a large number of module combinations can be created using a relatively small number of specially developed module variants. (Starr 1965 and Lee 2017)

Concrete research is currently additionally influenced by two major factors: The lack of qualified personnel and the awareness of environmental factors. Qualified specialists are primarily required to produce the formwork of the structures. The lack of these skilled workers can be counteracted by automation or substitution by adaptive formwork methods or formwork-free production processes. The improvement of environmental compatibility can be achieved primarily by reducing the amount of material used, for example by structural optimization. With regard to adaptive formwork, there are already several completed and ongoing research projects. In addition to textile formwork systems, there are systems of formwork which can be changed in their shape by actuators. The formwork can be reused as often as required, but the entire system is very cost-intensive and relatively limited in the changeability of the geometry. The basis is a flexible formwork skin, which is formed by lifting various points in a square grid (Michel et al., 2014). Another approach is the Smart Dynamic Casting process, in which a robot-controlled, movable, geometrically adaptive slipform is used to produce complex concrete structures. With the aid of the slipform, the concrete is built up continuously and with a variable cross-section around a previously erected steel reinforcement (Lloret E. et al, 2017).

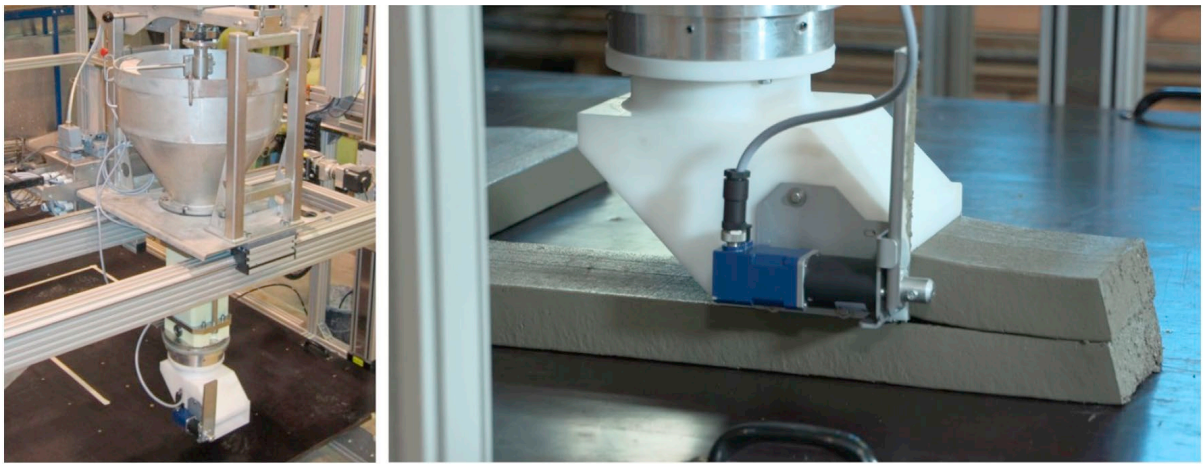

(a) (b)

Figure. 9: Current printhead for CONPrint3D a) general view including printhead and laboratory manipulation b) detailed view of the base nozzle with a nozzle closure (Mechtcherine et al., 2019)

3D printing offers even greater freedom in design while eliminating the need for formwork. The scientific investigations in this field of research currently focus on various methods for selective material deposition. In the most common method, the fresh mortar or concrete is conveyed as a material flow to the installation site and deposited there in a geometrically defined manner. In most cases, the material is deposited by extrusion. The material output, known as filament, receives its defined cross-sectional shape through an extruder nozzle. The spatial expansion of the produced components is created by layering the individual filaments (Mechtcherine V. et al, 2018). The selective bonding processes also lead to a layer-by-layer structure of the component. Here, the powdery matrix components are first spread out as a thin layer. Subsequently, the liquid component required for solidification is selectively added to the powder. After the matrix has set, non-wetted matrix components are removed and the desired structure is exposed (Lowke D. et al, 2018). However, the use of this process principle is limited to smaller components, because the production space is limited by the powder bed. In our opinion, concrete 3D printing based on extrusion holds the greater potential for successful practical application. In addition, for this group of processes, the technical development is most advanced and the approaches for economic implementation are promising (Mechtcherine V. et al, 2018).

In the following the concept CONPrint3D is presented, a method that is being developed at the TU Dresden. In most 3D printing processes the material is extruded from a circular and vertically oriented nozzle and applied in thin layers. The concrete is relatively soft and the shape defined by the nozzle opening is of minor importance. In terms of productivity and the desire to be able to print directly on the construction site, this process has major disadvantages. Existing concrete classes cannot be processed with this method. If one looks at the usual architectural standards, it quickly becomes clear that a defined, rectangular material flow is suitable for producing the most frequently required shapes. For this reason, CONPrint3D was developed for monolithic constructions with sharp edges and predominantly straight walls. The aim was to ensure that the process can be applied with common machines such as industrial robots and ordinary concrete pumps. Due to a relatively large cross-section of the filament, it can be applied to ordinary classes of concrete with largest grains up to 8mm diameter. The rheological properties of the concrete have been adjusted in such a way that the deformation of the cross section after discharge is negligible. In many situations this requires the addition of a (setting) accelerator in the print head. The print heads were therefore designed in such a way that the filaments emerge with a relatively large cross section (150x50mm) and a well-defined geometric shape with high surface quality, allowing the formation of sharp corners and precise terminations at the start and end of a path (Mechtcherine et al, 2019). A more detailed description of the rheological requirements in terms of yield stress, viscosity, elastic modulus, critical strain, and structuration rate can be found in Roussel (2018).

Like other 3D-printing approaches, CONPrint3D is not suitable for the installation of conventional reinforcement. For this reason, the investigation of highly ductile concretes with disperse synthetic fibre reinforcement is an essential part of the research. Extremely high strengths can be achieved with fibre-reinforced concrete, which already exceed the conventional requirements. The main weakness is the connection between the layers. This is because the fibres cannot cross the horizontal layers in the conventional printing process. For this purpose, a special fabric was developed which can be inserted between the layers and which "sews" the adjacent concrete layers by means of fibres protruding in both directions (Mechtcherine et al, 2018 (2)). The CONPrint3D

process is now to be adapted in order to be able to produce shell-like structures such as the concrete skeleton for Taut's Glashaus. Light, shell-like, double-curved and thus above-average performance structures from concrete are usually produced monolithically on site. To enable industrial prefabrication, the shells have to be divided into transportable modules which can then be assembled on site (design for assembly). The question here is, which modularization is best suited for flow production. Flat modules with four (or more) edges appear to be particularly suitable, in order to avoid too sharp corners and to reduce the complexity in fabrication. The following describes how the technology has to be further developed.

For the production of the modules, a series of automated or automatable process steps is planned, which are coupled to form a flow production. All process steps will be carried out under digital control. The combination of the process steps enables the structurally differentiated construction of the modules with differentiated edge zones and infills and also allows a high degree of flexibility with regard to geometric form and reinforcement and concrete quality. The fabrication of the modules is essentially divided into five process steps, whereby the work piece passes through at least three individual stations, see Figure 9. The first step involves the fabrication of the lower section of the edge zone from SHCC using a fully automated process based on extrusion. The shape of the edge in floor plan and cross-section is clearly defined geometrically by the position of the module within the overall structure and the connections to adjacent components. The extruded SHCC filament also serves as a component-integrated formwork, which is filled with concrete in the second process step. The distribution of a highly flowable fine concrete through a digitally controlled nozzle seems suitable, but low-pressure spraying is also possible. The reinforcement of the element is then installed with the aid of pre-fabricated textile layers or selectively deposited, mineral-impregnated carbon reinforcement. The installation of the reinforcement is driven digitally and the structure executed by a robot system. This technology promises a better bond between yarn and concrete matrix and a significantly higher temperature resistance of thin-walled elements. In addition to the reinforcement of the surface, the textile contributes to the creation of a tension-force bond between the edge zones and the infill. To complete the work piece, it passes through process steps 4 and 5, in which a further layer of material is added to both the edge zone and the infill.

In the further research the extruder has to be redesigned in order to be able to produce modules for a double curved shell structure. The current development status of the 3D printing process is limited to the extrusion of rectangular cross-sections. In order to be able to produce a segmented shell (gridshell), in which the facets vary in their surface angles, the connection geometries must be variably adapted. Two approaches can be examined for this purpose. In the first variant, the printed product is reshaped or cut to size while still soft, while in the second method an extruder is used, the geometry of which has to be continuously adjusted during operation.

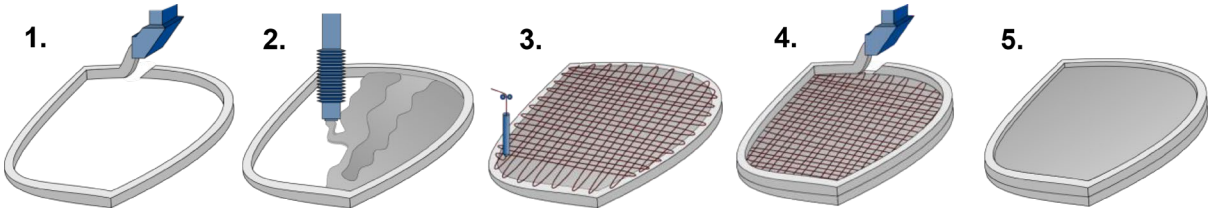

Figure. 10: Schematic representation of the aspired flow production of modules in five production steps

6. CONCLUSION AND OUTLOOK

We have shown, why the Glashaus by Bruno Taut is a good role model and testing field for our research project on gridshells from concrete. The geometric constraints and challenges have been discussed. In the further research we will adapt existing concepts to make the CONPrint3D production principle applicable to gridshell structures, especially domes. The focus must be on the design of the connections. It can be assumed that the distribution of the overall process to independent, networked processing stations is advantageous for the creation of a flexible, functional production chain. We assume that the potential of the methods presented is, in particular, being able to react to different structural conditions in great detail, while the production steps remain basically the same.

7. ACKNOWLEGEMENTS

This contribution is a result of the research project Adaptive Concrete Diamond Construction (ACDC), which is part of the priority programme SPP 2187: “Adaptive Modular Construction with Flow Production Methods – Precision High-Speed Construction of the Future” funded by the German Research Foundation (DFG).

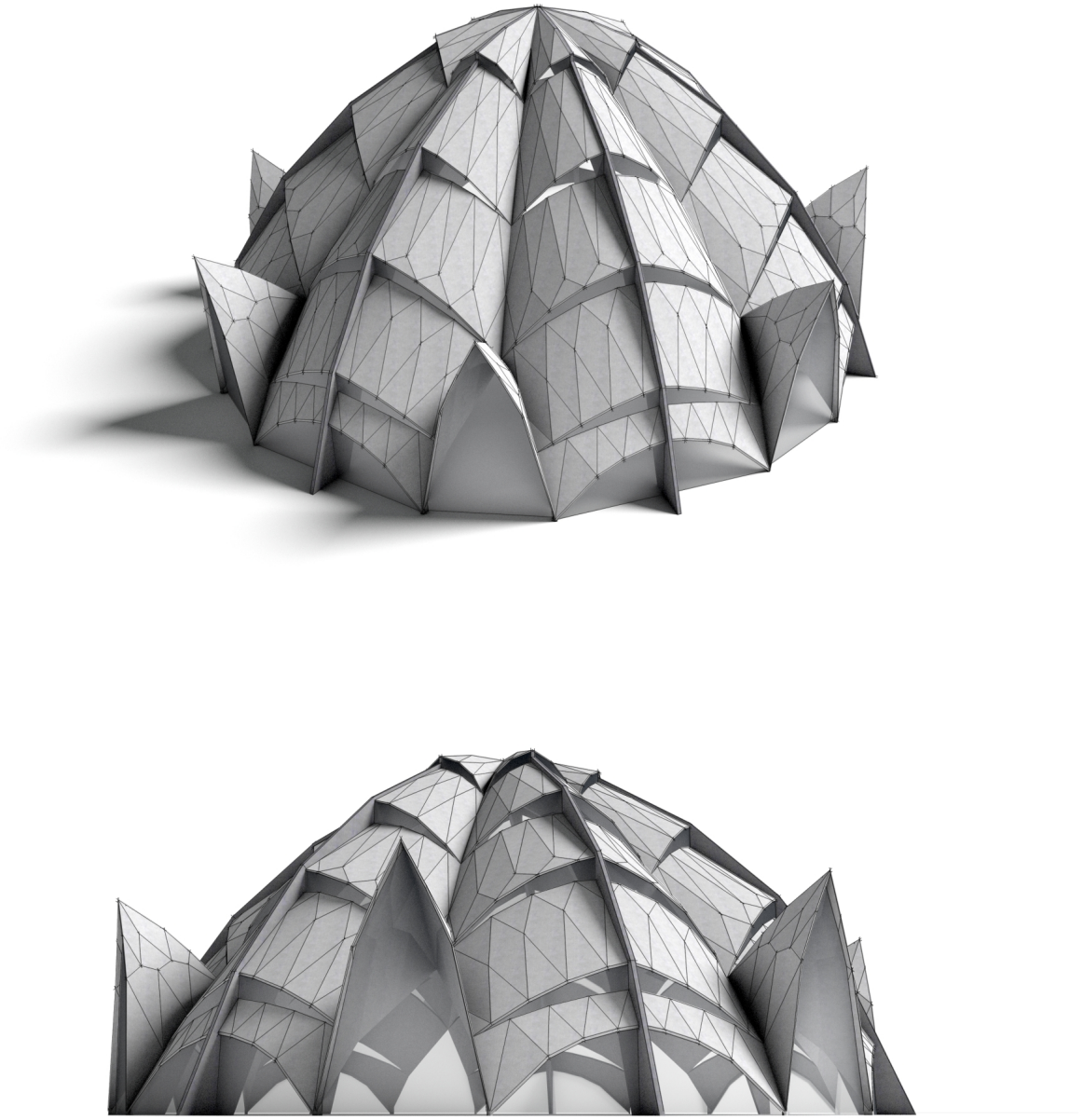

Figure. 11: Remodeled Sternkirche with planar modules for the aim of prefabrication

REFERENCES

1. Anonymous, 1914. Das Glashaus für die Kölner Werkbund-Ausstellung. *Die Bauwelt*, 1. pp 25–26.
2. TU Darmstadt, Otto Bartning Archiv.
3. Akademie der Künste, Berlin. Baukunstarchiv.
4. Engelbert A., Ramershover M. and Thiekötter A., 1996. Bauen in Licht – Das Glashaus von Bruno Taut: Eine multimediale Annäherung an das Glashaus von Bruno Taut auf CD-Rom. Duplicon, Berlin.
5. Heinle E. and Schlaich J., 1996. Kuppeln aller Zeiten, aller Kulturen. Deutsche Verlags-Anstalt, Stuttgart.
6. Herzogenrath, W., Hagspiel W. and Teubner D., 1981. Frühe Kölner Kunstausstellungen: Sonderbund 1912, Werkbund 1914, Pressa USSR 1928: Kommentarband zu den Nachdrucken der Ausstellungskataloge. Wienand, Köln.
7. Lloret E., Wangler T. P. and Flatt R. J., 2017. Smart dynamic casting slipforming with flexible formwork – Inline measurement and control. Proceedings of the Second Concrete Innovation Conference, Tromsø, Sveden.
8. Lordick D., 2009. Intuitive Design and Meshing of Non-Developable Ruled Surfaces. Proceedings of the Design Modelling Symposium, Berlin, Germany. pp. 248-261.
9. Lowke D., Dini E., Perrot A., Gehler C. and Dillenburger D., 2018. Particle-bed 3D printing in concrete construction – Possibilities and challenges. *Cement and Concrete Research*, 112. pp 50-65
10. Mechtcherine V., Nerella N. V., Will F., Näther M., Otto J. and Krause M., 2019. Large-scale digital concrete construction – CONPrint3D concept for on-site monolithic 3D-printing. *Automation in Construction*, 107.
11. Mechtcherine V., Nerella V. N., 2018 (2). Integration der Bewehrung beim 3D-Druck mit Beton. *Beton- und Stahlbetonbau*, 113. pp. 1-9.
12. Michel M. and Knaack U., 2014. Grundlagen zur Entwicklung adaptiver Schalungssysteme für frei geformte Betonschalen und Wände. *Bautechnik*, 91(12). pp 845-853
13. Pottmann H., Asperl A., Hofer M. and Kilian A., 2007. Architectural Geometry. Bentley Institute Press.
14. Pottmann H. and Wallner J., 2008. The focal geometry of circular and conical meshes. *Advances in Computational Mathematics*, 29. pp249-268.
15. Roussel N., 2018. Rheological requirements for printable concretes. *Cement and Concrete Research*, 112. pp. 76-85.
16. Schiftner, A., Leduc, N., Bompas, Ph., Baldassini, N. and Eigensalz, M., 2012. Architectural Geometry from Research to Practice: The Eiffel Tower Pavilions. In Advances in Architectural Geometry (Eds. H. Lars, S. Shrikant, W. Johannes, B. Niccolo, B. Prilippe amd R. Jacques). Springer, Wien, New York. pp. 213-228.
17. Thiekötter A., 1993. Kristallisationen, Splitterungen: Bruno Tauts Glashaus; eine Ausstellung des Werbund-Archivs im Martin-Gropius-Bau. Birkhäuser, Basel, Berlin, Boston.
18. Vischer J. and Hilberseimer L., 1928. Beton als Gestalter: Bauten in Eisenbeton und ihre architektonische Gestaltung; ausgeführte Eisenbetonbauten. Julius Hoffmann, Stuttgart.

HELICAL SURFACES AND THEIR APPLICATION IN ARCHITECTURAL PARAMETRIC DESIGN

Lidia Nataly Somarriba Sokolova
Department of Civil Engineering, Peoples' Friendship University of Russia (RUDN University),Moscow,Russia.
Master's Degree Student, lidiasomarriba@gmail.com

Marina Rynkovskaya
Department of Civil Engineering, Peoples' Friendship University of Russia (RUDN University),Moscow,Russia
PhD., Associate Professor, marine_step@mail.ru

ABSTRACT

The use of ruled surfaces has been common practice in architecture and design ever since first coliseums appeared. Most ruled helical surfaces, due to their visual, kinetic, and economic properties, have gained popularity over time. Nevertheless, its rationalization has not been fully displayed in recent years causing it to be a problem due to complex solutions when developing engineering or design projects. The overall picture that connects mathematical context and ready to use render visualizations are accompanied by some complexity in the process. As a consequence, parametric design and its technical characteristics cannot always be fully understood by the user.

This article aims to create a comprehensible model, which will show the overall process of parametrical shape-forming taking the developable and oblique type and its parametric equations with the initial conditions. Also, three case studies will be reviewed as part of the analysis. The main goal of this study is to make the parametrical algorithmic exploitation process easier to assimilate and utilize. Starting with some ground information about ruled helicoids and finishing the ready to use surfaces. Rhinoceros 6 and grasshopper are the main programs applied due to their visual simplicity and interactive usage. And finally, conclusions are made and recommendations given for further research.

Keywords: helical surfaces, ruled surfaces, helicoid, algorithm, Grasshopper, Rhinoceros, design, revolution surfaces, architecture, parametric design.

1. INTRODUCTION

Many statements have been known (J. A. J. Harmens, 2015; Oktan et al.., 2017; Scheeren et al.., 2015) concerning the right definition and term utilization for the parametric design process (Vlachodimos, 2015). Discussions have aroused whether it is a style or a method (Oktan et al.., 2017) and criticizing its dogmas for limiting the design process. Although interpretations still vary, this article is going to review it as a method by which we obtain the desired end result.

1.1 Parametrism

The method itself comes from the root word "parameter" and it is easier to understand as an approach of modeling architectural solutions, based on mathematical representations in computer programs. A parametrical methodology does not express a single shape, but a range of possibilities, that can be obtained by geometric schemes of mathematical dependencies. This type of modeling is well combined with pre-project analysis data, also expressed in digital form. The process of working with complex surfaces and their transformation is facilitated in order to achieve optimal values of the technical and economic indicators for the project.

Taking into account previous statements, the influence of parametrism is evident in architectural and urban educational programs. As seen in (Schnabel, 2007) educational institutions are opening each time more to parametrical architectural design studios where they assimilate, build, and blend parameters in order to come up with design proposals or large design-clusters as seen in Figure 1.

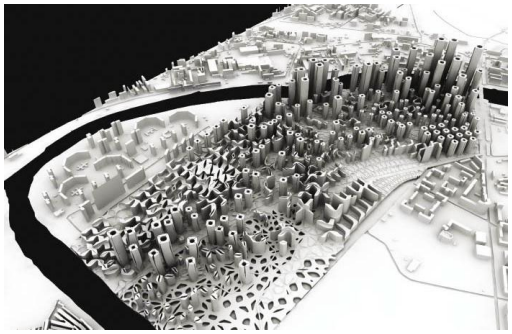

Figure. 1: Final urban design proposal for site in Moscow, Russia. (Source: (Schneider, Koltsova, and Schmitt, 2011).

Although advantages are evident at first impression there are some drawbacks when dealing with parametric design (Zarei, 2012). The previous level of preparation required in order to start adapting ideas into this type of model may take longer than traditional methods and most of times any new conception requires different algorithmic solutions. Furthermore, the exploitation process becomes more complex and traditional methods emerge as a more preferable choice in this context. This article addresses the issue by establishing a connection between parametric equations and parametric design, thus making the model more comprehensive for further use. Ruled helicoids are taken as the main modeling object due to their potential in areas of architecture and civil engineering.

1.2 Helical surfaces

Helical surfaces are characterized by the helical motion of the directrix line, or helical axis, which is a combination of revolution and translation movements (Krivoshapko et al.., 2015). If the speed and trajectory are constant then the surface and motion are denoted as *ordinary*. It is possible to alter the boundaries of each trajectory by changing the surface of revolution (Lăzureanu, 2014; Puig-Pey, et al.., 2004). Even though differentiating trajectories offer a great variety of choices, ordinary helical surfaces are going to be reviewed. Such trajectories are denoted as *Cylindrical lines of constant lead*.

With the directrix defined, another key factor is the type of generatrix implemented. According to (Krivoshapko et al.., 2015) there are three generatrix shapes for helical surfaces: Ruled, Circular, and General. The first one is defined by a straight line, the second one by a circle or a part of one, and finally the third one by an arbitrary curve. Ruled helical surfaces are review furtherly in the next chapter due to their feasibility in different architectural and engineering areas.

1.2.1. Ruled helicoids

Ruled surfaces are composed by a straight line, which moves in space according to given parameters mention in the previous section. In general, ruled surfaces are achieved by moving the generatrix along three guides and are divided into expandable and non-expandable or in surfaces of zero and negative Gaussian curvature (Flöry et al.., 2010; Lăzureanu, 2014). Ruled helicoids are classified depending on the position of the rectilinear generatrix relative to the axis of the spiral and from the end section. If the line intersects the helical axis, then the ruled helical surface is called closed, and if it does not intersect the axis, then it is called open (Krivoshapko, 2010). Closed ruled surfaces are always non-expandable while open are both expandable and non-expandable. From a technical point of view there are 5 types of ruled helicoids (Krivoshapko and Rynkovskaya, 2017): Right, oblique, developable, pseudo-developable of general type, and pseudo-developable. The first two belong to the group of closed ruled helical surfaces and the rest to open ruled helical surfaces.

1.2.1.1 Implementation of closed ruled helical surfaces

In social structures and industrial building reinforced concrete parking ramps are often used with the contoured surface of a right helicoid. The parking ramp is concentrated in an independent part of the building and is arranged separately from the parking area on the floors, this creates favorable conditions for car flow movement at the parking lot (Rynkovskaya, 2012).

Ruled closed helicoids are mostly known among civil engineers and architects in the construction of spiral staircases, and in some cases, helical surfaces are the main basic form of an entire public structure (Suyoto, et al.., 2015) or its main part. Moreover, there is a mix-use of structural design as seen in Figure 2(a). In the given example space is used primarily as a library and secondarily as a viewing platform and stage. This is done by turning the helicoid into the surface of the stairs and weaving open space within the building. Finally, right and oblique helicoids tessellations are used for urban and interior design spaces as illustrated in figure 2(b). This is possible due to the characteristics presented in both shapes (Allyn Polancic, 2014).

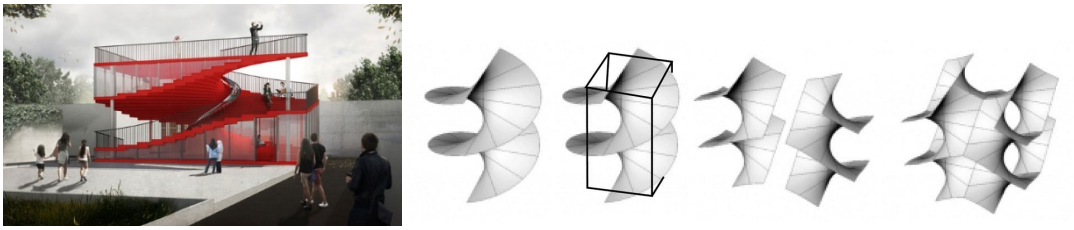

(a) (b)

Figure. 1: (a) Micro library – Helicoid library. (Source: (SHAU 2017), and (b) An illustration of oblique helicoid tesellations (Source: (Allyn Polancic, 2014)

1.2.1.2 Implementation of open ruled helical surfaces

Due to the simplicity of formation, torso surfaces are widely used in the aviation industry for specifying complex surfaces. The most common method is the construction of torsos by moving a straight line along two guiding initial sections. In shipbuilding, torso surfaces are formed using only rotating cylinders or presses. Heat treatment is used only to correct the overdue. Unfolding surfaces are an extremely flexible means to shape the ship. Particularly widely used by builders of yachts and boats, working in domestic terms (Abdel Gawad, 2015) with plywood and aluminum. In addition, the efforts that must be applied to form the torsos are less than in the manufacture of double curved surfaces.

As for developable helicoid surfaces, there are some cases in which they are used for staircase constructions as well as ramps but are not as widely applied as closed helicoids (Rynkovskaya 2019). Additionally, they are widely used in mechanical engineering for the creation of helical conveyers, support anchors and screws (Krivoshapko et al.., 2017).

2. MATERIALS AND METHODS USED

2.1 Software platforms

Rhinoceros (Rhino) is commercial software for three-dimensional NURBS-modeling, developed by Robert McNeel & Associates. It is mainly applied in fields of industrial design, architecture, ship design, jewelry and automotive design, CAD / CAM design, rapid prototyping, reverse engineering, as well as multimedia and graphic design. Rhino specializes in NURBS modeling and Plug-ins developed by McNeel, which include: Flamingo (ray tracing rendering), Penguin (non-photorealistic rendering), Bongo (animation), and Brazil (complex rendering). Along with over 1000 third-party plugins, Rhino has its own scripting language based on Visual Basic, and the SDK allows you to read and write files directly (Tedeschi et al..,, 2014).

One plugin that stands out the most in parametrical modeling is Grasshopper. Since it runs with Rhinoceros, Grasshopper is integrated into a reliable and versatile modeling environment and is used by creative professionals working in a wide range of professional areas, including, architecture, engineering, industrial design and so on. Grasshopper has its own series of plug-ins from which LunchBox is going to be applied. LunchBox is a tool for exploring surfaces, constructive exploitation, and workflow (LunchBox ,2015).

2.2 Governing equations

Parametric surfaces are widely used in applied geometry and computer graphics to represent complex forms. Parametrization makes such surfaces convenient for processing and display. When mentioning helical surfaces and preparing for modeling it is important to consider its classification according to the basic generatrix shape (Krivoshapko et al.., 2015) and the helical axis. The following equations are taken from (Krivoshapko et al.., 2017), where the geometry of ruled helical surfaces is further mathematically analyzed and calculated in (Krivoshapko, 2010). Two types of helicoids are going to be presented from each category mentioned above, and relevant points concerning surface modeling are mentioned as well.

2.2.1 Oblique helicoid

A helical surface whose profile is a straight line intersecting an axis at an angle $\alpha < {}^{\pi}/_{2}$. It has negative Gaussian curvature where $R < 0$. The traslation movement occurs parallelly to the cilinder's surface. The following parametric equations are given:

$$x(u,v) = u \sin a \cos v,$$
$$y(u,v) = u \sin a \sin v, \qquad \text{(Eq.1)}$$
$$z(v) = bv + u \cos a,$$

2.2.2 Developable helicoid

A helical surface whose profile is a straight line intersecting an axis at an arbitrary angle. Gaussian curvature equals zero, where $R = 0$. The traslation movement occurs adjacently to the cilinder's surface. The following parametric equations are given:

$$x(u,v) = a \cos v - \frac{au \sin v,}{\sqrt{a^2 + b^2}} \qquad \text{(Eq.2)}$$
$$y(u,v) = a \sin v - \frac{au \cos v,}{\sqrt{a^2 + b^2}},$$
$$z(u,v) = bv + \frac{bu,}{\sqrt{a^2 + b^2}},$$

Where the curvilineear coordinates are (as seen in figure 2):

u – rectilinear generatrix,
v – helixes

Variables

a – radius of the helicoid. Angle of generatrix closeness.
b – narrowness of the intercostal spaces of the helicoid

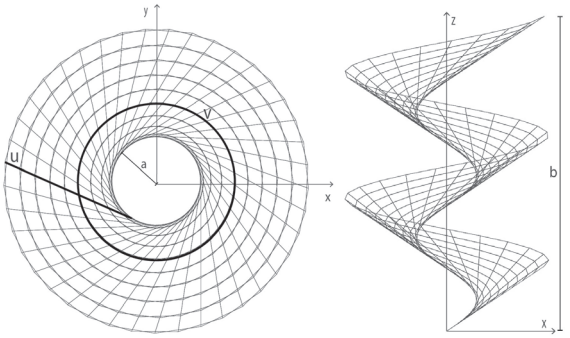

(a) (b)

Figure. 2: Depevopable helicoid diagram (a) Top view, and (b) side view. Source: Authors.

2.3 Methods

Parametrical designs encompass coding and generative modeling when summing and used in educational programs, which are constantly being evaluated. The given models help resolve problems in the design process. The method chosen for designing the following surfaces is generative modeling (Stavric et al.., 2011), which will use initial conditions and parametric forms as input data in rhinoceros 6 with grasshopper as a generative design editor. In practice, if grasshopper is being used parametrical surfaces are modeled with a mixture of operators, conditional statements, functions, and trigonometric curves. While Operators and conditional statements remain to be mostly used, functions and trigonometric curves are widely used for ruled surfaces.

After some consideration of research practices and accessible methods in surface design and evaluation such as reverse design(Cupar et al.., 2013), controlled tests(Palmirani et al.., 2011), case studies(Globa et al.., 2018), and others (Suyoto et al.., 2015). A case study analysis was the chosen methodology since it fulfills all the research requirements. In the following chapters the information will be presented according to the next approaches and then compared.

- Existing helicoidal algorithmic design cases.

- Helicoidal design algorithms using parametrical equations : (Eq.1) and (Eq.2). In Figure 3 the design method is presented along with the parameters mentioned in the previous chapter.

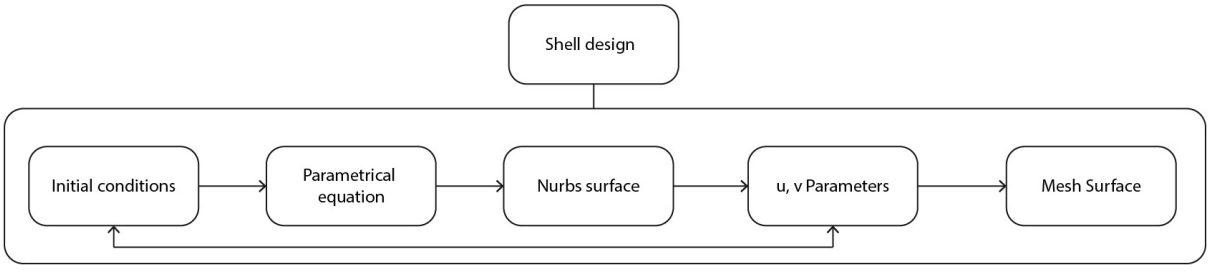

Figure. 3: Design methodology. Source: Authors.

3. RESEARCH STAGES PERFORMED

3.1 Case studies

The case studies presented are ordered by degree of complexity. Each algorithm is created according to the desired end product result. Therefore, each case uses different approaches.

3.1.1 Case 1

The first case (Capone et al.., 2018) presents an algorithm for the manufacturing of developable surfaces using kerfing technique. The generative algorithm seeks to solve the problem of generatrix overlapping while creating a developable surface division. This result is obtained by using the edge of regression which depends on the helical radius. In **figure 4** the design methodology is presented along the algorithm.

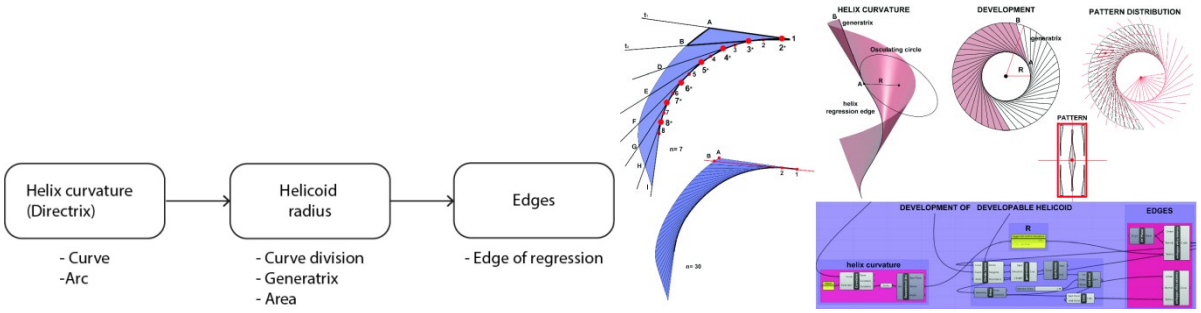

(a) (b)

Figure. 4: (a) methodology diagram, Source: Authors, and (b) Design of a developable surface in grasshopper. Source: (Capone and Lanzara 2019)

3.1.2 Case 2

The second case (Gómez Sánchez, et al.., 2019) presents an algorithm for three types of helicoids : right, oblique and developable. The generatrix definition diminishes complexity by creating all three helicoids simultaneously. Generatrices are defined with accuracy to create a constant surface division on a NURBS surface. In **figure 5** the design methodology is presented along the algorithm.

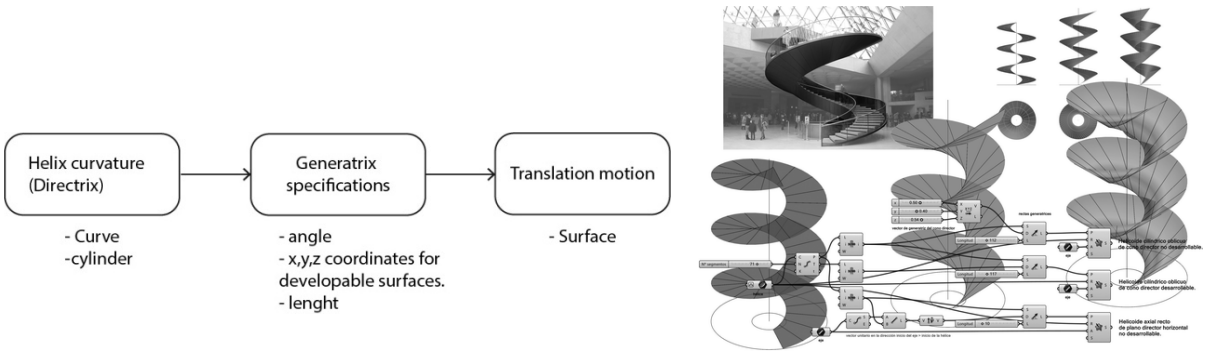

(a) (b)

Figure. 5: (a) methodology diagram, Source: Authors, and (b) Design of an oblique, right and developable helicoid surface in grasshopper. Source: (Gómez Sánchez, González Uriel, and García Ríos 2019)

3.1.3 Case 3

The third case presents the LunchBox plug-in, which has input values of two integers, three numbers and two intervals giving a surface as the output value. It creates non-developable surfaces. In **figure 6** the design methodology is presented along the algorithm.

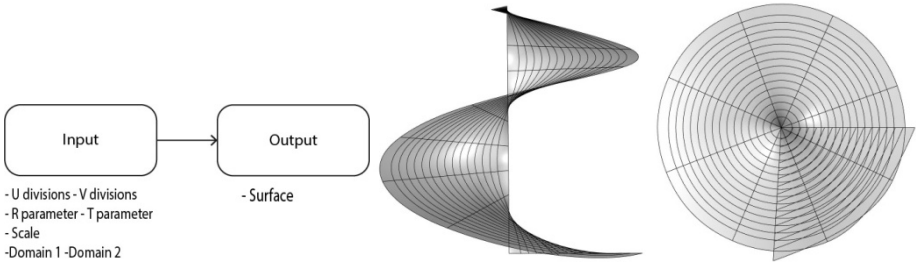

(a) (b)

Figure. 5: (a) methodology diagram, Source: Authors, and (b) Design of an oblique helicoid surface in grasshopper. Source: Authors.

3.2 Algorithmic design using parametrical equations

The directrix is set by the initial conditions defining the helicoid. Depending on its domain and range, the surface is able to be modifyed. The set of parametrical equations used (Eq.1) and (Eq.2) sets the points in relationship to the helix axis. Afterwards, a Nurbs surface is created from the given set. Finally, the Nurbs surface is able to be transformed into a Mesh and modified for further use. The given steps are showed in Figure 6 for the oblique helicoid. In Figure 7 it is showed the equation change for a developable helicoid.

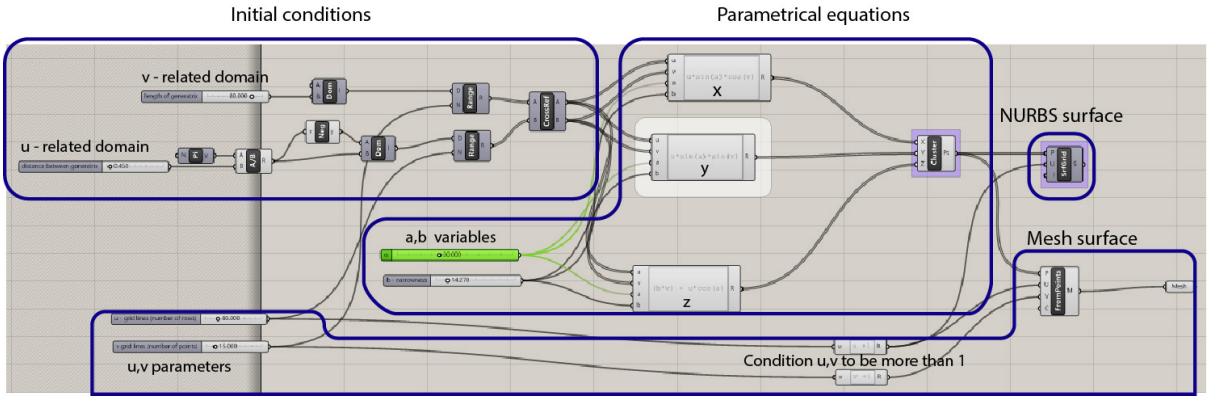

Figure. 6: (a) Logarithmic design for oblique helicoid. Source: Authors.

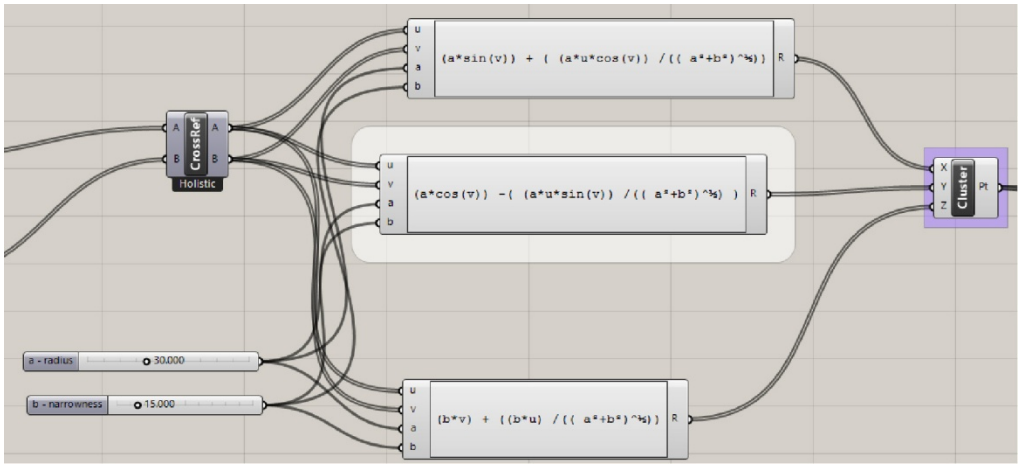

Figure. 7: Logarithmic design for developable helicoid. Source: Authors.

4. RESULTS AND DISCUSSIONS

After implementing several sets of values for u,v and a,b the following models where baked from the surface grid obtained as the final output.

4.1 Oblique helicoid

The following values where used for the surface:

u =80 , v = 15 ;
u – related domain = -π/0.45, v – related domain = 80;
a = 30, b = 15

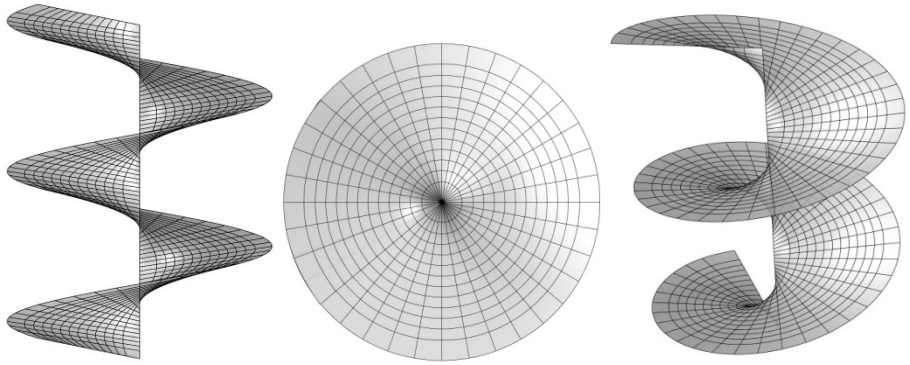

(a) (b) (c)

Figure. 8: Views of oblique helicoid model (a) side view, (b) top view, (c) isometric view.Source: Authors.

4.2 Developable helicoid

The following values where used for the surface:

u =30, v = 8 ;
u – related domain = -π/1.1, v – related domain = 90;
a = 30, b = 15

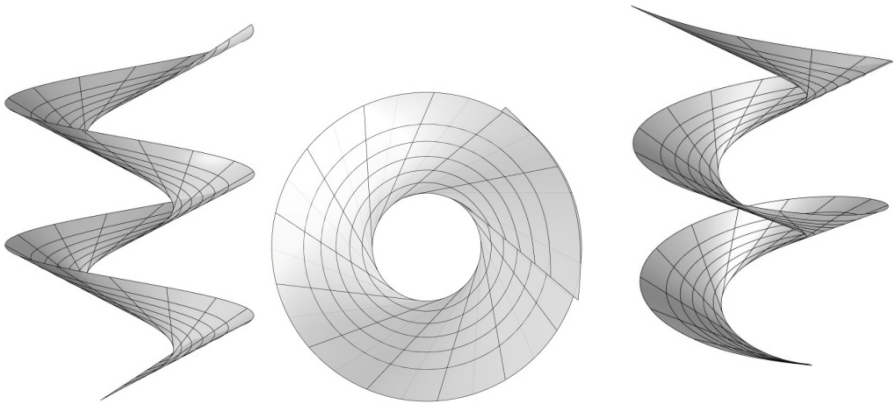

(a) (b) (c)

Figure. 8: Views of developable helicoid model (a) side view, (b) top view, (c) isometric view.Source: Authors.

5. CONCLUSIONS

Before making any type of surface using generative modeling, the classification and origin of it must be completely assimilated. Thus, giving a wider scope of possibilities for the logarithm to be sculpted. Another contributing factor is the specification of the end product. As seen in cases 1,2,3 each had different levels of immersion. Case 1 was the most accurate and complex due to its manufacturing exploitation which requires a precise level of surface definition. Case 2, despite not as accurate, provides a satisfactory system for surface comprehension. Case 3 showed its capacity for surface perception and how the parametric values affect it. But overall, the common value shared amongst the three cases was the logic dictated by descriptive geometry and the surface characteristics. The implemented design in section 3.2 has some minor drawbacks with overlapping and definition. But if used correctly is able to demonstrate the potential of modelling parametric surfaces. Initial conditions and variables showed how u, v coordinates relate to the actual surface.

Although coorditaed formulas are considered time consuming and risky in everyday work environment (Suyoto, Indraprastha, and Purbo 2015), they demonstrate their potential by giving new aesthetic value. Once automatized and assimilated it is conceivable to reuse the methodology, thus making the process of optimization part of the design process. Additionally, Grasshopper has the possibility of being used in educational programs for understanding descriptive geometry and parametric design. Its visuality makes it easier to interact and comprehend the logic that connects the user with the desired result.

6. ACKNOWLEDGEMENTS

This paper has bee prepared with the support of the “RUND University Program 5-100”.

7. REFERENCES

1. Abdel Gawad, Ahmed. 2015. “Hands-on Engineering Education by Construction and Testing of Models of Sailing Boats.” *American Journal of Aerospace Engineering* 2 (January): pp 11–30.

2. Allyn Polancic. 2014. “Oblique-Atory: Helicoid Tessellations.” Archinect. 2014. https://archinect.com/allyn/project/oblique-atory-helicoid-tessellations. [Accessed: 13th February, 2020].

3. Capone, Mara, and Emanuela Lanzara. 2018. “Kerf Bending: Ruled Double Curved Surfaces Manufacturing.” In *Blucher Design Proceedings*, pp 653–60.

4. Lanzara Emanuela and Capone Mara. 2019. “Parametric Kerf Bending: Manufacturing Double Curvature Surfaces for Wooden Furniture Design.” In *Digital Wood Design: Innovative Techniques of Representation in Architectural Design*, edited by Fabio Bianconi and Marco Filippucci, 415–39. Lecture Notes in Civil Engineering. Cham: Springer International Publishing.

5. Cupar, Andrej, Vojko Pogacar, and Zoran Stjepanovič. 2013. “Methodology for Analysing Digitised Geometry.” In , pp 903–20.

6. Globa, A.A., O.A. Ulchitskiy, and E.K. Bulatova. 2018. “The Effectiveness of Parametric Modelling and Design Ideation in Architectural Engineering.” *Scientific Visualization* 10 (1): 99–109. https://doi.org/10.26583/sv.10.1.08.

7. Gómez Sánchez, María Isabel, Ana González Uriel, and Ismael García Ríos. 2019. *Ruled Surfaces and Parametric Design*. Edited by Carlos L. Marcos. Springer, Cham. Cham: Springer International Publishing.

8. Krivoshapko, S. N., and V. N. Ivanov. 2015. *Encyclopedia of Analytical Surfaces*. Springer.

9. Lăzureanu, Cristian. 2014. "Spirals on Surfaces of Revolution." *VisMath* 16 (December): 1–10.

10. LunchBox. 2015. "LunchBox." *PROVING GROUND* (blog). June 20, 2015. https://provingground.io/tools/lunchbox/. [Accessed: 23rd March, 2020].

11. Palmirani, Monica, and Davide Sottara. 2011. Rule - Based Modeling and Computing on the Semantic Web: 5th International Symposium. Springer Science & Business Media.

12. Puig-Pey, Jaime, Akemi Galvez, and Andrés Iglesias. 2004. "Helical Curves on Surfaces for Computer-Aided Geometric Design and Manufacturing." In ,pp. 771–78.

13. Rynkovskaya, Marina. 2012. "On Application and Analysis of Helicoidal Shells in Architecture and Civil Engineering." *Bulletin of Russian Peoples' Friendship University* 4 (December).

14. Rynkovskaya, Marina. 2019. "Studying the Shape of a Helical Ramp." Proceedings of the IASS Annual Symposium 2019.Barcelona, Spain.

15. SHAU. 2017. "SHAU Projects." 2017. http://www.shau.nl/de/project/65. [Accessed: 2nd March, 2020].

16. Suyoto, William, Aswin Indraprastha, and Heru W. Purbo. 2015. "Parametric Approach as a Tool for Decision-Making in Planning and Design Process. Case Study: Office Tower in Kebayoran Lama." *Procedia - Social and Behavioral Sciences* 184 (May): pp 328–37.

17. Tedeschi, Arturo, and Fulvio Wirz. 2014. *AAD - Algorithms-Aided Design: Parametric Strategies Using Grasshopper*. First edition. Brienza: Le Penseur publisher. pp 100-101

SIMULATION OF THE CONTACT SURFACE BETWEEN THE HOBBING CUTTER AND THE WHEEL ON AN FD320A MILLING MACHINE

Alina Duta
Department of Automotive, Transportation and Industrial Engineering, University of Craiova, Romania
PhD., Associate Professor, duta_alina@yahoo.com

Ionut-Daniel GEONEA
Department of Applied Mechanics, Civil Engineering, University of Craiova, Romania
PhD., Associate Professor, igeonea@yahoo.com

Zorana Jeli
Faculty of Mechanical Engineering, University of Belgrade, Serbia
PhD., Associate Professor, zjeli@mas.bg.ac.rs

Ludmila Sass
Department of Automotive, Transportation and Industrial Engineering, University of Craiova, Romania
PhD., Associate Professor, ludmila_sass@yahoo.com

ABSTRACT

This paper is a result of numerous studies on the dynamics of the process on an FD320A milling machine. We also try to propose a method for the determination of the displacement of the contact surface using an analysis with finite elements. Before this, we outline an important problem of the achievement of a model with finite elements that must be the best approximation of the tool-machine structure first, and then the problem of making a geometric model for the contact surface. Additionally, we collected some experimental data. The findings of theoretical studies are mostly confirmed by experimental data, registered with an acquisition system set on the shaft's slides of the final elements for the milling machine. We performed a dynamic analysis with variable forces since it is, well known that the vibrations that appear may cause large displacements and severe stresses in the actual situations. The analysis proves that displacements are in admissible limits and do not exert major influence on the quality of the processing surfaces.

Keywords: finite element, displacements, milling machine, hobbing cutter.

RESEARCH PREMISES

An FD 320A milling machine is one of the most commonly used tools – machines in gear wheels processing. In a dynamic analysis it is necessary to determine the proper vibrations of the main chain, as well as the amplitudes of the forced vibrations which could appear in this chain due to the variation of cutting forces. If we want to determinate the right moment when dynamic instability appears, we also need to determine the proper vibration. [1]. The approach to the resonance domain has negative effects on the cutting process, as well as a direct influence on the processing precision [3].

Dynamical calculus is a form of calculus of free and maintenance vibrations of the main chain of the milling machine.

Hence, the motioned masses from the main chain are considered as elements with concise masses, in which every shaft is assimilated to a constant spring (k) and each dented wheel as a disk of inertia about J. In dynamical calculus and for the contact area, without making considerable errors, we take into account only the disturbance effect of the variable moments of cutting forces. At the same time, we can consider that the static behavior for different types of loading is also important. Additionally, we will determine the displacements on the contact point. The friction forces from the mechanisms of the main chain are variables, which means that it is possible for, the forced vibrations to appear. The sizes of these friction forces are superior, and it is for this reason that we do not take into account dynamical calculus [2]. On the other hand, we can say that friction in the mechanisms of the kinematic chain appear as a damper of vibrations, and, if oiled properly, their influence can be completely removed. In dynamic calculus, without making important errors, we will take into consideration only the disturbance effort of the variable moments of the splintering forces.

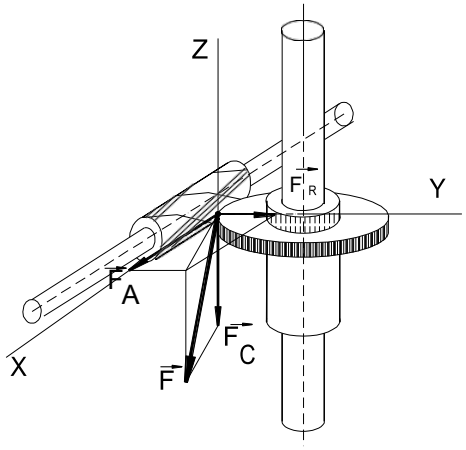

Figure. 1: The schematic representation of the splintering force

The resulting splintering force has the position and a momentary value as shown in Figure 1. It is practically impossible to determine the size and direction of this vector in space [4]. For this reason, for the complete determination of the F vector, it is necessary to determine its three components according to the three directions of the attached system. Finding momentary sizes of the projections F_A, F_R and Fc determines the F vector completely. As can be noticed, the main splintering force, Fc, solicits the holder tool–post shaft during torsion and flexure, the axial force F_A solicits the shaft of the piece during compression, and the radial force solicits both shafts during bending. The forces F_A and Fc are important as size, from the perspective of designing machine - tools. They are the forces that exert stress on the two ends of the kinematic rolling chain and upon the going out end of the main chain. We have done our experimental research using the FD320A milling tool–machine with the hobbing cutter with the characteristics mentioned in Table 1; the material of the gear wheels is steel C 45, not treated thermally.

Table 1: The hobbing cutter characteristics

Hobbing cutter module (mm)	*External diameter Φ_{ext} of the cutter Φext (mm)*	*Hobbing cutter mass (kg)*	*Inclination angle ω(°)*
3,5	*90*	*2,4*	*$2^0$31'24"*

To measure the Fc force, a dynamical strain gauge sensor system placed on the shaft of the gear was used. It measured the moment of torsion for the axle of the gear. [3], [5].

2. EXPERIMENTAL RESULTS

Processing of the results recorded using the analyzer was performed by means of a data acquisition plate mounted on an IBM-PC Pentium computer. Data processing yielded displacement diagrams in all the studied cases and for all the points considered (see figures below) on an IBM-PC Pentium computer. The analyzer sensor was mounted

at different points of the structure (Fig. 2, a), making recordings for different working situations: in the case when only the pump was started; with the machine running empty and then several determinations for different working regimes, mentioned in Table 2. The analyzer sensor located in measurement point 1 is shown in Fig. 2, a.

2.1. Experimental method to establish displacements

The measuring system is shown in Fig. 2, b. The analyzer sensor located in measurement point 2 is shown in Fig. 2, b.

(a) (b)

Figure. 2: (a) Measurement system (assembly view), and (b) Measurement system (detail view)

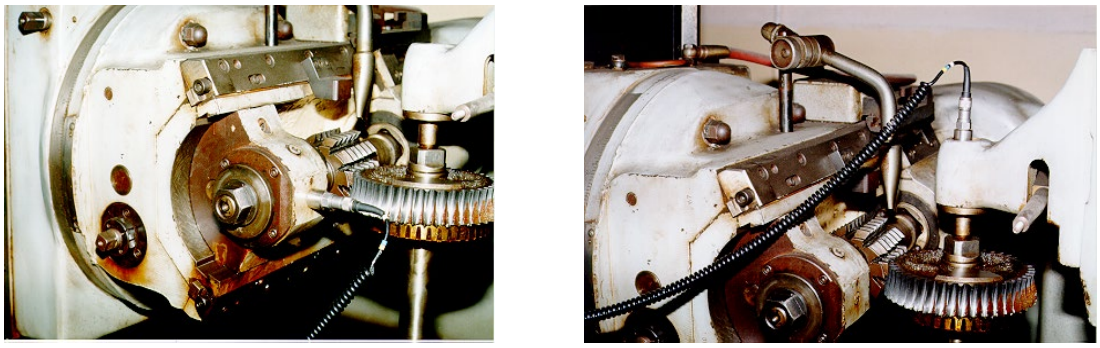

(a) (b)

Figure. 3: (a) Sensor located in measurement point 1 (detail), and (b) Sensor located in measurement point 2

The analyzer sensor located in the measurement point 1 is shown in Fig. 3, a. The analyzer sensor located in measurement point 3 is shown in Fig. 3, b.

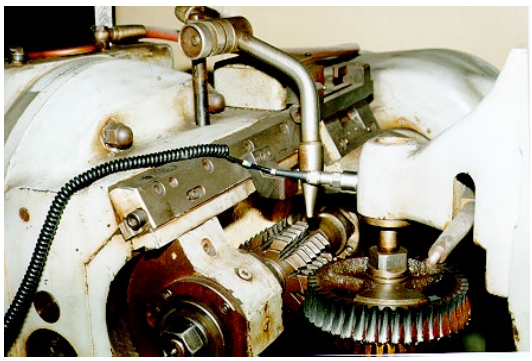

(a)

Figure. 4: (a) Sensor located on measurement point 4

The analyzer sensor located in measurement point 4 is shown in Fig. 4. Precise determination the dynamic behavior of the entire structure is not possible, primarily, due to the complex construction configuration and secondly, due to a relatively low level of knowledge regarding the rigidity and the damping properties in the

coupling places between the elements that transmit and transform the movement. Therefore, the only method for determining this behavior is the experimental method. However, a very important point should be raised here due to the fact that both the drill shaft and the tool shaft are in rotational motion, the analyzer sensor could not be positioned directly on them. The errors introduced in this way are relatively small, since the analyzer's sensor is near the area of interest. In addition to the four points considered important, a number of other points located on the structure of the toothbrush were also taken into account. In Fig. 2, b the positions of the points considered on the machine tool structure are schematically represented. Having analyzed the a first set of experimental determinations considering all these eight points, it was concluded [2] that differences of movements recorded in the case of points 5, 6, 7 and 8 for different types of loads are less important in the proposed study. As a result, the latter determinations were not taken into account.

Table 2: Experimental results

Module m (mm)	*RPM n (rot/min)*	*Feed rate w (mm/min)*	*Limit displacements Point 1 (μm)*	*Limit displacements Point 2 (μm)*	*Limit displacements Point 3 (μm)*	*Limit displacements Point 4 (μm)*
3,5	*95*	*4*	*-1.29⋯ 2.44*	*-1.31⋯ 1.01*	*-1.71⋯ 1.29*	*-1.17⋯ 1.02*
3,5	*95*	*8*	*-5.02⋯ 5.56*	*-3.32⋯ 1.36*	*-1.90⋯ 2.36*	*-1.88⋯ 1.72*
3,5	*150*	*4*	*-2.36⋯ 2.78*	*-2.22⋯ 3.25*	*-1.06⋯ 1.63*	*-1.56⋯ 1.89*

The first conclusion that can be drawn by examining the record diagrams (see figures below) is that displacements are variable within small limits. Higher displacements were recorded at the level of the port-tool shaft, compared to those at the level of the port-tool shaft, for the same working conditions, largely due to the increased value of the disruptive moment at the level of the port-tool spindle compared to that of the spindle port-track.

2.2. Experimental method for determining the torque moments

For the experimental determination of the torque moments on the shafts, strain gauge sensors were bonded. For transmitting the signal from the shafts in rotational motion to the fixed part, the systems with collecting brushes were used. This aspect is shown in Fig. 5.

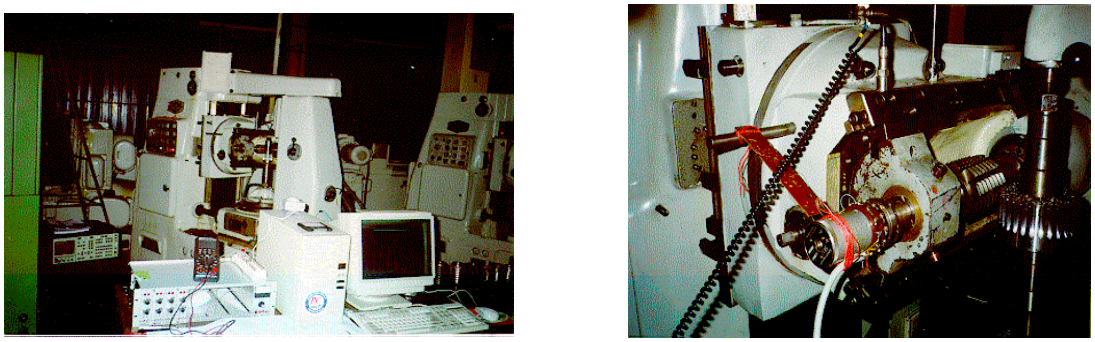

(a) (b)

Figure. 5: (a) Measurement system (assembly view), and (b) signal collecting system

Table 3: Measured torque results

Module m (mm)	*RPM N (rot/min)*	*Ap/Bp*	*Feed rate w (mm/min)*	*Measurement event*	*M_{tmax} (Nm)*
3,5	*95*	*24/34*	*4*	*49*	*52.95875*
3,5	*95*	*24/34*	*8*	*53*	*80.46825*
3,5	*150*	*31/27*	*4*	*61*	*67.47*

The graphs obtained for the experimentally determined torsion moments are shown in Fig. 6 and 7.

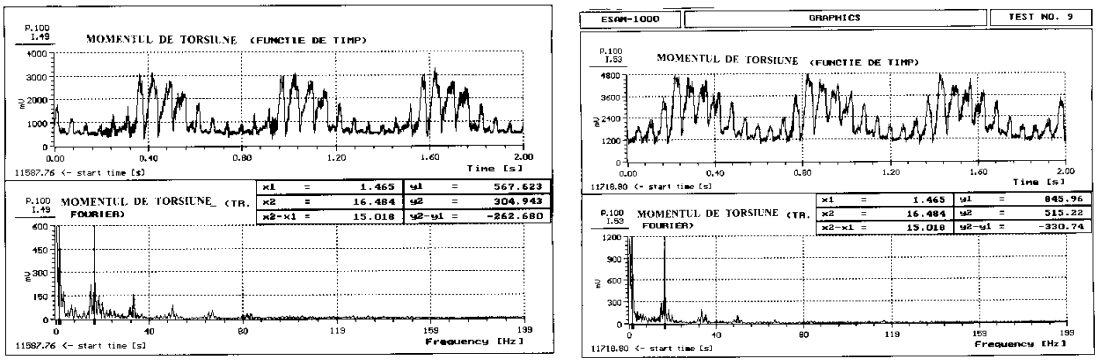

(a) (b)

Figure. 6: (a) Graphic for the torque variation for the case m=3,5 mm, n=95 rot/min, w=4 mm/min, and (b) for the case m=3,5 mm, n=95rot/min, w=8mm/min

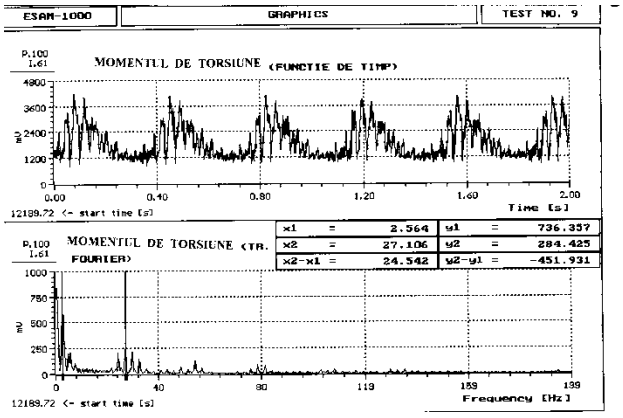

(a)

Figure. 7: (a) Graphic for the torque variation for the case m=3,5mm, n=150rot/min, w=4mm/min

From the interpretation of the diagrams resulting from the recordings of the cutting efforts Mt (Nm), based on the processing of the diagrams, the torque moments in their harmonic form have the expressions given in a synthetic form in Table 4.

Table 4: The measured torque numerical results

Module m (mm)	*RPM n (rot/min)*	*Ap/Bp*	*Feed rate w (mm/min)*	*Experiment number*	*Torque expression Mt (Nm)*
3,5	*95*	*24/34*	*4*	*49*	*18.2074+9.2239sin0.2331t+4.9553sin2.623t*
3,5	*95*	*24/34*	*8*	*53*	*36.3543+13.7468sin0.2331t+8.3723sin2.623t*
3,5	*150*	*31/27*	*4*	*61*	*30.3306+11.9658sin0.048t+4.6219sin4.314t*

The harmonic analysis indicated that the first two harmonics were important, for which the torque moments are written as follows:

$$M_t = M_0 + A_1 \sin \omega_1 t + A_2 \sin \omega_2 t \qquad \text{(Eq. 1)}$$

3. THE DETERMINATION OF THE DISPLACEMENT USING AN ANALYSIS WITH FINITE ELEMENTS

To model the machined gear wheel snail mill assembly, we used the SolidWorks software. The gear wheel is modelled very easily, using the tools in the SolidWorks toolbox. For this purpose, we specified the geometric parameters of the spur gear: the normal modulus, the number of teeth, the normal reference pressure angle and, the nominal diameter of the shaft on which the wheel was mounted. Through the set of modelling tools existing in SolidWorks we also modelled the hob gear cutter, which had the normal module of 3.5 mm. The next very

important aspect in defining the geometric model was the construction of the assembly. The appropriate geometrical constraints were placed in the model [5]. The interference between the two pieces must be avoided, as this may affect the correctness of the finite element analysis.[4], [6].

In Fig. 8, the geometrical models obtained for the spur gear, the hob gear cutter and, the overall model with two components are presented. The overall model incorporates geometrical constraints of the correct positioning of the two pieces [5].

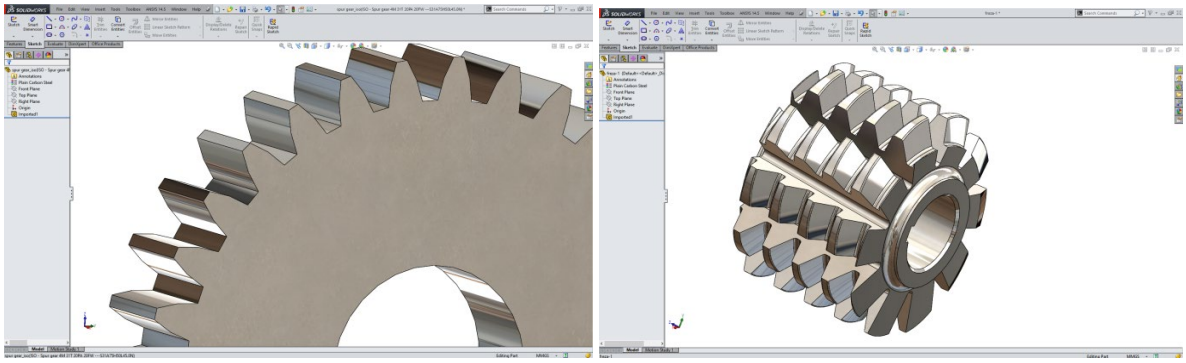

(a) (b)

Figure. 8: (a) Geometric models of the processed spur gear, and (b) hob gear cutter

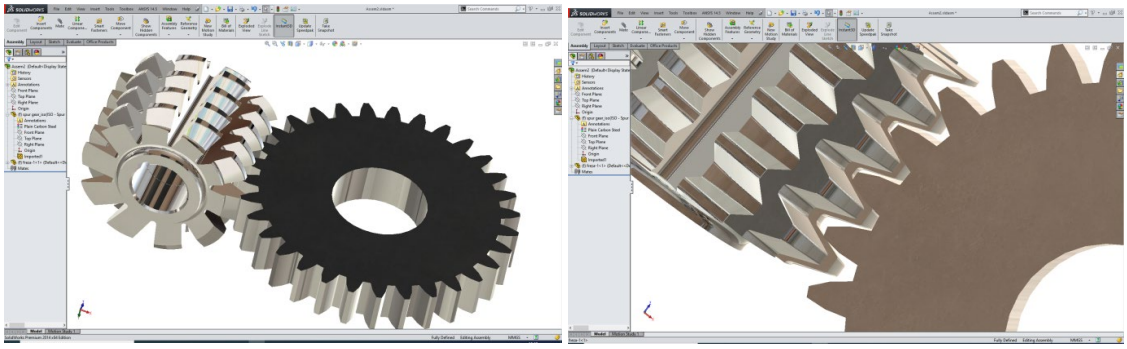

(a) (b)

Figure. 9: (a) Geometric model of the final assembly, and (b) detail of the spur gear tooth flanks contact

3. 1. The analysis of the structure of the tooth milling machine in a transient regime

In this section we present the aspects regarding the finite element analysis of the hob gear cutter and the spur gear assembly to be processed. We performed this analysis in the first stage in the transient structural regime, in the finite element analysis software environment, FEM, of ANSYS. In the first step, we had to make sure that the geometry built into the Solid Works was imported correctly into ANSYS. For this purpose, geometry can be checked in ANSYS Design Modeler. The geometry imported into ANSYS is shown in Fig. 10, where you can also see the global coordinate system, which is placed as a location in the hob gear cutter, and the orientation is with the Z-axis, the axis of rotation of the mill.

The next important step was choosing the appropriate materials from the ANSYS database [6]. The gear material is specified structural steel, with the nonlinear characteristics, with defined isotropic hardening characteristics. The hob gear cutter is made of metal carbides. Based on the geometry of the parts and the material characteristics (density), the software calculates the inertial properties of the parts (mass, moments of inertia). The appearance of the window of choice of materials from the ANSYS database is shown in Fig. 11.

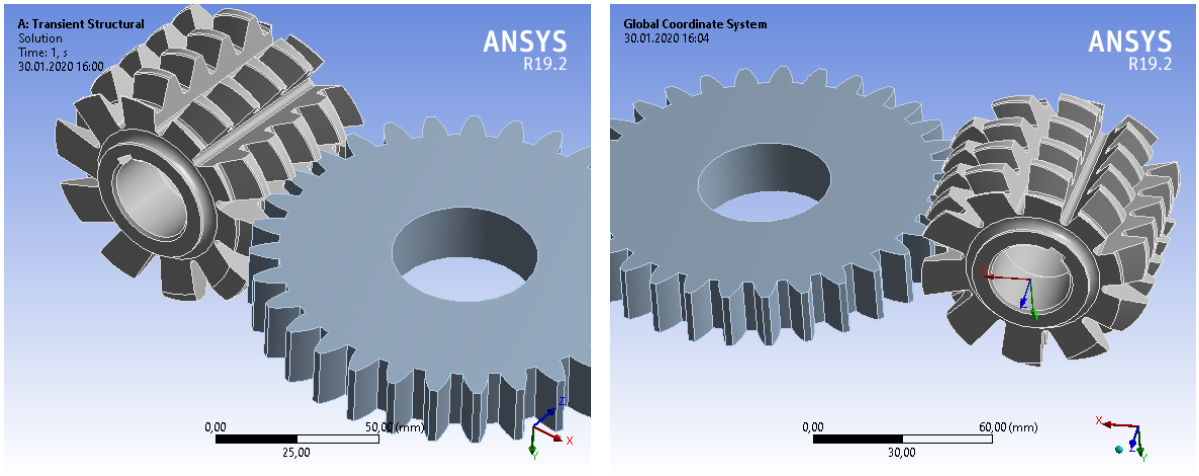

(a) (b)

Figure. 10: (a) ANSYS model of the assembly, and (b) coordinate system placement

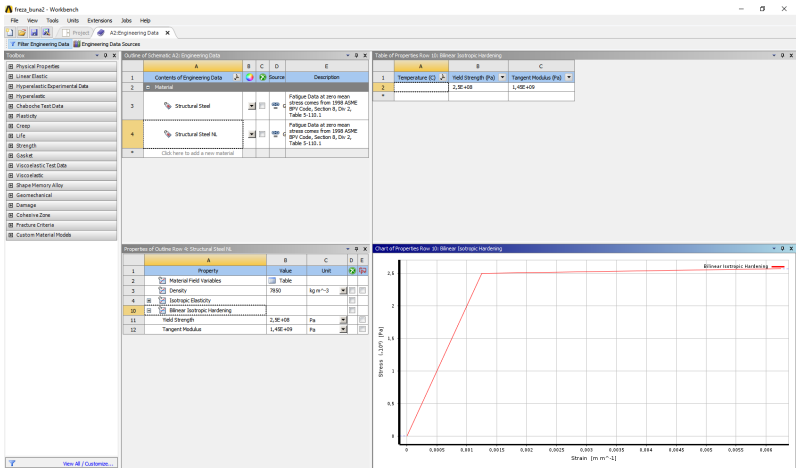

(a)

Figure. 11: (a) Choice of materials from ANSYS program database

The contact area between the flanks of the teeth is automatically detected by ANSYS. The type of contact is specified accordingly, for the specific situation, in this case, the type is frictional contact. The contact type is chosen as impact, with the dynamic friction coefficient of 0.2. The contact surface between the flanks is shown in Fig. 12.

Next the coordinate system was established: Ox is associated with directions 1 and 4, Oy for 2 and 3 of Fig. 13.

In order to model the virtual system strictly respecting the actual operating conditions, it is necessary to define the boundary conditions. For this, we need to define the kinematic joints in the system. Since we carried out a transient structural analysis in the first stage, we consider the gear set to be the base and the hob gear cutter is connected by a rotation joint to the base. Fig. 13 presents the windows defining the kinematic couples of the ensemble. For the hob gear cutter, it is observed that the allowed motion is the rotation along the Z-axis. In the rotation joint thus defined for the hob gear cutter, we will specify the loading conditions, i.e. define a torque.

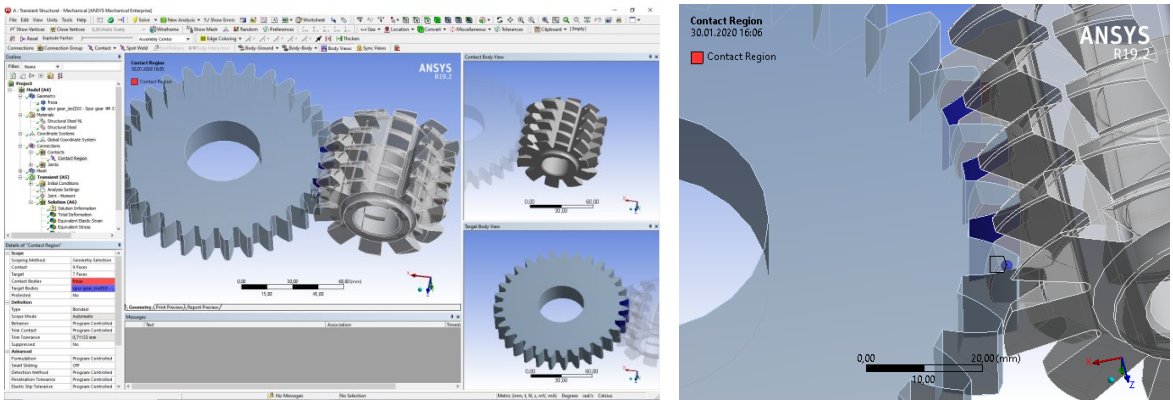

(a) (b)

Figure. 12: (a) The contact surfaces (region) between the hob gear cutter and the spur gear, and (b) contact detail

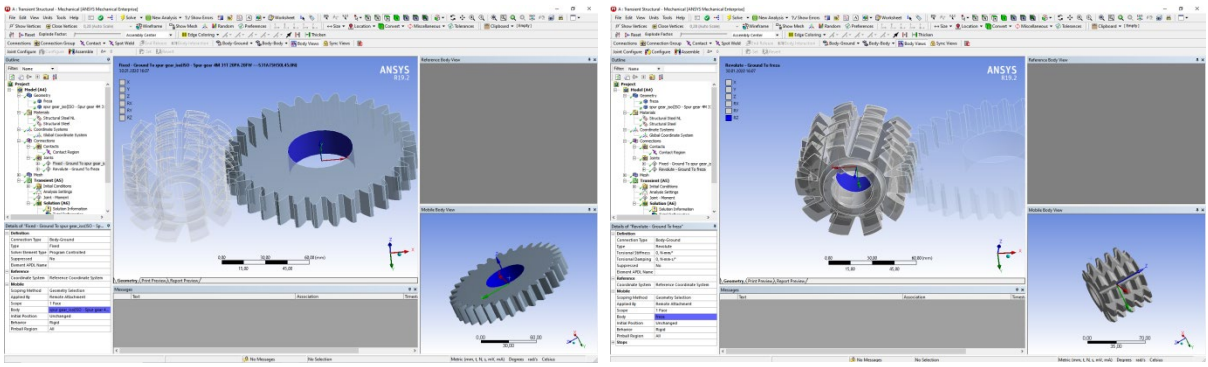

(a) (b)

Figure. 13: (a) Defining of the kinematic joints of the spur gear, and (b) joint of the hob gear cutter

The next step in the construction of the ANSYS model was the finite element meshing of the assembly. The discretized model in finite elements of the tetrahedral type is shown in Fig. 14. We performed an automatic discretization, specifying only the size of the element (element size) of 2 mm, as seen in Fig. 14. Another specified parameter is that we inserted a refinement mesh in the contact area of the flanks. To achieve a finer discretization, in the contact area of the teeth with the milling cutter, we used the Contact sizing option, available in ANSYS. We specified 0.2 mm as the size of the finished element in the contact area, as seen in Fig. 14.

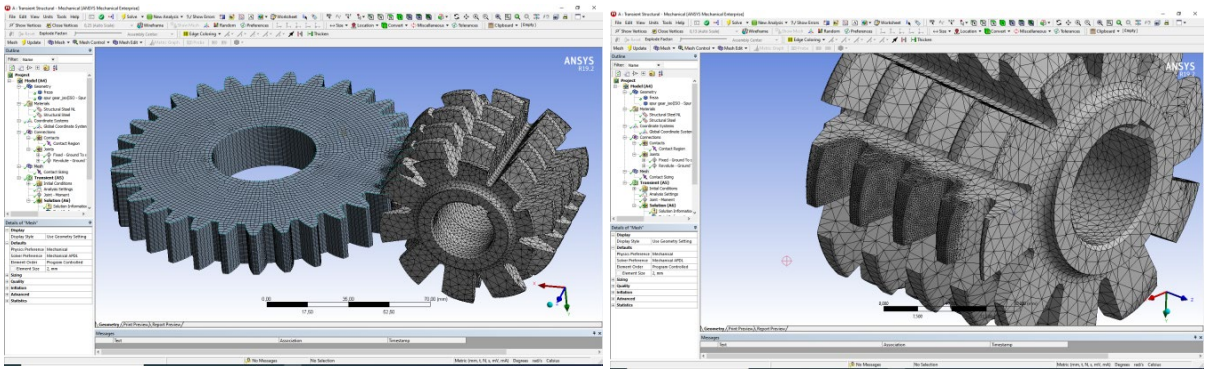

(a) (b)

Figure. 14: (a) Finite element meshing of the hob gear cutter and spur gear, and (b) detail of mesh refinement for the contact area

Based on the experimental determinations, regarding the moment of cutting, we defined a torque, with the value of 50 Nm as a load. For these purposes we used the joint load facility, existing in ANSYS. Thus, in the torque of rotation of the hob gear cutter we specified the torque, as seen in Fig. 15.

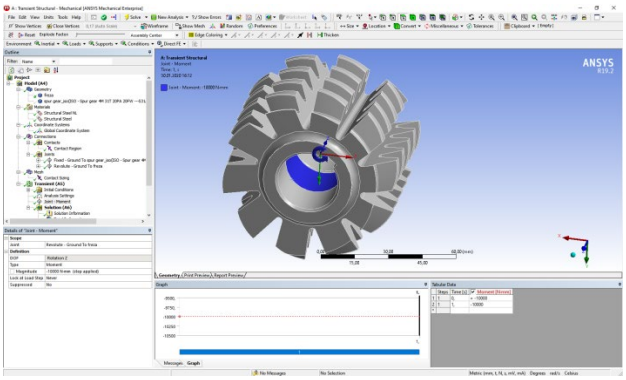

(a)

Figure. 15: (a) Specifying of the torque for the hob gear cutter

Due to the complexity of the model and, a large number of finite elements (approximately 300000), running the simulation takes approximately 16 hours. The results obtained are presented below. Total deformations of the hob gear cutter as well as those of the whole assembly are shown in Fig. 16. The maximum value of total deformations is 0.0066 mm.

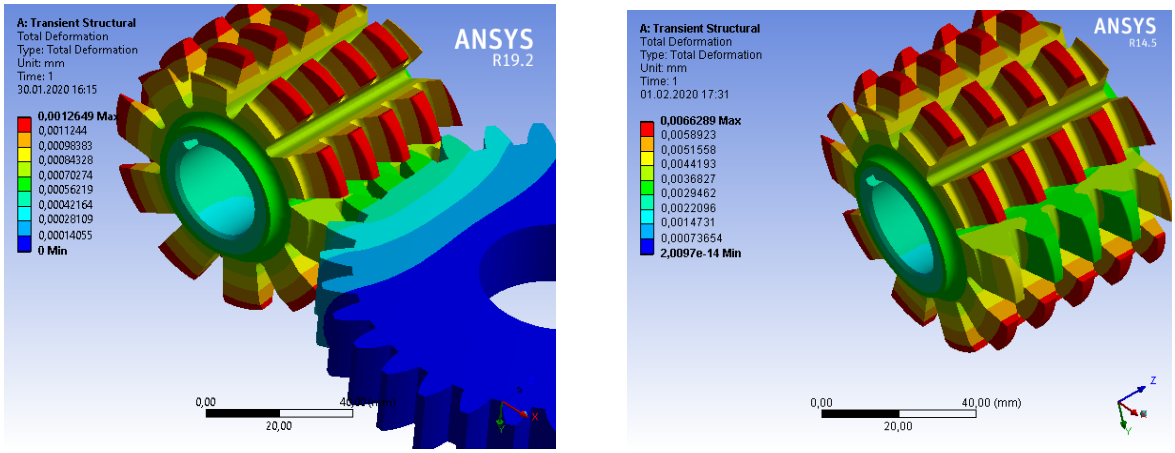

(a) (b)

Figure. 16: (a) Total deformation of the hob gear cutter and spur gear, and (b) hob cutter detail

The distribution of equivalent specific deformations (equivalent elastic strain) is shown in Fig. 17. It is observed that the maximum values are reached in the contact area of the flanks, in the value of 6.1 e-5 mm/mm.

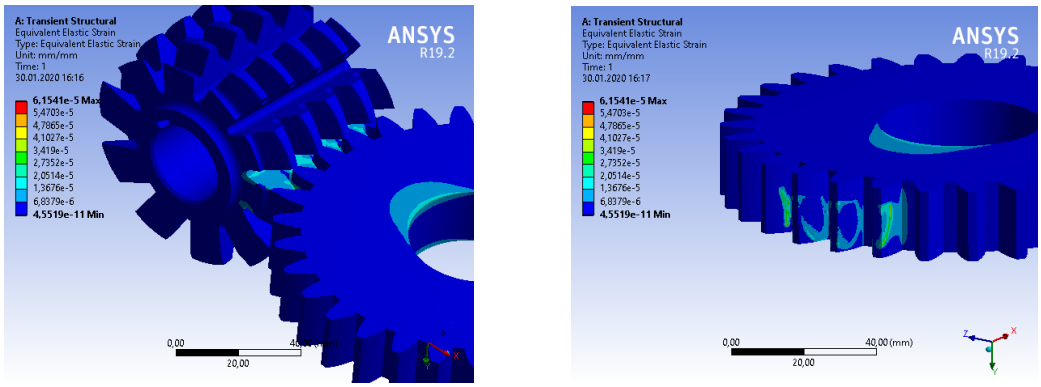

(a) (b)

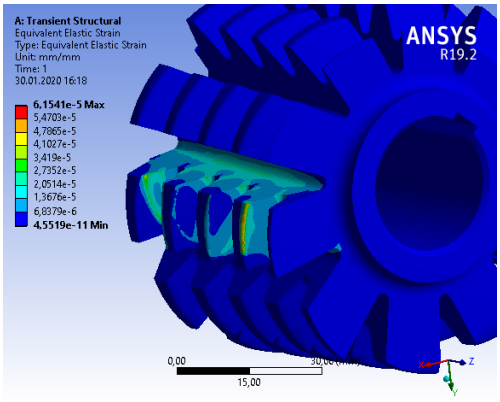

(c)

Figure. 17: (a) Equivalent elastic strain of the hob gear cutter and spur gear, (b) gear detail, and (c) hob cutter detail

For the considered load case, the distribution of equivalent stress is shown in Fig. 18. It can be noted that the maximum value of von Misses equivalent stress is 11 MPa.

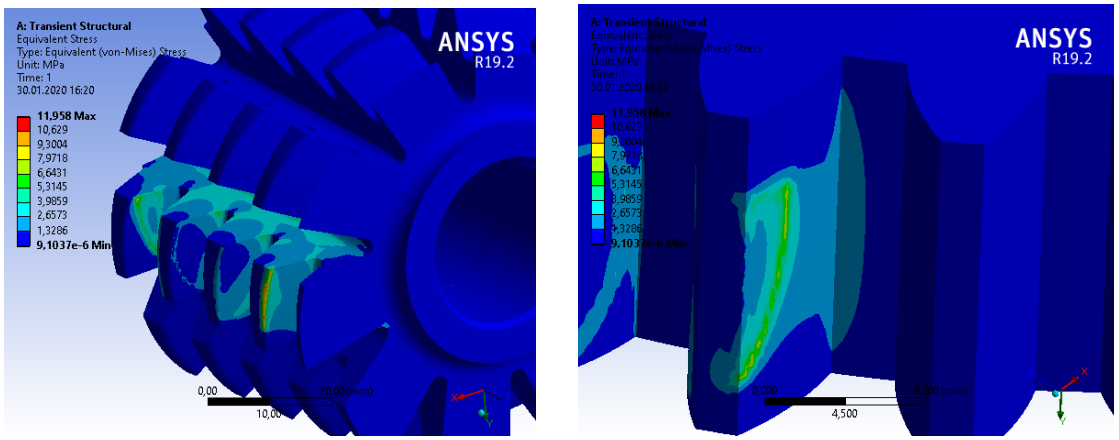

(a) (b)

Figure. 18: (a) Equivalent (von-Misses) stress distribution for the hob cutter, and (b) for the gear

We also present the displacements along three axes of the coordinate system for the processed gear, in Fig. 19. It can be observed that the highest values of displacements are recorded along the X and Y axes, with the values of 0.001 mm.

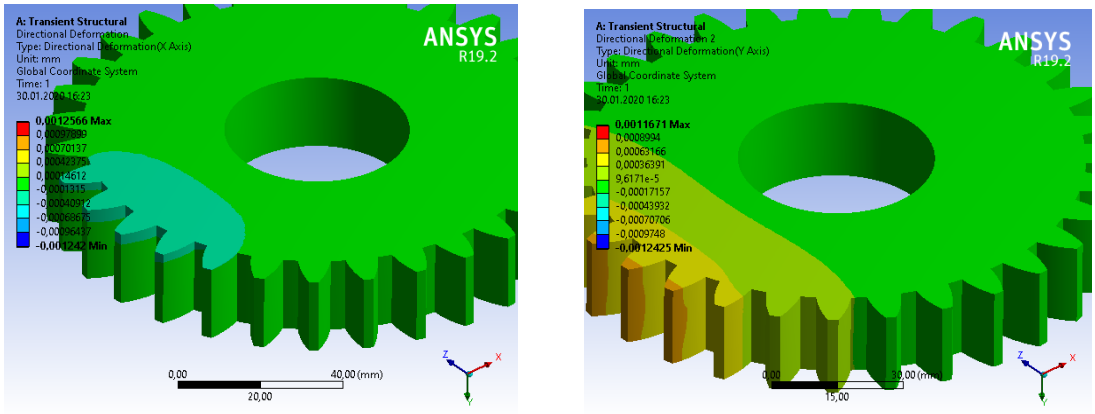

(a) (b)

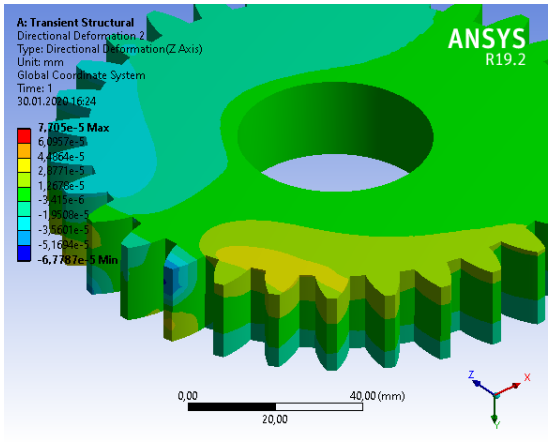

(c)

Figure. 19: (a) Spur gear directional deformation, upon X axis, (b) upon Y axis, and (c) upon Z axis

Table 4: Centralizing the results for the simulation performed

Module m (mm)	*RPM n (rot/min)*	*Feed rate w (mm/min)*	*Limit displacements for the hob gear cutter*			*Limit displacements for the part*		
			on Ox axis (μm)	*on Oy axis (μm)*	*on Oz axis (μm)*	*on Ox axis (μm)*	*on Oy axis (μm)*	*on Oz axis (μm)*
3,5	*95*	*4*	*0,0126*	*0,0112*	*7.4 e-5*	*0,012*	*0,0011*	*7.7 e-5*
3,5	*95*	*8*	*0,014*	*0,015*	*6.4 e-4*	*0,0125*	*0,0124*	*4-e-4*
3,5	*150*	*4*	*0,018*	*0,0198*	*5.6 e-3*	*0,0134*	*0,0168*	*5.9 e-3*

3. 2. The analysis of the structure of the tooth milling machine in a dynamic regime

In the next stage of the finite element analysis, we set out to simulate the process of cutting the spur gear teeth. For this purpose, we modelled the spur gear wheel half-finished, and used the analysis environment ANSYS explicit dynamics for the simulation. The manner of defining the contour conditions and loads corresponded to the real model. The rotation movements of the gear hob cutter and the processed gear were defined, as well as the milling speed. The obtained results are presented in Fig. 20.

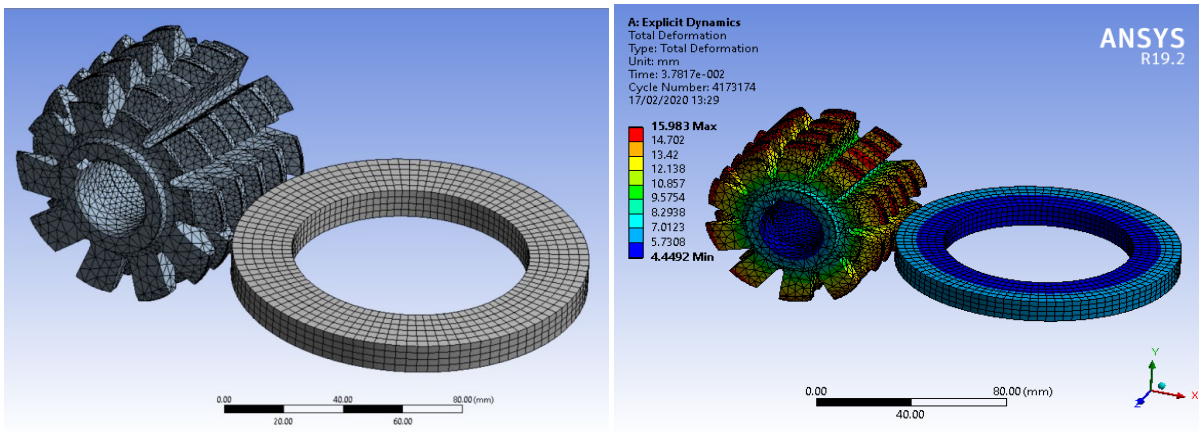

(a) (b)

Figure. 20: (a) Meshed assembly, and (b) total deformation distribution for the hob cutter and gear

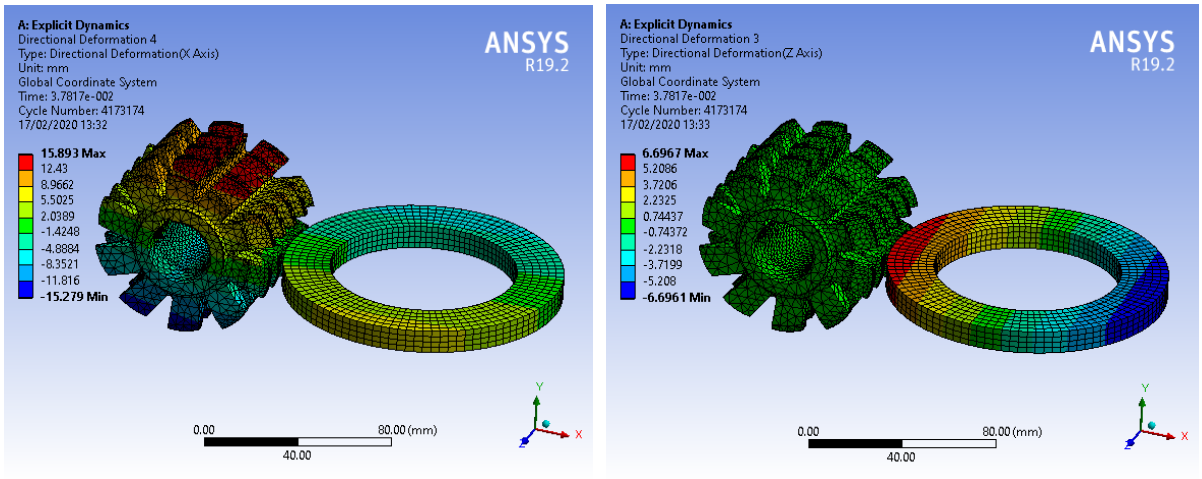

(a) (b)

Figure. 21: Spur gear directional deformation, upon X axis, and (b) upon Z axis

CONCLUSIONS

In this paper we presented experimental results regarding the determination of the rigidity of the milling machine system-the milling gear wheel. Further, the cutting torque that occurs during the machining of gear wheels was determined experimentally for the following set of parameters: milling speed and, feed rate. Further exploration of the rigidity of milling and gear wheels processing was performed by finite element analysis, in a structural transitional regime in the first stage, and then in an explicit dynamic regime. The results obtained by the simulation method with finite elements are comparable to those obtained by experimental means.

REFERENCES

1. Buculei, M., Bagnaru, D., 1980, Vibratii mecanice (Mechanical vibration), *Reprografia Universitatii din Craiova (University Publishing House)*,
2. Butu (Duta), A. and Minciu, C., 2002, A model of dynamic calculus of the main kinematic chain and of the roller chain, Politechnica University of Bucharest, 2-nd report of PhD thesis.
3. Ispas, C.; Simion, Fl..P, 1986, Vibratiile masinilor-unelte, teorie si aplicatii (Vibrations for tools-machines. Theory and application), *Editura Academiei R.S.R. (Romanian Academy Publishing House)*, Bucuresti.
4. Buciu, G., Popa, D.L., Grecu, D., Niculescu, D., Nemes, R., 2012. Comparative analysis of the three new designs of tibial nails which eliminate the use of orthopedic screws. Proceedings of The 4th International Conference "Advanced Composite Materials Engineering " COMAT 2012, Lux Libris Publishing House, Brasov, Romania, pp.387-392.
5. Tarniță, D., Popa, D., Tarniță, D.N., Grecu, D., Negru M., 2006. The virtual model of the prosthetic tibial components. *Rom J Morphol Embryol*, 47(4), pp. 339-344.
6. Popa, D.L., Duță, A., Tutunea, D., Gherghina, G., Buciu, G., Calin, D. C., 2016. Virtual Methods Applied to Human Bones and Joints Re-Construction Used for Orthopedic Systems, *Applied Mechanics and Materials*, 822, pp. 160-165

THE PRACTICE OF STRUCTURAL ANALYSIS AT THE "KULA" CONSTRUCTIONS

Anca Mihaela BARBU
Department of Applied Mechanics and Civil Constructions, University of Craiova, Romania
PhD, Associate Professor, ambarbu12@gmail.com

Alina DUTA
Department of Automotive, Transportation and Industrial Engineering, University of Craiova, Romania
PhD, Associate Professor, duta_alina@yahoo.com

Dragos-Laurentiu POPA
Department of Automotive, Transportation and Industrial Engineering, University of Craiova, Romania
PhD, Associate Professor, popadragoslaurentiu@yahoo.com

Ramona PINTOI
Department of Applied Mechanics and Civil Constructions, University of Craiova, Romania
PhD, Associate Professor, ramona.pintoi@icecon.ro

ABSTRACT

The study presents the "Kula" constructions from Romania, Oltenia region, and structurally analyses their long-term behaviour. The input parameters on which the behaviour of massive masonry buildings depends over time are analysed and taken into account. Heritage buildings of this type have been built in the Southwest of the Roumania for three centuries. The term "kula" refers to square or rectangular structures. These buildings can endanger the lives of a large number of people, first of all, their owners, but sometimes visitors and other people in their neighbourhood. Under these circumstances, the consolidation and maintenance of masonry construction is a major interest to groups of specialists. Through the obtained results and conclusions, valuable contributions are made to the lifetime estimation of heritage buildings by defining the exact role of each input parameter and the impact of each cause on the pre-collapse and collapse state.

Keywords: Kulas, degradation, descriptive statistics, seismicity, landslide

1. GENERAL INFORMATION

The influence of well-known parameters, the construction period, constructive system, seismicity of the area and seismic risk, is analysed in the paper. A statistical analysis of the kula is carried out according to the parameters mentioned in order to achieve the management of conservation and rehabilitation works of these historical monuments in order to prevent the structural collapse phenomena during their exploitation.

The term "Kula" has been borrowed from the Turkish-Bulgarian vocabulary, but as far as the structural and functional system is concerned, as well as architectural and aesthetic, the only thing the kulas in the South area of Danube have in common is the name. The word Kula itself refers to a citadel, a small fortress, which had the task of defending and was made of materials with significant resistance.

2. THE ORIGIN AND FUNCTION PERFORMED

In accordance with the way they were constructed and their placement on small fortresses, a specific purpose was imposed on kulas starting from the construction phase. Regardless of the purpose for which they were built, kulas are massive constructions, masonry, from their foundation.

Therefore, we can say that the most important functions of kulas are the following:

- Rescue and defence Kulas were built between 1516 and1806 for temporary shelter. They were built near mansions, with dominant height and well-protected doors, but with a limited living space. The place where they were built was carefully chosen in order to be easy to follow the surroundings where invaders were usually expected. This type of Kulas includes massive constructions with masonry thickness up to 1m and solid oak doors. Battlements were placed more in the corridors or on the access stairs [1];
- Alarm signalling Kulas were built between 1800 and1850. They did not have permanent dwelling rooms, their purpose being exclusively guard and watch for the area. In terms of function and position, the Alarm Kulas were quite high, with up to 4 levels, and a ground floor followed by three floors[1];
- Permanent dwelling-houses type of Kulas also performed the function of signalling and alarming. They were built between 1850 and1900 and became a place for living. Specific to them is that they all have massive masonry structures. On the ground floor, they have a cellar followed by three floors, and on the last floor they have a "veranda" resembling a balcony, with masonry columns that support trilobite arches, or form a semicircle [1].

(a) (b)

Figure. 1: (a) Rescue and defence Kula Cioaba-Chintescu, GJ-II-m-A-09392, Gorj County Romania, (b) Permanent dwelling-houses type of Kula VL-II-m-B-09977, Valcea Country, Romania

The kulas in Oltenia-Muntenia, built either for housing, defence or refuge, watch and alarm, are locally specific constructions. They were built in local ethnic style, the Oltenian style, and depict the talents and skills of local craftsmen who adopted the constructive system suited to the conditions of their time and place. All kulas have ramparts for defence, usually on the stairs but not in living rooms. Specific to these kulas is that they all have massive masonry structures.

3. STRUCTURE AND CONSTRUCTION TYPE

Generally, kulas, regardless of the purpose for which they were built, are still made of solid masonry. In the hill area, they were built of brick masonry, and those built in the mountains of stone quarry masonry [2]. Their shape was quadrilateral, with four levels at most, a ground floor, which was obligatory, and contained a cellar followed by a maximum of three floors. In some cases, the cover was made of fir tree with the length between 70 and75 cm or a wooden cutter [3]. Depending on the area where the arrangement was placed, it was either solved or in rows, and on the ridge there were beetles (beaten with profiles) [4].

Three ways of building methods were used to construct piles, which are no longer used for saving the execution time of a work.

Figure. 2: Alarm signalling Kula Cernătescu, DJ-II-m-A-08237, Dolj Country, Roamania,

4. DESCRIPTIVE STATISTICS IN THE OLTENIA AREA

The parameters according to which statistical analysis was carried out include: state of degradation; life span in the case of the pre-collapsed and missing Kulas; seismic risk; acceleration of foundation ground; risk landslide landslides; and constructive system.

- ✓ **Based on the analysis, it can be concluded that water is one of the most important factors in degradation of buildings, since it is one of the triggers for the degradation of quality and load-bearing capacity of foundation lands, and one of the catalysts of chemical reactions leading to a whole series of other chemical reactions. Water is also the main salt carrier that leads to degradation of masonry. Thus, we can argue that water is one of the main factors influencing the degradation and structural durability of buildings with massive masonry. The effects on humidity, the causes that determine it and the (lack of) existence of some remedial possibilities are necessary to determine if an effective modernization (rehabilitation) can take place or it is better to find other solutions (partial replacement).**
- ✓ **Structural degradation status: Depending on the state of degradation, varieties are divided into three categories: missing kulas, pre-collapsed kulas and kulas in good condition. These were also analysed in chronological terms, the construction period and the above categories. When it comes to missing kulas, the majority of them have actually been built most recently, which means that other parameters of influence (exceptional actions or poor management of the building) must be considered.**

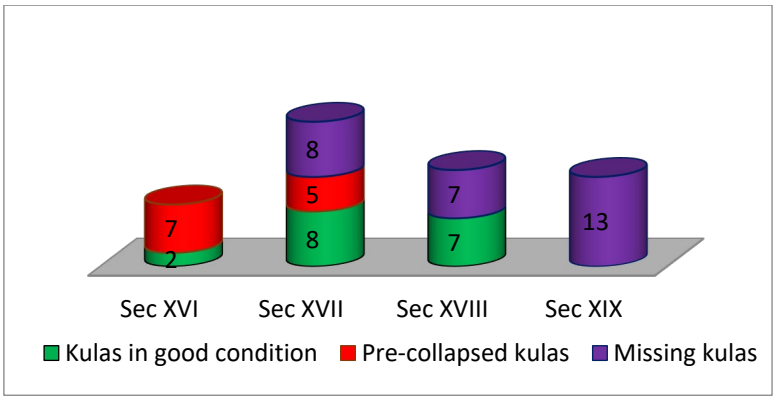

Figure. 3: Kulas hierarchy after the construction period

- ✓ **Life span. Concerning the missing kulas, there is 29% of those whose life span ranged between 250 and 300 years and 23% that lasted between 200 and 250 years. On the other hand, there are 6% of those that managed to survive for over 300 years and also those that disappeared in less than 50 years.**

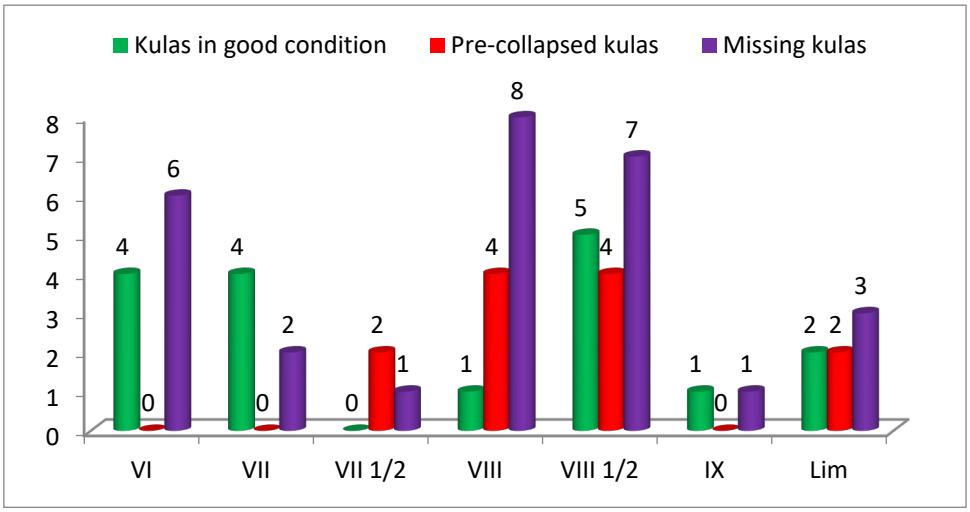

Figure. 4: Comparative seismic zoning for the studied objectives

- ✓ **Seismic Risk: There are 29 buildings in Zone VIII and VIII ½, which represents exactly half of the analysed constructins. At the opposite pole, we have areas IX - 2 and VII ½ which have 3 kulas each.**
- ✓ **Acceleration of the foundation ground: out of the total of 57 analysed objectives, 42% are in the area of 0.15g, 37% in the area 0.20g, 14% in the area 0.25g, and only 7% in the area of 0.30g;**
- ✓ **Risk of landslide slippage: considering the map of Romania that gives the probability of sliding the land in Fig.4, we have the following categories: Virtual zero, Low, Medium and High;**
- ✓ **The moisture and temperature content affects the slow flow in two different ways: directly, by altering viscosity of the material and indirectly, by the effects of aging. The hydration rate, associated with the aging and reduction of micro-pores in the microstructure of the mortar, decreases sharply as the moisture content of the pores decreases and when it reaches about 30%, this rate is neglected and there is no aging of the material.**
- ✓ **Constructive system: from the point of view of the constructive system, in keeping with the analysed objectives, three constructive types were identified, predominantly related to the geographical area of their location. The characteristics of each constructive system have been set out in subchapter 3 above and are denoted as follows: (a) the type of construction system specific to the plateau, respectively the hill; (b) the type of constructive system specific to the Oltenia middle area; (c) the type of construction system specific to the underground area.**

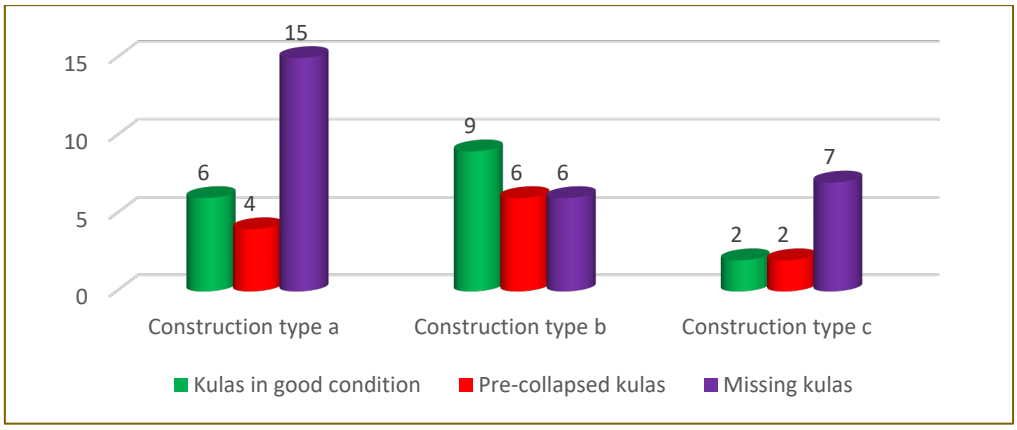

Figure. 5: Analysis of Kula buildings depending on the constructive type

- ✓ **The parameters involved in estimating the lifespan of heritage buildings made of massive masonry are taken into account in the statistical analysis of Kulas from Oltenia Region. In this paper, these types of buildings are studied in terms of degradation, lifespan in the case of pre-collapse and missing culverts, seismic risk, seismicity of the area, landslide risk, and the construction system.**
- ✓ **As a general conclusion, it can be said that, following the great earthquakes of 1838, 1940 and 1977, the studied buildings were damaged. The damages are not of a general character. Currently, the constructions show partial damages to both structural and non-structural elements. These data can be used as a management scheme for the activity of diagnosing the long-term behaviour of solid masonry walls.**

Figure. 6: Crăsnaru Rescue and defense Kula, GJ-II-M-A-09 309, affected by major earthquakes from 1780 to the present

5. CONCLUSIONS

In the engineering world, a major issue is to secure, maintain, strengthen and, above all, rehabilitate worship and patrimony buildings. This is due to the need for conservation and the need to assess seismic safety and vulnerability to environmental factors. as well as hygrothermal behaviour and the manner of maintenance and exploitation of heritage buildings in massive masonry is obvious. In this paper, these types of buildings were researched in terms of their degradation status, the lifetime of pre-collapsed and missing cells, seismic risk, seismicity of the area, landslide risk and the constructive system.

Out of the 57 kulas that were constructed, 21% are in ruins and 49% are missing. Concerning the missing kulas, 29% of them are those whose life span ranged between 250 and 300 years and 23% of those that lasted between 200 and 250 years. On the other hand, there are 6% of those that managed to survive for over 300 years and also 6% of those that disappeared in less than 50 years.

Situation is the same when it comes to pre-collapsed kulas, whose lifetime is between 143 and 212 years. It can be concluded that the average life of these patrimony buildings is between 150 and 300 years.

The analysis performed helps to precisely define the role of each input parameter that leads to the damage of massive masonry heritage buildings. The impact of each cause on the state of pre-collapse and collapse helps to develop new tools to assess the safety of such structures.

The long-term behaviour of constructions is a very important field, because it refers to the constructions in their place of existence, subject to the action of real natural and technological environmental agents and fulfilling their utilitarian functions in accordance with the purpose destination for which they were made. After all, all the studies and design and execution activities aim precisely at the realization of constructions able to be exploited in safe conditions and satisfying the requirements of the beneficiaries to the greatest possible extent. In fact, it can be said that only the insitu behaviour of buildings can give a valid verdict on the usefulness of research results and reveal the need for theoretical and applied research to improve their response to the requirements of beneficiaries.

During its lifetime, massive masonry is subjected to extraordinary loads, occasional loads (such as strong winds, massive accumulations of snow, earthquakes), movement of people and the like. Exposure to various environmental factors, such as the sun, temperature, frost and thawing, wind, rain and snow, erosion and biological degradation, is a variable load over time which greatly affects the structure when the number of charges or the effect is quite long. In most of the cases studied, it was proved that destruction or collapse of the masonry elements occurs due to the fatigue of the materials.

6. REFERENCES

1. Iancu Atanasescu, Pavel Popescu, Culeledin Oltenia...și evoluția lor până astăzi, ISBN 978-973-0-15178-7, Colecția Patrimoniu Cultural National, 2013, Craiova.
2. Monografie Prof. Alexandru Cișmigiu, editura Monitorul official.
3. Iancu Atanasescu, at all Culeledin Oltenia...și evoluția lor până astăzi, ISBN 978-973-0-15178-7, Colecția Patrimoniu Cultural National, 2013, Craiova.
4. Iancu Atanasescu, at all, Culele din Oltenia, Editura Scrisul Romanesc, 1974, Craiova.
5. Cule case boierești fortificate din Romania - Kule Boyar Fortified Houses in Romania, ISBN 978-973-87938-5-9, Igloo, 2007, București.
6. Anca Mogosanu, at all, Studii privind durabilitatea și degradarea consrucțiilor din zidărie masivă, International Congres S.M.A.T.23-25 oct 2014, Craiova.
8. Felician Eduard at all, Degradarea construcţiilor, Revista Construcțiilor, ian-feb 2011.
9. Mircea MIRONESCU, at all, Interventii structurale dupa cutremurele din 10 noiembrie 1940 si 4 martie 1977la bisericile de rit ortodox in România, Revist Construcțiilor nr.132/2016

GEOMETRY AND KINEMATICS OF HUMAN KNEE JOINT

Boris Kosic
Department of Theory of Mechanisms and Machines, Faculty of Mechanical Engineering, University of Belgrade, Republic of Serbia
PhD.student, Assistant, bkosic@mas.bg.ac.rs

Zorana Jeli
Department of Theory of Mechanisms and Machines, Faculty of Mechanical Engineering, University of Belgrade, Republic of Serbia
PhD., Associate Professor, zjeli@mas.bg.ac.rs

Aleksandra Dragicevic
Department of Biomedical Engineering, Faculty of Mechanical Engineering, University of Belgrade, Republic of Serbia
PhD.student, Research assistant, adragicevic@mas.bg.ac.rs

Misa Stojicevic
Department of Theory of Mechanisms and Machines, Faculty of Mechanical Engineering, University of Belgrade, Republic of Serbia
PhD., Assistant Professor, mstojicevic@mas.bg.ac.rs

Lidija Matija
Department of Biomedical Engineering, Faculty of Mechanical Engineering, University of Belgrade, Republic of Serbia
PhD., Full Professor, lmatija@mas.bg.ac.rs

ABSTRACT

At first glance, the human knee can look like a simple rotational joint but the real knee has more complex geometry and kinematics. Kinematics of the human knee depends on its geometry and applied analysis showed that it is a rolling joint, where the upper part of tibia rolling on femur lower end. Such kind of motion can be simply explained with rolling curves generation. In the simplest case, circle rotates on a flat surface and each point on circle circumference will generate one cycloid. Curves defined through this method highly depend on the shape of the rolling object and shape of the surface where the object roles.

In the literature complex, geometry and movement of the human knee can be solved with a relatively complex mechanism that can reproduce real movement or simply by replacing knee with one rotational joint. Application of the new popular technologies (3D printing, CAD) and new approaches of mechanisms design (where the mechanism is produced as one part, and its geometrical shape allows relative movement through elastics deformation), can simplify the overall geometry and kinematic of an artificial knee joint. This will further simplify manufacturing processes, lower costs of the knee and leg prosthetics, and increase its durability by reducing the number of movable parts.

Keywords: Human knee; rolling joint; simulation; 3D printing; CAD

INTRODUCTION

Each year in the world, there are a relatively large number of amputations made to save a patient's life. The most significant causes of amputation are diabetes. In the USA every year, more than 150,000 people lost their lower limbs due to amputation procedures [1]. Only in the USA, there are currently more than 2.1 million people

that have with an amputated limb. Expectations are that this number will be doubled in the next 30 years [2]. In Germany, more than 50,000 amputations are done per year from 2005 up to 2015, the most significant percentage (75%-78%) of those amputations are related to diabetes and peripheral artery diseases [3]. In those case, healthcare cost may be almost twice higher compared to people without limb loss [2]. According to [2], more than 1,000,000 amputations are done annually in the whole world. In India, where amputations are one of the biggest reasons for patient disability, only 5% of all amputees have access to the proper prosthesis. In most cases, for the patient with amputation, the only way to regain walking ability is the use of prosthesis limb (see figure 1) [4,5]. A properly designed knee joint is necessary and it is one of the most crucial components that impact walking performance for above-knee amputees. Optimally designed prosthesis and the knee joint is important for its functionality and aesthetic of patient locomotion. Design of knee mechanisms can differ according to the patient everyday routine [4,6].

Figure 1: Types of knee movement (Source: Sukanta S (2017)).

2. PROBLEM FORMULATION

Knee joint at first glance knee mechanism can look like simple rotational joint but in real life movement of the lower leg is much more complicated. Detailed analyses by Gunston have shown that motion in knee joint consist of gliding, rolling and axial rotation [7]. Types of movement depend on the angle between the upper and lower leg. In the first segment (0-10degrees) axial rotation will occur, form 10-20 degrees rolling is the dominant type of movement and from 20 degrees up to full flection of the leg, the main movement is sliding [7] (See figure 2).

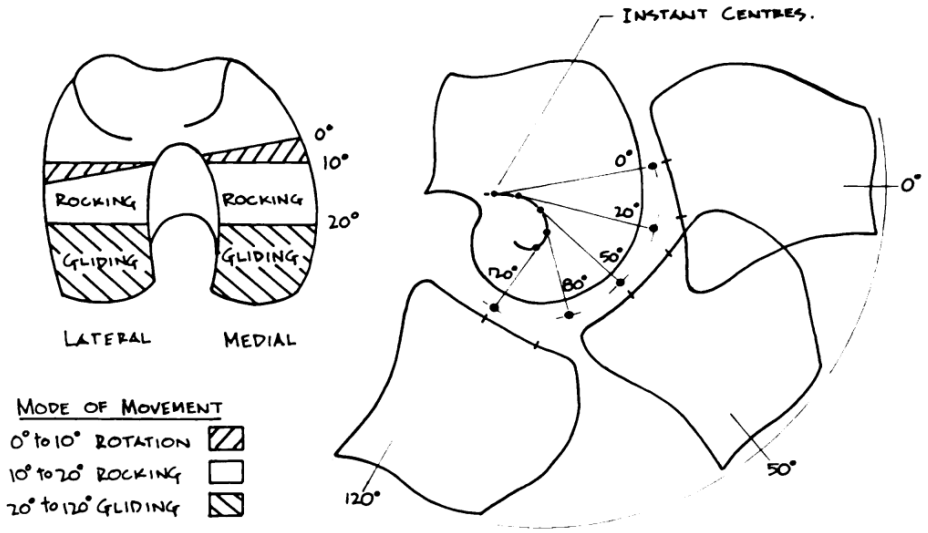

Figure 2.: Types of knee movement (Source: Gunston (1971)).

In literature, specific four-bar linkage mechanism are used for knee prosthesis due to its stability which depends on its relative position. Four bar linkage mechanism has four links joined with rotary joints where the length of those links determines its behaviour during patient motion. It this type of devices instantaneous centre of rotation changes its position as knee flexion angle changes (See figure 3). [8]. The good combination of factors such are simplicity, and sufficient stability with relatively good accuracy in replication of natural knee motion [8]. Recent research has shown improvements in prosthesis design where incorporated spring and damping elements are used to absorb impulse forces and regulate the speed of prosthesis swing [9]. On first glance, the four-bar mechanism looks relatively simple but engineering aspect can be highly complex to produce the optimal design. With the development of 3D printing and an increase in its application, new design approaches with complex geometry such are compliant mechanism and mechanical metamaterials should be investigated. In, the last decade, 3D printers have become one of the most popular and most perspective manufacturing technologies. Some types of 3D printing types have become cheap and affordable to almost everyone who tends to produce any kind of parts such are designers, architects, engineers and others. Those types of 3D printers use various types of thermoplastics, such as ABS and PLA, which are the two most common. Besides their affordability, most 3D printing techniques do not require any specialised type of knowledge to operate them, especially low-end printers that use ABS or PLA. Parts made from ABS or PLA have significant mechanical disadvantages, especially when printed with FDM (Fused model deposition) printers. Those types of printers are the cheapest one, and they produce parts when plastics filament is melted and extruded through the nozzle. Those parts have shown unusually low mechanical characteristics along with axis orthogonal on printing plane, where the most significant problem is layer separation. With all of those problems, the most considerable potential of 3D printers lies in their ability to produce parts with complex internal and external geometrical shapes relatively easy, this ability of 3D printing as manufacturing technology emphases research toward smart geometric design [10]. With the usage of advanced 3D modelling software, designing optimised parts for a specific application have become relatively easy. Those parts, in most cases, have complex natural geometrical shapes, that have better characteristics than any component with a regular geometric shape. Compliant mechanism and metamaterials are areas where 3D printing also have substantial potential, especially when those types of parts need to have significant displacements [10, 11, 12, 13].

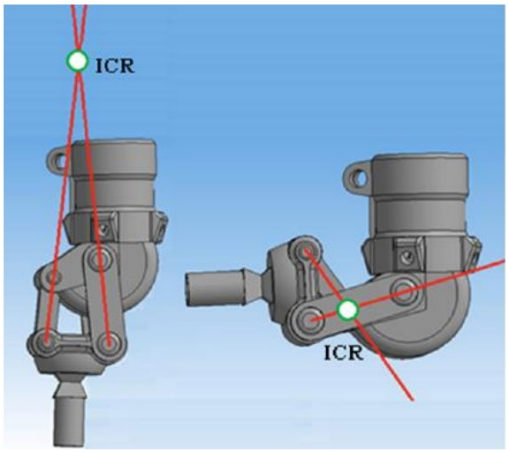

Figure 3. Definition of ICR (instantaneous centre of rotation) (Source: Sukanta S (2017)).

The compliant mechanism is the mechanism where all relative movement is achieved through its deformation. In this case, deformable components of mechanism must be carefully designed with such geometric shape that can allow required movement through deformation. In most cases, to perform movements with the compliant mechanism that match with a classical one, it is necessary to create a highly complex geometric structure of compliant mechanism that allows specific, precise movement [11]. In this paper, we investigate how much is the difference between real four-bar linkage mechanism used in knee prosthesis with a complaint mechanism where minimal changes are done to its geometry. This complaint mechanism is created in such a way that joints of real four-bar linkage are replaced with simple deformable shapes. Those shapes are thinned portion of the mechanism where its thickness is chosen with 3D printers nozzle diameter in mind because the main goal will be to design printable prosthesis on FDM 3D printers.

3. SIMULATION

All models were designed and simulation was created in SolidWorks 2020. In the modelling process, several assumptions are made:

- Materials used for simulation in this study is ABS with a linear stress-strain curve where Tensile strength is 30Mpa, Yield strength 20MPa, Elastic modulus 2000Mpa, Poison's ration 0.3 and density of 1020kg/m3. This material was chosen as one of the most popular 3D printing material. This material is affordable and has a satisfying mechanical characteristic
- All resulting stress is calculated according to Von-misses hypothesis.
- The force used for model testing was 6N this value was chosen to allow full swing prothesis
- Boundary condition has shown in figure 5.
- Stress simulation was using the module for nonlinear Finite element analysis is SolidWorks 2020. The nonlinear analysis was necessary to acquire accurate results because significant movement needs to achieve during a simulation. The simulation was done in calculation 13th steps within the virtual time from 0 to 1s where stepping was automatic with 0.01s initial time increase and 0.1s maximum time increase. During the simulation, default solver was used: FEEPlus.
- The model has meshed with standard solid mesh with high-quality mesh (16 jacobian points) where minimal element size was 0.057mm, and maximum size was 1.146mm.

Initial position and parameters of the four-bar mechanism are shown in figure 4. where point C represents the instantaneous point of rotation. According to these parameters compliant mechanism was designed as it is shown in figure 5.

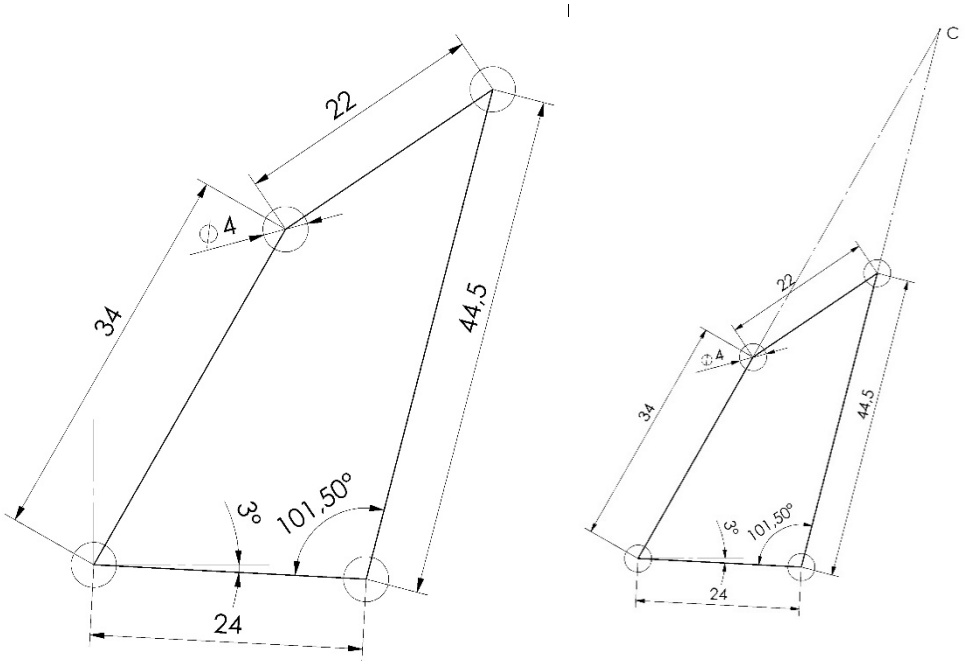

Figure 4. Mechanism definition. Mechanism lengths and initial position (Left). Position of ICR in initial position (Right)

4. RESULTS

As mentioned before nonlinear static simulation has 13 steps; in each step stress state for the whole model was calculated. After 4th step highest stress point on the model was over 37Mpa where up to 13th step highest stress was bigger than 126MPa. The applied force of 6N has moved the lower extension in a new position where the angle between upper and lower extension was 74 degrees which are a significant movement with a relatively small force, as shown on figure 6.

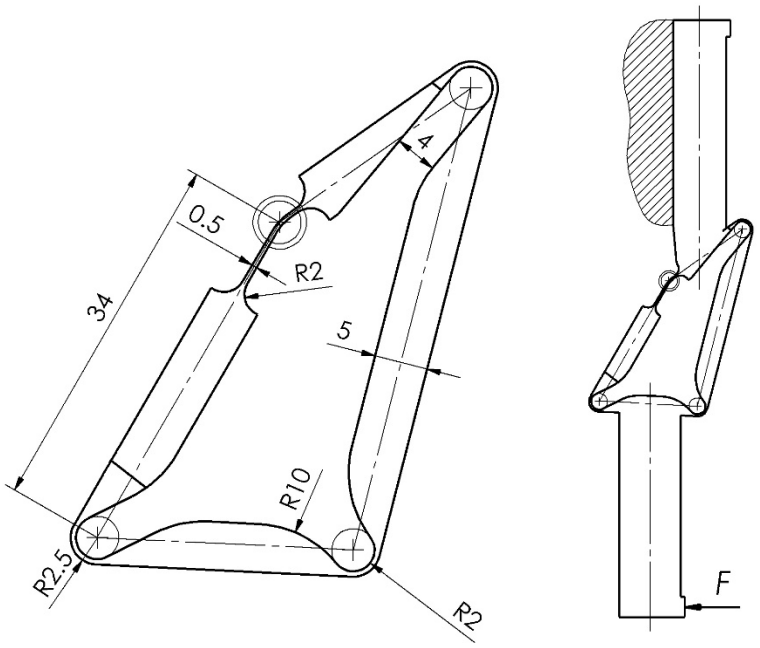

Figure 5. The compliant mechanism based on defined parameters (left), boundary conditions (right).

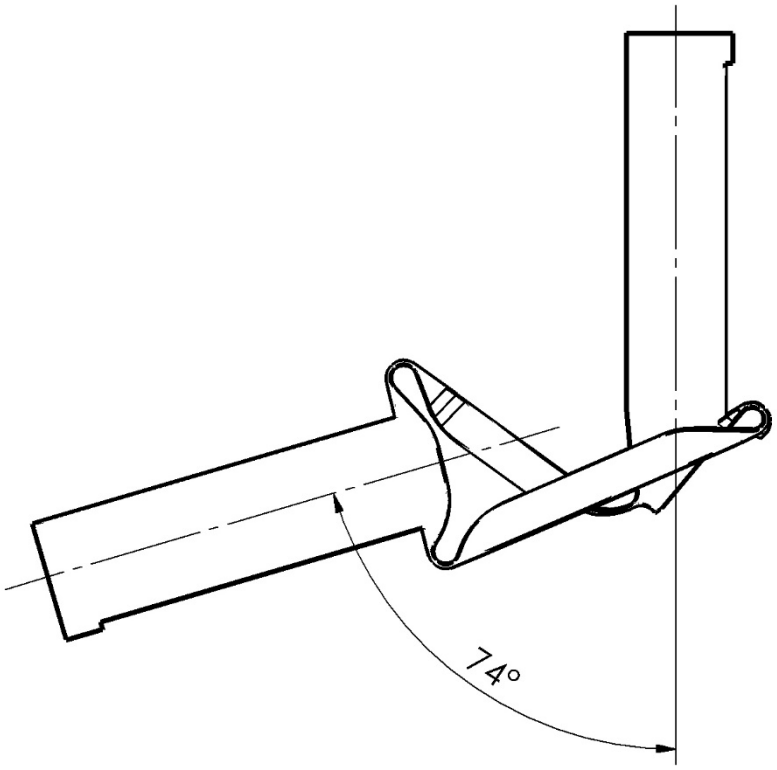

Figure 6. The final position of the compliant mechanism.

During each calculation step, a new mesh model is created that represent deformed mesh after force increment. Each of those models was used to construct the instantaneous centre of rotation. Those dots were traced with spline to approximate continuous movement of ICR. From simulation conditions first ICR for both mechanisms start at the same point (point C on the figure). In the beginning and up to 17.3 degrees (between

extensions) differences between paths of ICR are relatively small, where are the biggest distance between those paths was 0.4mm. At the point of ICR, where the angle between, the upper and lower extension is 17.3 degrees path of ICR for classical mechanism and compliant are crossed. After cross point "A" (see figure) difference between started to increase significantly and in the last step, it was about 2.5mm, as it is shown in figure 7.

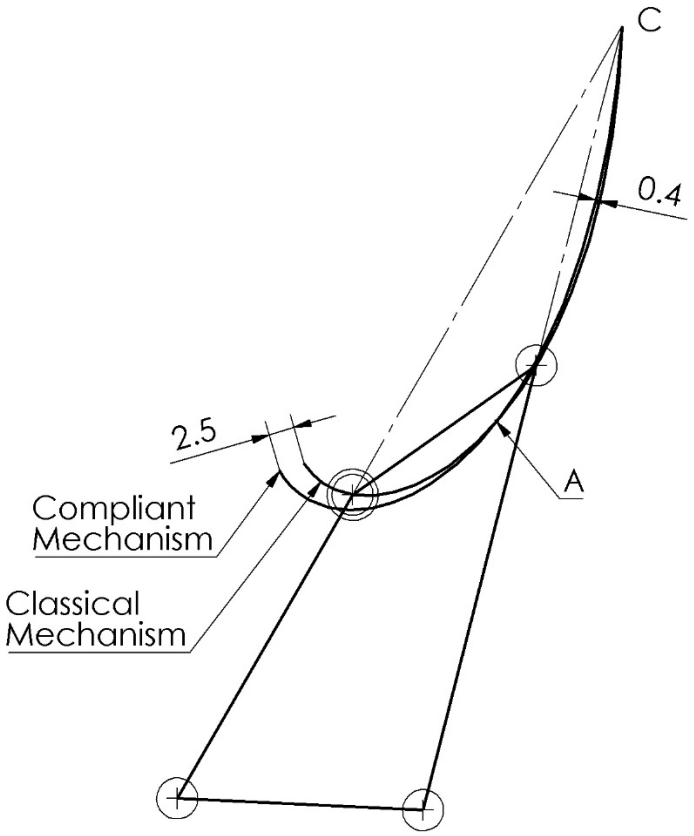

Figure 7. Traced paths of ICR.

5. CONCLUSIONS

In this study, a simple four-bar compliant mechanism was simulated to compare ICR paths with the same classical one. Large deformation dictated that nonlinear static simulation was necessary to get accurate results does not make small movement assumptions. Results obtained form all 13th steps have shown that maximal stress in the final step is more than four times larger than the tensile strength of simulated ABS plastic. Interesting results were occurred by comparing both ICR path, and those paths can be divided into two segments, before cross point "A" and after. The first segment has shown a relatively small difference between ICR paths (up to 0.4mm). In this segment path of ICR of the compliant mechanism is flatter than one from classical. After a cross point, "A", in the second segment, the path of ICR for the conventional mechanism was much more curved compared to compliant and in final step distance between points was 2.5mm. Analysing results, it is shown that with relatively simple compliant mechanism, it is possible to achieve a good comparison between ICR paths. Crosspoint between ICR paths at 17.3 degrees can be explained with higher stiffness in "joints" of compliant mechanism which has a consequence that ICR path of the compliant mechanism is much flatter. Large stress values have shown that significant redesign is necessary or change in material with lower Young modulus, which negatively will impact overall prosthesis stability and stiffness. In [14] have shown that the four-bar compliant mechanism can be used to increace impact resistance in fingers in hand prosthesis. Such result can imply that the application of compliant mechanism in prosthesis design can provide benefits that reduce the introduction of springs and dampers.

This result is the first step in the design and production of real prothesis compliant mechanism knee prosthesis, and it gave an overview of problems that can be solved in the final design.

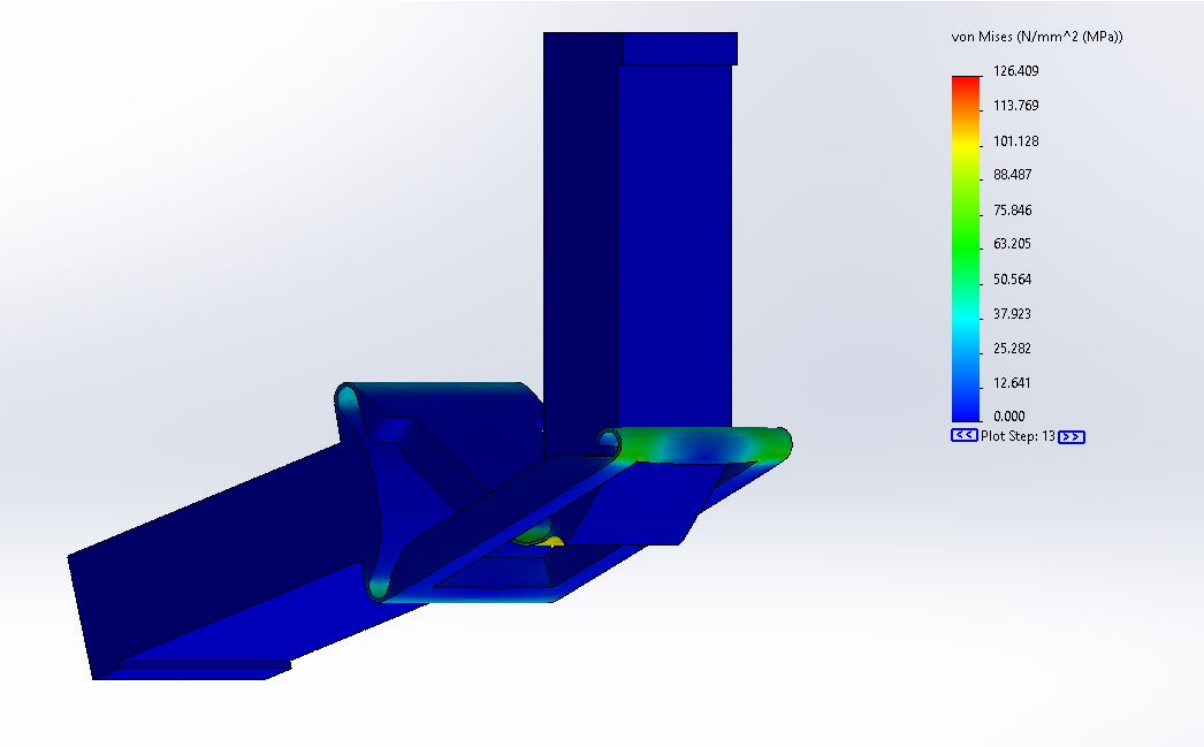

Figure 8. The mechanism in the final position with maximal stresse.

REFERENCES

1. Lower Extremity Amputation. https://www.ncbi.nlm.nih.gov/books/NBK546594/ [Accessed: 20th June 2020].
2. 15 Limb Loss Statistics that May Surprise You. https://accessprosthetics.com/15-limb-loss-statistics-may-surprise/ [Accessed: 20th June 2020]
3. Spoden, M., Nimptsch, U., & Mansky, T. 2019. Amputation rates of the lower limb by amputation level - observational study using German national hospital discharge data from 2005 to 2015. *BMC health services research*, 19(1), 8. https://doi.org/10.1186/s12913-018-3759-5
4. Sukanta S., & Rajesh M,. Mohanty, R.. (2017). Polycentric Prosthetic Knee Joint: A Review. *International Journal of Engineering, Science and Mathematics*, pp 503-509
5. Seymour R., 2002 Introduction of Prosthetics and Orthotics. In, Prosthetics and Orthotics Lower limb & Spinal, (Eds. T. Jules). Lippincott Williams & Wilkins, Philadelphia. pp 10–11.
6. N. Sancisi, R. Caminati, and V. Parenti-Castelli, 2009. Optimal Four-Bar Linkage for the Stability and the Motion of the Human Knee Prostheses, in Atti del XIX CONGRESSO dell'Associazione Italiana di Meccanica Teorica e Applicata. Ancona, pp. 1– 10.
7. Gunston FH. 1971. Polycentric knee arthroplasty. Prosthetic simulation of normal knee movement. *The Journal of Bone Joint Surgery,* 53(2):272-277.
8. Radcliffe CW. 1977. The Knud Jansen Lecture: above-knee prosthetics. *Prosthet Orthot Int*.;1(3) pp. 146-160. doi:10.3109/03093647709164629
9. Huiqun F., Xiufeng Z., Xitai W., Rong Y., Jian L., Li W., Ning Z., Guanglin L., Tao L., Bingfei F., Yoshio I., 2016. A novel prosthetic knee joint with a parallel spring and damping mechanism. *International Journal of Advanced Robotic Systems*.

10. Tsoulfas, G., Bangeas P. I., Suri J. S. 2020. 3D Printing: Applications in Medicine and Surgery. Volume 1, Amsterdam, Netherlands.
11. Howell L. L., 2001. Compliant Mechanisms, John Wiley & Sons, INC., New York, USA.
12. Kosic B., Dragicevic A., Jeli Z., Marinescu G. 2020. Application of 3D Printing in the Metamaterials Designing. In: Computational and Experimental Approaches in Materials Science and Engineering. (Eds. N. Mitrovic, M. Milosevic, G. Mladenovic), vol 90. Springer, Cham. https://doi.org/10.1007/978-3-030-30853-7_10
13. Kosic, B., Stoicevic, M., Jeli, Z., Popkonstantinovic, B., Duta, A., Dragicevic, A.: 3D Analysis of Different Materials Geometry and Simulation of Metamaterial Usage. *FME Transactions,* 47, 349-354 (2019).
14. K. Y. Choi, A. Akhtar and T. Bretl, 2017. "A compliant four-bar linkage mechanism that makes the fingers of a prosthetic hand more impact resistant," *2017 IEEE International Conference on Robotics and Automation (ICRA)*, Singapore, pp. 6694-6699, DOI: 10.1109/ICRA.2017.7989791.

CONTEMPORARY ARCHITECTURAL GRAPHICS THE IMPACT OF AVANT-GARDE MOVEMENTS

Vladan Nikolić
Faculty of Civil Engineering and architecture, University of Niš
PhD., Assistant Professor, vladan_nikolic@yahoo.com

Jasmina Tamburić
Faculty of Civil Engineering and architecture, University of Niš
PhD., Assistant, ministo@yahoo.com

Olivera Nikolić
Faculty of Civil Engineering and architecture, University of Niš
Assistant, o_milosavljevic@yahoo.com

Sanja Spasić Đorđević
Faculty of Civil Engineering and architecture, University of Niš
sanjaspasic@ymail.com

Sanja Janković
Faculty of Civil Engineering and architecture, University of Niš
sanja.jankovic@outlook.com

ABSTRACT

Until the 19thcentury, architecture was the determinant of stylistic changes, after which period painting took over. As a consequence, at the beginning of the 20thcentury, there was a gap between the condition in fine arts, on the one hand, and architecture and applied arts, on the other. Architecture was clearly behind, contributing to the emergence of many avant-garde movements across Europe. Such movements represented the leading force behind the development of architecture as well as new principles and techniques of architectural visualization and presentation. This paper analyzes the impact of avant-garde architectural movements on contemporary architectural graphics. Finding key visual specifics in the architectural representations of avant-garde architects of the 20thcentury, which are also applicable in contemporary visualizations, was the starting point of the analysis. After that, their systematization was carried out.

Keywords: contemporary architectural graphics; architectural visualization and representation; avant-garde movements

1. INTRODUCTION

The majority of avant-garde movements were active during the 20th century. However, the origins of the avant-garde itself may be traced back further in the past. The ideas promoted by the avant-garde proponents were always ahead of their time, innovative and experimental. They had an enormous impact on the future generations of architects. The avant-garde movements in architecture remained marginal initially. Yet, there are examples that confirm quite the opposite, like the development of the metabolist movement in Japan. Modernism and the avant-garde originated in the 18th century. A century before, the necessary philosophical and scientific preconditions

had been created aimed at separating architecture from religious dogma and boundaries of tradition (Butcher et al., 2019). This mainly referred to the perception and presentation of space. In the 17th century, Girard Desargues postulated the basics of projective geometry and established a connection between Euclidean geometry and perspective. A Cartesian coordinate system was defined, which determined the contemporary interpretation of Euclidean space. Jean Du Breuil systematized the rules of construction of linear perspective in architecture. In the early 18th century, Ferdinando Galli Bibien a devised the manner in which to construct perspective from an angle. Gaspard Mongedeveloped descriptive geometry as a branch of engineering in the 18th century, whereas in the 19th century, William Farishincited the contemporary application of axonometric projections (Tepavčević, 2010). Numerous visionary projects were initiated in France during the period of neoclassicism. Étienne-Louis Boullée, Claude Nicolas Ledoux, Jean-Jacques Lequeu etc., created a large number of architectural visualizations that influenced the development of the avant-garde thought in architecture. The 19th century architects had extensive knowledge related to the representation of space, which they exchanged and expanded globally. Significant technological innovations in the manufacture of equipment and materials were brought about by the Industrial Revolution. Architectural sketches were thus regarded not only as ordinary architectural drawings but also as works of art irrespective of objects they represented (Piedmont, 2007).

Figure 1: Visionary neoclassicism as a beginnings of avant-garde thinking and representation of architecture. River inspector's house, Claude Nicolas Ledoux and Temple of Divination, Jean-Jacques Lequeu

2. IMPACT OF AVANT-GARDE MOVEMENTS IN 20TH CENTURY ARCHITECTURE ON CONTEMPORARY ARCHITECTURAL VISUALIZATION

Architecture had been crucial in determining stylistic changes up to the 19th century, after which this role was adopted by painting. Therefore, the beginning of the 20th century witnessed a huge gap between painting, on one hand, and architecture and applied art, on the other. Architecture lagged far behind art, which gave rise to numerous avant-garde movements in the world. (Magomedov, 2000). These movements contributed to a powerful development of new architectural concepts and visualizations. Avant-garde movements completely redefined the principles and techniques of architectural visualization (Nikolić, 2012).

This paper presents several tendencies realized in the avant-garde movements of the 20th century, which are the basis of the contemporary architectural visualization. They are an intensive application of axonometric projections, the use of sketches and diagrams in architecture, the beginnings of the use of the hybrid techniques and composite representations and the definition of one's own visual expression.

2.1. Visual expression

Visual expression represents a recognizable "handwriting" of one architect or a group of architects, achieved by the adoption of certain principles and norms and through practice. It is reflected in the aesthetic and technical consistency of architectural visualizations. The fact that the architectural visualizations of the 19th and 20th centuries became art in their own right led to the creation of powerful and recognizable visual expressions of individual architects and groups of architects. The architects who were the members of the avant-garde movements were focused on presenting visionary projects that remained only on paper in most of the cases. This is the reason

why they were particularly absorbed in the aesthetic and technical aspects of representation. Their legacy had a powerful influence on the contemporary architectural visualization, redefined and improved after the digital turn.

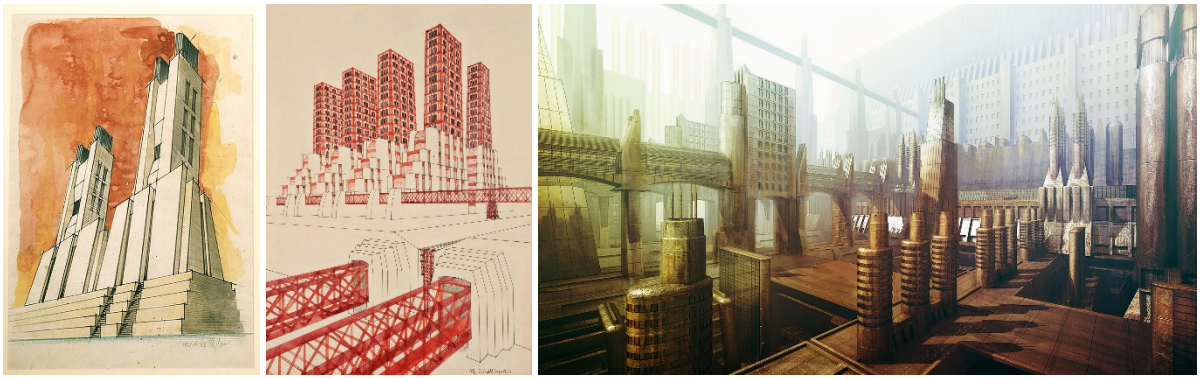

Figure 2: Architectural visualizations of Italian futurists from the beginning of the 20th century and their contemporary interpretation. Project for a monumental, 1914, Antonio Sant'elia (left), Bridge and Study of Volumes, 1914, Mario Chiattone (middle) and Tribute to Antonio Sant'Elia (La Città Nuova), 2017, Julien Berneron (right)

Figure 3: Bauhaus architectural visualisations. Double house, 1924, Carl Fieger (left) and Design for the Reconstruction of the August and Hilda Heriot House, 1936, Atelier Singer-Dicker (right)

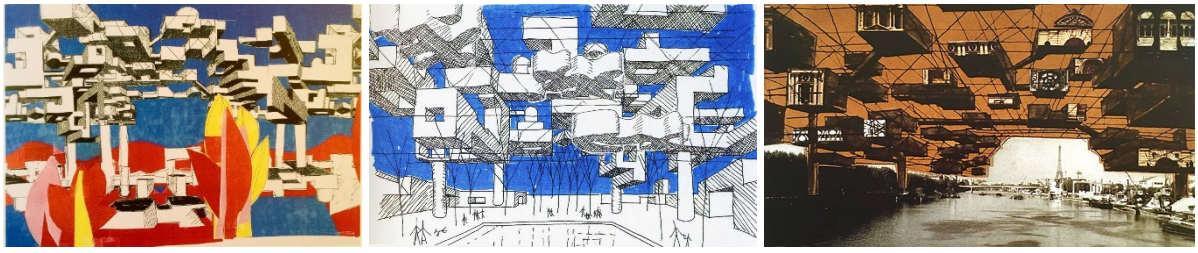

Figure 4: Yona Friedman avantgarde visual expression - a new manner in architectural representations of the 20th century, Spatial city, 1950s

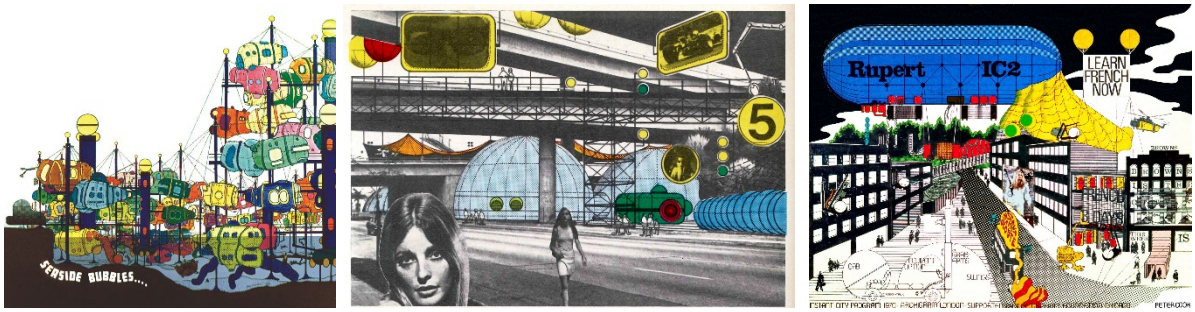

Figure 5: Architectural visualizations in Archigram manner, 1960s, Ron Herron (left) and Peter Cook (middle and right)

2.2. Application of axonometry

A projection system, known as *dengjiao toushi,* has been developing in China since the second century B.C. and corresponds to what is termed axonometry at present. The application of axonometric projections in Europe started in the Renaissance. They were instantly accepted by the engineers who were engaged in designing military buildings and forts, the fact which then determined their name – military perspective. William Farish published the book *On Isometrical Perspective* in 1822 and thus draw attention to the application of axonometry, which continued to develop considerably for the purposes of engineering during the 19th century (Tepavčević, 2010). Shoazi lent an architectural trait to axonometric drawings for the purposes of his illustrations of historical examples and objects. In the 20th century, axonometric projections became essential in architectural representation due to its simple construction and a realistic apprehension of spatial relations in the building in relation to the perspective. Sketches and drawings particularly dominated the works of the architects – members of the avant-garde movements. Axonometric projections are most commonly used for drawing diagrams in architecture in the contemporary architectural visualization (Scolari, 2012).

Figure 6: Application of frontal oblique projection in architectural visualizations
The Red Cube, 1923, Farkas Molnár (left), Spatial city, 1950's, Yona Friedman (middle)
and Part of visualisation, 2019, Emily Russell (right)

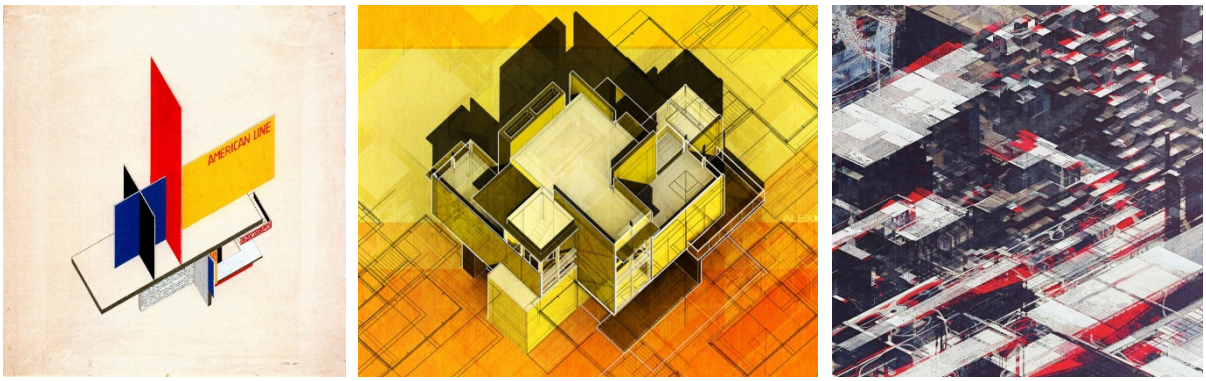

Figure 7: Application of axonometric projection in architectural visualizations
Kiosk, 1948, Herbert Bayer (left), Going Retro, 2012, Alex Hogrefe (middle) and Land of Pixels, Atelier Olschinsky, 2016

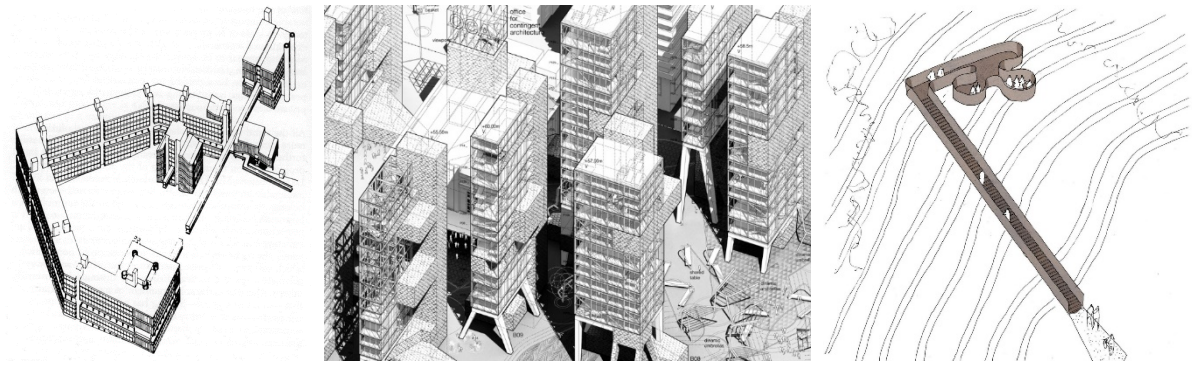

Figure 8: Application of axonometric projection in architectural visualizations
Sheffield University Extension, 1953, Alison and Peter Smithson (left), Badel site, 2012,
Alejandro Londoño, Gonzalo Gutierrez, Valentín Sanz, Toni Gelabert, Sergio del Castillo, Gonzalo del Val (midle)
and Portes Bonheur - le Chemin des Carrières, 2019, Reiulf Ramstad Architects (right)

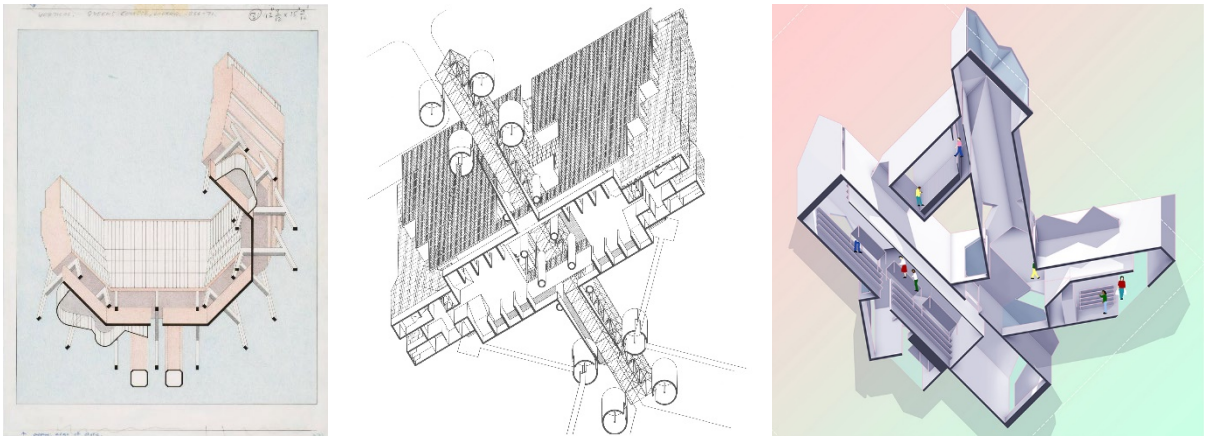

Figure 9: Application of worm's eye axonometric projection in architectural visualizations Queen's College, Oxford, UK, 1966, James Stirling (left), Nursing home, Agra, Switzerland, competition project, 1980, Mario Botta (middle) and Case Study, 2019, Tiffany Chien (right)

2.3. Sketches and diagrams

Sketches in architecture have multiple functions. They are used for the analysis and appreciation of the existing architecture, for the elaboration of new ideas and concepts, i.e. as part of the final presentation. Sketches were first used in the Renaissance, whereas they became an integral part of the process of architectural design in the 19th century. The reason lies in the education that architects gained at the Academy of Fine Arts in Paris. In the 20th century, the sketch became an important part of the research and creative process of the architects of the avant-garde and modernity. The sketches and other drawings created by the avant-garde architects represent preliminary drafts of numerous contemporary architectural visualizations. Particularly inspiring and significant are the works of John Friedman, which had an enormous impact on Archigram and Japanese Metabolist movement, while all influenced the architecture of the 21st century (Smith, 2008; Travis, 2015).

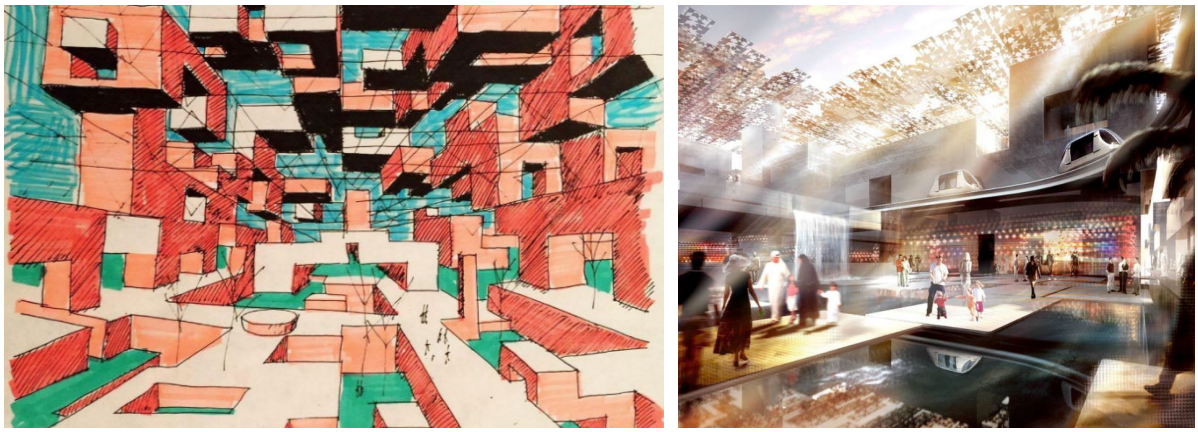

Figure 10: Architectural representation in the form of a sketch and an influence on contemporary visualization Spatial city, 1950's, Yona Friedman (left) and Masdar City, 2014, Foster + Partners (right)

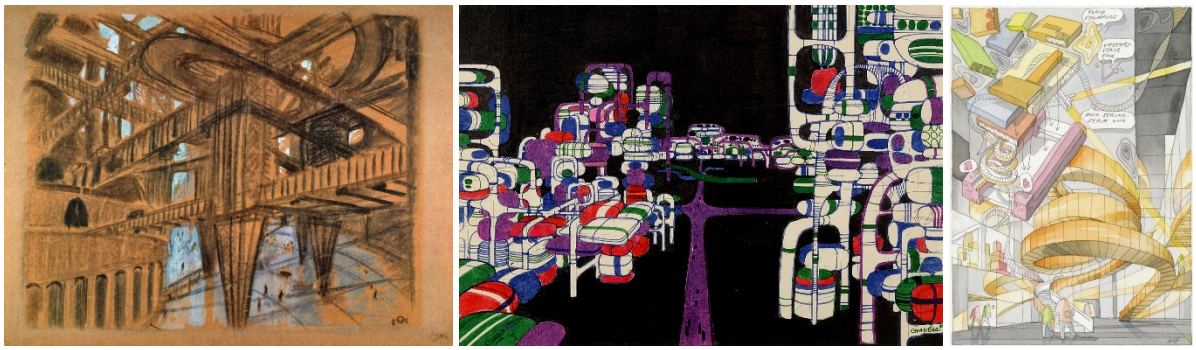

Figure 11: Scenography sketch, Metropolis, 1927, Otto Hunte, Fritz Lang (left), Projet de ville, 1966, Jean-Louis Chanéac (middle) and Experimentarium, 2017, CEBRA, drawing Mikkel Frost (right)

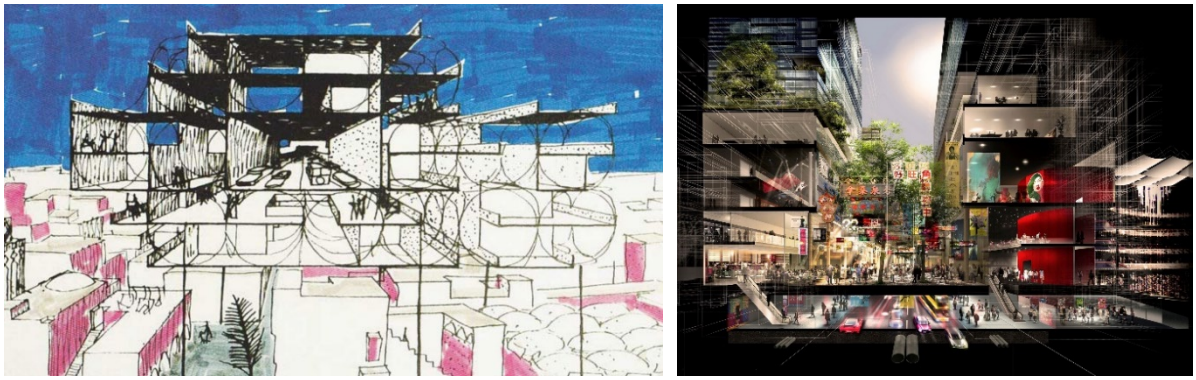

Figure 12: Architectural representation in the form of a sketch and an influence on contemporary visualization
Spatial city, 1959, Yona Friedman (left) and Masterplan for West Kowloon Cultural District, 2011, Foster + Partners (right)

Like the sketch, the diagram is a supplementary tool and visualization of thoughts. Its form can be a sketch or a schematic technical drawing, representing not just the form but also an architectural program. Louis Durand contributed significantly to the implementation of diagrams in architecture in the early 19th century. In the 20th century, diagrams were primarily developed in the avant-garde movements. They were particularly appreciated during the eighties of the 20th century in the works of Tschumi, Eisenman, Koolhaas, SANAA, etc. Toyo Ito was the first to use the term diagrammatic architecture describing the work of Kazuyo Sejima in 1996. The use of diagrams has become common in the works of numerous contemporary architects (Pyo, 2015; Pyo, 2019).

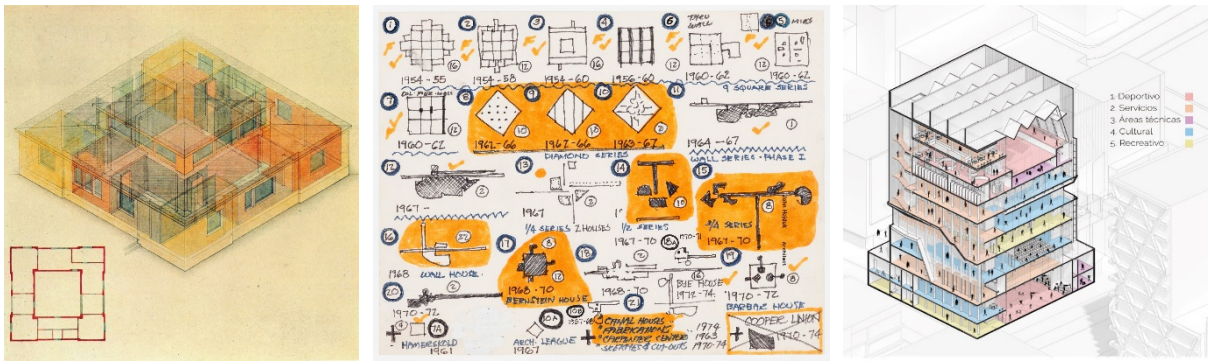

Figure 13: Application of diagrams from different periods of the 20th and 21st century - Haus am Horn, 1923, Georg Muche (left), Chronology of projects 1954–1974, c. 1975, John Hejduk (middle) and Centro de Felicidad, 2019, Arquitecto Luis Calderón (right)

2.4. Hybrid techniques and composite representations

A composite image in architecture is a graphic representation comprised of two or more images (layers). Therefore, the use of several graphic techniques is possible, which is defined as a hybrid image or hybrid graphics. In photomontage, the basis of the composite image is the photograph of the location and the second layer is the graphic representation of the building, both of these images being in the same spatial projection. Potential additional components contain secondary elements of architectural visualization. The examples of this particular type of architectural visualization are to be found in the 20th century architecture, especially the one that belonged to the avant-garde movement. In the time of the manual architectural graphics, this type of representation presupposed the technique of a mere overlapping of photographs, handmade drawings and printed clips. The technique and quality of the composite graphics has been improved by digitalization and has consequently become the dominant way of expression in the contemporary architectural visualization (Gorski, 2015; Nikolic et al., 2014).

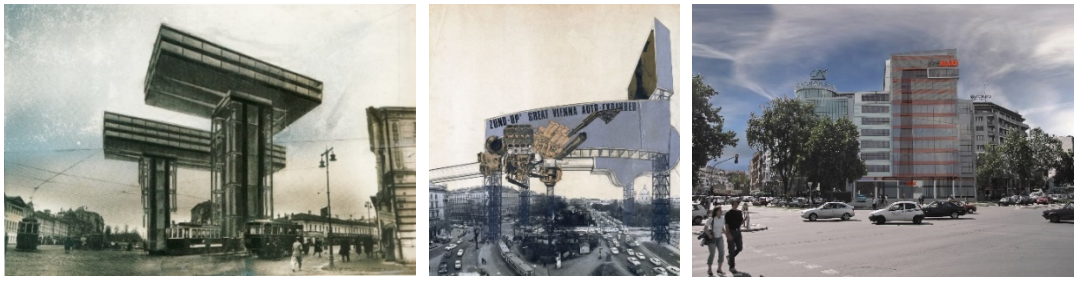

Figure 14: Composite architectural representations - Horizontal Skyscrapers, 1924, El Lissitzky (left), The Great Vienna Autoplatz, Austria, 1969, Zünd-Up (middle) and Office building EyeMaxx, Novi Sad, 2008, Vladan Nikolić (right)

Figure 15: Composite architectural representations - Golden Lane Project, 1952, Alison and Peter Smithson (left), Dwelling City, 1964, Kenji Ekuan (middle) and Daba Gardens, Dubai, UAE, 2009, Vladan Nikolić, Bojan Stojanović, Olivera Milosavljević, Predrag Milosević (right)

Figure 16: Composite architectural representations - Color Design for a Shopping Parade and Cafe-Restaurant, 1924, Theo van Doesburg and Cor van Eesteren (left), Swimming Pool Enclosure for Rod Stewart, 1972, Ron Herron, Archigram (middle) and Interior design, 2016, Taller Independiente (right)

Figure 17: Contemporary composite architectural representations - Pedestrian bridge in Knjaževac, 2020, Vladan Nikolić, Predrag Lukić

3. CONCLUSIONS

This paper analyzes the architectural visualizations created by the avant-garde movements of the 20th century and contemporary architectural visualizations created after the digital turn. The analyzed visualizations of the avant-garde movements, designed during the modern and postmodern periods, were innovative in both technical and aesthetic sense. Contemporary architectural visualizations reflect an evident influence of the avant-garde aesthetics. Certain visual characteristics, established in the 20th century, were transferred to the era of digital technologies. Several crucial tendencies postulated during the avant-garde period can be defined. They are the

necessity to define an innovative and authentic visual expression of representation, the use of axonometric projections in spatial representation, an intensive use of sketches, diagrams and composite graphics.

It is possible to recognize an authentic visual expression in the representations of the architects of each of the avant-garde movements active in the 20th century. Contemporary aesthetics of architectural visualizations developed under their strong influence. The authentic visual expression has been achieved by the innovative application of digital technologies and by redefining the aesthetic principles of the avant-garde movements of the 20th century.

The use of axonometric projections in representations of architectural objects became significant in the 20th century. They were used due to its simple constructions and a realistic presentation of spatial relations in relation to the perspective. In the 21st century, the technical performances of the CAD software have additionally contributed to a widespread use of axonometry, most commonly in creating diagrams.

The use of sketches, which represent an integral part of the process of research and design, has become an important segment of architectural visualization. Contemporary architectural sketches have been improved by digitalization and digital finishing. In the 20th century, the diagram was an essential tool of visual analysis of various characteristics of buildings and architectural objects. In the 21st century, the technology has enabled the creation of more complex and more advanced diagrams.

Architectural visualization in the form of the composite (hybrid) graphics is the result of the avant-garde movements in architecture. There was a series of various types of composite images and drawings that contributed to a realistic representation in the period of manual graphics. The process of digitalization has caused the greatest improvements in the techniques of creating composite graphics in particular.

Acknowledgements

The authors express their gratitude to the Ministry of Science and Technological Development of Serbia for providing partial support for this project (Grant No. TR 036037 and Grant No. TR 036045).

REFERENCES

1. Butcher, M. (Ed.), Pearson, L. (Ed.), 2019. Re-Imagining the Avant-Garde: Revisiting the Architecture of the 1960s and 1970s. Wiley: Architectural Design
2. Tepavčević, B., 2010. Influence of geometric representation of space on contemporary architecture. PhD thesis, University of Novi Sad, Faculty of Technical Science
3. Piedmont-Palladino, S. C., 2007. Tools of the Imagination: Drawing Tools and Technologies from the Eighteenth Century to the Present. New York: Princeton Architectural Press
4. Han-Magomedov, S. O., 2000. Ruski eksperiment u arhitekturi, Istorija moderne arhitekture - antologija tekstova, Knjiga 2/B. Kristalizacija modernizma. Avangardni pokreti, Beograd, Arhitektonski fakultet, pp 403-459
5. Nikolić, V., Nikolić, O., Marković, B., 2012. Human figure in contemporary architectonic presentation. Proceeding of 3rd International Conference on Geometry and Graphics, Mongeometrija 2012, Novi Sad, pp 459-470
6. Scolari, M., 2012. Oblique Drawing: A History of Anti-Perspective. The MIT Press
7. Smith, K. S., 2008. Architects' Sketches Dialogue and Design, Elsevier
8. Travis, S., 2015. Sketching for Architecture + Interior Design, Laurence King Publishing
9. Pyo, M., 2015. Architectural Diagrams 1: Construction and Design Manual. DOM Publishers
10. Pyo, M., 2019. Architectural Diagrams 2: Construction and Design Manual. DOM Publishers
11. Gorski, G., 2015. Hybrid Drawing Techniques: Design Process and Presentation. Routledge
12. Nikolić, V., Nikolić, O., Marković, B., Radović, Lj., 2014. Basic Principles and Techniques in Post Production of the Raster Images in Architectural Presentation. Proceedings of 4th International Scientific Conference on Geometry and Graphics, Mongeometrija 2014, Vol. 1, June 20- 22, 2014, Vlasina, Serbia, pp 354-362

MIMICRY OF GEOMETRY AND DESIGN FROM THE NATURE AND BIOLOGY TO MATERIAL SCIENCE AND ENGINEERING

Lidija Matija
Department of Biomedical Engineering, Faculty of Mechanical Engineering, University of Belgrade, Serbia,
PhD., Professor, lmatija@mas.bg.ac.rs

Boris Kosić
Department of Biomedical Engineering, Faculty of Mechanical Engineering, University of Belgrade, Serbia,
PhD., Assistant Professor, bkosic@mas.bg.ac.rs

Branislava Jeftić
Department of Biomedical Engineering, Faculty of Mechanical Engineering, University of Belgrade, Serbia,
PhD., Assistant Professor, bjeftic@mas.bg.ac.rs

Ivana Stanković
Department of Biomedical Engineering, Faculty of Mechanical Engineering, University of Belgrade, Serbia,
PhD., Assistant Professor, bjeftic@mas.bg.ac.rs

Djuro Koruga
Department of Biomedical Engineering, Faculty of Mechanical Engineering, University of Belgrade, Serbia,
PhD., Professor (retired), djuro.koruga@gmail.com

ABSTRACT

In this paper geometry and design in material science and engineering, which have been an inspiration from nature and biology is investigated. It is found out that symmetry, harmony, and perfection play crucial rule in this mimicry. In the symmetry approach not only symmetry of the crystallography group is included, but also molecular symmetry groups, Kugel and Curie symmetry groups. The criteria of harmony are based on Fibonacci sequences and Fibonacci numbers Φ,-Φ,ϕ,-ϕ. Symmetry and harmony are giving beauty to geometry and design in nature, biology, and engineering. However, in this investigation, perfection is also included (based on the perfect numbers) that gives, besides beauty, a new property of "sublime" to the objects and processes.

In this paper, a few examples of mimicry in relation to nature-biology-engineering based on symmetry, harmony, and perfection are presented. One of the examples of that kind of mimicry is a spiral galaxy- centrioles-solar plants. The second one is molecule C_{60} in space (in cosmic dust), clathrin in the human brain, and C60 in nanophotonics, nanocosmetics, and medicine. However, more examples of biomimicry (from biology to engineering) are presented. One of the more interesting examples is a container for cosmetically use with complex geometry and design based on the pentagonal-hexagonal organization of collagen in human tissue.

According to our investigation, we can conclude that optimization of mass-energy, energy-information, and information-control (regulation) in the nature, biology, and engineering are principle which determinate geometry and design of objects.

Keywords: symmetry, Fibonacci, applied geometry, mimicry, design, optimization

INTRODUCTION

When one observes the geometry of an object in nature or biology, one wonder why that object has that geometry and not some other. The answer to the question becomes even more difficult when one looks at dynamic objects such as insects, animals, and humans. However, the magic word that explains the connection between the geometry (shape of the object), kinematics (elements of the object) and dynamics (regulation of the relationship between parts - whole - environment) is optimization: mass, energy, information, organization, and control [1]. Optimization is a consequence of two pairs of internal opposites and one pair of external object-environment opposites. The first pair of internal opposites is symmetry/asymmetry, and the second pair is harmony/chaos. Depending on the function of the object in the environment, those opposites are reduced to a logical square: selectivity - evolution - overcoming - creativity.

For example, the science of deterministic chaos [2], which originated within metrology (Edward Lorenz), established that the dynamic systems, being nonlinear and dissipative, such as, for example, the atmosphere and biological systems, are sensitive to the initial conditions. Lorenz named this extraordinary sensitivity the 'butterfly effect: 'flapping of butterfly's wings on a flower in Japan causes a tornado in America after a few days, or in some other part of the planet. The human genome exhibits analogous behavior: the union of paternal and maternal chromosomes determines the characteristics of the new-born being. Therefore, the initial conditions of conception (union of maternal and paternal chromosomes), of embryogenesis (organization of the formation of the human organism, which is, as we shall see in the following chapters, actually a 'light being occupied by darkness'), and childbirth (influence of classical and quantum gravitational effects of the environment) are very significant regarding the life and health of the new-born organism. The science of deterministic chaos explains that if the formation of the human organism starts from 'two proximal points', they will be found, after a sufficiently long time, arbitrarily distant from each other, in the next phase becoming close again, finally becoming united. In other words, if the union of the genetic material (chromosomes) is not adequate ('two proximal points'), after the embryogenesis, the defect will be concealed and inactive ('arbitrarily distant'). However, eventually, it will be activated under stress ('re-established proximity'). Therefore, insight into the human genome, embryogenesis, and stress genic factors are of utmost importance for disease prevention, medical diagnostics, and therapy. Although, at first sight, everything seems chaotic, Einstein is right in saying: '...dear God does not gamble...', however, we must add: … although he throws dice. However, this dice throwing is the basis of the law of the distribution of large numbers that correspond to the law on the conservation of information, similar to the laws on the conservation of mass, energy, momentum, etc.

In this paper, we are primarily interested in objects in nature and biology whose principles we can use in engineering, or better understand their structures and functions in order to establish a proper diagnosis, or prescribe therapy.

GEOMETRY OF OBJECTS IN NATURE

Sunflower geometry we choose as an example of optimization in nature, than in biology and as human mimicry in engineering. The key point of understanding the sunflower geometry is icosahedral symmetry which is part of the point symmetry group.

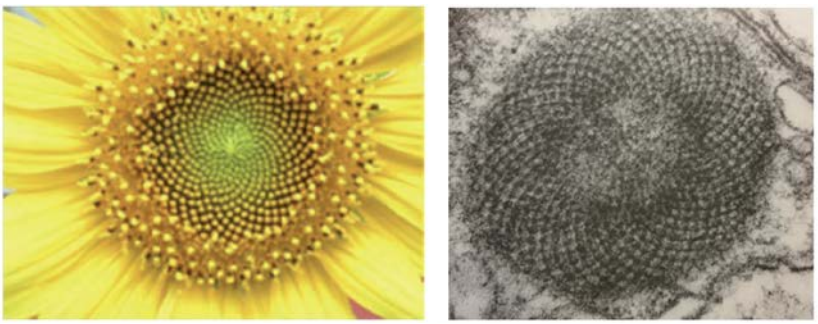

Figure 1. The sunflower seed (left), one of the most obvious examples of the realization of Fibonacci numbers in nature (realized in 2D), and the toroidal organelle (realized in 3D) within eye cells for night vision (rods) enabling hyperpolarization of the cell (right). These two examples demonstrate the realization of Fibonacci numbers as the mathematica naturalis in nature and biological systems.

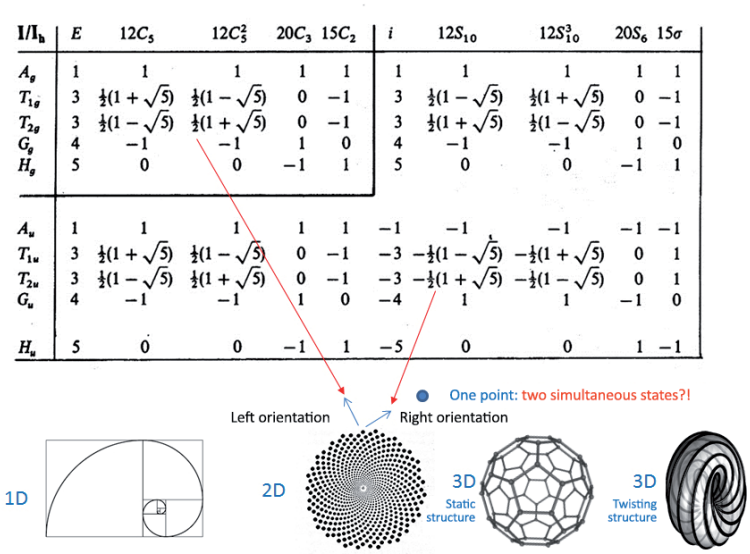

Figure 2: Realization of icosahedral symmetry geometry in 1-, 2- and 3D were geometry, internal structures, energy, and information are optimizing. As one can see only some of the energy states (T1g, T2g, T1u, and T2u) of structures and processes follow Fibonacci numbers.

OBJECT GEOMETRY IN BIOLOGY

As the essence of the photon and electron is unknown, neither are we aware of the essence of our existence, i.e., of the life phenomenon. However, we do know many characteristics of the proton and electron, and regarding life, we know that, according to Leibniz, after the peace of mind, health is the most important issue. This monograph originated from the need to contribute to as efficiently as possible health preservation in a natural way, using light. To achieve this, it is necessary to be well acquainted with structural, energetic, and informational foundations of biomolecules, that is, with organization and regulation mechanisms of the human organism. After we have understood the laws governing the main rules of biomolecules, which are essential as life itself, the next step is to design a device generating structural organization of photons according to the same laws that govern biomolecules' organization, that is, in the way biochemical/ physical processes are realized based on Gibbs free energy. Biomolecules are, by their structure and energy, via entropy, related to information. This will enable the newly created light to influence the information states, and thus act on structural-energy-information processes of biomolecules as well. Structuring photons, according to some of the biomolecular features, should follow the tally principle, the ancient method of recognition, pairing, i.e., identification of ownership (it was used by millers; a farmer would bring a sack of wheat, take a shorter slim stick, notches would be made on the stick, it would be split longitudinally so that on both parts notches would be visible.

Clathrin is one of the more important structures in the brain. It is a complex protein structure, composed of two main protein chains: the 'light' chain (25 000 D) and the 'heavy' chain (190 000 D). The overall molecular mass is about 215 000 D (Dalton: 1D ~weight of an atom of hydrogen), the size is 20 to 80 nm. Human chromosome 17 is responsible for the synthesis of the 'heavy' chain, and chromosome 22 for the synthesis of the 'light' chain. These two protein chains form a more complex structure called the triskelion (trimer). It was discovered in 1969 by the Japanese scientists Kamaseki and Kadota using the electron microscope [3] and extracted for the first time in 1975 by Barbara Pears. Clathrin is found in many human tissues as a carrier of substances such as neurotransmitters. It also clears the cell debris into the extracellular space. The triskelion forms pentagons and hexagons, so the clathrins in the CNS, composed of 36 triskelions, form 12 pentagons, and 20 hexagons, while in other tissues they are made of 12 pentagons and a varying number of hexagons (Figure 3). Clathrin of the CNS is the most perfect symmetrical structure that can exist in nature based on the law of point symmetry. This is the icosahedral symmetry group (dual to dodecahedron) whose energy states T_{1g}, T_{2g}, T_{1u} and T_{2u} are determined by the ordered quadruple Φ, $-\Phi$, φ, $-\varphi$ (1.61803…, -1.61803…, 0.61803…, -0.61803).

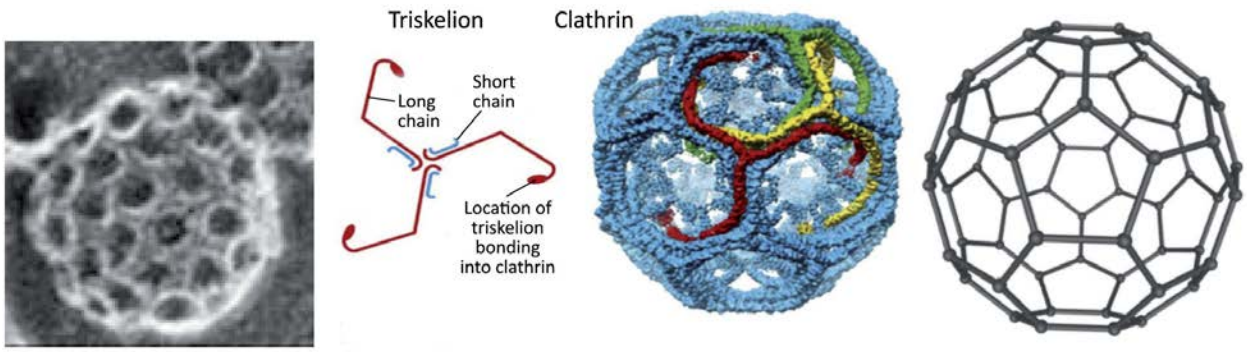

Figure 3. Microscopic image of clathrin (left), triskelion shape, and the network of 36 triskelions forming clathrin with 12 pentagons and 20 hexagons. Schematic structure with pentagons and hexagons (right) is displayed.

Microtubules did not attract attention until, in 1974, the New York Academy of Sciences organized the first scientific meeting on the subject, with the emphasis on the structural and biochemical aspects of microtubules. This topic aroused the interest of researchers all over the world, so the same Academy organized in 1986 a scientific conference on the dynamic aspects of microtubules [4]. It was demonstrated that microtubules have an important role in biology, in intracellular transport, cell shape definition, and as the main compound of the cell mitotic spindle. Microtubules also create more complex structures such as cilia, flagella, and centrioles [5].

The structural (spatial) packing of α and β tubulin into a protofilament of 13 subunits complies to the rule 1, 2, 3, 5, 8, 13..., followed by 4, 6, 7, and ending with 9, 10, 11 and 12. From this sequence we observe the ratios 1:2 = 0.500, 2:3 = 0.666, 3:5 = 0.600, 5:8 = 0.625, 8:13 = 0.615, 13:21 = 0.619, seeing they oscillate between 0.5 and 0.66 and that the convergence point belongs to the category of number φ = 0.61803. Observing inverse ratios, we have 2:1 = 2.000, 3:2 = 1.500, 5:3 = 1.666, 8:5 = 1.600, 13:8 = 1.625, 21:13 = 1.615, and the convergence point belongs to the category of number Φ = 1.61803. Since microtubules are structured as thirteens', the biophysical characteristics (dipole moments, temperature, magnetism, etc.) that depend on microtubules are within the limits $1.615 \leq \Phi \leq 1.625$.

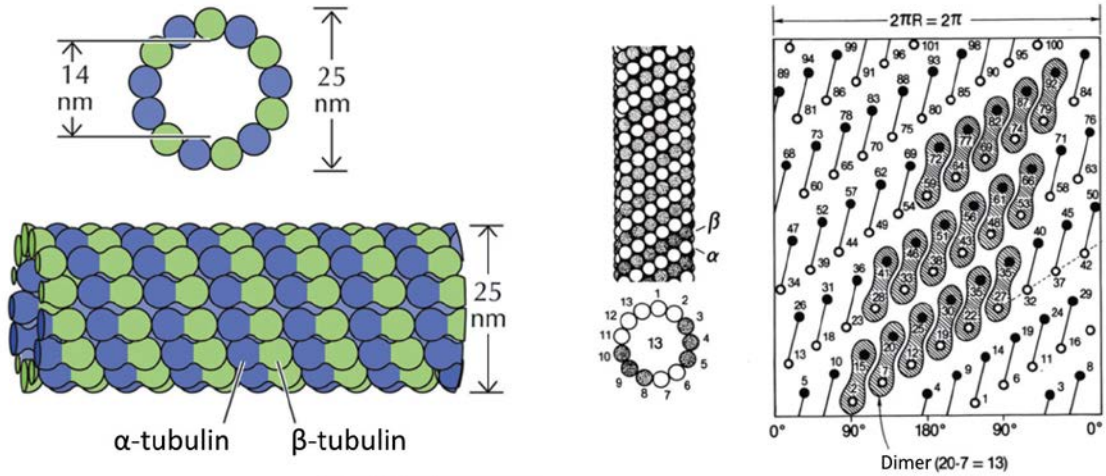

Figure 4: Schematic presentation of the microtubular configuration (MT) with 13 protofilaments, of the inner diameter 14 nm, outer diameter 25 nm, random length (from several nm to several tenths of μm) depending on cell type (left). When the microtubular cylinder is flattened in the plane (right), we obtain the packing sequence of subunits of α and β tubulin, which form a dimer. The packing sequence is such that the dimer always has the value 13, as the number of protofilaments in MT (15 - 2= 13, 20 - 7 = 13, etc.).

The centriole is the central enigma of molecular biology. What are the physical processes behind such a beautiful geometric figure, inciting not only a feeling of beauty but of sublime, because it resembles galaxies (‘a cosmic New York’)? This is the question we tried to answer 30 years ago. Ii is discussed this with many biologists, but no satisfactory answer was found; the majority displayed the attitude: it is a structure having a so and so function. Most of them were satisfied with this answer. Why is it so was not of much interest to them from the professional viewpoint (because they were taught so); however, some expressed interest to find out. Our model is based on the following mathematical and physical premises: for a random point having coordinates x, y, z, uniformly distributed within a sphere of radius r, the mathematical expectation of the point distance from the center of the sphere should be determined. Thus, the accumulation of points is at the sphere radius from its center which generates ‘the enneads’ with triplets (Fig.5).

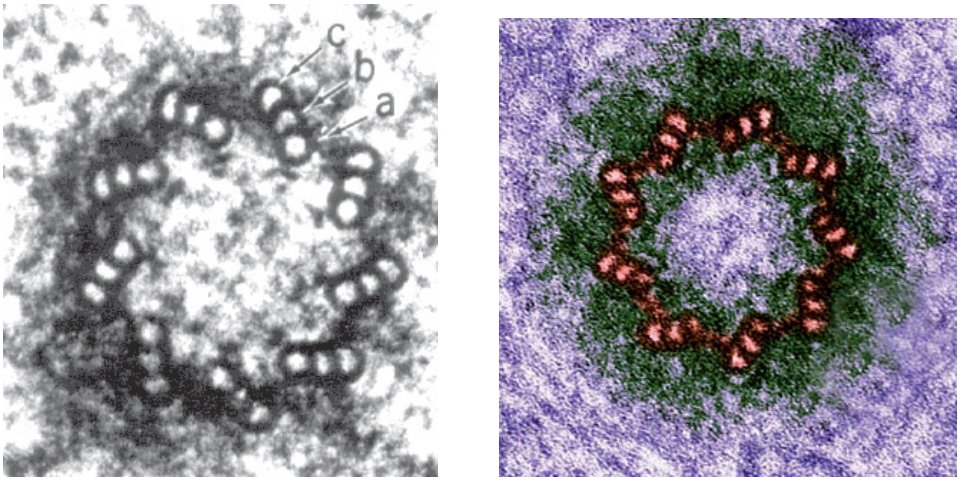

Figure 5. Left and right centriole organization: the microtubule a has 13 protofilaments, while microtubules b and c have 10 protofilaments each (left). The angle of the angulation of the microtubule triplet is 222.50, which is $360^0 \times 0.61803 = 222.5^0$ [5].

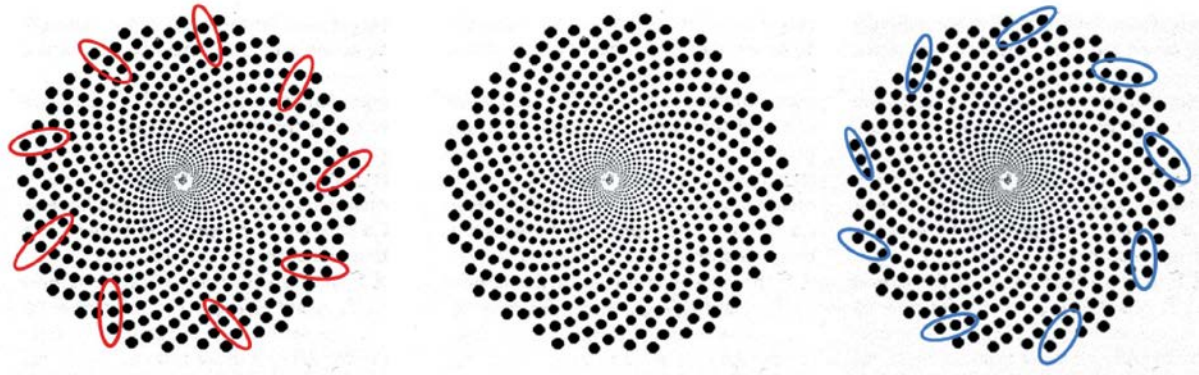

Figure 6: Discrete two-dimensional representation of the icosahedral energy eigenvalues T1g, T2u, T1g, and T2g, where the peripheral angle (of each point on the circle circumference) is 222.50 (middle). We observe left and right orientation (as in biology, Fig.5), where the three last points represent microtubular protofilaments forming centrioles.

Since the values generating φ and Φ are discrete, the curves oriented from the center (Figure 6, *left* and *right*) are also pointwise structures generating the law of icosahedral symmetry. This proves that in centrioles, the energy and structure are symbiotically coupled according to the icosahedral (dodecahedral) symmetry.

GEOMETRY OF OBJECTS IN ENGINEERING

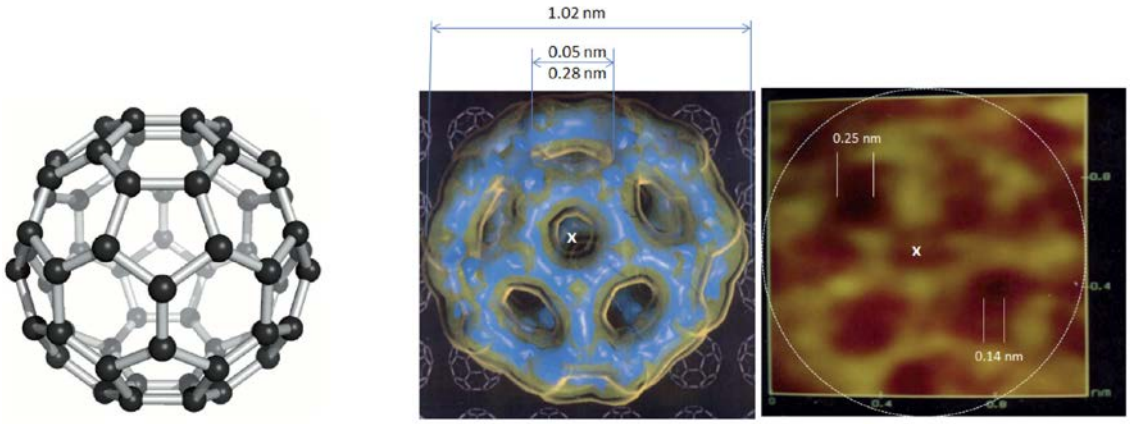

Figure 7: The theoretical model of the C60 molecule from 1985, immediately after it was discovered by Kroto, Curl, and Smalley of Rice University, USA (left); the C60 molecule model based on quantum-mechanical calculations from December 1991, the cover page of Science (middle); the first STM image of the C60 molecule, April 1992, Nano- Lab, Faculty of Mechanical Engineering, the University of Belgrade (right). It is striking that all three images of molecules are more than similar, and the most interesting fact is that quantum theory and experiment coincide completely [6].

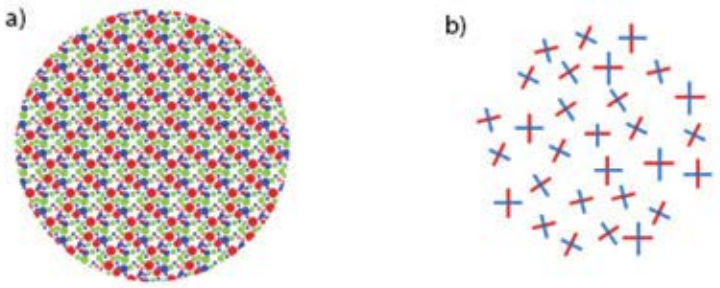

Figure 8: Geometry of electrical and magnetic planes of polychromatic diffuse light as a random set of photons with respect to energies, and **b)** random position of the electromagnetic photon rotating field (blue– electric photon field, red– magnetic photon field); photons have random orientation along the light propagation direction (rays are not parallel, they can intersect).

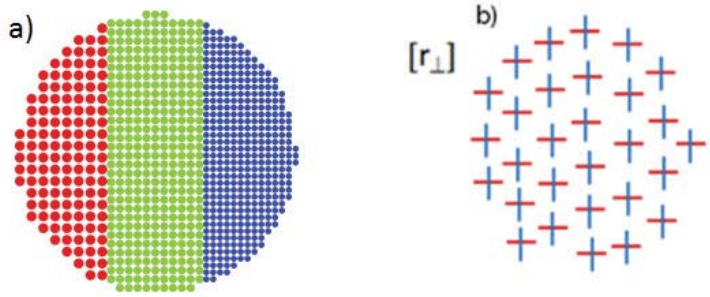

Figure 9: Geometry of electrical and magnetic planes of a) Polychromatic vertically polarized light as an ordered set of photons with respect to energies, and b) fixed position of the electromagnetic photon field (blue– electric photon field, red– magnetic photon field), and complete orientation of the electromagnetic photon field along the light propagation direction (rays are parallel). As the electrical field (blue) is vertical, this type of polarization is called the vertical linearly polarized light.

The basic similarities and differences between the vertically and horizontally polarized light and the hyperpolarized light were presented above. The hyperpolarized state of photons is the ground energy state of photons ($E0$) due to its structure based on the quantized *orbital angular momentum* (OAM) and *spin* (producing *half quantization* of the ground energy state of the photon $E0 = . hv$). Diffuse, vertically polarized, horizontally polarized, circular, etc., states are only possible particular solutions at higher energy levels $E1 = 3/2\ hv$, $E2 = 5/2\ hv$, $E3 = 7/2h\ldots$, (consequently, the difference between energy states is *one quant*, hv), therefore the basic principles of quantum mechanics are not violated.

Comparing Figures 8, 9, and 10 we observe basic similarities and differences. Diffuse light is, figuratively speaking, „wild“ regarding photon orientation, rotation of the electromagnetic photon field, and organization, while according to the overall effect it is very complex. In linearly polarized light „wild“ photons are ordered („militarization“), they are organized according to energies, oriented along a direction, no rotation of the electromagnetic photon field is present (it is fixed; when the electric component is vertical).

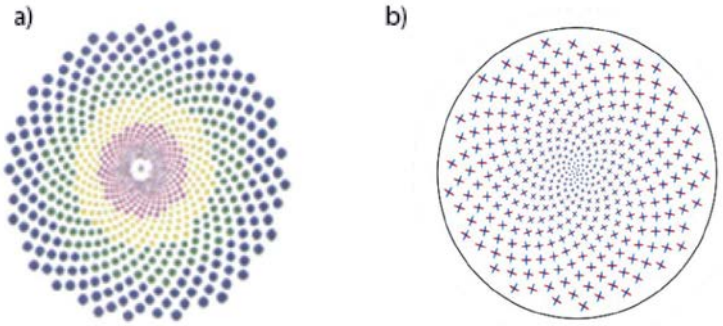

Figure 10: Comparative illustration of geometries of diffuse (Fig. 8), vertical linearly polarized (Fig.9), and hyperpolarized light. The major difference is in the orientation (geometry) and organization of electromagnetic photon fields. In all three cases, the electric (blue) and magnetic (red) field are mutually orthogonal. In diffuse light, the EM field of each individual photon is „twisting“, alternatively one moment to the left, one moment to the right; viewed in entirety, the EM photon fields are randomly oriented. In the vertical linearly polarized light, the EM fields are oriented strictly vertically, and photons are organized into planes according to energy levels (wavelength/frequency/wave numbers). In the hyperpolarized light, the EM photon fields are organized into curved planes according to the Fibonacci laws, photons are organized according to energies, so that the „half quantization“ principle holds for the total orbital angular momentum, consequently also for energy, based on Planck’s constant and frequency

The system for the generation of hyperpolarized light has three main elements: (1) diffuse light source, (2) polarizer transforming diffuse light into the vertical linearly polarized light, (3) nanophotonic polarizer transforming vertically polarized light into hyperpolarized light.

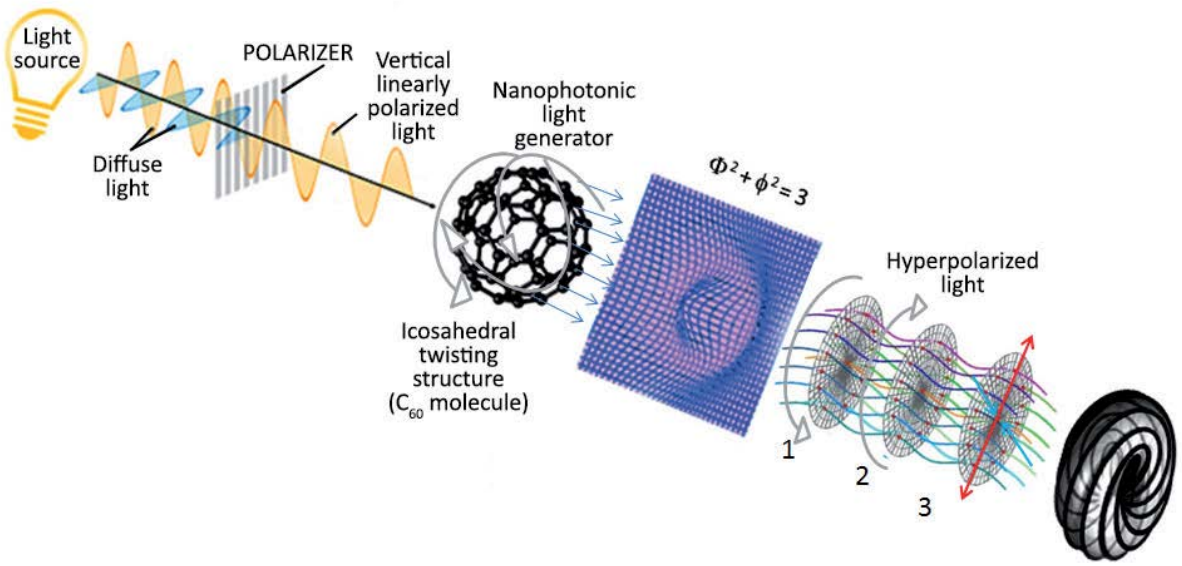

Figure 11: Schematic representation of how the geometry of electro-magnetic planes from diffuse trough polarized to hyperpolarized is changed. The key element is the icosahedral twisting structure (C60 molecules with icosahedral structure/energy properties incorporated into the polymer material) generating photon distribution by creating a 2D energy membrane [Φ2+φ2=3] which „filters" propagating photons according to the Fibonacci law [Φ, φ]. The final output is a Fibonacci twisting torus resulting from the dynamics of three (1, 2, 3) energy forms (left helix φ, right helix Φ, and attractive-repulsive interactions determining the value at each intersection of the left and the right helix).

Figure 12: Geometry of solar cells for optimal collection of solar energy: for half of the day, orientation to South (*left*), and for all-day (right). Solar cells have a position according to Fibonacci law. This 19.9MW Gemasolar Concentrated Solar Power (CSP) plant in Seville, Spain is the world's first commercial-scale CSP plant featuring a central tower receiver with thermal storage capabilities that have commenced supplying electricity to 25,000 homes in the Andalucia region of Spain. The plant is expected to save more than 30,000 tonnes of CO2 emission a year.

CONCLUSION

In this paper, we have shown how the geometry of objects or processes is related to its function in relation to the environment.

Nature and biological units are optimal systems in terms of mass, energy, information, organization, and management.

Engineering is inspired by the optimization of nature and biological systems in the creation of technical systems

REFERENCES

1. Koruga, Dj, 1992. Neuromolecular computing, Nanobiology, 1(1) pp.5-24.
2. Schuster, H.G. Just, W. 2005. Deterministic Chaos: An Introduction, Wiley-VCH Verlag GmbH &Co, Weinheim.
3. Kamaseki, T., Kadota T., The vesicle in a basket. *J. Cell Biol*, 42:202-220, 1969.
4. Soifer, D, 1986. Dynamic aspects of microtubule biology, Annals of the New York Academy of Sciences. vol. 466, New York.
5. Dustin, P., *Microtubules*. Springer-Verlag, Berlin, 1984.
6. Koruga, Đ. S. Hameroff, J. Withers, R. Loutfz, M. Sundershan, 1993. Fullerene C_{60}: History, Physics, Nanobiology, Nanotechnology. North-Holland, Elsevier, Amsterdam.

ON POSSIBILITIES TO ENCODE ARTISTIC STYLE AND MANNER PRESENT IN A CONCRETE ARTWORK USING MICRO-PHOTOGRAMMETRY AND MATHEMATICAL STATISTICS/PROBABILITY TO PROCESS THEIR GEOMETRIC DETERMINANTS

Djordje Djordjevic
University of Belgrade – Faculty of Architecture, Belgrade / Serbia
PhD., Assistant Professor, djordje@arh.bg.ac.rs

Mirjana Devetakovic Radojevic
University of Belgrade – Faculty of Architecture, Belgrade / Serbia
PhD., Assistant Professor, mirjana.devetakovic@arh.bg.ac.rs

Nikola Popovic
University of Belgrade – Faculty of Architecture, Belgrade / Serbia
Assistant, nikola.popovic.bk@arh.bg.ac.rs

Gordana Djukanovic
Faculty of Forestry, University of Belgrade, Serbia
PhD, Assistant Professor, gordana.djukanovic@sfb.bg.ac.rs

ABSTRACT

This paper defines a procedural approach intended to scientifically encode artistic style and manner exhibited in a concrete artwork - based on quantifying their descriptors of geometric nature previously professionally identified as subject-related due to their dominant presence and/or their value-wise importance. Such encoding is a specific authentication process whose purpose is to define an ID-card of a concrete artwork or an artist's overall creative epoch the analysed works belong to. Doing so, it also becomes feasible to scientifically determine the fact whether and with which level of probability ("threshold"), a particular artwork of an initially unknown artist, is possible to be classified in the opus of a presumed artist i.e. of her/his corresponding creative epoch.

To explain the procedure as comprehensively as possible, only one geometric-wise descriptor of artistic style and manner is analysed: "thickness of the painting-layer" – as their dominant indicator present on the chosen experimental painting. This quantifying is realized in a two-step activity which is carried out: (i) by using contemporary micro-photogrammetric technique and related equipment (to digitize the artwork, namely, to acquire and extract the mentioned descriptor), and (ii) by performing relevant statistical management that includes probability calculation, analysis and estimation of cross-referenced previously digitized data. Goal-directed Id-card is constituted by a set of those calculated outputs.

Keywords: Micro-photogrammetry, Geometry, Architecture, Fine & Applied Arts, Mathematical Statistics, Probability

1. PREVIOUS RESEARCH AND INTRODUCTION REMARKS

Sophisticated and extremely costly technology and equipment has been used for decades with limits in the field of visual arts, applied arts, including artwork curating and preservation, because only wealthy subject-related institutions might have the privilege to own it. Thus, for example, X-rays, laser- and MRI-scan technology (on one side) and radio-isotopes and spectral analysis (on the other side) are considered to be the leading techniques used for complex and extremely precise analysis of artworks and artefacts from various aspects (temporal, biochemical, physical and chemical, including morphological i.e. structural-geometrical). Once a set of relevant data has been acquired as described, it is possible to digitize entire subjects of interest (by generating precise 3D models), and, then investigate their outward and inward structure in real time, to date them and to define bio-chemical, physical-chemical characteristics of applied materials, including also the levels of spontaneous degradation as well as possible present (non)intentional damages (either visible or unnoticeable with the naked eye) (Chandler et al., 1996; Bennett, 2015; Rogerio-Candelera, 2015).

On the other hand, previous research pertaining to aspects of applying micro-photogrammetry in the aforementioned areas, is dominantly directed at finding a cost-effective (and, thus, more available) but also as exact methods to assess levels of structural degradation of materials, that the analysed artworks are made of (as consequences of an impact of a broad spectrum of inner and/or external factors of the aforementioned nature – revealed throughout their long-term exhibiting and/or in the course of conservation works) - all aimed at choosing a more appropriate manner to store, exhibit and preserve them in the future (Mancuso et al., 2015; Kumar et al.,2019; Cornille, 2005; Sims-Waterhouse et al., 2017; Guerra, 2018; Del Sette et al., 2017).

Additionally, Jiang & Kim (2019) demonstrated a method intended to recognise artwork paintings, as they are shown on panorama (360-degree) images. It was performed by applying a sophisticated ComputerVision technique, based on the usage of both: adaptive rectilinear projection and optimized affine scale-invariant feature transform (to efficiently rectify perspective distortions).

On the other side, there are several important investigations that more directly refer to the scope of this paper, but not completely - they "meet" it in some aspects only: (a) subjects of analysis were presented by flat/planar artworks (paintings) exclusively, and (b) presented colourisation (pigmentation) and brush stroke were primarily used as relevant authentication descriptors, capable to efficiently identify corresponding painters. So, Widjaja et al. established a method to identify painters using colour profiles of skin patches on painting images – based on exploration of various colour models which makes it possible to accurately represent the colour profiles (by comparing various implementations of multiclass support vector machine classifiers). Also, Montagner et al. (2016) investigated a tool to support authentication studies of paintings (attributed to the Portuguese modernist Amadeo de Souza-Cardoso). The aim was to find a quantitative indicator for authenticity, and to map the image of the analysed paining that indicates the areas where materials not coherent with the painter's palette were detected (if any). To do so, a set of information that relate to the presented pigment characteristics and analysed brushstroke characteristics were quantified (brushstroke analysis was performed by combining Gabor filter and Scale Invariant Feature Transform, while hyperspectral imaging and elemental analysis were used to compare the materials in the painting with those present in a database of oil paint tubes used by the artist himself).

Additionally, Hong and Kim (2019) investigated how to differentiate copyrighted art paintings from images that contained them (such as those placed in film scenes or TV programs, as a decoration), in order to prevent any copyrights infringement. They proposed a method based on comparison between local visual features of the examined image and the concrete, so called, "deep learning based object detector" - exercised with relevant data collected in advance (capable to represent the original artwork that relate to).

Having in mind the above mentioned, Djordjevic et al. (2019) tried to outline a more general and affordable concept intended to scientifically encode artistic style and manner exhibited in a concrete artwork (to authenticate it, namely, to define its ID-card) - based on quantifying their relevant descriptors of geometric nature previously professionally identified as subject-related due to their dominant presence and/or their value-wise importance. More precisely, introduced basic principles were general - ready to be applied with ease to all types and scales of artwork's mediums of physical nature (not only to paintings). Additionally, instead of operating an expensive ComputerVision Technology (otherwise, profusely employed nowadays as mentioned above), the authors' suggestions implied to use an affordable (money-consuming) photogrammetry technique, coupled with mathematical statistics and probability theory. To make it possible to easily recognize/extract/acquire relevant geometric-wise descriptors (as indicators of authenticity) from almost planar artworks (paintings, for example), that methodology alluded the usage of micro-cameras with large magnification (concretely, the usage of micro-photogrammetry).

The said investigation, as such, can be treated a conceptual foundation of the current research. So, the aim of this paper is to define concrete execution steps that rely on founded basic principles. To explain the procedure as comprehensively as possible, only one geometric-wise descriptor of artistic style and manner is analysed: "thickness of the painting-layer" – as their dominant indicator present on the chosen experimental painting. This overall quantifying is realized in a two-step activity carried out: (i) by using contemporary micro-photogrammetric technique and related equipment (to digitize the artwork, namely, to acquire and extract the mentioned descriptor), and (ii) by performing relevant statistical management that includes probability calculations, analysis and estimations of cross-referenced previously digitized data. The goal-directed Id-card is constituted by a set of those numerical outputs.

Bearing in mind the aforementioned, it can be expected that this research and its outcomes will also be innovative and important for the next reasons:

- for its topic-wise framework which steps out of the previously mentioned areas of existing researches and conceptual approaches – enabling thus the geometric descriptors of the artist's creative style and manner (either: of each of his/her separate work or of the overall creative epoch the analysed works belong to) to be practically used (extracted and quantified),
- for its principal goal, expressed in an ability to scientifically determine the fact whether and with which level of probability ("threshold"), a particular artwork of an initially unknown artist, is likely to be classified in the opus of a presumed artist i.e. of his/her corresponding creative epoch, and
- for an evident potential it be broadly applicable in museology/heritology practice in the future, because of the usage of sophisticated cutting-edge but cost-effective mathematical and micro-photogrammetry software (and related not-expensive equipment).

2. FUNDAMENTALS OF INVESTIGATED PROCEDURAL APPROACH

2.1. Initial Considerations

Depending on a concrete articulation of the artist's expression (related to the geometrical/texture—wise nature), her/his "fingerprint" can be defined/coded using various goal-relevant creative style and manner descriptors, such as:

- Thickness change over the finishing painting-layer, including brush stroke directions (as a part of paint-applying technical manner) /Fig. 1 (a, b) /, and
- Gouge change over the finishing material-layer (related to its shape and dimension), including inclination and direction change of the used carving tool (such as chisel), as part of an applied carving technical manner (Fig. 2 (a, b) – carving in wood and Fig. 3 – various forms of decorative picked/carved façade).

(a) (b)

Figure 1: **(a)** Painting made by Dragan Kunic (untitled). Oil on canvas /private collection of the author of this paper/ **(b)** Painting made by Biljana Damjanovic (untitled). Oil on chipboard /private collection of the author of this paper/

(a) (b)

Figure 2: **(a)** "The Witches". Author: Hans Baldung Grien. Relief on wood /New York Metropolitan Museum collection/ /photo downloaded from the website: https://www.metmuseum.org/art/collection/search/336235, Available on March, 2020/ **(b)** Wall art in wood. Author: Jude Fritts. Carving in wood /photo downloaded from the website: http://www.judefritts.com/safe-images/chisels%20&%20knives.jpg, available on March, 2020/

Figure 3: Various types of decorative picked/carved façade
(Author of the photos: arch. Mirjana Devetakovic Radojevic, Ph.D.)

For clarity reason, only one artistic style and manner descriptor: "thickness of the painting-layer" will be used here as a unique quantitative indicator of the authenticity of a geometric nature.

Also, it is important to underline that the achieved levels of reliability and accuracy of the performed coding are not focal points of this research and, thus, will not be evaluated and discussed here at all. Of course, as it has already been theoretically and practically known/proven, those levels depend on a variety of factors, such as: (a) relevancy and number of selected geometry-wise descriptors of the author's creative style and manner which are present on targeted artwork (evaluated previously as such after conducting a broad professional expertise), (b) possibility to measure (i.e. to scientifically quantify) the chosen descriptors - by applying an investigated methodological approach so as to achieve the estimated/wanted level of accuracy and precision of that measure, (c) number of analysed artworks of the same artist previously analysed by an expert and declared from statistical viewpoint adequate representative samples, namely, relevant "artistic style and manner fingerprints", (d) quality of used photo-equipment (respecting general close-range photogrammetry/micro-photogrammetry requests), (e) number and quality of digital micro-photos (taken in line with general shooting recommendations related to requirements of close-range photogrammetry/micro-photogrammetry), (f) achieved quality of micro-camera calibration outcomes, and (g) achieved quality of consequently photogrammetrically processed micro-photos (respecting general recommendations of both: close-range photogrammetry/micro-photogrammetry data acquisition and acquired data processing by using chosen photogrammetric software) (Sutton et. al., 2007; EosSystems Inc.: Photo modeler Scanner Tutorial; EosSystems Inc. (Expert's team)., 2012; Lopez, 2012).

2.2. Chosen Experimental Artwork/painting

In order to introduce procedural steps intended to code an artwork from the mentioned morphological, i.e. geometrical/texture-wise aspect: "thickness of the painting-layer", an experimental study-case relating to a painting by Biljana Damjanovic is singled out. It is naturally done as the chosen descriptor predominantly expresses the artist's technical-wise style and manner /Fig. 1 (б)/. The dimensions of the painting (in centimetres) are 17/24. Its painting-specificity is clearly visible on the presented segment of the said artwork, taken by a micro-camera under 1600x magnification / Fig. 4 /.

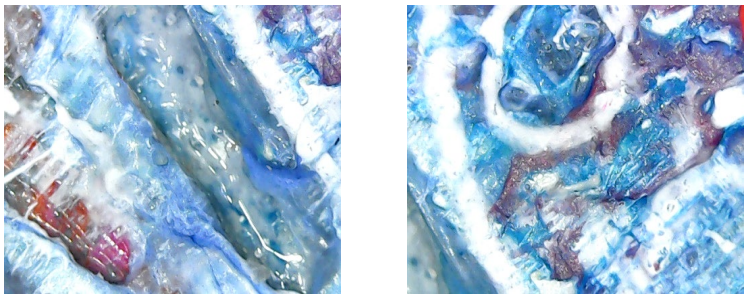

(a) (b)

Figure 4: Analysed aspect of artistic style and manner of Biljana Damjanovic is clearly visible on micro-photos of a randomly chosen representative segment of her painting (outlined by red-coloured oval visible on Fig. 1 (b))

2.3. Software and Equipment Needed

To efficiently investigate the chosen study-case, the following equipment is used:

- PC
- Hi-Res HD micro-camera (hereby, up to 1600x magnification),
- Photo reflector as a source of artificial lighting and uniform illumination,
- Photogrammetric software (hereby: EOS-Systems Inc. Photomodeler Premium), and
- Software used to analyse and mutually compare various characteristics of meshed 3D-models (hereby: CloudCompare /"C2C").

2.4. Main Procedural Steps

2.4.1. Micro-photographing and Photogrammetric Processing of the Photos Taken

Using a micro-camera and a source of artificial lighting (to achieve proper characteristics of illumination), it is necessary to take an adequate number of micro-photos of the entire painting's surface. According to both the dimensions of the finishing-layer and the recommendations that refer to stereoscopic photographing for the purposes of a close-range photogrammetry/micro-photogrammetry, the needed number of digital shots that ought to be taken is approx. 3264 (3264=34x96) (Rogerio-Candelera, 2015; Mancuso et al., 2015; Kumar et al., 2019; Cornille, 2005; Sutton et al., 2007**).** However, as concerns this experimental study-case, only an outlined segment of the artwork is micro-photographed (and consequently processed). The resolution of all stereoscopically taken digital images (in pixels) is 2560x1920.

Then, mentioned set of acquired "representative" micro-photos are processed using a chosen photogrammetric software, with respect to corresponding recommendations **(**Sutton et al., 2007; EosSystems Inc.: Photo modeler Scanner Tutorial).

The result/sub-output of that photogrammetric processing phase is a raw point-cloud which is triangulated consequently and converted into a photo-realistically textured 3D-model in the form of 3D-mesh (by using the same photogrammetric software) / Fig. 5/.

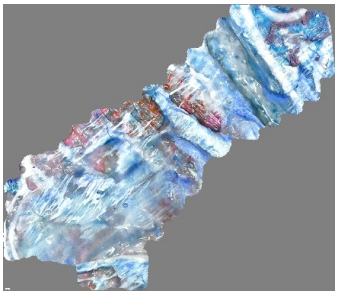

Figure 5: Output of the photogrammetrically processed set of "representative" micro-photos: photo-realistically textured 3D-model of the outlined artwork segment (generated in the form of 3D-mesh)

2.4.2. Subject-related Statistical Calculations of Photogrammetrically Processed Output-data: Probability Analysis

Once the analysed artwork's 3D-mesh is created (hereby, of the chosen segment only), for each of its surface points (namely, generated vertices) are quantified (calculated) concrete values of the analysed artistic style and manner descriptor ("thickness of the painting-layer"). Consequently, are also calculated statistical characteristics of the distribution of these values along the overall analysed painting-segment (chosen surface-part).

According to the fact that those descriptor's values are actually relative values of z-coordinates of generated 3D-mesh vertices - measured from a chosen referential entity (declared an origin of corresponding Cartesian coordinate system), such entity is firstly created and initially randomly positioned with respect to the 3D-mesh. Such tasks are performed by the mentioned "C2C" software. Then, by running the following procedures/modules as parts of the same software: "Match-bounding-box Centres Procedure" and "Fine Registration Procedure/Iterative Closest Point Procedure"/ "ICP", an adequate (the most appropriate) spatial re-positioning of the origin with respect to the 3D-mesh is done (Girardeau-Montaut: "CloudCompare" Tutorial; Zhang, 1994). After such re-position, needed relative distances between the origin-plane and each of the generated 3D-mesh vertices are calculated by the same software.

The final outputs of this stage are outcomes of statistical evaluation and estimation procedures, also performed by specific "C2C" software module. These outcomes, actually, represent characteristics of Gaussian/Normal distribution characteristics of previously found relative distances, including the calculated average value of their Mean as well as the calculated values of ±Sigma (standard deviation of that distribution).

A set of previously mentioned final outputs (in the form of z-coordinates/vertex "heights") and its global distribution are represented in the corresponding histogram /Fig. 6/.

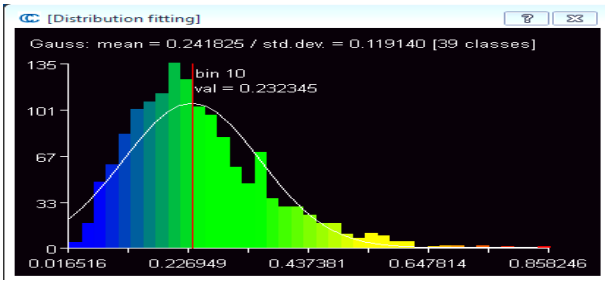

Figure 6: Histogram of statistical distribution of relative distances between the referential/zero plane (as origin) and vertices of the created 3D-mesh; white-coloured thin curve refers to the corresponding statistically defined Gaussian/Normal distribution of those relative distances.

The histogram consists of gradually coloured "vertical" bars: from orange (on its right-hand side), through yellow and green – to blue (left positioned), representing thus a gradient of change of the calculated values of vertex relative distances from the defined origin-plane (the orange colour on the histogram represents the highest value of that distance (its deviation), whereas the blue represents the lowest one). The thin white line shown there also refers to the curve of the statistically calculated Gaussian/Normal distribution of those relative distances. The corresponding values of Mean and Sigma are presented there as well (on-histogram position of Mean is defined by a thin "vertical" red line).

The characteristics of a statistically defined distribution of relative distances between the origin-plane and micro-photogrammetrically created 3D-mesh vertices (including values of Mean and standard deviation Sigma), may be considered a unique part of the artist's creative expression's ID-card related to the analysed artwork only (in accordance with the sole analysed descriptor: "thickness of the painting-layer"). To obtain a more complete and, thus, a statistically more reliable ID-card, additional relevant artistic style and manner descriptors of geometric nature have to be taken into account (for example: "roughness" of the painting-layer).

Provided that are used photogrammetric "micro-target" patterns of a „DOT-type" (created by laser beams projected onto a surface of the artwork prior to its being photographed), it becomes possible to scale the generated 3D-mesh and, thus, to convert relative values of calculated measures/distances into their absolute values (if needed). Accordingly, an input photo-set can be micro-photogrammetrically processed more precisely and accurately.

3. CONCLUSIONS AND OUTLOOK

The previous chapters demonstrated a sustainable possibility to scientifically encode various morphological aspects of artistic style and manner present in a concrete artwork (not only analysed one) – based on quantifying their descriptors of exclusively geometric nature (carried out by the usage of micro-photogrammetry and mathematical statistics/probability). A set of such coded aspects present in a concrete artwork, actually, defines its complex „ID-Card" (causally determined by the chosen geometric descriptors). In addition, the defining of ID-Card of a set of artworks that belongs to the same artist's creative epoch, makes it possible to generate in a sustainable way an ID-Card of that overall epoch (conform with the same aspects, namely descriptors). For this "overall" ID-Card to be defined with an expected/acceptable level of validity in a statistical sense, it is necessary that the representative sample to analyse and process, be adequately initially created (chosen) from a statistical point of view: both as regards the choice of artworks whose artistic style/manner it is possible to synthesize and describe with a set of analysed descriptors of geometric nature and as regards the issue of the needed number of available artworks that can be treated "artistic style and manner fingerprints". Finally, after creating a library of a variety of multi-authors' ID-Cards, it will become feasible to scientifically determine the fact whether a concrete artwork, made by an initially unknown author, can be treated a work of the known/assuming one (and with what level of certainty it is possible to accept it as a valid representative of his/her concrete creative epoch).

In order to create only standardized libraries of ID-cards of a larger number of artists and epochs they worked in, the focus of a future work in this field will be to create exact protocols of: (1) micro-photographing (regarding subject-related needs), (2) micro-photogrammetric processing (according to the same aspect), and (3) aim-directed statistical processing of obtained output-data. Those includes both a precise definition of all necessary methodological sub-phases and all relevant pre-sets that relate to procedural activities of taking photos and adjustments of necessary-to-use software modules. This makes it possible to create a common starting point which will enable not only to completely unify an overall processing of each separate artwork but also to scientifically mutually compare a larger number of artworks based on statistical correlations of obtained cross-referenced results (respecting and obtaining statistically acceptable levels of precision and accuracy). This will additionally increase the possibility to confirm the authorship in a most reliable way - by increasing the level of probability of estimation that a concrete artwork may be considered a part of the concrete creative epoch of an anonymous/unknown but presumed artist.

REFERENCES

1. Chandler, J. H. and Padfield, C. J., 1996. Automated digital photogrammetry on a shoestring. *Photogrammetric Record*, 15(88). pp 545–560.
2. Bennett, T., 2015. Photogrammetry and transmitted infrared imaging to document the support of a 19th c. British landscape painting. COSCH e-Bulletin. No. 2. pp 1-5.
3. Rogerio-Candelera, M.A., 2015. Digital image analysis based study, recording, and protection of painted rock art. Some Iberian experiences. *Digital Applications in Archaeology and Cultural Heritage*, 2(2-3). Pp 68-78.
4. Mancuso A., Pasquali A., 2015. New ways to dialogue with future researchers. University of Florence, Department of Architecture, Italy, https://www.academia.edu/19854847/Digital_Micro-Photogrammetry_new_ways_to_dialogue_with_future_researchers [Accessed: March 2020].
5. Kumar Verma, A., Bourke, C., 2019. A method based on structure-from-motion photogrammetry to generate sub-millimetre-resolution digital elevation models for investigating rock breakdown features. *Earth Surface Dynamics,* No. 7. pp 45-66.
6. Cornille, N., 2005. Accurate 3D Shape and Displacement Measurement using a Scanning Electron Microscope. *Signal and Image processing*. Institut Nationale des Sciences Appliquées (INSA Groupe) Institut de Toulouse, https://tel.archives-ouvertes.fr/tel-00166423/file/cornille_2005.pdf [Accessed: March 2020].
7. Sims-Waterhouse, D., Leach, R., 2017. Verification of micro-scale photogrammetry for smooth three-dimensional object measurement. In Precision Measurement and Metrology. *Science and Technology*, Vol.28. No.5.
8. Guerra, M. G., 2018. Analysis of a 3D optical scanner based on photogrammetry suitable for industrial applications in close and micro-range. Doctoral Dissertation, Politecnico di Bari, Italy,

https://www.dmmm.poliba.it/dottorati/pluginfile.php/255/mod_folder/content/0/PhDThesisGuerraMariaGrazia.pdf?forcedownload=1 [Accessed: March 2020].

9. Del Sette, F., Patané, F., Rossi, S., Torre, M., Cappa, P., 2017. Automated displacement measurements on historical canvases. *Heritage Science,* Vol. 2. No. 5(1):21. . pp 1-12.
10. Jiang, D. & Kim, J.W., 2019. Artwork Recognition for Panorama Images Based on Optimized ASIFT and Cubic Projection. *Multimedia Tools and Applications*, No.78. pp. 31893–31924.
11. Widjaja, I., Leow, W.K., Wu, F.C. , 2003. Identifying painters from color profiles of skin patches in painting images. Proceedings 2003 International Conference on Image Processing (Cat. No.03CH37429), IEEE (Institute of Electrical and Electronics Engineers), Barcelona/Spain (Print ISBN: 0-7803-7750-8, Print ISSN: 1522-4880).
12. Montagner, C., Jesus, R., Correia, N., Vilarigues, M., Macedo, R. & Melo, J.M., 2016. Features combination for art authentication studies: brushstroke and materials analysis of Amadeo de Souza-Cardoso. *Multimedia Tools and Applications*, No. 75. pp. 4039–4063.
13. Hong, Y. & Kim, J., 2019. Art painting detection and identification based on deep learning and image local features. *Multimedia Tools and Applications*, No.78. pp. 6513–6528.
14. Djordjević Dj., Ćirović I., Djukanović G., 2019. Osnovi zasnivanja metodologije definisanja identifikacione karte umetničkog dela – parametrizovanjem njegovih karakterističnih geometrijskih-morfogenih svojstava, primenom postupaka mikrofotogrametrije i matematičke statistike/verovatnoće. Zbornik apstrakata sa Prve nacionalne konferencije "Metodološka istraživanja u heritologiji i novim tehnologijama", Centralni institut za konzervaciju /CIK, Beograd/Srbija. (ISBN 978-86-6179-070-6, COBISS.SR-ID 281639180).
15. Sutton, M.A., Li, N., Garcia, D., Cornille, N., Orteu, J.J., McNeill, S.R., 2007. Scanning Electron Microscopy for Quantitative Small and Large Deformation Measurements. Part II: Experimental Validation for Magnifications from 200 to 10,000. *Experimental Mechanics*, No. 47. pp 775-787.
16. EosSystems Inc. Photo modeler Scanner Tutorial, www.photomodeler.com [Accessed: March, 2020].
17. EosSystems Inc., 2012. Quantifying the accuracy of dense surface modeling within PhotomodelerScanner. Vancouver, British Columbia, Canada, https://www.photomodeler.com/downloads/documents/applications/DSMAccuracy2012.pdf [Accessed: March, 2020].
18. Lopez, J.T.C., 2012. Fotogrametría practica, Punto Arquitectura S.L.P., Ediciones Tantin, Torrelavega/Cantabria, España.
19. Girardeau-Montaut D., CloudCompare Tutorial, http://www.cloudcompare.org/ [Accessed: March 2020].
20. Zhang Z., 1994. Iterative point matching for registration of free-form curves. *International Journal of Computer Vision*, Vol. 13. pp 119-152.

IMPLEMENTATION OF THE 3D MODEL COMPLEXITY IN VR ENVIRONMENT IN THE CASE OF NOVI SAD CITY CENTER

Miloš Obradović
Faculty of Technical Sciences, University of Novi Sad, Republic of Serbia
M.Sc., Teaching Assistant, milos_obradovic@uns.ac.rs

Jelena Kićanović
Faculty of Technical Sciences, University of Novi Sad, Republic of Serbia
M.Sc., Researcher, kicanovicj@uns.ac.rs

Marko Vučić
Faculty of Technical Sciences, University of Novi Sad, Republic of Serbia
M.Sc., Teaching Assistant, vucic.marko@uns.ac.rs

ABSTRACT

In this research, the aim is to create a large urban fragment representation with a lot of details and simultaneously with a low polygon count. Models of real-world objects with a high level of details are usually made by assessing and stored as a point cloud to preserve details. However, this can have an impact on the processing power of the computer. For that reason, a low poly model is preffered to be used, where the details were indicated by the material textures and not through geometry. Meanwhile, the lack of details in the geometry of the buildings can be compensated with urban furniture and tiling of the street in order to introduce more details and make the immersion adequate. In this paper, different objects and materials are used in the scene and the quality of immersion success is rated. The background of this research are ready-made 3D models of buildings in the pedestrian zone of Novi Sad, modeled by students. The link between the models and virtual reality was used to show the general public the city center of Novi Sad, without having to walk through it.

Keywords: Virtual Reality; Interactive Visualization; Architectural Visualization

1. Introduction

One of the ways a user can experience a space virtually is to feel it by walking through it. In this paper, an urban fragment of the city center of Novi Sad is presented through a virtual walk. The research is focused on finding a way of optimizing the virtual walk scene, as well as giving the user the best possible impression (Mah et al., 2019). Also, it refers to the specific segments of the space that affect the creation of a positive reaction on the user and points the details which should be stressed in the final presentation. The largest part of the scene is represented by 3D models of the objects, which can be made photogrammetrically (Pérez Ramos et al., 2016) or manually by using 3D modelling software. The difference between these strategies of modelling is analyzed in order to find out which is more cost-effective and useful for this type of presentation of an urban fragment.

As visualization is emerging as one of the important topics in architecture, any project can be presented in many ways - using orthogonal drawings, 3D rendering, photorealistic renders, animation, Augmented Reality (AR) or Virtual Reality (VR). In this paper, emphasis will be placed on VR, which is increasingly present as an integral part of many architectural projects. With VR, the user is transported to a different space in which he/she interacts with digital objects using assets in the virtual environment. In this way, the users change the way they look at a particular event, place and space, by interactively participating in it (Zhanga Y. et al., 2019) .

Virtual Reality is a term used to describe a computer-generated three-dimensional environment that a person can explore and interact with (Donovan, 2019). With the development of technology, architecture has evolved. Consequently, 3D presentation has become the main tool of architectural representation. One of the ways how visualization and the experience of space are dramatically developing is Virtual Reality. Nowadays VR technology has a lot of potential for application in architecture (TMD STUDIO LTD, 2017; Šiđanin et al., 2017). In the example of the 3D reconstruction of the old city of Xanthi (Koutsoudis, 2006), a 3D reconstruction of a settlement was attempted without the use of any expensive equipment. The goal was to make a low-budgeted 3D reconstructions project that still results in enough realism for cultural promotion. The fidelity and accuracy of the final 3D model is by far inferior to any other 3D models that could have been created by geodetic measuring techniques or terrestrial 3D laser range scanning. In the end, the attempt to use low cost infrastructure, like ordinary digital cameras and freely distributed software, proved to be good enough to promote cultural heritage over the Internet through a prestigious tool such as VR.

In a virtual urban environment of the old Calw (Balsa-Barreiro et al., 2018), in which the user can freely walk around, photogrammetrically made models were used. The models used for the virtual walk are low-poly with appropriate textures and the resulting 3D models are accurate, detailed and aesthetically pleasing. The utilization of VR can also be used as a medium for assessing the role of noise in the audio-visual design of an urban public space (Echevarria Sanchez GM. et al., 2017), as a stress relief application (Mattila, 2020) or to compare environmental perceptions and affective appraisals of contemporary versus traditional styles in architecture and public spaces (Mouratidis, 2020).

The aim of this paper is to create a large urban fragment representation with lots of details and with a low polygon count, using a headset and controllers for specific interactions in the virtual space. Also, the goal is to explore the difference between the low-poly models used in virtual walk and photogrammetrical models, as well as the way in which tiling, urban equipment and greenery affect the user experience. The research questions that are being adressed are what affects the perception of virtual space while the user is participating in a scene. Also, how paving and urban mobiles affect the user, as well as whether it is more efficient to use low poly models or photogrammetric models.

2. Methods used for optimizing the model and creating a virtual walk

For a scene to be created and implemented in a virtual environment, a proper 3D model must be created. In addition to the 3D models of objects in the scene, attention should be paid to urban equipment, greenery and paving, which affect the outcome of the final presentation. The process of creating a virtual scene can be divided into three segments. The first is the creation of a 3D model in Autodesk 3ds Max software (3DS MAX, 2020), the second is the implementation of the given assets in the software Unreal Engine 4 (Computer Hope, 2019), and the third part is the connection of the equipment with the software in order to form a virtual walk through the urban fragment of the center of Novi Sad. Given that object models represent the majority of the scene, an inevitable question is whether it was easier to create photogrammetrical models or to create them in 3ds Max.

Also, it is necessary to determine the relationship between the two programs mentioned above, as well as to find a way of implementing all the assets into a virtual scene. The user experience in the virtual space (Ferdani D. et al., 2020; Gaitatzes et al., 2001) is different from the experience in the real world, and it is necessary to determine how practical the use of a headset is to obtain a visual effect, and to what extent the effects affect the perception (Połap D. et al., 2020) of the space.

When it comes to creating 3D models (Smith et al., 2019) of objects in Zmaj Jovina and Dunavska street, there are several related questions. They concern the time it takes to create the model, the number of polygons and the adequate texture applied to each one of them. These parameters can be achieved in two ways - by creating a model in a modeling software or by a photogrammetrically created model.

The virtual walk might relate to cultural heritage and preservation, for the preservation of certain buildings, cultural monuments, etc. It should be considered, for example, creating a photogrammetric model of the monument within the given two streets, where they might also be preserved in that way. In that manner, the combination of low poly models and high poly models would have been made.

2.1. A model created in a modeling software

Models created in 3ds Max software have from 50,000 to 100,000 polygons, each. In order for one to be made, the object firstly had to be photographed and the relevant dimensions had to be determined. After that, the modeling process follows. With the help of photography, it is necessary to draw a facade in the AutoCad (Whyte et al., 1999) software and use it to create the final model. The advantages of this type of modeling are that a small number of polygons can be replaced with adequate texture, more complex shapes of objects that are not so visible can be simplified manually, and the model itself is much smaller and easier to manipulate further. Also, urban mobiles, as well as the greenery in front of an object can be neglected when modeling, and the hardware performance of computers does not greatly affect the speed of model making. The disadvantage lies in the fact that individual, more complex segments will not be persuasive from close range, because of the inability to easily control the model in 3ds Max software. Also, for each object it is necessary to find the appropriate texture, and since each model consists of multiple materials, this requires additional time.

Figure 1. Zmaj Jovina street in a Virtual Reality scene

2.2. Photogrammetric model

The photogrammetrically created model (Avşar et al., 2008) requires adequate equipment for photographing the current state, as well as the knowledge of working in the software for the creation of 3D models based on photographs (Metashape, 2020). Photogrammetrically created models are, unlike hand-modelled, high-poly models made with at least ten times more polygons (the façade in Figure 2 consists of 1,075,000 polygons). In order for a photogrammetric model to look adequate, it is necessary that the weather conditions are good, with no sunlight or rain, and that the photographer pre-calculates in order to be able to obtain a suitable 3D model in the software. Also, when creating this type of model, it is necessary to take into account everything that stands in front of the facade, such as the tables, chairs, umbrellas, trees, overpasses and similar. The given elements need to be further masked due to the preparation for the 3D model, and masking can be quite complicated due to, for example, the existence of leaves, branches, as well as other small details that need to be masked. The disadvantages are that even if the masking is done accurately, the point cloud may not be sufficiently cleaned and the model itself may not look as it should. In addition, a model created photogrammetrically takes up more memory on a computer than a model that is manually modelled, and in a scene of 56 models with a large number of polygons, it would certainly slow down the software. Also, the photogrammetric model has holes, bumps, and needs to be refined in some other software to look adequate. Non-planar models (Bruno et al., 2010) that are easier to photograph on all sides, as well as those that can be

located inside a closed space, are easier to create photogrammetrically than facades, which can be stated as one of the benefits of using this type of modelling for certain assets. However, when the focus is on creating a facade, the situation is different.

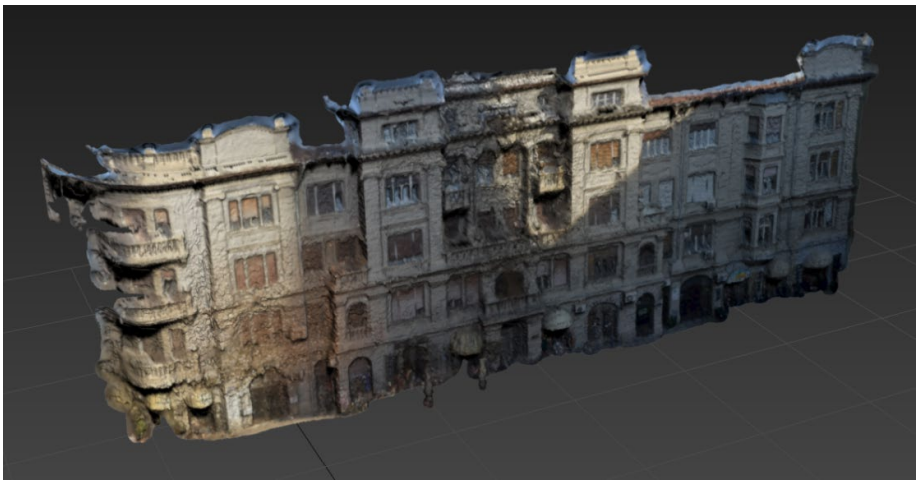

Figure 2. Facade of the building in the city center of Novi Sad

2.3. Additional segments that affect the way of presenting an urban fragment

In order to make the scene more complete, it is necessary to take into account some other segments, such as floor, paving, urban equipment and greenery. Without the substrate, the user would not be able to move through space, and the clay substrate does not have the same effect on the users, as does a substrate that has tiles that resemble the real world, as evidenced by experience.

The above fact also applies to the presence and absence of urban equipment and trees, since by the appearance of them the user gets the impression that he/she is in a space that is possible to exist in real world. However, in a space that contains only objects on both sides and he/she walks in an empty street, this does not give the impression of the space that can actually be possible. What should be taken into consideration are the spaces where the objects end, so that the user never has a glimpse of the empty space. This problem was solved by introducing additional geometry in the form of trees, or photographs that were placed at the ends of the scene, simulating the continuity of a street containing the objects in a row.

The models were created to be available to the public by using the VR headset, and they were used at several exhibitions in Novi Sad, such as Night of the museums in 2018 and Laboratory Space 2.0 in 2020.

Figure 3. Tiling, urban equipment and greenery in the VR scene

3. Conclusions

The photogrammetric model requires the possession of adequate equipment, the computers with good hardware performance, ideal photography conditions and the knowledge of using software to create 3D models based on images. Creating models in 3ds Max software, on the other hand, is a good option because the models will be low-poly and with adequate textures. They will look adequate for creating a virtual walk, while the scene will not be overloaded with a huge number of polygons. Also, no other software is required to modify the created 3D model.

For getting a the impression of immersion relapse and enhance the VR experience, there is a possibility of further exploration in the form of introducing interactivity, where the user could move models on the scene, such as chairs and tables located on the street, or change the color of the facade by clicking on a specific controller button. It is also possible to photogrammetrically model only single segments of the difficult-to-model objects and to place them on a pre-modeled object from 3ds Max software.

Tiling, urban equipment and greenery greatly affect the user experience of the space. Experience has shown that a virtual walk through an urban fragment of the city center of Novi Sad without these details does not give the user a sense of identification with the space, as when the details are present in the scene so that they are as important on the scene as the models of objects.

The future steps are to create more virtual walks of certain parts of the city, other cities, urban fragments of cultural heritage, in order to preserve those fragments in case they will not exist in the future, as well as to enable people who are not able to visit them, to see them virtually, etc.

REFERENCES

Avşar E. Ö., Duran Z., Akyol, O., Toz G. 2008. MODELING OF THE TEMPLE OF APOLLO SMINTHEUS USING PHOTOGRAMMETRY AND VIRTUAL REALITY. *The International Archives of the Photogrammetry, Remote Sensing and Spatial Information Sciences*, Volume 37, pp. 357-361.

Balsa-Barreiro J., Fritsch D. 2018. Generation of visually aesthetic and detailed 3D models of historical cities by using laser scanning and digital photogrammetry. *Digital Applications in Archaeology and Cultural Heritage*, Vol. 8, pp. 57-64.

Bruno F., Bruno S., De Sensi G., Luchi M. L., Mancuso S., Muzzupappa M. 2010. From 3D reconstruction to virtual reality: A complete methodology for digital archaeological exhibition. *Journal of Cultural Heritage*, Volume 11, pp. 42-49.

Computer Hope. Unreal Engine, 2019. https://www.computerhope.com/jargon/u/unreal-engine.htm [Accessed: 14th October 2019]

Donovan, A. How VR Technology Is Changing the Way Architects Design Your Home, 2019. https://interestingengineering.com/how-vr-technology-is-changing-the-way-architects-design-your-home [Accessed: 5th October 2019]

Echevarria Sanchez GM. et al. 2017. Using Virtual Reality for assessing the role of noise in the audio-visual design of an urban public space. *Landscape and Urban Planning*, Vol. 167, pp. 98-107.

Ferdani D. et al. 2020. 3D reconstruction and validation of historical background for immersive VR applications and games: The case study of the Forum of Augustus in Rome. *Journal of Cultural Heritage*, In Press, Corrected Proof

Gaitatzes A., Roussou M., Christopoulos D. 2001. Reviving the Past: Cultural Heritage Meets Virtual Reality. *Proceedings of the 2001 conference on Virtual reality, archeology, and cultural heritage*, pp. 103-110.

Koutsoudis A., Arnaoutoglou F., Chamzas C. 2006. On 3D reconstruction of the old city of Xanthi. A minimum budget approach to virtual touring based on photogrammetry. *Journal of Cultural Heritage*, Vol. 8, pp. 26-31.

Mah, O. B. P., Yan, Y., Tan, J. S. Y., Tan, Y. X., Tay, G. Q. Y., Chiam, D. J., Wang Y. C., Dean K., Feng, C. C. 2019. Generating a virtual tour for the preservation of the (in)tangible cultural heritage of Tampines Chinese Temple in Singapore. *Journal of Cultural Heritage*, Volume 39, pp. 202-211.

Mattila O. 2020. Restoration in a virtual reality forest environment. *Computers in Human Behavior*, Vol. 107, 106295

Metashape - photogrammetric processing of digital images and 3D spatial data generation. https://www.agisoft.com/ [Accessed: 3th March 2020]

Mouratidis K., Hassan R. 2020. Contemporary versus traditional styles in architecture and public space: A virtual reality study with 360-degree videos. *Cities*, Vol. 97, 102499

Pérez Ramos, A., Robleda Prieto, G., 2016. Only image based for the 3d metric survey of gothic structures by using frame cameras and panoramic cameras. *ISPRS - International Archives of the Photogrammetry, Remote Sensing and Spatial Information Sciences*, Vol. XLI-B5, pp. 363-370.

Połap D. et al. 2020. Strengthening the perception of the virtual worlds in a virtual reality environment. *ISA Transactions*, In Press, Corrected Proof

Smith M., Walford N.S., Jimenez-Bescos C. 2019. Using 3D modelling and game engine technologies for interactive exploration of cultural heritage: An evaluation of four game engines in relation to roman archaeological heritage. *Digital Applications in Archaeology and Cultural Heritage*, Volume 14, e00113

TMD STUDIO LTD. Virtual Reality Uses in Architecture and Design, 2017. https://medium.com/studiotmd/virtual-reality-uses-in-architecture-and-design-c5d54b7c1e89 [Accessed: 5th October 2019]

Whyte J., et al. 1999. From CAD to virtual reality: modelling approaches, data exchange and interactive 3D building design tools. *Automation in Construction*. Vol. 10, pp. 43–55.

Zhanga Y. et al. 2019. User-centered interior finishing material selection: An immersive virtual reality-based interactive approach. *Automation in Construction*, Vol. 106, 102884

Šiđanin P., Lazić M., Obradović R. 2017. Immersive Virtual Reality Course at the Digital Production Studies, *FME Transactions*, Volume 45, No. 2, pp. 205-208.

3DS MAX. https://www.autodesk.com/education/free-software/3ds-max [Accessed: 3th March 2020]

AUGMENTED REALITY KITCHEN DESIGN

Petar Pejic
Faculty of Information Technology, Metropolitan University, Belgrade, Serbia
PhD., Assistant Professor, petar.pejic@metropolitan.ac.rs

Jelena Pejic
Faculty of Sciences and Mathematics, University of Nis, Nis, Serbia
PhD. Student, Teaching Assistant, jelena.milovanovic@pmf.edu.rs

Miodrag Mikic
Faculty of Information Technology, Metropolitan University, *Belgrade, Serbia*
MSc. Student, Teaching Associate, miodrag.mikić@metropolitan.ac.rs

ABSTRACT

Kitchen represents a space with great importance for one family. That's why the goal is to have a kitchen with the best possible design. This implies the creation of a kitchen with the best possible organization, maximal space usage and aesthetic appearance in accordance with the owner's taste. The traditional kitchen design process assumes the use of professional services, such as an interior designer or architect. The kitchen design process consists of several steps:

Space measurement and initial design discussion;

2D / 3D design;

Design evaluation;

Technical drawing creation.

Professionals in the design phase use different manual and digital tools and software. Precise kitchen space measurement is done in a family home using measurement tools. Design discussion has a goal of understanding the homeowner's taste and desire for the kitchen appearance and functionality. Based on discussion and measurements, the designer creates first kitchen visualizations in the form of sketches, 2D images, or 3D models. This design is then discussed with the homeowner and readjusted several times until the final version. This final version is then used for the creation of technical drawings that are used for kitchen assembly.

The evolution of contemporary devices and computer graphics lead to the development and adaptation of Augmented Reality in design. Augmented reality (AR) is an emerging computer technology where the perception of the user is enhanced by the seamless blending between a realistic environment and computer-generated virtual objects coexisting in the same space. The resulting mixture supplements reality, rather than replacing it.

In this paper possibilities for Augmented Reality use in the kitchen design process are investigated. Analysis and comparison of currently available, state of the art solutions for Augmented Reality kitchen design are performed. State of the art in the field of AR space measurement, AR 3D model presentation, and AR kitchen design are investigated. Analysis of currently available solutions for Augmented Reality kitchen design is performed and compared.

Keywords: Kitchen Design; Augmented Reality; Computer Graphics; Visualisation

1. INTRODUCTION

Kitchen represents a space with great importance for one family. That's why the goal is to have a kitchen with the best possible organization, maximal space use, and aesthetic appearance in accordance with the owner's taste. In order to meet these criteria, homeowners in most cases decide to create a fully custom-made kitchen (Pejic, et al., 2019). This requires many elements disposition rules to be respected in order to get a functional kitchen (Pejic, et al., 2019).

The traditional kitchen design process assumes the use of professional services, such as an interior designer or architect. The kitchen design process consists of several steps:

- Space measurement and initial design discussion;
- 2D / 3D design;
- Design evaluation;
- Technical drawing creation.

Use of interior designer services for 360cm length, I-shape kitchen can be 30 days long process (Figure 1). The process starts with the first meeting between the homeowner and interior designer, space measurement, and design discussion. Based on homeowner preferences and dimensions, designer creates 2D drawings and 3D visualizations using architectural software's such as AutoCAD, SketchUp or 3D max. Created kitchen design is then evaluated by homeowners and usually redone a couple of times until final approval. The final design is then transformed into the kitchen project, which includes detailed technical drawings with a list and quantity of all parts and equipment needed for kitchen assembly.

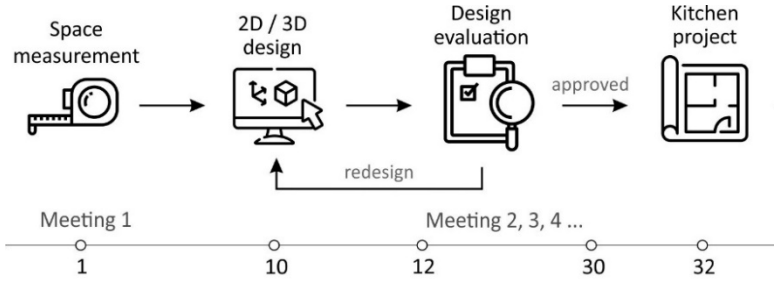

Figure. 1: Process of custom made kitchen creation

The current process of custom-made kitchen design is time-consuming, project completion timing is usually extended and budget surpassed because of two main challenges:

• **Miscommunication** between homeowner and designer results in multiple redesigns and a high level of stress;

• Need for **prior knowledge** for the use of complex 2D drawing, 3D modeling, and visualization software.

Solution for miscommunication can potentially be found in the application of Augmented Reality for kitchen design. Augmented Reality (AR) is an emerging computer technology where the perception of the user is enhanced by the seamless blending between a realistic environment and computer-generated virtual objects coexisting in the same space (Murru, et al., 2013). The resulting mixture supplements reality, rather than replacing it (Azuma, 1997), making it possible to supplement real space with a digitally created 3D model of kitchen. Augmented Reality enhances a user's perception of and interaction with the real world (Pejic, et al., 2014).

Augmented Reality allows intuitive presentation and manipulation of 3D models in a real environment. The use of Augmented Reality for kitchen design has the potential to bring new tools and possibilities for professionals. Intuitive use of Augmented Reality applications also allows everyday customers with average knowledge of smart device used to design a kitchen on their own.

There is plenty of research addressing the topic of interior design using Augmented Reality (Pejic, et al., 2020), (Samant, et al., 2019), (Sandu, et al., 2018), (Jani, et al., 2015), (Siltanen, 2012), (Phan, et al., 2010), (Woodward, et al., 2007), (Lee, et al., 2008). There are different approaches to the topic, one group of authors investigates the application of AR in renovation planning (Pinto, et al., 2007), (Saito, et al., 2007). Another group use AR to visualize building and construction projects (Woodward, et al., 2007), (Golparvar, et al., 2009). Some authors investigating the specifics of mobile Augmented Reality for interior design (Kilic, 2019) or application in education (Gurcinar, et al., 2018).

Recently AR furniture arrangement systems help users overlay virtual furniture onto the real world. Such systems allow people to see how the room will look with new furniture without actually buying or moving real furniture (Siltenen, et al., 2013). The majority of existing Augmented Reality applications are providing placement and preview of 3D furniture models in the interior. These applications are limited to provide furniture (e.g. table, chair, etc.) without the possibility to present custom made furniture (e.g. closet, kitchen, etc.).

In this paper possibilities for Augmented Reality use in the kitchen, the design process is investigated. State of the art in the field of AR space measurement, AR 3D model presentation, and AR kitchen design are investigated. Analysis of currently available, solutions for Augmented Reality kitchen design is performed and compared.

2. AUGMENTED REALITY SPACE MEASUREMENT

The process of custom-made kitchen design as one of the first steps requires precise space measurement. In order to measure existing space using Augmented Reality different approaches can be implied (Jamil, et al., 2019).

The simplest approach assumes the use of AR tape measure (Figure 2) which uses Augmented Reality technology and a smartphone camera to visually detect space and tape measure the real world. This approach allows users to replicate the same procedure as in the case of manual space measurement using tape, just in this case on a smartphone. The advantage comparing to the traditional approach is faster and easier measurement, especially in the case of hardly reachable parts of the space. The disadvantage is the precision of AR scene tracking, which can result in incorrect real space dimensions. This approach required the same steps and measurement one length at the time and manual sketching of geometry. Comparing to traditional, this AR approach can be a little bit faster, but less precise.

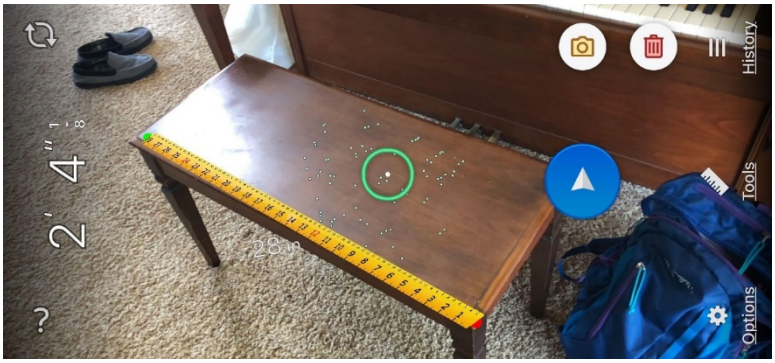

Figure. 2: AR tape measure (Broida, 2018)

More advanced approaches to the space measurement assume use Augmented Reality technology and smartphone camera to visually detect space and create a simple 3D model of the space (Figure 3). In this approach, user draw lines on the floor to mark the edges of the room and then extrude created shape to the height of ceiling inside AR. The next steps allow marking of additional details of the space such as doors and windows. The end result of this process is a 3D model of the space with all measurements which further can be exported and used in software for 2D drawing and 3D modeling. This approach is faster than traditional and AR tape measurement and requires less time for complete space measurement. It has some technical limitations as AR tape measurement regarding precession due to visual AR space tracking.

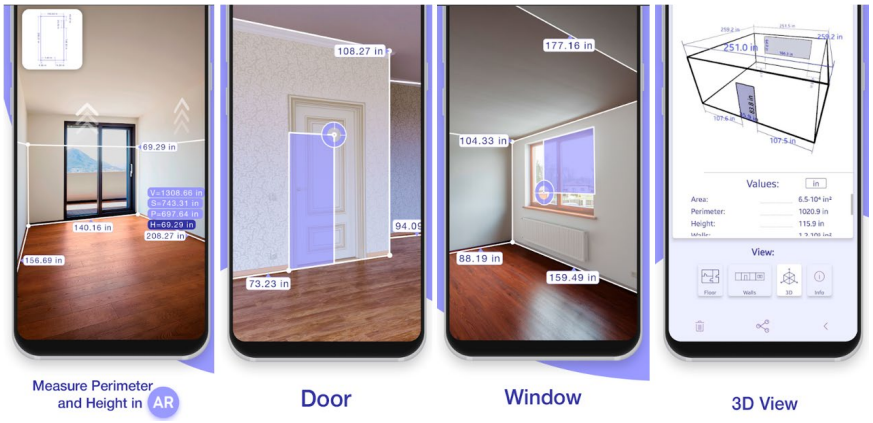

Figure. 3: AR 3D space modelling (Grymala, 2020)

The most advanced approach to the space measurement use Augmented Reality technology and smartphone TOF camera for space detection and virtual reconstruction (Figure 4). In this approach smartphones or tablet with TOF camera is used to scan and create a precise virtual 3D model of existing space (Nguyen, et al., 2018). This 3D model is then used for measurement of needed distances or export to the 3D modeling software. This approach is more precise and faster than AR tape measurement and AR 3D space modeling. The downside of this process is a need for a special device equipped with a TOF sensor, which is not widely present in smart devices.

Figure. 4: AR space capturing using TOF camera (O'Kane, 2016)

3. AUGMENTED REALITY INTERIOR DESIGN

Every interior space has a certain design, some simple and some complex. The design is created for the purpose of coordinating with the rules and technical regulations on construction and aesthetic appearances. The interior design is a trade dealing with creative and technical aspects of the creation of arranging interior space (Kymalainen, et al., 2012). The generally accepted method of presentation of the architectonic design of interior comprises the production of a design, which contains the 3D presentation of space. As architecture is dealing with the modeling of the actual world, the Augmented Reality is becoming an increasingly used method of design presentation (Pejic, et al., 2014). The application of augmented reality in the interior design can be with the goal of:

- Finished design presentation (Figure 5). This is applicable in the case that design and 3D models are done in some of the software such as SketchUp or 3D Max and then imported into the software for Augmented Reality presentation.

Figure. 5: AR finished design presentation (Johnston, 2017)

- Creation of design in real-time (Figure 6). This assumes the use of specially developed Augmented Reality based applications that allows interior design in real-time inside real space.

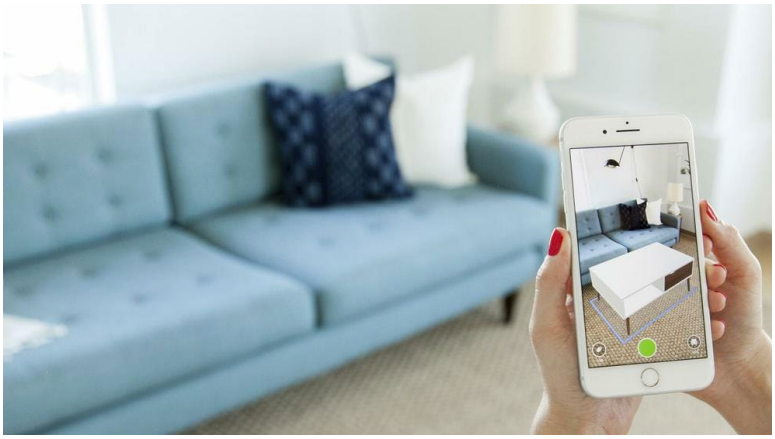

Figure. 6: AR real time interior design (Vania, 2019)

4. AUGMENTED DESIGN EVALUATION

Design evaluation represents an important step in the process of interior or kitchen design. In kitchen design, evaluation assumes presentation of kitchen 3D model to the owner in order to approve or request an additional correction in order to fit his requests. Presentation of final 3D models in Augmented Reality can be performed in two ways dependently of scale:

- In a small scale (Figure 7-a).
- In a 1:1 scale (Figure 7-b).

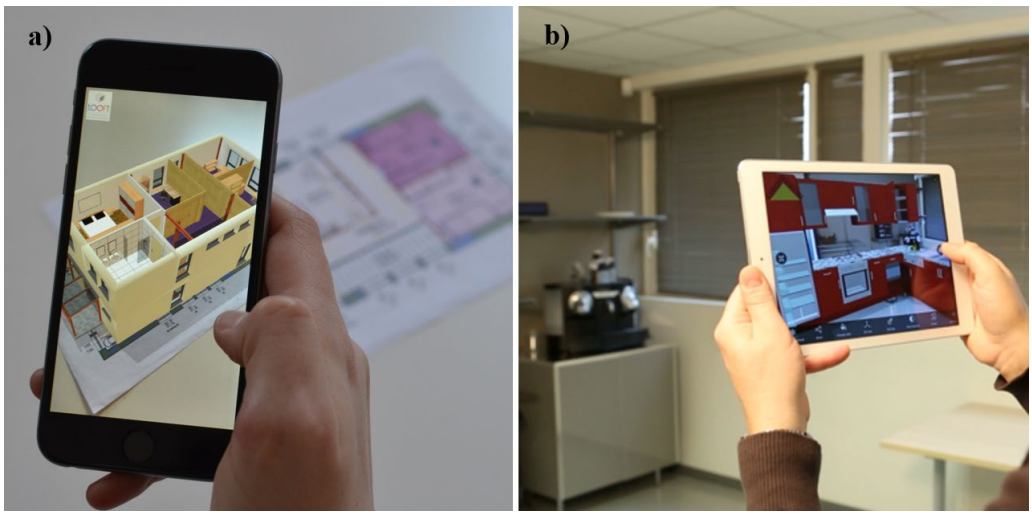

Figure. 8: 3D model evaluation in: a) small scale (Busta, 2015) and b) 1:1 scale (Koehler, 2018)

5. RESULTS AND DISCUSION

Traditional custom-made design requires a lot of time, previous knowledge, and experience in order to finalize the process. It requires a lot of digital 2D drawing and 3D modeling skills in order to transform kitchen design discussion and measurement of space into kitchen visualization. To reach a final design couple of meetings between homeowners and designers are needed because of common misunderstandings resulted from miscommunication.

Augmented Reality kitchen design has the potential to allow a much faster design process, due to intuitive use and a higher level of process automation. In theory, kitchen design can be performed on the first meeting between homeowner and designer, presenting and live designing a kitchen using 3D Augmented Reality. This can remove the possibility of misunderstanding because the homeowner takes part in the process of 3D modeling and can see the final kitchen design on the spot inside his home using AR.

Analysis of currently available android and iOS applications (Table 1) for smartphones and tablets does not show an existing solution that allows complete Augmented Reality kitchen design.

Table 1: Comparison of available smartphones and tablets applications for AR kitchen design

Application name	*Kitchen design*	*Space measurement*	*Space design*	*Design evaluation*	*Platform*
Kitchen planer 3D	*Yes*	*Manual*	*3D*	*3D*	*Android*
Kitchen design	*Yes*	*Manual*	*3D*	*3D*	*Android*
Kitchen design pro for Ikea	*Yes*	*Manual*	*3D*	*3D*	*Android / iOS*
Cambria AR	*Partly*	*AR Distance*	*AR*	*AR*	*iOS*
5D	-	*Manual*	*3D*	*3D / VR*	*Android / iOS*
Houzz	-	-	*AR*	*AR*	*Android / iOS*
Roomle 3D & AR Room planer	-	-	*AR*	*3D / AR*	*Android / iOS*
Augment	-	-	-	*AR*	*Android / iOS*
AR Ruler	-	*AR Distance*	-	-	*Android / iOS*
Measure (by Google)	-	*AR Distance*	-	-	*Android*
Measure (by Apple)	-	*AR Distance*	-	-	*iOS*
AR Plan 3D	-	*AR Space*	-	-	*Android / iOS*
Magic plan	-	*AR Space*	-	-	*Android / iOS*
AirMeasure - AR Tape & Ruler	-	*AR Space*	-	*AR*	*Android / iOS*
3D scanner for ARCore	-	*AR TOF*	-	-	*Android*
3D Scanner	-	*AR TOF*	-	-	*Android*
Structure Sensor	-	*AR TOF*	-	-	*iOS*

There are available kitchen design applications for Android and iOS smart devices but none of them are AR-based. This application requires user manual space measurement and input using the application interface. Space design and evaluation are performed in 3D on the device screen and their use requires a certain level of experience and previous knowledge. Smartphone application "Cambria AR" allow AR design and evaluation, but it is used only for kitchen countertop design.

On the market, there are available AR solutions for general purpose interior design and 3D model presentation, such as "5D", "Houzz", etc. These solutions do not address custom made kitchen design and allow the presentation of previously constructed furniture only. The joint characteristic of this group of applications is that they do not provide any possibility for space measurement.

There are many solutions for space measurement, with different approaches. The first group of applications allows simple distance measurement between two points in space. The second group represents applications that allow all room measurements and require user interaction and manual point of interest marking. The third group allows precise space reconstruction using a device TOF camera. None of these applications provide a possibility for the kitchen or any other space design. Only the "AirMeasure - AR Tape & Ruler" application allows the presentation of 3D models in AR, but they have to be created using some other software.

6. CONCLUSION

This research analyses possibility for Augmented Reality use in the kitchen design process and compares currently available, state of the art solutions for Augmented Reality kitchen design. The augmented Reality kitchen design has great potential compared to the traditional approach, which is much slower, requires a lot of prior knowledge and in most cases results in a misunderstanding between homeowner and designer. As presented, the Augmented Reality applications for kitchen design have the potential to significantly improve speed, make the process more intuitive, and easier to use. Analysis of available smart device applications show solutions for AR measurement, AR design, and AR design evaluation, showing technology readiness for AR kitchen design application. Unfortunately, the ultimate application with all these features integrated does not exist. The reason for this can be a need for a high level of precision during space measurement or the complexity of custom-made kitchen 3D modeling. Future research should be focused on the creation of the demo application that will integrate all mentioned features for Augmented Reality kitchen design.

REFERENCES

1. Azuma A. A Survey of Augmented Reality [Journal] // Teleoperators and Virtual Environments. - 1997. - 4 : Vol. 6. - pp. 355-385.
2. Broida R. How to measure things with your iPhone right now [Online] // Cnet. - 2018. - 2020. - https://www.cnet.com/how-to/how-to-measure-things-with-your-iphone-right-now/.
3. Busta H. Augmented and Virtual Reality Apps for Design and Construction [Online] // Architect Magazine. - 2015. - 2020. - https://www.architectmagazine.com/technology/products/three-augmented-and-virtual-reality-apps-for-design-and-construction_o.
4. Golparvar M., Pena F. and Savarese S. Application of D4AR - A4-dimensional augmented reality model for automating construction progress monitoring data collection, processing and communication [Conference] // ITcon . - 2009.
5. Grymala AR Plan 3D Ruler – Camera to Plan, Floorplanner [Online] // Google Play. - 2020. - 2020. - https://play.google.com/store/apps/details?id=com.grymala.arplan&hl=en.
6. Gurcinar E. and Esen O. The Application of Augmented Reality in Interior Design Education [Journal] // NordDesign 2018. - 2018.
7. Jamil F. and Marsh R. Distance Estimation In Virtual Reality And Augmented Reality: A Survey [Conference] // IEEE International Conference on Electro Information Technology (EIT). - Brookings, SD, USA : IEEE, 2019.
8. Jani B. [et al.] Interior Design in Augmented Reality Environment [Journal] // International Journal of Advanced Research in Computer and Communication Engineering. - 2015. - 3 : Vol. 4.
9. Johnston K. Explore Augmented Reality Features To Perk Up Your Event [Online] // Plannerwire. - 2017. - 2020. - https://plannerwire.net/explore-augmented-reality-features-perk-event/.

10. Kilic T. Investigation of mobile augmented reality applications used in the interior design [Journal] // The Turkish Online Journal of Design, Art and Communication - TOJDAC. - 2019. - 2 : Vol. 9.
11. Koehler S. A Superpower For Designers [Online] // Dream Kitchens. - 2018. - 2020. - https://www.dreamkitchenbuilders.com/blog/2018/6/19/a-superpower-for-designers.
12. Kymalainen T. and Siltanen S. Co-designing novel interior design service that utilises augmented reality, a case study [Conference] // CCGIDIS. - Italy : [s.n.], 2012. - Vol. 1.
13. Lee A., Hyun K. and Wookho S. MIRAGE: A touch screen based mixed reality interface for space planning applications [Conference] // VR '08 IEEE. - 2008.
14. Murru G., Fratarcsngeli M. and Empler T. Augmented Visualization on Handheld Devices for Cultural Heritage [Conference] // Skala (Eds.), WSCG 2013 - Communication Papers Proceedings. - Plzen, Czech Republic : University of West Bohemia, 2013. - pp. 97-103.
15. Nguyen T. and Meunier J. 3D Reconstruction with Time-of-Flight Depth Camera and Multiple Mirrors [Journal]. - [s.l.] : IEEE Access, 2018.
16. O'Kane S. You can now scan and measure your entire home with an iPad attachment [Online] // The Verge. - 2016. - 2020. - https://www.theverge.com/2016/11/10/13585786/occipital-ipad-structure-sensor-3d-scanning-augmented-reality.
17. Pejic P. [et al.] AUGMENTED REALITY APPLICATION IN ENGINEERING [Conference] // SMAT 2014. - Craiova, Romania : University of Craiova, Faculty of mechanics, 2014. - Vol. 1. - pp. 39-44.
18. Pejic P. [et al.] Parametric 3D modeling of I-shape kitchen [Journal] // Journal of Industrial Design and Engineering Graphics. - 2019. - pp. 155-158.
19. Pejic P. and Bavastro F. Augmented reality method and system for design [Journal] // US Patent 10580207. - [s.l.] : US patent office, 3 3 2020.
20. Pejic P., Krasic S. and Andjelkovic B. Application of Augmented Reality in interior design [Conference] // Mongeometija. - Vlasina : [s.n.], 2014.
21. Pejic P., Mikic M. and Milovanovic J. Automatic Rule-based Kitchen Layout Design [Conference] // PaKSom 2019. - Nis, Serbia : Research and Development Center “IRC ALFATEC”, Niš, Serbia, 2019. - pp. 199-203.
22. Phan V. and Choo S. Interior Design in Augmented Reality Environment [Journal] // International Journal of Computer Applications. - 2010. - 5 : Vol. 5.
23. Pinto I. [et al.] Dwelling renovation studio. Interactive tool for private residences renovation service [Conference] // Espoo> VTT. - 2007.
24. Saito S. [et al.] Indoor marker-based localization using coded seamless pattern for interior decoration [Conference] // Virtual Reality Conference. - [s.l.] : IEEE, 2007.
25. Samant T. and Vartak S. INTERIOR DESIGN USING AUGMENTED REALITY [Journal] // International Research Journal of Engineering and Technology (IRJET). - 2019. - 1 : Vol. 6.
26. Sandu M. and Scarlat I. Augmented Reality Uses in Interior Design [Journal] // Informatica Economica. - 2018. - 3 : Vol. 22.
27. Siltanen S. Theory and applications of marker-based augmented reality [Conference] // VTT Science 3. - Espoo, Finland : [s.n.], 2012.
28. Siltenen S. and Oksnab V. User-centered design of augmented reality interior design sevice [Conference] // International Journal of Arts & Science. - 2013. - Vol. UniversityPublications.net.
29. Vania A. Use Cases of Augmented Reality in Retail Sector [Online] // Trootech. - 2019. - 2020. - https://www.trootech.com/use-cases-of-augmented-reality-in-retail-sector-2020/.
30. Woodward C. [et al.] Virtual and augmented reality in the Digitalo building project. [Conference] // International Journal of Design Sciences and Technology. - 2007. - Vol. 14.

THE CONTEMPORARY VISUALIZATION AND MODELLING TECHNOLOGIES AND TECHNIQUES FOR THE DESIGN OF THE GREEN ROOFS

Aleksandar Čučaković
Department of Mathematics, Physics and Descriptive Geometry, Faculty of Civil Engineering, University of Belgrade, Belgrade, Republic of Serbia
PhD., Associate Professor, cucak@grf.bg.ac.rs

Biljana Jović
Department of Landscape Architecture and Horticulture, Faculty of Forestry, University of Belgrade, Belgrade, Republic of Serbia
PhD., Assistant Professor, biljana.jovic@sfb.bg.ac.rs

Mirjana Ocokoljić
Department of Landscape Architecture and Horticulture, Faculty of Forestry, University of Belgrade, Belgrade, Republic of Serbia
PhD., Full Professor, mirjana.ocokoljic@sfb.bg.ac.rs

Isidora Marković
Department of Landscape Architecture and Horticulture, Faculty of Forestry, University of Belgrade, Belgrade, Republic of Serbia
MSc., doraaa91@gmail.com

ABSTRACT

The contemporary design solutions are merging the boundaries between real and virtual world. The Landscape architecture like the other interdisciplinary field stepped in a contemporary technologies area focused on that, beside the good execution of works, designer solutions has to be more realistic and "touchable". The opportunities provided by Virtual Reality are certainly not negligible, it is common knowledge that the designs in the world are already presented in this way so the Virtual Reality increasingly used.

Following the example of the application of virtual reality in landscape architecture, this paper deals with proposals for the use of virtual reality in landscape architecture so that designers, clients and users would have a virtual sense of scope e.g. rooftop garden, urban areas, parks, roads, etc. It is a programming language that creates a series of images creating a whole, so certain parts can be controlled or even modified in VR. Virtual reality today requires a specific gadget, such as Occulus, HTC Vive, Samsung Gear VR and similar.

The aim of this paper is to acquire new theoretical and practical knowledge in the interdisciplinary field of virtual reality, the ability to display using virtual reality methods, and to present through a brief overview the plant species used in the design and construction of an intensive roof garden in a Mediterranean climate, the basic characteristics of roofing gardens as well as the benefits they carry.

Virtual and augmented reality as technology is a very powerful tool for landscape architects, when modeling roof gardens, parks, and urban areas. One of the most popular technologies used by landscape architects is Google Tilt Brush, which enables fast modeling. The Google Tilt Brush VR

app allows modeling in three-dimensional virtual space using a palette to work with the use of a three-dimensional brush.

The terms of two "programmed" realities - virtual reality and augmented reality - are often confused. One thing they have in common, though, is VRML - Virtual Reality Modeling Language.

In this paper are shown the ways on which this issue can be solved and by the way, get closer the term of Virtual Reality (VR), also all the opportunities which the Virtual reality offered us. As well, in this paper are shown the conditions of Mediterranean climate, the conceptual solution and the plant species which will be used by execution of intensive green roof on the motel "Marković".

Keywords: Visualization, Landscape architecture, Green roof, Virtual Reality

1. INTRODUCTION

Urban environments face many challenges, especially those related to the preservation of the green environment under the influence of infrastructure development and the rapid expansion of infrastructure facilities that have contributed to minimizing green spaces. In the absence of enough space to form new green spaces in the city, a good way to go back and create a better, more comfortable, healthier and more functional space in the city is to build green roofs, which do not take up additional space in urban spaces and have a great function in creating better microclimatic conditions of the city, reducing the reflection of the sun's rays, reducing the reflection of city noise and reducing the accumulation of heat in the summer. Green roofs represent a very profitable investment, because their lifespan is twice as long as the duration of a conventional roof, thus reducing the need to re-cover buildings [1]. The presence of plants has a positive effect on people by reducing stress and mental fatigue, which are the most common causes of the disease [2]. The notions of two "programmed" realities are often confused - virtual reality and augmented reality. One thing they have in common, though, is VRML - Virtual Reality Modeling Language. It is a programming language that is created through images that create a whole, and certain parts can be managed or even changed. Virtual reality in today's form requires a specific add-on (gadget), in the form of Occulus, HTC Vive, Samsung Gear VR and the like. Augmented reality today certainly requires a ubiquitous gadget - a smart phone. An ideal example of a well-known example of augmented reality is the world-famous game Pokemon GO. Global modernization and following trends subtly requires that the design solutions be as realistic as possible and that it represent a project that will be executed as faithfully as possible to the solution presented. For that reason, augmented and virtual reality can provide a lot to various disciplines, especially in Landscape-architectural projects. Augmented reality is a type of virtual reality in which certain information exists, imperceptible to the human senses, and which is observable and registered in an enlarged representation of reality with the physical world. The difference between virtual and augmented reality is that in virtual reality, the real world is completely replaced by the virtual [3]. Augmented reality has largely found application in a related discipline such as architecture. The big

get a sense of how big the room is [4]. Following the example of the application of augmented reality in architecture, this paper deals with proposals for the use of augmented reality in landscape architecture so that clients and users in a similar way, have a virtual sense of scope, e.g. roof garden, city urban areas, parks, roads, etc.

2. MATERIAL AND METHODS

The method of work is based on the study of professional literature and after the research of making a conceptual solution of the roof garden. The presentation of the conceptual solution in this paper is on the example of the motel Marković, which is located in Šušanj (municipality of Bar) Montenegro, on the coast, where it is planned to build an intensive roof garden so that motel users can additionally enjoy their vacation. Domestic as well as foreign literature related to climate, roof gardens, plants, ways of visualization and modeling was used. In addition to the available professional and scientific literature, consultations with experts in the field, internet portals with available information in the field of visualization, modeling and augmented reality were used. The aim of this paper is to acquire new theoretical and practical knowledge in the interdisciplinary field, with 3D model designed with chosen plant species used in construction of intensive roof garden in Mediterranean climate presentation using contemporary technologies, as well as to give a brief overview of rooftop gardens as well as the benefits they bring.

3. AUGMENTED AND VIRTUAL REALITY

The first system for displaying images of augmented and virtual reality with a head-mounted display (HMD) was developed in 1968 by Ivan Sutherland and his student Bob Sproule. The system worked on the basis of CRT technology and was primitive in terms of interface and realistic display, while the graphics showed the contours of a three-dimensional object. The model was named The Sword of Damocles because of its massive construction that descended from the ceiling to the user's head [5].

The term "augmented reality" is mentioned in the early 1990's, by Caudel and Meisel, scientists at the Boeing Corporation, who developed the unique AR a system that allows workers to connect wires more easily [6]. Virtual Reality (VR): providing information that changes in real time with the feeling and experience that the user is somewhere else. Augmented Reality (AR) is a supply of information that changes in real time with undisturbed observation of the real world and participation in it [7].The requirements that need to be met in order for virtual and augmented reality to be exploited are: Interactive action in real time; Combining real and virtual world in a real environment; and Matching real and virtual objects. The ability to implement computer graphics in the real world is collectively called augmented reality (AR). Unlike virtual reality, augmented reality interfaces at the same time allow users to see the real world as well as virtual recording related to real locations and objects. In the augmented reality interface, the world is viewed through a hand-held or head-mounted screen (HMD) through which the graphics can be seen or overlapped in a video of the surrounding environment. AR interfaces enhance the real world experience, unlike other computer interfaces that distract users from the real world into the virtual [8]. 1994 - Paul Milgram and Fumio Kishino define and present the Reality-Virtuality Continuum in their work [9] (Figure 1). Their continuum considers the space between the virtual and the real, within which there is augmented reality. This research of theirs is generally accepted and represents the unavoidable basis of all modern research in the field of augmented reality.

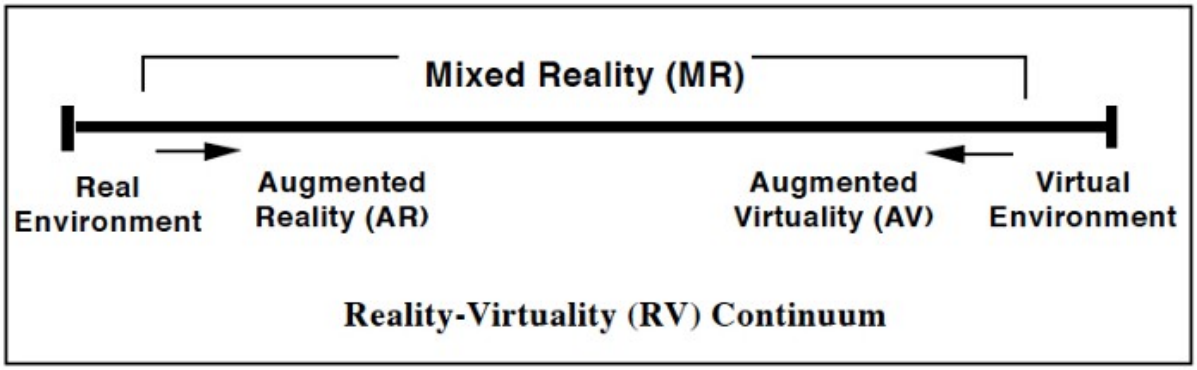

Figure 1: Real-virtual continuum (Milgram et.al. 1994)

The reality-virtuality continuum (Figure 3) ranges from the real, i.e. physical environment, all the way to the virtual environment. Between these extremes there is a mixture of the real and the virtual, the so-called mixed reality [9].

Mixed Reality - (MR Mixed Reality) presents:

-virtual continuum between completely virtual (VE Virtual Environments) and completely real scenes (RE Real Environments),

-inserting virtual elements into the real scene, AR augmented reality

-inserting real elements (images, videos into the virtual scene AV (audio-visual system) supplemented virtual scene (dominated by virtual scene)

-hiding (removing) objects of the actual scene is included (image processing is required) it is necessary to remove shadows of objects (other influences on the scene).

In order to bring the use closer to the users, in a later paper [10] Milgram lists seven types of MR images:

1. Monitor based (non-immersive) video displays. Showing a video about the real world to which digital images are superimposed.

2. The HMD displays the video. Same as type 1 but the content is in HMD.

3. Optical transient HMD. Transparent view that allowing virtual images to be displayed above the real world.

4. Transparent HMD video. It is same as 3, but displaying video from the real world in front of the users by virtual graphics.

5. Monitor-based AV system. Display 3D graphics on a monitor with superimposed video.

6. Full or partial AV that appears in the user environment. This way 3D graphics is shown on a display that turns into an impressive featuring video.

7. Partial AV systems. AV systems allow additional interactions in real objects, such as interaction with one's own real hand.

As the world is three-dimensional and interactive, it requires that the augmented reality system must have the following characteristics [10]:

-combines real and virtual,

-has real-time interaction, and

-functioning is three-dimensional.

The development of modern digital technology has enabled the creation and presentation of three-dimensional virtual models of objects. The basic division of methods for digital representation of objects is:

-Digital images,

-Animation,

-Virtual reality and

-Augmented reality

Virtual and augmented realities as a technology are a very powerful tool for landscape architects, when modeling roof gardens, parks, and urban areas. One of the most popular technologies used by landscape architects is Google Tilt Brush, which enables fast modeling. The Google Tilt Brush VR app allows modeling in three-dimensional virtual space using a work palette using a three-dimensional brush. This equipment was released by Google on April 5, 2016.

Required equipment for Google Tilt Brush VR app is [11]:

-HTC Vive hardware as a head set

-Controllers with motion tracking (brushes)

-Work space

Computer features that could handle these needs are presented on Fig. 2

Component	Recommended system requirements	Minimum system requirements
Processor	Intel Core i5-4590/AMD FX 8350 equivalent or better	Intel Core i5-4590/AMD FX 8350 equivalent or better
GPU	NVIDIA GeForce GTX 1060, AMD Radeon RX 480 equivalent or better	NVIDIA GeForce GTX 970, AMD Radeon R9 290 equivalent or better
Memory	4 GB RAM or more	4 GB RAM or more
Video output	HDMI 1.4, DisplayPort 1.2 or newer	HDMI 1.4, DisplayPort 1.2 or newer
USB port	1x USB 2.0 or newer	1x USB 2.0 or newer
Operating system	Windows 7 SP1, Windows 8.1 or later, Windows 10	Windows 7 SP1, Windows 8.1 or later, Windows 10

Figure 2: Minimum and optimal computer characteristics for using the Google Tilt Brush VR application (https://www.profweb.ca/en/publications/articles/forging-in-3-dimensions-using-vr-and-google-tilt-brush)

3.1. Virtual Reality and Augmented Reality center University of Arts in Belgrade

Within the research work, consultation with colleague from University of Arts in Belgrade was crucial for this paper. The most useful for the preparation of this work is access to the office and laboratory of associate professor Dr. Art Branko Sujić at the Faculty of Dramatic Arts in Belgrade, whose doctoral thesis was done using virtual reality called "Look into the infinity". In the professor's laboratory, there is also equipment that allows entry into the virtual world (Figure 3 and 4). Consultations with the professor were conducted on several occasions, as well as research and training on the use of equipment on the Oculus rift model with three sensors (Figures 5 and 6).

Figure 3: Oculus rift (Photo Isidora Marković)

Figure 4: Holder - *room scale* (Photo by Isidora Marković)

The first experience with virtual reality equipment was made possible by Professor Dr. art Branko Sujić, with a review of films from “Oculus studios”: “Oculus first contact”, “Lost”, “Oculus dream deck” as well as the professor's actual artwork entitled, “Look into the infinity” (Figures 5 and 6).

Figure 5: Testions Oculus rift Equipment in the laboratoire of the Faculty of Dramatic Art of the University of Belgrade (Photo by Branko Sujić)

Figure 6: Test of the Oculus rift Equipment in the laboratoire of the Faculty of Dramatic Art of the University of Belgrade (Photo by Branko Sujić)

3.1.1. TRACKING SENSORS

Monitoring sensors in virtual and augmented reality systems are:

• Camera (computer vision) - used to visually monitor the real world or its individual parts [12].

• Stereoscopic camera - allows visual monitoring of the real world and has the ability to determine the distance of real objects from the cameras [13].

• TOF (Time-of-Flight) camera - a camera that has the ability to detect the spatial distance of each pixel of the image it captures relative to it [14].

• Global Positioning System (GPS) - enables real-world global tracking [15].

• Magnetic compass - measures the magnetic field of the globe. It is used in the navigation process to determine and monitor the change of direction in real time [16].

• Gyroscope - a device for determining the direction of movement or a relative compass (because it only measures the movement of a plane as a result of the influence of force and does not coincide with the direction of the north) [16].

• Accelerometer - a device for measuring the acceleration of a moving body.

• MEMS (Micro-Electro-Mechanical-System) - a microchip for a complete navigation system with compact integration of several sensors simultaneously [16].

4. GREEN ROOF GARDENS

Green roofs date back to ancient times. The first known roof gardens were on the terraces of ziggurats in ancient Mesopotamia, and the ancient Romans planted plants on their flat roofs because they believed that greenery protected them from storms and thunder. Ornamental plants on the roofs were nurtured by the people of northern Europe, in Iceland, and in Scandinavia, within the framework of traditional architecture. The primary reason for this was the level of thermal protection of the roofs, which was so high that the buildings did not require intensive heating even in harsh winters. With the advent of the Renaissance in Italy, King Matthias was the first outside Italy to build hanging gardens at his court in Višegrad [17]. In modern times, the goal of roof gardens and plants on them is to enrich the urban environment as much as possible.

4.1. CLASSIFICATION OF GREEN ROOFS

There are two basic categories of roof green areas: green roofs and roof gardens. Green roofs are called extensive roof greenery, and roof gardens are called intensive roof greenery [18].

The main differences between these two categories of green areas on roofs stem from the type of construction and the category of plants used to raise them.

According to the International Green Roof Association (IGRA), roof gardens are divided into three categories: intensive, extensive and semi-intensive. The criteria for categorizing the types of green roofs according to the GAME are: maintenance intensity, irrigation, plants suitable for planting, depth of substrate, weight of the roof garden, lifting price and benefits of the roof garden.

Intensive roof garden is a garden that includes the use of trees, shrubs, grass areas, water surfaces, as well as the installation of park furniture and paths. This approach requires constant maintenance in terms of irrigation, plant care, maintenance interventions, etc. Maintenance costs are high and are more appropriate for public and commercial facilities [19].

4.1.1. General climatic characteristics of the Mediterranean area

A Mediterranean climate is any climate that resembles the climate of the countries of the Mediterranean basin that makes up half of the surface with this type of climate worldwide. Apart from the area along the Mediterranean Sea, this climate type is prevalent in the western parts of North America, in parts of western and southern Australia, in southwestern South Africa and in the central parts of Chile. The climate is characterized by hot, dry summers and cool, humid winters [20]. Climatic characteristics of Bar in Montenegro: The climate of the Bar area is defined by geographical position, in the zone of temperate climate zone, position right next to the Adriatic Sea and the existence and direction of the mountain range Rumija, which results in openness to maritime influences from the west and continental from east and northeast. The basic features of the Mediterranean climate are mild winters, warm summers, pleasant autumns, long and warmer than spring. For 300 days a year, average monthly temperatures above 10 ° C prevail here, and for 6 months, temperatures are above 15 ° C [21].

Roof gardens are characterized by low tree cultivars that are dwarf, spindle-shaped or mournful. Thin and brittle trees and leaves of light consistency cannot be used. Regardless of the lower height, the trees require additional anchoring (due to higher wind speeds) and increased depth of the substrate (which also increases the load on the roof structure). Therefore, a lighter substrate is used that contains enough nutrients necessary for plant

development. Shrubby plants are widely used in intensive roof gardens, but they must also be of smaller dimensions or dwarf, creeping forms. Creepers are also very often used in intensive roof gardens, but for their use it is necessary to provide adequate conditions, such as a solid and stable base with which to develop. In nature, vines often grow next to a tree; however, the trees used in roof gardens are not a good base. In roof gardens, pergolas or grilles made for this use (upright, in the form of bridges or frames) are a safe base for roofs. In addition to a stable base must also have a strong woody vase that will ensure safe growth. The basic function of woody plants in intensive roof gardens is not shading, but functionality and improvement of the space [22].

Selection of plant material for intensive roof gardens in the Mediterranean climate:

The use of woody plant material in intensive roof gardens depends primarily on the owner of the roof, his needs and desires when arranging. By using various decorative plants, the space on the roof can be enriched and made more pleasant to stay. Due to the specific conditions that prevail on the roof and the height at which the garden itself is located, woody plants of large dimensions are not used, but those of lower growth or different cultivars of dwarf growth. Light plants predominate due to the strong sun exposure of the roofs, but depending on the position of the roof and shading, semi-shade and shade plants can also be used [23].

5. THE CONCEPTUAL MODEL OF THE GREEN ROOF ON THE EXAMPLE OF THE MOTEL "MARKOVIĆ"

3D modeling of the garden (in the software designed for landscape architects) as one of the possible computer-graphic solutions, beside VR/MR/AR is used during design thinking. Main research and the final design solution is an obtained using an available software such as Realtime Landscaping Architect 2016. Realtime Landscaping Architect offers a wide range of plants, garden furniture, type of paving, etc. Photographs used as a background when creating the conceptual solution were made using a drone DJI SPARK Drone Controller Combo. The surface of the building is 950m^2, while the dimensions of the planned roof garden are 7.5m x 10m. The accommodation capacity of the motel is 80 people.

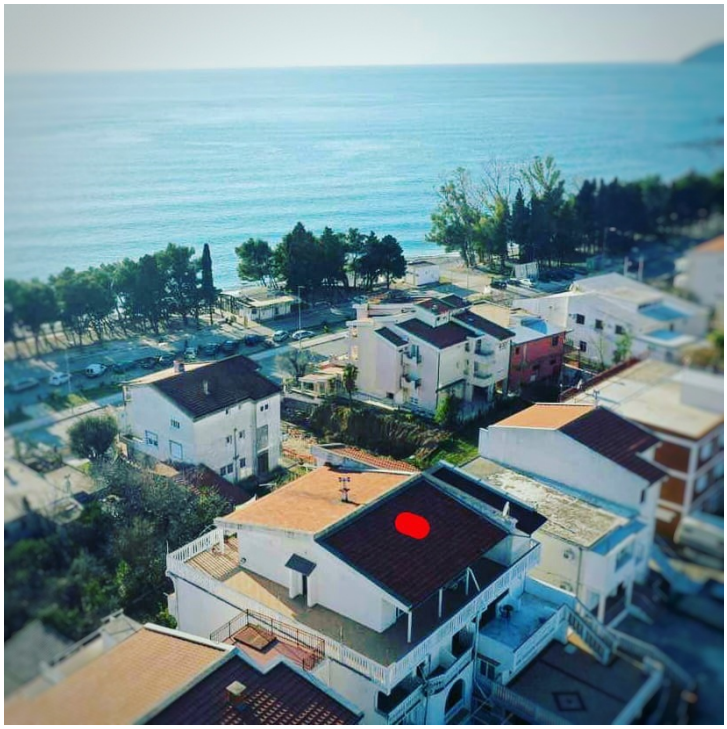

Figure 7: View of the location of the motel in relation to the promenade and the coast (Photo Isidora Marković)

The location of the motel "Markovic" is characterized by close proximity to the coast, promenade and the center of Bar (Figure 7). Due to the large number of visitors to the motel and the interesting location on the Adriatic coast, the following is a presentation of the conceptual solution of the roof garden. The selection of plant species was made on the basis of the climatic characteristics of the Mediterranean area, as well as on the type of roof garden that will be performed - intensive roof garden, which is shown in the legend of plant material (Figure 8).

The Realtime Landscaping Architecture software offers a wide range of plants, divided into groups into: annual plants, cacti, perennials, shrubs, trees, tropical plants, plants used for aquatic habitat, topiary plants and a search of plants by name (Figure 9).

Legend of plant material used in this conceptual design project:

1. *Laurus nobilis*L.

2. *Berberis vulgaris* L.

3. *Acacia decurrensvar.dealbata* (Link) F. Muell

4. *Rhus typhina* L.

5. *Prunus laurocerasus* L.

6. *Hibiscus syriacus* L.

7. *Yucca filamentosa* L.

8. *Clematis x jackmanii* T. Moore

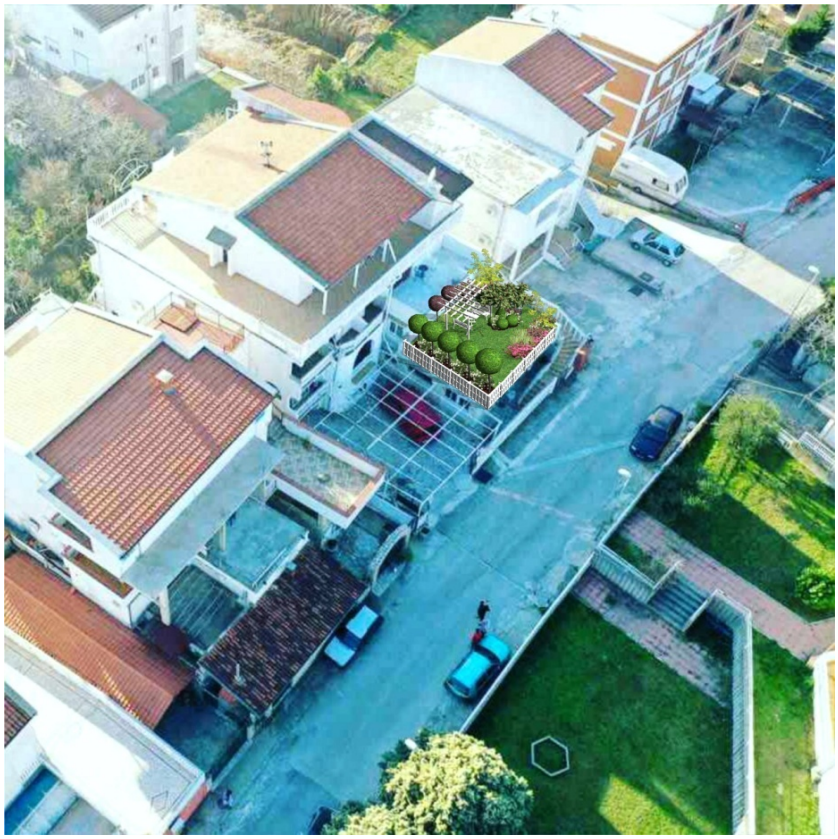

Figure 8: Conceptual design of rooftop garden

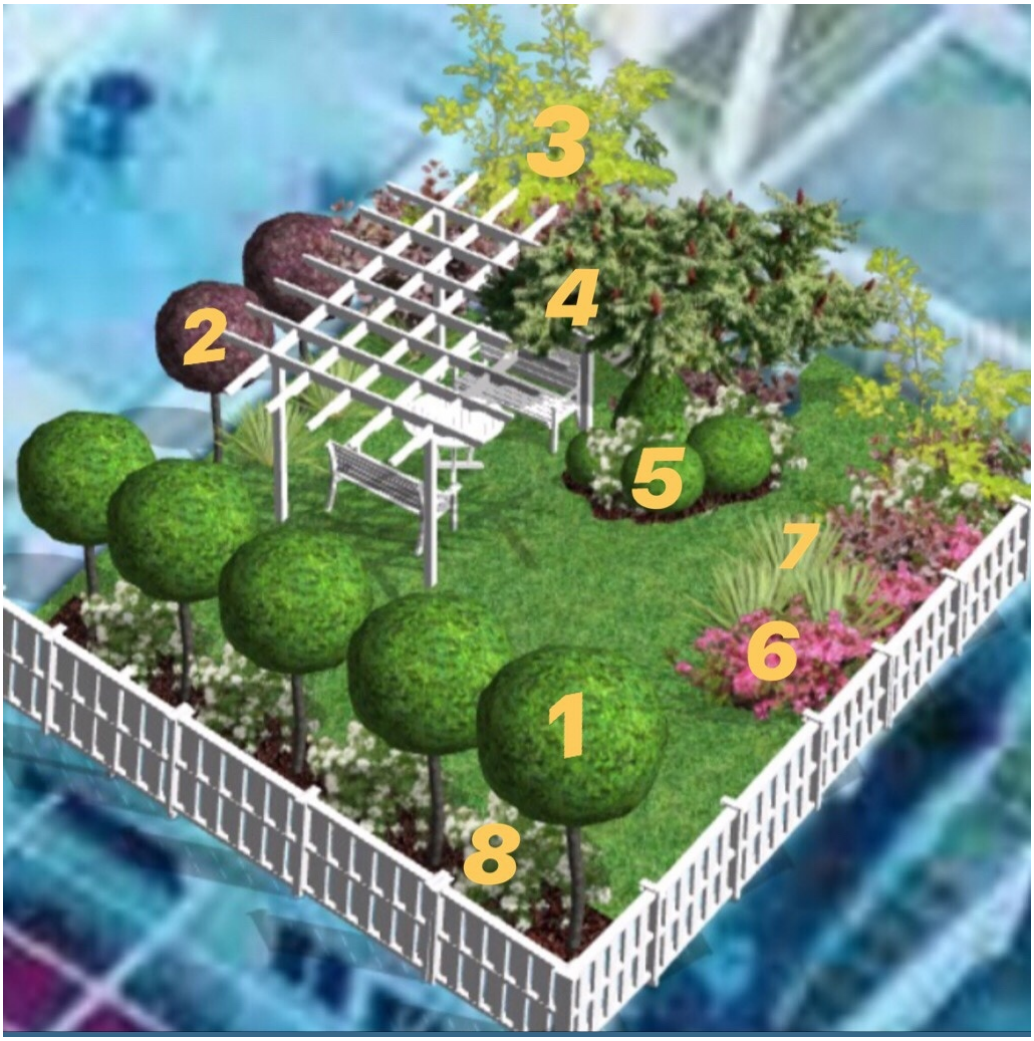

Figure 9: Detail of the conceptual design of rooftop garden with marked plant species 1-8

6. CONCLUSIONS

Virtual reality (VR) and Augmented reality (AR) already exists and will be more and more present, that is, there is a growing use in everyday life of a display system that implies some kind or elements of augmented reality. Therefore, landscape architecture as a modern and interdisciplinary science should follow new trends and be up to date with emerging innovations that are yet to be developed.

Since the Mediterranean is rich in greenery the green roof garden at the motel "Markovic" could give additional value to this specific landscape where there is no so many rooftop gardens in this area. Besides that green roofs also give a special function by providing better connected green system in this part of the city on the coast, following the best practice and actual trending.

Roof gardens are primarily efficient in urban, urban environments, given that roofs make up a large percentage of the city's area. Such roofs have economic (increase of energy efficiency of buildings), ecological (modification of climatic parameters and air composition, reduction of noise and in any form influence on improvement of living conditions in the city) and aesthetic significance, increase of decorative value of flat roof.

In this paper are shown the ways on which this issue can be solved and by the way, get closer the term of Virtual reality (VR) and Augmented Reality (AR), also all the opportunities which the Virtual Reality (VR) and Augmented reality (AR) offered us. As well, in this paper are shown the conditions of mediterran climate, the conceptual 3D design model and the plant species which will be used by execution of intensive green roof on the motel “Marković”.

Specific research questions in this paper are addressed to using contemporary technologies in 3D modeling design process green rooftop gardens. The main scientific contribution of this work is in the field of experimental design.

New knowledge is developed here as a result like experiments done in the VR lab at the University of Arts in Belgrade concerning applications of the various 3D modeling design solutions for rooftop gardens.

This research is first one connected to this inter or transdisciplinary landscape architecture topic done in cooperation between two Universities in Belgrade (University of Belgrade and University of Arts). So, it is just first step in future planned collaboration. Methodology is experimental design approach and evaluation as well as development of visualization techniques will be researched in next phase of common projects where students of landscape architecture and students of University of Arts will work together on new projects that are using VR technologies. Benefits and drawbacks will be investigated using questioners when more research results in the form of 3D models design projects of rooftop gardens will be done.

Acknowledgements

Authors are supported by the Ministry of Education, Science and Technological Development of the Republic of Serbia, Projects No. TP 36008 and project No. TP 31041 (451-02-68/2020/14/2000169).

7. REFERENCES

[1] Peck& Kuhn, 2003 Design Guidelines for Green Roofs, OAA, Home to Canadians, Canada.

[2] Gedge & Frith, 2004 Green Roofs-Benefits and Cost Implications, Birmigham City, Council, Birmigham.

[3] Čučaković A., Jović B., (2011): Constructive Geometry Education by Contemporary Technologies SAJ_2011_3_ Serbian Architectural Journal, original scientific article, approval date 12.06.2011. UDK BROJEVI 514.18:62 ID BROJ 184977420

[4] History of information, ' Ivan Sutherland and Bob Sproull Create the First Virtual Reality Head Mounted Display System', n.d. [Online]. http://www.historyofinformation.com/detail.php?entryid=1087, [visited 13.05.2019.]

[5]D.W.F. Krevelen, R. Poelman, "A Survey of Augmented Reality Technologies", *The International Journal of Virtual Reality,* vol. 9, no. 2, pp. 2, 2010.

[6] Zhou, Z.Y.,Karlekar J., Hii D., Schneider M., Lu W., Wittkopf S. Robust pose estimation for outdoor mixed reality with sensor fusion, 2009

[7]Augmented Reality in Education by Mark Billinghurs (https://s3.amazonaws.com/academia.edu.documents/4810740/ar_edu.pdf?response-content-disposition=inline%3B%20filename%3DAugmented_reality_in_education.pdf&X-Amz-Algorithm=AWS4-HMAC-SHA256&X-Amz-Credential=AKIAIWOWYYGZ2Y53UL3A%2F20190705%2Fus-east-1%2Fs3%2Faws4_request&X-Amz-Date=20190705T120750Z&X-Amz-Expires=3600&X-Amz-SignedHeaders=host&X-Amz-Signature=2ecfe7fd8c8c576fb52dded404d73b0a7fde9eb0a80ac2ddbeb109175c3f61ce–)

[8] Milgram, P. & Kishino, F., 1994. Taxonomy of Mixed Reality Visual Displays. IEICE Transactions on Information and Systems

[9] Milgram, P., Takemura, H., Utsumi, A., & Kishino, F. (1995). Augmented reality: A class of displays on the reality-virtuality continuum. In *Photonics for industrial applications* (pp. 282–292). International Society for Optics and Photonics.

[10]Craig, A., 2013. Understanding Augmented Reality - Concepts and Applications. 225 Wyman Street, Waltham, MA 02451, USA: Morgan Kaufmann, imprint of Elsevier.

[11]https://www.profweb.ca/en/publications/articles/forging-in-3-dimensions-using-vr-and-google-tilt-brush

[12]Grubert, J. & Grasset, R., 2013. Augmented Reality for Android Application Development. Livery Place, 35 Livery Street, Birmingham B3 2PB, UK.: Published by Packt Publishing Ltd..

[13] Kanbara, M., Okuma, T., Takemura, H. & Yokoya, N., 2000. A stereoscopic video seethrough augmented reality system based on real-time vision-based registration. Virtual Reality, 2000. Proceedings. IEEE, pp. 255-262.

[14]Fischer, J., Huhle, B. & Schilling, A., 2007. Using Time-of-Flight Range Data for Occlusion Handling in Augmented Reality. IPT-EGVE Symposium, Weimar, Germany.

[15]Parkinson, B. W., 1996. Introduction and Heritage of NAVSTAR, the Global Positioning System. U: Global Positioning System: Theory and Applications. Washington, D.C.: American Institute of Aeronautics and Astronautics, pp. 3-28.

[16]Rizov, T., 2014. ГЕОМЕТРИСКО ПРЕТСТАВУВАЊЕ НА ОБЈЕКТИ ВО ИНТЕРАКТИВНА АУГМЕНТНА РЕАЛНОСТ. Skopje: Univerzitet "Sv. Kiril i Metodij", Mašinski fakultet

[17]http://www.gradjevinarstvo.rs

[18] Anastasijević N.: (2011) Podizanje i negovanje zelenih površina, Šumarski fakultet u Beogradu, Beograd.

[19] Stevanović, J. (2011): "Zelena t(e)rasa- radionica o krovnim vrtovima", Šumarski fakultet, Beograd

[20]http://upoznajsvet.blogspot.com/2015/12/sredozemna-klima.html?view=magazine

[21] Fuštić, M. (2014): "Nautički marketing na primeru marine Bar", specijalistički rad, fakultet za mediteranske poslovne studije, Tivat

[22] Vukićević, E. (1996): "Dekorativna dendrologija", Univerzitet u Beogradu, Šumarski fakultet, Beograd.

[23] Ocokoljić M. i Ninić-Todorović J. (2003); Priručnik iz dekorativne dendrologije, Univerzitet u Beogradu, Šumarski fakultet, Beograd

PARAMETRIC ANALYSIS OF URBAN BLOCK GEOMETRY BASED ON VISUAL PRIVACY CONDITIONS PARAMETRIC - REFLECTING ON COVID-19 LOCKDOWN

Ana Perišić
Faculty of technical sciences, University of Novi Sad, Novi Sad, Serbia
PhD., Assistant Professor, anaperisic@uns.ac.rs

Marko Lazić
Faculty of technical sciences, University of Novi Sad, Novi Sad, Serbia
PhD., Assistant Professor, lazic.m@uns.ac.rs

ABSTRACT

This paper presents the results of the parametric analysis of visual privacy conditions in the case of three urban blocks with distinct geometry type. The influence of visual privacy on the health of the residents and the general living conditions is analyzed. The parameters are defined based on the results of research in the field of psychology, sociology, and medicine. Geometry and dimensioning of an urban block as the building element of the city environment is essential for the creation of a humane living environment. The built environment in terms of defining this aspect works on several generations of inhabitants and has long-term consequences. Computer graphics served as a framework for presenting the results of this research. Grasshopper and Rhino 3D software was used for simulation of visibility-vulnerability of the surface of the facade based on predefined conditions. The process is performed by determining critical points of the facade area of the urban block as part of the predefined grid. The grid applied in this analysis is at a macro level with a potential for resolution adjustments. The results are displayed in a form of graphs and as a graphical 3D model.

Keywords: computer graphics; simulations; computer science; urban block; privacy

1. INTRODUCTION

Considering the recent events during COVID-19 pandemic lockdown the research published (Perisic, 2016) has a new weight in evaluating the possible and longterm impact of the built environment on mental health and wellbeing. The need to protect privacy, in addition to access to daylight and ventilation, appears at an early stage in the history of settlement building. Territoriality was a key determinant of the rules of conduct in social communities both in the early stages of settlement and throughout history, in the form of choosing defendable places and marking the boundaries of a location belonging to an individual or group.

According to numerous researches, building density and population stand out as a factor that can endanger human mental health. Research confirms the link between privacy violations (physical or visual intrusion of personal space) and reduced ability to work and the occurrence of mental disorders in people.

2. RESEARCH BACKGROUND

The concept of territoriality refers to a physical place such as a home or a place in a business facility (Pluckhan, 1968; Altman, 1975). It is described as one of the essential human needs (Oland, 1978; Tate, 1980; Hayter, 1981). In scientific literature, territoriality is widely seen as belonging and control over a physical zone of space (Roberts, 1971). Territories are being used to regulate cooperation and maintain social order. The main division of territories based on (Lyman, et al., 1967) are: public spaces, home territory, interaction territory, and personal body zone. Personal space is (Gifford 2007: 135) defined as "a dynamic spatial component of interpersonal relationships". Territoriality is considered to be the ability to control and regulate the use of space (Evans, 2003).

2.1. Territoriality and the need to define the boundaries of the territory

Relaying on spatial boundaries often provides a definition, both individual and collective, of the territory owned or claimed. The physical dimension of privacy implies the degree to which a person is physically available to others. Privacy is closely related to the concept of personal space which is described as the basic premise of privacy.

Territories support social roles within the community. The specific context is always concerning specific roles (Prohansky et al., 1970) which implies that the significance of a place is defined by its exclusive use. A set of allowed behavior patterns is associated with each space.

A place belonging to a group is a space that is collectively inhabited and has a socioculturally controlled physical environment (Minami and Tanaka, 1995). Such a situation appears in the conditions of multi-family housing, where the inhabitants react negatively or suspiciously if an unknown person appears in the yard of the block. Territoriality in this sense serves as a basis for the development of personal and group identity. The links between group activity (a sense of belonging to a larger group of people) and spatial identity are of great importance for human health (Fried, 1982). In the early period of the theory of "defendable" places, according to Newman (Newman, 1972), it was considered that such space contains more housing units because residents have a greater sense of security, belonging to space, a sense of security and their engagement raises the level of informal surveillance. For that reason, Newman believed that the level of crime is declining in environments where residents feel not only their homes but also the surrounding areas as their own, as is the case with multi-family housing. He considers such spaces "defendable". Newman and Frank tested the relationship between physical design and its impact on crime levels by analyzing the testimonies and living environment of 2,655 Americans in the United States (Newman, et al., 1982). The results convey a partial agreement with the basic assumptions of the hypothesis (eg. a higher level of security in the case when the residents had a sense of control and the ability to monitor events in the surrounding areas). Later research, however, concurred that in the case of high housing density an aggressive behavior occurs.

Researchers, such as (Stokols, 1993), see the connection between grouping a larger number in one place (staying in crowds - crowding) and declining results at colleges and impaired student health. Preliminary research on human spatial behavior has concentrated on three causal factors: biological, cultural, and environmental conditioning. Crowding studies show contradictory evidence of hostility and reduced ability to act in adults and children (Griffitt, et al., 1971). According to research of neighborhoods and communities within apartment blocks, a more significant influence of the physical characteristics of the environment concerning the social condition and the quality of interpersonal relationships is shown (Fried, 1984). As social density (number of people) increases, satisfaction with the environment decreases (Duval, 2002), and the level of physical comfort decreases (Aries, et al., 2010). Lack of acoustic, and especially visual privacy - exposure to views, are cited as the most significant sources of stress in a densely populated environment. Privacy can encourage or limit human development depending on how accessible it is to the individual. Psychological stress, which arises in response to this situation, can over time affect mental health problems (Godin, et al., 2005). The density and great closeness of people leads to intense attention, because a person must unconsciously monitor a large number of potentially threatening stimuli in his environment. This environment leads to "cognitive exhaustion" and other effects such as impaired attention and concentration and decreased performance at work. A major psychological and sociological problem is the possibility of individual regulation of social contacts (Altman, 1975).

Stimulus overload is a typical condition in the case of crowding. Research in the field of psychology (Simmel, 1969) analyzes life situations in an urban environment in which people have a large number of daily contacts at a small distance from each other. Too many people in an environment that has many stimuli (noise, smells, colors ...) can lead to overloading the nervous system of individuals and often results in "social withdrawal" in an attempt to limit a person's involvement in associations or completely avoid interaction with others.

2.2. Territoriality and distance

Territoriality refers to the space that a person perceives as his own. The proportions of that space can vary from a residential unit, to an urban block, neighborhood, part of the city, etc. There is a form of territoriality that is associated with the human body defined by different distances and unwritten rules of conduct depending on the proximity to whom communication between an individual and a group takes place. Personal space is an invisible space around the human body, an individual zone that separates people from one another (Sommer 1969; Altman, 1975; Insel, 1978; Barron, 1990).

Hall defined four types of communication zones, ie distances (Hall, 1966):

1. intimate
2. personal
3. social
4. public

These zones are not strictly defined and vary depending on the individual, culture, social norms and space (Table 1).

Table 1: Tabular presentation of distance categories and types of interactions
(Source: Hall (1966))

Category	*Distance*	*Type of interaction*
Intimate distance	*from the body up to 45 cm (or 50 cm)*	*Confrontation, threatening.*
Personal distance	*45 to 120cm*	*Conversation among close friends.*
Social distance	*120 to 360cm*	*Informal and business conversation.*
Public distance	*360 to 450cm (or 750cm)*	*Addressing the audience, meeting strangers.*
Communication distance	*over 2000cm til 3000cm*	*At a distance of 30m, the need for communication ceases and privacy is protected.*

A popular trend of open-plan workspaces in modern design, is proven to be a psychologically stressful environment due to inadequate spatial distances between employees. This environment increases the level of anxiety, reduces the level of desirable communication, and increases the level of unwanted encounters and communication among employees (Zalesny, et al., 1987). As much as 70% of resigning is associated with some kind of feeling of invasion of privacy among employees (Perce, 2006).

Research argues that increasing visual exposure increases the number of interactions between people (Olson, et al., 2000). Visual accessibility to other people, especially in the workplace, intensifies verbal and nonverbal communication. In addition to close distances, there are other distances associated with human communication and privacy. Allen was among the first to explore further spatial distances and its impact on interpersonal communication (Allen, 1977). He presented the results of the research on the "Allen's curve" which describes the relationship between distance and intensity of communication (Figure. 1). Allen's classic curve shows that the possibility of communication between people decreases sharply at a distance of 30 meters and after that remains unchanged regardless of the increase in distance. This research has been confirmed by several authors (Kabo, 2006; Peponis, et al., 2007).

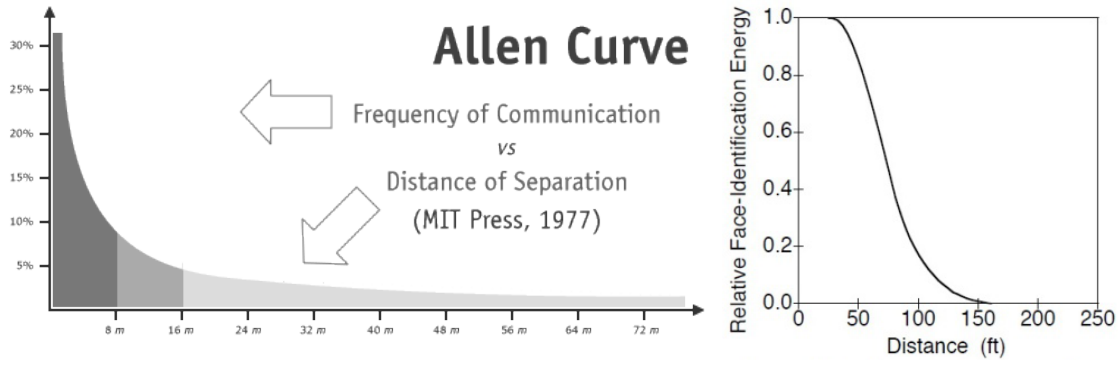

(a) (b)

Figure. 1: (a) Communication frequency curve concerning distance, and (b) Face-Identification curve concerning distance (Source: Allen (1977), Loftus, et al. (2004))

3. THE SIGNIFICANCE OF VIEW FOR HUMAN HEALTH

Housing satisfaction is determined by several parameters, including life stage, socioeconomic status, character, values and norms of the environment and society, and interpersonal relations with neighbors. Researches show that the physical characteristics of a house such as shape, architectural style, foundations, colors, and environment of a building as well as cultural background can influence housing preferences, choices, and satisfaction (Michelson, 1977). Numerous studies confirm that living in poor quality areas affects the socio-emotional health of children and adults (Evans, et al., 2000).

The literature related to the design of business premises is largely oriented towards factors that impair the mental health of employees (Veitch, 2011). Among the most important characteristics of the environment that can affect recovery from stress and increase work efficiency is, as shown by numerous studies, the window view (Ulrich, 1984). Ulrich demonstrated that hospitalized patients who had a view of nature through the hospital room window recovered much faster after surgery and used much less painkillers than those who had a view of the wall of a neighboring building from the window.

Research has shown that more than 35% of workers find extremely difficult working conditions in rooms without windows (Collins, 1975). During the research, children who stayed in rooms lit only by skylights displayed a higher level of anxiety, mental immaturity, increased aggression and irritability, when solving routine tasks and games, compared to their peers who stayed in rooms with a direct view of the external environment. Studies show that subjects who had a view of nature had lower blood pressure and better concentration compared to their counterparts who were in a windowless environment (Heerwagen, 1990). Studies have concluded that the introduction of daylight is better than fluorescent lighting, but also that the view through the window is important. Computer programmers who had a view through the window spend more than 15% of their time working on primary tasks, while employees who spent time in rooms without windows spent more than 15% of their time talking to each other and on the phone (Heschong, et al., 1999: 10).

In a study cited by Heerwagen, et al. (1986) conducted by the 1986 Veto, evaluated the effects of natural light and views on prisoners housed in different cells. Prisoners who had views of the field, mountains, and nature had significantly fewer calls related to stress-induced health problems than those who had views of the prison yard and buildings. Prisoners on the second floor also had fewer calls for medical assistance than prisoners on the ground floor and first floor. The reasons for this are the positive psychological impact of expanded views of the sky and the environment. Prisoners housed on the lower floors also reported feelings of stress due to lack of privacy and exposure to passers-by. These results can be registered without exception in the conditions of modern multi-family housing.

4. MATERIAL AND METHODS USED

The model for experimental verification illustrates the computer analysis of the degree of visual privacy in built urban environments. The theoretical part defines the distance limits for different types of communication. A distance of 30 meters is adopted as the limit of the need for communication ceases. The scope of observation must be wide enough to obtain valid results. In the case of simulation, it is necessary to observe objects that are located in a belt of 30 m from the boundaries of the urban block. The aim of the analysis is the localization and graphic presentation of areas that have an endangered level of privacy, ie they have facilities that are at a smaller distance from the facade.

The process of analysis of the facade implies its grid into observation zones arranged concerning the potential positions of the windows. In the direction of the normal concerning the plane of the facade cladding, for each part of the surface, an angle of observation is constructed that corresponds to the human view (cone of view) from one or more points on the divided surface of the facade (point of view). It is defined by the following measures: the angles of the human gaze (turquoise triangle in Figure. 2a), where 250º is lateral viewing on both sides from the axis, as well as for the view up, and 300º for the view down. The length of the view is 30 m, conducted from the research cited in the previous chapter (Allen, 1977). The top of the pyramid (the field of view defined in this way) represents the point of view, and view rays are formed from it in a 5x5 grid (a total of 25 rays) (Figure. 2b). The lengths of the lines are 30 m each, and their total length is 25 x 30 m = 750 m.

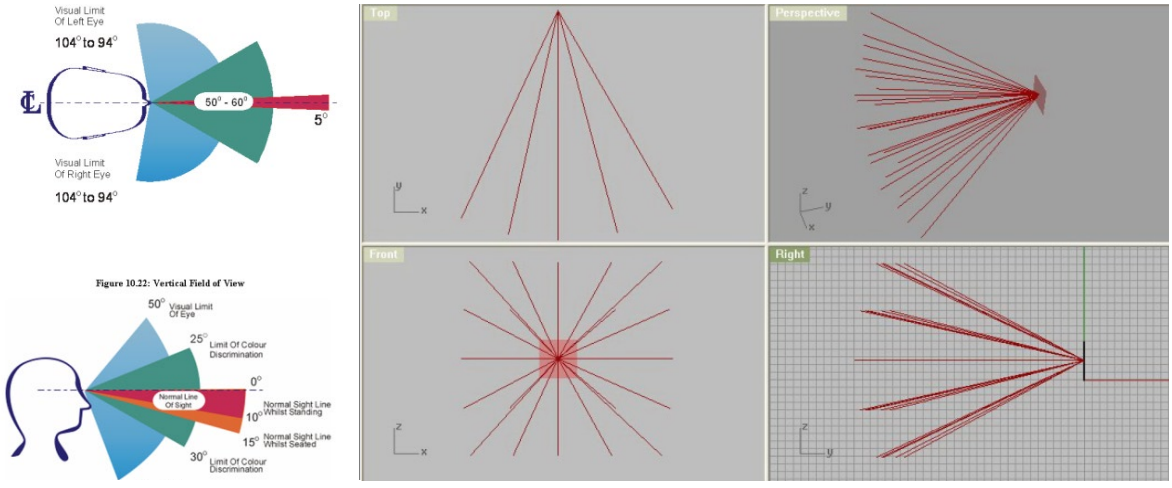

(a) (b)

Figure. 2: (a) The angle of a human's gaze, (Source: EIAR. (2007)) and (b) computer-generated geometry of view propagation

The next step is to detect the intersection of lines on the envelope surfaces of the formed 3D model. For each intersected line we calculate the length from the source (observation point) to the intersection with the first surface in the model, following the total sum of all line lengths is recalculated. The initial sum (of unobstructed view) is divided by 750, after that the percentage of the obscurity of the view is obtained.

The obtained value is converted into color chromatic scale where 0%, ie completely obscured view, corresponds to black color, and 100%, ie unobstructed view corresponds to white color, while other values are expressed by appropriate shades of gray.

The procedure is repeated for each surface of the divided facade. As a result of this processing, a visually modified initial 3D model was obtained, their envelope was colored depending on the views from different surfaces (Figures. 3,5,7).

A hybrid software environment for privacy analysis was formed based on the Rhinoceros 3D software package with the Grasshopper plug-in, using comparative analyzes of available simulation software tools.

5. MODEL ILLUSTRATION ON EXAMPLES OF TYPICAL URBAN BLOCKS

Analyzes of four typical urban block morphologies that occur in the area of Novi Sad were performed to illustrate the functioning of the model. The nature of the privacy parameters that were reduced to the geometry of the 3D model did not require the definition of other types of parameters. The geometry of the urban blocks is simplified, and the surrounding built environment is not included in the analysis. In the real situation, surrounded by the built environment, these results, depending on the morphology of the urban tissue in which the urban block is located, would have to be harmonized. Before analyzing the 3D model, its surfaces were divided by forming a grid with mesh elements measuring 5 m x 5 m. The dimensions of the grid can be changed arbitrarily, depending on the need. The grid dimension in this experimental simulation was taken as a boundary test to illustrate the functioning of the model and the capabilities of the hybrid environment. The simulation in real conditions, in usual construction conditions, would be provided by a higher density grid, e.g. reduced to 3 m x 3 m.

The level of details, the accuracy of the obtained results as well as the duration of the simulation, having in mind the semi-automatic correction of the results, are directly conditioned by grid density formed by the preprocessing step of the 3D urban block model. A visibility simulation is performed, with the support of Grasshopper software, and each surface is analyzed separately. The number of surfaces increases the duration of the analysis. The procedure begins with determining the geometric center of gravity of each surface that represents the viewpoint and from which the view cone is formed. The angle of observation of the human gaze (visual cone) is constructed from the center of gravity point of the surface in the direction of the surface normal.

The results of the research on the privacy conditions of 3 urban block types are presented in graphical form in the continuation of the experimental part of the paper. The degrees of privacy for different morphologies of urban blocks were determined based on the obtained graphs.

5.1. Urban block with multi-family residential towers

In the case of a typical block with multi-family towers (Figure. 3), the most endangered area is the ground floor and the first floor when it comes to exposure to views. Surfaces marked in black represent the most endangered areas on the facade when it comes to visual privacy. For that reason, they are suitable for rooms with secondary purposes, such as stairs, pantries, etc. They are not suitable for residential use.

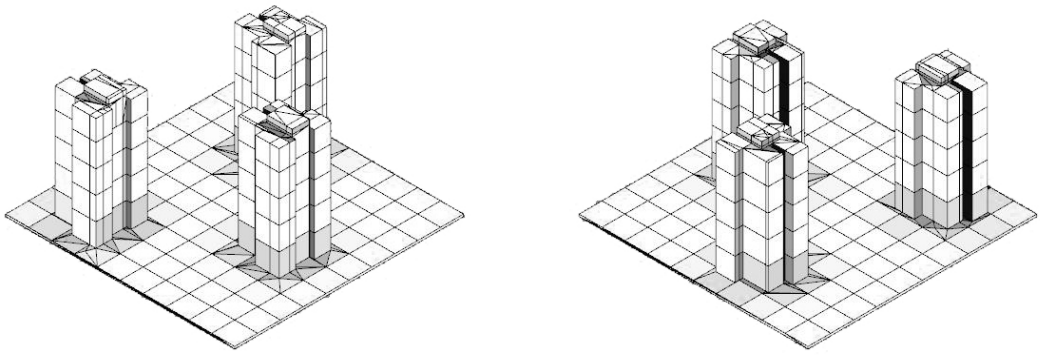

Figure. 3: The result of the simulation according to the model on the example: an urban block with multi-family residential towers

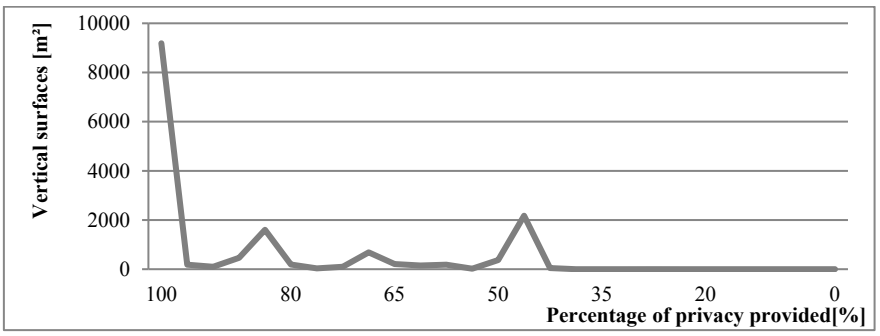

Figure. 4: Graph of the results of the percentage of provided privacy of urban block areas

The graph of the obtained results of the simulation of surface privacy conditions in the model of an urban block with multi-family residential towers (Figure. 4 and Table 2) shows that only 42% of the surfaces are exposed to views. It is designed for medium housing density (about 700 inhabitants/ha).

Table 2: Percentage of provided visual privacy of block surfaces

Percentage of visual privacy provided based on criteria	*Vertical surfaces of the block [m²]*	*Percentage of visual privacy of the total facade surfaces of the urban block*
>95%	*9187*	*58%*
85% - 95%	*745*	*5%*
70% - 84%	*1929*	*12%*
55% - 69%	*1229*	*8%*
40% - 54%	*2616*	*17%*
25% - 39%	*1*	*0%*
0% - 24 %	*0*	*0%*

In the case of multi-family housing, the ownership of the space of the housing unit is not strictly defined, but is of a communal character. A small percentage of occupancy of the plot (about 10%) can contribute to reducing the number of unwanted encounters.

5.2. Border urban block type with open space yards

In the case of a typical border urban block with an open yard space (Figure. 5), the most endangered area is the ground floor and the first floor when it comes to exposure to views. Residents who have residential units on the corner of two buildings overlooking the courtyard have the lowest level of privacy. The fascilities are at a proximal distance that does not compromise privacy when it comes to views.

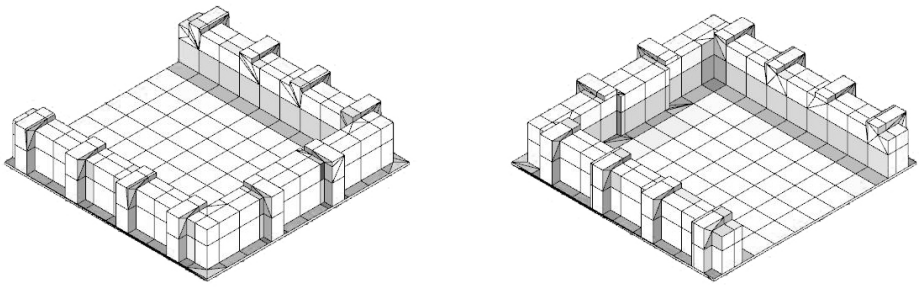

Figure. 5: The result of the simulation according to the model on the example: a boundary urban block with an open yard space

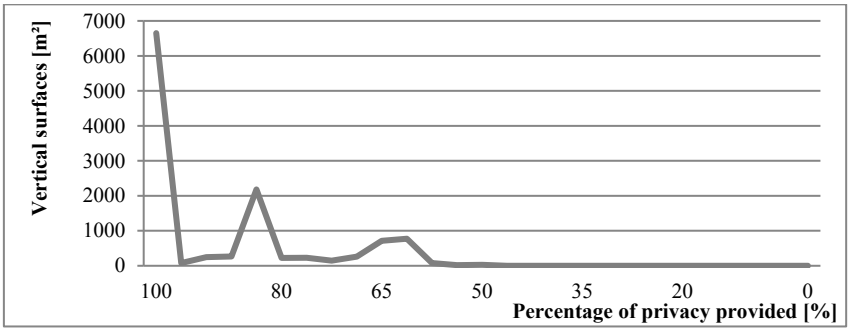

Figure. 6: Graph of the results of the percentage of provided privacy of urban block areas

The graph of the obtained results of the simulation of surface privacy conditions in the urban block model of the boundary urban block with open yard space (Figure. 6 and Table 3) shows that 44% of the surfaces have a compromised level of visual privacy.

Table 3: Percentage of provided visual privacy of an urban block surfaces

Percentage of visual privacy provided based on criteria	*Vertical surfaces of the block [m²]*	*Percentage of visual privacy of the total facade surfaces of the block*
>95%	*6650*	*56%*
85% - 95%	*589*	*5%*
70% - 84%	*2782*	*23%*
55% - 69%	*1827*	*15%*
40% - 54%	*48*	*0%*
0% - 39%	*0*	*0%*

There are no areas where privacy compromised below 50%, which makes this type of an urban block one of the better morphological solutions of the built environment based on the analysis criteria. The percentage of plot occupancy is low (about 30%) and the housing density (about 700 inhabitants/ha) is the same as the previous block type.

5.3. Densely constructed boundary urban block type

In the case of a typical densely constructed boundary urban block type (Figure. 7) the analysis shows that its morphology is poor when it comes to protecting the privacy of the occupants. A small number of housing units that have a view of the inner courtyard do not endanger privacy. The interior of the urban block is the most endangered, especially in the ground floor area. Everyone except the tenants on the top floors have their privacy compromised.

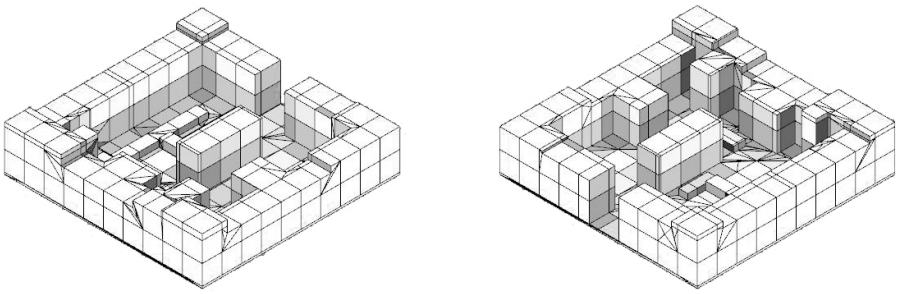

Figure. 7: Simulation result according to the model on the example: densely constructed boundary urban block

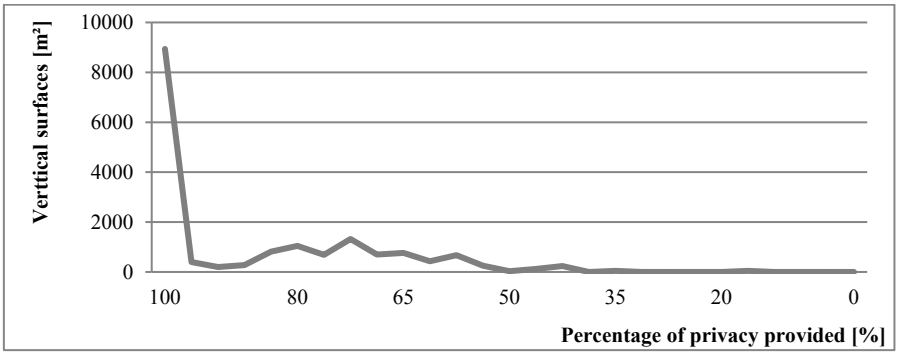

Figure. 8: Graph of the results of the percentage of provided privacy of an urban block areas

The graph of the obtained results of the simulation of the privacy conditions of the surfaces in the model of a densely built boundary urban block (Figure 8 and Table 4) shows that 47% of the vertical surfaces in the urban block do not have sufficient privacy conditions. The morphology of the urban block is insufficient when it comes to protecting the privacy of tenants.

Table 4: Percentage of provided visual privacy of the urban block surfaces

Percentage of visual privacy provided based on criteria	*Vertical surfaces of the urban block [m²]*	*Percentage of visual privacy of the total facade surfaces of the urban block*
>95%	*8937*	*53%*
85% - 95%	*871*	*5%*
70% - 84%	*3868*	*23%*
55% - 69%	*2561*	*15%*
40% - 54%	*639*	*4%*
25% - 39%	*49*	*0%*
10% - 24 %	*44*	*0%*
0% - 10%	*1*	*0%*

The percentage of plot occupancy is high (about 60%) and housing the density is also high (about 1400 inhabitants/ha) compared to the previous two examples analyzed.

6. CONCLUSIONS

The results of the analysis of experimental privacy simulations vary depending on the type of the urban block, in terms of healthy living conditions and the impact on mental health in correlation to geometry. The analysis display the maximum potential of the privacy conditions of each simplified urban block type 3D model, depending on their morphology. In conclusion of theoretical and experimental research the following relationships of 3D model measures have the greatest impact on privacy conditions:

- Density of construction,
- Disposition of buildings on plots, and
- Morphological characteristics of objects on the plot.

In the case of the morphology of the urban block with multi-family residential towers analysis, the tenants have the most sufficient visual privacy ambiance. The distances between the buildings and their disposition at the base of the urban block enable the protection of the visual privacy of the tenants. The small percentage of occupancy of the plot (about 10%) can contribute to reducing the number of unwanted encounters. The boundary type of the urban block with an open yard space based on the given criteria represents the second favorable type of morphology when it comes to the visual privacy of the inhabitants. Of the total area of the facade cladding, 56% of the area has sufficient privacy conditions. The percentage of plot occupancy is low (about 30%) and the housing density (about 700 inhabitants/ha) is the same as the previous block type. The most unfavorable results

were achieved by a densely-built border urban block. The high percentage of plot occupancy (about 60%) and housing density (about 1400 inhabitants/ha) additionally increases the number of unwanted encounters, which can be reflected in increased levels of anxiety and aggression among tenants. The number of possible interventions is limited since private property is limited to the residential area, and not to the free areas of the urban block, so the installation of effective visual barriers is disabled.

Reflecting on the period of lockdown during the COVID-19 pandemic, these results stress the need for reevaluating building density and its impact on mental health and wellbeing. By analyzing the window view, proven by numerous theoretical researches as one of the key components of children and adult mental health factors, further researches planned can locate the most critical areas in the city. As part of future experimental privacy research, it is necessary to include the links between the morphology of the urban block and its environment. There is also a need for preparation of the basis for creating conditions for parametric generation of different purposes of the premises within the buildings in the urban block depending on the degree of sufficient privacy conditions.

REFERENCES

1. Allen, T. J., 1977. Managing the flow of technology: Technology transfer and the dissemination of technological information within the R&D organization, MIT Press. Cambridge.
2. Altman, I., 1975. The Environment and Social Behaviour Privacy, Personal space, Territory, Crowding. Cole Publishing Company, Monterey, CA.
3. Aries, M. B., Veitch, J. A. and Newsham, G. R., 2010. Windows, view, and office characteristics predict physical and psychological discomfort. *Journal of Environmental Psychology*, 30(4), pp 533-541.
4. Baron, R. A. and Ransberger, V. M., 1978. Ambient temperature and the occurrence of collective violence: the "long, hot summer" revisited. *Journal of Personality and Social Psychology*, 36(4), pp 351.
5. Collins, B. L., 1975. Windows and people: A literature survey. Psychological reaction to environments with and without windows. Washington, DC: National Bureau of Standards.
6. Duval, C. L., Charles, K. E. and Veitch, J. A., 2002. A literature review on the effects of open-plan office density on environmental satisfaction. Ottawa, Canada.
7. EIAR, 2007. Environmental impact assessment report Landscape and Visual Impact Assessment, LVIA) for the construction and operation of the Proposed Beach Development at Lung Mei. http://www.epd.gov.hk/eia/register/report/eiareport/eia_1402007/For%20HTML%20version/Section10.htm [Accessed: 10th April 2020].
8. Evans, G. W., Wells, N. M., Chan, H. Y. E. and Saltzman, H., 2000. Housing quality and mental health. *Journal of consulting and clinical psychology*,68(3), pp 526.
9. Evans, G. W., 2003. The built environment and mental health. *Journal of Urban Health*, 80(4), pp 536-555
10. Fried, M., 1982. Residential attachment: Sources of residential and community satisfaction. *Journal of social issues*, 38(3), pp 107-119.
11. Fried, M., 1984. The structure and significance of community satisfaction. *Population & Environment: Behavioral and Social Issues*, 7(2), pp 61–86.
12. Gifford, R., 2007. Environmental psychology: Principles and practice, Optimal Books, Colville, Washington, USA.
13. Godin, I., Kittel, F., Coppieters, Y. and Siegrist, J., 2005. A prospective study of cumulative job stress in relation to mental health. *BMC Public Health*, 5(1), pp 67.
14. Griffit, W. and Veitch, R., 1971. Hot and crowded: Influence of population density and temperature on interpersonal affective behavior. *Journal of Personality and Social Psychology*, 17(1), 92.

15. Hall, E. T., 1966. Distances in man: The hidden dimension. Double Day, Garden City, New York.
16. Hayter, J., 1981. Territoriality as a universal need. *Journal of Advanced Nursing,* 6(2), pp 79–85.
17. Heerwagen, J. H. and Orians, G. H., 1986. Adaptations to Windowlessness A Study of the Use of Visual Decor in Windowed and Windowless Offices. *Environment and Behavior*, 18(5), pp 623-639.
18. Heerwagen, J. H., 1990. Affective functioning," light hunger," and room brightness preferences. *Environment and Behavior*, 22(5), pp 608-635.
19. Heschong, L., Mahone, D., Kuttaiah, K., Stone, N., Chappell, C., McHugh, J. and Holtz, M., 1999. Report on Skylighting and retail sales: an investigation into the relationship between daylighting. https://www.pge.com/includes/docs/pdfs/shared/edusafety/training/pec/daylight/RetailDetailed820.pdf [Accessed: 10th April 2020].
20. Insel, P. M., & Lindgren, H. C., 1978. Too close for comfort: The psychology of crowding. Prentice-Hall.
21. Kabo, F. W., 2006. Organizational analysis, part III: Spatial and socio-spatial relationships among housing sector organizations. In Low-cost housing design and provision: A case study of Kenya. Doctoral Thesis, University of Michigan.
22. Lyman, S. M. and Scott, M. B., 1967. Territoriality: A neglected sociological dimension. Social problems, pp 236-249.
23. Michelson, W., 1977. Environmental choice, human behavior, and residential satisfaction. New York: Oxford University Press.
24. Minam, H. i Tanaka, K., 1995. Social and Environmental Psychology Transaction between Physical Space and Group-Dynamic Processes.Environment and Behavior, 27(1), pp 43-55.
25. Newman, O., 1972. Defensible space. New York: Macmillan.
26. Newman, O. i Franck, K. A., 1982. The effects of building size on personal crime and fear of crime. Population and Environment, 5(4), pp203-220.
27. Oland, L., 1978. The need for territoriality. Human Needs and the Nursing Process. pp 97-140.
28. Olson, G. M. and Olson, J. S., 2000. Distance matters. Human-computer interaction, 15(2), pp 139-178.
29. Peponis, J., Bafna, S., Bajaj, R., Bromberg, J., Congdon, C., Rashid, M., et al., 2007. Designing space to support knowledge work. Environment and Behavior, 39(6), pp 815-840.
30. Perišić, A. 2016. The open conceptual model for parametric analysis and evaluation of urban blocks, Doctoral Thesis, University of Novi Sad, http://nardus.mpn.gov.rs/handle/123456789/4793 [Accessed: 12th May 2020].
31. Pierce, R. A., 2006. The 10 Keys to Effective Supervision http://www.risingsunconsultants.com/images/white_papers/PDFs/Supervision-Short.pdf [Accessed: 10th April 2020].
32. Pluckhan, M., 1968. Space:The silent language. Nursing Forum VII, (4), pp 386–397.
33. Prohansky, H. M., Ittelson, W. H. and Rivlin, L. G., 1970. Freedom of choice in a physical setting. Environmental psychology: People and their physical settings. Holt, Rinehart & Winston New York.
34. Roberts, J. M. and Gregor, T. A., 1971. Privacy: A cultural view. Cornell University, Latin American Studies Program.
35. Simmel, G., 1969. The metropolis and mental life. In Classic Essays on the Culture of Cities, ed. R. Senmett, pp 47- 60. New York: Appleton.
36. Sommer, R., 1969. Personal Space. The Behavioral Basis of Design, Englewood Cliffs, NJ, USA.

37. Stokols, D., 1993. Strategies of Environmental Simulation. In Environmental Simulation, pp. 3-21. Springer US.

38. Tate, J. W., 1980. The need for personal space in institutions for the elderly. *Journal of gerontological nursing*, 6(8), pp 439-449.

39. Ulrich, R. S., 1984. View through a window may influence recovery from surgery. *Science*, 224(4647), pp 420-421.

40. Veitch, J. A., 2011. Workplace design contributions to mental health and well-being. *Healthcare Papers*, 11(special issue), pp 38-46.

41. Zalesny, M. D. and Farace, R. V., 1987. Traditional versus open offices: A comparison of sociotechnical, social relations, and symbolic meaning perspectives. *Academy of Management Journal*, 30(2), pp 240-259.

GEOMETRIC PARAMETERS OF THE CLOCK DIAL

Rodoljub Milicevic
Faculty of Mechanical Engineering, University of Belgrade, Republic of Serbia
Master of science in mechanical engineering, rodoljub.milicevic95@gmail.com

Misa Stojicevic
Faculty of Mechanical Engineering, University of Belgrade, Republic of Serbia
PhD., Assistant Professor, mstojicevic87@gmail.com

Branislav Popkonstantinovic
Faculty of Mechanical Engineering, University of Belgrade, Republic of Serbia
PhD., Full-time Professor, dr.branislav.pop@gmail.com

Ivana Cvetkovic
Faculty of Mechanical Engineering, University of Belgrade, Republic of Serbia
MSc., Teaching Assistant, ivanacvetkovic1992@gmail.com

ABSTRACT

This paper deals with the geometric parameters required for the construction of a well-designed clock face as a part of pendulum wall clock described thoroughly in the master work. The face or dial of a clock is a circle whose circumference is divided into 60 equal parts, called minute spaces. A clock has two hands, the smaller one is called the hour hand or short hand while the larger one is called the minute hand or long hand. In order to determine the relation between the diameter of the clock and the distance from which one can clearly read position of its hands, it is necessary to adopt some of the basic geometric characteristics of minute and hour division on the clock face. Second important thing when it comes to the construction of a dial, is the height of the clock face. The criteria for dial height can be derived from the approved standards for the view field width of increased attention.

Keywords: clock; mechanisms; clock face geometry; clock hands; pendulum

1. INTRODUCTION

To make the clock usable, i.e. fit its purpose, it is necessary that the geometric parameters of its dial be consistent with certain requirements and recommendations. These requirements and recommendations derive directly from the physiological characteristics of normal human eyesight that today represent ophthalmic standards.

The first standard to be used in this simple calculation is the so-called visual acuity of the naked eye and is defined as the resolution of the eye or the visual power of detail separation. The average or adopted "normal" resolution of the human eye is about 1 angular minute. It is statistically determined and means that the "average" eye can distinguish between two contours if their distance is viewed at a viewing angle equal to or greater than one arc minute. Also, it means that the detail (point, line) is noticed and distinguished from the surrounding details if viewed at an angle of not less than one arc minute. If this angle is smaller, the "average" eye does not recognize the two contours, i.e. the details as separate.

Another standard that will be used in formulating recommendations for the geometric parameters of the dial refers to the width of the so-called field of vision of the heightened attention of the human eye. The width of the field of vision of the human eye is quite large: $\pm 110^0$ in the horizontal plane and $\pm\ 60^0$ in the vertical plane, measured from the optical axis of the eye. However, the observation of shapes, details, colours and movements is not evenly

distributed over the entire width of the field of vision, which is a direct consequence of the uneven density of optical sensors on the retina of the eye. The density of these sensors (the so-called cones and rods) is the highest on the macula of retina and decreases sharply with increasing radial distance from macula. Characters that fall on macula are the focus of the beholder's attention, and attention diminishes as the spotted characters are further away from it. It is adopted as a standard that the field of vision of increased attention lies within a rotating vision field of cone whose derivatives close a 30 degree angle with the optical axis of the vision cone. If the observed objects are within this cone, the observer will notice them with increased attention. If it is outside, the observer may notice the object, but unconsciously, so they will not pay attention to it.

2. GEOMETRY AND VISUAL CHARACTERISTICS OF THE CLOCK DIAL

In addition, it is necessary to highlight some recommendations regarding the geometry of the dial itself. It is advisable for the dial to be circular and not any other (triangular, square, rectangular ...) shape, because only the circular shape ensures the uniformity of the hour and minute markings and their equal distance from the center of the clock dial.

The clock dial should have 12 hour markings and 60 minute markings [1]. Divisions can be realized as points or lines of appropriate dimensions. The lengths of the divisions into 12 may be all the same, but for clarity the division into 4 can be highlighted (12, 3, 6, and 9 hours) by the increased length of the lines. The size (length and width) of the 60-minute dividing lines must be at least twice the size smaller than the 12-hour dividing lines.

The clock must have a clock and a minute hand, and a secondary if needed [2]. The clock hand should always be shorter than a minute one, approximately equal to one quarter of the diameter of the clock and a thickness equal to or greater than the thickness of the hour markings. The length of the minute hand must not be smaller than 3/4 nor greater than 5/6 of the radius of the clock, and a thickness of at least equal to the thickness of the minute markings. The secondary hand, if any, should be the thinnest and longest, but highlighted with a specially selected colour, marking, or shape. These recommendations are of a practical nature: the observer should first notice the hours and, if able, because of the distance, the minutes and finally the seconds.

In accordance with the aim of the observer to read the time on the dial of the clock effortlessly, precisely and quickly, it is necessary to ensure a sufficiently high contrast of markings. It has been experimentally determined that the greatest contrast is provided by the combination of black and yellow with the black background of the dial and the yellow division markings. Somewhat less contrast is created by the black background and white markings [3]. The combination of a black marking on a white background, although widespread in use, causes the eye of the viewer to be dazzling, thus not contributing to the clarity of time reading. If, for aesthetic or any other reasons, a black background is not acceptable, dark blue with yellow or light orange markings may be used. Also, dark green or even dark red (burgundy), with white or yellow markings for hours and minutes, may be adopted for the background colour of the dial. All colours should be matte in order to prevent reflections that impair the clarity of reading of the hands positions.

Public clocks should be placed in illuminated places, not shaded or obscured by other objects [1], [4]. It is important that they be adequately lit at night, with special lighting or pre-existing street lamps. If the dial is white and the markings are black, it can be made of matt glass, which allows it to be illuminated at night by the light sources behind the dial. The light should never be too strong, dazzling or of colour that is not white or light yellow. The public clock dial should not be glazed, protected by a glass window, because of reflections.

Numbered markings, although regularly present on many public clocks and wristwatches, are not necessary. Namely, the division into 12 ordinary lines (or circles - dots) achieves an unambiguous orientation on the dial so that the observer will be able to observe and read clearly and infallibly the positions of hour and minute hands without numbers as well. The following example illustrates that the numbered markings are not necessary. If the minute hand points to 3, it reads "... and fifteen", if it shows 4, we say "... and twenty", if it is at 6, we say "half", if it stands at 8, we read "twenty to ...", if the minute hand shows 9, we say "fifteen to ..." etc. Thus, the numbered markings may be present, but they are not necessary because they are not read, but the geometric division of the circle into quarters, thirds, and halves.

In order to establish the relationship between the diameter of the clock and the distance from which the position of its hands can be read clearly, it is necessary to first adopt some basic geometric characteristics of the minute and hour divisions on the dial. To distinguish the hour division from the minute one it is sufficient to assume that the thickness of the hour division line is twice the thickness of the minute line. It is also accepted that the distance between any two nearest lines on the division of the dial should not be shorter than the thickest line, ie. the thickness of the hour division line.

If the arc distance between the axis of symmetry of any two lines on the division of the dial is divided into seven equal parts and if it is chosen that the thickness of the line of the hour division is 4/7 and minute 2/7, then the recommendations adopted in the previous chapter are met. This division can be expressed in angular measures: the thickness of the line for the hour division corresponds to the central angle of the dial of α =(4 · 360 °)/(420 = 3.43 °), and for the minute division β=α/2= 1.71 °. A smaller and larger division is also possible, but it would be at the expense of resolution or visibility. Figure 4.1 shows the basic geometric characteristics of the minute and hour divisions on the dial. If the diameter of the dial is D, then the thickness of the minute division line is 2Dπ/((7 · 5 · 12)) = 2Dπ/420 and, in order to be viewed from a distance l at a viewing angle of one arc minute, the following equality must be applied:

$$\frac{2D\pi}{420} = l \cdot tan\, tan\, \frac{1}{60\,°}$$

The relation follows directly from the above equation and that is

$$\frac{l}{D} = \frac{\pi}{210 \cdot tan\, tan\, \left(\frac{1}{60\,°}\right)} = 51.42 \approx 50.$$

So, if the visual conditions are good (brightness, the air is free of smog and fog), the minute division of the dial of a clock whose diameter is D will be seen clearly and effortlessly at a distance of l = 50D. The clock with the dial of diameter D will be usable under good light conditions and at a distance of 100D, since the lines of the hour division are twice as thick as the minute lines, and no minute reading is required for approximate reading of time. As the lighting conditions are often poor (dusk, dawn, the dial is not illuminated or is in shadow, there is fog or smog in the air, rain, snow, etc.), it is correct for safety reasons to adopt a recommendation that for the maximum reading distance of time l a clock dial of diameter D =l/50 is provided and designed.

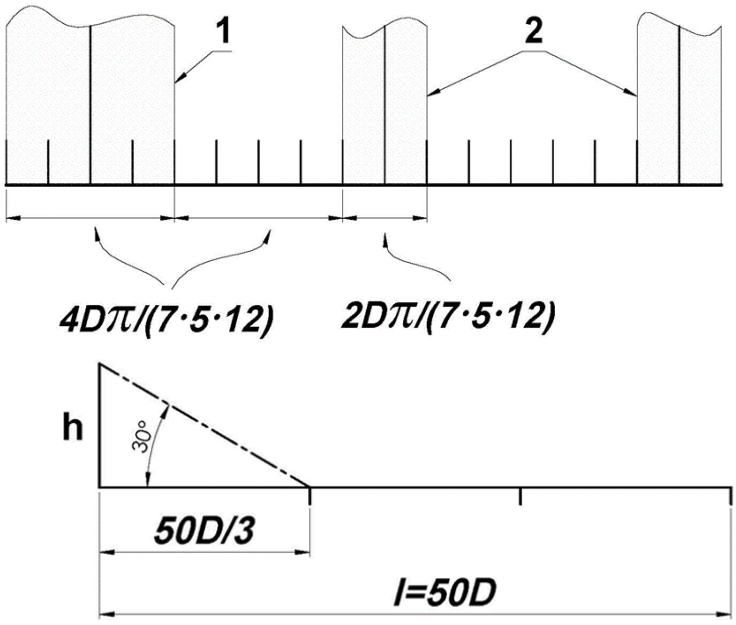

FIGURE. 1: Parameters for determining the visibility of the clock.

For the selected diameter of the clock dial D, it is also necessary to establish a recommendation for the height at which the clock (axis of the clock hands) will be set. Ideally, every clock should stand at the height of a human face - at eye level. However, such clocks would rarely be usable as they would be regularly obscured by other numerous objects. Therefore, it is necessary to set the clock to a higher altitude, but again not too high. The height criterion can be derived from the adopted standard for the width of visual field of increased attention.

3. NUMERICAL EXAMPLE

Let us suppose that the clock dial of diameter D has been designed according to the rules already described. A reasonable recommendation for the height of installation h of such a dial is that the dial should be placed at that

height h so that, from a third of the length l = 50D, it is visible at the border of the visual field of increased attention. From this recommendation the following expression is derived:

$$\frac{3h}{50D} = tan\ \tan 30\,^{\circ},$$

From which it directly follows that installation height of the dial is

$$h = \frac{50D}{3}\ tan\ tan\ 30\,^{\circ} = 9.62D.$$

Thus, if the dial of the clock of diameter D is placed at a height h which is 9.62 times bigger than its diameter, it will be viewed at the boundary of the field of vision of increased attention, or at an angle of 30 °, from a third of the distance l = 50D. As the dial is viewed from the surface of one circular sector of radius l = 50D and if raised to the height h = 9,62D, it will be within the visual field of increased attention of the observer with 8/9 of the total area of the said sector. If necessary and if circumstances permit, the dial can be set to a lower altitude but not to a higher altitude.

Public clocks are set up as façade, street clocks or clocks at squares [5]. If the clock is on the facade, it has only one dial, the street ones have two dials that look on both sides of the street, and the clocks at squares should have four dials that are turned in all four cardinal directions.

For example, if the square is approximately circular in diameter of 100 meters, the clock should be placed in the center of the square, it should have four dials of 1 meter in diameter each, rising to a height of 9 or 10 meters. They will be in the visual field of increased attention from an area of almost 7000 of a total of 7854 square meters. Home clocks - alarm clocks, desk clocks, wall clocks, etc., should have dial diameters tailored to the dimensions of the rooms. In most cases, it is sufficient that their diameters are not shorter than 80 to 100 millimeters.

Figure 2. - Large façade clock at the beginning of Knez Mihailova Street

All of these recommendations should be followed in practice because there is no reasonable reason not to do so, except through negligence or ignorance. Also, the stated and explained requirements are sufficiently mild and general, thus providing designers with ample space for the freedom of additional aesthetic expression and artistic creativity. Nonetheless, there are too many examples, especially public clocks, where these recommendations are not respected at all or are hardly met. Thus, for example, a rectangular façade clock at the main post office in Belgrade, approximately one meter in diameter, has been set at a height of about thirty meters. Most passers-by have never even become aware that the clock exists at all. The clock at the top of the Railway Museum building in Nemanjina Street, Belgrade, has also been set disproportionately high for the diameter of its dial. The large façade clock at the beginning of Knez Mihailova Street in Belgrade (Figure 2) does not meet most of the recommendations highlighted here. Yet, because of its dimensions and the small height at which it has been set, it would justify the purpose of its existence, had it not been for one but the worst possible mistake: two trees have been planted directly in front of it, as if it had been intended for the clock not to be seen at all during the whole spring and summer. The damage has been made greater due to the fact that this clock has become a kind of symbol of the city of Belgrade, just at a time when there were no treetops in front of it.

4. EXAMPLES OF PUBLIC CLOCKS IN SERBIA

Fortunately, there are also examples in Serbia where public clocks do their part correctly. Thus, for example, the old, large façade-tower clock at the Palace of Justice in Niš has been designed correctly Belgrade (Figure 3). It would be better if the background of the dial was black and the markings were white or yellow. No objection can be made to the ecclesiastical, quadruple dial of the tower clock at the Cathedral in Novi Sad (Figure 4). The big black clock at Petrovaradin Fortress (Figure 5), a symbol of Novi Sad, is also an example of a well-designed public clock. The facade clocks at the old Belgrade train station building were also excellent by all the criteria set out here. Our hope remains that they will not be removed upon completion of the ongoing reconstruction.

There are public clocks in the hallways on each floor at the Faculty of Mechanical Engineering in Belgrade (Figure 6). They are blue with white markings, which is commendable. The serious complaint is that they haven't been working for decades. The only thing worse than that would be that they work, but inaccurately, which luckily is not the case. In all three amphitheaters of the aforementioned faculty, it would be useful to place clocks with dials of diameter not shorter than one meter, at the maximum height that the amphitheater allows.

Figure 3. - Large façade-tower clock at the Palace of Justice in Niš

Figure 4. - The tower clock at the Cathedral in Novi Sad

Figure 5. - The big black clock at Petrovaradin Fortress

Figure 6. - Clock in the hall of the Faculty of Mechanical Engineering, University of Belgrade

4. CONCLUSION

This paper deduces, derives and discloses the geometric and other visual parameters required for the construction of a well-designed clock face. In particular, the formulas for the correct clock face diameter, the height of the dial, dimensions of the division marks and clock hands are obtained from two important ophthalmological parameters: visual acuity and field of vision of the heightened attention of the naked human eye. The relationship between the diameter of the clock and the distance from which the position of its hands can be read clearly is also emphasized. In addition, regarding the sufficiently high contrast of clock face markings, the appropriate and applicable combination of colours and illumination of the clock dial parts are also discussed and recommended. Finally, a few examples of public clocks in Serbia are presented and the correctness of their design are considered and criticized.

REFERENCES

[1] Čučaković, A., Popkonstantinović, B. 2006, *Projekat i konstrukcija velikog vestminsterskog časovnika,* Proceedings of MoNGeometrija,Novi Sad, Serbia.

[2] Стојићевић, М. *PhD dissertation: Нелинеарна динамика сатних механизама,* Belgrade, Serbia, 2018.

[3] Lecture material from course Product aesthetic at Mechanical faculty, University in Belgrade, Serbia. Author: prof. Branislav Popkonstatinović

[4] Popkonstantinovc, B., Miladinovic, Lj., Jeli, Z., Stojicevic, M. 2016, Event Based Motion Analysis of Escapement Mechanism 3D Model, Proceedings of MonGeometrija, Vlasina, Serbia

[5] Popkonstantinovic, B., Miladinovic Lj., Obradovic M., Stojicevic M., 2014. Geometrical Characteristics and Solid Modeling of the Grasshopper Escapement Mechanism, Proceedings of MonGeometrija, Vlasina, Serbia.

TOPIC 3: ENGINEERING COMPUTER GRAPHICS AND GEOMETRY

CONTENT

CAD STRUCTURAL OPTIMIZATION OF LARGE CANTILEVER GIRDERS ON CRANES

Vlada Gašić
Department of Material Handling, Faculty of Mechanical Engineering, University of Belgrade
PhD, Associate Professor, vgasic@mas.bg.ac.rs

Ivan Milenović
Department of Material Handling, Faculty of Mechanical Engineering, University of Belgrade
PhD Student, Research Assistant, imilenovic@mas.bg.ac.rs

Miloš Jovanović
Department of Material Handling, Faculty of Mechanical Engineering, University of Belgrade
MSc student, jmilosh35@gmail.com

ABSTRACT

The paper deals with the structural optimization of the cantilever girder. Standard CAD optimization tool is used for the model of the main girder on a large jib crane. The objective function is the minimum weight of the girder subjected to the given payload, while constraint functions are postulated according to the usual structural rules and regulations. The illustrative example shows an easy way of optimization which can be used in everyday CAD designing practice. It gives practical recommendations in the selection of variable parameters. The obtained results indicate that the algorithm is time-saving when compared to the analytical approach, especially when variability of the section needs to be included in the design.

Keywords: Structural optimization, CAD, FEA, CATIAV5, jib crane, cantilever

INTRODUCTION

Optimization is an everlasting tendency in mechanical engineering. Having started as an empirical approach, optimization in the modern age has brought the techniques which are fully related to applied mathematics. As in all other fields of engineering, the methods of optimization can be classified into analytical and numerical methods.

Analytical methods played an important role in structural optimization in the 20th century. However, their limitations in finding a close-formed solution for the given problem opened up the space for a strong development of numerical methods. Nowadays, in structural analysis, the numerical method implies the usage of Finite Element Analysis (FEA) with the accompanying Computer Aided Design (CAD). They are used as an engineering tool for design in almost all fields of mechanical engineering because they offer a simple way of representing complex structures. The modern CAD software also stands for a product development tool for mechanical structures, i.e. for optimization. The related studies were numerous in the last twenty years and can be easily found.

Within the structural optimization problems, there is a following classification (Spillers, 2009): (1) size optimization, which deals with the calibration of cross-sectional properties and structural elements dimensions, (2) shape optimization, which deals with the optimization of the boundary shape of the structure, and (3) topology optimization, which consists of the distribution of material within the structural space.

CAD is used for the design of "heavy" machinery jib cranes as well (Fig. 1). However, designers of such structures tend to follow the usual recommendations which reduce the possibility for structural optimization.

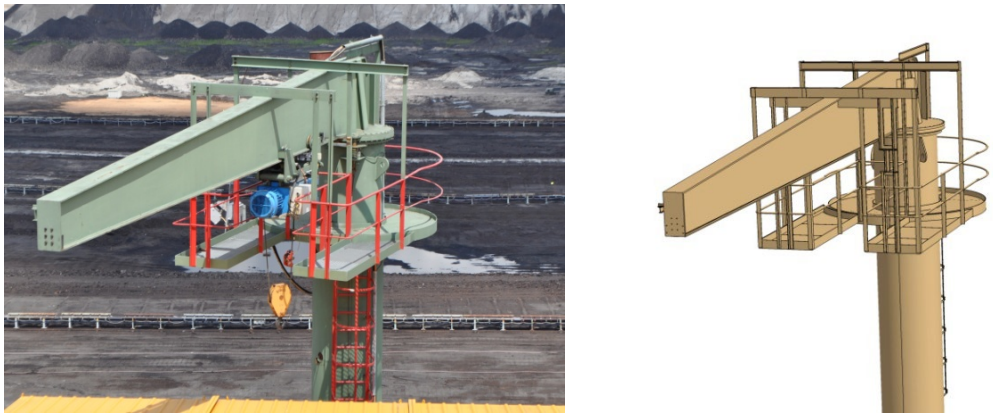

(a) (b)

Figure 1: Foot-mounted jib crane: a) Real model, b) CAD model

The aim of this paper is to show one way of structural optimization of cantilever girders on big jib cranes subjected to the main vertical load (payload). The authors are fully aware that the calculation model belongs to the class of "simple" models, but the safety of these cranes highlights the importance of this topic. The postulation brings this problem into the field of variability of the cross-sections over span. It has to be pointed out that design examples are based on the realistic/possible object of the jib cranes. Of course, the goal is the reduction of girder mass with the preservation of the constraints which are defined by main structural proofs.

CATIA implemented Simulated Annealing optimizer is used as one of the basic algorithms within the Product Engineering Optimizer workbench. Due to the class of the title problem, this can be adopted as a sufficient enough postulation of the optimization tool.

Further, this paper is aimed at encouraging the designers of big jib cranes to include the variability of dimensions of structural elements, which is rarely done in practice (Fig.1).

RESEARCH BACKGROUND

Many analytical approaches can be found when it comes to the problems of structural optimization. Mostly, they deal with the method of Lagrange multiplication for the optimization of structural cross-sections asin research (Šelmić et al., 2006) or (Anđelić et al., 2007). The constraints in those cases correspond to main safety requirements, such as the allowed stresses and displacements. This kind of approach belongs to the class of size optimization. In spite of the fact it is carried out manually, this technique can be a good basis for the improvement of structural products.

Another kind of approach, used in this paper, is the consideration of variability of the cross-section over length of structural elements. Theoretically, this idea is covered within the topic of strength of materials. However, it can be used only for simple models of beams (usually made of I-sections) under very few constraints. This kind of postulation belongs to the class of shape optimization. The addition of constraints, such as the effect of torsion on open beams, increases the complexity of the postulated problem, as shown in research (Gašić et al., 2018).

In practice, the tendency for variation of the cross-section over length has been present since the beginning of the industrialization of structures. In early stages, it was strongly connected with the limits of production technology for steel beams as in the book (Kurt, 1969), which forced engineers to tailor beams with the existing ones.

However, the above-mentioned possibilities are often neglected in structural design due to a missing link in the calculation of manufacturing costs vs. operational costs between the manufacturer and the user.

Hence, one may find the following characteristics of structural optimization as an overview of the mentioned techniques:

- minimal mass of structure is almost always the priority,
- optimization is often done manually and is a time-consuming process,
- class of optimization is mostly separated.

Here, some of the disadvantages with analytical methods will be avoided with the CAD based optimization. The object of optimization is a cantilever girder of the big jib crane. The weight of the girder does not influence the

performance of the crane and any reduction of the weight has a positive effect on the energy consumption-cost within the operation of the rotation of the girder (Fig 1.a). The task is to adjust the structural parameters of the existing girder and to save the material, with the preservation of the given requirements and product performance.

The idea is not to go towards the truss structure, which would lead to topology optimization (Marjanović et al., 2009), but to maintain the beam-like element due to the manufacturing cost.

Firstly, the variation of height comes as a natural and known way for the shape optimization of the given problem. However, it is rarely done in practice. Schematically, the postulation is depicted in Fig. 2a, where the girder has a left (clamped) end-L, right (free) end-R, length *l* and (payload) capacity *Q*. The usual cross-section of these cantilevers is made of wide I-sections or box sections (Fig. 2b). The first class is generally used in jib cranes because the production process requires only the purchase of the rolled section girder. Thus, variation of height would increase the manufacturing costs in that case. For the jib cranes with a bigger length/reach and high capacity, the box section has to be involved. It is made by welding of the sheet metal plates. Even in this case, manufacturers tend to make a uniform section over length. The only excuse for this kind of production postulation can be found in the fact that these cranes are not subjected to mass production and that the calculation method comes from the standard analytical approach.

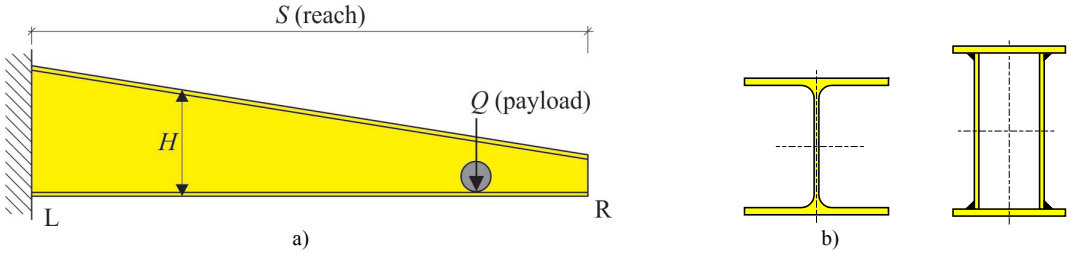

Figure2: a) Schematic model of jib (cantilever), b) Typically used sections

The objective function is the minimal mass (volume) of structure, which obviously corresponds to the minimal weight. The constraint functions are defined as:

$$g_1 = f_R - f_d \quad \text{(Eq.1)}$$

$$g_2 = \sigma_L - \sigma_d \quad \text{(Eq.2)}$$

$$g_2 = \tau_R - \tau_d \quad \text{(Eq.3)}$$

where f_R is the displacement of the free end, σ_L is Von Misses stress at the clamped section, τ_R is shear stress near the free end and the corresponding values (noted with index *d*) are the allowed values coming from structural rules and regulations. This can be considered as basic and sufficient enough conditions for the dimensioning of the main girder on cranes.

The first constraint function, in analytical formulation, has challenges in the determination of the cantilever flexibility when complex variational section is introduced. In addition, one has to calculate the influence of both the payload and load due to self-weight of the girder. Therefore, one may use approximative/substitutional models, which are presented in book (Tuma et al., 1971). However, they are time-consuming and require a large number of iterations/rehearsals. This is the main difficulty when variability of the section is included. The effect of the carrying capacity due to bending is simple and obvious even with the analytical approach and the authors will not emphasise this furthermore. Constraint functions can be added by implementing the effects of local bending stresses, lateral buckling, etc. However, this can be considered as a disadvantage of the CAD optimization because of the limits with FEA when different structural phenomena have to be considered. According to the authors, in that case, the CAD optimization should be used to get a good enough model under basic constraints and to perform additional checks afterwards.

THE CANTILEVER MODEL

The title problem deals with big jib cranes, which stand for long reach and high capacity. In practice, this can be represented by the jib cranes with the payload capacity of 5 t (*Q*) and reach of 6 m (*S*). According to the authors, this can be established as a starting point, where the inclusion of the variation of height and cross-section properties can give benefits versus increased costs due to the manufacturing process of such a cantilever. Thus, in order to follow the effects of mass minimization with CAD optimization, one illustrative model of the cantilever beam is given (Fig.3a). The material is common structural steel S235, with the following nominal

characteristics: yield strength f_y = 235 MPa, modulus of elasticity E = 210000 MPa and Poisson's ratio v = 0.3. It is considered a box cross-section, with symmetry over vertical axis and with the geometry postulated in Fig. 3b. With respect to practical aspects of the trolleys which are mounted on the bottom flange on the jib section, some parameters have to be constants like B_1, B and t_1.

It should be pointed out that basic knowledge of the beam-like structures is important in this phase, in order to avoid misleading or impractical design results. The optimization workbench requires the starting parametric model, which is here designed in CAD and noted as V-1.

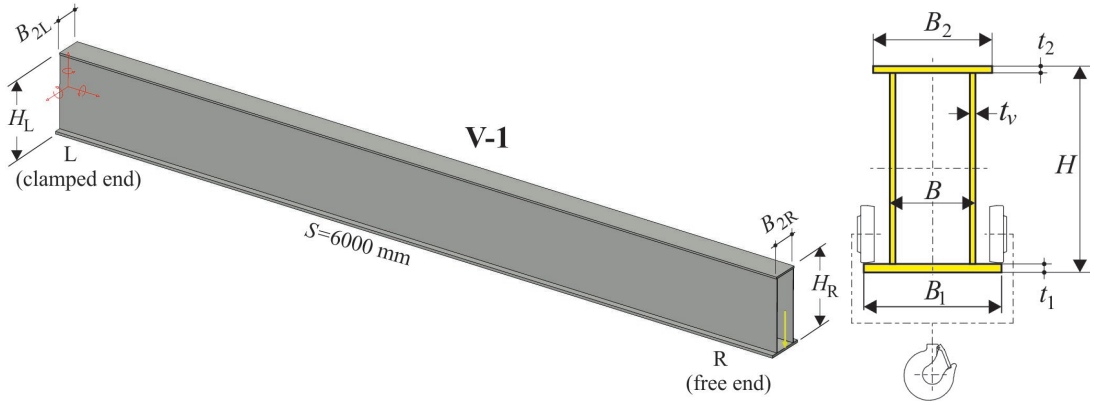

Figure 3: a) Starting model of jib (cantilever), b) Parameters of the jib sections

The main parameters are given in Table 1. It starts with the uniform girder model where height is chosen as the S/10 as a general starting point for the beam-like structure.

CAD OPTIMIZATION

CATIA implemented Simulated Annealing optimizer is used, as one of the basic algorithms within the Product Engineering Optimizer workbench. The advanced algorithms can be used as an addition, as shown in research (Konig et al., 2004) or (Park et al., 2010). The variational parameters are taken to be H, t_2, t_v, and B_2. The lower limits are chosen upon the practical consideration of the sheet metal design, along with the geometrical postulations of the cross-section due to adopted constant parameters (Table 1).

The objective function is the minimal mass of the girder, while constraint functions are as follows: (1) allowable deflection of f_d=30 mm, which is taken upon the recommendation of S/200, (2)normal stress of σ_d =157 MPa and (3) shear stress of τ_d =90 MPa.

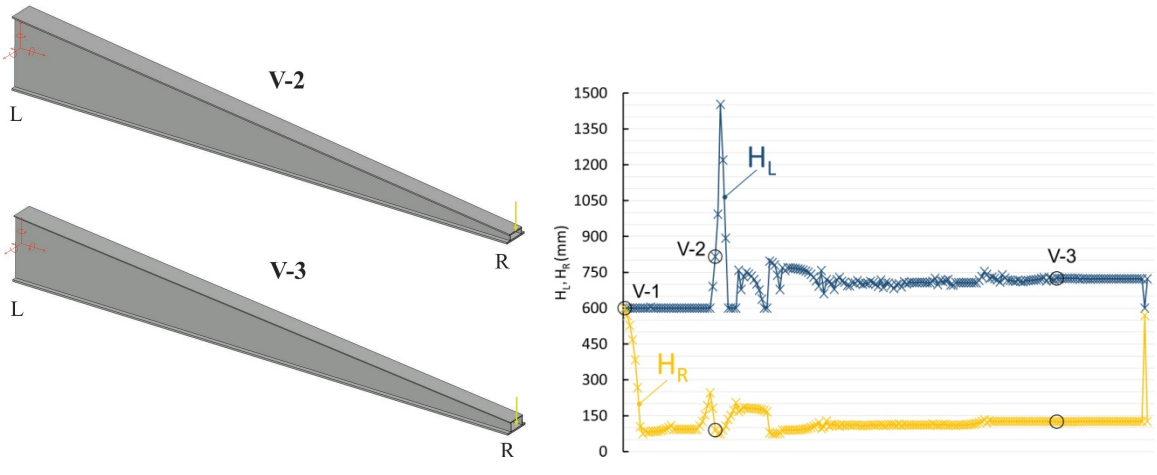

Figure 4. a) Variational models of jib (cantilever), b) Height variation in CAD algorithm

The Optimizer starts to change the given parameters and follows the value of the mass. It intermittently makes variations/attempts of all the parameters along with the measurement of sensitivity. Thus, one may find peaks in

the beginning as shown for values of the heights in Fig. 4b. Any variant which exceeds the constraint function returns the process to recalculating. An algorithm ends if the model satisfies all the conditions for 20 iterations.

The model noted as V-2 is provided here for descriptive purpose only, while the end-optimized model is here presented as V-3 (Fig. 4.a).

NUMERICAL RESULTS AND DISCUSSION

Next, the CAD optimization of the model of the jib girder with given basic parameters and under basic structural regulations is performed. The starting and optimized parameters of the model, along with the obtained jib mass, are shown below in the tabular form.

Table1: The parameters of the optimization model

	Constants			*Variable parameters*						
	B_1 (mm)	t_1 (mm)	B (mm)	H_L (mm)	H_R (mm)	t_2 (mm)	t_v (mm)	B_{2L} (mm)	B_{2R} (mm)	*mass* (kg)
V-1	*300*	*20*	*200*	*600.0*	*600.0*	*15.0*	*10.0*	*220.0*	*220*	*970.26*
V-2	*300*	*20*	*200*	*816.1*	*90.5*	*14.3*	*6.0*	*300.0*	*212*	*691.81*
V-3	*300*	*20*	*200*	*722.3*	*126.3*	*10.0*	*6.0*	*265.0*	*212*	*617.77*

The reduction of mass is obvious throughout the whole process. The values cannot be compared directly because the starting model (V1) is checked to satisfy the postulated constraint functions, but presents only an initial model. The scope of the model was not an improvement of the specific design but aimed at making easy arrangements of the optimization of structural parameters under basic crane requirements. It is obvious that the workbench makes for easy dimensioning of the model within the given limits.

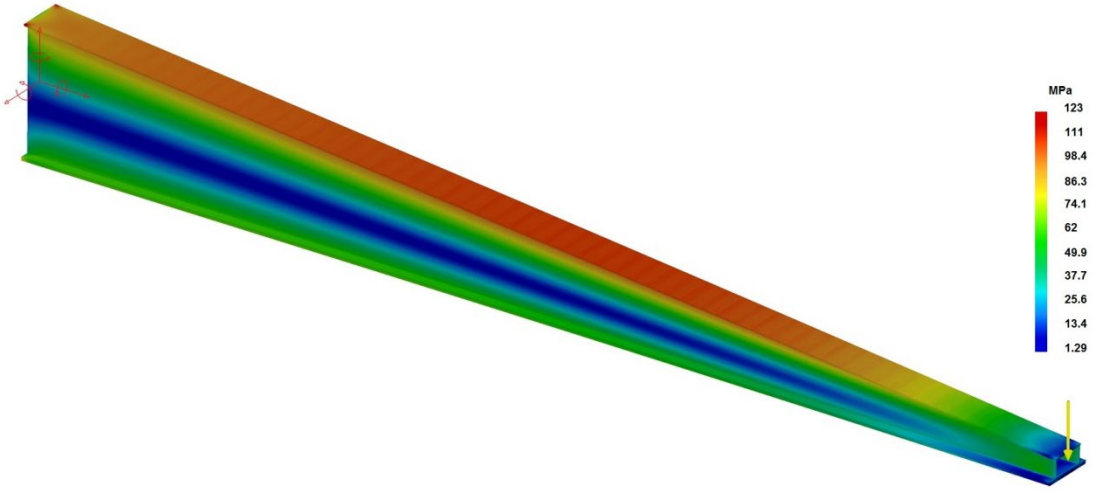

Figure 5. Stress state in the cantilever girder-V3

The stress state of the obtained model is shown (Fig. 5) in order to perform visual validation of the given constraints (Eq.2) and (Eq.3). The shape optimization, which corresponds here to the variation of height over length of the girder, has a positive effect on the utilization of the material. This is well-known from experience, but it can be noticed easily in the previous picture, where the allocation of high stresses is situated all over the upper flange of the girder. However, the governing constraint for this kind of structure is usually (Eq.1), which depends on the postulated deflection limit that is in direct relation with the crane load class.

CONCLUSION

The simple way of structural optimization of the cantilever girder on a jib crane is shown in the paper. Using CATIA Product Engineering Optimizer workbench, one illustrative model is subjected to optimization in order to obtain the minimum mass of the girder under given constraints. It combines the size and shape optimization, which is very difficult to achieve with the analytical approach. The procedure is also easy-to-use for the designers that use FEA and CAD in everyday practice and requires basic knowledge in mechanical engineering. Apart from that, it gives benefits in time-saving when variability of the cross section over span has

to be considered because it demands a large number of manual hand iterations. Thus, time-consuming process is transferred to a computer.

The optimization of a beam section should always be the goal for designers in order to reduce weights and, consequently, operational costs which save energy. Even for the aesthetic purpose, under preservation of the mechanical/structural regulations and rules, the consideration of variability of geometrical parameters in engineering CAD designs produces ingenious designers and separates them from ordinary practice.

ACKNOWLEDGMENT

This work is a result of the research supported by the Ministry of Education, Science and Technological Development of the Republic of Serbia by the Contract 451-03-68/2020-14/200105.

REFERENCES

1. Anđelić, N., Milošević-Mitić, V., 2007. The optimization of a thin walled I-beam subjected to displacement constraint, Proceedings of the 1st International Congress of Serbian Society of Mechanics, Kopaonik, Serbia, pp. 359-366.
2. CATIAV5
3. Gašić, V., Ćoćić, A., Anđelić, N., 2018. Consideration of the Horizontal Inertial Effects at Cantilever Beams with Non-uniform Open Sections, *FME Transactions* 46(3), pp. 342-346.
4. Kurt,T., 1969. Stahl imHochbau, Verein Deutscher Eisenhuttenleute,Verlag Stahleisen, Dusseldorf, Deutschland.
5. Konig, O, Wintermantel, M, 2004. CAD-based Evolutionary Design Optimization with CATIAV5, 1st Weimar Optimization and Stochastic Days.
6. Marjanović, N, Isailović, B, Blagojević, M, 2009. Structural optimization in CAD software, *Machine Design*, Faculty of Technical Sciences, Novi Sad.
7. Park,H.S., Dang X.P., 2010. Structural optimization based on CAD-CAE integration and metamodeling techniques, *Computer-Aided Design* 42, pp. 889-902.
8. Spillers, W., MacBain, K., 2009. Structural Optimization, Springer.
9. Šelmić, R., Cvetković,P., Mijailović, R., 2006. Optimization of the cross sections of metal structures (in Serbian), Faculty of Transport and Traffic Engineering-University of Belgrade.
10. Tuma, J.J, MunshiR.K, 1971. Advanced structural analysis, McGraw-Hill.

SYNTHESIS OF EPICYCLIC GEAR TRAIN AS A DRIVE FOR GENEVA MECHANISM

Maja Čavić
Faculty of Technical Sciences, University of Novi Sad, Republic of Serbia
PhD., Associate Professor, scomaja@uns.ac.rs

Marko Penčić
Faculty of Technical Sciences, University of Novi Sad, Republic of Serbia
MSc., Assistant, mpencic@uns.ac.rs

Milan Rackov
Faculty of Technical Sciences, University of Novi Sad, Republic of Serbia
PhD., Associate Professor, racmil@uns.ac.rs

Dijana Čavić
Faculty of Technical Sciences, University of Novi Sad, Republic of Serbia
MSc., Assistant, dijana.cavic@uns.ac.rs s

Vladimir Algin
Joint Institute of Mechanical Engineering of National Academy of Sciences of Belarus, Republic of Belarus
PhD., Full Professor, vladimir.algin@gmail.com

ABSTRACT

While the Geneva mechanism is a staple in many industries, there are two main drawbacks to its use. The first is the existence of impact loads, and the second are velocity and acceleration jumps, both of which lead to the appearance of vibrations and wear. This paper shows the synthesis of an epicyclic gear train as the driving component for a conventional Geneva mechanism. Based on a number of proposed requirements, two solutions of the modified Geneva mechanism were considered, with one and with two planet gears. Both variants completely eliminate the impact loads, and significantly decrease the velocity and acceleration jumps. Aside from this, the variant with one planet gear offers lower angular velocity and acceleration values in general, while the variant with two planet gears offers a decrease in the size of the mechanism.

Keywords: Geneva mechanism; epicyclic gear train; synthesis; kinematics;

1. INTRODUCTION

Intermittent mechanisms transform the continuous movement of an input link into intermittent motion of the driven link. These mechanisms are widely used in contemporary machinery for food processing, packaging, production engineering, automotive industry etc. [1–3]. Intermitent motion can be achieved by a variety of mechanisms, for example by lever mechanisms, cams, Geneva crosses etc. However, these mechanisms are characterized by impact loads, and sudden changes in both velocity and acceleration. The most notable consequences are significant loads which cause vibrations and wear, especially if there is significant backlash between the elements. Even with the drawbacks, these mechanisms are irreplaceable in practical use, especially in high-speed machinery working with heavy loads, where the use of electronics in the control of the working element motion isn't reliable (highly precise positioning which enables high accuracy and repeatability of the motion is key).

A Geneva drive is one of the simplest and least expensive off intermittent mechanisms. It transforms the continuous rotational movement of the crank into intermittent rotational motion of the Geneva cross. A pin, which is situated on the crank and traverses a circular trajectory subsequently enters the slots on the cross thus producing its movement. Such a mechanism is known as the classic Geneva mechanism and it has certain unfavourable characteristics, most notably the existence of an acceleration jump at the start and end of the Geneva cross interval of motion [4].

In this paper, the use of an epicyclic gear mechanism with constant output angular velocity as a drive for the Geneva cross is proposed. Thus enabling smooth, non-impact engagement/disengagement of the pin and cross, as well as an elimination of the acceleration jump at the beginning and end of the Geneva cross motion.

2. STATE OF THE ART

Several mechanisms have been proposed to reduce or eliminate acceleration jump in Geneva mechanisms. Linkage mechanisms [5, 6], mechanisms with elastic elements [7] and cam mechanisms [8], have been proposed to replace the crank in order to improve the dynamic behaviour of the Geneva cross. A number of authors also proposed crosses with curved slots and a slot offset to improve the motion characteristics of the Geneva cross [8, 9], but such designs proved to be cumbersome, problematic with respect to dynamic behaviour, complicated and expensive. Another method of modifying the Geneva cross motion is to use variable speed input – noncircular gears [10, 11]. This way, the Geneva mechanism can be realized for an arbitrary value of the working coefficient and extreme values of acceleration and jerk can be reduced but complete elimination of the acceleration jump requires noncircular gears with a complicated shape, which can be a challenge to produce.

3. MODIFIED GENEVA MECHANISM

Figure 1 shows the conventional Geneva mechanism in the starting – Figure 1a and an arbitrary position – Figure 1b. It consists of three elements, the input link – the crank, the output link – the cross and the fixed link. Pin A situated on the crank enters the groove on the cross, thus moving it. After the carrier traverses angle $2\alpha_1$, and the cross angle $2\varphi_1$, pin A leaves the groove and the cross comes to a halt.

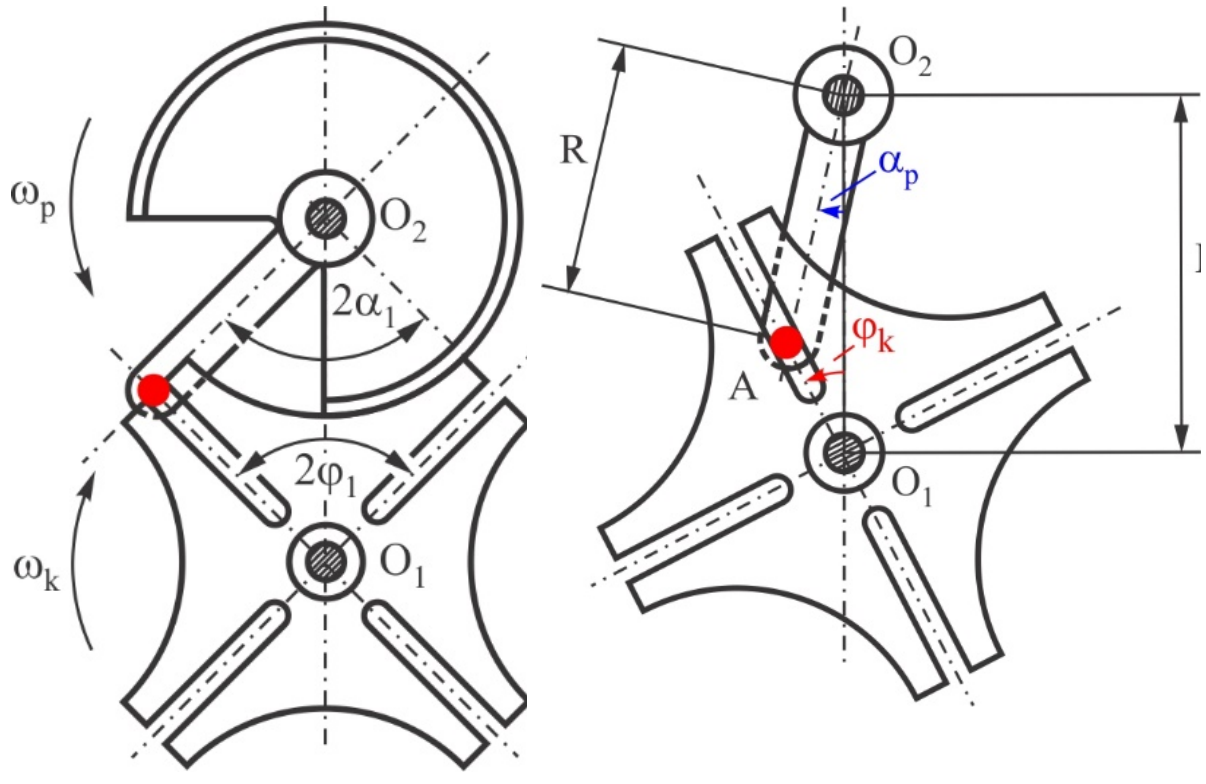

(a) (b)

Figure. 1: Conventional Geneva cross: (a) starting and (b) arbitrary position

The cross rotation angle φ, expressed using the input parameter – the carrier rotation angle α, is:

$$\varphi_k = \arctan\left(\frac{\lambda \sin\alpha_p}{1-\lambda\cos\alpha_p}\right) \quad \text{(Eq.1)}$$

where λ is a parameter dependent on the number of grooves on the cross, z. Therefore:

$$\lambda = \frac{R}{L} = \sin\frac{\pi}{z} \quad \text{(Eq.2)}$$

By differentiatin Eq. (1), the angular velocity of the cross is obtained, and in a similar fashion, the angular acceleration as well:

$$\omega_k = \frac{d\varphi_k}{dt} = \left(\frac{\lambda\left(\cos\alpha_p - \lambda\right)}{1-2\lambda\cos\alpha_p+\lambda^2}\right)\omega_p \quad \text{(Eq.3)}$$

$$\varepsilon_k = \frac{d\omega_k}{dt} = \left(\frac{\lambda\left(\lambda^2-1\right)\sin\alpha_p}{\left(1-2\lambda\cos\alpha_p+\lambda^2\right)^2}\right)\omega_p^{\,2} \quad \text{(Eq.4)}$$

Based on Eqs. (1–4), the usual diagrams of the Geneva cross motion are obtained – Figure 2, dependant on the number of grooves z and the angular velocity of the carrier ω_p (which is constant), expressed using the angle α, from $-\alpha_1$ to α_1. It is evident that there is an acceleration jump in the initial and final position, which is unfavourable.

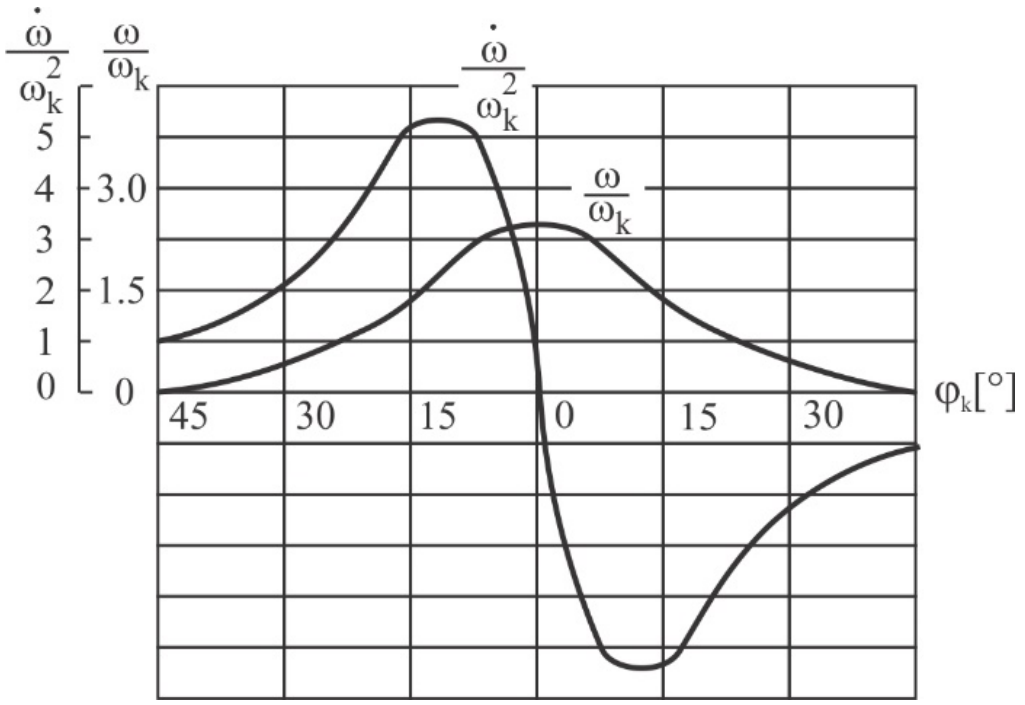

Figure. 2: Diagram of the angular velocity and angular acceleration of the Geneva cross, z=4

3.1. Modification

Figure 3 shows the proposed modification to the Geneva mechanism – two solutions. Cross c is driven by a set of planetary gears consisting of carrier k, central gear 2 and a single planet gear 3 (Figure 3a) or two planet gears 3 and 4 (Figure 3b). Located on the planet gear 3(4) is pin B which enters the groove on the cross, thus moving it. The configuration with two planet gears is somewhat more complex, but decreases the space requirements of the mechanism significantly.

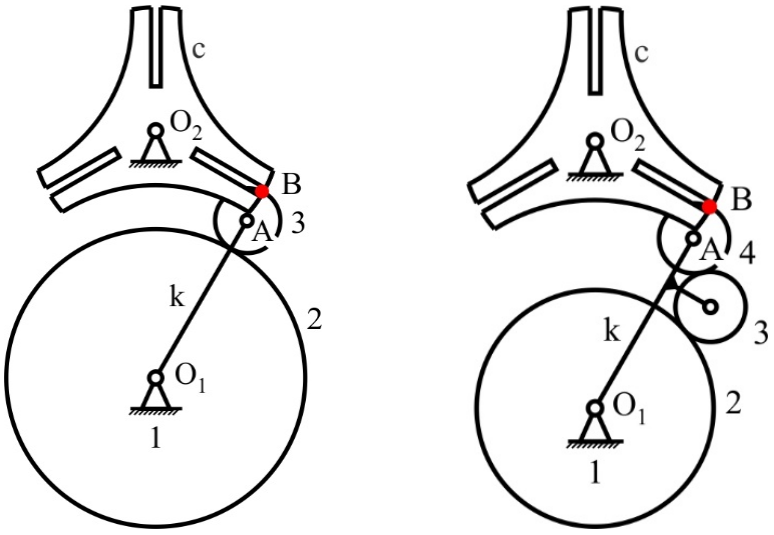

(a) (b)

Figure. 3: Modified Geneva mechanism: (a) with one planet gear and (b) with two planet gears

2.3. Synthesis

There are two main requirements the modified Geneva cross must fulfil. The first is to enable smooth, non-impact engagement/disengagement of the pin and cross, and the second to eliminate the acceleration jump at the beginning and end of the Geneva cross motion.

Based on the stated requirements, two solutions are proposed, in the form of modified Geneva crosses in arbitrary positions. Figure 4a shows a Geneva mechanism with one planet gear 3, while Figure 4b shows a mechanism with two planet gears 3 and 4. When the input link – carrier R, rotates by angle φ_k, then the planet gear 3(4) which drives the cross rotates by angle $\varphi_3(\varphi_4)$. The angle between the start and end positions of the carrier is α_k, and the angle between the start and end positions of the cross is α_c. Finally, the end position is defined by the point in time when pin B located on the planet gear 3(4) leaves the cross and the motion of the cross is halted.

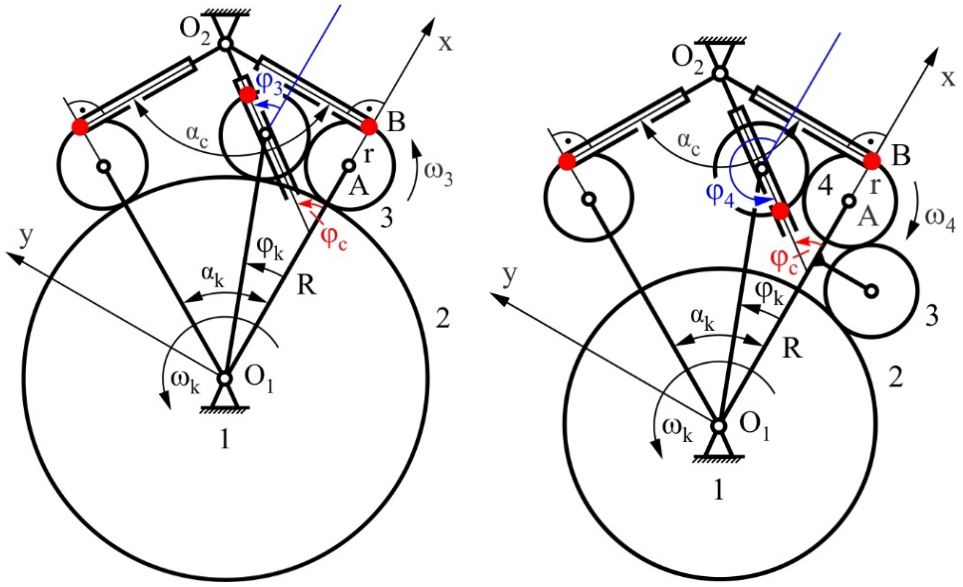

(a) (b)

Figure. 4: Modified Geneva mechanism a) with one planet gear, b) with two planet gears

The characteristic dimentions of the mechanism are the length of the carrier R and the position of the pin on the planet gear, defined as distance r. Therefore:

$$\overline{OA} = R \tag{Eq.5}$$

$$\overline{AB} = r \tag{Eq.6}$$

The angle that the cross rotates for per cycle depends on the number of grooves, z. Therefore:

$$\alpha_c = \frac{2\pi}{z} \tag{Eq.7}$$

The first design requirement is ensured when the velocity vectors of the carrier and the groove on the cross are perpendicular to one another at the beginning and the end of the contact. Consequently, the angle that the carrier rotates for per cycle is:

$$\alpha_k = \pi - \alpha_c \tag{Eq.8}$$

More specifically:

$$\alpha_k = \frac{\pi(z-2)}{z} \tag{Eq.9}$$

Planet gear 3(4), when moving relative to carrier R, needs to make one full rotation per cycle. Therefore, the absolute rotation angle of the planet gear is:

$$\alpha_{p3} = \alpha_k + 2\pi \qquad \alpha_{p4} = \alpha_k - 2\pi \tag{Eq.10}$$

More specifically:

$$\alpha_{p3} = \frac{\pi(3z-2)}{z} \qquad \alpha_{p4} = -\frac{\pi(z+2)}{z} \tag{Eq.11}$$

The ratio of the absolute rotation angles of the planet gear and the carrier are:

$$\frac{\alpha_{p3}}{\alpha_k} = \frac{\varphi_{43}}{\varphi_k} = \left(\frac{3z-2}{z-2}\right) \qquad \frac{\alpha_{p4}}{\alpha_k} = \frac{\varphi_4}{\varphi_k} = -\frac{(z+2)}{(z-2)} \tag{Eq.12}$$

Keeping in mind that the angular velocity of the carrier is constant, the following is stated:

$$\frac{\omega_3}{\omega_k} = \left(\frac{3z-2}{z-2}\right) \qquad \frac{\omega_4}{\omega_k} = -\left(\frac{z+2}{z-2}\right) \tag{Eq.13}$$

The Willis equations can be writted for the gear train in Figure 4 in the following way:

$$\frac{\omega_3 - \omega_k}{\omega_2 - \omega_k} = -\frac{z_2}{z_3} \qquad \frac{\omega_4 - \omega_k}{\omega_2 - \omega_k} = \left(-\frac{z_2}{z_3}\right)\left(-\frac{z_3}{z_4}\right) = \frac{z_2}{z_4} \tag{Eq.14}$$

Therefore:

$$\omega_3 = \frac{z_2}{z_3}\omega_2 + \left(1 + \frac{z_2}{z_3}\omega_k\right) \quad \omega_4 = \frac{z_2}{z_4}\omega_2 + \left(1 - \frac{z_2}{z_4}\omega_k\right) \tag{Eq.15}$$

By introducing this substitute:

$$\omega_2 = k\omega_k \tag{Eq.16}$$

Eq. (15) then becomes as follows:

$$\omega_3 = \omega_k\left(k\frac{z_2}{z_3} + \frac{z_2}{z_3} + 1\right) \quad \omega_4 = \omega_k\left(k\frac{z_2}{z_4} - \frac{z_2}{z_4} + 1\right) \tag{Eq.17}$$

Combining Eq. (13) and Eq. (17) yields the dependency between the number of grooves on the cross and the number of teeth of the central and planet gear that enables the pin to enter and exit the groove on the cross without impact (the first equation is for the gear train with one planet gear, and the second one with two planet gears):

$$\frac{3z-2}{z-2} = k\frac{z_2}{z_3} + \frac{z_2}{z_3} + 1 \qquad -\frac{z+2}{z-2} = k\frac{z_2}{z_4} - \frac{z_2}{z_4} + 1 \tag{Eq.18}$$

To fulfil the second requirement, the elimination of the acceleration jump at the beginning and the end of the cross motion, the equations describing the acceleration of the pin on the planet gear 3(4) need to be formed. The

following equations (19–24) define the position, and the velocity and acceleration components of pin B in the xOy coordinate system.

$$x_B = R\cos\varphi_k - r\cos\varphi_4 \quad \text{(Eq.19)}$$

$$y_B = R\sin\varphi_k - r\sin\varphi_4 \quad \text{(Eq.20)}$$

$$\dot{x}_B = R\omega_k\left(-\sin\varphi_k\right) + r\omega_3\left(-\sin\varphi_4\right) \quad \text{(Eq.21)}$$

$$\dot{y}_B = R\omega_k\cos\varphi_k + r\omega_3\cos\varphi_4 \quad \text{(Eq.22)}$$

$$\ddot{x}_B = R\omega_k^2\left(-\cos\varphi_k\right) + r\omega_3^2\left(-\cos\varphi_4\right) \quad \text{(Eq.23)}$$

$$\ddot{y}_B = R\omega_k^2\left(-\sin\varphi_k\right) + r\omega_3^2\left(-\sin\varphi_4\right) \quad \text{(Eq.24)}$$

To prevent the acceleration jump at the begingin and end of the contact, the acceleration vector of pin B must be in the direction of the groove. Since the velocity of pin B is, based on the first requirement, also in the direction of the groove, the acceleration and velocity must be in the same diretion – the acceleration must have only the tangential component, meaning the normal component must be equal to zero, $\vec{a}_B = \vec{a}_{BT}$ and $\vec{a}_{BN} = 0$. Therefore:

$$a_{BN} = \frac{\dot{x}_B\ddot{y}_B - \dot{y}_B\ddot{x}_B}{\sqrt{\dot{x}_B^2 + \dot{y}_B^2}} = 0 \quad \text{(Eq.25)}$$

Meaning:

$$\dot{x}_B\ddot{y}_B - \dot{y}_B\ddot{x}_B = 0 \quad \text{(Eq.26)}$$

The previous equation represents the condition that needs to be fulfilled to prevent the acceleration jump at the beginning and end of the cross motion. At the begining of the contact φ_k=0. The velocity and acceleration components of pin B are:

$$\dot{x}_B = 0 \quad \text{(Eq.27)}$$

$$\dot{y}_B = R\omega_k + r\omega_3 \quad \text{(Eq.28)}$$

$$\ddot{x}_B = -R\omega_k^2 - r\omega_3^2 \quad \text{(Eq.29)}$$

$$\ddot{y}_B = 0 \quad \text{(Eq.30)}$$

The condition (Eq. (26)) yields:

$$\left(R\omega_k + r\omega_4\right)\left(R\omega_k^2 + r\omega_4^2\right) = 0 \quad \text{(Eq.31)}$$

By introducing the following substitution:

$$\omega_4 = A\omega_k \quad \text{(Eq.32)}$$

Eq. (36) becomes:

$$A^3r^2 + A^2rR + ArR + R^2 = 0 \quad \text{(Eq.33)}$$

or:

$$A^3\left(\frac{r}{R}\right)^2 + \left(A^2 + A\right)\left(\frac{r}{R}\right) + 1 = 0 \quad \text{(Eq.34)}$$

Introducing the following substitution:

$$\frac{r}{R} = t \quad \text{(Eq.35)}$$

Yields the following equation:

$$A^3t^2 + \left(A^2 + A\right)t + 1 = 0 \quad \text{(Eq.36)}$$

With the solutions being:

$$t_{1,2} = \frac{-\left(A^2 + A\right) \pm \sqrt{\left(A^2 + A\right)^2 - 4A^3}}{2A^3} \quad \text{(Eq.37)}$$

Solving Eq. (37) yields the ratio between the contructive parameters R and r which enables the Geneva mechanism to function without the acceleration jumps at the begining and end of the contact.

3.3. Kinematics

The position angle of the cross, and its angular velocity and angular acceleration are defined as:

$$\varphi_c = \frac{x_B}{\overline{O_1O_2} - y_B} \tag{Eq.38}$$

$$\omega_c = \frac{a_1}{a_2}\omega_k \tag{Eq.39}$$

$$\varepsilon_c = \frac{a_1a_3 + a_2a_4}{2a_2^2}\omega_k^2 \tag{Eq.40}$$

where:

$$x_B = x_B \sin\frac{\alpha_k}{2} - y_B \cos\frac{\alpha_k}{2} \tag{Eq.41}$$

$$y_B = y_B \sin\frac{\alpha_k}{2} - x_B \cos\frac{\alpha_k}{2} \tag{Eq.42}$$

$$A = -\frac{z+2}{z-2} \Big/ \frac{3z-2}{z-2} \tag{Eq.43}$$

$$a_1 = -Ar^2 - R^2 + rR(1+A)\cos(1-A)\alpha + R\cos\alpha - Ar\cos A\alpha \tag{Eq.44}$$

$$a_2 = 1 + r^2 + R^2 - 2rR\cos(1-A)\alpha - R\cos\alpha + r\cos A\alpha \tag{Eq.45}$$

$$a_3 = rR(1-A)\sin(1-A)\alpha + R\sin\alpha - Ar\sin A\alpha \tag{Eq.46}$$

$$a_4 = rR(1-A^2)\sin(1-i)\alpha + R\sin\alpha - A^2r\sin\alpha \tag{Eq.47}$$

4. EXAMPLE

For a cross with 6 grooves, in the case where the central gear is fixed and there are two planet gears, the ration between the number of teeth of the central and planet gear is:

$$z = 6 \qquad -2 = 1 - \frac{z_2}{z_4} \tag{Eq.48}$$

$$k = 0 \qquad z_2 = 3z_4 \tag{Eq.49}$$

For a cross with 6 grooves, in the case where the central gear rotates with the same velocity but in the opposite direction to the carrier (this variant is easily realized), the ration between the number of teeth of the central and planet gear is:

$$z = 6 \qquad -2 = k\frac{z_2}{z_4} - \frac{z_2}{z_4} + 1 \tag{Eq.50}$$

$$k \neq 0 \qquad -3 = \frac{z_2}{z_4}(k-1) \tag{Eq.51}$$

$$k = -1 \qquad z_2 = \frac{3}{2}z_4 \tag{Eq.52}$$

The benefits of the mechanism with a rotating central gear are clear. This variant yields a planetary-differential mechanism that requires significantly less space.

For a cross with 6 grooves, in the case where the central gear is fixed and there is only one planet gear, the ration between the number of teeth of the central and planet gear is:

$$z = 6 \qquad 4 = 1 + \frac{z_2}{z_3} \tag{Eq.53}$$

$$k = 0 \qquad z_2 = 3z_3 \tag{Eq.54}$$

Applying Eq. (37) yields two solutions of the ratio r/R; for the mechanism with one planet gear: r/R= –0.0625 and r/R= –0.25. The solution r/R= –0.0625 offers a smooth curve for the path of point B, so it is adopted as the final solution – Figure 5a, and for the mechanism with two planet gears: r/R=0.5 and r/R= –0.25. The solution r/R= –0.25 offers a smooth curve for the path of point B, so it is adopted as the final solution – Figure 5b.

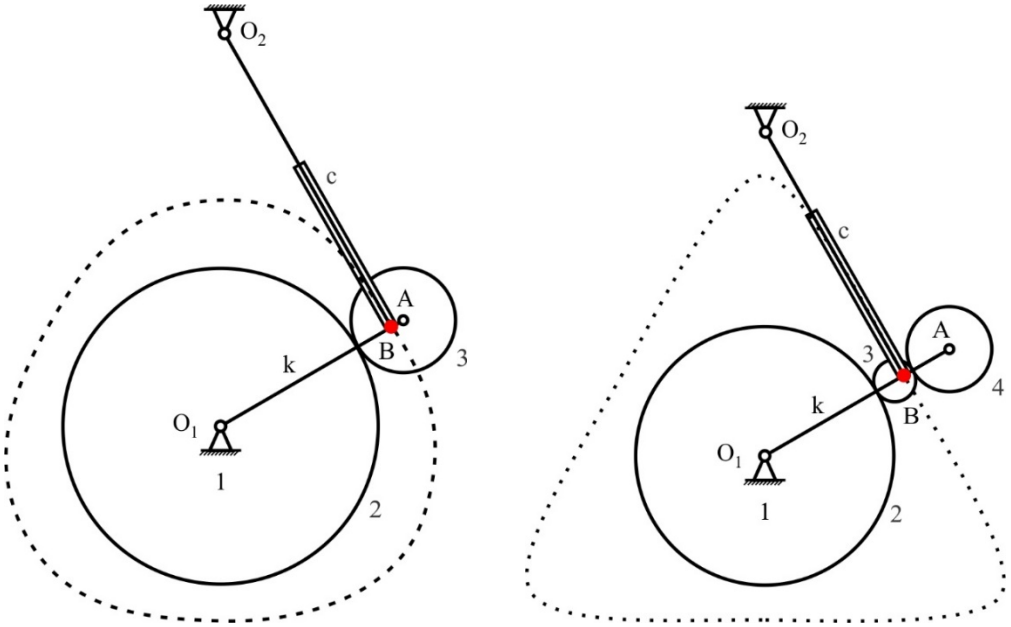

(a) (b)

Figure. 5: Modified Geneva mechanism a) with one planet gear, b) with two planet gears

Figure 6 shows the change of the position angle, the angular velocity and the angular acceleration of the cross of the modified Geneva mechanism with one planet gear 3 – Figure 6a and with two planet gears 3,4 – Figure 6b. The angular velocity of the carrier is adopted as 10°/s, while the length of the carrier is R=5m.

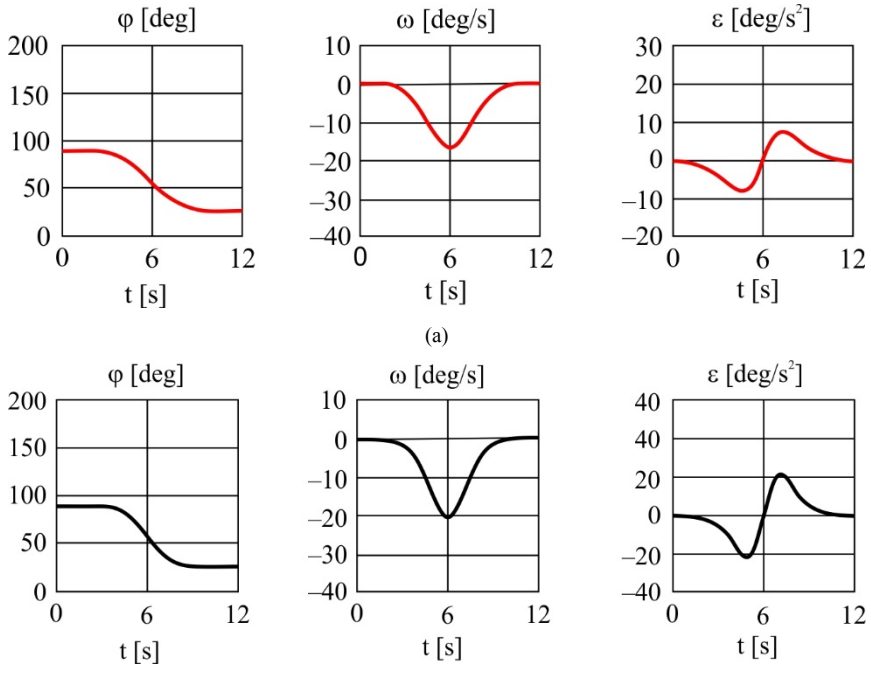

(a)

(b)

Figure. 6: Time histories of the position, angular velocity and angular acceleration of the modified Geneva mechanism: (a) with one planet gear 3, and (b) with two planet gears 3,4

Both solutions fulfil the requirement for no-impact contact between the pin and the cross. The variant with one planet gear offers lower values of angular velocity and acceleration, but requires more space. The planet gear needs to mesh with the central gear, meaning the central gear must be large enough to allow this. The choice between the two proposed variants depends on other factors as well. If there is a requirement for a smaller sized mechanism, the variant with two planet gears will be chosen, and if the value of the angular velocity and acceleration is more important, the variant with one planet gear will be chosen.

4. CONCLUSION

The paper shows the synthesis of an epicyclic gear train as the driving component for a conventional Geneva mechanism. Based on existing works on the subject, it was established that there are two main drawbacks to Geneva mechanisms, the first being impact loads, and the second velocity and acceleration jumps which lead to vibrations and wear. Therefore, there are two requirements that the mechanism is modified to achieve – smooth, non-impact engagement/disengagement of the pin and cross, and the elimination of the acceleration jump at the beginning and end of the Geneva cross motion. Based on these requirements, two solutions of the modified Geneva mechanism were proposed, with one and with two planet gears. The synthesis and kinematic analysis was conducted for both variants. Aside from this, an example was analysed that illustrated that both variants of the modified mechanism completely eliminate the impact loads and greatly decrease the velocity and acceleration jumps. The variant with one planet gear was shown to offer a general decrease of the angular velocity and acceleration values, while the variant with two planet gears offers a decrease in the size of the mechanism. Further study is planned to examine the possible use of epicyclic gears with internal meshing.

REFERENCES

1. Bickford, J. H.,1972. Geneva mechanisms. Chapter 9 in Mechanism for Intermittent Motion (Ed. J. H. Bickford). Industrial Press Inc., New York. pp. 127–138.
2. Sclater, N., 2011. Cam, geneva and ratchet drives and mechanisms. Chapter 7 in Mechanisms and Mechanical Devices (Ed. N. Sclater). McGraw-Hill Companies Inc., New York. pp. 180–210.
3. Zhang, D., Reed, M., Li, B., Gao, Z. and Ge, Y., 2009. Design optimization of a geneva mechanism for internal combustion engine application. Proceedings of ICIA International Conference on Information and Automation, Macau, China, pp. 649–654.
4. Hunt, K.H., 1978. Kinematic Geometry of Mechanisms. Clarendon Press/Oxford University Press, Oxford/New York.
5. Dijksman, E.A., 1966. Jerk-free Geneva wheel driving. Journal of Mechanisms, 1(3–4). pp. 235–283.
6. Sujan, V.A. and Meggiolaro, M.A., 2000. Dynamic optimization of geneva mechanisms. Proceedings of the International Conference on Gearing, Transmissions and Mechanical Systems, London, UK, pp. 687–696.
7. Cheng, C.-Y. and Lin, Y., 1995. Improving dynamic performance of the geneva mechanism using non-linear spring elements. Mechanism and Machine Theory, 30(1). pp. 119–129.
8. Heidari, M., Atai, A. A. and Panahi, M. S., 2012. An improved geneva mechanism for optimal kinematic performance. Proceedings of the Institution of Mechanical Engineers, Part C: Journal of Mechanical Engineering Science, 226(6). pp. 1517–1525.
9. Fenton, R.G., Zhang, Y. and Xu, J., 1991. Development of a new geneva mechanism with improved kinematic characteristics. Journal of Mechanical Design, 113(1). pp. 40–55.

10. Figliolini, G. and Angeles, J., 2002. Synthesis of conjugate geneva mechanisms with curved slots. Mechanism and Machine Theory, 37(10). pp. 1043–1061.
11. Lee, J.-J. and Jan, B.-H., 2009. Design of geneva mechanisms with curved slots for non-cutting manufacturing. Mechanism and Machine Theory, 44(6). pp. 1192–1200.
12. Lee, H. P., 1998. Design of a geneva mechanism with curved slots using parametric polynomials. Mechanism and Machine Theory, 33(3). pp. 321–326.
13. Hsieh, J., 2014. Design and analysis of geneva mechanism with curved slots. Transactions of the Canadian Society for Mechanical Engineering, 38(4). pp. 557–567.
14. Shen, S. H. and Cai, J. F. 2013. Kinematic analysis on series combined mechanism of elliptic gear and outer geneva. Applied Mechanics and Materials, 312(1), pp. 42–46.
15. Dooner, D. B., Palermo, A. and Mundo, D., 2014. An intermittent motion mechanism incorporating a geneva wheel and a gear train. Transactions of the Canadian Society for Mechanical Engineering, 38(3). pp. 359–372.

DESIGN OF A GAME CONTROLLER FOR PEOPLE WITH MOTOR IMPAIRMENT

Tashko Rizov
Faculty of Mechanical Engineering - Skopje, University "Ss. Cyril and Methodius" in Skopje, Skopje, Republic of North Macedonia
PhD., Associate Professor, tashko.rizov@mf.edu.mk

Risto Tashevski
Faculty of Mechanical Engineering - Skopje, University "Ss. Cyril and Methodius" in Skopje, Skopje, Republic of North Macedonia
PhD., Professor, risto.tashevski@mf.edu.mk

Martin Zhivskovski
Faculty of Mechanical Engineering - Skopje, University "Ss. Cyril and Methodius" in Skopje, Skopje, Republic of North Macedonia
MSc., student, martin.zhivskovski@students.mf.ukim.mk

ABSTRACT

The entertainment industry is one of the largest and most profitable industries today. A great portion of that industry involves video games that are designed with the intent to be played using a game controller. The designers of games usually include options to improve the gaming experience of people with visual or hearing impairments, but the population with motor impairments are left to be dealt by the producers of the game controllers. A number of solutions exist today on the market that tackle this issue, but there is still a good possibility for improvement mainly from the possibilities offered by advanced technologies like 3D printing.

The paper analysis the needed assistance for game controllers for people with motor impairment using the universal design methodology. Furthermore, using the advantages of 3D printing technology, the paper analysis the possibilities for custom design of game controllers according the needs and requirements of the users. After that, the paper presents a design solution for game controller for people with motor impairment together with the methodology for production of a prototype. With a detailed analysis of the improvement effects the game controller introduces to the focus group, the authors conclude on the key elements for design of game controller for people with motor impairment as well as possibilities for further research and development of the product.

Keywords: engineering design; rapid prototyping; 3D modelling; motor impairment;

1. INTRODUCTION

Much progress has been made in building interfaces for people with visual, auditory and motor disabilities, both for day to day activities and for computer interaction. Despite these advances, videogame interaction is highly dependent on hand movement for control. This makes it almost impossible for individuals with motor disabilities to play videogames. In this paper we describe the design of an interaction device for individuals with severe motor disabilities. Through interviews and discussions with a motor-impaired user, we created a device that enables them to play a videogame (Pereira et al., 2011).

Video games, as an entertaining media, dates back to the '50s and their hardware device underwent a long evolution starting from hand-made devices such as the "cathode-ray tube amusement device" up to the modern mass-produced consoles. This evolution has, of course, been accompanied by increasingly specialized interaction mechanisms. As of today, interaction with games is usually performed through industry-standard devices. These devices can be either general purpose (e.g., mouse and keyboard) or specific for gaming (e.g., a gamepad). Unfortunately, for marketing reasons, gaming interaction devices are not usually designed taking into consideration the requirements of gamers with physical disabilities (Maggiorini et al., 2019).

1.1. Video game consoles development

The earliest video game that was publicly presented in 1950 was Bertie the brain (Fig.1-a). It was consisted of a computer tall 4m with vacuum tubes enabling the user to play the well-known tic-tac-toe game. The interaction was with buttons placed in front of the machine. In 1951 at the Britain science festival Nimrod game machine was presented playing the game Nim. In 1958 the first game console is presented, named Tennis for two. The biggest evolution in this industry segment comes in 1971 with the first game designed with integrated circuits – Computer Space. In 1972 on the same hardware design the game Pong is presented – the first coin based game console. In the end of 1972 the first game console that was able to connect to a home TV set was presented. That was the game Magnavox Odyssey and it was sold in 35.000 copies. In 1977 the game console Atari 2600 was presented (Fig. 1-b). This was the first console of the so called second generation with standardized socket for game controller.

(a) (b)

Figure. 1: (a) Bertie the Brain, and (b) Atari 2600
(Source: R. Chikhaniet 2015);

The third generation of video consoles started in 1983 with the boom of Nintendo and Sega. The Nintendo Famicom was the first game console to include a controller with a direction pad. In 1988 for the first time ever Nintendo presented a controller for impaired people. With the continuous development of microprocessors more advanced consoles appear in 1988 which is called the forth generation game consoles. In this generation, Nintendo is the first company to introduce the shoulder buttons on its controller in the Super Nintendo Entertainment System. With the introduction of the CD as a medium the fifth generation of consoles appeared where Sony takes the lead with the Play Station. With the new millennium the sixth generation appears alongside Microsoft's Xbox. The seventh generation of consoles is characterized with motion sensors instead of physical controllers. The last one is the eight generation where the focus is on the social interaction of the players. The three biggest competitors are Nintendo, Sony and Microsoft.

1.2. Video game controllers development

The Tennis for two game developed in 1952 used two controllers, with aluminum casing with one rotating potentiometer and one switch. The potentiometer defined the direction of the ball and the switch was used to give the command to hit the ball. The design in this controller did not play any role since the game was not mass produced. The first commercial game, Magnavox Odyssey introduced the first designed and mass produced controller consisted of three potentiometers and one switch integrated in a plastic box that stands on a flat surface. The revolution comes with the controller of Atari 2600 (Fig. 1-b). This game console had a controller designed according the controls of the aircrafts with so called joystick. His simplicity enabled people who never played a video game to play them with ease and to understand the concept immediately since the movement of the stick was according the desired direction of movement in the game. This controller became a symbol of videogames. The next big innovation was the D-Pad (direction pad) of Nintendo (Fig. 2-a). The joystick was meant for analogue signals, giving simultaneously the command for direction and intensity. For digital signals only the information of the direction was needed therefore the joystick was replaced by the D-pad. With this the player had better control, could change directions faster and the controller had smaller dimensions. Sega for its console Genesis presented the first ergonomic controller (Fig. 2-b). It had a C-shape with buttons placed under an angle making it easier to reach. The next biggest revolution were the motion controllers (Fig. 2-c). With them the interface became wireless and gave a wide array of commands available.

(a) (b) (c)

Figure. 2: (a) Nintendo D-Pad, (b) Sega Genesis and (c) Nintendo Wii motion controller.
(Source: Kyle et al. 2007);

1.3. Disabilities and Video Games

The disabilities as a concept have different meaning in different communities around the World. The disability can be referred to mental or physical properties that some institutions (especially medical) consider that need to be improved. This is referred as medical model. Also, it can refer to the limitations imposed to people by the physical demands of the society – referred as the social model. The United Nations' World Health Organization (WHO) has prepared and International Classification of functioning, disabilities and health that serves as unified platform for describing health and health conditions of an individua (Fig.3). This block-diagram describes human functioning or an individua through three perspectives: body, human and society. The information are organized in two parts: functional disabilities and contextual factors.

The components of the functional disabilities are divided in body functions and structure which also includes anatomic strictures like pain in joint, impaired sight, impaired hearing etc. Activity and participation are components where "activity" is defined as execution of certain task like inability to grasp small objects, lost perception of depth, inability to locate sound etc. Participation is defined as participation in a life situation like socialization, attending a competition, participate in choir etc. Each of these categories are filled in with terms that are chosen from a detailed list which is unified and categorized by short codes.

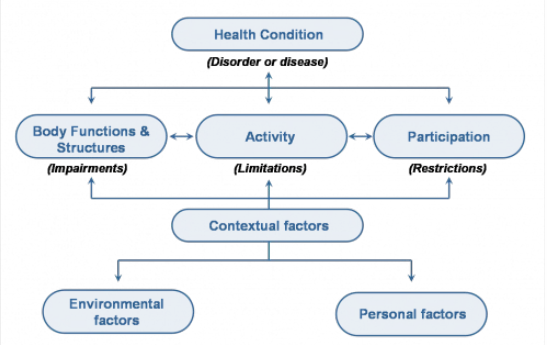

Figure. 3: WHO's International Classification of functioning, disabilities and health. (Source: WHO. 1980);

The video games accessibility is considered as a separate subgroup of the computer accessibility since video games are a sort of software controlled by specific hardware. Video games accessibility is becoming a major research interest due to two factors: increase of the number of people interested in playing video games and the fact that video games are used for other purposes besides fun, like education, rehabilitation and development. Since video games and gamification are becoming part of formal education, they will have to become accessible to all, including people with disabilities.

Accessibility in video games in general could be categorized in three categories depending on the impairment:

- Could not get feedback from the game due to sensor impairment. For example a user is not able to hear the dialogue between characters in the game, or an audio effect like explosion due to hearing impairment. Similar for visual impairment the player could not recognize the colours or distinct elements of the game.

- Could not provide the needed input signal to the game using conventional device due to physical impairment. Usually, the special devices for input signals for people with physical impairment like the switch controller or the eye tracker are not suitable for games where complex commands are necessary.

- Could not understand the game play or to understand the controls due to cognitive impairment. People with difficulties in learning or poor coordination could have difficulties playing the video games.

The game controllers for impaired people have travelled a significant road of improvement since their beginnings in the 80's. In 1988 Nintendo produced the first game controller for physical impaired people called NES Hands Free . Although it was only made by order and pretty expensive, it was an important milestone in the process of further development of this category of controllers because it caught the attention of other game controllers manufacturers. In the years to come, companies are exploring the combination of voice, electromyography, biting, chin movements etc. One of the latest development in this filed is Microsoft's Xbox Adaptive Controller where by combination of interfaces and programable buttons users can get better game control.

Users, on the other hand, have developed various modifications of the standard controllers to make them suitable for players with physical impairment. By adding specially designed livers or enlargement of the pushing surface of existing buttons. These type of solutions have become more present with the availability of 3D printing. The ability to produce inexpensive plastic parts according custom design have provided users with the ability to make tailor-made controllers according the abilities and impairment of a single user.

Figure. 4: Modifications of standard controllers with custom made masks/elements.
(Source: Maggiorini et al. 2019);

2. DESIGN OF THE CONTROLLER

In order to create a successful product, the universal design (UD) framework has been used. This methodology is most suitable for inclusive design and design for all which are the major elements of our focus. One of the elements of UD are the human factors principals where the accent is on the human-system integration. In order to analyse the human factor principals, the Inclusive Design Toolkit (IDT) was used. This toolkit is specifically focused on the human abilities putting forward the user ability to complete a task. Using the toolkit, the following factors have been analysed: sight (size, shape, contrast, colour, position of graphical versus text elements), sound (volume, tone, clearness, location of sound source), cognitive (memory, interface, attention), reach and agility (force, movement, grasp), mobility (should the user move while using the device).

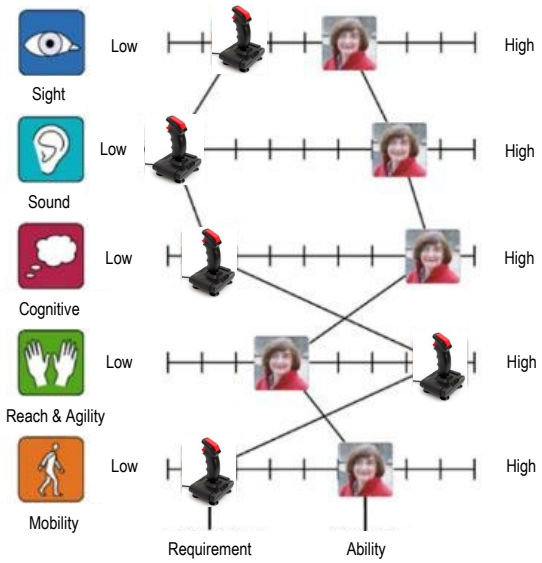

Figure. 5: IDT used to analyse human-system integration.

Each of the factors has been ranged on a scale from low to high for the requirement and ability of a selected focus group (Fig .5). Although this analyse is rough it is a good starting point for the further steps in the design process. In the next steps the "waterflow" method for product development was used in order to precisely define the needs, requirements, concepts and solutions. The user-centric design method was used to analyse the ergonomic properties needed for this product. The final element of the design methodology was the user interview. A focus group of people with motor impairment were selected and a structured interview was conducted. The first target of the interview was to examine different shapes and select the most suitable shape for a controller (Fig. 6).

The second target of the interview was to analyse the difficulties that they face when playing video games. The third target was to investigate if they have made modifications of existing controllers and what can be learnt from that.

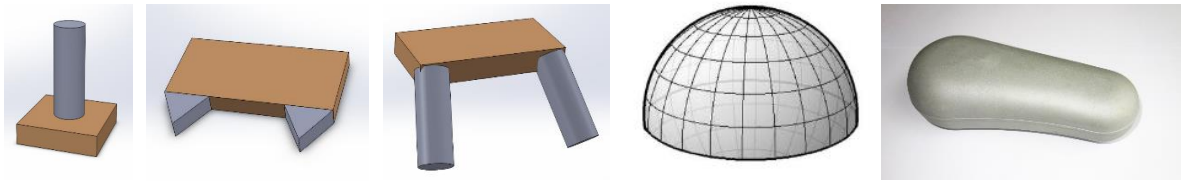

Figure. 6: Different shapes analysed during the structural interview.

The conclusion of the interview was that all users use their hands when interacting with objects, but they all have limited radius of reach. The difficulties they face when playing video games are complexity and reaction speed. This limits them to playing video games controlled only by touch screen. None of the interviewees has made modifications of a controller so far. Regarding the shape, it was a clear selection of the spherical shape as most suitable. The advantage of this shape was that it could be placed on a supporting surface and place the hand over it (Fig. 7). In this way the controller will also support the hand of the user without resulting in joint strain. Also, the fingers have a natural position and the user does not need to move the fingers a lot to reach the buttons of the controller. The spherical shape is most suitable for all users regarding their difference in size of hand making it universal.

Figure. 7: Spherical shape test while interview with focus group.

Finally, the complete analysis gave the following guidelines for the design of the game controller: spherical shape, use only one hand, support the controller firmly on a surface, use dent buttons, use buttons with higher sensitivity, avoid cylindrical shapes. Having all this in mind, the first sketches of the game controller were created.

The first element of the design was the base of the controller. This element should provide the user with the ability to place the controller on a table and to provide a fix and stable support. Also, the base element has to include the control mechanism and the supporting electronics and switches (Fig. 8-b). By modelling this element in CAD, the best design was selected. For inputting the direction control the system would use a liver that is rotating 12° in each direction. The spherical element was designed based on this function, matching the axis of the two elements to use less force for inputting the command (Fig. 8-a). In order to satisfy the requirement for lower force needed to press the buttons, a microswitch with leaver was selected. The leaver decreases the needed force to activate the switch, i.e. the buttons. Ergonomic research shows that all people have better control on the thumb, the index and the middle finger. The last two fingers are not the best solution for pressing a switch. Having this in mind, this feature was incorporated in the design of the controller.

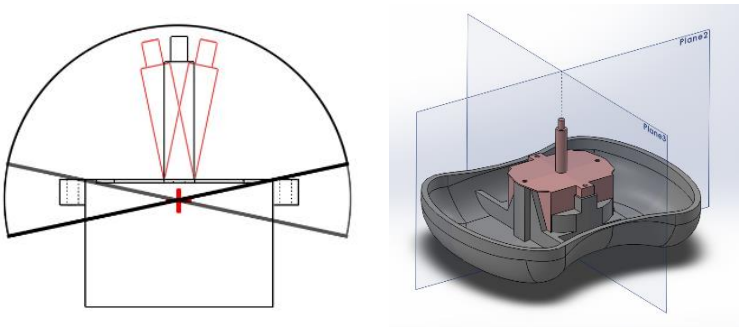

(a) (b)

Figure. 8: (a) Spherical element with a direction control liver, (b) CAD model of the base element of the controller.

In order to design the dents on the spherical element a clay model was used. The clay element was modelled so it would provide a natural fit of a hand placed on it (Fig. 9). By adding material and changing the radius an optimal shape of this element was achieved. The clay model also served for defining the dents for switch controls as well as the distance between these dents to fit the hand naturally. When an optimal design was achieved the dimensions were recorded and a CAD model was created. In all elements of this process the focus was also to create a controller that can be produced using additive manufacturing technologies. The 3D printing has become so accessible that it this case it could provide with the ability to print spherical elements custom made to the size and shape of the user.

Figure. 9: Clay model of the spherical element to determine optimal dimensions.

3. PROTOTYPE PRODUCTION

In order to produce a prototype the technology for Fused Deposition Modelling (FDM) was used. Using the 3D printer Ultimaker and the accompanying slicer software the three designed elements of the prototype was created. The print out is not used right away, since the shape of the elements is complicated with round edges and wholes. The model is printed with supporting material in order to achieve the desired form (Fig. 10). Also, the model has to be additionally processed in order to achieve the desired quality of the surfaces.

Figure. 10: 3D printed model of the base, subassembly and the final prototype of the controller.

In the next step, the liver for inputting the direction commands is installed, together with the circuit board and the switches for the thumb and the index finger. In the final step, the electronics was wired to the liver and

the switches, and the controller was calibrated using the standard tools for controller calibration in Windows operating system. The assembled controller was tested using several video games with different complexity.

4. CONCLUSION

The paper presents the development of video games and video controllers through history focusing on the activities in this area for impaired people. The paper continues with analysis of the International Classification of functioning, disabilities and health that serves as unified platform for describing health and health conditions of an individua. In addition, it utilizes the Universal Design methodology and the Inclusive Design Toolkit to define and determine the requirements of video game players with motor impairment.

Furthermore, using the advantages of 3D printing technology, the paper analysis the possibilities for custom design of game controllers according the needs and requirements of the users. After that, the paper presents a design solution for game controller for people with motor impairment together with the methodology for production of a prototype. With a detailed analysis of the improvement effects the game controller introduces to the focus group, the research provides a list of key elements for design of game controller for people with motor impairment as well as possibilities for further research and development of the product.

REFERENCES

1. Orland Kyle, Thomas Dave, Steinberg Scott. (2007). The Videogame Style Guide and Reference Manual. ISBN 9781430313052
2. Bianca O. Pereira, Cristiano Expedito, Fabrício Firmino De Faria, and Adriana S. Vivacqua. (2011). Designing a game controller for motor impaired players. In Proceedings of the 10th Brazilian Symposium on Human Factors in Computing Systems and the 5th Latin American Conference on Human-Computer Interaction (IHC+CLIHC '11). Brazilian Computer Society, Porto Alegre, BRA, 267–271.
3. Maggiorini, Dario & Granato, Marco & Ripamonti, Laura & Marras, Matteo & Gadia, Davide. (2019). Evolution of Game Controllers: Toward the Support of Gamers with Physical Disabilities. 10.1007/978-3-030-32965-5_4.
4. Riad Chikhani (2015): The History Of Gaming: An Evolving Community; Techcrunch.com
5. World Health Organisation (WHO). (1980). International Classification of Impairments, Disabilities, and Handicaps, WHO Press.
6. Martin Zhivskovski: Development of methodology for designing a game console controller intended for people with impaired motor functions; University "Ss. Cyril and Methodius" in Skopje (2019).

PARAMETRIC DESIGN AS AN APPROACH FOR DESIGN FOR ADDITIVE MANUFACTURING

Jelena Djokikj
Faculty of Mechanical Engineering, Ss. Cyril and Methodius University in Skopje, RNM
PhD, Teaching Assistant, jelena.djokikj@mf.edu.mk

Tatjana Kandikjan
Faculty of Mechanical Engineering, Ss. Cyril and Methodius University in Skopje, RNM
PhD, Professor, tatjana.kandikjan@mf.edu.mk

ABSTRACT

Additive Manufacturing (AM) refers to a group of processes that experienced rapid development over the last decade. This enabled their applicability in various areas. Their specific manner of functioning through adding material is the reason why they are so versatile. Still, at the same time, this specific manner of functioning demands a different approach in the design process, the so-called design for additive manufacturing (DfAM). DfAM is an approach based on the principle of the well-known DFM (Design for Manufacturing) and DFMA (Design for Manufacturing and Assembly). The aim of the DfAM is to help designers to adapt more easily to AM and fully exploit its possibilities. One of the most important AM advantages is the fabrication of complex geometries, which is particularly interesting to designers. Regardless of all the advantages, there are some restrictions to the AM processes that need to be taken into consideration in the design process.

In this paper, we propose the use of parametric design for designing unique models with complex geometries. Through designing the parameters, we can implement the AM restrictions in the early stages of the design process without affecting the complexity of the shape. Another advantage of the parametric design is the possibility of easy manipulation of the CAD model and a change of the parameters, so that a whole collection of unique products can be created.

Keywords: design for additive manufacturing (DfAM); parametric design; design process

1. INTRODUCTION

Additive manufacturing is a group of processes in which the model is built by adding material in layers (Gebhardt, 2011). This manner of functioning is completely opposite to the traditional manufacturing processes. One of the key opportunities stands in the AM's flexibility potential (Gardan et al., 2016; Thompson et al., 2016). While other technologies impose strict technological or economic constraints on the production of variants, AM offers an unprecedented level of freedom in this regard (Gibson et al., 2015; Lipson, 2012). AM processes are well-suited to customized products and small-series production down to lot size one (Friesike et al., 2019), and, at the same time, they lower the overall manufacturing cost. AM's main capabilities and advantages include the following: shape complexity, hierarchical complexity, material complexity and functional complexity (Gibson et al., 2015). This creates new opportunities, but also, at the same time, poses challenges when designing for AM.

1.1. Design for Additive Manufacturing (DFAM)

Freedom offered by AM can be treated as a threat for the industrial design, caused by the lack of structured procedures and tools to easily adapt the new technologies (Friesike et al., 2019). When it comes to these structured procedures and tools, few studies were published concerning the breakthrough into the designing

process (Vayre et al., 2012). Bourell et al. (2009) suggest developing new design methodologies dedicated to additive manufacturing and inspired by the Design for Manufacturing and Design for Assembly; they call it DFAM. DFAM is a methodology which tends to maximize product performance through the synthesis of shapes, sizes, hierarchical structures, and material compositions, enabled by the AM technologies (Gibson et al., 2015). Laverne et al. (2014) suggest an extension of this definition to the tools that support the DFAM methodologies. According to them, DFAM is a set of methodology and tools that help the designer to take into account the specificities of additive manufacturing during the design process.

1.2. CAD modelling

The opportunities occur in the form of freedom for complex shapes creation, allowing the designers to set their imagination free in the design process. The first steps in the concept generation phase are the most creative; the designer imagination is at the highest level and there are no obstacles. In the next step, sketches need to be transferred to CAD software. This is the moment when designers usually encounter difficulties. The reason is that the available CAD software packages are designed to address the needs and requirements, but also restrictions of the traditional manufacturing processes. This means that the working principle should be changed, but, more importantly, flexibility in the form creation should be enabled (Gibson et al., 2015). The challenges that the user encounters with CAD can be stated as: geometric complexity, physically based material representations and physically based property representations (Gibson et al., 2015).

Yang and Zhao (2015) classify contemporary design tools (different modelling software) for AM into four groups, depending on their main characteristics. The first group consists of systems (i.e., Geomagic Design (3DSYSTEMS, n.d.) and Meshlab (ISTI-CNR, n.d.)) intended for point cloud (received from 3D scanning) editing. The second group consists of solid based CAD systems (Solidworks, CATIA), which, although they use parametric modelling, still follow the rules of modelling for traditional manufacturing. The third group contains systems that are intended for process-oriented design (i.e., Magics). These kinds of systems are mainly used to check the model's manufacturability; they are not intended for modelling. These three types of design systems enable modelling, visualization, mesh, and converting of the 3D model into STL files, which is important for the transformation from conceptual ideas to implementable files for AM systems. Nevertheless, with the growth in the number of physical features and the increase in the hierarchical order of magnitude, conventional solid-modelling-based systems run slowly and consume too much memory. Another problem is the difficulty in manipulating the interior volume to form internal structures in the AM design. Since the possibilities of software's part of the presented three groups do not satisfy the needs of designers when designing for AM, new design tools have emerged in recent years. The design tools of the fourth group come across the problems that the tools from the first three groups cannot solve. They propose a new way of designing which exploits the AM's advantages. In this group, two main courses can be identified: topology optimization (i.e. HyperWorks's Altair (Altair HyperWorks, n.d.)) and lattice structure. The topology optimization solutions are based on the finite element analysis in order to optimize the use of material and final design output. In spite of that, the lattice structure software or modules generate cellular structures in the predefined model shape. These design tools change the design process and the design approach involving the designers in the early stages to think about the AM considerations and manufacturing. This is an appropriate approach when designing for AM, as stated previously. However, one key ingredient is absent in the working process with these tools and that is designer's creativity. These tools do not help the designer in the modelling phases of creating more complex and organic shapes. Friesike et al. (2019) have an interesting approach in the design for additive manufacturing in order to increase creativity and productivity. At the moment, designers are left to their own devices in CAD modelling to find alternatives. They often use CAD software intended for animation since it allows for better surface modelling but that can result in an inappropriate STL file (not closed boundaries). Hence, this kind of software should be used with caution and the file should be verified before slicing and sending it to the machine. At Loughborough University, researchers work on the development of new software as an appropriate answer to the AM development (evoShape, n.d.; Retzepi et al., 2017) and its opportunities for application in customization and personalization (Ariadi, 2016).

In this paper, we propose the use of software for parametric or algorithmic software for the design in AM. With parametric modelling, the designer can combine mathematical equations in order to create rhythmic and complex shapes. This offers multiple possibilities: with parametric models, a whole series of unique models can be created without the need of additional modelling.

2. METHODOLOGY

The research methodology proposed by Gibson et al. (2015) is used in the paper. The methodology is designed so that it can be applied for designing various products for AM. As implied by (Gibson et al., 2015), the proposed DFAM methodology includes the design process, concept generation, solid modelling and process planning. All the elements have the same level of importance and all of them should be taken into consideration. The most important characteristic of this methodology is that process planning should be a part of the design process. The design process starts with problem synthesis, using an existing problem template. According to the problem definition, different interconnections of elements are made. Figure 1 presents the model that we propose for the implementation of parametric design in the DFAM.

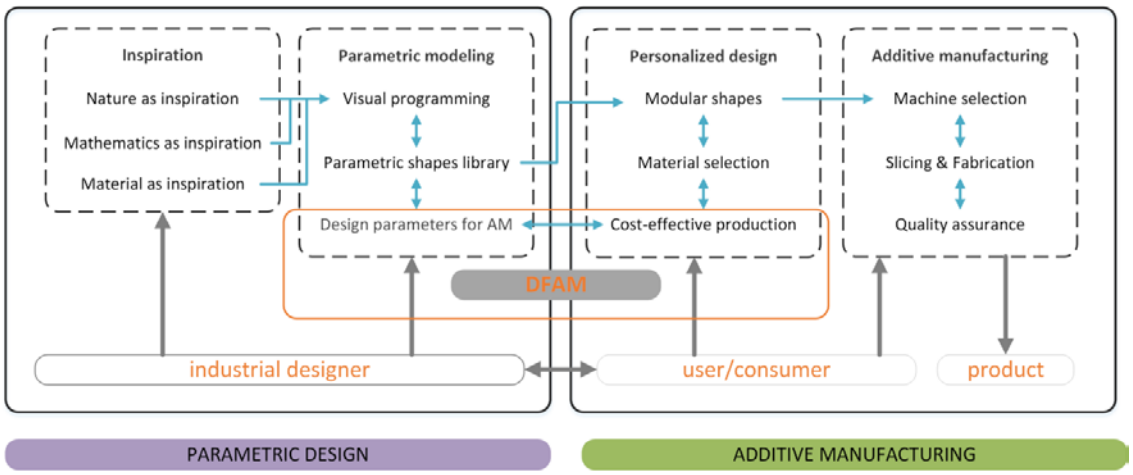

Figure 1. The proposed model for the integration of parametric design in the DFAM

3. PARAMETRIC DESIGN

Abdullah and Kamara (2013) propose the procedures for parametric design in order to increase the idea generation in the conceptual phase. Dean (2009, 2006) uses parametric and generative modelling to fully exploit the AM's possibilities and to offer personalized products to users. The design studio Nervous Systems offers an interesting approach, by applying parametric and generative design to their products inspired by nature (Nervous System, n.d.).

Rhinoceros and its visual editor Grasshopper were used for parametric modelling. The possibilities offered by the combination of Rhino and the Grasshopper provide an adequate response to AM requirements (Akos and Parsons, 2014). Rhino is used for modelling complex freeform shapes, while Grasshopper is utilised for additional mathematical modelling or even programming (Khabazi, 2009). Still, Grasshopper on its own can be used for the modelling of the whole part. Rhino offers more subtle and straightforward options for freeform modelling. In Figure 2-a, the algorithm for one model is presented. With simple manipulation of the already created algorithm, multiple variation of the initial model can be created. In Figure 2-b, one variation of the model is presented.

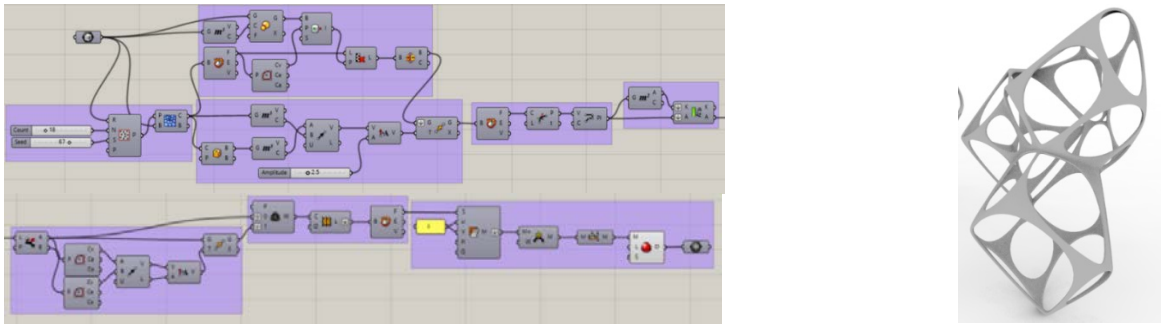

a) b)

Figure. 2: The algorithm created in Grasshopper for complex voronoi structure:
a) the Grasshopper algorithm, and b) one variation of the model
(Source: Djokikj, 2020)

Figure 3 presents the sphere model so as to demonstrate the creation of different variations with the change of one parameter. In order to create variance with less resemblance, several parameters can be varied. In the example shown in Figure 3, the parameter for the space between the holes has been varied.

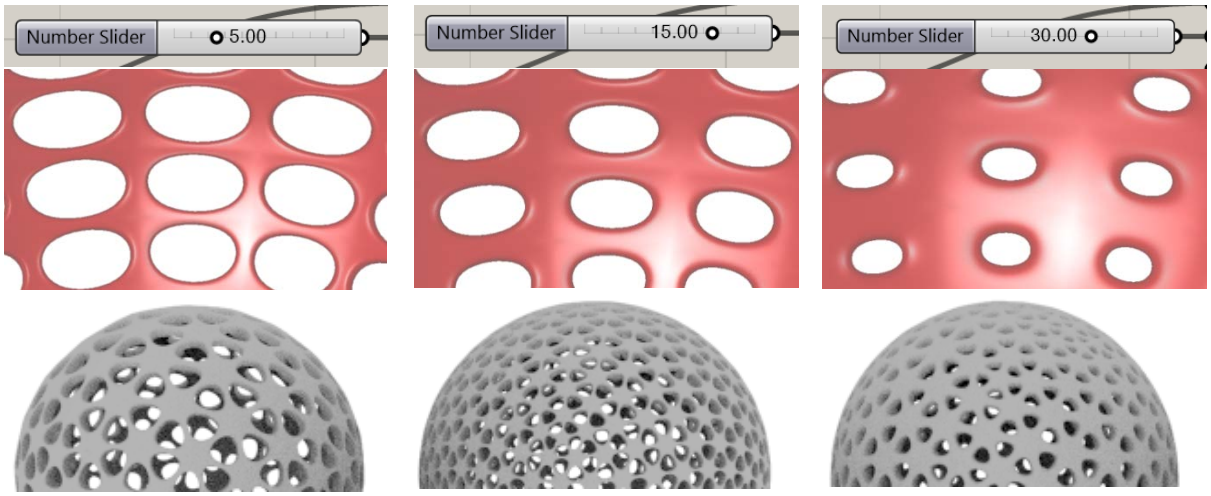

a) b) c)

Figure. 3: Variation in output depending on one parameter of the sphere model:
a) Variation 1, b) Variation 2, and c) Variation 3

4. RESULTS AND DISCUSSION

It has been proved over time that parametric modelling is a great opportunity to create complex shapes. Additionally, it is a very powerful tool in the concept generation phase. In this paper, we have aimed at proving that it is also an appropriate solution when designing for AM.

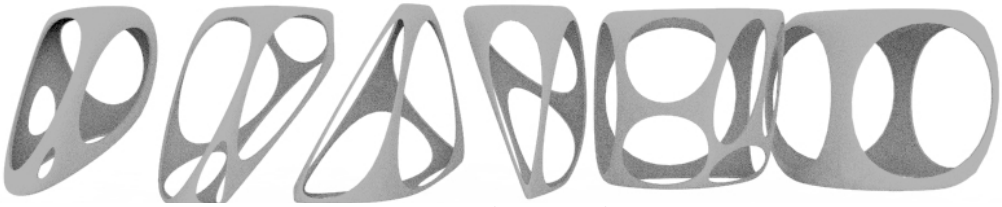

Figure. 4: Example of shape modification on one model

Using parametric modelling, designers create the initial shape of the parameterized model, which can be modified using the parameters in order to explore the options (Fig. 3, Fig. 4). The first model from Figure 4 was manufactured using the machine for fused filament fabrication (FFF) in order to check the quality of the model and manufacturability. FFF is one of the most often used AM processes. The models are designed as polygonal mesh, which is the most suitable for STL conversion. The STL file is the universal file format needed for the AM processes. The parts are fabricated using different methods, as shown in Figure 5. Different methods and process parameters are applied in order to find the most suitable one.

a) b) c)

Figure. 5: Different fabrication methods using the FFF machine
a) without support, b) with tree support, and c) with soluble support
(Source: Djokikj, 2020)

The changes in the support material options affect printing time and the used material, but, at the same time, surface quality as well. In Figure 5-a, the model was manufactured without the support material and printing time was four hours. In comparison, printing time of the second option, with three supports (Figure 5-b), is eight hours, which is double. In the last option, fabrication with the soluble support material, printing time is 12 hours. It is important to mention that the parts were fabricated using the FFF machine with one extruder. If there had been two extruders, printing time would have been decreased.

a) b) c)

Figure 6c: Manufactured outputs using different parameters:
a) without support, b) with support, and c) with soluble support
(Source: (Djokikj, 2020))

In Figure 6, outputs of the fabricated parts obtained by using different methods are presented. All models were manufactured on the same machine, using the same material – only working parameters were modified. The results are satisfactory, although the best results regarding surface quality are achieved with the use of the soluble support material.

Still, the main purpose of this paper has been to check whether the parametrically designed model is suitable for this purpose to be manufactured using AM. Based on Figure 6, it can be concluded that the models designed parametrically as a polygonal mesh are an appropriate solution for AM and the printed result is fully satisfactory.

5. CONCLUSION

On the basis of the findings presented above, it can be concluded that parametric modelling is an appropriate tool for the designers to use when designing forms in AM. This kind of modelling gives the designer the freedom that he/she needs and, at the same time, exploits the possibilities of the AM technologies. As stated previously, there are other software solutions that exploit the possibilities of AM, like topology optimization software or lattice structure modelling, but they restrict designer's creativity.

In this paper, we used Rhino's Grasshopper, since if offers multiple modelling techniques. At the same time, openness of the plug-in allows for the creation of individual modules and components or the use of the third party components. This flexibility enables numerous different applications for any type of design or product.

Additionally, there is always an option to use multiple software solutions for one model. This means that the initial shape of the model or one component can be designed in one software package and the more complex operations, such as panelling or morphing, can be done in the software for parametric design.

REFERENCES

1. 3DSYSTEMS. Geomagic Design X. http://www.rapidform.com/products/xor/overview/. Accessed: 18th November 2019
2. Abdullah, H.K., Kamara, J.M., 2013. Parametric design procedures: A new approach to generative-form in the conceptual design phase. AEI 2013 Build. Solut. Archit. Eng. - Proc. 2013 Archit. Eng. Natl. Conf. 333–342.
3. Akos, G., Parsons, R., 2014. Foundations: The Grasshopper primer third edition. Modelab.
4. Ariadi, Y., 2016. Facilitating consumer involvement in design for additive manufacturing / 3D printing products, PhD Thesis, Loughborough University, Loughborough, UK
5. Bourell, D.L., Leu, M.C. and Rosen, D.W., 2009. Roadmap for additive manufacturing: identifying the future of freeform processing. The University of Texas at Austin, Austin, TX, pp.11-15.
6. Dean, L.T., 2006. Designing for RM: " Entropia " A Case Study. In: TCT2006 RM Conference.

7. Dean, L.T., 2009. Futurefactories: The application of random mutation to three-dimensional design. The University of Huddersfield. PhD Thesis
8. Djokikj, J., 2020. Form design for Additive Manufacturing. Ss. Cyril and Methodius University.
9. Friesike, S., Flath, C.M., Wirth, M., Thiesse, F., 2019. Creativity and productivity in product design for additive manufacturing: Mechanisms and platform outcomes of remixing. J. Oper. Manag. 65, 735–752.
10. Gardan, N., Schneider, A., Gardan, J., 2016. Material and process characterization for coupling topological optimization to additive manufacturing. Comput. Aided. Des. Appl. 13, 39–49.
11. Gebhardt, A., 2011. Additive Manufacturng. Hanser Publishing. Munchen.
12. Gibson, I., Rosen, D., Stucker, B., 2015. Additive Manufacturing Technologies: 3D Printing, Rapid Prototyping and Direct Digital Manufacturing, Second Edi. ed. Springer Science+Business Media, New York.
13. evoShape. https://www.lboro.ac.uk/microsites/lds/dprg-projects/digital_evoshape.html/. [Accessed 10th December 2010].
14. HyperWorks. Altair. https://www.altairhyperworks.com/. [Accessed: 18th November 2019].
15. ISTI-CNR. Meshlab. https://www.meshlab.sourceforge.net/. [Accessed: 18th November 2019].
16. Khabazi, M., 2009. Algorithmic modelling with Grasshopper (Vol.1). Bukupedia.
17. Laverne, F., Segonds, F., Anwer, N., Coq, M. Le, 2014. DFAM in the design process: A proposal of classification to foster early design stages. *CONFERE, Sibenik, Croatia*.
18. Lipson, H., 2012. Design in the age of 3-D printing. *Mechanical Engineering.* 134(10).
19. Nervous System, I., n.d. Nervous System. https://n-e-r-v-o-u-s.com [Accessed: 10th December 2019].
20. Retzepi, T., Goh, Y.M., Graham, I.J., 2017. 3D object comparison with geometric guides for Interactive Evolutionary CAD. Advances in Manufacturing Technology XXXI: Proceedings of the 15th International Conference on Manufacturing Research, Incorporating the 32nd National Conference on Manufacturing Research, University of Greenwitch, UK (6), pp.421–426.
21. Thompson, M.K., Moroni, G., Vaneker, T., Fadel, G., Campbell, R.I., Gibson, I., Bernard, A., Schulz, J., Graf, P., Ahuja, B., Martina, F., 2016. Design for Additive Manufacturing: Trends, opportunities, considerations, and constraints. *CIRP Annals*, 65(2), pp.737–760.
22. Vayre, B., Vignat, F., Villeneuve, F., 2012. Designing for additive manufacturing. *Procedia CIRP*, *3*, pp. 632–637.
23. Yang, S., Zhao, Y.F., 2015. Additive manufacturing-enabled design theory and methodology: a critical review. *Journal of Advanced Manufacturing Technology*, 80(1-4), pp.327–342.

THE METHODS OF 3D MODELING OF SEVERAL TYPES OF HELICOIDS

Vladimir Jean Paul
Department of civil Engineering, Peoples' Friendship University of Russia (RUDN University), PhD student
jeanpaulvladimir@yahoo.fr

Marina Rynkovskaya
Department of civil Engineering, Peoples' Friendship University of Russia (RUDN University), Associate Professor

Fabrice Mayaki Domingo
D. E. A industry inc of Canada, Designer and project manager.

Timur Elberdov
Department of civil Engineering, Peoples' Friendship University of Russia (RUDN University), master student

ABSTRACT

This article discusses the methods of 3D modeling of several types of helicoids with their subsequent printing on a 3D-printer. For printing traditional 3D models, it is proposed to use SolidWorks software, which allows to perform parametric modeling of mechanical objects with the help of engineering computer graphics, while for printing more complex 3D models, other software tools are required. In this article, there is a review of the software tools which allow to model complex forms for further exporting into SolidWorks and additive technologies. It is also described in detail by the construction of different types of helicoids. The process of 3D modeling of helicoids is described step-by-step and is divided into two stages: parametric modeling of the helicoid in SCAD Office Software, editing of the obtained model in AutoCAD and its export to a special format for 3D printing. Some problems in creating the models suitable for 3D printing are also discussed.

Keywords: 3D modeling; helicoids; SolidWorks; additive technology; computer graphics.

INTRODUCTION

To print the three-dimensional model by 3D-printer it is necessary to introduce the model in .stl file format [1]. The file format .stl is widely used for storing three-dimensional models of objects for use in additive technologies. The vast majority of modern software for three-dimensional geometry have the ability to export the models to the .stl format [2].

In case of a 3D shell model, there are two options [3]. The first option (the easiest one) is to build a shell model in any program that implements the construction of 3D geometry like SketchUp, 3ds Max or more engineering programs like SOLIDWORKS, Autocad, Revit and others, and then export the model to a .stl file. However, these programs do not implement the construction of surfaces using mathematical equations. The second option is to build a shell model in a program that has the ability to build geometry using mathematical equations, and then transfer this model to the .stl file. Among the software systems that are widely used in the CIS countries, only SCAD Office has the function of constructing geometry using mathematical equations. The COMSOL Multiphysics and ANSYS Workbench programs also have such functionality, but they do not have Russian localization and are used little in the CIS countries.

1. SOFTWARE SYSTEMS FOR MODELLING SHELLS OF COMPLEX GEOMETRY

Autodesk 3ds Max is a professional 3D modeling, animation, and visualization software for game development and design. 3ds Max has extensive tools for creating a diverse in form and complexity of three-dimensional computer models, real or fantastic objects of the surrounding world, using a variety of techniques and mechanisms. 3ds Max is widely used by architects to create complex expressive forms that are very difficult to model in other programs and supports exporting the model to .stl format.

SolidWorks is a hybrid parametric modeling system designed to create parts and assemblies in three-dimensional space. In SolidWorks, it is possible to work equally well with both solids and surfaces. Typically, a part is a solid, surface, or a combination of a solid and a set of surfaces. The process of constructing a 3D model is based on creating elementary geometric primitives and performing various operations between them [5]. The software package is most often used in mechanical engineering, but thanks to its wide functionality for building three-dimensional geometry, it is excellent for modeling shells of complex geometry [6]. The program supports export to .stl format.

Speaking about programs for 3D - modeling, it is necessary to mention the well-known software AutoCAD. AutoCAD, a product of Autodesk, is a universal base package containing almost all the fundamentals that are embedded in specialized packages of computer-aided design (CAD) systems of a higher level. The breadth of opportunities, the prevalence and openness of AutoCAD make it the preferred software product for the development of the technology of geometric modeling of objects. The program also supports its own programming language AutoLISP, which significantly expands the basic capabilities of AutoCAD not only in the field of automation, but also when creating geometry [7]. The program also supports export to .stl format.

SCAD Office is a software package designed for strength analysis of building structures using the finite element method, as well as their design according to existing building codes. One of the main advantages of SCAD is the ability to construct not only simple shells of revolution, but also shells of complex geometry, while the program allows you to use both analytical and parametric methods for specifying the surface [9]. However the program doesn't support export to .stl format.

COMSOL Multiphysics is a universal environment for the numerical simulation of systems, devices and processes in all areas of design, production and scientific research. The basic COMSOL Multiphysics package contains geometric modeling tools for creating geometry elements based on solids, surfaces, curves, and Boolean operations. The program has the ability to build surfaces in the parametric way of the job and supports export to .stl format.

ANSYS is a universal software system of finite element analysis (FEM) analysis, is quite popular among specialists in the field of automated engineering calculations [11]. ANSYS software products include specialized applications for the preparation of computational models, work with geometry and modeling at the system level. The program also supports the construction of surfaces using parametric equations and export to .stl format [13].

2. BUILDING A MODEL USING SCAD OFFICE

If it is necessary to get a 3D model defined by a parametric or analytical equation, then the easiest way to do this is to use the SCAD Office software package. As already mentioned, it is widely distributed in the CIS countries and, unlike other programs with the necessary functionality, has Russian localization.

The authors created five models of different types of helicoids: Torso-, Pseudo-developable, Right, Oblique, Convolute. These five types of helicoids differs due to their geometry and each of them has some specific features different from others. More information on the differences in geometry and analysis of these five types of helicoids can be found in [14, 15]. The chosen parametric equations for the models are presented in Table 1.

Table 1: Types of helicoids and their equations

Torso-helicoid	*Pseudo-developable*	*Right helicoid*	*Oblique*	*Convolute*
$x(u,v)=a\cos v-au\sin v/m$ $y(u,v)=a\sin v+au\cos v/m$ $z(u,v)=bv+bu/m$	$x(u,v)=a\cos v-u\sin v$ $y(u,v)=a\sin v+u\cos v$ $z(u,v)=cv$	$x(u,v)=u\cos v$ $y(u,v)=u\sin v$ $z(u,v)=cv$	$x(u,v)=u\cos v$ $y(u,v)=u\sin v$ $z(u,v)=cv+ku$	$x(u,v)=a\cos v-u\sin\alpha\sin v$ $y(u,v)=a\sin v+u\sin\alpha\cos v$ $z(u,v)=cv+u\cos\alpha$

Here the parameters for all helicoids are assumed to be the same, $u\in[4;12]$, $v\in[0;6\pi]$ which corresponds to the helicoid with an inner radius 4 m, outer radius 12 m and the number of turns 3. The constant coefficients taken arbitrarily, so that the difference between the visual geometry of helicoid was clearly visible.

The construction of shells by parametric equations in SCAD Office is described for the purpose of this study and there are almost no differences. Furthermore, this paper notes that the number of steps to tab a variable containing the angle of rotation of the generatrix around the axis (in this case: the variable v) is better to set as large as possible to maximize approximate resulting shape to a smooth curve. If set a large value for parameter v, then SCAD can make an error, so sometimes it is better to split the shape into several parts and build them separately, that will reduce the number of tab steps. The number of tabulation steps of another variable (u) must be set not very large, because it will increase the number of schematic nodes, negatively affect the creation of solid geometry in Autocad and increase the speed of model processing in it. When building models, the number of tabulation steps is taken as Ns = 90 (for variable v), Nt = 8 (for variable u) [17]. The created helicoids models are presented in Figure. 1.

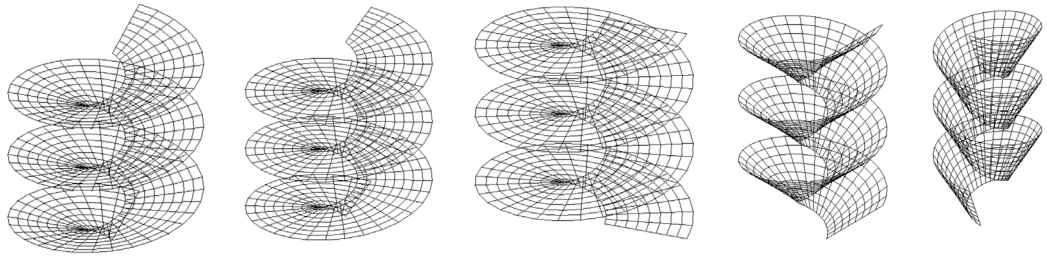

(a) (b) (c) (d) (e)

Figure. 1: The models of helicoid constructed in SCAD Office: (a) Torso-helicoid, (b) Pseudo-developable helicoid, (c) Right helicoid, (d) Oblique helicoid, (e) Convolute helicoid

SCAD Office, unfortunately, does not allow exporting models to format files .stl, so there is a need to use the intermediate step - export the model to a program that has the ability to export to .stl [18]. The easiest option for this is Autocad. To transfer the model to it, the format .dxf a universal format responsible for the exchange of information between various design systems were used [10].

3. EDITING A MODEL IN AUTOCAD AND EXPORTING TO .STL

After import, .dxf file in Autocad gets only flat geometry in the form of separate 3D-faces. Such a model, even if converted to .stl file cannot be printed on the 3D-printer. It is necessary to convert separate 3D-faces into one 3D-object (Figure. 2).

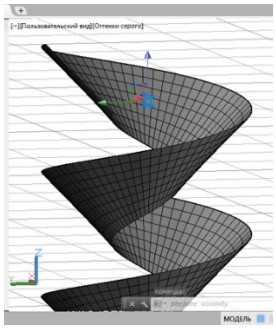

Figure. 2: Example of a model in Autocad immediately after import .DXF file.

To do this, it is necessary first to switch the workspace from “Drawing and Annotations” to “3D Modeling” using the corresponding item in the lower right menu of Autocad. After switching, special toolbars for working with 3D-geometry will appear.

Next, select all the elements of the model and use the “Convert to Surface” command in the “Solid Editing” panel. As a result, all elements are transformed from 3D faces in the surface. This action is necessary because it is impossible to get a 3D object in Autocad from elements of the “3D face” type, but from “Surfaces” it is possible.

Having selected all the elements again, the “Thickness” command in order to obtain a 3D-object by specifying a surface of a certain thickness is implemented. At this step Autocad prompts to enter a value by which the thickness of the surface will be increased. This results in multiple 3D objects of a specified thickness. To export the model to a file .stl, it is necessary to combine it into one object: using the “Body, union” command in the “Edit body” panel. Autocad asks to select the objects that to be combined. This results in one 3D object that can be exported to a .stl file. The helicoid models in Autocad obtained after the decribed operations are shown in Figure. 3 [12].

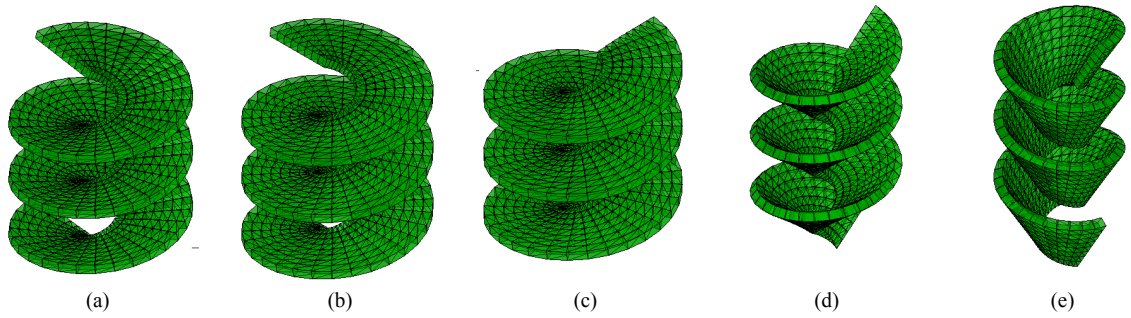

Figure. 3: The models of helicoids at Autocad after processing for export at the format .stl: (a) Torso-helicoid, (b) Pseudo-developable helicoid, (c) Right helicoid, (d) Oblique helicoid, (e) Convolute helicoid

After that, it remains only to select the “Export” command in the AutoCAD menu, in the drop-down menu – “Other formats”, then in the window that opens, select the file type “Lithography (*.stl)” and save it under the desired name [16]. When AutoCAD asks to select “bodies or tight networks” for export it is necessary to select the object and press the “Enter” button. If an error message does not appear on the command line, the export was successful. The resulting file can be opened in any program designed to print 3D-objects, and then can be printed [19]. Figure. 4 shows a preview of a 3D print on a printer of a convolute helicoid model in the MakerBot Print program [4].

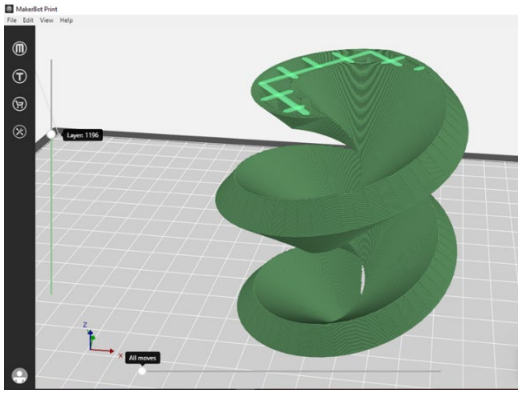

Figure. 4: Model of convolute helicoid in print preview on 3D-printer

4. BUILDING A MODEL USING SOLIDWORKS

The SolidWorks software complex is a hybrid parametric modeling system designed to design parts and assemblies in 3D space with the possibility of carrying out various types of analysis (the parametric modeling is not available for all types of figures), also allows to draw up design documentation according to the requirements of the Unified System of Design Documentation (USDD). The SolidWorks is implementing a classic process of

3D parametric design - from idea to volume model, from model to draw. The complex provides development of products of any complexity and purpose.

Different types of helicoids can also be construct in SolidWorks program by the following steps:

1. Create a circle (inside diameter), and then on Toolbar, select “Helix and Spiral”, and set the desired parameters (pitch, revolution, direction and etc.).
2. Create a plane perpendicular to the origin point and inside diameter.
3. Create a circle (outer diameter) and, if necessary, select “Taper angle”, “Taper outward”, etc. Using steps 1, 2, 3, it is possible to create a framework of helicoid.
4. To create the surface of the helicoid, click “Swept Surface”, and then create the thickness of the helicoid (button “Thicken”) [8, 20].

However in SolidWorks there is no possibility to create a helicoid by parametric equations.

Examples of the helicoids that are constructed by the steps described above are shown in Figure. 5.

(a) (b) (c) (d) (e)

Figure. 5: The models of helicoids constructed in SolidWorks: (a) Torso-helicoid, (b) Pseudo-developable helicoid, (c) Right helicoid, (d) Oblique helicoid, (e) Convolute helicoid

CONCLUSION

This article discusses two methods of 3D modeling of the helicoid for subsequent 3D-printing:

- The first method is to construct a helicoid using SCAD Office and AutoCAD programs (using parametric equations of the surfaces);
- The second method is to construct a helicoid using a SolidWorks program.

Each method has specifis features:

- The first method is more precise because each type of helicoid is constructed using its parametric equations, but more time-consuming, and requires three software (Scad Office, AutoCAD, and programm for 3D printing).
- The second method is easier because one software (SolidWorks) is used, but less precise because it is impossible to construct a helicoid according to the parametric equations. The different types of helicoid are modeled by converting a right helicoid by changing of the certain parameters (pitch, revolution, direction, taper angle, taper outward and etc.), and the final geometry of the models should be further verified.

ACKNOWLEDGEMENTS

This paper has been prepared with the support of the “RUDN University Program 5-100”.

REFERENCES

1. Šljivić, M., Pavlovic, A., Ilić, J., Stanojević, M. and Todorović, S., 2017. Comparing the Accuracy of Professional and Consumer Grade 3D printers in Complex Models Production. FME Transactions, 45(3). pp. 348-353.
2. Topçu, O., Taşcıoğlu, Y., and Ünver, H. O., 2011. A Method for Slicing CAD Models in Binary STL, Format, 6th Int. Adv.. Technol. Symp. pp. 141–148.
3. Belter, J. T. and Dollar, A. M., 2015. Strengthening of 3D printed fused deposition manufactured parts using the fill compositing technique. PLoS One, 10 (4). pp. 1-19.
4. Vlajkov, V., Desnica, E., and Palinkas, I., 2017. 3d modeling of casting tool using software package solidworks. Annals of Faculty Engineering Hunedoara – International Journal of Engineering. Tome XV.
5. Staneva, N. N., 2008. Approaches for generating 3D solid models in AutoCAD and solid works. J Eng, VI(3). pp. 28–31.
6. Busygina, G. M. and Dremova, O. V., 2015. Application of the SCAD Office software package for calculation of rod structures: educational and methodical manual for students of construction specialties. Barnaul. Russia.
7. Rynkovskaya, M. I., Elberdov, T., Sert, E. and Öchsner, A., 2020. Study of modern software capabilities for complex shell analysis. Structural Mechanics of Engineering Constructions and Buildings, T. 16. № 1. pp. 45–53. http://dx.doi.org/10.22363/1815-5235-2020-16-1-45-53.
8. Krivoshapko, S. N. and Rynkovskaya, M., Five Types of Ruled Helical Surfaces for Helical Conveyers, Support Anchors and Screws, MATEC Web Conf., 95 (2017) 06002, pp.1-5.
9. Zivanovic, S. T., Popovic, M. D., Vorkapic, N. M., Pjevic, M. D. and Slavkovic, N. R., 2020. An overview of Rapid Prototyping Technologies using Subtractive, Additive and Formative Processes. FME Transactions, 48. pp. 246-253.
10. Jean Paul, V., 2017. On the investigations of ruled helical shells in 2000-2017. Structural Mechanics of Engineering Constructions and Buildings, 3. pp. 9-11.
11. Chaudhary, D. G. and Gawali, B. W., 2018. Design and Modeling with Autodesk 3DS Max. International Journal of Computer Science and Information Security (IJCSIS), Vol. 16, No. 6, June.4 COMSOL Multiphysics Software for Optimizing Designs, 2018. https://www.comsol.ru/comsol-multiphysics?utm_ source=GT_5&utm_campaign=ru_GT_2018&utm_medium =Other&utm_content=1 [Accessed: 1st May 2020].
12. Butorina, I. V. and Vasilieva, V. N., 2018. Surface modeling in AutoCAD for architectural and structural design. IOP Conf. Ser.: Mater. Sci. Eng. 451 012125.
13. Pavlovic, A., Šljivić, M., Kraisnik, M., Ilić, J. and Anić, J., 2017. Polymers in Additive Manufacturing: The Case of a Water Pump Impeller, FME Transactions, 45(3). pp. 354-359.
14. Krivoshapko, S. N. and Ivanov, V. N. 2015. Encyclopedia of Analytical Surfaces. Springer. Moscow. Russia. p.752.
15. Karpilovskyy, V. S., Kryksunov, E. Z., Maliarenko, A.A., Perelmuter, A.V., Perelmuter, M.A. and Fialko, S.Y., 2015. SCAD Office. V. 21. System Scad++. SCAD Office Publ. Moscow. Russia.
16. Learch, J. A., Lockhart, S. and Tilleson, E., 2019. AutoCAD 2020 Instructor. SDC Publications.
17. Planchard, D., 2019. Engineering Design with SOLIDWORKS 2019. SDC Publications.
18. COMSOL Multiphysics Software for Optimizing Designs, 2018. https://www.comsol.ru/comsol-multiphysics?utm_ source=GT_5&utm_campaign=ru_GT_2018&utm_medium =Other&utm_content=1 [Accessed: 1st May 2020].
19. License, implantation, consulting - CADFEM. Program package ANSYS, 2020. https://www.cadfem.net/en/our-solutions/ansys-academic-software.html [Accessed: 1st May 2020].
20. Solidworks help, 2018. http://help.solidworks.com/2018/english/SolidWorks/sldworks/c_introduction_toplevel_topic.htm [Accessed: 1st May 2020].

moNGeometrija 2020

THE SYNTHESIS AND MOTION STUDY OF THE ASTRONOMICAL CLOCK MECHANISM

Branislav Popkonstantinović
Faculty of Mechanical Engineering, University of Belgrade, Republic of Serbia
PhD, Full-time Professor, dr.branislav.pop@gmail.com

Ratko Obradović
Faculty of Technical Sciences, University of Novi Sad, Republic of Serbia
PhD, Full-time Professor, obrad_r@uns.ac.rs

Branko Malešević
School of Electrical Engineering, University of Belgrade, Republic of Serbia
PhD, Full-time Professor, branko.malesevic@etf.bg.ac.rs

Miša Stojićević
Faculty of Mechanical Engineering, University of Belgrade, Republic of Serbia
PhD, Assistant Professor, mstojicevic@mas.bg.ac.rs

Ivana Cvetković
Faculty of Mechanical Engineering, University of Belgrade, Republi
Teaching assistant, ivanacvetkovic1992@gmail.com

Ivana Vasiljević
Faculty of Technical Sciences, University of Novi Sad, Republic of Serbia
M.Sc., Teaching Assistant, ivanav@uns.ac.rs

ABSTRACT

This paper describes and explains the synthesis of the astronomical clock mechanism on which face the mean position of the Sun, Moon, lunar nodes, zodiac circle and Moon phases and their motion during the year are displayed as seen from the Earth. The clock face represents the stereographic projection of the celestial equator, meridian celestial tropics, Zodiac circle (Ecliptic) and horizon for the latitude of Belgrade from the north celestial pole to the Equator plane. This type of projection is particularly useful for the astronomical clock faces because it is conformal and thus preserves the angles at which celestial circles cross each other. The observed motions of the Sun, Moon, lunar nodes and Zodiac circle are realized by the set of clock gear trains with the carefully and properly calculated gear ratios. Since the gear ratios are rational numbers and the angular velocities ratios of the observed celestial objects are real numbers, each gear ratio is determined as the approximation of the corresponding real one. The method of continued fraction is applied to computation of proper and practically applicable gear ratios of the clock gear trains since this calculating technique produces the best possible rational approximation of the real number. The fully operational 3D model of the astronomical clock is created and the motion study of its operation is accomplished and documented by using SolidWorks 2016 application. The simulation results are compared with the astronomical ephemeris data and the detected differences are used to inspect, evaluate and discuss the long term accuracy of the Astronomical clock operation.

This work is important for the education in the field of theory of mechanisms, 3D modelling, simulation, as well as for teaching courses in astronomy. Moreover, the exposed methods of the synthesis of mechanisms can be useful for the design, construction and reparation of the large scale city astronomical clocks.

Keywords: astronomical clock, continued fractions, mechanisms, motion study, stereographic projection

INTRODUCTION

This paper describes the synthesis of the astronomical clock mechanism and explains the design and of its dial. This astronomical clock determines and displays the mean position of the Sun, Moon, lunar nodes, zodiac circle and their motion during the year as seen from the Earth. Moreover, its mechanism calculates the phases of the Moon and demonstrates the evolution of its shape on additional screen. The content of this work is divided on several chapters. After short historical considerations of the design of some significant astronomical clocks which were installed in European cities during the past centuries, the features of the modelled astronomical clock are presented. Next chapter explains the geometrical and astronomical characteristics of the astronomical dial and discloses and visually demonstrates its design. Astronomical data important for the design of the astronomical clock mechanism and approximations of their ratios by the method of continued fractions are exposed in the succeeding chapters. The synthesis of the clock gear trains, simulation and the motion study of the clock mechanism operation are disclosed and explained in next chapters. Finally, the simulation results are analyzed and compared with the astronomical ephemeris data. The detected differences are used to inspect, evaluate and discuss the long term accuracy of the Astronomical clock operation.

2. HISTORICAL BACKGROUND

Astronomical clocks or horologia appeared in Europe as a reflection of the cultural and scientific revival during the period of Renaissance. One of the earliest known astronomical clocks is Le Gros Horloge in Rouen Le Gros-Horologe , probably one of the oldest in France which movement was made in 1389. The mechanism of this astronomical clock is very large but quite simple. It displays only the daily motion of the Sun and lunar phases. The Strasbourg astronomical clock (The astronomical clock), installed in the Cathédrale Notre-Dame of Strasbourg in 17th century, is the third on this location. The first clock had been built in the 14th century and the second one in 16th century. The current clock computes and demonstrates many astronomical data including the correct dates of Easter. The most famous astronomical clock in Europe is the Old-Town Hall clock in Prague (Czech Republic), also known as the Prague Orloj (Prague astronomical clock), built in 1410. Its most recognizable characteristic is the dial designed as stereographic projection of the Celestial sphere. Interesting enough to be mentioned is the horologium in Czech Republic as well, but in the city of Olomouc (Orloje v Olomouci). It is the rare example of a heliocentric astronomical clock. Contrary to the fact that vast majority of astronomical clock were built in the past centuries, there are some examples of modern samples. One of recently constructed (in the year of 2009) astronomical clock, installed in the municipality of Stará Bystrica (Slovenský orloj v Starej Bystrici), is the only astronomical clock in Slovakia. Similarly to face of the Prague Orloj, its display consist of an astrolabe but, unlike the Prague Olrloj, its mechanism is controlled by computer using German longwave time signal.

Figure. 1: Le Gros Horloge in Rouen, France [1]

Figure. 2: The Strasbourg astronomical clock (The astronomical clock)

Figure 3: The Prague Orloj, Czech Republic (Prague astronomical clock)

Figure 4: The clock of Stará Bystrica, Czech Republic (Slovenský orloj v Starej Bystrici)

Astronomical clock were important horological and astronomical instruments in the past centuries. Today, they represent precious historical and cultural heritage of European civilization. That is the main reason why the art of the astronomical clocks design and skills for maintenance and conservation of their mechanisms should not be forgotten.

3. FEATURES OF THE MODELLED ASTRONOMICAL CLOCK

The astronomical clock which design and motion study are presented in this paper will be capable to determine the mean position of the Sun, Moon, lunar nodes, Zodiac circle and their motions during the year as seen from the Earth. The mean locations and movements of the previously mentioned celestial objects are displayed on the astronomical clock face which represent the stereographic projection of the celestial sphere from the North celestial pole to the Equator plane. In particular, the clock face indicates the celestial equator, meridian of a place, celestial tropics (Tropic of Cancer and Tropic of Capricorn), Zodiac circle (Ecliptic), horizon and set of almucantars above the horizon, as well as the almucantars of civil, nautical and astronomical twilights for the latitude of Belgrade. Moreover, the clock mechanism determines the phases of the Moon and displays them on additional and separated screen.

Since the modelled astronomical clock indicates simultaneously the mean positions of the Sun, Moon and Zodiac circle during the year, the following data can be observed straightaway on its dial: local mean solar time, local mean sidereal time, the position of the Sun and Moon on Ecliptic (in Zodiac circle), the angular distance between Moon and Sun which determines the phase of the Moon, the altitude of the Sun, the local time of sunset, sunrise, dusk and down. The date of the winter and summer solstices, as well as the date of vernal and autumnal equinoxes can also be detected and shown on the clock dial. Besides this, the date of Lunar and Solar eclipses can also be predicted and determined sufficiently accurate because the clock mechanism indicates the position of the lunar nodes.

4. THE FACE OF THE ASTRONOMICAL CLOCK

The positions of the celestial objects on the celestial sphere are determined by angular coordinates (altitude - azimuth, declination – right ascension or ecliptic latitude and longitude.) Since the stereographic projection is conformal and thus preserves angles, it can be used for the design of the astronomical dial. The construction of the astronomical dial for the latitude of Belgrade (44.8^0) will be exposed and explained in this paper in all necessary details.

Since Celestial sphere rotates around the Celestial axis *NS*, the dial of this astronomical clock can be geometrically constructed by the stereographic projection of characteristic circles on the Celestial sphere from the Celestial pole *N* or *S* to the plane of Celestial equator *e*. From the reason that Belgrade is located on the northern hemisphere, the stereographic projection is obtained from the northern pole *N*. As is shown on Fig. 5, Zodiac circle (circle of Ecliptic) z, Celestial Tropic of Capricorn t_S, Celestial Tropic of Cancer t_N, and horizon *h* for the latitude of Belgrade are stereographically projected from the pole *N* to the plane of Celestial equator *e*. The circles of Ecliptic *z* and Celestial equator *e* intersect in two points: one of them is the First point of Aries or Cusp of Aries ♈ and the second one is the First point of Libra ♎. As usual, the astronomical dial is rimmed by the Celestial Tropic of Cancer since the Sun and the Moon, as observed from the Earth, never exceeded this circle. The Zodiac circle (the circle of Ecliptic) *z* just touches both Celestial Tropics and intersects equator *e* and horizon *h* in the same pair of points – ♈ and ♎

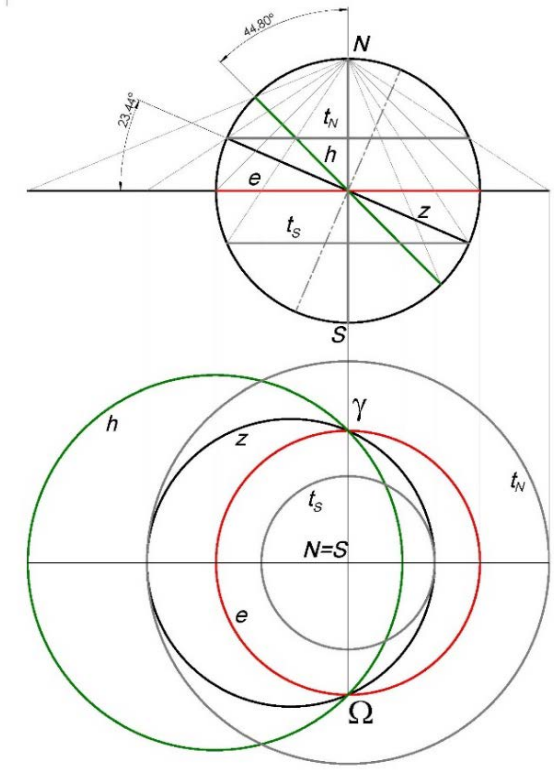

Figure 5: The stereographic projection of the Celestial sphere

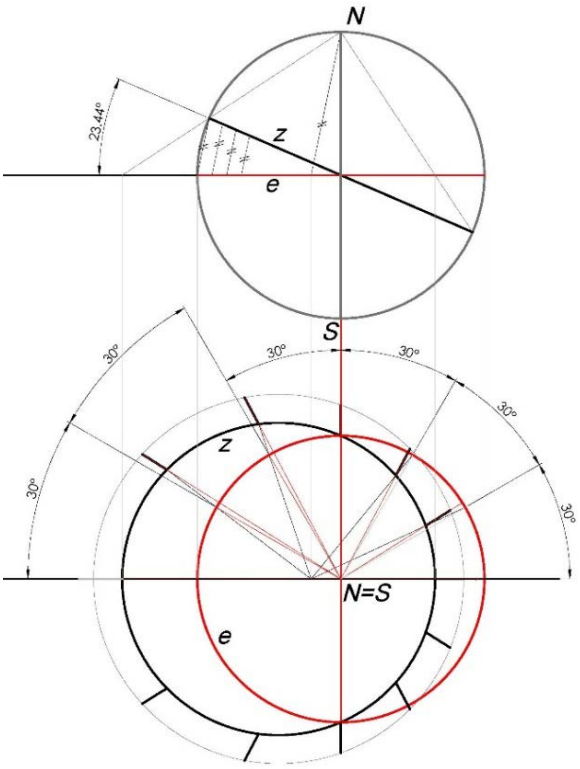

Figure 6: The stereographic projection of the Zodiac and its division on 12 equal segments

Due to the fact that the position of the Sun and the Moon are determined on this astronomical dial by the ecliptic longitude, the representation of the Ecliptic circle (Zodiac) is crucially inevitable part of its face. Thus the Zodiac circle must be geometrically constructed as well. The stereographic projections of the Zodiac circle and its division on 12 equal segments from the pole *N* to the plane of Celestial Equator are given on Fig. 6. The Zodiac circle is stereographically divided on 12 equal segments each of which is 30 degrees of Ecliptic longitude wide. These segments are named after well-known astrological signs: Aries, Taurus, Gemini, Cancer, Leo, Virgo, Libra, Scorpio, Sagittarius, Capricorn, Aquarius, and Pisces. All segments are equally graduated with 6 divisions of 5 degrees each. It is important to emphasize what can be easily seen on the Zodiac circle that stereographic projection of these divisions are unevenly distributed, since the stereographic projection is not affine but central.

On Fig.7, the model of the astronomical dial created by the SolidWorks application is shown. The Sun 4 and the Moon 16 symbols (icons) are attached on clock hands which rotates around the clock axis 13. The Zodiac (Ecliptic) circle 14 also rotates around the axis 13 and supports the Sun and the Moon icons by the two circular grooves. By the position of the Sun pointer, the local mean solar time can be ridden on the 24 numeral division placed at the edge of the Celestial tropic of Cancer 3. By the position of the arrow mark 2 (♈) at the Zodiac 14, the local mean sidereal time can also be determined on the same division 3 or on the Equator circle 8 scale. Ring 12 is the Celestial tropic of Capricorn and represents the inner border of the dial. The position of the Sun 4 on the Ecliptic circle 14 discloses the current date of the year. The apparent angular distance between Sun 4 and Moon 16 hands determines the Moon phase. This angular distance can be ridden out directly in days on the tiny ring 17

attached to the Sun pointer. The Moon phases can also be seen more pictorial and vivid on separate display equipped with rotational sphere 9 which is painted half white and half dark blue. The astronomical dial has the projection of the local horizon 6 and five almucantars 5 on angular distance of 12^0. The daytime period 1 and astronomical night 10 are indicated by the position of the Sun icon above and below the horizon respectively.

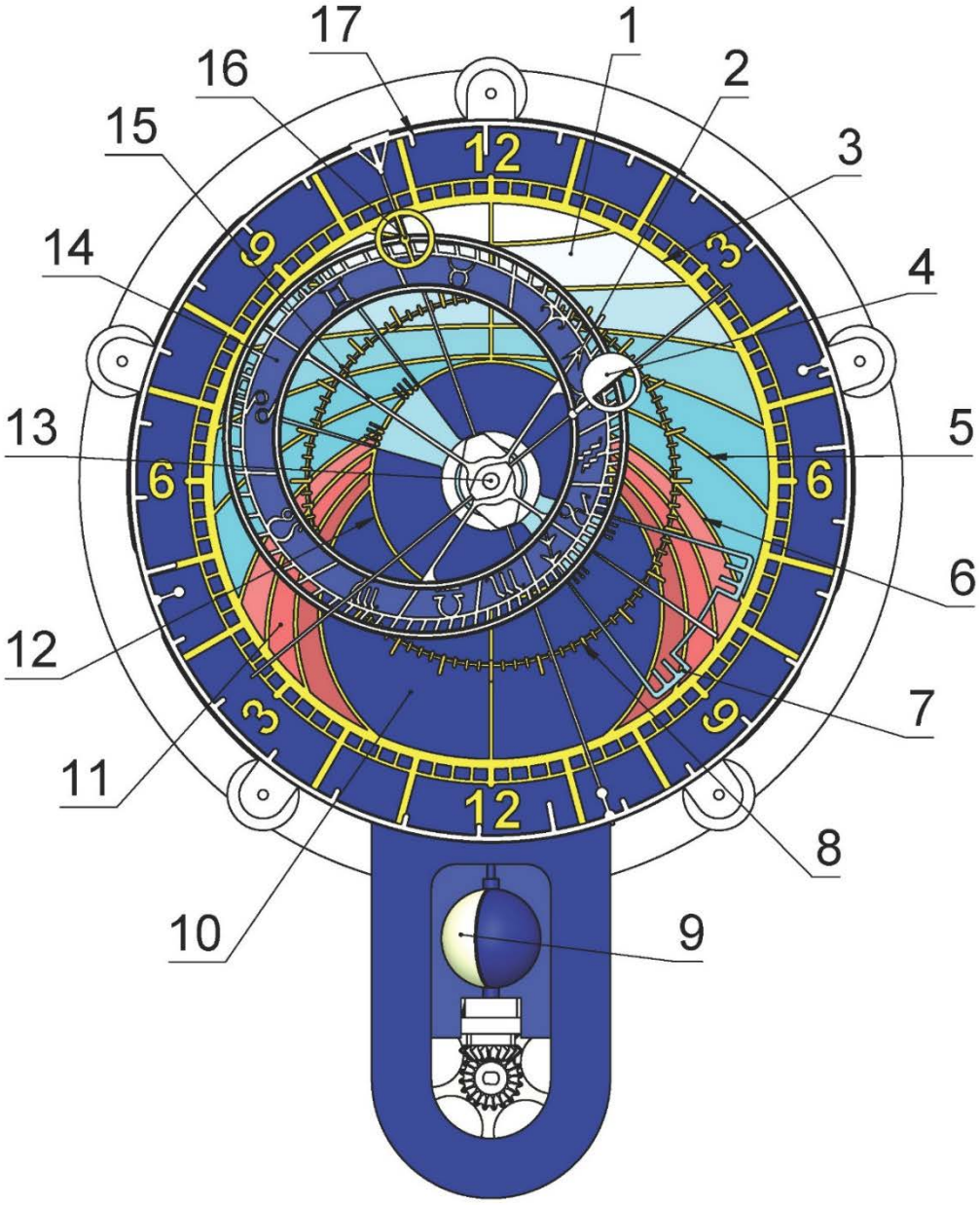

Figure 7: The model of the astronomical dial

The altitude of the Sun can be determined approximately correct by the aforementioned almucantars. The Sun icon positioned on the horizon determines the time of sunrise or sunset. Three almucantars 11 are also displayed below the horizon, on angular distance of 6^0, which illustrate the periods of civil, nautical and astronomical twilights 11. The interval between sunset and dusk is determined on the right side of the dial, while the interval between dawn and sunrise on its left side. The astronomical dial is equipped with the lunar nodes pointer 15 and corresponding circular sectors 7 which play an important role in prediction of lunar and solar eclipses. The meaning of these sector will be explained in the next chapter dedicated to the astronomical data necessary for the proper construction of the astronomical clock mechanism.

4. THE ASTRONOMICAL DATA

It is evident that all the intended features of the astronomical clock disclosed and explained in chapter 2, can be obtained not just by the proper construction of the dial, but also by the correct design of the clock mechanism. The synthesis of the astronomical clock mechanism is based on certain well-known astronomical facts and numerical data. The ratio between these data will be interpreted and realized by the clock mechanism gear ratios. Therefore, all astronomical data which are necessary for the design of the clock mechanism must be carefully considered and properly selected.

First, the Earth rotates around its axis which is currently tilted 23.444 degrees from its orbital axis (Reingold M. et all, 2018). From the viewpoint on the Earth, the Sun rotates from the east to the west with the period known as a solar day which mean length is 24 hours. The apparent path of the Sun during the year, as seen from the Earth, passes through the Zodiac which is divided into 12 signs and form the ecliptic coordinate system. The Sun's position at vernal equinox is the origin of ecliptic longitude. From an observer on the Earth, the Zodiac rotates daily to the west with the period known as sidereal day which mean length, determined for the year 2019, is 23 hours 56 minutes 4.09053 seconds or 23.934469592 seconds (Astronomical Almanac, 2018).

The period of Moon's orbit respecting the line which connects the Earth and the Sun, or the period of lunar phases is called Synodic month. This period varies during the time but its mean value calculated for long period of time is extremely stabile. Currently, the average duration of the synodic month is $T_{Ph} = 29.530589$ days (Reingold M. et all, 2018), (Reijs V) and is decreasing in mean length by about 3.6 10-7 solar days per century (Reingold M. et all, 2018) or by about 0.311 seconds per millennium.

Since the astronomical clock displays the daily motion of the Moon, it must be calculated the average period of the Earth rotation relatively to the Moon or tidal lunar day. From the fact that angular distance between Sun and Moon determines the lunar phase, the mean value of the tidal lunar day can be find out from the equation (Eq.1):

$$T_L = 24\left(\frac{1}{T_S} - \frac{1}{T_{Ph}}\right)^{-1} = 24\left(1 - \frac{1}{29.530588}\right)^{-1} = 24.8412024\ hours \qquad \text{(Eq.1)}$$

The orbit of the Moon is inclined to the ecliptic and crosses the ecliptic in two lunar nodes: the ascending node and the descending node (Eclipses and the Moon's Orbit). The lunar nodes revolve slowly around the ecliptic (Eclipses and the Moon's Orbit) in the direction opposite to the direction of the Earth's revolution. The period of lunar node cycle determined for the year 2019 is $T_N = 18.612952$ years (Reijs V). The mean interval of time between two successive conjunctions of the Sun with the same lunar node is called the eclipse year and lasts $T_E = 346.620067$ days (Reijs V). It is a little bit shorter than the solar year because the directions of nodal precession and Earth's revolution are opposite. Lunar nodes play an important role for an explanation of phenomena called lunar and solar eclipses. From the viewpoint of an observer on the Earth, a solar eclipse can occur only when the Moon and the Sun are both near the same node, and a lunar eclipse can only happen when the Sun and the Moon are close to an opposite lunar nodes. If the angle between the line of nodes and the Moon or the Sun is less than 9°30' a lunar eclipse must occur, while if it greater than 12°15' a lunar eclipse is not possible (lunar eclipse limit). If the above-mentioned angle is less than 15°23' a solar eclipse must happen, while if it is more than 18°35' a solar eclipse cannot occur (solar eclipse limit) (Lunar and solar eclipses).

All astronomical data important for the synthesis of the astronomical clock mechanism are given in Table 1.

Table 1: The parameters defined for different tests

Astronomical data	Duration
Solar day	$T_S = 24$ hours
Sidereal day	$T_{SID} = 23.934469592$ hours
Synodic month	$T_{Ph} = 29.530588$ days
Lunar tidal day	$T_M = 24.8412024$ hours
Lunar nodal cycle	$T_N = 18.612952$ years
Eclipse year	$T_E = 346.620067$ days

6 APPROXIMATIONS OF ASTRONOMICAL DATA

It is important to emphasize that astronomical clock which design is exposed in this work determines and displays geocentrically not apparent or true but the mean position of the Sun, Moon, lunar nodes, zodiac circle and their motion during the year. All irregularities of the Sun, Moon and lunar nodes celestial motions are neglected for this mechanical model. Otherwise speaking, it is presumed that the observed movements of aforementioned objects across the celestial sphere are circular and uniform. These uniform circular motions are realized by a set of clock gear trains with meticulously calculated gear ratios.

Since the number of gear teeth is an integer, the gear ratios must be approximated by rational numbers. The proper gear ratios of the mechanism gear trains are determined by the method of continued fractions since this calculation technique was mathematically proven (Khinchin Y. A, 1964) to produce the best possible rational approximation of a real number (Малешевић Б.: , 1998). But, for this objective, the method of continued fractions is not sufficient. Since the diameter of the gear cannot be arbitrarily large nor gear modulus arbitrarily small, the number of gear teeth is always limited by the clock dimensions and by the method of gears production. Thus, it is necessary to introduce an additional criterion which will determine the practically acceptable rational approximation obtained by the method of continued fractions. Basically, this precautions can be formulated as a limitation of gear teeth number, and depends on gear production technology, gear modulus and dimensions of the clock. In this case, we are planning to produce gears by ABS filament 3D printing and since the clock face dimeter is approximately 400 mm large, the gear diameter should not be greater than 150 mm and modulus not less than 1 mm.

Briefly, the previous consideration can be summarized as follow:

1. The proper gear ratio of the particular gear train must be determined by the method of continued fractions. This method generates the set of convergents or semi-convergents of the continued fraction representation of the real ratio (Малешевић Б.: , 1998), (Malešević B. , 2014).
2. The error of the chosen rational approximation should be sufficiently small.
3. The rational approximation should be selected in such a way that prime factors of their enumerators and denominators are less than 150.

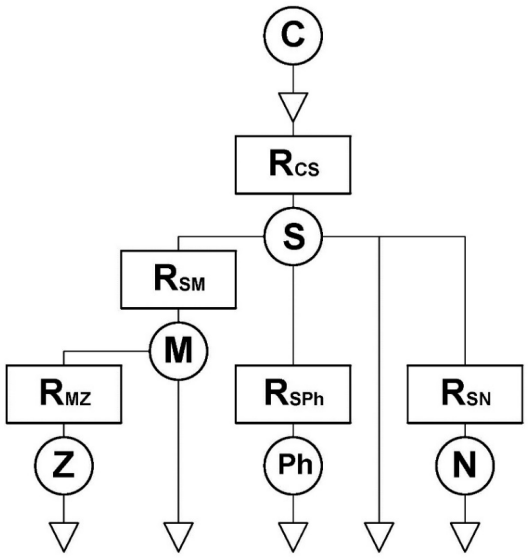

Figure 8: The operational scheme of the astronomical clock mechanism

The operational scheme of the astronomical clock mechanism which consists of a set of gear trains is given on Fig. 8. On this figure, *C* is the input hour shaft of the ordinary clock, *S* is the Sun, *M* - Moon, *Z* – Zodiac, *Ph* – lunar phases and *N* represents lunar nodes. On the same figure, $R_{CS} = 2{:}\,1$ is the ratio between angular velocities of the clock hour shaft and the astronomical clock Sun pointer. R_{SM} is the ration between angular velocities of the Sun and the Moon pointers, R_{MZ} – the Moon and the Zodiac, R_{SPh} – the Sun and the lunar phases and R_{SN} is the

ratio between angular velocities of the Sun and the lunar nodes pointers on the same astronomical dial. These ratios will be approximated by the set continued fractions convergents and semi-convergents and the prime factors of their enumerators and denominators will be determined. To demonstrate this calculations more concise, not all convergents and semi-convergents will be presented, but only the range from the first to one which is accepted as sufficiently correct approximation.

The set of best rational approximations of the ratio R_{SPh} =29.530589 is given in Table 2.

Table 2: The best rational approximations of the ratio R_{SPh}

Type	*Approximation*	*Type*	*Approximation*
C	$29/1$	*SC*	$384/13 = 2^7 \cdot 3/13$
C	$30/1 = (2 \cdot 3 \cdot 5)/1$	*C*	$443/15 = 443/(3 \cdot 5)$
C	$59/2$	*C*	$502/17 = 2 \cdot 251/17$
SC	$266/9 = 2 \cdot 7 \cdot 19/3^2$	*SC*	$945/32 = (3^3 \cdot 5 \cdot 7)/2^5$
SC	$325/11 = (5^2 \cdot 13)/11$	*C*	$1447/49 = 1447/7^2$

The semi-convergent $945/32$ is chosen to approximate the ratio $R_{SPh} = 29.530589$. The error of this approximation is 0.000662 days per lunation or less than 12 minutes per year.

The ratio R_{SM} between angular velocities of the Sun and the Moon clock pointers is determined by the equation (Eq.2):

$$R_{SM} = \frac{T_L}{T_S} = \frac{24.8412024}{24} = 1.0350501 \qquad \text{(Eq.2)}$$

The set of best rational approximations of the ratio R_{SM} is given in Table 3.

Table 3: The best rational approximations of the ratio R_{SM}

Type	*Approximation*	*Type*	*Approximation*
C	$1/1$	C	$30/29 = (2 \cdot 3 \cdot 5)/(2^2 \cdot 7)$
SC	$16/15 = 2^4/(3 \cdot 5)$	C	$59/57 = 59/(3 \cdot 19)$
SC	$17/16 = 17/2^4$	SC	$266/257 = (2 \cdot 7 \cdot 19)/257$
SC	$18/17 = (2 \cdot 3^2)/17$	SC	$325/314 = (5^2 \cdot 13)/(2 \cdot 157)$
SC	… … …	SC	$384/371 = (2^7 \cdot 3)/(7 \cdot 53)$
SC	$27/26 = 3^3/(2 \cdot 13)$	C	$443/428 = 443/(2^2 \cdot 107)$
SC	$28/27 = (2^2 \cdot 7)/3^3$	C	$502/485 = (2 \cdot 251)/(5 \cdot 97)$
C	$29/28 = 29/(2^2 \cdot 7)$	SC	$945/913 = (3^3 \cdot 5 \cdot 7)/(11 \cdot 83)$

The semi-convergent $945/913$ is selected as the approximation of the ratio R_{SM}. The absolute value of the error of this approximation is calculated from the expression (Eq.3)

$$\left|24 \cdot \frac{945}{913} - 24.8412024\right| = 1.949 \cdot 10^{-5}\ hours \approx 0.07\ seconds \qquad \text{(Eq.3)}$$

This error denotes that the mean position of the Moon will be determined by the clock mechanism with the error of approximately 0.07 seconds per day or within 30 seconds per year.

Regarding operational scheme of the astronomical clock mechanism given on Fig. 6, the ratio R_{MZ} between angular velocities of the Moon and the Zodiac pointers is calculated by the following expression (Eq.4):

$$R_{MZ} = \frac{T_{SID}}{T_S} \cdot {R_{SM}}^{-1} = \frac{23.934469592}{24} \cdot \frac{913}{945} = 0.963499592 \quad \text{(Eq.4)}$$

The set of convergents and semi-convergents by which the ratio R_{MZ} is approximately determined is given in Table 4.

Table 4: The best rational approximations of the ratio R_{MZ}

Type	*Approximation*	*Type*	*Approximation*
C	$0/1$	SC	$1003/1041 = (17\cdot59)/(3\cdot347)$
C	$1/1$	SC	$1135/1178 = (5\cdot227)/(2\cdot19\cdot31)$
SC	$13/14 = 13/(2\cdot7)$	SC	$1267/1315 = (7\cdot181)/(5\cdot263)$
SC	$14/15 = (2\cdot7)/(3\cdot5)$	SC	$1399/1452 = 1399/(2^2\cdot3\cdot11^2)$
SC	… … …	SC	$1531/1589 = 1531/(7\cdot227)$
SC	$24/25 = 2^3\cdot3/5^2$	C	$1663/1729 = 1663/(7\cdot13\cdot19)$
SC	$25/26 = 5^2/(2\cdot13)$	C	$1795/1863 = (5\cdot359)/(3^4\cdot23)$
C	$26/27 = (2\cdot13)/3^2$	C	$3458/3589 = (2\cdot7\cdot13\cdot19)/(37\cdot97)$
C	$53/55 = 53/(5\cdot11)$	SC	$15627/16219 = (3\cdot5209)/(7^2\cdot331)$
C	$79/82 = 79/(2\cdot41)$	SC	$19085/19808 = (5\cdot11\cdot347)/(2^5\cdot619)$
C	$132/137 = (2^23\cdot11)/137$	SC	$22543/23395 = 22543/(5\cdot4679)$
SC	$871/904 = (13\cdot67)/(2^3\cdot113)$	C	$26001/26986 = (3^5\cdot107)/(2\cdot103\cdot131)$

The convergent $26001/26986$is selected as the approximation of the ratio R_{MZ}. Since the ratio between this convergent and the semi-convergent $913/945$ produces the rational approximation $\bar{T}_{SID}$ of the sidereal day by the following expression (Eq.5)

$$\bar{T}_{SID} = 24 \cdot \frac{26001/26986}{913/945} = 23.93446961\ hours, \quad \text{(Eq.5)}$$

the absolute value of the error obtained by this approximation can be calculated from the expression (Eq.6).

$$|\bar{T}_{SID} - 23.934469592| = 2\cdot10^{-8}\ hours = 7.2\cdot10^{-5}\ seconds \quad \text{(Eq.6)}$$

This value means that the clock mechanism determines the mean sidereal day with the error of approximately $7.2\cdot10^{-5}$ seconds per day or within 0.03 seconds per year.

In accordance to the operational scheme of the clock mechanism, astronomical data given in Table 1 and the fact that lunar nodal cycle is k=18.612952 times longer than a year, the ratio R_{SN} between angular velocities of the Sun and the lunar nodes pointers can be determined by the expression (Eq.7).

$$R_{SN} = \left[\frac{T_S}{T_{SID}} + \left(\frac{T_S - T_{SID}}{T_{SID}}\right) \cdot \frac{1}{k}\right]^{-1} = 0.997123293 \quad \text{(Eq.7)}$$

The best rational approximations of the ratio $R_{SN} = 0.997123293$ are given in Table 5. The convergent $2773/2781$ is chosen as the best applicable approximation of the ratio R_{SN}. Since the difference between angular velocities of the Sun and lunar nodes pointers represents the approximation of the lunar nodes angular velocity relative to the Sun, next equation (Eq.8) determines the approximation of the Eclipse year $\bar{T}_E$.

$$\bar{T}_E = \left(\frac{2781}{1773} - T_S\right)^{-1} = \left(\frac{2781}{1773} - 1\right)^{-1} = 346.6250162\ days \qquad (\text{Eq.8})$$

Thus, the mechanism of the astronomical clock approximates the Eclipse year with the error which absolute value is determined by the expression (Eq.9).

$$|\bar{T}_E - T_E| = |346.6250162 - 346.620067\ | = 0.0049492\ days \approx 7.13\ minutes \qquad (\text{Eq.9})$$

Table 4: The best rational approximations of the ratio R_{SN}

Type	Approximation	Type	Approximation
C	$0/1$	C	$346/347 = (2{\cdot}173)/347$
C	$1/1$	C	$347/348 = 347/(2^2{\cdot}3{\cdot}29)$
SC	$173/174 = 173/(2{\cdot}3{\cdot}29)$	C	$693/695 = (3^2{\cdot}7{\cdot}11)/(5{\cdot}139)$
SC	$174/175$	C	$1040/1043 = (2^4{\cdot}5{\cdot}13)/(7{\cdot}149)$
SC	… … …	C	$1733/1738 = 1733/(2{\cdot}11{\cdot}79)$
SC	$345/346 = (3{\cdot}5{\cdot}23)/(2{\cdot}173)$	C	$2773/2781 = (47{\cdot}59)/(3^3{\cdot}103)$

The reciprocal value of the ratio $(T_S - T_{SID})/T_{SID}$ which appears in equation (Eq.7) determines the duration of the Solar or Tropical year. Consequently, the clock mechanism produces the approximation of the mean Tropical year $T_T = 365.242189$ days (Reingold M. et all, 2018) with the error which absolute value can be determined by the equation (Eq.10)

$$\left| T_T - \frac{\bar{T}_{SID}}{T_S - \bar{T}_{SID}} \right| = |365.242189 - 365.2422884\ | = 9.94{\cdot}10^{-5} days \approx 8.6\ seconds \qquad (\text{Eq.10})$$

After all calculations and evaluations exposed in this chapter, it can be concluded that rational approximations of real ratios R_{MZ}, R_{SPh}, R_{MZ},R_{SN} are not perfect, but sufficiently good and practically applicable for the synthesis of the astronomical clock mechanism. The next chapter is dedicated to this task.

7. THE CLOCK GEAR TRAINS

In accordance with exposed astronomical data and their approximated ratios the design of the astronomical clock mechanism is realized and a fully operational 3D model of this mechanical device is created by using the Solid Works 2016 application.

As is shown on Fig.6, the mechanism of the clock consist of five gear trains. Each gear train has its specific speed ratio determined in previous chapter by the method of continued fractions as the best rational and practically applicable approximation of the real ratios. The prime factors of the enumerator and denominator of these approximated ratios are also calculated and the proper gear modulus and teeth numbers are determined. These ratios, gear teeth numbers and gear modulus are given in Table 5. It must be emphasized again the problem of selecting the best but practically applicable convergents or semi-convergents of the continued fractions approximation for the construction of the clock gears. Obviously, the higher terms of this rational approximation produces the smaller error. But, the higher terms have larger enumerator and denominator and, very often, their prime factors are also extremely huge. Since these prime factors have to be realized directly and precisely by the gear teeth numbers, extremely high terms of continued fraction approximations are not practical and useful. At the other hand, the lover terms of rational approximation are usable, but produces larger errors. Thus, the problem of selecting the best but practically applicable convergents or semi-convergents of the continued fractions approximation must be solved as compromise between two opposite demands.

The mechanism of the astronomical clock has four coaxial shafts which hold the lunar nodes, the Sun, the Zodiac and the Moon pointers. Also, the clock mechanism is equipped with one separated shaft which controls the rotation of the sphere, painted half white and half dark blue and displays the lunar phase. As is already emphasized and shown on operational scheme of the clock mechanism on Fig.6, shafts are mutually connected by five previously

mentioned gear trains. The clock mechanism has two five-pointed frames which support the astronomical face, all shafts and gear trains as one functional block.

Table 5: The rational approximations of the gear train ratios of the clock mechanism

	Approximated ratio	*Approximated ratio indicated by the gear teeth numbers*	*Modulus [mm]*
R_{CS}	$\frac{2}{1}$	$\frac{40}{60}\cdot\frac{60}{80}$	2
R_{SPh}	$\frac{945}{32}=\frac{3^3\cdot5\cdot7}{2^5}$	$\frac{50}{20}\cdot\frac{50}{20}\cdot\frac{45}{20}\cdot\frac{42}{20}$	2
R_{SM}	$\frac{945}{913}=\frac{3^3\cdot5\cdot7}{11\cdot83}$	$\frac{70}{83}\cdot\frac{81}{66}$	1.5 – 70, 83 scaled up – 81, 66
R_{MZ}	$\frac{26001}{26986}=\frac{3^5\cdot107}{2\cdot103\cdot131}$	$\frac{60}{131}\cdot\frac{81}{103}\cdot\frac{90}{60}\cdot\frac{107}{60}$	1
R_{SN}	$\frac{2773}{2781}=\frac{47\cdot59}{3^3\cdot103}$	$\frac{59\cdot94}{103\cdot54}$	1.5 - 59, 103 scaled up – 94, 54

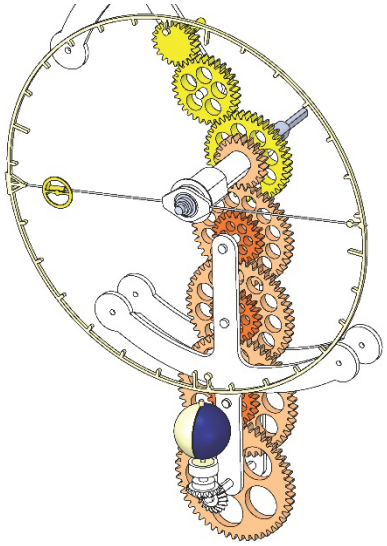

Figure 9: The Sun and the lunar phase gear trains

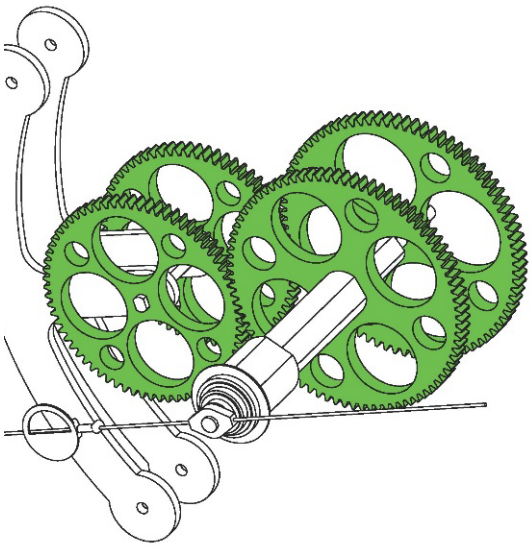

Figure 10: The Moon gear train

The gear trains which control the motion of the Sun pointer and lunar phase's spherical display are shown on Fig.9 and the related gear numbers are given in Table 5. The gear modulus for both trains are 2 mm. The Sun gear train consists of three gears, first of which is connected to the hour shaft of the ordinary clock. This shaft holds the Sun pointer equipped with the small gold-plated symbol of the Sun. The hour shaft of this clock drives all gear trains of the astronomical clock. The lunar phase train have four pairs of gears and takes the power from the Sun shaft. The last shaft of the lunar phase's gear train is connected to the small spherical pointer which displays the current Moon phase.

The Moon gear train is shown on Fig.10. It consist of two pairs of gears, first of which have modulus 2 mm and the modulus of the second pair is scaled up in such a way that the shafts of the first and the last gear are coaxial. The first gear of the Moon gear train is driven by the Sun shaft and the last gear drives the Moon pointer equipped with the small silver-plated symbol of the Moon. The teeth numbers for each gear in the Moon gear train are given in Table 5. The support for this train is connected to the main pair of the astronomical clock five-pointed frames.

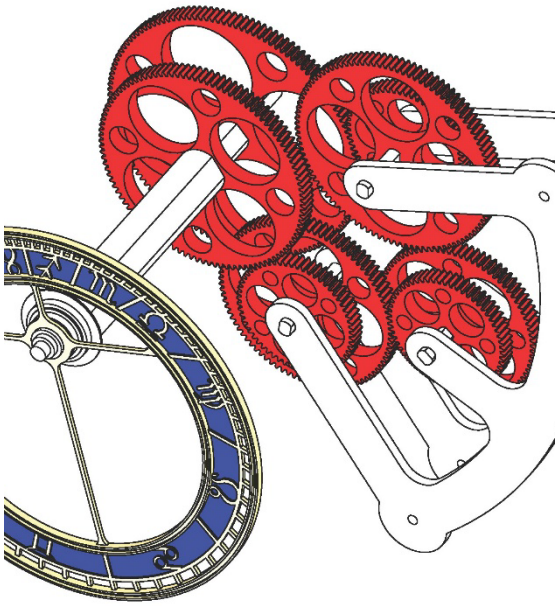

Figure 11: The Zodiac gear train

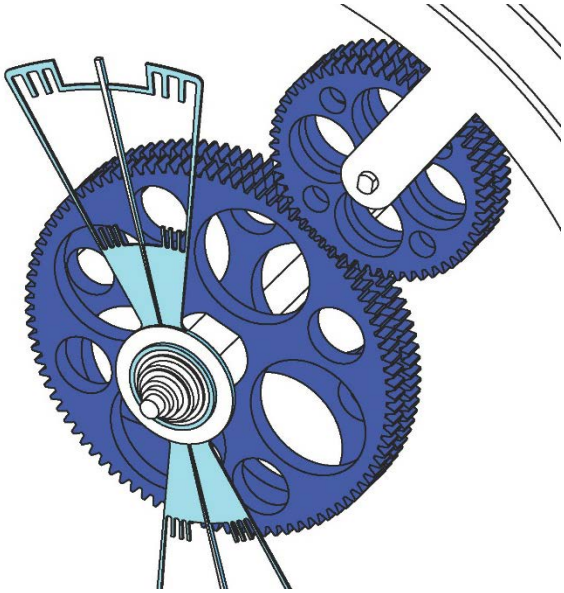

Figure 12: The lunar nodes gear train

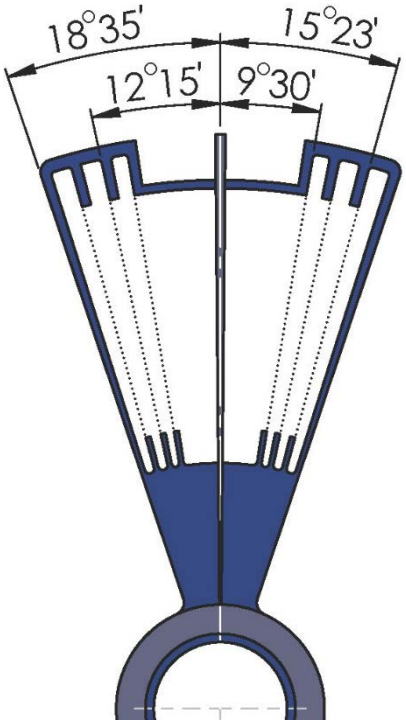

Figure 13: The lunar node and eclipse sector

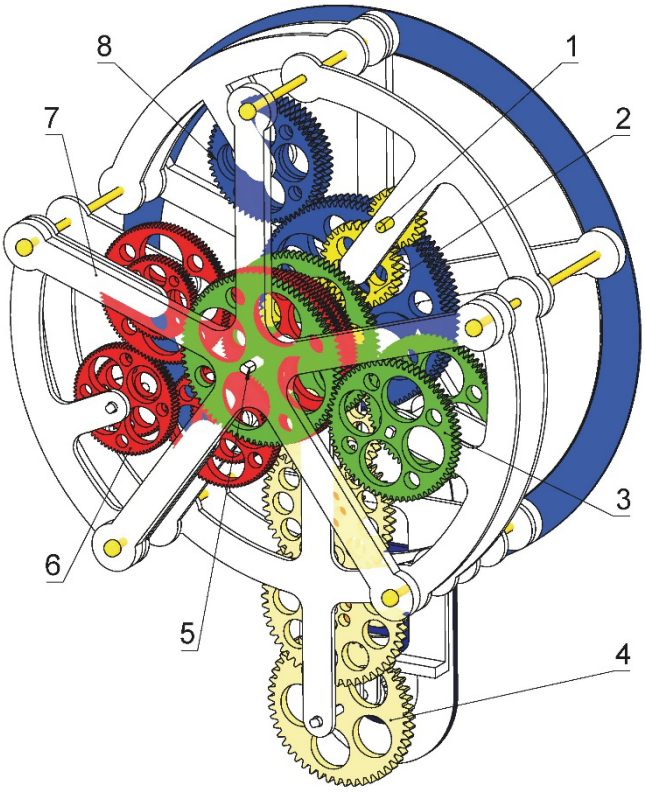

Figure 14: The clock face during the motion study

The Zodiac gear train is shown on Fig 11. It consist of four pairs of gears which modulus is 1 mm. The teeth numbers for each gear of this gear train are also given in Table 5. The first gear of the Zodiac train is driven by the Moon shaft and the last gear drives the Zodiac shaft on which the Zodiac circle is attached. As is previously mentioned, the Zodiac circle is divided on twelve equal segments which are equally graduated with 6 divisions of 5 degrees each. It measures the Ecliptic longitudes of the Sun, Moon and lunar nodes.

Table 6: Differences between ephemeris astronomical data and data generated by the motion study of the astronomical clock mechanism

Date	A-*Eph*	A-*S*	ΔA	K-*Eph*	K-*S*	ΔK	N -*Eph*	N -*S*	ΔN
18.5	♌ 27.52	♌27.52	0	♍ 5.13	♍ 5.13	0	♎ 0.93	♎ 0.93	0
19.5	♌ 28.48	♌ 28.51	+0.03	♍ 17.00	♍ 18.31	+1.31	♎ 0.88	♎ 0.88	0
20.5	♌ 29.44	♌ 29.49	+0.05	♍ 28.92	♌ 1.48	+2.56	♎ 0.83	♎ 0.83	0
21.5	♎ 0.41	♌ 0.48	+0.07	♌ 10.92	♌ 14.66	+3.74	♎ 0.77	♎ 0.77	0
22.5	♎ 1.37	♌ 1.46	+0.09	♌ 23.07	♌ 27.83	+4.76	♎ 0.72	♎ 0.72	0
23.5	♎ 2.33	♌ 2.45	+0.12	♎ 5.35	♎ 11.01	+5.66	♎ 0.67	♎ 0.67	0
24.5	♎ 3.29	♌ 3.44	+0.15	♎ 17.80	♎ 24.19	+6.39	♎ 0.62	♎ 0.62	0
25.5	♎ 4.25	♎ 4.42	+0.17	♏ 0.45	♏ 7.36	+6.91	♎ 0.57	♎ 0.56	+0.01
26.5	♎ 5.22	♎ 5.41	+0.19	♏ 13.30	♏ 20.54	+7.24	♎ 0.50	♎ 0.51	+0.01
27.5	♎ 6.18	♎ 6.39	+0.21	♏ 26.38	♐ 3.71	+7.33	♎ 0.45	♎ 0.46	+0.01
28.5	♎ 7.14	♎ 7.38	+0.24	♐ 9.72	♐ 16.89	+7.17	♎ 0.40	♎ 0.40	0
29.5	♎8.09	♎ 8.37	+0.28	♐ 23.30	♑ 0.06	+6.76	♎ 0.35	♎ 0.35	0
30.5	♎ 9,05	♎ 9.35	+0.30	♑ 7.15	♑ 13.24	+6.09	♎ 0.30	♎ 0.30	0
31.5	♎ 10.01	♎ 10.34	+0.33	♑ 21.27	♑ 26.41	+5.14	♎ 0.25	♎ 0.24	-0.01
1.6	♎ 10.97	♎ 11.32	+0.35	♒ 5.63	♒ 9.59	+3.96	♎ 0.18	♎ 0.19	+0.01
2.6	♎ 11.93	♎ 12.30	+0.37	♒ 20.18	♒ 22.77	+2.59	♎ 0.13	♎ 0.14	+0.01
3.6	♎ 12.89	♎ 13.29	+0.40	♓ 4.83	♓ 5.95	+1.12	♎ 0.08	♎ 0.08	0
4.6	♎ 13.84	♎ 14.28	+0.44	♓ 19.50	♓ 19.17	-0.33	♎ 0.03	♎ 0.03	0
5.6	♎ 14.82	♎ 15.27	+0.45	♈ 4.07	♈ 2.30	-1.77	♎ 29.98	♎ 29.98	0
6.6	♎ 15.76	♎ 16.24	+0.48	♈ 18.42	♈ 15.48	-2.94	♎ 29.93	♎ 29.93	0
7.6	♎ 16.72	♎ 17.24	+0.52	♑2.47	♈ 28.65	-3.82	♎ 29.87	♎ 29.87	0
8.6	♎ 17.67	♎ 18.22	+0.55	♑16.18	♑11.83	-4.35	♎ 29.82	♎ 29.82	0
9.6	♎ 18.63	♎ 19.21	+0.58	♑29.50	♑25.00	-4.5	♎ 29.77	♎ 29.77	0
10.6	♎ 19.58	♎ 20.19	+0.61	♒ 12.47	♒ 8.18	-4.29	♎ 29.72	♎ 29.71	-0.01
11.6	♎ 20.54	♎ 21.18	+0.64	♒ 25.08	♒21.36	-3.72	♎ 29.67	♎ 29.67	0
12.6	♎ 21.49	♎ 22.16	+0.67	♓ 7.40	♓ 4.53	-2.87	♎ 29.60	♎ 29.61	+0.01
13.6	♎ 22.01	♎ 23.15	+1.14	♓ 19.50	♓ 17.71	-0.79	♎ 29.55	♎ 29.55	0
14.6	♎ 23.41	♎ 24.14	+0.73	♈ 1.47	♈ 0.89	-0.58	♎ 29.50	♎ 29.50	0
15.6	♎ 24.36	♎ 25.12	+0.76	♈ 13.35	♈ 14.06	+0.71	♎ 29.45	♎ 29.45	0
16.6	♎ 25.32	♎ 26.11	+0.79	♈ 25.23	♈ 27.24	+2.01	♎ 29.40	♎ 29.40	0
17.6	♎ 26.27	♎ 27.01	+0.74	♉ 7.18	♉ 10.41	+3.23	♎ 29.35	♎ 29.34	+0.01
18.6	♎ 27.23	♎ 28.08	+0.85	♉ 19.28	♉ 23.59	+4.31	♎ 29.28	♎ 29.29	+0.01
19.6	♎ 28.18	♎ 29.06	+0.88	♎ 1.55	♎ 6.77	+5.22	♎ 29.23	♎ 29.24	+0.01
20.6	♎ 29.14	♏ 0.05	+0.91	♎ 14.03	♎ 19.94	+5.91	♎ 29.18	♎ 29.18	0
21.6	♏ 0.09	♏ 1.04	+0.95	♎ 26.77	♏ 3.12	+6.35	♎ 29.13	♎ 29.13	0
22.6	♏ 1.05	♏ 2.02	+0.97	♏ 9.75	♏ 16.29	+6.54	♎ 29.08	♎ 29.08	0
23.6	♏ 2.00	♏ 3.00	+1.00	♏ 22.98	♏ 29.47	+6.49	♎ 29.03	♎ 29.03	0
24.6	♏ 2.95	♏ 3.99	+1.04	♐ 6.45	♐ 12.65	+6.20	♎ 28.97	♎ 28.97	0
25.6	♏ 3.91	♏ 4.98	+1.07	♐ 20.13	♐ 25.82	+5.69	♎ 28.92	♎ 28.92	0
26.6	♏ 4.86	♏ 5.96	+1.10	♑ 4.02	♑ 9.00	+4.98	♎ 28.87	♎ 28.87	0
27.6	♏ 5.82	♏ 6.95	+1.13	♑ 18.05	♑ 22.17	+4.12	♎ 28.82	♎ 28.82	0
28.6	♏ 6.77	♏ 7.93	+1.16	♒ 2.20	♒ 5.35	+3.15	♎ 28.77	♎ 28.76	-0.01
29.6	♏ 7.72	♏ 8.92	+1.20	♒ 16.43	♒ 18.53	+2.10	♎ 28.70	♎ 28.71	+0.01
30.6.	♏ 8.68	♏ 9.91	+1.23	♓ 0.72	♓ 1.70	+0.98	♎ 28.65	♎ 28.66	+0.01

The lunar nodes gear train is shown on Fig. 12. It consists of two pairs of gears, first of which have modulus 1.5 mm and the modulus of the second pair is scaled up in such a way that the shafts of the first and the last gear are coaxial. As is done for the others gears, the teeth numbers of the lunar nodes gear train are given in Table 5. The first gear of the lunar nodes train is driven by the Sun shaft and the last gear drives the lunar nodes pointer, shown in Fig. 13. This pointer is equipped with two circular sectors which have ±9°30' ±12°15' ±15°23' and ±18°35' marks the meaning of which has been explained earlier. The angular span of this circular sector corresponds to a certain interval of time called the eclipse season during which the condition for the occurrence of a solar or lunar eclipses are satisfied.

The Fig.14 exposes the complete assembly of the astronomical clock mechanism with the disposition of all gears. On this figure, 1 is the input shaft driven by the hour arbour of the ordinary clock, 2 - the Sun gear train, 3 – the Moon gear train, 4 – the lunar phase train, 5 – the main shaft of the astronomical clock, 6 – the Zodiac gear train, 7- the clock five-pointed frame and 8 - the lunar nodes train.

8. THE MOTION STUDY OF THE CLOCK MECHANISM

For the correct operation of the Astronomical clock mechanism, the initial positions of the Sun, the Moon, Zodiac, lunar phase and the lunar nodes pointers must be chosen first. The best way to accomplish this task is to adjust the pointers positions for the datum in which the Moon is located in its orbital perigee or apogee. This decision is reasonable since the modelled clock mechanism determines exclusively the mean motions and positions of the aforementioned astronomical objects and the true and mean position of the Moon in its orbital apogee or perigee is approximately the same. The Moon is in apogee on 18 May 2020 (Lunar perigee and apogee calculator) and this datum has been chosen for the Astronomical clock set up. The ecliptic longitudes for The Sun, Moon and lunar node ☊ are taken from Ephemeris tables for 2020 (Ephemeris tables for the year 2020) which are calculated for each day at Greenwich Mean Midnight. On 18 May 2020 at midnight 00:00 UT, the ecliptic longitude of the Sun is ☌ 27.52^0, of the Moon ☽ 5.13^0**,** and the mean longitude of the lunar node ☊ is ♋ 0.93^0. If the clock is located in Belgrade, latitude 20^0 28', it is necessary to calculate the local mean solar time for this place. This is done by the following calculation (Gronbeck C):

$$LSoT = LST + 4'(LL - LSTM) + ET = 1 + 4'(20.467 - 15) + 0 = 1{:}21{:}52 \qquad \text{(Eq.11)}$$

In equation (Eq.11), *LSoT* is the local solar time, *LST* the local standard time, *LL* the local longitude, *LSTM* the local standard time meridian, measured in degrees, which runs through the center of each time zone and *ET* is the equation of time. Neglecting *ET*, the local solar time becomes local mean solar time. In accordance to these data, the initial positions of the Sun, the Moon, Zodiac, and the lunar nodes pointers are adjusted on the astronomical clock face. The correct lunar phase is determined by the angular distance between Sun and Moon pointers.

After the clock has been adjusted, the motion study of its mechanism is accomplished by the use of the Solid Works 2016 application and the accuracy of its predictions is demonstrated, documented and inspected. The simulation of the mechanism operation has been performed continuously for 44 days, from 18 May to 30 June 2020 and the differences between ephemeris astronomical data and data generated by the motion study of the astronomical clock mechanism are disclosed in Table 6. Columns ☌-*Eph,* ☽-*Eph* and ☊ *–Eph* collect ecliptic longitude for the Sun, Moon and lunar node respectively taken from Ephemeris data. Columns ☌-*S,* ☽-*S* and ☊-*S* gather the corresponding ecliptic longitudes obtained by the clock mechanism motion study and columns Δ☌, Δ☽ and Δ☊ collect the the differences between them.

First, as is shown in Table 6, through the duration of 44 days, the differences for the Sun longitudes between ephemeris data and data obtained by the motion study of the clock mechanism operation gradually grow from 0^0 to $+1.23^0$. This divergence occurs because the clock mechanism neglects the equation of time and tracks only the mean motion of the Sun. This error inducts the difference between the true and the mean local time. Second, during the 44 days, the differences for the Moon longitudes between ephemeris data and data obtained by the simulation have positive and negative signs and their absolute values are larger than those calculated for the Sun. This errors are expected since the orbit and the motion of the Moon have many irregularities and the Moon gear train of the clock mechanism displays only its uniform motion and determines its mean positions. Moreover, since the clock is adjusted for the datum in which the Moon is located in its orbital apogee, the Moon mean positions obtained by the simulation "oscillates" around the correct positons on both sides, between -4.36^0 and $+7.35^0$. Third, the mean longitudes of the lunar node ☊ determined by the mechanism motion study are identical to those given in Ephemeris tables. This means that lunar nodes gear train generates good approximation for the mean precession of the lunar nodes.

During the June 2020, two significant and interesting astronomical events occur, first of which is the lunar and the second one is the solar eclipse. The eclipse of the Moon is penumbral and takes place on 5-6 June 2020 (Penumbral Lunar Eclipse) and the solar eclipse is annular and occurs on 21 June 2020 (Annular Solar Eclipse). Since equipped with the lunar nodes pointer, the astronomical clock exposed in this work is capable to predict these events acceptably accurate. In Belgrade, the lunar eclipse begins on 5 June at 19:45:51 CET, reaches its maximum at 21:24:55 CET and ends at 23:04:03 CET. The Astronomical clock predict the beginning of the lunar eclipse on 5 June 2020 at approximately 16:42 when the Moon pointer enters the eclipse sector and, the maximum at 23:16 when the Moon pointer overlaps the Sun pointer inside the eclipse sector as is shown on Fig.15. (The clock says local mean solar time for Belgrade.) The end of the eclipse cannot be determined by the positions of the Sun, Moon and lunar node pointers of the clock. The error of the clock prediction is visible but it is not too large. In Belgrade, the annular solar eclipse reaches maximum on 21 June 2020 at 8:40:04 CET and, as is shown on Fig.16, the astronomical clock predict that this maximum will occur on 20 June 2020 at 17:58 when the Moon icon overlaps the Sun icon, inside the eclipse sector and almost overlaps the nodal pointer. The error is quite large, more than 12 hours ahead, but it is expected since the error range for the Moon longitude is also large (-4.36^0, $+7.35^0$). The predictions of the lunar and solar eclipses with similar values of error are obtained by the entirely different mechanical device described and explained in paper (Popkonstantinović B. et al, 2018).

Figure 15: Full moon and penumbral lunar eclipse 5-6 June 2020

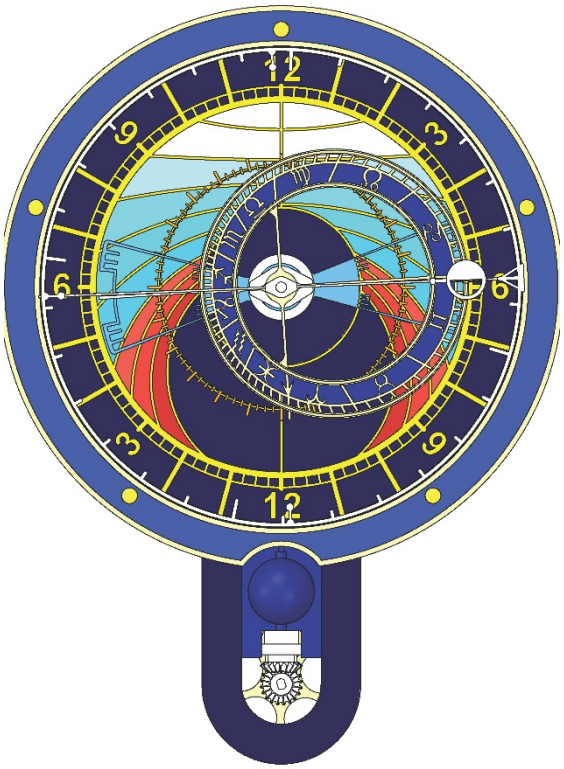

Figure 16: New Moon and annular solar eclipse 21 June 2020

7. FINAL REMARKS AND CONCLUSION

This work discloses the design of the Astronomical clock which displays the mean position of the Sun, Moon, lunar nodes, Zodiac circle and their motions during the year geocentrically. Since the mean periods of these motions are approximated by the method of continued fractions and realized by the set of gear trains with great accuracy, the clock mechanism determines the mean positions of aforementioned astronomical object correctly. Nevertheless, the accuracy of the presented Astronomical clock can be improved by the more advanced and delicate mechanism which will consider non-uniform motions of the Moon and the Earth. For this purpose, the paper (Addomine M. et al, 2018) is of great interest, since it discloses the kinematical structure of Dondi's astronomical clock, which gear trains are equipped with the non-circular gears, for tracking the motion of the Moon and the planet Mercury. Author of this paper have already examined and prepared several epicyclical mechanisms which take into account the equation of time as well as the first and the second lunar anomalies. By

the use of these mechanical devices the novel astronomical clock will be capable to simulate and display apparent motions of the Earth and the Moon more accurately.

This paper can be important mostly for the education in the field of mathematics, geometry, theory of mechanisms, 3D modelling, motion study, as well as for teaching courses in astronomy. Moreover, the exposed methods of the clock mechanism synthesis can be useful for the design, maintenance and conservation of the large scale city astronomical clocks since these clocks represent precious historical and cultural heritage of European civilization.

ACKNOWLEDGMENTS

This research is supported by the Ministry of Science and Education of the Republic of Serbia, Grant No. III 44006.

REFERENCES

1. Addomine M., Figliolini G., Pennestri E.: A Landmark in the History of Non-Circular Gears Design: The Mechanical Masterpiece of Dondi's Astrarium, Mechanism and Machine Theory, Elsevier, April 2018, DOI: 10.1016/j.mechmachtheory.2017.12.027
2. Astronomical Almanac for the Year 2019, Dept. of the Navy; Annual edition (January 4, 2018),
3. Ephemeris tables for the year 2020, https://www.astro.com/swisseph/ae/2000/ae_2020.pdf
4. Gronbeck C., Time Basis, https://susdesign.com/popups/sunangle/time-basis.php
5. Khinchin Y. A. Continued fractions, University of Chicago, USA, 1964
6. Le Gros-Horologe http://www.rouen-histoire.com/GHorloge/
7. Lunar perigee and apogee calculator: https://www.fourmilab.ch/earthview/pacalc.html
8. Малешевић Б.: Рационалне апроксимације реалних бројева и неке примене, Настава математике, XLIII, 3, 1998., стр. 20–31
9. Malešević B., Milinković L., Simpozijum MATEMATIKA I PRIMENE, Matematički fakultet, Univerzitet u Beogradu, 2014, Vol. V(1)
10. NASA - Eclipses and the Moon's Orbit. https://eclipse.gsfc.nasa.gov/SEhelp/moonorbit.html
11. Orloje v Olomouci http://www.orloj.eu/cs/olomouc.htm
12. Popkonstantinović B., Miladinović Lj., Obradović R., Jeli Z., Stojićević M., The Eclipses Abacus, the mechanical predictor of the solar and lunar eclipses, SAGE journals, Simulation, 2018, https://journals.sagepub.com/doi/abs/10.1177/0037549718798040?journalCode=simb
13. Prague astronomical clock https://www.amazingczechia.com/sights/prague-astronomical-clock-orloj/
14. Reijs V, Mean lunar and solar periods http://www.iol.ie/~geniet/eng/moonfluct.htm
15. Reijs V. Lunar and solar eclipses, http://www.archaeocosmology.org/eng/eclipse.htm
16. Reingold M. E, Dershowitz N, Calendrical Calculations: The Ultimate Edition, Cambridge University Press; 4 edition (April 27, 2018)
17. Slovenský orloj v Starej Bystrici http://www.orloj.sk/index.php/slovensky-orloj
18. The astronomical clock https://www.visitstrasbourg.fr/en/things-to-see-and-do/visiting/places-to-visit/other-places-to-visit/f223007613_the-astronomical-clock-strasbourg/
19. Time and date AS: 21 June 2020 Annular Solar Eclipse, https://www.timeanddate.com/eclipse/solar/2020-june-21
20. Time and date AS: 5-6 June 2020 Penumbral Lunar Eclipse, https://www.timeanddate.com/eclipse/lunar/2020-june-5

DESIGN OF AN ACCURACY EVALUATION SYSTEM FOR SURFACE FLATTENING METHODS

Peng-Fei Zheng
Department of Mechanical and Power Engineering, East China University of Science and Technology, China,
Department of Mechanical and Information, Yiwu Industrial & Commercial College, China
Associate Professor, pfzheng@126.com

Jing-Jing Lou
Department of Mechanical and Information, Yiwu Industrial & Commercial College, China
Associate Professor

Da-Jun Lin
Department of Mechanical and Power Engineering, East China University of Science and Technology, China,
Full Professor

Qi An
Department of Mechanical and Power Engineering, East China University of Science and Technology, China,
Full Professor

ABSTRACT

Based on the analysis of the existing methods for estimating the surface flattening error, they can be roughly classified into two types of estimation methods: the relative area error analysis method and the relative length error analysis method. The advantages and disadvantages of these methods are summarized in the paper. Combining the general surface flattening methods and sheet metal stamping forming process, a more reasonable, scientific and comprehensive evaluation system for the accuracy of surface flattening is proposed. In line with the unfolding characteristics of the grid surface, the relative average area error of triangles is used instead of the traditional area error estimation method. The accumulated length error is replaced by the relative length error of each triangle in the estimation method, and the value of the change in the orientation (direction, position) relationship between the triangles is increased to assess the deformation error of the surface flattening method. The mass attributes of the patch are introduced. The minimum displacement energy method is used to supplement the evaluation of surface flattening accuracy. Finally, a comprehensive evaluation system is established and proposed, which takes into account the accuracy of local and global surface flattening.

Keywords: *surface flattening; triangle; area error; length error; deformation error; evaluation system*

INTRODUCTION

The problem of surface expansion is often involved in the field of mechanical manufacturing, especially approximate expansion of non-deployable surfaces. The approximate expansion of non-deployable surfaces is an important technology in the aerospace, shipbuilding, and chemical equipment industries. Scholars at home and abroad have conducted extensive research for this purpose and proposed various methods and techniques for surface flattening [1-5], such as the finite element method, the geometric approximation method [6], the mechanical model method [8-9], the energy equation method [11-12], the 3D software method [7], the triangle mesh method [10,13], etc. Among them, the energy model method is utilised to triangulate a surface, using triangle points as particles and triangle edges as springs, to construct an energy equation, to calculate the binding force of the particles, and optimally unfold surface patches in the form of energy release.

Although the analysis of the surface development error is mentioned in these surface flattening algorithms, the accuracy analysis of surface development has not been introduced as a research focus. Based on the research of the free-form surface flattening algorithm of multi-point forming plate parts, Zhang [14] theoretically analysed the reasons that caused the free-form surface expansion error. Mao [15] established a comprehensive error analysis mathematical model based on different emphases on various error requirements, and designed an error analysis system for free-form surface approximate flattening. A new Isogeometric Analysis (IGA) beam element was developed by integrating the displacement field of the element, which was approximated by the NURBS basis, with the internal work formula of Euler-Bernoulli beam theory with the small deformation and elastic assumptions. An effective alternative to standard Finite Element Analysis for shape error analysis of functional surface was proposed [16]. However, most of these studies only describe the accuracy of surface development as an evaluation of the effectiveness of the surface flattening algorithm. For the evaluation of the development accuracy of non-developable surfaces, the effectiveness of a flattening method is evaluated by indicators such as the area change rate and the edge length change rate. However, the currently widely used evaluation methods of the area change rate and the edge length change rate have some limitations, and cannot comprehensively reflect the accuracy of surface development. Therefore, based on the geometric changes of the graphics involved in the process of surface flattening, an evaluation system for the accuracy of surface flattening is designed and established in this paper. Additionally, the errors of surface development accuracy from the shape and position changes of the graphic geometry are comprehensively measured.

1. THE SURFACE FLATTENING DEFORMATION

In the process of surface flattening, subdivision and development are commonly used in the form of 3D mesh surfaces. The area of the triangle in the 3D mesh surface and the area of the flattened triangle will be different. Similarly, the length of the edge of the 3D mesh triangle will change before and after unfolding. These are the two most obvious deformation indicators, and hence this indicator is often used as an evaluation basis for measuring the accuracy of development in general surface flattening algorithms.

1.1. Primitive position change

Being the smallest graphic unit, points are often called primitives. Almost all complex graphics can be composed from or expressed by points. Two points can form a line, three points can form a plane, and countless free points can form a complex surface or body. Taking the common triangular surface in the calculation of surface expansion as an example, it involves many primitive deformations. As shown in Figure 1, $\triangle p_1 p_2 p_3$ is connected by points p_1, p_2, p_3; when the position of the primitive p_1, p_2, p_3 changes, it causes the deformation of the triangle. Since $\overline{p_{1'}p_{3'}} < \overline{p_1 p_3}$, $\overline{p_{1'}p_{2'}} < \overline{p_1 p_2}$, $\overline{p_{2'}p_{3'}} < \overline{p_2 p_3}$, and $s_{\triangle p_{1'}p_{2'}p_{3'}} < s_{\triangle p_1 p_2 p_3}$, and the centroid positions of the two triangles change accordingly. This kind of deformation, caused by the change of the position of the primitive, is obvious, and its deformation can also be measured by the change of the edge length and the area.

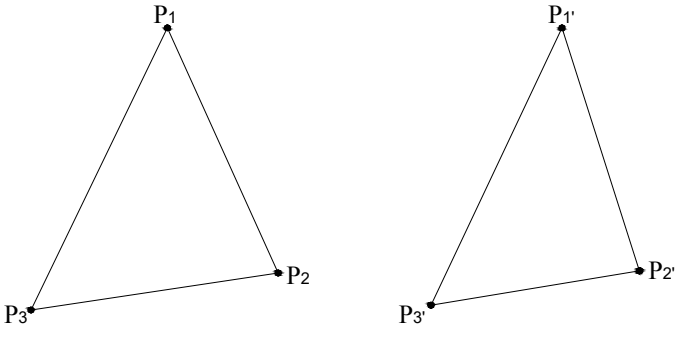

Figure 1: Primitive deformation (dominant deformation) in triangles:
(a) the triangle before deformation, (b) the triangle after deformation.

1.2. Graphic deformation

Generally speaking, changing the position of the primitive will cause the deformation of the graphics. Still, sometimes the relative position between the primitives does not change, but it can cause another hidden deformation of the graphics. Since this kind of recessive deformation cannot be judged or measured by the commonly used indicators such as the change in edge length and area, it is called recessive deformation in this paper. As shown in Figure 2, there are two right-angled triangles $\triangle abc$,$\triangle def$, where $ab = ef, bc = ed, ac = df$. It can be seen that when $\triangle abc$ changes to $\triangle def$ after a certain transformation, the edge length and area of the two triangles do not change. Does this form of primitive change belong to the category of deformation? The obvious answer is yes. Clearly, $\triangle abc$ and $\triangle def$ are not the same graphic, the shapes of the two are very different, as well as their centroid positions. Therefore, the triangle has substantially deformed during this change.

The above is the analysis of the deformation of a single primitive (a point or a triangle). When multiple primitives form a graphic, its deformation meaning will be further enriched and extended. As shown in Fig. 3, two triangles $\triangle s_1 s_2 s_3$ and $\triangle s_1 s_3 s_4$ intersecting in space have an angle of α, and they are flattened to a plane to obtain an expanded view of $\triangle p_1 p_2 p_3$ and $\triangle p_1 p_3 p_4$. Because the triangular sheet flattening process is an equal area expansion, the length and area of each edge of the triangular sheet do not change before and after the expansion. However, the relative positional relationship of the two triangles has changed. The change in the positional relationship has a huge impact on the flattening result of the surface, and sometimes even exceeds the damage brought about by the deformation of a single element, which, in turn, causes the surface development to fail.

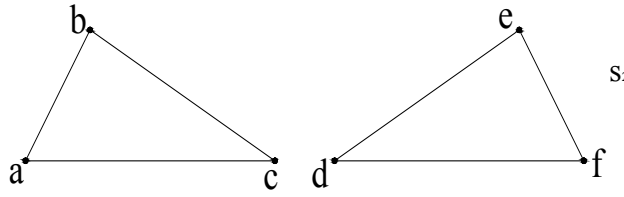

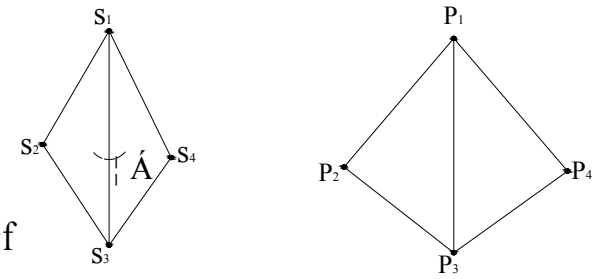

Figure 2: Recessive deformation of triangles **Figure** 3 Expanded deformation between triangles

2. ESTABLISHMENT OF AN EVALUATION SYSTEM FOR SURFACE FLATTENING ACCURACY

In order to evaluate the accuracy of surface development more comprehensively and scientifically and to measure the effectiveness and practicability of a surface flattening algorithm, this chapter will introduce in detail four technical indicators that affect the accuracy of surface development. It will also use these indicators to establish the corresponding evaluation model of the surface development accuracy system, enrich the evaluation method of surface development accuracy, and provide some help to further optimize the improvement of a surface flattening algorithm.

2.1. Relative edge length error index (single object evaluation)

Since free-form surfaces are often theoretically non-developable, the flattened view will inevitably be deformed. For the evaluation of the development accuracy of non-developable surfaces, the relative edge length change rate is often used to evaluate the surface development accuracy. In the process of surface flattening, the triangular mesh model is frequently used for expansion. The length of the edge of triangles in a three-dimensional mesh surface undergoes a change before and after the expansion, which results in some edges being stretched and some others being squeezed to get shortened. This deformation is caused by the change in the position of the primitives, which is a local deformation of a single object. This edge length variable can be calculated by equation (1).

$$e_l = \sum_{i=1}^{n} \left| l_i - l_i^p \right| \Big/ \sum_{i=1}^{n} l_i \qquad (1)$$

where e_l is called the average value of the relative edge length error of the surface; l_i is the actual edge length of the 3D mesh triangle; l_i^p is the flattened edge length of the triangle, and n is the number of triangle grid edges.

2.2. Relative area error index (single object evaluation)

During the development of the surface, due to the deformation force, the triangles will deform correspondingly, and cause their area to change. This is also the evaluation point that many surface flattening algorithms focus on. The effectiveness of the algorithm is directly evaluated by the area change of the entire surface before and after the expansion, or the deformation change of the entire surface is calculated by calculating the area change of each triangle. Therefore, the relative area error index is also an indispensable index in the evaluation system of the accuracy of surface development. The deformation can be calculated by equation (2):

$$e_s = \sum_{i=1}^{n} \left| s_i - s_i^p \right| \Big/ \sum_{i=1}^{n} s_i \qquad (2)$$

where e_s is the average value of the relative area error of the surface; s_i is the actual area of the 3D mesh triangle; s_i^p is the area of the flattened triangle; and n is the number of triangles.

2.3. Relative displacement error index

Flattening the space surface to a plane is the process of flattening the subdivided triangular meshes to a plane one by one. The deformation of a single triangle has been included in the evaluation system of the accuracy of the surface expansion in the above process. However, due to the local deformation of a single triangle, the interaction between the triangles will occur, and this local deformation is caused by the adjacent relationship between the triangles. Propagation affects the deformation of adjacent triangles and even the entire mesh surface. As shown in Fig. 4, according to a certain surface flattening method, the space curved piece is flattened. It can be seen that the relative positional relationship between the spatial triangle m、n and the flattened triangular piece m'、n' has changed. The relative displacement between such triangles has also been changed. Such changes are common in the process of surface flattening. They are one of the causes of surface development errors. In order to introduce such a relative displacement error between triangles into the evaluation system of surface development accuracy, as well as to globally evaluate the accuracy of surface development, it is necessary to find a constant reference point for the quantitative calculation of relative displacement. During the surface development process, a single triangle will change, and the position of the primitive will also move with it. However, a reference point or a starting point for stepwise flattening will be generally chosen for surface development, so this reference point is the most suitable reference point. As shown in Fig. 4, the relative displacement offset of the centroid of the triangular plate before and after the development is calculated using the development reference point bp as a base point. The specific computation method can be counted by using formula (3):

$$e_d = \sum_{i=1}^{n} \left| d_i - d_i^p \right| \Big/ \sum_{i=1}^{n} d_i \qquad (3)$$

where e_d is the average relative displacement error of the surface; d_i is the distance between the centroid of a triangle in a three-dimensional grid and the unfolding reference point; d_i^p is the distance between the centroid of the plane triangle corresponding to the flattened space triangle and the unfolded reference point; and n is the number of triangles.

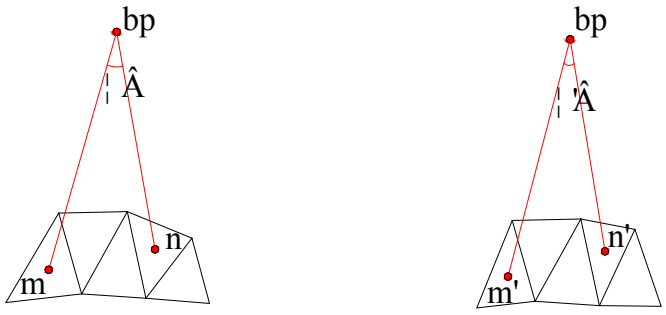

(a) (b)

Figure 4: Relative orientation deformation of triangle: (a) the graph before flattening, the directional angle between triangle m and n is β , (b) the graph after flattening, the directional angle between triangle m' and n' is β' .

2.4. Relative direction error index

Since the relative area error (e_s) and the relative edge length error (e_l) are only used to evaluate the development accuracy of a single triangle, they are, in fact, two local accuracy evaluation indicators, and cannot fully measure the development accuracy of a flattening method. Therefore, this article introduces a more accurate evaluation index, the relative angle change rate. Before and after the surface has been unfolded, the relative orientation between the triangles changes accordingly, and that is why e_s and e_l cannot reflect this change. Still, the change in the orientation between triangles has a huge impact on the overall development result. The flattening graphic is determined by the positional relationship between the triangles.

In order to reflect the change of this relative positional relationship, the development surface is taken as a whole, and the reference point of the development is used as a reference. The change in the relative angle between the centroid of the triangle and the development reference point (β as shown in Figure 4) is evaluated, unfolding accuracy. The relative direction error (e_a) can be calculated by formula (4), so that the local and global comprehensive evaluation of the unfolding graph can be realized:

$$e_a = \sum_{i=1}^{n} \left| ang_i - ang_i^p \right| \Big/ \sum_{i=1}^{n} ang_i \qquad (4)$$

where e_a is the average relative direction error of the surface; ang_i is the connection angle between the centroid of the three-dimensional grid triangle and the unfolding reference point; ang_i^p is the connection angle between the centroid of the flattened triangle and the unfolded reference point; and n is the number of triangles.

In order to further evaluate the accuracy of surface development, the quality attributes of patches are introduced, and the accuracy of surface development is supplemented by the minimum displacement energy of triangular patches. During the flattening process of the surface, all patches are finally located on the same plane, so the change of the displacement energy in the z direction can be ignored, and only the displacement energy in the x and y directions should be considered. The specific calculation method is shown in formula (5):

$$e_g = \sum_{i=1}^{n} \left| g(x,y)_i - g(x,y)_i^p \right| \cdot v_x \cdot v_y \Big/ \sum_{i=1}^{n} g(x,y)_i \qquad (5)$$

where e_g is the average relative displacement energy of the surface; $g(x,y)_i$ is the displacement energy at the centroid of a triangle in a three-dimensional grid (x , y direction); $g(x,y)_i^p$ is the flattening displacement energy at the centre of the triangle; v_x, v_y are unit vectors in the x and y direction, n is the number of triangles.

3. QUANTITATIVE DESIGN OF AN EVALUATION INDEX OF SURFACE DEVELOPMENT ACCURACY

In order to further quantify the evaluation index of surface development accuracy, a scientific, reasonable and comprehensive evaluation model of surface development accuracy has been constructed, and the surface development accuracy is quantified by expression (6):

$$e_{flattening} = k_1 \cdot e_l + k_2 \cdot e_s + k_3 \cdot e_d + k_4 \cdot e_a + k_5 \cdot e_g \,, \quad k_1 + k_2 + k_3 + k_4 + k_5 = 1 \qquad (6)$$

where $e_{flattening}$ is the comprehensive evaluation value of surface development accuracy; k_1 is the relative edge length error weight value of the surface; k_2 is the surface relative area error weight value; k_3 is the surface relative displacement error weight value; k_4 is the surface relative direction error weight value; and k_5 is the surface relative displacement energy weight value.

According to formula (6), the error of surface development can be calculated and the effect of surface development can be evaluated, but different values of the weight coefficients k_1, k_2, k_3, k_4, k_5 will directly affect the comprehensive evaluation value of surface development accuracy, and thus affect reasonable judgment. Therefore, further selection of the reasonable weight coefficient value through surface expansion experiments is needed. This makes the evaluation system more instructive and improves its practical value.

As shown in Fig. 5, a partial spherical surface has been used for the flattening test, and, according to different weight coefficients, the unfolding accuracy values of the same model surface have been calculated. After plenty of tests and comparisons (some test results are listed in Table 1), a more appropriate weight reference value has finally been selected: $k_1 = 0.25$, $k_2 = 0.25$, $k_3 = 0.20$, $k_4 = 0.20$, $k_5 = 0.10$.

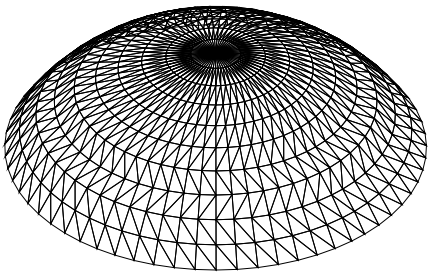

(a)

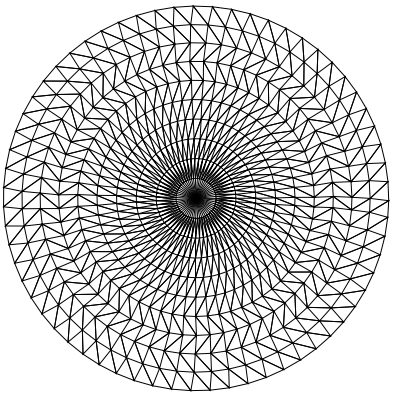

(b)

Figure 5: Flattening of a partial sphere: (a) a mesh of partial-sphere, and (b) the flattening result of (a).

Table 1: The related parameters determination experiment

Model	K_1	K_2	K_3	K_4	K_5	$e_{flattening}$
Partial-sphere	*0.30*	*0.35*	*0.15*	*0.10*	*0.10*	*0.01087344*
Partial-sphere	*0.30*	*0.30*	*0.20*	*0.10*	*0.10*	*0.01123564*
Partial-sphere	*0.25*	*0.30*	*0.25*	*0.10*	*0.10*	*0.01824917*
Partial-sphere	*0.35*	*0.35*	*0.10*	*0.10*	*0.10*	*0.00617236*
Partial-sphere	*0.30*	*0.25*	*0.25*	*0.10*	*0.10*	*0.00712849*
Partial-sphere	*0.25*	*0.25*	*0.20*	*0.20*	*0.10*	*0.00302347*
Partial-sphere	*0.20*	*0.20*	*0.20*	*0.20*	*0.20*	*0.02346912*
Partial-sphere	*0.25*	*0.25*	*0.15*	*0.15*	*0.20*	*0.01136527*

4. CONCLUSION

This paper has analysed the existing evaluation methods of surface development error, the deformation nature of the primitives and the graphics from the entire surface development process. It has studied the causes of a single deformation and deformation transmission from the perspective of local deformation and global deformation. A comprehensive evaluation system for the accuracy of surface development has been proposed, using five indicators, which include the relative edge length error index, the relative area error index, the relative displacement error index, and the relative direction error index. The reference values of the relevant weight coefficients are provided as parts of flattening experiments. The surface development accuracy evaluation system proposed in this paper not only overcomes the limitations of the existing area and edge length errors as evaluation methods, but also provides some reference for the reasonable evaluation of surface development accuracy and the optimization and improvement of surface flattening algorithms. Thus, it bears certain practical value.

REFERENCES

1. Gan, M. C., Tan, S. T., Chan, K. W., 1996. Flattening developable bi-parametric surfaces. Computers& Structures, 58(4). pp 703-708.
2. Zhang, Q. L., Luo, X. Q., 2003. Finite element method for developing arbitrary surfaces to fattened forms. *Finite Elements in Analysis and Design*, 39. pp 977-984.
3. Zhang, W. J., Liu, T., Zhang X. J., Li, R.H., 2016. Digital Development Modeling Method on Integral Panel. *Aeronautical Manufacturing Technology*. 508(13). pp 56-61.
4. Pan,W.,Wu,H.,Li,T.R.,Gao,B.Q.,2016.Grid generation on free-form surface based on surface flattening. *Journal of Zhejiang University (Engineering Science)*. 50(10). pp 1973-1979.
5. Cui, X. K. and Chen, M., 2012. Efficient developable strip surface design. *Application Research of Computers*. 29(10). pp 3997-4000.
6. Jin, L., Chen, H., Zhang, Y.F., 2010. Curved Surface of Steel Construction with Computer Development. *Journal of Shanghai Institute of Technology (Natural Science)*.10(2).pp 97-100.
7. Huang, P. 2014. Surface Flattening Problem and Research of Flattening Method on Template Design. *Aeronautical Manufacturing Technology*. S1. pp 155-157.
8. Han, L. and Liu, B. 2011. An Algorithm of Triangular Mesh Surface Flattening Based on Spring-Mass Model and Its Application. *Journal of Huaqiao University (Natural Science)*.32(6).pp 601-606.

9. Liang, Y. B., Xu, W. C., Li, J. G., Yang, Q., 2012. General surface flattening algorithm based on mechanical model. *Computer Engineering and Design*. 33(9).pp 3539-3543.

10. Zhan, W., Zhou, L. S., Chen, G., 2007. A General Algorithm of Complex Surface Development. *Machine Building & Automation*. 36(1). pp 83-87.

11. Wang, C. C. L., Smith, S. S. F., Yuan, M. F., 2002. Surface flattening based on energy model. *Computer-Aided Design*. 34(11). pp 823-833.

12. Yan, G. B. and Liu, B. 2011. An Improved Algorithm for Surface Flattening Based on Energy Model. *Journal of Huaqiao University (Natural Science)*.32(2).pp 135-139.

13. Chen, G., Zhou, L. S., An, L. L., Zhan, W., 2007. Study on a General Method on Flattening of Complex Surfaces. *Chinese Journal of Mechanical Engineering*. 18(24).pp 2914-2920.

14. Zhang, D. J. and Cui, Z. S. 2005. Unwrapped dimension tolerance analysis of multi-point forming workpiece surface. *Journal of Plasticity Engineering*. 12(4). pp 24-27.

15. Mao, X., Mao, P. Y., Sun, J., 2007. Free- form surface approximate development and error analyses system. *Machinery Design & Manufacture*. 12(12). pp 201-203.

16. Yuan, P., Liu, Z. Y., Tan, J.R., 2017. Shape Error Analysis of Functional Surface Based on Isogeometrical Approach. *Chinese Journal of Mechanical Engineering*. 30. pp 544–552.

VIRTUAL AND EXPERIMENTAL TESTS APPLIED ON A REVISION PROSTHETIC HIP

Dragoş-Laurenţiu Popa
Department of Automotive, Transportation and Industrial Engineering, University of Craiova, Craiova, Romania
PhD., Associate Professor, popadragoslaurentiu@yahoo.com

Branislav Popkonstantinović
Faculty of Mechanical Engineering, University of Belgrade, Belgrade, Serbia
PhD., Professor, dr.branislav.pop@gmail.com

Gabriel Buciu
Faculty of General Health Care, Titu Maiorescu University, Targu Jiu, Romania
PhD., Lecturer, buciugabriel@yahoo.com

Daniel Cosmin Calin
Faculty of Medicine, University of Medicine and Pharmacy of Craiova, Craiova, Romania
PhD. Student, calindanielcosmin@yahoo.com

ABSTRACT

The hip joint is a complex structure consisting of bones covered with cartilage, muscles and their tendons, fascia and ligaments. It is a typical spherical joint with three axes of motion and has a great importance in statics and locomotion. In this joint, the femoral head and the acetabulum are joined. The role of the pelvis as an intermediate segment, belonging to both the trunk and the inferior member, should be specified. From a biomechanical point of view, it performs the role of a mobile platform curving on the ends of the femurs and implanting the spine as a supporting body.

But, this biological structure can be damaged, due to age or physical activity. The hip revision prosthesis is a viable option when the initial prosthesis is damaged. The paper presents the model of a stand that can test the hip prostheses made with a three-dimensional modeling program. Also, this stand has been tested virtually using the finite element analysis method. The bone component and the elements of the prosthesis are in fact tested, the virtual bone component being taken and reconstructed from CT images, of the Dicom type. A technique was used that is based on identifying different tissues based on shades of gray and then transforming them into "point cloud" type structures similar to those obtained by three-dimensional scanning. These structures have been transformed into surface-type geometries, consisting of triangular meshes. Using certain CAD techniques, these geometries were processed, applying different methods of filling the gaps, finishing and reducing the number of elementary triangular surfaces. These models formed from closed surfaces were loaded into a CAD program where they were transformed into virtual solids. This virtual bone component was attached to the elements of the prosthesis and to the components of the test stand. Several virtual tests were defined and simulations were performed using the finite element method. A number of results were obtained which were analyzed and several important conclusions were underlined. Also, the metal components of the device have been manufactured, as it was performed real test using EDZ 20 Universal Testing Machine. Main conclusions were underlined.

Keywords: computer graphics; virtual hip; revision prosthesis; virtual test; virtual reconstruction

INTRODUCTION

The hip joint is a complex structure consisting of bones covered with cartilage, muscles and their tendons, fascia and ligaments. It is a typical spherical joint with three axes of motion and has a great importance in statics and locomotion. In this joint, the femoral head and the acetabulum are joined (Bîzdoacă, 2008; Buciu, 2012).

The biomechanics of this important joint are also very important. In the biomechanics analysis, the contact between the bone components and muscle action is relevant. Around the coxofemoral joint, the strongest muscle groups are placed: the pelvic muscles and a part of the thigh muscles, along with the abdominal and back muscles, which also participate in the swinging movements of the pelvis. The total number of muscles with action on the joint amounts to 54 (Vatu, 2019; Popa, 2016).

The pelvic and thigh muscles perform: Static contraction of the two body segments, the movements of the pendulum thigh against the trunk, the movements of the trunk against the fixed thigh (the spindle) (Tarnita, 2010; Vatu, 2019).

Thigh movements are complex. These can be reduced to the three fundamental torques of movement performed around the three main axes of the joint: 1) in the sagittal plane: the flexion (120°) and the extension (113°) around the axle transversally disposed; 2) in the front plane: abduction (40°) and adduction (10°) around a sagittal shaft; 3) inward rotation (36°) and outward rotation (13°) around a longitudinal axis (Tarnita, 2010; Tarnita, 2016; Tarnita, 2019; Tarnita, 2009).

Having the fixed point distal (on the fixed thigh), the muscles provide either trunk movements or balancing the pelvis while preserving trunk recurrence (by dynamic contraction), or stabilizing any baseline position on the fixed member (by static contraction) (Tarnita, 2006; Tarnita, 2009; Tarnita, 2015; Tarnita, 2010).

The role of the pelvis as an intermediate segment, belonging to both the trunk and the inferior member, should be specified. From a biomechanical point of view, it performs the role of a mobile platform curving on the ends of the femurs and implanting the spine as a supporting body (Popa, 2016; Vatu, 2019).

The affections of the hip that need to be prosthesis present a modified joint morphology. Among the most common disorders in medical practice that have as final therapeutic solution the arthroplasty of the hip balance: coxarthrosis primary but also secondary, followed by the traumatic disorders: fracture of the femoral neck and pseudarthrosis of the femoral neck, aseptic necrosis of the femoral head stage III as well as the rheumatic cochetes from rheumatoid arthritis, ankylopoietic spondylitis or juvenile artery (Buciu, 2012).

2. EXPERIMENTAL TEST MADE ON A HIP ORTHOPEDIC SYSTEM

To determine the mechanical behavior of the orthopedic system for the revision of the hip prosthesis, a universal testing machine EDZ 20 was used. The main components of this machine are shown in Figure 1.

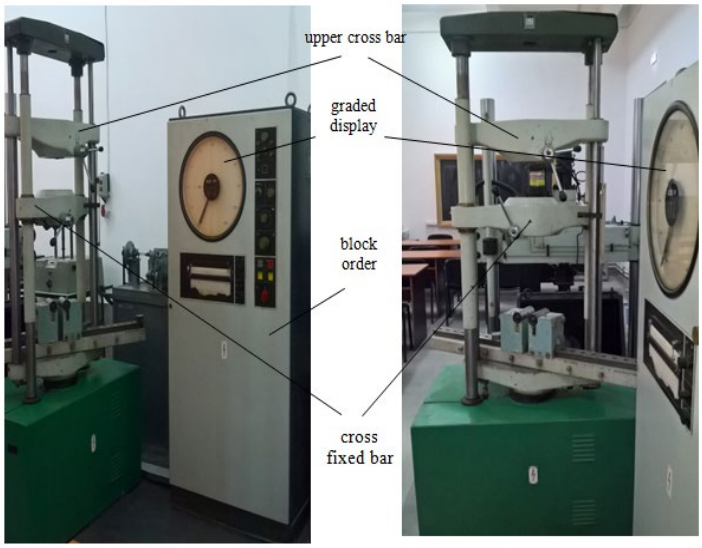

Figure.. 1: EDZ 20 **u**niversal testing machine

For fixing the orthopedic assembly, a device was imagined and designed that could be adapted to the universal test machine using the SolidWorks CAD program. The main elements are shown in Figure 2.

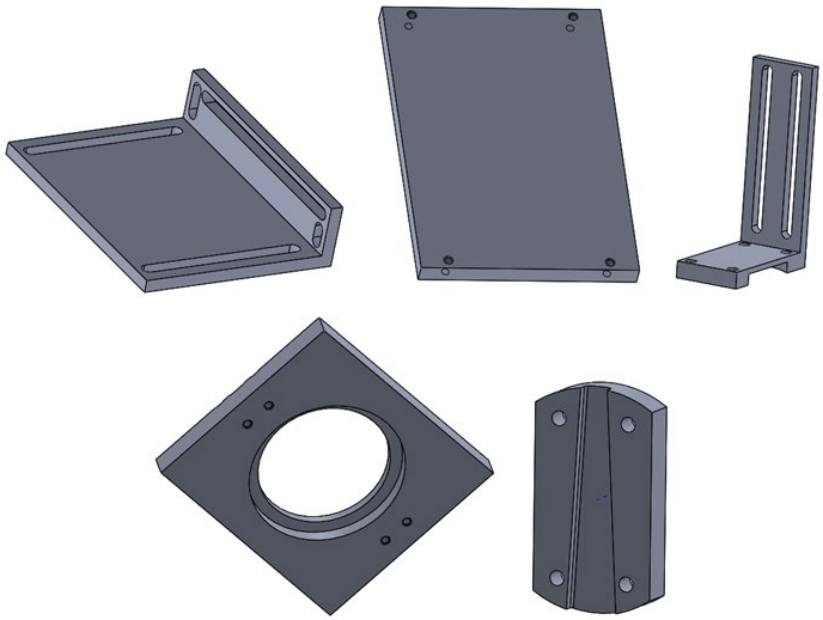

Figure. 2: The main components of the fixing device

Very important was the positioning and fixation of the hip prosthesis stem. Because the position of the stem was not known exactly, an assembly was designed to allow rotation of the prosthesis stem, and then fixing it (Jeli, 2017; Kosić, 2019). This fixing assembly is shown in Figure 3.

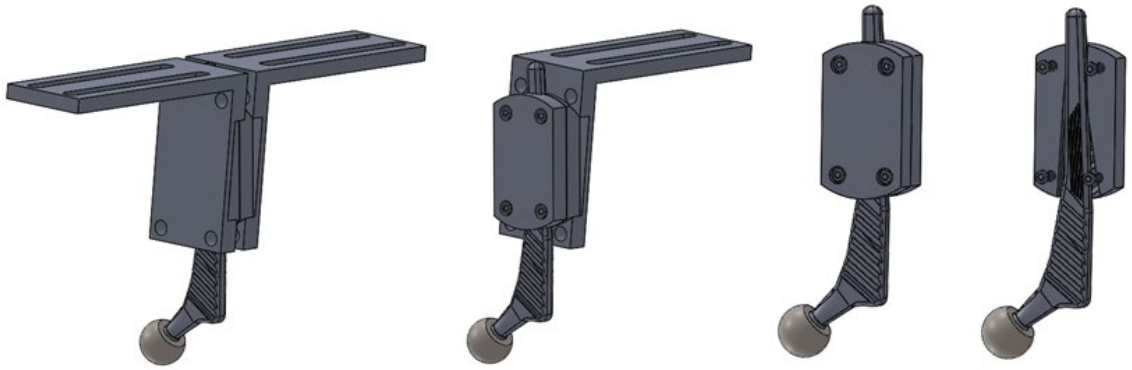

Figure. 3: The fixing assembly of the prosthesis stem (some parts were artificially removed

These components, but also the locking elements (screws and nuts) were assembled in SolidWorks. Also, the bone component (colored in yellow) and the elements of the prosthesis were loaded (Popa, 2016). The final assembly is shown in Figure 4. The blue colored elements are the two main tables of the universal testing machine.

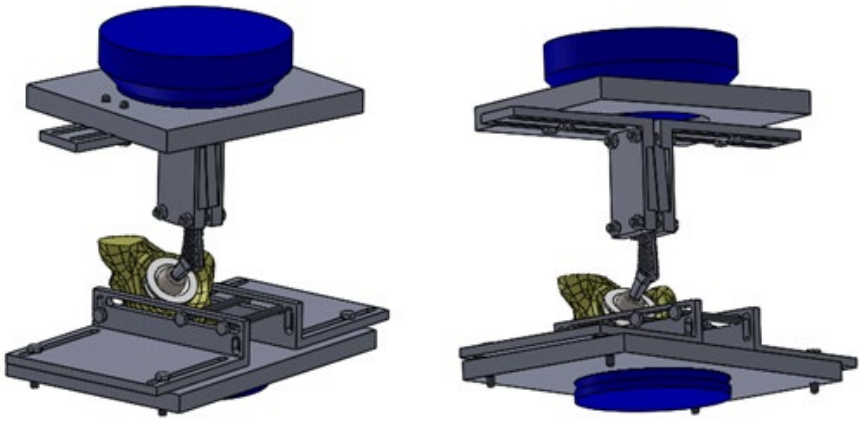

Figure. 4: The final assembly of the fixing device of the orthopedic system (two spatial views)

These components and, of course, the entire fixing device were manufactured using numerically controlled machines. Some elements were welded. Figure 5 shows the components of this assembly.

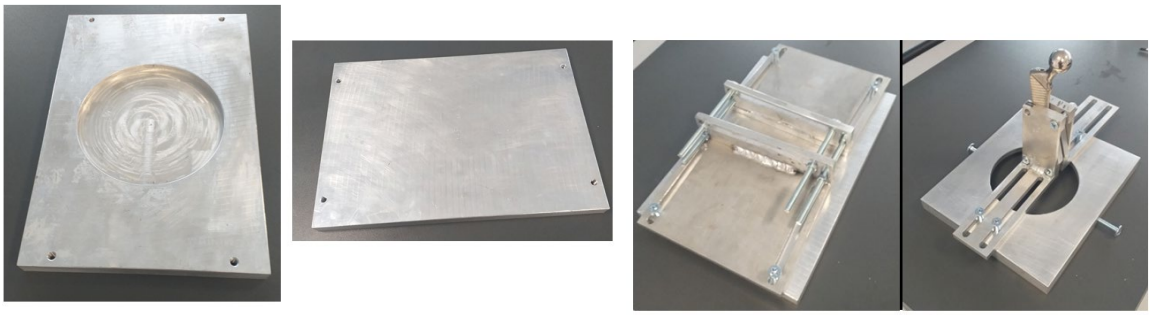

Figure. 5: Components of the fixing device

In parallel, the bone component was prepared. It was taken from a cow and consists of the pelvic bone. The orthopedic assembly was done 5-6 hours after the sampling, so it was done on a fresh component. This component was chosen because the cow acetabulum is close in size to the human one, and the mechanical properties are similar. Figure 6 shows the pelvic bone and a piece of the femur taken from the animal.

Figure. 6: Parts of the femur and pelvic bone taken from the animal

Figure 7 shows the hip prosthesis but also the revision component and the orthopedic screws used.

Figure. 7: Components of the revision prosthesis

For the preparation of the pelvic bone component taken from the animal, but also for the orthopedic installation, the instruments and materials that are commonly used in the orthopedic surgical clinic were used. Also, surgical gloves and orthopedic cement were used to fix the prosthesis. These elements, tools and materials are shown in Figure 8.

Figure. 8: The tools and materials used to prepare the bone component and obtain the orthopedic assembly

The pelvic bone component has undergone a series of operations to adapt it to the acetabular component. Some of these steps are shown in Figure 9.

Figure. 9: Steps to prepare the pelvic bone component.

An orthopedic cement was used to attach the elements of the prosthesis to the pelvic bone component. This cement was prepared from two components and was deposited on the bone component, but also on the elements of the prosthesis. The additional revision component was attached to the acetabulum through two orthopedic screws (Figure 10).

Figure. 10: Stages of attachment of the elements of the prosthesis using orthopedic cement

Because the universal testing machine allows the verification of samples less than 27 cm in height, the orthopedic system has been adapted to this constraint (Figure 11).

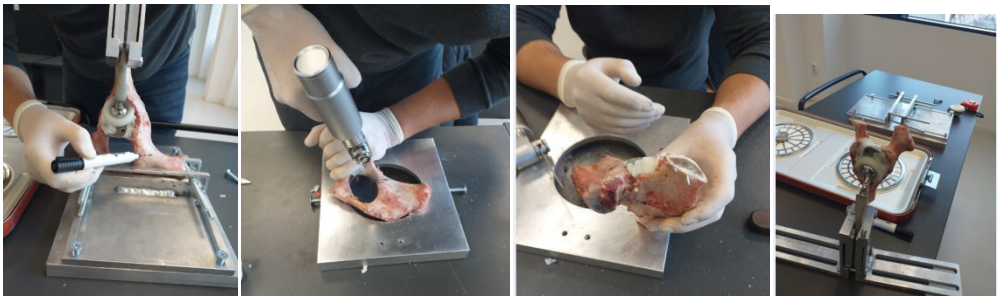

Figure. 11: Adaptation of the assembly to the dimensions required for testing

The metal components of the fixing system were mounted on the test machine, then they were adapted to the orthopedic assembly so that the applied force is approximately vertical (Figure 12).

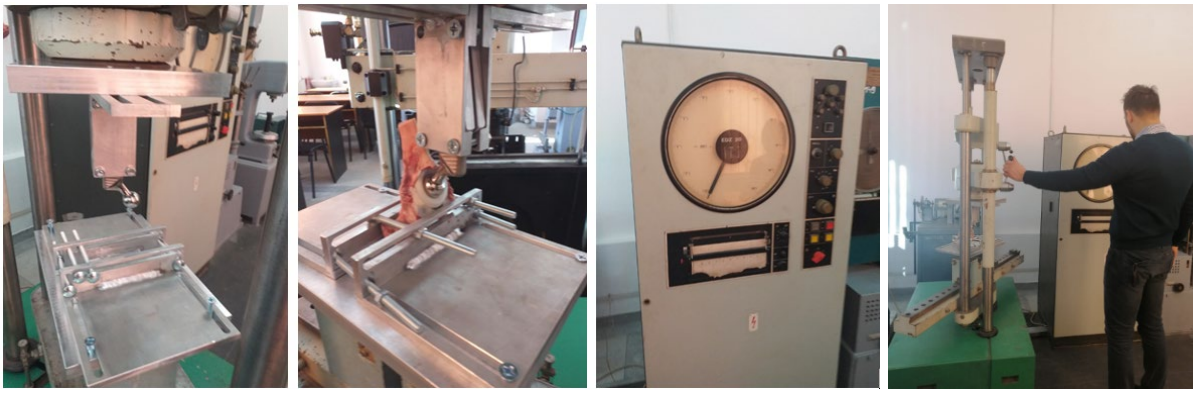

Figure. 12: Mounting and adapting the orthopedic system on the test machine

The force applied through the prosthesis stem was increased in very small steps until the system failed. This whole process was filmed with several cameras. The force at which the orthopedic system failed was 450 kgf, approximately 4500 N. Figure 13 shows images obtained immediately after the failure of the analyzed system.

Figure. 13: The orthopedic system tested on the universal machine after failure

3. VIRTUAL TEST MADE ON A HIP ORTHOPEDIC SYSTEM

3.1. FEM test made on hip orthopedic system with normal walking loading

For the FEM testing in static regime, a simplified model, similar to the real one, composed of a bone segment and revision revision prosthesis was used (Figure 14). The model was initially created in the SolidWorks program, then imported into Ansys Workbench, the programs having common interfaces. The Ansys module in which the analysis and simulation was performed is Static Structural, and the contact between the solid components was of the Bonded type and was defined automatically. The simulation duration with the finite elements method was considered to be 1 sec.

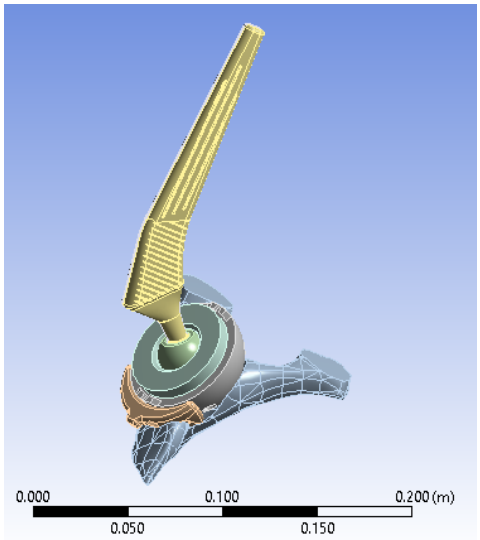

Figure. 14: The model of the analyzed system in Ansys Workbench

The system was loaded using the evolution of the force determined on the pelvic bone at normal walking. The graph of this force is shown in Figure 15.

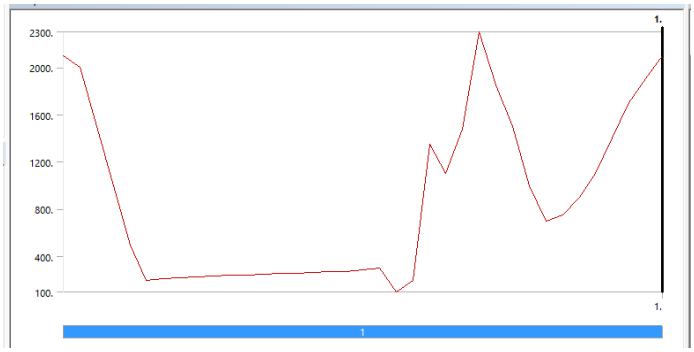

Figure. 15: The evolution of the force during the analysis

The materials used in the simulation are different, and of course they are biocompatible. The properties and components that are part of the analyzed system are shown in Table 1.

Table 1: The used materials and the main mechanical properties

Component	*Material*	*Density (kg/m3)*	*Young's modulus (Pa)*	*Poisson's Ratio*	*Bulk Modulus*	*Shear Modulus (Pa)*
Revision metal cup	*Titanium Alloy*	*4620*	*9.6 E+10*	*0.36*	*1.142 E+11*	*3.529 E+10*
Pelvic bone	*Bone*	*1400*	*1 E+10*	*0.3*	*8.3331 E+9*	*3.846 E+9*
Spherical couple	*Stainless Steel*	*7750*	*1.93 E+11*	*0.31*	*1.693 E+11*	*7.366 E+10*
Additional revision component	*Titanium Alloy*	*4620*	*9.6 E+10*	*0.36*	*1.142 E+11*	*3.529 E+10*
Polyethylene cup	*Polyethylene*	*950*	*1.1 E+9*	*0.42*	*2.291 E+9*	*3.873 E+8*
Femoral stem	*Stainless Steel*	*7750*	*1.93 E+11*	*0.31*	*1.693 E+11*	*7.366 E+10*

The first operation prior to running the simulation was the division into finite elements. The finite element used was the tetrahedron obtaining 148542 nodes and 91045 elements. The finite element structure of the analyzed system is shown in Figure 16.

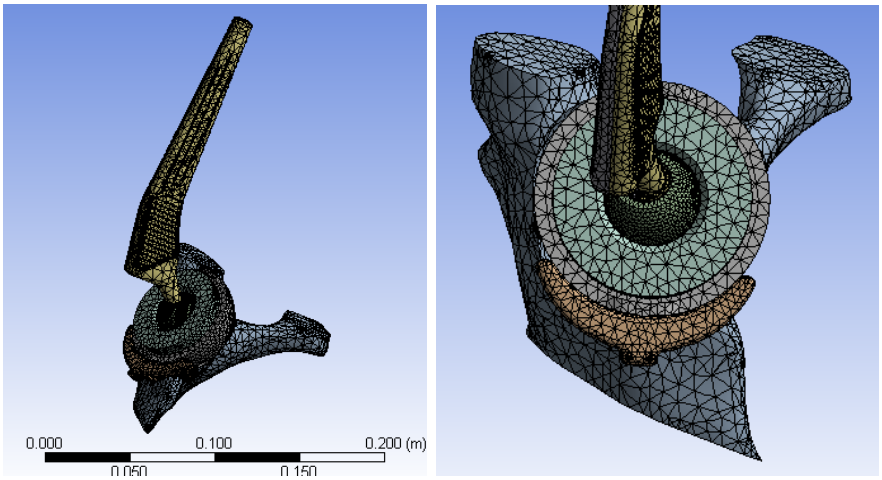

Figure. 16: The structure of the finite elements

The position and direction of the force, but also the constraints of movement are identical to those used in the real experiment and similar to the loads of the normal gait. After running the application, maps of stresses, displacements and strain were obtained (Figure 17).

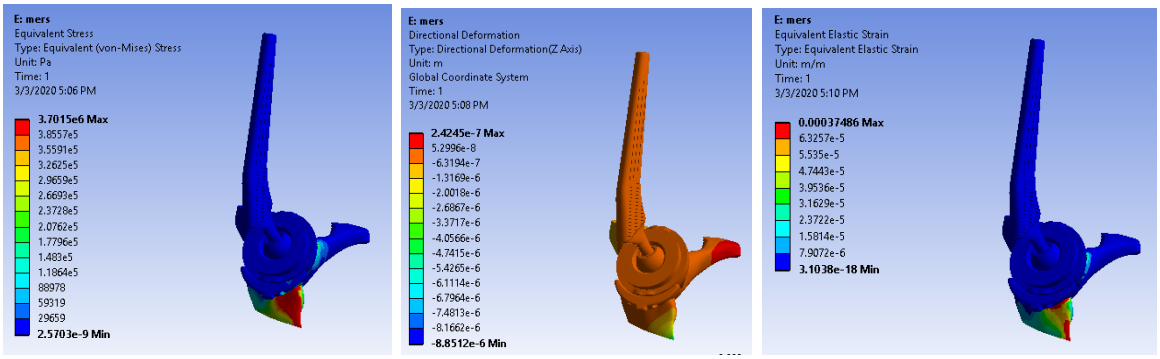

Figure. 17: The stress, displacement and strain maps

3.2. FEM test made on hip orthopedic system with a very high load until the materials fail

To perform such a simulation, the Explicit Dynamics module of Ansys Workbench was used. This module requires a very high computing power and consumes hardware and software resources. By default, running such a simulation takes at least several tens of hours. Therefore, to capture in the simulation the failure of materials was analyzed a very small period of time, that is 0.1 sec. Also, an increase of force up to 1.65E + 08 N was used (Figure 18).

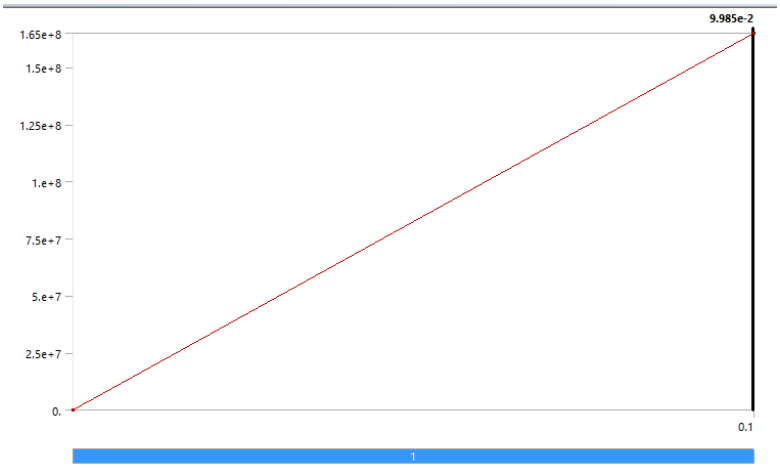

Figure. 18: The evolution of the force

The other settings, movement constraints, materials, finite element structure were similar. After running the application were obtained maps of stresses, displacements and deformations. Figure 19 shows some stress maps, and in figure 20 the displacement and deformation maps.

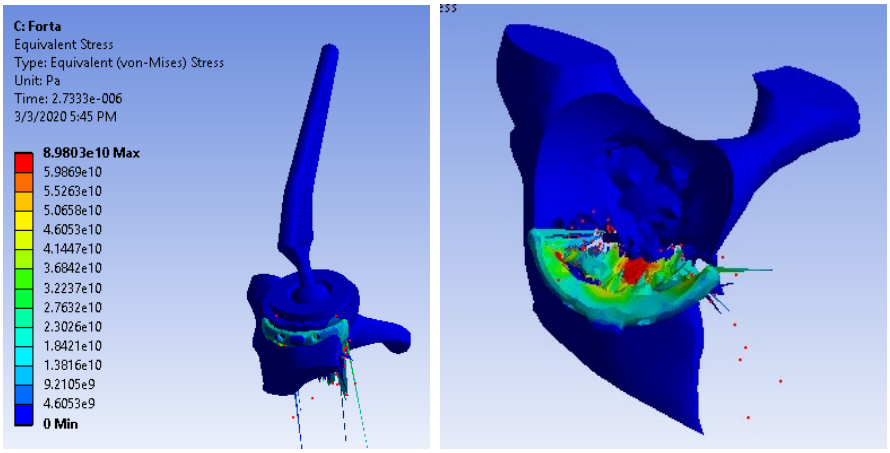

Figure. 19: The stress maps.

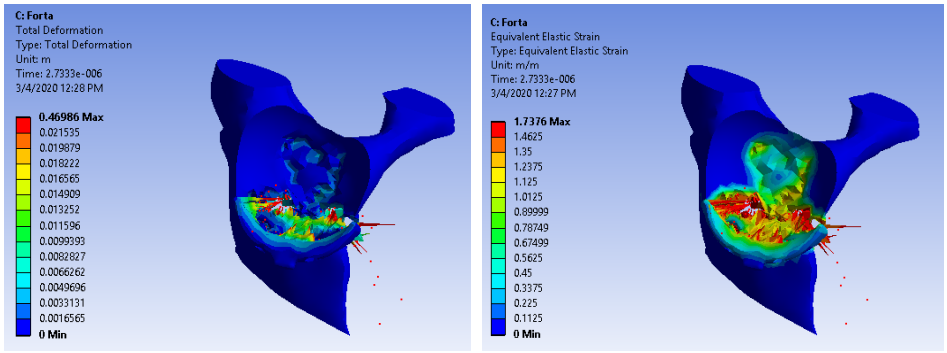

Figure. 20: The deformation and strain maps

Knowing the moment when the system failed at t = 0.00000273 sec. one can determine the force value at this time as F = 4504.5 N, compared to the experimentally determined force that was 4500 N. The error becomes 0.09% in this case, which validates the simulation with the finite element method.

4. CONCLUSIONS

Analysing the obtained results in this paper, the following conclusions were drawn:

- using parameterized CAD programs can be modelated complicate biological systems;
- applying CAD methods and medical imaging techniques can lead to personalized models at the patient's level. These methods can do even more, bringing these virtual models to the virtual reality where medical diagnosis can be sensitively improved;
- It was found that approximately equal values were obtained for the force that causes the orthopedic system to fail, both in the real and virtual experiments. This validates the virtual model presented in this paper.
- Analyzing the stress maps for the two simulations it was found that the stress to which the system fails are 24271 times higher than in the case of normal gait;
- Also, it was observed that in the situation in which the orthopedic system fails the displacements are greater than 1937966.5 times compared to the normal walking load;
- From the study of the deformation maps it is observed that they have 4635.3 higher values in the situation when the orthopedic system fails.
- From the analysis of the images obtained after breaking the bone component, both in the real experiment and in the virtual one, the cracks were obtained in the proximity of the additional revision element as can be seen in Figure 21. The image on the left was made with digital stereo microscope INSIZE ISM-PM200SB.

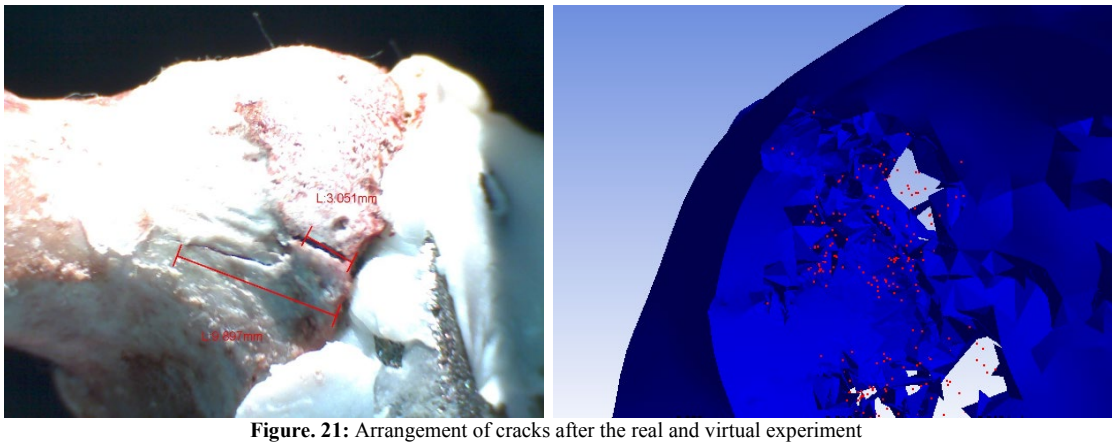

Figure. 21: Arrangement of cracks after the real and virtual experiment

REFERENCES

1. Bîzdoacă, N.G., Tarniţă, D.N., Tarniţă, D., Popa, D.L., Bîzdoacă, E., 2008. Shape memory alloy based modular adaptive ortophedic impants, Proceedings of the 1st WSEAS international conference on Biomedical electronics and biomedical informatics, World Scientific and Engineering Academy and Society (WSEAS), pp. 188-195.
2. Buciu, G., Popa, D.L., Grecu, D., Niculescu, D., Nemes, R., 2012. Comparative analysis of the three new designs of tibial nails which eliminate the use of orthopedic screws. Proceedings of The 4th International Conference "Advanced Composite Materials Engineering ", COMAT 2012, Lux Libris Publishing House, Brasov, Romania, pp. 387-392.

3. Jeli, Z., Stojićević, M., Cvetkovic, I., Duta, A., Popa, D. L., 2017. A 3D analysis of geometrical factors and their influence on air flow around a satellite dish, *FME Transactions*, 45(2), pp. 262-267.
4. Kosić, B., Stojićević, M., Jeli, Z., Pokonstantinović, B., Duta, A., Dragičević, A., 2019. 3D analysis of different metamaterial geometry and simulation of metamaterial usage, *FME Transactions*, 47(2), pp. 349-354.
5. Popa, D.L., Duță, A., Tutunea, D., Gherghina, G., Buciu, G., Calin, D. C., 2016. Virtual Methods Applied to Human Bones and Joints Re-Construction Used for Orthopedic Systems, *Applied Mechanics and Materials*, 822, pp. 160-165.
6. Tarnita, D., Berceanu, C., Tarnita, C., 2010. The three-dimensional printing–a modern technology used for biomedical prototypes, *Mater. Plast.*, 47**(**3**)**, pp 328-334,
7. Tarnita, D., Catana, M., Tarnita, D.N., 2016. Design and Simulation of an Orthotic Device for Patients with Osteoarthritis, in New Trends in Medical and Service Robots, Springer Publishing House, pp. 61-77.
8. Tarnita, D., Pisla, D., Geonea, I. Vaida, C., Catana, M., Tarnita, D.N., 2019. Static and Dynamic Analysis of Osteoarthritic and Orthotic Human Knee, *J Bionic Eng* 16(3), pp. 514-525.
9. Tarnita, D., Popa, D., Boborelu, C., Dumitru, N., Calafeteanu, D., Tarnita, D.N., 2015. Experimental bench used to test human elbow endoprosthesis, in New Trends in Mechanism and Machine Science, Springer Cham, pp. 669-677.
10. Tarniţă, D., Popa, D., Tarniţă, D.N., Grecu, D., Negru M., 2006. The virtual model of the prosthetic tibial components. *Rom J Morphol Embryol*, 47(4), pp. 339-344.
11. Tarnita, D., Tarnita, D.N., Bizdoaca, N., Popa, D., 2009. Contributions on the dynamic simulation of the virtual model of the human knee joint, *Materialwissenschaft und Werkstofftechnik*, Materials Science and Engineering Technology, Special Edition Biomaterials, Willey-Vch., 40(1-2), 2009, pp. 73-81.
12. Tarnita, D., Tarnita, D.N., Bizdoaca, N., Tarnita, C., Berceanu, C., Boborelu, C., 2009. Modular adaptive bone plate for humerus bone osteosynthesis, *Rom J Morphol Embryol*, 50(3), pp. 447-452.
13. Tarnita, D., Tarnita, D.N., Hacman, L., Copilusi, C., Berceanu, C., Cismaru, F., 2010. In vitro experiment of the modular orthopedic plate based on Nitinol, used for human radius bone fractures, *Rom J Morphol Embryol*, 51(2), pp. 315-320.
14. Tarnita, D., Tarnita, D.N., Popa D., Grecu, D., Niculescu, D., 2010. Numerical simulations of human tibia osteosynthesis using modular plates based on Nitinol staples, *Rom J Morphol Embryol*, 51(1), pp 145-150.
15. Vatu, M., Vintila, D., Mercut, V., Popescu, S.M., Popa, D.L., Petrovici, I.L., Vintila, G., Pitru, A., 2019. Three-dimensional modeling of the dental-maxillary system, *Journal of Industrial Design and Engineering Graphics*, 14(1), pp. 207-210.
16. Vatu, M., Vintilă, D., Popa, D.L., Mercuţ, V., Popescu, S.M., Vintila, G., 2019. Simulations Using Finite Element Method Made on a Personalized Dental System, *Advanced Engineering Forum*, Trans Tech Publications Ltd, 34, pp. 175-182.

COMFORT AND ELEGANCE IN AUTO DESIGN

Contoloru Violeta
University of Craiova, Faculty of Mechanics, Craiova, Romania
PhD., Lecturer, dumitru.violeta@yahoo.com

Didu Anca
University of Craiova, Faculty of Mechanics, Craiova, Romania
PhD., Assistant Professor, ankadidu11@gmail.com

Rotea Cristina
University of Craiova, Faculty of Mechanics, Craiova, Romania
PhD., Lecturer, ccploscaru@yahoo.ro

Magdalena Dragovic
Faculty of Civil Engineering University, Belgrad, Serbia
PhD., Associate Professor, megi188plus@gmail.com

Duta Alina
University of Craiova, Faculty of Mechanics, Craiova, Romania
PhD., Associate Professor, duta_alina@yahoo.com

ABSTRACT

Today, we are witnessing a strong combination between industry and art. It can even be argued that authentic artistic industry is being created, which consists of the manufacturing of products that combine useful qualities with aesthetic ones, all the way to the deep psychological comfort that product creates with the help of aesthetic value.

This paper presents the concept of industrial aesthetics, argumentation of the beauty problem, aspects, guidelines and personal observations. Additionally, we provide an algorithm for the aesthetic evaluation of a product (beauty, attractiveness),which reveals numerous possibilities that designers haves at their disposal to meet product aesthetic requirements (e.g. comfort, elegance). Aesthetic indicators include appreciation criteria regarding the shape of the product, the ratio of shape-structure-functionality, shape-material, shape-colour-ornament, shape-colour-fashion-details, environmental form, appearance and finish, packaging and presentation of the product, expressivity trademarks etc. The design and aesthetics of the products are assets in the competitive struggle and elements of real differentiation of the products.

Keywords: car products, design for aesthetics, comfort, elegance

1. INTRODUCTION

Practice has shown that a car whose design is made according to market preferences, may not necessarily be a market success. An eloquent example was the launch of the Ford EDS 44, designed in detail after a long and expensive market study, which was a financial failure for the Ford trust. The conclusion is that the creative genius of a designer cannot be replaced.

Industrial aesthetics, or engineering design is aesthetics (the science of beauty) that deals with the artistic features of products. It harmoniously combines art with technique, the beautiful with the functional. In both pure aesthetics and industrial aesthetics, some fundamental notions are used, such as: harmony, proportion, symmetry, rhythm, contrast.

Beauty, as a fundamental component of aesthetics, is an intrinsic feature (property) of a product capable of awakening the states of satisfaction, emotion and aesthetic joy in users.

The aesthetic component [1] plays two primary roles in the life cycle of a product:

(A). Engineer's discovery of solutions with aesthetic value;

(B). Products user's discovery of the meaning with aesthetic value.

The basic aesthetic components of products include: shape-volume-spatiality; external detailed appearance and significant sensory and emotional content. Aesthetic products display specific features such as: diversity, originality, uniqueness and creativity of constructive solutions.

One of important aspects that can elevate the aesthetic value of a product is its elegance. It consists of: (a) the simplicity of the structural solution - a simpler solution that corresponds correctly to the loads and forces applied ; (b) clarity of the solution - a solution that directly resolves mechanical requirements; (c) economics - to use components as little as possible and require labor as little as possible; and (d) - harmonious properties - dimensions, distribution and density of the constructive elements.

Aesthetics is not attached to a construction as an ornamental detail. It must be integrated into the objective. Structural elements cannot be treated as decorations. Also, the beauty of the product is not a luxury to the good constructive solution. It is a consequence of the mechanical form, spatiality, costs and harmony of the elements. Goldman [2] proposed a classification of aesthetic evaluation terms into the following eight categories: evaluation (beautiful, ugly, sublime, frightening); formal (balanced, graceful, concise); emotional (sad, angry, cheerful, clear); evocative (powerful, agitated, funny, hilarious, boring); behavioural (slow, bouncy, jaunty); representation (realistic, distorted, artificial); perceptual (alive, boring, bright); historical (derivative, original, conservative).

The product model defines the structure and association of the elements (components) in a system, specifying the interfaces (connections) of the elements with the outside. The association of elements is realized along the connections through relations. In Figure 1, we can see: (a) the component representing an identifiable material assembly, which may be: a single part (gear) or a group of parts (gearbox); (b) the linkage that is a feature of a component, which allows an outside view of the component; (c) the relationship expresing a union between two or more links.

The multi-product model represents the product seen from a specific point of view of each specialist participating in the design, based on entities [3].

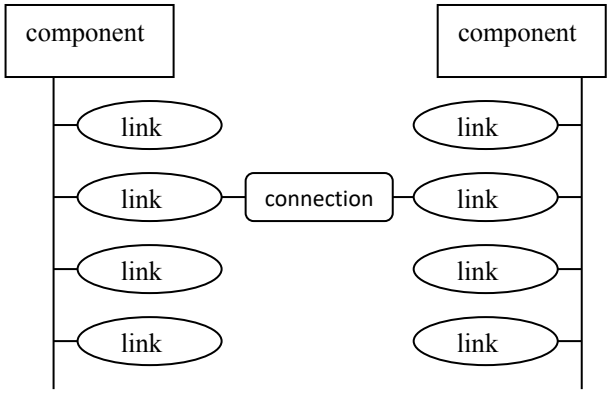

Figure. 1 The structure of a product model

2. DESIGN FOR AESTHETICS

The real motivation in the case of designing a product is the fulfillment of the needs of the human society, the needs not only related to the functions of the product, but going all the way to deep psychological comfort that the product has with the help of aesthetic value.

Aesthetics is a necessity as important as the functions, safety in operation or the cost of execution. The attribution of primacy of one of these aspects leads to a visible imbalance in the final solution.

Figure 2 shows the basic needs pyramid, as identified by Maslow [4]: the need for personal fullness; the need for esteem: self-esteem and respect for others, power, success; the needs of affection: couple, family, community, society, cohabitation, love; security needs: survival, comfort, peace; physiological needs: hunger, thirst, sleep.

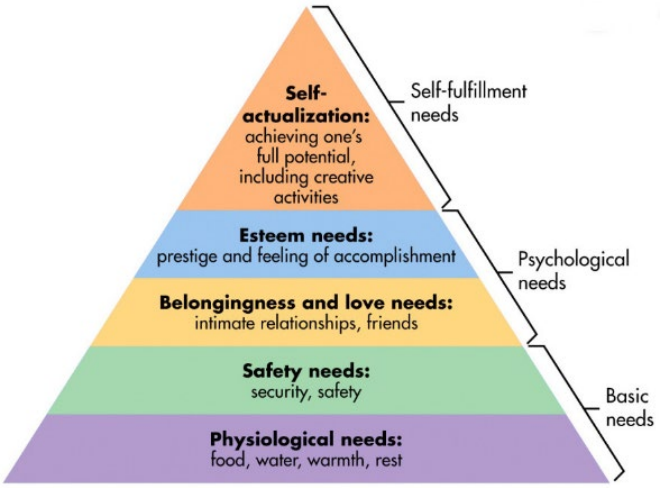

Figure. 2 Pyramid of human needs identified by Maslow [4]

For each product, when it is designed and executed, there are several obstacles that an engineer must overcome, such as:: financial, political, cultural, ecological, and environmental obstacles, the lack of imagination and overall vision, etc.

A product engineer must find the most appropriate technical solutions, following guidelines that also include the concern for beauty. The aesthetic solution of the product must be representative for the level of evolution of the company. The specialist must adapt to the changes that the company goes through, in order to be able to offer optimal solutions suited to its needs.

Each action, from the moment of generating an idea, has a potential that must be properly exploited, in order to create products that will meet the highest needs of the clients. This involves establishing an operational engineer-producer-user feedback.

Figure 3 proposes a potential information flow for the process of creating aesthetic products [5].

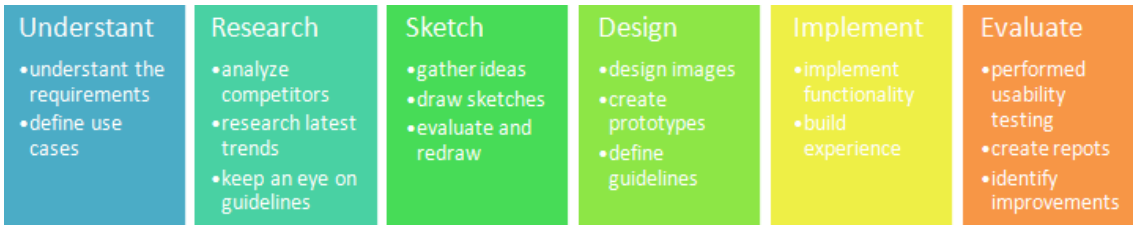

Figure. 3 Information flow in the process of creating aesthetic products

The solution of the aesthetic quality of a contemporary product is based on a series of criteria, namely:

- technical criteria: qualitative performances, their correspondence with the requirements of the beneficiaries, the degree of capitalization of the resources;
- market criteria: customer interest, demand size, competitiveness;
- economic criteria: economic efficiency;
- social criteria: raising the standard of living, avoiding pollution, disturbing the ecological balance.

It is imperative to know the tools, means, resources, freedoms and restrictions that have an impact on the project, from the beginning of the design process.

The design of products implies the harmonization of the following factors:

- Technical and scientific basis (structure, materials);
- Execution technologies (processes, technologies);
- Methods for designing and rendering shapes (dimensions, proportions).

The aspects to be considered include: the trust between the designer and beneficiaries; professional ethics; compliance with the laws; judicious exploitation of resources; the social factor; aesthetic component; exploitation of current technologies; logistics; sensory effects; physical reasoning; the laws of kinematics; spatial limitations.

Here are some principles [6] that can lead to the successful design of products with aesthetic value:

Order. The spatial arrangement of the structural components ensures the product visual comfort. However, a too strict abordation of rules for aesthetic design can lead to the eclipse of other values. Besides the order that brings unity and balance, disorder can be used to the advantage of the product if it brings visual tension;

Proportions, rhythm, symmetry / asymmetry. Proportions must be fair and can have different and relative values for each particular case in order to be expressive. The golden section is a solution that reflects a fair proportionality. Where possible, symmetry is recommended;

Generating surfaces and choosing colours. If the structural form of the product responds and expresses its behaviour (static, dynamic), then, that structure is the most mechanically best solution. From a chromatic point of view, it is desirable that the product usses the colors of the palette in the vicinity or the environment, or to choose light colors.

The conformation, the unit. The form must follow the function in the context of respecting the other aesthetic parameters. If a shape is functionally correct, the result does not necessarily have aesthetic value.

Functionality. The functional purpose of the product must be reflected by the attention paid to the other aspect.

Repeatability. Sometimes, it is appropriate to introduce repetitiveness of similar elements, but taken to the extreme it generates monoton. Designing the product with an increased dose of creativity and fantasy turns the product into an interesting one.

Lighting. For each particular product, some structures have either higher transparency, which gives them elegance, or a higher dose of massiveness, which increases the feeling of stability.

The feeling of stability. Structural elements of the product must inspire resistance, stability and general safety, in order to create mechanical, physical, visual and psychological comfort.

Product integration in the environment. The product must integrate harmoniously with the environment, paying attention to the volume occupied in space, the materials used and the colors.

Responsibility, novelty and progressive vision. The engineer must be a man/woman of his/her time, keeping up with the innovations in the field;

In the modern era, engineers had begun to exploit the source of inspiration that the living world represents. Bodies capable of self-generation, creatures with special physical and mechanical properties, respectively different species of animals can generate a large number of solutions for aesthetic products. There are numerous ways of implementing the beautiful in engineering, such as:

- Choosing a material and experimenting with its possibilities of use;
- Concentration of attention and interest in lowering the cost of making the product;
- Production of prototypes and direct studies on them for modelling the aesthetic solution.

The digital revolution well known to the contemporary society needs to be exploited in favour of identifying, designing and executing structural solutions of products that correspond to the current demands of the company. The parametric approach is one of possible solutions.

Aesthetic appreciation. Next, we propose an algorithm for the aesthetic evaluation [7] of a product (beauty, attractiveness):

Step 1. Identify all different properties (i = 1, 2, 3, ..., n) that determine the aesthetic quality of the product. Normally, proportionality of component elements, the color contrast, the optical corrections, the color range, the nature of the surfaces, are alltaken into account. Establishing the "n" properties, as a rule, remains unchanged and is applied for the appreciation of all types of models made.

Step 2. For each "i" quality, the mass M_i is established experimentally, using the relation:

$$\sum_{1=1}^{n} M_i = 1 \quad \text{(Eq.1)}$$

Step 3. Experimentally evaluate the k_i qualities for each property "i" (points, percentages, units). For each example, this appreciation may be different. Thus, the structure shape of a product will be appreciated with the index K_i.

Step 4. Determine the aesthetic index K_{EI} for the quality "i" with the relation:

$$K_{EI} = f(K_i \cdot M_i) \quad \text{(Eq.2)}$$

in which, K_i – is the aesthetic index for the quality „i"; M_i – is the mass for each „i" quality.

The evaluation of the aesthetic indicator is performed using mathematic modell. Thus, the complex aesthetic appreciation K_{EP} of the product is calculated with the relation:

$$K_{EP} = \sum_{i=1}^{n}(K_i \cdot M_i), \text{ where } 0 \ll K_i \ll 1 \quad \text{(Eq.3)}$$

There are three levels of models that can be combined:

(a) Working models. Sometimes called "white models" or "volume models", they correspond to the realization, a more or less completed project in three dimensions. The materials used are various: cardboard, wood, resin, etc. The objective of this type of models is to be able to touch the product (before the final one), to mold the outline and evaluate the overall appearance, the lines and surfaces respectively. The realization costs are lowl and companies can achieve more for different solutions.

(b) Appearance models. These may or may not be functional. The cost is generally high. They simulate the whole together with accessories and markings. These models are necessary because they highlight the future product before its realization or technical development. Such a model is needed in the following situations: presentation in front of the management, clients, preparation of the catalogue, tests for the acceptance of concepts, etc.

(c) Functional models (prototypes). In industry, a prototype has tot be identical to the future product that will be manufactured in series. Generally, it has an approximate appearance of the product and includes all the functions of use. Its purpose is to validate, on the one hand, the implantation of different product components (internal / external architecture) and, on the other hand, the operating modes of the product. Prototypes serve to validate the chosen options.

The computer offers wide possibilities of expression in the design of the form, choice of the material and movements simulation for flexible elements.

3. SHAPE, AS AN ELEMENT OF AESTHETIC ASSURANCE

Products are designed to perform certain functions. Functions will be performed by certain structures (e.g. mechanical, electrical, electronic).

A structure in space results in a certain external form. The structure and form are found in relationships of mutual determination. The structure requires a certain organization of the form, but there are cases when the form can change the structure.

Shape of the products is used to pleasantly impress the user. The following things are required in order to achieve his impresion: the chosen form has to be unitary; the details have to be clear and logical to highlight the functions of the platform; it has to suggest how it should be used; it needs to have economic justification; finnaly, it ha to be simple and easy to use.

When creating the aesthetic aspect of an industrial product [8], elements that are used in works of art have some particularities: (a) the chosen materials need to fulfil three criteria: the functional criterion (the material first has to meet the purpose for which was chosen and also for manufacturing technology); the aesthetic criterion (the material has to be pleasant - visual or tactile-); and the economic criterion (to combine functional and aesthetic in an economic result); (b) the line gives the impression of movement; geometric shapes that include lines are recommended because they generate a sense of balance; (c) colour is the element that defines the aesthetic value of the industrial product. There must be a harmony in form and color constructed in such a way that two aesthetic elements are congruent with each other. When choosing colors, space rules are taken into account for an optimal visualization, as well as an emotional value;

The implications of applying industrial aesthetics are economic (productivity, operating life), social (labor humanization) and educational (product care, aesthetic values).

Shape, as an element of ensuring a pleasant aesthetics of cars, must fully correspond to their respective function and execution technology. Structural elements of the contour as well as other objective elements of the form, exert important influence on the human psyche. This must be taken into account in the elaboration of the form of products.

Size is an important means of composition, one of the principles that organize the shape of the manufactured product. A proportionally designed car has the best indicators of rigidity. The following types of proportions are distinguished: the arithmetic ratio, H1 - H2 = H2 - H3; geometric ratio, H1: H2 = H2: H3; eight harmonic proportions, a: c = (a-b) (b-c); a: c = (b-c): (a-b); b: c = (b-c): (a-b); a: b = (b-c): (a-b); a: c = (a-c): (b-c); a: c = (a-c): (a-b); b: c = (a-c): (b-c); b: c = (a-c): (a-b).

In the stage of engineering composition, the designer begins the processing of the form considerinf the human body. His/her sketches differ from the engineering ones (establishes first of all human figure - the "humanization of the car" begins). Due to different destinations (ordinary, sports, racing) the position of the human body changes. in each case, this determines the shape and dimensional structure of the car [9] (Figure 4).

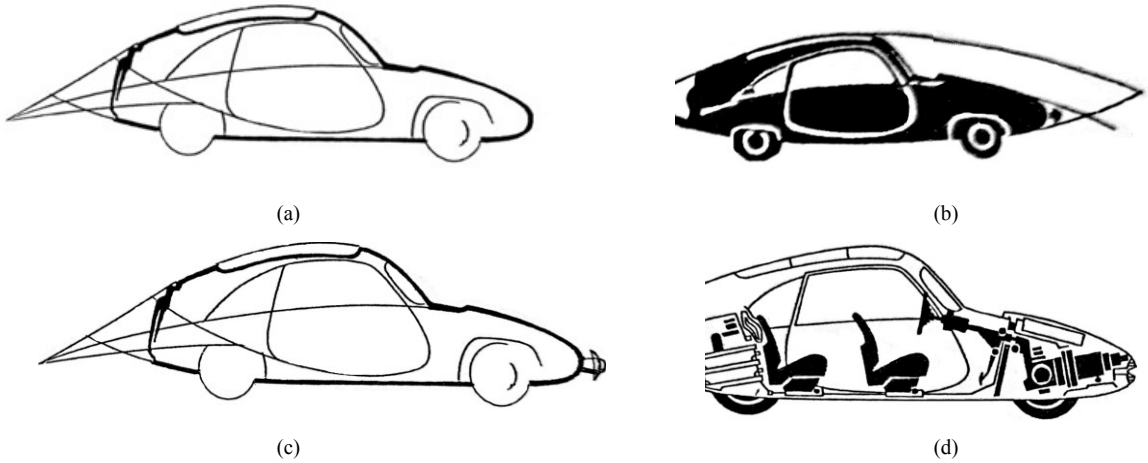

(a) (b)

(c) (d)

Figure. 4 The structure and form of a car [9]

Another aspect of aesthetics is the effect of colour on the shape of products. Compensatory or contrasting colours, for example, carefully chosen, according to scientific criteria, act effectively on the form. Complementary colours, light and color density create harmony and beauty.

Cars from the begining of the century were characterized by monochrome colours, the majority being black (90%) and only a few in white. Technical considerations prevented the appearance of bright colours until 1936, when the use of organic pigments made their existence possible. Only the 1960s brought eesential changes in the habits of consumers and producers. It is considered that the '70s led to light and vibrant colours, partially confirmed in the' 80s. The last period was dominated by slightly more discreet colors. Beyond statistics, we can say that the use of a wide range of colours, with good taste and discernment, is a factor in promoting these products, contributing to the increase of the environment quality .

Exterior design.Car design targets not only the form of the car, but also the combination of form and function. Aesthetics value also has to correspond to ergonomic functionality and utility functions. In particular, electronic components provide more challenges for car designers (displays, GPS navigation, satellite radio, HD radio, mobile TV, MP3 players, video playback and smartphone interfaces). Car design includes: exterior design, interior design, color and total design.

Detailed drawings are executed and approved and digital models are developed together with the drawings (Figure 5). The clay model is still the most important tool to evaluate the design of a car and is therefore used in industry. The data from these models are then used to create the dimensions and layout of the final design (Figure 6).

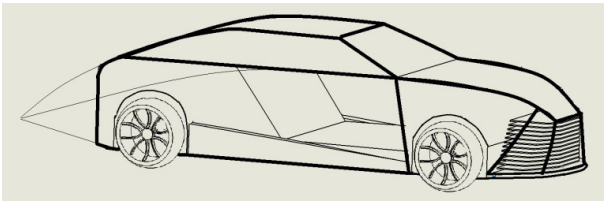

Figure. 5 Structure body for a car

Figure. 6 Final design model

Interior design. The engineer responsible for designing the interior of the car develops the proportions, shape, placement and surfaces for the instrument panel, chairs, doors, poles, ornaments, etc. The priority is to create a balance between the functional elements and passenger comfort.

(4) THE FINAL COLOR AND DESIGN

The designer is responsible for research and design, as well as for the development of all interior and exterior colours and materials used on a car. These include paints, plastics, fabric designs, leather, carpet, headliner, wood trim, colour, contrast, texture and pattern. They must be carefully combined to give the car a unique indoor environment experience. Final designers work closely with exterior and interior designers. Designers are inspired

by other disciplines, such as: industrial design, fashion, home furniture and architecture. Trend components are researched in order to track design influences that relate to the automotive industry. The designer then uses this information to develop themes and concepts that are then further refined and tested on car models.

Car bodies can be created in a variety of different styles and bodies. These styles are largely dependent of a car's classification in terms of price, size, and overall market destination. In car engineering, the body of a car (Figure 7) is the structure that protects the occupants structural panels, doors and other movable panels.

Style of color. The chromatic arrangements should be viewed from the following points of view: functional - utility; physio - psychological; aesthetic - artistic. The red colour is perfectly perceived in the morning. The green colour is very well perceived throughout the day. The blue colour is perceived well in the morning, but the quality of perception increases in the afternoon. Blue has a good influence on vision. Good visibility is an essential quality, mandatory in conventional signalling systems or for highlighting the parts, levers or control panels. One method for increasing colour visibility is contrast. The following scale of chromatic contrast visibility was formed: yellow on black is the most visible combination; white on blue; black on orange; black on yellow; orange on black; black on white; white on red; red on yellow; green on white; orange on white; red on green; the latter becomes increasingly difficult to distinguish. According to general considerations, the usual functional colours for cars include: blue (light blue - Figure 7a, medium blue - Figure 7b); green in different shades (dark green - Figure 7c, varnish - Figure 7d); red (Figure 7e); silver (Figure 7f); dark with warm shades; turquoise blue in different shades. The requests for other colours refer to turquoise and especially orange-brown.

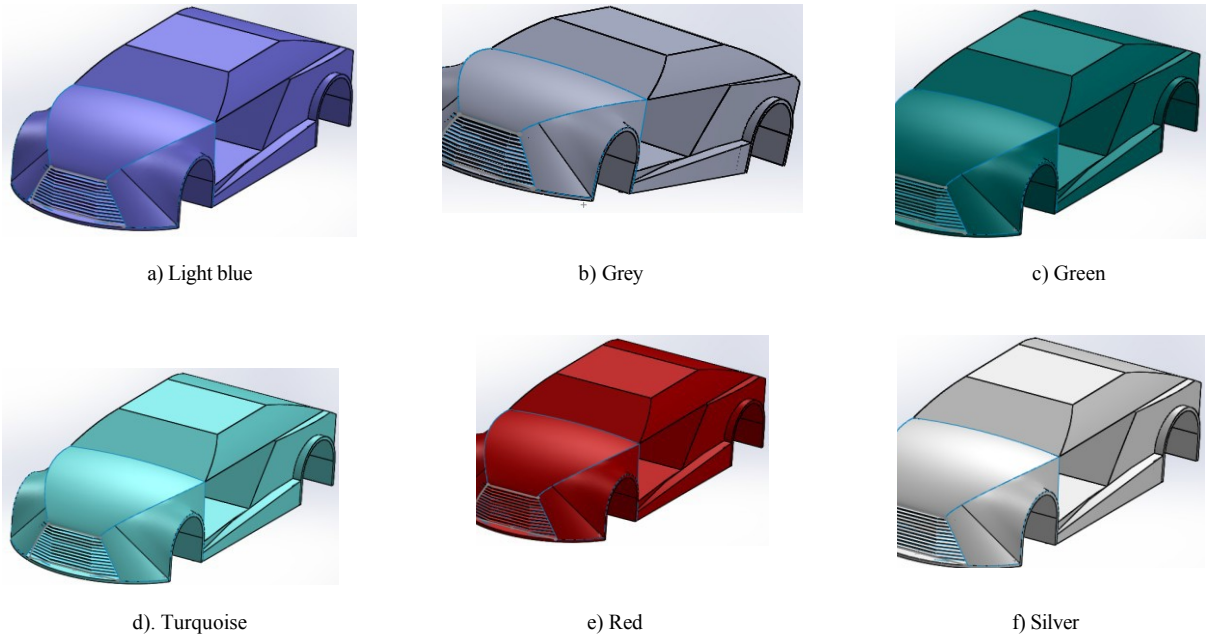

a) Light blue b) Grey c) Green

d). Turquoise e) Red f) Silver

Figure. 7 Style of colour

5. CONCLUSIONS

Industrial products, through their functional role, offer users certain services in response to their demands. Products can be completely new or improved variants of some already existing products. They can have important functional characteristics, obtained by the incorporated technologies or modern approaches to quality, cycle and life, design, aesthetics etc.

Regardless of the car segment we refer to, we allow ourselves to maintain a close connection between the car's design and its technical and performance requirements, fuel consumption, comfort and safety, ergonomic and ecological restrictions.

The process of technical creation (innovation), which is an investment in the long term future, has be conducted like any other activity that brings benefit to the company. Therefore, the industry needs specialized engineers in the field, i.e. design engineers. A design engineer is vital for doing research activities, needs to have a thorough

knowledge of marketing, and be proficient in the legislation governing, the financing of innovation at different decision levels, technological principles of product development and their limitations.

Every creative process is influenced by marketing studies, i.e. by the wishes of potential buyers. We are astonished by the speed of changes and innovations in the mass of production cars. The global trends aim at developing the urban cars segment with comfortable interior space, with reduced exterior dimensions, lack of sobriety and particularly low-cost finishing elements. The studies of different companies propose original and advantageous solutions, including those related to modularity and flexibility.

Increasing the number of models with family tint, either monovolume or estate cars, characterized by a generous interior space is another goal for companies. Further goals include: increasing the sales of electric vehicles and the segment of minivans, 4x4s and pickups and transforming the jeep into family sedans (opinion polls show that only about 10% of the owners use this kind of vehicles for their original destination). These small 4x4 cars used in the city, have the following advantages: high position of the driver, large loading space, increased safety in winter due to a large ground guard and all-wheel drive.

REDERENCES

1. Wladyslaw, T., The history of aesthetics, Merdiane Publisher, Bucharest, 1978;
2. Goldman “Aesthetic Value”, Westview Press, Colorado, 1995;
3. Draghici, G., Product modeling in integrated engineering, https://ibn.idsi.md/sites/default/files/imag_file/Modelarea%20produsului%20in%20ingineria%20integrata.pdf
4. Maslow, A., H., A Theory of Human Motivation, The journal of Psychology nr. 50(1), 1943; https://www.simplypsychology.org/maslow.html
5. Goldman “Aesthetic Value”, Westview Press, Colorado, 1995;
6. Coelho, D., Industrial Design - New Frontiers , InTech Open Access Publisher, 2011. ISBN 978-953-307-622-5, https://books.google.ro/books?isbn=9533076224;
7. Bodack, K. D., Aesthetic Measurement and Subjective Evolution of Visual Objects. University of California, Berkeley, 1967
8. Mayall, WH, Industrial design for engineers, Londra: Iliffe Books, 1967, ISBN 978- 0592042053;
9. Garnich, R, “Construction, Design und Aesthetic”, Stuttgart, 1968
10. Fiell, Ch. & P., Industrial Design A - Z, Taschen, Köln 2000;
11. Walker, S., The cage of aesthetic convention – Stasis in industrial design and the necessity of the avant-garde, The Design Journal Vol. 5 Issue 2, 2002;
12. Ionescu-Muscel, M., The technology of applied product research,TechnicalPublisher, Bucharest, 1981;
13. Karjalainen, Toni-Matti, It Looks Like a Toyota: Educational Approaches to Designing for Visual Brand Recognition, Vol. 1(1) April 2007. http://www.ijdesign.org/index.php/IJDesign/article/view/43;
14. Dumitru, C., Product engineering. Principles of design, management and design, Universitaria Publisher, Craiova 2002, ISBN: 973-8043-86-6;
15. Madan, E., Ergonomics and industrial aesthetics:Course notes, UTM Publisher, Chişinău, 2011;
16. Owain, F., P., Influence of Stakeholders on Industrial Design Materials and Manufacturing Selection Vol. 3(1) April 2009, http://www.ijdesign.org/index.php/IJDesign/article/view/453;

*** Dictionary of general aesthetics, ed. Politică, Bucharest, 1972;
*** British encyclopaedia, London, 2002;
*** Interntional Journal of Design, http://www.ijdesign.org/index.php/IJDesign.

ACQUISITION OF PHOTOGRAPHS FOR PHOTOGRAMMETRIC RECONSTRUCTION OF SCULPTURE IN DIFFERENT LIGHTING CONDITIONS – INDOOR AND OUTDOOR PHOTOGRAPHY

Ivana Vasiljević
Faculty of Technical Sciences, University of Novi Sad, Republic of Serbia
M.Sc., Teaching Assistant, ivanav@uns.ac.rs

Ratko Obradović
Faculty of Technical Sciences, University of Novi Sad, Republic of Serbia
PhD, Full-time Professor, obrad_r@uns.ac.rs

Isidora Đurić
Faculty of Technical Sciences, University of Novi Sad, Republic of Serbia
M.Sc., Teaching Assistant, isidoradjuric@uns.ac.rs

Željko Santoši
Faculty of Technical Sciences, University of Novi Sad, Republic of Serbia
M.Sc., Teaching Assistant, zeljkos@uns.ac.rs

Miloš Obradović
Faculty of Technical Sciences, University of Novi Sad, Republic of Serbia
M.Sc., Teaching Assistant, milos_obradovic@uns.ac.rs

Igor Budak
Faculty of Technical Sciences, University of Novi Sad, Republic of Serbia
PhD, Associate Professor, budaki@uns.ac.rs

ABSTRACT

To obtain a set of photos suitable for photogrammetric reconstruction, in addition to determining the exact positions from which the photos will be taken, it is also necessary to adjust the camera parameters according to the lighting conditions in the recording environment. The aim of this paper is to compare the results of taking photos of the same sculpture under different lighting conditions. Therefore, in the first case, the photos of the sculpture were outdoor photos where the light source was the Sun. The sculpture was placed on a pedestal in the centre of a circle of a calculated diameter and the camera was moved around it with a certain increment of angle. Another case was taking photos in a laboratory where the light was diffuse, the camera was static, and the sculpture rotated on a turntable. To align the camera parameters with the lighting conditions in the recording environment, the first thing we need to do is to measure the light intensity. The measurement is done automatically or manually, but the camera parameters must be constant during the shooting. The reconstructed object is dominated by darker shades of brown and golden-yellow colour, composed of complex free-form surfaces that faithfully depict the upper part of the human figure, exactly the head, neck and torso.

Outdoor photographing process

When shooting is done in daylight, light conditions cannot be affected. The best light source is sunlight because it has the widest spectrum, but an object should not be exposed to such light directly. The reason is the sharp shadows on the parts of the reconstructed object and the reflection on flat and shiny surfaces. The most preferred type of light for photogrammetric reconstruction is diffuse light. The shooting was done on a sunny day in the courtyard of the Gallery of Matica srpska in Novi Sad between 10am and 12pm (August 2019). The camera was moved around the sculpture following a circular path. During this process, a reflection occurred so that some parts of the sculpture were more in shade because of the position of the Sun which did not change significantly. A white canvas was used to mask the background but also to block the reflection. Such uneven lighting had an impact on the results obtained.

Photographing under laboratory conditions

Photographing in the laboratory was performed under diffuse illumination. In this case, the camera was static while shooting and the recorded subject was on a turntable. To provide the required level of coverage for all surfaces, the photos were taken at five different height levels, with a 20° turntable rotation increment. Also, additional photos were taken in the face region.
For both shooting cases, the light parameters were measured in aperture priority mode so they are further manually customized and adjusted. Manual mode was used during capturing photos to ensure that the set parameters remain securely fixed.
Based on the results we have come to the conclusion that shooting outside produces worse results regardless of the ideal weather conditions. The point is that the position of the Sun does not change in such a short period of time but that the surrounding objects make shadows or reflections. Because of this, parts of the sculpture were in marked shade resulting in fewer points in the point cloud in these areas due to lack of data. Also, the texture in these areas is darker and in some places completely black. The laboratory photographing showed that a 3D model of uniform quality was obtained over the entire scope of the shooting, i.e. per unit area, there was a similar number of points in the cloud. Also, the texture is uniform in quality and brightness.

Keywords: photogrammetry, sculpture, 3D model, texture

1. INTRODUCTION

The use of 3D photogrammetric reconstruction has increased significantly in recent years [1], [2]. Photogrammetry is a low-cost and flexible modeling technique, where, as a result of a realistic representation of an object, both geometry and texture are obtained [3], [4]. Photogrammetry is a contactless and non-destructive method, which is of great importance for the reconstruction of cultural heritage objects [5], such as sculptures. There is no possibility of object damage.

Successful photogrammetric reconstruction requires a detailed approach when creating a shooting plan, i.e. a plan for photos acquisition related to access and lighting conditions and camera settings. The number of photos and the angles from which the photos will be recorded can ensure comprehensive coverage of the object [6]. Careful planning and correct photos acquisition allow the generation of accurate and realistic 3D textured models with low-cost photographic equipment [7], [8]. Using multi-group photo processing in photogrammetric reconstruction software provides satisfactory results in 3D reconstruction even on average computer performance hardware [9]. Choosing the optimal method for surveying depends on a number of factors, such as object geometry, object size, the shape of the object, mobility, and surrounding, as well as the properties of the surface material and lighting conditions [10], [11].

The aim of this paper is to compare the results of taking photos of the same sculpture under different lighting conditions. Namely, 3D models of the same sculpture but of different quality are obtained when outdoor shooting and in the laboratory. This difference is observed in the different density of point clouds on the two models. Structure from Motion (SfM) algorithm was used for photogrammetric data surveying. The object for reconstruction is an art sculpture, cast in plaster. Special attention was devoted to the analysis and comparison of the obtained results and the impact the lighting conditions on the quality of the model.

2. PHOTOGRAPHING

2.1. Outdoor photographing process

For a successful photogrammetric reconstruction, it is very important that the shooting plan is well designed. The shooting plan includes determining the appropriate positions for taking the photos and determining the camera parameters that should be consistent with the shooting conditions. The key requirement is that there should be an overlap between two adjacent photos, meaning that two adjacent photos must have a minimum of 60% of the same pixels (the same dots on the object) and an optimum of 80%.

Ground Sample Distance (GSD) was determined first in order to obtain the desired model details. After the GSD is determined, the amount of space that the photo will occupy is checked, which is determined using the GSD and the number of pixels of the camera sensor. After defining a certain area that covers the photo, it is checked whether it is better to turn the camera horizontally (landscape mode) or vertically (portrait mode).

The sculpture is freestanding, with its dimensions of approximately width $\mathbf{28}\boldsymbol{cm}$, the height $\mathbf{47.5}\boldsymbol{cm}$ and the depth $\mathbf{23}\boldsymbol{cm}$.The sculpture is composed of complex free-form surfaces, which faithfully depict the upper part of the human figure, exactly the head, neck and torso.The reconstructed object is dominated by darker shades of brown and golden-yellow colour which are partly conducive to the application of the photogrammetry based on Structure from Motion algorithm. In this step, the focus was on photographing the head of the sculpture. Based on the geometry of the object, a convergent imaging plan was used.The convergent approach is used for freestanding objects, and the camera positions are arranged around the object. The sculpture is made of plaster, with a coating that emulates old gold. The first shooting took place outside on a sunny day between 10am and 12pm in August 2019. The sculpture is mounted on a pedestal. A sketch of the shooting plan and camera position is shown in Figure 1.

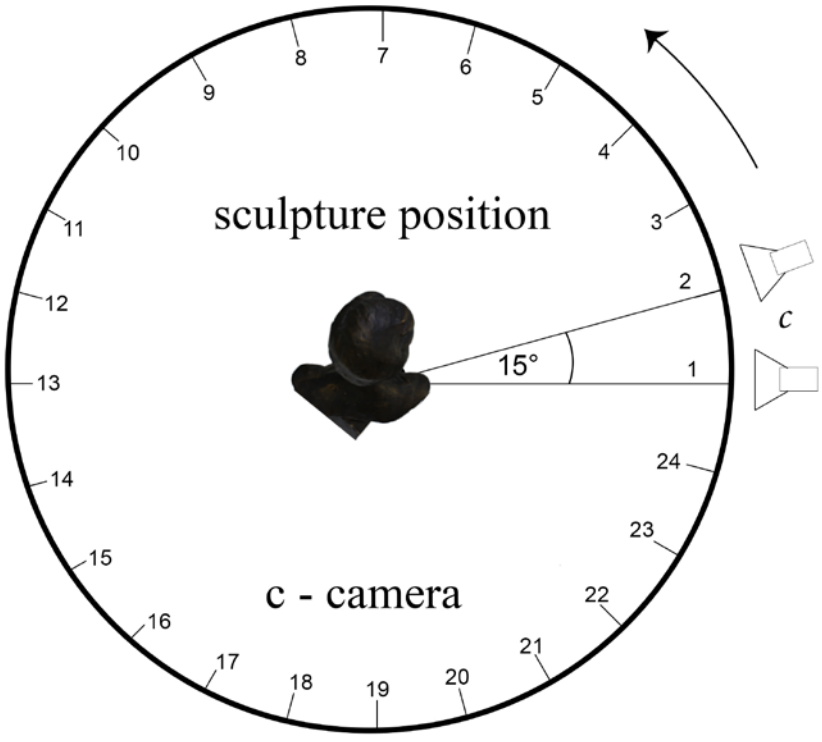

Figure 1. Sketch of the shooting plan for photographing outside

The equipment used for shooting: tripod and NIKON D7000 camera (pixel size - 4.78μm, sensor size - 23.6 × 15.6mm, focal length range - 18 - 109mm, crop factor - 1.53), with manual settings of the following parameters: f-stop, ISO speed, Exposure time.

The selected GSD value is 0.1mm because the 0.1mm details on the object should be visible. The covered space (D) in the photos is determined by considering the number of pixels of the camera:

$$D = pixel\ number \cdot GSD\ .$$

In that case, the covered space is $(0.1mm \cdot 4928) = 492.8mm$ (portrait mode) and $(0.1mm \cdot 3275) = 327.5mm$ (landscape mode). Landscape mode was used for the shooting. When GSD was determined, the scale (m) was calculated

$$m = \frac{GSD}{pixel\ size} = \frac{0.1}{4.78 \cdot 10^3} = 0.0209 \cdot 10^{-3}$$

and the camera distance from the subject (h) is

$$h = \mathrm{m} * \mathrm{c} = 0.0209 \cdot 10^{-3} \cdot 35 = 0.735m$$

where the focal length (c) is 35mm.

The radial distance from the camera to the sculpture should be the same on all sides. The total circumference of the circle is 2rπ = 2 · 0.735 · 3.14 = 4.615m, so for a 15° shift, the distance between the photos is the length of the circle tendon b = 19cm. Three strips were created for covering the whole sculpture height (Figure 2), and this is the first stripe that covers the middle of the sculpture, that is, the height of the nose. The second stripe was created for covering height that encloses the top of the head to prevent the hole on the 3D model from the top due to the insufficient number of points in dense cloud. The third stripe was created from the camera position at the height of the collarbone with the camera oriented at a certain angle so that the part of the chin and the part of the neck below the chin are covered.The number of photos in one stripe is 24.

Based on the sketch shown in Figure 1, the layout of the elements (object, camera, and white canvas) was realized in the field. A circle with a 0.735m radius is drawn on the ground because this value represents the camera distance from the sculpture (Figure 2).

Figure 2. Setting up the elements during outdoor photographing

The shooting was performed on a sunny day in the courtyard of the Matica Srpska Gallery in Novi Sad between 10am and 12pm, in August 2019 following the created shooting plan. As can be seen from the sketch, the trajectory while photographing the sculpture was a circle. During the shooting, a reflection occurred so that some parts of the sculpture were more in shade because of the position of the Sun which did not change significantly. A white canvas was used to mask the background but also to block the reflection. Such uneven illumination had an impact on the obtained results. The Depth of Field (DoF) was checked to obtain the proper sharpness of the photos.The DoF value was checked for the distance of 0.735m from the object. For $f/11$ the near focus plane is at the distance of 0.65m and the far focus plane is at the distance of 0.84m.The distance of 0.7m was used as the focal point of the camera because it is in the specified range. Figure 3 shows the photos from the set of photographs taken outside, which clearly show the difference in brightness depending on the position of the camera on a created circular path.This difference in the brightness of the photos resulted in different point densities on some segments in the point cloud. The 3D software for model creation recognized a smaller number of points on the parts of the sculpture which were in the larger shade,which reflected in the appearance of visible uneven surfaces and cavities on the model.

Figure 3. Exterior illumination of the sculpture

2.2. Photographing under laboratory conditions

Photos acquisition was done with a fixed camera and a sculpture mounted on a turntable, which was at height H (Fig. 4), using a previously created shooting plan. The Canon 1200d DSLR camera was used for photographing, which was equipped with a CMOS APS-C sensor with a crop factor of 1.6 and an EFS lens with an 18-55mm focal length range.This camera supports capturing high-resolution photos (4608x3456 pixels). The photographing was done under diffuse lighting conditions.

The focal length is fixed to a minimum value of 18mm, which provides the highest Field of View (FoV). The camera was initially placed at a distance of approximately 0.5m so that the FoV into which the complete sculpture should be located could be adjusted. The DoF was calculated after placing the camera at the initial distance with the following parameters: $f/11$, shutter speed $0.3''$and ISO 100. Since the camera was mounted on a tripod, the photographing was done through a computer and it was possible to set any exposure time and to adjust the DoF through the aperture. The sketch of the shooting plan is shown in Figure 4.

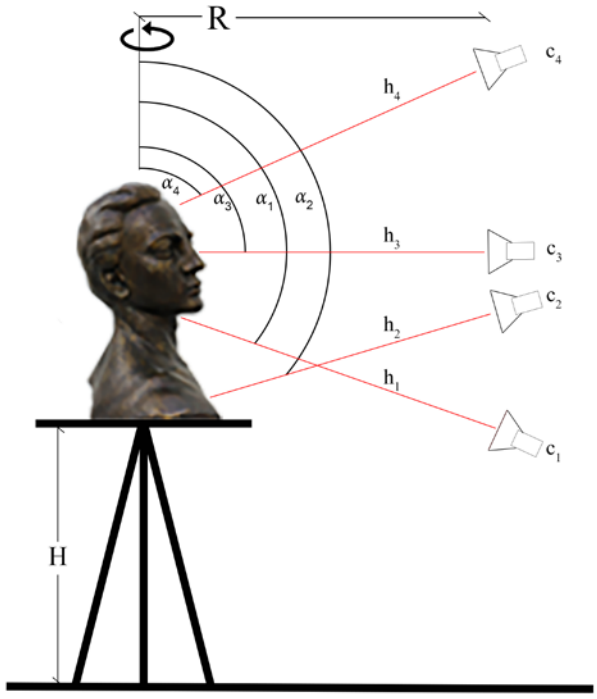

Figure 4. Sketch of the shooting plan in the laboratory

The final camera distance was set at 0.5m, so a compromise was made between FoV and depth of field (DoF). In order to provide the required level of coverage of all surfaces of the sculpture with photographs, the photographs were taken in four different stripes in height, with the turntable increment of 20◦. In the face region, the turning increment was less than the predicted 20◦. In Figure 4, four camera positions, denoted $C_1, \dots, C_4$ are shown, and the distances along the optical axis from the camera to the sculpture are indicated respectively by $h_1, \dots, h_4$. The first stripe is also the lowest stripe in which the camera was placed. The second stripe was set up to photograph the pedestal. At the third level, the camera is positioned at the level of the face with an optical axis of 90° relative to the axis of rotation, and at the fourth and highest level, the camera is positioned above the sculpture, so that the optical axis closed a sharp angle (α_4) with the axis of rotation of the turntable.Additional photographs in the region of the face and the crown of the head were taken to gather as much information as possible from the surface of the object. After the photographing 100 photographs were used to create the 3D model in the appropriate software.

Figure 5 shows the interior where the sculpture was photographed, placed in the laboratory at the Faculty of Technical Sciences in Novi Sad. The shooting was done during September 2019.

Figure 5. Setting up the elements during photographing in laboratory

Figure 6 shows three photographs of the sculpture,which show that the diffused light in the laboratory produced better results than the results obtained by outdoor shooting. Specifically, the luminance of the sculpture is more uniform in scope, which is why a 3D model with a point cloud of uniform density throughout the sculpture will be obtained. Also, the texture will be more uniform in brightness, i.e., colors and details will be displayed more faithfully.

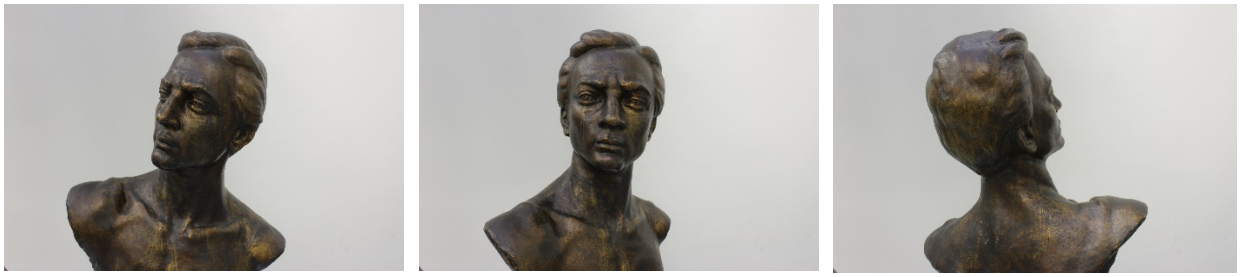

Figure 6. Illumination of the sculpture in laboratory conditions

3. RESULTS

Figures 7 and 8 show, respectively, the results obtained from the photos taken outside and in the laboratory. Figures 7 (a, b, c) and 8 (a, b, c) show dense point clouds and Figures 7 (d, e, f) and 8 (d, e, f) show 3D textured models. It can be seen in Figure 7(a, b, c) in the area of the nose, chin, left eyebrow and the whole right side of the face, there is a cloud of points of lower density, i.e. it is poor quality. Concerning the texture shown in Figure 7 (e), the poor illumination of the texture is particularly noticeable, while in Figure7 (d) the result is relatively good and in Figure 7(f) the texture is of satisfactory quality.

These results have been caused by problems arising from the uneven illumination of the object being photographed in the exterior, in the sunlight. With this method of shooting, the camera was moved around the sculpture along the circle with the sculpture located in its center, and in some positions of the camera, parts of the sculpture were in accentuated shadows.

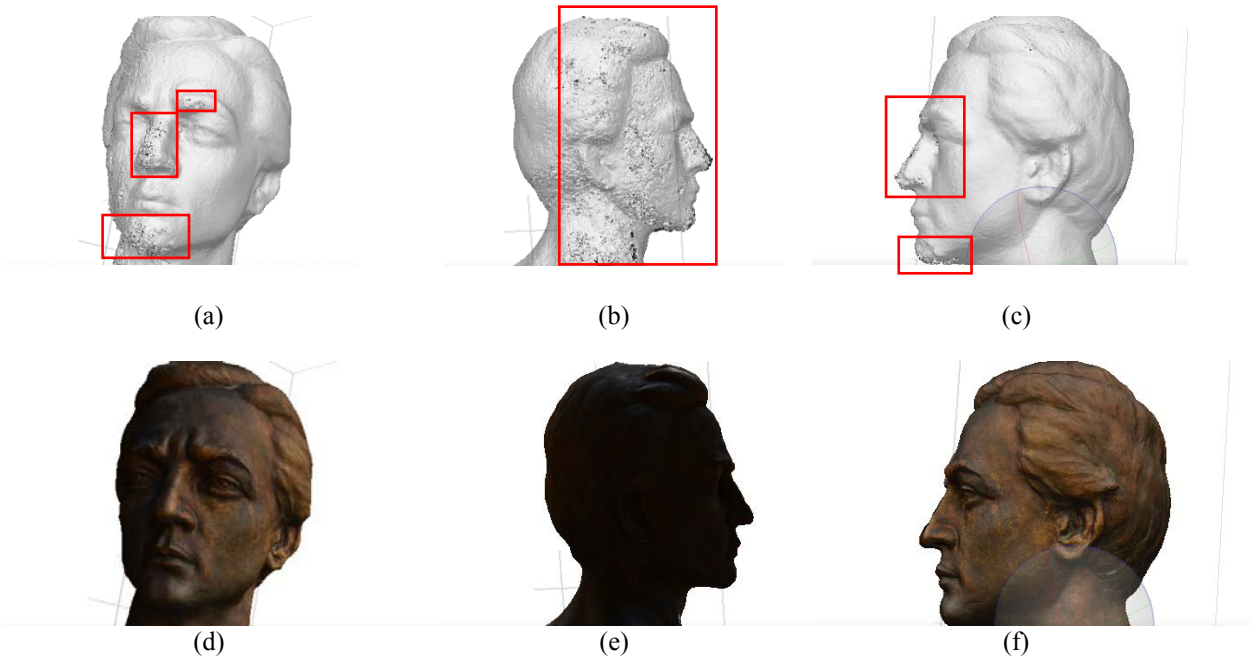

Figure 7. Results obtained with photos taken outside: (a) Details on character's chin, nose and arcade; (b) Character's left profile; (c) Holes on character's chin and nose; (d) Textured model from Figure 7(a); (e) Textured model from Figure 7(b); Textured model from Figure 7(c)

Figure 8 (a, b, c) shows that the point cloud is of uniform quality through the entire scope of the sculpture. Figures 8 (d, e, f) show the obtained texture of uniform luminance and satisfactory quality, better than Figures 7 (d, e, f), but not of ideal quality. It is certain that a better quality of model and texture could have been obtained by using a camera with better performance and professional diffusion lighting equipment.

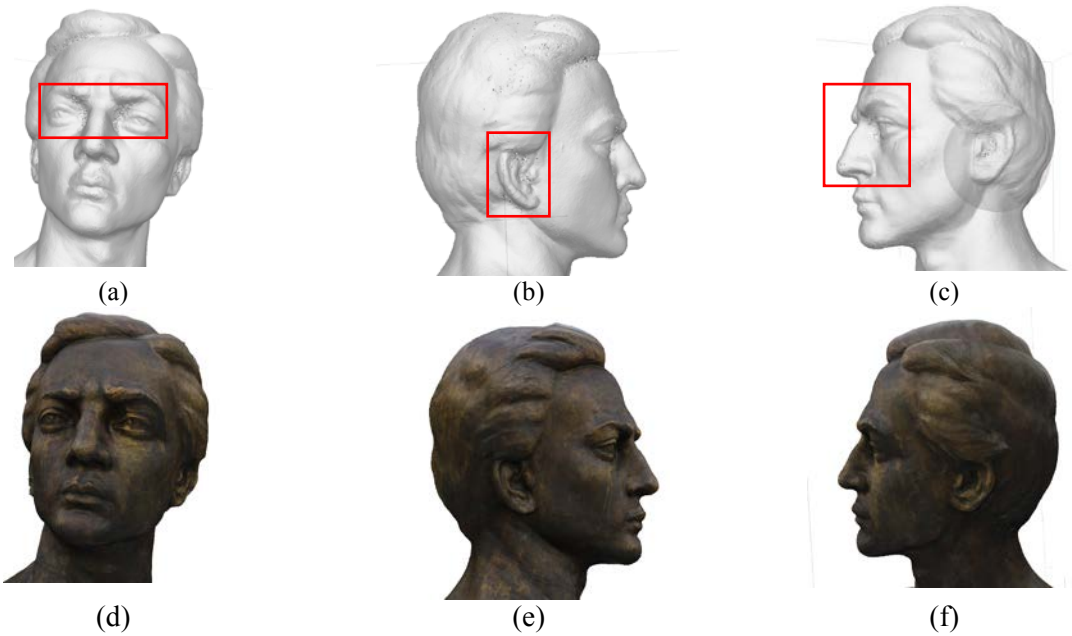

Figure 8. Results obtained with photos taken in laboratory conditions: (a) Details around the character's eyes; (b) Details on the character's ear; (c) Details around the eyes and on the nose of the character; (d) Textured model from Figure 8(a); (e) Textured model from Figure 8(b); Textured model from Figure 8(c)

4. CONCLUSION

Based on the results shown in Figures 7 and 8, it can be concluded that the point cloud obtained from the photos of the sculpture taken in the laboratory had a higher density than the point cloud created from the photos of the sculpture taken outside. Although the lighting in the laboratory was diffuse, it is important to note that it was not ideally diffuse and that no professional reflection blocking equipment was used. When parts of the sculpture were exposed to reflections or were in their own shadow during outdoor shooting, this resulted in fewer dots in the point cloud in these areas due to lack of data. Also, in these parts, the texture is darker and in some parts it is completely black.The uniform lighting in the laboratory affected the quality of the photos and the texture, and therefore also the point cloud. In this case, a similar number of points per unit area of the point cloud was obtained. Also, it should be said that different cameras were used for photographing outside and in the laboratory. This is because the software that was programmed for Canon 1200d camera model was used to synchronize the turntable and the camera. Outdoor shooting,which was chronologically done first, was performed using Nikon D7000 camera which has better technical characteristics than Canon 1200d. Certainly, the comparison of the results would have been more credible if the same equipment had been used for both ways of photographing, and if professional diffused light was used in the laboratory.

REFERENCES

[1] Gómez, F. D., Peiró, J. J., Benavent, A. B., Recuenco, B. A. and Juan, J. H., 2015. 3D modeling for the generation of virtual heritage. *Virtual Archaeology Review*, *6*(12).pp 29-37.

[2] Clini, P., Ruggeri, L., Angeloni, R.andSasso, M., 2018. INTERACTIVE IMMERSIVE VIRTUAL MUSEUM: DIGITAL DOCUMENTATION FOR VIRTUAL INTERACTION. *International Archives of the Photogrammetry, Remote Sensing & Spatial Information Sciences*, *42*(2).Pp 251-257.

[3] Caro José L., 2012. Fotogrametría y modelado 3D: un casopráctico para la difusión del patrimonio y supromociónturística.

[4] Sacra, P. C. A., 2017. 3D photogrammetric reconstruction by "Structure from Motion" as a monitoring technique for safety, conservation and improvement of the fruition of cultural heritage.

[5] e Sá, A. M., Vila, A. B. I., Echavarria, K. R., Marroquim, R., & Fonseca, V. L., 2019. Accessible Digitisation and Visualisation of Open Cultural Heritage Assets. In *Eurographics Workshop on Graphics and Cultural Heritage*. The Eurographics Association.

[6] Nicolae, C., Nocerino, E., Menna, F. and Remondino, F. 2014. Photogrammetry applied to problematic artefacts. *The International Archives of Photogrammetry, Remote Sensing and Spatial Information Sciences*, 40(5).pp 451-456

[7] Abed, F. M., Mohammed, M. U. andKadhim, S. J. 2017. Architectural and Cultural Heritage conservation using low-cost cameras. *Applied Research Journal*, 3.pp 376-384.

[8] Santoši, Ž., Šokac, M., Korolija-Crkvenjakov, D., Kosec, B., Soković, M. and Budak, I. 2015. Reconstruction of 3D models of cast sculptures using close-range photogrammetry. *Metalurgija*, 54(4).pp 695-698.

[9] Samaan, M., Héno, R. and Pierrot-Deseilligny, M. 2013. Close-range photogrammetric tools for small 3D archeological objects. *International Archives of the Photogrammetry, Remote Sensing and Spatial Information Sciences*, XL(5/W2). pp 549-553.

[10] Crkvenjakov, D. K., Santoši, Ž., Budak, I., Sladoje, N. and Stojaković, V. 2016. 3D DIGITIZATION AS A TOOL IN THE CONSERVATION AND RECREATION OF CULTURAL HERITAGE-A CASE STUDY OF THE ICONOSTASIS OF A DESTROYED SERBIAN ORTHODOX CHURCH IN BUDA, pp 23-31.

[11] Đurić, I. and Letić, J. 2016. IMAGE-BASED MODELING OF COMPLEX GEOMETRIC FORMS IN RESTRICTED SURVEYING CONDITIONS–A CASE STUDY OF THE COACH OF METROPOLITAN OF KARLOVCI IN THE MUSEUM OF VOJVODINA. *Between Computational Models and Performative Capacities*, pp 62-74.

SHAPING THE PERCEPTION OF ENGINEERING OBJECTS BASED ON GEOMETRICAL MODELING

Anita Pawlak-Jakubowska
Department of Building Processes and Building Physics, Silesian University of Technology, Faculty of Civil Engineering
PhD., anita.pawlak@polsl.pl

Ewa Terczyńska
Department of Building Processes and Building Physics, Silesian University of Technology, Faculty of Civil Engineering
PhD., ewa.terczynska@polsl.pl

ABSTRACT

In the process of engineering designing, a well-developed spatial imagination is a necessary pre-requisite for correct perception of three-dimensional space. Moving objects or changing the perspective of looking at them in our mind is easier for people whose sense of spatial vision is well developed. The correlation between understanding space or moving in it and the ability to reproduce it in projection methods and graphic notation is inseparable.

The main objective of research studies carried out in the work is the issue of developing and shaping spatial imagination and its impact on the ability to think creatively. The search for new ideas together with the simultaneous ability to combine existing facts often leads to the development of innovative solutions for engineering objects. Currently, rapid technological development imposes on the designers the capacity of being able to move freely in three-dimensional space. They work using advanced computer programs for spatial modeling, in which they often realize complex visions of engineering structures. The requirements demanded from Engineers involve the ability to construct flat images and transform their location with respect to one another. Therefore, they must be practical and creative, and their decisions must be quick and error-free.

The considerations undertaken in the work are intended to prepare the student for proper perception of engineering objects and to practice the ability to read them based on the drawings presented in the technical documentation. The work makes use of a model, a cubic block presented in an axonometric projection and its mapping in the expanded form. Models of various difficulty level were used. Then we related the skills developed by the student to the mapping of other objects such as roofs or buildings. The final stage of the considerations comprised a summary of the work with students in the form of carried out tests. On their basis, it was assessed whether the work with models improved their perception of engineering objects.

Keywords: geometry and engineering graphics; spatial perception; 3D geometric model; spatial ability

1. INTRODUCTION

The development of spatial ability and spatial perception of engineering objects is one of the learning outcomes which is included in most teaching programs of descriptive geometry at technical universities. In the education process, an important role in terms of shaping the profiles of future engineers is played by the capability to develop features that facilitate the learning process of science subjects. Indisputably, they include perceptiveness, logical thinking or spatial imagination that characterize people aspiring to work as engineers. Spatial ability and perception of space are helpful in adopting flexible approach and accuracy in making decisions. Such skills are essential in the process of innovative technical problem solving at the design stage. Albert Einstein

said "imagination is more valuable than knowledge because knowledge is limited". However, it is knowledge combined with imagination that is the basis of creativity. Creativity, imagination, space perception and innovative thinking are closely interrelated and form an inseparable dependence between the effectiveness of studying and the obtained results.

Spatial abilities are viewed as one of the main elements of human intelligence, which are manifested in various aspects. Some of them refer to tasks that require mental rotation of simple two-dimensional or three-dimensional objects and the ability to manipulate complex objects to obtain the right solution, and others refer to spatial orientation, in which elements must be imagined from a different perspective. The combination of imaginative and creative thinking skills with the use and application of tests supports the development of spatial imagination. Problem solving requires an interdisciplinary approach, i.e. the involvement of own experience combined with the use of modern techniques. The development of computer technologies and numerous programs enabling 3D modeling along with animations or virtual walks has provided a very easy and fast way to support perception without the need for spatial thinking. In research studies (Godfry, 1999; Sorby, 1998) have demonstrated that the use of solid modeling alone is less effective for the development of spatial thinking as compared to traditional techniques - sketching, freehand drawing, analysis of a spatial elements created on a flat piece of paper supported, e.g. by a physical model.

The concepts of space perception and imagination were discussed by such philosophers as Plato and Aristotle. The Briton Francis Galton (1879) in their research identified “originally conceived the idea of spatial ability”. In work (Seery et al.., 2018), defined the framework for spatial imagination based on literature review. They also conducted detailed research in this area. In the book „Psychology of cognition” Maruszewski (2016) points out to the ambiguity of the term imagination. On the one hand, it is the ability to create mental images, and on the other hand it is the ability to make conjectures, hypotheses, to pretend and think creatively. In classical psychology, imagination was treated as a phenomenon closely related to seeing or perception of space. Definition given by Kopaliński (1994) defines perception as "perception and conscious reaction of the sense organ to an external stimulus, how to react ... used to recognize geometric figures, simple characters.” In order to enrich and develop the imagination and perception of space, constant creative work is required which stimulates people to think and act in many areas of life.

The research on spatial ability and spatial perception has been combined with the considerations on human intelligence since 1905, is proved by the works of such researchers as Binnet, (1905) or Quaiser-Pohl (2003). Education methods in universities, including polytechnics have undergone rapid transformations, forcing scientists to search for other, more flexible methods of knowledge transfer. In response to the changes, research staff of technical universities who teach descriptive geometry and geometry-related subjects such as engineering geometry, engineering graphics or geometric CAD design, have been conducting a wide range of research on the issues of spatial imagination development and research methods enabling to verify that development. Scientists from various countries of the world have been discussing how to effectively prepare students for the profession of engineer. The results of the studies (Miller, 1991) prove that the most important feature involves the critical ability to perceive as an ability of spatial vision. Other studies (Lohman, 1983) demonstrate the relations that are taking place while testing spatial abilities, e.g. the ability to recognize an object when it is seen from different angles, or the ability to imagine an object when it is moving. Important seem to be mental skills that make it possible:

- to make a projective record of a spatial object created in the imagination,
- to reproduce the shape and spatial form recorded in the projections (e.g. in orthogonal projections),
- to combine individual elements together into one unit.

Howard Gardner (1995) created the theory of Multiple Intelligences, which revolutionized the way of thinking about intelligence and learning. Visual-spatial intelligence is found in people who can think in pictures, they use maps, diagrams, tables and their imagination. Such people are sensitive to details, draw a lot, graphically present their ideas and orientate themselves easily in three-dimensional space. They have the ability to create images in their minds, spatial relations and visualizations. Numerous scientific studies carried out in recent years are very important for broadly understood research on the abilities in the development process of spatial skills and for identifying relationships between them. Many researchers have proved that this ability is very complex and undeniably needed.

In research (Sorby, 2009; Maier, 1996) they pay attention points out to the division between "spatial ability" and "spatial skills" in research works on psychology. He states that spatial ability can be understood as talent, something which people are born with and they have this talent without any training or practice. And spatial skills

can be placed in a group of skills that you can train, develop, and practice. In the article Sorby (1999) introduces the concept of "spatial visualization skills" and proposes their division into the following categories:

- spatial perceptron - which could be described as space perception,
- spatial visualization - the skill to visualize spatial issues,
- mental rotations - the ability to rotate an object in your imagination,
- spatial orientation - the ability to orientate oneself in space.

Most technical universities have been carrying out research studies using Mental Rotation Test (MRT) (Vandenberg et al.., 1978), which tests the perception ability, and Mental Cutting Test (MCT) (CEEB, 1939), which tests the level of spatial imagination. They are most frequently applied, and they confirm the relationship between the obtained results and the effectiveness of studying. Also other tests are available that have been used for educational purposes to validate practical thinking in various engineering professions:

- The Differential Aptitude Test: Space Relations (DAT:SR) (Bennet et al.., 1973),
- The Purdue Spatial Visualization Test: Rotations (PSVT:R) (Guay, 1977),
- 3-Dimensional Cube (3DC) (Gittler, 1990),
- The Mental Cutting Test “Schnitte” (Fay et al.., 1999). This method has been described and investigated by many authors, including Górska, (2005),
- Purdue Visualization of Rotations Test (PVRT) (Bodner et al.., 1997), and its implementation in the group of chemistry students was investigated by the authors (Merchant et al.., 2012).

The subject of perception and spatial intelligence was examined in (Erkan Yazici, 2016). It defines the relationship between cognitive styles and visual spatial intelligence. The author argued after the conducted research that “Overall performance of the students at answering the questions indicates that a significant portion experienced difficulties in perceiving and working with three-dimensional geometrical objects. It was observed that some student had problems with depth perception and struggled with assigning a third dimension to planar figures.”.

The purposefulness of undertaking research in this field seems to be grounded. To ensure a comprehensive and knowledgeable approach to the issue of spatial perception and its impact on human cognitive development, it is necessary to analyze the topic within the area of interests. Furthermore, the research on the perception of space and its impact on human development is complex and important in the era of changes taking place in the world around us. "The situation today shows that the know descriptive geometry is even more necessary than before" (Leopold, 2005). Technological development means that the generation of young engineers, who from an early age use the images seen in telephones, tablets and computers, perceive space differently. Our task is to learn about this "world" and to prepare educational material that will allow students to understand the discussed topics. The current considerations are the continuation of research involving the perception of vision and the development of spatial imagination analyzed in the past (Sroka-Bizoń et al.., 2013). The discussed problem concerns all engineering and technical sciences and the subject matter falls within the area related to the application of geometry and graphics as well as education and teaching methodology.

The main objectives of the research work are as follows:

- developing an authorial test that will allow to get oriented in the level of advancement in the field of space perception by students and to what extent the descriptive geometry course influenced the development of spatial imagination in students of the first semester,
- obtaining information on how to direct further classes in this subject for the examined group of students and to prepare them for further work. The ability to use spatial imagination - understanding the surrounding world in relation to engineering objects - reducing them to simple solids. Input base – a cube block,
- obtaining answers to the question involving the differences in visual perception among students depending on age, gender and whether the person works in their profession or has participated in specialized internships.

The main research problem investigated in the work involves the search for the best solutions for the realized tasks in the authorial test and their verification (testing) on a target group of students. Indirectly, the research problems in the work are related to the realization way of the tasks contained in the test and with determination of difficulty levels for the tasks.

2. METODOLOGY

The main research method used in the work was the experimental method in which the applied technique was in the form of an authorial test on imagination. Based on the test, data was collected and the results were elaborated on how graphic problems were solved by students after the completion of the courses of descriptive geometry and engineering graphics. The obtained information is a valuable source of knowledge for geometry and engineering graphics teachers, guiding them towards the introduction of changes in the education of young engineers during the first semester of engineering studies. The questions in the test were prepared in the computer program AutoCAD 2018. Numerical sheets were made in Microsoft Excel 2010, and based on them the graphs and tables were prepared in Microsoft Word.

2.1. Participants

The research study involved 100 students participating in descriptive geometry classes at the University of Technology in Katowice. The said classes took place during the first semester of full-time first-cycle studies in 2019. The investigated group was divided according to age, gender, type of completed secondary school (divided into grammar schools and secondary technical schools) and design experience or lack thereof. The tests were carried out in one trial, after the course of descriptive geometry and engineering graphics. 60% of the participants were female and 40% male. Participants of different age took part in the study (Table 1). Most of the 72 students were in the 19-25 age range, which is due to the fact that a significant proportion of the participants started their studies immediately after finishing the secondary school. 31 students had apprenticeship or were employed in design offices. Most students 64 in the group graduated from grammar schools.

Table 1: Test participants
(Source: own study)

	Participants number of people	*Age*				
		19-25 years old	*26-30 years old*	*31-35 years old*	*36-40 years old*	*over 40 years old*
Female	*60*	*44*	*4*	*4*	*4*	*4*
Male	*40*	*28*	*2*	*0*	*6*	*4*

2.2. Material

Based on the analyzed tests (MCT, MRT, DAT:SR, PSVT:R, 3DC, PVRT) and years-long didactic experience in conducting courses in geometry and engineering graphics - for 13 years at the Faculty of Civil Engineering at the Silesian University of Technology in Gliwice, and 15 years at the University of Technology in Katowice - the test examining space perception was developed. The purpose of its realization is to obtain information on how to orientate classes in the following semester for the examined group of students. The test carried out after the completed geometry course is a source of valuable information about the changes that should be made for the following semester in terms of the curriculum and the direction of modifications of the prepared tasks and work with students.

2.2.1 Test

The idea of preparing tests for students is not new. During the classes in descriptive geometry and technical drawing, principally the existing Mental Cutting Test (MCT) is applied, which is taken by students during the initial meetings. It has been used for many years, and it is widely available both in the Internet and in paper version. Since it can be easily downloaded, students can prepare the answers beforehand. Therefore, the need to introduce a "new test" was noted. The developed authorial test of imagination presents a spatial element - a cube as the simplest spatial form. Lines were placed on the particular walls of the cube in various ways. The student's task is to imagine the cube net together with the lines applied on the walls (Fig. 1).

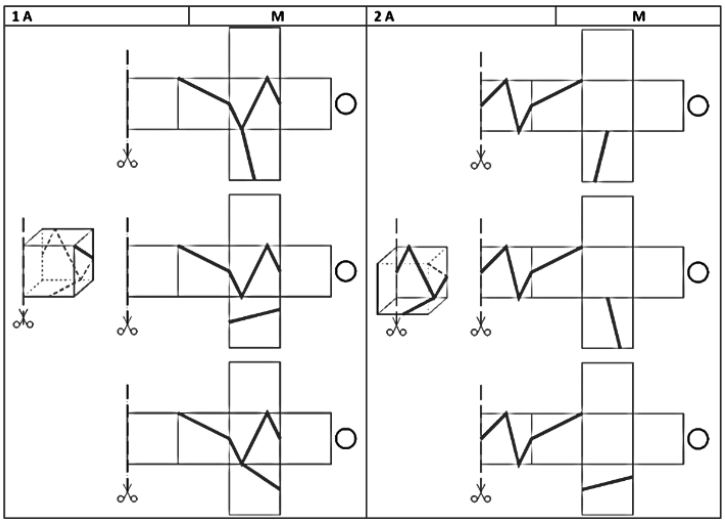

Figure. 1: The student determines the grid on the basis of a cubic element, depending on the cut line introduced.
(Source: own study)

By entering the cutting line and by indicating the direction and method of unfolding, the students receive unambiguous information on how to proceed in order to obtain its flat net (Fig. 2).

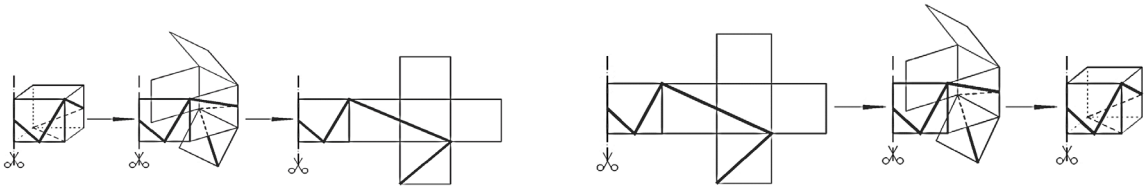

(a) (b)

Figure. 2: (a) The way the net is laid out, and (b) The way the net is folded.
(Source: own study)

Other tasks illustrate the opposite situation. On the basis of a flat net, the students must imagine a spatial element in the form of a cubic block with lines applied on the walls (Fig. 3). The developed test consists of 16 questions. Each of them is based on multiple choice - 3 answers – and only one is correct. One point is scored for each correct answer.

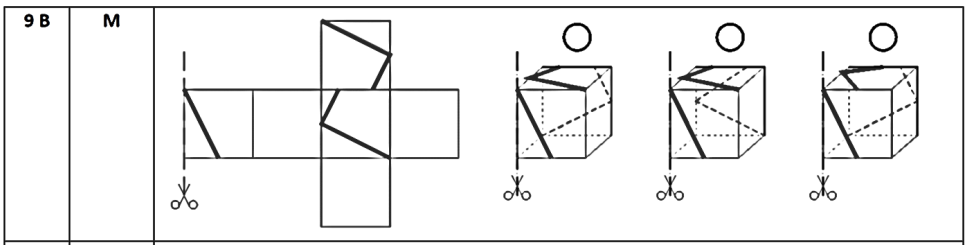

Figure. 3: On the basis of a flat net, the students must imagine a spatial element in the form of a cubic block with lines applied on the walls.
(Source: own study)

The test was divided into two parts A and B, in which two levels of difficulty were distinguished. The first part of the test, marked with the letter A, contained easy questions 1-4 (section A1) and difficult questions 5-8 (section A2). In this section, based on the presented spatial element, its net must be indicated. The second part, marked with the letter B, comprised respectively sections B1 - easy questions from 9 to 12 and B2 - difficult questions from 13 to 16. In this part of the test, basing on the presented net, a model should be built. Both in the sections A and sections B, easy examples have lines introduced only on three walls of the cube, while difficult examples have lines introduced on each wall.

Furthermore, the tasks were constructed in two ways. First, the observer of the cube element looks at the cube in which the front wall is a front view (Fig. 4a) - these are tasks 1A, 3A, 5A, 7A, 9B, 11B, 13B, 15B. The next example involves the same element but the front view is represented by its back wall (Fig. 4b). The observer does not change their position. Such a form is represented by the examples 2A, 4A, 6A, 8A, 10B, 12B, 14B, 16B. The tasks constructed in this way are intended to illustrate which of the presented cases are more understandable for students. In addition, the analysis of these tasks is to show the student that a given spatial element can be examined in a different way, obtaining a different result. 30 minutes were allocated to do all tasks, whereof 5 minutes were taken to explain the idea of the test and the solving method. The test is anonymous, it is done independently by the student and does not affect the grade in a given subject.

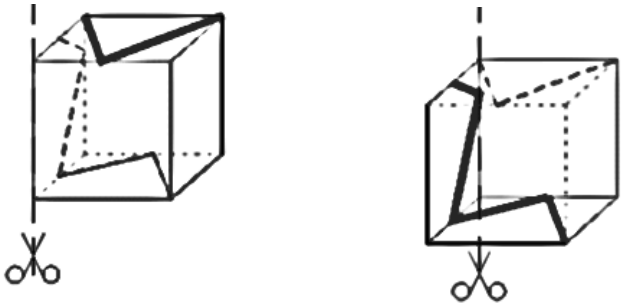

(a) (b)

Figure. 4: (a) The observer of the cube element looks at the cube in which the front wall is a front view, and (b) The same element but the front view is represented by its back wall.
(Source: own study)

2.2.2 Physical model

For all tasks, next to the number, the letter M is given as a designation of the model. In the course of the test, students can use the physical model M prepared by the teacher. It is made in the form of a net that can be folded into a cubic block. The student can apply lines on the cube's walls with a pencil, in line with a particular case and observe the correctness of solution. The net (physical model M) aims to encourage the student to analyze each case (even the most difficult ones) and solve them independently using the deduction process.

3. RESEARCH FUNDAMENTALS

The tasks comprised in the test involved a spatial element on the basis of which a flat net should be read, and then the other way round. Research fundamentals of the conducted research were based on studies in which the authors used a similar technique – a test with tasks. In the work (Baranova et al.., 2018) the impact of descriptive geometry on the ability of spatial vision of students was examined at the Faculty of Civil Engineering of the Technical university of Košice. The research was carried out using the test which was conducted before and after classes in that subject. In one of the questions from the test "students were required to "mentally fold" a two-dimensional (2D) pattern and choose the correct 3D objects" (Tab.2 item 1). The test was a multiple-choice test in which only one answer was correct. Similarly, in the work (Uygan et al.., 2016), the authors used the same system to check the level of spatial perception of students (Tab. 2 item 2). The Santa Barbara Solids Test (SBST) and Purdue Spatial Visualization Test (PSVT) were applied for the measurements, where in the questions also the developments of spatial models are applied. In addition, the (PSVT) test was used in the research studies presented in the work (González Campos et al.., 2019) (Tab. item 3), in which the authors obtained very interesting results and „support the claim that studying computer graphics has an impact on visual-spatial abilities, making them stronger for most of the students". The test DAT:SR is a test in which questions contained a net on the basis of which a spatial element must be built in the imagination (Tab. 2, item 4). It was also applied in the research studies by the authors of the work (Martı´n-Gutie´rrez et al.., 2010) who, using the tests for first-year students of the Faculty of Mechanical Engineering, also wanted to orientate themselves in the level of expanded spatial imagination. The said research subject is also consistent with the work (Marunić et al.., 2014) (Tab. 2 item 5).

Table 2: Tests where part of the questions concerned the grid from which the spatial element was mapped (Source: own study)

Lp.	*Test name*	*Data*	*Answer*
1	-	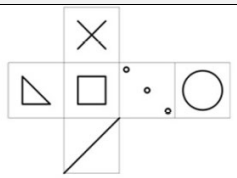	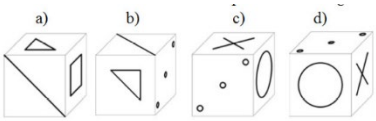
2	*PSVT*	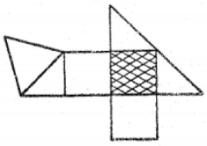	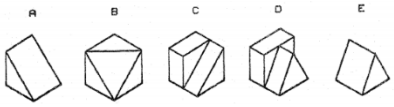
3	*PSVT*	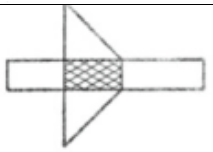	
4	*DAT-5:SR*	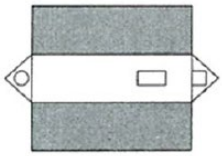	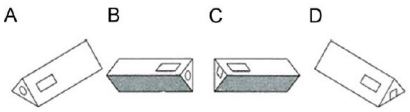
5	*DAT:SR*	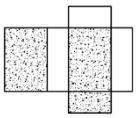	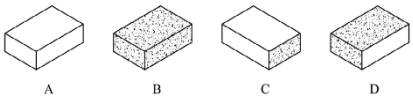

The above works do not exhaust the discussed subject. Another research study is presented in the (Buckley et al.., 2019), which examined "how the levels of spatial ability influenced both performance and the approach to problem solving". The inclusion of that problem in the work gave rise to undertake further research by the authors in the field of space perception. Many years of observation and the work with students was the driving force for the preparation of material suitable for them. We know that with each subsequent decade the way people look at the world and understand it is changing.

4. RESULTS

One of the objectives of the conducted test was to check to what extent the descriptive geometry course influenced the development of spatial imagination in the first-semester students. The issues presented in the test were not contained in the subject material, yet they related to the content of the course. The questions were constructed in such a way that the student could answer the asked questions by analyzing them step by step in terms of difficulty level (from easy to difficult questions). To make the task easier for students, they could use the model to define their visual ability - the transition from the 2D image to the 3D structure.

We evaluated the conducted tests by dividing them according to the following criteria.

1. The first criterion (Chart 1) involved the level of difficulty of the tasks, with the division into easy and difficult tasks in the particular sections A1, A2, B1 and B2.

- In section A1, the easiest task was task 1 – the students gave correct answers in 93%, while task 4 proved to be the most difficult. Only 12% of students answered that question correctly,
- In section A2, the easiest were the tasks 5 and 7 - 81% of correct answers, and the most difficult was the task 8 - 43% of correct answers,
- In section B1, the easiest was the task 10 - 87% of students gave correct answers, while the most difficult task turned out to be the task 12 - 75% of students gave correct answers,

- In section B2, the easiest task was the task 14 - 88% of correct answers, and the most difficult task was the task 13 - 69% of correct answers.

It follows from the above that in the entire test the easiest turned out to be the question 1, and the most difficult was the question 4. Both questions are from section A1, where basing on the spatial element, the net solved correctly should be indicated. Some people in section A1 had the result at 100%, i.e. they answered all 4 questions correctly. There were also people who in that section did not give any correct answer, obtaining 0%. Yet, having analyzed all sections, the collected results demonstrate that section A1 proved to be the most difficult to solve. This is most likely due to the fact that the line drawn on the net is on three walls, and it does not form one sequence. It is disconnected by introducing walls without any applied lines, whereby it is difficult to reconstruct the element. The cube on which the line forms the whole section A2 and B2 is read in a different way. Having analyzed the test, it can be seen that in order to make the task easier, the students solving the task followed the course of the line by numbering the lines on the model, simultaneously transferring them on the net.

As to the tasks from Part A, students gave 62% of correct answers, and in Part B 81% of correct answers. Thus, the sections B1 and B2 turned out to be much simpler. A large number of students answered all 8 questions correctly. In that group no participant received 0%. It means that the transition from flat drawings to axonometric drawings is easier to perceive and it bespeaks of clear understanding of the content without confusions or faulty representation of the object.

As to the way of looking at the element, the situation in which the observer of the cube element looks at the block in which the front wall is the front view, turned out to be easier to perceive (tasks 1A, 3A, 5A, 7A, 9B, 11B, 13B, 15B). The average of correct answers was at 83%. In the second case, when the front view is the rear wall of the element (examples 2A, 4A, 6A, 8A, 10B, 12B, 14B, 16B), there were 60% of correct answers. Therefore, we can conclude that that way of looking at the spatial element was more difficult for them.

Chart 1: Percentage of people giving correct answers
(Source: own study)

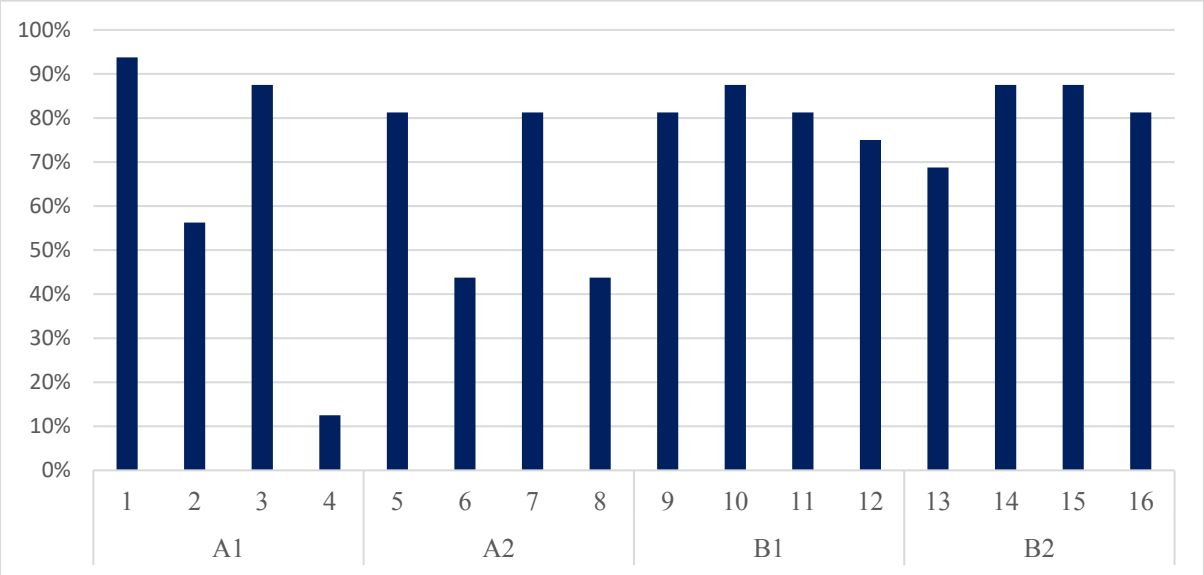

2. The second criterion (Chart 2) involved the assessment of the solutions of the individual parts of the test (A and B) and the sections (A1, A2, B1, B2) divided by gender.
The average of correct solutions is definitely better for men in Part A, in which the following results were obtained:

- in section A1 - 68% of correct answers for men with 58% for women,
- in section A2 - 71% to 56% respectively.

In Part B the advantage in providing correct solutions belongs to women. The obtained results are as follows:

- in section B1 - 82% of correct answers for women with 68% for men,

- in section B2 - 82% of correct answers for women with 75% for men.

Section B turned out to be easier for women, while section B2 for men.

Generally, adding up parts A and B of the test in view of the division of the students according to gender and type of the applied tasks:

- in part A of the test the following results were obtained - women 57% of correct answers and men 69.5% of correct answers,
- in part B of the test the following results were obtained - women 82% of correct answers and men 71.5% of correct answers.

For women and men, part B of the test turned out to be easier, in which the spatial model was identified based on the flat element (net).

As to the division into easy questions for sections A1 and B1, the following results were obtained:

- Women had 70% of correct answers, while men had 68.5% of correct answers.

As to the division into difficult questions for sections A2 and B2, the following results were obtained:

- Men had 72.5% of correct answers, while women had 69% of correct answers.

The conclusion from the above is as follows - for women, it is easier to answer questions in which the line was drawn on 3 walls. In turn, for men it was less difficult to answer questions where the line was on 6 walls of the element.

Chart 2: Percentage of persons giving correct answers by gender
(Source: own study)

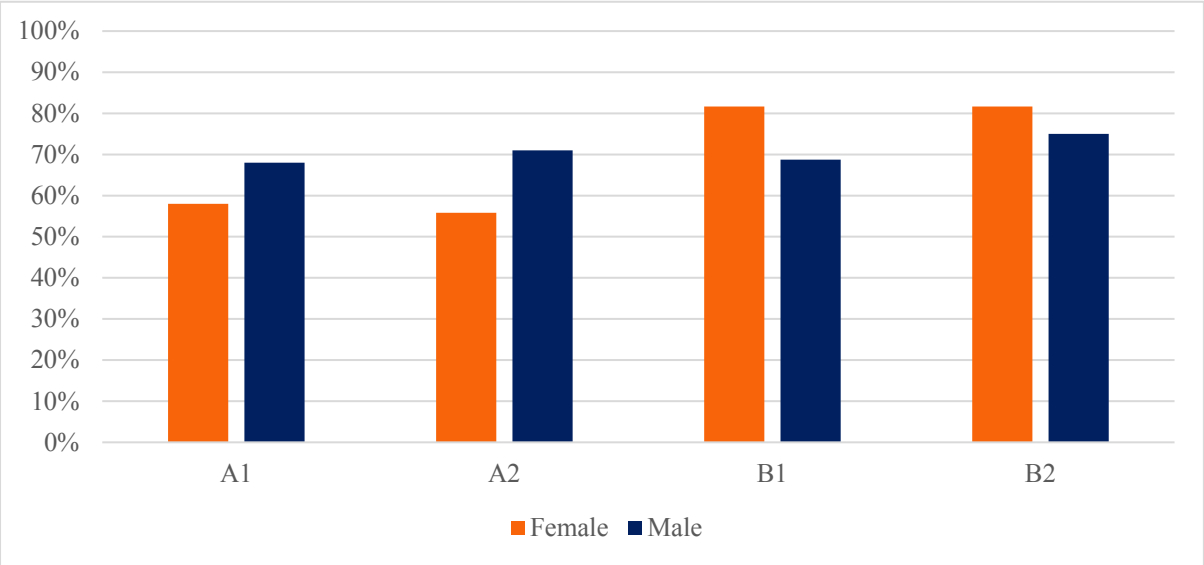

3. Criterion involving vocational training (Chart 3).

The percentage share of people who had design experience was 31%. Working people obtained in Part A a larger number of correct answers, amounting to 77% as compared to people without vocational training (53.5%). Similarly, in Part B, definitely more correct answers (92.5%) were provided by working students, while students without vocational training had 68.5% of correct answers. The research also demonstrates that, depending on the difficulty level of the questions for easy questions, sections A1 and B1, much better answers were provided by working students - 89% of correct answers. Students who do not work obtained 61%. For the sections with more

difficult questions, A2 and B2, as above, the working students received better results, at 80.5% compared to non-working students who provided correct answers at 61%.

Chart 3: Percentage of correct answers by working and non-working persons
(Source: own study)

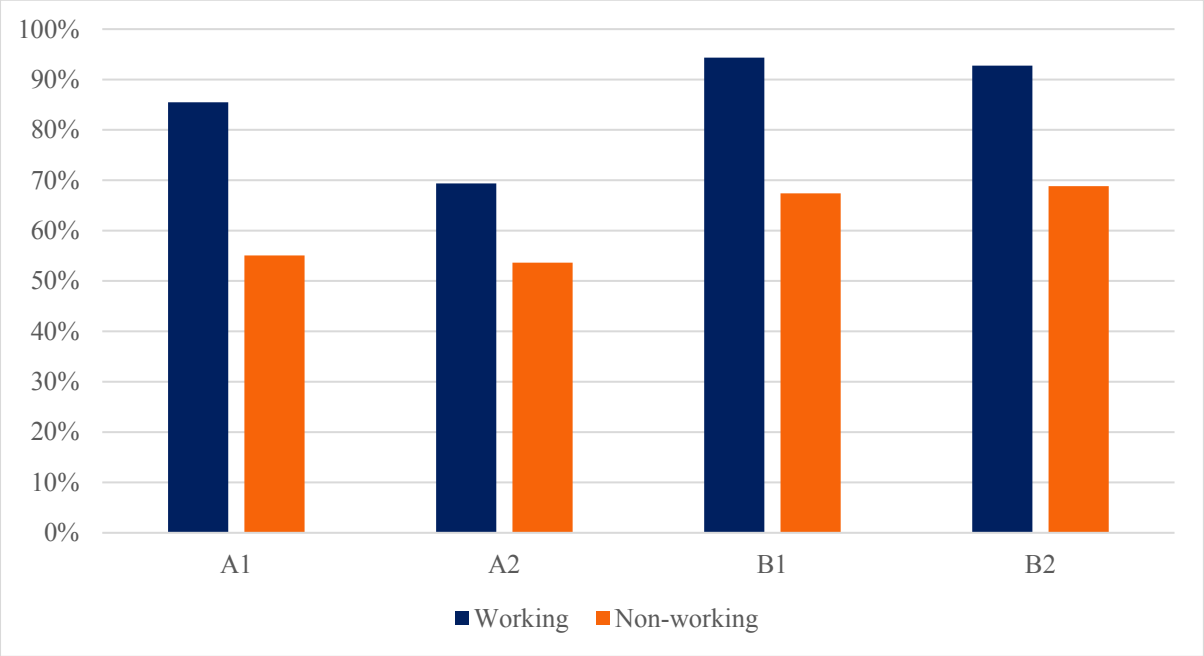

Based on the results, we can conclude that working people were much better at solving the prepared test. Among the working group, there were people who solved the tasks in a very short time and returned their work before the time limit, obtaining a faultless result, i.e. 100% of correct answers. Those people had previously completed the 1st and 2nd degree studies in Civil Engineering and were in active working life. This probably accounts for their easiness and effortlessness when taking the test. In comparison to people starting their studies without vocational training, their abilities are definitely dominating.

It was surprising that none of the examined persons wanted to use the physical model when analyzing the examples.

4. Criterion according to the type of completed high school - divided into grammar schools (GS), secondary technical schools (STS) (Chart 4) and age (Chart 5).

In each of the sections A1, A2, B1, B2 persons, who graduated from secondary technical schools outweigh correct answers persons who completed grammar schools (Chart 4):

- in section A1 - 74% of correct answers for secondary technical school with 68% for grammar school,
- in section A2 - 76% of correct answers for secondary technical school with 55% for grammar school,
- in section B1 - 81% of correct answers for secondary technical school with 72% for grammar school,
- in section A2 - 84% of correct answers for secondary technical school with 74% for grammar school,

The data in Chart 5 show that the group of students who graduated from technical secondary school in the 26-30 age group is definitely the best. The correctness of the answers in each section is 100% in their case. Students over 40 years old after both secondary technical schools and grammar school also responded well. The group in the 31-35 years after the graduation of grammar school in sections A1 and A2 did not get well, obtaining only 37% of correct answers. However, the same group in sections B1 and B2 obtained 87% and 100% respectively.The worst result in the whole test was obtained by students in section A2 in the 26-30 age group after graduating from grammar school - only 25%. The result is a surprise, since the same group in section A1 obtained 75%.

Chart 4: Percentage of correct answers by division to a finished school
(Source: own study)

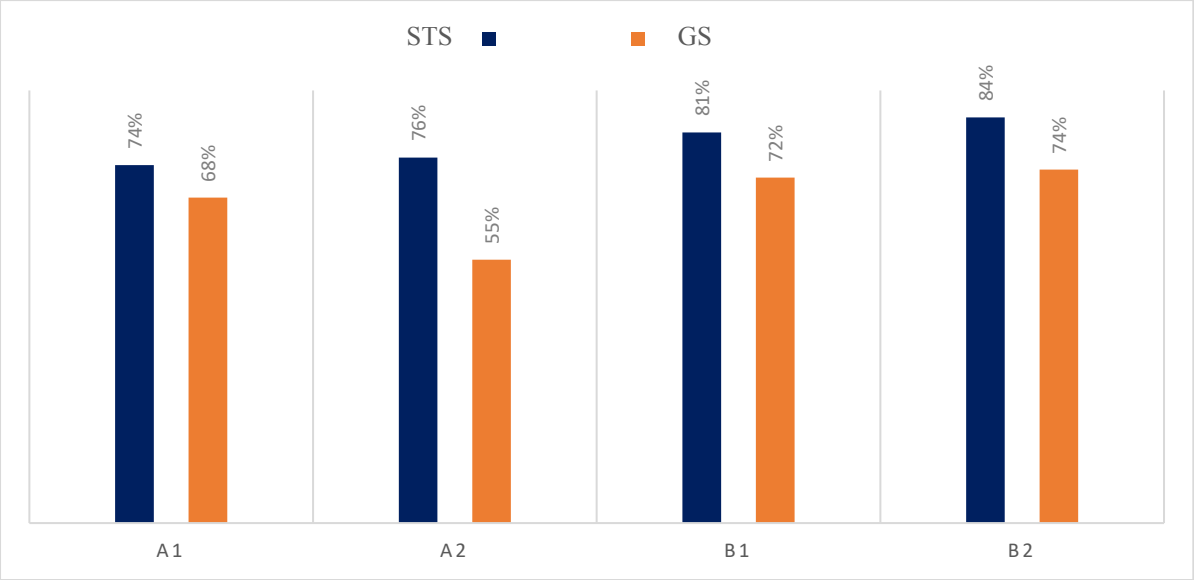

Chart 5: Percentage of correct answers by division to a finished school and age
(Source: own study)

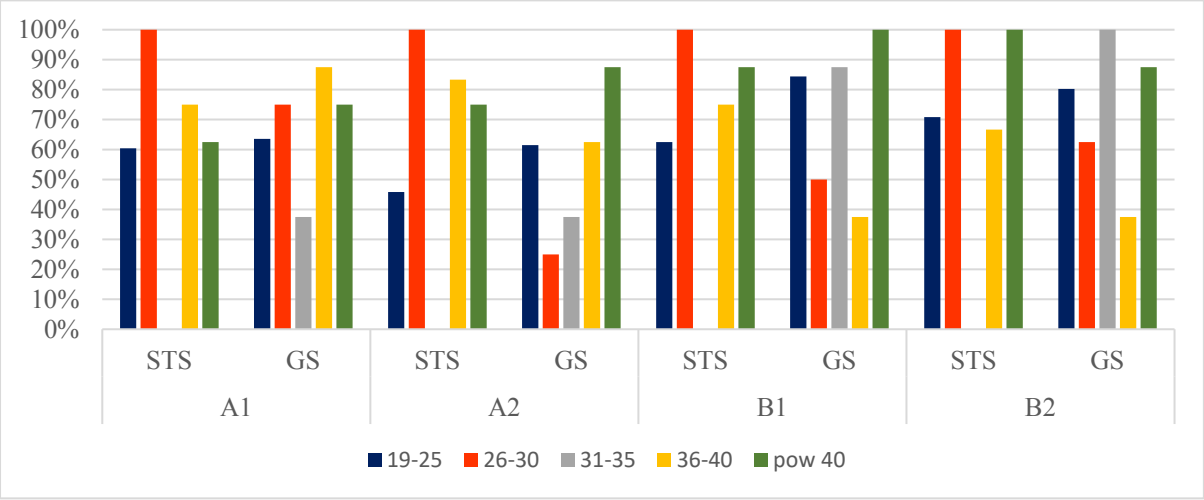

5. DISCUSSION

The conducted experimental research based on the completed test have demonstrated that many students have problems with spatial mapping. This is particularly evident with respect to students who start their education immediately after secondary school. The mapping skills of people who start studies, but who have completed apprenticeships, e.g. in design offices, looks completely different. In their case, changing the position of objects, rotating them in different planes is not an obstacle to spatial vision.

The test results in terms of the correctness of answers indicate that a significant proportion of students have difficulties in perceiving and working with three-dimensional objects. In addition, there are big problems in understanding depth perception and adding the third dimension. The scale of the difficulty also results from the observation position of the element and its complexity.

Based on the conducted tests, the lecturer can define how and which issues of the teaching curriculum in the course should be modified to improve spatial perception among young people. The results (Chart 1, Chart 2, Chart3, Chart 4, Chart5) have identified problems that require deeper analysis.

The authors of the article propose several solutions, the introduction of which may result in the improvement of effectiveness in teaching:

- reinforcement of the emphasis on shaping the work with a model, where physical models are used for both reading and drawing up technical documentation. Working with a model as a process of accurate association and development of spatial thinking. The construction of a model generates many benefits in the process of describing three-dimensional space through better understanding of structure and form. The introduction of paper, plasticine or spatial elements (e.g. blocks) to reinforce the emphasis on shaping the imagination by constructing and using the model, both for drawing purposes and reading of drawings. Such work should convince students about the flexibility and universality of its application.
- Additional training for people who received the lowest number of points in the test. Here, the such meetings would be conditioned by the need to carry out tests which would not be anonymous. During the workshops, the task can be corrected many times and students can work step by step with the possibility to consult the teacher at any time. Such a system will allow the students to eliminate mistakes and to have them explained. Such a form of work with students increases the likelihood of raising the level of their awareness and provides better results in further work.
- teamwork - working in a group viewed as an opportunity to adapt one's capability and knowledge to the level of others, with simultaneous consultation with the teacher. The unquestionable advantage of this method is the ability to raise students' own competences through competition in a group (I want to match others and I will do everything to be appreciated). Work in small groups enforces active behavior and promotes practical action.
- dividing the students into laboratory groups in line with the level of knowledge (determined on the basis of test result). The realization of the teaching curriculum should be universal and flexible with the possibility to modify and adapt to changing needs. As an example, we can mention advanced laboratory groups for whom the realized tasks should provide the opportunity to broaden the development of space perception and not slow it down. Education focused on solving problems by choosing effective teaching methods in accordance with the level of knowledge of students and by developing interesting support materials encouraging further work.

6. CONCLUSIONS

The tests had very positive opinions obtained from the students. A large part of them wanted to know their results and discuss individual tasks. The students wanted to take the test again so that they could confront their results. Therefore, we can conclude that they would be interested in the future in the testing system in which the test is not anonymous.

The main conclusions of the research are as follows:

- in the entire test the easiest question turned out to be question 1 and the most difficult question 4. The authors' assumption regarding the division into easy and difficult questions was incorrect. For students, the questions in which the line is located only on 3 walls were more difficult, which the authors initially described as easy examples,
- with respect to the way of looking at the element, the situation in which the observer of the cubic element looks at the block in which the front wall is the front view was easier to handle (Fig. 3a),
- part B of the test proved to be easier for both men and women, where the spatial model was indicated based on the flat element (net). Yet, for women it was easier to answer questions where the line was drawn on three walls. In turn, for men it was less difficult to answer questions in which the line was introduced on 6 walls of the element,
- working people were much better at solving the prepared test,
- persons, who graduated from secondary technical schools outweigh correct answers persons who completed grammar schools,
- the group of students who graduated from technical secondary school in the 26-30 age group is definitely the best,
- it was surprising that none of the examined persons wanted to use the physical model when analyzing the examples.

The assessment of the students' solutions of the tests demonstrates that spatial imagination is an individual feature of each person. The conducted research resulted in the implementation of the authorial test, based on which answers were obtained on the advancement level of space perception of the first semester students. In addition, the direction for further classes in the subject of descriptive geometry and technical drawing for the examined group of students (semester II) was defined. At this stage of studies, teaching should be focused on practicing visual perception of engineering objects, i.e. the reception of space using the sense of sight and mapping the seen image onto a flat sheet of paper. Furthermore, the realization of the test provided answers on the subject of differences in visual perception of students depending on gender, and whether a given person works in the profession or has completed specialist internships, which is presented in the results of this study. Particular attention should be paid to encouraging students to work with a physical model. The test results demonstrated that they were reluctant to resort to such teaching aids. It should be remembered that using a model generates many benefits involving better understanding of spatial structure, construction and function.

Further research will be focused on the implementation of the test by the authors of the research study for students starting studies at the faculties where they teach, i.e. civil engineering, architecture and urban planning. Such an approach is effected by very positive feedback involving the test, provided by the students. In the following years, the authors want to focus on taking the test before and after the course in the first semester of engineering studies. In this way, we can gather a lot of information about the way classes are conducted and about the progress in the development of space perception by students during the course of descriptive geometry and engineering graphics. The results obtained by the authors are motivating to introduce changes in the implementation of tasks for students of various levels of advancement and for people who have vocational experience. The obtained data has clearly indicated that such persons are better at solving spatial tasks. In addition, conducting workshops for students with the lowest number of points scored in the test will make it possible to better understand the issues raised in the following semesters. Another direction of further research involves the expansion of the scope of questions and the development of tests in the electronic form. Such a form of training in space perception undoubtedly appeals to students nowadays. They represent a generation for whom working with a smartphone can be a pleasant form of acquiring knowledge and training of spatial imagination. Another direction of research that the authors will present in the next study is the development of a test for students, which will be corrected by the student - they check their works by themselves. This will allow them to independently analyze and evaluate the made mistakes based on the physical model, which they will be permitted to use to find the correct answer. This approach teaches the students analytical work and allows them to define the problem which they find difficult to deal with.

Students with a high level of visual-spatial intelligence, i.e. people who according to H. Gardner "are sensitive to details, draw a lot, present their ideas graphically and orientate themselves in three-dimensional space without problems" should be able to perform tasks requiring three-dimensional thinking. The skills they possess provide ease of orientation and mental rotation. Students who have lower level of that relation have much bigger problems in the reception of information between a two-dimensional drawing and a spatial image. The presentation method of the test, 3D model and net unfolding – they represent the correlation that is taking place in engineering projects between the model and the drawing (building and design) and their interrelationship.

References

1. Baranová, L. and Katrenicová, I., 2018. Role of Descriptive geometry course in development of students' spatial visualization skills. *Annales Mathematicae et Informaticae*, 49. pp 21-32.
2. Bennett, G. K. and Seashore, H. G. and Wesman, A. G., 1973. Differential aptitude tests, forms S and T. The Psychological Corporation, New York, USA.
3. Binnet, A and Simon, T., 1905. Sur la necessite d'etablir un diagnostic scientifique des etats infereurs de l'intelligence. *L'annee Psychologique*, 11. pp. 163-190.
4. Bodner, G. M. and Guay, R. B., 1997. The PurdueVisualization of Rotations Test. *The Chemical Educator*, 2(4). pp 1-17.
5. Buckley, J. and Seery, N. and Canty, D., 2019. Investigating the use of spatial reasoning strategies in geometric problem solving. *International Journal of Technology and Design Education, 29. pp* 341- 362.
6. College Entrance Examination Board. (1939). CEEB special aptitude test in spatial relations. New York, USA.
7. Erkan Yazici, Y., 2016. The Relationship Between Cognitive Style and Visual Spatial Intelligence of First Year Architectural Students. *Kastamonu Eğitim Dergisi*, 25(2). pp 805-820.
8. Fay, E., and Quaiser-Pohl, C., 1999. Schnitte—Ein Test zur Erfassung des räumlichen Vorstellungsvermögens. Frankfurt, Germany: Swets Test Services.

9. Galton, F., 1879. Generic images. *The Nineteenth Century*, 6(1). pp 157–169.
10. Gardner, H., 1995. Frames of Mind: Theory of Multiple Intelligences. Fontana Press, New York, USA.
11. Gittler, G. 1990. Dreidimensionaler Würfeltest 3DW. Beltz Test. Weinheim, Germany.
12. Godfry, G. S., 1999. Three-Dimensional Visualization Using Solid-Model Methods. A Comparative Study of Engineering and Technology Students. Unpublished PhD dissertation. Northern Illinois University, USA.
13. González Campos, J. S. and Sánchez-Navarro, J. and Arnedo-Moreno, J., 2019. An empirical study of the effect that a computer graphics course has on visual-spatial abilities. *International Journal of Educational Technology in Higher Education*, 16(41). pp 1-21.
14. Górska, R. A., 2005. Spatial Imagination | an Overview of the Longitudinal Research at Cracow University of Technology. *Journal for Geometry and Graphics*, 9(2). pp 201-208.
15. Guay, R. B., 1977. Purdue spatial visualization test: Rotations, West Lafayette: Purdue Research Foundation.
16. Kopaliński, W., 1994. Dictionary of foreign words and synonyms. WP, Warsaw, Poland.
17. Leopold, C., 2005. Geometry education for developing spatial visualisation abilities of engineering students. *The Journal of Polish Society for Geometry and Engineering Graphics*, 15. pp 39-45.
18. Lohman, D. F. and Kyllonen, P. C., 1983. Individual differences in solution strategy on spatial tasks. In Dillon R. F. and R. R. Schmeck R. R., Individual Differences in Cognition. First edition. Academic Press. New York, USA.
19. Maier P.H., 1996. Spatial geometry and spatial ability: How to make solid geometry solid? In E. Osnabrück, Cohors-Fresenborg, K.Reiss, G. Toener, & H. Weigand (Eds.), Selected papers from the annual conference of didactics of mathematics, Germany.
20. Martı´n-Gutie´rrez, J. and Luı´s Saorı´n, J. and Contero, M. and Alcan˜iz, M. and Pe´rez-Lo´pez, D.C. and Ortega, M., 2010. Design and validation of an augmented book for spatial abilities development in engineering students. *Computers & Graphics*, 34. pp 77-91.
21. Marunić, G. and Glažar, V., 2014. Improvement and assessment of spatial ability in engineering education. *Engineering Review,* 34(2). pp 139-150.
22. Maruszewski, T., 2016. Psychology of cognition. The mind and the world. GWP, Gdansk, Poland.
23. Merchant, Z. and Goetz, E. T. and Keeney-Kennicutt, W. and Kwok, O. and Cifuentes, L. and Davis T. J., 2012. The learner characteristics, features of desktop 3D virtual reality environments, and college chemistry instruction: A structural equation modeling analysis. *Computers & Education*, 59. pp 551-568.
24. Miller, C. L. and Bertoline, G. R., 1991. Spatial visualization research and theories: Their importance in the development of an engineering and technical design graphics curriculum model. *Engineering Design Graphics Journal*, 55(3). pp 5–14.
25. Quaiser-Pohl, C., 2003. The Mental Cutting Test „Schnitte" and the Picture Rotation Test – Two New Measures to Assess Spatial Ability. *International Journal of Testing*, 3(3). pp 219-231.
26. Seery, N. and Canty, D. and Buckley, J., 2018. A Heuristic Framework of Spatial Ability: a Review and Synthesis of Spatial Factor Literature to Support its Translation into STEM Education. *Educational Psychology Review*, 30. Pp 947-972.
27. Sorby, S. A., and Górska, R. A., 1998. The Effect of Various Courses and Teaching Methods on the Improvement of Spatial Ability, The 8th International Conference on Engineering Design Graphics and Descriptive Geometry, Austin, USA.
28. Sorby, S. A., 1999. Developing 3-D spatial visualization skills. *Engineering Design Graphics Journal*, 63(2). pp 21-32.
29. Sorby, S. A., 2009. Educational research in developing 3–D spatial skills for engineering students. *International Journal of Science Education*, 31(3). pp 459-480.
30. Sroka-Bizoń, M. and Terczyńska, E., 2013. Perception of View – How to Develop Spatial Imagination. *The Journal Biuletyn of Polish Society for Geometry and Engineering Graphics*, 25. pp 19-26.
31. Uygan, C. and Kurtuluş A., 2016. Effects of Teaching Activities via Google Sketchup and Concrete Models on Spatial Skills of Preservice Mathematics Teachers. *Turkish Journal of Computer and Mathematics Education*, 7(3). pp 510-535.
32. Vandenberg, S. G. and Kuse, A. R., 1978. Mental rotations, a group test of three dimensional spatial visualization. *Perceptual and Motor Skills*, 47. pp 599–604.

ONE METHOD FOR REAL TIME VISUALISATION OF EEG DATA

Bojan Banjac
Computer graphics chair, Faculty of Technical Sciences, University of Novi Sad, Novi Sad, Serbia
PhD., Assistant Professor, bojan.banjac@uns.ac.rs

Miljan Đorđević
Student at Faculty of Electrical Engineering, University of Belgrade, Belgrade, Serbia
dm170264d@student.etf.bg.ac.rs

Milica Janković
Signals and systems Department, University of Belgrade, Belgrade, Serbia
PhD., Assistant Professor, piperski@etf.bg.ac.rs

Branko Malešević
Department of Applied mathematics, University of Belgrade, Belgrade, Serbia
PhD., Full Professor, malesevic@etf.bg.ac.rs

Jelena Sučević
Department of Experimental Psychology, University of Oxford, Oxford, United Kingdom
PhD., Postdoctoral Research Associate, jelena.sucevic@psy.ox.ac.uk

ABSTRACT

Human brain wave reading instruments have been around for quite some time, although many of the imaging tools currently used are limited in their scope and often produce data that is hard to read. In this paper, we aim at creating a real time platform for brain wave visualization. Electroencephalograms come in many different forms, the main differentiator being number of electrodes featured. This platform is mainly targeted at the researchers in this field and people who work with electroencephalographic devices on a regular basis, but struggle with currently available visualizing software. It is developed using open source solutions. Visualization is done in 3D, with five different types of brain waves – alpha, beta, gamma, delta and theta, visualized in a distinct manner.

Keywords: computer graphics; electroencephalography; brain waves; 3D imaging;

1. INTRODUCTION

Electroencephalography (EEG) has found many applications. Its primary area of application is neuroscience. Today EEG is used in areas of research such as observing cognitive functions of the children (Taylor et al., 2002), study of brain functions of persons with Schizophrenia (Stelt, 2007) and search for markers of chronic pain and sleepiness (Camfferman et al., 2017), but it can also be used as a tool to help patients with Alzheimer's disease (Ienca et al., 2017). It has even found its way to the neuromarketing (Yadava et al., 2017). From EEG was developed one of its most used applications – brain computer interface (BCI).

Brain computer interfaces were discussed very quickly with the rise of digital computers (Vidal, 1973). It took two decades for BCI to reach the level of development for the real time data reading (Lotte et al. 2015). There are many engineering problems that are still present even with the current systems, and very broad expert knowledge

will be needed to solve them. One of the most obvious examples is that the different systems of the electrodes are still being discussed, as they all have their cons and pros (Chi et al., 2010). Electrical engineers are working on removing artefacts and noise that appears on BCI readings (Janani et al., 2018). Researchers in machine learning are working on ways to classify different pattern that appear in read data (Tsuji et al., 1999, Roy et al.,2019, Craik et al., 2019).

While there is still great space for improvements of BCI, they attract great attention, and present us with many possibilities. Application to prosthetics, such as those shown in paper of Guger et al., 1999, were one of first to be presented. While they are still in development, they show great promise. Some software applications as interface for users to interact with graphical environment in 3D and 2D applications were discussed by Rai et al., 2016. Gaming industry has also shown interest in BCI as these devices can be used as control interface (Kerous et al., 2018), way to measure difficulty level (Girourard et al., 2009) or to simply, quantifiably and impartially measure user experience (McMahan et al., 2015). Even researchers from data protection and identity verification fields are considering using these devices as means for identity authentication (Ashby et al., 2011, Pham et al.,2013).

Most research in EEG today is conducted using BCI. These devices measure the electrical activity of brain on the large number of points along the scalp. Frequency of this electrical activity is then analyzed, as to determine activity of in some spectral range. Most common classification is to Alpha (from 8Hz to 12Hz), Beta (from 12Hz to 35Hz), Gamma (above 35Hz), Delta (less than 4Hz) and Theta waves (from 4Hz to 8Hz) according to Abhang et al., 2016. It has been shown that activity on certain frequencies corresponds to specific brain and body function. Thus, researchers do not analyze one wavelength but values on these ranges.

Goal of research presented in this paper is to develop new approach to visualization of EEG data. While there are many researchers who work on visualization of EEG data (such as Schreiber et al., 2017, O'Brien et al., 2019, Hassan et al., 2015, Anderson et al., 2013) most of these visualizations focus on traditional methods for representing signals. Idea that we present here is to use 3D graphics to represent data in such a way that it allows users to spot significant patterns that appear in EEG data.

2. SUPERSHAPES AND SUPERFORMULA

One of first things that can be seen when working with standard tools for EEG data acquisition and processing is that most of them use analogue electrical signal representation techniques. These representations are great at observing the singular aspect of obtained signal (as shown in Figure 1.). Frequency analysis shows which frequency is the most present in signal. Wave form graph gives change of the value over time. Histogram gives which the value is most present in some time window. All of these methods can show patterns in the singular aspect, but it is very hard to find patterns formed over several aspects of signal.

As basis for our visualization we used Supershape (Matsuura, 2015). Supershape is generated by the following equation (also called Superformula):

$$\frac{1}{r} = \sqrt[q]{\left|\frac{1}{a}\cos\left(\frac{m_1\varphi}{4}\right)\right|^{p_1} + \left|\frac{1}{b}\sin\left(\frac{m_2\varphi}{4}\right)\right|^{p_2}}.$$

Supershape has shown some great properties for data visualization. It can change significantly with change of single parameter. On Figure 2. we can see several different Supershapes. They have very different shapes, and all were obtained by slight change of parameters. By observing different shapes, and parameters that lead to them, users can with time learn how each parameter affects the shape. They can also quickly assess the activity in each of the observed frequency ranges. This creates more intuitive way to observe the different wavelength activity of EEG than the several separated waveform diagrams. Color of figures can be also used as one of the parameters, as humans are very perceptive to it.

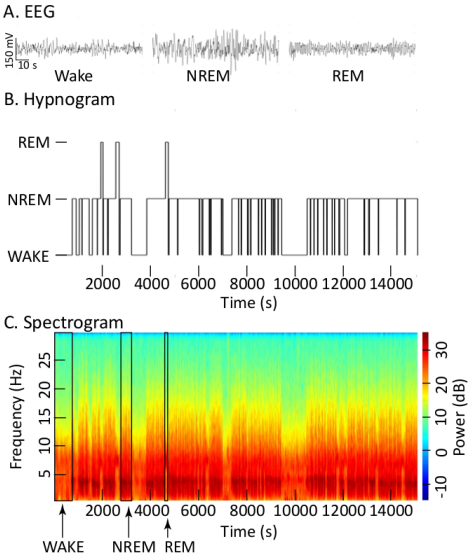

Figure 1: Standard ways of presenting EEG data (Source: O'Brien, 2019)

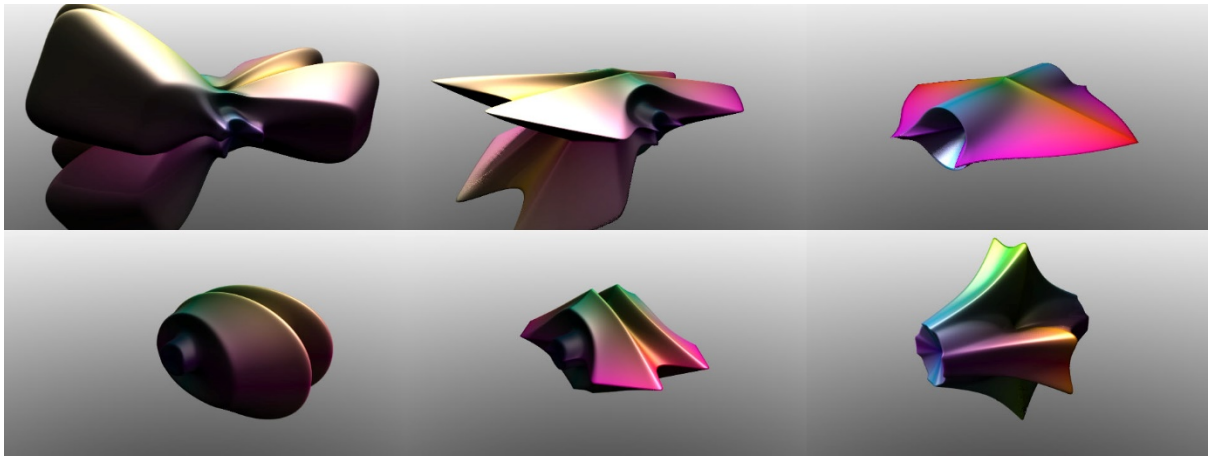

Figure 2: Supershape with different parameters (Source: renderings created by online application www.shadertoy.com)

3. APPLICATIO OF SUPERSHAPE FOR EEG DATA VISUALIZATION

Our visualization uses open source solution for obtaining EEG data. We selected OpenBCI as a good starting point. It allows researchers to write their own data processing code in programming languages Java and Processing. While it has limited number of data acquisition nodes, it still allows us to demonstrate the principles of our visualization. With more nodes it is possible to use aggregation functions that would show data from several nodes on same supershape.

EEG channel values dictate the change of the parameters in the superformula and dictate the look of the supershape. Supershape is always changing color, and the speed of the change is dictated by one of the channels. User can change the neutral look of the supershape by changing the default values of parameters used in the supershape formula. Values of parameters impact the size, whether surface consists of the blobs or the spikes, surface smoothness, spike/blob size, the density, the length and the number of symmetry axis on the sphere. Parameters can be set in such a way that we can see the object from inside, or make the object have holes. System in its current state uses prerecorded data which it reads from textual files, but a real time expansion would consist of simply changing the input stream to a desired EEG device. As we used Processing programming language for coding of visualization, code can easily be embedded into webpage code using p5.js Javascript library, or used for some embedded device. As shown in Figure 3. shape can dramatically change with change of input data. Users

are able to select which type of waves and with what intensity affects parameters, so they can control shapes which will appear. This helps users to see patterns with much more ease.

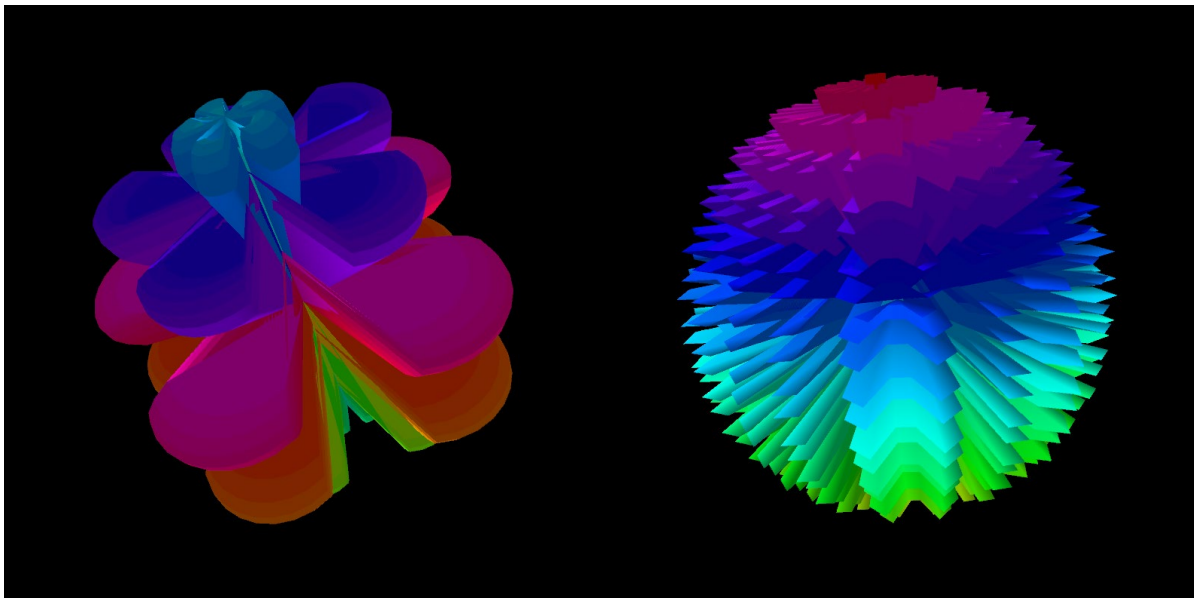

Figure 3: The properties of the supershape for different values of EEG channels varies greatly

4. CONCLUSION

We have successfully created an EEG data visualizer which can be used to monitor brain wave activity in real time. Our system gives new approach to data representation and it allows researchers in this field observe data about all frequency ranges in single image. System is written in such a way that it can be easily transferred to some other platform. Some further research goals are to allow for several nodes to be represented in simple way as well as to even further improve quality of visualization.

REFERENCES

1. J. J. Vidal, 1973. *Toward direct brain-computer communication*, Annual review of Biophysics and Bioengineering, vol. 2, no. 1, pp 157–180.
2. C. Guger, W. Harkam, C. Hertnaes, and G. Pfurtscheller, 1999. *Prosthetic control by an eeg-based brain-computer interface (bci)*, in Proc. aaate 5th european conference for the advancement of assistive technology. Citeseer, , pp 3–6.
3. F. Lotte, L. Bougrain, and M. Clerc, 2015. *Electroencephalography (eeg)-based brain–computer interfaces*, Wiley Encyclopedia of Electrical and Electronics Engineering, pp. 1–20
4. B. Kerous, F. Skola, and F. Liarokapis, 2018. *Eeg-based bci and video games: a progress report*, Virtual Reality, vol. 22, no. 2, pp 119– 135
5. T. McMahan, I. Parberry, and T. D. Parsons, 2015. *Modality specific assessment of video game players experience using the emotiv*, Entertainment Computing, vol. 7, pp 1–6,
6. Y. Roy, H. Banville, I. Albuquerque, A. Gramfort, T. H. Falk, and J. Faubert, 2019. *Deep learning-based electroencephalography analysis: a systematic review*, Journal of neural engineering
7. D. Camfferman, G. L. Moseley, K. Gertz, M. W. Pettet, and M. P. Jensen, 2017. *Waking eeg cortical markers of chronic pain and sleepiness*, Pain Medicine, vol. 18, no. 10, pp 1921–1931
8. R. Rai and A. V. Deshpande, 2016. *Fragmentary shape recognition: A bci study*, Computer-Aided Design, vol. 71, pp 51–64
9. M. Ienca, J. Fabrice, B. Elger, M. Caon, A. S. Pappagallo, R. W. Kressig, and T. Wangmo, 2017. *Intelligent assistive technology for alzheimers disease and other dementias: a systematic review*, Journal of Alzheimer's Disease, vol. 56, no. 4, pp 1301–1340,

10. A. Girouard, E. T. Solovey, L. M. Hirshfield, K. Chauncey, A. Sassaroli, S. Fantini, and R. J. Jacob, 2009. *Distinguishing difficulty levels with non-invasive brain activity measurements*, in IFIP Conference on Human-Computer Interaction. Springer, pp 440–452
11. A. Craik, Y. He, and J. L. Contreras-Vidal, 2019. *Deep learning for electroencephalogram (eeg) classification tasks: a review*, Journal of neural engineering, vol. 16, no. 3, p. 031001
12. Y. M. Chi, T.-P. Jung, and G. Cauwenberghs, 2010. *Dry-contact and noncontact biopotential electrodes: Methodological review*, IEEE reviews in biomedical engineering, vol. 3, pp. 106–119
13. A. S. Janani, T. S. Grummett, T. W. Lewis, S. P. Fitzgibbon, E. M. Whitham, D. DelosAngeles, H. Bakhshayesh, J. O. Willoughby, and K. J. Pope, 2018. *Improved artefact removal from eeg using canonical correlation analysis and spectral slope*, Journal of neuroscience methods, vol. 298, pp. 1–15
14. Toshio Tsuji, Osamu Fukuda, Hiroyuki Ichinobe, and Makoto Kaneko, 1999. *A Log-Linearized Gaussian Mixture Network and Its Application to EEG Pattern Classification*, IEEE Transactions on systems, man and cybernetics – Part C: Applications and reviews, , vol. 29, no. 1
15. M.J. Taylor. T. Baldeweg, 2002. Application of EEG, ERP and intracranial recordings to the investigation of cognitive functions in children, Developmental Science 5:3, pp 318–334
16. Mahendra Yadava, Pradeep Kumar, Rajkumar Saini, Partha Pratim Roy, Debi Prosad Dogra, 2017. *Analysis of EEG signals and its application to neuromarketing,* Multimedia Tools and Applications 76:19087–19111
17. Odin van der Stelt, Aysenil Belger, 2007. Application of Electroencephalography to the Study of Cognitive and Brain Functions in Schizophrenia, Schizophrenia Bulletin vol. 33 no. 4 pp 955–970
18. Tien Pham, Wanli Ma, Dat Tran, Phuoc Nguyen, and Dinh Phung, 2013. *A Study on the Feasibility of Using EEG Signalsfor Authentication Purpose,* ICONIP 2013, Part II, LNCS 8227, pp 562–569
19. Corey Ashby, Amit Bhatia, Francesco Tenore, and Jacob Vogelstein, 2011. *Low-Cost Electroencephalogram (EEG) based Authentication,* Proceedings of the 5th International IEEE EMBS Conference on Neural Engineering Cancun, Mexico
20. Masaya Matsuura, 2015. *Gielis' superformula and regular polygons*, Journal of Geometry, 106, pp 383–40
21. Schreiber G., Lin H., Garza J., Zhang Y., Yang M., 2017. *EEG Visualization and Analysis Techniques.* In: Xu D., Wang M., Zhou F., Cai Y. (eds) Health Informatics Data Analysis. Health Information Science. Springer, Cham
22. O'Brien, C. B., Baghdoyan, H. A., Lydic, R., 2019. *Computer-based Multitaper Spectrogram Program for Electroencephalographic Data*. Journal of Visualized Experiments. (153), e60333
23. Hassan M, Shamas M, Khalil M, El Falou W, Wendling F, 2015. *EEGNET: An Open Source Tool for Analyzing and Visualizing M/EEG Connectome*. PLoS ONE 10(9): e0138297.
24. E. W. Anderson, C. Chong, G. A. Preston and C. T. Silva, 2013. *Discovering and visualizing patterns in EEG data*, IEEE Pacific Visualization Symposium (PacificVis), Sydney, NSW, pp 105-112
25. OpenBCI – open source BCI headset https://openbci.com/
26. Priyanka A. Abhang, Bharti W. Gawali, Suresh C. Mehrotra, 2016. *Technological Basics of EEG Recording and Operation of Apparatus*, Editor(s): Priyanka A. Abhang, Bharti W. Gawali, Suresh C. Mehrotra, Introduction to EEG- and Speech-Based Emotion Recognition, Academic Press, pp 19-50,

TOPIC 4: GEOMETRY, GRAPHICS EDUCATION AND TEACHING METHODOLOGY

CONTENT

DIAD-TOOLS PLATFORM AS A REALIZATION OF THE IDEA OF EDUCATIONAL COOPERATION

Monika Sroka-Bizoń
Department of Building Processes and Building Physics, Silesian University of Technology, Gliwice, Poland
PhD., Associate Professor, monika.sroka-bizon@polsl.pl

Piotr Dudzik
Department of Building Processes and Building Physics, Silesian University of Technology, Gliwice, Poland
PhD., Lecturer, piotr.dudzik@polsl.pl

Tatjana Sankauskiene
Vytautas Magnus University. Agriculture Academy, Kaunas, Lithuania
PhD., Associate Professor, tatjana.sankauskiene@vdu.lt

Ewa Terczyńska
Department of Building Processes and Building Physics, Silesian University of Technology, Gliwice, Poland
PhD., Assistant Professor, ewa.terczynska@polsl.pl

Jolanta Tofil
Department of Building Processes and Building Physics, Silesian University of Technology, Gliwice, Poland
PhD., Assistant Professor, jolanta.tofil@polsl.pl

Krzysztof Tytkowski
Department of Building Processes and Building Physics, Silesian University of Technology, Gliwice, Poland
PhD., Senior Lecturer, krzysztof.tytkowski@polsl.pl

Antanas Vansevicius
Vytautas Magnus University. Agriculture Academy, Kaunas, Lithuania
PhD., Associate Professor, antanas.vansevicius@vdu.lt

ABSTRACT

Education is all activities and processes that enable people to get to know nature, society, and culture, and at the same time participate in their transformation, as well as the most comprehensive development of their physical and mental fitness, interests and abilities. The education process is based on teaching and learning and involves the participation of teachers and learners. General education enables the acquisition of general qualifications (knowledge, skills and values) necessary for everyone, regardless of their social and professional role. Vocational education ensures qualifications in the chosen specialty. The content and forms of education processes are determined by the general learning objectives formulated as part of individual concepts of general and vocational education. Traditionally, three levels of education are distinguished: basic, also called elementary, secondary, i.e. enabling preparation for higher and higher studies. The idea of the concept of vocational education implemented at two complementary levels of education, secondary and higher, is one of the main objectives of the project No2017-1-LT01-KA202-035177 "Development of Interactive Animated Teaching Tools - DIAD-tools, implemented from October 1, 2017 to 31 March 2020, as part of the Erasmus + Strategic Partnership program, by partners from

Estonia, Latvia, Lithuania, Slovakia and Poland. Representatives of technical secondary vocational schools and technical universities participate in the design work. The cooperation of teachers conducting vocational education at two levels of education has enabled the identification of basic thematic issues, which as the content of education appears in the curricula of subjects such as drawing, technical drawing or engineering graphics, at the secondary and higher level of vocational education. The authors will present the implementation of the concept of the internet platform developed as part of the DIAD-tools project containing interactive and animated teaching materials supporting the independent learning of secondary technical school pupils and technical university students in the field of geometry and technical drawing. The article will present: the idea of compiling and complementing the process of vocational education implemented at secondary and higher levels in the field of geometry and technical drawing, four main thematic blocks within which didactic materials were developed, and the scope of detailed issues developed in individual blocks.

Keywords: geometry, technical drawing, architectural drawing, constructional drawing, CAD, teaching tools

1. INTRODUCTION

Education is all activities and processes enabling people to get to know nature, society, and culture, and at the same time to participate in their transformation, as well as the most comprehensive development of their physical and mental fitness, interests, and abilities. The education process is based on teaching and learning. The implementation of the education process involves the participation of teachers and learners. General education allows the acquisition of general qualifications (knowledge, skills) necessary for everyone, regardless of their social and professional role. Vocational education ensures qualifications in the chosen specialty. The content and forms of education processes are determined by the general learning objectives formulated as part of individual general and vocational education concepts. Traditionally, three levels of education are distinguished: basic, also called elementary; medium, i.e. enabling preparation for university and higher education, among others. Higher education implemented as part of technical universities is largely conducted within scientific disciplines in the field of engineering and technical sciences, and a graduate of a technical university has the opportunity to obtain a professional title - engineer. The education programs for particular fields of engineering studies are formulated in such a way that the future engineer obtains qualifications enabling conducting professional activities in the field of broadly understood technique. One of the basic skills of an engineer is the ability to use technical drawing, which is *the basic form of expressing the creative thought of an engineer - designer. With the help of a drawing the engineer - the designer presents to the engineer - the contractor his concept of the building e.g. a house, machine, road, bridge, river regulation, spatial development of a certain area and many, many other three-dimensional works that work of engineering art. Drawing plays the role of a means of mutual communication among engineers and technicians, just as the written word fulfills this goal among all humanity* (Szerszeń, 1955) (Sroka-Bizoń, et al., 2019).

Technical drawing in educational programs of various fields of engineering studies occurs under many names - as a classic "technical drawing", extremely popular in the 90s of the 20th century and used to date now, the "engineering graphics", "CAD mapping" or "description of the construction". Regardless of the names of the subjects in the curricula, careful study of the curriculum content of these subjects and the objectives and learning outcomes adopted in the curriculums allows us to state that each time we are dealing with the subject of the teaching that is to ensure a person who is studying the subject acquires skills related to passive and active use of technical drawing. The technical drawing as an important subject for engineering education, in some measure basic in vocational education, is conducted in the first years of study, thanks to which students, with appropriate initial preparation, can participate in classes in design subjects that are envisaged in higher education programs years.

Studies at technical universities are undertaken by persons with secondary or higher education, which may have the character of general or vocational education. They can be graduates of various types of secondary schools - artistic, general, technical. Often students of the first year of study with an engineering profile become those persons already studying at a technical university or university, undertaking studies in the second field of study. Technical studies are also undertaken by graduates of universities or technical colleges. Therefore, the student group joining the first year of technical studies is often an extremely diverse group in the skills that individual members have. The "boon" of the variety of skills students have at their disposal also applies to technical drawing classes. One group of students can comprise of people who have not yet encountered the issues of mapping spatial objects on the drawing plane, as well as skilled draftsmen, authors of drawing studies related to the design of machinery or structures. Conducting the course of the subject in a way that allows all students to broaden their knowledge and acquire new skills is a great challenge for academic teachers. Additional

aspects hindering the implementation of education in the field of technical drawing to the satisfaction of all participants in this process are the duration of the course and continuous, over recent years, limiting the number of teaching hours allocated to classes.

In the dynamically changing reality of the modern world, the learner's ability to self-educate is becoming increasingly important in the education process. The independent acquisition of knowledge by students from various sources: from traditional printed textbooks and task sets, electronic versions of these studies and teaching materials available on the Internet, is becoming an indispensable part of learning.

Especially that every teacher knows that you cannot teach anyone anything, you can only help those who want to learn by themselves (Cieśla, 2020).

2. DIAD-TOOLS PLATFORM

At present, the Internet is one of the basic sources in which pupils and students look for materials that support learning. (Klok, 2018) Extensive resources of online educational materials also include technical drawing issues. Materials available on the web have a diverse character, including websites devoted to various issues such as orthographic views or axonometry; payable internet courses dedicated to the use of computer programs; materials developed by individual Internet users, commercial companies, and educational institutions. The wealth of resources of online materials can be a boon for a network user, but the conscious use of these resources requires the user to be able to search and select materials in terms of their reliability and substantive correctness. Therefore, an extremely valuable supplement to educational online resources is the dissemination of materials developed by specialists from individual scientific disciplines.

The main goal of the project No 2017-1-LT01-KA2020-035177 "Development of Interactive and Animated Teaching Tools" - DIAD-tools, implemented from October 1, 2017, to March 31, 2020, as part of the Erasmus + Strategic Partnership program, was to create an online platform containing interactive and animated materials supporting the study process of technical drawing, which would be characterized by the following values:

- usefulness - the selection of issues enabling the use of materials by both technical secondary school students and technical university students,
- comprehensiveness - the selection of issues in the field of technical, mechanical as well as architectural and construction drawing,
- substantive - verified content of materials in terms of scientific correctness and compliance with applicable European standards,
- accessibility - materials developed in the form of short films and interactive exercises available in 6 different languages - English, Estonian, Lithuanian, Latvian, Polish and Slovak,
- openness - open access to materials.

The concept of developing online teaching materials for pupils and students was also the implementation of the idea of the concept of vocational training in technical drawing, implemented at two complementary levels of education, secondary and higher.

The project partners:

- Vilnius Builders Training Centre (the project coordinator, Lithuania),
- Slovak University of Technology in Bratislava (Slovakia),
- Ida-Virumaa Vocational Eduaction Centre (Estonia),
- Vytautas Magnus University. Agriculture Academy (Lithuania),
- The Lithuanian Society of Engineering Graphics and Geometry (Lithuania),
- Riga Technical University (Latvia),
- Panevezio kolegija/University of Applied Sciences (Lithuania),
- Silesian University of Technology (Poland),

from 5 European Union countries, represented 7 medium and higher education institutions and a scientific association of Lithuanian specialists in the field of engineering graphics and geometry. Each of the partners involved in project implementation activities involved project participants, who were: teachers of technical secondary schools, teachers of technical universities, pupils of technical secondary schools, students of technical universities, and entrepreneurs. Establishing cooperation between technical teachers of secondary schools and academic teachers of technical universities dealing with education in the field of technical drawing, engineering graphics, and geometry enabled the analysis of the program scope of the subject 'Technical drawing' implemented at two levels of vocational education. The cooperation of partners and project participants also made it possible to examine the applied teaching methods in the field of the subject, which are used in technical

secondary schools and technical universities. Surveys conducted in the first stage of the project in a group of 56 entrepreneurs, 149 teachers and 349 pupils/students were the basis for distinguishing:

- issues in technical drawing courses at both levels of education for which the development of interactive and animated teaching materials would be particularly useful,
- issues with the highest degree of difficulty in assessing pupils / students,
- the preferred form of teaching materials to support learning (Vansevicius A., 2018 The Report of the Needs Analysis Survey, February 2018, pp. 1-42).

The presented charts are part of the full report of the need's analysis survey, they show divergence in the assessment of difficult issues in the field of technical drawing indicated by students and teachers (**Fig.** 1, **Fig.** 2).

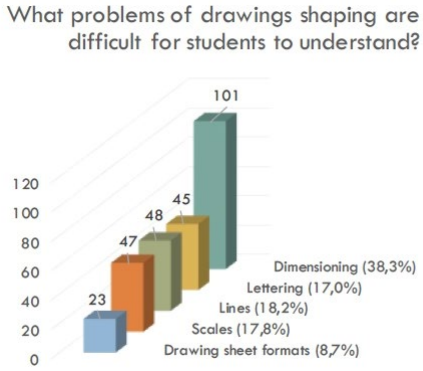

Figure. 1. A graph showing the percentage distribution of answers listing the difficulty of individual issues in the basics of technical drawing – based on teacher's responses.

(Source: Vansevicius A., 2018, The Report of the Needs Analysis Survey, p. 11, February 2018, p. 1-42)

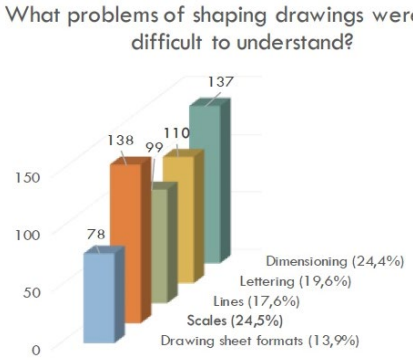

Figure. 2. A graph showing the percentage distribution of answers listing the difficulty of individual issues in the basics of technical drawing – based on student's responses.

(Source: Vansevicius A., 2018, The Report of the Needs Analysis Survey, p. 20, February 2018, pp. 1-42)

In the group of teacher answers, the leading issue is dimensioning, in students' assessment dimensioning and scales are equally difficult issues. All difficult issues identified by students and teachers were included in the developed didactic materials of the project.

2.1. The interactive and animated didactic materials

For the needs of the online DIAD-tools platform, project partners have developed, in 6 languages 37 animated and interactive materials presenting selected issues in the field of technical drawing, which create a universal set of teaching materials for pupils and students.

The developed animated materials fall into four main thematic groups (**Fig.** 3):

- Execution of drawings. Geometric drawing – 13 animated material developed by Vytautas Magnus University. Agriculture Academy, Lithuania,
- Basics of projection drawing. Views. Sectional Views. Sections – 5 animated materials developed by Slovak University of Technology in Bratislava, Slovakia,
- Joints of parts. Working drawings parts – 5 animated material developed by Riga Technical University, Latvia,
- Construction drawing – 6 animated materials developed by Silesian University of Technology, Poland.

The interactive material developed by Slovak University of Technology in Bratislava, include the following issues:

- Monge Method,
- Multiview Projections EU norm,
- Multiview Projections – USA norm,
- Intersections of solid,
- Object reconstruction,
- Reconstruction in Monge method,
- Cube planar cuts.

Figure. 3: The English version of the DIAD-tolls platform – four main groups of topics

(Source: https://liggd.lt/diad-tools/gb/training-materials)

2.2. The adopted concept of the structure of animated teaching materials on the example of two thematic groups

2.2.1. Execution of drawings. Geometric drawing

It was planned to create 5 interactive learning tools to enable learning to draw both by hand and using a computer (AutoCAD program). The materials were to cover the following basic issues:

- scales,
- lines on engineering drawings and their application in practice,
- dimensioning,
- curves and smooth connections and their application in practice,
- dividing the circles into equal parts and drawing polygons.

In total, 13 tutorials were created: 5 focused on hand-drawing, 3 focused on drawing construction realized with AutoCAD, and 5 focused on the method of designing based on full cloud computing system Onshape.

According to the basic assumption of the DIAD-tools project, the latest ISO system requirements have been taken into consideration when preparing the material. One of the other assumptions adopted in the structure of materials was to present the basic issues of technical drawing in relation to examples occurring in the reality surrounding the pupil/student (**Fig.** 4).

Figure. 4: The graphic layout used in the material titled "Polygons" dedicated to basic definitions of polygons.

(Source: https://liggd.lt/diad-tools/gb/training-materials)

5 tutorials from the group "Execution of drawings. Geometric drawing" are examples of the use of the relatively new Onshape 3D CAD system, a full cloud computing data system (**Fig.** 5) (Vansevicius, 2019).

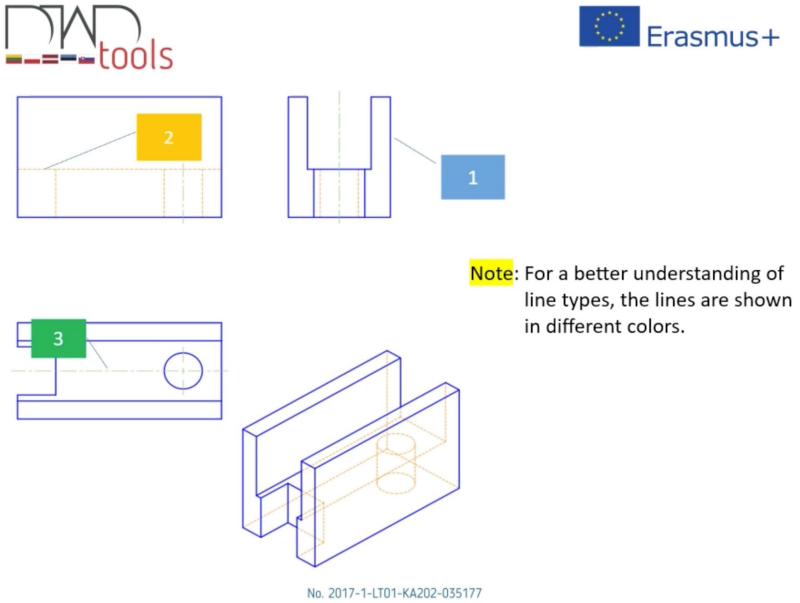

Figure. 5: The graphic layout used in the material titled "Lines on engineering drawings – Onshape". The spatial object designed in Onshape was presented in orthographic projections (main views) and in axonometry - the teaching material presents the structure of the object and the automated process of creating drawing project documentation.

(Source: https://liggd.lt/diad-tools/gb/training-materials)

2.2.2. Construction drawing

The concept of developing didactic materials in the form of short animated instructions presenting the basic issues of individual thematic blocks was adopted in three instructional parts:

- part 1. Architectural and construction drawing general principles,
- part 3. Dimensioning at architectural-construction drawings,
- part 5. Construction elements,

the same concept of material distribution was adopted - the axonometric drawing illustrates the spatial problem of the discussed topic, and the orthographic projection of the building object is used to present the method of preparing the architectural drawing. The verbal commentary in the form of a description of the drawings describes the problem presented (**Fig.** 6.).

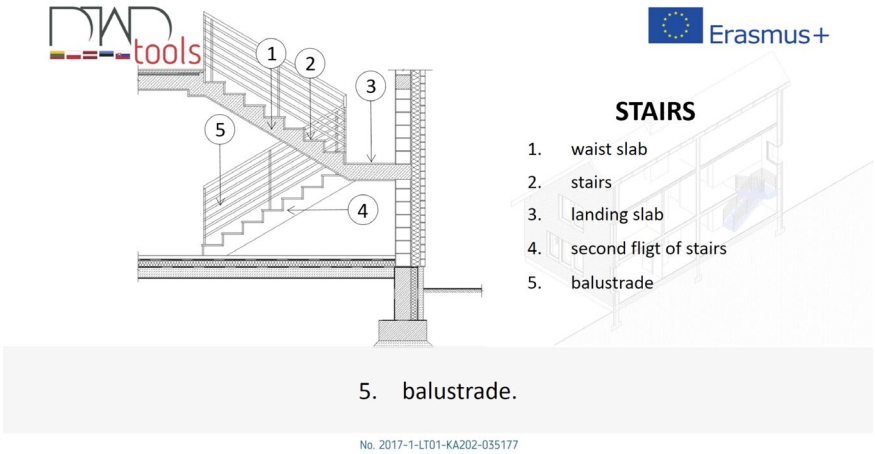

Figure. 6: The graphic layout used in three parts of teaching materials in the field of architectural-construction drawing - axonometric drawing, orthographic projection of a building object and verbal commentary discussing the presented issue

(Source: https://liggd.lt/diad-tools/gb/training-materials)

Parts related to the scales used in architectural and construction drawings and the graphic designation of building materials required the adoption of a different arrangement of materials because they are a form of an illustrated dictionary of terms. Also, the part devoted to the test in the field of architectural and construction drawing was developed in a different layout, because it is a compilation of thematic issues discussed in other parts of materials (**Fig.** 7.). As in all didactic materials developed under the project, the musical background was introduced in all parts of the teaching materials from the thematic group "Construction drawing". This was one of the general technical assumptions adopted in the project.

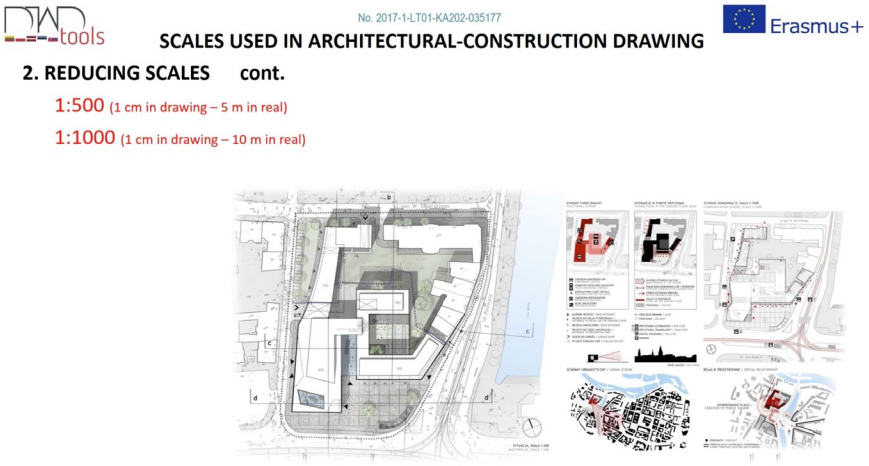

Figure. 7: The graphic layout used in the didactic material dedicated to scales used in architectural-construction drawing – the illustrated dictionary of terms.

(Source: https://liggd.lt/diad-tools/gb/training-materials)

CONCLUSIONS

Based on the research carried out as part of the project and the cooperation established between the partners and project participants, it can be concluded that there is a strong need to integrate various activities within education. Identifying the needs for planned educational activities is extremely important.

The cooperation between teachers of technical secondary schools and academic teachers of technical universities gives the opportunity to develop universal teaching materials in the field of technical drawing that can be used by pupils of technical secondary schools as well as students of technical universities.

Changes in the methods of learning and teaching in all fields of science related to the dynamic dissemination of Internet access, the constantly decreasing number of hours allocated for learning technical drawing in curricula and study plans make it necessary to develop professional teaching materials for self-study. Didactic materials in the field of technical drawing developed as part of the DIAD-tools project can constitute such materials.

Open access to developed didactic materials and their availability in six languages suggest that they will constitute a significant supplement to the existing didactic offer on the Internet. The advantage of the developed materials may be the fact that they have been prepared by teachers, practitioners from specific fields.

A huge problem in the field of learning and teaching technical drawing is the lack of open access to ISO and EU standards. This also applies to the possibility of comparing the full content of drawing standards valid in the countries of project partners. This was particularly important in the context of developing teaching materials in the field of construction drawing.

Some tutorials from the group "Execution of drawings. Geometric drawing" are examples of the use of the relatively new Onshape 3D CAD system, a full cloud computing data system. This system is still difficult to accept for some users, because *old habits die hard, and many designers will prefer to continue using software they are most familiar with* (Bethany, 2016). Teaching materials were prepared for pupils and students who begin studying technical drawing. Therefore, in ~~a~~authors' opinion, the presentation of the basic issues of technical drawing in relation to the latest computer technologies is extremely important. Especially today in the context of the COVID-19 pandemic and the resulting need for remote work, the special advantages of cloud data computing have been particularly evident (Vansevicius, 2019).

Based on the evaluation of the didactic materials developed in the DIAD-tools project, which was carried out in spring 2018, it can be concluded that the materials were developed correctly in terms of methodology and content.

Pupils and students from all countries of the project partners assessed them directly in the formulated assessments as useful and helpful in the independent learning of drawing.

Materials were evaluated in a similar way by experts from individual project partner countries. The expert assessment was carried out in parallel with the assessment of project participants, which are pupils and students from Estonia, Latvia, Lithuania, Poland and Slovakia.

In authors' opinion, it would be valuable to develop and improve already developed materials and expand the thematic scope not included in the didactic materials developed as part of the project.

REFERENCES

1. Cieśla, J., 2020. E-studia, czyli eksperyment na studentach, p. 29, Tygodnik POLITYKA No 18 (3259), pp. 29-30.
2. Sroka-Bizoń, M., Tytkowski, K., Vansevicius, A., Velichova, D., Dobelis, M., 2019. Do engineers use an international language? Construction drawing as a way of communication between engineers. Journal for Geometry and Graphics 2019, vol. 23, No 1, pp. 115-126.
3. Vansevicius, A., 2019. Cloud-based technologies in technical drawing. The Journal of Polish Society for Geometry and Engineering Graphics Volume 32 (2019), pp. 35 – 38.
3. Szerszeń, S., 1955. Geometria Wykreślna. Studium Zaoczne Politechniki Warszawskiej, Warszawa, Polska.
4. DIAD-tools platform, 2020, https://liggd.lt/diad-tools/gb/training-materials [Accessed: 14st May 2020].
5. Klok, B., 2018 Internet jako wiarygodne źródło informacji, *intromedia*, https://www.intro.media/artykuly/internet-jako-wiarygodne-zrodlo-informacji [Accessed: 14st May 2020].
6. Bethany, Jul 28, 2016 How Will the Cloud Impact on CAD? https://www.scan2cad.com/cad/will-cloud-impact-cad/ [Accessed: 14th May 2020].

PERFORMANCE-BASED DESIGN IN ARCHITECTURAL AND URBAN PLANNING EDUCATION

Ivana Bajšanski
Department of Architecture, University of Novi Sad, Novi Sad
PhD., Assistant Professor, ivana_b@uns.ac.rs

Bojan Tepavčević
Department of Architecture, University of Novi Sad, Novi Sad
PhD., Associate Professor, tepavcevicb@uns.ac.rs

ABSTRACT

In the previous several years, performance-based design becomes very important area of research in the field of architectural and urban planning education. In contemporary practice, this approach is used as a method for modelling sustainable and intelligent urban design. Taking into account rapid development of various software applications for solar and computational fluid dynamic (CFD) simulations, students are able to create different urban designs with different geometry, and select the final design with optimal performances. In order to obtain the best solution, user has to consider climate and weather data, location, position, orientation and geometry of an urban fabric. The aim of this paper is to emphasize the importance of introducing performance-based design and software applications into student's education. Contrary to traditional procedure of urban modelling, computational parametric modelling in combination with solar and CFD simulations allows a lot of opportunities as well as fewer mistakes in the beginning of urban planning process. In this paper will be shown how urban area can be redesigned in order to minimise or maximise solar or CFD influence on selected urban area. Students used the geometrical parameters of width and height of buildings, streets, change position and geometry of urban furniture and find the best solution.

Keywords: performance-based design; urban design; solar simulations; CFD simulations; architectural education

1. INTRODUCTION

In the previous several years, performance-based design is very important area of research in the field of architectural and urban planning education (Klemm et al., 2015; Taleb and Musleh, 2015). There are a several various methods to improve human thermal comfort in open urban spaces. Some of these are insolation mitigation during summer period or wind reduction during winter period (Li et al., 2007; Amado and Poggi, 2014; Benni et al., 2016) or improvement of outdoor thermal comfort during both periods (Bröde et al., 2012; Blazejczyk et al., 2012; Yahia and Johansson, 2014). Based on geometrical characteristic of urban environment and possibility to change it, issue which implies uncomfortable conditions of stay on urban spaces could be solved. Geometrical characteristics are height and position of buildings (Bajšanski et al., 2015), disposition, size and number of trees (De Abreu-Harbich et al., 2015; Bajsanski et al., 2016; Milošević at al., 2017) and shape of urban mobiliar, such as canopies, pergolas (Bajsanski et al., 2017). In contemporary practice, rapid development of computer software applications in previous decades lead to a numerous programmes which have opportunity to examine some performance of urban environment based on climate and geographical data (Shi and Yang, 2013). Among these, in combination with parametrical and procedural modelling, a lot of combination which implies geometry

changing can be simulated interactively. For insolation analysis, user can used Ecotect software, which is connected with Grasshopper, software application for parametrical modelling. CFD (Computational Fluid Dynamics) analysis enables wind simulations in various software applications, eg. Simulation CFD 2015. For thermal comfort analysis, Ladybug, Grasshopper add-on, is used in research (Roudsari, 2013). Climate and geographical data of selected location or city are necessary part of each type of simulation.

Performance-based design is a powerful method for architectural and urban planning practice in the beginning of designing process, in order to prevent mistakes which are reflected on comfortable condition in open urban spaces. In this paper are presented various types of performance-based design application through students' works. The aim of this paper is to emphasize the importance of introducing performance-based design into students' education and practice as efficient method for creating more conscious urban design.

2. PERFORMANCE-BASED DESIGN IN ARCHITECTURAL AND URBAN PLANNING EDUCATION

Contrary to traditional ways to design architectural and urban environment, academic course Representation of Wider Spatial Environment at the Faculty of Technical Sciences explore new methods and software applications for design which is connected with parametric modelling. The course is a part of master programme Digital Techniques, Design and Production in Architecture and Urban Planning where students can learn about parametrical and procedural modelling, also. In order to find useful method to learn performance-based design, the issues refer to insolation mitigation, wind minimisation or improvement of outdoor thermal comfort during summer or winter period. The main point is to notice several parameters in urban environment which can be changed and which influences on final results. After every change of the geometry of urban environment, the software performs insolation simulation, wind analysis or simulation of outdoor thermal comfort. Some of students groups, for analysis selected various city areas and focused on changing geometry of buildings, streets and urban blocks. Other groups selected to analyse location and geometry of canopies.

3. STUDENT'S WORKS

In order to present the different methods and various approaches of performance-based design in architectural and urban planning education, students selected to perform insolation simulations of urban block of Grbavica (Novi Sad district), wind analysis on Petrovaradin fortress and simulation of outdoor thermal comfort on Podbara (Novi Sad district). Students used summer climate data for Novi Sad, in order to mitigate insolation and wind as well as improve outdoor thermal comfort conditions. The software applications enable a selection of year period (0-365 days) and day period (0-24 hours). Among these, climate data for any other city can be downloaded from internet (https://energyplus.net/weather).

a. Insolation analysis

Insolation analyses were performed on the urban block in Novi Sad, Grbavica district. The main aim of this project is changing buildings heights, slope and shape of the roofs in order to mitigate insolation on the ground during summer period. Geometry of 3d models is created in City Engine, where parameters of the mentioned geometrical characteristics are determined in some range. Buildings heights are defined in the range from 3m to 18m, the roof slope is in range from 0° to 60° and the shape of the roof could be flat, gable, pyramid or hip. The design of 3d model is changed after every slider movement and for each design the insolation analysis is performed in Ecotect software. Mentioned software applications are selected for teaching because they are applied in contemporary architecture and urban practice as well as many modern school of architecture. Very important in students future practice is to connect procedural with parametrical modelling in order to perform complex environmental analysis. Figure 1a-c show various cases of insolation depend of the selected geometry. The results shown, on the insolation mitigation the most influence has buildings heights and slope of the roof. Students performed around 50 simulations, but only three representatives are showed.

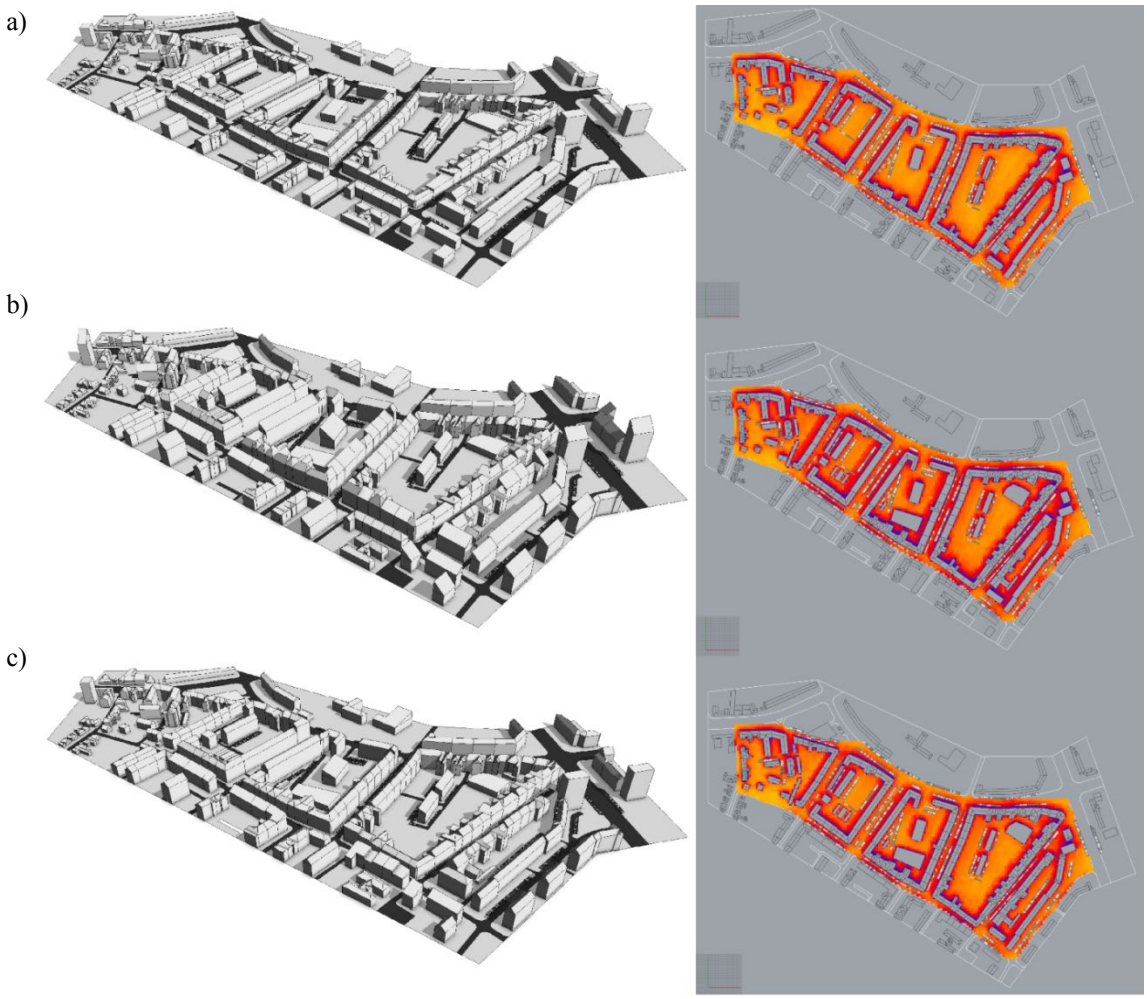

Figure 1. Insolation analysis of urban blocks with changing of floors number, slope and shape of the roofs. a) insolation result 1928Wh/m², b) insolation result 1678Wh/m², c) insolation result 1747Wh/m². Retrieved from students Nela Novakovic, Ognjen Jokic and Djordje Miletic.

b. Wind analysis

Wind simulations are performed on different places on the Petrovaradin fortress in order to find the best place to positioning scene stage. To find possible solution, it is necessary to examine more location and several shapes of the scene stage. The wind speed is approximately 20 m/s with northwest direction, characteristically for area of Novi Sad, and CFD simulations are performed in Simulation CFD software. Due to possibility to change 3D model of urban environment and noticing very small differences, this software application is appropriated for wind analysis in detailed urban areas. On the figure 2a and b are presented same locations with two different geometries of stage scene. Results show that free form stage design is better than cubical design, because the wind is slower in front of the stage, where the audience will stand and sit.

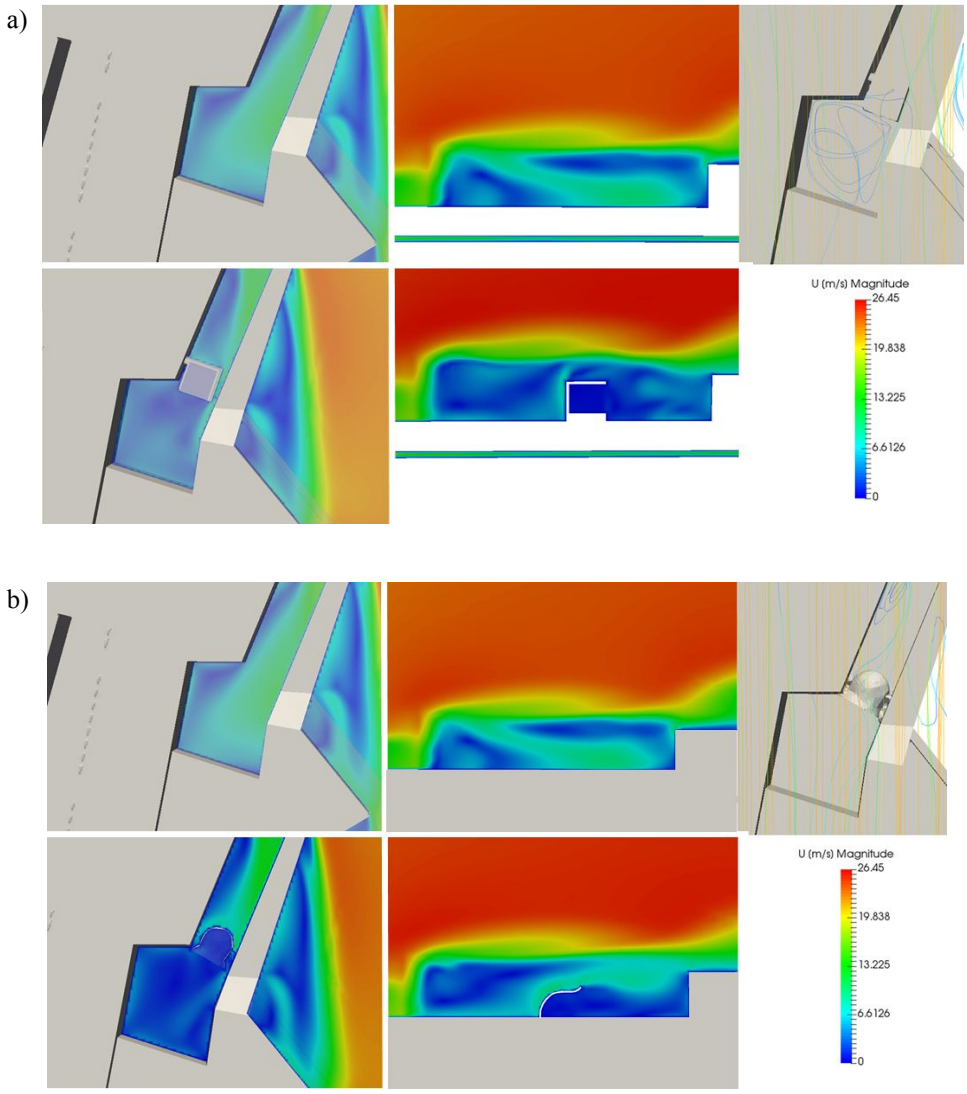

Figure 2. Wind simulation of two different geometries of scene stage: a) floor plan and section through cubical form, b) floor plan and section through free form. Retrieved from students Jovana Plavsic and Andrija Mihelcic.

c. Outdoor thermal comfort analysis

Simulations of outdoor thermal comfort are performed in Ladybug software application (Grasshopper add-on). Ladybug is directly connected with Rhinoceros, which allows noticing of outdoor thermal comfort results with any geometry changing. The aim of this project is to improve outdoor thermal comfort conditions in pedestrian zone, during summer period, by changing urban block typology. On the figure 3a are presented two blocks with different buildings locations and designs. On the figure 3b one block is shown also with three different buildings locations and designs. In order to examine level of outdoor thermal comfort, scale of universal thermal climate index (UTCI) has to be used. Depends on UTCI index values, the outdoor thermal comfort is evaluated. After a huge number of simulations, the best solution is selected.

a)

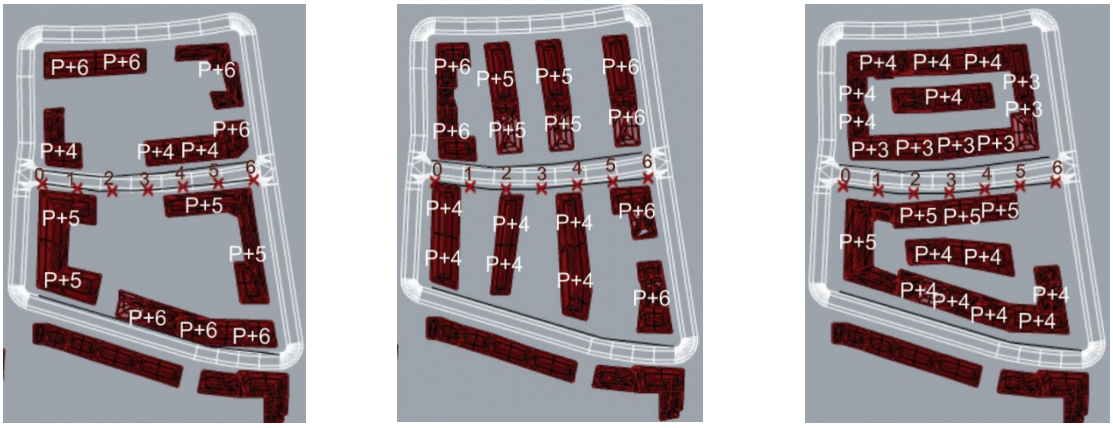

b)

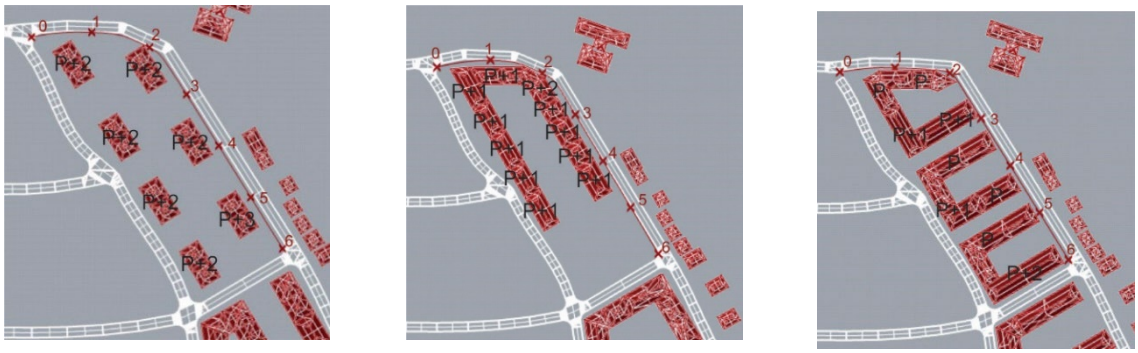

Figure 3. Simulations of outdoor thermal comfort with different building disposition within the urban block. Retrieved from students Biljana Cvijanovic, Milica Pajic, Dejana Cecavac and Jelena Maric.

4. CONCLUSION

Environmental simulation parameters such as wind flow, solar radiation or outdoor thermal comfort level are not often used in urban modelling process and in urban and architectural practice. In this research we have shown that various performance-based design tools can be used in the process of urban planning and design. Through the process of design optimization outdoor thermal comfort and urban planning can be improved in beginning stage of urban design. The advance of this novel approach is that computational parametric modelling in combination with solar and CFD simulations allow a lot of opportunities as well as fewer mistakes in the beginning of urban planning process.

In order to minimise or maximise solar or CFD influence on selected urban area this paper show various students work and investigation in different types of urban area. The significantly influence of wind and solar radiation is presented trough geometrical parameters and its change. The heights of buildings and roof slope have effect on results and can improve quality of outdoor thermal comfort conditions at public spaces. Additionally, such tools can be efficiently used in urban planning and architectural education. By using contemporary software applications students improve and wide their knowledge and observe urban design another way. After course of Representation of Wider Spatial Environment, students have very good knowledge about mentioned software applications, which allows a lot ideas to use software in architectural and urban practice. Knowledge about

softwares and its application is measured by high grades, from 8-10 in more than 80% of one student generation (about 20 students).

Software appliications allows import of climate and geographical data for any city and allows simulation performing on any world location. Further research will be directed toward implementation of these tools for different urban typologies on micro and macro level of the city.

REFERENCES

Amado, M. and Poggi, F., 2014. Solar urban planning: a parametric approach. Energy Procedia, 48, pp.1539-1548.

Bajsanski, I., Stojakovic, V. and Jovanovic, M., 2016. Effect of tree location on mitigating parking lot insolation. Computers, Environment and Urban Systems, 56, pp.59-67.

Bajsanski, I., Stojakovic, V., Tepavcevic, B., Jovanovic, M. and Mitov, D., 2017. An application of the shark skin denticle geometry for windbreak fence design and fabrication. Journal of Bionic Engineering, 14(3), pp.579-587.

Bajšanski, I.V., Milošević, D.D. and Savić, S.M., 2015. Evaluation and improvement of outdoor thermal comfort in urban areas on extreme temperature days: Applications of automatic algorithms. Building and Environment, 94, pp.632-643.

Benni, S., Tassinari, P., Bonora, F., Barbaresi, A. and Torreggiani, D., 2016. Efficacy of greenhouse natural ventilation: Environmental monitoring and CFD simulations of a study case. Energy and Buildings, 125, pp.276-286.

Blazejczyk, K., Epstein, Y., Jendritzky, G., Staiger, H. and Tinz, B., 2012. Comparison of UTCI to selected thermal indices. International journal of biometeorology, 56(3), pp.515-535.

Bröde, P., Krüger, E.L., Rossi, F.A. and Fiala, D., 2012. Predicting urban outdoor thermal comfort by the Universal Thermal Climate Index UTCI—a case study in Southern Brazil. International journal of biometeorology, 56(3), pp.471-480.

De Abreu-Harbich, L.V., Labaki, L.C. and Matzarakis, A., 2015. Effect of tree planting design and tree species on human thermal comfort in the tropics. Landscape and Urban Planning, 138, pp.99-109.

Energy Plus weather data, https://energyplus.net/weather, Accessed June 2019.

Klemm, W., Heusinkveld, B.G., Lenzholzer, S. and van Hove, B., 2015. Street greenery and its physical and psychological impact on thermal comfort. Landscape and Urban Planning, 138, pp.87-98.

Li, W., Wang, F. and Bell, S., 2007. Simulating the sheltering effects of windbreaks in urban outdoor open space. Journal of Wind Engineering and Industrial Aerodynamics, 95(7), pp.533-549.

Milošević, D.D., Bajšanski, I.V. and Savić, S.M., 2017. Influence of changing trees locations on thermal comfort on street parking lot and footways. Urban forestry & urban greening, 23, pp.113-124.

Roudsari, M.S., Pak, M. and Smith, A., 2013, August. Ladybug: a parametric environmental plugin for grasshopper to help designers create an environmentally-conscious design. In Proceedings of the 13th international IBPSA conference held in Lyon, France Aug.

Shi, X. and Yang, W., 2013. Performance-driven architectural design and optimization technique from a perspective of architects. Automation in Construction, 32, pp.125-135.

Taleb, H. and Musleh, M.A., 2015. Applying urban parametric design optimisation processes to a hot climate: Case study of the UAE. Sustainable Cities and Society, 14, pp.236-253.

Yahia, M.W. and Johansson, E., 2014. Landscape interventions in improving thermal comfort in the hot dry city of Damascus, Syria—The example of residential spaces with detached buildings. Landscape and Urban Planning, 125, pp.1-16.

TEACHING RIGGING FOR ANIMATION AT THE COMPUTER GRAPHICS - ENGINEERING ANIMATION STUDIES

Jelena Letić
Computer Graphics Chair, Faculty of Technical Sciences, University of Novi Sad
PhD Student, Teaching Assistant, jelena.letic@uns.ac.rs

Filip Mirčeski
Computer Graphics Chair, Faculty of Technical Sciences, University of Novi Sad
MSc Student, Teaching Associate, mirceski.filip95@gmail.com

IsidoraĐurić
Computer Graphics Chair, Faculty of Technical Sciences, University of Novi Sad
PhD Student, Teaching Assistant, isidoradjuric@uns.ac.rs

Ivana Vasiljević
Computer Graphics Chair, Faculty of Technical Sciences, University of Novi Sad
PhD Student, Teaching Assistant, ivanav@uns.ac.rs

Igor Kekeljević
Computer Graphics Chair, Faculty of Technical Sciences, University of Novi Sad
PhD., Assistant Professor, igor.kekeljevic@uns.ac.rs

Ratko Obradović
Computer Graphics Chair, Faculty of Technical Sciences, University of Novi Sad
PhD., Full Professor, obrad_r@uns.ac.rs

ABSTRACT

Rigging is a well-known process in the computer graphics field and represent an essential step in creating 3D animation. The technique is most common in games and movies, as well as in educative animations. Rigging is the process of the creating a virtual skeleton, composed of interconnected bones, for a character 3D model. The primary goal of rigging is to make it as easy as possible for the animator to do the animation (Maestri, 2002). Basic rigging involves building a skeleton and skinning the character. Both processes can be performed inside a software for 3D modeling which provides required modifiers and controllers. This paper present a teaching process of rigging for different types of the 3D models through the contents of undergraduate subjects of the Computer Graphics study program at the Faculty of Technical Sciences, at the University of Novi Sad. The paper presents examples of rigged models created by the second and third year students, as the supervised projects, done through three subjects of the Computer Graphics study program: Character Animation, Fundamentals of Engineering Animation and Aesthetics of Visual Communications. After completing these three courses, students acquire enough skills and knowledge for studying the basics of animation of rigid bodies and 3D characters.

Keywords: computer graphics; rigging; 3D animation; teaching

1. INTRODUCTION

The program for academic studies in Engineering Animation was established at the Faculty of Technical Sciences, University of Novi Sad in 2011 as an interdisciplinary program which connects the courses of electrical engineering and computer science with mathematics. This study program is designed to enable high quality education in interdisciplinary visualizations and in applying Computer Graphics in interdisciplinary researches in different fields (Obradović et al., 2010, Obradović et al., May 2019.).

Undergraduate Academic Studies last for four years and comprise 40 subjects, of which 31 are compulsory subjects and nine elective positions with a choice of several subjects (Obradović et al., 2012, Obradović et al., May 2019). During the studies, especially in professional courses, independent work is highly rated, students are encouraged to participate in professional and development projects, and the focus is on the development of the skills for solving real problems.

2. STUDY COURSES

By describing three assignments which students completed within three different courses during the fourth, the fifth and the sixth semester, we will present the process of developing the skills of rigging and skinning different types of characters. These subjects are studied through the following three courses: Character Animation - in the second year of study, Fundamentals of Engineering Animation and Aesthetics of Visual Communications, both in the third year. During the 15 weeks of a semester, the students have 60 classes of practical exercises in the computer laboratory for each of these courses (Obradović et al., 2019). Independent student work is accentuated, still it is supervised by teachers and teaching assistants.

2.1. Character Animation course

In the second year of study, students attend a Character Animation course which deals with following topics: drawing the basic 3D shapes and manipulation with basic 3D shapes, drawing the basic shape of 3D animation and animation of the basic figure. The students learn as well about rigid body animation, animal rigging with a relatively simple system of movement, and the creation of short films on these two topics (Stajić et al., 2016). The goal is to enable students to create characters and introduction to the basic requests of motion and frame, as well as study the space in the animated form.

The practical part of the course consists of two assignments and a Course project. The task in the Second assignment is to model, rig and animate animal character - the fish. Students can choose one of 80 offered fish types or create their own. After modeling the character, students practice rigging and skinning in order to animate the movement of the fish through the water as well as changing expression of its face. They are required to show a minimum of 7 different facial expressions and animation of transitions between them.

Process of rigging and skinning a fish character will be explained in detail in the next section.

2.1.1. Rigging and skinning a fish character

The aim of the Second assignment is to create and apply a simpler rig to the character of the fish. Details of the rig will be shown and explained on the 3D fish model that is shown in Figure 1.

Before starting the rigging process it is very important to explore how characters move, find a good anatomical reference, notice the different skeleton joint types and how to represent them best into the rig. Since a real fish has dozens of bones in spine only, it is necessary to do approximation of bones that will be sufficient to achieve the desired movement. Bones should be placed on key parts of the character, specifically, moving parts of body: spine, fins, head, and tail. Figure 2(a) shows the entire digital skeleton of a fish.

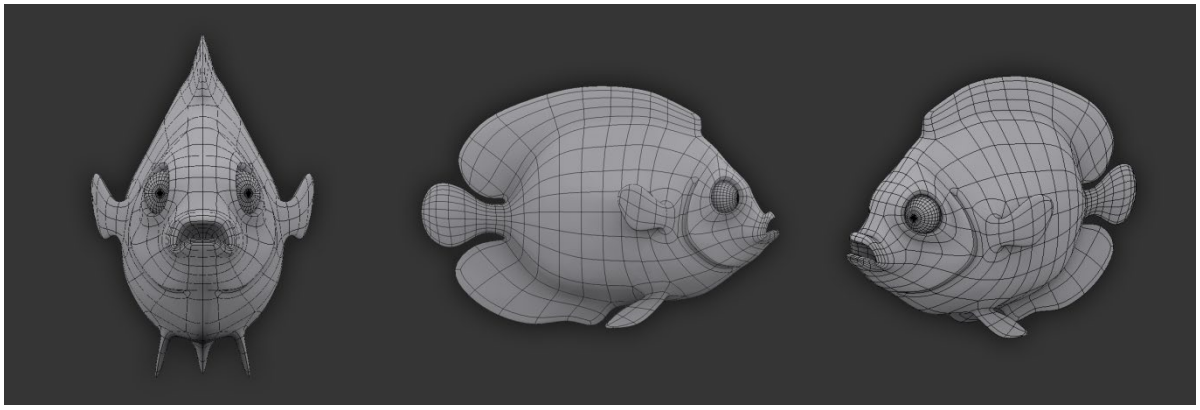

Figure. 1: Fish Character mesh

The bones in a rig are connected to form a hierarchical structure. The hierarchical structure can be seen metaphorically as 'a parent-child' relationship. 'A parent' is an object at the top of the hierarchy, while 'a child' is an object at the bottom of the hierarchy. In the digital skeleton of a fish, the spine represents 'the parent' in the hierarchical structure, and the fins are 'the child'.

After placing and connecting the bones, it is necessary to create controls outside of the geometry of the character in order to allow the animator easier control over the bones of the digital character. A well-organized control design is important topic - everything from the placement and shape of controls, to the level of detailed settings for control systems. Manipulation of numerous digital skeleton controls allows animator to move the character to the desired position. Figure 2(b) shows the controls of the digital character of the fish.

Specific requirements necessary to fulfill in this assignment are:

- Use *Morph Modifier* to present different facial expression,
- Use *Dummy/Helper* objects within the process of rigging and setting controls. It is necessary to place all helpers in a separate layer,
- Use *Freeze Transform/Transform to Zero* actions for each object within the process of rigging, and
- All elements and sub-elements of the 3D model(geometry, bones, controls and helpers) should be named according to the given specification. All elements should be arranged in layers and sub-layers

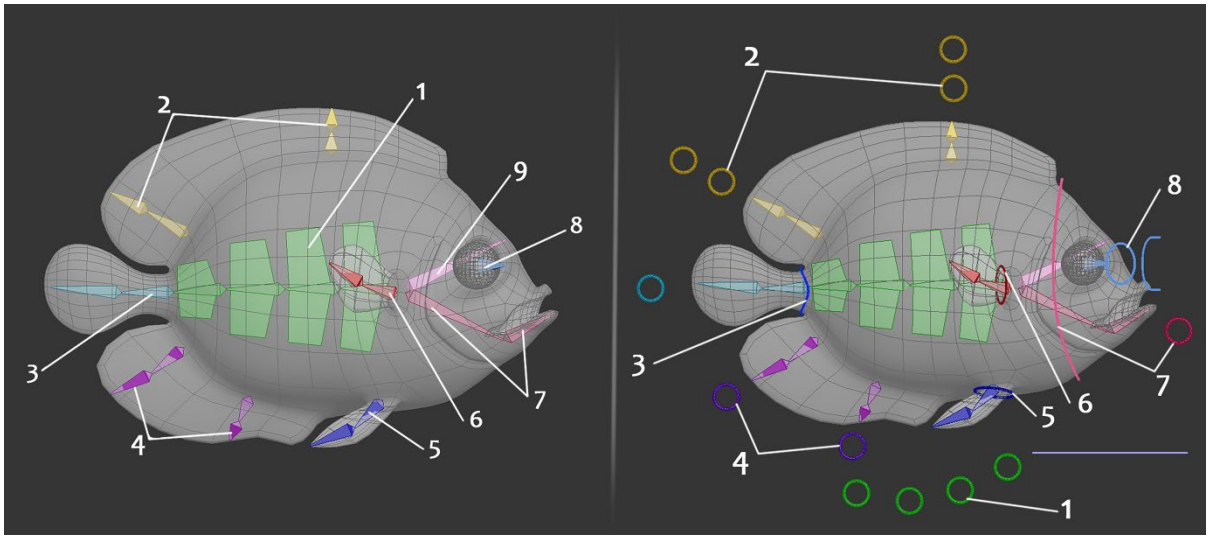

(a) (b)

Figure. 2: (a)Bones, and (b) Controls

Table 1

a.	*b.*
1. Spine bones	*1. Spine controls*
1. Top fins bones	*2. Top fins control*
2. Tail bones	*3. Tail control*
4. Down fins bones	*4. Down fins control*
5. Side fins down bones	*5. Side fins down control*
6. Side fins bones	*6. Side fins control*
7. Jaw bones	*7. Jaw control*
8. Eye bones	*8. Eye control*
9. Head bone	*9. Head control*

Skinning is the process of attaching the geometry (mesh) of a 3D model to the digital skeleton. For polygonal mesh character, the bone is associated with a group of vertices. Portions of the character's skin can be associated with multiple bones, each one having an influence factors called vertex weights.

Correct modeling and clean topology is important in order to make the skinning process easier and to create more realistic muscle movement and skin motion of the character. Topology should supports the correct creasing in required areas, thus an edge loops must be created around mouth, tail and fins. The influence of individual bones on the geometry of the model can be seen in Figure 4.

2.2. Fundamentals of Engineering Animation course

The course Fundamentals of Engineering Animation (FEA) is studied in the fifth semester and covers all the topics students learn in relation to different movements of manlike characters. The FEA course are the continuation of the previous three courses: Spatial Shape Design, 3D Modeling, and Character Animation (Obradović et al., 2019). Within these subjects, students are taught following topics: various techniques for modeling 3D shapes, texturing and mapping, various techniques of lighting and rendering, animations with rigid bodies and the use of constraints as well as rigging and controllers creating for animal with relatively simple skeleton.

The main topics covered in the FEA course are complex movements of manlike characters which are studied over four interconnected tasks. The first student task in fifth semester, called Project, is to model, rig and animate humanoid character. Students can create caricature or realistic character, with two legs, feet (with or without fingers), two hands and fingers (three or more), waist, chest, neck, head, two eyes on a head. Finally, rigged and skinned character should be set in 5 different poses. The advice to students is to choose the character pose and camera position for renders in which a character has aesthetically beautiful silhouette (Obradović et al., 2019). Process of rigging and skinning a humanoid character will be explained in detail in the next section.

2.2.1. Rigging and skinning a humanoid character

The humanoid character rig is more complex than the fish example shown in the previous section. Digital skeleton for humanoid character, in addition to hierarchical structure of bones, also contains more complex systems such as constraints and inverse kinematics. Details of the rig will be shown and explained on the 3D model that is shown in Figure 6.

Bones should be placed on moving parts of body. With reference to fish, the humanoid character also requires an approximation of the bones. For example, the human spine has 33 vertebrae, while the digital skeleton shown in Figure 7 has only 5 spine bones.

Constraints limits bone position, rotation, and scaling depending on parental bones. Among many different constraints, in this particular rig example it have been used: LookAt Constraint (used for eye rig), Position and Orientation Constraint (used for hand rig).

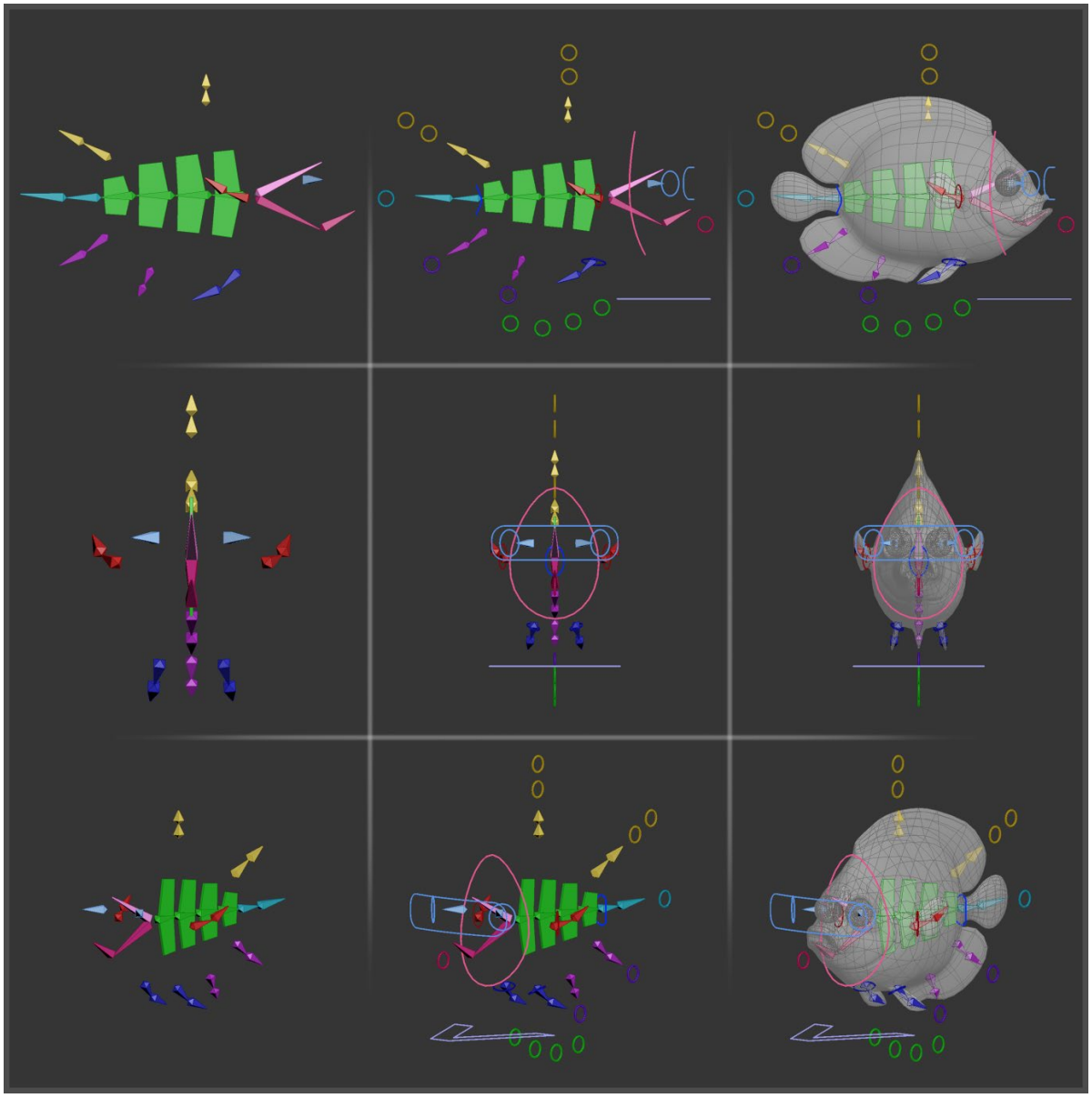

Figure.3: Fish rig from left, front and perspective view

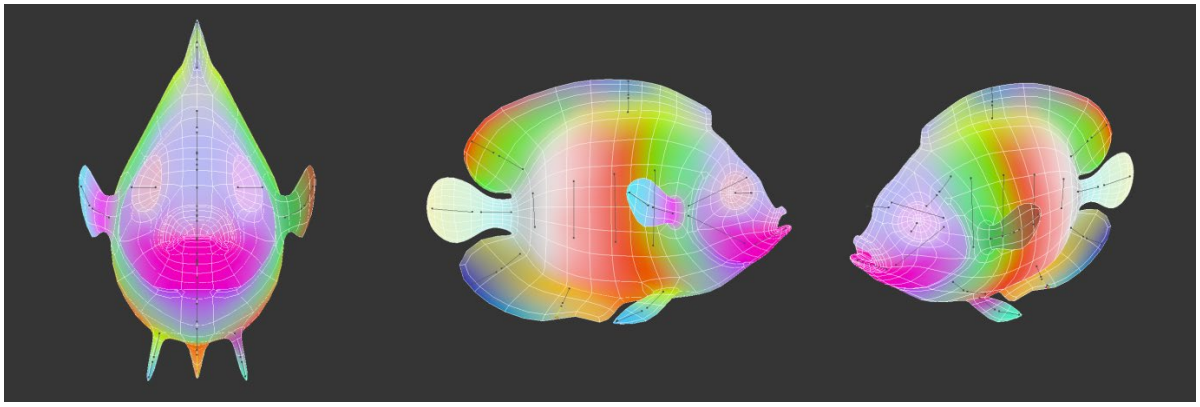

Figure. 4: Fish character skin preview

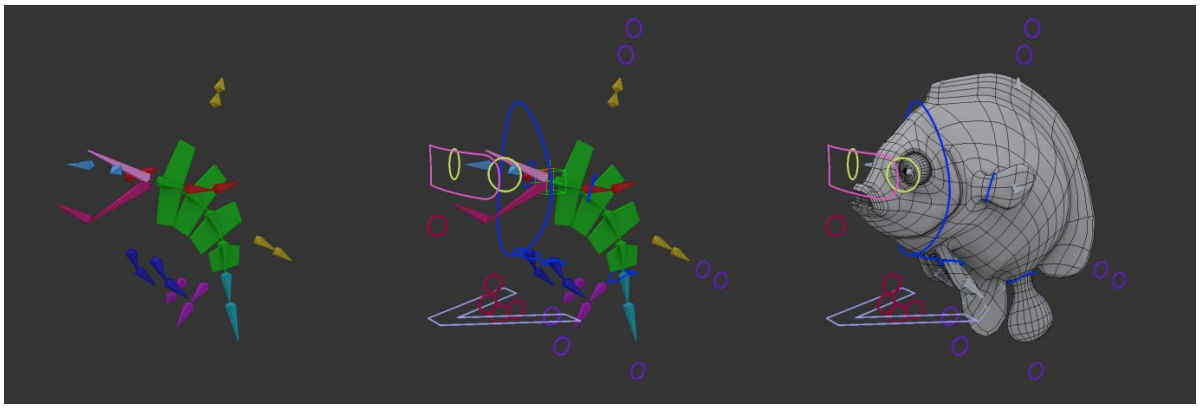

Figure. 5: Fish character in pose

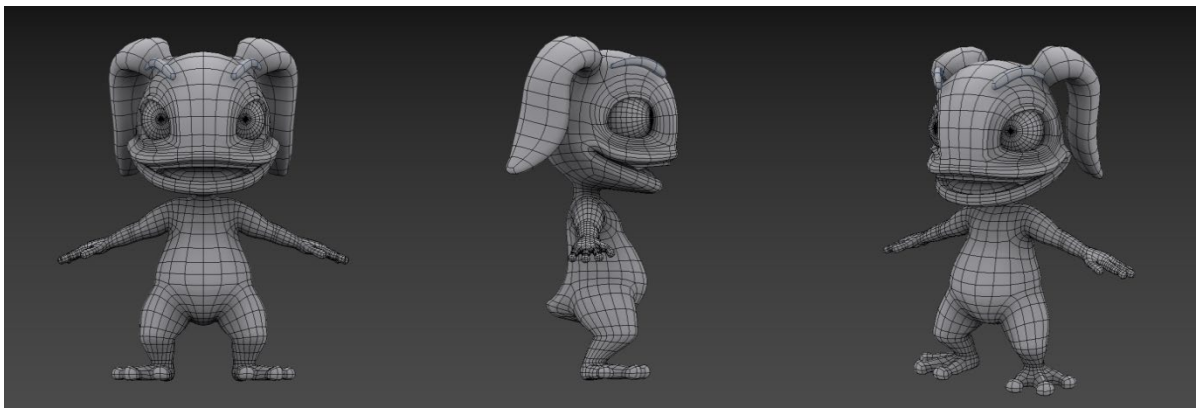

Figure.6: Humanoid character mesh

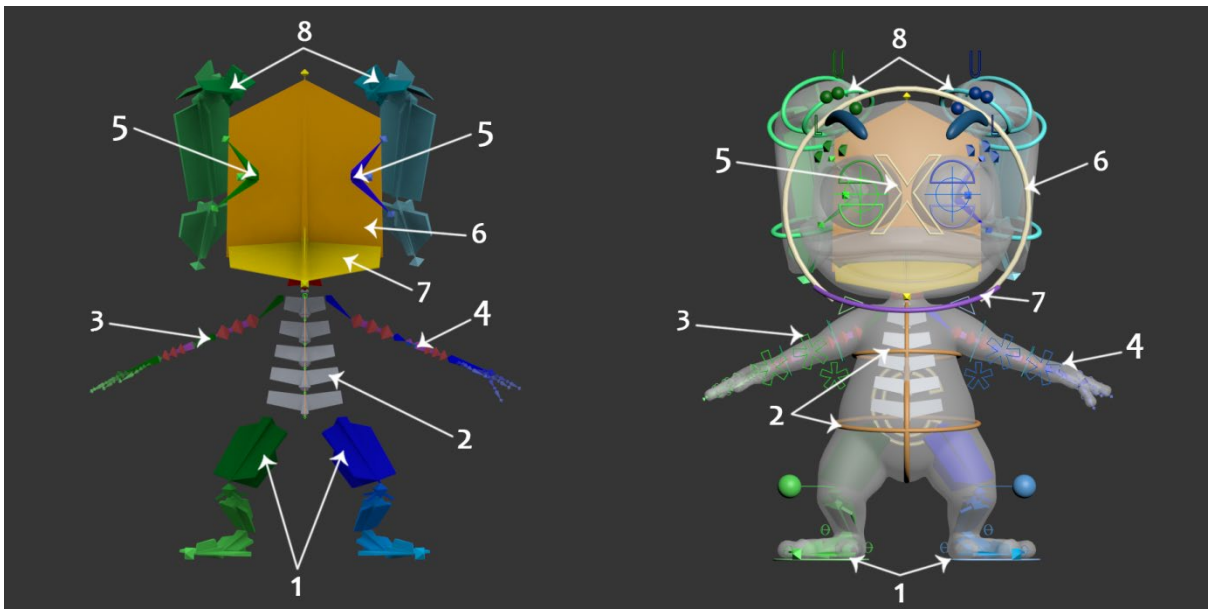

(a) (b)

Figure.7: (a)Bones, and (b) Controls

Table 2

a.	*b.*
1. Leg bones	*1. Leg control*
2. Spine bones	*2. Spine control*
3. FK arm bones	*3. FK arm control*
4. IK arm bones	*4. IK arm control*
5. Eyes bones	*5. Eyes control*
6. Head bone	*6. Head control*
7. Jaw bone	*7. Jaw control*
8. Ears bone	*8. Ears control*

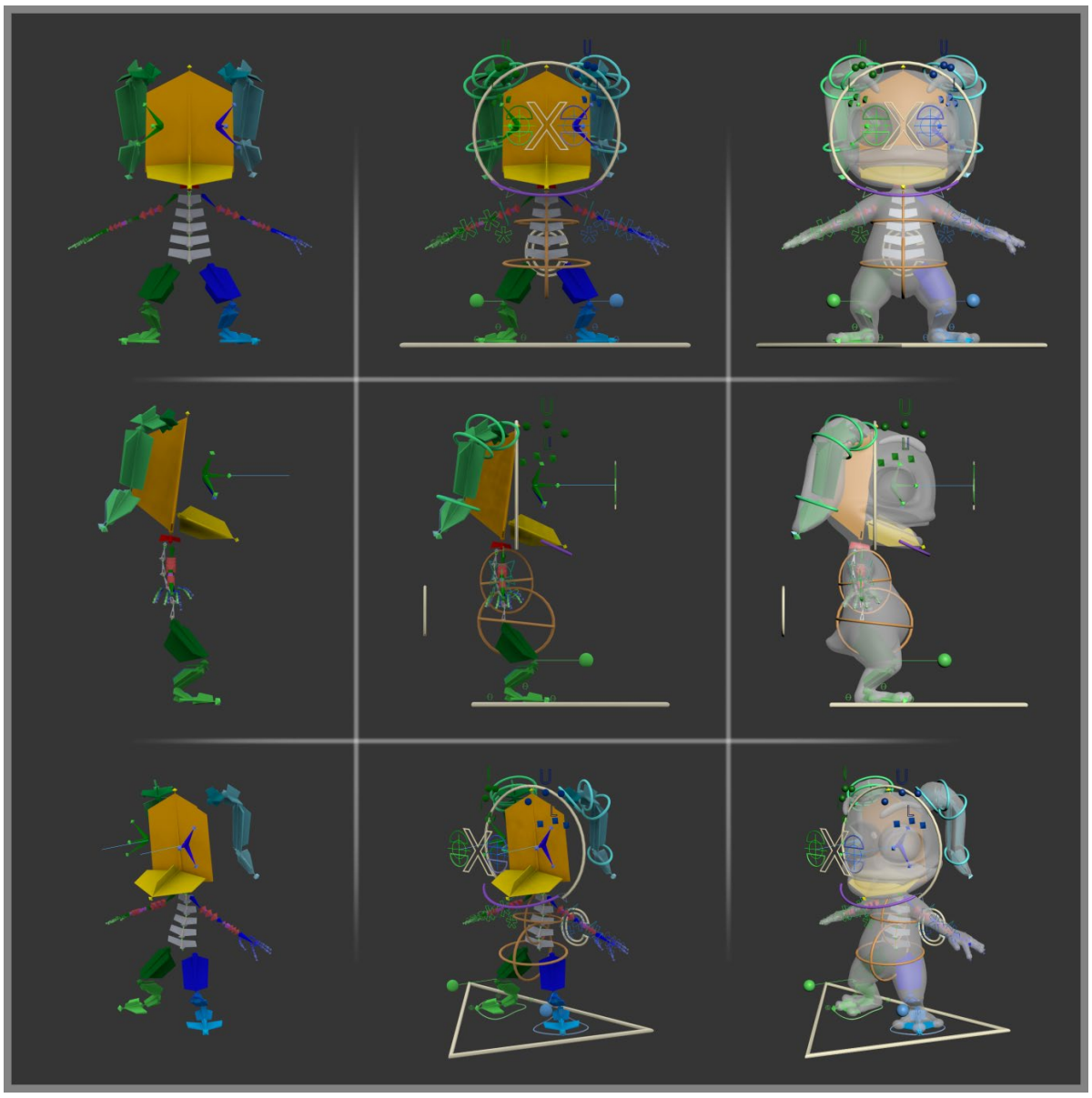

Figure.8: Humanoid character rig from left, front and perspective view

The basic kinematic systems in the rigging process are Forward Kinematic (FK) and Inverse Kinematic (IK). Forward kinematics is the most straightforward method for animating hierarchies, such as a digital skeleton. With FK, transforms applied to the parent are also transmitted to child objects. It is based on rotation, which

means that the joints need to be rotated to position the bones. This is how human joints function, and FK therefore provides us with a good simulation of reality. Inverse kinematics (IK) is a method of animating that reverses the direction of the chain manipulation, i.e. the last bone in the chain controls the bones above. IK requires more setup than FK, but is more intuitive for complex tasks such as character animation. The IK system is mostly used for leg rig. For example, moving the foot would cause the lower leg and thigh bone to follow its movement. Furthermore, an example where both FK and IK systems are used is hand of digital character. The FK would be used when a character needs to pick something up from the table and the IK would be applied when the fist need to be fixed while the body moves.

Regarding skinning process, a proper topology is essential for more realistic and efficient skin deformations. Compared to a fish muscular system, human body is more complex, thus the skinning process requires more time and effort. The most challenging are the bending parts of the character (shoulders, elbows, knees etc.) and face. For these parts, edge loops must be created in order to follow roughly the form of the muscles and their movement. The distribution of weight for 3D-humanoid skin deformation can be seen in Figure 9.

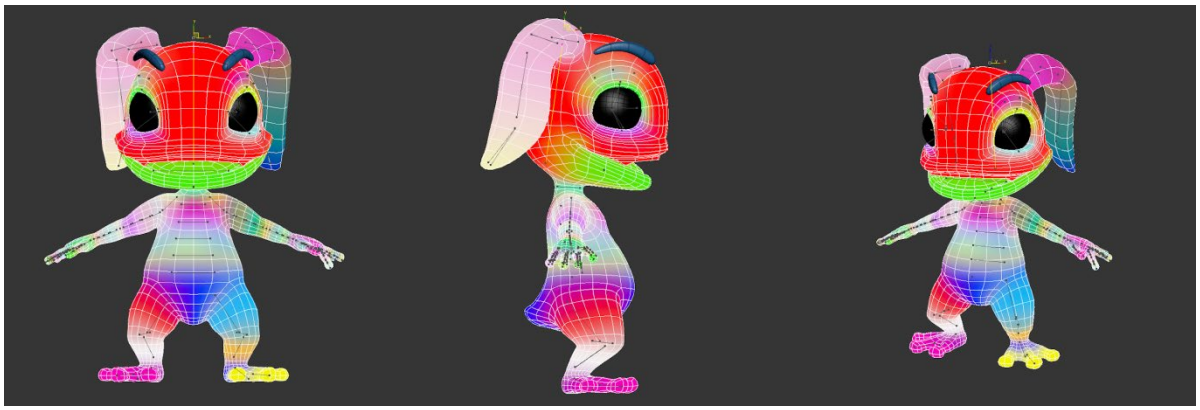

Figure. 9: Humanoid character skin preview

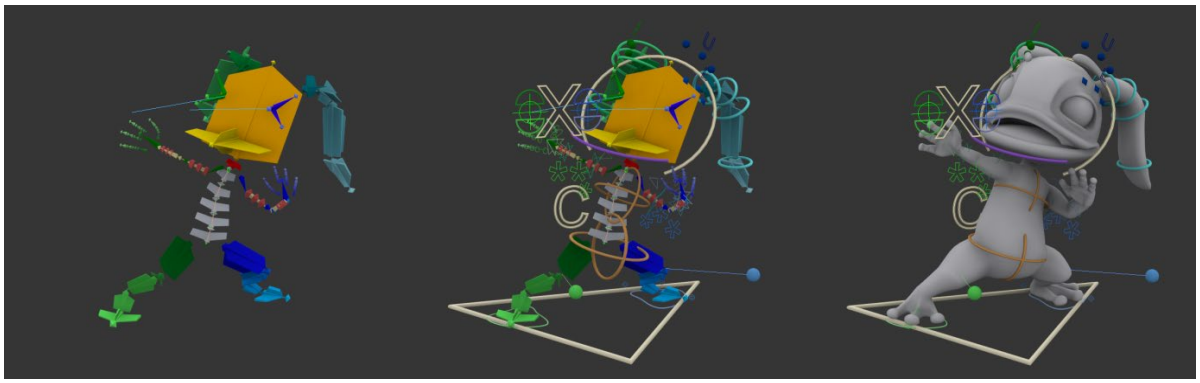

Figure. 10: Humanoid character in pose

2.3. Aesthetics of Visual Communications course

The last course of the study program Engineering Animation that include rig topics is Aesthetics of Visual Communications. This subject is studied in the sixth semester and covers different definitions, concepts and principles of aesthetics of visual communications (Faculty of Technical Sciences, 2020). In order to develop the skills for forming the judgment of aesthetic evaluation of visual impression in all forms of visual communications, within the practical part of the course, student are required to do three projects on different topics.

The task in the First assignment is to rig and animate the car or vehicle of their choice. The vehicle should have a minimum of 4 wheels, with wheel steering. Animation should include driving along a given path, over rough terrain, with bends on the road. Vehicle animation should correspond to realistic model of vehicle behaviour. It is necessary to animate basic vehicle movements such as: wheel rotation, front-wheel steering, shock absorbers function, vehicle body roll and drifting (Computer Graphics - Engineering Animation, 2020). Good animation requires correct rig which will be presented in the next section.

2.3.1. Rigging a vehicle

Although the car is not a living being, we can observe it in the same way as the previous two examples i.e. as a 'character'. Unlike the previous two, 'living' characters, the car rig, shown in Figure 11, does not contain any bones. Considering that fact, locator objects (helpers) are used as intermediaries between the controls and geometry of 3D model. Each individual vehicle movement (wheel rotation, wheel steering, body roll, etc.) should be controlled by one control which manipulates the part of the vehicle geometry (Figure 12 and 13). Some controls affect the position and rotation of other controls. This is because the controls are arranged in a hierarchy. It is very important to link all the elements into a whole to form a hierarchical structure.

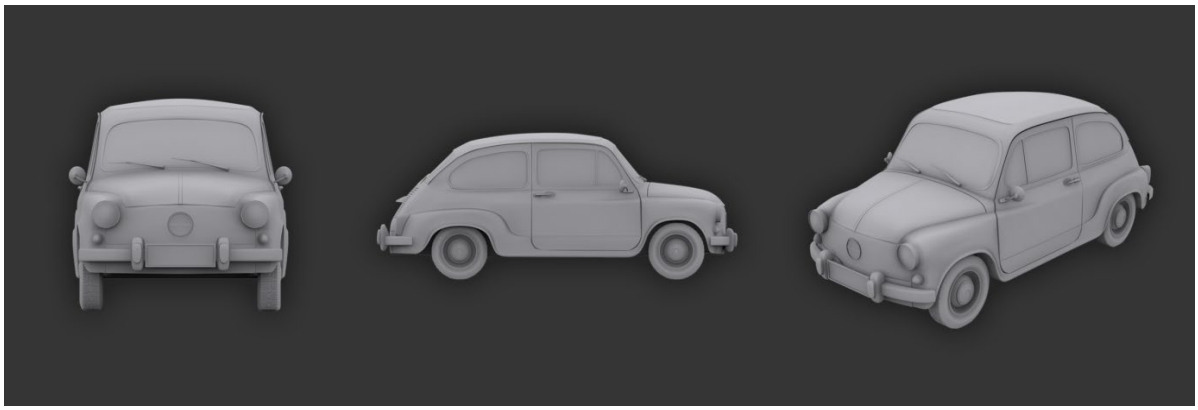

Figure. 11: Car 3D model

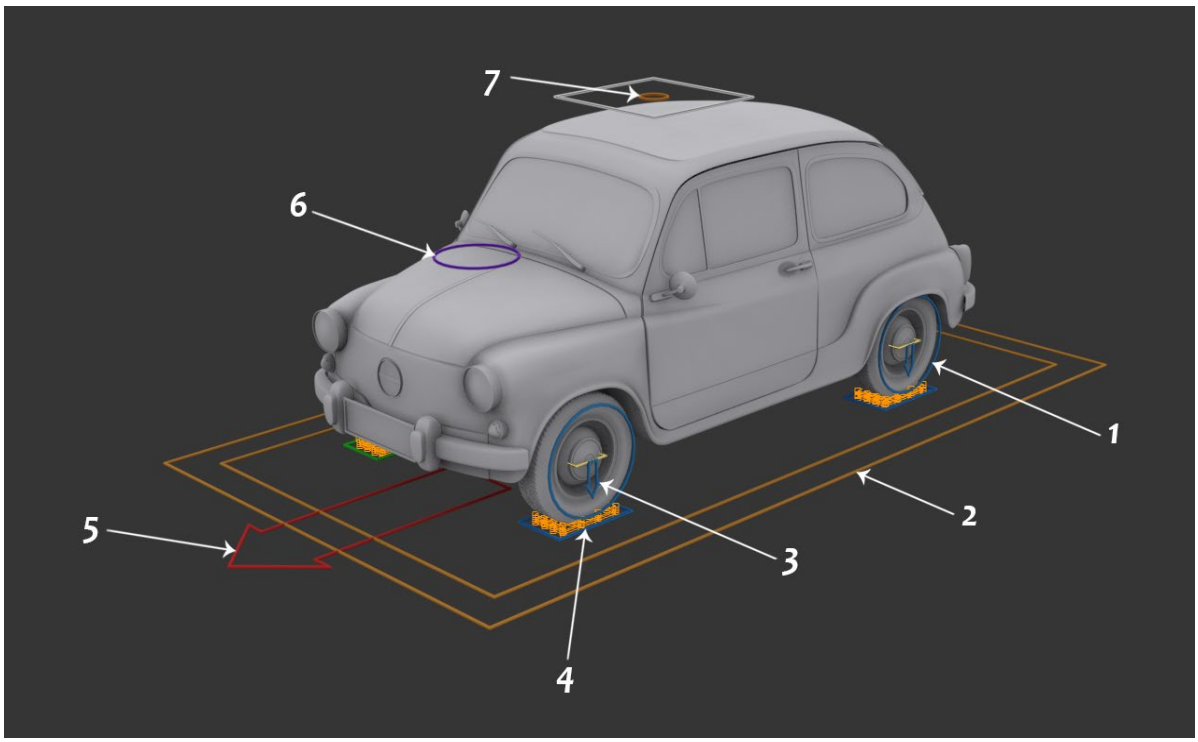

Figure. 12: Controls

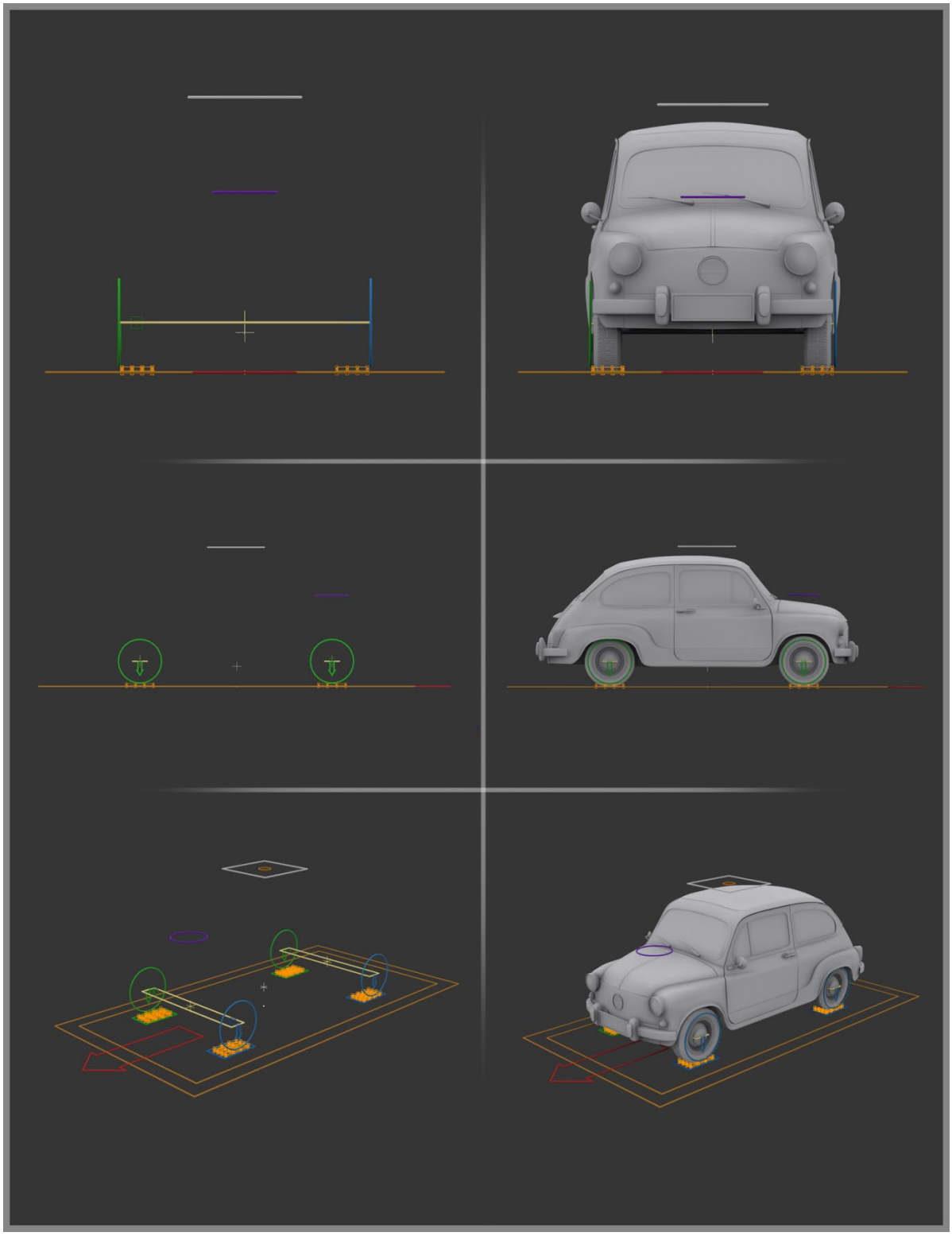

Figure. 13: Car rig from left, front and perspective view

Table 3

1. Wheel rotation control
2. Global control
3. Tire pressure control
4. Wheel grip control
5. Front wheel control
6. Drift control
7. Roll control

In the previous examples, after the rigging, process of skinning was required, whereas in this case it is not. Skinning process for the vehicle is not required to be done if the task is to animate a realistic car, as solid body. In the case of a stylized vehicle that has, for example, mouth and eyes, the skinning process is mandatory, because it has the characteristics of a living character.

3. RESULTS

In this section we will present the most successful and most attractive student projects that have been done in the last two academic years.

Figure 14 shows the renders of the fish character with characteristic facial expressions. Figure 15 presents renders of humanoid character in three different key poses. In Figures 16 moving car is shown with several characteristics key frames.

(a) (b) (c)

Figure.14: Fish character;(a) Scared,(b) Stunned, and (c) Angry, by student Nataša Sremac

Figure. 15: Human character, by student Aleksa Paunović

4. CONCLUSION

This paper present a teaching process of rigging for different types of the 3D models through the contents of three undergraduate courses of the Computer Graphics study program at the Faculty of Technical Sciences, University of Novi Sad: Character Animation, Fundamentals of Engineering Animation and Aesthetics of Visual Communications. Through the implementation of these courses, a gradual learning of the addressed topics was achieved. Different rigging processes are covered through three mandatory projects during the second and third year of study, and they are all presented in detail in this paper.

Figure.16: Car in motion, by student Nikola Milinković

The most significant outcomes of this method of teaching are:

- The majority of students successfully complete the courses
- Interesting and properly completed students' projects, and
- Distinct progress in learning process of the specified topic.

In addition, this methodology of the courses is well accepted by the students, and they are motivated in the work which is interesting for them.

REFERENCES

1. Computer Graphics - Engineering Animation, http://www.racunarska-grafika.com [accessed on March, 2020]
2. Faculty of Technical Sciences, Undergraduate Academic Studies Engineering Animation, http://www.ftn.uns.ac.rs/2028806618/engineering-animation [accessed on March, 2020]
3. Maestri G., 2002. Digital Character Animation 2, Volume II: Advanced Techniques, New Riders, Indianapolis, USA.
4. Obradović, R., Popkonstantinović, B., Šidjanin, P., Vujanović, M., Milojević, Z., 2010. Computer graphics and computer animation studies at Serbian faculties. In: Popkonstantinović, B. (ed.) 2nd International Scientific Conference on Geometry and Graphics moNGeometrija 2010. University of Belgrade, Belgrade, Serbia
5. Obradović, R., Vujanović, M., 2012. New curriculum at the faculty of technical sciences: computer graphics—engineering animation. In: Obradović, R. (ed.) 3rd International Scientific Conference moNGeometrija 2012, pp. 481–486. University of Novi Sad, Faculty of Technical Sciences, Novi Sad, Serbia
6. Obradović, R., Vujanović, M., Kekeljević, I., 2019. Teaching 3D Character Animation Through Four Related Tasks, Advances in Intelligent Systems and Computing 809, ICGG 2018—Proceedings of the 18th International Conference on Geometry and Graphics, pp. 1671–1681
7. Obradović, R., Vujanović, M., Popkonstantinović, B., Ivetić, D., Šiđanin, P., May 2019. Computer Graphics - Engineering Animation study program at the Faculty of Technical Sciences in Novi Sad, JIGED, Volume 14, Issue 1, pp. 319-326.
8. Stajić, B., Šunjka, N., Mijatov, J., Perišić, A., Obradović, R., 2016. 3D modeling course at the computer graphics—engineering animation studies. In: Tepavčević, B., Stojaković, V. (eds.) Between Computational Models and Performative Capacities 4th eCAADe International Regional Workshop, pp. 124–138. University of Novi Sad, Novi Sad, Serbia

APPLICATION OF ADVANCED TEACHING METHODS IN DESCRIPTIVE GEOMETRY II ACADEMIC COURSE AT THE FACULTY OF CIVIL ENGINEERING AND ARCHITECTURE IN NIŠ

Sonja Krasić
Faculty of Civil Engineering and Architecture , University of Niš, Niš, Republic of Serbia
PhD., Associate Professor, krasic.sonja@gmail.com

Zlata Tošić
Faculty of Civil Engineering and Architecture, University of Niš, Niš, Republic of Serbia
PhD Candidate, zlata10@live.com

Jovana Stanković
Faculty of Civil Engineering and Architecture, University of Niš, Niš, Republic of Serbia
PhD Candidate, jovana__stankovic@hotmail.com

Nastasija Kocić
Faculty of Civil Engineering and Architecture, University of Niš, Niš, Republic of Serbia
PhD Candidate, nadja93.al@hotmail.com

ABSTRACT

Theoretical and practical teaching in Descriptive Geometry II academic course, at the study program Architecture, at the Faculty of Civil Engineering and Architecture, University of Niš, is performed using advanced teaching methods. These methods imply the use of digital drawings, which are projected onto the screen via video bim. The didactic principle of step-by-step problem solving was applied for creation of digital presentations in teaching, as in the classical teaching method. The application of step-by-step presentations has advantages compared the classical method, drawing on a board, because the drawings are larger, more precise and there is ability to move back and forth on the slides. The step-by-step presentations have been applied in the last 10 academic years in theoretical teaching, and in the last 2 academic years also in practical teaching.

The goal of the paper is to show what are the benefits of applying advanced teaching methods, which are individual work with students and better acquired knowledge in the subject. An indicator of the quality of student's' knowledge is a better average grade which students achieved in the exam, during the last two academic years, when advanced teaching methods have been applied in practical teaching too.

Keywords: Teaching, Advanced Methods, "Step-by-step" Presentations, Exam Average Grade

1. INTRODUCTION

Descriptive Geometry II academic course, which is taught in the first year of the study program Architecture, at the Faculty of Civil Engineering and Architecture in Niš, covers areas of perspective and shading in parallel projections and in perspective that are required for realistic representation of architectural objects. This academic course with the same number of classes (1 + 2), had been taught using the classical methods until the academic year 2009/10, with tendencies to introduce advanced methods into the teaching process, which started that year. Presentations with the theoretical base are presented on specific examples, which are then solved step by step. These presentations are shown on the screen via video bim. Advanced methods have been introduced into the practise classes in the last two academic years 2017/18 and 2018/19.

Instead of classical drawing on the blackboard, the assistants presented solving the tasks by digitally made drawings "step by step", which are projected on the screen via video bim. During the preparation of presentations, for the theoretical and practical part of teaching, the didactic principle was retained, which was applied in the classical teaching methodology, gradualy solving the tasks. The drawings in the presentations were done on a computer, in AutoCAD program, and current step in solving problems is shown with a single slide and with lines of different colors. The usage of digital presentation technique make it easier for students to visually follow up the solution. Students draw graphical tasks, manually on paper. The experience that the authors of the paper had on the course, Descriptive Geometry in the study program Civil Engineering, at the same faculty (Krasić S. at all 2019), where advanced teaching methods were introduced in order to achieve better quality of student's knowledge, which is reflected in better average grades achieved in the exam, it was necessary to compare to another subject, with students in the Architecture study program. A comprehensive analysis of the introduction of advanced teaching methods in the subject Descriptive Geometry in the study program Civil Engineering has shown that students have gained multiple benefits from their application (Krasić S. at all 2019, Căuneac, D. at all 2014). Higher quality of knowledge was shown through better exam results (average grade), higher percentage of students passing the exam are just some of the benefits. This method of teaching provided additional time for individual work with students, which is beneficial for teachers and associates. (Krasić S. at all 2019, Krasić S. at all 2016, Krasić S. at all 2015).

In this paper, the analysis was performed only on the final results, for average grade achieved in the exam. Input data, such as previous school success, students' perceptual and spatial abilities (Wolf, B at all 1992), were not taken into account, as no student surveys and tests were conducted (Krasić S. at all 2019, Holland, J. L.at all 1997). This will be the topic of further research by the team of authors.

2. ADVANCED METHODS IN THEORETICAL TEACHING

Theoretical teaching is performed with 11 Units on PowerPoint presentations, five for perspective and six for shading. Each presentation contains drawings and textual explanations of the theoretical bases, and several examples within use of these basics, step by step. The paper presents only characteristic steps in solving problems, and representative examples are selected.

All 11 Units presentations in the academic course for theoretical teaching were posted on the Faculty's website (http://rc5.gaf.ni.ac.rs/dec/viscom/system/index.php). The students are facilitated to follow the classes, prepare and take the exams. The exam in Descriptive Geometry II consists of two parts. The exam assignments are similar to the practical class assignments.

2.1. Perspective Presentations

Perspective is a type of projection in which objects are presented as we see them in nature. Within this area, students are initially introduced to the basic elements of perspective and the elements of space in perspective (point, straight, plane). The greatest attention being paid to geometric, linear perspective. According to the position of the projection plane, the perspective is divided into frontal, perspective „from the corner“ and oblique perspective. The first two are studied within the course syllabus, where the projection plane is vertical. This is followed by the rules for constructing a frontal perspective, in which the two axes of the object coordinate system are coincident with the projection plane. Finally, a frontal perspective of the selected interior is constructed, step by step.

The next type of perspective "from the corner" is dealt with in a little more detail as it is used more in architectural practice. In this type of perspective, one axis of the object's coordinate system is coincident with the projection plane. All methods of constructing perspective "from the corner" were mentioned, and only two of them were discussed in more detail, the method of breakthrough of visible rays and vanishing points and the coordinate method (Fig. 1). Perspective images of the same simple object were gradually constructed, using these two methods.

The coordinate method has greater advantages, so it will be used for graphical tasksOf great importance is the final perspective image to which a lot of attention has been paid. Each architectural object should be placed in a natural environment, so that students should be introduced with the way of presenting the environment.

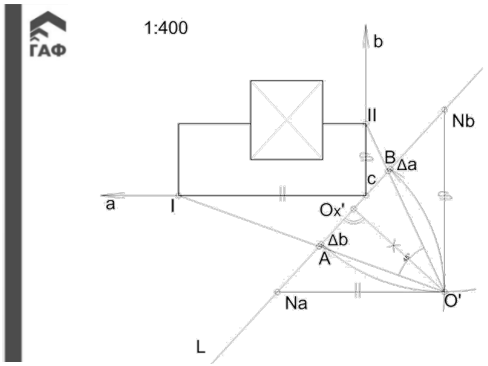

Determining all elements of a perspective image, **A**, **B**, $\mathbf{N_a}$, $\mathbf{N_b}$, **Δa** i **Δb**, in basis on a smaller drawing scale **R=1:400**.

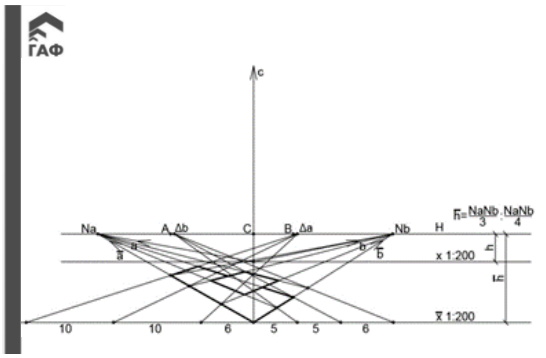

Drawing a lowered basis in perspective in drawing scale **R=1:200**, using the axis $\bar{x}$ and proportional points **Δa** and **Δb**, and vanishing points $\mathbf{N_a}$ i $\mathbf{N_b}$.

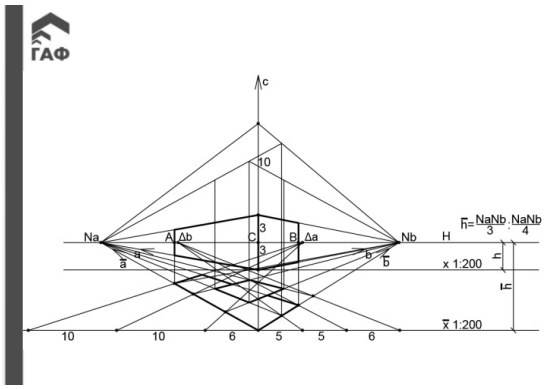

Drawing a lower part of object in perspective. Heights are applied to a proportional vertical line **c** from the basic stright line **x**.

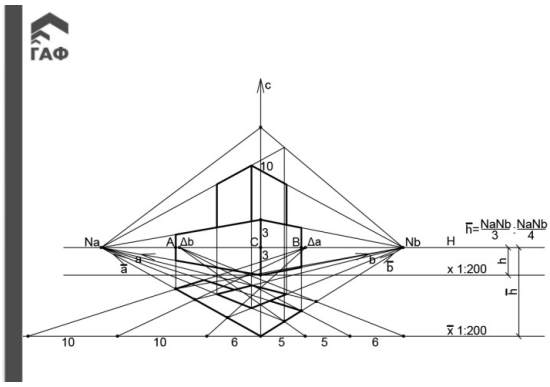

Drawing a higher part of object, using the auxiliary vertical line in **bc** plane and marking the visibility of the whole object.

Figure. 1: Perspective Presentation „Unit V" – Solution to the task of constructing a perspective image „from the corner" of an object using coordinate method, in steps

2.2. Shading Presenatations

For a realistic representation of objects, in addition to drawing them in perspective, they need to be illuminated by some light source and complemented by shadows on the object itself and the surrounding surfaces. Shading was applied to specific architectural objects and details. Therefore, this area is also represented in the course. Students are first introduced to the shadowing rules of parallel illumination (light source - sun) in parallel projections, and then to central (light source - lamp) and parallel illumination (light source - sun) in perspective. Solutions to specific tasks that follow the theoretical basis are presented step by step in the presentations. All methods of constructing cast shadows apply, but the most direct method.

Figure 2 shows one specific example, from several represented in Presentation VI, of constructing cast shadows for architectural detail, a staircase, in parallel projections for arbitrary, parallel illumination, which is solved step by step in the lecture. Special cases of parallel illumination in parallel projections, "under 45^0" shadowing and frontal illumination were also presented in the shading presentations. For these cases several examples have been made, with detailed construction, step by step, of which only characteristic steps are shown in this paper, in one example.

In addition to the shading in the parallel projections, the presentations dealt with the shading in perspective, where central (light source - lamp) in interiors and parallel (light source - sun) illumination in exteriors are also represented. The paper will show only one example (Fig. 3) of shading in perspective for a light source sun, which is in an arbitrary position relative to the projection plane, for a simple object in the exterior.

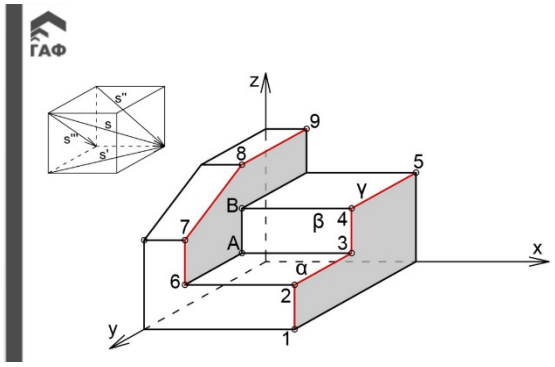

Marking the illuminated part, its core shadow and the separate line on the staircase for a given arbitrary, parallel illumination, in oblique frontal projection.

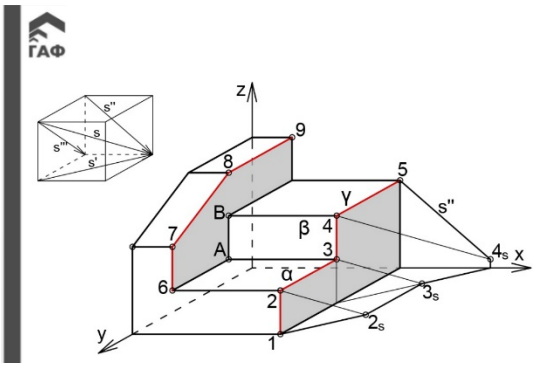

Determination of cast shadow from a separate line (**1-5**), on horizontal and frontal plane. Light rays were used **s** and $\mathbf{s^I}$ to determine the cast shadows of points.

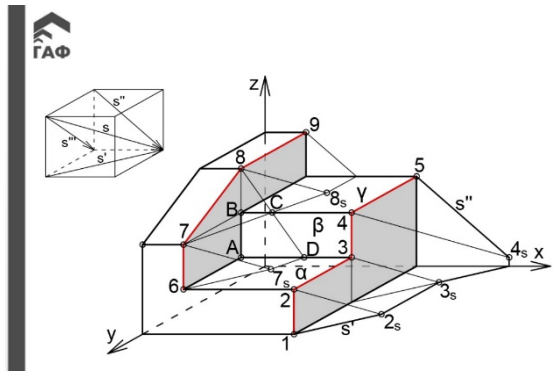

Determination of cast shadow from a separate line (**6-9**), on frontal plane and staircase. Light rays were used **s,** $\mathbf{s^I}$ and $\mathbf{s^{II}}$, as well as breakthroughs of the inclined stick through the horizontal and vertical planes of the stairs, to determine the shadows of the points.

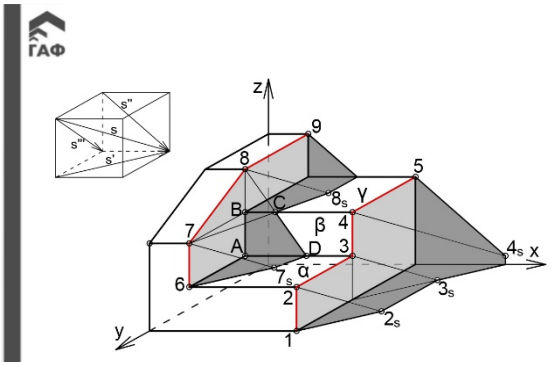

Marking the visibility of core and cast shadows on the staircase and surrounding planes from arbitrary, parallel illumination in oblique frontal projection.

Figure. 2: Shading Presentation „Unit VI“ – Solution to the task of determining core and cast shadow of the staircase from parallel illumination, in parallel projections, in steps

Advanced methods in presenting materials, digital drawings for solving tasks, step by step, displayed onto the screen via video bim, have great benefits. The presentations are easier to follow, and there is more time to renew the course material, the topic of each unit.

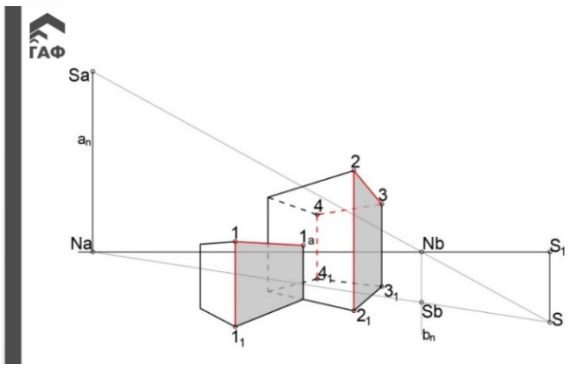

Determination of core shadow and separate lines, polygonal lines, on prismatic objects and solar figures $\mathbf{S_a}$ and $\mathbf{S_b}$.

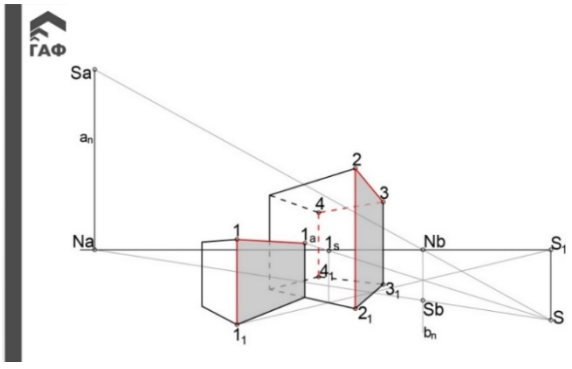

Determination of cast shadow from a separate polygonal line, $\mathbf{1_1 11_a}$, of lower object on horizontal plane and higher object.

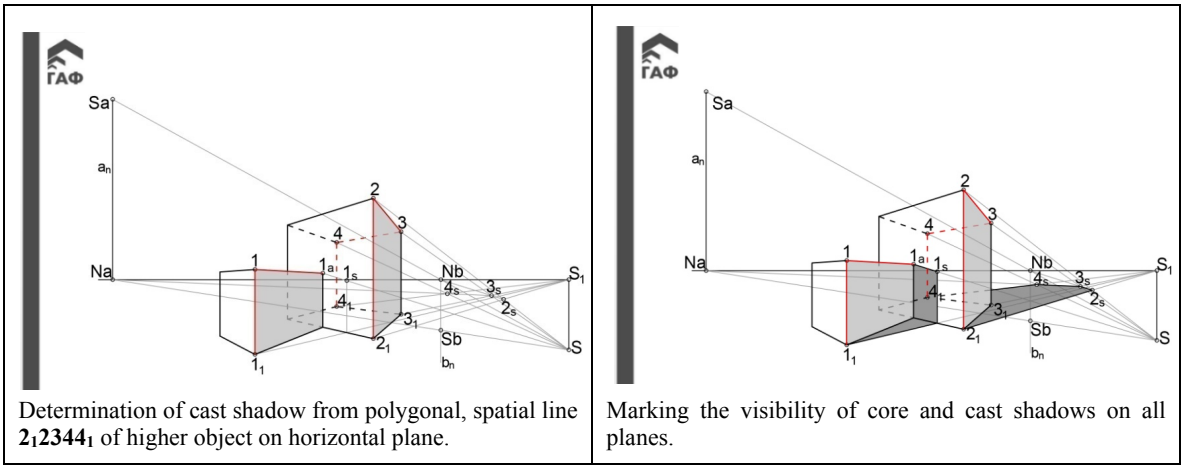

Determination of cast shadow from polygonal, spatial line **$2_1 2 3 4 4_1$** of higher object on horizontal plane.

Marking the visibility of core and cast shadows on all planes.

Figure. 3: Shading Presentation „Unit X" – Solution to the task of determining core and cast shadow of the object from parallel illumination, in perspective, in steps

3. ADVANCED METHODS IN PRACTICE CLASSES

Practical teaching is performed with 11 Units on Presentations in pdf format. Five of them are in the perspective, and six are in the shading area. Each presentation represents the production of one graphical assignment, which follows theoretical teaching. The graphical assignments were produced with precise digital drawings, by step by step method, showing new lines in different colors, in each subsequent step. Advanced methods applied in practical teaching are the presentation of step by step graphical assignments onto the screen via video bim. The didactic principle applied in the preparation of presentations for practical teaching is the same as in the classical teaching method. There are one or more tasks on graphical assignments, which are solved gradually.

In this academic year, an online publication, collection of tasks of "Perspective and Shading - Step by Step" has been published and can be found on the website of the University Library "Nikola Tesla" in Niš (https://www.ubnt.ni.ac.rs/images/pdf/Udzbenici/Zbirka%20za%20biblioteku%20NEW.pdf). This collection of tasks contains all 11 presentations of graphical assignments from the subject Descriptive Geometry II, with a brief introduction to perspective and shading and with textual explanations of the solution of the tasks. The authors hope that the results achieved in the exam in this academic year 2019/20 will improve as the collection of assignments can be downloaded free of charge from the library website and it is available to all students.

3.1. Perspective Graphical Assignments

The tasks in graphical assignments are designed to draw specific architectural objects in the frontal perspective - 1 interior example and in the perspective "from the corner" - 3 exterior examples (Fig. 4). Architectural objects on graphical assignments should be placed in a natural environment, with human figures. Units from the theoretical teaching are applied to graphical assignments. The exam assignments are similar to the practice classes assignments.

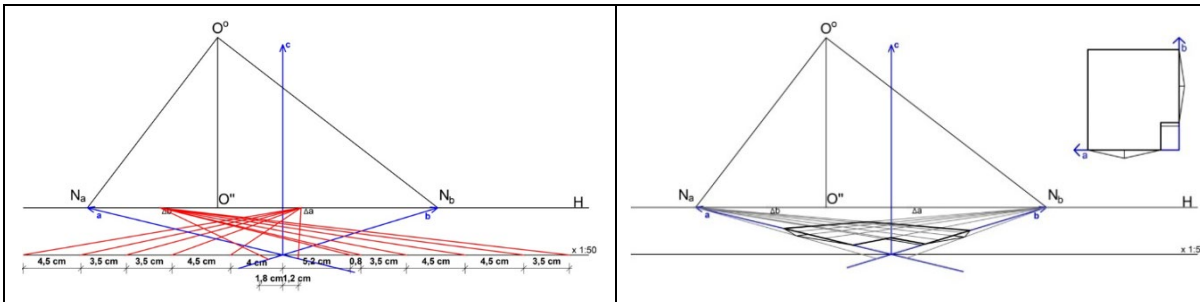

Applying coordinates to the axis **a** using the proportional point **Δa** and coordinates to the axis **b** using the proportional point **Δb**, in drawing scale **R=1:50**. It is shown how to enter positive and negative coordinates.

Drawing roof basis of an object with overhangs on the ridges, using the coordinates of the axes **a** and **b** and vanishing points of their directions **N_a** and **N_b.**

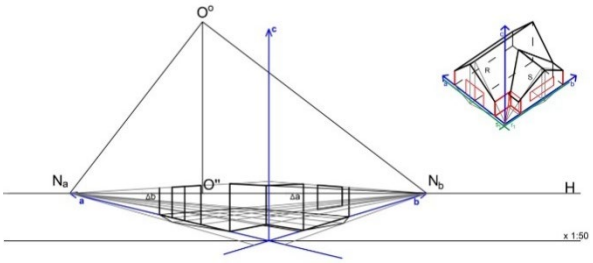

Drawing vertical planes **a** and **b** directions, with double lap doors and window. Heights are applied to the axis **c** from the axis **x** in drawing scale **R=1:50**. Using the horizontal **a** and **b** directions, the heights of all the verticals in these planes are determined.

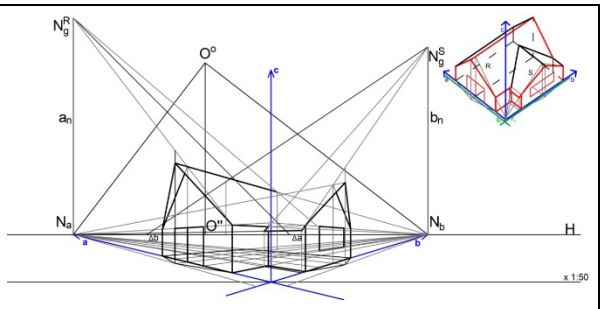

Determining the vanishing points of a slope lines of roof planes **R** and **S**, using the slope construction according to the plane of the basis. Drawing roof planes **R** and **S**, with overhang on the gutter of roof plane **S**.

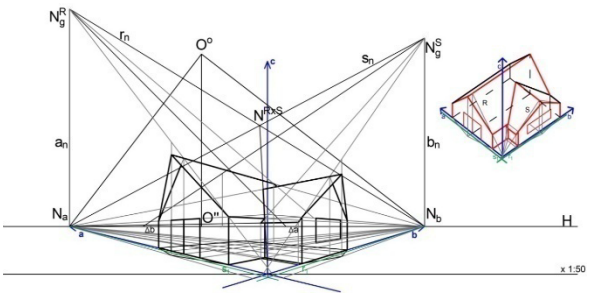

Determination of intersection of roof planes **R** and **S**, using the intersection point **N** of vanishing lines $\mathbf{r_n}$ and $\mathbf{s_n}$ and intersection point of first traces $\mathbf{r_1}$ and $\mathbf{s_1}$ of this roof planes.

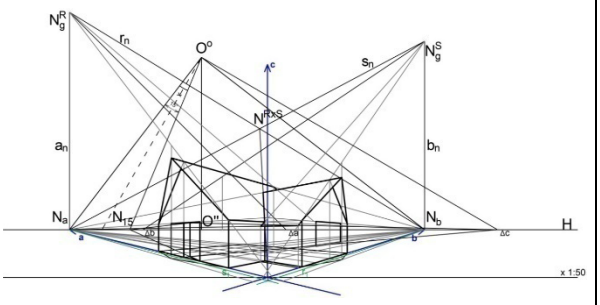

Opening door right wing inwards for angle of $\mathbf{15^0}$, using vanishing point $\mathbf{N_{15}}$ and vanishing point of bisectrics rays **Δc**. Marking the visibility of the whole object.

Figure. 4: Graphical Assignment „Unit V"– Solution to the task of constructing a perspective image „from the corner"of an object using coordinate method, in steps

3.2. Shading Graphical Assignments

Within the shading in parallel projections for parallel illumination (light source - sun), two tasks on one graphical assignment designed on template. Students learn to determine core and cast shadows from arbitrary and special lighting on specific architectural objects or details (Fig.5). Within the shading in perspective one task on one graphical assignment designed on template, (Fig.6). Students learn to determine core and cast shadows from central illumination (light source - lamp) in one interior and for parallel illumination (light source - sun) in two exteriors (Fig.6), on specific architectural objects. The paper shows only some characteristic steps in solving problems, and representative examples are selected.

The application of advanced teaching methods in practical teaching has its advantages, one of them being more time for individual work with students. In addition, it is easier for students to keep up with production of their assignments, as on-screen drawings are larger, more accurate, and they can move back and forth through slides.

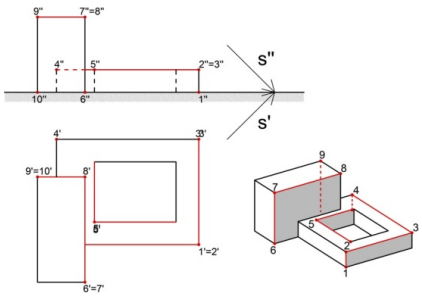

Marking the illuminated part, its core shadow and the separate line on the object for a given arbitrary, parallel illumination, in parallel projection.

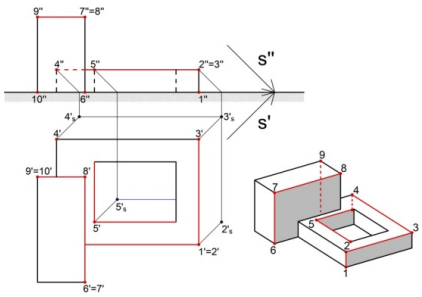

Determination of cast shadow from a separate spatial polygonal line (**1-4**), and two horizontal lines through point **5** on horizontal plane. Light rays $\mathbf{s^I}$ and $\mathbf{s^{II}}$ were used to determine the cast shadows of points.

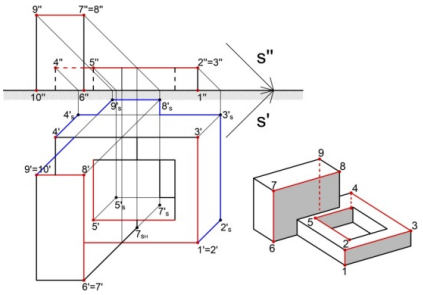

Determination of cast shadow from a separate spatial polygonal line (**6-10**), on horizontal plane and on lower part of the object

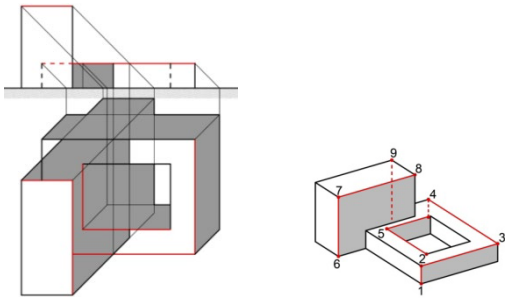

Marking the visibility of core and cast shadows on all planes.

Figure. 5: Graphical assignment „Unit VI“ – Solution to the task of determining core and cast shadow of the object from parallel illumination, in parallel projections, in steps

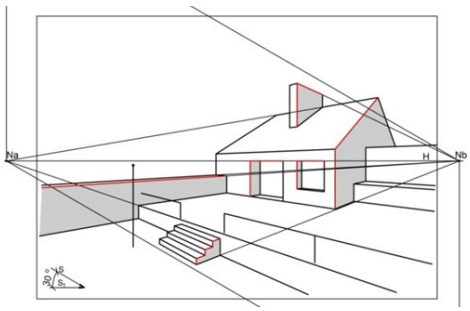

Marking the illuminated part, its core shadow and the separate line on the object for a given arbitrary, parallel illumination, in perspective.

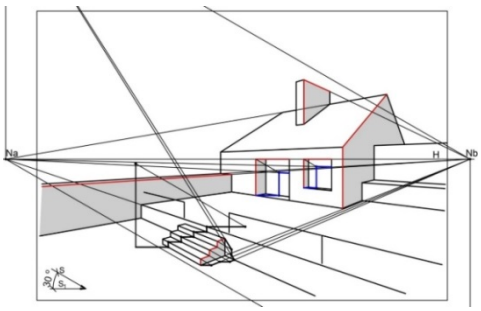

Determination of the cast shadow from the separate line on staircase, door and window and vertical rod on all horizontal and vertical planes.

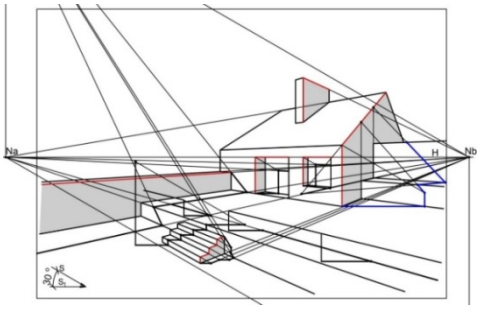

Determination of cast shadow from the separate line on the object, full fence on all horizontal and vertical planes.

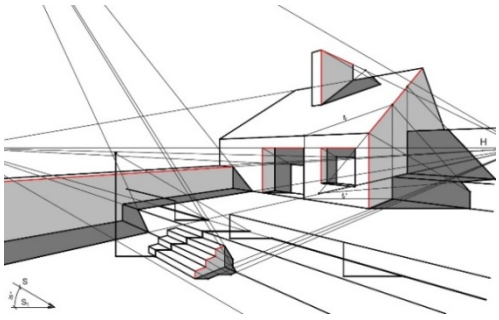

Marking the visibility of core and cast shadows on all planes.

Figure. 6: Graphical assignment „Unit XI“ – Solution to the task of determining core and cast shadow of the object from parallel illumination, in perspective, in steps

4. EVALUATION

Since the advanced methods in theoretical teaching of the course Descriptive Geometry II, introduced in the academic year 2009/10, it was possible to analyze the success of students who achieved at the exam, in the last 10 years. The analysis was made on the basis of the results in all exam periods in one academic year, when a large percentage of enrolled students of that generation passed the exam (Table 1). Based on Table 1, it can be concluded that the average grade in the exam was the lowest in the first academic year 2009/10 (7.96), to increase gradually (8.43 - 8.68). Such a high average grade in the exam is a result of the higher quality of students' knowledge, which was followed after application of advanced teaching methods.

In the last two academic years 2017/18 and 2018/19 were applied advanced methods in practical classes. Analyzing the average grade achieved on the exam, it was concluded that it increased significantly to 8.90, in the first (2017/18) and to 8.95 , in the second (2018/19) academic year. The authors 'assumption that the students' acquired knowledge of the subject will be greater, using advanced methods, is proven by this analysis.

Students are more satisfied with these teaching methods because more time is devoted to working with them individually, as shown by the final results.

Table 1: Average grades in last 10 academic years on the subject Descriptive geometry II

Number of enrolled students	***122***	***101***	***102***	***93***	***134***	***128***	***157***	***156***	***151***	***146***
Enrolment year	***2009/10***	***2010/11***	***2011/12***	***2012/13***	***2013/14***	***2014/15***	***2015/16***	***2016/17***	***2017/18***	***2018/19***
Average grade	***7.96***	***8.57***	***8.84***	***8.59***	***8.68***	***8.80***	***8.43***	***8.51***	***8.90***	*8.95*

5. CONCLUSION

Advanced methods of presented subject matter, which is using digital drawings that are made step by step, which are projected via video beam on the screen, allow students to better monitoring theoretical and practical teaching. The drawings on the screen are larger, more accurate and can move back and forth, so more time is devoted to working with students individually.

This makes it easier for students to complete their graphical assignments obligations and have plenty of time to devote to preparing the exams which are available now in the form of PowerPoint Presentation, posted on the Faculty's website (http://rc5.gaf.ni.ac.rs/dec/viscom/system/index.php), and from this academic year a textbook ”Descriptive geometry II” in CD version and collection of tasks of “Perspective and Shading - Step by Step” (https://www.ubnt.ni.ac.rs/images/pdf/Udzbenici/Zbirka%20za%20biblioteku%20NEW.pdf).

REFERENCES:

1. Căuneac, D., Chiliban, B., Chiliban, M., 2014, Modern educational instruments and blended-learning technologies in descriptive geometry teaching, The 5th International Conference on Engineering and Business Education &, Sibiu, Romania. pp 1-4.
2. Clivel, D., Alicem, A., Ozgureris, Danield, F., Larryj, L., 2005, Engineering Design Thinking, Teaching, and Learning, Journal of Engineering Education 103.
3. Di Paola, F., Pedone, P., Pizzurro, M.R., 2013, Digital and interactive Learning and Teaching methods in descriptive geometry, Proceedings of 4th International Conference on New Horizons in Education, Education and Technology-TASET, Sakarya Universitesi, Turkey. pp 873-885
4. García, R., R., Quirós, J., S., Santos, R., G., González, S., M., Fernanz, S., M., 2007, Interactive multimedia animation with Macromedia Flash in Descriptive Geometry teaching, Computers & Education, Vol. 49, 3, pp. 615-639
5. Gittler, G., Gluck, J., 1998, Differential Transfer of Learning: Effects of Instruction in Descriptive Geometry on Spatial Test Performance, JGG 2(1), pp. 71-84
6. Gorjanc, S., Halas, H., Jurkin, E., 2014. Introducing 3D Modeling into Geometry Education at Two Technical Faculties at the University of Zagreb, 16th International Conference on Geometry and Graphics ISGG, 4–8 August, 2014, Innsbruck, Austria. pp 2-9.
7. Gutierrez, J., M., Gil, F., A., Contero, M., Saorin, J., L.,2013, Dynamic Three-Dimensional Illustrator for Teaching Descriptive Geometry and Training Visualisation Skills, Computer Applications in Engineering Education, Volume 21, Issue 1, pp. 8–25
8. Holland, J. L., 1997, Making vocational choices: A theory of vocational personalities and work environments. Odessa, F.L.: Psychological Assessment Resources, Inc.
9. Krasic, S., Pejić, P., Krstić, H., 2015. Implementation of Contemporary Methods in Teaching Descriptive Geometry at the Faculty of Civil Engineering and Architecture of Niš, Book of abstracts, 18th Scientific-Professional Colloquium on Geometry and Graphics, Croatia. pp 21-22
10. Krasić, S., Pejić, P., Veljković, M., 2016, A Comparative analysis of Contemporary and Classical Teaching methods of Descriptive geometry at the Faculty of Civil Engineering and Architecture in Niš, Book of abstracts, Proceedings of International scientific conference moNGeometrija 2016, pp.43-45
11. Krasić S., Pejić P., Stojiljković S., Dosković M., Tošić Z.: Advanced Teaching Methods Application and its Benefits in Descriptive Geometry at the Faculty of Civil Engineering and Architecture in Niš ,

Technical Gazette, Vol.26/No.6, 2019, ISSN 1330-3651 (Print), ISSN 1848-6339 (Online), pp.1814-1820, DOI: https://doi.org/10.17559/TV-20180628135401, http://tehnicki-vjesnik.com/web/public/page

12. Krasić S.: *NACRTNA GEOMETRIJA II (Perspektiva i senčenje u paralelnim projekcijama i perspektivi),* Osnovni udžbenik, Građevinsko-arhitektonski fakultet Univerziteta u Nišu, 2020, 160 str., ISBN 978-86-88601-47-4, COBISS.SR-ID 282987276
13. Krasić S., Tošić Z., Stanković J., Kocić N.: *Perspektiva i senčenje – korak po korak*, Zbirka zadataka, Univerzitetska biblioteka "Nikola Tesla", Niš, 2020, 1070 str., ISBN 978-86-7500-021-1,COBISS.SR-ID 534204822, https://www.ubnt.ni.ac.rs/images/pdf/Udzbenici/Zbirka%20za%20biblioteku%20NEW.pdf
14. Wolf, B., Momirović, K., Džamonja, Z., 1992. KOG 3. Baterija testova inteligencije. Beograd: SDPS – Centar za primenjenu psihologiju.

TEACHING PERCEPTION AS MOTIVATION FOR STUDENTS TO APPLY DESCRIPTIVE GEOMETRY AND PERSPECTIVE

Vesna Stojaković
Department of Architecture, Faculty of Technical Sciences, University of Novi Sad, Serbia
PhD., Associate Professor, vesna100@uns.ac.rs

Radovan Štulić
Department of Architecture, Faculty of Technical Sciences, University of Novi Sad, Serbia
PhD., Full Professor, *stulic@uns.ac.rs*

ABSTRACT

For Descriptive Geometry and Perspective, traditionally regarded as difficult subjects, the introduction of perception related topics may lead to better motivation of students in mastering the topics and in further applying the gained knowledge. In this paper some general perception theories together with the accompanying principles and examples are presented, as well as the selection of the topics which appear to be the most attractive to the students. Such topics, being most visually intriguing, seem to maximize the extrinsic motivation by the social context and therefore they are selected as the most important driver for self-determined learning.

Keywords: education; perspective; descriptive geometry; perception

INTRODUCTION

The motivation as the concept of intention is in the core of many theories about the education and learning (Deci, 1991). The teaching mainly addresses understanding as a main goal. However, the need for the application of science knowledge is just as important (Hutton, 1998), especially in the field of technical disciplines (Gallagher, 2000). Aside from learning about possible application, building a knowledge, generate understanding, finding and creating applications can be a valuable driver for students' motivation to put the effort to the certain subject.

When learning Descriptive Geometry and Perspective students often find geometry hard to learn and miss to notice possible application of the subject. The lack of application demonstration in the study program can lead to the decreased interest in students. These courses are usually taught in the beginning study years which is why it is hard to include application since advanced knowledge in the certain technical discipline would be required. The experience in teaching Descriptive geometry and Perspective within the different technical disciplines, especially the ones design oriented, showed that the students are attracted to the topics involving relationship between geometry and human perception.

The perception of the shapes, defined as geometrical properties of a specific three dimensional object, has a unique place in the perception studies (Pizlo, 2008). Understanding the perception of the shapes is aimed to develope mechanisms which provide humans with accurate information about the surrounding objects. The perception mechanisms, the way we experience size, distance and orientation, are developed during human evolution in order to produce information that are veridical in most cases (Howe & Purves, 2005). If the visual system fails to provide veridical information about the stimuli and perception of space, which differs from the reality, such phenomenon is called optical illusion. Studying optical illusions can trigger "the effect of magician" in which the audience seeks to understand how the trick works (Schott, 2010). Same effect can be used to stimulate students to gain more interest in shape perception understanding and underlying geometry.

The aim of this paper is to explain the perception related topics, especially shaped based optical illusions, and how they can be used to motivate students to apply their knowledge of Descriptive Geometry and Perspective.

General perception theories are interesting to the students, but the topics which are visually intriguing maximize the extrinsic motivation by the social context and therefore are selected as the most important driver for self-determined learning. The selection of the topics which appear to be the most attractive to the students will be presented in the paper. The importance of the paper is to outline the main perception related themes and examples which can be used for students' motivation improvement.

2. SHAPE PERCEPTION

The basic perception knowledge is useful for a creative application of descriptive geometry and perspective. Explanation of the perception theories evolution and how the ideas favored the figure-ground organization or depth cues are good for basic understanding of the different approaches (Pizlo, 2008). In figure-ground organization it is assumed that the recognitions of the figures representing different shapes have to be determined first, and the shape properties are assumed after. In contrast in theories which favor depth cues (such as binocular vision, textures, shades, etc.) assume that the shape recognition is done based on the determined properties of the shapes.

Figure-ground organization is related to gestalt theory. One of the main principles of gestalt theory is that the whole is greater than its parts (Koffka, 1935). This means that the shape itself is more important and primarily perceived than its geometrical properties. One of the questions that was debatable in gestalt theory is why do we see what we see. At first it is thought that we choose to see the simplest figure, but with the development of the computers the simplicity principle could be easily measured and it has been noticed that the figures people see are often not the simplest figures. Simplicity principle is replaced with veridicality principle.

In the middle of the 20th century the creation of the random dot stereograms (Julesz, 1960) changed the course of perception theories. The 3D shape in random dot stereograms can be perceived in spite of the fact that figure-ground organization cannot be performed because there is no shape contour. The shape is perceived only by usage of the binocular disparity. Only after the depths of all segments of the surface are determined, the shape can be isolated from the background. This research influenced that majority of the perception researches orient towards the depth cues rather than figure-ground organization (Pizlo, 2008).

With the development of the computer graphics it is noticed that depth cues alone are not powerful enough to be the base for the image recognition algorithms. During the end of the 20th century both approaches of perception are developing and have application in different cases.

3. CONNECTING PERCEPTION WITH DESCRIPTIVE GEOMETRY AND PERSPECTIVE

In the connection with the shape perception theoretical branches, depth cues a well as figure-ground organization, can be explored. Most interesting depth cue which can be studied in perceiving geometry is the binocular vision. The binocular vision represents our ability to sense depth by using disparity between two images perceived by two eyes in different positions. Interesting applications for the students are the representation techniques in which the left and the right eye receive different images and we get the impression of depth even though the medium in which the images are shown is flat and there is no real spatial depth. Some of the examples of such stereo representation methods are anaglyphs (Figure 1), stereograms, holograms and virtual reality. Understanding and creating anaglyphic line drawings is a very good practice for students since they have to use perspective and descriptive geometry to draw correct anaglyph. Other methods for stereo representations rely mostly on analogue or computer automation and because of that thay are not suitable for learning descriptive geometry or perspective.

Figure 1: Anaglyph drawing (Pal, 1966)

Optical illusions are also very interesting for the understanding of the perception and application of the knowledge gained in Descriptive Geometry and Perspective. One of the main phenomenon on which the illusions rely on is the shape ambiguity. The shape ambiguity represents a situation in which two or more 2D figures/images having different shapes produce perception of the identical image. The observer would have a problem to determine which 3D shape produces the given image.

The simplest representation of the shape ambiguity is inability to determine the shape orientation when silhouette (orthogonal projection) is presented. Since the silhouette is the same if the shape is observed, for instance, in front (view) or in back view, the observer can imagine the object perceived from the front and at the same time the mirrored object observed form the back. The famous illusion using only silhouette ambiguity is the gif animation "Dancer" made by Japanese web designer Nobuyuki Kayahara in 2003. One frame of this illusion is presented in Figure 2: depending on the imagined orientation of the object with respect to the view direction, the dancer can be seen as standing on the right or on the left leg. The observer can also be under the impression that the dancer is changing legs (and the direction of spin) depending of the personal interpretation of the direction of view (Guillen, Marquez, & Bernal, 2014). Another interesting example is the Necker cube published by Swiss crystallographer Louis Albert Necker in the 19th century. The cube can be geometrically interpreted in two ways eather as a possible figure or an impossible figure (Figure 3). Humans tend to see both possible shapes equally and also strikingly change the appearance during prolonged viewing as a sudden switch to different interpretation of the shape position (Kornmeier & Bach, 2005).

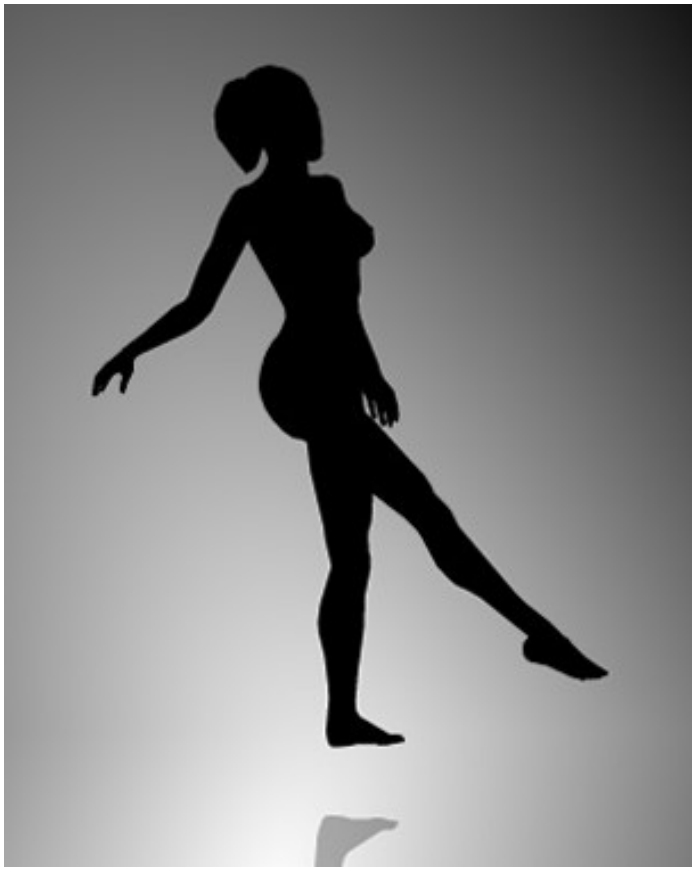

Figure 2: Dancer illusion

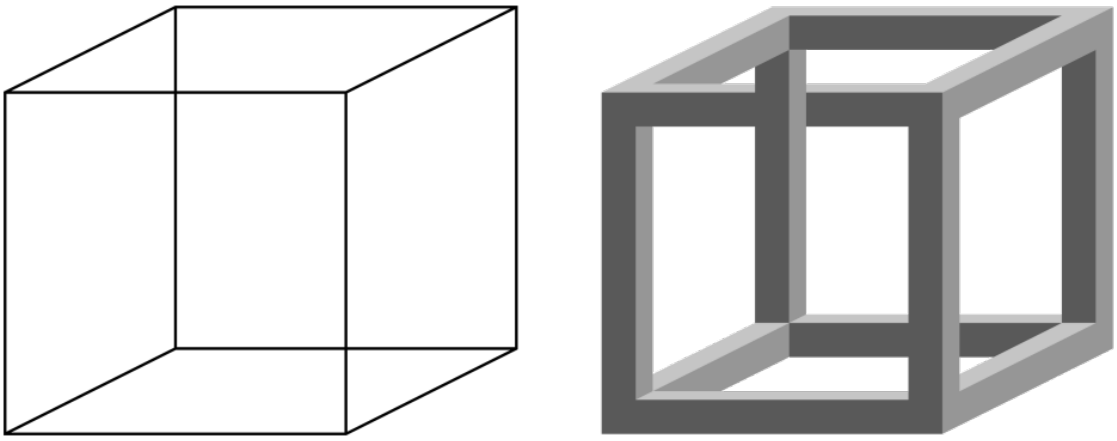

Figure 3: Necker cube and impossible figure

Some illusions include the expectation of the usual perspective perception as a base. The famous illusion using the convergent lines to distort the perception of the size was created by Mario Ponzo in 1982 (Leibowitz, Brislin, Perlmutrer, & Hannessy, 1969). The object closer to the vanishing point seems larger than the object of the same size placed further away of the vanishing point. There are multiple variations of the Ponzo illusion, the simple one is shown in Figure 4. One natural phenomenon is the moon illusion – the effect of the moon which appears as much larger when it is near horizon (Ross & Plug, 2002). One of the reasons is that the moon looks larger when it is close to clouds near the horizon which appear smaller to the observer (Figure 5).

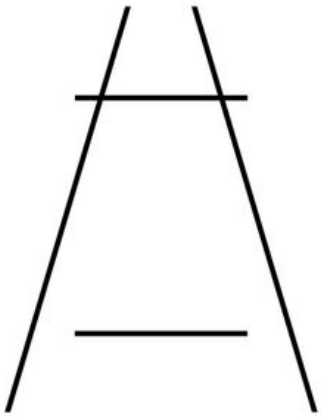

Figure. 4: Ponzo illusion

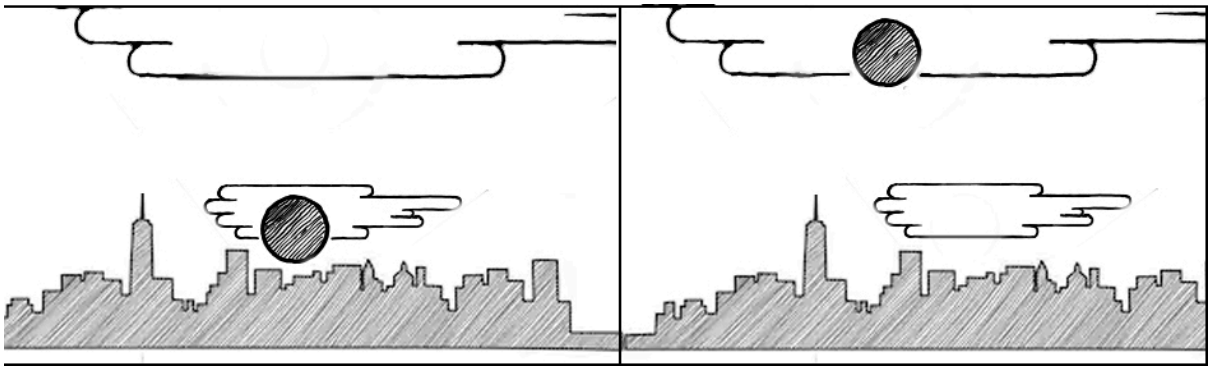

Figure 5 Moon illusion

Shepard tables is an optical illusion created in 1990 by psychologist Roger Shepard (Bach & Poloschek, 2006).The illusion is interesting because it combines orthogonal view with the perspective constrained perception. The tabletops are identical parallelograms, just rotated by 90 degrees. However when the tabletops are put in realistic surrounding (e.g. by adding legs) the perspective perception is triggered. The effect is that one table looks elongated while other look as almost a square (Figure 6). The reason is that dimensions naturally get much more shorten in near-far direction (towards the horizon) than in frontal position.

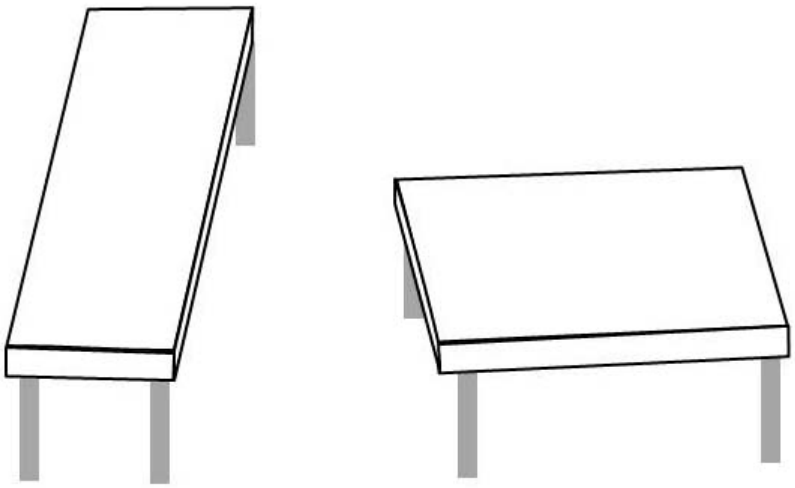

Figure 6: Shepard tabletop illusion

Forced perspective is an applicable illusion in which the size is differently perceived because of the presumed relationships between elements. It became very popular for tourist photographs in which people pretend to hold

Pisa tower or that the sun is between their fingers. Except for the fun with photographs, forced perspective has important role in architecture, theatre plays and movie production. Disney castles often use forced perspective to appear larger (Figure 7). The fake scale models of the castle parts are put on the top of the real building. In order to make the impression that such sculptural scale models are integral part of the castle several main ideas are implemented. The scale model has to be in the right position considering the view from the entrance. The repetition of the elements that differ only in size (windows, bricks) is used because we assume that same shaped elements have the same size too. In movies same principles of the forced perspective can be used to make actors to appear larger or smaller than they really are (e.g. it is used in Lord of the Rings to make hobbits look smaller).

Figure 7: Disneyland Beast castle, a) illusion of size, b) real size presented in comparison to human figure

One of the most interesting illusions to the students are an anamorphosis. An anamorphic image is the image which appears normal when viewed from a particular point or with a suitable mirror. Anamorphosis made on planes are actually perspective projection, just highly distorted, so that the shape cannot be perceived from any point of view, but from the predefined point of view the image seems like it is in a different plane. In order to connect the creation of the illusions with the Descriptive Geometry and Perspective, it is encouraged that an anamorphosis is created by the construction of vanishing points in orthogonal views and afterwards, constructed as perspective projection drawings (Figure 8).

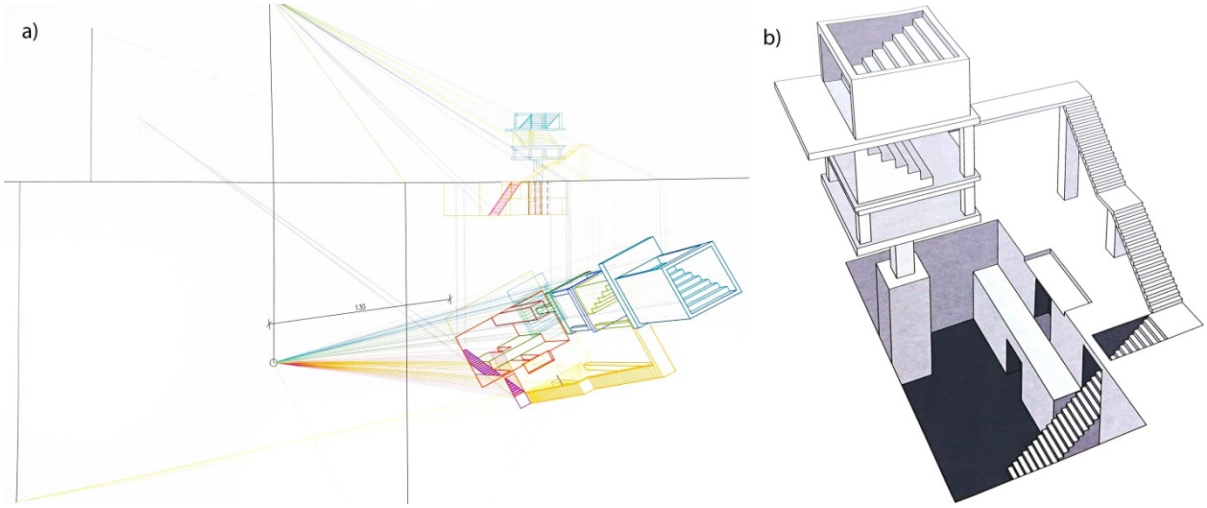

Figure 8: Student's project a) anamorphic drawing and construction, b) illusion of depth observed from the predetermined view point

Three dimensional models are also very interesting to experiment on, because the shape ambiguity, perspective perception and distortions can be combined. Shapes perceived as a different can be used to make the illusions in which it looks like the water flows or ball slides upwards or to perform other similar tricks. The main point in such a trick is to use the expectations of the brain to assume that the retinal image represents the familiar shapes

based on perpendicular planes and angles, circles, etc. Three dimensional illusions can be perceived form the two points of view which make the illusion even more intriguing (Figure 9).

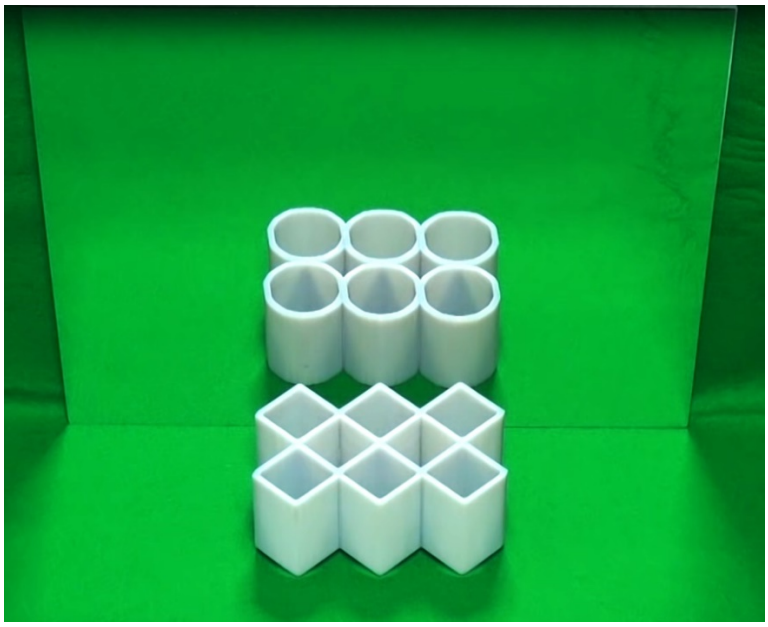

Figure 9: Mirror illusion (Kokichi Sugihara, 2016)

CONCLUSION

In this paper the main theories of perception are presented and the relationship with the illusions is explained. The illusions which appear to be most interesting to the students are shortly described.

Study of the perception can be used as a motivation for students in the area of technical disciplines to put more effort in understanding both Descriptive Geometry and Perspective. Optical illusions are the main driver for the students because of its intriguing nature. Some illusions are interesting to show, study and understand the mechanism behind while others are good practice for direct application of the methods learned in Descriptive Geometry and Perspective.

The limitation of this research is that the effect of the perception teaching has not been not measured, it relies on the subjective interpretation of the teacher-students communication, so that the future work is to be focused on a careful defining appropriate themes which might be given to students that are interested in additional research as an optional activity. Further, thorough analysis and comparison during examination of both groups of students, i.e. those who worked on extra research and those who did not, should be carried out, so that the results of the examination might give opportunity for collecting more objective conclusions on the learning outcomes.

REFERENCES

1. Bach, M., & Poloschek, C. (2006). Optical illusions. *Advances in Clinical Neuroscience & Rehabilitation, 6*(2), 20-21.
2. Deci, E. L. (1991). Motivation and Education: The Self-Determination Perspective. *Educational Psychologist, 26*(3-4), 325-346
3. Gallagher, J. J. (2000). Teaching for Understanding and Application of Science Knowledge. *School Science and Mathematics*, 310-318.
4. Guillen, M., Marquez, J., & Bernal, B. (2014). The spinning dancer illusion and spontaneous brain fluctuations: an fMRI study. *Neurocase, 20*(6), 627-639.
5. Howe, C., & Purves, D. (2005). Perciving Geometery: Geometrical Illusions Explained by Natural Scene Statistics. New York: Springer.

6. Hutton, M. (1998). Nursing mathematics: The importance of application. *Nursing standard, 13*(11), 35-38.
7. Julesz, B. (1960). Binocular depth perception of computer-generated patterns. *Bell System Technical Journal, 39*, 1125-1162.
8. Koffka, K. (1935). Principles of Gestalt psychology. NY: Brace.
9. Kokichi Sugihara, M. U. (2016). *Illusion of the year*. Retrieved from "Ambiguous Cylinder Illusion": www.illusionoftheyear.com
10. Kornmeier, J., & Bach, M. (2005). The Necker cube—an ambiguous figure disambiguated in early visual processing. *Vision research, 8*, 955-960.
11. Leibowitz, H., Brislin, R., Perlmutrer, L., & Hannessy, R. (1969). Ponzo perspective illusion as a manifestation of space perception. *Science, 166*(3909), 1174-1176.
12. Pal, I. (1966). *Nacrtna geometrija u anaglifskim slikama.* Zagreb: Tehnicka knjiga Zagreb.
13. Pizlo, Z. (2008). 3D Shape: Its Unique Place in Visual Perception. London: MIT Press.
14. Ross, H., & Plug, C. (2002). The Mystery of The Moon Illusion-Exploring Size Perception.
15. Schneider, W. (1998, September 1). Anamorphoses for games, education and promotions. *U.S. Patent 5,799,939*, pp. 1-16.
16. Schott, P. (2010). The use of magic in optics in higher education. *Creative Education, 1*, 10-17.

THE BENEFITS OFAN ADDITIONAL PRACTICE IN DESCRIPTIVE GEOMETRY COURSE: NON OBLIGATORY WORKSHOP AT THE FACULTY OF CIVIL ENGINEERING IN BELGRADE

Magdalena Dragović
Faculty of Civil Engineering, University of Belgrade, Belgrade, Serbia
PhD., Assistant Professor, dim@grf.bg.ac.rs

Svetlana Čičević
Faculty of Traffic and Transportation, University of Belgrade, Belgrade, Serbia
PhD., Professor, s.cicevic@sf.bg.ac.rs

Aleksandar Čučaković
Faculty of Civil Engineering, University of Belgrade, Belgrade, Serbia
PhD., Associate Professor, cucak@grf.bg.ac.rs

ABSTRACT

At the Faculty of Civil Engineering in Belgrade, in the Descriptive geometry (DG) course, non-obligatory workshops named "facultative task" are held for the three generations of freshman students with the aim to give students the opportunity to get higher final grade on the exam. The content of this workshop was a creative task, performed by a group of three students, offering free choice of a topic, i.e. the geometric structure associated with some real or imagery architectural/art-work object.

After the workshops a questionnaire (composed by the professors at the course) is given to the students, in order to get their response on teaching/learning materials for the DG course and the workshop. During the workshop students performed one of the common tests for testing spatial abilities, named "paper folding".

Based on the results of the questionnairethe investigation of the linkages between:students' final achievements and spatial abilities, as well as students' expectations of their performance on the exam, and how the students' capacity to correctly estimate their grades were associated with expected and final grades, is provided. The goal was to give an evidence that a creative work, performed by a small group of students and self-assessment of their performances are a good way of helping students to maintain motivation and to accomplish their achievement.

The final conclusion is addressed to the benefits of additional workshops employment in the course, which confirmhigherfinal scores-grades, achievement of creative results (facultative tasks) and confirmation of DG knowledge adaption.

Keywords: Descriptive geometry course; workshop; spatial ability test; questionnaire; self-assessment.

INTRODUCTION

The ultimate goal of education is to help students become self-sufficient learners (Karably et al., 2009). Modern teaching methods aim to facilitate this process in order to improve students' learning success. They achieve this by using student-centered learning arrangements but also assign more responsibility to studentsfor their own learning outcome (Beumann et al., 2018).The creation of pedagogical conditions for successful self-independent construction and growth of students' knowledge is of key importance (Voronina et al., 2018)

Students' ways of approaching their studies influence their academic outcomes. Expecting high grades and having the skills to steer learning activities towards assessment demands seem to be important components of academic success (Öhrstedt et al., 2019). However, our knowledge about students' capacity to predict academic achievement is still limited.In the era of fast modern technologies, there is a need to hold students' interest and motivation on a subject matter which requires much attention and deep cognitive actions (Dobelis et al., 2019).

Expecting high grades seems to be an important component for achieving high grades (Dochy, et al.,1999; Hattie 2015). In his comprehensive review of 800 meta-analyses related to education, Hattie (2008) found that self-reported grades (a weak form of self-assessment where students simply predict their own grades and then try to achieve them) were one of the single-most important strategies for improving student achievement. To be able to assess and value their academic outcomes, students need to assess their learning. This requires that students have self-assessment skills.

Self-assessment and goal setting are two strategies employed by educators to assist in the task of developing self-regulated learners. A key type of student self-judgment is self-assessment, which refers to students comparing their learning outcomes with a goal or standard (Labuhn et al., 2010). During self-assessment, students are responsible for interpreting their own results, explaining what the results mean, and determining what actions to take to improve their learning (O'Brian et al., 2010). Self-assessment is important as it complements learning goals and helps students maintain high levels of self-efficacy, including both reflections on and evaluation of one's work; it helps to develop feelings of ownership, and build responsibility for learning (Paris et al., 2001).

LeBlanc et al., (1985) define self-assessment as procedures by which the learners themselves evaluate their skills and knowledge. Harris et al., (1994) regard self-assessment as a self-directed and determined learner setting his/her own assessment criteria, judging his/her learning processes (or product) against these criteria, and making decisions based on these judgments. Self-assessment is more accurately defined as a process by which students 1) monitor and evaluate the quality of their thinking and behavior when learning and 2) identify strategies that improve their understanding and skills. That is, self-assessment occurs when students judge their own work to improve performance as they identify discrepancies between current and desired performances (McMillan et al., 2008; Lee, 2009).

A second component of self-assessment, self-judgment, involves identifying progress toward targeted performance. These judgments give students a meaningful idea of what they know and what they still need to learn (Bruce 2001; McMillan et al., 2008).

Students with high expectations are more likely to persist; those with low expectations often avoid tasks or give up (Brophy, 2004). Positive self-evaluations encourage students to commit more resources to continued study and set higher goals in the future (Schunk, 1995). When involved in assessing their own academic growth, students become more aware of their learning goals and the results of their efforts (Joseph, 2006), thus developing their skills as agents of learning.

It is well established that student engagement depends upon students' self-efficacy beliefs- perceptions of their ability to do well on a specific task, and the value of doing well (Pintrich et al., 2002; Schunk 2004). Self-efficacy involves students estimating what they can do and the likelihood of successful performance. Students achieve more when they set specific goals for themselves (Zimmerman et al., 1989; McMillan et al., 2008). Also, performances can be improved simply by having students self-report their learning.

Students who believe that they can successfully complete a task are more motivated and engaged. What are more important, self-assessment skills can be trained and such training also improves learning and academic performance. Motivation leads to enhanced performance, persistence, and creativity. Therefore, it is important to provide strategies that affect cognitive engagement and motivation (Park, 2018).

High-achieving students could be characterized as highly self-regulated learners. Self-regulated learners could be distinguished by their systematic use of metacognitive, motivational, and behavioral strategies; by their responsiveness to feedback regarding the effectiveness of their learning; and by their self-perceptions of academic accomplishments (Zimmerman, 1990; Panadero, 2017).Metacognition, which has been widely investigated and reported in both educational and psychological literature, involves the capacity to monitor, evaluate, and know what to do to improve performance. This includes conscious control of specific cognitive skills such as checking understanding, predicting outcomes, planning activities, managing time, and switching to

different learning activities. It is a set of skills that relate positively to increased achievement, and such skills can be taught to students (Schunk 2004; Panadero, 2017).

Learner autonomy, the development of study skills, the concept of life-long learning, and increased motivation were found by Oskarsson (1989) to be some of the benefits of self-assessment. Self-assessment fosters the development of the meta-competencies—like self-efficacy, self-confidence, and motivation. Self-assessment encourages the students not just to maximize the teacher-assigned grade but to learn the subject on a level of deep understanding (Beumann et al.,2018).

Currently, in most undergraduate curricula students' active participation in their learning process means much more than just attending lectures. Despite lectures still being widely used, other more interactive learning activities that provide opportunities for peer learning, as students working in small groups searching for the solution of contextualized problems are increasingly being used (Ramirez 2015,Voronina et al. 2018).

Descriptive Geometry is an educational course that provides a training of the students' intellectual capability of space perception, important for the variety of engineering professions, and it opens an insight into the structure, and metrical properties of spatial objects, geometric procedures and principles for their design. In the new context of technological environment, beside classical projections of a spatial object, DG improves students' skills in 3D modeling of various curves, surfaces and solids, by employing logical reasoning between 3D structure and 2D projection, and activating students' spatial abilities(Stachel 2007).

At the Faculty of Civil Engineering in Belgrade, in the Descriptive geometry (DG) course, non-obligatory workshops named "facultative task" are held for the three generations of freshman students with the aim to give students the opportunity to get higher final grade on the exam. The final outcome of the students' task was devisedas a creation and representation of a geometric structure applicable in architecture or other type of design.

This study is set out to investigate the linkages between their final achievement and spatial ability, as well as students' expectations of their performance on an exam, and how the students' capacity to correctly estimate their grades were associated with expected and final grades. The goal was to provide an evidence that a creative work, performed by small group of students and self-assessment of their performances are good way of helping students to maintain motivation and to accomplish their achievement.

2. MATERIAL AND METHODS

At the Faculty of Civil Engineering in Belgrade, in the Descriptive geometry (DG) course, non-obligatory workshops named "facultative task" are held for the three generations (total of 50 students) of freshman students with the aim to give students the opportunity to get higher final grade on the exam. The content of this workshop was a creative task, performed by a group of three students, offering free choice of a topic, i.e. the geometric structure associated with some real or imagery architectural object. The task consisted of: creation of 3D model of coordinate system (cardboard model)with 2D drawings-orthogonal projections of a chosen structure – 1(Fig.1a), its geometric modelling in AutoCAD software (Fig 1b) or the optional card-board model -2 and a poster presentation of the overall creative process -3 (Fig. 2). The final result was enriched by architectural/art-work examples of similar objects (buildings/art piece) and images obtained by AR application "Augment" for smart-phones aimed for the visualization of 3D objects (Fig. 1c).The workshop was performed during two days (approx. 12 hours of work in the classroom) at the end of the two near exam terms (January and February).

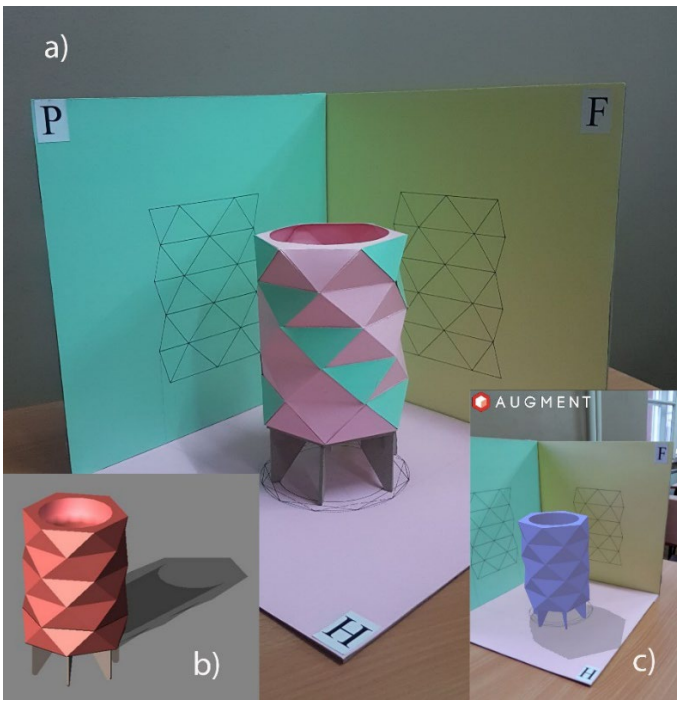

Figure 1: Students creative tasks: (a) Physical model of the art-work piece; (b) 3D model in Auto CAD software; (c) AR application (Source: authors' photo images of the students' work)

At Descriptive Geometry course at the Faculty of Civil Engineering, the students gained theoretical knowledge and were taught the methods and principles of graphical representations of various types of geometric solids and surfaces. The knowledge related to the basic ones, such as prism, pyramid, cone, cylinder, sphere, polyhedrons (cube, tetrahedron and icosahedron), and more complex ruled surfaces, as well as geometric operations that enable variety of their spatial settings, were the students' base for the investigation of a chosen inspiration – the structure that appears in the literature, or in real, or imagery world of architecture/design. Prior to the workshop students did not have the opportunity to test their actual knowledge in the practical – engineering/design manner.

In reality, most of the architectural or design/artistic structures are rather combinations or multiplications of the elements (the whole element, or its parts), either of the same type or different, and additionally, often specifically set in a spatial surroundings. One of the "problematic" issues of this experimental work with freshman students was their actual ability to recognize the exact geometric characteristics of a chosen (realistic) structure (or its elements), and to adopt an adequate approach for its' graphical representation, specifically because of the lack of their practical experience. The workshop was an ideal opportunity for the testing of students' skills and even more, their creativity.

In order to inspire students, challenge and encourage them to participate in the workshop, prior to its realization date, several examples - images of the structures (roofing structures or design creations) were made available as teaching materials at the Faculty's website (http://grf.bg.ac.rs). Some of the most creative examples were chosen from the book "Geometric surfaces in architecture" by Sonja Krasić (2012) (geometric roofing structures which combine: Plato's solids, cylinders, hyperbolic paraboloids, conoids, etc., set over regular polygonal bases or in some other spatial arrangements). Other practical instructions for the creation of a 3D physical (card-board) model of coordinate planes and several illustrations for the other parts of the task, were given along with an example of the final poster presentation (containing all the elements of the task).

The realization of the workshop assumed several practical conditions: the two available classrooms, one for the realization of the manual drawings and the other one aimed for computer drawing/modeling additionally supported by internet access (1); the two professors conducted the work of the workshop simultaneously, during all working hours, by instructing, guiding and helping students in solving the main issues of the tasks, while several (3-5) associates-older and experienced students supported the practical performance (2).

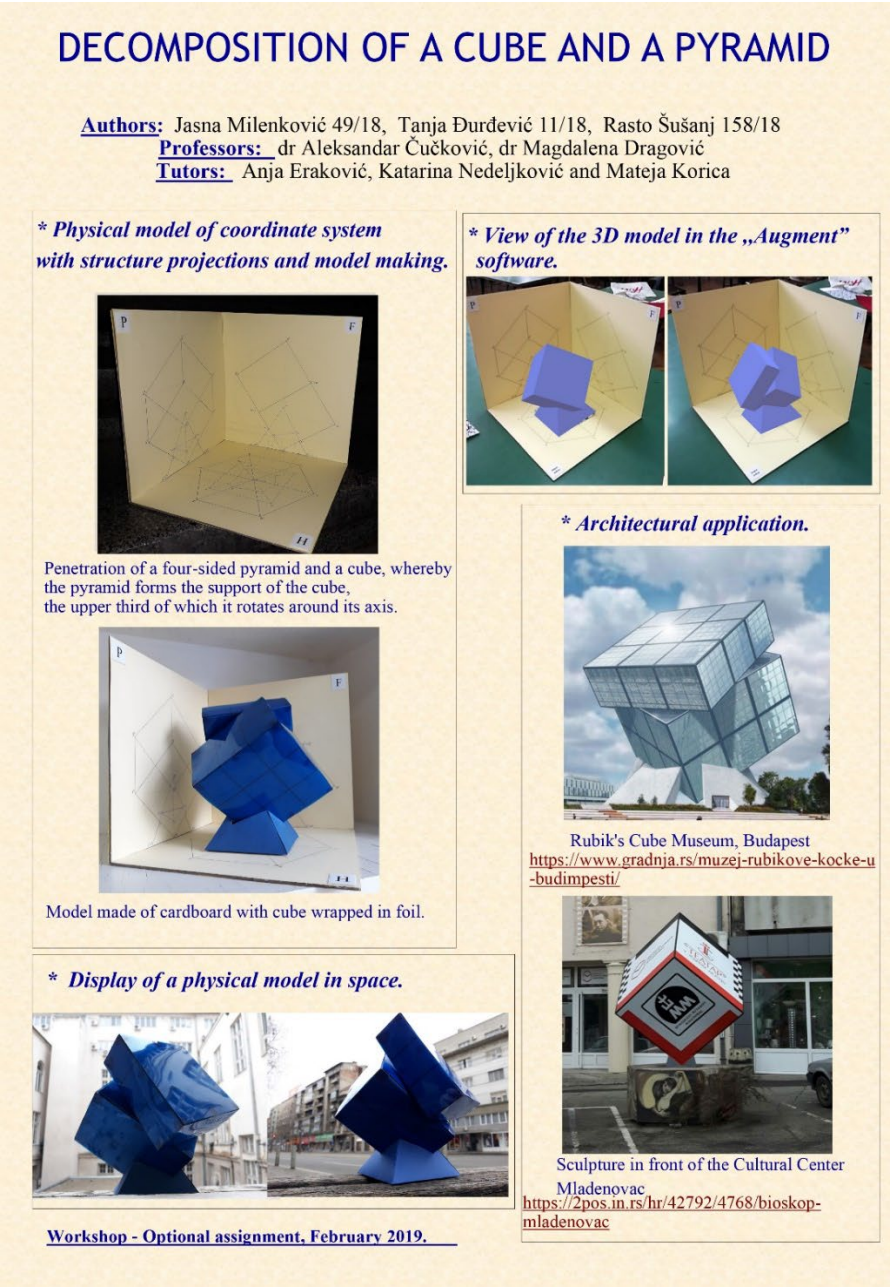

Figure 2: Final poster-presentation of one of the representative students' workshop tasks

After each of the workshops a questionnaire (composed by the professors at the course) is given to the students, in order to gather their response upon teaching/learning materials for the DG course and the workshop. During the workshop students performed one of the common tests for testing spatial abilities, named "paper folding" (PF), as one of the most important ability in working with Descriptive geometry is spatial ability which has a substantial position in human thought and for engineering students is very desirable. Variables covered by the questionnaire were students self-assessment of their own performances on the workshop, previous experience with spatial ability tests, with 3D software, mobile and AR application, as well as with teamwork, visibility and problems with projections, subjective assessment whether DG course is interesting and difficult, time necessary for exercise preparation, creativity self-assessment and overall satisfaction with workshop results. The questionnaire comprised several open-ended questions, so that the respondents had the opportunity to describe what they liked about the participation in the workshop, to give their comments and suggestions for improving the workshop quality.

3. RESULTS AND DISCUSSION

Package for the Social Sciences (SPSS) was used to code and tabulate scores collected from the survey. First, descriptive statistics were employed to take a general view of students' responses. Further, grades can be considered ordinal level data, thus demanding Spearman correlations. However, grades can be analyzed using Pearson correlations and so both Pearson and Spearman coefficients were computed. Two-tailed *P* values of 0.05 were considered statistically significant.

This paper presents some of the most important results from the very extensive research undertaken. Of the total number of students who participated in the workshops, 52.5% achieved the highest overall final grade, while 30% of students received a grade of 9. The highest grade for the project was given to 42.5% of participants, and 35% received a grade of 9.Near half of the of students (55%) rate themselves with a grade of 9, and 30% of them think that they deserve the highest grade.

On the PF test, 25% of students have the maximum achievement, while 30% of workshop participants solved the test with 90% success, although 70% of them have never had experience with aptitude tests before.

Further, the results show that 40% of the students provided perfect ratings of their final grades, among them, half of the students awarded themselves a grade of 10, 37% a grade of 9, and finally, 13% a grade of 8. 38% underestimated, while 22% of the students overestimated their final grade. Within the group who misjudge the final grade, 63 % underestimated their final grade(Figs.2a-d).Thus, the most common form of misjudgment (63 per cent of the students) involved underestimating the final grade; that is, they expected a lower grade but received a higher grade. In comparison, only 37% of the students overestimated their final grade, thus they expected a higher grade than the one they received.

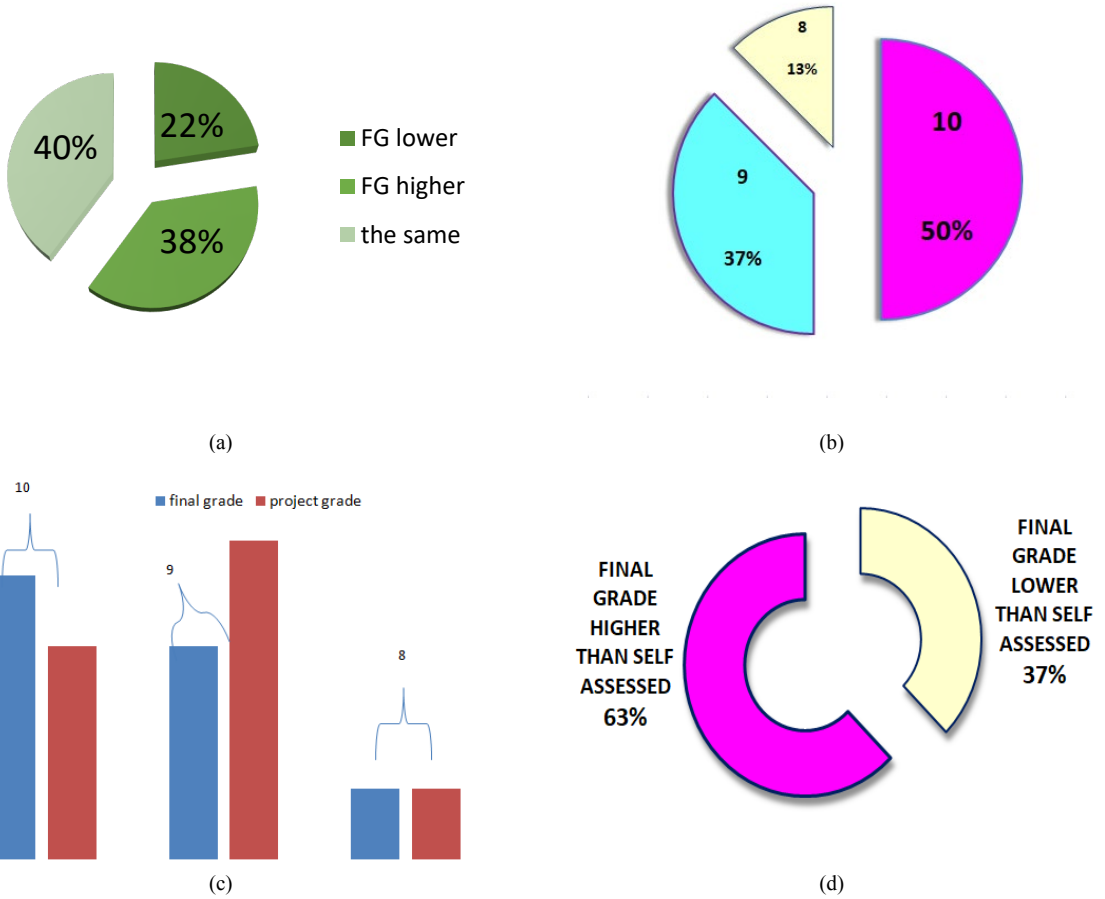

Figure 2:(a) Relationship between self-assessed and final grade, (b) Percent of cases where self-assessed and final grade are equal, (c) Relationship between project and final grade, and (d) Percent of students that misjudge the final grade

When it comes to the comparison of the project grade (all the phases of a creative task) in relation to the self-assessed, 43% of the students made perfect estimations of their project grades, among them, 35% of the students awarded themselves a grade of 10, 53% a grade of 9, and finally, 12% a grade of 8. Within the group who misjudge the final grade, there are almost the same percentage of students who under or overestimated their project grades(Figs.3 a-c).

The overall percentage of the students who provided perfect ratings of their final and project grades is almost the same, but there are differences in the ratio of the grades they awarded themselves. Namely, higher number of students assigned the grade of 10 as a final grade, while, for the project grade the majority of the assigned grades belong to category 9.

During the completion of the questionnaire, respondents had the opportunity to describe what they liked about their engagement in the workshop, to give their comments and suggestions for improving the work in the workshop. Out of the total number of students who took the opportunity to answer these open-ended questions, 47% highlighted teamwork, as well as, teamwork combined with the opportunity to express their creativity. A quarter of students emphasize the creation of 3D models as a great advantage of participating in the workshop, the final result, i.e., the realization of the idea to the end, and mastering new skills emphasizes 6.25% of participants (respectively), while close to 10% of respondents pointed out the choice of important and interesting topics. Students' open-ended comments also suggest that using self-assessment has helped them to maintain their motivation and to become more aware of their participation and involvement in the learning, thus indicating more learner autonomy.

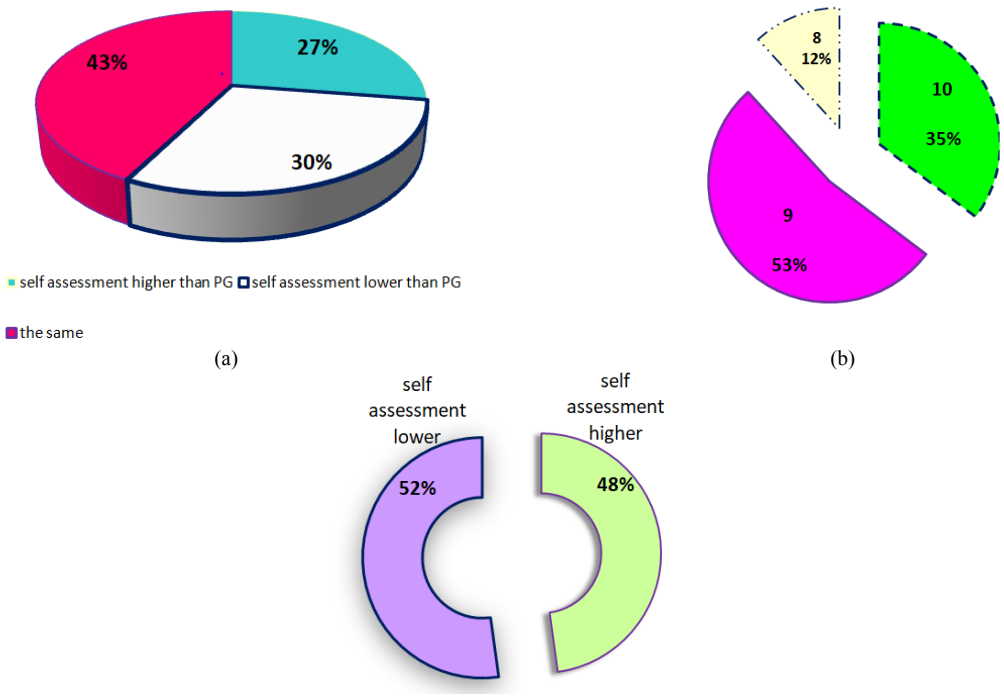

Figure 3: (a) Relationship between self-assessed and project grade, (b) Percent of cases where self-assessed and project grade are equal, and (c) Percent of students that misjudge the projectgrade

Correlation coefficients show the highest positive values for the relationship between grades for practice exercises in DG and the final course grades, and also high correlations exist between achievement on the test of spatial abilities and final grades, as well as with grades for practice exercises (Figs.4 a - b).

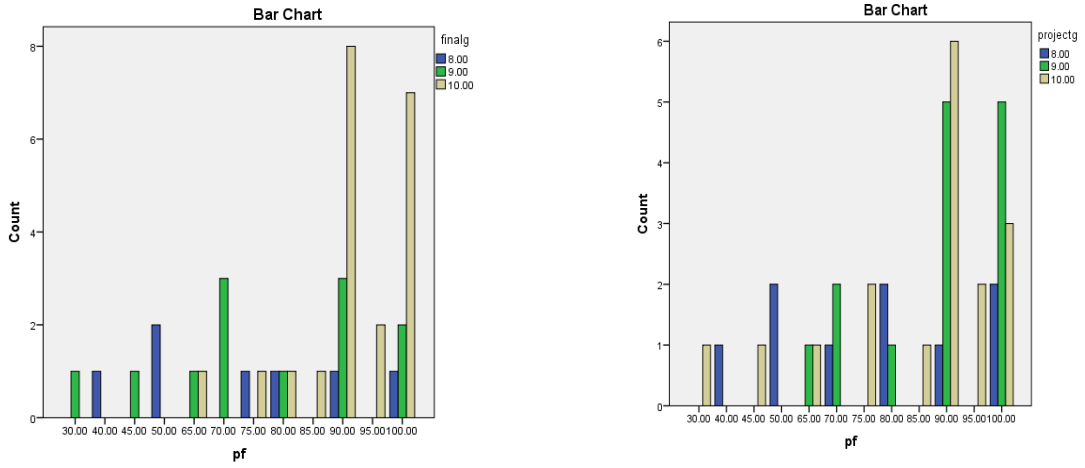

Figure 4:(a) Relationship between the paper folding test scores and the final grade, (b) Relationship between the paper folding test scores and the project grade

Negative association appear between grades for exercises and experience in teamwork, suggesting that students who participated in teamwork earlier show higher average grades for practice exercises (M=9.51) compared to those who do not have teamwork experience (M=8.6) (Table 1).

Table 1: Significant associations among variables

Site	*Final grade*	*Exercises grade*	*Project grade*
PF	*.495***	*.356**	
Final grade		*.600***	*.430***
Teamwork		*-.585***	
**. Correlation is significant at the 0.05 level (2-tailed).*			
***. Correlation is significant at the 0.01 level (2-tailed).*			

Öhrstedt et al. (2016) reported a negative association between the surface approach and expected grades, but also found positive associations between both the deep and strategic approaches to learning, respectively, and expected grades. Meta-analyses of students' capacity to predict examination grades have shown a mean correlation of r ≈ .40 (Mabe et al., 1982; Boudet al., 1989; Falchikov et al., 1989). Comparing the present findings with previous research, the correlation coefficients show somewhat higher values.

All this leads to the conclusion that, in addition to acquiring specific skills necessary to master the material on the DG course, abilities, communication skills, careful selection and cooperation among team members play a significant role, in the success and satisfaction of students. Self-assessment can increase the interest and motivation level of students for the subject leading to better academic performance and enhanced learning. It can also help in development of critical skills among students to assess and analyze their own work, an essential component of self-directed lifelong learning. Self-assessment encourages the students not just to maximize the teacher-assigned grade but to learn DG on a level of deep understanding.

CONCLUSIONS

Beside their practical role, to achieve the connection of the "world" of an engineering practice with Descriptive Geometry knowledge from students point of view, the workshops employed in the teaching/learning process at the Faculty of Civil Engineering gave significant insight into achievements of several educational goals. This paper described positive students' attitude toward DG after their participation in the motivational workshop. Namely, when students were actively engaged in the task which employed their creativity and other personal capacities, they eagerly participated, which consequently led to the positive attitudes. Results indicated that teaching DG through a motivational workshop model was more acceptable to students than traditional

teaching/learning methods (Dragović et al., 2019). Evaluating what they have learned, what they still need to work on, and how they can get there can all support deeper understanding rather than superficial knowledge.

Students' open-ended comments also suggest that using self-assessment has helped them to maintain their motivation and to become more aware of their participation and involvement in the learning, thus indicating more learner autonomy. Students benefit from explaining their work and their own evaluation of quality through reflective activities and they are more satisfied with their performance when they can evaluate their work. Correctly implemented, student self-assessment can promote intrinsic motivation, internally controlled effort, a mastery goal orientation, and more meaningful learning (Mc Millan et al., 2008).Overall, students displayed good ability to self-assess accurately, variations probably relate to the discipline (DG) being specific, as well as, to circumstances characterizing the local educational setting. From a practitioner's point of view, students' ideas of assessment and their assessment literacy are of interest for the improvement of learning conditions.

It is important to train students self-assessment practices which should no longer be treated as an assessment, but instead as an essential competence for self-regulation which are to be focused throughout the learning cycle rather than at the final result. Workshops in which participants present their accomplishment are an opportunity for students to formally reflect on the learning that has taken place. This reflection occurs when students prepare themselves for the project, as well as during the presentation itself when they show and explain what they have done. Thus, a curriculum for self-assessment competence would be of great benefit to educational practice and will trigger significant developments, especially in online learning environments where teachers and learners interact in real time, and which requires new teaching and communication skills. Teacher's assistance is even more important if we want learners to develop high levels of competence and confidence. Effective online teacher finds ways to give every sort of feedback about their work to individual, as well as to groups of learners, facilitate mutual understanding, communication and learning experience which will contribute to improved classroom practice in Descriptive Geometry courses, as well as in general educational practice.

Acknowledgements

This work is partially supported by the Ministry of the Science and Technological Development of the Republic of Serbia under No. 036022, No. 036006 and No. 36008.

REFERENCES

Beumann, S. and Wegner, S-A. 2018. An outlook on self-assessment of homework assignments in higher mathematics education. *International Journal of STEM Education,* 5(55). https://doi.org/10.1186/s40594-018-0146-z.

Boud, D. and Falchikov, N. 1989. Quantitative Studies of Student Self-Assessment in Higher Education: A Critical Analysis of Findings. *Higher Education,* 18(5). pp 529–549. Doi:10.1007/BF00138746.

Brophy, J., 2004. Motivating Students to Learn. Second edition. Lawrence Erlbaum, Mahwah, N.J.

Bruce, L. B. 2001. Student Self-Assessment: Making Standards Come Alive. *Classroom Leadership,* (5)1. pp. 1–6.

Dochy, F. Segers, M. and Sluijsmans, D. 1999. The Use of Self-, Peer and Co-Assessment in Higher Education: A Review. *Studies in Educational Evaluation*, 34(3). pp 331–350. Doi:10.1086/250095.

Dragović, M., Čičević, S., Čučaković, A., Trifunović, A. and Gramić, F., 2019. Positive Impact of 3d Cad Models Employment in Descriptive Geometry Education. *The Journal of Polish Society for Geometry and Engineering Graphics,* 32. pp. 11-16. Doi: 10.36176/96.PTGiGI.2019.32.2.02.

Dobelis, M., Sroka-Bizon, M., Bfanoff, T., 2019. How to boost the students' interest to engineering graphics? IOP Conference Series: Materials Science and Engineering, 660, 012013.

Falchikov, N. and Boud, D. 1989. Student Self-Assessment in Higher Education: A Meta-Analysis. *Review of Educational Research*, 59(4). pp 395–430. Doi:10.3102/00346543059004395.

Harris, D., Bell, C. 1994. Evaluating and Assessing for Learning. Nichols Publishing, East Brunswick, NJ.

Hattie, J. A. C. 2008. Visible learning: A synthesis of over 800 meta-analyses relating to achievement. First edition. Routledge, London.

Hattie, J. A. C. 2015. The applicability of Visible Learning to higher education. *Scholarship of Teaching and Learning in Psychology,* 1(1). pp 79–91. https://doi.org/10.1037/stl0000021.

Joseph, N. 2006. Strategies for success: Teaching metacognitive skills to adolescent learners. *The NERA Journal, 42*(1). pp 33-39.

Karably, K. and Zabrucky, K. M. 2009. Children's metamemory: A review of the literature and implications for the classroom. *International Electronic Journal of Elementary Education, 2*(1). pp 32-52.

Krasić, S. 2012. *Geometric surfaces in architecture*/*Geometrijske površi u arhitekturi*, Faculty of Civil Engineering and Architecture/Građevinsko -arhitektonski fakultet, Niš.

Labuhn, A. S. Zimmerman, B. J. and Hasselhorn, M. 2010. Enhancing students' self-regulation and mathematics performance: The influence of feedback and self-evaluative standards. *Metacognition Learning, 5*. pp 173-194. Doi:10.1007/s11409-010-9056-2

Leblanc, R. and Painchaud, G. 1985. Self–assessment as a second language placement instrument. *TESOL Quarterly,* 19(4). pp 673–305.

Lee, Y-H. 2009. Self-assessment in Interpreter Training: Student-teacher Interface Model of Assessment. Université de Genève Ecole de traduction et d'interprétation.

Mabe, P. A. and West, S. G. 1982. Validity of Self-Evaluation of Ability: A Review and Meta-Analysis. *Journal of Applied Psychology*, 67(3). pp 280–296. Doi:10.1037/0021-9010.67.3.280.

McMillan, J. H. and Hearn, J. 2008. Student Self-Assessment: The Key to Stronger Student Motivation and Higher Achievement. *Educational Horizons*, 87(1). pp 40-49.

O'Brian J. R., Nocon, H. and Sands, D. I. 2010. The use of dialogue and tools to develop students' mathematical language and meta-cognition. *Teacher Development, 14*(4). pp 447- 466. Doi: 10.1080/13664530.2010.533487.

Öhrstedt, M. and P. Lindfors. 2016. Linkages between Approaches to Learning, Perceived Stress and Expected and Actual Academic Outcomes among First-Semester Psychology Students. *Journal of Further and Higher Education*, 42(1). pp 116–129. Doi:10.1080/0309877X.2016.1206856.

Oscarson, M. (1989). Self-assessment of language proficiency: Rationale and implications. *Language Testing*, *6*(1). pp 1-13. Doi: 10.1177/026553228900600103.

Panadero E. (2017). A Review of Self-regulated Learning: Six Models and Four Directions for Research. *Frontiers in psychology*, *8*, 422. https://doi.org/10.3389/fpsyg.2017.00422

Paris, S. G. and Paris, A. H. 2001. Classroom applications of research on self-regulated learning. *Educational Psychologist, 36*(2). pp 89-101.

Park, S.W., 2018. Motivation Theories and Instructional Design. In Foundations of Learning and Instructional Design Technology (Ed. R. West). Available at https://lidtfoundations.pressbooks.com/.

Pintrich, P. R. and Schunk, D. H., 2002. Motivation in Education. Englewood Cliffs, NJ: Prentice Hall.

Ramirez, B. U. 2015; Correlation of self-assessment with attendance in an evidence-based medicine course. *Adv Physiol Educ* 39. pp 378–382, Doi:10.1152/advan.00072.2015.

Schunk, D. H. 1995. Inherent details of self-regulated learning include student perceptions. *EducationalPsychologist,* 30. pp 213-216.

Schunk, D. H. 2004. Learning Theories: An Educational Perspective. Sixth edition. Pearson/Merrill/Prentice Hall. Upper Saddle River, N.J.

Stachel, H., 2007. The status of today's DG related education (CAD/CG/DG)*Journal of Graphic Science of Japan* 41.Supplement 1, pp. 15-20. Doi: 10.5989/jsgs.41.Supplement_15

Voronina, M. V., Ignatiev, S. A., Merkultova, V. A. 2018. Systematic review of a flipped learning model for the courses of Descriptive Geometry, Engineering and computer graphics. *Advances in Intellignet Systems and Computing 809,* pp. 1765-1776. https://doi.org/10.1007/978-3-319-95588-9_158

Zimmerman, B. J. and Schunk, D. H. 1989. Self-regulated learning and academic achievement: Theory, research, and practice. Springer-Verlag. New York, NY.

Zimmerman, B. J. 1990. Self-regulated learning and academic achievement: An overview. *Educational Psychologist, 25*(1). pp 3-17.

DIDACTIC VIDEO-MATERIALS FOR TEACHING CONSTRUCTIVE GEOMETRY COURSES

Daniela Velichová
Department of Mathematics and Physics, Faculty of Mechanical Engineering, Slovak University of Technology in Bratislava, Slovakia
Doc. RNDr. CSc., Associate Professor, daniela.velichova@stuba.sk

ABSTRACT

These paper is aimed to present information about on-line educational materials developed in the Erazmus+ project DIAD-Tools to support teaching of subjects such as Technical Drawing, Descriptive Geometry, or Constructive Geometry at secondary and tertiary level in engineering educational programmes. DIAD-tools project is an international project joining powers of secondary and tertiary school teachers to improve the situation in geometric knowledge and technical skills of graduates at both types of schools, technical secondary schools and technical universities. In addition to videos, interactive materials developed in GeoGebra environment are available for on-line use, providing opportunity to investigate presented information in step-by-step mode and with individual speed. Another benefit might be seen in possibility of augmented reality usage. Investigation of all geometric constructions is possible observing 3D-scenes, as GeoGebra application provides stereoscopic view representation for red-green glasses on one click, which might improve spatial understanding, imagination and abilities of respondents.

Keywords: descriptive geometry; constructive geometry; video materials; augmented reality; 3D stereoscopic view; interactive applets

1. INTRODUCTION

In the beginnings of higher technical education and engineering schooling, Descriptive geometry used to be a compulsory subject proudly called „the queen of all technical disciplines“, and not so long ago it was also one of the important subjects at the secondary schools. Nowadays, hardly any of the secondary school graduates heard the name of this discipline. Only few of them could experience subjects related to technical drawing at the professionally oriented secondary schools, perhaps with an exception of those aimed at civil and mechanical engineering domains. However, every professionally reliable engineer should be aware of space relations, as constructor of space objects and designer of the space arrangement itself. Lack of spatial abilities and understanding may lead to many problems also in a lot of other domains, not only those related to technical disciplines.

Consequently, teachers of subjects such as Technical drawing, Descriptive or Constructive geometry and others, related to spatial stereo-metric relations, projection methods or 3D objects representation and properties, strive to develop and use didactic materials supporting spatial imagination and understanding. Lack of innovative learning materials suitable for introduction of available ICT and bringing active learning elements to educational process resulted in the establishment of a consortium of representatives of educational institutions from five EU countries. This professionally well balanced consortium succeeded in submitting a project proposal that was accepted and funded by the European program Erasmus+.

Erasmus+ project DIAD-Tools is an international project joining powers of secondary and tertiary school teachers to improve the situation in geometric knowledge and technical skills of graduates at both types of schools, technical secondary schools and technical universities. Consortium of partners consists of teachers and experts from five European countries – Lithuania, Latvia, Estonia, Poland and Slovakia. The main goal of the project was to develop sample examples of instructional materials, interactive and dynamic, which could be used as introduction to teaching, learning and training subjects related to Descriptive geometry and Technical drawing. The idea was to establish an open learning platform available on web with a variety of training materials, see (1).

Finally, the realistic expectations went to development of about 20 dynamic videos bringing basic information on different topics from the above disciplines. All materials are available in all 5 language mutations and in English version. Materials were tested and updated according to needs of customers from all participating countries and at both levels of respective educational institutions, secondary and tertiary. Learning platform is free to visit and materials can be used by all interested community. Therefore, the main idea of the present paper is to inform about form and contents of these project results.

2. EDUCATIONAL VIDEOS

Videos are lasting about 5 minutes each, and intended to bring informative text introducing short factual pieces of knowledge, possibly enriched by dynamic figures interpreting presented facts in more illustrative way. Scenarios and design of all videos were carefully planned in advance and discussed among the project partners. Practical examples were invited, suitable for the chosen domains and level of foreseen target group of students. Each partner was responsible for one separately chosen group of related topics covering the 4 main domains:

1. Execution of drawings, geometric drawing
   Some of the most important basic information on drawing practise is presented in videos from this part, and normative about used lines, scales and dimensioning principles in accordance to EU ISO standards.

- Scales
- Lines on engineering drawings
- Dimensioning
- Geometric relationships
- Polygons

2. Basics of projection drawings, views and sectional views, solids

   Videos contain information on basic projection methods mostly used in mechanical, construction and architectural engineering drawings. Animated pictures are intended to help students in understanding e.g. Monge method or Multiview projection, basic principles of linear perspective or object reconstruction from related views. Elementary solids and animated developments of their nets are presented, too.

- Projections
- Variations of prism
- Sectioning
- Reconstruction
- Solids and nets

3. Joints of parts, working drawings of parts

   Educational videos bring detailed information on threads and various types of joints and their parts, and they contain many practical examples about rules for marking and presenting joints on working drawings.

- Threads and threads representation in drawings
- Threaded fastenings
- Separable and permanent joints
- Assembly drawing
- Detailing assembly drawing

4. Construction drawings

   Materials in this group are aimed to bring practical examples of general principles in architectural and construction drawings, special markings and dimensioning rules and construction elements.

- Architectural and construction drawings general principles
- Graphic designations of the building materials
- Dimensioning in architectural-construction drawings
- Scales at architectural-construction drawings
- Construction

Additionally developed materials are available as tutorials on how to use some of the commands and related geometric constructions in the most used and popular CAD systems, e.g. AutoCAD or Onshape, innovative on-line design system available on any device that unites modelling tools and design data management in a secure cloud workspace, which never loses data and eliminates design gridlock.

Examples of some video shots from the second part – Basic of projections are presented in the figures below.

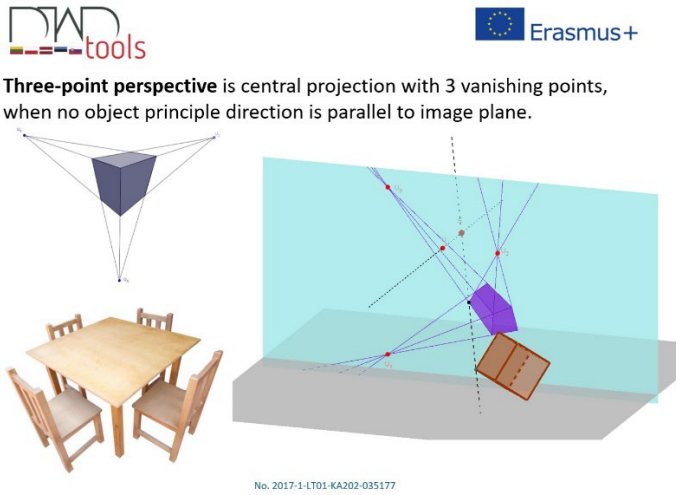

Figure. 1: Video Projections - linear perspective

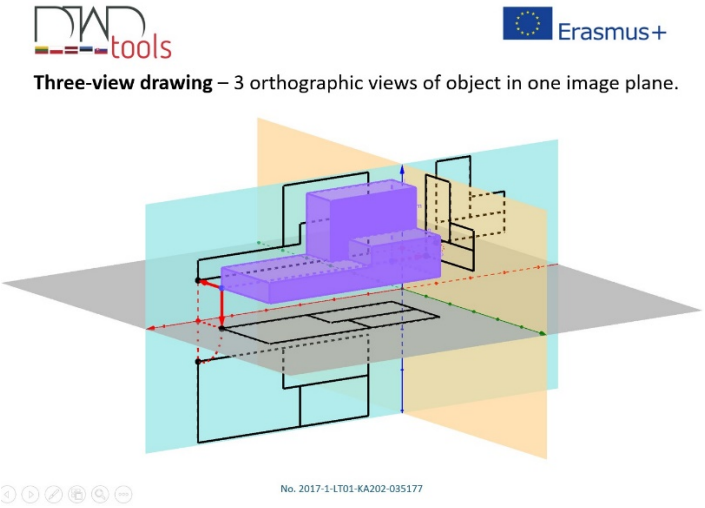

Figure. 2: Video Projections – Monge method with additional side view

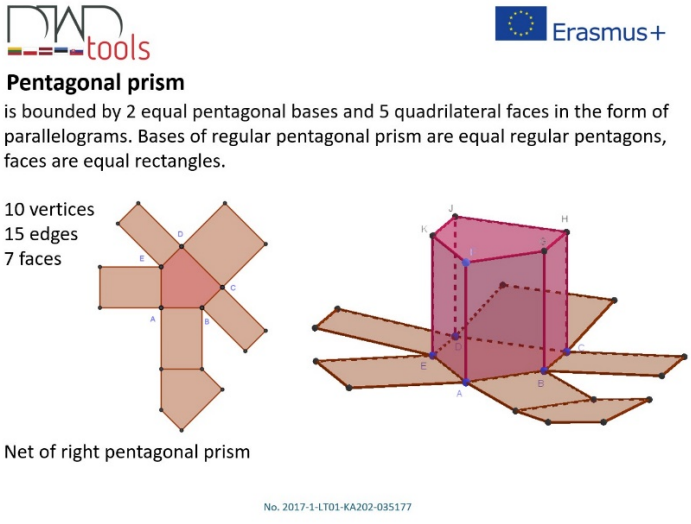

Figure. 3: Video Solids and nets

Arrangement of the presented pieces of information can be seen in the video illustrations in Figures 1 or 2, where explanatory text describing certain type of projection method is accompanied by dynamic illustration of this process, e.g. revolution of top and side projection planes to vertical image plane in case of Monge method with additional side view. Basic information about elementary solids is introduced in video Solids and nets, illustrated in Figure 3. Here, in addition to solid classification of regular solids, solids with polyhedral boundaries and round solids, detailed description of various solids with their nets in animated form is presented.

Video Variations of prism was designed to bring examples of various forms of solids that can be achieved from basic prism by planar cuttings and removing of solid parts. Orthographic views of resulting solids are placed on the left, while their 3D views on moving pictures is placed on the right. 3D scene rotates around vertical axis *z*, and it might help students to comprehend better the process of truncated solid generation and to understand form of its views, see example in Figure 4.

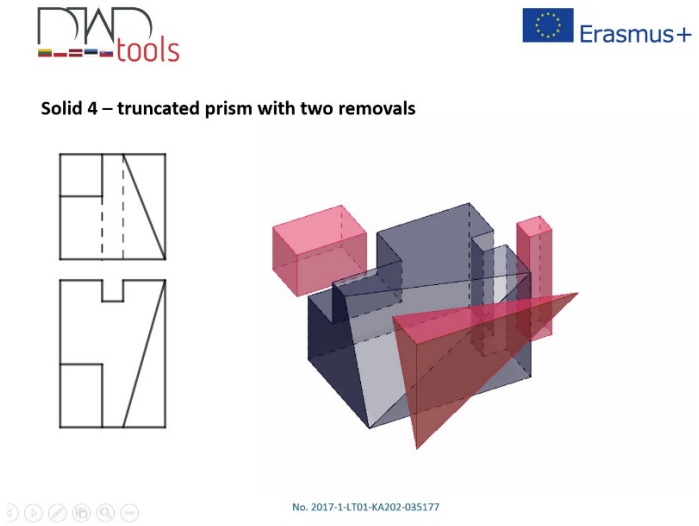

Figure. 4: Video Variation of prism

Educational videos included in other three parts are focused merely on details of technical documentation development, as used types of lines, dimensioning rules, drawings layout and design, sections and cross sections representations and other technical specifications for applications in mechanical and construction engineering and in architecture. In some of these videos, many practical information on machine parts, namely threads and joints and about architectural specifications in technical documentations is available.

Design and contents of presented videos and applets was influenced by various constraints, while differences in the basic curricula of the above mentioned subjects in partner countries were one of the most limiting, as described in (Sroka-Bizoń et al., 2019). Materials were designed to be as short as possible, the final decision was to make them about 5 minutes long, but to bring important pieces of information to support general understanding of principles and rules for production and reading of technical documentation. One of the most important aspects of these videos is their focus on animations of presented facts. They enable better insight into the presented theoretical material, 3D effect of illustrated scenes and support contextual synergy of illustration image and informative text.

3. INTERACTIVE APPLETS

In addition to videos, interactive materials developed in GeoGebra environment are available for on-line use, providing opportunity to investigate presented information in step-by-step mode and in individual speed. Interactive GeoGebra applets are dynamic training materials available at the server, which can be interactively used by students in the process of knowledge acquisition. Users can freely manipulate sliders, construction steps, zooming and revolution of the 3D scene about vertical axis *z* in the graphical window. Another benefit might be seen in possibility of augmented reality usage. Investigation of all geometric constructions is possible by observing 3D-scenes with a real 3D effect, as GeoGebra applications provide stereoscopic view representation for red-green glasses on one click. This augmented reality experience might improve spatial understanding, imagination and skills of respondents, and their ability to read and comprehend 2D representations of 3D objects.

Main design strategy of interactive applets was to allow users to investigate 3D scenes by haptic manipulations of presented constructions with their individual speed and by their own manipulations and steps forward. Students can use step-by-step construction, manually, or automatically if choosing the speed of slide changes by determining the time interval in the graphical window. Text in the left window appears synchronically with the sequence of respective construction steps. Manipulations with objects in the scene are provided by sliders in the text window on the left. 3D scene can be manipulated using mouse buttons and scroller in the graphical window. It can be rotated about vertical axis z, in order to investigate the relations in the space, and zoomed for adjustment to the screen size. Other functions provided by software can be utilised as well, e.g. one can choose desirable projection method, where anaglyph, stereoscopic projection of the 3D scene, is available. The spatial sensation can be achieved while observing this view through 2-coloured glasses, as true spatial perception through augmented reality experience. This feature could positively influence and support imagination, and develop better spatial abilities of students, who might have problems with visualisation of objects from their views.

Instructions how to start construction animations and manipulate 3D scene are available in all applets and they are marked in red colour to avoid misunderstandings. Users can use applets directly from the web, there is no need to install GeoGebra software in their own computer. Applets are fully functional also on iPads and in mobile phones with access to internet. Therefore, this learning material is freely available for anybody interested to obtain information as introduced in (Velichová, 2019) and (Velichová at al., 2019).

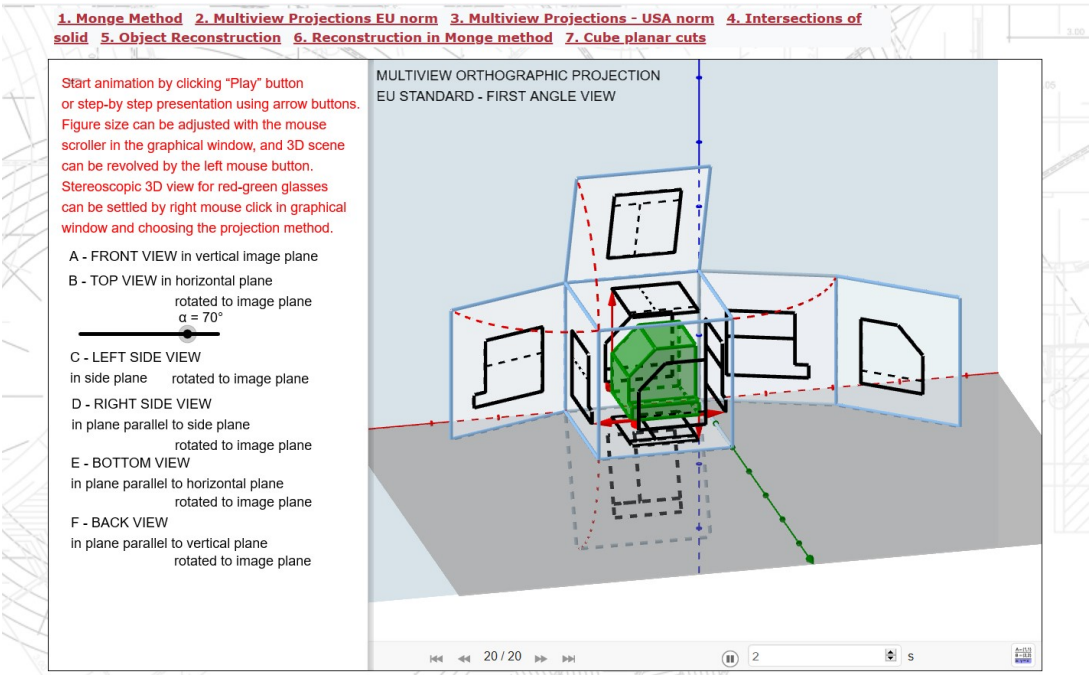

Figure. 5: Interactive applet Multiview Projection EU norm

Illustrations in Figure 5 shows construction of 6 orthographic views of an object positioned in the first octant (formed by positive semi-axes x, y and z of the Cartesian coordinate system) onto the faces of a cube and their revolution to the image plane (xz) in the vertical position, forming thus EU normalised Multiview orthographic projection – first angle view. It is possible to manipulate revolution of cube sides by slider showing the size of angle of rotation α. Users can also revolve the whole scene to observe it from various directions to understand the views layout in the image plane, by clicking the left mouse button in the graphical windows.

One of the greatest advantages of GeoGebra program are 3D graphics possibilities, which enable presentation of three-dimensional problems. In addition to various projections of 3D scenes, such as orthographic mapping, linear perspective and axonometry, users can benefit also from available stereoscopic view. Here 2 coloured images, separately for left and right eye in complementary green and red colours are automatically generated. These can be viewed through colour glasses and provide thus an excellent real 3D vision, even when projected via data projector to a large screen. Printed form is also working well, when read with suitable glasses. Thus, a very powerful didactic tool is available for teaching geometry, enabling not only to explain better various relations in 3D, but also to attract students in an unusual way, visiting 3D cinema and enjoying augmented reality to study and understand space relations more actively.

While teaching subject of Constructive geometry at the Faculty of Mechanical Engineering, Slovak University of Technology in Bratislava, Slovakia, we have benefited from the project platform and enlarged group of available Interactive materials in Slovak versions by many more materials that have been developed to support our students. There are 28 learning applets in total, covering many topics from the subject in Slovak language.

These are: Cylindrical helix and its properties, Planar cuts on cylindrical surface of revolution, Elliptic sections on conical surface of revolution, Parabolic sections on conical surface of revolution, Hyperbolic sections on conical surface of revolution, Planar cuts on ellipsoid of revolution, Elliptic sections on paraboloid of revolution, Parabolic sections on paraboloid of revolution, Elliptic sections on one-sheet hyperboloid of revolution, Parabolic and hyperbolic sections on one-sheet hyperboloid of revolution, Planar sections on two-sheets hyperboloid of revolution, Planar cuts on torus, Helicoids – Line helicoid, Planar cuts on line helicoid, Cyclical helicoid -Vault surface, Planar cuts on Vault surface, Cyclical helicoid - Winded column, Planar cuts on Winded column, Surface of tangents to helix, Planar cuts on surface of tangents to helix, Archimedean serpentine.

Some of applets allow simple manipulations with the 3D scene, while no explanatory text is available, and they are meant to serve for students own discovery and understanding. Applets are used as motivational illustrations during lectures in lecture theatre, while students receive red-green glasses and enjoy a 3D performance on the large screen, see Figure 6. They can of course use these materials in their self-study after lessons, in their own way, speed and mode. Sliders serve for changing the intersected surface, their values determine semi-axes of the surface generator - revolving hyperbola. Intersection plane position can be change by moving indicated red points that are pierce points of the plane and coordinate axes x and y. Users can observe changing form of elliptic intersection on the defined one-sheet hyperboloids.

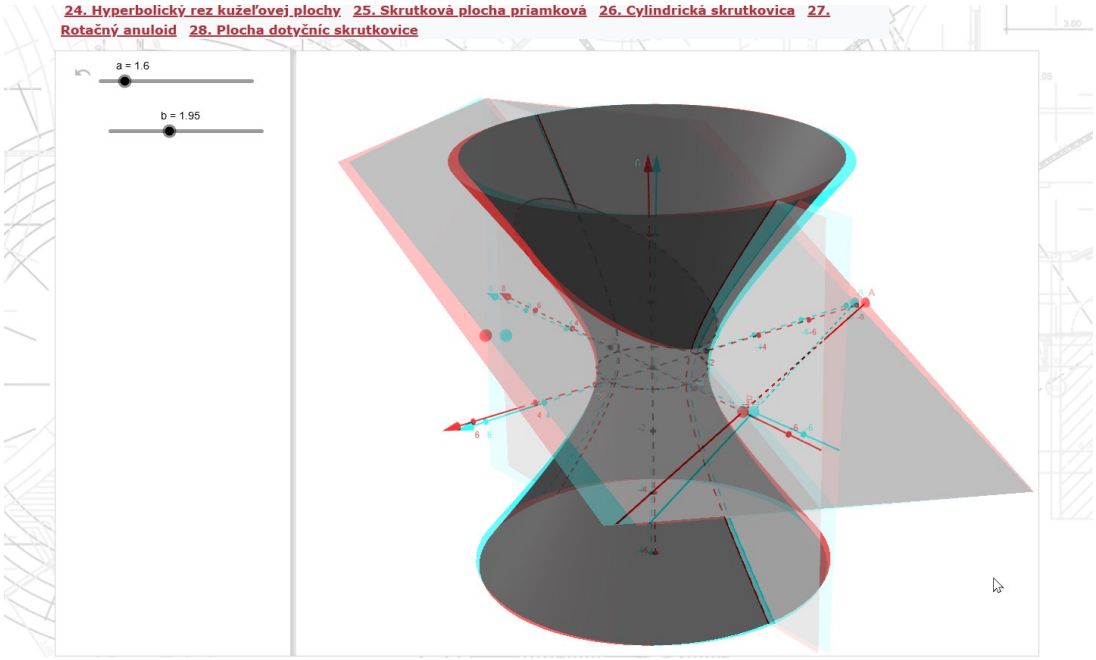

Figure. 6: Interactive applet Elliptic sections on hyperboloid of revolution

A different situation can be seen in Figure 7, where a cyclical helicoid – winded column is presented, generated by helical movement of a circle positioned in the plane perpendicular to the axis of this movement. Surface cuttings by plane are constructed. Here, manipulation sliders represent shaping parameters of the helicoid. First, the position of the generating circle centre moving on coordinate axis x and circle radius are determined. Next, the reduced pitch of the helical movement with axis in the coordinate axis z can be chosen. Intersection plane is meridian plane passing through axis of helical movement in axis z and it can be revolved around this axis by moving its point indicated in red. Two other parameters represent curvilinear coordinates of an arbitrary surface point, as intersection of surface parametric curves - position of generating circle in the movement and respective helix. One can observe how any point on the intersection curve of the plane and surface can be obtained as pierce point of this two parametric curves, and the skew symmetry of the two parts of intersection meridian curve.

Intersections on all other helicoids can be investigated in a similar way, while surface shape can be adjusted according to user needs and ideas. Students enjoyed to work and play with these applets, and they tried to investigate special outrages situations, where the solutions were not straightforward and easily foreseen.

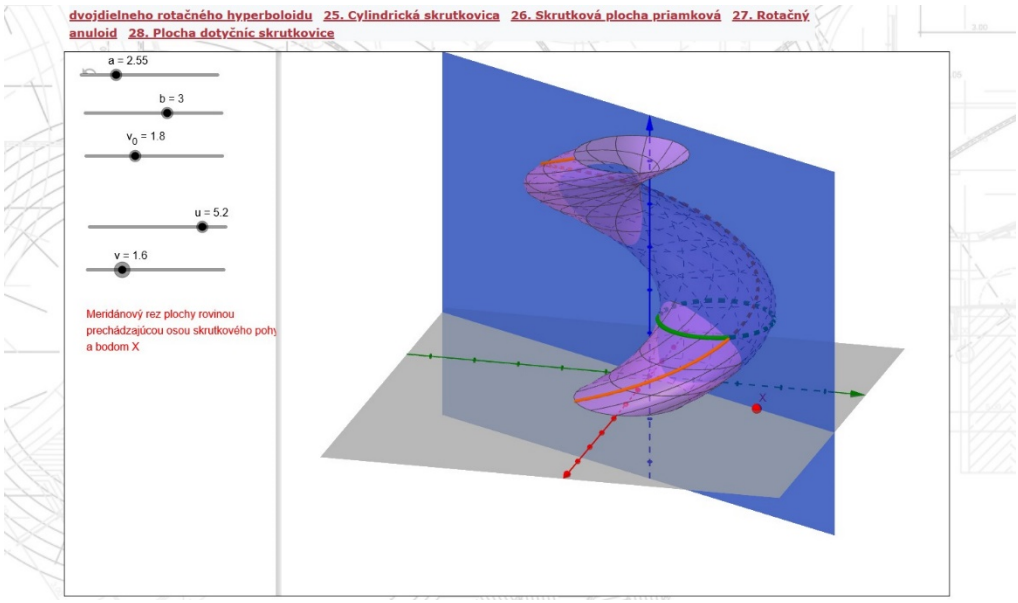

Figure. 7: Interactive applet Cyclical helicoid – winded column

In the last illustration in Figure 8, Archimedean serpentine is presented. This surface can be generated as an envelope surface of a spherical surface helical movement about coordinate axis z with the pitch defined by slider v_0. Spherical surface radius and position of its centre sliding on coordinate axis x can be chosen to determine the Archimedean serpentine shape. The same surface can be obtained also by moving a generating circle that is a planar cutting on the spherical surface by plane passing through its centre and perpendicular to the tangent line of a helical trajectory of this centre. Any point on the surface can be determined by position on this generating circle while moving. Tangent plane to the Archimedean surface at this point is determined by two depicted lines. One is tangent to the helix of movement perpendicular to cutting plane at the current position, and the other one is tangent to the moving circle. This relation can be well understood by exploring the applet, playing with parameters and observing all special superpositions. Students have to investigate and describe special situations and combination of parameters, when generated helical surface collapses to be a cylindrical surface or a torus.

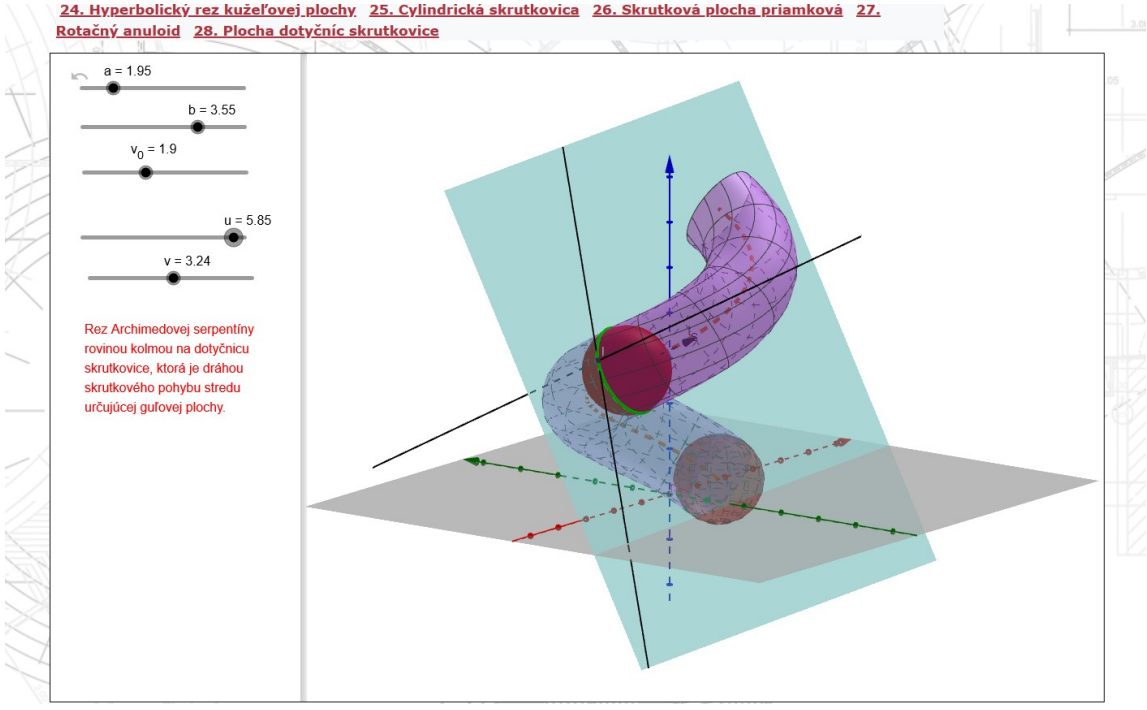

Figure. 8: Interactive applet Cyclical helicoid – winded column

4. CONCLUSIONS

Research in the domain of cognitive psychology shows that human brain stores knowledge in two forms: in the graphical form as images, or in the form of words. It has been documented that methods of education, which are oriented to development of both of these forms of knowledge acquisition, in a considerable way influence quality and depth of understanding and sustainability of acquired knowledge. Dynamics opens way to discover connections, and to understand mutual dependencies, which is often more important than a detailed fragmented knowledge. Dynamic tools enable changes and motion in geometric constructions, better spatial understanding and comprehension in often very difficult spatial tasks and help to improve spatial understanding. Many constructions used in classical descriptive geometry can be easily presented here and explained to students with not well developed spatial abilities and thus help them to generate mental images of spatial relations.

Development of interactive applets, and their introduction to classical subjects as Technical drawings, Descriptive geometry or Constructive geometry enable better insight to the topics of 3D geometry, which became recently a nightmare for many students at technical universities specialised on mechanical or civil engineering and architecture. There are more reasons of this unfavourable situation, but it does not help to cry over the spilt milk. It is more efficient to provide innovative study materials in order to attract our students and to prevent the geometric illiteracy of the future generations. Author hopes to have made some steps in this direction.

REFERENCES

1. Project DIAD-Tools, 2020. http:// www.liggd.lt/diad-tools [Accessed: 1st February 2020].
2. Sroka-Bizoń, M., Tytkowski, K., Vansevicius, A., Velichová, D., Dobelis, M., 2019. Do Engineers Use International Language? Construction Drawing as a Way of Communication Between Engineers. *Journal for Geometry and Graphics*, Volume 23 (2019), Number 1, Helderman Verlag, pp. 115-126.
3. Velichová, D., 2019. Educational Videos – Products of DIAD-Tools Project. Proceedings of Slovak-Czech Conference on Geometry and Graphics, Slovak Society for Geometry and Graphics, Bratislava, Slovakia. pp. 183–190.
4. Velichová, D., Záhonová, V., 2019. Learning Materials for Teaching Constructive Geometry Course. Proceedings of Aplimat 2019 Conference on Applied Mathematics, Slovak University of Technology in Bratislava, Slovakia. pp. 1302–1309.

DEVELOPMENT OF A VACUUM DRYING MODEL WITH A FOCUS ON 3D MODELING

Aleksandra Joksimović
Department of Theory of Mechanisms and Machines, University of Belgrade-Faculty of Mechanical Engineering, Republic of Serbia
MSc., Research Assistant, ajoksimovic@mas.bg.ac.rs

Ivana Medojević
Department of Agricultural Engineering, University of Belgrade-Faculty of Mechanical Engineering, Republic of Serbia
MSc., Teaching Assistant, imedojevic@mas.bg.ac.rs

Nikola Veličković
Department of Agricultural Engineering, University of Belgrade-Faculty of Mechanical Engineering, Republic of Serbia
Student, velickovnikola94@gmail.com

Nikola Beljanski
Department of Agricultural Engineering, University of Belgrade-Faculty of Mechanical Engineering, Republic of Serbia
Student, belja913@gmail.com

Nikola Jovanović
Department of Agricultural Engineering, University of Belgrade-Faculty of Mechanical Engineering, Republic of Serbia
Student, jovniki@gmail.com

ABSTRACT

With the development of technology, we are forced to develop teaching in the same direction, introducing modern 3D tools and examples that are close to those in practice. For this reason, this paper will explain the development and design of a model of a vacuum food dryer, with an emphasis on 3D modeling. The model of the vacuum dryer consists of a glass base which has the function of a drying chamber, and the vacuuming is achieved by means of a compressor. The base is positioned on a wooden structure to which an electric heater is attached, on the upper side of which slices of raw fruit are placed to be dried. Humidity, temperature and pressure sensors are installed in the chamber, which are connected to the control panel of the microcontroller via a hermetically sealed cover. The task of the microcontroller is to compare the previously defined parameters with the measured values in a given time cycle. The whole process and design development was done by the students in the 3D package Solid Works, as well as the accompanying documentation necessary for making the model. After the design is completed, it is planned to test the operation of the model of the vacuum dryer. The importance of this approach in working with students is reflected in increasing student interest and encouraging ideas for independent development and design using modern tools and methods acquired in teaching.

Keywords: education; 3D modelling; new approach;

1. Introduction

Guided by the idea of implementing as many realistic examples as possible in teaching, this paper will present the work and students' reactions to this type of teaching. As part of the course "Design of plants and process and energy systems", at the Department of Agricultural Engineering, University of Belgrade, as one of the tasks, students were given to make a model of a vacuum dryer in the SolidWorks (SW) package. With this type of teaching, students are encouraged to apply the theoretical knowledge acquired in the lectures on a specific example and the design of one of the dryers they learned about. In this way, students gain knowledge for handling the SW package that is generally applicable for future independent work. The paper presents a modification of an existing vacuum dryer solution, which was done by one student as part of his final work [1].

2. Vacuum drying

The drying process is intended to remove water from foodstuff in order to prevent microbial spoilage and chemical alterations thus prolonging shelf-life while realizing space and weight saving. [3].

Drying of the material can be achieved by evaporation of moisture, which can be achieved faster than by diffusion of water vapor into the environment, which occurs in dryers in which air is introduced. At atmospheric pressure, boiling occurs at a temperature of 100 o C, that is, at a temperature that for many materials that dry above the allowable heating temperature. Some materials need to be dried at low temperatures, as a slight increase in temperature causes a sharp deterioration in their technological properties. Drying at low temperatures and at atmospheric pressure is very slow. Therefore, in order to intensify the drying process of such thermo sensitive materials, vacuum drying is used. A decrease in pressure abruptly increases the intensity of evaporation at the expense of an increase in the transport coefficient of matter which is inversely proportional to the pressure in the first approximation. Since vacuum drying takes place in a hermetically sealed device, heat transfer is neglected. Therefore, in order to maintain a significant intensity of drying in vacuum, the heat necessary for the evaporation of the liquid is supplied to the material to be dried, by conducting from the heating surface (contact drying) or by radiation from heated screens (drying by infrared radiation). [2]

In vacuum dryers, the heating of the material is achieved by contact, radiation or direct electric current, where the heating and radiation take place simultaneously. In order to maintain the required vacuum, it is necessary to continuously suck out the generated vapors. Due to the large specific volume of steam generated, a large capacity pump is required, so it is more economical to condense the steam between the drying chamber and the vacuum pump in a chiller. The vacuum dryer in most cases consists of a drying chamber, a condenser and a vacuum pump [2].

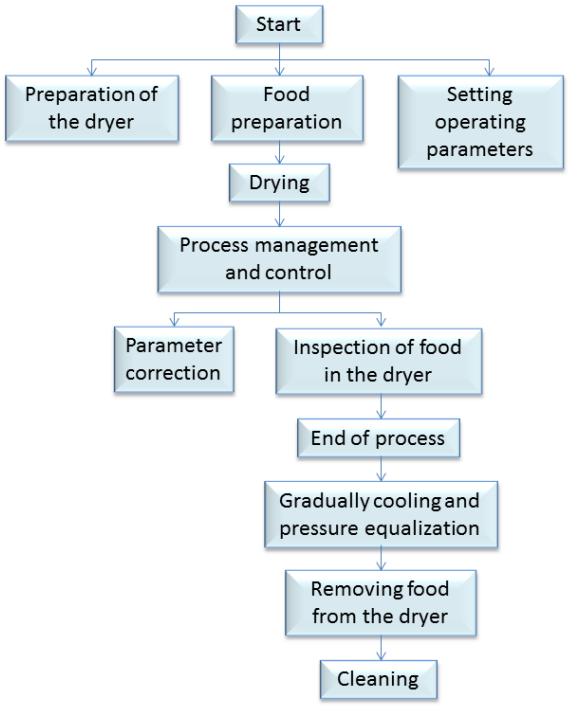

Figure. 1: Block diagram of the drying process [1]

3. EXISTING SOLUTION (model base)

The already existing solution gave excellent guidelines to students for design, on which they applied their ideas, observations and knowledge gained during the semester. The real challenge was to design a model of a vacuum dryer with an already good base, which additionally presented to the students the difficulty and importance of designing from the beginning. Certainly the idea was two-way, on the one hand to give students a sense of design, and on the other hand, to master modelling and making technical documentation in SW.

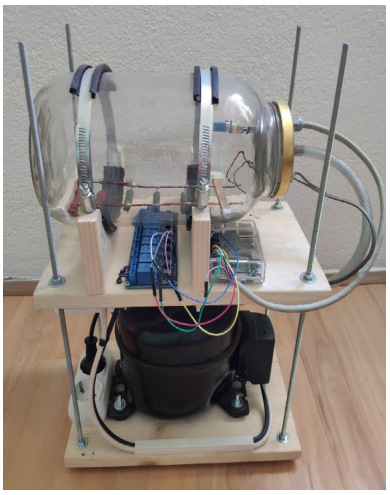

Figure. 2: Existing solution – model base [1]

The model base (Figure 2) consists of several segments, each representing a specific, separate system. The model presented in this way can be divided into three parts: construction, control and drive. In this paper, students focused on the modification of the structural unit of the observed model and made certain corrections to the observed model in a 3D environment. The development of the 3D model is reflected in the need to improve the internal construction of the vacuum chamber, performance, ergonomics, modularity and safety. As already mentioned, the students focused on the parts of the model that have constructional significance, and those parts are the following: the stand, the protection system and the internal construction of the vacuum chamber. The internal construction of the already existing solution is made of wood (Figure 3), with certain rubber, wire-profiled inserts, which are bent into a shape that corresponds to the drying of fruit slices. Heaters (resistors) are also placed under the wooden beams, which are soldered between two parallel copper wires (Figure 4).

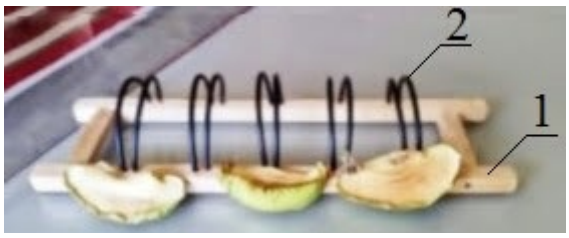

Figure. 3: The internal timber construction (1), profiled inserts a wire (2) [1]

Figure 4. Heaters (wirewound resistors) [1]

The method of making these parts, as well as the choice of materials, is such that, at the limit of acceptability, it ensures uninterrupted operation of the dryer. The advantage of making such a construction is reflected in its

economy and fast realization. While the protection is at the questionable level, ie. From Figure 2 it can be seen that in case of breakage of the chamber (jar) there is no adequate protection system. Also, the approach to the working parts is questionable and dangerous due to the non-existence of this system.

4. NEW SOLUTION OF THE VACUUM DRYING MODEL

Modifications of the existing model of the vacuum drying model of the existing model are based primarily on the design and construction of a new stand with protection, as well as modifications of the internal wooden structure of the vacuum chamber. The basic improvement of the internal construction is reflected in the improvement of heat transfer from the heater (heat source) to the fruit (dried object). In the observed chamber of Figure 5, air is the main medium for heat transfer, and this transfer takes place by natural flow where there is heat dissipation from a solid body surrounded by air.

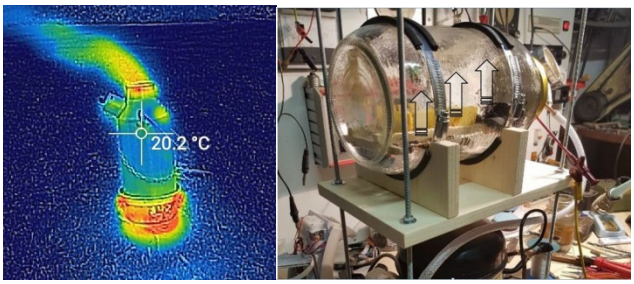

Figure 5. Natural heat transfer in a vacuum chamber, Figure 5a. Convection [1]

In our case we have the working fluid being drawn out of the chamber. As air is expelled from the chamber, the consequence is that the heating of the working medium takes place more slowly, which is also shown in the paper. The air temperature of 45 °C is reached in a time interval of 100 min. Which is a direct consequence of the discharge of air, as well as its thermal conductivity. On the other hand, this refers to the discontinuous principle of operation of a vacuum dryer where there is condensation of water (originating from the product) on the wall of the chamber, which can be removed only by interrupting its operation.

The conceptual solution from the view is that the internal construction is made of sheet metal 0.40 mm thick and is so profiled (Figure 6), to achieve as much as possible direct indirect heat transfer (reduce air dependence) from the heater to the product, as well as heat accumulation in the central core of the chamber. In this way, the heating time of the localized air would be reduced to a greater extent.

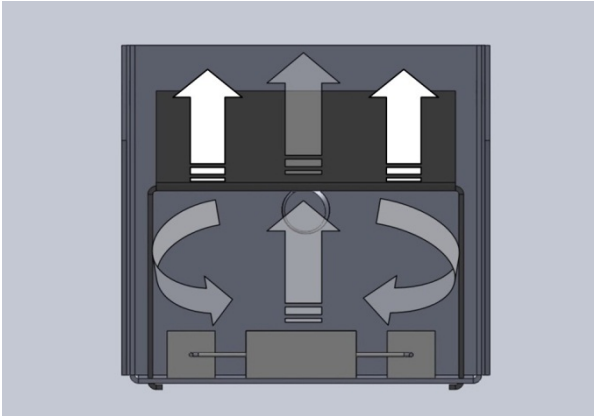

Figure 6. Thermal tunnel (air heating)

This design of the internal structure would provide a controlled contact temperature. One part of the heat would go to heat metals and products, while the other part of the heat would go to heat the surrounding air. In this way, the air temperature inside the chamber would be about 10^{o}C lower, but the local heating (in the zone of the dried product) could be many times higher. In this way, it is possible to provide amortization of losses caused by air extraction, it also opens the possibility of continuous operation of the vacuum dryer, which is an improvement over the existing solution.

4.1. MODELING OF NEW SOLUTION

The components of the internal structure are:

- Supporting part
- Modular part
- Resistors for conductors

Supporting part

The supporting part (Figure 7) is U-shaped, cantilever type. It is fastened with an M10 screw to the lid of the jar and is glued on the inside in contact with the lid with two-component glue. It is made of 0.40 mm thick sheet metal, and the profile is obtained by bending and riveting technology.

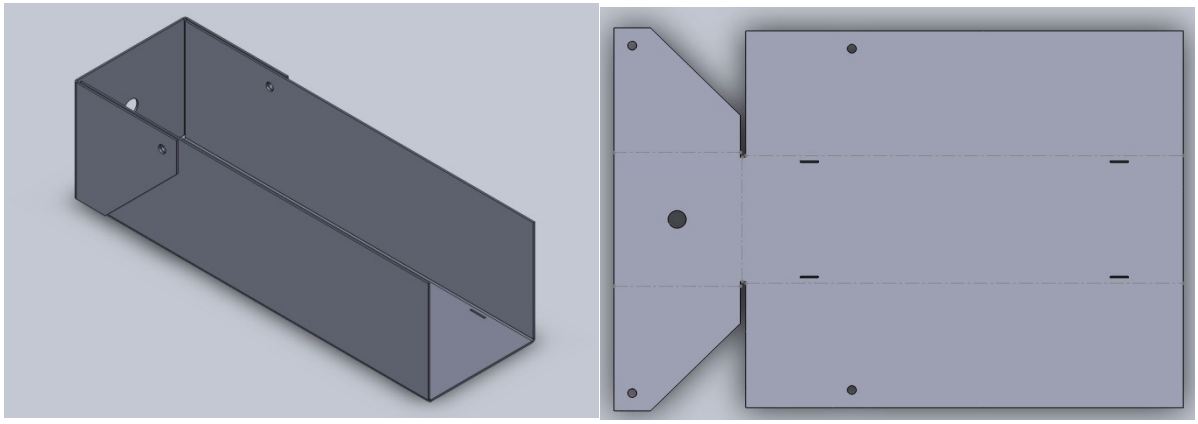

Figure 7. Cantilever part of the internal structure (sheet metal)

Modular part

The modular part (Figure 8) is also profiled as the supporting part. The product we want to dry is placed on it (this part can be considered as an elementary part of a vacuum dryer). There is a possibility of drying several types of fruits and vegetables, regardless of their shape. The fixing of this part for the supporting part is done with the help of feet, which rotate when placed in the openings on the supporting structure, which achieves the locking of this part. The surface on which the product is placed can also be perforated, which achieves the modularity of the entire internal structure. Another advantage is reflected in the protection of the heaters themselves from condensate, ie. this construction protects the heaters from contamination.

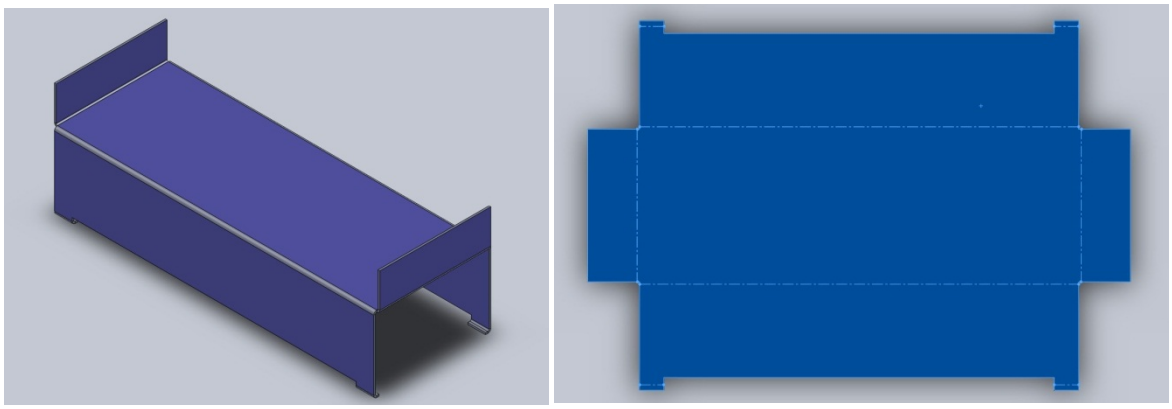

Figure 8. Contact part of the internal structure (sheet metal)

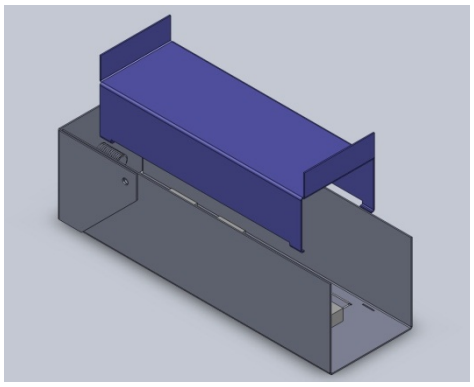

Figure 9. Separate view of the internal structure

Heaters (resistors)

As part of the internal construction, there are resistors on the lower surface of the supporting part (Figure 10). These resistors are ceramic, positioned (connected) so as to ensure the highest degree of their utilization, ie. to make the most of their dissipative power. The resistors are fastened with heat-resistant glue and fixed in some places with galvanized wire.

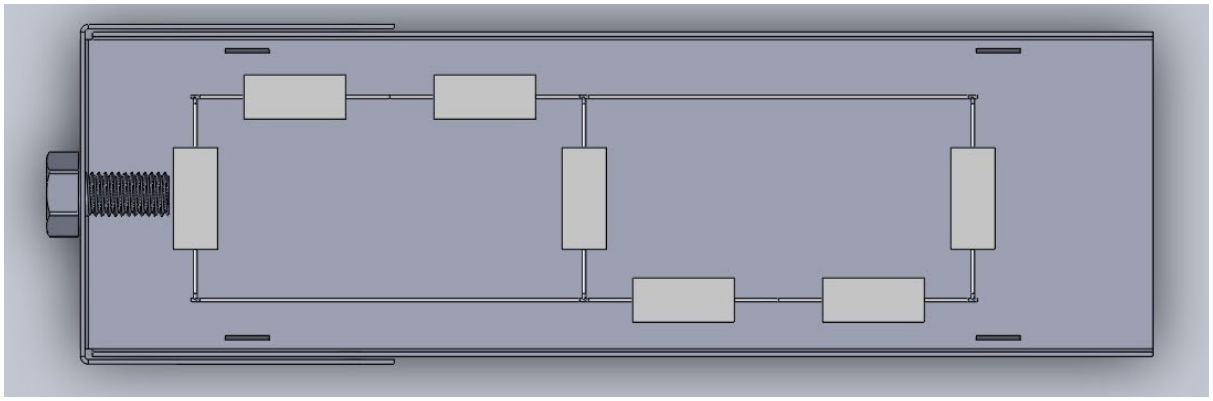

Figure 10. Arrangement of resistors along the supporting structure

The external supporting structure(Figure 11.) of all parts of the model is made of wood and designed so that all parts are placed in a minimal space, so that they are easily interconnected and at the same time the construction represents protection.

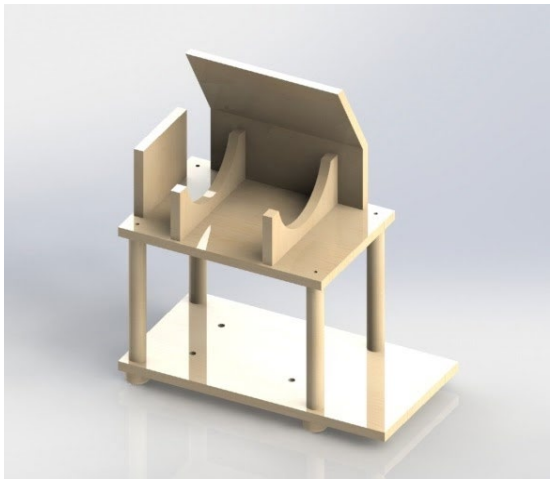

Figure 11. The external supporting structure

4.2. CONCEPTUAL DESIGN - ASSEMBLY

The conceptual solution is a set of the following elements:

1. Pedestal
2. chamber with internal construction
3. slope within the base place for electronics
4. pneumatic hose
5. liquid accumulator and
6. compressor

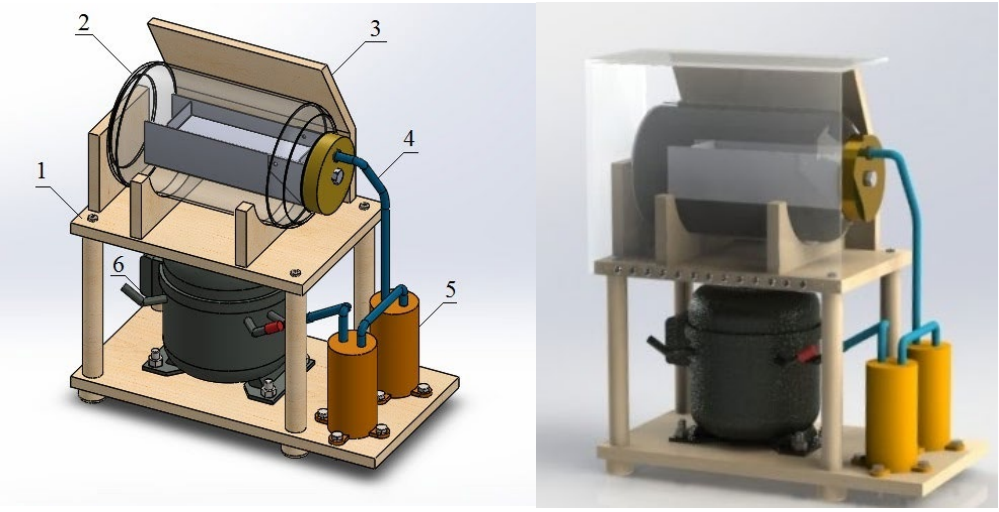

Figure 12. Conceptual design – Assembly

5. Conclusion

From all the above, we can conclude that working in a 3D environment SW in many ways gives a great picture of what should actually be realized. Also, the natural phenomena themselves can be considered, which can occur with the introduction of new materials and similar corrections. This way of working opens discussions between several branches of mechanical engineering, electrical engineering, design, etc., in order to find the optimal solution that is acceptable to everyone. At first glance, the 3D model of the conceptual solution (Figure 12) does not differ much (in relation to the number of components for production) from the already existing model from Figure 1. However, the essential difference is reflected in improvements such as: continuous operation, better efficiency , modularity, better ergonomics as well as greater safety. Also, according to the 3D model of the conceptual design, a prototype was made on which the thermal parameters were checked, in order to support the theory of heat transfer by convection. From this experiment, it is concluded that it is possible to accumulate heat in the central core of the chamber and its local distribution to the dried object. In this way, it is much easier to see the construction problems that would occur with certainty, if, instead of making a 3D model, we immediately went to making a real model. Going through this experience, students learned to apply the theory to a real solution. Also, they learned to use the SW package and came to the conclusion how much knowledge and use of such packages saves time and money, because in a real 3D environment [4] irregularities are easily spotted and even easier to correct.

ACKNOWLEDGEMENT

This work has been performed within project TP35043, supported by the Ministry of Education, Science and Technological Development of the Republic of Serbia, whose financial involvement has been gratefully acknowledged.

6. References

1. Ambrinac .F., 2018. Model of vacuum dryer-final work, - Josip Jurj Strossmayer University of Osijek Faculty of Electrical engineering

2. Prof. dr Radivoje M. Topić, 2013. Special techniques and technologies of the drying process, Book, Belgrade

3. G. Cuccurullo a, L. Giordano a, D. Albanese a,⇑, L. Cinquanta b, M. Infrared thermography assisted control for apples microwave drying

4. R.P.F. Guine´ a,*, A.E. Rodrigues b, M.M. Figueiredo Modelling and simulation of pear drying

5. Joksimović A., Veg E., Simonović V., Regodić M., Šiniković G., 2019. Implementation of inverted classroom methodology in 3D modeling course, - FME Transactions, 47(2), pp. 310 - 315

STUDENT`S PAPERS

CONTENT

PERFORATED PANEL DESIGN FOR DAYLIGHTING CONTROL

Nikoleta Stamenković,
Department of Architecture, Faculty of Technical Sciences, University of Novi Sad, Novi Sad, Serbia
B.Arch, nikoleta.nina.stamenkovic@gmail.com

Marko Jovanović
Department of Architecture, Faculty of Technical Sciences, University of Novi Sad, Novi Sad, Serbia
PhD, Assistant Professor, markojovanovic@uns.ac.rs

ABSTRACT

Contemporary architecture exhibits structures with glass facades due to aesthetic reasons and the need to provide adequate interior daylighting. However, glass facades can also bring discomfort in everyday life - excessive room heating or cooling, reflection, glare, and loss of privacy. In order to solve these listed issues, architects created passive and active shading systems. Most of the existing active shading systems are powered by electrical and operated via mechanical drive, which requires a lot of energy and money. In order to achieve more energy-efficient and cost-effective solution, in this research a passive facade system, i.e. perforated screen is suggested. This research is concentrated on designing and calculating the efficiency of an optimal perforated screen that minimizes direct sunlight. The perforations are inclined, due to the hypothesis that more direct sun rays are blocked in that manner. By changing the values of the perforation inclination angle, perforation size, and screen thickness, different exposure to direct sun rays is observed and compared. Getting countless combinations is made possible by using a parametric design approach.

Keywords: perforated panel, passive facade system, sun rays, direct light

1. INTRODUCTION

There has always been the need to explore the building's relation to light through the facade. Nowadays, the introduction of stronger materials, such as steel, allows the construction of curtain walls. The benefit of using glass in a curtain wall is viewed through the control of natural light into the building - daylighting. Adequate daylighting can be observed as the amount of natural light required to conduct a specific task related to the purpose of the space (Phillips, 2004) as well as the user's needs. Therefore, the adequate daylighting cannot be uniform. By having proper daylighting, the necessity for artificial light is reduced, aiding the energy preservation (Goia, 2016). Furthermore, adequate interior daylighting broadly affects the improvement of health and lifestyle (Fournier et a., 2010; Boubekri, 2008). However, large glass openings can lead to discomfort pertaining to loss of privacy (Alkhalili et al.,2018) and inadequate daylighting in forms of glare (Jakubiec et al., 2012; Cantin et al., 2011) overheating (De Herde et al., 2010; Nebia et al., 2017; Altan et al., 2008) or loss of thermal energy (Hee et al., 2015). In order to mitigate such discomforts, architects have implemented passive and active shading measures throughout the centuries.

Both passive and active shading measures include the design of building elements that mitigate or dissipate the solar energy and control the natural light intake (Bainbridge et al., 2011). However, passive measures achieve this through stationary systems and without tracking the sun as opposed to the active measures. Regardless of the system, one of the most recognizable forms of shading elements is the brise soleil (sun breakers) in form of louvres. Louvres can mitigate the solar exposure (Hashemi, 2014) with regards to the environment (Gutiérrez et al., 2019) but also raise the aesthetical appeal as well. By using simple rotation of the panels, different lighting and appearance features can be achieved in general (Giovannini at al., 2015), as seen in the active shading systems of RMIT Design Hub and Kolding Campus projects (Fig. 1a and 1b respectively).

(a) (b) (c) (d)

Figure. 1: Active shading systems – a) RMIT Design Hub, Melbourne, Sean Godsell, 2012 (source: Through Vin's Lens, 2018); b) Kolding Campus, Kolding, Henning Larsen, 2014 (source: ArchDaily, 2015); c) Al Bahar Towers, Abu Dhabi, Aedas architects, 2012 (source: Middle East Architects, 2014); d) Arab World Institute, Paris, Jean Nouvel,1987 (source: Depositphotos, 2015)

Al Bahar Towers project in Abu Dhabi exhibits an active shading system using triangular louvres that open and close following an origami folding principle (Fig. 1c). By observing the louvre openings as facade perforations in the previous examples, a contemporary interpretation of the mashrabiya (Akçay et al., 2017) can be recognized. The mashrabiya is a passive shading system used in traditional Islamic architecture and it has served as an inspiration for a multitude of active facades. One of the most significant examples is the Arab World Institute in Paris, by Jean Nouvel in 1987 (Fig. 1d). The malfunction of the used mechanism indicates a problem with mechanically operated systems. Moreover, active shading systems exhibit major issues in terms of cost effectiveness and high maintenance, which is why using passive shading systems is considered as a better solution for everyday daylighting control.

By using movable perforated screens (PS), without using electric energy, the size of the perforations as well as the inclination angle can be varied to achieve optimal daylighting efficiency (Karamata et al., 2014). The approach can be simplified even further, where the perforations are fixed in size and inclination. This approach reduces the shading measures to passive ones, designing the openings for average lighting conditions and requirements, instead of adapting them to in situ ones. The design is still based on the optimal results procured through extensive simulation calculations and analysis with rectangular (Kotbi et al., 2016; Lavin et al., 2017), circular (Pool, 2019) and more classical looking mashrabiya (Aljawder et al., 2019). A lot of previous research relies on optimal results, based on the diffuse daylighting and solar radiation calculations pending software capabilities, which can differ from real life circumstances. Regardless of the daylighting efficiency, simple application of rectangular or circular openings as shading devices can lead to monotonous appearance, while smaller openings in classical mashrabiya can limit the connection with outside, i.e. the view of exterior.

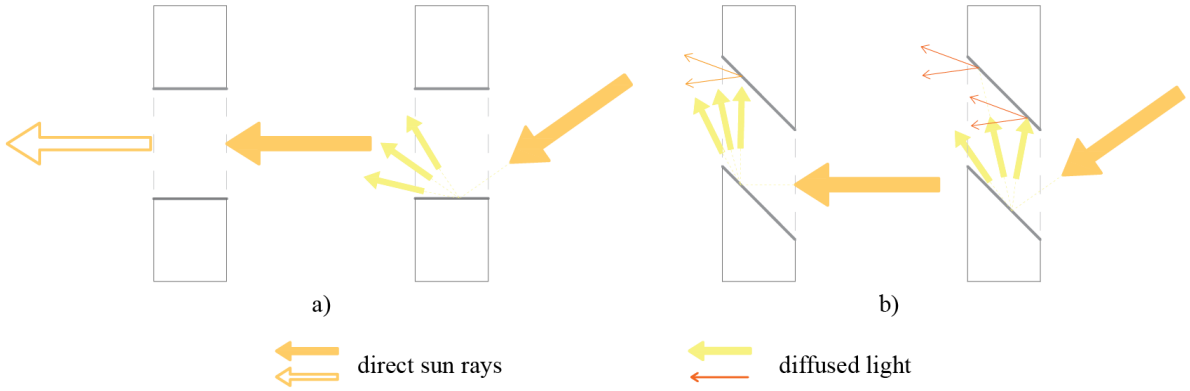

Figure. 2: direct sun rays scattering shown on horizontal section of the panel a) without perforation inclination b) with perforation inclination

In this research, the goal is to design an optimal perforated screen that minimizes direct sunlight, generates an interesting and aesthetically appealing look, but still allows for a fair outside connection and view. The design opening is based on random Voronoi cell disposition, bringing it somewhere between the large rectangular and circular openings on one side and small classical mashrabiya on the other.

The design parameters including the size and the inclination angle of the openings and the thickness of the screen will be discussed in Section 2. The research is based on the hypothesis that the inclined planes of the perforation sides can scatter the direct sun rays and mitigate direct exposure while allowing diffuse lighting altogether (Fig. 2). Therefore, this research is mainly focused on concluding whether, and to what degree the inclination influences the room shading. The efficiency of using a specific perforated screen design is calculated based on the geometry design and sun rays, avoiding solar radiation and diffuse daylighting calculations present in other researches. In this manner, the procedure shows the exposed and occluded parts of the interior as straightforwardly as possible, given that it is based on shadows, which will be discussed in Section 3. The direct solar exposure results of the perforated screen variations are achieved through comparative analysis shown in Section 4. The paper is concluded in Section 5, with discussions and future work.

2. PERFORATED SCREEN DESIGN

As indicated above, in this section the emphasis is placed on how to design the PS. Given the existence of three parameters - size of the perforations, inclination of the perforations and the thickness of the screen, the use of parametric modelling is chosen. This approach allows for quick changes in variation generation in real time, which is important for time efficiency and calculation manipulation. The Rhinoceros and Grasshopper software package is chosen for its parametric modelling capabilities. Alongside the parametric approach through visual programming, it offers the calculation of shadows and their depiction in a visual and quantitative manner that can be used for comparative analysis later on. In order to start designing the PS, a general room depiction is chosen through a box measuring 400 cm in width, 250 cm in height and 700 cm in length i.e. the depth of the room. The shorter vertical side of the box, the screen surface (SS), is chosen to be replaced by the perforated screen (PS), with the exploration of the three design parameters in the following section.

2.1. The Perforation Size

Many researchers explore the proper size ratio of the openings, settling on rectangular or circular shapes and varying the sizes according to requirements. In this approach, the emphasis is placed on generating an appealing interior look through diversity. The driving factor is to avoid monotonous and repetitive patterns that most approaches use and to make a shift towards randomly displaced Voronoi cells. Due to the random disposition of the Voronoi cells, it can be difficult to set a specific size of the opening, like it can be done with common shapes, such as a rectangle or a circle. For that reason, the procedure is done in the following manner.

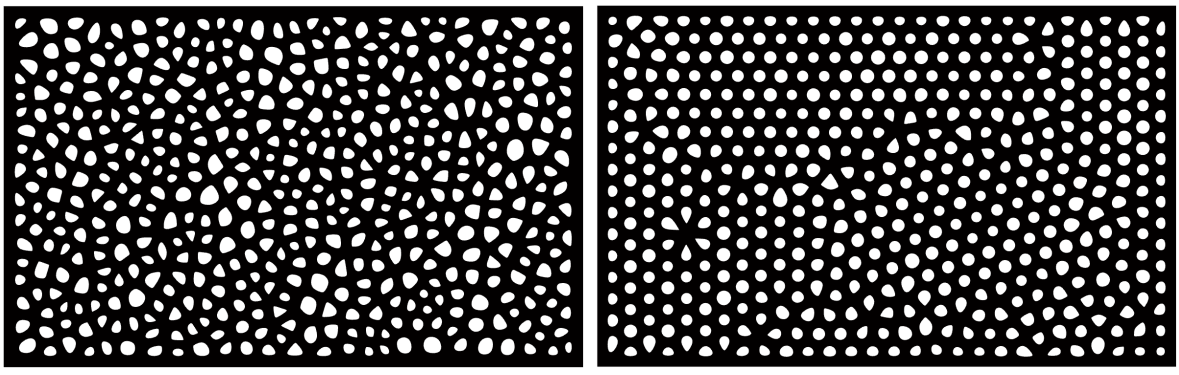

(a) (b)

Figure. 3: The depiction of the perforation; (a) the random disposition of Voronoi cell which shows diversity; (b) optimized disposition of Voronoi cell which shows uniformity

The SS is offset inwards by a certain constant, in this case 5cm, to avoid the perforations being too close to the brim and for later perforation inclination. The offset SS is populated with a certain set of randomly placed points. The randomness is achieved through generic Grasshopper components and is not the topic of this paper. The number of points is determined as a quotient of the total area of the offset SS and the circular cell area of a desired radius. The cell radius is determined as the sum of the perforation radius and the space between the perforations i.e. the offset of each Voronoi cell. For the purposes of this specific case, the space between perforations is set to 2.5cm and the radius is set to be 5cm, 7.5cm and 10cm. Using Voronoi cells cannot produce exact perforation sizes, so in order to mitigate the perforation size discrepancy, each point that is closer than the cell radius is culled from the population producing a diverse and randomized perforation pattern (Fig. 3a). Optimizing the disposition of the Voronoi cells to accommodate for the size uniformity and not diversity produced repetitiveness, while the average size remained the same (Fig. 3b). Perforations done in this manner have an average area that corresponds to the desired cell radius, while the space between perforations can differ due to the cell shape irregularity. By changing the radius, other depictions can quickly be generated. Once the perforations are determined, it is also necessary to address the perforation inclination, and its role in transforming direct light into diffuse light.

2.2. The Perforation Inclination

The key factor in producing diffuse light lies in the creation of surfaces which the direct sun ray can scatter against and lose its strength. With the secondary scattering, the sun ray creates an equally illuminated surface without a glare, and transforms into diffuse lighting. Since the sun ray inclination is changing on a daily basis, the research hypothesis is that more sun rays are blocked if the perforations are also inclined. The perforation inclination (Fig. 4) refers to the angle between two vectors - the perforation extrusion vector and a specific vector (the projection of extrusion vector on horizontal or vertical plane) located in the SS. The perforation extrusion vector is the vector which the perforations are extruded along thus generating the perforation sides for sun ray dissipation (Fig. 4a). The specific vector aligns with either of the two perpendicular isocurves in the SS, producing the inclination in reference to the horizontal and vertical axis (Fig. 4b and 4c respectively).

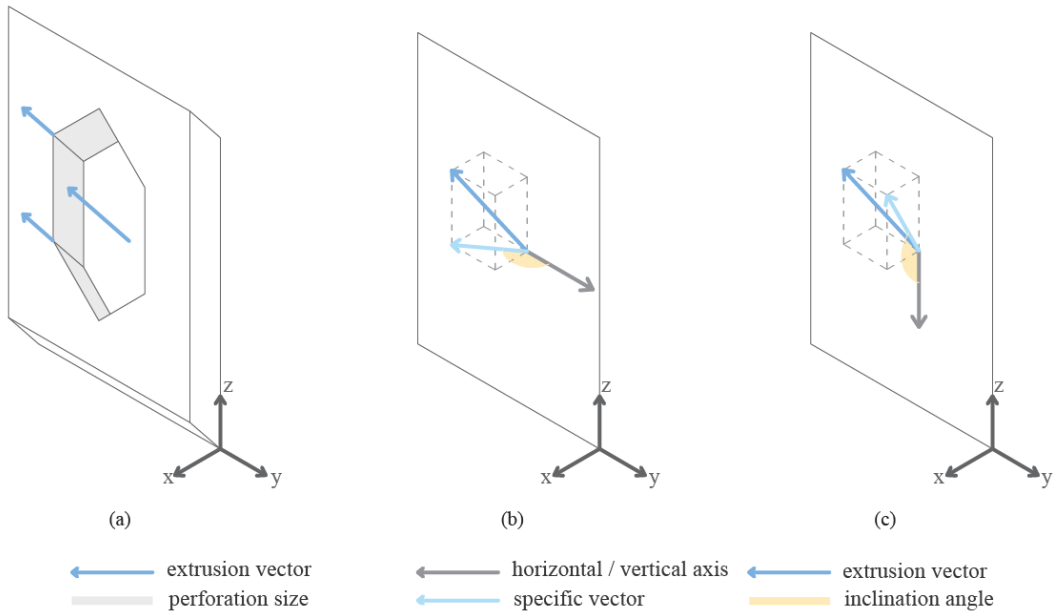

Figure. 4: vertical inclination of perforation lateral sides with a depiction of extrusion and specific vector

The choice of whether to include both horizontal and vertical inclinations has to be considered in reference to the screen's orientation to the sun. This is important since the sun rays change throughout the year meaning that perforation inclination has to be designed to fit multiple situations. In order to test the Voronoi perforation in reference to the largest set of sun rays, a south facing facade is chosen, given its sun ray diversity throughout the year. Since the south side is the most illuminated one on the northern hemisphere, adequate daylighting is provided, while simultaneously achieving protection from direct sunlight.

As for the horizontal and vertical inclination, it is possible to deduce that horizontal rotation i.e. the angle extrusion inclination vector forms in reference to the specific SS angle in the horizontal plane, does not make much of an influence on interior exposure and daylighting pertaining to south facing facades. This derives from the fact that

any horizontal inclination angle is at one time directly aligned with the horizontal sun ray vector projection, meaning that using 0 as the horizontal inclination angle can be considered similar to it being any other angle. This is why, for the purposes of this research, only vertical inclination angles are going to be considered. The range of angles for the inclination vector spans from -45 to 45 degrees, with negative values indicating direction below the horizontal plane i.e. away from the sky and positive values indicating direction towards the sky. This range is chosen empirically, given that angles larger than 45 degree tend to disable view from the inside out (Fig. 5a and 5b).

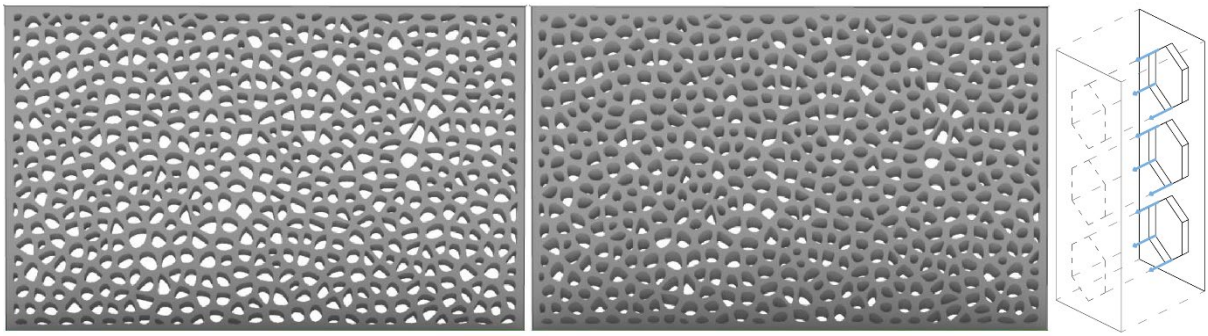

(a) (b) (c)

Figure. 5: The depiction of different inclination vector angles a) -45 degree vertical inclination of the perforation sides; b) -60 degree vertical inclination of the perforation sides

Since the extrusion produces only the sides of the perforations, but not the screen as a solid, which is needed for later shadow and viewing analysis, the perforations are projected along the perforation extrusion angle onto a plane parallel to the SS at a distance of the desired thickness (Fig. 5c). The extrusion is performed away from the initial box depicting the room, so that the results can be comparable, without the room losing a percentage of its area with the increasing PS thickness. The thickness is set to be 5cm, 10cm or 15cm which are values that are realistically used in similar scenarios. With these parameters defined and the ranges set, the calculation and analysis part can be introduced.

3. DAYLIGHTING ANALYSIS

Once the PS is generated, it needs to be evaluated with regards to its efficiency for controlling direct interior daylighting. The evaluation is done in reference to the shadow the PS casts in the following manner. The bottom side of the initial box depicting the room (Section 2) is chosen as the evaluation surface (ES). The ES forms a planar region where the PS shadow, cast with a specific sun ray, is going to be considered. This is done in order to have comparable data later on. The sun ray represents a vector, related to the geographical position of where the PS is evaluated for and changes throughout the year. For this research, the data for Belgrade in Serbia is chosen, where the vertical inclination of the sun in reference to the ground (altitude angle) changes from 23 degrees in the winter time (December 22nd), passing 45 degrees in the spring and autumn (March 20th and September 21st respectively) with the largest inclination of 67 degrees occurring during the Summer (June 22nd). These four dates are chosen as the start, middle and end angle values for sun ray's vertical inclination. For the horizontal inclination, in order to have comparable data, a time frame from 8AM to 5PM is chosen for all above mentioned dates, with sun rays being determined for every hour, thus having 10 values in total for each day. This time frame is used due to the fact that there is daylight during this period throughout the year.

By using a parametric approach, the geographical position can be updated for any location. Before the shadows can be cast, the remaining sides of the initial box are used as the obstructing geometry, along with the PS. Once all 10 sun rays are used for casting a PS shadow onto the ES, a screenshot of a shadow map is generated for a specific date (Fig. 6a), with black parts showing no direct exposure and white parts showing direct exposure. However, this depiction is not the best choice for comparison later on, since the area of white parts consists of a larger or smaller overlap of shadows for different sun rays throughout the day. Because of that, the ES is divided into a square grid with adjustable sizes, where the center of each square is checked for sun ray exposure. For the purposes of this research, the square edge is set to 5cm. Depending on the number of sun rays that reaches each center, the square surfaces are colored a different shade, with green having no exposed squares, yellow having five and red having all ten sun rays reach the square center, with shades in between (Fig. 6b and 6c).

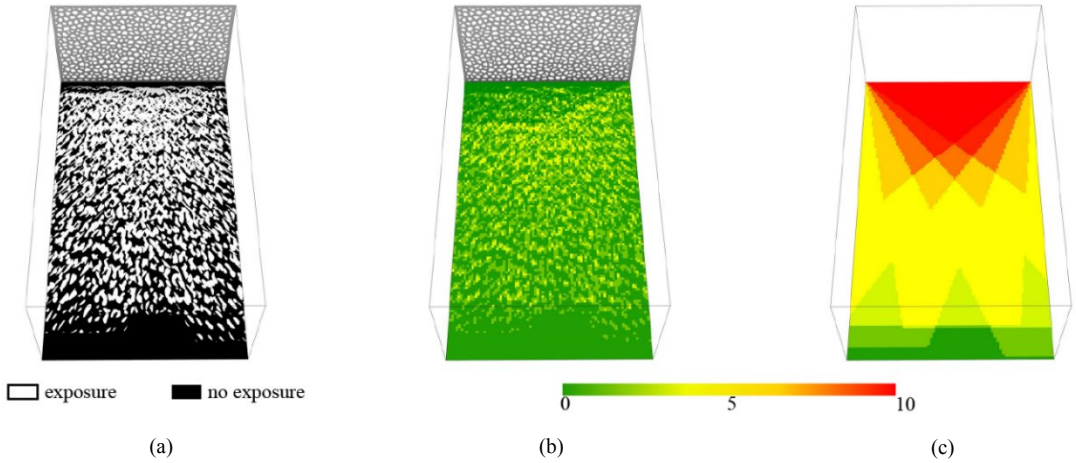

Figure. 6: The exposure of the interior ES for sun rays on December 22nd (a) shadow map created by PS consisting of overlapped and joined shadow areas with black having no exposure and white showing exposure; (b) The depiction of the exposure with the PS color graded; (c) The depiction of the exposure without the PS color graded

In order to check the impact of the PS application can have on the room interior, a control exposure is done without the PS shown in Figure 6c. Even though this color graded depiction is easy to understand visually, it still requires a quantitative representative in order to be comparable. That is why, the number of rays that reaches each square center is calculated (r_{sr}) and compared to the total number of rays that can reach each square in the grid (t_{sr}). This is determined with a simple equation (1):

$$\frac{r_{sr}}{d_{sr}*\left(\frac{b_l}{g}*\frac{b_w}{g}\right)} \qquad \textbf{(Eq. 1)}$$

where r_{sr} is the total number of sun rays that reaches each square center in the grid, t_{sr} represents the total daily number of sun rays, with b_l and b_w showing the length and width of the initial box room respectively and g showing the size of the square grid edge. In such a manner a visual representation of the exposure is reduced to a numerical value which can be compared much easier later on. Following this procedure, coupled with the variations pending parameter changes explained in Section 2.1 and 2.2., the analyses are conducted and presented in the following section.

4. RESULTS

The parameters and values used in this research are specified in each section. However, in order to make the overview more organized for the analysis process, they are laid out in three separate categories - the geometry, the sun rays and the evaluation. The geometry part refers to the room depiction and the PS. The box depicting the room is set to 400 cm width, 700 cm length and 250 cm height. The shorter vertical side of the box, measuring 250 cm in height and 400 cm in width is chosen for placing the PS instead. The size of the perforations is set in increments of 2.5cm in the range between 5cm and 10cm for the radius. The inclination angle is set in increments of 15 degrees in the range between -45 degrees and 45 degrees. The thickness of the PS is set in increments of 5 cm in the range from 5 cm to 15 cm. The sun rays part refers to the vectors at which the sun is shining at a specific geographical location and a specific time of the year. The geographical location is set to be Belgrade in Serbia and the times of the year are planned to be the two equinoxes and two solstices during the year. However, since the vertical inclination of the sun in reference to the ground is the same for spring and fall, only one equinox is chosen for the analyses. To sum up, the chosen dates are March 20th, June 22nd and December 22nd. Times during the day are set for each hour in the range between 8AM and 5PM. The evaluation part refers to the square grid, with the edge length of 5 cm, located on the ES, meaning 140 squares in one direction and 80 squares in the other direction, with a total of 11.200 squares. The following tables shows the percentages for a specific combination of the above mentioned parameter values (Tables 1, 2 and 3).

The perforation size and inclination is changed, as well as the sun ray inclination represented with dates, for a PS thickness of 5 cm, then 10 cm and finally 15 cm. The percentages are shown in the colored table cells, with the first group (light orange) showing results of the calculation with the PS, the second group (light yellow) without the PS and the third (blue), the difference that a PS makes on the interior exposure. As can be seen, the highest percentage (dark orange) of occluded rays per panel thickness is calculated for the inclination of -45 degrees regardless of the perforation size and time of the year. Following this percentage result, it is calculated what is the maximum difference that a PS makes when compared to a control case of a sun exposed room without a PS.

Table 1 - numerical data, percentage of blocked direct sun rays and panel efficiency; PS thickness 5 cm

PS thickness 5 cm		*With panel [%]*							*Without panel [%]*	*Difference [%]*
Season	*Perforation size [cm]*	*Perforation inclination [degrees]*								
		-45	*-30*	*-15*	*0*	*15*	*30*	*45*		
Spring	*10*	99,73	99,12	98,39	97,44	96,45	95,44	94,41	75,86	23,87
	15	97,95	96,72	95,75	94,78	93,78	92,94	92,09		22,09
	20	95,89	94,57	93,61	92,74	91,88	91,04	90,38		20,03
Summer	*10*	100	100	100	100	100	99,97	99,85	92,08	7,92
	15	100	99,97	99,93	99,87	99,75	99,6	99,32		7,92
	20	99,87	99,76	99,61	99,46	99,31	99,08	98,73		7,79
Winter	*10*	87,38	83,38	79,93	76,83	75,04	75,62	79,34	41,69	45,69
	15	81,85	77,92	74,73	72	70,46	71,15	74,3		40,16
	20	77,41	73,8	71,03	68,62	67,39	67,94	70,72		35,72

Table 2 - numerical data, percentage of blocked direct sun rays and panel efficiency; PS thickness 10 cm

PS thickness 10 cm		*With panel [%]*							*Without panel [%]*	*Difference [%]*
Season	*Perforation size [cm]*	*Perforation inclination [degrees]*								
		-45	*-30*	*-15*	*0*	*15*	*30*	*45*		
Spring	*10*	100	100	99,99	99,82	99,31	97,96	96,52	75,86	24,14
	15	100	99,85	99,44	98,57	97,5	95,92	94,65		24,14
	20	99,79	99,05	98,02	96,92	95,66	94,22	92,98		23,93
Summer	*10*	100	100	100	100	100	100	100	92,08	7,92
	15	100	100	100	100	100	100	99,98		7,92
	20	100	100	100	100	99,99	99,96	99,83		7,92
Winter	*10*	90,91	90,28	87,26	82,61	79,29	80,25	85,66	41,69	49,22
	15	89,93	86,52	82,24	77,48	74,7	75,61	81,02		48,24
	20	86,73	82,17	77,79	73,43	71,06	71,98	77,05		45,04

Table 3 - numerical data, percentage of blocked direct sun rays and panel efficiency; PS thickness 15 cm

PS thickness 15 cm		*With panel [%]*							*Without panel [%]*	*Difference [%]*
Season	*Perforation size [cm]*	*Perforation inclination[degrees]*								
		-45	*-30*	*-15*	*0*	*15*	*30*	*45*		
Spring	*10*	100	100	100	100	99,94	99,24	97,51	75,86	24,14
	15	100	100	99,99	99,83	99,19	97,78	96,04		24,14
	20	100	99,98	99,76	99,1	97,94	96,26	94,61		24,14
Summer	*10*	100	100	100	100	100	100	100	92,08	7,92
	15	100	100	100	100	100	100	100		7,92
	20	100	100	100	100	100	100	100		7,92
Winter	*10*	90,93	90,89	90,22	86,06	82,11	83,1	88,29	41,69	49,24
	15	90,92	90,32	87,33	81,69	77,89	78,95	85,32		49,23
	20	90,58	87,89	83,52	77,69	74,19	75,39	81,82		48,89

The table data show the efficiency in blocking direct sun rays. By changing the angles for the inclination from positive to negative values, the percentage of blocked direct sun rays is increasing, if the results for summer and spring are observed. During winter, if the observation is based on the same principles, the percentages are firstly decreasing until the result calculated for 0 degrees value. By changing the angles from 0 to negative values, the percentages are increasing, as is the case for other seasons. The best results are achieved for negative values taken for the inclination angle, regardless of the season. Therefore, when calculating the difference that PS makes, the result from the column with the inclination of -45 degrees (dark orange) is chosen. The panel efficiency in relation to the seasons will be compared and discussed below.

The differences that PS makes are not significant during the summer. Namely, by comparing all the calculated values for every combination of parameters, in the orange part, the maximum difference is less than 2%. The percentage of occluded sun rays calculated without the presence of PS is 92,08%. This means that most of the direct sun rays cannot reach the room, due to the altitude angle during summer (the sun is at its highest). The PS application improves protection from direct sun rays by only 8%. The biggest difference in the blue column between the calculated values, if all three tables are observed, is less than 0,2%. That means that the impact of the perforation size and screen thickness parameters is barely noticeable. The impact of the inclination parameter is calculated by comparing the highest and the lowest percentage of each row in the orange part. The biggest difference is about 1% if the row with the 20 cm for perforation size parameter, i.e. the third row in Table 1 is observed.

A greater difference in the prevention from direct sun rays than in summer is achieved during spring. The percentage of occluded sun rays calculated without the presence of PS is 75,86%. The difference with applied PS is between 20% and 24%. The biggest difference in the blue column between the calculated values is about 4% which means that changing parameters such as screen thickness and perforation size, in this case, has more influence than during the summer. This case scenario corresponds to the values of altitude angles during seasons. The value of the altitude angle during spring passes 45 degrees, but it is still smaller than in summer. The impact of the inclination parameter, observed for each row in the orange part, is between 2,5% (Table 3, first row) and 7,5% (Table 1, second row), if the comparison is based on the same principles as for the summer. If the PS efficiency is observed throughout the day, the values from the tables show that the maximal number of direct sun rays is prevented from reaching the room floor.

The biggest difference that a PS makes is achieved during winter. The percentage of occluded sun rays calculated without the presence of PS is 41,69%. The difference with applied PS is between 35% and 50%. The combination of -45 degrees for the inclination parameter, 10 cm for the perforation size parameter, and 15 cm for the screen thickness parameter gives the biggest difference achieved with the PS application - 49,24%. During winter, the high percentage of occluded sun rays (70-80%) is calculated even for the positive values of the inclination parameter, regardless of the screen thickness. The main reason is the value of altitude angle during winter (23 degrees). The impact of both, PS thickness and perforation size parameters, is between 1% and 10%, if values from the blue column in all three tables are observed. The impact of the inclination parameter is calculated by comparing the highest and the lowest percentage for each row in the orange part. The difference obtained is between 9% (Table 3, seventh row) and 16% (Table 3, ninth row).

5. CONCLUSION

This research was concentrated on designing and calculating the efficiency of an optimal perforated screen that minimizes direct sunlight. The PS designed for this research, represents the contemporary interpretation of mashrabiya combined with inclined perforations. The improvement of blocking direct sun rays by placing the PS on the south side of the room is calculated and it is between 8% and 50%, depending on the season. If the impact of PS thickness is observed, the highest percentage of occluded sun rays is achieved with the value of 15 cm, and the lowest percentage with the value of 5 cm. The most efficient perforation size in blocking direct sun rays is the value of 5 cm, and the least efficient is the value of 20 cm. The impact of perforation size and PS thickness is the same, regardless of the season. However, the impact of perforation inclination angle depends on the season. During winter, the highest percentage of occluded sun rays is for the inclination angle of -45 degrees, and the lowest percentage for the inclination angle of 15 degrees. During spring and summer, the most efficient value of the inclination angle is the value of -45 degrees, and the least efficient is the value of 45 degrees. Analyses proved that the perforations inclination is an important parameter as well as the cell size and the panel thickness. The inclination effect can be seen by comparing the values obtained for the angle measuring 0 and for all other angles. Future research will focus on incorporating both direct and diffuse daylighting calculations. The illumination level in the room with several variations of PS will be analyzed, and then compared with the required illumination level.

ACKNOWLEDGEMENTS

This research (paper) has been supported by the Ministry of Education, Science and Technological Development through the project no. 451-03-68/2020-14/200156: “Innovative scientific and artistic research from the FTS (activity) domain”.

REFERENCES

1. Akçay, A.Ö. and Alotman, H., 2017. A Theoretical Framework for the Evaluation from the Traditional Mashrabiya to Modern Mashrabiya. Journal of History Culture and Art Research, 6(3), pp.107-121.
2. Aljawder, H.M. and El-Wakeel, H.A.,2019. Evaluating the Performance of a Daylighting Traditional Device “The Mashrabiya” in clear sky conditions: Case Study of a Traditional Bahraini House. Structural Studies, Repairs and Maintenance of Heritage Architecture XVI, 191. p. 395.
3. Alkhalili, N., Kesik, T., O'Brien, W. and Peters, T., 2018. Developing and testing visual privacy metrics. Proceedings of 7th International Building Physics Conference, Syracuse, New York. p. 703.
4. Altan, H., Ward, I., Mohelníková, J. and Vajkay, F., 2008. Daylight, solar gains and overheating studies in a glazed office building. International journal of energy and environment, 2(2). pp. 129-138.
5. Bainbridge, D. and Haggard, K., 2011. Passive solar architecture: heating, cooling, ventilation, daylighting and more using natural flows. Chelsea green publishing, White River Junction, Vermont.
6. Boubekri, M., 2008. Daylighting, architecture and health: building design strategies. First edition. Routledge, Abingdon, United Kingdom.
7. Cantin, F. and Dubois, M.C., 2011. Daylighting metrics based on illuminance, distribution, glare and directivity. Lighting Research & Technology, 43(3). pp. 291-307.
8. De Herde, A. and Nihoul, A., 1994. Overheating and daylighting in commercial buildings. Renewable energy, 5(5-8). pp. 917-919.

9. Fournier, C. and Wirz-Justice, A., 2010. Light, Health and Wellbeing: Implications from chronobiology for architectural design. World Health Design: Architecture, Culture, Technology, 3(1). pp. 44-49.
10. Giovannini, L., Verso, V.R.M., Karamata, B. and Andersen, M., 2015. Lighting and energy performance of an adaptive shading and daylighting system for arid climates. Energy Procedia, 78. pp. 370-375.
11. Goia, F., 2016. Search for the optimal window-to-wall ratio in office buildings in different European climates and the implications on total energy saving potential. Solar Energy, 132. pp. 467-492.
12. Gutiérrez, R.U., Du, J., Ferreira, N., Ferrero, A. and Sharples, S., 2019. Daylight control and performance in office buildings using a novel ceramic louvre system. Building and Environment, 151. pp. 54-74.
13. Hashemi, A., 2014. Daylighting and solar shading performances of an innovative automated reflective louvre system. Energy and Buildings, 82. pp. 607-620.
14. Hee, W.J., Alghoul, M.A., Bakhtyar, B., Elayeb, O., Shameri, M.A., Alrubaih, M.S. and Sopian, K., 2015. The role of window glazing on daylighting and energy saving in buildings. Renewable and Sustainable Energy Reviews, 42. pp. 323-343.
15. Jakubiec, J.A. and Reinhart, C.F., 2012. The 'adaptive zone'–A concept for assessing discomfort glare throughout daylit spaces. Lighting Research & Technology, 44(2). pp. 149-170.
16. Karamata, B. and Andersen, M., 2014. Concept, Design and Performance of a Shape Variable Mashrabiya as a Shading and Daylighting System for Arid Climates. Proceedings of 30th International Passive and Low Energy Architecture conference, Ahmedabad, India. pp. 344-351.
17. Kotbi, A. and Ampatzi, E., 2017. Using solar screens in school classrooms in hot arid areas: the effect of different perforation on daylighting levels. Proceedings of 33rd Passive and Low Energy Architecture International conference, 2. Edinburgh, United Kingdom. pp. 3253-3260.
18. Lavin, C. and Fiorito, F., 2017. Optimization of an external perforated screen for improved daylighting and thermal performance of an office space. Procedia engineering, 180. pp. 571-581.
19. Nebia, B. and Tabet Aoul, K., 2017. Overheating and daylighting; assessment tool in early design of london's high-rise residential buildings. Sustainability, 9(9). p. 1544.
20. Phillips, D., 2004. Daylighting: natural light in architecture. Routledge, Abingdon, United Kingdom
21. Pool, D.A.C., 2019. A Comprehensive Evaluation of Perforated Façades for Daylighting and Solar Shading Performance: Effects of Matrix, Thickness and Separation Distance. Journal of Daylighting, 6(2). pp. 97-111.
22. Through Vin's Lens, 2018. http://www.throughvinslens.com/rmit-design-hub.html [Accessed: 13th May 2020]
23. ArchDaily, 2015. https://www.archdaily.com/590576/sdu-campus-kolding-henning-larsen-architects [Accessed: 13th May 2020]
24. Middle East Architects, 2014. https://www.middleeastarchitect.com/portfolio/in-pictures-mashrabiya-in-contemporary-architecture/attachment/al-bahr-towers-7-d378-682 [Accessed: 13th May 2020]
24. Depositphotos, 2015. https://depositphotos.com/77668708/stock-photo-facade-of-arab-world-institute.html [Accessed: 13th May 2020]

AUTOMATION AND PARAMETRIC DESIGN IN ARCHITECTURAL EDUCATION

Sanja Janković
Faculty of Civil Engineering and Architecture, University of Nis, Serbia
PhD. student, sanja.jankovic@outlook.com

Vladan Nikolić
Faculty of Civil Engineering and Architecture, University of Nis, Serbia
PhD., Associate Professor, vladan_nikolic@yahoo.com

Sanja Spasić Đorđević
Faculty of Civil Engineering and Architecture, University of Nis, Serbia
PhD. student, sanjaspasicdjordjevic@gmail.com

ABSTRACT

Many forms in architecture, and therefore constructions, are so complex today that they cannot be construct without some kind of automation, and this is an opportunity for architects to engage more in this area. In this sense, the subject of this research is the importance of programming use in architecture, ie in parametric design of biomimicry forms. Emphasis in this paper is placed on the efficiency of automation, because it refers not only to generated geometries but also to production. The aim of this paper is to highlight own interpretations related to the problem, ie the importance of automation in biomimicry design. The main contribution of this paper should be the proposal of programming introduction at faculties of architecture in order to effectively understand parametric design and automation.

Keywords: automation; parametric design; biomimicry; programming; education

1. INTRODUCTION

In modern architecture, biomimicry forms are so complex that it is not possible to intuitively design construction and predict what the optimal construction would look like. In this case, parametric design and automation are indispensable as a tool that generates millions of different solutions and suggests optimall one.

In order to understand automation in parametric design of biomimicry forms, it is not enough to be an expert in some scientific field, but it is necessary knowledge in the field of architecture, construction and basic programming. The subject of this research work is about importance of parametric tools and automation in biomimicry design. In the first part of the paper it will be exposed the role of automation and coding in parametric design. Also, it will be indicated on significance of multidisciplinary work and collaboration between engeneers in design process. In the second part of the paper, emphasis is placed on studies of automation application in digital education. The aim of the paper is to highlight our view about the importance of automation and multidisciplinary design in engineering, as well as programming introduction at faculties of architecture in order to understand parametric design and automation.

2. THE ROLE OF AUTOMATION AND CODING IN PARAMETRIC DESIGN

"I want to own the automation of my own profession…" (Mario Guttman, Architect, Programmer).

The onset of digital design has enabled a new level of experimentation with freeform shapes in contemporary architecture, which has made geometry a fertile area of research over the last decade or so. Today, with various parametric tools also coming into the picture, an architect is easily able to establish parameters and constraints on dynamic geometries, to seamlessly produce convoluted designs. Now the question arises as to whether the credit should go to the architect or to the programmer who scripted the tool which contains the algorithms embedded in its code. To solve this dilemma, it would just make more sense if the architects, themselves, had the liberty of creating the tools required to design their own building spaces. Besides, a lot of the design tools, out there now, are open source (encourage third party development) and come with their respective APIs (Application Programming Interfaces) and SDKs (Software Development Kits), and that is an advantage that should be utilized.

Coding helps you explore new architectural forms and investigate how architecture can evolve and adapt to the ever-changing. Usually, design tools use various complex automation routine algorithms which many architects fail to understand, hence their usage of the tool is limited and their overall efficiency is reduced. If they know exactly what these algorithms represent and how they influence the outcome of a geometry, they can make much more conscious and efficient decisions in the design process. Coding Knowledge gives the architect complete control over the whole form generation process, as the architect would know exactly what to expect out of the tool and so, tailors it to their specific needs. The tool becomes unique to the architect's style and screams originality on a whole new level. A designer is encouraged to analyze the problem at hand and solve it in a step by step process in contrast to what he typically does – intuitively or creatively approach the problem, which is very subjective (https://www.arch2o.com/5-reasons-architects-learn-to-code/, Accessed: 1st March 2020).

Helmut Pottmann describes how geometry not only has the potential to inform a more exciting generative approach for architects, but can also make design much more construction aware for the whole design team, enabling a wholly digital work flow from design to fabrication.

The logic of parametric modeling offers a new way of thinking in the design process, and digital fabrication is a way to perform that design. Detail of the technical drawing of a parametric designed structure: all the elements in the drawing are similar but mutually different to give the final shape after assembly. Therefore, an algorithm that automatically generates a 3d structure also makes numbers that allows construction to be easily assembled after fabrication. The cost of projects based on parametric modeling and application of digital fabrication need not be more expensive than the traditional construction method. Parametric design enables automation in the design process. Automation therefore also saves a lot of time. Automation is applicable at different levels in architecture, both on large structural systems and in furniture design where software analyzes parameters and allows statically optimal structures.

Parametrically generated curved shapes can save a lot of energy, offer new efficient and elegant structural solutions, save on the amount of material used, or allow better natural lighting and ventilation. Quite simply, it allows you to create countless variations of geometric shapes that meet certain criteria defined by the design assignment. It is up to the architects to choose the variant that is best suited for the particular project task. They are not necessarily a symbol of a new aesthetics in architecture, but of a new way of thinking and building.

It is also true that the process of fabricating curved shapes can be significantly more expensive than construction based on traditional shapes and methods. Therefore, it is necessary to know the techniques of fabrication as well as the methods of geometric optimization, because in this way it can be adjusted to be the same or even cheaper in the production process compared to traditional construction methods (Tepavčević, 2019).

In addition to this, knowledge of structure (skeleton) is of great importance. The design of complex three-dimensional shapes is among the most interesting challenges for structural engineers. Irrespective of whether a structure is visible, it forms the skeleton for the architecture and the basis for geometric coordination. Design strategies are required for this intelligent engineering that embrace the inherent structural behaviours of such complex geometries from the start and allow the coordination of structure, architecture and fabrication. Studying their basic principles, communalities and differences, one can develop a classification of the different types of surfaces and geometries and derive from them the right modelling approaches (Mangelsdorf, 2010).

3. AUTOMATION AND STRUCTURAL ENGINEERING AS INTEGRATIVE DESIGN PROCESS

The new understanding of architecture, emerging production technologies and parametric design tools have to go hand in hand with the traditional understanding of engineering and detailing. For complex geometry structures, analytical knowledge and understanding of the structural behavior, due to the complex nature of the geometry, is in most cases missing. Research in this field is important for engineers and designers to give them the insight and the necessary knowledge for designing an efficient and aesthetically pleasing structure and the understanding that structures are an integral part of the building design process. Therefore it is of utmost importance to educate engineers not only in working with FEM programs, but also facilitating the means for them to develop an analytical understanding of the structural behavior which is the key to the correct interpretation of the analysis results (Borgart et all., 2007).

Programmers generally do not understand space well enough, do not understand how construction works, or the basic static principles. Civil engineers, on the other hand, generally ignore aesthetic aspects of architecture, that are very important. Construction has to follow architecture above all else, and today we have tendency to merge the construction and facade into one - the construction becomes façade, ie envelope of the object. In this regard, parametric architecture should not be separated from its important advantage, which is production at any level; it's a façade, a detail, energy efficiency. It is also important to emphasize biomimicry in architecture as an discipline that contribute to this creative process using analogy and mathematical-geometric model. Biomimetic study by system analysis in nature strives for better exploitation and lower energy consumption.

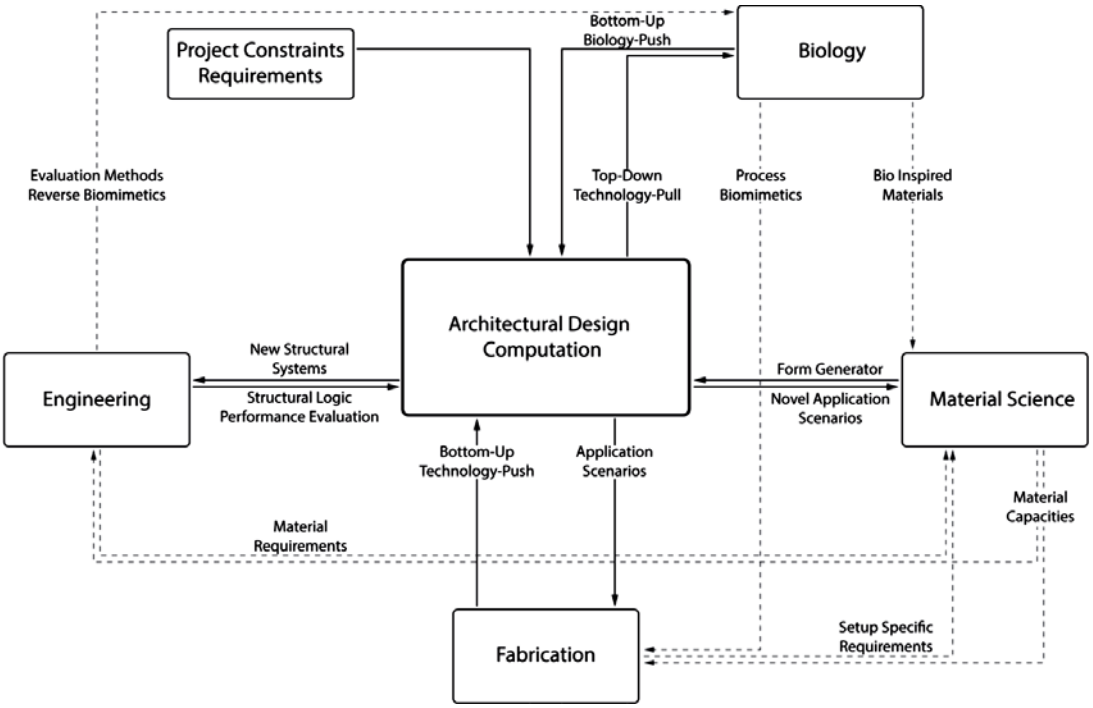

Figure. 1: Generic integrative design process (Source: Dörstelmann et all., 2014)

In order to orchestrate the complex network of interrelations within a multidisciplinary design and construction process, design computation is used to translate various process inputs into tool parameters and encoding the interrelations into an algorithmic framework (Figure 1) (Dörstelmann et all., 2014). The integration of structural design into a multidisciplinary design process through novel simulation tools permits engineers and architects to explore structural systems beyond predetermined typologies, as well as enabling them to include precise and meaningful structural analysis into the formally decoupled design process (Knippers, 2013).

When designing complex threedimensional shapes and geometries, structural engineering has to be a creative contribution to the design process, so that a full integration and coordination of aesthetical and physical aspects can be achieved. This relies completely on the development of engineering concepts that understand and facilitate the design, and at the same time close collaboration with the architect, manufacturer and other design disciplines. The engineering modelling and realisation strategies outlined here help to create that important conceptual clarity

behind the development of the design – the basis of a constructive dialogue between the design partners and a trusting relationship between architect and structural engineer.

Also, this opens up greater potentials for the transfer of functional principles from biology to novel material and structural systems within a multidisciplinary process, while generating potential biological insight through the use of cross-disciplinary methodologies within a reverse biomimetic process.

4. IMPORTANCE OF PROGRAMMING IN ARCHITECTURAL EDUCATION AND PRACTICE

In accordance with these tendences, programming should be included from the beginning in parametric design. As a starting strategy in development of this idea, it would be of great importance to learn programming in faculties of architecture. "Creative collaboration" and various forms of ways in which the parties in the building process collaborate – is not yet a part of the formal architectural and/or engineering education (Borgart et all., 2007).

As noted by Moneo (2005), it has become fashionable to design organic-shaped buildings. However, Di Cristina (2001) emphasizes that this "topological tendency" does not simply mean curved surfaces, but the study of the geometrical properties that remain unchanged when figures undergo continuous transformations, something that requires computational knowledge for understanding and implementing.

The new generation of architects must be able to develop designs that are adaptable to a continuously changing urban environment, and programming may play an important role in modeling these concepts to develop design through conditional dependencies. In other words, contemporary, architecture is fundamentally about relationships, and state of the art construction is characterized by the use of expensive materials produced with great acuracy, frequently through automated processes. A new generation of CAD software is being currently developed to respond to these new requirements.

However, until now there exists neither a framework nor a fundamental structure for the use of computer in architectural education, most of architectural schools and departments, especially in developed countries, have developed their criteria in the educational schedules by integrating more computer courses (Zhi-Ting Zhu et all., 2016)

A proper understanding of architecture schools pedagogies can be a start to discover when, where and how the computer applications should be implemented in architectural education. Hence at first, the current status for the architectural education should be examined and analyzed through a theoretical and analytical investigation of the architectural schools. Then, understanding the architectural profession needs is the second step towards an ideal framework to integrate the computer applications with architectural curriculum (Soliman et all., 2019).

4.1. Automation and parametric design in architectural curriculum

This chapter presents studies of computer applications integration in the top 20 international architecture schools, with the aim of understanding the current level of automation application in digital education.

The survey examines 20 international schools from 9 different countries; 9 architectural schools from USA, three from England UK, two from Australia and a single school from each China, Singapore, Italy, Netherlands, Germany and Canada. The sample is chosen according to Quacquarelli Symonds (QS) World University Ranking by Subject (2017) and Times Higher Education University Ranking (2017). Then it is summarized to the common top 20 schools in both ranking systems.

The architectural schools covered by this research are: University of Hong Kong, MIT, University of California - LA, Cornell University, National University of Singapore, Manchester School of Architecture, Columbia University, Milano University, University of Cambridge, University of Melbourne, UCL, UCB, Delft University, Harvard school of Architecture, ETH Zurich- Swiss Federal, University of Sydney B. Design Computing, University of Georgia, University of Toronto, Princeton University,University of Pennsylvania.

On the international level, it was found that the 2D&3D representation applications stand for 50 percent of all computer application courses all over the threephases. Digital fabrication courses take 13 percent from the architecture curriculum followed by nine percent for programming, seven percent forsimulation courses and five percent for environmental technologies. While parametric design, building technologies and communication take four percent (Figure 2). Finally GIS and BIM courses account for the least computer application courses in the curriculum.

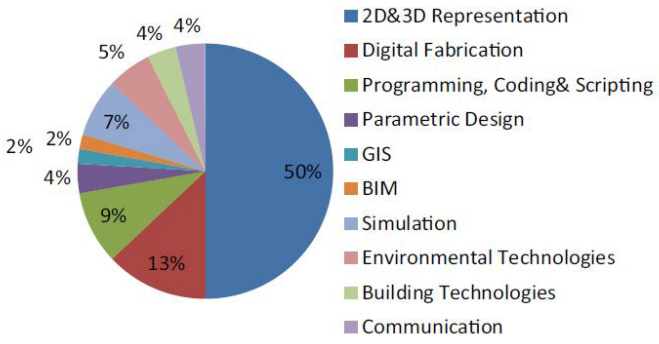

Figure. 2: Computer application disciplines in the international level (Source: Soliman et all., 2019.)

On the international level, it is noticed that parametric design and digital fabrication courses are needed in the final year(s) (aside to the 2D&3D representation) more than in sophomore or preparatory years unlike the simulation and building technologies which take place in sophomore years as the matrix shows (Figure 3). But 2D&3D representation is found in the three phases, mainly in the preparatory year (Soliman et all., 2019) .

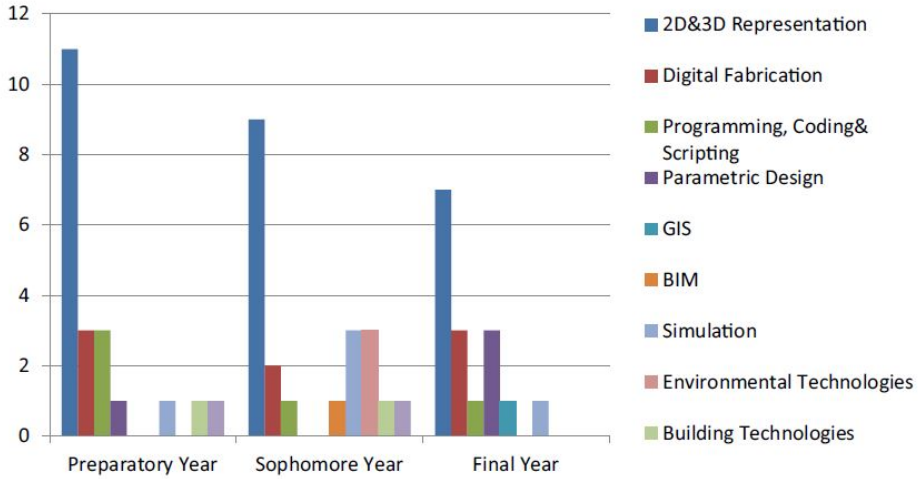

Figure. 3: International computer applications courses in study years (Source: Soliman et all., 2019.)

At the faculties of architecture in Serbia, the aim is to improve the field of computer programs application for visualization in architecture. For the most part, this refers to the application of 2D and 3D representation. However, the field of biomimicry and automation is not still enough included in education. An example of good practice is the architecture department, FTS from Novi Sad, which has a Digital Design Center. The Center is conducting research on when and how to apply innovative design approaches, that is, parametric design and digital prefabrication. So far, they have had several successfully implemented architectural projects in which the aforementioned methods have been applied. One of these "Shark skin" project is related to biomimicry and illustrates very well the application of automation in parametric design.

Shark Skin panels represent biomimetic structure designed, analyzed and generated by digital tools and technology. Specific characteristics of shark skin denticles are inspiration for the designed biomimetic panels (Figure 4a left). Shark skin denticles geometry minimizes the turbulence of the water in micro scale. The aim of this project is to transfer the analogies shape in macro scale in order to reduce unfavorable wind velocity in urban areas. Computational fluid dynamic analysis proved the significant wind reduction of the shark skin panels compared to other surfaces (Figure 4b). Base plane of the designed panels use the irregular hexagonal tessellation, such as sharkskin itself, and surface is generated as a section of two ruled surfaces with mutually orthogonal directrix and generatrix. The panels are made by industrial robot using the hotwire styrofoam cutting technique (Figure 4a right).

Project is conducted over the 4th eCAADe International Regional Workshop held in Novi Sad 19th and 20th May 2016 (http://www.arhns.uns.ac.rs/cdd/shark-skin-panels/#content-wrapper, Accessed: 1st March 2020).

(a)

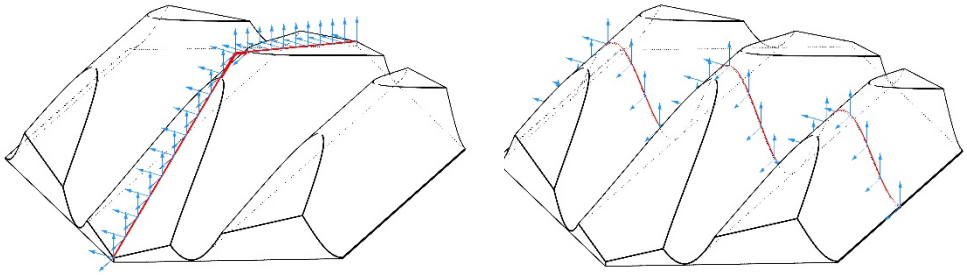

(b)

Figure. 4: Shark skin – biomemtic structure, (a)panels and industrial robot, (b) fluid dynamic analysis (Source: http://www.arhns.uns.ac.rs/cdd/shark-skin-panels/#content-wrapper, Accessed: 1st March 2020)

4.2. "Programming architecture" and automation in practice

Programming Architecture is a company that solves problems in the design and construction phase of complex architectural objects, they generate complex geometries, optimize their form or their structure statically and eventually automate the production of technical drawings and the CNC production of architectural elements (facade, structure, etc..).

Programming Architecture focuses on developing custom software for specific projects, using C# and C++ in combination with diverse, industry recognized, software (Rhino, Revit, Tekla, RFEM, Unreal, etc.) in order to:

- Generate architectural and structural elements with maximum precision and prepare them for fabrication, and
- Perform Statical and Geometrical Optimization using cutting edge methods and FEM software (http://www.programmingarchitecture.com/publications/ControlledParametricalDesign.pdf, Accessed: 1st March 2020)

On the project of the Bao'an International Airport there was limited space to change the design and all problems arising from the complex geometry of the facade and the structure had to be solved by programming (Figure 5). In analogy to biological shapes Massimiliano Fuksas decided to break up the symmetry and many conventions of traditional airport buildings and to go for a free form shape with more then 60.000 different facade elements. The same number of different glass panes is carried by a light steel structure of around 400.000 individual structural members.

The main focus was on the geometrical development of the steel structure and the façade. The generation of the façade and roof elements of the Shenzhen Bao'an International Airport, has been automated with bespoke in-house software tools. This enabled to generate a double truss structure over a given free form surface, including aspects of sustainability, day light control, energy gain and architectural design intends were influencing the final design which required several adjustments of façade layout. The manual drawing of structure and facade would

take an unacceptable amount of time especially once it comes to changes. The only possible way to deal with this kind of task is to parametrically define the entire structure so that with each change of the form all elements can be generated within hours, or even minutes.

Figure. 5: Bao'an International Airport structure and geometrical development (Source: http://www.programmingarchitecture.com/publications/ControlledParametricalDesign.pdf, Accessed: 1st March 2020)

The 300.000m2 of free form surface was divided into a huge point cloud. This system of points was arranged in four layers. Two inner layers served as the basis for a double-layered grid structure and two outer layers for the generation of facade elements. The free form surface was unrolled so that the facade elements can be represented in an Excel spread sheet, and since there were 20 different types of façade panels (with different angles and openings), architects were able to simply fill the spread sheet with different colours and numbers, representing different elements (Figure 8). The software written for this purpose was able to extract that information from an Excel file, generate appropriate facade elements on the desired spot and fix all problems that arose in the process. Fixing problems refers to the adjustment of the connections between different elements and automated geometry perturbations performed in order to always keep the glass part of the facade planar - which was one of the main conditions and one of the biggest challenges, considering the double curvature of the surface and the complexity of the elements.

Combining different software, like in this case, enables an efficient cooperation between designers and engineers. There is one core software, programmed to automatically generate the structure and facade and there are many input branches that allow the definition of new elements, new structural pattern, the entire facade element disposition (like the Excel sheet shown in Figure 8), etc. This provides the flexibility to experiment with different settings, because after each change of the element, the definition of a new element type or structural system, the entire system can be generated automatically within a very short time. Today parametric design programs are conquering the market, but are often used for some basic design development. In this case, heavy steel and aluminium parts without any space for errors in the geometry had to be produced. That is why original methods had to be developed in order to deal with specific problems of this project.

The fixed shape approach is a design driven method where structural efficiency and production abilities come second. The main advantage is the enormous freedom in sculptural expressiveness of the architect. The disadvantages are the bigger programming efforts required to generate a statically efficient structure and automatically fix all the geometrical difficulties that could cause problems with fabrication of elements. There is basically always a trade-off between the freedom of the architect in shaping the form and the effort needed to program methods that will automate the generation and production of structural and facade elements (http://www.programmingarchitecture.com/publications/ControlledParametricalDesign.pdf, Accessed: 1st March 2020)

5. CONCLUSION

Automation in engineering represents optimization, sustainability, efficiency... Design in architecture is increasingly turning to nature and biomimicry. Due to the possibilities of automation in parametric design, forms from nature are much easier to transpose into architecture. Analytical understanding of form design, structure, programming with multidisciplinary work enables successful design of biomimicry forms. Such a concept results in original organic forms, leading to design solutions that can significantly affect the quality of architectural and urban spaces. Implementation of automation and programming in the architectural curriculum should be emphasized as a starting strategy in developing this approach to design. Automation in parametric design offers

unique methods that combine Design and Static Analysis software in order to achieve statically and geometrically efficient biomimicry structures.

REFERENCES

1. Borgart, A. and Kocaturk, T. 2007. Free form design as the digital "zeitgeist", *Journal of the international association for shell and spatial structures*, 48(4), pp.3-9
2. Di Cristina, G., 2001.The Topological Tendency in Architecture. *Architecture & Science*. New York: Wiley, pp.21-53.
3. Dörstelmann, M., Parascho, S., Prado, M., Menges, A., and Knippers, J., 2014. Integrative Computational Design Methodologies For Modular Architectural Fiber Composite Morphologies, ACADIA 2014 Design Agency, At USC, Los Angeles
4. Knippers, J., 2013. "From Model Thinking to Process Design." Architectural Design, Wiley, 83(2), pp. 74–81.
5. Moneo, R., 2005. Theoretical Anxiety and Design Strategies in the Work of Eight Contemporary Architects, Cambridge, MA: The MIT Press.
6. Mangelsdorf , W., 2010. Structuring Strategies for Complex Geometries, *The new structuralism design, engineering and architectural technologies*, 80(4), pp. 40-45.
7. Pottman, H., 2010. Architectural geometry as design knowledge, *The new structuralism design, engineering and architectural technologies*, 80(4) , pp. 72-77.
8. Soliman, S., Taha, D., El Sayad, Z., 2019. Architectural education in the digital age; Computer applications: Between academia and practice, *Alexandria Engineering Journal, 58(2),* pp.809-818
9. Tepavčević, B., 2019. Od VR-a, do izmenjene realnosti: Digitalne tehnologije u prodaji i posredovanju nekretnina , Build Up conference, panel Proptech, Belgrade
10. Zhi-Ting, Z., Yu, M.H., Riezbos, P,. 2016. A research framework of smart education, *Smart Learning Environments,* 3 (1), pp.1-17
11. https://www.arch2o.com/5-reasons-architects-learn-to-code/ [Accessed: 1st March 2020]
12. http://www.arhns.uns.ac.rs/cdd/shark-skin-panels/#content-wrapper, [Accessed: 1st March 2020]
13. http://www.programmingarchitecture.com/publications/ControlledParametricalDesign.pdf [Accessed: 1st March 2020]

moNGeometrija 2020

PARAMETRIC MODEL OF A RECTANGULAR FLAT VAULT

Teodora Nikolić
Department of Architecture, Faculty of Technical Sciences, University of Novi Sad, Novi Sad, Serbia
B.Arch, Master's student, niktea96@gmail.com

Dimitrije Nikolić
Department of Architecture, Faculty of Technical Sciences, University of Novi Sad, Novi Sad, Serbia
PhD, Assistant with PhD, dima@uns.ac.rs

Marko Jovanović
Department of Architecture, Faculty of Technical Sciences, University of Novi Sad, Novi Sad, Serbia
PhD, Assistant Professor, markojovanovic@uns.ac.rs

Vesna Stojaković
Department of Architecture, Faculty of Technical Sciences, University of Novi Sad, Novi Sad, Serbia
PhD, Associate Professor, vesna100@uns.ac.rs

ABSTRACT

Unlike the usual shape of vaulted structures, so called flat vaults are planar and are formed out of voussoirs cut in a specific way, which combines the material's properties and the needed geometrical, i.e. structural logic. Thus, the shape of the stone blocks enables their interlocking without the use of any kind of bonding agents. In this paper, the analysis of the flat vault's shape and its fundamental elements is conducted. The analytical model regarding geometric constrains of the vault over rectangular floor plan is derived and the corresponding parametric model is developed. Contrary to the common use of uniformly shaped voussoirs, which produce a strictly repetitive pattern in the ceiling appearance, the model includes the application of two systems of voussoirs. Such an approach enables various ceiling appearances suitable for diverse use in contemporary architectural design. In addition, through the parametric model, the variety of vault's form is inspected, and the physical model is digitally fabricated.

Keywords: flat vault; geometric analysis; masonry structures; parametric design

1. INTRODUCTION

Since ancient times, masonry systems, made out of individual elements, enabled easy and swift building of diverse types of structures. Conceivably the most distinctive ones are massive vaulted structures, whose appearance of intrados, being the interior soffit of a vault, is defined by the applied craft technique known as stereotomy (Gojković, 1976). Unlike beam systems, which transmit vertical loads, vaulted systems produce horizontal thrust, whose overcoming has been one of the greatest problems in building history. In the interest of successfully transmitting the forces, as well as forming the space, different shapes of vaults and voussoirs were developed. However, the zone above the extrados of a vaulted floor demanded a fill to make it planar and usable, consequently that meant a lot more material and space were needed.

In order to resolve this issue, shallower vaults were built. At the end of the thirteenth century, in Crusaders castle Crac des Chevaliers in present-day Syria, a shallow dome was built and described as flat due to its slight curvature (Fig. 1a). Later, in the sixteenth century, in El Escorial monastery in Spain, a stone ceiling with one entirely flat segment was built (Fig. 1b). Further, the Abeille vault, proposed at the end of the seventeenth century, was created in a way that enabled uniformly shaped voussoirs to interlock reciprocally, i.e. to support one another (Fig. 2a). Thus, the problem of occupying space and a needed fill was resolved by designing a flat vault, whose intrados and extrados are planar. Aside from its planar shape, relatively low height of constituent elements provided the

greatest possible usage of space even though, as a consequence of a specific type of stereotomy, the transmission of forces was similar to other vaulted structures.

(a) (b)

Figure. 1: (a) Shallow dome in Crac des Chevaliers, Syria, (b) vault in El Escorial monastery, Spain (Source: Alkhataeb et al., 2006)

Keeping in mind the complex process of the construction in the past and the stereotomy constrains, the design and aesthetics were limited in order to make it cost and time-efficient. Despite all the advantages, such as the uniform shape and the disposition of elements, not a lot of built examples of flat vaults remained. However, new ways of adapting stereotomy and flat vaults to the contemporary demands of the architectural design are being developed (Etlin et al., 2008). In recent years, this topic has become more interesting and researchers in the field of construction history have analysed the mechanical behaviour of flat vaults (Brocato et al., 2011; Fleury, 2009; Sakarovitch, 2006; Uva, 2003), as well as the new ways of their construction and development (Brocato et al., 2014; Piekarski, 2018; Estrin et al., 2011). Thus, using parametric design, adaptable models can be developed, novel disposition of elements can be enabled and the design can be accelerated, while providing the necessary models and drawings for the fabrication phase. Consequently, the adaptability to different spaces can be increased. For example, in the monastery shop, within the St Mary of the Resurrection Abbey in Jerusalem (The flat vault - AAU ANASTAS, 2018), the ability of a flat vault with reinforcement to span the area of even 50 m^2 is demonstrated (Fig. 2b).

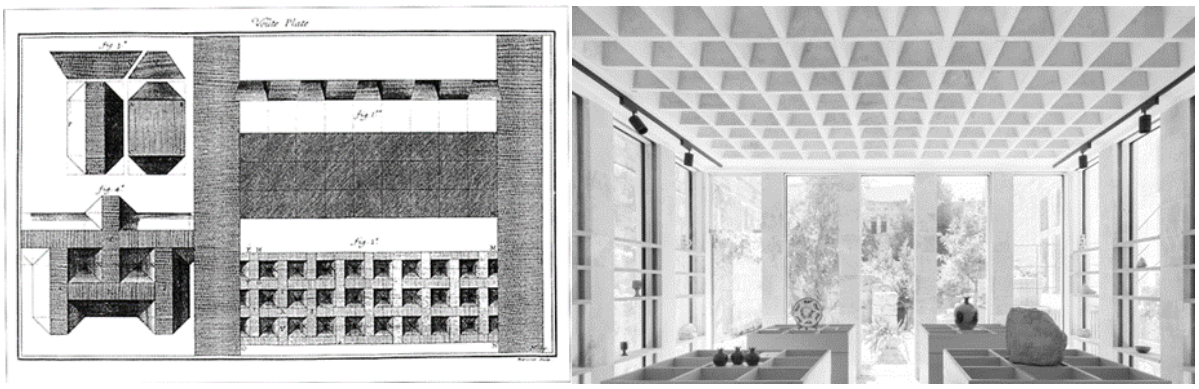

(a) (b)

Figure. 2: (a) Drawing of Abeille vault (source: Gallon, 1735); (b) flat vault in the monastery shop, Israel (source: AAU ANASTAS, 2019)

In accordance with the abovementioned principles and the architectural design progress, the aim of this research is creating a model of a ceiling made of both uniformly and non-uniformly shaped voussoirs above strictly rectangular floor plan. Additionally, due to the advantages of parametric design, an algorithm for the model is developed.

2. METHODS

In order to achieve appropriate parameterization of the flat vault, the design process is divided into several phases which can be separately analysed:

- parameterization of a rectangular floor plan by defining it as a uniform rectangular grid,
- parameterization of two fundamental elements (voussoirs), i.e. determination of dimensions of their longitudinal and transverse section through different parameters,
- defining the reciprocal arrangement of elements and embedding elements into an enclosing frame by trimming elements extending over the floor plan.

Accordingly, the algorithm was developed in visual programming language and environment Grasshopper connected to 3D modelling software Rhinoceros. As a result of using the abovementioned parameters, modification of the initially set conditions during the design process was enabled.

2.1. Rectangular Floor Plan Parameterization

The starting point of this research was defining the space in a geometric sense. Thus, exclusively, floor plans of rectangular shape are considered. Namely, the parameterization of a rectangular plan is conducted in order to ensure the adaptability of flat vaults to rooms of different dimensions. In accordance with Fig. 3, the floor plan is represented by a rectangular grid, for which the following geometric parameters are needed: (i) the length of a plan's side in the direction of the *x*-axis and *y*-axis (*a* and *b*, respectively), and (ii) the number of cells in the direction of the *x*-axis and *y*-axis (N_a and N_b, respectively). Combining these four starting parameters, an infinite number of possible rectangular floor plans can be obtained, where the dimensions of the cells constituting the grid are determined by l_x and l_y.

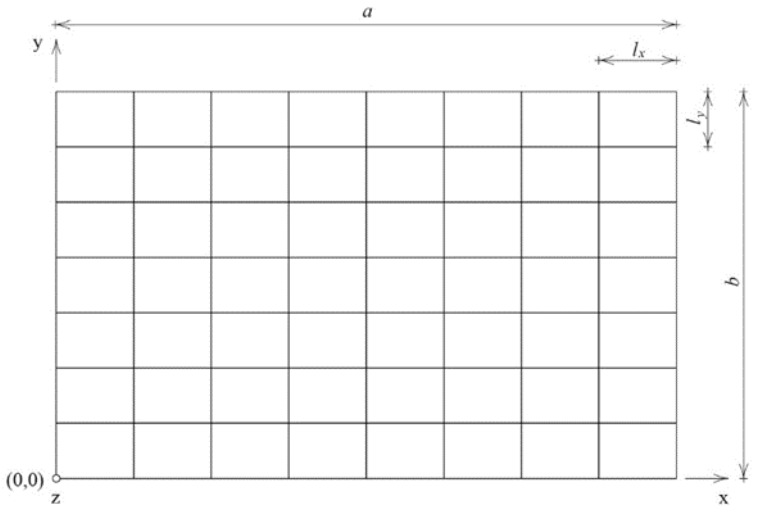

Figure. 3: Rectangular grid where $N_a = 8$ and $N_b = 7$

Throughout the parameterization, a certain number of limitations, regarding the number of cells in both directions and their size, could be set in order to ensure the stability of the flat vault. Namely, the they should be determined by conducting structural analyses, albeit only geometrical analysis was considered in this research. Once the grid has been defined through adequate parameters, it is possible to address the generation of the fundamental elements.

2.2. Shaping of Two Fundamental Elements

The parameterization of a floor plan produces in general a rectangular grid. The centre of each rectangular cell in the grid is used for determining the size and shape of the fundamental elements in their respective direction, i.e. the *x* and *y* direction. This is achieved by aligning the centre of the fundamental element's bottom side to the centre of the cell. Since the grid is comprised of rectangular cells, two fundamental elements are needed – one forming the system of elements in the direction of the *x*-axis and the other in the direction of the *y*-axis. Due to

the nature of the present design, several variations of these two fundamental elements will be needed when positioning them near the brim of the grid which will be addressed in section 2.3. Aforementioned rules of stereotomy demand a specific shape of the elements in order to ensure their reciprocal stability. Hence, in accordance with Fig. 4, the shape of the element's longitudinal and transversal section is a trapezium determined by combining several parameters – ones taken over from the parameterization of a floor plan (l_x and l_y), together with three new parameters: (i) trapezium height, h, (ii) trapezium's shorter base length, b_1, and (iii) trapezium's legs tilt, φ.

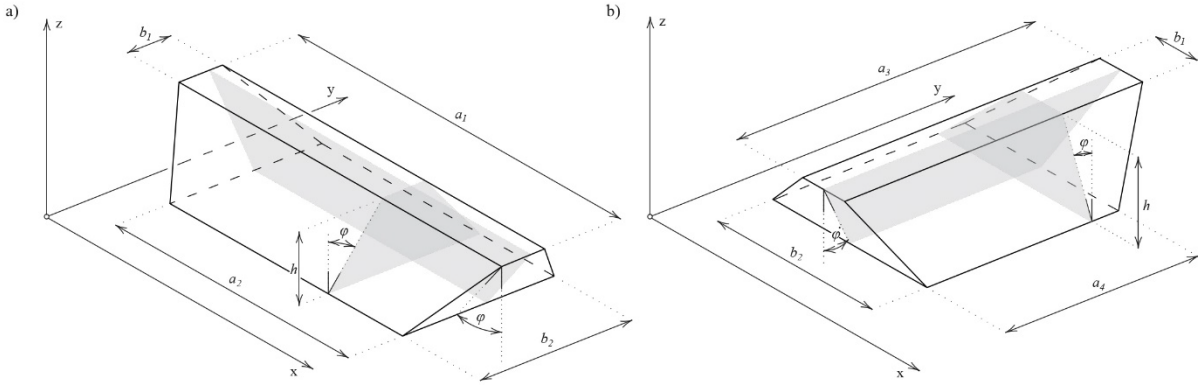

Figure. 4: (a) The fundamental element in the *x* direction; (b) the fundamental element in the *y* direction

Element's upper zone is defined by the length of the shorter base in transversal section, b_1, and the longer base in longitudinal section, a_1 (Fig. 5a), which represent the width and the length of the fundamental element in its upper zone, respectively, where the longer base is defined by the following expression:

$$a_1 = 2l_x - b_1. \quad \text{(Eq. 1)}$$

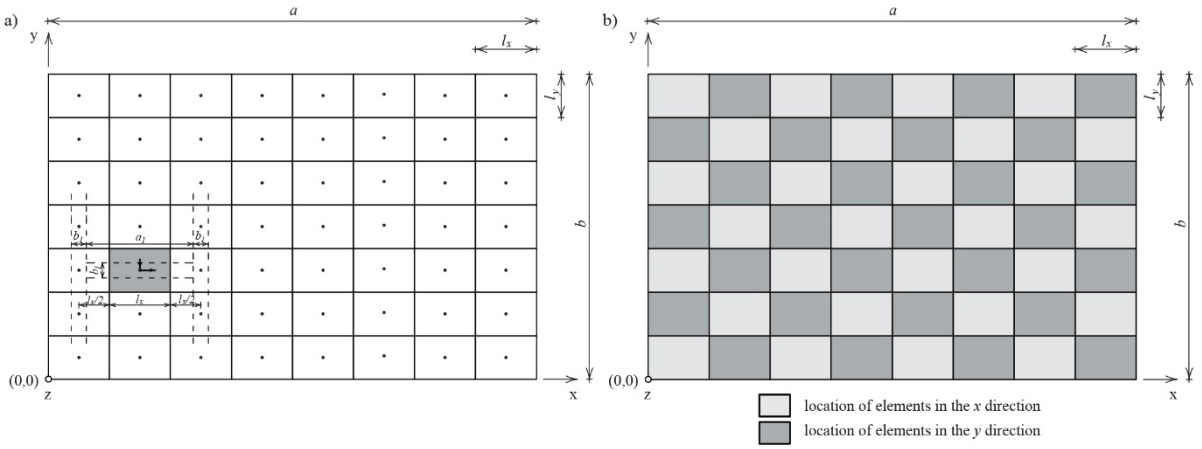

Figure. 5: (a) Construction of the longer base in longitudinal section, a_1; (b) element placement locations in the direction of two main axes

Similarly, the lower zone of the element is defined by the length of the longer base in transversal section, b_2, and the shorter base in longitudinal section, a_2, which represent the width and height of the element in the lower zone, respectively (Fig. 4a). The length of the lower (longer) base of the transversal section, b_2, is determined by the geometry of the trapezoidal transversal section; more precisely it is obtained from the following expression:

$$b_2 = b_1 + 2h\cot\varphi. \quad \text{(Eq. 2)}$$

Indirectly, the length of the fundamental element (the length of the longitudinal section's base) is affected by the abovementioned parameters. This way, the length of the element in the lower zone, a_2, is defined by:

$$a_2 = 2l_x - b_2, \quad \text{(Eq. 3)}$$

where the value b_2 is defined by Eq. 2 (Fig. 4a).

Shaping of the element oriented in the *x* direction is described in the abovementioned process. Likewise, the shaping of the element in the *y* direction (Fig. 4b) relies on initial parameters – ones taken from the rectangular grid and three new parameters. Also, the length of the lower (longer) base of the transversal section, b_2, is the

same in both types of elements. In accordance with the stated procedure, only the longitudinal section of the element in the z direction needs to be defined as follows:

$$a_3 = 2l_y - b_1 \quad \text{(Eq. 4)}$$

$$a_4 = 2l_y - b_2, \quad \text{(Eq. 5)}$$

where the value a_3 is the longer base in longitudinal section of the element oriented in the direction of the y-axis, and the value a_4 is the shorter base in longitudinal section of the same element. After the two fundamental elements are defined, positioning of elements, i.e. forming of the flat vault is enabled.

2.3. Flat Vault Shaping

The initial step for shaping the entire vault is defining the disposition of two systems of elements which follow a checkerboard pattern over the floor plan (Fig. 5b). The number of elements per row in the direction of the x-axis and the y-axis, is defined by the value N_x and N_y, respectively. Afterwards, the fundamental elements in x and y direction are placed in every other cell of the grid according to the checkerboard disposition as shown in Fig. 6a.

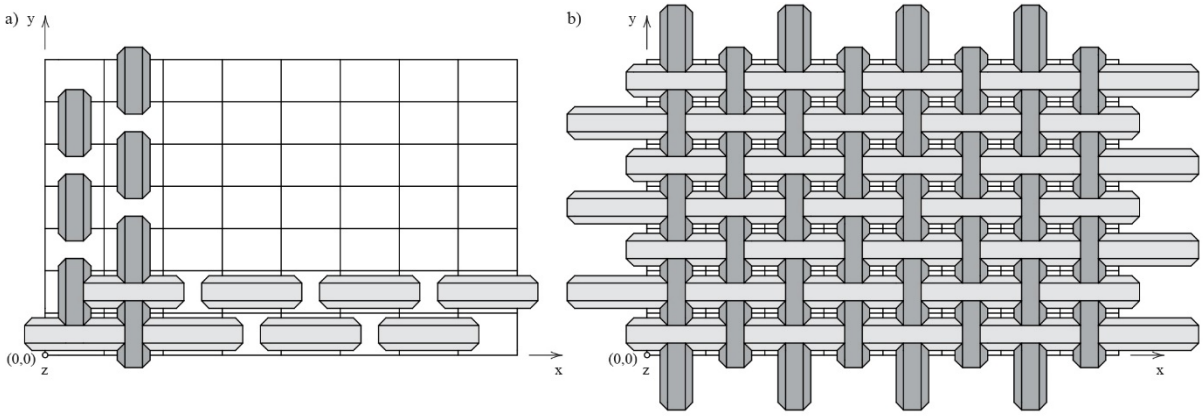

Figure. 6: (a) Positioning of elements in two directions; (b) shaped vault

Since this type of disposition would leave gaps in the arrangement of the fundamental elements, the same elements are added spanning over the grid border (Fig. 6b). Namely, if the number of cells per row is an even number, then one additional element will be needed at the end of every row. However, if the number is odd, two additional elements will be placed in every other row, alternately, to fully infill the vault.

In order to place the vault exactly over the desired floor plan, trimming the elements extending over the border is needed. Trimming is carried out with the planes located along the brim of the vault, inclined at an angle equal to the tilt of trapezium's legs, φ (Fig. 7a).

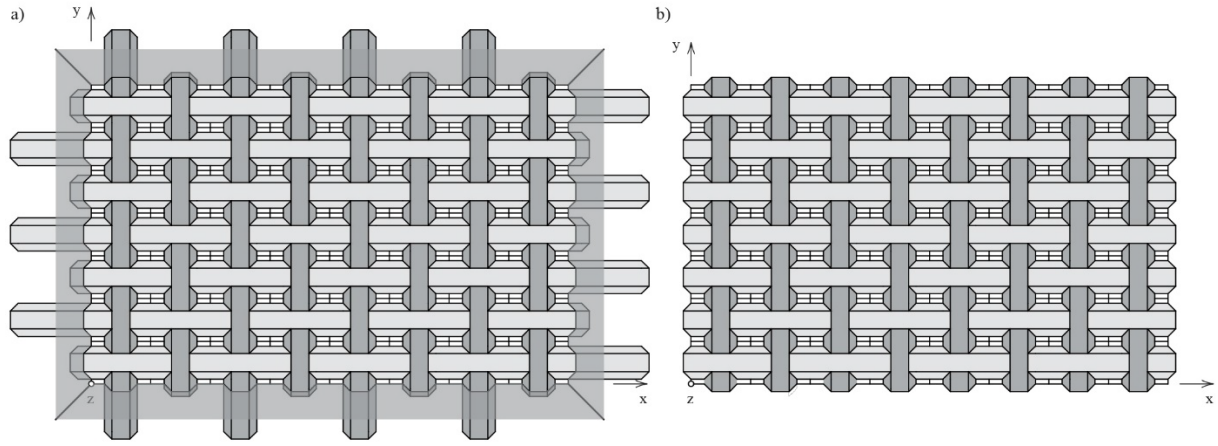

Figure. 7: (a) The vault with the trimming planes; (b) final shape of trimmed vault

After the trimming process, besides two fundamental elements, there are four new types of elements, i.e. a pair of new elements in the *x* direction, and a pair of new elements in the *y* direction (Fig. 7b). These elements are located around the perimeter of the vault and are resting on the supports. Hereby, the trimmed flat vault has covered the desired floor plan and the design is finished. Lastly, as a remaining part of the whole process is the fabrication phase which is made efficient by developing the parametric model of the flat vault.

3. RESULTS

According to the aforementioned principles, the parametric model for the rectangular flat vault is developed, enabling numerous adjustments of the vault by changing the cell shape (from square – Abeille vault, to rectangle), i.e. the ratio of the length and the width of the used voussoir. Thus, a novel type of flat vault based on two similar fundamental elements is produced (evoking the flat vault in Lugo Cathedral). Varying input parameters regarding the rectangular cell, two different kinds of the flat vault are generated – one with closed cells (the whole cell area is occupied, i.e. the ceiling is flat) and the other with open cells (the whole cell area is not occupied, i.e. the ceiling is partially filled, with voids). The first kind corresponds to the usual one, covering the entire ceiling over the desired floor plan without any cavities at the intrados. A few possible examples are obtained by modifying the cells' number, size, shape, defined by voussoirs' width, b_1, height, h and the tilt, φ, respectively (Fig. 8).

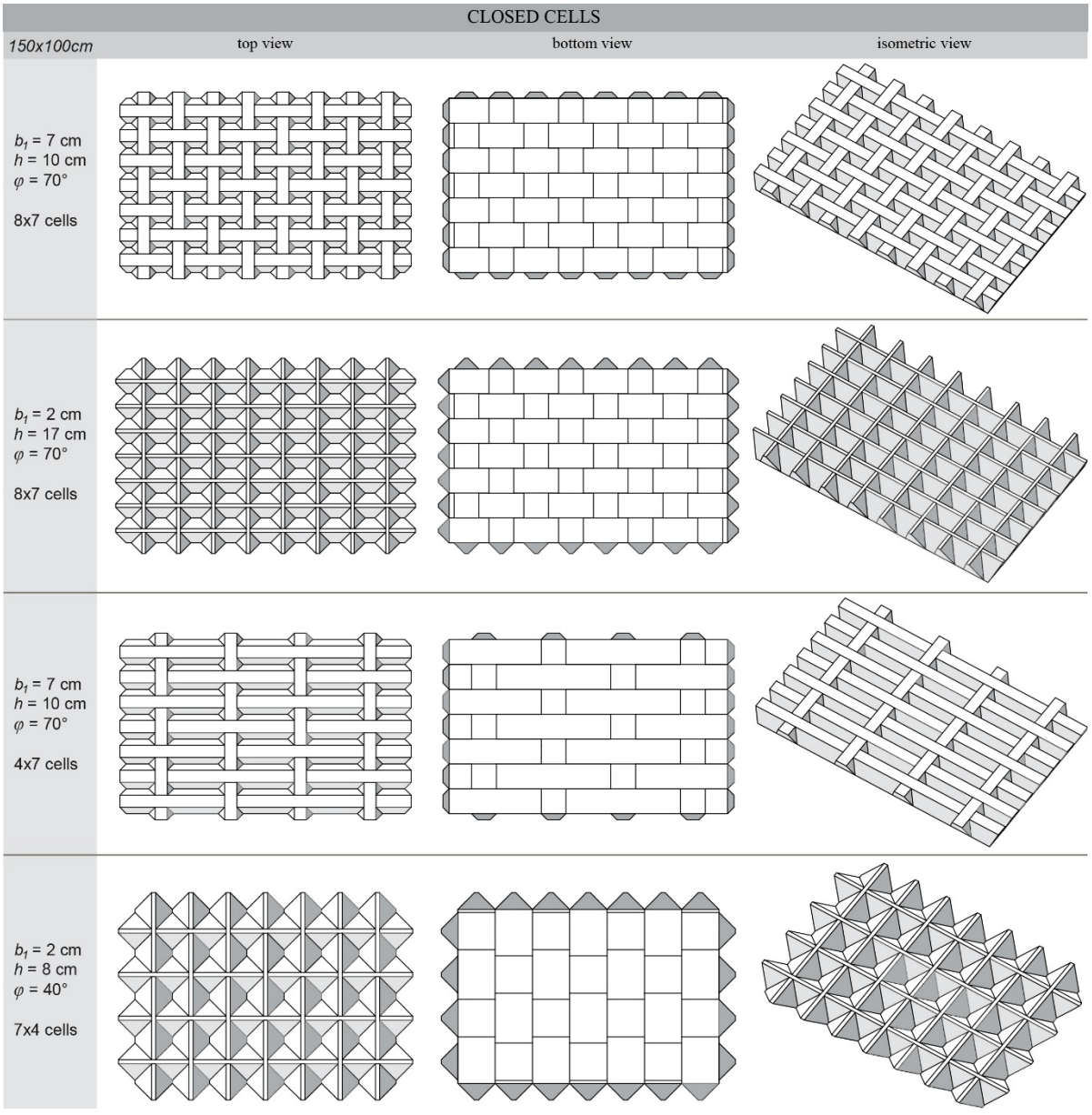

Figure. 8: Flat vault with closed cells

The ceiling of the second type is not covered to the full extent; the voids differing in size and shape depend on the values of input parameters, as shown in Fig. 9. The flat vault developed in this manner could be adaptable to covering various architectural spaces.

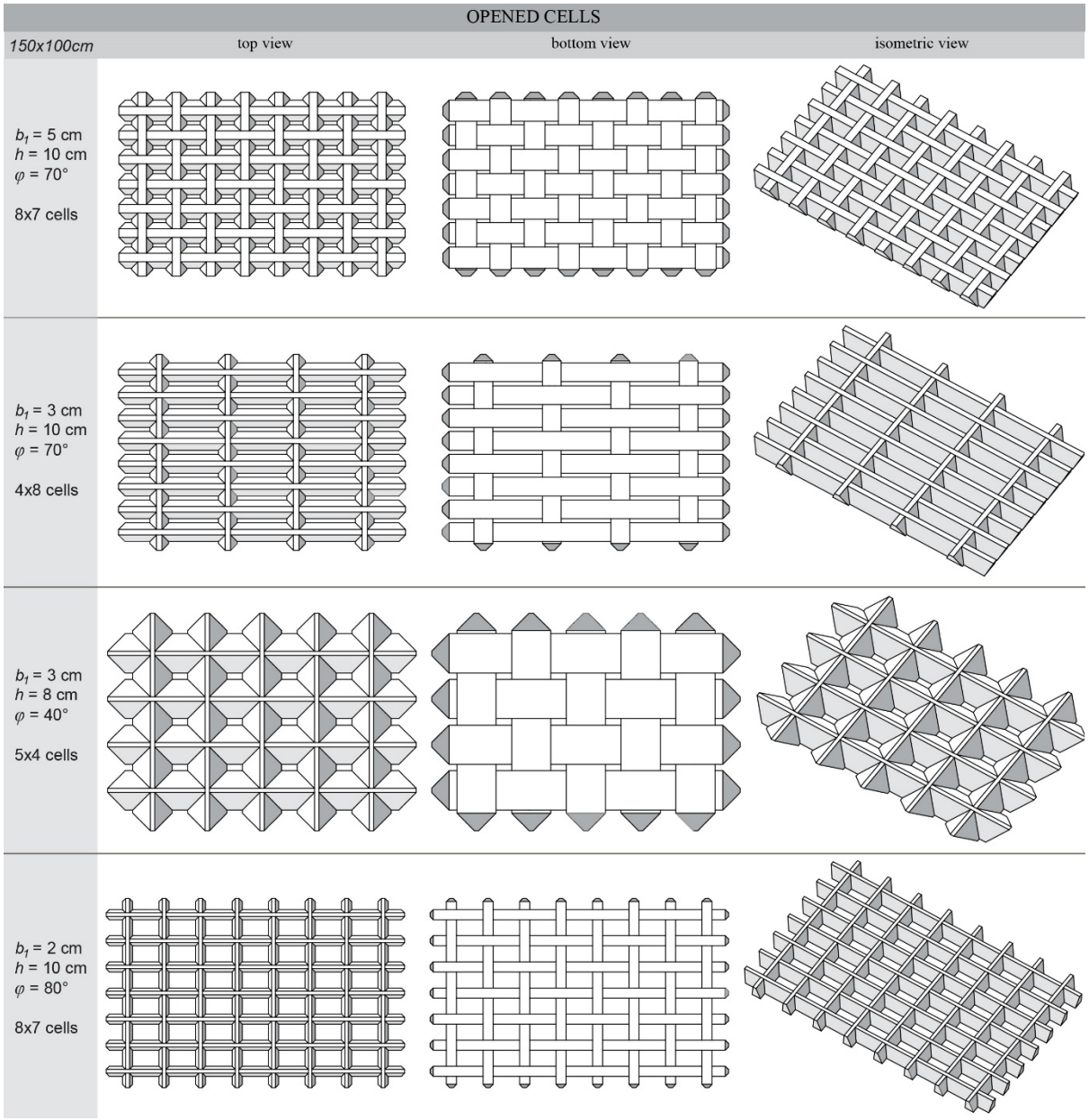

Figure. 9: Flat vault with open cells

Special case of flat vault, being a variation which can be generated with the developed algorithm, is, unlike aforementioned types, made of uniform voussoirs (Fig. 10). Namely, dividing a floor plan into a square grid enables the production of uniform elements in the direction of both main axes. In addition, a scale model of such vault has been fabricated as shown in Fig. 11.

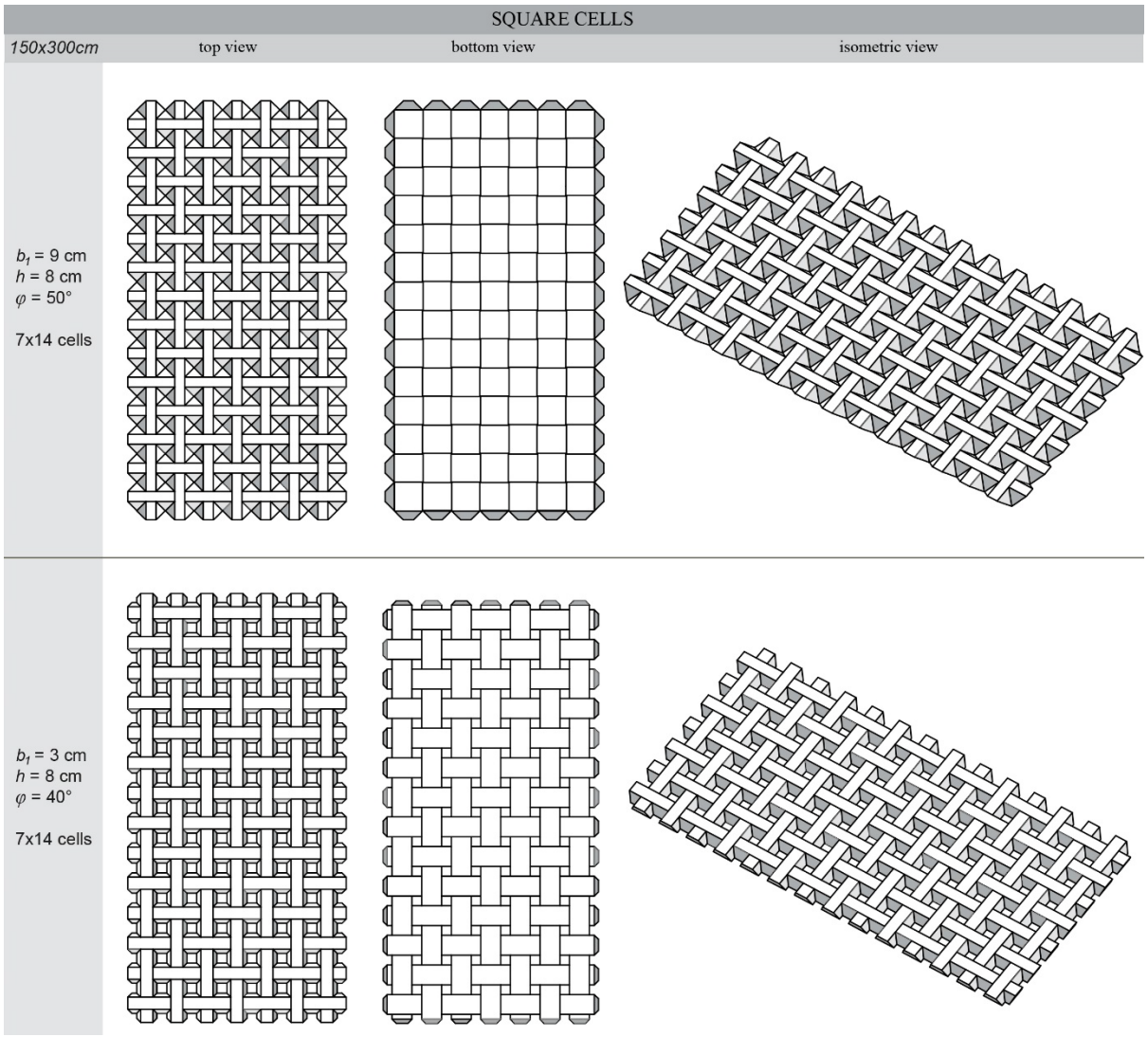

Figure. 10: Flat vault with square cells

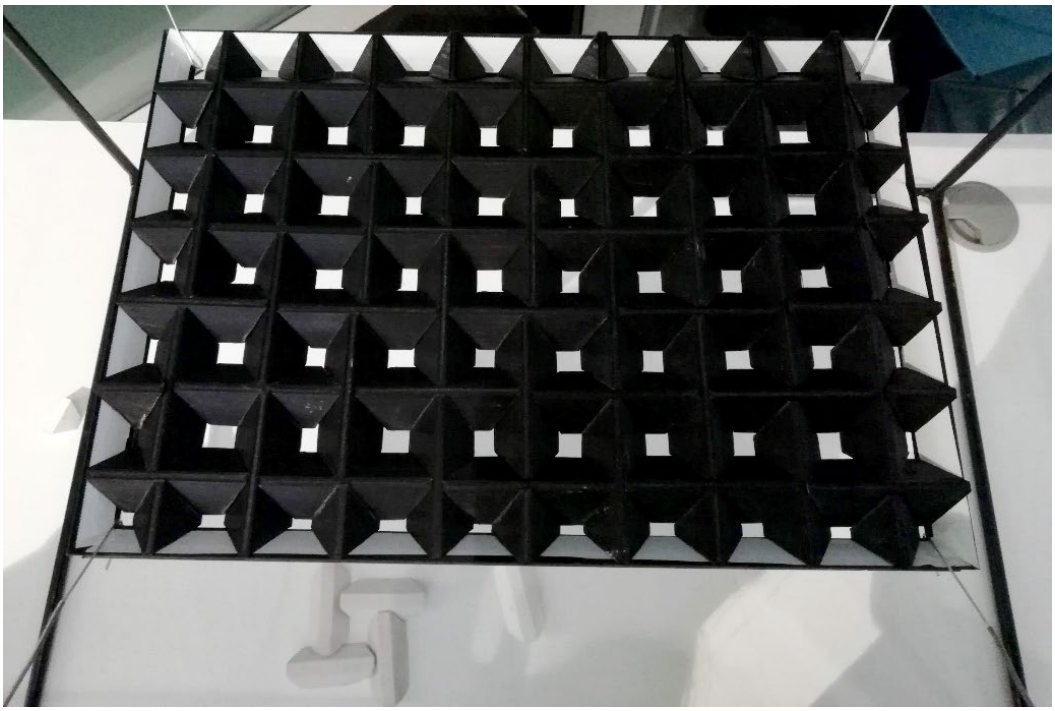

Figure. 11: Scale model of the flat vault

4. CONCLUSION

In this paper, flat vaults with voussoirs of uniform cross-section were considered. The formerly known uniformly shaped flat vaults were enhanced by envisioning a floor plan not as a square grid but as a rectangular one, in order to enable adaptability of the said structure. The parametric model of a rectangular flat vault, with two systems of elements positioned in two perpendicular directions, was created. Using the developed algorithm, more diversity in the appearance, i.e. the solutions for the construction of stone ceilings of the flat vault and its voussoirs was achieved. Thus, the design process is significantly made easier and quicker compared to the past building experience. Consequently, a lot more attention can be paid to the fabrication itself.

Further extension of the developed parametric model will address the adaptation of flat vaults to the demands of contemporary architecture, by making every voussoir unique in its size, as a consequence of the distance between the voussoir and an introduced attractor. Bearing in mind the advances in the fabrication techniques, non-uniformity of voussoirs would not represent a flaw to the popularization of this structure. Additionally, an upgraded model should enable the inverted position of the vault in order to obtain flat extrados and coffered intrados.

REFERENCES

1. Alkhataeb, E., Wendland, D., 2006. A Flat Vault in the Crac des Chevaliers and Some Considerations on the Development of Vault Geometry and Stereotomy in Mediaeval Masonry Structures in Syria. Second International Congress on Construction History, Cambridge. pp 3279–3296.
2. Brocato, M., Mondardini, L., 2011. A new type of stone dome based on Abeille's bond. *International Journal of Solids and Structures*, 49. pp 1786–1801.
3. Brocato, M., Mondardini, L., 2014. Parametric analysis of structures from flat vaults to reciprocal grids. *International Journal of Solids and Structures*, 54. pp 50–65.
4. Estrin, Y., Dyskin, A. V., Pasternak, E., 2011. Topological interlocking as a material design concept. *Materials Science and Engineering: C*, 31. pp 1189–1194.
5. Etlin, R., Fallacara, G., Tamborero, L., 2008. Plaited stereotomy, Stone Vaults for the Modern World, Aracne editrice S.r.l., Rome
6. Fleury, F., 2009. Evaluation of the perpendicular flat vault inventor's intuitions through large scale instrumented testing. Proceedings of Third International Congress on Construction History, BTU Cottbus, Cottbus, Germany. pp 611–618.
7. Gallon, J., 1735. Machines et inventions approuvées par l'Academie Royale des Sciences depuis son établissement jusqu'à présent. Académie des Sciences, Paris
8. Gojković, M., 1976. Kamene konstrukcije. Izdavačko-informativni centar studenata (ICS), Beograd
9. Piekarski, M., 2018. New Concepts for Application of Topological Interlocking in Architecture, 36th eCAADe Conference, Łódź, Poland
10. Sakarovitch, J., 2006. Construction history and experimentation. Proceedings of Second International Congress on Construction History, Queen's College Cambridge, Cambridge. pp 2777–2791.
11. Uva, G. R., 2003. Learning from traditional vaulted systems for the contemporary design. An updated reuse of flat vaults: Analysis of structural performance and recent safety requirements. Proceeding of First International Congress on Construction History, Instituto Juan de Herrera, Madrid. pp 2015-2021.
12. AAU ANASTAS, 2018. http://aauanastas.com/project/the-flat-vault/ [Accessed: 20. 11. 2019]

APPLICATION OF GEOMETRIC SURFACES IN THE MUSEUM BUILDINGS OF DANIEL LIBESKIND

Jovana Stanković
Faculty of Civil Engineering and Architecture, University of Niš, Niš, Republic of Serbia
PhD Candidate, jovana__stankovic@hotmail.com

Sonja Krasić
Faculty of Civil Engineering and Architecture, University of Niš, Niš, Republic of Serbia
PhD., Associate Professor, krasic.sonja@gmail.com

Marko Nikolić
Faculty of Civil Engineering and Architecture, University of Niš, Niš, Republic of Serbia
PhD., Assistant Professor, marko.nk@hotmail.com

Zlata Tošić
Faculty of Civil Engineering and Architecture , University of Niš, Niš, Republic of Serbia
PhD Candidate, zlata10@live.com

Nastasija Kocić
Faculty of Civil Engineering and Architecture, University of Niš, Niš, Republic of Serbia
PhD Candidate, nadja93.al@hotmail.com

ABSTRACT

The form of contemporary architecture structures has changed over time, from simple to complex shapes that were used in the design. It is noted in the works of numerous world architects that the form of structures does not have to strictly follow the function, but can be considered at the same time. When designing, it is started with a volume that can be of regular or irregular geometry. Complex geometric shapes and deviation from the conventional way of thinking about the facade of a structure are the basic features of deconstructivism. One of the most famous deconstructivists of today is Daniel Libeskind, who designed a large number of museum buildings of attractive design. He applies simple geometric surfaces, their basic shapes and parts, obtained by intersections or breakthroughs with other surfaces.

Museums are the topic of research in this paper, where the analysis of the form and geometry of completed structures will find concrete types of geometric surfaces and the methods of their merging, cutting and combining applied by Daniel Libeskind in his work. Therefore, this will point out his methodology for designing these types of structures. His museum buildings can serve as inspiration for future architecture engineers to design numerous types of public buildings.

Keywords: form in architecture; geometric surfaces; Daniel Libeskind; museums;

1. INTRODUCTION

Function, construction and form are the key aspects of architecture. At the beginning of the twentieth century, as a result of social, technical and technological changes, a modernism movement arose. This movement in architecture is characterized by a functional organization of space, the simple form of structures of regular geometry and linear elements, as well as the use of new materials such as reinforced concrete, steel and glass, which enabled a new construction of structures. Therefore, the principle of modern architecture is that form follows function, because it is considered that the shape and volume of a structure are conditioned by the basic purpose of the space that is being designed. '***It is the pervading law of all things organic and inorganic, of all things physical and metaphysical, of all things human and things superhuman… that form ever follows function, This is the law …***' (Sullivan, 1896).

At the end of the twentieth century, postmodernism emerged, which contained multiple movements, Hi-tech, deconstructivism, critical regionalism, and neo-modernism. What is common for all these movements is the rapid development of technology that enables the construction of intelligent buildings in which structures and installations are an integral part, and the use of new materials, such as steel sheets, prestressed concrete, laminated wood, plastics, special tarpaulin, etc. All this influenced the architects to pay more attention to the shape of the structures when designing, due to the fact that much more complex geometric surfaces could be used with the new materials and construction systems (Krasić, 2012).

Another feature of the postmodern era in architecture is that the architect expresses his thoughts, ideas and feelings with his architectural work, and interprets them with the observers of the relation of function, i.e. the way space is organized, and the form of the structure, i.e. by shaping the facade. (Alfirević, 2012). In this creative design process, new concepts emerge, where the layout and relationship of some spatial units can be conditioned by form, or where they are considered at the same time, which in the end gives the best results (Trisno et al, 2019). Based on the above-mentioned concepts, the meaning is realized, i.e. the meaning of the designed architectural structure introduces a new key concept in understanding and perceiving architecture (Alihodžić et al, 2010). The function is somewhat eliminated, leaving space for understanding the form in its symbolism (Erzen, 2015).

The movement of releasing the infinite possibility of playing with the shapes, form and volume appeared after an exhibition on Deconstructive Architecture at the Museum of Modern Art in New York in 1988, which featured works of world-famous names, pioneers of this movement in architecture (Frank Gehry, Daniel Libeskind, Rem Koolhaas, Peter Eisenman, Zaha Hadid, Coop Himmelblau, and Bernard Tschumi). Therefore, the form plays a key role in the design process of the structure, so that the somewhat functional organization is overshadowed by the visual phenomenon, but by no means omitted. Architects choose complex geometric surfaces, which allow them abstract and attractive forms, thus visually communicating with the observers, conveying to them their ideas, concepts and meaning. Such experimentation with a design is inherent in the public buildings, i.e. museums, libraries, cultural centres, etc., which underwent an expansion during the deconstructionist period.

Of the public buildings, each of the pioneers of deconstructivism in architecture designed at least one museum building. They all use a specific design method to meet the new requirements of museum architecture and identify it with the aesthetics of the art, located inside the building, which is imposed as a principle of deconstructivism in the architecture of new museums. Therefore, deconstructivists design museums as spectacular, unrepeatable architectural forms, omitting a neutral container or multifunctional box (Milojković et al., 2012). In this way, architecture takes on the features of sculpture, structures become representatives of the city and the state in which they are located (Krasić, 2012).

The application of complex geometric surfaces results in unique architectural works of public buildings. However, the abstract form of numerous deconstructivist architectural works is based on the use of simple general geometric solids such as a prism, pyramid, and sphere, with their proportions and dimensions changing from their original basic shape (Hegzi et al, 2018; Ching, 2015). In such case, cutting, folding, breaking throw, merging, adding, wrapping and curving are some of the guiding principles of this movement in architecture (Tepavčević, 2010; İnceköse, 2007). Consequently, the model of a public building is started from a simple form and, with the appropriate transformations, acquires a finite complex shape.

Taking into account a large number of museum buildings and authentic expression in architecture, the subject of this paper will be the built museums of Daniel Libeskind in order to find out what geometric surfaces he uses in his work and what design principles he uses to get a distinct form, that can serve as an inspiration to other architecture engineers.

2. MUSEUM BUILDINGS OF DANIEL LIBESKIND

Daniel Libeskind is one of the most famous deconstructivists of today. Unlike many world architects, who began their careers by designing residential buildings, Daniel began with public buildings at the 1988 World Design Contest for the Jewish Museum in Berlin, which he won. The project of this museum has made him one of the greats of world architecture. Also, it represents the basis for future projects and the remarkable affirmation of Daniel Libeskind in the field of designing this type of buildings.

The reason for his many successes in this field is the methodology he applies in his many years of work and his unique approach to problem-solving. The innovation of his design is reflected in the fusion of the history and tradition of the place in which he designs, with the art exhibited in the structure in question, into his architectural work and the way he wants to awaken emotions in the user i.e. the desire to feel that space. Applying 95% of the old and 5% of the new architecture, Daniel emphasizes that his ideas are always new in their context, but also that they are always connected to the past, i.e. traces in history (Qabanis et al).

As an architect of deconstructivism, he applies the concept that the form of a structure must follow the idea. He uses distinct forms, which are not a goal by themselves, but a product of reflecting on the content displayed in that structure and context (Gössel et al, 2001). For Libeskind, all the components within his work have meaning in another sense as well. The position of the components within the plan of the ground floor and the other floors, as the layout and relationship of the functional units, indicates these meanings, but also the volume and geometry of the structure.

When it comes to the form of a structure as a physical phenomenon, Daniel Libeskind's museums are authentic because of the permeation of acute and curved architectural forms (Alfirević, 2012). The complexity of this architectural form encourages the user to remember such structures and to wonder which meaning they convey through their appearance. However, understanding this architecture is only possible through logical thinking and the conscious intention of the visitor. Logical thinking dictates that complex forms are perceived better when visually separated into simpler parts (Hegzi et al, 2018). In the case of Daniel Libeskind's museums, complex forms can be separated from each other by mass ratio, i.e. volume, and then researched individually to find out about their geometric characteristics, applied shaping processes, and how to merge simple parts into complex shapes. Masses and volumes are characteristics of a 3D model of a structure, the creation of which is an initial step in the design process and the way in which the architects of the Libeskind studio present their ideas and communicate with each other (Swickerath, 2017).

Of the many built museum buildings, the subject of geometry analysis in this paper is the Royal Ontario Museum, Extension to the Denver Art Museum, and the Contemporary Jewish Museum.

2.1. The Royal Ontario Museum, Toronto, 2007

The extension to the Royal Ontario Museum (ROM), now named the Michael Lee-Chin Crystal, is the largest Museum in Canada. It is situated at one of the most prominent intersections in downtown Toronto. The extension provides 9300 square meters of new exhibition space, a new entrance and lobby, a street-level retail shop and three new restaurants. Its new name is derived from the building's five intersecting metal volumes, which are reminiscent of crystals—inspired by the crystalline forms in the ROM's mineralogy galleries (Studio Libeskind, 2020). In this way, Daniel Libeskind merges art that is exhibited within the museum with the context in which the structure is built, and with its form differentiates the old from the new architecture. The Crystal presented a unique challenge to build and was among the most complicated construction projects in North America. There are no right angles and only one vertical wall in the structure—the five crystals are designed as interlocking self-supported structures (Studio Libeskind, 2020).

2.1.1. Steps of the form- modelling process

Regardless of the purpose of the space, each building has general physical characteristics, such as the dimensions of the building, proportions, number of storey, construction system, materials of which it was built, etc. The shape of the architectural building, the size, the layout of the masses, the geometry, the volume and the character of the architectural form are represented by a 3D model of the structure. The starting point in this process is to observe and perceive the 3D model of the building in order to decompose its complex form into simpler parts. In this way, the relation of individual masses is emphasized as a characteristic of the 3D model, which conditioned the procedure of analysis of this building and the division of volumes into Crystal 1, Crystal 2, Crystal 3, Crystal 4 and Crystal 5.

From the research materials, technical drawings of the site plan, ground floor, sections and facades are used (from the website https://arqa.com/english-es/architecture-es/the-royal-ontario-museum-in-toronto-canada.html). Of computer-aided design programs to test the form were used AutoCAD and Rhinoceros. The orthogonal projections of the museum building were made in AutoCAD, while the 3D model was developed in Rhinoceros. Initially, each of the crystals is marked with a special colour on the site plan of the museum building (Figure 1a). With the help of orthogonal projections of the site plan, i.e. x and y-coordinates, the characteristic points of each crystal on its roof planes are determined. From all these points, vertical lines were drawn. The ground floor plan is used in the same way as the site plan, where it is necessary to identify the first trace intersection of each of individual crystals with a horizontal projection xy-plane and mark their characteristic points (Figure 1b). In this way, the points on the horizontal projection xy-plane are determined, from which the crystalline forms originate as well as the extreme points on the roof planes, where the crystalline forms end, in the horizontal xy-plane.

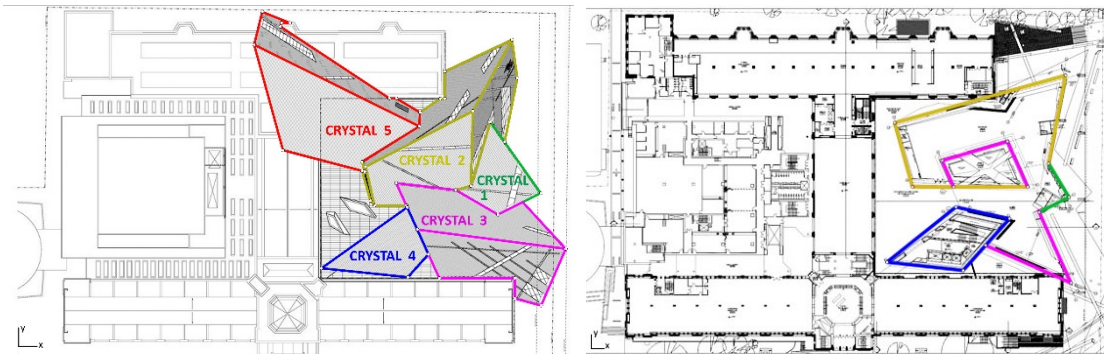

(a) (b)

Figure. 1: (a) Site plan of the model, the xy-plane, and (b) Ground floor plan of the model, the xy-plane

Each of these characteristic points should be moved by the corresponding distance defined by the z-coordinate. This coordinate is obtained by the technical drawings of cross-sections and longitudinal sections, representing the xz (Figure 2a) and the yz-planes (Figure 2b). These technical drawings redefine the characteristic points of these crystals on their respective planes. From these points, horizontal lines must be drawn.

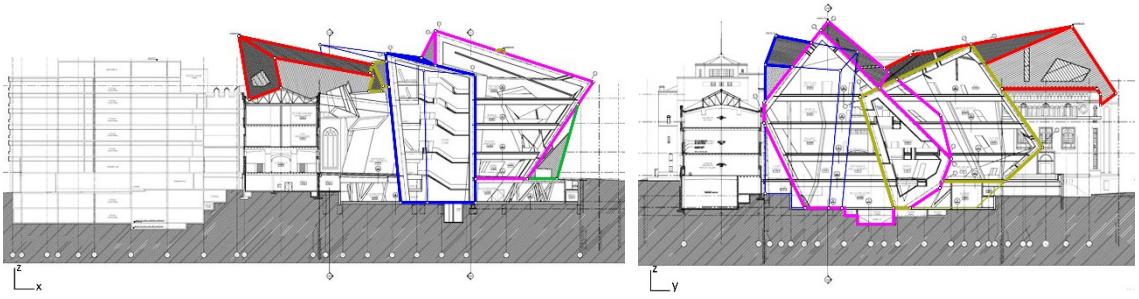

(a) (b)

Figure. 2: (a) Section 1-1, the xz-plane, and (b) Section 2-2, the yz-plane

The intersection of the horizontal and vertical lines, which were previously placed on the points of the site plan, ground floor plan, sections and facades, gives the exact position of all characteristic points in space. The next step is to connect characteristic points with polylines to get the polygons, which are faces of polyhedral surfaces (corresponding crystals). Finally, the surfaces (Figure 3) are obtained by the Planar Curves option, thus confirming that the points are taken as relevant lie in the same plane, i.e. they are coplanar. However, tracing over the technical drawings cannot give reliable results. It is sufficient that the position of one point is not well established and the plane will not be obtained with the Planar Curves option, which further implies that the points used are not coplanar. The surface may, in this case, be obtained by Surfaces option from 3 or 4 points (by merging 4 points), but it will not be the result of a regular geometry, which is a characteristic of this Daniel Libeskind museum building. So for each surface of the crystal three points were taken as relevant to obtain the right shape with the Planar Curves option, and then changed the position of the other points (Figure 3).

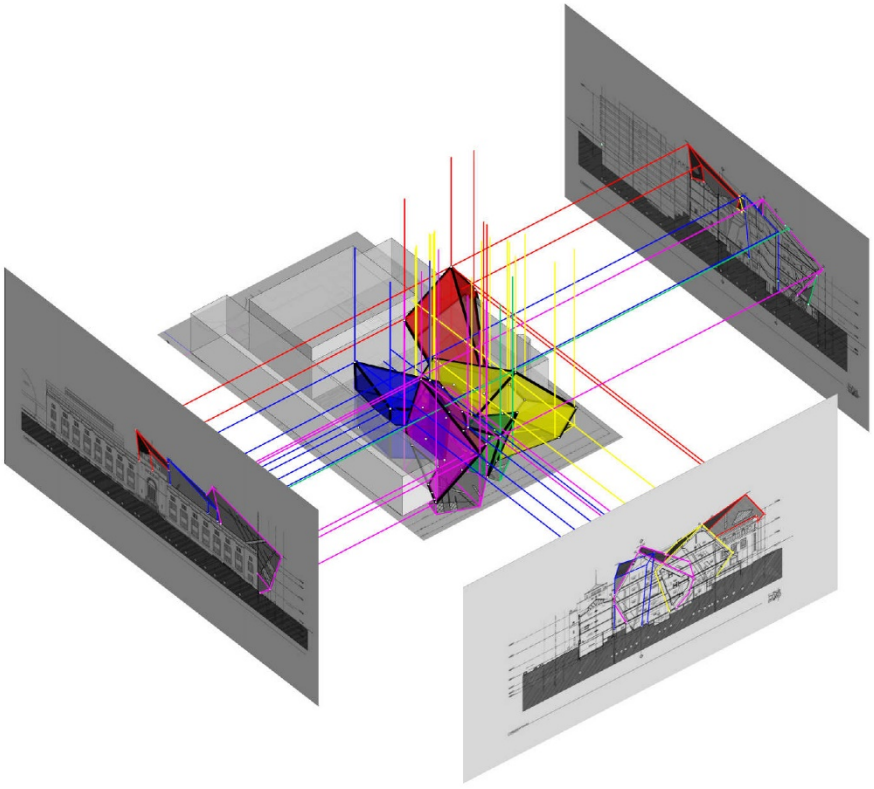

Figure. 3: 3D model of the museum building

Therefore, with the help of orthogonal projections, it was discovered which geometric surfaces these are, i.e. geometric analysis determined the shape of a crystal-like structure, which was served an architect as an inspiration for work. The hypothesis is that Daniel Libeskind used 5 prisms in the design. For this reason, we analyse the given surfaces, i.e. crystals, which we eventually obtained. The paper will show how each crystal was obtained individually, via a model in the Rhinoceros software. For easier following step-by-step of the modelling process, each crystal is labelled with a different colour and number.

2.1.1.1. Modelling of Crystal 1

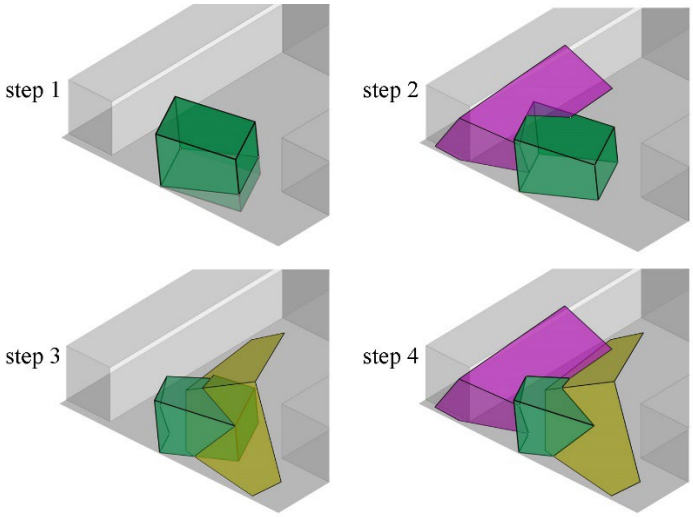

Figure. 4: Steps of the form-modelling process – Crystal 1

Based on the orthogonal projections (Figure 1, Figure 2), it was concluded that Crystal 1 is an oblique four-sided prism, with a regular basis in the vertical plane. It is cut with a horizontal projection plane per quadrilateral (step 1). It is then broken through Crystal 3 along the spatial polygon (step 2). On the other side, it is broken through Crystal 2 (step 3) along the spatial polygon. Figure 4 shows the final shape of Crystal 1 in the final form (step 4).

2.1.1.2. Modelling of Crystal 2

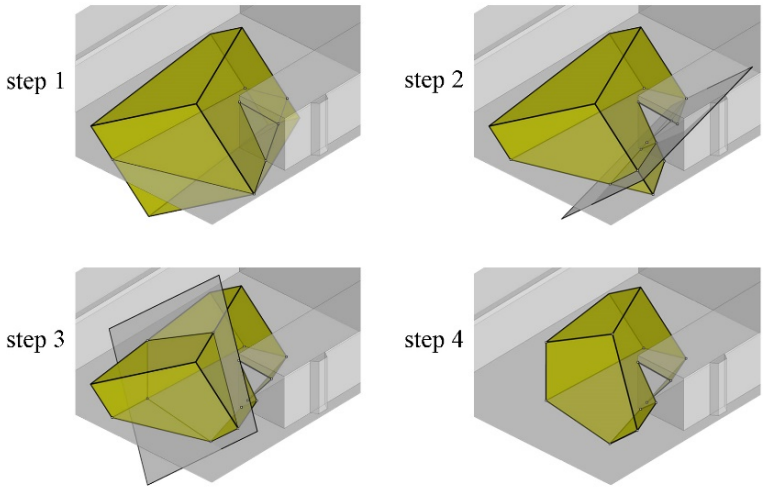

Figure. 5: Steps of the form-modelling process – Crystal 2

Based on the orthogonal projections (Figure 1, Figure 2), it is concluded that Crystal 2 is an oblique four-sided prism with an irregular base in an oblique plane, breaking through with the three-sided pyramid. The intersection with the basic horizontal projection plane is along an irregular quadrilateral (step 1). The intersection with the first oblique plane is along the two quadrilaterals (step 2). The intersection with the other oblique plane is along an irregular pentagon (step 3). Figure 5 shows the final shape of Crystal 2 in the final form (step 4).

2.1.1.3. Modelling of Crystal 3

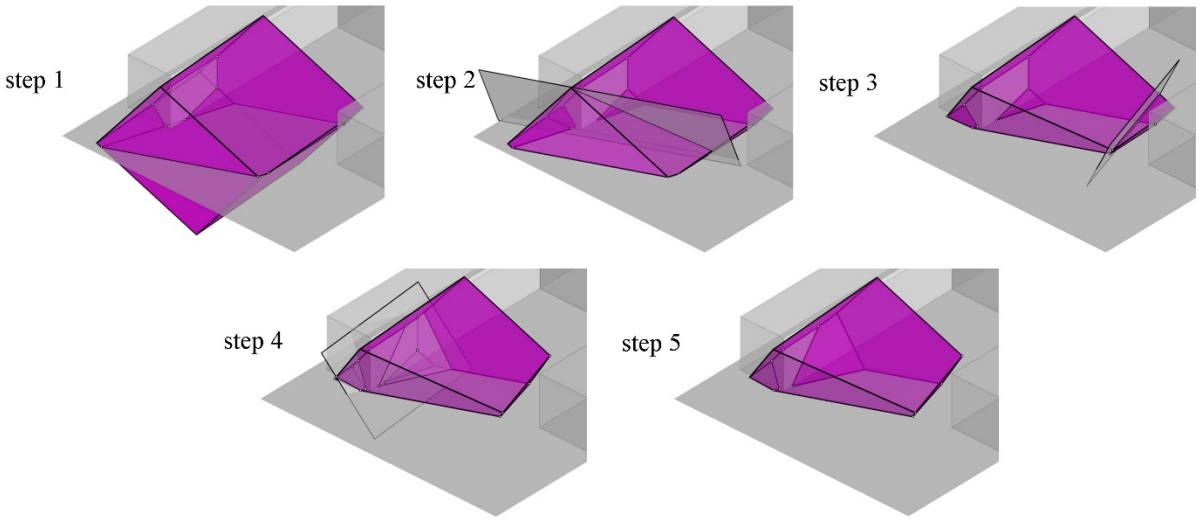

Figure. 6: Steps of the form-modelling process – Crystal 3

Based on the orthogonal projections (Figure 1, Figure 2), it was concluded that Crystal 3 is an oblique four-sided prism that breaks through a right four-sided prism of an existing structure along a spatial polygon, and with the basic horizontal projection plane intersected along an irregular quadrilateral (step 1). Afterwards, the first oblique plane is cut with an irregular quadrilateral which is extended to the space polygon (breakthrough with an existing prism – step 2). Steps 3 and 4 show the intersection with two more oblique planes along irregular quadrilaterals. Figure 6 shows the final shape of Crystal 3 in the final form, with all intersections and breakthroughs (step 5).

2.1.1.4. Modelling of Crystal 4

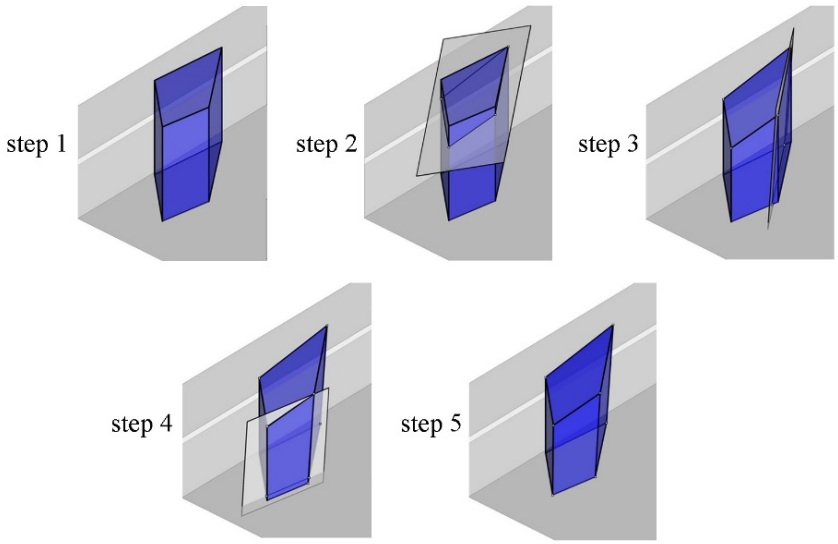

Figure. 7: Steps of the form-modelling process – Crystal 4

Based on the orthogonal projections (Figure 1, Figure 2), it was concluded that Crystal 4 is a regular four-sided prism with an irregular basis in the horizontal projection plane (step 1). Afterwards, it was cut with the first oblique plane along the irregular quadrilateral (step 2). Steps 3 and 4 show the intersections with two more oblique planes along the irregular quadrilaterals. Figure 7 shows the final shape of Crystal 3 in the final form, with all intersections (step 5).

2.1.1.5. Modelling of Crystal 5

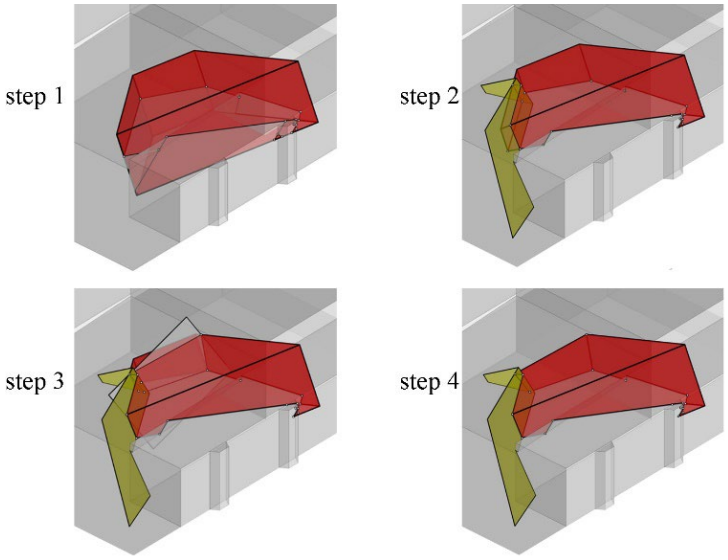

Figure. 8: Steps of the form-modelling process – Crystal 5

Based on the orthogonal projections (Figure 1, Figure 2), it was concluded that Crystal 5 is a right four-sided prism with an irregular basis that breaks through the right four-sided prism of an existing structure along a spatial polygon (step 1). It is then broken through Crystal 2 along the spatial polygon (step 2). In step 3 is shown an intersection with an oblique plane along the irregular quadrilateral. Figure 8 shows the final shape of Crystal 5 in the final form with the intersection and breakthroughs (step 4).

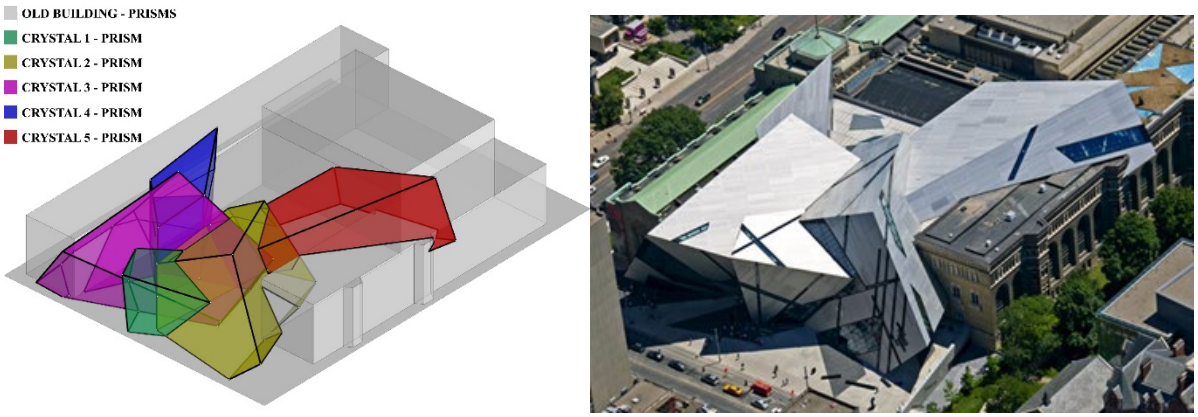

(a) (b)

Figure. 9: (a) 3D Model of the Royal Ontario Museum, and (b) the Royal Ontario Museum in the photo

Daniel Libeskind starts designing process with the prism as its basic shape and by its breakthroughs and intersections with the planes obtains the form (Figure 9) he wants, i.e. the form by which he conveys meaning. The conclusion is that each of the crystals was obtained by the transformation of a prism.

2.2. Extension to the Denver Art Museum, 2006

The extension to the Denver Art Museum is the Studio Libeskind's first building to reach completion in the USA. It is located in the Civic Center of Denver, Colorado. The peaks and valleys of the mountain range of the Rocky Mountains were an inspiration for a series of specific geometric volumes. As an extension of the institution's original building by Gio Ponti in 1971, it presents 13,500 square meters of new exhibition space, art studios, cafes, and gift shops. The Frederic C. Hamilton Building, as this extension of the Denver Art Museum is named, is clad in an innovative new surface with 9,000 titanium panels, which is the reason why the project was recognized by the American Institute of Architects as a successful Building Information Modelling project (Studio Libeskind, 2020).

2.2.1. Steps of the form-modelling process

The geometric analysis process begins by diving the volume into Mountain 1-9. Based on their orthogonal projections, it was concluded that in this project (Figure 10, 11), Daniel Libeskind used two right four-sided prisms with a regular basis in a horizontal projection plane (Mountain 8, Mountain 9), and seven oblique four-sided prisms with regular or irregular basis intersected by many oblique planes with each of the volumes breaking through each other along the spatial polygon.

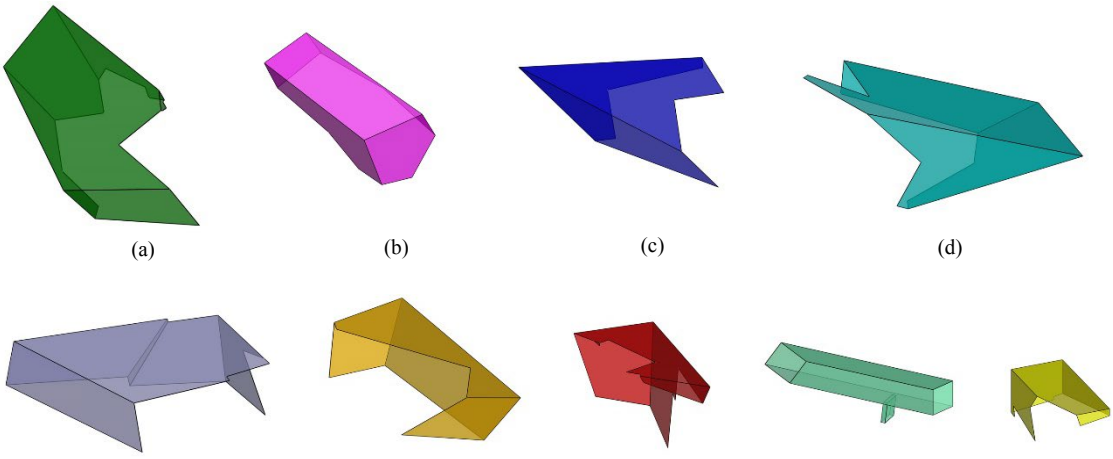

(a) (b) (c) (d)

(e) (f) (g) (h) (i)

Figure. 10: Steps of the form-modelling process: (a) Mountain 1, (b) Mountain 2, (c) Mountain 3, (d) Mountain 4, (e) Mountain 5, (f) Mountain 6, (g) Mountain 7, (h) Mountain 8, (i) Mountain 9

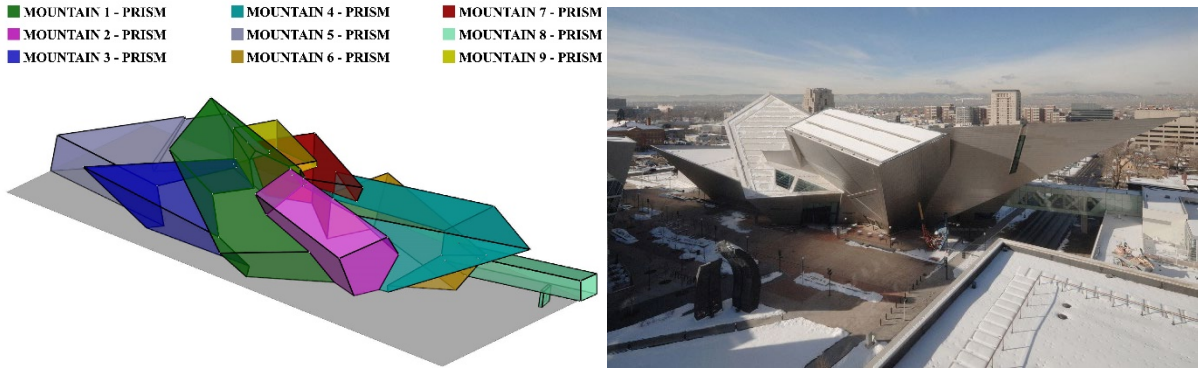

(a) (b)

Figure. 11: (a) 3D Model of Extension of the Denver Art Museum and (b) Extension of the Denver Art Museum Museum in the photo

2.3. The Contemporary Jewish Museum, San Francisco, 2008

Studio Libeskind designed this new museum as an addition to the historic red-brick power plants from the 19th century. The 8,800-square-meter building is situated in the heart of downtown San Francisco, California. The building design is based on the two Hebrew letters spelling "L'Chaim," which means "To Life", because Daniel wanted to merge art and history in one space. Following the Jewish tradition, the eighth letter of Hebrew alphabet 'chet' provides an overall continuity for the exhibition and educational spaces, and the tenth letter 'yud,' with its 36 windows, serves as event space, special exhibition and performance (Studio Libeskind, 2020). These forms are clad in luminous blue steel panels, finished in a unique cross-hatching surface that distinguishes from old building design. The steel panels change colour depending on the time of day, the weather, and the viewer's position.

2.3.1. Steps of the form-modelling process

The geometric analysis process begins by dividing the volume into Old building, Letter chet and Letter yud. Based on their orthogonal projections, it was concluded that in this project, Daniel Libeskind used two oblique four-sided prisms with a regular basis in oblique planes (Figure 12, 13), with each of them breaking through each other along the spatial polygon, as well as the Old building.

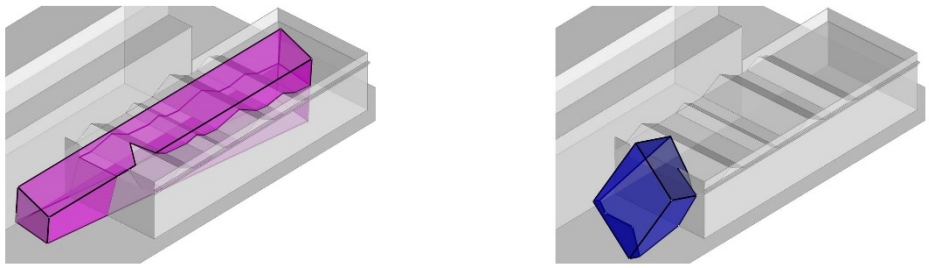

(a) (b)

Figure. 12: Steps of the form-modelling process: (a) Letter chet and (b) Letter yud

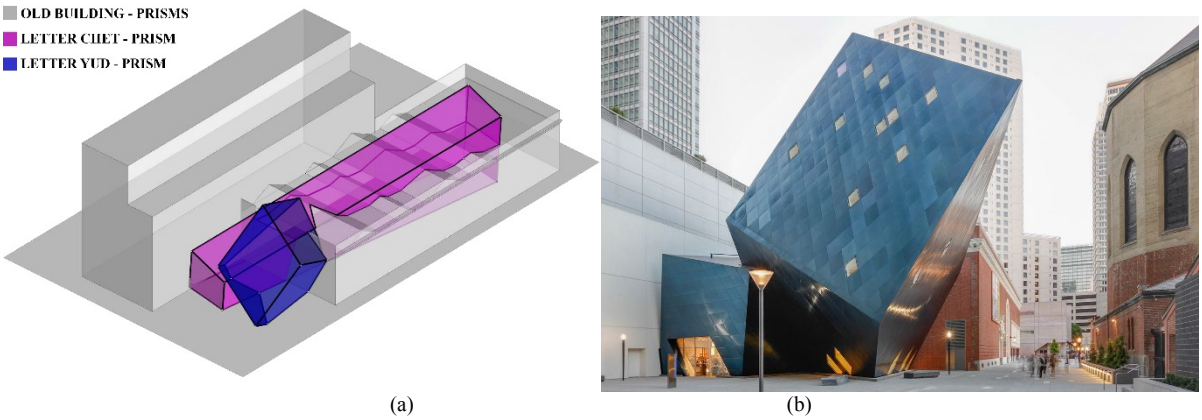

(a) (b)

Figure. 13: (a) 3D Model of the Contemporary Jewish Museum and (b) the Contemporary Jewish Museum in the photo

3. CONCLUSION

Daniel Libeskind is a renowned world architect. His architectural works have an authentic expression because he uses attractive architectural form and through them conveys his feelings, ideas, thoughts, and concepts. Museum buildings are special because he combines ideas with art that is exhibited inside a building with an architectural form into one unity and connects on them at the same time. His deconstructivist approach contributes to the architecture of new museums, which underwent expansion during this period. As the architectural form is accomplished by geometry, the analysis of his museum buildings leads to the conclusion that the complex geometric appearance seems to originate from simple geometric solids, which in his case is a prism. A different approach to intersecting a prism, as the simplest geometric solid, with other planes yields the final shape of the structure. The conclusion is that complex forms can be obtained by using simple forms. Symbolism is that the architectonic objects will be recognized as a representative of the country, i.e. the city in which it is located. Future architectural engineers who are engaging on the process of designing public buildings can use these examples to make complex structures using simple forms that would be worthy of attention.

4. REFERENCES

1. Alfirević, Đ., 2012. Ekspresionizam kao radikalna stvaralačka tendencija u arhitekturi. Arhitektura i urbanizam, 34, p.14-27.
2. Alihodžić, R. and Kurtović-Folić, N., 2010. Phenomenology of perception and memorizing contemporary architectural forms. Facta universitatis-series: Architecture and Civil Engineering, 8(4), pp.425-439.
3. Erzen, J. N., 2015. Form and meaning in architectural theory. Serbian Architectural Journal, 7(1), pp.75-84.
4. Gössel, P. and Leuthäuser, G., 2001. Architecture in the twentieth century (Vol. 1). Taschen.
5. Hegzi, Y.S. and Abdel-Fatah, N.A., 2018. Quantifying students' perception for deconstruction architecture. Ain Shams Engineering Journal, 9(4), pp.2745-2754.
6. İnceköse, Ü. and Campus, G., 2007. Geometrical Transformation: A Method for the Creation of Form in Contemporary Architecture. In Tenth Annual Bridges Conference, Bridges: Mathematical Connections in Art, Music, and Science.
7. Krasić, S., 2012. The geometrical surfaces in Architecture (Geometrijske površi u arhitekturi), Građevinsko-arhitektonski fakultet, Niš.
8. Milojković, A. and Nikolić, M., 2012. Rethinking museum architecture – Art museum at the beginning of the 21 century. International Conference on Architectural Research: (Re)writing History.
9. Studio Libeskind, 2020. https://libeskind.com/ [Accessed: 15th Januar 2020].
10. Sullivan, L., 1896. The tall office building artistically considered. Lippincott's Monthly Magazine. 339, 403-409. Philadelphia, J.B. Lippincott Co.
11. Swickerath, C., 2017. Reinventing design with Daniel Libeskind. https://youtu.be/TRsULc30Fbg [Accessed: 21st Februar 2020].
12. Trisno, R. and Lianto, F., 2019. Relationship Between Function-Form in The Expression of Architectural Creation. SageSubmissions. Preprint. https://doi.org/10.31124/advance.8275322.v1
13. Qabanis J. and Yeorgios Nikolaos Kampanis Y. N., https://www.academia.edu/10960271/Daniel_Libeskind_spears_to_the_future [Accessed: 1st March 2020].

SHAPE AND ACOUSTIC INTERACTION IN LARGE CONCERT HALLS

Evgenia Ermakova
Department of Civil Engineering, Peoples' Friendship University of Russia, Moscow, Russian Federation
Master Student, evgenia.er@mail.ru

Marina Rynkovskaya
Department of Civil Engineering, *Peoples' Friendship University of Russia*, *Moscow, Russian Federation*
PhD., Associate Professor, marine_step@mail.ru

ABSTRACT

In this work there is an effort to fully analyse the entire evolution of a concert hall formation and to identify the main typological shapes, which permitted exploring the revolution in the architecture of the concert halls in the 20th century taking as an example the Berlin Philharmonic hall by Hans Scharoun. Similarly, the configurative development in the auditorium of the concert hall and its gradual complication are evaluated. Additionally, special attention is paid to the acoustics properties of the halls and different methods of acoustic improvement are identified. The main purpose of this study is to develop a comparative analysis of both architectural and acoustic aspects through a review of historical forms and to determine the most appropriate shapes for concert halls.

Furthermore, architectural and construction systems of the "shells" type are taken into account. The use of shells in the halls contributes not only to the beautiful image of the interior, but also to the creation the effective and comfortable acoustic mode of the halls. This article discusses the issues of effective compositional and constructive application of the shape of the hall space in which the shells of the simple and complex geometry are used. Examples of successful combination of architectural expressiveness and acoustic properties are given, such as National Kaohsiung Center for the Arts (Mecanoo, Taiwan), Elbe Philharmonic (Hamburg, Germany), House of Music and Zaryadye (Moscow, Russia) and so on. The project of a concert hall for 1500 seats (diploma project of Evgenia Ermakova) in the city of Petrozavodsk, Republic of Karelia is also given as an example.

Keywords: concert hall; shape; acoustic; shells of the simple and complex geometry

INTRODUCTION

1.1. Greek and Roman period

The process of forming the architectural space of concert spectacles began in the age of antiquity. At first, these were temporary wooden structures that were built for the opening of important events. In the V century BC, the plan of spectacular buildings already acquires an elongated asymmetric shape, which by the end of the century is formed into a stable type of structure, including such elements as the orchestra(stage), the theatron (seats for spectators) and the skena (warehouse of scenery). The shape of the visual space itself was a semicircle that slightly exceeded 180° (Fig.1). The seating was steeply sloped in these structures, typically 2:1, which afforded good sight lines and reduced grazing attenuation [18]. The acoustic system of this time had a very simple scheme. The stone surfaces of the orchestra, stage, and structures behind the stage sent sound reflections to the audience, amplifying

the direct sound. There are theatres carved on native stone and others constructed on hill-sides from marble or stone seats joined together [13].

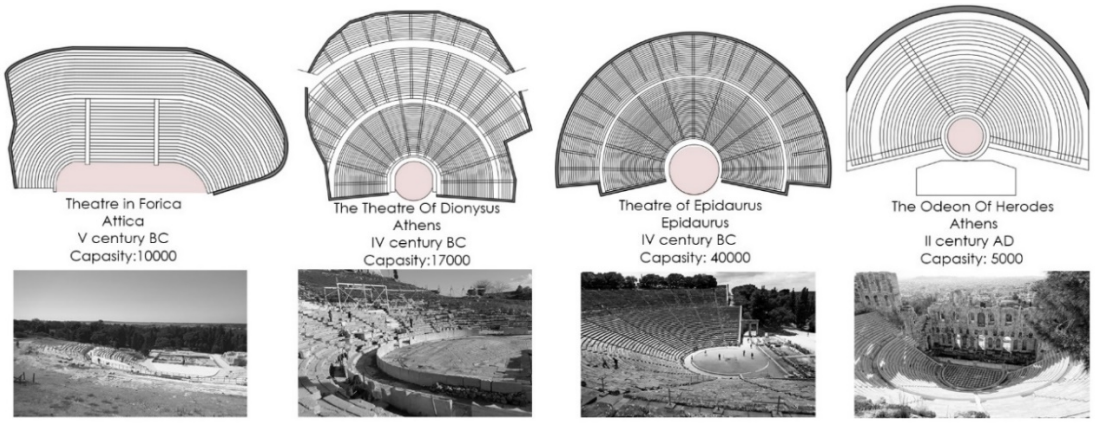

Figure. 1**:** The concert halls in Greece

Later, in Ancient Rome, there was the appearance of a complete ellipsoid shape, where seats for spectators and high walls surrounded the arena for performances. The most magnificent buildings-amphitheatres, such as the Roman amphitheatre in Capua and the Colosseum, could accommodate up to 50,000 people (Fig.2). The building itself was built on a flat platform, and the auditorium had a steep rise, which contributed not only to good visibility of what was happening on the stage, but also good audibility. Even then, the ancient architects were aware of the role of the correctly chosen area, the angle of the auditorium and the sound reflection from the floor. In the "ancient architectural acoustics," the concepts of reverberation, interference, echo disturbance, and clarity of voice were described [1]. Despite the inability to perform appropriate calculations, in Roman theatres, optimal acoustics was of greater importance than visibility [14]. The shape of the Roman amphitheatre: from a semicircle to an ellipsoid was later reflected in the configuration of the audience space of the concert halls.

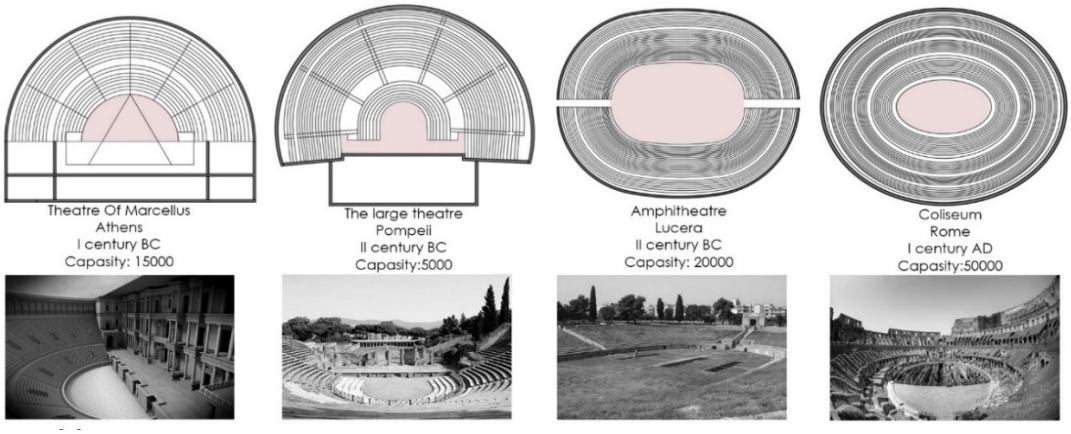

Figure. 2**:** The concert halls in Rome

Ancient theatres are the best example in achieving good audibility and still amaze with excellent acoustics. The cup-shaped plan, a certain height between the stone benches, and their heterogeneous structure created conditions for additional amplification of sounds coming from the stage, as well as for a kind of filtering out of the background low-frequency noise.

This article describes such an important acoustic parameter as the reverberation time T (in seconds), which characterizes the time for the sound level to decay to one millionth of its energy. Despite the many advances of recent years, reverberation time remains the single most valuable measurable quantity for the acoustics of an enclosed space [3]. The authors conducted a study of changes in reverberation time depending on the shape of the concert hall in the acoustic program EASE and for the ancient theatre it was quite short and did not exceed 1 min (Fig 3).

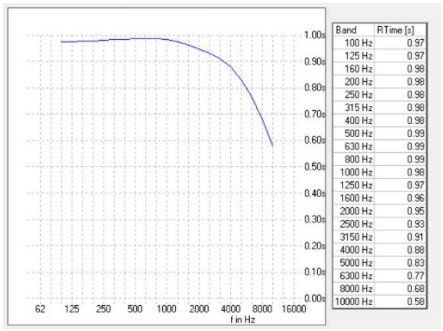

Figure. 3: Reverberation scheme of the ancient theatre

1.2. The Middle Ages

The gradual decline of the Roman Empire, combined with the expansion of Christianity, led to a loss of interest in the ancient theatre in favour of the development of choral music. To X-XIV century it acquires an independent character with the appearance of wandering musicians, communities of music lovers. There is a practice of holding musical events both on the street and in city public spaces as taverns or cathedrals. Churches, built in the first half of the fourth century, were elongated rectangular halls with a single apse and a raised floor. The evolution of space has led to more complex spatial forms with side naves and transepts (Fig.4 a). In Orthodox churches in order to create a good natural acoustics, ceramic jugs were used in the style of ancient amphora, which were laid in the walls of the building to enhance the echo from the choir and increase the reverberation time (Fig.4 b).

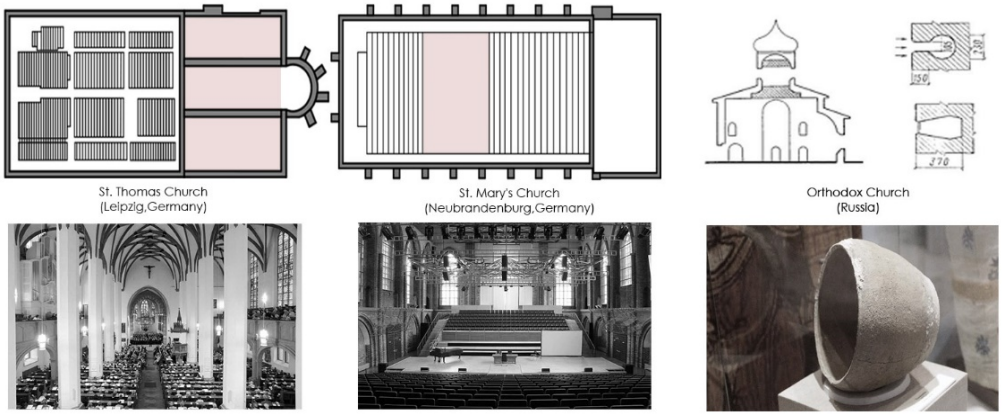

(a) (b)

Figure. 4: (a) The ancient churches, and (b) An image example of ceramic jugs in the orthodox churches

Due to the large isolation of the spatial environment, Church buildings facilitated multiple reflections of sound waves, as well as reverberation. Later, the rectangular shape of the Church buildings will become the basis for the classic " box " shape in the architecture of the concert hall.

1.3. XVIII century. Appearance of the first specialized concert buildings

With the beginning of the New century, music was finally separated from the theatre, it became completely independent and an integral part of the cultural life of people. Opera, a genre of musical and dramatic work, appears there, and various buildings for chamber concerts are designed and built. Many elements are borrowed from the theatre's architecture, such as a raised stage, U-shaped Seating, concave walls, and a high domed ceiling. In the future, the composition of concert halls will still have all this predominant characteristics, which are going to be further developed

In the 18th century, the first specialized concert buildings with a small capacity and simple shape appeared as seen in Fig.5. Compared to the halls of antiquity, the 18th-century hall takes on a U-shaped shape with rounded

sides to create the effect of an "acoustic lens" that collects sound in the centre of the hall and diffuses sound relatively evenly to all the walls. The development of the hall's composition is in length. The U-shaped amphitheatre will soon get a complete rectangular shape.

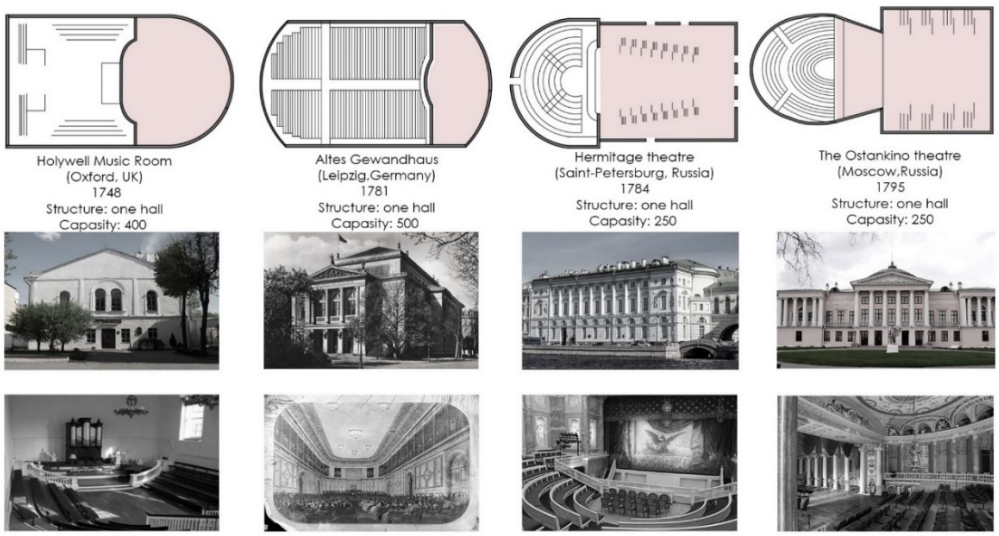

Figure. 5: The concert halls of the 18 century

1.4. XIX century. The appearance of the halls of the great capacity

In the 19th century, the concert hall was universalized and the aspirations of architects and composers to change the form, as well as social conditions, led to completely more grandiose spaces for musical performance. The big halls with a large capacity were created, which played the role of necessary architectural experiments for the further development of the concert hall. Such buildings as the Crystal Palace (London, England), the Albert Hall (London, England), and the Trocadero Palace (Paris, France) were not specialized buildings for the musical performances, but their halls were used for mass concerts (Fig 6 a). The shape of the Crystal Palace was an elongated rectangle with dimensions 550x137x40 m with galleries on both sides. For this building, a special project of an amphitheatre was developed with the arrangement of seats in the form of an ‘isoacoustic curve’. Each level of the amphitheatre on the line of this curve should give the same ‘acoustic picture’ for the listener (Fig 6 b). This scheme was firstly introduced by Russell (1838) who calculated the optimum floor profile in long section for good vision and hearing [8]. The concert halls Albert Hall and Trocadero Palace had an elliptical shape.

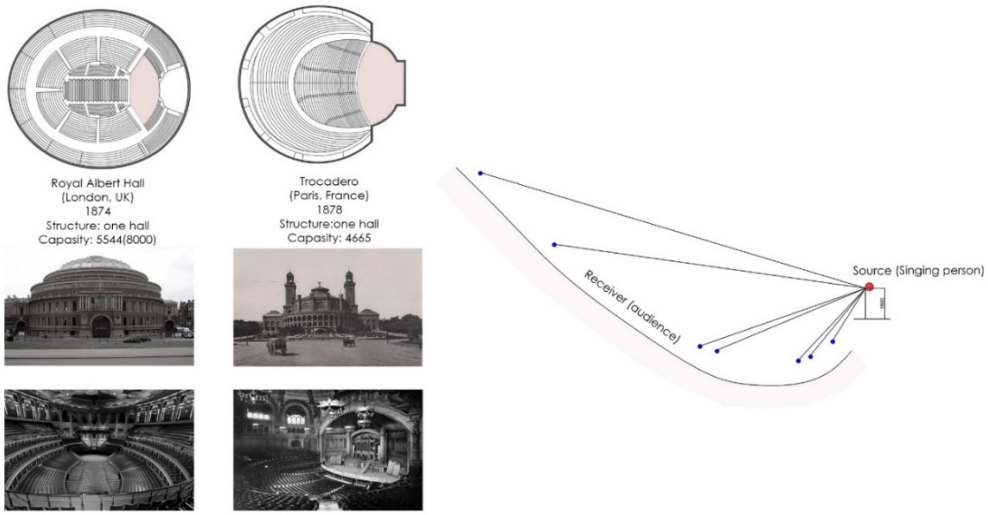

(a) (b)

Figure. 6: (a) The concert halls of the 19 century, and (b) the ‘isoacoustic curve’ in the Crystal Palace

After designing such buildings as Crystal Palace, Royal Albert Hall and Trocadero, it became clear that the concert hall can be multifunctional and at the same time with this universalization the designer's task to ensure adequate acoustics came to the fore. With the appearance of such big halls, the limits of the estimated capacity of the music hall began to be formed, which were established experimentally and amounted to from 2200 to 2700 people for one large symphony orchestra and a mixed choir. Otherwise, with an increase in size, the hall reaches a limit, after crossing which it stops to meet the requirements of sound intelligibility and there is an extremely strong echo.

1.5. The appearance of the four great halls in terms of acoustics

In the 19th century, the first radical revolution in the design of concert halls took place. The end of the era was marked by the appearance of the big five halls, such as Grosser Musikvereinssaal (Austria, Vienna), Neues Gewandhaus(Leipzig, Germany), Concertgebouw (Amsterdam, the Netherlands), Carnegie Hall (New York, USA), Symphony Hall Boston (Boston, USA) (Fig 7). All the halls have a trapezoidal-sector shape and are mainly built on a two-hall structure except for the Carnegie Hall and Symphony Hall Boston, which have only one hall. Boston Symphony hall is considered to be the first concert hall where the young scientist William Sabine performed reverberation calculations already at the design stage. Sabine's great achievement was to develop a rational understanding of acoustic behavior and thereby lay a solid foundation for its later study [4]. These halls showcase very ornamented combinations of the same few architectural elements such as a stage, parterre and balconies. However, despite this ornamentation, the structure and the embedded engineering techniques are relatively simple [6]. Also, the design practice includes such a form as 'theatre form'. The Carnegie Hall and Usher Hall are built according to this scheme. The theatre form is designed as a theatre with one or two balconies with curved balcony fronts, which extend some way along the side walls from the back; the stage is in a recess [5].

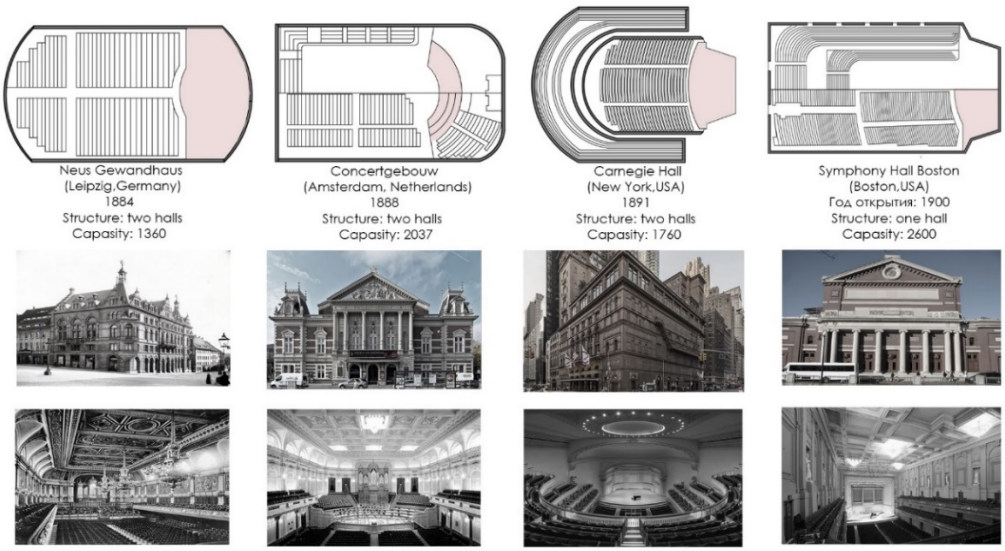

Figure. 7: Four great halls in terms of acoustics

It should be noted that using such elements as columns, semi- columns, pilasters and molding is done in order to make the form more acoustically suitable. All these additions to the interior are necessary to achieve a good sound. The introduction of non-linear walls is also important. A good solution is to round the walls on the sides. This way the reflections will come earlier than from the ceiling and there will be no sound delaying. As we can see in the Figure 8 (a), a rectangular shape with rounded sides has a much shorter reverberation time than simple 'shoebox form' in the Figure 8 (b). This type of form with rounded sides is currently used in the concert hall model.

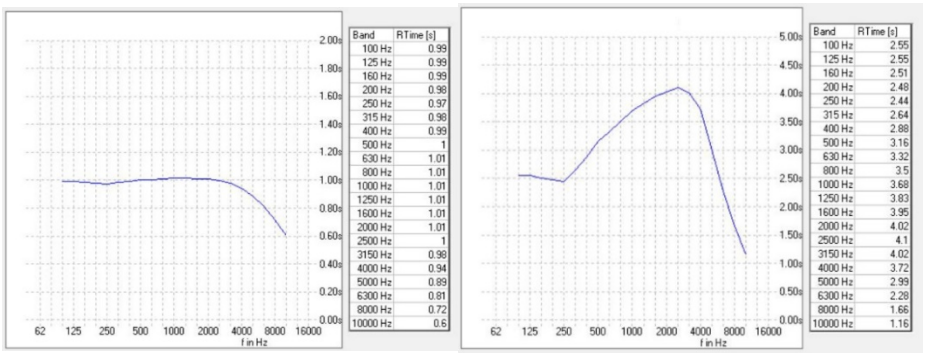

(a) (b)

Figure. 8: (a) Reverberation scheme of 'shoebox form' with rounded sides, and (b) Reverberation scheme of 'shoebox form'

The dynamic development of music and acoustics in the second half of the nineteenth century led to the need to expand existing concert halls. A growth in cubature in the shoebox, fan or horseshoe – shaped layouts posed a threat of an overly prolonged reverberation time as well as of an echo [14]. All of this will further have an influence on the development of a completely different form that will be applicable to large halls.

1.6. New configuration of the concert halls by Hans Scharoun

In the twentieth century, architectural acoustics came to be recognized as a science as well as an art [18]. With the beginning of construction of concert halls with the possibility of audio recording or radio broadcasting of events, the audience space became more complicated [9]. Architects and constructors felt the need to escape from traditional rules of architectural composition involving Classical orders of columns, symmetry and axes [3]. There are various variations of forms created on the basis of simple ones (Fig 9). For example, the Radio City Music Hall has a double segment-ellipsoid shape with three circles of cantilever balconies. In this period such form as 'fan-shape" was appeared. A good example is the hall Salle Pleyel in Paris. The plan form allows for a maximum audience within a certain angle centred on the stage [5].

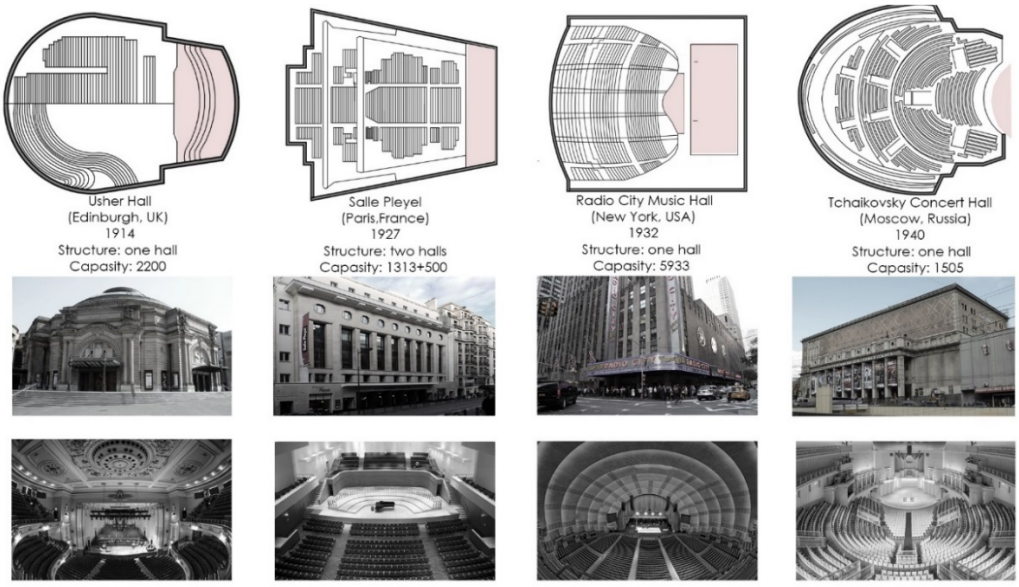

Figure. 9: The concert halls in the beginning of the XX century

In the 60s, there was a second significant revolution in the design of the concert halls. In 1963, the building of the Berlin Philharmonic, designed by Hans Scharoun with acoustician Lothar Cremer, was opened. This concert hall is a real challenge for the generally accepted architectural and acoustic standards. With the appearance of this building, the internal and external composition of the space was changed and a new era of designing concert halls began [9]. Scharoun completely changed the configuration of the auditorium and stage. In the traditional hall, a single mass of the listeners is located opposite the orchestra and exceeds it in number. At the same time in the

Philharmonic the new principle of 'circular sound' was firstly applied, when the audience surrounds the orchestra and all the seats are located in close proximity to the sound source. From an acoustic perspective, Cremer knew of the importance of early reflections, which necessitated in this design placing the audience blocks at different levels so that surfaces separating them could be used to provide additional early reflections [3] (Fig 10 a, b). The Philharmonic hall hasn't got parallel walls in interior to avoid standing waves and vibrating echoes. Vineyard terraces are local reflectors, transmitting reflections to each other. All surround halls sacrifice acoustical excellence mainly in the side and rear seating areas for audience proximity and visual stimulation [18]. The unusual ceiling of the building also performs its acoustic function. It provides strong overhead reflections to remote seats and helps maintain loudness [6].

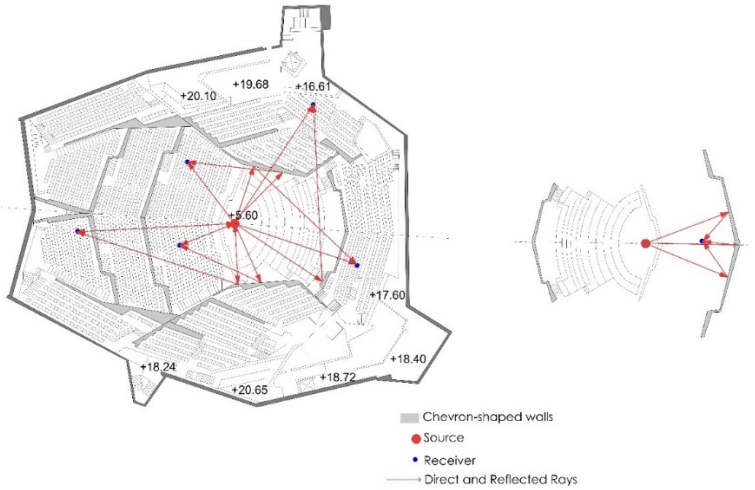

Figure. 10: General acoustic scheme of the Berlin Philharmonic Hall with the reflecting surfaces (chevron-shaped walls) near the listener

A complex shape based on the principles of the Berlin Philharmonic with non-parallel walls and with an orchestra in the center of the composition has a very acceptable reverberation time (Fig 11). Bringing lateral reflection surfaces closer to the listeners allows dividing the interior of the room into smaller, acoustic segments acting individually [14].

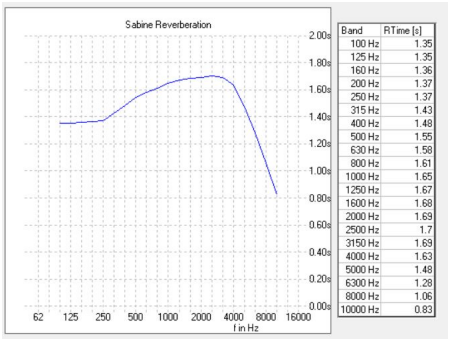

Figure. 11: Reverberation scheme of complex form

1.7. The modern concert halls

Nowadays the acoustics of the hall has become one of the main elements in architecture and with the advent of the vineyard configuration, the beauty of architectural forms began to connect with the acoustics in concert halls. Shells in particular have a long tradition of being structurally sound as well as architecturally significant [10]. The architects of the modern world use a variety of shapes and transformations to create rooms with unique audio data The principle of centric location of the stage, the asymmetric configuration of the audience seats that surround the orchestra on all sides in the Berlin Philharmonic is currently actively used in the design of modern halls. Bright examples are the concert halls: National Kaohsiung Center for the Arts (Kaohsiung, Taiwan), Elbe Philharmonic (Hamburg, Germany), House of Music and Zaryadye (Moscow, Russia). Table 1 shows the most

expressive examples of using shells in the concert hall. Also, the surfaces with identical slopes [25] or ellipsoidal surfaces [18] can be used. Furthermore, such complicated spatial structures as focal-directorial models in a spherical grid [24] can form the shell of a building. Inventing and using your own original scientific and creative fundamental basis of morphogenesis — a direct way to create a very large complex of architectural and design solutions of new shells that can dramatically affect the formation and development of stylistic artistic concepts-design of interiors and small forms that reflect cultural-aesthetic demands of the future society [16].

(1) **Table 1:** The use of different shells in the concert halls

Concert hall	*Capasity of the large hall*		*Plan*	*Type of surface*	*Model*
Berlin Philharmonic (Berlin, Germany) 1963	*2440*		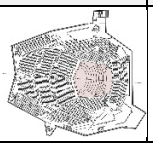	*Elliptical paraboloid*	
After					
Sydney Opera House (Sydney, Australia) 1973	*5738*		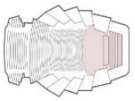	*spherical surface*	
Roy Thomson Hall (Toronto, Canada) 1982	*2630*		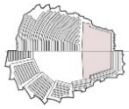	*The surface of conjugation of the coaxial cylinder and the cone*	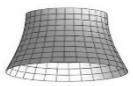
Elbe Philharmonic Hall (Hamburg, Germany) 2017	*2100*			*Elliptical paraboloid*	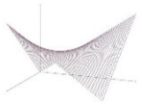
The concert hall of the National Kaohsiung Centre (Kaohsiung,Taiwan) 2017	*2300*		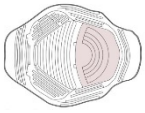	*The connection of three velaroids on a rectangular plane*	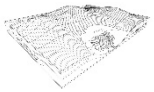
Zaryadye Concert Hall (Moscow, Russia) 2018	*1500*		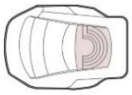	*The complex form of shell*	
The concert hall (Petrozavodsk, Russia) The project of Ermakova Evgenia	*800*	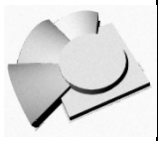	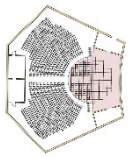	*Conoid surface*	

As an example, the diploma project of the concert hall of the author of the article Ermakova E. V. is also given. The structure of the building contains 4 shells: three conoid surfaces with different rises (18 m, 14 m and 11 m respectively) and one cylindrical with a radius of 30 m. All of these elements form a single composition together and create unique concert venues for concerts of different genres: the main hall with 1,800 seats for large symphony concerts and a small hall with a capacity of 800 seats for chamber music performances. The main hall is the basic part of the composition and is located in the centre of the cylinder, and the small hall is located inside the largest of the three conoid surfaces. The chosen shape of the building perfectly fits into the surrounding landscape, emphasizing the relief of the existing area on the river bank. This concert hall is a stunning space for all kinds of performance and musical productions, combining the person, art and unique personality of the city of Petrozavodsk.

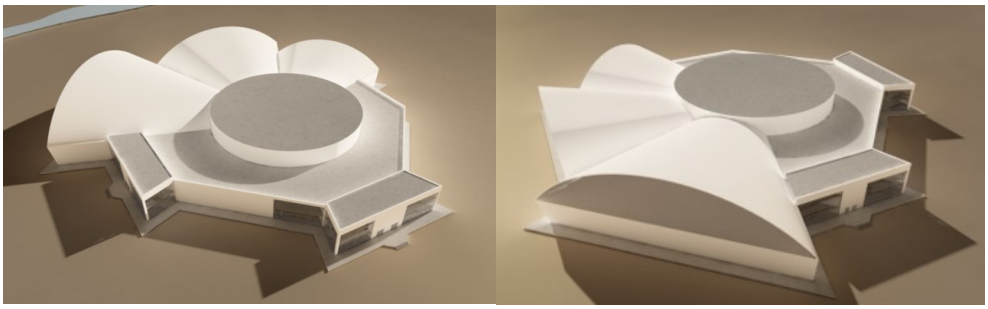

Figure. 12: The project of the concert hall

2. AN OVERVIEW OF MEASURES TO CREATE A GOOD ACOUSTIC PERFORMANCE IN A CONCERT HALL

2.1. A method of computer modelling of the acoustic qualities of the form

Acoustic performance in buildings is of major importance since it provides the necessary comfort and fundamental essentials for an optimal work environment. What makes a good concert hall is a combination of many acoustic and nonacoustic attributes perceived by an audience member in a complex manner [8]. The acoustic consideration played a key role in determining the shape of the hall [2]. From the beginning of creating the form of concert halls it is very important to take into account its acoustic suitability. It is now a common practice to simulate the impulse response and, the deriving room acoustic parameters, using computational models [11].

Currently, this can be checked not only in special acoustic programs such as EASE or ODEON, but also using the Pachyderm Acoustics application in the Rhino Software. This app is a collection of acoustics simulation algorithms which can be used to predict noise, visualize sound propagation, and critically listen to designed spaces. The main aim of the program is to combine geometry and acoustics together in order to speed up the architectural design process.

In this program, two simple shapes were modelled: the classic shoebox form with columns (Fig 13) and the oval one (Fig 14). Dimensions of a rectangular hall are 40 x 24 x 14 m with 32 columns. The oval form has following dimensions: 50 x 40 x 18 m without the introduction of reflective surfaces. The task was to check how much the introduction of additional reflective surfaces improves the reverberation time and compare it with the form in which there are only walls.

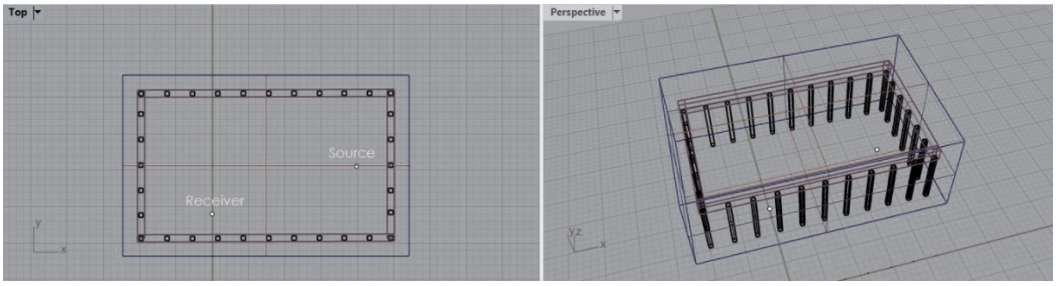

Figure. 13: The classic shoebox form

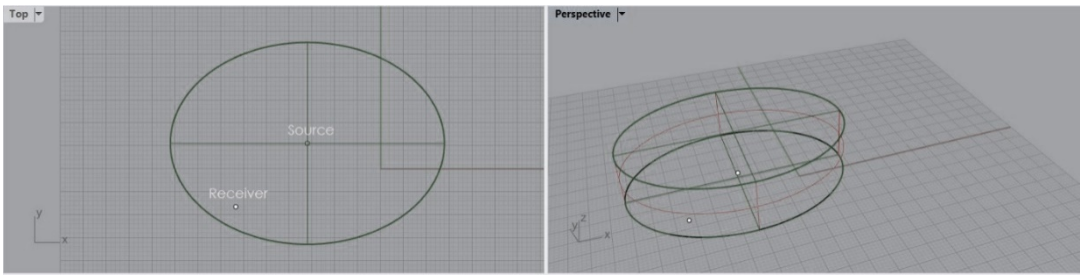

Figure. 14: The oval form

After modelling the geometry, the transition was made directly to the Pachyderm Acoustics application and two points were placed: Source (Singing person) and Receiver (Listener). Next, materials were selected for all enclosing surfaces of the room. After that, an acoustic shape analysis was performed directly and three logarithmic ETC curves (energy time curve), which measure room decay time graphically, were constructed for each hall at a frequency of 500 Hz. In contrast to the frequency response, which shows the level of sound pressure at different frequencies of the spectrum, the ETC curve gives an idea of how the spectrum is constructed. Each peak on the curve is a reflection. The model of sound wave construction is shown in the Table 2.

(2) Table 2: The graph of construction ETC and the values of reverberation at frequency 500 Hz

Form	Logarithmic Energy Time Curve on 500 Hz	T_{500}
Shoebox form with columns	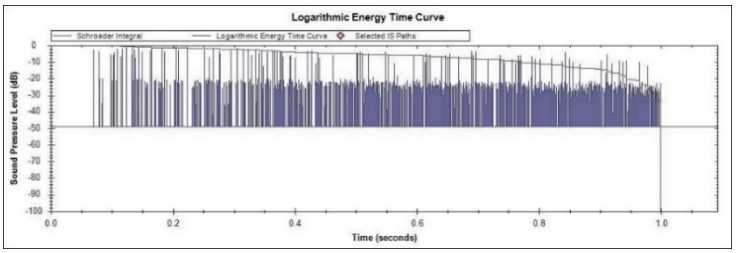	**1.8**
Oval form	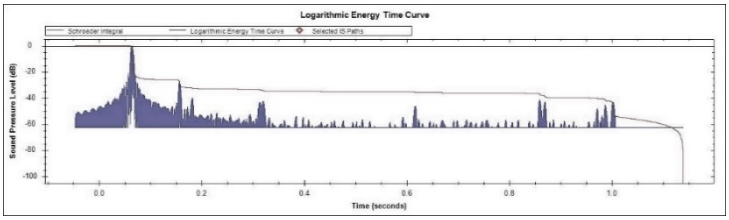	**2.4**

In these calculations, we can see that the rectangular shape has more complex and long curves from -10 dB and below. The oval shape has early attenuations and there is a high probability of an echo. Thus, the introduction of additional enclosing elements improves the acoustic conditions in the hall.

2.2. The possibilities of the improvement of the acoustics

Creating perfect acoustics in a concert hall is not an easy task. There are not many acoustically suitable buildings for concerts in all of Europe and Russia. However, technologies for improving acoustics have been constantly developing since the 20th century. The creation of an effective / comfortable acoustic mode for the venues of public buildings is absolutely impossible today without the use of advanced structural and technological solutions for interior shells [16]. The interior of a building can include such shells as cyclic surfaces of revolution or an elliptical paraboloid. For example, in the Sydney Opera concert hall a set of 18 acrylic rings, or 'clouds' provides a height-adjustable canopy intended to reflect sound back to the stage [26]. These elements form the shape of a cyclic surface of revolution (Fig.15 a, b)

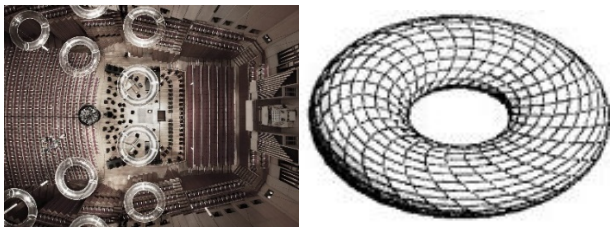

(a) (b)

Figure. 15: (a) The "clouds" canopy, and (b) The cyclic surface of revolution

An extremely strong echo was detected in the Royal Albert Hall concert building after the opening, which can naturally decrease to acceptable only when the audience seats are occupied by 90% due to sound absorption. To eliminate this effect, special fibreglass acoustic diffusers ('mushrooms') were introduced under the ceiling in the amount of 135 pieces, located in the centre of the dome, which eliminated excess echo and redirected the sound to the galleries (Fig 16 a, b). In 2001, following more advanced acoustic testing by Peutz Associates, 50 diffusers were removed and the remaining 85 were reconfigured [20]. This system of 'mushrooms' improved the quality and immediacy of sound for the audience. In addition to increasing sound level, the reflections are useful for providing a degree of reverberation and are beneficial in allowing the performers to hear each other [2].

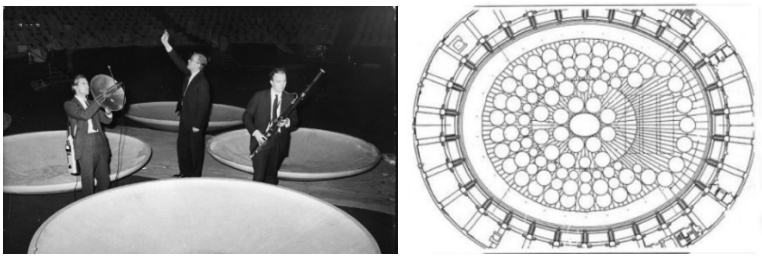

(a) (b)

Figure. 16: (a) Acoustic tests in the late 1960s, and (b) ('mushrooms')

Also, the acoustics can be adjusted using the special Meyer Sound Constellation system, which is able to adapt to any shape and size of the hall, giving full architectural freedom to designers. Constellation is a digital way to control reverberation time, early reflections, and other key parameters that determine the intelligibility and comfort of sound perception through the resonant properties of the room [21]. The system is based on a large number of microphones and speakers located in the visual space and directly near the stage. This system is very successfully used in the Logomo Concert hall (Turku, Finland), the House of Music (Moscow, Russia). Constellation's tasks do not include amplifying or changing the sound-only correcting acoustic defects or creating a new hall geometry.

In the Logomo hall, the entire transformation process is linked to the constellation adaptive system provided by the Meyer Sound d-Mitri digital audio platform. The ambient sound is picked up by 76 microphones and returned back to the hall in the form of early reflections and late reverberations via 223 self-powered discrete speakers and 12 compact subwoofers [22]. The system is equipped with programs for nine hall and stage configurations, each of which already has ready-made acoustic parameters, including reverberation time, early decay time, power and frequency (Fig. 17 a).

In order to eliminate problems with sound distribution in the area of the stage and orchestra seats, the concert hall of the House of Music also has a Constellation system installed (Fig. 17 b). The introduction of this system made it possible not to rebuild the hall and keep everything in its original form. The use of mobile microphones and speakers mounted on winches can be considered a distinctive feature in the hall that allow you to quickly change the position, namely to raise or lower all the equipment.

A total of 48 microphones are installed in the hall-32 in the visual part, and the remaining 16 above the stage [23]. Microphones in the hall above the audience are responsible only for reverberation, and above the stage for reverberation and early reflections. After that, the sound goes to a special reverb and early reflection processor, and is then output to more than 200 speakers. As a result normal reverberation and early reflections were restored, "volume of sound" was added, and the previously "dead" zone under the balconies was voiced with the installation of this system [23].

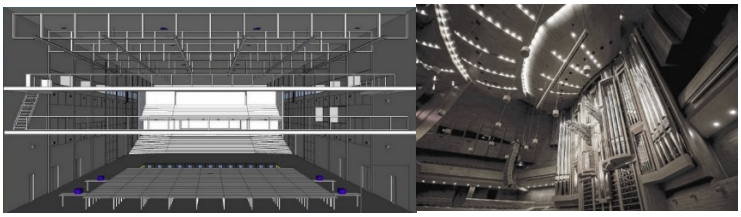

(a) (b)

Figure. 17: (a) Constellation system in the concert hall Logomo, and (b) Constellation system in the House of music

Also, internal transformation of elements of the concert hall space is a very common phenomenon for improvement of the acoustics. This can be a change in the configuration of the stage, as is done in the Zaryadye Concert hall in Moscow, where lifting platforms are created for large group concerts, in order to evenly distribute the sound from high to low frequencies and are located along the radius, dividing into the independently working elements. The first rows are intended for stringed instruments, and the top ones for wind instruments, in order to avoid overlapping the sound. The lifting height of each platform is 1500 (Fig 18 a, b, c, d). These elements are equipped with an electro-mechanical drive with a reduced noise level. Platforms can work synchronously or asynchronously in any configuration and they are integrated into the lower stage mechanization control system.

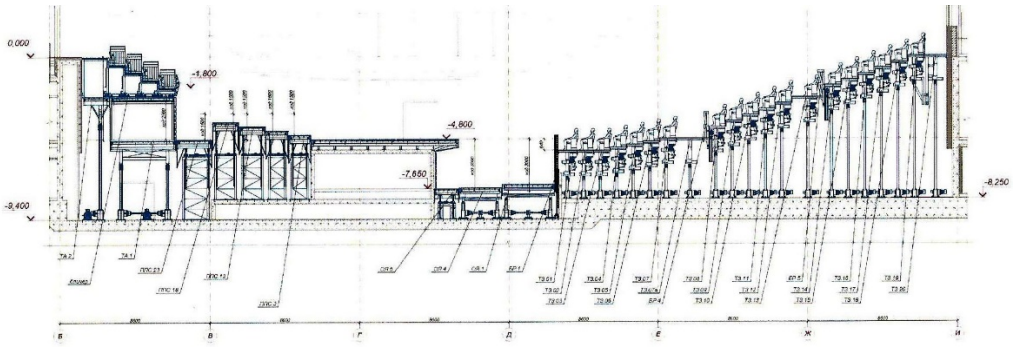

(a)

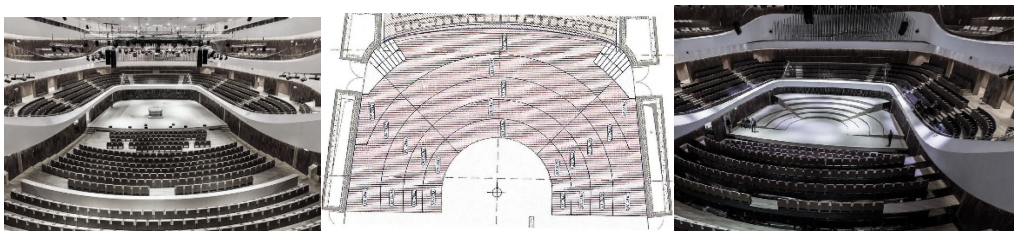

(b) (c) (d)

Figure. 18: (a) The section of the Philharmonic hall, (b) Lifting platforms are down, (c) The plan, and (d) Lifting platforms are up

Transformation in this concert hall is also present in the space of the orchestra pit, which is divided into 3 parts. The first part consists of three independent lifting and lowering platforms. The second part consists of a single lifting and lowering platform for the entire width of the orchestra pit. The third part is a stationary platform located under the stage. The platform is used for entering the orchestra and providing the necessary lifting of the orchestra pit. This arrangement of the orchestra pit allows to form an orchestra pit in its various configurations, depending on the number of musicians and the purpose of the orchestra, which undoubtedly has an impact on the sound process (Fig 19).

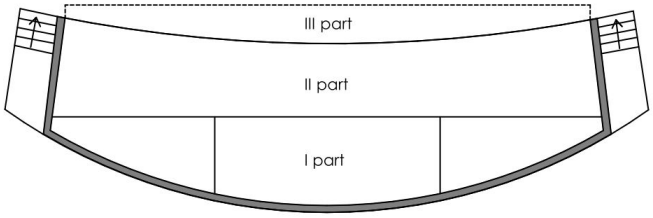

Figure. 19: Separation of the orchestra pit

3.1. Materials and Methods

This study is primarily based on the study and comparison of scientific, literary and graphic sources. The work uses a comparative method to analyse the full development of the form of concert halls in the historical aspect. On this issue, the study is based on researches by Marshall L [2], Barron M [3, 5], Beranek L [4], Jablonska J et al. [14,15]. The following shows an overview of the shells that form the basis of modern concert halls after the opening of the Berlin Philharmonic and the designation of these forms is based on research Krivoshapko S.N

and Ivanov V.N [17]. Acoustic form analysis is applied using special programs EASE 4.3.8 and Rhino with a Pachyderm connection.

3.2. Research Fundamentals

This research topic is based on the correlation between form and acoustics in concert halls. Throughout the historical centuries, the form has repeatedly undergone significant changes. Many factors have influenced its development, but the most important is the acoustics. The purpose of this study is to develop a comparative analysis of both architectural and acoustic aspects through a review of historical forms. The scientific novelty of the work consists in a complete review given above of the evolution of the formation of concert halls both externally and internally in conjunction with acoustic parameters. In this paper also special attention is paid to shells and a detailed description of these systems in the form of a table was provided. The paper showed the advantages of Pachyderm for architects in calculating acoustics in the Rhinoceros program.

3.3. Results and Discussion section

The shape of the concert hall at the turn of the 25th century was repeatedly changed, improved and became more and more acoustically suitable. In the XIX century, after the construction of Boston Symphony Hall, the architects used a scientific method for calculating the acoustic properties of the designed hall.

The special acoustic calculations helped to correctly design the form and even led to unexpected decisions in the appearance of the auditorium (Concert hall of the Berlin Philharmonic). The ideas of Hans Scharoun and Cremer's acoustical schemes were widely used in the design of subsequent halls. The author 's concert hall was also designed according to their principles, which are based on the complexity of external and internal forms with an introduction of shells. These elements are responsible not only for the beauty of the building, but also for the creating good audibility in the hall.

In this study the analysis of several forms was done using two programs (EASE 4.3 and Pachyderm acoustics app for RHINO) in order to estimate the reverberation time as the most important factor for determining the acoustic quality of the room. The calculations on the historical development of the form in the concert hall were made using the EASE program. First, the reverberation time for the ancient form of the theater was calculated, then the same calculations were done for the traditional rectangular form and for the complex one. Also, a calculation was made in Pachyderm Acoustic for a rectangular shape with columns and for an oval shape to see how different the results of a hall with columns will be from a hall with concave walls. The results obtained allow us to conclude that in an oval shape, due to the long reverberation time, an echo will be created, while in a rectangular shape with columns, the sound will be dispersed evenly due to the introduction of additional architectural elements. This study confirmed the excellent sound in the theaters of Ancient Greece and Rome, and that the shape of the hall with rounded sides and complex ones are the most favorable for good audibility in the hall.

At the moment the practice of designing concert halls is dominated by a complex form of spectator space and the creation of a large number of terraces of different directions. However, a rectangular plan or 'shoebox type' is also still used, because of its good acoustic qualities with a small width at a relatively high height, columns, and plaster, which contribute to earlier reflections from the walls than from the ceiling.

Nowadays, there are many ways to improve acoustic qualities of any form without its changing. These could be special shells with a reflection function, the introduction of electroacoustic systems with ready-made settings for any concerts or the transformation of elements in the stage space. With computer modelling in Rhinoceros, using the Pachyderm acoustics app, you can quickly interact with form building and acoustic analysis.

3.4. Acknowledgements

This paper has been prepared with the support of the "RUDN University Program 5-100".

REFERENCES

1. Ando, Y., 1998. Architectural acoustics: blending sound sources, sound fields and listeners. Springer–Verlag, New York, USA.
2. Blundell, J. P. and Kang, J.,2003. Acoustic form in the Modern Movement. Architectural Research Quarterly, 7(1). pp.75–85.
3. Barron, M.,2009. Then and now–how concert hall design of the 1960s and '70s compares with the present. Proceedings of NAG/DAGA, Rotterdam, Netherlands. pp. 4–8.
4. Beranek, L.L., 2008. Concert Hall Acoustics. Journal of the Audio Engineering Society, 56. pp 532-544.
5. Barron, M., 2006. The development of concert hall design - A 111 year experience. Proceedings of the Institute of Acoustics, 28. pp. 1-15.
6. Barron, M., 1996. Loudness in concert halls. Acustica-acta acustica, 82. pp. 21-29.
7. Barron, M., 1993. Auditorium Acoustics and Architectural Design. Spon Press, New York, USA.
8. Cox, T.J. and D'Antonio,P.,2003 Engineering art: the science of concert hall acoustics. Interdisciplinary science reviews, 28. pp. 119-129.
9. Ermakova, E.V. and Rynkovskaya, M.I., 2019. Formation of shell's plasticity in the concert hall. Izvestiya KGASU, 3(49). pp.53–61.
10. Echenagucia, T. M. et all, 2014. Multi-Objective Acoustic and Structural design of shell structures for concert halls. Proceedings of the IASS-SLTE Symposium 'Shells, Membranes and Spatial Structures: Footprints', Brazilia, Brazil. pp. 1-12
11. Echenagucia, T. M. and Block, P., 2015. Acoustic optimization of funicular shells. Proceedings of the International Association for Shells and Spatial Structures (IASS), Amsterdam, Netherlands. pp. 1-13
12. Garcia Comez, J.O., 2016. Shaping concert halls. Proceedings of EuroRegio, Porto, Portugal. pp. 1–11.
13. Goussios, C. et all, 2009. Epidaurus: Comments on the Acoustics of the legendary ancient Greek theatre. Proceedings of AES 126th Convention, Munich, Germany. pp. 1–6.
14. Jablonska, J. et all, 2015. Sound and architecture–mutual influence. Energy Procedia, 78. pp 31-36.
15. Jablonska, J., 2018. Architectural Acoustics in Vineyard Configuration Concert Hall. Journal of Architectural Engineering Technology, 7(2). pp 1–6
16. Korotich, A.,V., 2015. Innovative solutions of architectural shells: alternative to traditional building construction. Akademicheskij vestnik URALNIIPROEKT RAASN, 4. pp 70-75.
17. Krivoshapko, S. N. and Ivanov, V. N., 2015. Encyclopedia of Analytical surfaces. Springer International Publishing, Switzerland.
18. Krivoshapko, S. N., 2007. Research on general and axisymmetric ellipsoidal shells used as domes, pressure vessels, and tanks. Applied Mechanics Reviews (ASME), 60(6). pp 336–355.
19. Marshall, L., 2006. Architectural Acoustics. Elsevier Academic Press, London, UK.
20. Mushrooms (acoustic diffusers). https://www.royalalberthall.com/about-the-hall/our-history/explore-our-history/building/acoustic-diffusers-mushrooms/ [Accessed: 1st March 2020].
21. Meyer Sound Constellation. https://showcraft.ru/meyersound/constellation [Accessed: 1st March 2020].
22. Meyer Sound Constellation Tailors Acoustics for Finland's Shape-Shifting Logomo Hall. https://meyersound.com/news/logomo/[Accessed: 1st March 2020].
23. MMDM: There are no limits to perfection. https://inavate.ru/site/content/view/4636/ [Accessed: 1st March 2020].
24. Petruševski, L.,S. et all, 2017. Modeling of Focal-Directorial Surfaces for Application in Architecture. FME Transactions, 45 (2). pp 294–300.
25. Romanova V. A., Rynkovskaya M., Ivanov V.N., 2019. Automatic Modeling of Surfaces with Identical Slopes. Advanced Structured Materials, 92. pp 143–156.
26. Taylor, L. and Claringbold, D.,2010. Acoustics of the Sydney Opera house concert hall. Part One: The Client's Perspective. Proceedings of 20th International Congress on Acoustics, ICA, Sydney, Australia. pp. 1–8.

DISCRETIZATION AND OPTIMIZATION OF FREEFORM SURFACES WITH CIRCULAR MESHES FOR ADAPTING TO GRID SHELL STRUCTURES

Zlata Tošić
Faculty of Civil Engineering and Architecture, University of Niš, Niš, Republic of Serbia
PhD Candidate, zlata10@live.com

Sonja Krasić
Faculty of Civil Engineering and Architecture , University of Niš, Niš, Republic of Serbia
PhD, Associate Professor, krasic.sonja@gmail.com

Daniel Lordick
Geometric Modeling and Visualization (GMV), Institute of Geometry, TU Dresden, Germany
Prof. Dr.-Ing., Head of the Research Group GMV, daniel.lordick@tu-dresden.de

Jovana Stanković
Faculty of Civil Engineering and Architecture, University of Niš, Niš, Republic of Serbia
PhD Candidate, jovana__stankovic@hotmail.com

Nastasija Kocić
Faculty of Civil Engineering and Architecture, University of Niš, Niš, Republic of Serbia
PhD Candidate, nadja93.al@hotmail.com

ABSTRACT

Freeform surfaces play a significant role in contemporary architecture. Organic shapes, often inspired by nature, seem to have an appealing effect, especially to attract audience to the buildings of cultural institutions. In this context, shell structures have an additional advantage of being constructively effective, especially for widespan roof structures. To adapt freeform surfaces to shell-properties, it is necessary to modify both shape and structure.

The approach given here makes use of mesh representations with circular meshes. Circular meshes are planar quad (PQ) meshes, which have the additional property that each face has a circumcircle. Consequently, discrete differential geometry is the basis for the actual construction and the discretization of the given surfaces. The aim is to approximate the surfaces with freeform grid shells. Starting from principal curvature lines, we optimize the structural properties, as well as the supporting beam layout, with respect to optimal node properties. The circular mesh approach enables the generation of a PQ mesh with (nearly) planar faces.

The goal of the paper is to show how the combination of the applied methods can help to optimize freeform grid shell structures with respect to geometric properties (high level of mesh planarization, small deviation from the initial design), as well as structural properties (low deformation, low stresses). In this respect, the application of circular mesh optimization has a positive aesthetic impact and is also essential for building these shapes.

Keywords: grid shell structures; shape optimization; structural optimization; circular mesh systems; free-form geometry.

1. INTRODUCTION

Shells are structures that need a multidisciplinary overview in order to be built efficiently. They are a good representation of both structure and contemporary architecture design. Shells can be defined as a connection of three elements: *shape design*, *construction solving* and *geometry definition*. The first element reflects the problem that an architect faces and serves as an illustration of the story about the building that has to be told. When the idea has been defined, it is necessary to put construction to the test and see in which way the shell will be built and of which elements. The size, number and type of connections are crucial in this phase. The element's static efficiency is going to determine whether the structural strategy is beneficial or not. The geometry definition and optimization actually comes in the end of this process as a tool to reconcile the first two. In other words, if we start from the initial design, the analysis of the geometry is going to define what position is the best one for the elements in order to fulfil the architecture needs.

The PQ mesh optimization for equilibrium and face planarity is provided by Tang et al. (2014), where the success of this method is dependent on the initial mesh connections. Schiftner and Balzer (2010) propose a method for planar quad-remeshing of given surfaces, guided by principal stress lines. Pellis and Pottmann (2018) succeeded in designing principle meshes in equilibrium by aligning the membrane surface stress and curvature, although not all shapes are aesthetically appropriate given the variation in the element's size and number. For an introduction to principal meshes in architecture, we refer to (Pottmann 2012; Tošić et al. 2019).

These meshes are computed by a combination of optimization and subdivision and have been successfully introduced by Pottmann and Liu (2007). This optimization procedure does not convert any mesh, and there are some restrictions to the initial design. Moreover, precise geometric results and relations offered by discrete differential geometry are of high importance in architectural design (Brell-Cokcan et al. 2006; Cutler et al. 2006; Glymph et al. 2002; Liu et al. 2006; Pottmann et al. 2006; Pottmann et al. 2007), because their mesh representation (i) is visible and greatly influences the aesthetics and (ii) forms the basis for the actual construction (Pottmann et al. 2007; Tošić et al.2019).

There are two directions that can be taken when it comes to designing free-form grid shell structures. The first is to take inputs for designing efficient geometry for the best structural results. Inputs can be more regular shapes, such as translation surfaces, ruled surfaces, rotational surfaces and minimal surfaces, or just some limitations when it comes to boundary conditions, heights, area, curvature. With this approach, both structural and geometry results of individual elements but also the overall construction can be very satisfactory.

The second direction is to start from an already predetermined shape that has to be implemented as a design inspiration (*it is possible to deviate from it*). As a result, there has to be some compromise between the initial shape and the structural and geometry properties of the elements. The authors of the paper use this method and will show which methods are used to achieve the results and in which way by dealing with both the requirements of the individual elements and overall shape. Contributions of the paper are the following:

- Geometrical optimization of the free-form geometry to a circular PQ mesh system,
- Size, shape and number of the initial and final elements are similar,
- Construction properties are optimized (deformation is lowered),
- The final shape preserves the idea of the initial architecture design,
- Optimization algorithms are elaborated in C# and Grasshopper for Rhino.

2. RESEARCH METHODS USED FROM DISCRETE DIFFERENTIAL GEOMETRY

When it comes to a free-form shape in an arbitrary sense, i.e. the shape that does not have any distinctive properties, discrete differential geometry contributes with one of the largest ranges of methods for defining the characteristics of these shapes. The network of curves that are displayed on the surface is one of the most beneficial ways for free-form surface analysis. Nevertheless, it is very important to know which curves to choose. Conjugate curve network consists of two family curves with the following property: "*If we pick the first family of curves called A, the second one B is determined by connecting the vertices where the tangents of the first family A can be drawn, so that they can form a developable surface (Figure 1)* (Pottmann et al. 2012)." As a result, we obtain the tangent developable surface of the initial free-formed one. Although it does not seem like that, there is a variety of curves with this property on the surface. On the other hand, one must be very careful because not every curve network can be helpful for geometry analysis.

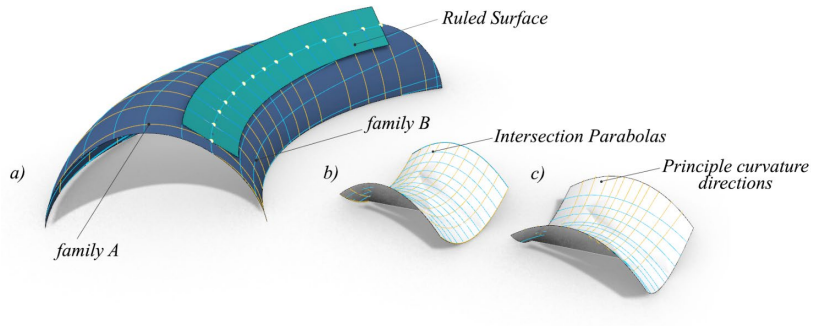

Figure. 1: a) Arbitrary geometry with the conjugate curve network of two family curves A and B. Tangents of the family curve A drawn on the points of the family curve B give the tangent ruled surface (green); Two examples of the conjugate curve network on a hyperbolic paraboloid: b) Translational curve network formed with parabolas as an intersection with vertical planes; c) Principal curvature lines; (reproduced from Pottmann et al. 2012)

Figure 1 represents two solutions for conjugate curve networks. The first is the intersection with vertical planes and an HP (hyperbolic paraboloid), which gives two direction parabolas. It can be seen that this one cannot be helpful in the determination of PQ systems of the surface, for example, because the rulings of the same family are skewed (Pottmann et al. 2012). The most important is the second example, which represents the principle curvature lines of the surface. For the arbitrary free-form surface, these curves present the most important property. They can be computed for every chosen point in the surface. Firstly, it is necessary to determine the direction with the biggest and lowest curvature. They are usually orthogonal, k1 and k2. That is done by establishing the tangent plane for the surface in the chosen point. The curve that is the result of the intersection of the orthogonal plane and the surface which has the biggest and lowest curvature in that point determines the directions of principle curvature lines. As a result, the radius of the curvature (tangent circle for the intersection curve) has to be the smallest (inverted function) (Figure 2).

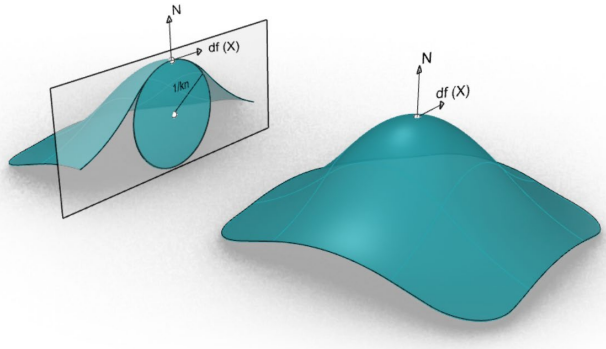

Figure. 2: The display of the procedure for finding the principle curvature direction on the arbitrary surface. It can be seen that the size of the radius of circle (kn) is inversely proportional to the curvature in the chosen point (1/kn)

2.1. Geometry benefits of circular meshes

There are multiple geometrical benefits when using principle curvature lines for the analysis of free-form surfaces. Firstly, discretization of the surface in the direction of the principle curvature lines results in the PQ mesh system (Pottmann et al. 2006). These PQ strips are actually tangent planes of the surface. Moreover, principle curvature lines are discretized edges of circular mesh systems (Pottmann et al. 2012). That means that every quad/face has a circle drawn around it, circumcircle (Figure 3). The same goes for the conical system, as circular and conical meshes are in a polar duality and can be easily transformed from one to another. Both of them have beneficial geometrical properties, which leads to a recommendation to use them for the free-form surface discretization. Their property of discrete normal that is defined as a radius (r) on the unit sphere is the direct consequence of the vertex mesh offset – a parallel mesh at the constant vertex-vertex distance (d=r). This means that every vertex belongs to the sphere and if the face is planar, a circle can be drawn around it (*proof lies in the intersection of the plane and sphere*). The vector that connects four vertices of the face and the centre of the sphere is one of discrete normals. The other system of discrete normals is the vector determined by two points, the centre of the circumcircle and sphere centre (Figure 3). As a result, circular mesh systems are very suitable for computation and optimization when it comes to free-form geometry (Pottmann et al. 2006).

Figure 3: Display of two sets of discrete normals of the circular mesh system

2.2. Construction benefits of circular mesh systems

Although very interesting and beneficial from the geometry point of view, circular meshes also possess certain properties that can exert substantial influence on the structural characteristics of the grid shells in free-form shape. Principal curvature lines are particularly suited for freeform structures in architecture, since they allow for a supporting beam layout with optimal node properties (Pottmann et al. 2012). Moreover, the offset mesh property brings several advantages when it comes both to individual elements and the overall structure. Firstly, as elements are flat, the production process is less complicated. One of the biggest problems is geometric torsion in the rod elements which can increase stress in elements during different loading cases. This happens if symmetry planes of the cross-sections of the four elements in a node do not intersect at a single line (Figure 4 right). Nevertheless, because of the offset mesh property, this can be avoided, as the vertex-vertex distance (Figure 4 left) actually defines the node axis and is at the same time the normal of the surface in the chosen point. Direction of offsets can be easily defined through the mapping of the parallel mesh system in the unit sphere (Figure 4 right).

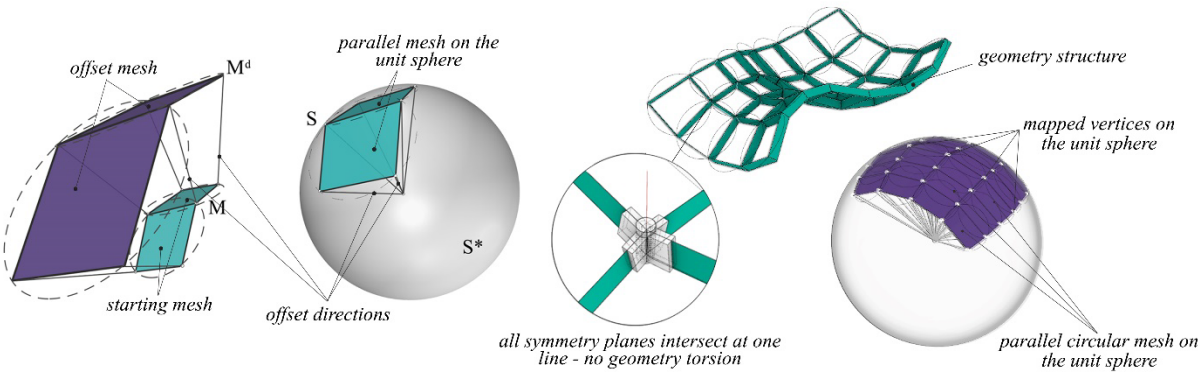

Figure 4: Mesh offset properties of the circular mesh system within the unit sphere (left) and computed for the entire structure (right)

As a consequence of the previously mentioned issues, in the case of double facades, the nodes can be at the same distance as well. Since the intersection of principle curvature lines is usually close to the orthogonal, this prevents the possibility of the existence of sharp angles between the edges in the grid shell. All this enables more uniformed prefabrication of both the elements and their connections. One of the methods that can be implemented is Christoffel duality as an inverted version of the construction process of parallel meshes in the unit sphere in order to obtain discrete minimal surfaces (Pottmann et al. 2006). This method cannot be implemented for the arbitrary mesh system but it may help in this case to achieve better edge guidance during the process of optimization (Tošić et al. 2019).

2.3. Christoffel duality method

This method has intrigued the authors as the one that connects the geometry and structural property of designed construction, when overlooking the statics response of the whole structure. It can be implemented entirely on isothermic surfaces (*surfaces of revolution, quadrics and constant mean curvature surfaces without umbilics (Bobenko et al. 1994)*), where, as a result, the reciprocal mesh, called a discrete minimal surface, is constructed. Such meshes are called *reciprocal parallel* and arise as *reciprocal force diagrams in graphical statics* (Pottmann et al. 2012). The starting and final one are both in static equilibrium and represent bijection functions. Figure 5 a) shows the mesh *S* that can be mapped on the unit sphere and the *M* is reciprocal one. In order to show the transformation procedure, Figure 4 b) shows the transformation of only one quad and a four-quad rule that posits the reciprocal relation as a method for testing. It can be seen from these drawings that a reciprocal quad is defined by drawing the reverse orientation of the edges with opposite diagonals parallel (Figure 5 b). Although this procedure can be performed for each quad separately, the real test of the transformation is whether this can be done for four quads. If the points do not overlap in the reciprocal one, this means that the rule cannot be implemented. It is then necessary to "fix" the starting meshes so they can adhere to the rule (Figure 5 c).

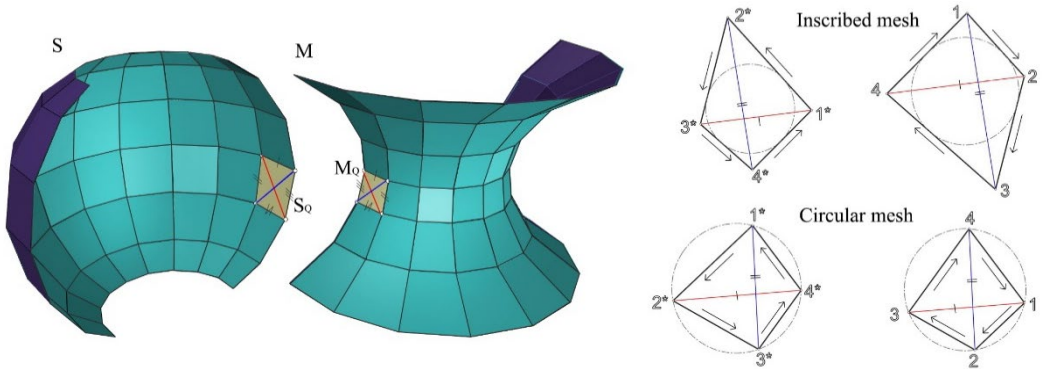

Figure 5: a) Koebe mesh (left) with its discrete minimal surface (right), b) Two parallel quads with reverse diagonals and vertex directions, c) the four-quad rule shown on the example of circular meshes (Tošić et al. 2019)

After the introduction to the methods that can be used for defining arbitrary free-form surface, the choice seems clear. The usage of principle curvature direction is necessary. If the analysis is done for the initial surface, the result usually leads to a very chaotic distribution of the curves (Figure 6 left). Even though they possess all the properties that were mentioned, it cannot be neglected that there are several downsides: *multiple elements per node*, *ununiformed size* and *shape of the elements*. This can be a crucial problem for the production and assembly processes. On the other hand, the standard u, v division of the surface possesses a more *uniformed size and shape of the elements*, *four elements per node*, but without planar elements or an optimal position of the rod elements for structural characteristics (Figure 6 right). The goal of the research is to take the best from both and make suitable compromises in order to utilize the benefits from the two.

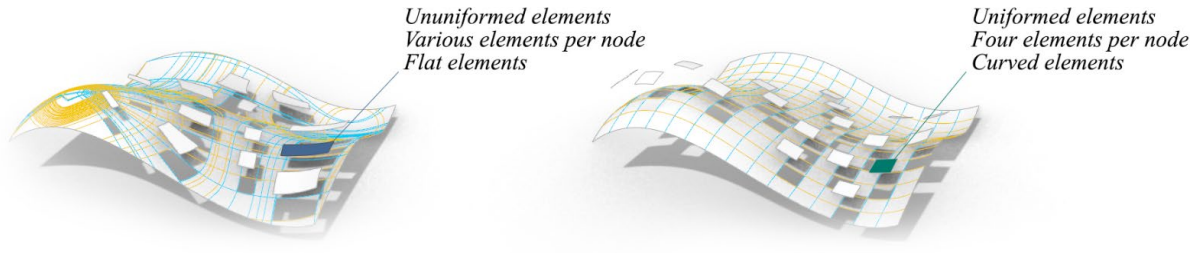

Figure 6: The division on the arbitrary free-form surface in the direction of principle curvature directions (left), regular u and v division of the same surface (right) with the characteristic of their elements

3. WORKFLOW OF THE RESEARCH

In this section, the workflow with the step-by-step process is going to be implemented on the first example of an arbitrary free-form surface. The goal is to show the combination and usage of the methods that have been presented, with their results showed in the end. The task states: "*Starting from the arbitrary free-form surface, optimize it into a circular PQ mesh for a grid shell structure while improving the structural characteristics of the overall shape and at the same time increase production benefits for individual elements.*" The workflow consists of the following steps:

1. Analysis of the initial geometry for principle curvature lines and making the starting u, v division in those directions.
2. Working on the "*quad by quad*" optimization by making every face PQ.
3. Checking the Christoffel duality for the *four-quad* rule and, if necessary, modifying the edge direction.
4. Transforming the mesh system into a grid shell construction and calculating stresses and deformation.
5. Comparing the geometrical and construction properties with the starting surface.

3.1. The first step – Analysis of the geometry

In this step, it is important to analyse the geometry of the initial surface that has been designed for the grid shell. This example is defined as a roof-like structure and it is a completely arbitrary free-form shape with a rectangular basis from the top view. The surface is double-curved, with both positive and negative curvature. Even though there are some concentrations and overlapping in the principle lines, two dominant directions can be seen (Figure 7 left). In this case, they are the usual u and v division of the surface. As a result, the starting division for the optimization is shown in Figure 7 right.

When it comes to the number of surface division, it can depend on more than one factor: for instance, the desired size of the elements, construction conditions (*stress in elements*, *type of cross section*, *mass, deformation*), span of the grid shell, etc. On the other hand, it also depends on the optimized construction and the way in which the number of division influences the characteristic, in this case, the circular mesh system. Several cases have been tested: u= v = 34, 30, 25, 20, 15 and 10. The highest number 34 is due to the calculation which has shown that after a larger division results are degrading. Cases 34, 30 and 25 are rejected since the production characteristics of elements are not suitable (*elements too small and very large number of elements*). Moreover, in order to fulfil the construction conditions (*the maximum allowed deformation*, *L/300*), the utilization of elements is not optimal. In the following phases, the remaining three cases are taken into consideration (n=*20, 15, 10*). All these analyses were conducted on the starting construction only in order to extract the unnecessary cases for further steps.

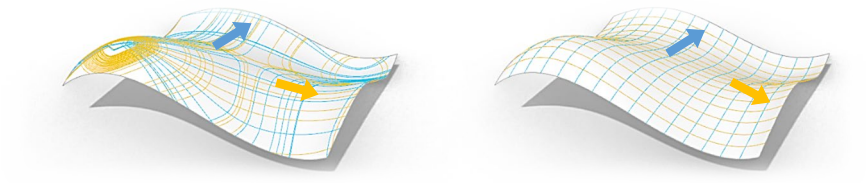

Figure 7: Analysis of the designed arbitrary free-form surface with principle curvature directions (left), the starting division of the surface in two dominant directions (right).

3.2. The second step – Making the division and optimizing the initial mesh into a circular one

After the ordinary u, v division, the obtained faces are not PQ and circular. The next step would be the "*quad by quad*" optimization system. Considering that the procedure happens as the name says "quad by quad", different effects and results can be gained depending on the starting position of the process. That is why the system is tested for various possibilities (Figure 8). There are three types of quads, and their definitions are provided in the following section. The position of the starting quad is marked in red, followed by the first columns and rows optimized (*orange*). The rest of the quads type three are yellow. The criterion for the most effective one is based

on the construction properties, which is the most important feature, but also the deviation from the starting shape (*the grey surface in Figure 8*) was tested. After the analysis, it has been concluded that the fifth procedure is the most effective one.

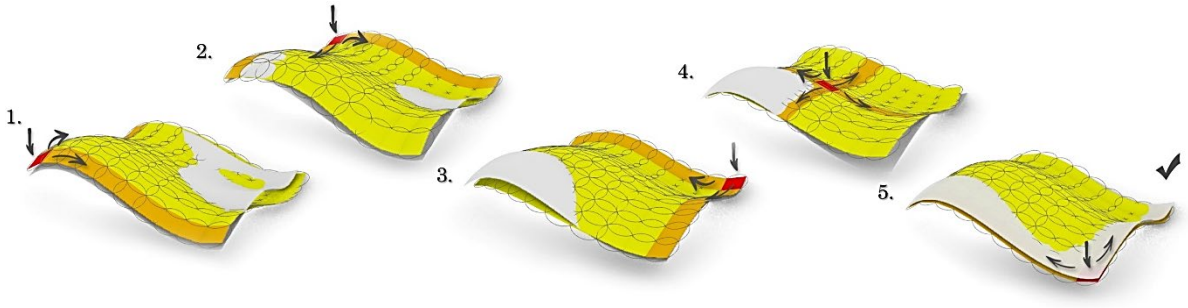

Figure 8: Analysis of the starting position of the "quad by quad" optimization process (coloured) with the overlapping starting shape of the surface design (grey).

"*Quad by quad"* optimization is an iterative process where we start from one quad mesh, map it into a sphere and perform projective transformations so that the final circular and planar mesh quad is as close as possible to the vertices of the initial quad (Figure 9) (Tošić et al. 2019). Throughout the process, there are four types of quads that are named by the number of fixed vertices. Depending on the number and position of those vertices in a quad, we have a free quad (*no fixed vertices – red*), quad-one (*one fixed vertex – does not exist in this example*), quad-two (*two fixed vertices – orange*) and quad-three (*three fixed vertices – yellow*) (Figure 9). The number of fixed vertices depends on the quad position in the mesh and the starting position of the optimization. Fixed vertices are the ones that optimized quads (*circular*) have determined and where the procedure continues. In Figures 8 and 9, it can be seen that most of the quads are type 3, as they have three fixed vertices from the previous iteration steps. This means that the final shape result largely depends on the starting position. That is why this was important to test in the previous step. (Tošić et al. 2019).

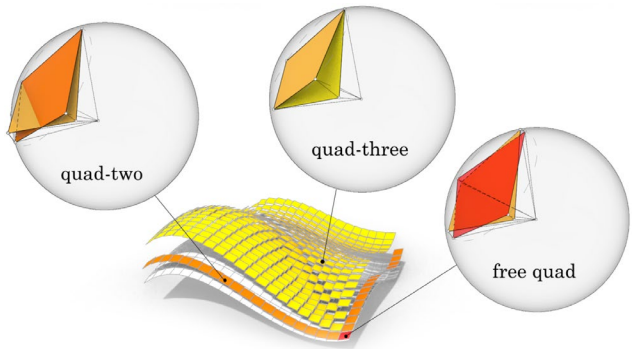

Figure. 9: "Quad by quad" optimization with the display of three types of circular quads depending on their position in the chosen starting procedure

3.3. The third step – Checking the edge directions with the help of the Christoffel duality method

During the process of transformation of curved quads into circular ones, one other method has been implemented. The above-mentioned Christoffel duality serves as a check-in within the four-quad rule that was shown in the previous section. It makes it possible to guide the direction of the mesh edges to the optimal one and prevent the quads to move zigzag while getting circular. This process is performed for every four-quad mesh, one by one. The transformation is done in Grasshopper and it guides the fourth quad in gravitating to establish the Christoffel duality. This is a part where circularity of the quad helps in guiding the vertices into proper dual quads, as it has a defined path (*circle*) to move. As a consequence, this works as in plane transformations and not the spatial transformation. Moreover, the final mesh does not deviate significantly from the initial shape, number and length of the elements. On the other hand, it is not possible to reach complete duality for the entire mesh. That is

why the mesh is not in complete equilibrium and the entire dual quad is not connected in each vertex. The steps are implemented on the example of the free-form shape displayed in Figure 10 (Tošić et al. 2019).

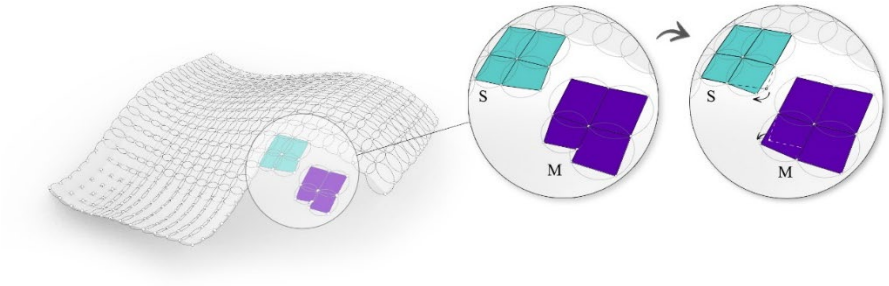

Figure 10: The display of the implementation of the Christoffel duality four-quad rule in the circular mesh

3.4. The fourth step – Calculation of both the initial and final construction for comparison

After a complete circular mesh system has been defined, it is materialized into a construction. Now the structure can be calculated and compared with the initial one. The used material is steel S355, with a tube cross-section and rigid connections between the elements. The support is placed on the boundary points of the mesh (Figure 12). The same characteristics are given to both constructions. Table 1 shows mass and deformations for four examples of the division: u=v= 10, 15, 20, along with the characteristics of the elements (*number and size*). As an addition, the fourth example is a transformed circular mesh from the same initial surface with 2% PQ deviation (Schober 2016) (*from the average diagonal length per face*). This solution is included here in order to analyse the construction conditions when compromises are made in geometry.

4. RESULTS AND DISCUSSION

The overview of the results is evaluated by two different criteria: *geometry and construction*. Four examples are compared in order to conclude how the changes in geometry, size, number and shape of the elements influence the construction properties and results.

Geometry optimization results: Properties of the elements of all seven grid shells can be seen in Table 1. The number of elements is the same when comparing the shells with the same number of division; the average length per element is quite similar as well. This was one of the goals from the start since it has been noticed that optimal direction for arbitrary shells was not so flattering when it comes to these properties. The average deviation of the PQ mesh (S_1, S_2, S_3) from the initial shape (S^*_1, S^*_2, S^*_3) increases until the number of division has been reached 15 (S_2). After that, it gets lower and stabilizes approximately around 1.64 m (S_3). The seventh example with the maximum 2% PQ deviation (M_3) shows that the final shape is two times closer to the starting one.

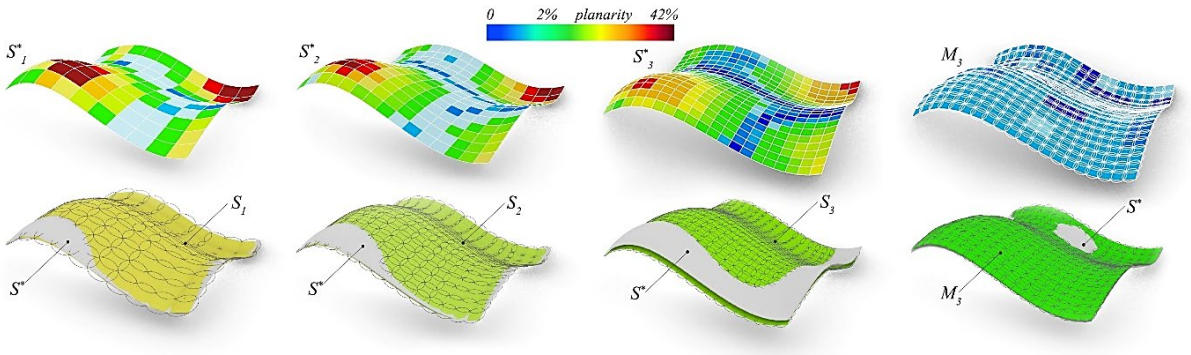

Figure 11: Display of the planarization of mesh panels in the initial shape S* and the optimized S (left), the overlapped S* with the new grid shell S and N overview of A circular mesh on the right

Construction optimization results: When it comes to the construction properties of grid shells, mass and deformation are presented. The difference in mass is not more than 1% between the matching examples. In all cases except the first one, the mass of the final (S_1, S_2, S_3) is larger than in the starting one (S^*_1, S^*_2, S^*_3). The difference in deformation is in favour of PQ meshes (S^*_1, S^*_2, S^*_3), but the percentage of optimization gets lower (27%, 17%, 4.5% etc.) as the number of division gets larger (n=10, 15, 20…). This means that if elements are larger (i.e. *number of division is smaller*), the effect of the PQ mesh optimization is bigger for the construction. We can conclude that the number and size of the elements and span of the construction will determine the limit for the number of division, but it is better to keep it as small as possible in order to get better construction results. When it comes to the way in which a slight change in the PQ mesh (*max 2% from PQ deviation*) can influence the construction, the last example (M_3) shows that the mass is 1% larger and deformation 0.5% lower when compared to a regular PQ mesh. In this case, production conditions, as well as the other stresses in elements, will have the biggest impact in the determination of whether this geometry compromise is beneficial for the final result.

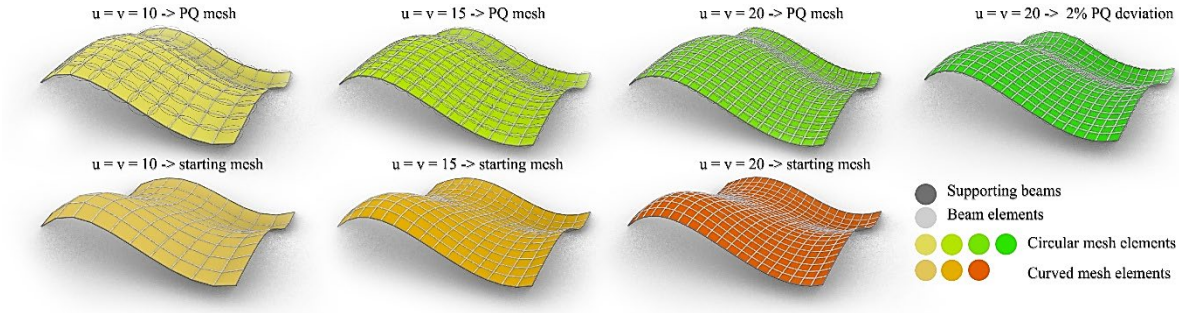

Figure 12: Display of all seven grid shells with their construction elements depending on the number of the elements and planarity

Table 1: The results of geometry and construction properties in the first example of all seven grid shells

Construction and geometry properties	S^*_1	S_1	S^*_2	S_2	S^*_3	S_3	M_3
Mass (kg)	*63 134 kg*	*63 08 kg*	*90 452 kg*	*91 913 kg*	*118 75 kg*	*119803kg*	*120 347 kg*
Deformation (cm)	*36.50 cm*	*26.60 cm*	*25.75 cm*	*21.30 cm*	*19.54 cm*	*18.66 cm*	*18.56 cm*
Number of division	*N= 10*	*N=10*	*N=15*	*N=15*	*N=20*	*N=20*	*N=20*
Number of elements	*400*	*400*	*900*	*900*	*1600*	*1600*	*1600*
Elements size (m)	*5.72 m*	*5.80 m*	*3.80 m*	*3.87 m*	*2.86 m*	*2.88 m*	*2.88 m*
Planarity deviation (%)	*0 – 45 %*	*0*	*0 – 32 %*	*0*	*0 – 23 %*	*0*	*0 – 2 %*
Average deviation from the initial shape (m)	*/*	*1.64 m*	*/*	*1.71 m*	*/*	*1.64 m*	*0.88 m*

5. THE SECOND EXAMPLE

For the second example, the two-axis symmetry arbitrary surface is given, also double curved. After the analysis of the principle curvature directions, two dominant directions are used for the initial surface division (Figure 13 a). The process of the "quad by quad" optimization is determined by the symmetry mesh that is made circular with all fixed vertices (Figure 13c) green), so that the starting quad is at the bottom of the shell and located on all four sides of the symmetry axis (Figure 13c) red). The quad-two (orange) is in the blue direction and most of the quads are type three (yellow) (Figure 13c)). Surface is optimized by two examples of division, N=13 and 22 (Figure 15), which are determined by the suitable size, number of elements as well as the cross-section utilization and maximum deformation construction properties. Results are shown in Table 2 and evaluated through geometry and construction characteristics.

Geometry optimization results: When it comes to the geometry properties of the initial shape, it can be seen that in the case of the lower division N=13 (S^*_1, S_1), there is a bigger difference in the number and size of elements. The reason is that sometimes more elements are needed to cover the whole starting surface in the direction of the division. This difference is smaller in the case of N=22 (S^*_2, S_2). Planarity is lowered from the maximum 66% (in N=13) and 28% (in N=22) to a totally planar PQ mesh (Figure 14). For this particular shape, the deviation from

the starting mesh is not that high. In both cases, the average is d≈0.90m and it can be noticed that the final shape did not change the initial design idea. On the other hand, the boundary shape does not overlap with the starting Top view square (Figure 15).

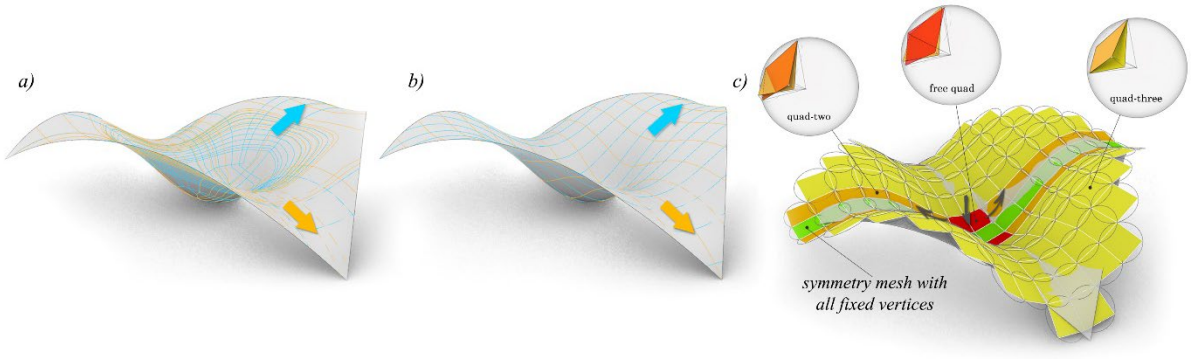

Figure 13: a) Surface analysis of the principle curvature directions; b) initial division in two dominant directions; c) display of the chosen "*quad by quad*" optimization process

Table 2: The results of geometry and construction properties in the second example of all four grid shells

Construction and geometry properties	S^*_1	S_1	S^*_2	S_2
Mass (kg)	*89 356 kg*	*89 876 kg*	*135 168 kg*	*137 968 kg*
Deformation (cm)	*9.19 cm*	*7.96 cm*	*5.75 cm*	*4.87 cm*
Number of division	*N= 13*	*N=13*	*N=22*	*N=22*
Number of elements	*676*	*608*	*1936*	*1952*
Elements size (m)	*4.96 m*	*5.40 m*	*3.80 m*	*3.87 m*
Planarity deviation (%)	*66 %*	*0 %*	*28 %*	*0 %*
Average deviation from the initial shape (m)	/	*0.87 m*	/	*0.88 m*

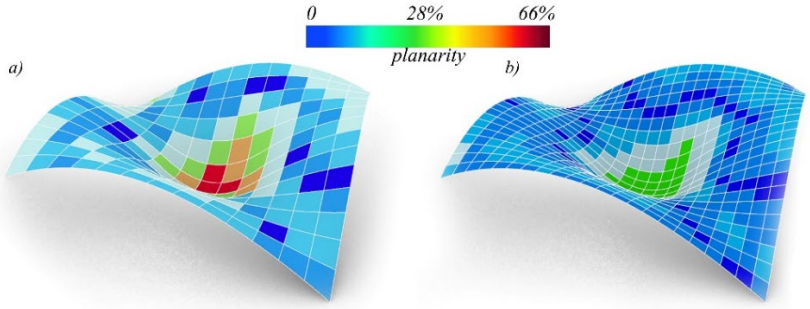

Figure 14: Display of planarity of the initial shapes with the number of division: a) N=13 and b) N=22

Construction optimization results: The complete construction is calculated as stated in the first example. There is a bigger difference in mass in the case of S^*_2, S_2 than in the first one S^*_1, S_1, where it is quite similar. In this example, optimization of the deformation is bigger (15%) when the number of division is bigger (N=22) than in the division N=13 (13%) (Figure 15).

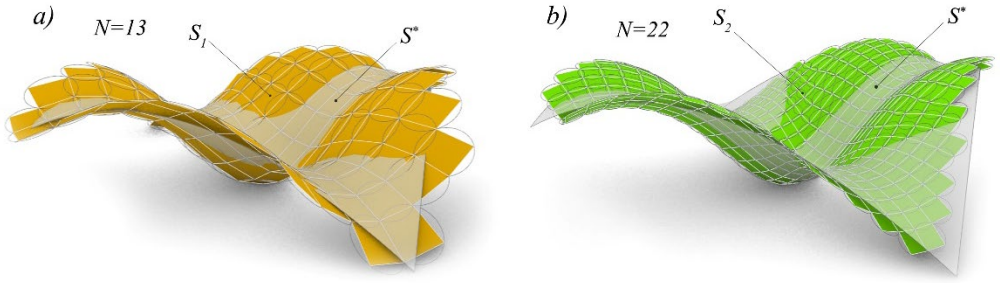

Figure 15: a) Optimized PQ circular meshes S_1 for N=13 (orange), b) S_2 for N=22 (green) with the overlapped initial shape S^* (grey)

When comparing this case with the first example, where the change in results had a different direction, it can be concluded that every example must be considered differently and that the results and the input depend on the initial geometry conditions. In both examples, the utilization of elements is larger in the PQ mesh system while getting a lower deformation, which also means that the forces are larger compared to the starting shape. This is one of the crucial things to work on in the future research.

6. CONCLUSION AND FUTURE IDEAS

A combination of methods from discrete differential geometry was used in this paper in order to create circular mesh systems and show how the grid shell structure can be optimized both geometrically and structurally. The main goal was to balance between the number of surface divisions and their size and topology, but also to improve the construction properties while obtaining a PQ mesh system from the arbitrary surface. This goal was achieved. It can be noted that the efficiency of construction results is directly influenced by the size and number of elements. When it comes to geometry, PQ mesh systems have a better potential for glazing grid shell structures, which can also make the elements' production easier and more efficient. On the other hand, by making some compromises in the geometry, such as in the M_3 example, there are more benefits for the construction and the final shape design. The limitations of this method lie in the nature of the principle curvature directions from the starting analysis. In some cases, it is not possible to have only two dominant directions to start from. Moreover, as the geometry goals are very predetermined, the final PQ circular meshes did not exploit all the property benefits presented in the second section of the paper. To achieve better results with this respect, future research should focus more on the starting topology division, which may be more adequate for a variety of the shapes and, at the same time, utilise the geometry input better. This is also closely related with the moment stresses in the elements whose results, in some cases, are not better in the final construction. In order to achieve better results, the input surface data have to be less strict and the focus has to be shifted from the entire surface shape to some necessary geometry conditions that are crucial to the architectural project. The main goal will also be to explore similar examples and attract better potential surfaces.

7. ACKNOWLEDGEMENTS

This contribution is a part of the priority project SPP 2187: Adaptive Modular Construction with Flow Production Methods – Precision High-Speed Construction of the Future in the subproject Formwork-free Flow Production of Adaptive Supporting Structures from Variable Frame Elements – Adaptive Concrete Diamond Construction (ACDC) funded by the German Research Foundation (DFG).

Dieser Beitrag ist Teil des Schwerpunktprojektes SPP 2187: Adaptive Modulbauweisen mit Fließfertigungsmethoden – Präzisionsschnellbau der Zukunft im Teilprojekt Schalungsfreie Fließfertigung adaptiver Tragstrukturen aus variablen Rahmenelementen – Adaptive Concrete Diamond Construction (ACDC) gefördert durch die Deutsche Forschungsgemeinschaft (DFG).

8. REFERENCES

1. Bobenko, A. and Pinkall U., 1994. Discrete Isothermic Surfaces. Göttingen Niedersächsische Staats- und Universitätsbibliothek Berlin SFB 288.

2. Brell-Cokcan, S., and Pottmann, H., 2006. Tragstruktur für Freiformflächen in Bauwerken. Patent No. A1049.
3. Cutler, B. and Whiting, E., 2006. Constrained planar remeshing for architecture, In Symp. Geom.Processing, Montréal, poster.
4. Glymph, J., et al., 2002. A parametric strategy for freeform glass structures using quadrilateral planar facets, In Acadia, pp. 303–321. ACM.
5. Liu, Y., Pottmann, H., Wallner, J., Yang, Y.L., and Wang, W., 2006. Geometric modeling with conical meshes and developable surfaces, ACM Trans. Graphics, 25(3): pp. 681–689.
6. Pellis, D., Pottmann, H., September 2018. Aligning principal stress and curvature directions, Advances in Architectural Geometry, Chalmers University of Technology, Gothenburg, Sweden, pp. 22-25;
7. Pottmann, H. and Wallner, J., 2006. The focal geometry of circular and conical meshes, Advances in Computational Mathematics, v29 n3 (200810). pp 249-268.
8. Pottmann, H., Bentley, D. (eds.), 2012. Architectural Geometry, Exton: Bentley Institute Press;
9. Pottmann, H., Brell-Cokcan, S., and Wallner, J., 2006. Discrete surfaces for architectural design. In Curve and Surface Design: Avignon, Nashboro Press, pp. 213–234.
10. Pottmann, H., Liu, Y., 2007., Discrete Surfaces in Isotropic Geometry, Berlin; New York: Springer Verlag, Lecture notes in computer science. no. 4647: pp. 341-363.
11. Pottmann, H., Liu, Y., Wallner, J., Bobenko, A., and Wang, W., 2007. Geometry of multi-layer freeform structures for architecture, ACM Trans. Graphics, 26(3).
12. Schiftner, A. and J. Balzer, 2010. Statics-sensitive layout of planar quadrilateral meshes, In C. Ceccato et al. (Eds.), Advances in Architectural Geometry, Springer, pp. 221–236.
13. Schober H., 2016. Transparent shells form topology structure, 1 Edition. Ernest & Sohn GmbH & Co. KG.
14. Tang, C., X. Sun, A. Gomes, J. Wallner, and H. Pottmann, 2014., Form-finding with polyhedral meshes made simple, ACM Transactions on Graphics 33(4), pp. 1–9.
15. Tošić, Z., Krasić, S., Kostić, D., 2019. Design and optimization of grid shell structures using Christoffel duality, Proceedings of IASS Annual Symposia, Barselona, pp 1-8.

ISOPHOTES OF ROTATIONAL CONE FOR CENTRAL LIGHTING

Isidora Ratajac
Department of Architecture, Faculty of Technical Sciences, University of Novi Sad, Novi Sad, Serbia
Undergraduate student, isidora.ratajac99@gmail.com

Dimitrije Nikolić
Department of Architecture, Faculty of Technical Sciences, University of Novi Sad, Novi Sad, Serbia
PhD, Assistant with PhD, dima@uns.ac.rs

ABSTRACT

Isophotes represent the locus of surface's points of equal brightness, and are originally considered in descriptive geometry problems regarding shadow determination. They are applied in computer graphics for producing more realistic presentation of illuminated objects and their spatial relation.

In the present paper, the determination of the isophotes of rotational cone is considered. It is shown that the descriptive geometry method of auxiliary spheres' isophotes, commonly applied to parallel lighting, can also be used when central lighting is present. Namely, contrary to parallel lighting, in which the spatial relation between the spheres and the light source is constant, in the case of central lighting, this relation becomes variable. Accordingly, the corresponding parameters are noted and the suitable method for the determination of the sphere's isophotes is derived. Since it enables the direct construction of the desired angle between the light ray and the auxiliary spheres' tangent plane, the developed procedure is applied to rotational cone. Furthermore, admissible shapes of cone's isophotes as well as the corresponding characteristic elements are inspected.

Keywords: isophote; descriptive geometry; shadows; central lighting

1. INTRODUCTION

When presented objects are pictured illuminated with light rays, they become more realistic and textured. Shadows of the observed and surrounding objects give the image better notion of spatial relations. It is common for light rays to come from one light source, and in geometric optics are considered as limit cases of a light cone the opening angle of which tends to zero (regardless of the dimensions of the light source, being considered as a point) (Anagnosti, 1966). Long distance of a light source (the sun or the moon that are considered as infinitely distant points), indicates parallel lighting with cylindrical beam of (parallel) light rays (Fig. 1a). Alternatively, if the source (candle, lamp) is close to the object, there is a bundle (cone) of light rays – central lighting (Fig. 1b).

Solid's sides can either be illuminated or in self-shadow, depending whether light rays reach the surface. The border between those two parts is called illumination dividing line – spatial curve or polyline in which light rays are tangential to the surface. When the direction of (parallel) projection coincides with the direction of parallel lighting, illumination dividing line and the surface's contour (visibility dividing line) also coincide, and are, accordingly, determined the same way (s. Brauner 1986). The intensity of surface illumination depends on the glancing angle of the light ray, i.e. its inclination with respect to tangent plane at the piercing point. Greater angle implies higher intensity of illumination, the brightest point then being the one in which light ray is perpendicular to the surface. In the case of parallel lighting, every plane forms one angle with the given light ray (Fig. 3a), while for a given central lighting, since light rays are not parallel, each ray has a different inclination, giving a unequally illuminated plane.

Isophotes represent curves, the locus of surface's points of equal brightness (points in which light rays form the same angle with the surface). Therefore, surface is divided by isophotes into parts more or less illuminated. For curved solids, the glancing angle is variable all along the surface, whereas in the case of polyhedron, the change of the rays' inclination occurs at the edges (s. Niče, 1967, p. 318). Isophotes of rotational surfaces are commonly

determined using the method of auxiliary spheres and its characteristic elements. These problems have been considered in the case of parallel lighting and solved accordingly (s. Niče, 1967; Štulić, Atanacković, 2003). Namely, the position of the sphere does not affect its brightness, since the orientation does not change with respect to the given direction of light rays. Therefore, isophotes retain the same proportions, i.e. disposition along the spheres, regardless the sphere's diameter or position (s. Figs. 2a and 7).

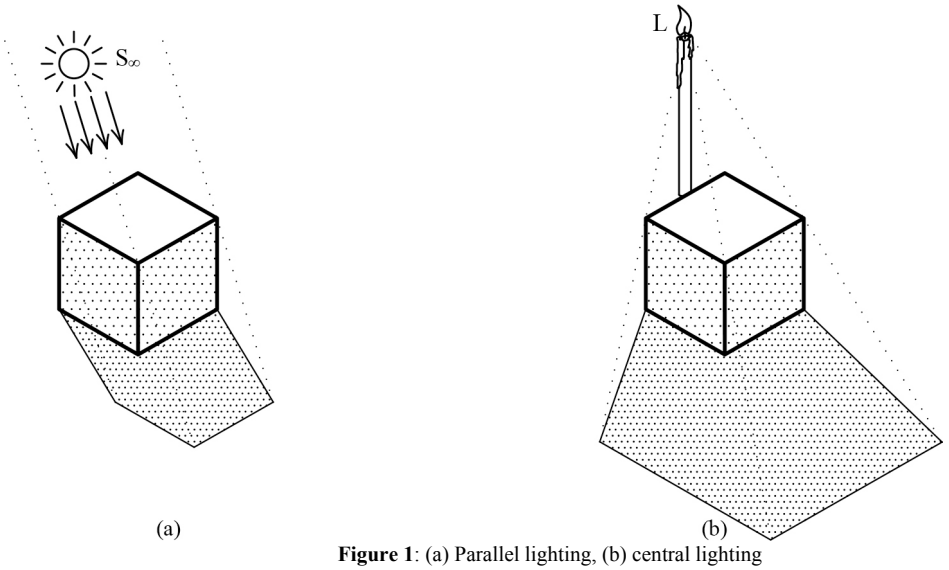

Figure 1: (a) Parallel lighting, (b) central lighting

A sphere with the centre *O* and the light ray *s*, representing the direction of parallel lighting, are shown in Fig. 2a. In order for isophotes to be determined, it is necessary for the light ray to be seen in true size (or the characteristic projection to be chosen). The piercing point of light ray that contains centre of the sphere defines the brightest point, whilst the dividing line is sphere's great circle perpendicular to the ray. In accordance with the desired frequency of isophotes, the sphere has been divided so that inclined angle of the light rays differentiates by 15°. Thus, between dividing line and the brightest point, five isophotes, represented as parallels (circles) that are in view position in characteristic projection, have been set. The angle between the light cylinders and the corresponding tangent cones is easy to construct, as shown in Fig. 2b. However, since in the case of central lighting, by changing the position of the sphere relative to the light source, the light rays' inclination alters, and therefore the determination of isophotes becomes more complex (Fig. 2c).

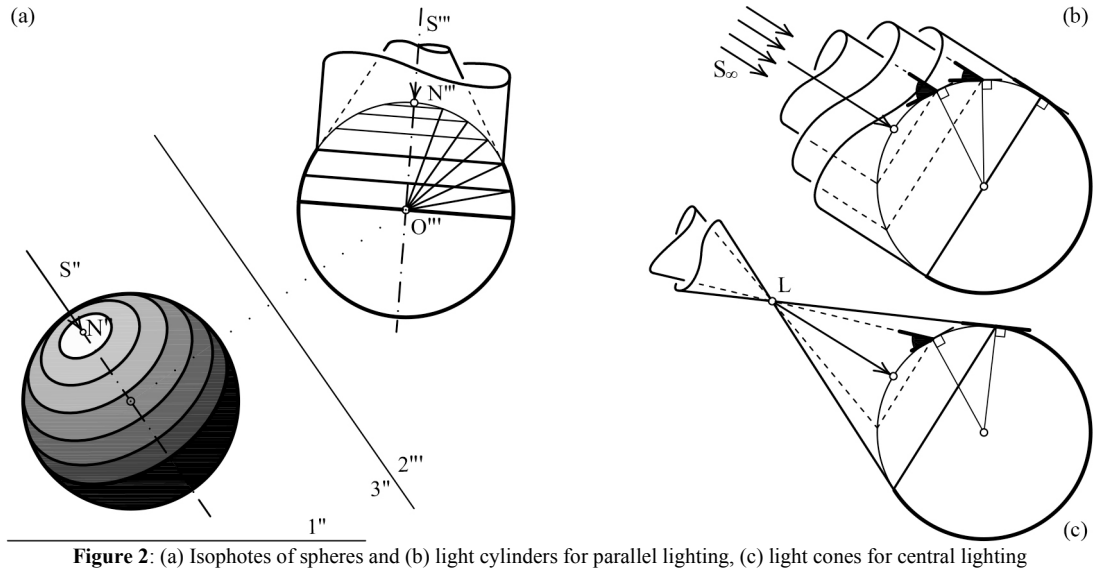

Figure 2: (a) Isophotes of spheres and (b) light cylinders for parallel lighting, (c) light cones for central lighting

Accordingly, isophotes of rotational cone for central lighting have been chosen as the subject of the present research. The aim is to derive a general method for determining sphere's isophotes for a given central lighting and

its use within noting characteristic elements of rotational cone's isophotes. The elaboration of the problem will be within methods of descriptive geometry, considering characteristic elements of auxiliary spheres.

2. ISOPHOTES FOR CENTRAL LIGHTING

When the light source is at a finite distance, certain parameters that are valid for parallel lighting, are changed. Since the inclination of light rays differs, a plane is not equally illuminated. The plane's isophotes are obtained as a intersection of the plane and a light cone whose rulings (generatrices) have the same inclination; consequently, the isophotes have the shape of concentric circles. When the plane is in view position, light rays of desired inclination can be set directly. Thus, the ray perpendicular to the plane gives the brightest point, while other rays are set stepwise (15°) in Fig. 3b. Extreme points – highest and lowest, are defined as the piercing points of light rays.

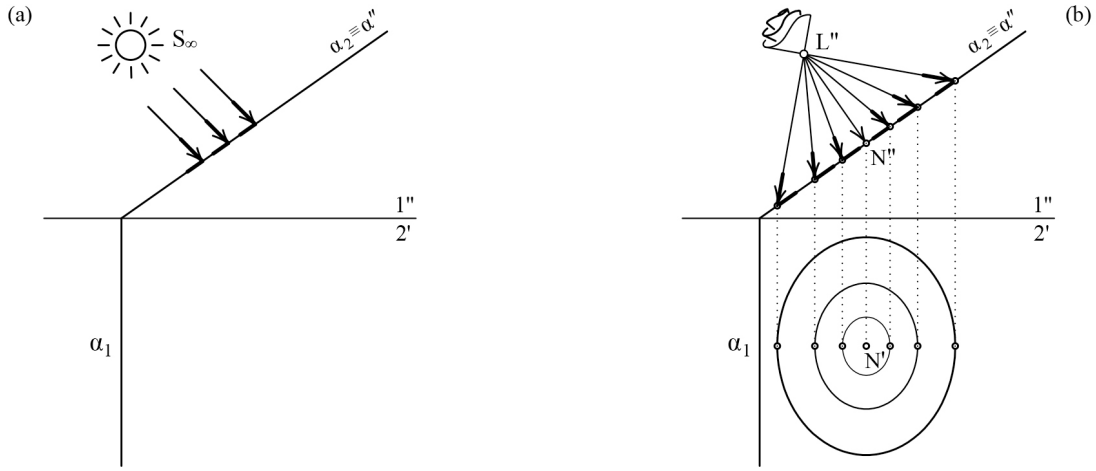

Figure. 3: Illumination of a plane: (a) parallel lighting, and (b) central lighting

The determination of the brightest point and dividing line on the sphere in the case of central lighting is identical to the parallel lighting: the brightest point is given by the light ray passing through the centre of the sphere, while the dividing line is the sphere's circle in which the corresponding light cone is tangential to the sphere. The change of the position of the sphere relative to the light source, affects the opening angle of the tangent light cone, as well as the position of the dividing line. As stated, opposed to parallel lighting, where the inclined angle between the light ray and tangent plane of the sphere can be directly determined, in the case of central lighting, it is not known how to appoint the light ray for the wanted angle. Therefore, the construction of wanted angle between the light cone and the sphere's tangent cone has been set as the primary task of the present research.

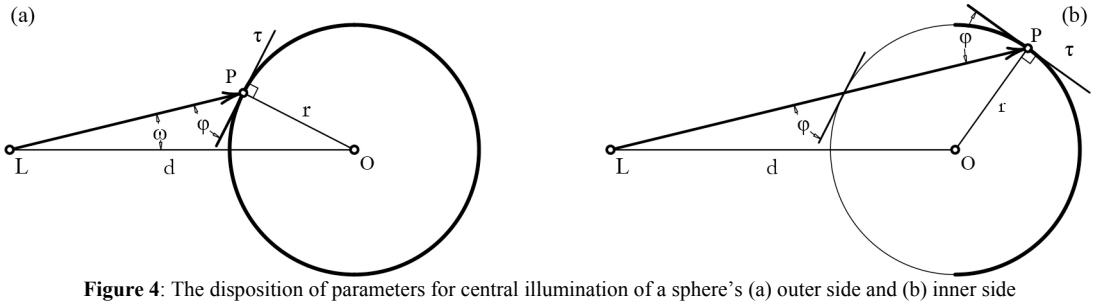

Figure 4: The disposition of parameters for central illumination of a sphere's (a) outer side and (b) inner side

The parameter *d* describes the distance between the sphere's centre *O* and the lamp *L*, the value *r* denotes the diameter of the sphere. The angle φ represents a desired angle between the light ray *s* and the tangent plane τ, while the angle ω is an angle with respect to the direction *d*. Considering the triangle *OLP*, the relation between the specified parameters can be established with the sine theorem:

$$\frac{d}{sin(90° + \varphi)} = \frac{r}{sin\,\omega} \qquad \text{(Eq. 1)}$$

Hence, the value of the desired angle can be expressed as follows:

$$\omega = arcsin\left(\frac{r}{d}cos\,\varphi\right) \qquad \text{(Eq. 2)}$$

Moreover, this equation can be represented by a geometrical construction where four parts can be distinguished:

- The cosine of an arbitrary angle, which can be defined by the trigonometric unit circle (Fig. 5a);
- The ratio between two lengths, which can be represented by the hypotenuse of a right triangle having sides equal to these lengths (Fig. 5b);
- The product of two values is obtained on the base of the similarity between the triangle *OLM* and the corresponding triangle having one side equal to cosφ (Fig. 5c);
- Arcus sine of the previously obtained value is also determined on the trigonometric circle (Fig. 5d).

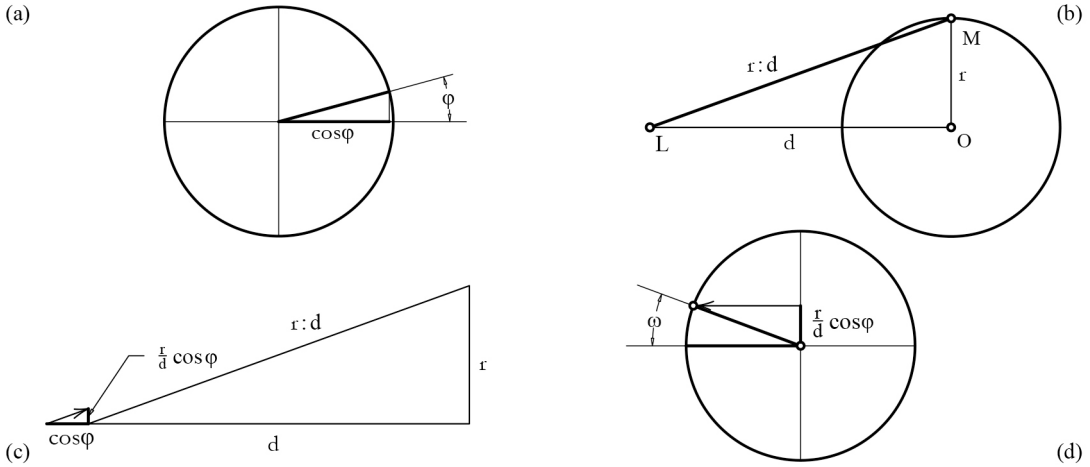

Figure 5: Geometric constructions: (a) cosine of the angle φ, (b) the ratio between sphere's radius and the distance of a lamp, (c) the product of two values, (d) arcus sine

These individual geometric constructions can be combined into a single construction shown in Fig. 6, outlining the overall procedure for determining the isophote referring the desired angle. This method is valid for one isophote on the sphere and must be repeated for each isophote on one or another sphere which is in a different position to that of the lamp.

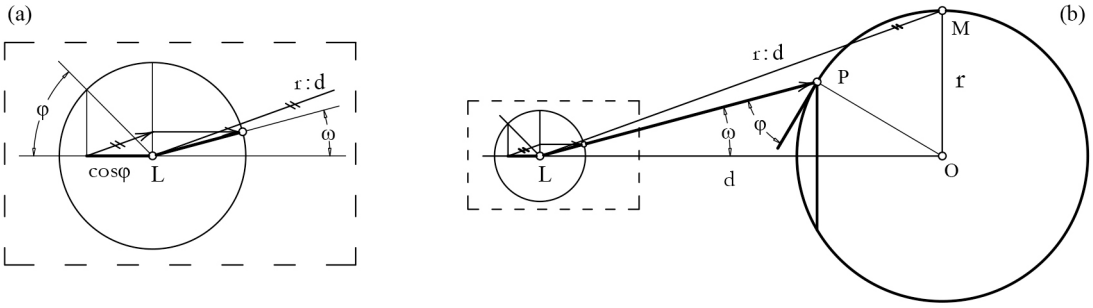

Figure 6: (a) Enlarged view of construction detail, (b) overall geometric construction for determining a sphere's isophote under central lighting

3. ISOPHOTES OF ROTATIONAL CONE

As mentioned, isophotes for rotational surfaces can be solved by the use of auxiliary sphere method. Thus, along every parallel of the cone, a coaxial sphere has common tangent planes as well as the points of the corresponding isophotes. Depending on the wanted level of detail, the number of parallels (and corresponding auxiliary spheres) is presented accordingly.

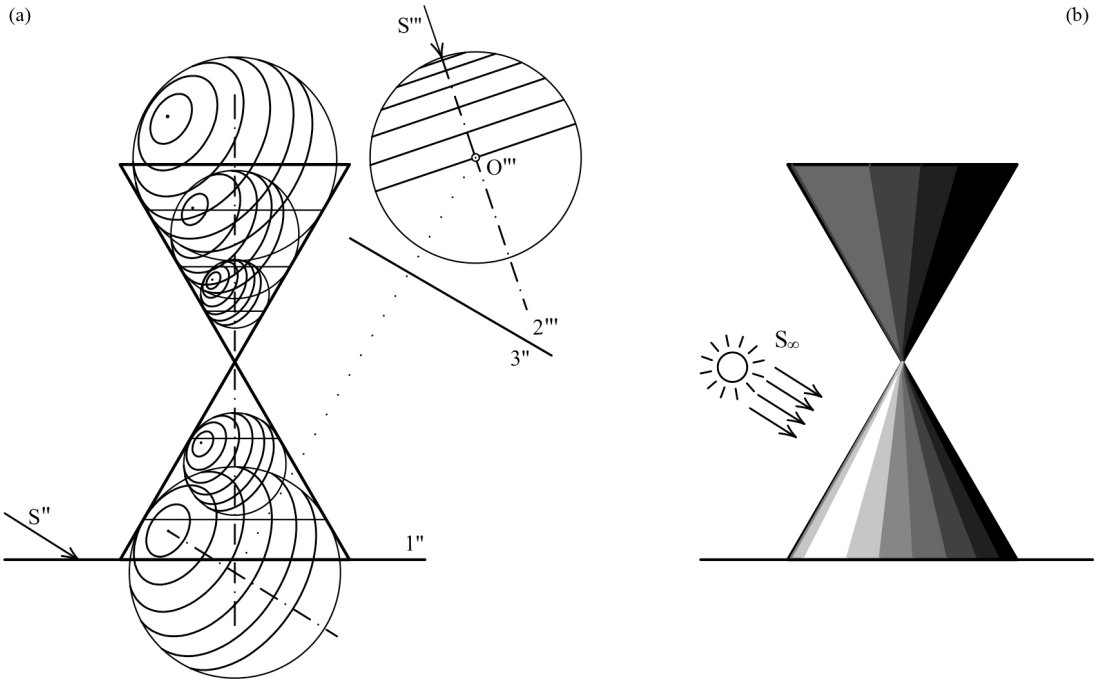

Figure 7: (a) Auxiliary spheres for the determination of rotational cone's isophotes under parallel lighting, (b) shaded rotational cone

A vertical rotational cone and its auxiliary spheres with isophotes under parallel lighting, are shown in Fig. 7a. However, central lighting alters relation between the lamp and the rotational cone, which determines the shapes of isophotes. When the lamp is at the level of the cone's apex, both cone's branches are identically illuminated and have symmetrical isophotes, with one brightest point each (Fig. 9a). On the contrary, the lamp may be higher or lower with respect to the cone's apex, in which case isophotes are not the same and the brightest point could occur only on one branch of the cone (Fig. 9b,c). Since both branches behave equally when illuminated, henceforth only one branch will be considered.

With no effect to the generality of the solution, the lamp and the (vertical) axis of the cone are placed in a frontal plane. Front view then being characteristic, hence the lowest and highest points can be directly determined at the contour generatrix (cf. Fig. 3b and Fig. 8). It is convenient to allocate those points as the determinants of the cone's and auxiliary spheres parallels on which the isophotes will be found. Since the radius of the sphere, its orientation and distance from the light source change, the spheres act differently and therefore the previously shown construction must be applied for each sphere separately. Spheres which tangent planes form an angle with the light rays of 15, 30, 45, 60, 75 and 90 degrees are presented in Fig. 8a. By connecting the points of corresponding isophotes on the parallels, isophotes of the cone are obtained (Fig. 8b).

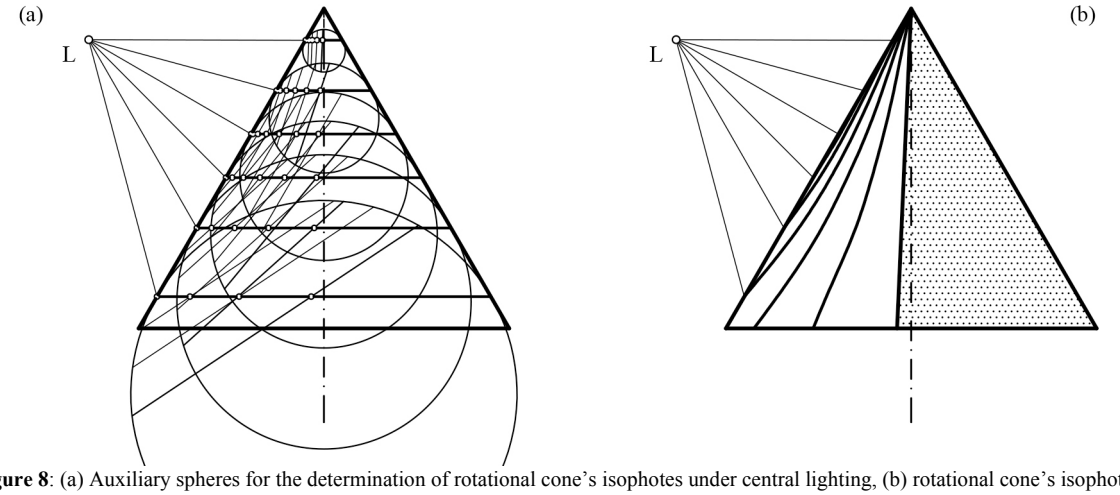

Figure 8: (a) Auxiliary spheres for the determination of rotational cone's isophotes under central lighting, (b) rotational cone's isophotes

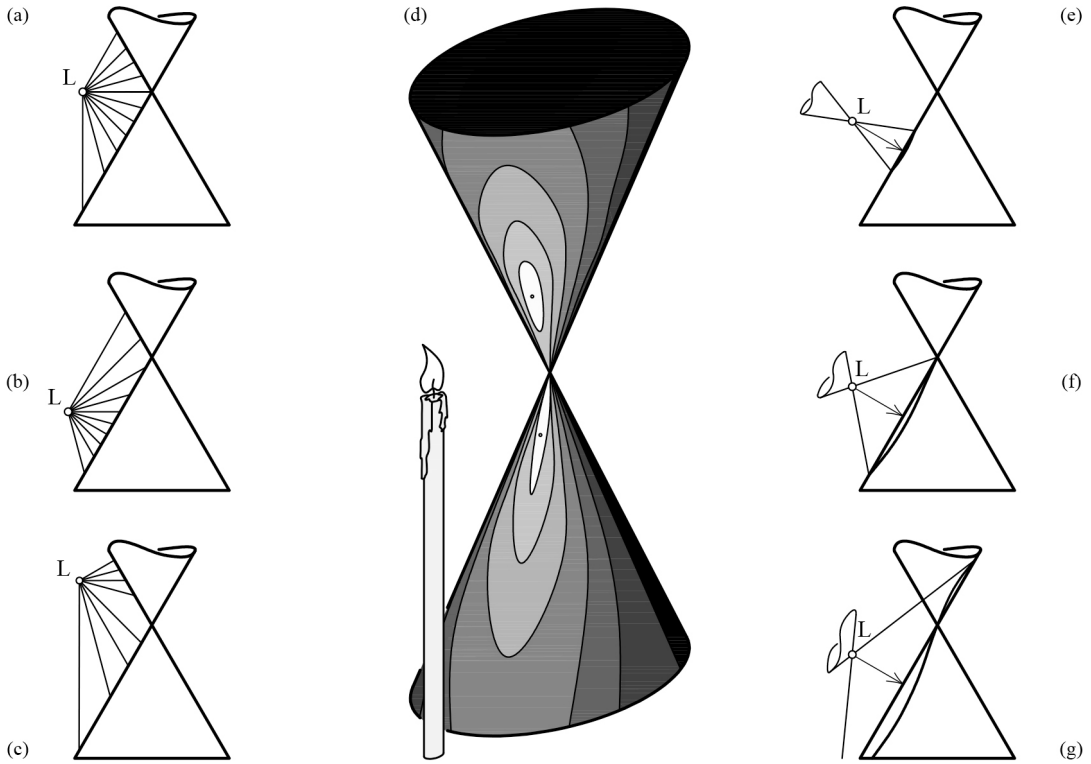

Figure 9: (a) The lamp and the cone's apex at the same height (symmetrical isophotes), (b,c) the lamp and the cone's apex at the different heights (asymmetrical isophotes), (d) rotational cone's isophotes shown in oblique projection, (e) oval isophote, (f) isophote with a cusp,(g) lemniscate-like isophote

Depending on the relative position of the light and the given (illuminated) cone, the following shapes of isophotes may be noticed:

- Point – limit case of isophote which corresponds to the brightest point;
- Spatial oval curve – the light cone penetrates only one branch of the given cone (Fig. 9e);
- Spatial curve with a cusp (at the cone's apex) – the light cone contains the apex of the given cone (Fig. 9f);
- Spatial lemniscate-like curve – a light cone cuts both branches of the given cone. Namely, if the intersection of two cones are considered (along the same rulings of both branches), two parts of the intersecting curve are formed: real part – on the one branch of the cone, lying at the (outer) side closer to the lamp, and imaginary part – on the other cone's branch, lying on the (inner) side further from the lamp. The characteristic elements of the imaginary part of the curve can also be determined by the auxiliary sphere method, with the inner side of the sphere being considered in this case (cf. Fig. 4b and Fig. 9g). It should be noticed that the derived analytical expression as well as the procedure for constructing the desired inclination of light ray are also valid in this case.
- A pair of straight lines – a limit case in which the light cone degenerates into the light plane and the lemniscate splits into two cone's rulings.

In order to represent isophotes more accurately, it is necessary to determine their behaviour, i.e. tangent lines at some of their points. Characteristic points of the isophotes are the highest and the lowest one, having horizontal tangent lines. Since the isophote is the intersection of two cones, the tangent line at a arbitrary point is defined by the intersecting line between the corresponding tangent planes of the cones, which is determined by the usual procedure for the intersections of two curved solids (s. Brauner 1986; Dovniković 1994).

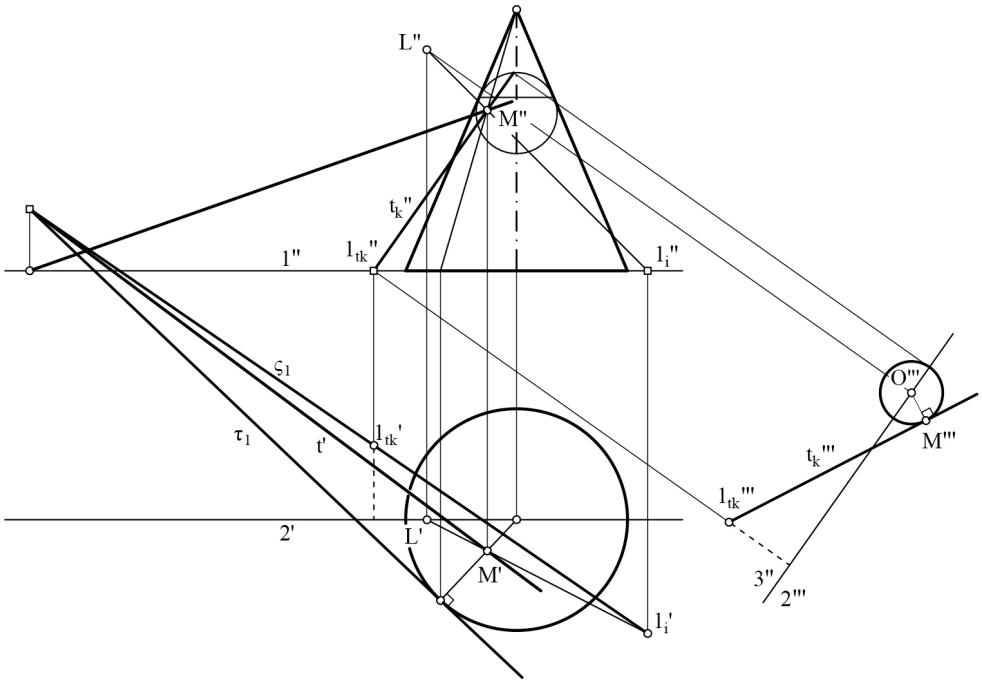

Figure 10: The determination of the tangent line at an arbitrary isophote's point

Tangent plane of the light cone can be defined by its generatrix and isophote's tangent line of the auxiliary sphere's circle. Let the point *M* represent an arbitrary point of the isophote. To determine the tangent line of the auxiliary sphere's isophote through the point *M*, the projection in the direction of the axis of the light cone is introduced in order for the sphere's isophote (circle with the centre *O*) to be seen in true size (Fig. 10). The circle's tangent line, being incident to the tangent plane of the light cone, can be directly set in that projection. Its piercing point through the horizontal plane (containing cone's base) is noticed in front view (where the circle's plane is in view direction), and along with the piercing point of the light cone's generatric (being incident to the point *M*) defines the trace of the light cone's tangent plane. Moreover, the trace of the given cone is presented by the tangent line of the base circle. The straight line which is defined by the point *M* and the intersecting point of the two traces, represents the tangent line of the cone's isophote at the point *M*.

4. CONCLUSION

In the present paper, the problem of the determining the rotational cone's isophotes has been elaborated. It has been shown that the method of auxiliary spheres, commonly applied to parallel lighting, can also be used in the case of central lighting. However, the occurrence of new parameters has been noticed, with respect to the variable mutual relation between the sphere and the light source. Hence, the procedure for defining the sphere's isophote, by which the desired angle between the light ray and the sphere's tangent plane can be directly constructed, has been derived. Accordingly, characteristic elements have been analysed and possible shapes of rotational cone's isophotes have been considered.

The derived method can also be applied to the solving of more complex rotational surfaces' isophotes. Therewith, during computational processing, the analytical expression derived in the present paper would be more appropriate than the geometrical construction. Furthermore, the properties of the lines thus obtained, representing isophotes, may be inspected in further research.

ACKNOWLEDGEMENT

This research has been supported by the Ministry of Education, Science and Technological Development through the project no. 451-03-68/2020-14/200156: "Innovative scientific and artistic research from the Faculty of Technical Sciences (activity) domain".

REFERENCES

1. Anagnosti, P., 1966. Nacrtna geometrija. Naučna knjiga, Beograd.
2. Brauner, H., 1986. Lehrbuch der Konstruktiven Geometrie. Springer-Verlag, Wien New York.
3. Niče, V., 1967. Deskriptivna geometrija. Školska knjiga, Zagreb.
4. Dovniković, L., 1994. Nacrtna geometrija. Univerzitet u Novom Sadu, Novi Sad.
5. Štulić, R., Atanacković, J., 2003. Implementation of computer technologies in descriptive geometry teaching: surfaces of revolution. *Facta Universitatis, Series: Architecture and Civil Engineering*, 2(5), pp. 379–385.

moNGeometrija 2020

DESIGN STYLES IN LANDSCAPE ARCHITECTURE

Radenka Kolarov
Department of Fruit growing, Viticulture, Horticulture and Landscape architecture, University of Novi Sad, Faculty of Agriculture, Novi Sad, Serbia
MSc., PhD student, Junior Researcher, kolar.rada@gmail.com

Milena Lakićević
Department of Fruit growing, Viticulture, Horticulture and Landscape architecture, University of Novi Sad, Faculty of Agriculture, Novi Sad, Serbia
PhD., Associate Professor, milenal@polj.uns.ac.rs

Beata J. Gawryszewska
Department of Landscape Art, Warsaw University of Life Sciences, Warsaw, Poland
PhD., Associate Professor, beata_gawryszewska@sggw.pl

ABSTRACT

Since ancient times, landscape design has developed along the lines of two basic styles: geometric and landscape design style. The geometric style encompasses elements of order, proportion, rational planning and often symmetry; and has reached its peak in the period of French baroque. The landscape style is usually irregular, "informal" and simple, and is commonly related with the English romantic gardens. Since the modern art period, these two styles merge into what we recognize as the combined (mixed) design style and nowadays, the combined style is commonly seen in urban landscapes. This paper analyses the basic principles of designing a space in: geometric, landscape and combined style, with main references from history of landscape architecture. As a case study, we have selected an atrium space in Novi Sad, Serbia. On one hand, this paper describes basic principles for designing a space in a particular style, and on the other hand paper analysis main differences in between above mentioned landscape styles. The main goal of the paper is to provide guidelines for designing a space in different styles, and to emphasize its importance in terms of biodiversity preservation, social interaction, and improving visual qualities of urban landscapes.

Keywords: landscape architecture; geometric style; landscape style; combined style; visual impact

INTRODUCTION

Landscaping, landscape gardening, landscape engineering, landscape design, landscape planning are just some of the names under the field of landscape architecture. Importance of landscape architecture is often easy to explain comparing buildings that has been adequately landscaped with those in which the landscaping has been neglected or missing. Such comparison will show that a poor arrangement of the landscape can certainly decrease the value of a well – designed building. Design of a landscape in ancient times was determined under the regulation of cities. The gardens of ancient times, especially Egypt and Persians, are characteristics with a geometric shape of a garden with irrigated agriculture (Lakićević and Kordić, 2018). Such gardens reflected climatic, religious and physical influence and they were not part of a natural landscape. The gardens occupied a square or rectangle shape of a land and were surrounded by lofty (Egypt) or mudy (Persia) walls (**Figure.** 1). In the middle of the gardens, especially in Egypt, were vineyards and rows of trees. Buildings within the walls were shaded by high trees, mostly palm trees. The grounds were divided by intersecting raised paths with low fences and enhanced with water

features (ponds, waterfalls, blue tiled pools) and green borders. In Persian time a structures started to occur as a precursor of a nowadays mobiliar, such as pavilions, kiosks, small summer houses etc.

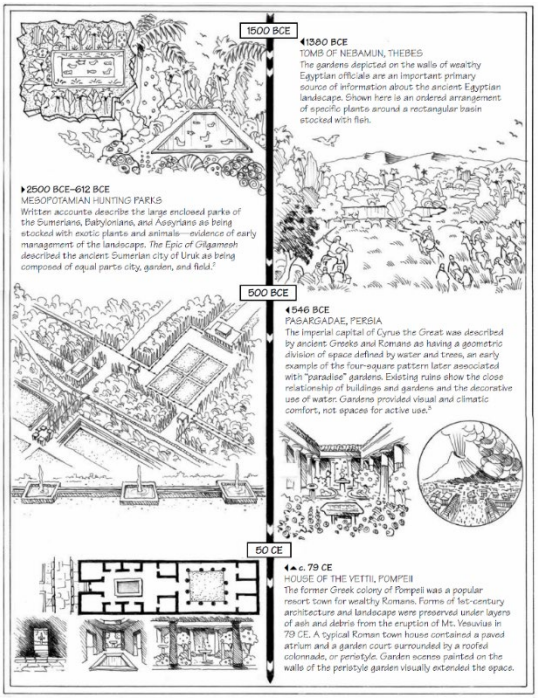

Figure. 1: Ancient gardens
(Source: Boults, 2010)

In the early Greek cities has progressed and they included baths, stadiums, open-air theaters and colonnades, still maintained in the geometric shape. In a point from Middle Age to Modernity occurred Renaissance. Gardens in that period were constructed around the villas and were closely adapted to the Italian hillsides. Main keys to determination of Renaissance gardens: contracted on a slopes that gardens naturally followed, including three or more terraces faced with stone and equipped with staircases (Newton, 1971). Each terrace had its purpose, for instance, the lower level contained the flower garden and the principal approach, on the second level were a buildings and the upper levels included the woodland, and the water was an indispensable element in the whole garden. The Spanish gardens of the Renaissance were also notable. They occupied lofty sites and had arcaded courts. They made use of channels, fountains, and jets of water, rows of potted plants and tile decorations. Palms and orange trees framed more distant vistas. Some of the Renaissance gardens of France achieved great distinction. The grounds at the Palace of Versailles (**Figure.** 2) were among the most distinguished and spectacular. Their most outstanding features were an intricate pattern of cross-connecting avenues, an amazing display of statues, cascades, and fountains, and a canal a mile or more in length (Lohmann, 1963). The basic characteristic of the Renaissance gardens was its formality; it was balanced and orderly. Its planes, patterns and shapes were still in a geometric style.

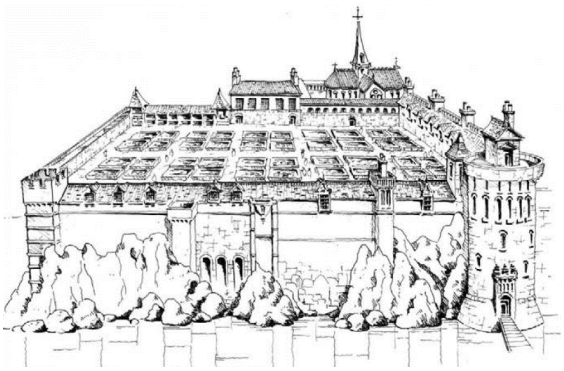

Figure. 2: Renaissance garden: Ambroise
(Source: Boults, 2010)

On the other side of developed European culture, Chinese culture and gardens were established (**Figure.** 3 (a)) 1600 BC – 1100 BC. When people think of Chinese traditional landscape they think of natural landscape, but actually it is not the real nature, but rather an artificial natural landscape. Such landscape is not completely changed nature by humans, but rather an attempt to improve and develop nature, and make the artificial landscape that look like nature, especially compared with Western formal landscape. Chinese painting reflects this attitude toward nature. These gardens represented or suggested actual scenes, hills, and streams. Paths ran through the gardens in pebbled patterns with doors often circular, or octagonal. Weird, contorted, water-worn rocks and petrified plant forms were used as sculpture, along with guardian dogs and other features of stone. Water flowed quietly, or lay calmly in lakes or ponds. The Japanese gardens (**Figure.** 3 (b)) derived their landscape inspiration from the Chinese and included in their layouts meaningful stones and stone lanterns, trees, pagodas, arched bridges, and characteristic fences and gates. While much of the spirit of the informal and naturalistic garden came from the Far East, it was developed in 18th century in England (Weiss, 1998).

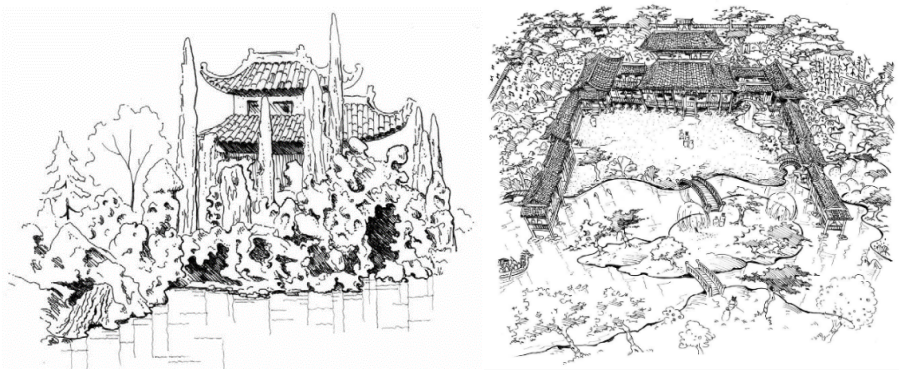

(a) (b)

Figure. 3: (a) Chinese garden, and (b) Japanese garden
(Source: Boults, 2010)

The notion of Chinese gardens in England in the 17th was based on letters and tales. English landscape gardens (**Figure.** 4) informal and natural style had been partially inspired by Chinese traditional landscape. The English understanding of the meaning of Chinese traditional landscape was conjectured as unsymmetrical or gracefully careless patterns or decorative arrangements (Weiss, 1998). The English landscape garden emerged in the early period of 18th century, the style was totally different then till then known geometric style, and it rejected the imposition of any foreign geometry whatsoever in landscape design. These landscapes were noticeable by used winding path, natural woods and grass, wriggle stream to make harmonious scenery with nature.

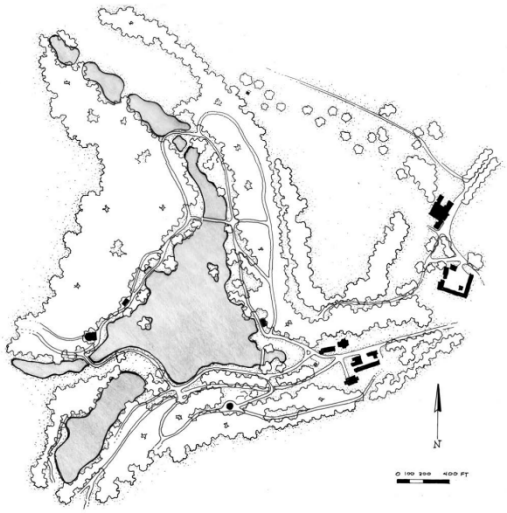

Figure. 4: Stowe - English landscape garden
(Source: Boults, 2010)

Until now we discuss how landscape design has developed along the lines of two principal traditions, the formal and the informal. The formal tradition has behind it elements of order, proportion, rational planning and symmetry. The informal type of landscape design was irregular, naturalistic and simple. Today we have a new conception of landscape design, in which not just views but also the use of space, space relations and new materials, as well as freedom of form are important considerations (Alle, 2014). The design may be formal or informal, or a combination (**Figure.** 5) of the two. Perhaps the biggest change that has occurred in landscape architecture is in the concept of the relation between house and garden (Lohmann, 1963). Until recent years the garden was designed to walk in or through. Today the garden is designed to live in and the use of glass walls has made the garden a part of the living area of the house. The use of glass, more than anything else, is responsible for the great interest today in Japanese gardens, since the Japanese with their sliding walls have for centuries done away with the iron clad division between the indoors and the outdoors.

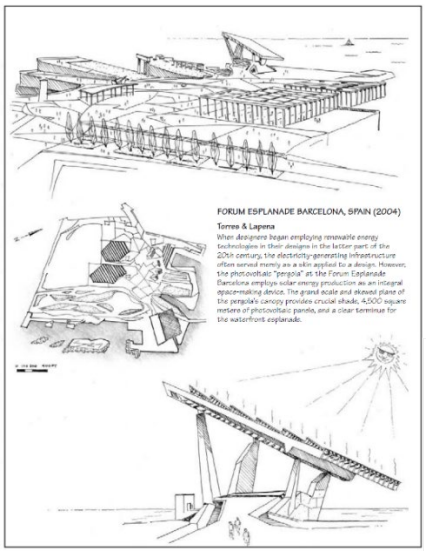

Figure. 5: Modern landscape design
(Source: Boults, 2010)

MATERIAL AND METHODES USED

The aim of this paper is to analyze and compare two basic design styles in landscape planning, geometric and landscape style, along with third - combined style. Based on the example of an atrium space in Novi Sad (**Figure.** 6), bordered by residential buildings, three styles - geometric, landscape and combined style, are shown and analized graphically and schematic, with included plant specification for each style. Methodology included all aspects of systematization of available data from written literature on history of landscape architecture, which considered insight into detailed observation of design styles. Of great importance was understanding of main principles while planning certain space and ideology behind it. Studying of setting directions of movement in different styles, usage of a plant material in different manners, setting a pavement and materials in order to compliment design style were one of the main guidelines for this research paper. For that purpose, we used several softwares: AutoCAD 2017, Realtime Landscaping Architect 2018 and Photoshop 2020.

Figure. 6: Border lines of atrium
(Source: https://geosrbija.rs/)

DISCUSSION

The atrium space selected for this paper is 20 x 13m long, in a rectangular shape. In the new design proposal for geometric style (**Figure.** 7) it has been inspired by a combination of ancient gardens in geometric style and a more modernistic geometric inspired approach. In the front part of the courtyard with the main entrance to the atrium are present elements of a geometrically oriented combination of green hedge border (*Buxux sempervirens* L.) in contrast to the red mulch, in symmetric order. While on the right repeats the geometric shape framed by a stone structure with a floral parterre in bright red (*Salvia splendens* L.) that complements the red color of the mulch on the other side. It is well known that water is one of the crucial elements in this type of garden, and for this reason a fountain of circular form is symbolically foreseen. The atrium tiling is made of stone cubes, rectangular in shape and simple in form. It primarily connects the main entrances to the atrium by straight lines, and it also gives a secondary path through the atrium. These directions, both main and secondary, are centered around the central part of the atrium, which is oriented towards a more modernist approach. Two mini amphitheatres are planned, one above ground level and one below ground level. The paving in this part is designed as a combination of grassy surface and stone paving with the aim of breaking the monotony of non-natural material. Plants are intended to complete the ambient of a space and allow a pleasant living in the urban environment. Topiary forms, that descend from a Renaissance gardens, are an indispensable element of geometric style, so they appear along the main path in order to separate the space into two parts, the front part being more common space and the back part having a more intimate character (**Figure.** 8). This part is also bordered with a hedge with suitable plant species. Species that are well tolerated to pruning - topiary forms chosen for this project are *Robinia pseudoacacia*. L. and *Buxus sempervirens* L. located in the middle of hedge borders at the entrance to the atrium. Plants also appear in containers in a combination of citrus (*Citrus limon* L.) and hibiscus (*Hibiscus syriacus* L.) species. In the rear of the courtyard are provided two trellis with integrated benches for a more intimate socializing. This segment is framed by a green surface consisting of several segments of floral parterrels, each characterized by a single plant species in order to achieve a uniform monochrome surface with clear borders. The species used are *Monarda didyma* L., *Hemerocallis fulva* L. and *Canna indica* L., and also a conifer species (*Thuja occidentalis* L.) to bring dynamics to the composition.

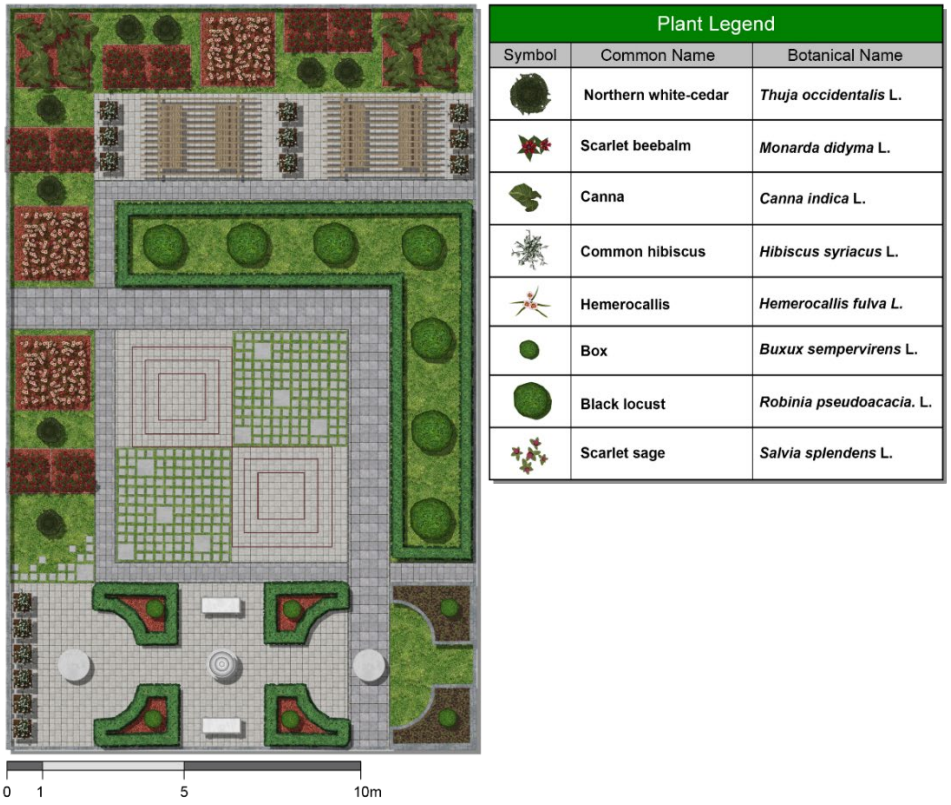

Figure. 7: Example of formal landscape design
(Source: original by authors)

Figure. 8: 3D of the formal landscape design
(Source: original by authors)

Atrium space was also designed in informal style (**Figure.** 9), inspired by English garden, circular forms and a golden ratio – so is the nature. The main path that connects the two entrances to the atrium is semicircular, made of natural material - wood. It is designed in order to be a part of a whole space while connecting the two sides of the atrium. Informal style is dominated by natural materials, so mobiliar is made of wood in an organic form. It is a typical occurrence in nature that however dynamic a process or change is, there is always some harmony, which was our guiding idea. The goal was to obtain a more natural look of the space, so the bench layout was inspired by the image of abandoned boulders in the forest, for example. The plant material is foreseen in the front of the atrium as a natural shift of the meadow landscape of species that build a harmonious composition, from taller to lower species. The types that fit this idea are *Hosta crispula* L., *Muscari armeniacum* L. and *Delphinium grandiflorum* L. Additionally, the planned plant species are also characterized with colorful leaves, besides interesting flower features. The water element is also important when it comes to natural informal style, with a free-form pond with stone elements (**Figure.** 10). Whereas in the upper part of the atrium a different approach was applied. Namely, most of it is covered with white stone paving, and a segments of green surface with middle tall trees (*Cercis siliquastrum* L.), a circular bench with a shorter tree (*Syringa vulgaris* L.) and a circular parterre with a bench and a pergola are inserted. In order to break up a bigger pavement area, three lines of greenery are planned that intersect and further refine the space.

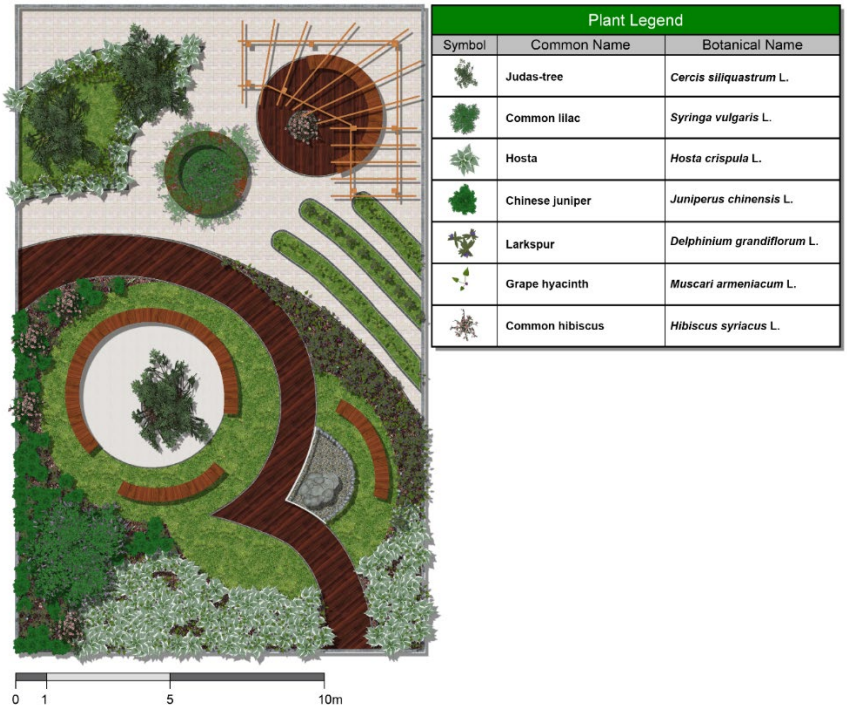

Figure. 9: Example of informal landscape design
(Source: original by authors)

Figure. 10: 3D of the informal landscape design
(Source: original by authors)

We aimed to show an example of a combined style (**Figure.** 11) that was created much later than formal and informal style. This style is characterized by the use of newly discovered materials and is inspired by the previous two styles (**Figure.** 12). The main directions of movement in the atrium were planned as a combination both of geometric and organic forms, and the material used was printed concrete in orange and brown color. As a newer technology, it has a very effective visual impression in the refinement of space. In the second half of the atrium, the goal was to create a dynamic effect using colorful pavement and to calm an ambient with simple structures. Benches and seating elements are all formed of the same material, but in different forms with the aim of leaving the choice of usage of these elements to visitors of the atrium. The structures used for this project are metal arbor, glass structure with bench - as more modern elements in the landscape design. The use of glass in a combined style is common, as are other recently discovered materials. The water element is optional in this landscape style, but a fountain in the form of a sculpture was used here, which in addition to the function of water stabbing and adds to the visual effect of the space. The plants in the project were planned by combining the previous two styles, with geometric forms of the parterre with a variety of plant species such as *Iris pumila* L., *Hosta crispula* L. and *Muscari armeniacum* L. Besides monochrome and multi-colored parterres, woody species (*Cercis siliquastrum* L. *Syringa vulgaris* L.) were used in order to create a complex, yet simple form.

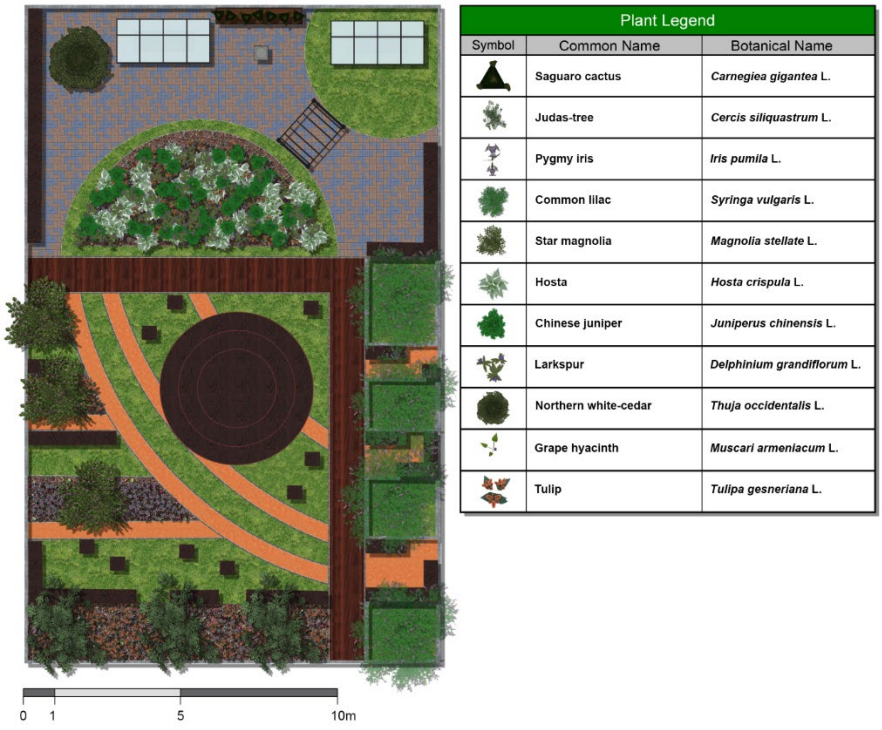

Plant Legend

Symbol	Common Name	Botanical Name
	Saguaro cactus	*Carnegiea gigantea* L.
	Judas-tree	*Cercis siliquastrum* L.
	Pygmy iris	*Iris pumila* L.
	Common lilac	*Syringa vulgaris* L.
	Star magnolia	*Magnolia stellate* L.
	Hosta	*Hosta crispula* L.
	Chinese juniper	*Juniperus chinensis* L.
	Larkspur	*Delphinium grandiflorum* L.
	Northern white-cedar	*Thuja occidentalis* L.
	Grape hyacinth	*Muscari armeniacum* L.
	Tulip	*Tulipa gesneriana* L.

Figure. 11: Example of combined landscape design
(Source: original by authors)

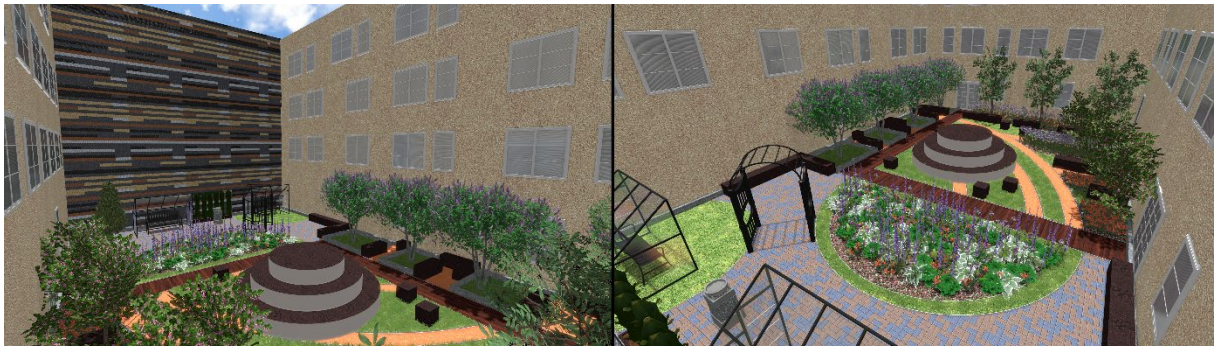

Figure. 12: 3D of the combined landscape design
(Source: original by authors)

CONCLUSIONS

Throughout the history of landscape planning, we have seen that the design process took place in two main directions, formal (until the 17th century) and informal (from the 18th century). As an expression of the new age, the use of glass and materials that were not previously applied in architecture also resulted in a change in landscape design and thus a combined style was created. On the example of an atrium in an urban area, we wanted to show basics of landscaping in the three different styles mentioned above. The aim was to show that the same plants can be applied in all three styles, but that schedule and combination with other landscape elements play a key role. The geometric-style features are more oriented towards stricter lines, cooler materials and increasingly leads to minimalism (like the example of an outdoor amphitheater). The landscape style has warmer features, using natural materials in organic forms that are integrated into the whole composition. For a combined style, it is possible to apply the characteristics of the two styles described above or use a completely new expression.

REFERENCES

1. Alle, E., 2014. Contemporary Art in Cultural Landscape: Experience and Opinions. *Scientific journal of Latvia*, 4(4). pp 49-57
2. Boults, E. and Sallivan, C., 2010. Illustrated History of Landscape Design. John Wiley & Sons, Inc.
3. Lohmann, K.B., Fundamentals of Landscape Architecture. 1963. Second edition. International Correspondence Schools, Scranton, Pennsylvania, USA
4. Lakićević, M. and Kordić, D., 2018. Geometric style in design of urban landscapes. GRID, Novi Sad, Serbia. pp 519-523
5. Newton, N. T., 1971. Design on the Land; The Development of Landscape Architecture. Harvard college. Massachusetts, USA
6. Weiss, A. S., 1998. Unnatural horizons; Paradox and contradiction in Landscape Architecture. Princeton Architectural Press, New York, USA

USE OF MACLAURIN GEOMETRIC TRANSFORMATIONS IN 3D SYNTHESIS OF MECHANISMS

Marko Rusov
Zuhlke Engineering, Belgrade, Serbia, Faculty of Mechanical Engineering, University of Belgrade, Republic of Serbia
M.Sc., Ph.D. student, markorusov@yahoo.com

Boris Kosić
Faculty of Mechanical Engineering, University of Belgrade, Republic of Serbia
M.Sc., Teaching Assistant, bkosic@mas.bg.ac.rs

Dušan Berdić
Chamber of Comerce of, Serbia, Belgrade, Serbia, Faculty of Mechanical Engineering, University of Belgrade, Republic of Serbia
M.Sc., Ph.D. student, dusan.berdic@pks.rs

ABSTRACT

This paper describes and explains MacLaurin's transformations and their use in a 3D synthesis of mechanisms. An overview of the high order curves is provided, along with their degradation to the curves of the lower order. MacLaurin's transcriptions are used to degrade the curves of the higher order to the desired curves of the lower order. This will allow us to generate different kinds of trajectories and, therefore, different kind of mechanisms. Furthermore, the implementation of the obtained curves into the CAD pragmas and 3D environment is presented. This allows a quick synthesis of a mechanism, its adaptation and simulation in order to get the desired final trajectories. Different kinds of trajectories implemented in a 3D environment are shown in this paper. Fully operational 3D models of mechanism trajectories and simulation are created and documented in the SolidWorks application.

This research could be used further in the theory of mechanisms, 3D modelling, simulations and the synthesis of mechanisms. The exposed methods of the synthesis of mechanisms may be used in the design and construction of new mechanisms or the redesign of the existing mechanisms.

Keywords: *computer graphics; 3D modelling, mechanism synthesis, MacLaurins's transformations.*

1. INTRODUCTION

The need to create a viable product and get it on the market as soon as possible is higher than ever in modern industry. In order to shorten this time and learn as much as possible about the behaviour and characteristics of the product (in this paper, to learn about the mechanism), modern software tools are used. In general, software tools can shorten the time needed for calculation or the time needed for drawing different models. However, tools alone cannot give answers to the questions how we can create the wanted movement of the mechanism. Even today it is still difficult to translate common rotational movement to the straight-line movement in a plane mechanism.

In the following chapters it will be shown how we can use knowledge about the curves of the higher order and their characteristics when they break to the curves of the lower order to obtain the desired movement of the mechanism. Synthesis of the mechanism will be performed without the use of analytical and differential geometry.

We did great research in field of geometrical transformations and mechanisms synthesis. Dovnikovic L. in [1] provides an overview of the curves and describes restitution of the curves of the higher order. Radnovic G.

and Popkonstantinovic B. in the paper [2] describe a synthesis of uniform mechanisms, by which all kinds of second-order curves can be generated. Dovnikovic L. in paper [4] shows space restitution of the plane curves. Artobolevsky I.I. in [4] provides the foundation of the theory of the mechanism synthesis. Hunt K.H. in [5] presents the specifics of geometry for the synthesis of mechanisms. Shiwalker P.B. et al in the the paper [6] show the problems of the straight line movement obtained in crank mechanisms and offer solutions for approximate straight line movement. Kiper G. et al in the paper [7] show how to obtain defined trajectories and movements. Shaoping Bai in paper [8] gives synthesis of the mechanism to visit 10 poses. Urizar M. et al in the paper [9] show synthesis of the mechanisms with specific software tool. Babichev D. et al in the paper [10] show methodology of a structural-kinematic mechanism synthesis. Villegas C. in the paper [11] optimize link lengths of the function generation four bar linkages.

Combining the theoretical knowledge based on these ideas we aim to creating the mechanisms which will have any given trajectory as final movement, even the straight-line movement which is almost impossible to get in any other way. This paper relies on the synthesis of the mechanisms obtained through some of MacLaurin's transformations. The concrete mechanism to obtain a straight line trajectory as a final movement has not been obtained yet. We prepared drawings for two kind of movement for this paper as an example, starting from basic geometrical transformation thru Sketch in CAD software tool (Solid Works2019), and at the end we created two mechanisms for receiving trajectory as we wanted.

2. RESTITUTION OF CURVES OF THE 4TH ORDER TO THE CURVES OF THE LOWER ORDER

A detailed analysis of the restitutions of the curves of the higher order into the curves of the lower order in [1, 3] has lead us to the idea to use some of the restitutions during the synthesis of mechanisms. The given geometrical transformations are used as an input parameter for a geometrical synthesis of the mechanism which translates rotational movement into the chosen movement of the final trajectory. This is maybe only way to receive straight line movement of point from basic rotation. Using some transformations we will explain geometrical bases and restitutions for receiving some movement of the point, but in this paper we didn't made synthesis of straight linear movement of mechanism. For this paper we used two different restitutions (Fig. 1 and Fig. 2).

Space curve of the 4th order is restituted in the curve of the 3rd order. The condition for this restitution is that the circle of mapping goes through point V (Fig. 1).

Space curve of the 4th order is restituted in curve of the 3rd order. The curve is breaks it into the curve of the 3rd order and the line (Fig. 2).

Since that we can choose conditions such as placement of the points and placement of the circle we can generate wanted trajectories for specific mechanism. Here are only two of restitutions presented such as an idea.

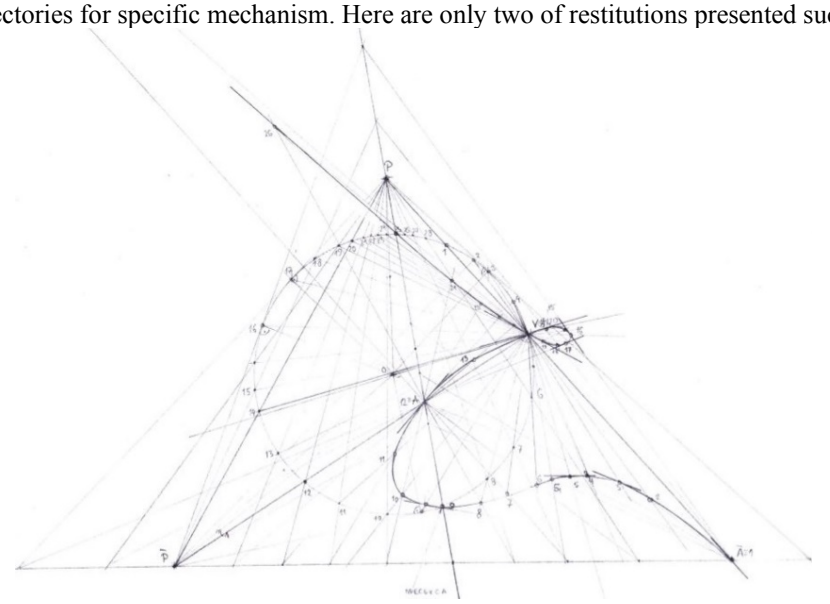

Figure 1 - Space curve of the 4th order is restituted in the curve of the 3rd order

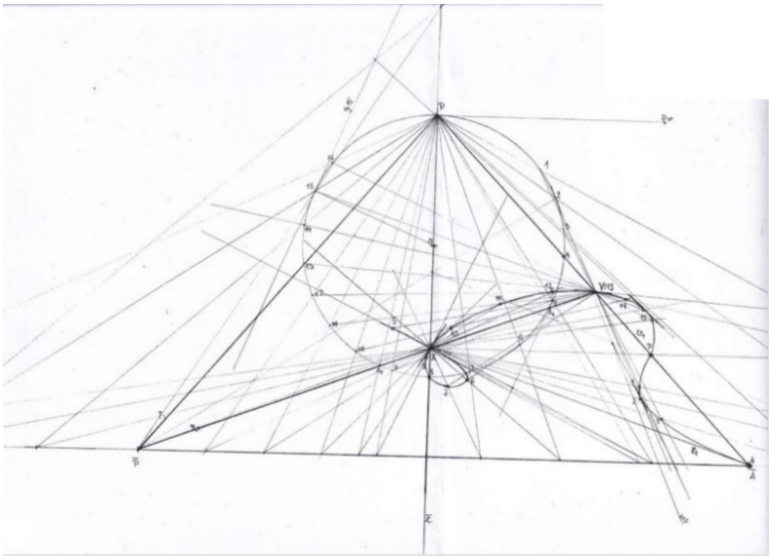

Figure 2 - Space curve of the 4th order is transforming into the curve of the 3rd order.

3. CAD OF THE MECHANISMS OBTAINED THROUGH MCLOREN GEOMETRIC TRANSFORMATIONS

Having obtained geometrical transformations in the previous chapter, we can proceed further to the theoretical synthesis of the mechanism. In this paper do not use an analytical synthesis of the mechanism, but focus on a 3D computer synthesis of crank mechanisms. For these purposes we are use the software package SolidWorks2019.

Primary, we made graphs using geometrical trasnformations from drawings presented in previous chapter (sketch in software for future usage of mechanism synthesis) as a basement for mechanism synthesis. After computer checking of Motion Analysis we made a mechanism with wanted movement of some point. In this paper we will present two examples, as we choose two geometrical transformations (fig. 1 and fig. 2).

Example 1: To generate a knot, the circle of mapping should cut $P\bar{P}$ like shown in the sketch. Sketching of the graph the in the SolidWorks 2019 package provides us various options for changing and adopting the final movement of the mechanism to the desired movement. The dot at the end of the line starting from point $\bar{A}$ gives the desired trajectory while M_0 rotates around circle diameter. Considering that we are choosing the placement of the dots for transcription and placement of the projection circle we can control the final trajectory (Fig. 3).

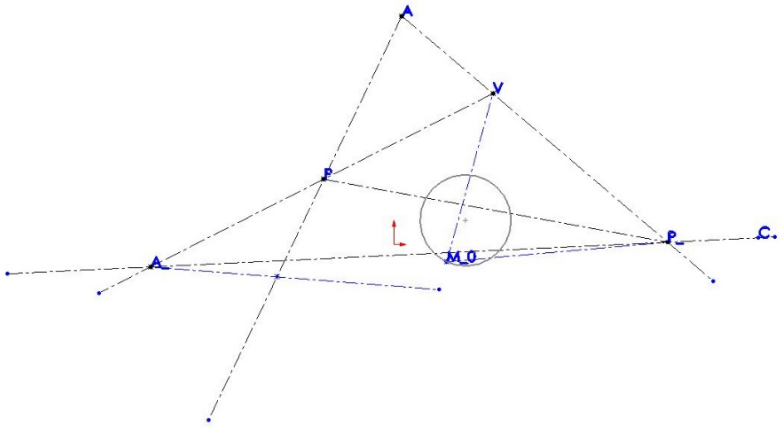

Figure 3 - SolidWorks2109 graph for geometrical transformation from fig. 1

Using the sketch, from *Fig. 3* we can easily create the mechanism as it is shown in next figure (fig. 4). Rotational movement is translated into the shown curve, which creates a knot in dot V. Points $\overline{A}$, V, $\overline{P}$ and centre of the circle are used as joints for the parts of mechanism while. Line AP is used as a slider so that the movement could replicate transcription. In fig. 4 the trajectory of wanted movement I presented, and we proved that it is possible to receive any kind of movement from rotation.

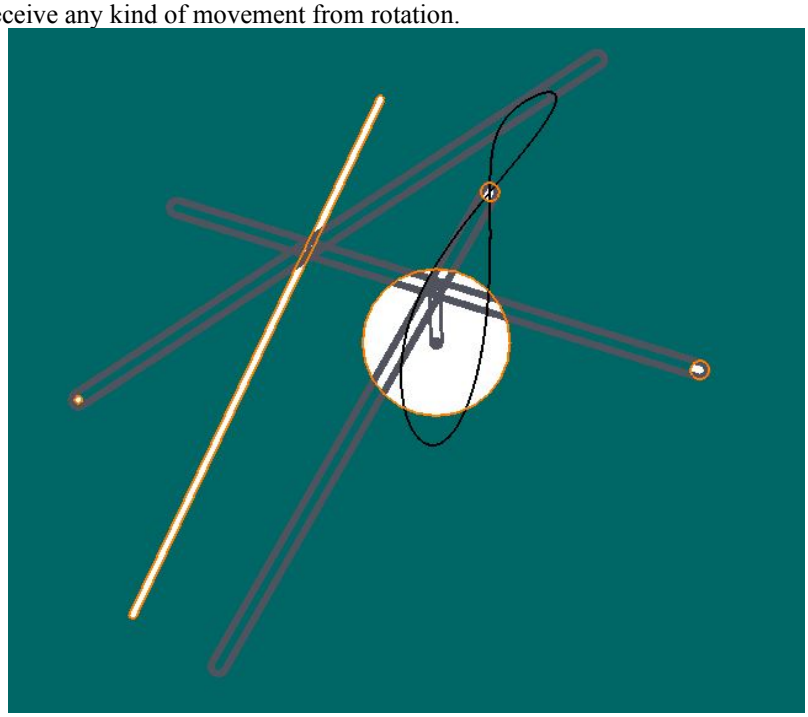

Figure 4 – SolidWorks2019 mechanism created from sketch fig. 3.

Example 2: Mechanism creates spike in dot V. To obtain this movement, a circle needs to be placed in tangent position to the $P\overline{P}$, as shown in Figure 5. For this we used geometrical tansformation from fig. 2. After Motion Analysis we started to create the mechanism**.**

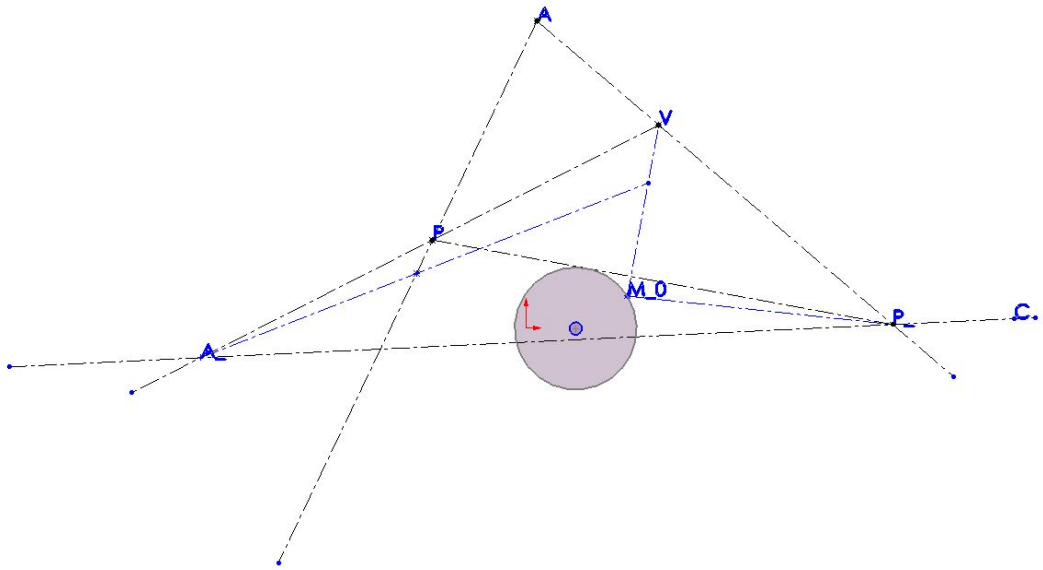

Figure 5 - SolidWorks2109 sketch for geometrical transformation from fig. 2

Using the sold bodies are used to create and simulate mechanism movement. Which is shown in *Figure 6*. In some point it is obvious that we receive one pick, and a trajectory of curve line 3th order.

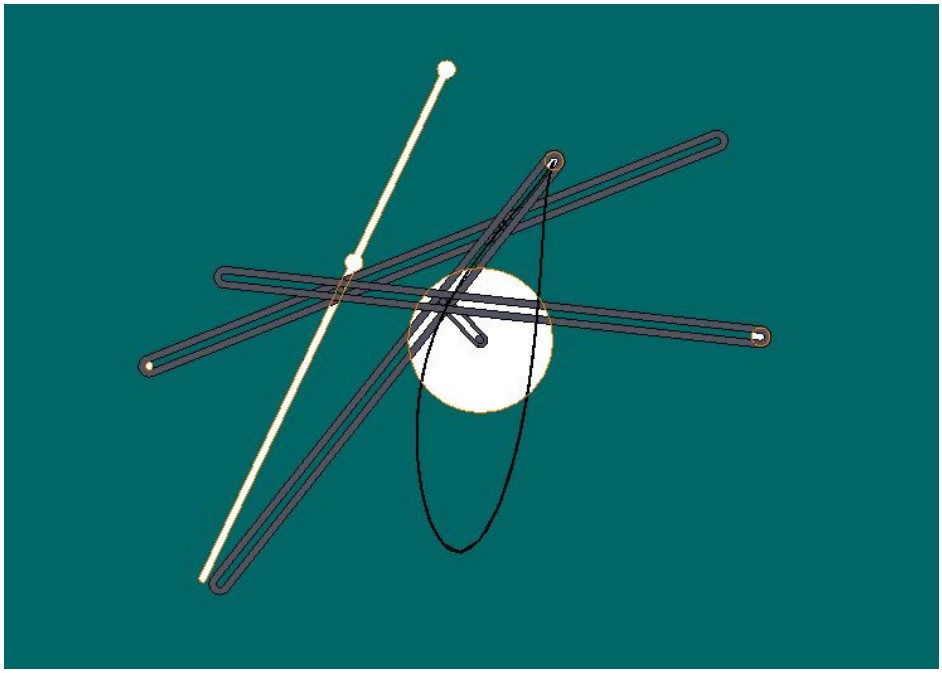

Figure 6– SolidWorks2019 mechanism created from sketch fig. 5.

The given examples show that it is possible to obtain a mechanism with the desired movement in CAD relatively easy. The generated assembly could be further used to obtain various pieces of information, such as speed or acceleration of the parts of the mechanism trough CAD simulation. Additionally, the forces and stress of the parts could be later simulated and adjusted to the needs.

Combining new software technology with theoretical geometry significantly decreas the time to obtain the first results. If we consider that real life test could have variations in results compared to CAD simulation, but we try to make it real as much as it's possible. The possibility to adapt and change a mechanism quickly is even more important. Using this approach together with production technologies like 3D printing highly reduces the time from a theoretical concept to the physical proof that we can test in real life environment.

4. CONCLUSION

MacLaurin geometric transformations offer a wide range of possibilities to transform the common rotational movement to the desired final movement of the mechanism. For the purposes of this paper, a synthesis of two mechanisms was performed and the desired final trajectory was obtained. We confirmed the assumption that there was a possibility of obtaining the final movement of the wanted linkage by the given trajectory. In further research, more attention should be placed on obtaining non-conventional movements or a straight-line movement of the plane mechanism from the rotational movement of engine.

Acknowledgements

This work was supported by the Ministry of Education, Science and Technological Development of the Republic of Serbia (Contract No. 451-03-68/2020-14/200135)

REFERENCES

[1]. Dovnikovic L., 1977. Descriptive Geometrical Treatment and Classification of Plane Curves of the Third Order, Reprint from Proceedings of natural sciences, Matica Srpska, SFRJ.

[2]. Radnovic G. and Popokonstantinovic B., 1998. The Geometrical Synthesis of Conicographs Based on MacLaurins transformations. Proceedings of 8th ICECGDG Conference, July 31-August 3, 1998, Austin, Texas, USA
[3]. Dovnikovic L., 1988. Descriptive Geometrical Methods of Space Restitutions of Algebraic plane curves Proceedings of 3rd International Conference on Engineering Computer Graphics and Descriptive Geometrz, Vol. 1, Vien-Austria, pp.109-116
[4]. Artobolevsky I.I., 1988.Teoriya Mehanizmov i Mashin, Nauka, Moskva, SSSR
[5]. Hunt K.H., 1978. Kinematic Geometry of Mechanism, Clarendon press, Oxford, UK
[6]. Shiwalker P.B. Moghe S. D., Shiwalkar J. P., Modak P., 2019 Inflection Circle Based Approach to Synthesis of Approximate straight line Mechanisms , Springer Nature Switzerland AG 2019 T. Advances in Mechanism and Machine Science, Mechanisms and Machine Science 73, Proceedings of 15th IFToMM World Congress, Krakow, Poland, https://doi.org/10.1007/978-3-030-20131-9_154
[7]. Kiper G. Soylemey E., 2019 Kinematics synthesis of Planar 4-Bar Path Generators for Finite Line Positions Springer Nature Switzerland AG 2019 T. Advances in Mechanism and Machine Science, Mechanisms and Machine Science 73, Proceedings of 15th IFToMM World Congress, Krakow, Poland, https://doi.org/10.1007/978-3-030-20131-9_134
[8]. Shaoping Bai, 2019 Exact Synthesis of a 1-dof Planar Linkage for Visiting 10 Poses, Springer Nature Switzerland AG 2019 T. Advances in Mechanism and Machine Science, Mechanisms and Machine Science 73, Proceedings of 15th IFToMM World Congress, Krakow, Poland, https://doi.org/10.1007/978-3-030-20131-9_127
[9]. Urizar M. Munoyerro A., Ameyua E., Hernandez A., 2019. Optimal dimensional Synthesis using GIMSYNT software Springer Nature Switzerland AG 2019 T. Advances in Mechanism and Machine Science, Mechanisms and Machine Science 73, Proceedings of 15th IFToMM World Congress, Krakow, Poland, https://doi.org/10.1007/978-3-030-20131-9_78
[10]. Babichev D., Evgrafov A., Lebedev S., 2019. Lever mechanisms: the new approach to structural synthesis and kinematics analysis] Springer Nature Switzerland AG 2019 T. Advances in Mechanism and Machine Science, Mechanisms and Machine Science 73, Proceedings of 15th IFToMM World Congress, Krakow, Poland, https://doi.org/10.1007/978-3-030-20131-9_56
[11]. Villegas C., Husing M., Corves B., 2019 Dynamic Synthesis of a Crank-Rocker Mechanism Minimizing its Joint-Forces. Advances in Mechanism and Machine Science, Mechanisms and Machine Science 73, Proceedings of 15th IFToMM World Congress, Krakow, Poland, https://doi.org/10.1007/978-3-030-20131-9_312

moNGeometrija 2020

THE INTEGRATED DESIGN AND FABRICATION PROCESS FOR PLANAR MORPHING TESSELLATION

Radmila Đurašinovič
Department of Architecture, Faculty of Technical Sciences, University of Novi Sad, Serbia
B.Arch., M.Arch. Student, radmila-d@hotmail.co.uk

Marko Jovanović
Department of Architecture, Faculty of Technical Sciences, University of Novi Sad, Serbia
PhD., Assistant Professor, markojovanovic@uns.ac.rs

ABSTRACT

In contemporary architectural practice, the tessellation of planar surfaces, such as walls or floors is usually done by using a uniform triangular, rectangular or hexagonal tile as a template. This approach, albeit the most efficient, relies mostly on colours to induce the experience of a pattern and as such is limiting. By using differently shaped tiles, the possibilities are increased, but at the cost of time and mould fabrication. In this paper, the focus is placed on integrating the design and fabrication process in order to create a morphing tessellation from differently shaped triangular tiles, by fabricating them from a single mould with adjustable edges. The design concept was based on triangular shaped tiles where the edges morph into a curved shape created by rotating the curves around the centre-point of each side of the triangle. By generating a parametric model, the possibility for creating quick design variations is introduced by adjusting the shape of the edges through predetermined parameters. The final design consisted of ten different tile shapes, each of which would require a separate mould. However, by developing a mould with walls that can be adjusted i.e. bent according to a predetermined template, it was possible to fabricate all of the different shapes in plaster. The final result of the project took the form of a physical model of the chosen tessellation design with 336 plaster tiles produced with the adjustable mould. This demonstrates the possibility of incorporating interesting and more dynamic, but seemingly complicated designs in interior and exterior tiling along with an efficient fabrication process.

Keywords: tessellation; digital design; mould; plaster; cast

1. Introduction

Tessellation, or the tiling of a plane using geometric shapes with no overlaps or gaps, has been a part of architectural decoration for thousands of years. The origins of tessellation can be traced back to 4000 B.C. to the Sumerian civilization (Pickover, 2009), and its development followed throughout the ancient world in various forms of colourful mosaics and tiling. In fact, tessellation has played a large role in the decoration of buildings throughout history, reaching a particularly high level of sophistication in medieval Islamic art, most notably the Alhambra palace (Lovric, 2003). A visit to this palace in 1936 greatly influenced the work of Dutch graphic artist M. C. Escher, whose artistic contribution to this geometrical field is of great importance in the modern world (Escher & Locher, 1974). Also, in 1936, the earliest known spiral tessellation was developed by mathematician H. Voderberg, eponymously known as Voderberg tiling, shown in Figure 1a. This type of tessellation is significant for its use of monohedral tiles to create a dynamic pattern. Later developments by B. Grünbaum and G. C. Shephard (1987) made significant further progress in this field.

(a) (b)

Figure. 1: (a) Spiral tiling discovered by mathematician Heinz Voderberg (1936) (Source: Grünbaum, Shephard 1987, pg. 521)
(b) Mosaic in the Hall of the Two Sisters, Alhambra Palace, Granada (Source: Giordano et al 2018, pg. 121)

Tessellation is found in all areas of architecture, from the simplest monohedral tiling found in daily architectural practice (interior tiling mainly of kitchens and bathrooms, as well as exterior paving), to the opulent mosaics adorning important sacral and secular buildings all over the world (Alhambra palace, Figure 1b). However, while substantial funds for important public commissions allow for a greater scope of artistic freedom resulting in more elaborate and interesting designs, more often than not, budgetary constraints limit possibilities in this field. In contemporary architectural practice, the tessellation of planar surfaces, such as walls or floors in interiors and exteriors is usually done by using a uniform triangular, rectangular or hexagonal tile as a template. This approach, albeit the most efficient, relies mostly on colours to induce the experience of a pattern and as such is limiting. By using differently shaped tiles, the possibilities are increased, but at the cost of time and mould fabrication. Adjustable moulds are a production method which is gaining traction for its advantages in overcoming these limitations. For example, research conducted by van der Weijst (2019) saw the development of an adjustable mould for the casting of glass voussoirs of varying geometries, applied on a tessellating shell structure.

The focus of this paper is on the decorative application of tessellation within architecture and interior design. In this research, the aim was creating a morphing tessellation from differently shaped triangular tiles, while integrating the design and fabrication process in a time and cost-efficient manner. By casting the tiles from a single mould with adjustable edges, the expense of mould fabrication could be reduced. This would ultimately allow for greater possibilities in contemporary practice, creating more dynamic and elaborate designs for commonplace spaces.

2. The Integrated Process

The integrated process merges the design and the fabrication process into a complete whole. It implies adapting both of these processes to the other in the aim of achieving optimal results. The first phase of research consisted of exploring the different results that could be obtained by varying the basic parameters of tessellation – the prototile and type of transformation. The aim was to create a dynamic design through geometric transformation, but one that was practical enough for a feasible fabrication process. The second phase involved realizing the design in a cost and time efficient way. In this paper, both processes will be broken down as separate subheadings, explaining the complete design process from conceptualizing the design to its rationalization for the fabrication process, and finally the fabrication process itself.

2.1. The Design Process

The design developed for this research drew inspiration from M. C. Escher's tessellation "Liberation" (see Fig. 2a). Often depicting animal and human motifs in his designs, Escher gave a new lease of life to geometry-based tessellation. The design created for this research represents a reduced geometric interpretation of Escher's design, with the aim of fabrication for practical use. A triangular grid was chosen as the foundation, which gradually transitioned to a curved form reminiscent of the bird in "Liberation". The form was obtained through rotational symmetry with the midpoints of each side of the triangle being the rotational centre (see Fig. 2b).

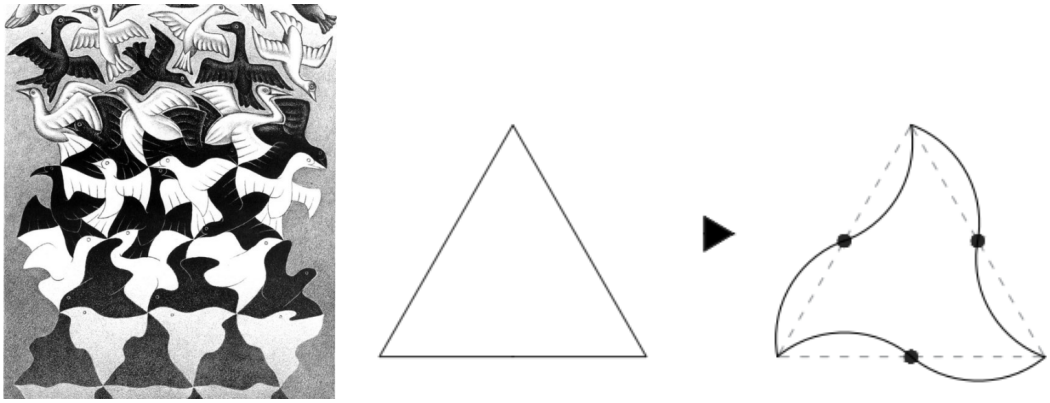

(a) **(b)**

Figure. 2: (a) Liberation by M.C. Escher, Lithograph (1955) (Source: Gorini 2018, pg. 28)
(b) Transformation of initial shape into curved variant in this research

In order to allow for a larger number of variations in a time efficient manner, the possibilities of a parametric design approach were explored using Rhinoceros and Grasshopper. By using simple affine transformations and a set of actions, it enabled the design process to be observed both qualitatively and quantitatively at the same time. In generating a parametric model in Grasshopper, the possibility for creating quick design variations was introduced by adjusting the shape of the edges through predetermined. The most important one was the introduction of a Bézier curve. By varying its tangent, the shape of the Bézier curve was impacted which enabled different aesthetic qualities to be investigated. Additional parameters will be explained in more detail in the following section. Upon finalizing the final shape, the next step consisted of determining the rule according to which the triangle morphed into its curved variant i.e. the final shape. A curve attractor was chosen as the determinant of this rule.

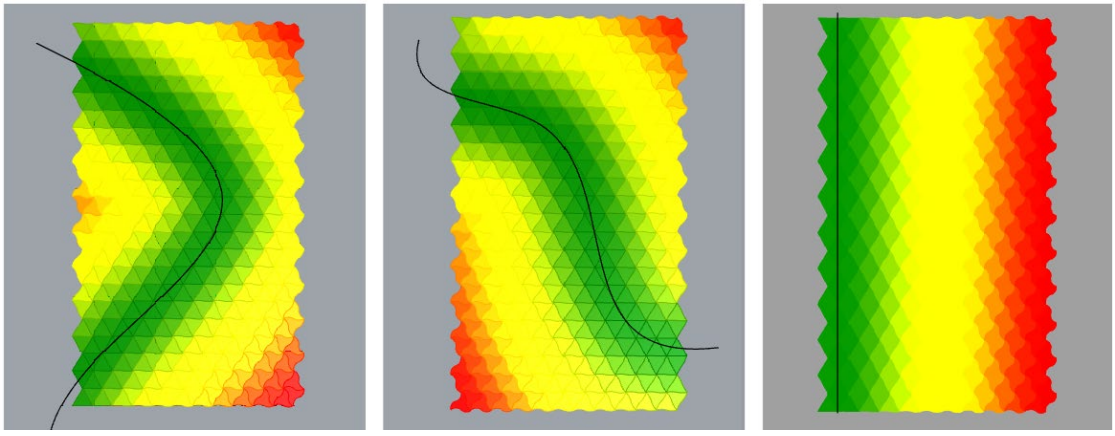

Colour gradient enabling clearer visibility of the morphing pattern. Green tiles represent the initial triangular shape, while red depicts the final curved variant. The shades in between represent the transitional shapes.

Figure. 3: Manipulation of the design with various forms of curve attractor, resulting in different patterns

The edges closest to the curve attractor retained the initial triangle shape, while the edges furthest away had the final shape, with a set of transitional shapes in between. As shown in Fig. 3. various forms of a curve attractor (depicted as a black curve) were explored,

before settling on the final design which demonstrated a proportionate ratio of the different shapes and dynamic aesthetic qualities. The result was a tessellation which gradually morphs from triangular shaped tiles into the curved variant with parametrically controlled edge curves.

Grasshopper proved to be a valuable tool in aiding the design process, generating results of adjustments in real-time. The different parameters Grasshopper enabled to be adjusted included changing the size and number of tiles in x and y direction, the shape and curve degree of the Bézier curve and the shape and position of the curve attractor. These variable parameters allowed for the possibility of the final design being adapted for application on different dimensions of surfaces, as well as creating different visual effects. Once the triangular pattern was chosen it was necessary to make certain adjustments before proceeding to the fabrication phase.

2.2. Adapting the Design for Fabrication

At this point, the design consisted of a large number of different shapes. The aim of this phase of research was to adapt the design for a more efficient fabrication process without compromising the aesthetic qualities. This was done by reducing the amount of differently shaped tiles to a viable number for practical application, but which was ultimately high enough to retain the dynamic character of the morphing design.

By rationalizing the curve extremes - the maximum distance curve points can have in reference to the initial straight edge of the tiles i.e. restricting it to certain intervals, the number of different tiles was reduced to ten. The intervals were marked by the numbers 0 through 3, 0 being the straight edge of the triangular tile, with a value of 0mm, and 3 the edge with the greatest curve extreme at 11mm, while 1 and 2 were linearly interpolated. By using basic Grasshopper tools, it was possible to examine all tiles generated in such a manner, create an annotation based on the edge shape and label each triangle accordingly (see Fig. 4) so the proper number can be noted and later on fabricated with the draft of implementation to follow. In addition, a list of the number of each combination was generated, further aiding the logistical aspect of preparing the design for fabrication.

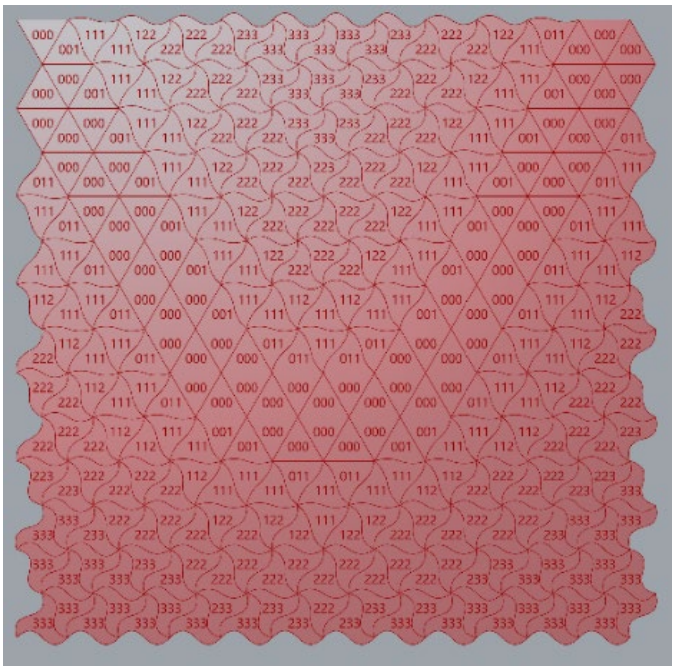

Figure. 4: Final design in Rhinoceros with tiles labelled accordingly

3. Practical Application

The final design consisted of ten different tiles, each of which would normally require a separate mould. However, the development of a mould with walls that can be adjusted i.e. bent according to a predetermined template opened the possibility of producing all of the different shapes in one mould. The aim of this phase of the research was to devise a mould which could successfully be used to produce all ten of the tiles. The mould developed consisted of two components – a fixed plywood base and adjustable walls made of ABS.

3.1.1. Mould Development - Base

The mould was conceived around the idea of inserting the adjustable ABS walls into grooves engraved in the plywood base, forming a perimeter for the casting of the tiles. As the mould needed to allow for the fabrication of all the different tiles, the first step in creating the mould was to overlap the shapes labelled 000, 111, 222, 333, as these can be considered the baseline shapes from which the other variants can be obtained. The chosen length of the sides of the equilateral triangle prototile was 8cm. On overlapping, the shapes converged in all three corners of the initial triangle shape. Furthermore, the design of the mould was devised to accommodate the interlocking of the ABS strips with a waffle joint (Fig. 5a,b). For this, continuing each edge in the direction of the tangent of the end vertex point was necessary. To prevent the damaging of the mould i.e. chipping of the sharp corners in the converging points of the overlapping edges during use, circles were incorporated into the engraving template, which is shown in Fig. 5c. This proved to be effective in reducing damage to the mould in the later phase of its practical application.

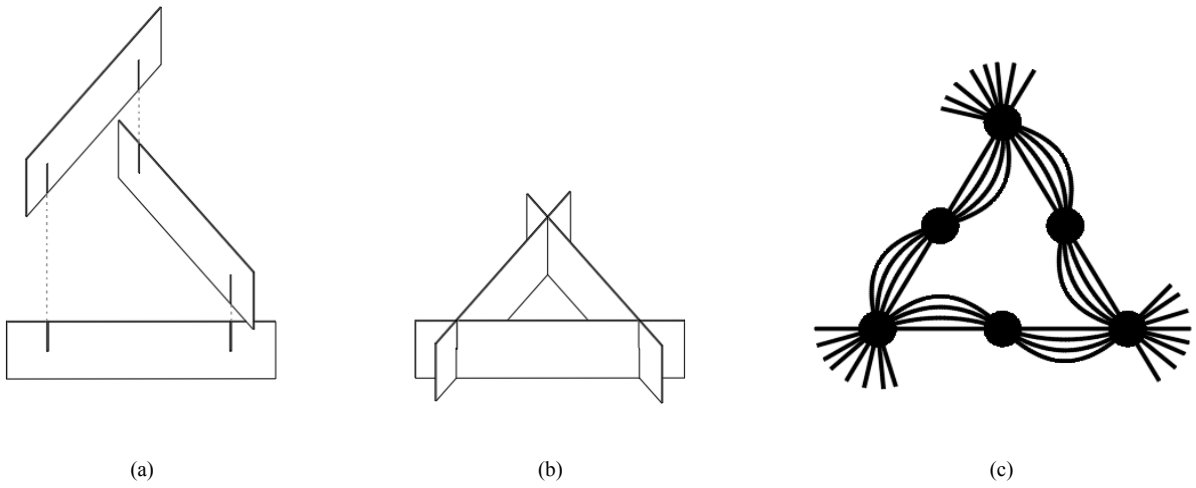

(a) (b) (c)

Figure. 5: (a,b) Graphic depiction of the interlocking of ABS strip walls with a waffle joint and (c) Graphic depiction of the template for engraving

There were also two additional parameters to consider when designing the mould for fabrication which could affect its functioning. Firstly, the thickness of the grooves engraved into the plywood by a laser cutter needed to precisely correspond to the thickness of the ABS strips which were to be inserted. The strips used had a thickness of 0.45mm, thus the grooves in the plywood needed to be slightly wider, allowing some room for manoeuvring. Taking into consideration an approximate kerf width of 0.2mm on each side, the resulting width of the grooves was 0.9mm. This width proved to enable smooth insertion of the ABS strips, without being too loose. Secondly, the depth of the grooves was an important aspect to factor into the design of the mould. The course of the research led to the conclusion that the deeper the groove, the more securely the ABS strip remained in place. The minimal depth empirically proved from the findings is 6mm, which is the depth used in the research. Fig. 6 depicts a side by side comparison of the engraved base, and the mould in use during casting upon insertion of the ABS strips.

During the fabrication process of the mould, there were certain issues relating directly to the method of engraving. In this case, the 3D engraving possibilities of the laser cutter available were used, testing its performance for a task more commonly done with a CNC milling machine. Namely, to achieve the desired groove depth of 6mm, several rounds of engraving were required. The focal length of the laser proved to be an issue, as it affected the width of the groove, making it narrower with each subsequent engraving job. This resulted in a groove with a cross-section shaped like an isosceles trapezoid - widest on the surface and tapering downwards. Inevitably, this partially affected the ability of the ABS strip to be inserted all the way through. Another issue encountered related to the build-up of residue in the grooves from the engraving process, which, due to the small width of the grooves, wasn't viable for removal.

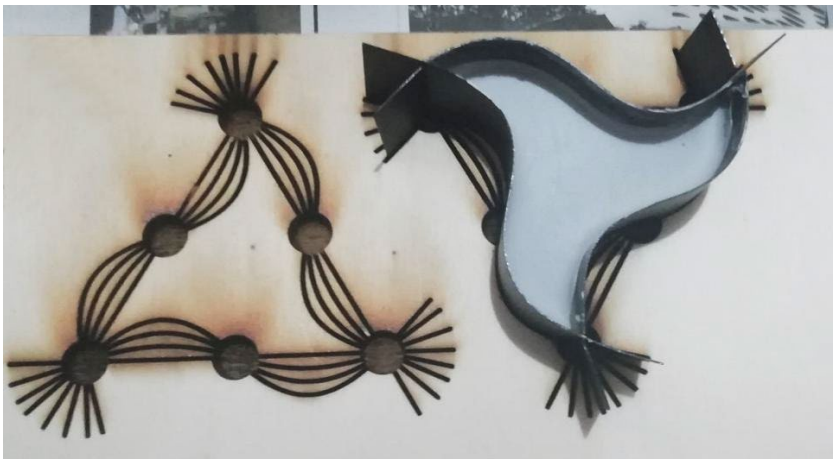

Figure. 6: Engraved base of the mould on the left, and mould with inserted walls in use on the right

Furthermore, the mould required an additional element in order to be functional. Once the adjustable walls were set in the corresponding grooves of the base, parts of the "unused" grooves in the interior of the mould needed to be covered to prevent the plaster from seeping into these crevices. Several methods were tested to resolve this issue, including a plastic film overlay and a removable disc in the shape of the tile being made. In the end, a laser-cut acrylic disc was used for this element and proved to be favourable not only for this function, but also instead of a mould-release agent, which will be addressed in more detail in section 4.

Despite these issues during the development process, the plywood mould performed adequately in the tile fabrication phase. Further research could include exploring a different engraving method, i.e. a CNC milling machine, which would solve problems regarding the focal length or residue build-up.

3.1.2. Mould Development - Adjustable Walls

The adjustable walls were the key feature in fabricating all of the differently shaped tiles from one mould. Different materials were investigated for the walls, including PVC foam boards and A-PET sheets. The material chosen was ABS edging tape for its range of thicknesses, flexible quality and shape, i.e. it is pre-cut into strips.

Initially, a thickness of 0.6mm tape was tried for the walls. However, this thickness proved to be too rigid for the relatively small dimensions of the tiles. 0.45mm thick tape resolved the flexibility issues and was easily able to be bent and inserted into the grooves of the base. Four different lengths of the tape were cut, corresponding to the lengths of each edge from the shortest to the longest and labelled L0, L1, L2, L3, L4 respectively. In order to "seal" the corners of the tile where the three walls met, slits were created through the tape. Interlocking the individual strips in a waffle joint. This type of joint proved to be an efficient method of fixing the strips in place, as well as acting as a leak-proof barrier for the tile casting process.

While the results achieved using the ABS edging tape as a wall for the mould were satisfactory, minor difficulties were encountered in the way the tape interacted with the base of the mould, mostly due to the aforementioned engraving issues. As explained in the previous section, the tapered cross-section of the grooves limited the ability of the ABS tape to be inserted completely. This caused the tape to occasionally pop out during the assembling of the mould. This affected the time required to put together the mould, but didn't create problems during the casting process. However, the limited insertion capacity of the grooves did negatively affect the tile casting process in another way. Given the 3.3cm height of the ABS walls and the fact that they weren't completely secured in the grooves, they tended to tilt outwards slightly towards the top. While this problem was not initially observed, it led to issues upon the assembling of the tiles which will be presented in the Results section.

3.2. The Casting Process

Once a mould had been developed, the next phase consisted of testing its functionality through the tile casting process. The final result of the research is presented in the form of a physical model consisting of 336 tiles of the selected tessellation design. For the material of the tiles, plaster was chosen for its favourable casting qualities, quick hardening time and light mass.

To begin with, several ratios of plaster to water were tested to determine the desired consistency. According to the manufacturer (plaster used was model plaster produced by Rigips) a plaster to water ratio of 2:1 is recommended. However, due to the thicker consistency and rapid hardening of the plaster, the ratio used throughout the casting process was closer to 1,5:1. Measurements were made approximately throughout the process, and variations in consistency weren't found to affect the aesthetic or durable qualities of the final tiles.

A step that can be an issue with plaster in general is releasing the form from the mould. Often, a mould release agent is used to aid this part of the casting process. However, as both the walls of the mould and the removable disc forming the base are made of plastic, this was not an issue. The smooth surface of these elements provided favourable circumstances for releasing the tiles from the mould without damaging them. Approximately 25 minutes was necessary for the plaster to harden sufficiently before removal from the mould.

Overall, the number of defective tiles was less than 10% and most likely due to several factors in play, not one in particular. Human error can be considered the cause of the majority of defects i.e. inaccurate ratio of plaster to water, less than optimal hardening time or improper handling of the mould upon tile removal. Therefore, the method can be considered adequate in producing differently shaped tiles from one mould.

In order to speed up the casting process, which in this case relied on manual labour, silicone moulds were developed from the plaster tile prototypes obtained from the adjustable mould. This proved to be effective in that it eliminated the time required to set up the adjustable walls from the process after the prototypes had been created.

3.3. Results

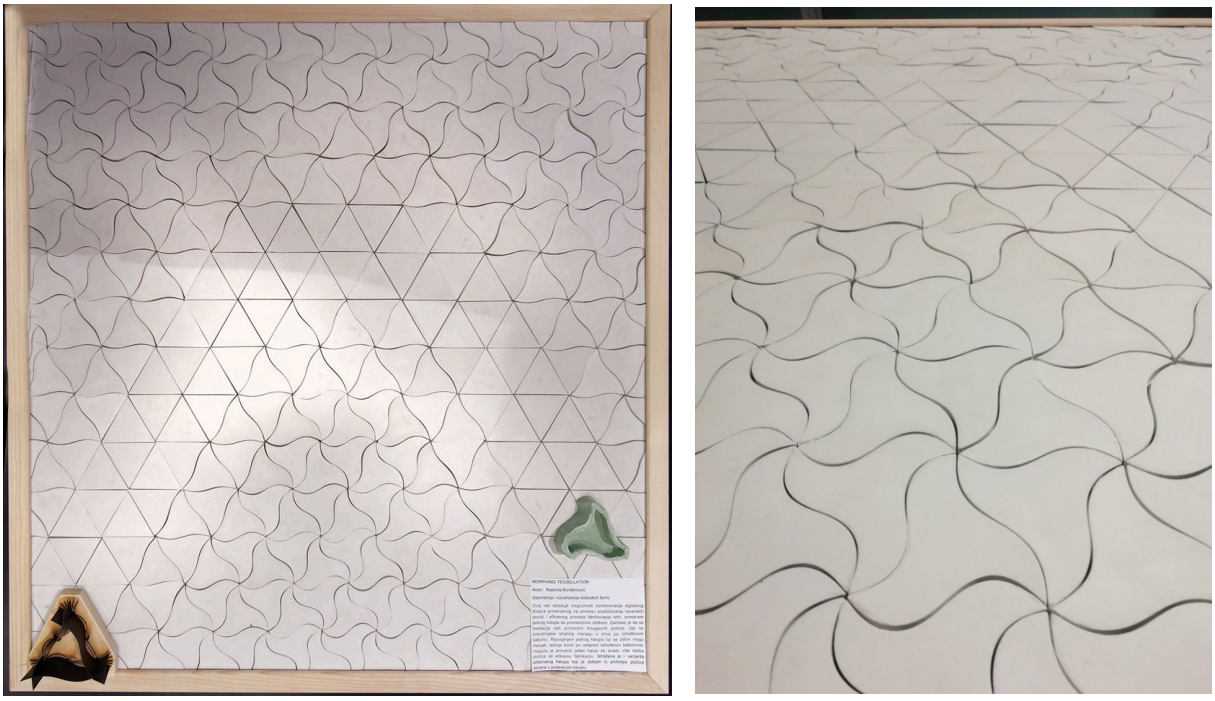

(a) (b)

Figure. 7: (a) Final model (Image from Digital Lab 2.0 Exhibition 2019, by Vesna Stojakovic) and (b) Detailed view of interlocking tiles

Once all 336 of the tiles were fabricated in the adjustable and silicone moulds, the following and final step consisted of assembling the tiles according to the chosen design. The final assembled model is shown in Fig. 7a. The practical application of the presented research was a success in that the tiles were easy to assemble and interlocked without major deviations. However, the walls of the tiles not being completely vertical with a slight tilt did cause slight variations in the width of the gaps between tiles (see Fig. 7b).

This stemmed from the aforementioned issues regarding the tilt of the adjustable walls of the mould. Overall, the entire composition was able to be assembled with minor discrepancies in fit, resulting from the handmade nature of the practical research.

4. Conclusion

The results of the research showed that Grasshopper is an invaluable tool for aiding the design process. It allowed for easy and quick changes to the initial design, as well as rationalizing the design for preparation for fabrication. In addition, the adjustable mould developed was successful in producing the differently shaped tiles. The research process showed that the thinner ABS edging tape proved more effective, without compromise on sturdiness. Furthermore, plastic in general, was a good choice of material in combination with the plaster as it provided a smooth base and easy release for the tiles. The project resulted in an aesthetically pleasing design using geometry as the sole variable parameter and was successfully fabricated in the form of a model, integrating these two processes for more efficient use in the fields of architecture and design in future.

The varying parameters set up in Grasshopper make the design easily adjusted for future research or projects, making it adaptable for a wide range of surface dimensions and visual effects. However, further investigation of different engraving methods could lead to improvement. Future research could involve testing the design of the adjustable mould base using a CNC milling machine as the engraving method, and seeing whether it solves problems regarding the focal length or residue build-up.

Acknowledgement

This research(paper) has been supported by the Ministry of Education, Science and Technological Development through the project no. 451-03-68/2020-14/200156: “Innovative scientific and artistic research from the FTS (activity) domain” and the University of Novi Sad, Faculty of Technical Sciences - Department of Architecture and Urban Planning.

References

Escher, M. C., Locher, J. L. (1974). The world of M.C. Escher. New York, H.N. Abrams; distributed by New American Library.

Giordano, C., Palmisano, N., Caruncho, D. R., Giordano Jones, C. (2018). Tilework in the Alhambra of Granada: visual edition. Barcelona, Dosde Publishing.

Gorini, C. (2018). Geometry for the Artist: An Interdisciplinary Consciousness-Based Course. 3. 1.

Grünbaum, B., Shephard, G. C. (1987). Tilings and patterns. New York, W.H. Freeman.

Lovric, M. (2003) “Magic Geometry: Mosaics in the Alhambra,” in: Meeting Alhambra, ISAMA - Bridges Conference Proceedings, University of Granada.

Pickover, C. A. (2009) The Math Book: From Pythagoras to the 57th Dimension, 250 Milestones in the History of Mathematics. New York, Sterling Publishing Co.

Van der Weijst, F. (2019) Glass Vaults: Introducing an Adjustable Mould for Casting Glass Voussoirs for Transparent Shell Structures, Master’s thesis, Delft University of Technology, Delft.

COMPARATIVE ANALYSIS OF METHODS FOR BLOOD VESSEL DETECTION IN RETINAL IMAGES

COMPARATIVE ANALYSIS OF METHODS FOR BLOOD VESSEL DETECTION IN RETINAL IMAGES

Radovan Turović
University of Novi Sad, Faculty of Technical Sciences, Novi Sad, Serbia
MSc, Teaching Assistant, radovan.turovic@uns.ac.rs

Gorana Gojić
University of Novi Sad, Faculty of Technical Sciences, Novi Sad, Serbia
MSc, Teaching Assistant, gorana.gojic@uns.ac.rs

Dinu Dragan
University of Novi Sad, Faculty of Technical Sciences, Novi Sad, Serbia
PhD, Assistant Professor, dinud@uns.ac.rs

Veljko Petrović
University of Novi Sad, Faculty of Technical Sciences, Novi Sad, Serbia
PhD, Assistant Professor, pveljko@uns.ac.rs

Dušan Gajić
University of Novi Sad, Faculty of Technical Sciences, Novi Sad, Serbia
PhD, Assistant Professor, dusan.gajic@uns.ac.rs

Ana Oros
Institute of Neonatology, Dept. of Retinopathy of Prematurity and Retinal Development, Belgrade, Serbia
MD, PhD*, annaoros03@yahoo.com*

ABSTRACT

Images of the back part of the eye, also known as retinal images, are the basis for the diagnosis of many systemic and eye diseases such as glaucoma, diabetic retinopathy, and retinopathy of prematurity. Disease indicators may be found by observing the blood vessel network in the retinal image. A failure of an ophthalmologist to correctly identify a disease, due to fatigue or a low-quality image, may lead to severe health damage. To address this problem, many methods for automatic vessel detection in retinal images have been proposed. Among those, machine learning approaches based on convolutional neural networks have proven to yield the best results. Often, these methods require some sort of input retinal image preprocessing, such as transformation to grayscale, to emphasize blood vessels on images and reach their full potential. In this paper, we employ a subset of general-purpose algorithms for edge detection to produce retinal images with an emphasized retinal blood vessel network, which can be used for convolutional neural network blood vessel detection training. We test Canny, Sobel, Scharr, and Hollisticaly-Nested Edge Detection algorithms on the DRIVE dataset. Resulting images produced by these four algorithms are evaluated by an experienced ophthalmologist. Each image was graded and the time required to make the decision was measured. The ophthalmologist (who operated under double-blind test conditions) was later interviewed and qualitative data was collected. The data was then analyzed showing a clear win for the Sobel algorithm which, according to the post-test interview, preserves more fine detail.

Keywords: computer vision; retinal images; blood vessel; edge detection

1. INTRODUCTION

Medical image analysis is a crucial factor in the diagnosis and treatment of many diseases. By looking at the retinal image showing the back part of the eye, an ophthalmologist can assess some of widespread diseases such as glaucoma, diabetic retinopathy, and retinopathy of prematurity. To determine the diagnosis, the ophthalmologist observes the density and spatial distribution of the blood vessel network in the image. It can be a challenging task to precisely identify the complete blood vessel network due to a low and inconsistent contrast between finer blood vessels and the image background, blurred retinal images, ophthalmologist's fatigue, etc. A failure to correctly identify segments of the blood vessel network may result in severe eye damage due to disease progression, which eventually can lead to blindness. To help early disease diagnosis and treatment, many automated, image-based systems for blood vessel segmentation have been developed. These systems are intended to assist the ophthalmologist in blood vessel segmentation.

Early work in automatic blood vessel detection was based on classical methods for image analysis, such as hand-crafted filters (Budai et al. 2013; Fraz et al. 2011, 2012; Soares et al. 2006) and line detectors (Nguyen et al. 2013; Ricci and Perfetti 2007). However, recent state-of-the-art solutions for this task are based on deep learning and convolutional neural networks (Leopold et al. 2019; Maninis et al. 2016; Oliveira, Pereira, and Silva 2018). Given enough image data and corresponding outputs, a neural network can learn important features required to map an input image to the corresponding output image. Typically, neural networks for vessel detection receive a color retinal image as an input and, as a result, output a vessel segmentation mask or a probability map. If the input image is too complex or features that the network should learn are not expressive enough in the color image, the image is usually transformed to other, more expressive domains, and used as a standalone or an extra input to the neural network. In the particular case of blood vessel detection, the input color image is transformed to enhance blood vessels on the retinal image. Stationary Wavelet Transform (SWT) is used in (Oliveira et al. 2018) to transform the image to a grayscale space which is later used to train the convolutional neural network for blood vessel detection. In (Leopold et al. 2019), the image is also converted into grayscale by extracting a green channel of the image, which is further enhanced by different filters.

The ability of the chosen transformation to emphasize image features that should be learned directly affects the performance of the neural network that is trained using transformed data. Although classic approaches for blood vessel detection are well behind deep learning approaches, they can still be used in a data preprocessing step, as is demonstrated by their common usage in existing methods. Inspired by this fact, we compare multiple well-established, general-purpose edge detection algorithms for automatic blood vessel enhancement on grayscale retinal image. The study is performed in a context of preprocessing transformations for retinal images used to train convolutional neural networks for automatic detection of a blood vessel network from a color image. Among classical edge detection algorithms, we choose Canny (Canny 1986), Sobel (Kanopoulos, Vasanthavada, and Baker 1988), and Scharr (Scharr 2000) edge detectors since they are proven to be the most widely used of all non-machine-learning algorithms. We also include the Holistically-Nested Edge Detection (HED) (Xie and Tu 2015) algorithm as a representative of general-purpose, deep learning algorithms for edge detection. All experiments are performed on images from DRIVE dataset (Soares et al. 2006). We apply all four edge detection algorithms on each color retinal image to obtain images showing blood vessel edges. The results are then graded by an experienced ophthalmologist according to how faithfully they display the blood vessels visible on the corresponding color retinal image. In our experiment, we assume that the method with the best grades by the expert is the best preprocessing transformation among suggested due to the best emphasis on blood vessels.

The findings of this research are interesting not only for its application to retinal image analysis but as a way to analyze the geometric properties of edge-detection filters—what is preserved and what is lost and how this level of detail interacts with various requirements edge detection may pose.

The rest of the paper is organized as follows. In Section 2, we present an experimental setup used in this paper, including the retinal image dataset used and methods tested. Section 3 gives a brief theoretical overview of the methods used in this research. Next, in Section 4, we present the statistical and visual results of our experiment. Section 5 closes the paper with the main conclusions and plans for future work.

2. MATERIALS AND METHODS USED

The experiments are performed on retinal images from the DRIVE dataset. The dataset was collected as a part of a screening program conducted by the Netherlands and comprises of 40 color retinal images, including 7 images with pathology. All images are captured by a Canon CR5 nonmydriatic 3CCD camera at 45º field of view. For each image, a blood vessel network is manually annotated by three observers, including one expert in the

field. The dataset is split into training and testing subsets, but since our experiment does not require training, all images are used for testing. Four characteristic images from the DRIVE dataset are shown in Figure 1.

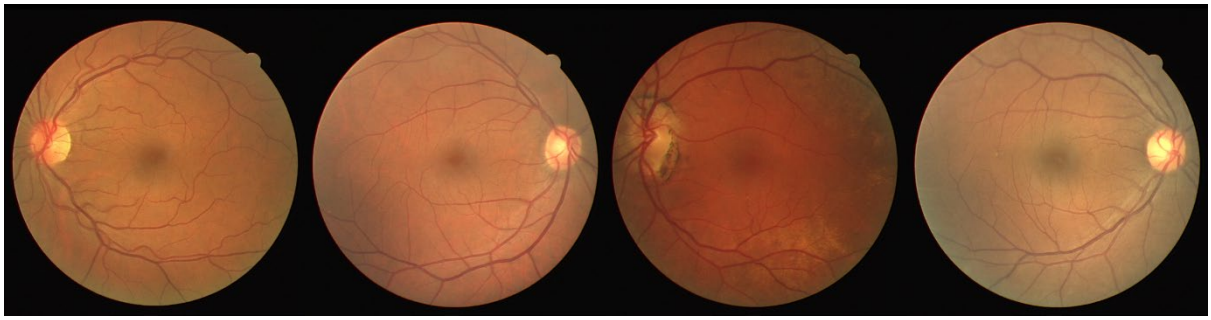

Figure. 1: Examples of images used in the experiment from the DRIVE dataset

The experiment was conducted on a workstation with the hardware specifications shown in Table 1. The operating system of the workstation is Ubuntu 18.04.3. All code used was written in the Python programming language, version 3.6 using version 4.8.2 of the Anaconda framework. The implementation of the Sobel, Scharr and Canny filters were the ones publicly available as part of the OpenCV library, version 3.4.2 through the Anaconda python wrapper.

Table 1: Hardware specification used in the experiment

CPU	*GPU*	*RAM*
AMD Ryzen 7 1700	*NVIDIA GeForce GTX TITAN X 11GB*	*32 GB*

Every image in the DRIVE dataset was used during the experiment. The experiment was conducted in the following steps, also shown in Figure 2:

1. All the images that are used as the input for the algorithms tested are first preprocessed.
2. Preprocessed images are fed into the Sobel, Scharr, and Canny filters, and the HED neural network.
3. All the resulting images are collected and assembled into a survey. Observers are asked to grade how easy it is for them to evaluate the condition of the blood vessels based on the shown images.
4. The data acquired as part of the survey which included the grades and the precise time needed for grading was analyzed statistically.

The concrete use of all the methods was based on the online documentation available for the OpenCV[1] library and the HED Git-hub repository[2] separately. For the classical methods, in all three cases, the first two steps were to smooth the image using a Gaussian filter in order to remove edge noise pixels and to convert the smoothed images from color to grayscale. Preprocessing for HED consists of simply turning images to grayscale to reduce color space complexity. From this step onwards, each method applies its own specific edge filter on the prepared input image. Parameters for each of the filters were selected independently. For Sobel, kernels of size 5x5 were used for calculations of second derivatives in both horizontal and vertical directions. In case of Scharr, for both directions first derivatives were used. Finally, Canny was used with lower and upper thresholds of 20 and 60. For Canny, thresholds were chosen based on the analysis of the histograms of grayscale images. Other parameters of these methods, if not listed, are left with their default values. For the HED neural network, the model used is the latest publicly available pretrained model[3]. Last step of all methods was to persist resulting edge-detected images.

[1] https://docs.opencv.org/ [Accessed: 17 January 2020]

[2] https://github.com/ashukid/hed-edge-detector [Accessed: 17 January 2020]

[3] Referenced from https://github.com/s9xie/hed [Accessed: 17 January 2020]

COMPARATIVE ANALYSIS OF METHODS FOR BLOOD VESSEL DETECTION IN RETINAL IMAGES

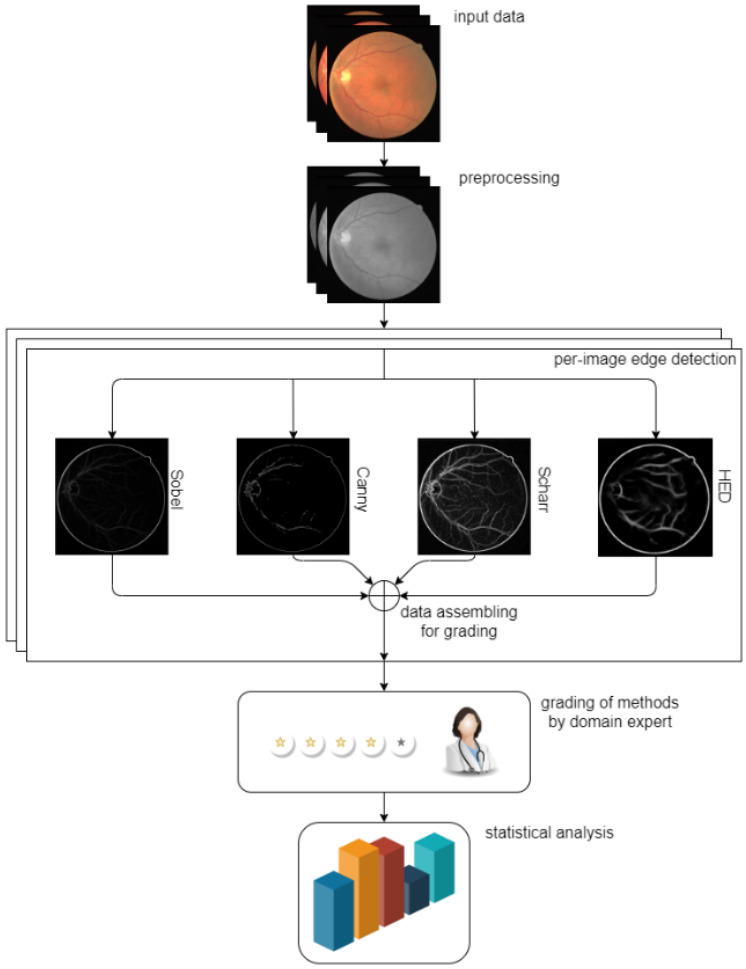

Figure. 2: General workflow of the experiment

The survey includes the original images and the transformed images. Each question of the survey contains the original image, the transformed image, and the grading scale. We used a grading scale from 1 to 5, where one means that it was very hard and five means that it was very easy for them to evaluate the condition of the blood vessels based on the shown images. Example of a question from the survey is shown in Figure 3. Unfortunately, in this experiment, only one ophthalmologist participated, although in the future we plan to include more domain experts. The participating ophthalmologist is an expert in the field with particular expertise in the retinopathy of prematurity (ROP) and with more than 25 years of experience. The survey is in Serbian language for the benefit of the observer who is a native Serbian speaker. In the example in Figure 3, we did not translate the text, because we wanted to show the original survey in the form presented to the observer.

3. RESEARCH FUNDAMENTALS

Edge detection is a class of methods in Computer Vision that examine images for existence of edges. The core idea is to map every pixel to the probability that the pixel is a part of the edge. The edge is a border between two neighboring groups of pixels with a significant change in color or color intensity.

Generally speaking, there are two classes of edge detectors to consider:

- Classic straightforward methods, such as Sobel, Scharr and Canny.
- Machine learning methods, such as the HED neural network.

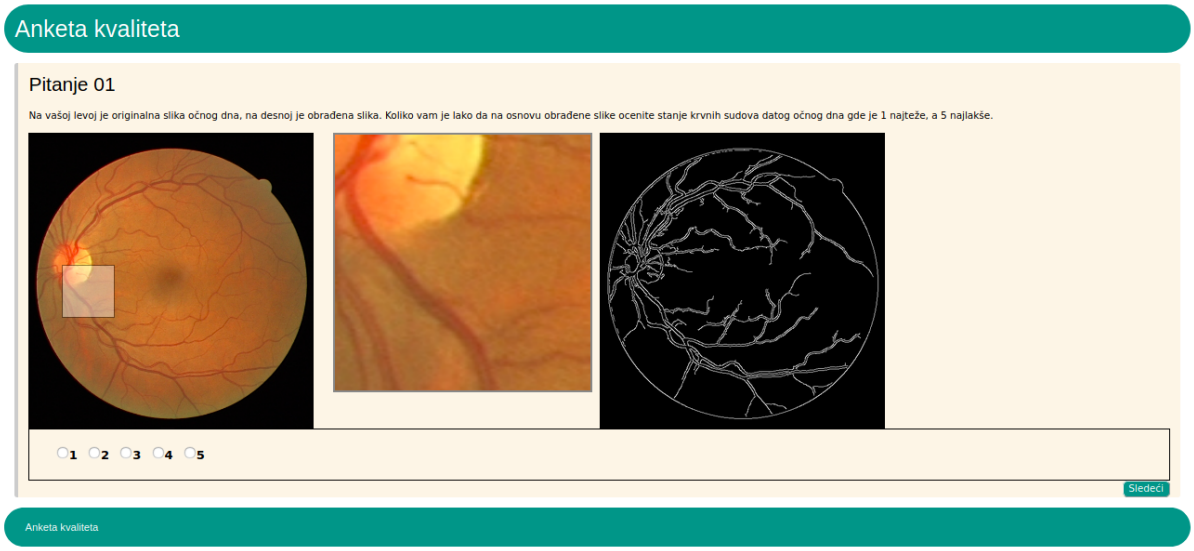

Figure. 3: Example of a question used in the survey which the ophthalmologist had to answer (the question is in Serbian and has the following translation: "On the left side is the original retinal image and on the right side is the processed image. How easy it is for you to evaluate the condition of the blood vessels in the processed retinal image, where 1 means very hard and 5 means very easy")

The first class of methods proved themselves insufficient for detecting edges between objects with insufficient pixel differences in their edge regions. Consequently, various machine learning methods for edge detection in images were developed to tackle this problem. Since machine learning methods also look for the context of the image, it is common to train domain specific machine learning models. For example, in the case of edge detection described in this paper, there is a specific use-case of discerning blood vessels in retinal images.

Sobel (Kanopoulos, Vasanthavada, and Baker 1988), Scharr (Scharr 2000), and Canny (Canny 1986) are based on a derivative analysis of an image. If an image is viewed as a discrete 2D function, whose inputs are the x and y coordinates of a pixel and whose output is the value of the pixel at [x, y]. An edge can then be modeled as a significant change in value of the function. Given that derivatives measure the rate of change of functions, they can be used to detect edges. In those regions of an image where edges are present, the derivative function reaches a local maximum, indicating that the relevant pixel belongs to the edge. To simplify calculation, the derivative is calculated from the partial derivatives over x and y, or in other words, in horizontal and vertical directions. Partial derivatives are calculated by means of convolution of each pixel with its neighboring pixels against a kernel as can be seen in Figure 4.

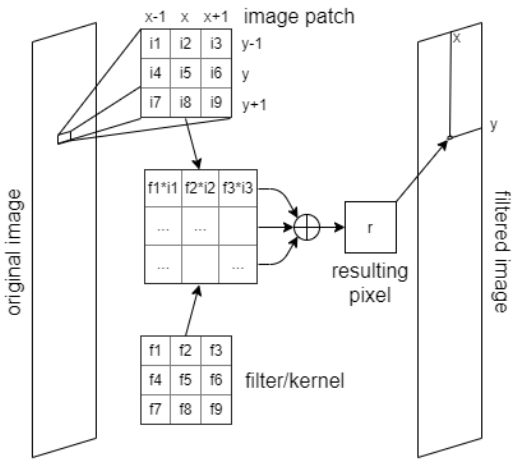

Figure. 4: Filtering image by using convolution

The kernel is an approximation of a derivative, enhanced with smoothing perpendicular to the direction of the derivative, so as to form a matrix. The total value of a derivatives indicates the probability of a given pixel belonging to the edge. The symmetrical Sobel kernels, used to implement the Sobel operator, can be seen in Figure 5. A linear combination of results after convolving a part of the image of the same size as the kernels, yields derivative value for a given pixel, i.e., edge probability.

a)

-1	*-2*	*-1*
0	*0*	*0*
1	*2*	*1*

b)

-1	*0*	*1*
-2	*0*	*2*
-1	*0*	*1*

Figure. 5: 3-by-3 Sobel operator; a) derivative in y direction; b) derivative in x direction

Scharr in his thesis explored ways of optimizing kernels. His main contribution was rotational invariation of kernels. This practically means that kernels for edge detection should return the same probability without respect to angle at which an edge is observed in an image. The OpenCVs implementation of a 3-by-3 Scharr optimization of the Sobel operator can be seen in Figure 6.

a)

-3	*-10*	*-3*
0	*0*	*0*
3	*10*	*3*

b)

-3	*0*	*3*
-10	*0*	*10*
-3	*0*	*3*

Figure. 6: 3-by-3 Scharr operator (OpenCV implementation); a) derivative in y direction; b) derivative in x direction

Canny filter is an upgrade to Sobel filter with additional steps. Canny aims to emphasize the "significant" edges more, so in its two additional steps it removes insignificant edges and noise and assimilates edges that are in immediate proximity to each other. The first step is based on hysteresis. Using two thresholds, pixels are divided in three groups, as "not edges" if the computed probability is below the lower threshold, as "sure edges" if the probability is over the higher threshold, and the rest are labeled as potential edge pixels. Potential pixels are accepted as edges if there is a path of only potential pixels to one of the "sure edge" pixels. It should be noted that Canny edge detection is based on removing insignificant and duplicated edges. This removes smaller details from resulting image.

HED is a neural network for general purpose edge detection (Xie and Tu 2015). It is a deep fully convolutional neural network. Here deep means that there is a large number of layers and that the network has high computational and memory complexity. Fully convolutional means that from start to end, every layer is convolutional, excluding pooling and activation layers. Convolutional layers have images as inputs and outputs, and the output is calculated using filters/kernels as in Figure 4. Main difference as compared to simple filtering is that parameters of kernels are learned in the process of training the neural network. Concretely, HED tackles the problems of different scales of objects, complex feature learning, and comprehending an image as a whole. The HED architecture consists of stacked activation and pooling layers and mini-stacks of convolutional layers. HED outputs multiple images in various sizes each produced by a mini-stack of convolutional layers. The final output aggregates all the mini-stack outputs into a single image with the same dimensions as the input image.

4. RESULTS AND DISCUSSION

The first step of the analysis of the grading data is the computation of summary statistics and basic visualization. To this end, we produced the results visible in Table 2 and Figure 7. As it can be seen from Table 2 and Figure 7, the confidence intervals do not overlap indicating a high probability of statistically significant difference in the grade averages. Given the relatively small size of the sample, and the experimental design, it was decided that robust methods would be called for. In the end Wilcox's implementation of Yuen's method for comparing means (Mair, Schoenbrodt, and Wilcox 2014; Wilcox 1997, 2012; Wilcox and Tian 2011) using pooled variance for repeated measures design with 10% trimmed means was employed with a *post-hoc* comparison design corrected using Holm's method. These results are presented in Table 3.

COMPARATIVE ANALYSIS OF METHODS FOR BLOOD VESSEL DETECTION IN RETINAL IMAGES

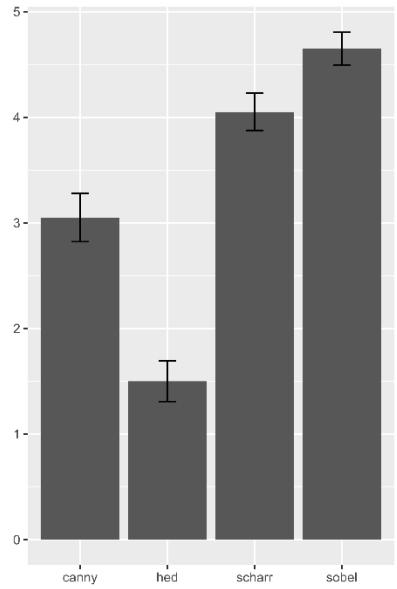

Figure. 7: Mean plot of grades with 95% CIs, $n = 40$.

Table 2: Descriptive statistics of ophthalmologist grading data, $n = 40$.

Filter	*Grade Mean ± 95% CI*	*Grade Standard Deviation*
Canny	*3.05 ± 0.22*	*0.71*
Sobel	*4.65 ± 0.15*	*0.48*
Scharr	*4.05 ± 0.17*	*0.55*
HED	*1.5 ± 0.19*	*0.60*

When dealing with time, the methods were the same, albeit with more modest success. Figure 8 and Table 4 demonstrate the descriptive statistics done on the data.

Table 3: Result of group mean comparison, ophthalmologist grade, $n = 40$. A measure of zero for the probability indicates a probability value too small for the algorithm to detect.

Filter comparison	$\hat{\psi}$	$\hat{\psi}$ *95% CI lower bound*	$\hat{\psi}$ *95% CI upper bound*	*p*	*Significant?*
Scharr vs. Sobel	*-3.190*	*-3.560*	*-2.820*	*0*	*Yes*
HED vs. Sobel	*-2.500*	*-2.780*	*-2.220*	*0*	*Yes*
HED vs. Scharr	*-1.590*	*-1.980*	*-1.210*	*3.15e-12*	*Yes*
Canny vs. Sobel	*-0.969*	*-1.400*	*-0.541*	*8.22e-7*	*Yes*
Canny vs. HED	*-0.625*	*-0.901*	*-0.349*	*8.22e-7*	*Yes*
Canny vs. Scharr	*1.590*	*1.20*	*1.99*	*5.16e-12*	*Yes*

Given the partially overlapping confidence intervals and the unpromising nature of the stats, it is to be expected that the results of statistical analysis are similarly dubious. Indeed, as Table 5 shows, the results are unclear. While it is clear that the times are mostly different, it is impossible to differentiate between HED and Scharr and Canny and Sobel. In other words, there are two groups, the slow and the fast, but within those groups there is no difference that the statistical instruments used within this paper can detect.

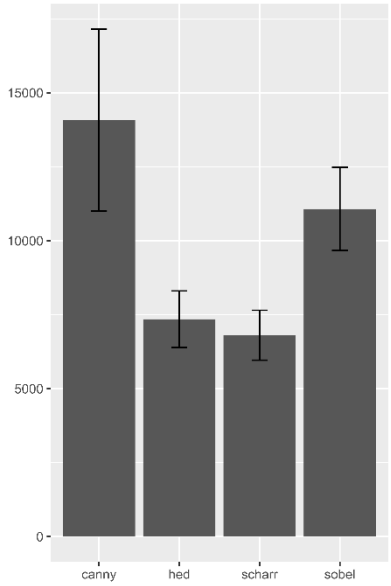

Figure. 8: Mean plot of times with 95% CIs, $n = 40$. Time measured in ms.

Table 4: Descriptive statistics of ophthalmologist time data, $n = 40$.

Filter	*Time Mean ± 95% CI*	*Time Standard Deviation*
Canny	*14080 ± 3067*	*9591*
Sobel	*11073 ± 1404*	*4390*
Scharr	*6808 ± 843*	*2635*
HED	*7350 ± 953*	*2981*

Table 5: Result of group mean comparison, ophthalmologist time, $n = 40$.

Filter comparison	$\hat{\psi}$	$\hat{\psi}$ *95% CI lower bound*	$\hat{\psi}$ *95% CI upper bound*	*p*	*Significant?*
Scharr vs. Sobel	*-4329*	*-6711*	*-1947*	*9.11e-5*	*Yes*
HED vs. Sobel	*-3821*	*-6208*	*-1434*	*3.47e-4*	*Yes*
HED vs. Scharr	*452*	*-911*	*1815*	*3.99e-1*	*No*
Canny vs. Sobel	*1770*	*-2036*	*5575*	*3.99e-1*	*No*
Canny vs. HED	*4831*	*1680*	*7982*	*4.47e-4*	*Yes*
Canny vs. Scharr	*5631*	*2213*	*9048*	*2.98e-4*	*Yes*

To visually illustrate the effects of the chosen methods on the retinal images, we provide Figure 9. The first row shows four randomly selected images from the DRIVE dataset, while the rows from the second to the fifth show corresponding result images produced by Canny, Sobel, Scharr, and HED methods, respectively.

5. CONCLUSION

From the presented experimental results, we can clearly conclude that, when it comes to quality, the Sobel edge detection is by far the best, followed by Scharr, and then trailed by Canny. HED is simply not worth using in this context. The results of the time comparison are less clear, but a possible interpretation of the results is that slower response times correspond to the level of detail, on the one hand, and the level of contrast, on the other. The experimental design did not allow us a way of determining if this interpretation is true. Therefore, more research is clearly required if this problem is to be solved.

The results of the grading are counterintuitive. Scharr is an upgrade of Sobel and yet is rated a little bit worse. Canny is an even further upgrade and is worse still. HED is a modern, machine-learning powered method, and yet it ranks worst of all. This is precisely the opposite of the expected results. Some additional context is accessible through the qualitative data gathered in a post-test interview with the ophthalmologist, expert. It turns out that the more advanced models that emphasize edges and clear out the noise also remove vital detail that the expert needs to make a diagnosis. The expert identified HED as completely lacking the small details needed for diagnostics (indeed, HED depicts only the broad outlines of an image: precisely what it has been designed to do), and Canny's

COMPARATIVE ANALYSIS OF METHODS FOR BLOOD VESSEL DETECTION IN RETINAL IMAGES

thresholding approach creates what the expert called “empty areas”, void of any texture or detail that is needed to characterize a retinal image. It should also be noted that HED, provided as-is, is a general-purpose edge detector CNN. There is a possibility that, should HED get explicitly trained for this use-case, it may yield better performance.

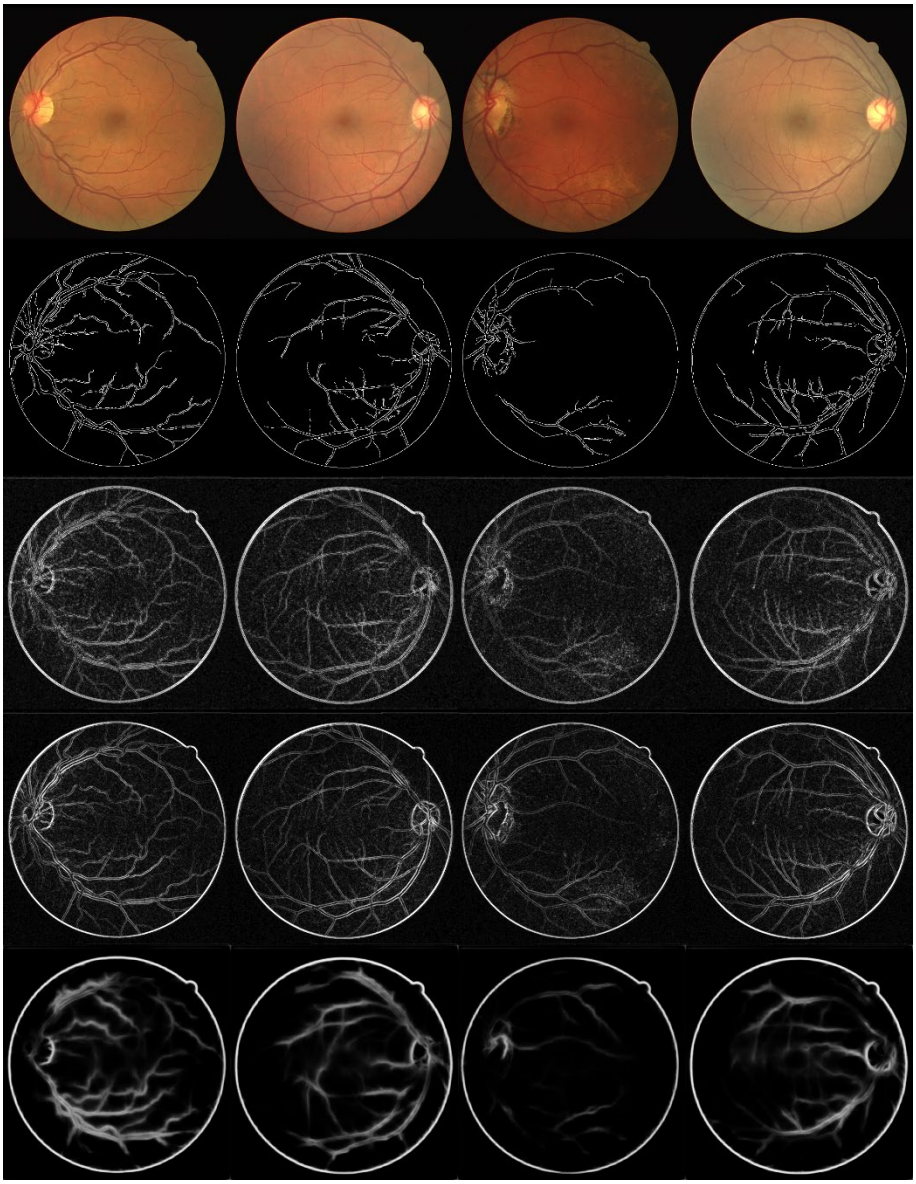

Figure. 9: Original images (the first row) and resulting images (Canny, Sobel, Scharr and HED edge detectors respectively)

From graphics standpoint pixel color and intensity values do not depict the difference between small blood vessels which form the region of interest from the background in a straightforward way. This renders classical edge detection methods unable to differentiate edges of the small blood vessels, while HED is unable to by design. With this fresh insight, we can conclude that general-purpose edge algorithms are not appropriate even for the pre-processing step. Methods which perform well for regular photographs are not suitable in the considered case. Filters used to prepare medical images of this type for machine learning model training need to preserve texture, small details, and to differentiate between thicker and thinner blood vessels. To this end, more research is needed in the construction of a custom-designed filter made to dramatically increase contrast and isolate precisely the features of interest in input images.

COMPARATIVE ANALYSIS OF METHODS FOR BLOOD VESSEL DETECTION IN RETINAL IMAGES

REFERENCES

1. Budai, A., R. Bock, A. Maier, J. Hornegger, and G. Michelson. 2013. "Robust Vessel Segmentation in Fundus Images." *International Journal of Biomedical Imaging* 2013.
2. Canny, John. 1986. "A Computational Approach to Edge Detection." *IEEE Transactions on Pattern Analysis and Machine Intelligence* PAMI-8(6):679–98.
3. Fraz, M. M., P. Remagnino, A. Hoppe, B. Uyyanonvara, Christopher G. Owen, Alicja R. Rudnicka, and S. A. Barman. 2011. "Retinal Vessel Extraction Using First-Order Derivative of Gaussian and Morphological Processing." *Lecture Notes in Computer Science (Including Subseries Lecture Notes in Artificial Intelligence and Lecture Notes in Bioinformatics)* 6938 LNCS(PART 1):410–20.
4. Fraz, M. M., P. Remagnino, A. Hoppe, B. Uyyanonvara, A. R. Rudnicka, C. G. Owen, and S. A. Barman. 2012. "Blood Vessel Segmentation Methodologies in Retinal Images - A Survey." *Computer Methods and Programs in Biomedicine* 108(1):407–33.
5. Kanopoulos, Nick, Nagesh Vasanthavada, and Robert L. Baker. 1988. "Design of an Image Edge Detection Filter Using the Sobel Operator." *IEEE Journal of Solid-State Circuits* 23(2):358–67.
6. Leopold, Henry A., Jeff Orchard, John S. Zelek, and Vasudevan Lakshminarayanan. 2019. "PixelBNN: Augmenting the Pixelcnn with Batch Normalization and the Presentation of a Fast Architecture for Retinal Vessel Segmentation." *Journal of Imaging* 5(2).
7. Mair, Patrick, Felix Schoenbrodt, and Rand Wilcox. 2014. "WRS2: Wilcox Robust Estimation and Testing."
8. Maninis, Kevis Kokitsi, Jordi Pont-Tuset, Pablo Arbeláez, and Luc Van Gool. 2016. "Deep Retinal Image Understanding." Pp. 140–48 in *Lecture Notes in Computer Science (including subseries Lecture Notes in Artificial Intelligence and Lecture Notes in Bioinformatics)*. Vol. 9901 LNCS. Springer Verlag.
9. Nguyen, Uyen T. V., Alauddin Bhuiyan, Laurence A. F. Park, and Kotagiri Ramamohanarao. 2013. "An Effective Retinal Blood Vessel Segmentation Method Using Multi-Scale Line Detection." *Pattern Recognition* 46(3):703–15.
10. Oliveira, Américo, Sérgio Pereira, and Carlos A. Silva. 2018. "Retinal Vessel Segmentation Based on Fully Convolutional Neural Networks." *Expert Systems with Applications* 112:229–42.
11. Ricci, Elisa and Renzo Perfetti. 2007. "Retinal Blood Vessel Segmentation Using Line Operators and Support Vector Classification." *IEEE Transactions on Medical Imaging* 26(10):1357–65.
12. Scharr, Hanno. 2000. "Optimale Operatoren in Der Digitalen Bildverarbeitung." University of Heidelberg, Germany.
13. Soares, João V. B., Jorge J. G. Leandro, Roberto M. Cesar, Herbert F. Jelinek, and Michael J. Cree. 2006. "Retinal Vessel Segmentation Using the 2-D Gabor Wavelet and Supervised Classification." *IEEE Transactions on Medical Imaging* 25(9):1214–22.
14. Wilcox, Rand. 1997. "Pairwise Comparisons Using Trimmed Means or M-Estimators When Working with Dependent Groups." *Biometrical Journal* 39(6):677–88.
15. Wilcox, Rand R. 2012. *Introduction to Robust Estimation and Hypothesis Testing*.
16. Wilcox, Rand R. and Tian S. Tian. 2011. "Measuring Effect Size: A Robust Heteroscedastic Approach for Two or More Groups." *Journal of Applied Statistics* 38(7):1359–68.
17. Xie, Saining and Zhuowen Tu. 2015. "Holistically-Nested Edge Detection." *Proceedings of the IEEE International Conference on Computer Vision* 2015 Inter:1395–1403.

GEOMETRY USAGE FOR THE DESIGN OF STREAMLINED BODY

Aleksandra Stakić
Department of Theory of Mechanisms and Machines, Faculty of Mechanical Engineering, University of Belgrade, Republic of Serbia
PhD.student, Research Assistant, aleksandrastakic@yahoo.com

Ognjen Scepanović
Faculty of Mechanical Engineering, Belgrade, Republic of Serbia
M.Sc. student, scepanovic.ognjen@gmail.com

Lazar Vidosavljević
Faculty of Mechanical Engineering, Belgrade, Republic of Serbia
B.Sc. student, lazar19a@gmail.com

Stefan Berdić
Faculty of Mechanical Engineering, Belgrade, Republic of Serbia
B.Sc. student, stefanberdic@gmail.com

ABSTRACT

Almost all modern industries, from manufacturing industries to movie making companies, use some kind of graphic design software. Designing a new product via graphic software can reduce a lot of time in the manufacturing processes. Further, new shapes and more complex geometries can be created to improve the overall aesthetics. Complex geometry created in the designing process does not need to be a simple combination of standard geometric shapes (a cube, cylinder, sphere), much more complex curves can be used as well. Complex curves can be created using splines, which are defined piecewise by higher-order polynomials. The surfaces constructed by splines will have a smooth curvature transition without sharp edges, which plays a significant role in its light reflection. The mathematical definition of splines allows easy implementation in computer graphics, especially in the cases when it is necessary to trace the predefined curves or contours of objects. Using this method, it is possible to convert any object from its picture into a 3D model. This paper will present the modelling processes of a sports car from its pictures, where surfaces are created with splines in SolidWorks 2018.

Keywords: 3D modelling, geometric elements in costume design, applied geometry

1. INTRODUCTION

Body design in the automotive industry is a creative process which, in addition to the development (aesthetics of the product) of visual appearance, is accompanied by a number of other challenges that designers face during its creation. A team of experts from various disciplines participates in the design process. It all starts with an idea that is transferred to paper in the form of hand-drawn sketches. The path that the idea must take is a development path during which a series of changes will occur as a result of a compromise between the design and functionality of the vehicle. According to the conventional method, the initial idea of the model is realized by sketching, and then the process of clay modelling visualizes the car body [1]. Given the fact that this modelling process takes a lot of time and resources, it was necessary to improve it [2]. With the advent of CAD software, there is a possibility of creating a virtual 3D model based on 2D sketches. This raised the design process to a higher level, and the use of clay modelling patterns was pushed into the background. Thanks to simulations that are an integral part of the CAD software, it is possible to analyse 3D models from various aspects, including the kinematic, dynamic, thermodynamic ones etc. This results in greater cost-efficiency through reducing the time of development of the

design process. In this way, from the initial idea of the designer through functional studies, a perfect combination of quality, safety, functionality and, of course, good taste is reached.

2. PROBLEM FORMULATION

As part of the Aesthetic Design course in the first year of Master studies, Professor Popkonstantinović insists on creating an original product design. The task is to make a 3D model of the design of a machine assembly, where one of the basic requirements is not to use simple combinations of standard geometric shapes such as cubes, cylinders, spheres, etc. but instead use more complex surface curves, which will result in an improvement in the overall aesthetics of the product. Taking into account the set requirements, a 3D model of a sports car of the Lamborghini Aventador make was made. The idea of the design, as well as the modelling process, was performed based on YouTube tutorials [3]. Regardless of the above, the design presented in this paper is original and was made by a group of students in their graphic work developed for the needs of an aesthetic design course.

Figure 1. Lamborghini Aventador /Source: Lamborghini/

3. FORMING OF THE CONCEPTUAL DESIGN

In addition to aesthetic qualities, a well-designed product includes many other characteristics that are a response to different needs. Therefore, the initial phase in the process of designing a new product primarily includes its specification. This means that, at the very beginning, all the requirements that can be set and which can affect the quality of the finished product, must be clearly defined. In this phase, communication with customers is of special importance, after which the needs of clients are clearly defined and then the production of drawing begins. During the development of the idea, the emphasis is placed on the conventional methods of making drawings, and not on the digital ones, so the designer has several techniques at his/her disposal that help him/her in the process of forming the concept. One of these techniques is freehand sketching, which enables the rapid development of an idea and its presentation to others. In addition, it is the easiest and freest form of expression for a designer, because his/her idea is translated into paper by use of a pencil. A good sketch should contain three basic characteristics: quick preparation, simplicity and easy interpretation [4]. An example of freehand sketching of a machine part is given in Figure 2.

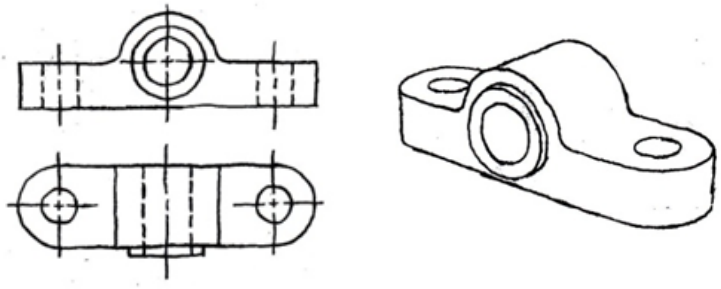

Figure 2: A 2D and 3D view of the machine part in a freehand sketch [4]

During the creation of a drawing, the moment of visualization is very important. It refers to the ability of a designer to come up with a conceptual solution for the design of a model. It is possible to make a design of a product on the basis of an already existing model, and, when making such a drawing, there is a direct connection between the designer's hand and the object he/she is drawing (Figure 3). However, the visual image of that object in the

designer's head and mind plays a major role in the process of creating the idea. During this process, the sketch begins to adapt to the new visual form of the object formed by the mind and thus creates the original form of the object in relation to the object used by the designer when he/she started the drawing (Figure 4).

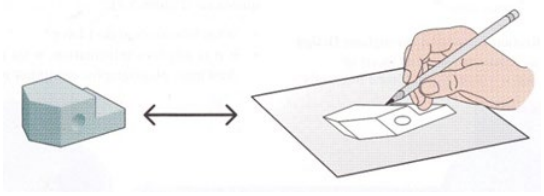

Figure 3: The eye-hand connection [4]

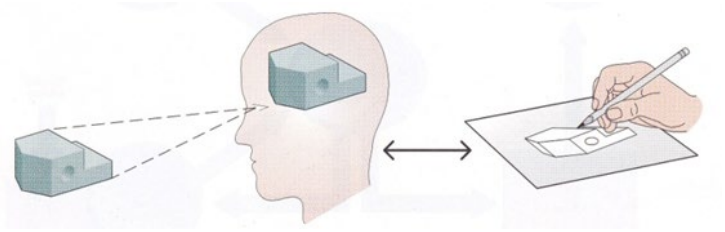

Figure 4: The eye-mind-hand connection [4]

In this paper, the method of freehand sketching was used in the initial phase of the design process (Figure 5). During this phase, the previously mentioned requirements defined by the clients were taken into account, as well as the requirements that take into consideration the functional characteristics of the car that should be met (good aerodynamics, symmetry, etc.). Certainly, the inspiration in these moments is the most deserving for the formation of the original idea. Designers find their inspiration in a variety of sources that are all around us, but at the heart of it all is geometry.

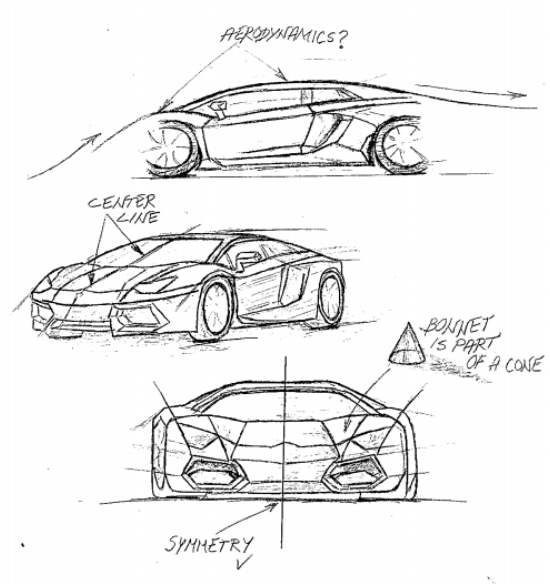

Figure 5: Freehand sketching

When forming a conceptual solution, special attention is paid to determining the ideal proportions. Whether it is designing a car or some other product, choosing a harmonious relationship of the dimensions is considered to be the key to aesthetics and harmony. The use of the golden ratio in the design gives the viewer a visual sense of natural elegance. Figure 6 shows the idea of applying the golden ratio using a Fibonacci spiral, in an infinite series of golden rectangles, during the design of a Lamborghini Aventador car.

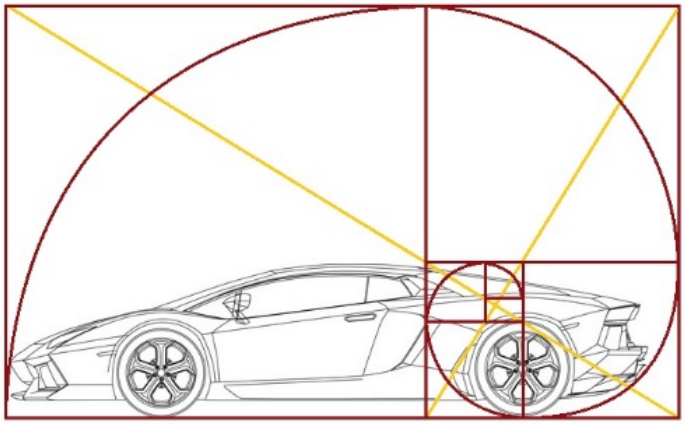

Figure 6: Presentation of the application of the Fibonacci spiral in an infinite series of golden rectangles

4. DRAWING CURVES

In this paper, a 3D software package SolidWorks 2018 was chosen for the purpose of forming a car model. At the very beginning, it was most important to collect the best possible blueprints with a clearly defined design idea. Therefore, the first step was to prepare blueprints whose lines would be monitored throughout the modeling process. The collected group of blueprints must have a sufficient number of views, and most often this includes a side, top, front and rear view. The next step was to properly position the 2D drawing in adequate positions (Figure 7).

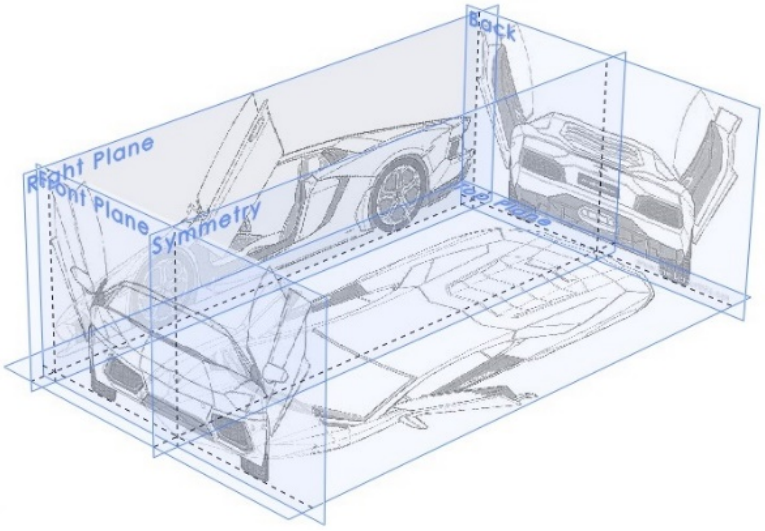

Figure 7: 2D blueprints positioned in 3D space

A 3D sketch and a spline option were used to draw curved lines according to the already created sketch. In order to obtain a curved surface that connects two adjacent curved lines, the boundary surface option was used (Figure8). This way of forming the curved surfaces was used during the creation of the whole model with minor variations.

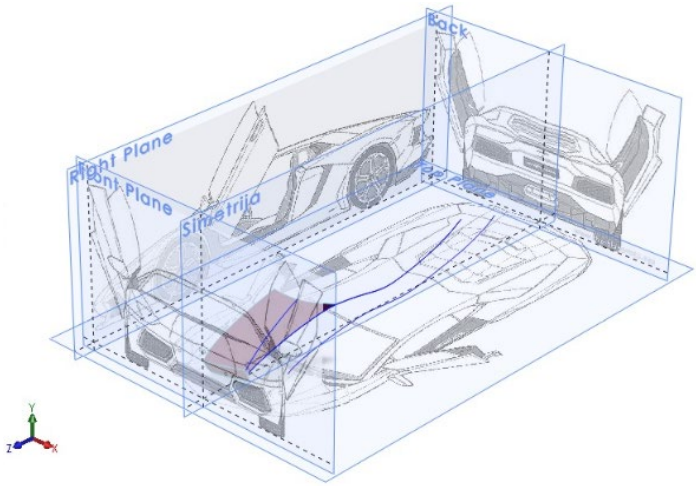

Figure 8: Forming of the curved surfaces

Considering the unusual design of the hood of the car and not at all simple contour, it was necessary to introduce an additional surface (Figure 9) which would allow easier and more accurate mirroring of the idea from the draft to the car model itself. This procedure achieves the desired effect of the distance between two curved surfaces, i.e. a clear contour of the car hood.

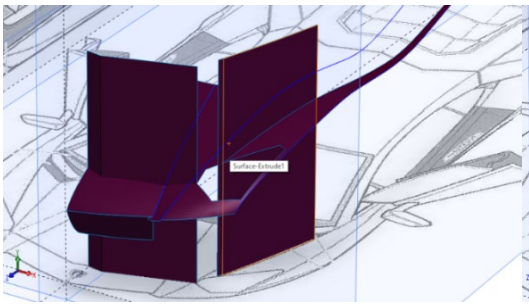

Figure 9: Introducing an additional surface

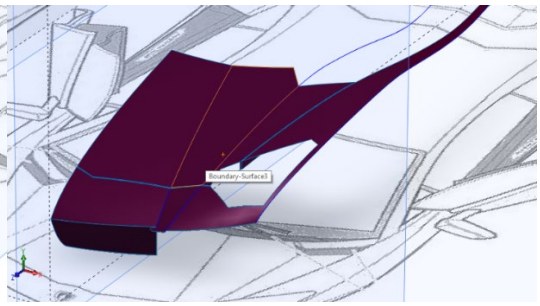

Figure 10: Formed contour

First, one side of the car model was formed, after which the whole model was completed thanks to the plane of symmetry and the use of the mirror option, which allows the surface to be mirrored (Figure 11).

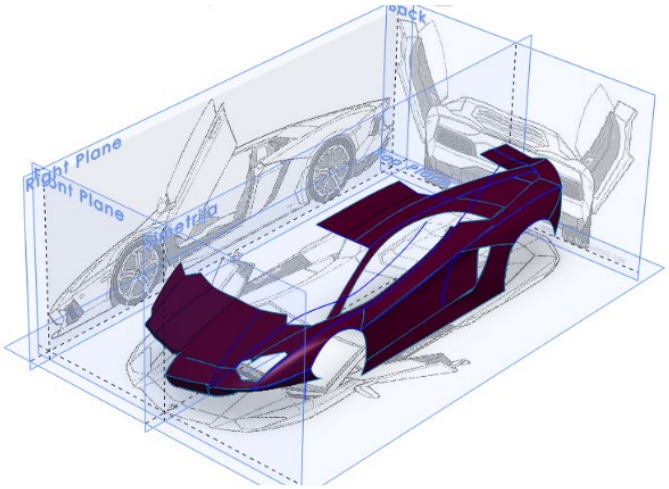

Figure 11: The use of plane of symmetry in the process of forming a 3D model

As this is a complex model of a large number of different curved surfaces, it was necessary to combine them into one whole, which was made possible by using the Knit Surface option, offered by SolidWorks. The final phase of 3D modeling is the generating, using the "Wireframe" model (Figure 12). Functionality and interaction with customers are an imperative, so we must not allow them to remain in the shadow of the visual appearance of the final product. Wireframe models can also be used as input geometric data for the finite element model analysis [6].

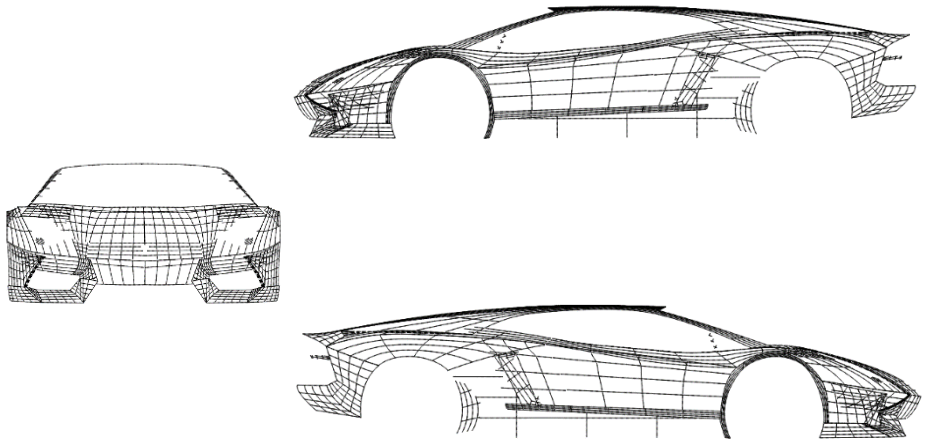

Figure 12: 2D view of Wireframe model

5. MODEL PRESENTATION

In order to present the final product in a way that will create an image of the model in a real environment in the eyes of viewers, it is necessary to fill the entire space with photorealistic effects. Adding effects such as lighting, with the proper choice of materials, will bring the final product to a photorealistic look thanks to the reflection of the light from the surface of the model. In addition to lighting, a background effect is introduced, which can greatly determine the visual display of the created design. The final step in forming a three-dimensional visualization is a rendering process that generates a predefined 3D scene.

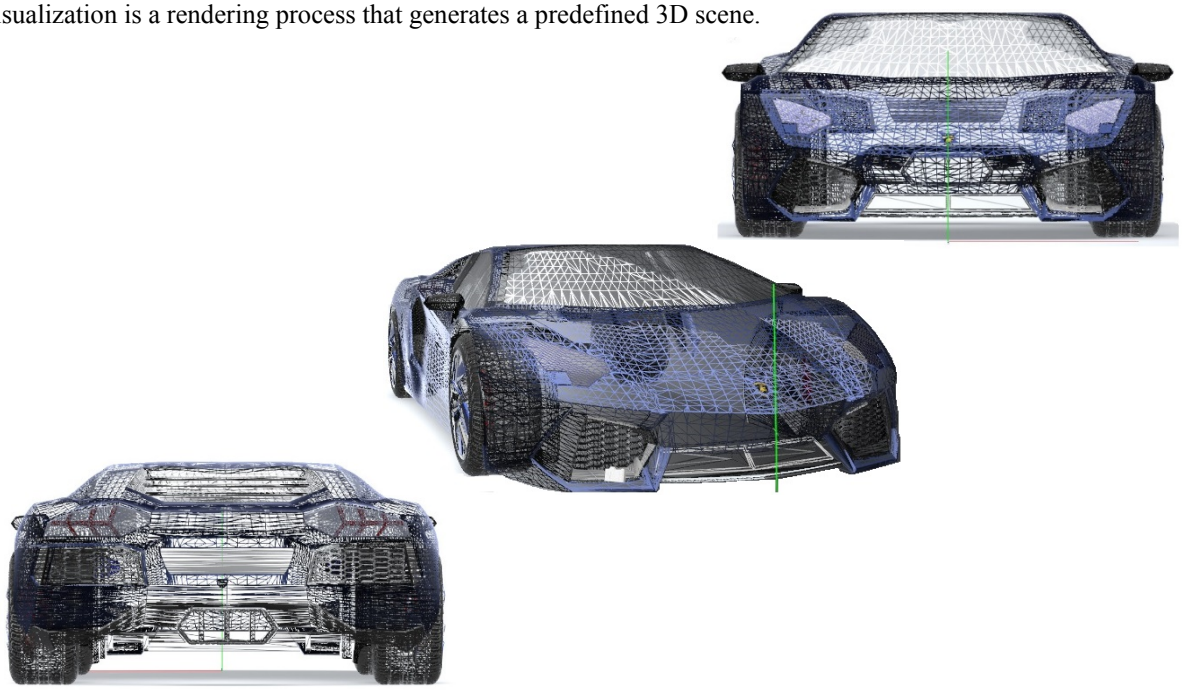

Figure 13: A 3D view of the wireframe model

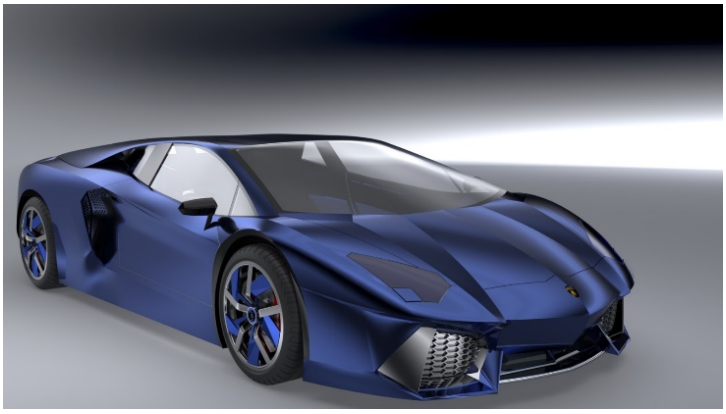

Figure 14: View of the car model after rendering

The 3D plane bilateral symmetry of the car model shown in Figure 15 is conditioned by the constructive dynamic characteristics of lateral stability [5].

Figure 15: Frontal central projection and symmetry of the Lamborghini Aventador car

Since this is a model whose main functional characteristic is movement, the model would fit the view that contains reflections of aerodynamic forms which suggest movement and speed, as well as the view of the specific visual relationship of the movement of the model in relation to the stationary environment [5] (Figure 16).

Figure 16: Frontal projection of a Lamborghini Aventador car

REFERENCES

[1] Georghina G., Tutunea D., Dima A., Popa D.: 3D model based process in automotive industry, Applied mechanics and materials, Volume 880, 2018, Pages 151-156, ISSN 1660-9336,

[2] Sibois R., Salminen K., Siuko M., Mattila J., Määttä T.: Enhancement of the use of digital mock-ups in the verification and validation process for ITER remote handling systems, Fusion Engineering and Design, Volume 88, 2013, Pages 2190-2193, ISSN 0920-3796,

[3] Ginestou Romain:

https://www.youtube.com/watch?v=LloKqeikZZM&list=PLUgk_zEXfs_UQE35wUr0QEuCbJbefs0NX

[4] Jeli Z., Popkonstatinović B., Stojićević M.: Usage 3D Computer Modeling in Learning Engineering Graphics,

[5] Popkonstatinović B, Aesthetics of visual communications, University of Novi Sad, Faculty of Technical Sciences, Serbia, 2013

[6] Jeli Y., Graphic communications and virtual reality in the development of technical systems [doctoral dissertation], Mechanical Engineering Faculty, University of Belgrade, 2013.

PRINCIPLES OF TRANSFORMATION USED IN ARCHITECTURAL DESIGN AND THEIR IMPACT ON THE FORMS OF BUILDINGS

Sanja Spasić Đorđević
Faculty of Civil Engineering and Architecture, University of Niš
PhD student, sanjaspasicdjordjevic@gmail.com

Vladan Nikolić
Faculty of Civil Engineering and Architecture, University of Niš
Professor, vladan_nikolic@yahoo.com

Sanja Janković
Faculty of Civil Engineering and Architecture, University of Niš
PhD student, sanja.jankovic@outlook.com

Olivera NIkolić
Faculty of Civil Engineering and Architecture, University of Niš
PhD, Assistant professor, o_milosavljevic@yahoo.com

ABSTRACT

The development of modern technologies, industry, but also greater possibility of application of technical mechanisms had considerable influence on the deviation from the traditional architectural structures. The ability to move, rotate, modify parts of buildings until recently represented only a futuristic approach to design on paper, without clear and workable solutions in practice. Transformation as a method which is applied in architectural design, push the boundaries when it comes to the form of the object. The possibilities of applying this method are significant, they are used in the visual improvement of the project, in order to increase the functional parameters of the buildings, but also to achieve energy efficient buildings. The purpose of analyzing these principles, as well as their effects on the shape of an individual object, the paper presents some of the examples that are built around the world. This work highlights the possibilities offered by transformability as a method used in architecture, as well as the impact of these on the design process and the visual identity of built objects.

Keywords: transformation, architectural design, buildings, geometry forms

1.0. INTRODUCTION

Designing architectural objects has always been considered a creative process that has adapted to the modernization of technical capabilities, research about new materials, and also the development of human

knowledge. However, despite this, "architectural object for a long time was considered a static category."[1] Transformation of objects and change of form after construction are ideas that were previously considered impossible or used to a small extent as technical support and part of the construction of the object, rather than as a product of a specific design. In recent years there has been an expansion of objects that by changing their geometry affected also the functional change, energy and aesthetic requirements of the building. For this reason, a transformable and transportable architecture should be distinguished. While transformable architecture refers to the ability to change location and facility re-use, here we are talking about methods to improve the performance of the object itself. New, bold ideas adapt the architectural design of the building to the specific requirements of the customer, which increases the quality of stay in such buildings. "Transformability can be considered as an important way to respond to the building user's ambitions."[2] For all these reasons, transformability is an architectural process that uses different methods as a creative expression of architects, but also opens up new opportunities for further research. This paper will discuss the methods used in applying the principles of transformability, as well as specific solutions that are used at already constructed buildings.

The aim of the paper is to analyze methods that support the principle of transformable architecture from the aspect of changing geometric shapes, more precisely, at what level transformable architecture can affect the form and the visual identity of an object.

2.0. PRINCIPLES AND APPLICATION OF TRANSFORMABLE ARCHITECTURE

For the moving design of parts of an object, changing the geometry of an object, modifying a built object, various terms are often used in the literature. Often these terms do not have the same meaning and need to be distinguished (kinetic architecture, variable, adaptable, interactive, transportable, modular, transformable, rotating ..). According to R. Kronenburg[3], the whole term for user-friendly architecture is flexible architecture. In one of his works, he states that flexible architecture represents " buildings that are intended to respond to changing situations in their use, operation, or location. This is architecture that adapts rather than stagnates; responds to change rather than rejects it; is motive ratherthan static. It is a design form that is by its essence cross disciplinary and multi-functionaland consequently, is frequently innovative and expressive of contemporary design issues"[4].

Transformable architecture, the theme of our work, is only one part of flexible architecture. In his research, Lee[5] divides flexible architecture into:

- **Adaptable** - the name for a flexible architecture that can be customized to the user (open plan space where it is possible to modify the partitions and furniture layout, or use modules that would be added to the base unit and to adjust that way). The most famous example of this type is Le Corbusier's Domino House.

[1] Kondić S. (2009): The application and importance of the principle of kinetic architecture in the design of family housing, nauka+praksa, Niš, Serbia
[2] Asefi M. (2012): Transformation and movement in architecture: the marriage among art, engineering and technology, Procedia - Social and Behavioral Sciences, Volume 51, 2012, Pages 1005-1010
[3] Kronenburg R. (2008): Portable ArchitectureDesign and Technology, book, Springer Science & Business Media
[4] Kronenburg, R. H. (2004). Flexible Architecture: The Cultural Impact of Responsive Building. In 10th International Conference on Open Building (pp. pp). Paris, France: CIOB.
[5].Lee J.D. (2012): Adaptable, Kinetic, Responsive, and Transformable Architecture: An Alternative Approach to Sustainable Design , Phd thesis

- **Kinetic** - The basic feature of this subtype is the motion. Kinetic architecture is the ability of an object to move some of its parts or the entire object with the help of energy. The most famous examples of this subtype are the pavilions.
- **Responsive** (in some papers used the term interactive[6]) - the ability for an object to respond to and adapt to environmental conditions.
- **Transformable** - refers to changing the shape of a building and will be discussed further in the future.

According to Kronberg's definition[7], transformable architecture refers to "buildings that change shape, space, form or appearance by the physical alteration of their structure, skin or internal surface, enabling a significant alteration in the way it is used or perceived." A more detailed and complete definition of this subtype of flexible architecture is provided by Lee[8] "Transformable architecture: buildings and structures that are able to rapidly take on new shapes, forms, functions, or character in a controlled manner through changes in structures, skin and / or internal surfaces connected by articulated joints. " Based on these definitions, we can see that it is about the integration of technology into architectural objects, where the object can be adjusted to the user by means of joint connections and structural elements that can be moved. Based on the categories of flexible architecture, we can see that the boundaries between these categories are clearly defined, yet often some objects can be categorized into several categories at the same time.

In the case of transformable architecture, the method of performing object transformation (figure 1) can be classified into the following categories:[9]

1. The principle of joining and division: refers to adding or subtracting elements of an object
2. The principle of pulling in and drawing out: the ability of an object to extend and shrink joints according to user needs
3. The principle of opening and closing: this principle refers to the ability to open and close elements of an object. may refer to doors, windows or roof.
4. The principle of expanding and contracting: the principle which leads to modification of form building.

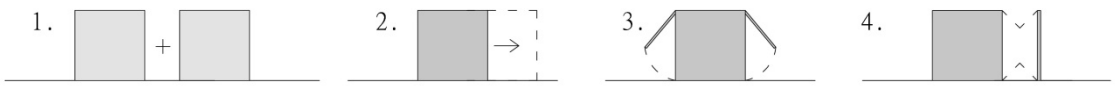

Figure 1: Categories of transformable architecture

In the following sections of the paper, the examples for each category are going to be analyzed. By examining various examples, the idea of the paper is to answer the following questions:

[6] Aishwarya B.K (2013).: Flexible architecture: What value does flexible architecture add to dwelings?, Phd thesis
[7] Kronenburg R (2007): Flexible: architecture that responds to change , book, Laurence King; First Edition edition
[8] Lee J.D. (2012): Adaptable, Kinetic, Responsive, and Transformable Architecture: An Alternative Approach to Sustainable Design , Phd thesis
[9] Anđelković V.(2016): Transformation principles in the architectural design of a contemporary house, Archi Doct, Vol. 4 (1), pp 87-107

- How the transformation of the building affects the shape of the analyzed object and how there has been a transformation
- What is the category of the analyzed objects and which method was used to produce a particular form,
- What are the reasons for the application of transformable architecture, is the function of the object or is it creative expression from the architect.

2.1. APPLICATION OF TRANSFORMATION METHODS IN ARCHITECTURAL DESIGN

The implementation of transformable elements is increasingly being implemented in practice. The analyzed examples were selected according to the specificity of the solution, and sorted by the categories given in the previous chapter.

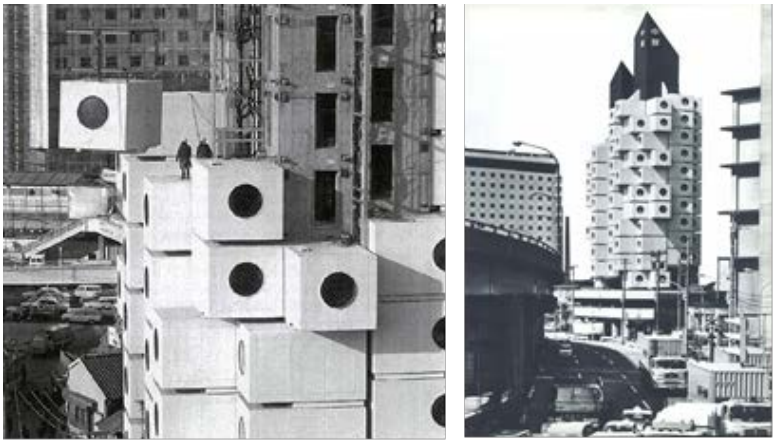

Figure 2: The principle of joining and division, Nakagin Tower, https://archeyes.com/wp-content/uploads/2016/03/nakagin-capsule-tower-tokyo-kisho-kurokawa-archeyes-23.jpg

The principle of joining and division affected the greatest change regarding shape of the object. It include modular architecture models, where by adding or subtracting a particular unit, the object is transformed according to user needs. The most famous example belonging to this type of building is certainly the Nakagin tower (figure 2), which was built in 1970. It is a groundbreaking project where the architect's idea was that units would further be merged and added, but unfortunately it wasn't implemented in practice. The shape of the module is cube, which was multiplied to build a shattered form around the central communication core. Latter examples remained at the concept level and did not come into practice. We're not talking here about shipping containers, which can be used as modular blocks for the construction of temporary structures.

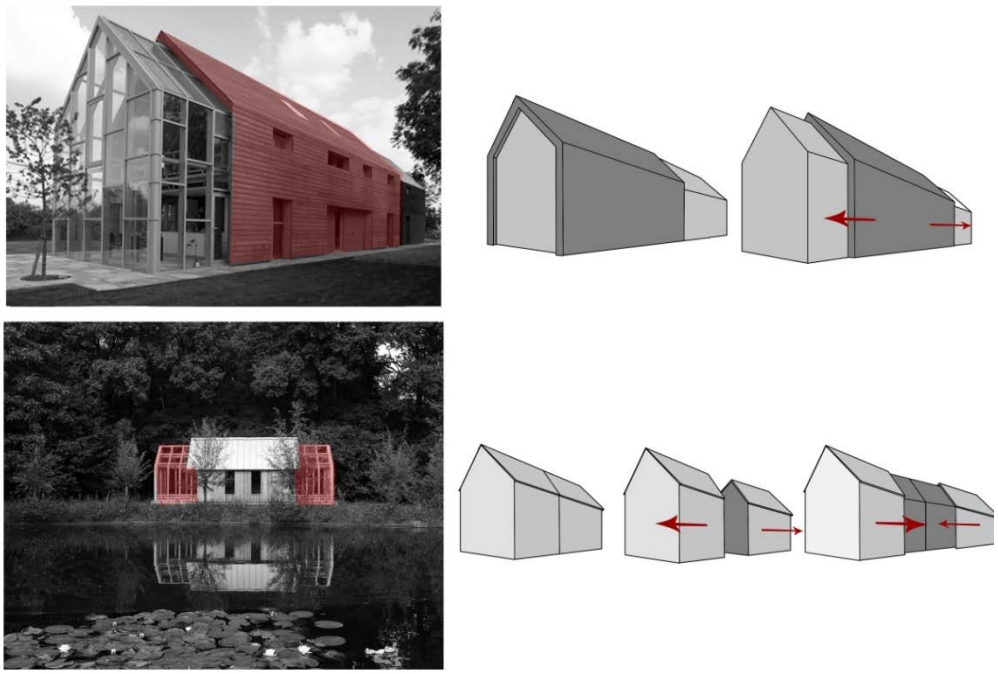

Figure 3: The principle of pulling in and drawing out, Sliding house and Sliding walls garden house

The principle of pulling in and drawing out (figure 3) very often used in residental projects. One example is the Sliding house, where the architects have formed two separate facilities, residential building made of glass and a garage that separates the interspace intended for communication between the two buildings. The objects are positioned linearly and covered with a membrane. This membrane follows the shape of the objects and with the help of rails, it can be moved according to the needs of the user. The shape of the building is unchanged, but this project represents the architectural seal of an architect who combined functionality, technical capabilities and creativity. A similar example is the sliding wall house, but in this project there is a change of form. From a traditional gable roof house, comes a prismatic shape where the height of the prism changes according to the needs of the user. The object can be separated into two sides, and since below the basic structure of the object is a glass membrane, it can close the object again, even though the object is now twice it's length before.

The most famous examples of transformable objects in the world of modern architecture relate to sports facilities.[10] The way in which transformative architecture is used to construct sports event facilities is most often in terms of moving the roof covering, actually by applying the principle of opening and closing (figure 4). The basic idea of these projects is to adapt in the best way to the needs of sporting events and weather conditions. Quizong stadium is one of the most famous examples of sports facilities with the principle of transformative connection. The base of the building is circular in shape and corresponds to the classic appearance of a sports facility intended for tennis. The articulated connection was applied in the roof cover that adapts according to the

[10] Mohamed M.A.A., Esam Hussein (2013): Transformable Architecture, A key to Improve stadiums & sports buildings, Hosting Major International, Innovation, Creativity and Impact Assessment, Egypt

events that are happening here, changes in climate and weather conditions. The specificity of this solution is the visual identity which is achieved by a specific form of roof coverings. The inspiration for the roof covering comes from the magnolia flower. Segments of the cover (membrane) are projected as petals that expand or shrink when we opening and closing the roof. The form of the petals is made of folds of prism and pyramid, identical in size that are radially placed from the center of the building. In the shrunken form they form a closed crown, which by rotating around the central axis results in the formation of a "flower" which gives the object an irregular shape and makes the object attractive to the viewer. Within public buildings where the roof can be opened and closed, we have another similar example. The Sjorstrom Stharling Theater also opens and closes segments of the roof covering, in which case there are 6 parts. The difference between the two examples is that here it is done only by raising and lowering and not by rotation as in the first example.

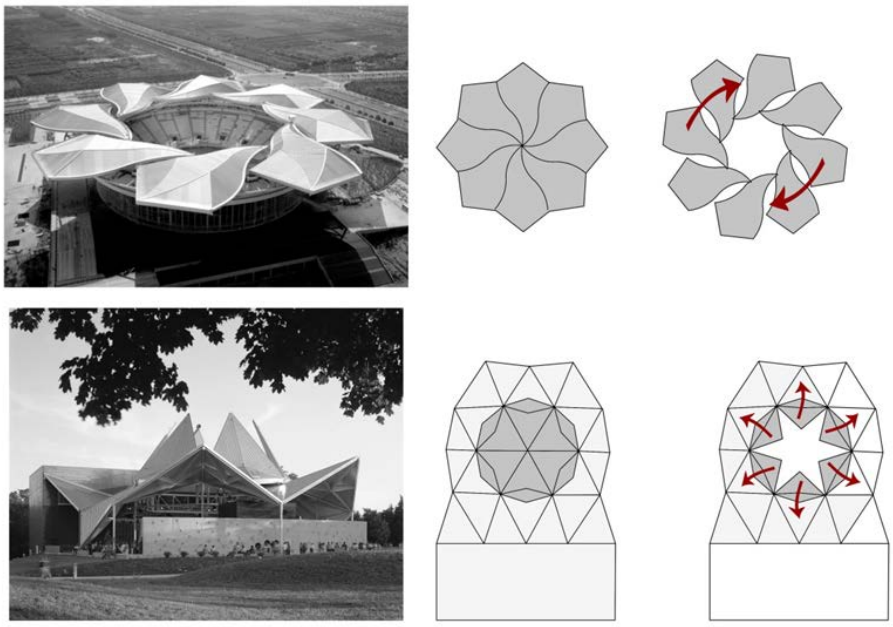

Figure 4: The principle of opening and closing, Quizong stadium and Sjostrom starling theatre

The method of opening and closing is often used in residential architecture. The membranes, which are placed over the opening elements are made of different elements and we can modify their position according to the needs of the user. In this case, there is minimal impact on form. It depends on the chosen form and method of implementation of that element, as shown in the selected examples (Ballet house, Tokyo Steel house, House in Smilovci, (figure 5)).

Figure 5: The principle of opening and closing, Ballet house, Tokio Steel house, House in Smilovci

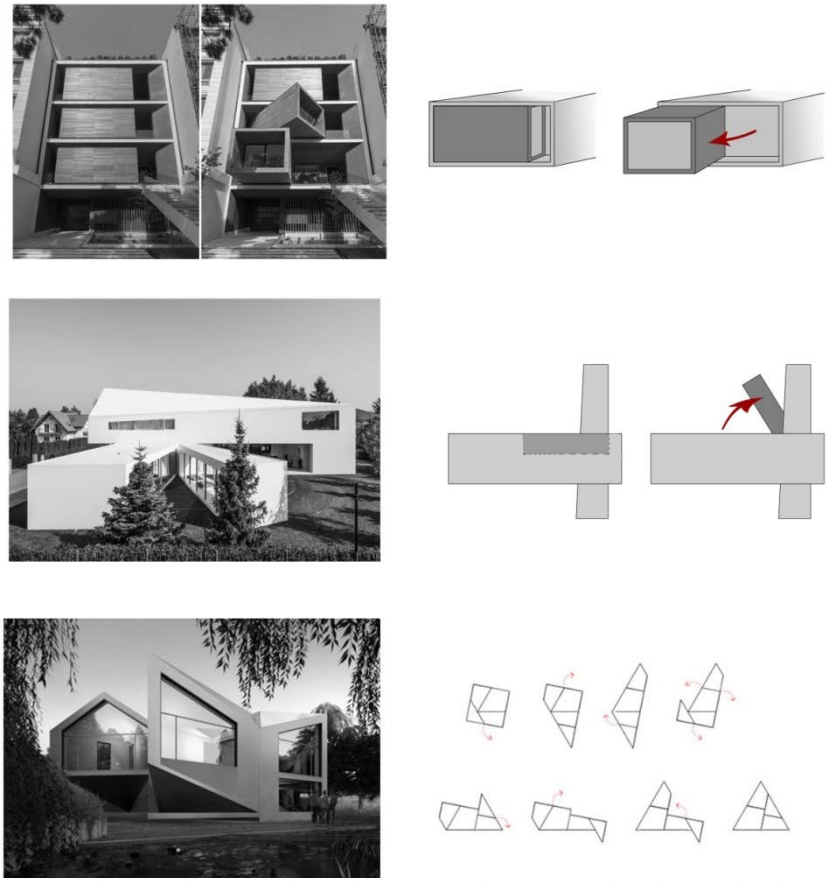

Figure 6: The principle of expanding and contracting, Sharifa Ha, Quadrant house and D+ house

The last category, the principle of expanding and contracting (figure 6), consists of objects that have a significant impact on the shape of the object itself. Projects HA Sharif house and Quadrant house at the first sign is a classic example of modern architectural practice. Both projects have flexible parts, which are rotated to fit the needs of the residents of those facilities. Square form is attached to the basic object, which can be rotated in all positions up to an angle of 90 degrees from the starting position. D house is a concept project which in its basic or zero position is cubed. However, according to user needs, weather conditions, this facility can be transformed into 8 positions. It is made up of 4 prisms, which can be moved by rotation so that the subject receives a variety of forms. The specificity of this solution is that in every position the object retains its functionality and aesthetics.

3.0. DISCUSSION - TRANSFORMABILITY IMPACT ON THE SHAPE OF THE OBJECT

Transformable architecture represents the integration of technology into a home, where the user is enabled to transform the object from a zero, initial position, which represents a simple structure, into a more complex system. From a zero position, objects can be transformed into one or more positions, which has a great impact on changes in the geometry of the object. With the changes that have taken place in geometry and the shape of the object comes to changes in the internal organization of space, where there is a modification in the dimensions of the rooms or modification of the position of walls and openings. Based on this case, we can see that architects use a simple form of a cube, a prism, or a combination of them, and to emphasize the aesthetic impression of a transformation and selected forms.

Based on the examples presented in the previous chapter, we can conclude that modification of a form by transformation takes place in two different ways by:

- *Rotation*: as in the example of Quizong stadium, Sjostorm theatre but also in residential buildings such as D +, Sharifa HA and Quadrant house. More influence on the shape is achieved by rotation, where it is possible to transform the shape into multiple positions and change more geometric shapes. In the analyzed examples where rotation is performed to achieve the effect of a transformable object, the elements are set in two ways:
    1. about a defined center, around which the rotation is made (Quizong stadium.Sjostrom starling theater, house D +, Ballet house)
    2. or attached to a basic object by a specific joints connection (Quadrant house, Sharifa Ha house)
- *by translational movement* of a certain element (Sliding house, sliding wall house, House in Smilovci, Tokyo steel house) when the objects are positioned linearly. The impact on the shape of the objects is minimal, mostly they are elements of the same geometric shapes that do not change the shape, only the dimension of the object is affected.

In the examples analyzed, we notice two models of how transformation is applied:

- by the change of particular element, or more precisely when part of the object transforms in accordance with the design and function, and in line with the project, leads to the greater influence on the shape of the object itself (Sharif Ha, Quadrant house and D + house)
- by using membrane (like roof or some other part of the object) as an element of transformation. Regarding these facilities there are two cases:
    1. when moving the entire membrane (Sliding house and Sliding walls garden house, Quizong stadium)
    2. when there are displacements of its parts, when there are no changes in the geometry of the object. In these cases, there is a change in the structure of the building, when by closing and opening certain parts (roof, doors, windows) it is possible to adapt the space to the external influences, weather conditions and needs of the user. Examples: Sjostrom starling theater, Ballet house, Tokyo Steel house, House and Smilovci.

The reason why architects choose to apply some transformable elements in all examples is mainly due to the connection of the outer and the inner space. The architect's vision of adapting his project to the weather conditions and enabling the user to use the space at all times during the year and easier connection with the natural environment can be seen in all the examples analyzed. One of the main reason is the higher utilization of natural light. In the first place, the reason for using such methods is certainly the functionality, but along with the functionality there is an aesthetic character, where the architects used their creativity to come up with interesting solutions. In all projects, there is a change in the composition of the object, which creates both a functional benefit and a visual atmosphere, and therefore we can conclude that this is a strong link between technology, geometry and aesthetics when we talk about transformable architecture.

4.0. CONCLUSION

Transformable architecture was in the first concepts solely for the purpose of function. Today, in addition to its functional features and construction, a large space is given to visual comfort. First of all, each of the projects certainly has an increase in functionality, but the way to apply transformability and how it has a design character. The use of transformable architecture can be called a combination of design and construction, where the main architectural method in the project is the specific form used as in the examples.

Based on the examples analyzed, we can conclude that architects dare to go beyond the traditional frameworks of static architecture and increasingly use transformable elements that fit into movable joints so they can easily adapt to the user. This is also the main purpose of transformable architecture, to increase usable space and to make it more usable in the event of weather changes. In public spaces benefit is the use of facilities

in all conditions, the facility operates as a closed hall and an open atrium. In residential projects, there is interaction with the external environment and a better involvement of yards and interiors. Based on the examples mentioned in the paper, we can see that as a consequence of transformability, a larger or smaller change in the geometry of the object occurs. When we talk about the geometry of the object, depending on the category to which the objects belong, we can see that there are different levels of transformation of the form. In some it is possible to transform an object into only two positions, while in some it is possible to transform in more positions (D+ house can be transform in 8 positions) , and there are more complex form occurs. Based on the analyzed examples, we can conclude that in transformable architecture, architects choose simple forms (box, prism) and achieve aesthetic experience by transforming these elements. The ways in which the form is transformed are the rotation and translation of the individual elements, while either the corresponding element that is attached to the basic object or the protective membrane is used as a moving element. Transformable architecture is used in all segments of architectural design, we have seen from the examples that it has been used equally in both public and residential buildings.

REFERENCES

1. Anđelković V.(2016): Transformation principles in the architectural design of a contemporary house, Archi Doct, Vol. 4 (1), pp 87-107
2. Asefi M. (2012): Transformation and movement in architecture: the marriage among art, engineering and technology, Procedia - Social and Behavioral Sciences, Volume 51, 2012, Pages 1005-1010
3. Aishwarya B.K (2013).: Flexible architecture: What value does flexible architecture add to dwelings?, Phd thesis
4. Kronenburg R (2007): Flexible: architecture that responds to change , book, Laurence King; First Edition edition
5. Kronenburg R. (2008): Portable ArchitectureDesign and Technology, book, Springer Science & Business Media
6. Kronenburg, R. H. (2004). Flexible Architecture: The Cultural Impact of Responsive Building. In 10th International Conference on Open Building (pp. pp). Paris, France: CIOB.
7. Kondić S. (2009): The application and importance of the principle of kinetic architecture in the design of family housing, nauka+praksa, Niš, Serbia
8. Lee J.D. (2012): Adaptable, Kinetic, Responsive, and Transformable Architecture: An Alternative Approach to Sustainable Design , Phd thesis
9. Web:
    - https://www.archdaily.com/917957/quadrant-house-kwk-promes/5cee9b5e284dd1f7c5000008-quadrant-house-kwk-promes-photo
    - https://www.mydesignweek.eu/architecture-design-the-sharifi-ha-house-in-tehran/
    - https://www.designindaba.com/articles/creative-work/house-turns-inside-out-summer
    - http://www.orangesmile.com/extreme/en/magnificent-stadiums/qi-zhong-stadium.htm
    - https://www.arch2o.com/bengt-sjostrom-starlight-theater-studio-gang/arch2o-ebengt-sjostrom-starlight-theatre-studio-gang-05/
    - https://www.archdaily.com/875241/house-in-smilovci-modelart-arhitekti/595dc918b22e38537c000073-house-in-smilovci-modelart-arhitekti-photo
    - https://www.archdaily.com/299403/tokyo-steel-house-mds/50b6b009b3fc4b7c990000a0-tokyo-steel-house-mds-photo
    - https://www.archdaily.com/909097/ballet-mechanique-manuel-herz-architects

APPLYING OF GRASSHOPPER IN GEOMETRIC OPTIMIZATION OF TORUS SHELL

Nastasija Kocić
Faculty of Civil Engineering and Architecture, University of Niš, Niš, Republic of Serbia
PhD Candidate, nadja93.al@hotmail.com

Sonja Krasić
Faculty of Civil Engineering and Architecture, University of Niš, Niš, Republic of Serbia
PhD., Associate Professor, krasic.sonja@gmail.com

Zlata Tošić
Faculty of Civil Engineering and Architecture, University of Niš, Niš, Republic of Serbia
PhD Candidate, zlata10@live.com

Jovana Stanković
Faculty of Civil Engineering and Architecture, University of Niš, Niš, Republic of Serbia
PhD Candidate, jovana__stankovic@hotmail.com

ABSTRACT

In contemporary architecture, where function often follows the form of an object, the use of curved structures is increasingly present. The development of new technologies and software enables faster and easier creation of planned forms of objects. In some cases, modeling limits us to reduced forms with planarization of curved surfaces.

Planarization can be obtained with combination of some software and their extensions. In this paper, the authors used a canopy obtained from a torus shell. Segments of torus are determined by intersecting with vertical planes. Since the torus is a double curved surface, Grasshopper was used to obtain the planar elements of which the torus shell would be made.

As a graphical algorithm editor, Grasshopper is tightly integrated with Rhinoceros's 3D modeling tools. Because of that, Rhinoceros was used in design and Grasshopper was used in optimization and planarization of curved shape. The goal of the paper is to show how planar elements can obtain a stable, curved surface.

Keywords: torus shell; curved surfaces; geometric optimization; Rhinoceros; Grasshopper

1. INTRODUCTION

The use of curved surfaces in architecture is increasing, because when it comes to a perceptual process, form is the most important element of the design. Some of the great architects used the elements of curved surfaces, combining them to get attractive objects. The design process is one problem, but quite another emerges when it comes to the performance of the actual objects [1].

Curved surfaces may be optimized in a number of ways. One method results in planar panels. The initial surface form is approximated in order to obtain planar elements, and depending on the size of individual elements, a greater or lesser distortion in the geometry of the set form occurs [2]. Whereas Torus shell used in this paper, was modelled in Rhinoceros, software that offers simple options for complex freeform structures with knowledge of their geometry. Torus shell was divided into segments to form a pavilion canopy [3]. Our approach to the

geometric optimization is based on the use of Grasshopper, a modelling plugin for Rhinoceros and a structure of planar elements was obtained [4]. This paper presents a simple geometric approach to optimize torus shell, using planar elements, with the goal of obtaining a stable curved structure. In our work we would like to give the opportunity to choose the planar elements size. The other part of project is model making with the aim of showing the stability of such a construction.

2. THE WORKFLOW

In order to work with curved surfaces, it is necessary to know their geometry and the way they are obtained. Torus belongs to special surfaces of revolution, generated by rotating a circle in three-dimensional space about an axis that is coplanar with the circle. In this paper, parts of torus shell were used to construct a canopy that can be used as a pavilion [5]. The torus measuring 14 meters in outer diameter and 5 meters in inner diameter of the circle. Then the uper half torus shell was divided into 12 parts, by vertical planes and was cut by quadrilateral prism with side 14 m. Eight elements were trimmed, while the other 4 elements remained whole to form a canopy (Figure 1).

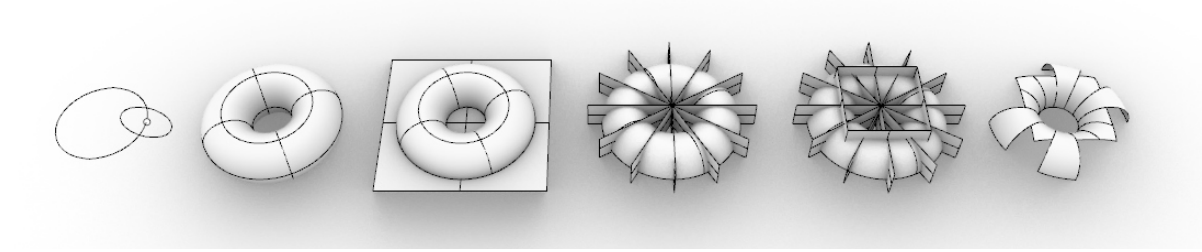

Figure. 1: The workflow of the pavilion canopy

2.1. Modelling in Rhinoceros

Rhinoceros is a program where curved and double-curved surfaces can easily be obtained. It has the tools to form a desired surface with specific dimensions in a few steps (Figure 2). With other tools it is possible to modify them, break them down into sections, gain intersections and breakthroughs. As the torus shell is the topic of this research, it was modelled in Rhinoceros with tool "Torus", using the Perspective view:

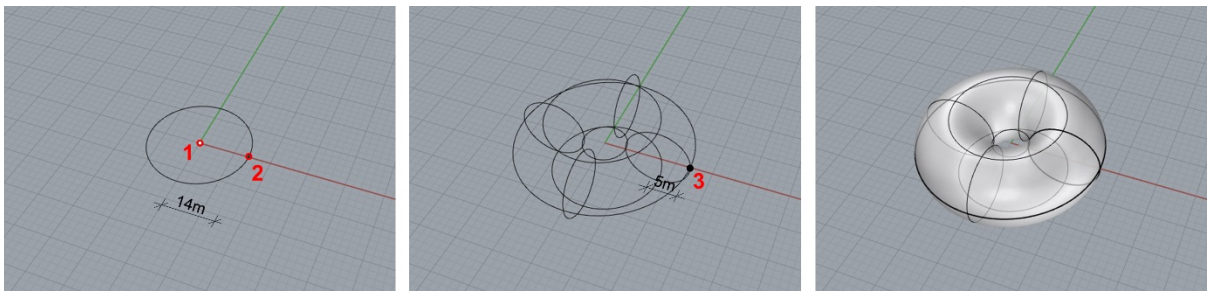

(a) (b) (c)

Figure. 2: (a) Determining the center and the first radius, (b) the size of the second radius, and (c) the final appearance of the torus; Rhinoceros

2.2. Optimization with Grasshopper

In Grasshopper, we want to obtained the torus shell to get a surface that will contain planar elements, but also to maintain the original shape. From tab Params, in section Geometry, the option Surface was choosen. To connect Grasshopper with Rhinoceros, the torus was selected as a setting surface. The option Divide Domain2 from Maths/Domain tab was choosen to divide a two-dimensional domain into equal segments. Then, the surface was pluged in with Base Domain (Figure 3). In order to specify the number of segments in U and V direction, one division was started with minimum 30 and ended with 50 parts (Figure 4). By trying different numbers of segments, it was found that it is most rational to choose a division into 48 parts in both directions.

Figure. 3: Option Divide Domain[2] connected with Surface; Grasshopper

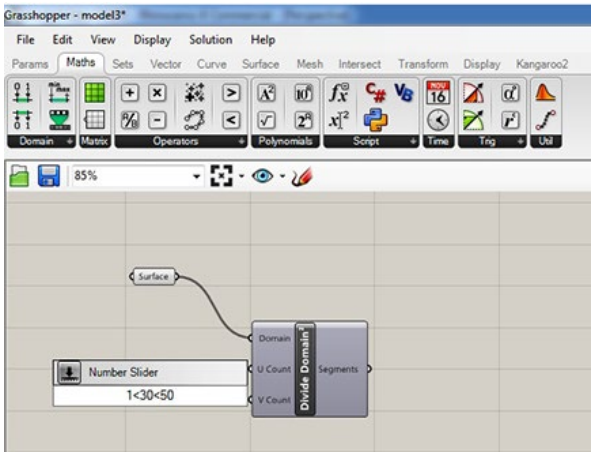

Figure. 4: Number Slider in the range of 1 to 50; Grasshopper

Two slider controls with U and V count were pluged in. For this work we will set 48 number of segments for both directions (Figure 5). Under Surface/Utilities, Isotrim was used, which allows to extract an isoparametric subset of the surface. We plug in the original surface with input for Isotrim and connect Segments with Domain (Figure 6).

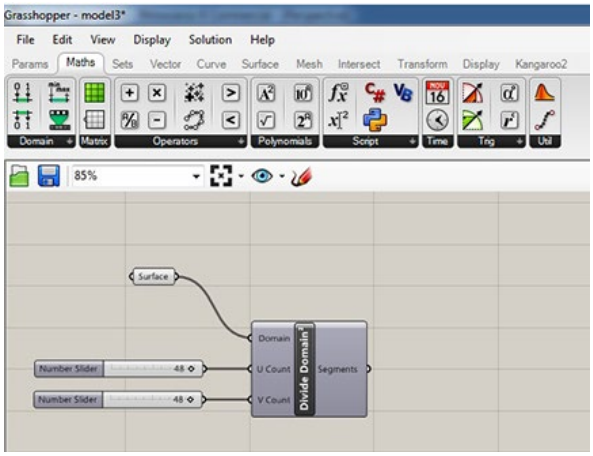

Figure. 5: Number of segments-48 connected with U and V direction; Grasshopper

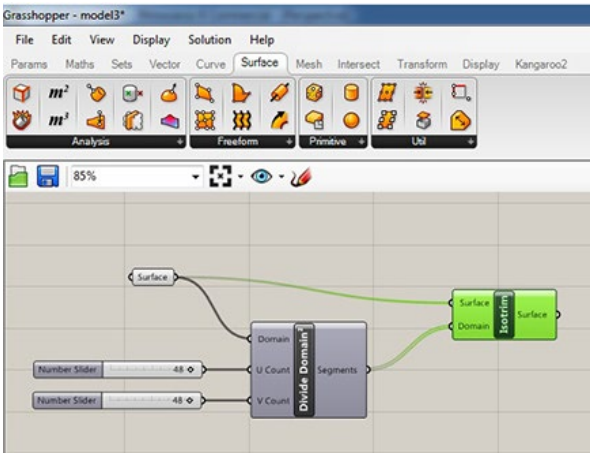

Figure. 6: Option Isotrim, connected with Surface and Segments; Grasshopper

We can “bake” on Isotrim option to see what we have for now. The panels were obtained as a subportions of the original surface (Figure 7). But, in order to obtain planar surfaces, it is necessary to reduce the curve order.

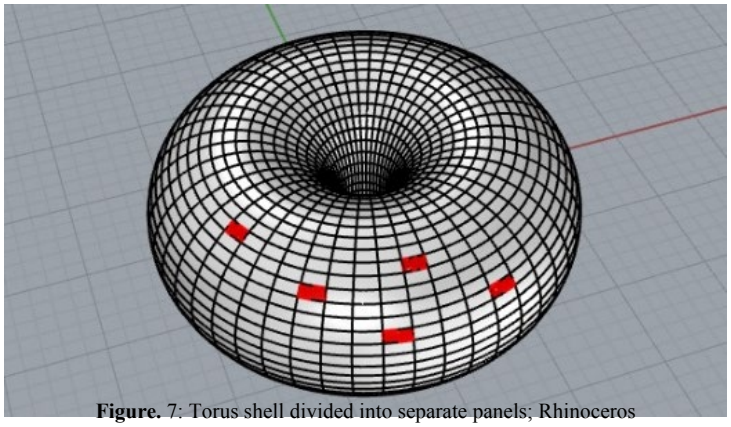

Figure. 7: Torus shell divided into separate panels; Rhinoceros

We want to obtained torus surfaces by the curve intersections. To obtained prism surface it was used the option 4Point Surface was used (Surface/Freeform/4Point Surface). For input, there are corners A, B, C and D. Therefore, four List Items are required (Sets/Items/List Item) (Figure 8).

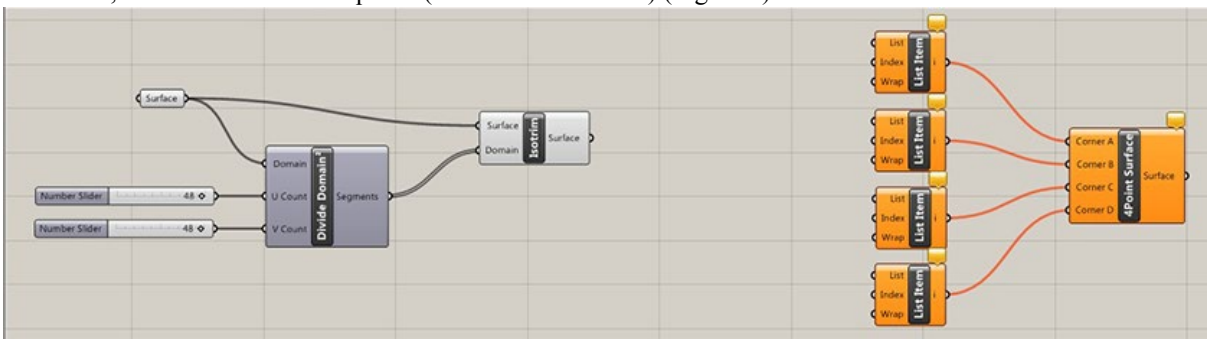

Figure. 8: Four List Items pluged in to option 4Point Surface; Grasshopper

To mark intersection vertices and connect them with List Items, the option Deconstruct Brep was used (Surface/Analysis/Deconstruct Brep). The surface from Isotrim was pluged in and Vertices was connected with Lists (Figure 9).

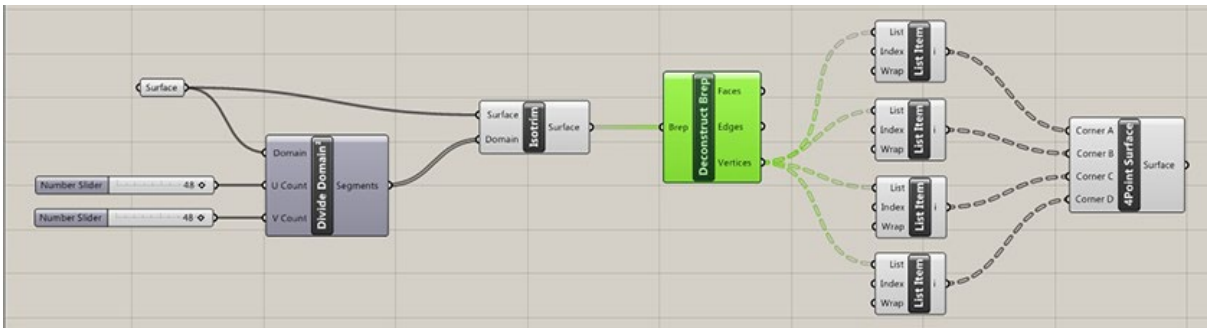

Figure. 9: Deconstruct Brep connected with surface and List Items; Grasshopper

The final appearance obtained with option Bake shows torus shell, which now consists of planar segments (Figure 10).

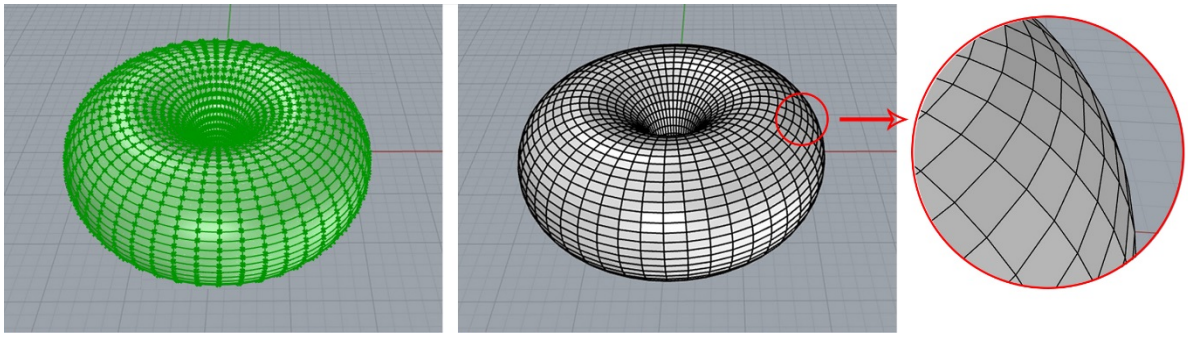

(a) (b)

Figure. 10: (a) The intersection points selected in Grasshopper, and (b) baked torus shell consisted with planar surfaces; Rhinoceros

2.3. Canopy formation

First, all the parts were connected into one whole with option Join. The torus was cut with a horizontal plane. After that, the bottom part of the surface was removed (Figure 11).

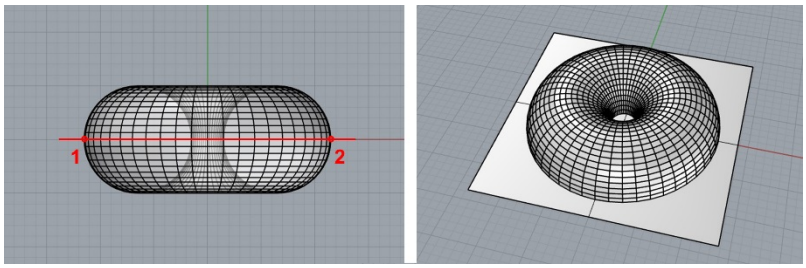

(a) (b)

Figure. 11: (a) Positioning of horizontal cutting plane, and (b) perspective view; Grasshopper

Afterwards, the surface was divided into 12 equal parts by copying the vertical cutting surface (In Top view) relative to the center with option Transform/Array/Polar. The center of polar array coincides with the center of the torus. The chosen angle is 360, and number of cutting planes is 12 (Figure 12).

The surface was divided by vertical planes with option Split. The next step is to draw the square in the Top view, whose sides are aquidistant from the center of torus and with length of 14m. Then, the square was extruded, to cut the shell (Figure 13). Unnecessary parts were removed by option Trim (Figure 14).

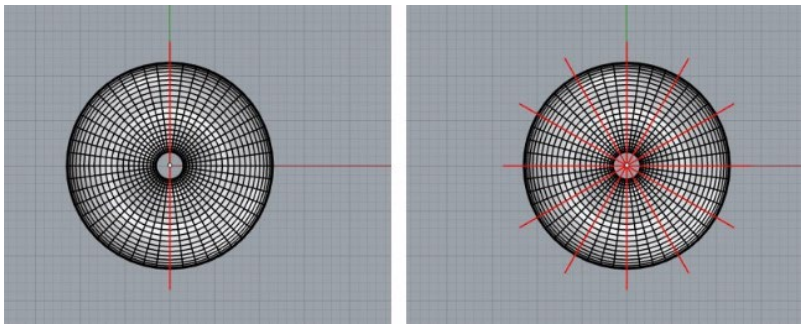

Figure. 12: 12 vertical cutting planes; Grasshopper

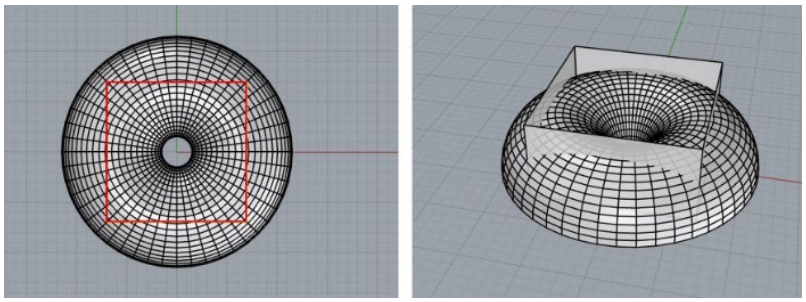

Figure. 13: Extruded square; Grasshopper

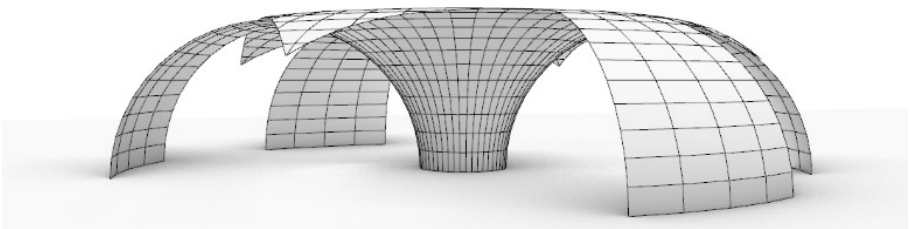

Figure. 14: Perspective view of the canopy; Rhinoceros

2.4. Model making

In order to check the stability of the structure, we made a scale model. Since the elements would be too small, we reduced the number of segments to 12 for making 3D model of the canopy with laser cutter. Half of the original torus was extracted, openings were added, and preparation for cutting was done in the Grasshopper (Figure 14).

(a) (b)

Figure. 14: (a) Laser cutter operation, and (b) scale model of canopy structure

3. CONCLUSION

To solve the problem of performing of curved surfaces objects can be optimized in a number of ways. In this paper, we worked on a geometric optimization of torus shell to make a canopy. The Rhinoceros softwer has proven as exelent in modelling of complex geometric surfaces, such as double-curved, so we used it for modelling of a torus shell.

With a number of options in Grasshopper, planarization of curved surface was performed and we obtained a structure of planar elements. In this way we made a canopy that can be made of planar elements and can be stable. With the Grasshopper algorithm we have enabled easy change of the number of segments in both directions.

This was checked on the 3D model, where a smaller number of panels were chosen. With the model, we determined that the structure is statically stable, and by increasing the number of planar elements, a structure even closer to the initial curved shape can be obtained, what will be the goal of further research.

REFERENCES

1. Tošić Z., Krasić S.,Ando N., Milić M. (2018). Geometrical and construction optimization of church St. Joseph the Craftsman in Mexico of architect Felix Candela, MoNGeometrija 2018., Serbia;
2. Stavrić M., Wiltsche A. (2015). Ornamental plate shell structures, Institut for Architecture and Media, Faculty of Architecture, Graz;
3. Krasić S., (2012). Geometrical surfaces in Architecture (Geometrijske površi u arhitekturi), Faculty of Civil Engineering and Architecture, Unversity of Niš, Serbia;
4. http://grasshopperdocs.com/ [Accessed: 10th March 2020];
5. Veljković M., Krasić S., Pejić P., Tošić Z., (2012). A case study of modelling torus in different modelling softwares, VOLUME 7 ISSUE 1 JIDEG.

CIP - Каталогизација у публикацији - Народна библиотека Србије, Београд

514.18(082)(0.034.2)
004.92(082)(0.034.2)

INTERNATIONAL Scientific Conference on Geometry and Graphics (7 ; 2020 ; Beograd)

Proceedings [Elektronski izvor] / The 7th International Scientific Conference on Geometry and Graphics, moNGeomatrija2020, September 18th - 21st 2020, Belgrade, Serbia ; [conference organizers Serbian Society of Geometry and Graphics (SUGIG) [and] Faculty of Mechanical Engineering, University of Belgrade] ; editor-in-chief Zorana Jeli]. - Belgrade : Serbian Society for Geometry and Graphics (SUGIG) : Faculty of Mechanical Engineering, University, 2020 (Belgrade : Planeta print). - 1 elektronski optički disk (CD-ROM) ; 12 cm

Sistemski zahtevi: Nisu navedeni. - Nasl. sa naslovne strane dokumenta. - Tiraž 80. - Bibliografija uz svaki rad.

ISBN 978-86-6060-046-4 (FMEU)

1. Serbian Society for Geometry and Graphics (Beograd)

a) Нацртна геометрија - Зборници
b) Рачунарска графика - Зборници

COBISS.SR-ID 19970825

www.mongeometrija.org